THE FLEXIBILITY AND STRENGTH OF CORRUGATED DIAPHRAGMS AND FOLDED PLATES

VOLUME 1.

A Thesis Submitted for
the Degree of
DOCTOR OF PHILOSOPHY

by

Robert Mark Lawson, B.Sc., A.C.G.I.

Department of Civil Engineering,
University of Salford

September 1976

C O N T E N T S

Page No.

DECLARATION ..... (i)

ABSTRACT ..... (ii)

ACKNOWLEDGEMENTS ..... (iv)

LIST OF SYMBOLS ..... (v)

LIST OF FIGURES ..... (ix)

LIST OF PLATES ..... (xv)

CHAPTER 1: INTRODUCTION

1.1. General Concepts 1
1.2. The Stressed Skin Approach in Framed Buildings 2
1.3. The Strength of Corrugated Diaphragms 6
1.4. Shear Flexibility 9
1.5. Applications of Corrugated Sheeting in Frameless Structures 12
1.6. Limitations of Present Knowledge 13

CHAPTER 2: THE DISTORTIONAL FLEXIBILITY OF TRAPEZOIDAL SHEET PROFILES FASTENED IN EVERY TROUGH

2.1. Simplified Approaches 16
2.2. Methods due to Libove, Strehl and Others 20
2.3. Energy Method of Assumed Displacement Functions 24
2.4. Influence of Sheet Length, Thickness and Number of Fourier Terms 34
2.5. Possible Energy Method of Localized End Distortion 36
2.6. Experimental Determination of Flexibility 38
2.7. Finite Element Method for Determining Corrugation Distortion 40
2.8 Effect of Edge Beam Restraint on Shear Distortion 41
2.9. Effect of Fastening to Intermediate Purlins 44
2.10. Sheets Fastened in Intermediate Purlins in Alternate Troughs and in Every Trough at their Ends 49
2.11. Longitudinal Variation of Cross-Section Displacements 50
2.12. Comments on the Distortional Flexibility as Determined by the Energy Method 54

Page No.

2.13. Comparison of Energy Method Results with Libove and Strehl Methods 56
2.14. Comparison with Finite Element Results 57
2.15. Comparison of 'Purlin-Prop' Reduction of Flexibility with other Theories 58
2.16. Discussion of Experimental Observations for Every Trough Fastening with no Intermediate Purlins 59
2.17. Discussion of Experimental Observations for Every Trough Fastening for up to Four Intermediate Purlins 62

CHAPTER 3: THE SHEAR FLEXIBILITY DUE TO DISTORTION OF SHEETS FASTENED IN ALTERNATE OR EVERY THIRD TROUGH

3.1. General Solution 65
3.2. Alternate Trough Fastening 67
3.3. Fastening in Intermediate Purlins 75
3.4. Effect of Length, Sheet Thickness and Number of Fourier Terms for the Energy Method Derivation 77
3.5. Effect of Intermediate Purlin Fixings 78
3.6. Edge Beam Reduction Factor due to Fastening in Alternate Troughs 79
3.7. Testing by Experiment and Finite Elements 83
3.8. Purlin Prop Reduction Comparison with Finite Elements 84
3.9. Discussion of Experimental Results for no Intermediate Purlins 85
3.10. Discussion of Experimental Results for up to Three Intermediate Purlins 86
3.11. Fastening in Every Third Corrugation 87
3.12. Edge Beam Restraint for Fastening in Every Third Trough 90
3.13. Discussion of Test Results for Every Third Corrugation Fastening 92
3.14. Excessive Deformation due to Concertina Action 93

CHAPTER 4: THE SHEAR FLEXIBILITY OF SINUSOIDAL CORRUGATIONS

4.1. Theories due to McKenzie and Libove 96
4.2. Energy Method Solution for Every Trough Attachment 97
4.3. Intermediate Purlin Fixings in Every Corrugation 102

Page No.

4.4. Effect of Sheet Length, Thickness and Number of Intermediate Purlins 103
4.5. Comparison of Theory with Libove's, McKenzie's and Experimental Results 105
4.6. Fastening in Alternate Troughs at Intermediate Purlins 108
4.7. Discussion of Energy Method Results for Alternate Trough Fixing and Comparison with Experiment 111

CHAPTER 5: METHODS OF REDUCING SHEAR DISTORTION

5.1. 'Folded-Down' Corrugation Ends 112
5.2. Discussion of Energy Method and Experimental Results for Folded Down Corrugations 115
5.3. Double Trough Fastened Corrugations 117
5.4. Discussion of Theoretical and Experimental Results for Double Fastened Corrugations 118
5.5. Effect of Sheet Overhang Beyond Purlins 119
5.6. Effect of Insulation Resistance to Deformation 121
5.7. Curved Down Corrugation Overhand Ends 126

CHAPTER 6: OVERLAPPING SHEETS

6.1. Overlaps Fastened in Every Corrugation 129
6.2. Overlaps Fastened in Alternate Corrugations 133
6.3. General Interaction Formula for Over-Lapping Sheets 136
6.4. Formulae for any Number of Overlapping Sheets 137
6.5. Formulae for Overlapping Sheets of Different Lengths 140
6.6. Effect of Sheets Fastened in Every Trough at their Ends and Alternate Troughs at the Overlaps 143
6.7. Comparison with Experimental Results for Overlaps Fastened in Every Trough 146
6.8. Comparison with Experimental Results for Overlaps Fastened in Alternate Troughs 147
6.9. Comparison with Experimental Results for Sheets Fastened in Every Trough at their Ends and Alternate Troughs at the Overlaps 148

Page No.

CHAPTER 7: CONTINUOUS DIAPHRAGMS

7.1.	Modified Shear Distortion Flexibility due to Sheets Spanning Across a Central Rafter	150
7.2.	Discussion of Experimental and Theoretical Observations for Two and Three Bay Continuous Diaphragms	157
7.3.	Inertia of Purlins in Simple Diaphragms	159
7.4.	Inertia of Purlins Spanning Across Rafters	160
7.5.	Effect of Sheet Overlaps	165
7.6.	Overlapping Sheets with Variations in the Fastening Arrangement	167

CHAPTER 8: THE SHEAR STRENGTH OF CORRUGATED DIAPHRAGMS

8.1.	Connections	171
8.2.	Possible Diaphragm Failure Modes	173
8.3.	Indirect Shear Transfer Through Purlins	174
8.4.	Effect of Laterally Weak Purlins	179
8.5.	Discussion of Theoretical Results for Diaphragm Strength	184
8.6.	Comparison of Differential Equation and Finite Element Results for Diaphragm Strength	187
8.7.	Effect of Holes in Diaphragms (Isolated Opening; Periodic Openings)	188
8.8.	Discussion of Differential Equation Results for Openings in Diaphragms	198
8.9.	Comparison of Differential Equation and Finite Element Results	200

CHAPTER 9: SHEAR BUCKLING OF CORRUGATED SHEETING

9.1.	Review of Theoretical Investigations for Flat Diaphragms	203
9.2.	Special Notes on the Shear Buckling Formula	206
9.3.	Effect of Periodic Intermediate Purlin Fasteners	208
9.4.	Effect of Sparce Perimeter Attachments	210
9.5.	Discussion of Theoretical and Experimental Results for Shear Buckling	212
9.6.	Shear Buckling of Hyperbolic Paraboloid Shells	215

Page No.

CHAPTER 10: FOLDED PLATE ROOFS

10.1.	The Folded Plate concept	220
10.2.	Folded Plate Analysis as Applied to Concrete Roofs	223
10.3.	Folded Plate Roof Design using Corrugated Steel Sheeting	226
10.4.	Formulae for Steel Folded Plate Roof Design	229
10.5.	Prototype Folded Plate Roof Design	234
10.6.	Design of Specially Pressed Sheeting	237
10.7.	Erection of Prototype Folded Plate Roof	240
10.8.	Design of Loading System	242
10.9.	Testing Procedure	244
10.10.	Discussion of Experimental Results	245
10.11.	Limits of Viability of Folded Plate Roofs	247
10.12.	Comparison with Portal Frame Construction	253
10.13.	Design Summary for Folded Plate Roof using Open Profiled Sheeting	254

CHAPTER 11: SPECIAL PROBLEMS RELATED TO FOLDED PLATE ROOFS

11.1.	Holes in Folded Plates	260
11.2.	General Approach for Holes in Folded Plates	267
11.3.	Lateral Instability of Edge Beam	271
11.4.	Variations in Sheet Flexibility along the Roof Length	275

CHAPTER 12: EXPERIMENTAL TESTING OF CORRUGATED WEB GIRDERS

12.1.	Tests on Pressed Sheeting and Standard Open Profile	280
12.2.	Discussion of Deflection Comparisons	282
12.3.	Corrugated Web Beam Test Results	284
12.4.	Comparison of Failure Loads with Theory	286

CHAPTER 13: CONCLUSIONS TO THESIS

13.1.	Conclusions of Main Topics	289
13.2.	Design Calculations	293

REFERENCES: 297

VOLUME 2

C O N T E N T S

LIST OF FIGURES

FIGURES

APPENDIX 1

Experimental Test Results

APPENDIX 2

Design Data for Corrugated Sheeting Flexibility

APPENDIX 3

Sheet Overlap Design Data

APPENDIX 4

Folded Plate Roof Design

APPENDIX 5

Computer Programs

D E C L A R A T I O N

None of the material contained in this thesis has been submitted in support of an application for another degree or qualification of this or any other university or institute of learning.

Robert Mark Lawson
September, 1976

A B S T R A C T

Trapezoidally corrugated sheeting has been previously studied with regard to applications in shear diaphragms, making use of its inherent strength and stiffness properties by suitable connections. The in-plane deflection is an important design factor and the shear distortion component, due to eccentric transfer of fastener force into profile shear, is a major contributor to the total. A design formula is developed for the distortional shear flexibility for sheets fastened in every trough and in intermediate purlins which takes account of the localized distortion at the sheet ends by using an energy method analysis of assumed displacement functions to represent plate bending.

For fastening in alternate or multiple of troughs, an additional profile concertina distortion occurs, resulting in a large increase in the shear flexibility. A similar energy method is performed as for the previous case, developing the same basic formula for the distortional deflection. A corresponding study is made for sinusoidally corrugated sheeting.

A number of practical design factors have been examined - including the effect of longitudinally overlapping sheets, and purlin restraint on profile distortion. For sheets spanning over rafters into different shear fields, the expressions for shear flexibility have been modified.

The strength of diaphragms has been investigated, especially with regard to fastening on two sides only, which includes the torsional and bending stiffness of laterally weak purlins. Diaphragm openings cause an increase in the sheet flexibility and constrain purlins to follow the resulting displaced shape. Consequently locally high purlin bending stresses and sheet-purlin forces may be generated, as revealed by differential equation and finite element studies.

Corrugated sheeting has many applications in frameless structures such as folded plates and hyperbolic paraboloids. The flexibility and strength expressions have been used to design a prototype three bay folded plate roof which utilizes specially pressed sheeting to reduce the shear distortion component of roof deflection.

The shear buckling strength of corrugated diaphragms is an important factor in such construction. For larger roof diaphragms with only periodic intermediate fixings to purlins, buckling may occur over the complete diaphragm depth rather than separately in each bay, and design tables are shown for this condition.

A C K N O W L E D G E M E N T S

I am especially grateful to Dr. J. M. Davies, my supervisor, who helped me throughout my theoretical work. I also thank Professor E. R. Bryan who gave invaluable advice in the selection of the topic for this thesis and the consequent experimental study.

I also wish to express my appreciation to:

- The staff of the Fitton Structures Laboratory in the charge of Mr. W. H. Deakin for their assistance during the experimental testing and construction.

- Mr. J. Grimshaw for his management of the folded plate roof construction project.

- Mr. F. Ogden and his Mechanical Workshop Team, for the fabrication of the steelwork for the test rigs and roof.

- Mr. T. Clark, for overall supervision of the Technical staff during the research project.

- Mr. C. Tivey for the preparation of the photographs.

- Mrs. J. Kenworthy, who typed the manuscript.

I also acknowledge the financial and technical assistance given to me by various outside bodies, such as:

British Steel Corporation Product Development Centre, Shotton, Clwyd.

Hawker Siddeley Aviation Company, Greengate, Manchester.

F. E. Titmus Company Ltd., Wellinborough, Northants.

The Institution of Structural Engineers, Lancashire and Cheshire Branch.

The Science Research Council.

LIST OF SYMBOLS

a	panel or sheet width, mm
a^1	- sheet overhang
a_1, a_2	- imaginary roots of differential equation
a_1^1, a_2^1	- real roots of differential equation
a_i	- energy method parameter
A	- fold line or purlin area, mm^2
b	- sheet length, mm
b^1	- distance between outer purlins
$2b_T$	- profile crest width, mm
$2b_S$	- profile side plate width, mm
$2b_L$	- profile trough width, mm
b_1, b_2	- imaginary roots of differential equation
b_1^1, b_2^1	- real roots of differential equation
B	- folded plate roof column spacing, m
c	- corner uplift of hyperbolic paraboloid
C	- total panel flexibility, mm/kN
$C_{1.1}$	- flexibility due to sheet distortion, mm/kN
$C_{1.2}$	- flexibility due to shear strain
$C_{1.3}$	- flexibility due to axial strain in the purlins
$C_{2.1}$	- flexibility due to sheet-purlin fastener slip
$C_{2.2}$	- flexibility due to seam slip
$C_{2.3}$	-flexibility due to sheet-shear connector slip
$C(i, j)$	- profile distortion energy terms
d	- profile pitch, mm
$d_{1.1}$	- central folded plate deflection due to sheet distortion
$d_{1.2}$	- etc., as above for $C_{1.2}$, etc.
$D(i, j)$	- total energy terms for every trough attachment flexibility

$\bar{D}$ - profile inertia per mm sheet thickness

D - sheet bending stiffness, kN mm

D_x - orthotropic sheet minor bending stiffness, kN mm

D_y - orthotropic sheet major bending stiffness, kN mm

E - Young's modulus kN/mm^2

E_d - internal energy due to sheet distortion

E_b - internal energy due to plate bending

E_{Tot} - total internal energy

f - side plate uplfit for unit concertina displacement

F_S - seam fastener capacity

F_p - sheet-purlin fastener capacity

F_{sc} - sheet-shear connector fastener capacity

g - proposed factor for effect of purlins on diaphragm slip and strength

g_1 - factor for influence of sheet-purlin fasteners on seam slip, etc.

G - shear modulus kN/mm^2

G_i - insulation shear modulus

$\bar{G}$ - effective shear modulus

h - profile depth

I - purlin lateral inertia

I_S - sheet bending inertia

J - purlin torsional inertia

k - slope of buckling wave

K - rigid plate movement distortion parameter

$\bar{K}$ - localized end distortion parameter

$\bar{K}_A$ - $\bar{K}$ value due to concertina action of alternate trough fixing

$\bar{K}_E$ - $\bar{K}$ value due to fastening in every trough

$\bar{K}_{EN}$ - $\bar{K}$ value due to fastening in every trough to N intermediate purlins

l - pitch of buckling wave

L - length of folded plate roof, m

M_i - cross-section bending moments using in analysis

M - number of continuous diaphragm bays with alternate trough fastening at the sheet overlap

n - number of sheet-purlin fasteners

n_p - number of purlins

n_e - number of sheet-purlin fasteners / mm

n_s - number of seam fasteners

n_{sc} - number of sheet-shear connector fasteners

n_{sh} - number of sheets in folded plate span

N - number of bays between purlins or rafters

p - profile dimension, equals to tan θ .h

p^1 - fastener pitch mm

P_1, P_2 - uplift forces due to purlin restraint kN

P - axial force in member kN

q - local in-plane loading kN/mm^2

q_f - vertical fold line loading, kN/mm

Q - diaphragm shear force, kN

Q_S - seam shear force capacity, kN

Q_{sc} - sheet-shear connector force capacity, kN

Q_{cr} - critical buckling load, kN/mm

r - flexibility reduction factor due to fastening in every trough at the sheet ends and alternate fastening at the overlaps

r_E - flexibility reduction due to 'purlin-propping' for fastening in every trough

r_A - as above, for fastening in alternate troughs

r_T - as above, for fastening in every third trough

R - diaphragm reaction

S - co-ordinate around profile

$\bar{S}$ - profile perimeter, mm

t - sheet thickness, mm

t_i - thickness of insulation, mm

U_T - top plate displacement for every trough fixing analysis

U_S - side plate displacement

U_B - trough plate displacement

$\bar{U}_T$ - end top plate movement

V_O - purlin centroid displacement

V_E - purlin top flange displacement

V_S - sheet displacement

W - normal loading, kN/mm^2

x - co-ordinate along purlin

x_d - distorted length

X_1, X_2 - overlap restraints

y - co-ordinate along sheet from mid-span

z - co-ordinate normal to profile

ε - overlap slip factor

θ - side plate slope to the vertical

θ^1 - folded plate inclination to the horizontal

ϕ - parameter in 'purlin-prop' reduction analysis

δ_{ij} - profile displacement at i due to a force at j

γ - ratio of major to minor bending stiffnesses

χ - buckling parameter

σ - bending stress N/mm^2

τ - shear stress N/mm^2

Δ - shear displacement

ν - poisson's ratio

LIST OF FIGURES

CHAPTER 1.

1. A typical roof diaphragm
2. Equilibrium of sheet and members
3. A practical diaphragm arrangement
4. Diaphragm restraint of frame sway
5. Sheet flexibilities in normal directions
6. Flexibilities due to fastener slip
7. Complete lateral stability of roof provided by the sheeting
8. Spread of pitched roof portal frame under normal load
9. Forms of frameless structure - folded plate roof
10. Hyperbolic paraboloid
11. Cylindrical shell

CHAPTER 2.

1. Shear distortion for every trough fixing
2. Warping due to plate movements
3. Cross-sectional bending moments
4. Superposition of Fourier terms
5. Asymptotic behaviour of shear distortion
6. Standard test rig
7. Finite element representation
8. Edge beam restraint due to every trough fixing
9. Summary of cross-sectional bending moments
10. Profile displacements along sheet length
11. Effect of profile shape and sheet length on K parameter
12. End cross-section displacements
13, 14. Variation of K parameter with number of Fourier terms
15. Effect of pitch and thickness
16. Variation of K with sheet thickness
17. Purlin prop reduction of K value
18. Effect of profile shape on $\bar{K}$ parameter

19. Trough movement restrained at two intermediate purlins

20. Fastening in every trough at the ends and in alternate troughs at the intermediate purlins

21. Effect of increasing number of intermediate purlins

22. Effect of increasing number of Fourier terms, for above

23. Effect of profile shape and number of intermediate purlins on $\bar{K}$

24. Variation of $\bar{K}$ with sheet length.

25, 26, 27. Profile displacements for up to four intermediate purlins

28. Comparison of effective shear modulus with Strehl's results

29, 30, 31, 32. Experimental, energy method and finite element K value comparisons

33, 34, 35. As above for intermediate purlin attachments

36. 37, 38. Comparison between finite element and energy methods

CHAPTER 3.

1. Fastening in a multiple of troughs

2. Alternate trough fastening

3. Superposition of Fourier terms

4. Variation of K value with length

5. Effect of number of Fourier terms

6, 7. Trough displaced shapes

8. Effect of number of intermediate purlins

9. Variation of $\bar{K}$ parameter with length

10. Effect of sheet thickness

11. Effect of trough pitch

12. Effect of fastening to an end purlin

13. Effect of profile shape on $\bar{K}$ parameter

14. Trough displaced shapes for 2 and 3 intermediate purlins

15. Purlin-prop reduction in flexibility

16. Bending moments used in alternate trough fastening analyses

17, 18. 19. Experimental energy method and finite element comparisons

20. Purlin-prop reduction in flexibility for every third trough fixing

21. Bending moments used in every third trough fixing analyses

CHAPTER 4.

1. Sinusoidal corrugation geometry
2. Energy method displacements
3. Effect of profile, length and number of intermediate purlins on K value
4. Effect of sheet thickness
5. Displaced shapes of sinusoidal profiles
6. Alternate trough fastening displacements
7. Effect of thickness for alternate trough fixing
8. Effect of profile, length and number of intermediate purlins for alternate trough fastening

CHAPTER 5.

1. Shear deformation of a 'closed-end' corrugation
2. Cross-section displacements
3. Comparison of open and 'closed' profiles
4. Shear deformation of a double fastened corrugation
5. Cross-section displacements
6. Comparison with a profile fastened in every trough
7. Effect of sheets extending beyond purlins
8. As above, for rigid plate movements
9. Effect of insulation covering
10. Composite shear action
11. Insulation bending
12. Curved end sheeting - every trough attachment
13. As above, for alternate trough fixing

CHAPTER 6.

1. Overlapping corrugations
2. Model for every trough fastening
3. Model for alternate trough fastening
4. Longitudinal warping
5. Unequal sheet lengths

6. General interaction expression for rigid plate movements
7. As above, for localized end distortion
8. Variations in fastening arrangement

CHAPTER 7.

1. Continuous diaphragm displacements for every trough fixing
2. As above, for alternate trough attachment
3. Plate displacements
4. Test apparatus for 2 and 3 bay diaphragms
5, 6. Modified shear flexibility
7. Inertia of purlins
8. Contribution of sheet to beam inertia
9. General formularion for sheet inertia
10. Sheet displacements in web
11. Overlapping sheets
12. Beam on elastic foundations analogy
13. Formulae for central deflection
14. Variations in the fastening arrangement

CHAPTER 8.

1. Overlap seam performance
2. Upstand seam performance
3. Performance of button punched seams
4. Indirect shear transfer
5, 6. Purlin displacements
7. Effective sheet widths
8. Variation with bending and torsional stiffnesses
9. Influence of sheet flexibility
10. Tabulation of g_1 parameter
11. Comparison of differential equation with finite element results

12. Holes in diaphragms; simple shear deflection
13. Isolated opening in diaphragm
14. Periodic openings in diaphragm
15. Shear force variation
16. Purlin displacements for single opening
17. Purlin displacements for periodic openings
18. Comparison of periodic and isolated hole solutions
19. Maximum purlin bending stress variation
20. Maximum sheet-purlin fastener force variation
21. Effect of parameters on purlin bending
22. Finite element representation of shear panel with opening
23. Finite element results and theoretical comparisons
24, 25, 26, 27. Matrices for single and periodic opening solutions

CHAPTER 9.

1. Shear buckling of corrugated sheeting
2. Buckling of various profile shapes
3. Derivations from uniform or the tropic medium
4. Buckling between intermediate purlin fasteners
5. As above, for three bays
6. Possibility of uplift between sparce perimeter fasteners
7, 8. Curves for buckling between intermediate purlin fasteners
9, 10. Curves for buckling between perimeter fasteners
11. Shear buckling of hypar shells
12. Shear buckling of cylindrical shells

CHAPTER 10.

1. Forms of folded plate roofs
2. Resolution of forces and deflection
3. Concrete folded plate roof theory
4. Axial stress and deflection in folded plates
5. Axial stresses in prototype folded plate roof
6. Pressed sheeting

7, 8. Vertical loading system
9, 10. Elastic tests on folded plate roof
11. Centre section deflections
12. Wind load deflections
13. Bending and shear deflections for uniform loading
14. Bending and shear deflections for wind loading
15. Test to failure
16. Centre section deflections prior to collapse
17, 18. 19.
20. Maximum folded plate roof span
21. Fold area at a given span and inclination
22. Typical section through folded plate roof bay
23. Weight of steel comparison for folded plate and portal frame
24, 25, 26, 27. Folded plate roof details
28. Stress-strain curve for steel used in sheeting
29. Load-slip curve for upstand seam

CHAPTER 11.

1. Holes in folded plate roofs
2. Fold line deflections
3. Local fastener forces and fold line stresses
4. Variations in fold line fastening
5. Lateral instability of edge beam

CHAPTER 12.

1. Equivalent beam test for pressed sheeting
2, 3, 4. Equivalent beam tests for open profiled sheeting

CHAPTER 13.

1. Design examples for profiled sheeting

LIST OF PLATES

2.1. Shear distortion of open profile fastened in every trough

2.2. Unclad test rig, showing the full range of purlin positions

2.3. Test rig is shown clad with profile 1

2.4. Insitu measurement of the seam slip on modified test rig

5.1. Sheeting fastened in alternate troughs with insulation covering

5.2. Sheeting with curved overhangs

5.3. Mould for pressing 'closed-end' sheeting

5.4. Corrugation folded-down after forming

6.1. Interaction of overlapping sheets fastened in alternate troughs

7.1. Three bay continuous diaphragm apparatus

8.1. Collection of fasteners used in testing

8.2. Apparatus for determining the ultimate fastener strength

9.1. Local buckling around trough fasteners

9.2. Buckling wave passes between the sparce fastenings at the intermediate purlin

9.3. Buckling wave passes through alternate fastenings at two intermediate purlins

9.4. Buckling wave passes between alternate trough perimeter fasteners

10.1. Sheeting between the fold lines in operation

10.2. Jacking of the roof in stages from moveable knees

10.3. Roof ready for testing with side sheeting and loading system attached

10.4. Wind loading system connected to the eaves fold line

10.5. Seam failure of the central bay

10.6. View along the valley member at failure

12.1. Plate girder test showing buckling of standard sheeting

12.2. Seam failure in pressed sheeting

C H A P T E R 1.

INTRODUCTION

1.1. General Concepts:

Corrugated sheeting is a structural commodity of wide application. Its use as roofing and decking is well established, relatively thin sheets spanning between purlins owing to the bending rigidity of the formed profile. Insulation and weather proofing layers may be attached, and the sheets themselves are easily fastened to their supporting members by self tapping screws etc.[1]

In recent years the diaphragming capabilities of complete panels has been realised,[2, 3] and by making specific fastening arrangements, the shear strength and stiffness of corrugated units, may be utilized in integral building design. The 'stressed skin' approach[4] has proved successful in establishing the flexibility of corrugated diaphragms due to a number of different factors, and allows the sheeting to make a positive contribution by reducing the bare frame moments and forces throughout the structure.

The inherent in-plane stiffness of a panel is mobilized wherever relative movement occurs between frames or members in single or multi-framed buildings. Low rise, large plan structures, typical of industrial buildings benefit most from the diaphragm action of corrugated panels. For example, horizontal wind forces may be transfered as in-plane shear by roof cladding to stiffened end gables, eliminating the need for complex wind bracing arrangements. Similarly, the differential spread of frames under normal load is resisted by the roof deck.

The high relative stiffness ratio between diaphragm and frame ensures that considerable force will be attracted to the roof sheeting whether accounted for in design or not, and hence some benefit will accrue from comprehensive stressed skin analyses with very little alteration to the normal sheet fastening arrangement.

In multi-storey buildings, floors, walls and roofs all have

considerable in-plane strength and stiffness which are mobilized through the connections, producing a complex interaction of plates and members [5].

Frameless structures of all types extend the category of 'surface active' structures by relying completely on membrane resistance to loads, obviating the need for a framing system, which is designed to be independent of the cladding. In frameless construction the primary load carrying system is also the skin of the completed roof. Thus the philosophy is one of interaction of planes or surfaces by their geometry to produce a load bearing unit where in-plane stresses dominate.

Cylindrical shell, folded plate and tent roofs all provide an efficient method of covering relatively large areas with low material cost. Ease of erection, inherent simplicity of fastening, and prefabrication are important considerations for such modern construction, especially in repetitive design for hospitals and schools, where economy is important.

Corrugated sheeting is ideally suited for medium span folded plate roofs to cover gymnasia, swimming baths etc. By twisting the profile along its length, hyperbolic paraboloid units may be constructed, [6] making use of the shear stiffness of the medium and the strength of the connections. Curved units have been developed for corrugated steel 'Nissen' huts [7] and grain silos which utilize the in-plane as well as the bending properties of the sheeting.

Thus, corrugated sheeting has the ability to provide a number of functions and its continued and varied use is made more amenable by accurate quantification of its in-plane strength and stiffness properties as well as those of the connection arrangement.

1.2. The Stressed Skin Approach in Framed Buildings:

A roof diaphragm consists of bounding members to which corrugated sheets are attached by rigid connections. Even the sparsest distribution of fastenings will induce shear resistance in the cladding providing that the framing members are capable of maintaining equilibrium. The simplest

diaphragm consists of a rectangular assemblage of pin-jointed members with inter-connected sheeting fastened on all four sides, which generates a uniform shear field.

The acceptable mechanical fastenings are those which provide a definite fixing between sheet and member or neighbouring sheet and whose strength and slip characteristics can be reliably determined. The performance of the individual fasteners[8] and welding pattern[3] as used in practice has been the subject of much investigation in Europe and North America. For a simple diaphragm, the overall capacity is dependent on the type and number of connections given that all four sides and seams must resist the same uniform shear flow. (Fig. (1.2(a)).

A major requirement of all diaphragm design is that failure should occur by ductile sheet tearing rather than brittle shearing of the fasteners.

The shear deflection of a corrugated membrane is largely controlled by the degree of trough fastening. The sheet is relatively flexible perpendicular to the corrugations, and the profile is easily compressed and extended by the net fastener force as in Fig. (3.1). Similar to an accordion, this concertina action is manifested as a shear displacement. Hence, the usual fixing arrangement for deflection limitation is in alternate or third troughs.

A typical roof diaphragm behaves like a deep plate girder within which the framing members absorb the axial force and the cladding is subjected to shear forces only (Fig. (1.1)).

Two distinct categories of roof design exist and are:

(a) where the diaphragm provides the complete roof stability for resistance against wind loading. This is illustrated in Fig. (1.7) for a flat roof diaphragm and pin-jointed frame. Wind load is transmitted through the roof by beam action and hence to the end gables.

(b) where the roof and frame act in conjunction. Flat or pitched portal roofs may be designed individually to

resist wind loading, but when coupled by roof sheeting, the lateral force is shared between the diaphragm and frame according to their relative stiffness. Fig. (1.4) shows for a four bay roof, how frame sway is resisted by diaphragm action between stiffened end gables. Clearly the penultimate frame is subject to the greatest relief of sway bending moment and consequently the end diaphragm suffers the greatest shear force.

A plastic method of design has been proposed[9] for the second category which shows that, for uniform frames and loading, all the frames have the same cladding resistance. The shear panel must be sufficiently ductile in failure to allow all the frames to develop their respective plastic hinges. Brittle forms of failure such as global buckling or fastener shear would make the design method unreliable and hence these modes should have a greater factor of safety.

For pitched roof portal frames[4] the spread of the eaves under normal loading may also be resisted by diaphragm action again dependent on the relative spread stiffnesses of frame and sheeting as shown in Fig. (1.8). In this case the inclined diaphragm is reduced to the appropriate flat diaphragm flexibility.

The equilibrium requirements and the compatibility of frame and diaphragm movement may be solved for each frame according to.

$$\Delta_o - X_i \Delta = \delta_i \qquad \text{where } X_i = \frac{-2\delta_i + \delta_{i-1} + \delta_{i+1}}{C/\cos^2\theta}$$

where X_i and δ_i are the net diaphragm reaction andspread deflection for the ith frame.

Δ_o, and Δ are the applied loading spread and the frame spread flexibility, respectively. C is the roof diaphragm's own flexibility, as shown in Fig. (1.8).

Establishing an equation for each intermediate frame, assuming

zero end movement, yields a solution for the final diaphragm displacements and also the relief of frame spread bending moment. Reduction factors have been tabulated by Bryan for the spread bending moment as a function of frame-diaphragm relative stiffness and frame position. The roof, of course is designed primarily for its simple bending properties and may consist of purlins spanning across rafters, with profiled sheeting spanning perpendicular to the purlins (Fig. 1.3(a)). The plane of shear resistance may thus be significantly higher than the rafter thrust, and this imposes a twisting tendency on the purlin-rafter connections. If the cladding is fastened on two sides only to the purlins, shear connectors running along the rafters are usually advisable to transfer the sheet shear directly along all four edges.

The 'stressed-skin' nature of buildings, taking into account the diaphragm action of corrugated panels, requires that the sheeting be permanently in place and is treated as a primary structural member. Where both frame and diaphragm act together it has been suggested that the bare frame should resist the design load and that the sheeting ought to merely contribute to the factor of safety.[4]

Quite apart from its membrane strength and stiffness, the attachment of corrugated sheeting to purlins and columns, ensures that there is some degree of lateral and torsional restraint to buckling of light cold formed members.[10]

American diaphragm practice often specifies puddle welding of an upstand overlap seam to reduce the risk of poor fusion, and this is reflected in a high strength factor of 2.5 to account for the variability of site welding.[3] Canadian practice involves the combination of welding and button punching of seams to lower site costs.[11] Of course, much higher snow and wind loads are experienced in North America and this may make welding appear more viable than in Britain, where self-tapping screws are the most popular fixing.

Historically the stressed skin application to buildings was first used by consultants in California in 1949 as diaphragm resistance for wind and seismic loading. Nilson,[3] at Cornell University began an extensive program of research into welded diaphragms in 1956 and tabulated the strength and deflection of various gauges of standard diaphragms

from experimental data. Luttrell[12] continued this work in 1965 firstly at Cornell and later at West Virginia University.

Many companies[11, 13] in North America use extra-polated experimental observations to design large scale diaphragms and it seems that the theoretical approach is overlooked.

In 1964 Bryan[14] at Manchester began to study mechanically fastened prototype sheeted buildings and obtained good agreement between experimental and theoretical deflections for full scale tests. His approach still forms the basis of all future study.

Recently the finite element analysis has revealed new information about the internal force distribution within diaphragms. Nilson[15] and Sved[16] in Australia have modelled the individual corrugations and fasteners and studied sheeted buildings by this method.

Davies[17] used finite element and other computational techniques to verify simplified design formulae for the strength and flexibility of corrugated diaphragms.

1.3. The Strength of Corrugated Diaphragms:

A general diaphragm arrangement is shown in Figure (1.1). As a guide to optimum proportions Bryan suggests that for flat roofs the overall length should be no more than four times the width and 2.5 times for pitched roofs. Using the deep girder analogy, the purlin axial stresses are dependent on the diaphragm bending moment, and also on their position from the neutral axis. Assuming a linear variation of axial strain, then the outer purlins are most highly stressed. The consequent distribution of shear stress within the roof diaphragm is a step-wise function, each additional increment being related to the axial stress in the intermediate purlins.

This is a purely an observation from statical equilibrium considerations, which takes no account of the compatibility requirements of shear strain between each section. Nevertheless, as a lower bound to

to the diaphragm capacity, the worst conditions should be taken for initial failure of the seams or edge fastenings. However, the ultimate strength of the whole diaphragm may be significantly higher as seam failure spreads out from the centre into the lower shear regions. Seden[18] has studied these elastic-plastic characteristics of diaphragm failure.

The idealized transfer of rafter thrust into diaphragm shear is dependant on certain practical considerations. As in Fig. (1.3(a)), shear connection directly between rafters and sheeting is advisable so that the diaphragm is fastened on all four sides. In some cases, the loading may be low enough to permit shear connections in the end roof bays only, the local rafter force being absorbed through the purlin-rafter connections, and spread into the panel by the sheet-purlin fasteners, (Fig. (1.3 (b))).

For a simple diaphragm connected on all four sides, the required number of fasteners on each perpendicular edge are given by:-

$$n_B = \frac{Q}{F_R} \quad \text{and} \quad n_A = \frac{Qa/b}{F_P}$$

where F_R and F_P are the ultimate loads of the individual sheet-shear connector and sheet-purlin fasteners respectively and a and b are the panel width and length respectively. Q, the panel ultimate load, is applied in direction b.

Bryan[4] suggested that for self-tapping screws in sheet steel $F_P = F_R = 6$ KN/mm thickness, but this is only a typical value. Nilson[3] expressed the complete panel strength graphically for various configurations of welded diaphragms.

The number of seam fasteners required may be conservatively given by,

$$n_s = \frac{Q}{F_s}$$

where F_s is the characteristic seam fastener ultimate strength. Again, as a very rough guide Bryan suggested $F_s = 2.5$ KN/mm thickness of sheet steel.

Ellifritt and Luttrell[19] proposed experimental failure curves for welded diaphragms corresponding to weld-sheet tearing and inter-weld buckling. A typical curve for this second failure mode might be,

$$Q = \frac{3.22}{L/t} + \frac{41.1 \times 10^3}{(L/t)^2} \quad kN$$

where t is the sheet thickness and L the weld spacing.

For diaphragms fastened on two sides only as in Fig. (1.2(b)) the overall equilibrium is maintained by fastener forces normal to the purlins as well as those in line with the member. The extreme fastener is most highly stressed and the sheet shear force builds up from zero at the ends to a medium at the centre, consistent with the application of the sheet-purlin force. For a linear distribution of forces perpendicular to the purlins as assumed by Bryan, the sheet shear force is parabolic in nature and increases to 1.5Q at the centre of the diaphragm. Davies[17] examined the effect of purlin bending on the expressions for ultimate load and concluded that for the indirect shear transfer case due to fastenings on two sides only, the assumption of a linear distribution of forces normal to the purlin was in gross error.

Considerable purlin bending was revealed by finite element study, which tends to magnify the extreme fastener force. Indeed, the capacity of a diaphragm due to indirect shear transfer would seem to remain constant independent of the diaphragm width.

He suggested that for fastening on all four sides seam failure occurs at,

$$Q = (n_s F_s + n_p F_p) \cdot \frac{(2n_s s + g_1 . n_p . s_s)}{(2n_s s + n_p s_s)}$$

where n_s, s_s, n, s are the number and slip of the seam and sheet-purlin fastenings respectively. g_1 accounts for the effect of the sheet-purlin connections on the seam strength. Some shear force is transferred by the purlins (of number n_p) away from the seam, and for a linear distribution of sheet-purlin forces g_1 tends to $n/6$. A similar expression may be derived

for failure of the sheet-shear connector fasteners.

In general, sheet-shearing is the most ideal failure, but other possible modes include global or local shear buckling, and serviceability limits such as excessive corrugation distortion.

1.4. Shear Flexibility

The shear deflection of corrugated diaphragms is composed of a number of different factors such as the slip of the seams and edge fasterings and the pure shear strain within the sheeting. Also the beam type deflection may be considered as an additional component due to axial strain on the purlin members.

The depth of the corrugation is important for its own bending properties, but under shear the open profile is able to distort and warp as in Fig. (2.1 (a)). This is because the plane of shear resistance is different from the line of action of the fasteners, producing profile twisting and a consequent longitudinal shear displacement. Distortional flexibility is only a part of the total but is usually the major component and the deeper or more sparcely fastened the profile, the more distortion dominates. Based on linear movement along the sheet length Bryan[4] derived the shear flexibility due to distortion as,

$$C_{1.1} = \frac{0.144ad^4}{Et^3b^3} K f_1$$

where a, b, d, t, E are as defined, and K is a dimensionless parameter dependent on the fixings and profile shape. The factors f_1, f_2, f_3, are due to the effect of a number of intermediate purlins.

The shear strain component is,

$$C_{1.2} = \frac{2a(1 + \nu)\ (1 + 2h/d)}{btE} f_2$$

where ν, b, etc., are as defined.

The flexibility due to axial strain is

$$C_{1.3} = \frac{2a^3}{3b^2 AE} \cdot f_3$$

where A is the purlin cross-sectional area.

The flexibility due to the sheet purlin fastenings is, as in Fig. (1.3),

$$C_{2.1} = \frac{2asp'}{b^2} f_3$$

where s is the characteristic fastener slip and approximately equals 0.15 mm/KN for self tapping screws[4] in sheet steel, and p is the fastener pitch.

For fastening on two sides only $C_{2.1}$ is modified to,

$$C_{2.1} = \frac{2sp'}{a} \left(\frac{6}{n_p} + \frac{a^2}{b^2} \right)$$

where n_p are the number of purlins.

The component due to seam slip is,

$$C_{2.2} = (n_{sh} - 1) \frac{s_s}{n_s}$$

where n_{sh} is the number of sheets and s_s is the characteristics seam slip taken as 0.35 mm/KN for poprivets and screws.[4]

Finally, the flexibility due to sheet-shear connector slip is,

$$C_{2.3} = \frac{2s_{sc}}{n_{sc}}$$

where n_{sc}, and s_{sc} are the number and slip value of these fasteners.

The total flexibility is the sum of all these constituent parts, and the deflection per bay is obtained by multiplying by the diaphragm

shear force.

The theoretical distribution of shear force within a diaphragm as in Fig. (1.1) is controlled by the linear variation of axial force in the purlins. To maintain equilibrium there must be an increase or shear flow towards the sheet centre and hence Bryan[4] modifies his component flexibilities by the factors f_1, f_2, and f_3 which are all equal to a value less than unity, to approximately account for this effect.

The basic sheet flexibility, c is defined as being in line with a force applied along the corrugations. To obtain the transverse flexibility a modification factor $(b/a)^2$ is introduced as in Fig. (1.5).

American diaphragms often use a flat sheet spot welded along its length to the base of the profile, producing a very rigid membrane by eliminating the $C_{1.1}$ flexibility.

For puddle welding, the slip per seam on roughly 1.2 mm thick steel sheet may be taken according to Nilson[3] as,

$$23.1 \times 10^{-3} \frac{Qw}{a} - 0.105 \text{ mm},$$

which if negative, becomes zero. Where Q is the external shear force in kN, w the weld spacing and a the panel width in mm.

American standards state that the lateral roof deflection for masonary walls should be less than,

$$\frac{h^2 f}{.0004Et} \text{ mm}$$

where h, f, E, t are the wall's height, allowable compressive stress, Young's modulus and thickness respectively.

Sheet shear flexibility is a design parameter in order to determine the overall force distribution between frame and diaphragm. Underestimating the deflection in design would in practice attract more force to the frame and vice-versa perhaps producing a dangerous over-loading in the elastic range.

1.5. Applications of Corrugated Sheeting in Frameless Structures

The in-plane and bending properties of profiled sheeting may be utilized in many frameless forms of construction. Folded plate roofs as in Fig. (1.9) rely on the beam action of equivalent girders spanning between stiffened end frames. These inclined deep plate girders are composed of fold line members which attract the axial stresses, and sheeting spanning between, which resists the shearing force. Thus the skin is both stressed and acts as a covering.

The sheeting spreads load back to the fold members, where the total reactions are split as in-plane components into the neighbouring roof sheets according to the parrallelogram of forces. Hence, each roof plate is subjected to uniform, in-plane loading along its length, and consistent with beam statics, the sheeting is subjected to a maximum shear force at its ends. The fold lines are naturally most highly stressed at mid-roof span. In addition the shear proportion of central roof sag adds considerably to the overall deflection and often represents a limitation to the permissible roof span.

The overall roof capacity is generally determined by the fastener resistance along the edges and seams or the shear buckling strength. Easley[20] derived a useful expression for the global shear buckling load of,

$$Q = \frac{36}{b} Dx^{1/4} Dy^{3/4} \quad kN$$

where Dy and Dx are the major and minor sheet bending stiffnesses respectively, and b the sheet span.

Thompson[21] studied the effect of variations in fastening arrangement along the roof length. This may be necessary if the cost of fixing is prohibitively high, especially for the seams, which may reduce in number according to the decline in shear force.

Hyperbolic paraboloid units may be formed by twisting corrugated sheets along their length, (Fig. (1.10)). Load resistance, in theory, occurs

by membrane shear forces generated according to,

$$\tau t = w \left(\frac{ab}{4c}\right)$$

where w is the normal sheet loading per unit area and τt the sheet shear flow. c is corner uplift defined by the generators according to Fig. (1.10),

$$z = 2c \frac{xy}{ab}$$

The overall shear flow is constant and hence the shear deflection components are of the same form as a flat diaphragm.

In California there are examples of 70m cantilevered folded plate modules[22] used as aircraft hangars. The sheeting spanning between fold lines is twisted differentally along the roof producing a hyper-shape. An advantage of curved membranes is not only in their load bearing capabilities but also in their buckling strength compared to flat sheets. Gergely[23] has studied the buckling characteristics of highly orthotropic hyperbolic paraboloids.

Cylindrical sheets as in Fig. (1.11) spanning directly between end frames utilize the orthotropic properties of corrugated sheeting. Stiffening ribs are usually necessary to transfer in-plane forces across the weak sheet direction, and the sheeting is then subject to shear and arch action. The non-uniform shear strain suggests that the distortion components $C_{1.1}$ for an equivalent flat sheet cannot be used. Abdel Sayed shows that the shear buckling strength is greatly enhanced by the curvature.[24]

Young[25] has studied cylindrical shell barrel vaults which may be designed more economically by including the shear stiffness of the sheeting.

1.6. Limitations of Present Knowledge and Aims of this Study

In designing corrugated sheets to resist in-plane forces it is

necessary to quantify their own shear flexibility which not only controls the roof deflection but also determines the relative distribution of load between the frame and diaphragm in traditional buildings. The flexibility due to distortion is an important factor in shear diaphragm analysis and its control by suitable choice of profile and fixing arrangement may be necessary in structures where in-plane forces dominate.

A number of theories have been proposed to model this shear distortion, which lack either accuracy or simplicity of formulation in accounting for the effects of profile shape, sheet length and thickness as well as fastener pitch.

The use of profiled sheeting is subject to many practical considerations such as the effect of discrete fastenings, intermediate purlins, overlapping of sheets, openings for roof lights and the suitability of the shear transfer between sheeting and rafter.

Diaphragm openings are often necessary and apart from the finite element method, no analysis is available to predict the effect of a flexible band within a stiffer roof diaphragm. Light cold formed purlins are constrained to follow the shear deflection of the sheeting which causes locally high fastener and purlin bending stresses.

The purlins also contribute to the strength of the seams by spreading some shear force to the sheet-purlin fasteners. For diaphragms fastened on two sides only, the lateral bending and torsional stiffness of the purlins is an important factor in determining the degree of shear transfer to the sheet purlin fastenings, which had been neglected in the previous simplified analyses.

In many applications, finite sheet lengths must be overlapped to produce the complete diaphragm depth. However, the distortion component of flexibility is extremely dependent on the length and number of sheets, and this is further complicated by the interaction of neighbouring corrugation distortions.

Sheets usually span across purlins, but in other forms of construction the corrugations span directly between rafters. The problem of sheet span across different shear intensity regions makes quantification of the corrugation flexibility more difficult especially if this is associated with

overlaps at the rafter-points.

Folded plate roofs using mechanical fixings have been examined by single plate tests,[21] but no full scale building has yet been constructed to verify the design philosophy, and to show that the basic diaphragm properties may be extrapolated, for design of a frameless structure.

The shear buckling capacity of corrugated sheeting has been determined but only for idealized constraints. The effect of discrete parameter and intermediate purlin fastenings may cause a sizeable deviation from the simple formulation. Although not normally a failure criterion for mechanical fixings, welded diaphragms may be sufficiently strong to permit failure by global shear buckling.

The overall aim of the study is to account for the practical considerations of roof design using corrugated sheeting, as well as to more accurately determine strength and deflection, with regard to use in frameless forms of construction.

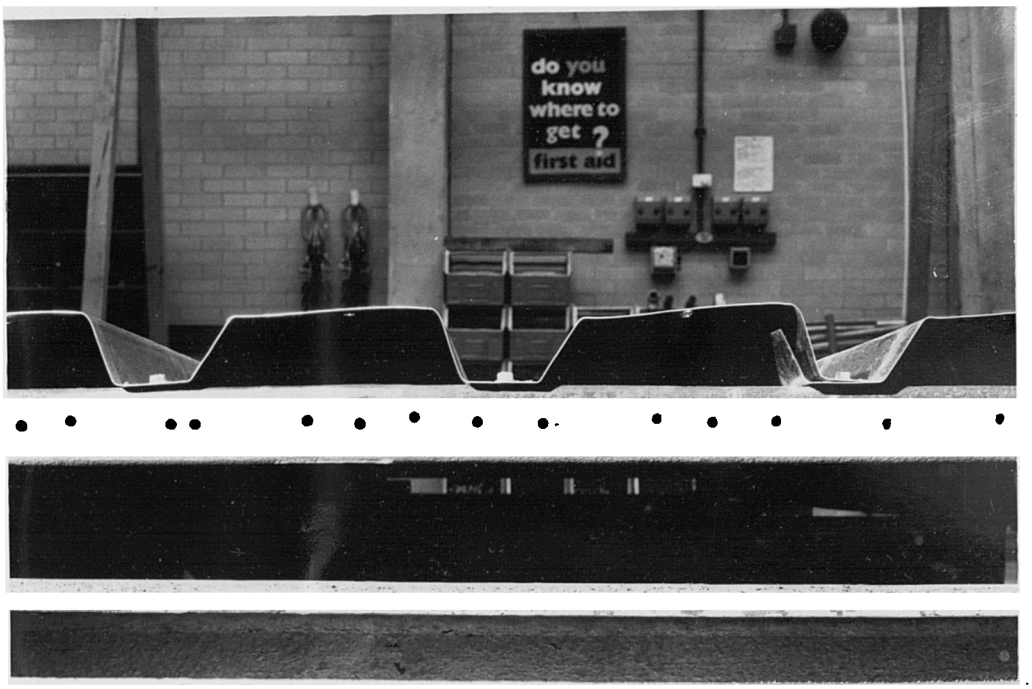

Plate (2.1) Shear distortion of an open profile fastened in every trough

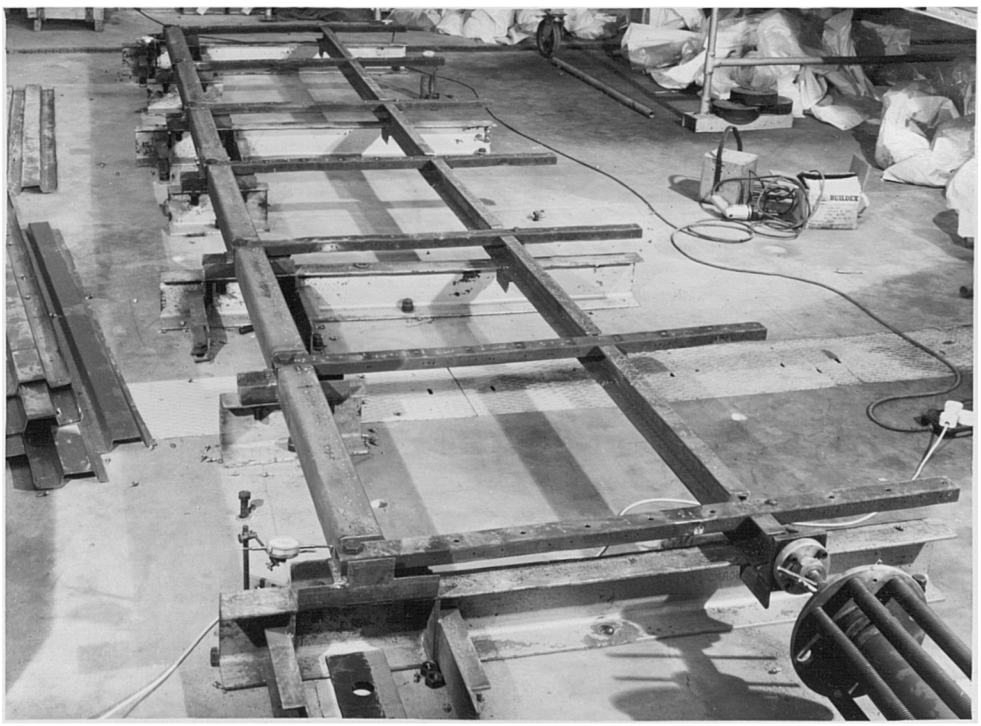

Plate (2.2) Unclad test rig, showing the full range of purlin positions. The left hand rafter is fixed and all connections are pinned

CHAPTER 2

THE DISTORTIONAL FLEXIBILITY OF TRAPEZOIDAL SHEET PROFILES FASTENED IN EVERY TROUGH

2.1. Simplified Approaches

The shear flexibility of corrugated sheeting fastened on discrete points to a bounding member system is dependent on the profile shape, the panel dimensions and also on the fastening arrangement. The shear distortion component derives from the fact that the centre of shear resistance of the profile is different from the plane of force application and the corrugation is twisted out of shape by its own shear flow. The individual plates, whilst moving laterally, also rotate and bend inplane which produces longitudinal warping, and hence shear displacement across the profile.

Naturally, the degree of end fastening controls the shear distortion, the every trough fixing case twisting due to movement of the top and side plates (Fig. (2.1 (b))). Alternate trough fastening, however, is much more flexible as an additional concertina action occurs, resulting from the freedom of the unfastened bottom plate (Fig. (3.1)).

The methodsof evaluating the shear flexibility due to corrugation distortion vary in their complexity, some permitting a whole range of fastening and end forming conditions to be examined. Others make simplifying assumptions about the physical process of deformation. In general, energy methods of assumed displacement functions would seem to be the most suitable for analysing shear distortion as a complicated relationship exists among the internal forces within the corrugation.

Hlavaceck[20] considered the cross-section to deform due to a uniform shear flow transferred from the fasteners which causes a linear movement of the top and side plates along the panel depth. The transverse bending moments around the profile can be obtained by statics from the shear flow and hence the bending strain energy is a function of the shear force only. Equating the internal to the external work gives an expression for the shear flexibility due to a unit force parallel to the corrugations.

Rigid plate movements, where all sections contribute to the total energy, generates a shear stiffness in terms of the panel length cubed, as shown later.

In Hlavacek's analysis the side and top plates are separately allowed to move and the flexibilities of the two cases added. The case where only the top plate shear force is considered, corresponds to the analysis of Bryan and Jackson.[27] The first attempt to analyse the shear flexibility of a flat sided corrugated sheet was performed by Rothwell[28] who considered a pointed profile ($b_T = 0$) which has applications on the aeronautics industry, where the primary design factor was to relieve thermal stresses and improve the skin's buckling strength. Rothwell also assumed rigid plate generators and the derivation is merely a special case of other theories which make this simplified observation.

A more general extension of the assumptions of linear plate movement caused by uniform profile shear flow was presented by Bryan who was able to evaluate the work done in deforming the cross-section as a function of the end shear flow, q. Top and side plate end deflections may be obtained by,

$$\bar{U}_T = \int_o^s M_2 M_o \frac{q}{EI_S} ds = \phi_1 \frac{q}{EI_S}$$

$$\bar{U}_S = \int_o^{s/2} M_1 M_o \frac{q}{EI_S} ds = \phi_2 \frac{q}{EI_S}$$

where $\int_o^s ds$ represents integration around the profile. The plate stiffness $I_S = \frac{t^3}{12(1-\nu^2)}$ per mm sheet length.

The bending moments M_o, M_1, M_2 are shown in Fig. (2.9).

The expression for in-plane warping due to plate movements $\bar{U}_S$ and $\bar{U}_T$, as shown in Fig. (2.2 (a)), is,

$$\Delta = \frac{4h}{b} \bar{U}_S + \frac{4b_T}{b} \bar{U}_T$$

where b is the sheet length and the profile geometry is given in Fig. (2.1(a)).

The internal work due to cross-section twist is obtained by multiplying the side and top plate forces by their respective displacements at any section y, and integrating over the complete length. Equating to the external work gives,

$$\frac{\Delta^2}{2C_{1.1}} = \int_o^{b/2} (2b_T.\bar{U}_T + 2h.\bar{U}_S)\ q.(\frac{y}{b/2})^2\ dy$$

Hence

$$\frac{\Delta^2}{2C_{1.1}} = \Delta^2 \int_o^{b/2} \frac{y^2 EI_S}{2h\emptyset_2 + 2b_T\emptyset_1}\ dy$$

The total energy equation yields the flexibility per corrugation as,

$$C_{1.1} = 288\ (h\emptyset_2 + b_T\emptyset_1)\ \frac{(1 - \nu^2)}{Et^3 b^3}$$

The flexibility expression may be rearranged in terms of a dimensionless parameter K defined by,

$$C_{1.1} = \frac{0.144\ ad^4K}{Et^3b^3}$$

where d is the trough pitch and a is the sheet width. The K value is now only a function of the cross-sectional shape and the fastening conditions. This expression for shear flexibility due to distortion has formed the basis for Bryan's study[29] of prototype panel and building tests. It is apparent that the distortion deflection falls rapidly with sheet length, b, and at about 8 metres for a 35 mm. deep profile is of the same magnitude as the other factors due to fastener slip and pure shear strain.

It should be noted that the deformation pattern assumed in all the simplified analyses implies that the downward side plate movement is unrestrained by fastening to a rigid purlin member, which disrupts the antisymmetry of deformation as in Fig. (2.1 (a)) and Plate (2.1).

If the aspect ratio of the plates increases Horne and Raslan[30] first showed the presence of non-linear plate movements (Fig. (2.2 (b))).

Rather than assuming a uniform cross-section shear flow, the portal frame type bending energy was expressed in terms of in-plane displacements of each plate. Non-linear longitudinal flexure and shear strain were included as contributors to the total internal energy by establishing additional simusoidal forms for the movements along the sheet length.

Thus, the overall strain energy may be expressed in terms of displacement parameters. Minimization of the total energy with respect to each variable, and including the condition that the shear deflection should remain constant throughout the sheet length reduces the energy expression to simultaneous equations in the independent variables to solve for the corrugation flexibility.

The shear flow is no longer constant but can be redetermined from the transverse bending moments. Unfortunately Horne and Raslan only carried out their analysis for the case where side plate uplift is prevented, but as will be shown later, the approach of assuming displacement parameters has a number of attractive features.

These same authors[31] also performed a finite difference analysis of the controlling differential equations of plate movement in terms of three chosen plate displacement parameters. Each side is under the equilibrium of in-plane moments and forces, as in Fig. (2.3 (b)). The local forces, q, derive from the transverse portal frame bending moments of cross-section distortion. Thus equilibrium is maintained when the forces producing in-plane plate flexure are compatible with the profile distortion. The three resulting fourth order differential equations require twelve geometrical or force boundary conditions for solution.

Horne and Raslan's energy method analysis may be easily adapted to cope with rigid plate movements alone and it may be shown that the results do not differ markedly from Bryan's method. However, Horne did indicate that above a 2 metre sheet length, plate linearity breaks down, mainly due to trough bending, and that the flexibility rises above Bryan's formulation.

The physical interpretation of plate bending is that for long panels, distortion becomes localized near to the end of the sheet where

the discrete fasteners absorb the sheet shear force. This phenomena was also realized by Libove, a summary of whose analysis follows. With various co-authors he derived a rigorous method for evaluating the sheet effective shear modulus, which defines its reduced stiffness compared to that of a flat sheet of the same thickness.

2.2. Methods due to Libove, Strehl and Others

The most comprehensive analysis of the shear flexibility of corrugated sheeting to date was performed by Libove[32] who established the total energy of plate distortion in terms of three longitudinal and three transverse displacements. Portal frame bending, longitudinal plate flexure, shear and torsion energy were all included by establishing differential forms such as,

$$\left(\frac{d^2U_T}{dy^2}\right)^2 \quad \frac{2}{3} b_T{}^3 tE,$$

(which represents the bending energy of an element of the top plate due to an in-plane displacement , U_T).

Thus, the total energy is expressible in certain orders of differentials of the parameters and by applying the calculus of variations, six differential equations are generated corresponding to the minimized total potential energy.

The necessary force and geometrical boundary conditions are obtained, and the six simultaneous differential equations may be solved in terms of their complementary functions and particular integrals. Any boundary conditions can be selected to represent, for example, methods of fastening or processes designed to reduce deformation.

Libove has studied a number of different cases for both trapezoidal and sinusoidal profiles corresponding to free deformation of troughs and corrugation ends, the longitudional restraint of trough bending, and the effect of purlin restraint on side plate depression.

Translating his graphical representation of effective shear modulus into shear flexibility, seems to indicate non-linearity of plate displacements for panels longer than 1.5 metres. The stiffness, a function of length cubed for straight line generators falls rapidly to a power of length squared: for longer panels and the flexibility factor K increases correspondingly. His experimental results are confined to relatively short panels, and given that the factors due to fastener slip and strain on purlins are accurately quantifiable, it does appear that the flexibility factor K rises with length. However, the relative stiffness concept used by Libove does not make the results more amenable to interpretation, as he was unable to develop a controlling parametric equation for the shear stiffness.

Strehl[33] uses an approach based on the beam on elastic foundations analogy. The stiffness of the beam is provided by the inertia of the plates of the corrugation and the elastic medium is represented by the effect of cross-section distortion. Of course, the interaction between the movements of each plate is complex as each one acts like a beam on its own foundation. The disturbing force is provided by the trough fastener which both bends the beam and depresses the elastic medium.

A number of other analyses have been presented notably by Baere,[34] Ting[35], and Falkenberg[36], but all lack the confidence of a rigorous derivation.

Libove's approach may be summarized by the following section which uses three in-plane displacements and three shear strains to define the total internal energy making use of the inherent anti-symmetry of deformation as in Fig. (2.1(a)). The method outlined illustrates the collection of individual energy terms and their minimization to evaluate the shear flexibility.

Firstly, cross-section distortional energy may be expressed as,

$$E_d = \int_o^b a_{11}U_T^2 + a_{12}U_TU_S + a_{13}U_TU_B + a_{22}U_S^2 \text{ etc.,} \quad dy$$

where $\int_o^b$ implies integration over the whole sheet and U_T, U_S and U_B are

the respective top, side and bottom plate movements. The in-plane bending energy longitudinally is,

$$E_b = \int_o^b b_1 \left(\frac{d^2U_T}{dy^2}\right)^2 + b_2\left(\frac{d^2U_S}{dy^2}\right)^2 + b_3\left(\frac{d^2U_B}{dy^2}\right)^2 \, dy$$

The shear strain energy is,

$$E_S = \int_o^b d_1 \gamma_T^2 + d_2\gamma_S^2 + d_3 \gamma_B^2 \, dy$$

where γ_T, γ_S, γ_B are each plates' respective shear strain.

An additional axial strain component is caused in the side plates by the bending strain incompatibility of top and bottom plate movement. It is a necessary condition to ensure similarity between neighbouring corrugation movement, that the shear displacement Δ is constant over the sheet length. So if,

$$\Delta = 2b_T(U_T^1 + \gamma_T) + 4b_S(U_S^1 + \gamma_S) + 2b_L(U_B^1 + \gamma_B)$$

then according to Fig. (2.4(b)) the axial strain energy in the side plates may be taken as,

$$E_a = \int_o^b C_1(b_T U_T^{11} + b_T\gamma_T^1 - b_L U_B^{11} - b_L\gamma_B^1)^2 \, dy$$

where $U_T^{11} = \frac{d^2U_T}{dy^2}$ etc, and $\gamma_T^1 = \frac{d\gamma_T}{dy}$ etc.

The total internal energy is $E = E_a + E_b + E_d + E_s$ and $E = \Delta^2/2C$, where C is the shear flexibility which includes both the pure shear strain and the distortion components.

Taking small changes in each variable corresponding to $\delta E = 0$ when the internal energy is at a minimum, then small changes in the individual energy components yields, for example,

$$\delta\left\{\int_o^b (U_T^{11})^2\,dy\right\} = 4\left[U_T^{11}\frac{d}{dy}\delta U_T - U_T^{111}\delta U_T\right]_o^{b/2} + 2\delta U_T \int_o^b U_T^{1v}\,dy$$

$$\text{and } \delta\left\{\int_o^b U_T^{11}\gamma_B^{1}dy\right\} = 2\left[\gamma_B^{1}\frac{d}{dy}\delta U_T - \gamma_B^{11}\delta U_T\right]_o^{b/2} + \delta U_T\int_o^b \gamma_B^{111}\,dy$$

$$\text{and } \delta\left\{\int_o^b U_T^{2}\,dy\right\} = 2\delta U_T \int_o^b U_T\,dy$$

where $\left[\quad\right]_o^{b/2}$ is the function value at the sheet end minus that in the centre. Combining for each incremental displacement δU_T, δU_S $\delta\gamma_B$ etc., yields typically.

$$\delta E = \delta U_T \int_o^b 2a_{11}U_T + a_{12}U_S + a_{13}U_B + 2b_1U_T^{1v}$$

$$+ 2C_1b_T\,(b_TU_T^{1v} + b_T\gamma_T^{111} - b_LU_B^{1v} - b_L\gamma_B^{111})\,dy$$

$$+ \frac{d}{dy}(\delta U_T)\left[2U_T^{11}b_1 + 2C_1b_T\,(b_TU_T^{11} + \gamma_T^{1}b_T - b_LU_B^{11} - b_T\gamma_B^{1})\right]_o^{b/2}$$

$$+ \delta U_T\,[\ldots\ldots]_o^{b/2}$$

where $U_T^{1v} = \dfrac{d^4U_T}{dy^2}$, $\gamma_B^{111} = \dfrac{d^3U_B}{dy^2}$ etc

For minimum potential energy δE is zero and hence the right hand side of the equation must also vanish. For δU_T non-zero if follows that at all points along the sheet length.

$$2a_{11}U_T + a_{12}U_S + a_{13}U_B + 2b_1U_T^{1v} + 2C_1(b_TU_T^{1v} + b_T\gamma_T^{111} - b_LU_B^{1v} - b_LU_B^{111})b_T$$

$$= 0$$

Similarly the boundary conditions at the sheet end resulting from the constant terms $\left[\quad\right]_o^{b/2}$ must also be zero for $\delta E = 0$.

At the sheet ends, the axial strain in the side plate is necessarily zero, as is the plate bending strain and so the boundary conditions are automatically satisfied. Solution proceeds by solving the six simultaneous differential equations which result in twelfth order differential equations in each of the variables.

Each displacement may be expressed in terms of complementary functions and particular integrals. The differential equations, themselves, resulting from this energy method derivation correspond to Horne and Raslan's equilibrium analysis for each of the plates of the corrugation, which were solved by finite difference approximation.

It may be noted that the complementary functions of solution correspond to the plate bending displacements and the particular integrals to the linear plate generator theory.

2.3 Energy Method of Assumed Displacement Functions

For most practical applications of corrugated steel sheeting, the fastenings are not merely at the extremities of single span sheets. Many variations from the simple arrangement are experienced and it is normal for roof sheets to be continuous over three or four supports. In addition, due to locally high wind suction forces, fasteners may be more frequent near the sheet ends than at the intermediate purlin points. Fastenings in a multiple of troughs may be suitable from a strength requirement but for insulated panels, the resulting high degree of end deformation may cause serviceability problems by breaking the bond between sheet and covering.

All these factors contribute to the difficulty in deriving the sheet flexibility of a practical shear diaphragm. Often every corrugation fastening is preferred at the sheet ends but the internal purlin fastenings are usually more sparce.

It was for this reason that the analysis of corrugation distortion due to fastening in every trough was considered by an energy method of

assumed displacement parameters in terms of Fourier series to represent the individual plate movements. This method has thefacility of modelling internal restraints by adjusting the variables to satisfy the geometry of deformation.

Although the shear stiffness of corrugated sheeting has been the subject of much research, especially with regard to its application in aeronautics, no comprehensive study has been performed of its use in relatively long lengths with the possibility of intermediate fixings. Libove, especially, places rather more emphasis on the types of end attachment for both sinusoidal and trapezoidal profiles in order to limit excessive shear distortion for the shorter lengths required for aircraft applications.

The energy method analysis by Horne and Raslan offers a number of advantages in that, although by implication approximate, it is a common property of assumed displacement functions that they often present a reasonably close answer to the principal displacements providing that the chosen shapes roughly model the actual deformation. The approach follows that of a Ritz technique whereby the geometrical boundary conditions are satisfied, but the internal force conditions can only be approximated.

As with Libove's analysis the main energy components must be expressed in terms of the chosen displacement parameters.

All these may be described by six parameters which are the in-plane and shear displacement of each plate, taking into account the inherent geometrical and deformational anti-symmetry, omitting the effect of end purlin restraint on side plate depression.

The portal frame bending energy of cross-sectional deformation is determined by the displacements U_T, U_S, U_B as shown in Fig. (2.3(a)). If Θ_B, Θ_C are the joint rotations then the transverse moments are,

$$\frac{M_B}{D} = \frac{3V_2}{b_L^2} + \frac{3\Theta_B}{b_L} \quad ; \qquad \frac{M_C}{D} = \frac{3V_1}{b_T^2} - \frac{3\Theta_C}{b_T}$$

where $D = \frac{Et^3}{12(1 - \nu^2)}$ corresponding to the plane strain bending stiffness

and $V_1 = U_T \tan\theta - U_S \sec\theta$

$V_2 = U_B \tan\theta - U_S \sec\theta$

$V_3 = (U_T - U_B) \sec\theta$

If equilibrium of the side plate is expressed according to,

$$\frac{M_B}{D} = \frac{6V_3}{(2b_s)^2} - \frac{2\theta_B}{b_s} - \frac{\theta_C}{b_s}$$

$$-\frac{M_C}{D} = \frac{6V_3}{(2b_s)^2} - \frac{2\theta_C}{b_s} - \frac{\theta_B}{b_s}$$

Solving for M_B and M_C in terms of U_S, U_B, and U_T by eliminating θ_B and θ_C, gives,

$$\frac{M_B}{D} = \frac{1}{b_s^2 F}\{-G_1(U_T + U_B) + J(U_T - U_B) + GU_S\}$$

$$\frac{M_C}{D} = \frac{1}{b_s^2 F}\{-H_1(U_T + U_B) - K(U_T - U_B) + HU_S\}$$

where $G_1 = \frac{p}{2d}\{\frac{2b_s + b_s}{b_L} - \frac{b_s}{b_T}\}$; $H_1 = \frac{p}{2d}\{\frac{2b_s + b_L}{b_T} - \frac{b_s}{b_L}\}$

$$J = \frac{b_s}{d}\left[3 + \frac{b_T}{b_s} + \frac{p}{2b_s} \cdot \{\frac{2b_s + b_T}{b_L} + \frac{b_s}{b_T}\}\right]$$

$$K = \frac{b_s}{d}\left[3 + \frac{b_L}{b_s} + \frac{p}{2b_s} \cdot \{\frac{2b_s + b_L}{b_T} + \frac{b_s}{b_L}\}\right]$$

$$G = \frac{2b_s}{d}\{\frac{2b_s + b_T}{b_L} - \frac{b_s}{b_T}\}; \qquad H = \frac{2b_s}{d}\{\frac{2b_s + b_L}{b_T} - \frac{b_s}{b_L}\}$$

$$F = (1 + \frac{2b_L}{3b_S}) \cdot (1 + \frac{2b_T}{3b_S}) - \frac{b_L b_T}{9b_S^2}$$

Knowing these cross-sectional bending moments, the distortion energy may be evaluated by integration around the section according to,

$$E_d = \frac{2}{2 \times 3} \times \frac{1}{D} \{(b_L + 2b_S) M_B^2 + (b_T + 2b_S) M_C^2 + 2b_S M_B M_C \}$$

Using $M_B/D = A_1 U_T + A_2 U_S + A_3 U_B$

$M_C/D = B_1 U_T + B_2 U_S + B_3 U_B$

then $E_d = C(1,1) U_T^2 + C(1,2) U_T U_S + C(1,3) U_T U_B$

$+ C(2,2) U_S^2 + C(2,3) U_S U_B + C(3,3) U_B^2$

where typically,

$$C(1,2) = \frac{D}{3} \cdot \{(b_L + 2b_S) 2A_1A_2 + (b_T + 2b_S) 2B_1B_2 + 2b_S(A_1B_2 + B_1A_2) \}$$

The individual plate displacements may be expressed as a finite Fourier series expansion superimposed on linear plate movements as shown in Fig. (2.4(a)). Thus, as stated in references (37) and (38),

$$U_T = a_1 y + a_2 \frac{b}{2\pi} \sin \frac{2\pi y}{b} + a_3 \frac{b}{34\pi} \sin \frac{4\pi y}{b} + a_4 \frac{b}{6\pi} \sin \frac{6\pi y}{L} + a_5 \frac{b}{58\pi} \sin \frac{8\pi y}{b}$$

$$+ a_6 \frac{b}{10\pi} \sin \frac{10\pi y}{b}$$

$$U_S = a_7 y + a_8 \frac{b}{2\pi} \sin \frac{2\pi y}{b} + a_9 \frac{b}{4\pi} \sin \frac{4\pi y}{b} + a_{10} \frac{b}{6\pi} \sin \frac{6\pi y}{b}$$

$$+ a_{11} \frac{b}{8\pi} \sin \frac{8\pi y}{L} + a_{12} \frac{b}{10\pi} \sin \frac{10\pi y}{L}$$

$$U_B = a_{13}\frac{b}{2\pi}\sin\frac{2\pi y}{b} + a_{14}\frac{b}{4\pi}\sin\frac{4\pi y}{b} + a_{15}\frac{b}{6\pi}\sin\frac{6\pi y}{b}$$
$$+ a_{16}\frac{b}{8\pi}\sin\frac{8\pi y}{L} + a_{17}\frac{b}{10\pi}\sin\frac{10\pi y}{b}$$

The plate shear strains are,

$$\gamma_T = a_{18} + a_{19}\cos\frac{2\pi y}{b}$$

$$\gamma_S = a_{20} + a_{21}\cos\frac{2\pi y}{b}$$

$$\gamma_B = a_{22} + a_{23}\cos\frac{2\pi y}{b}$$

The length of the Fourier series for the plate displacements is a very important parameter, as will be discussed later. The truncation at the sixth term was merely an observation from the convergence of the solution towards a constant value for the shear displacement at a suitable length of about 6 metres. It was found that for longer lengths that more terms would be needed to model the increased localization of end distortion.

The influence of the 'purlin prop' end restraint has again been omitted to be included later as a constant flexibility reduction factor dependent only on the profile shape and fixing arrangement. It has been assumed that no rotational restraint occurs at the fastener points but as may be observed in practice, decking profiles with a relatively narrow trough width are stiffened by the clamping nature of the fasteners.

The total deformation of the single corrugation is expressed in terms of the 23 variable coefficients, as a vector V where,

$$V = (a_1, a_2, a_3 \ldots\ldots\ldots\ldots a_{23}, a_{24})$$

It follows that the end shear displacements is,

$$\Delta = 2b_T(a_1 - a_2 + a_3 - a_4 + a_5 - a_6 + a_{18} - a_{19})$$

$$+ 4b_S(a_7 - a_8 + a_9 - a_{10} + a_{11} - a_{12} + a_{20} - a_{21})$$

$$+ 2b_L(-a_{13} + a_{14} - a_{15} + a_{16} - a_{17} + a_{22} - a_{23})$$

A necessary requirement for compatibility between adjacent corrugations is that the relative shear displacement between the two longitudinal edges should remain constant along the total length. Using $\frac{d\Delta}{dy} = 0$, the above equation may be simplified by grouping each of the sine and linear terms together, giving,

$$\Delta = 2b_T(a_1 + a_{18}) + 4b_S(a_7 + a_{20}) + 2b_L\, a_{22}$$

$$0 = 2b_T(a_2 + a_{19}) + 4b_S(a_8 + a_{21}) + 2b_L(a_{13} + a_{23})$$

$$0 = 2b_T a_3 + 4b_S a_9 + 2b_L\, a_{14}$$

$$0 = 2b_T a_4 + 4b_S a_{10} + 2b_L a_{15}$$

$$0 = 2b_T a_5 + 4b_S a_{11} + 2b_L\, a_{16}$$

$$0 = 2b_T a_6 + 4b_S a_{12} + 2b_L\, a_{17}$$

Knowing these basic compatibility conditions the total strain energy may be expressed as the sum of energies due to,

(i) bending of the cross-section
(ii) longitudinal bending of the plate elements
(iii) longitudinal axial strain on the side plate
(iv) shear strain in the plate elements
(v) torsion of the sides of the profile.

The distortional energy of cross-section bending has been derived in terms of the three characteristic plate displacements U_T, U_S, U_B. It follows that the total energy may be obtained by integration along the sheet length according to the variation of the assumed displacements.

$$E_D = 2\int_0^{b/2} \left[C(1_1 1) U_T^2 + C(1_1 2) U_S U_T + C(1_1 3)\ U_T U_B \right.$$

$$\left. + C(2_1 2) U_S^2 + C(2_1 3) U_S U_B + C(3_1 3) U_B^2 \right]\ dy$$

A typical integration takes the form,

$$2\int_0^{b/2} C(1_1 2) U_S U_T\ dy = C(1_1 2) \left[\frac{b^3}{(2\pi)^2}\ (a_1 a_8 + a_2 a_7) + a_1 a_7 \frac{b^3}{12} \right.$$

$$+ \frac{b^3}{2(2\pi)^2}\ a_2 a_8 - \frac{b^3}{(4\pi)^2} \cdot (a_1 a_9 + a_3 a_7) + \frac{b^3}{2(4\pi)^2}\ a_3 a_9$$

$$+ \frac{b}{(6\pi)^2}\ (a_1 a_{10} + a_4 a_7) + \frac{b^3}{2(6\pi)^2}\ a_4 a_{10} - \frac{b^3}{(8\pi)^2}\ (a_1 a_{11} + a_5 a_7)$$

$$\left. + \frac{b^3}{2(8\pi)^2}\ a_5 a_{11} + \frac{b^3}{(10\pi)^2}\ (a_1 a_{12} + a_6 a_7) + \frac{b^3}{2(10\pi)^2}\ a_6 a_{12} \right]$$

The sinusoidal displacements give rise to in-plane bending energy according to,

$$E_B = 2\Sigma_i \frac{EI_i}{2} \int_0^{b/2} \left(\frac{d^2 U_i}{dy^2}\right)^2\ dy$$

where I_i refers to the inertia of the top, side and bottom plates respectively.

$$\text{Therefore, } E_B = \frac{2\pi^2 Et}{3b} \left\{ b_T^3 (a_2^3 + 4a_3^3 + 9a_4^3 + 16a_5^3 + 25a_b^3) \right.$$

$$+ 2b_S^3\ (a_8^3 + 4a_9^3 + 9a_{10}^3 + 16a_{11}^3 + 25a_{12}^3)$$

$$\left. + b_L^3\ (a_{13}^3 + 4a_{14}^3 + 9a_{15}^3 + 16a_{16}^3 + 25a_{17}^3) \right\}$$

The bending displacements imply a longitudinal strain incompatibility at the plate joints, and it is therefore necessary to include the appropriate membrane extension of the side plate (Fig. (2.4 (b)) which takes the form,

$$\text{Axial strain} = \left\{ b_T U_T^{11} + b_T \gamma_T^{1} - b_L U_B^{11} - b_L \gamma_B^{1} \right\}/2$$

$$\text{Strain energy, } E_A = \frac{\Pi^2 b_S E t}{b} \left\{ (a_2 + a_{19}) b_T - (a_8 + a_{23}) b_L \right)^2$$

$$+ 4(a_3 b_T - a_{14} b_L)^2 + 25(a_6 b_T - a_{17} b_L)^2 \}$$

The total shear strain energy is simply,

$$E_S = \frac{G}{2} \int_o^s \int_o^b \gamma^2 \, ds \, dy$$

where $\int_o^s$ means integration around the section

$$E_S = Etb \left[b_T a_{18}^2 + \frac{b_T}{2} a_{19}^2 + 2b_S a_{20}^2 + b_S a_{21}^2 \right.$$

$$\left. + b_L a_{22}^2 + \frac{b_L}{2} a_{23}^2 \right]$$

The torsion energy of the sides is given by,

$$E_T = \frac{t^3 G}{6} \left[\left\{ \frac{2b_T}{b_T^2} + \frac{2b_L}{b_L^2} \right\} \int_o^b \dot{U}_S^2 dy + \frac{4b_S}{(2b_S)2} \int_o^b (\dot{U}_T - \dot{U}_B)^2 \, dy \right]$$

$$E_T = \frac{t^3 b G}{3} \left\{ \frac{1}{b_T} + \frac{1}{b_L} \right\} \left[a_7^2 + \tfrac{1}{2} a_8^2 + \tfrac{1}{2} a_9^2 + \tfrac{1}{2} a_{10}^2 + \tfrac{1}{2} a_{11}^2 + \tfrac{1}{2} a_{12}^2 \right]$$

$$+ \frac{t^3 b G}{6 b_S} \left[a_1^2 + \tfrac{1}{2}(a_2 - a_{13})^2 + \tfrac{1}{2}(a_3 - a_{14})^2 + \tfrac{1}{2}(a_4 - a_{15})^2 \right.$$

$$\left. + \tfrac{1}{2}(a_5 - a_{16})^2 + \tfrac{1}{2}(a_6 - a_{17})^2 \right]$$

The total internal energy is thus,

$$E_{tot} = E_d + E_b + E_a + E_s + E_t = e(1,1) a_1^2 + e(1,2) a_1 a_2, \text{ etc}$$

and may be expressed as,

$$E_{tot} = V.(D).V^T = \frac{\Delta^2}{2C}$$

where V is the vector of displacement parameters, a(i) and (D) is a square symmetric matrix whose terms are derived from the coefficients of the variables according to,

$$\sum_{i=1}^{23} \sum_{j=1}^{23} a(i).D(i.j).a(j) = \frac{\Delta^2}{2C}$$

where $D(i, i) = e(i, i)$

and $D(i, j) = e(i, j)/2$ for $i \neq j$

The minimum potential energy condition is obtained by differentiating the internal energy with respect to small variations in each of the displacement coefficients. The matrix D(i,j) is shown in Figs. (2.36) and (12.37).

Thus,

$$dE_{tot} = 2da(i). \sum_{j=1}^{23} D(i, j).a(j)$$

However, due to the compatibility conditions, six of the parameters are no longer independent and the 23 equations may be reduced to 17 by applying the conditions in differentiated form according to,

$$da_7 = \frac{-b_T}{2b_S} (da_1 + da_{18}) - da_{20} - \frac{b_L}{2b_S} da_{22}$$

$$da_{13} = \frac{-b_T}{b_L} (da_2 + da_{19}) - da_{23} - \frac{2b_S}{b_L} (da_8 + da_{21})$$

$$da_{14} = \frac{-b_T}{b_L} da_3 - \frac{2b_S}{b_L} da_9$$

$$da_{15} = \frac{-b_T}{b_L} da_4 - \frac{2b_S}{b_L} da_{10}$$

$$da_{16} = \frac{-b_T}{b_L} da_5 - \frac{2b_S}{b_L} da_{11}$$

$$da_{17} = \frac{-b_T}{b_L} da_6 - \frac{2b_S}{b_L} da_{12}$$

Eliminating these differentials gives a set of 17 independent simultaneous equations in terms of 23 unknowns.

Again, by expressing the dependant displacements in terms of the others, the 23 unknowns may be reduced to 17 and left in matrix form as,

$$(H)\bar{a} = B$$

where (H) is a 17 x 17 square symmetric matrix and B is a column vector.

$$\bar{a} = \begin{bmatrix} a_1/\Delta \\ a_2/\Delta \\ a_3/\Delta \\ \vdots \\ a_6/\Delta \\ a_8/\Delta \\ \vdots \\ a_{12}/\Delta \\ a_{18}/\Delta \\ \vdots \\ a_{23}/\Delta \end{bmatrix}$$

The equations may then be solved in terms of the unit applied shear force parallel to the corrugations, and reinserting into the total energy expression, the flexibility c is obtained as,

$$C = \frac{\Delta^2}{2E_{tot}}$$

To extract the distortional flexibility $C_{1.1}$, the pure shear strain flexibility must be subtracted where,

$$C_{1.2} = \frac{2(b_L + 2\,b_S + b_T)}{tbG}$$

Thus, corresponding to Bryan's formulation,

$$C_{1.1} = \frac{0.144ad^4}{Et^3b^3}K$$

where K is a parameter reflecting the distortion of the cross-section.

2.4 Influence of Sheet Length, thickness and Number of Fourier Terms

If, in the above analysis only a_1 and a_7 are retained then the solution degenerates to the rigid plate movement theory, and K remains at a steady value. Fig. (2.13) shows how, for a typical profile, an increase in the number of Fourier terms (a_i) used results in an increase in the apparent value of the sheeting constant, K. With each additional parameter the K value rises and flattens off as the length increases, which physically implies that the model of the localized distortion by sinusoidal terms becomes less exact. The asymptotic behaviour is revealed by the six Fourier terms used and it is clear that K becomes approximately linear with length, and that there is a quick transition from the rigid plate theory at about 1.5 metre sheet length.

The most important single factor influencing the increase of K with length appears to be the horizontal displacement of the bottom plate which is wholly caused by plate bending. If a_{13}, a_{14} to a_{17} are removed from the analysis, consistent with the trough lines being held straight, then K reduces almost to its base value as given by Bryan's theory. Indeed, observing the profile displaced shapes (Fig. (2.1)) it is apparent that the top plate undergoes relatively little bending. The trough width however, seems to be a more important parameter, as revealed by the greater number of Fourier terms required, as shown in Fig. (2.14), for convergence for decking profiles ($b_T > b_L$). Physically, this is probably due to the influence of the discrete fastener force which causes more localised trough bending as b_L becomes small.

In general, energy methods of geometrically satisfactory displacement functions give a smaller solution than in practice to the chosen characteristic displacement which, in this case, is shear movement parallel to the corrugations. The only yardstick to the accuracy of the approach, apart from Libove's theory, is some independent technique such as the finite element method, or experimental testing, which is itself prone to error.

Figs. (2.15) and (2.16) show how the sheet thickness also influences the rise of K, for the useful range of thickness between 0.5 and 1.25 mm. In addition the trough pitch is an important parameter as revealed by Fig. (2.15).

Examination of the variation of K with length reveals that the slope passes through the origin. For lengths of less than 1.5 metres the rigid plate assumption holds but this is trivial as regards practical shear diaphragms.

Bryan suggested that,

$$C_{1.1} = \frac{0.144ad^4K}{Et^3b^3}$$

However, K may be shown to be proportional to length and the square root of thickness as in Fig. (2.16(b)), and hence maintaining the dimensionless property of the sheeting constant, a new parameter $\bar{K}$ may be derived, according to,

$$\bar{K} = \frac{Kd^{1.5}}{t^{0.5}b}\ 0.144$$

and $$C_{1.1} = \frac{ad^{2.5}\bar{K}}{Et^{2.5}b^2}$$

Qualitatively as the length increases it may be expected that the shear distortion will be confined to a fixed distance from the end, and this is consistent with the shear stiffness proportional to b^2.

In the following sections, the energy method solutions for the distortional flexibility will be separately compared to the alternative approaches such as Libove's energy derivation, the finite element method, and experimental observations. Although, the existing K value parameter will be used as a basis for comparison, the endeavour will be to show that the proposed formula for shear distortion flexibility utilizing $\bar{K}$ is more suitable as a dimensionless relationship.

In Appendix 2 tables are given of $\bar{K}$ for a range of profile shapes and fastening arrangements.

2.5. Possible Energy Method of Localized End Distortion

The Fourier series analysis reveals that the flexibility perpendicular to the corrugations remains constant, which according to the shear orthogonality factor of $(a/b)^2$ gives a longitudinal distortion flexibility in proportion to $(1/b)^2$.

Observing the corrugation displaced shapes, as in section (2.11) for the energy and finite element methods, justifies the assumption that for sufficiently long sheets, distortion soon dies out away from the effect of the fastener force. In retrospect, knowing the physical nature of corrugation distortion, an alternative theory could have been proposed whereby deformation is assumed to occur over an end distance x_d as shown in Fig. (2.5).

The influence of the fastener is to cause in-plane bending of the trough, and as confirmed in section (2.11) the top plate remains relatively rigid. To simplify the approach, the trough displacement may be assumed to be parabolic decaying to zero at x_d from the sheet edge and the top plate displacement is zero throughout. The end bottom plate movement is half the sheet flexibility perpendicular to the corrugations.

The side plates must also bend parabolically to ensure compatibility for zero longitudinal shear displacement, and hence the only variable parameter in the total energy expression is the distorted length x_d. As previously, the longitudinal and transverse bending energies may be evaluated

according to the same expressions as in section (2.3). The shear and torsion energies are neglected.

Distortional energy due to transverse bending varies as t^3. In-plane bending energy, is in proportion to t, the sheet thickness.

If the trough movement is given by a parabolic form as,

$$U_B = \left(\frac{x}{x_d}\right)^2 \Delta_1$$

then the side movement is,

$$U_S = \frac{b_L}{2b_S} \left(\frac{x}{x_d}\right)^2 \Delta_1$$

where x_d is the distorted length.

The distortion energy is thus,

$$E_d = 2 \int_o^{x_d} C(2,2) U_S^2 + C(3,3) U_B^2 + C(2,3) U_S U_B \quad dx$$

$$= Cd \int_o^{x_d} \frac{x^4}{x_d^4} \cdot dx = Cd \frac{x_d}{5} \Delta_1^2$$

The longitudinal bending energy is thus,

$$E_b = \frac{8Et}{3} (b_L^3 + 2b_S^3 \left(\frac{b_L}{2b_S}\right)^2) / x_d^3 = C_e \frac{\Delta_1^2}{x_d^3}$$

If $E_{tot} = E_b + E_d$ only,

therefore, $$\frac{\Delta^2}{2C'} = \left\{\frac{Ce}{x_d^3} + \frac{Cd}{5} x_d\right\} \Delta_1^2$$

$$\frac{dE}{dx_d} = -\frac{3Ce}{x_d^4} + \frac{Cd}{5} = 0, \quad \text{Therefore, } x_d = \sqrt[4]{\frac{15Ce}{Cd}}$$

thus $C^1 \propto C_e^{-3/4} C_d^{-1/4}$

As $C_e \propto t$ and $C_d \propto t^3$

$\therefore \quad C^1 \propto t^{-3/2}$

Using the expression for flexibility parallel to the corrugations as,

$$C = C^1 \frac{a^2}{b^2}$$

then $C \propto \frac{1}{t^{3/2} b^2}$ as indicated from the previous energy method analysis of Fourier series displacement functions.

2.6. Experimental Determination of Flexibility

Ideally the testing apparatus should have sufficient dimensional variability to observe the flexibility of as many different lengths of standard sheets as possible, with widths based on multiples of the trough pitch. A suitable test rig was developed as in Plate (2.2) with an ultimate jack capacity of 100 kN when extended to its maximum size. The left hand longitudinal member and jacking point were bolted down to the strong floor, and the right hand member was free to slide over needle bearings.

The following provisions were made:-

(a) The framing members were of substantial proportions in order to limit flexibility due to axial strain.

(b) The joints between the framing members were pinned so that the unclad rig had negligible resistance.

(c) The rigid body rotations could be measured and subtracted from the rafter movement in order to obtain the shear displacement as in Fig. (2.6).

(d) The rig width could be altered from 150 mm to 1,250 m in steps of 150 mm.

(e) The length could be varied from 1 to 6 metres. Intermediate purlins are shown in all possible positions. In some tests on very long sheets, a single purlin would also be used at mid span to prevent excessive sagging.

(f) The tops of the purlins were set at the same level as the tops of the rafters in order to eliminate any eccentricities of loading.

(g) Where seams between adjacent sheet widths were necessary, a large number of seam fasteners were used in order to limit the influence of seam slip.

A number of sheet profiles were *examined with depths ranging from* 19 mm to 65 mm, and thicknesses of nominally 0.5, 0.6 and 0.7 mm. Each sheet was used in both decking ($b_T > b_L$) and roofing ($b_L > b_T$) configurations.

In Plate (2.3) the entire rig is shown clad with a 35 mm deep decking profile number 1 which is 1.25 m wide times 6.1 m long. Each sheet was tested in order to establish the shear flexibility over the whole range from one to six metres, as well as for various widths of sheet. For all tests the load was increased in increments and unloaded several times until a linear steady response was obtained so that the bedded-in value of fastener flexibility could be confidently used in subsequent analysis. It should be noted that 0.07 mm/kN and 0.03 mm/kN were taken as the respective slip values of the seam and edge fasteners respectively after a few loading cycles.

As a standard fixing arrangement, seam fastenings were made at 150 mm centres and longitudinal edge fastenings at 300 mm. The seams were stiched by 'Tucker' blind pop rivets and for the perimeter fixings, 'Tek 4' self tapping screws, were used.

For each test, the components of shear deflection other than that due to corrugation distortion were calculated from current theory and

deducted from the measured flexibility. The observations were then expressed as effective values of the sheeting constant K, and the results and appropriate theoretical comparisons are given in Section 2.15. Alternatively, the theoretical and experimental total flexibilities may be compared.

The likely errors are much greater for longer sheet lengths when the distortion component may be of similar magnitude as the minor flexibilities. On the other hand, for short lengths of about 1 metre, the inaccuracy of jack loading in the smallforce range is a variable factor. In general the rig could accommodate shear displacements of about 100 mm, and proved to be a very versatile piece of apparatus.

2.7. Finite Element Method for Determining Corrugation Distortion

Simple rectangular elements may be pieced together to represent the faces of the corrugation. In order to model the actual deformation the condition of zero strain must be maintained along the trough centre line, and the trough allowed to bend freely. This was best achieved by attachment to a hypothetical member of high axial but zero bending stiffness (Fig. (2.7(a))). The fasteners where replaced by single point constraints and those on the moveable side given one degree of freedom. In addition, the effect of purlin restraint on side plate depression could be modelled by simply removing the vertical degree of freedom of the last element in the side plate.

Each element has five degrees of freedom per node and a finite element mesh generator was specially written by Dr. J. M. Davies which avoided tedious checking and eliminated the possibility of data errors. Thus only a small amount of data was required corresponding to the geometry, boundary conditions, material properties and element distribution.

Convergence tests were carried out for two sheeting profiles to determine the best arrangement of elements. It has been shown[37] that two elements per face gives a reasonably close approximation to the shear flexibility, which is remarkably insensitive to the number of elements on the cross-section.

The number of elements in the length is rather more critical, in order to keep a suitable aspect ratio of element size. Fig. (2.7(b)) shows the K value plot against number of elements which indicates that for maximum economy 60 elements gave sufficient accuracy for practical pruposes for a length of 4 metres. This corresponds to an element aspect ratio of about 4 and thus approximately 900 elements would be needed to represent a length of 6 metres.

2.8. Effect of Edge Beam Restraint on Shear Distortion

The problem of edge beam reduction of shear flexibility is due to restraint against depression of one side plate. As previously outlined, end deformation occurs by top and side plate movement, and the upward force provided by the edge beam disrupts the basic antisymmetry of distortion (Plate (2.1)).

The proposed energy method in Section (2.3) can only analyse idealized antisymmetic end movements, but it will be shown that the effect of edge beam restraint due to 'purlin-propping' may be separately accounted for as an independent flexibility reduction factor.

A useful model for analysis is to consider the resisting force at the base of the side plate as the sum of a symmetrical and anti-symmetrical pair of forces as in Figs. (2.8). The energy method cannot easily take this effect into account which would require double of the number of parameters for a comprehensive analysis.

An alternative method may be suggested based on rigid plate movements. This is not so unreasonable as it may be expected that, as all the applied forces are at the ends of the corrugation a direct ratio of end movements to shear displacement based on more rigorous functions would be the same as for the linear case. Thus any end forces can be expected to modify the overall shear flexibility independent of length.

This uniform edge beam reduction factor assumption is in fact borne out by alternative energy[32] and finite element methods.[37]

Libove[39] has studied the shear stiffness of trapezoidal corrugations with discrete attachments to a rigid flange. He considers the anti- and symmetrical components of edge beam uplift force separately which are of such a magnitude to reduce the free side deformation to zero. His approach is a comprehensive energy analysis similar to that outlined in Section (2.2), the symmetrical component of uplfit involving only three rather than six independent displacements.

The rigid plate movement theory is in principle the same although it is merely a simple means of extracting a solution to this complex deformational problem. Its use is really only justifiable by the very close comparisons with Libove and finite element results for the complete range of profile shapes. Falkenberg[36] did propose a similar energy method based on rigid generators.

For simplicity alone, Bryan's assumption of a uniform cross-sectional shear flow was utilized, after it had been observed that Horne's approach with linear plate movements gave almost identical answers. Thus the free side plate displacement due to a unit fastener force could be easily determined from the bending moments of Fig. (2.9).

$$\bar{U}_S = \int_o^{s/2} M_1 M_o \frac{q}{EI_S} ds = \phi_2 \frac{q}{EI_S}$$

where $q = \frac{1}{d}$, and $I_S = \frac{Et^3}{12(1-\nu^2)}$ per mm. length

The anti-symmetric loading component due to a force $\frac{P_1}{2}$ as in Fig. (2.8(b)), gives,

$$\bar{U}_{S_1} = \int_o^{s/2} M_1 M_1 \frac{P_1}{2EI_S} ds = \phi_3 \frac{P_{1/2}}{EI_S}$$

The symmetrical component due to $\frac{P_1}{2}$ is, as in Fig. (2.8(c)),

$$\bar{U}_{S_2} = \int_o^{s/2} M_3 M_3 \frac{P_1}{2EI_S} ds = \phi_4 \frac{P_{1/2}}{EI_S}$$

where $\int_o^{s/2} ds$ implies integration over the half profile.

It should be noted that the symmetrical displacements are in the same direction at each end of the sheet, whereas the anti-symmetic components are linear along the length from the centre. Thus, in theory, if uplift is constant along the length, then $\bar{U}_{S_2}$ will be a much stiffer displacement than $\bar{U}_S$ and $\bar{U}_{S_1}$ by the ratio 1/2 to 1/6. However, as the symmetrical uplift is only restrained by the end fasteners it may be expected that the deformation will soon die out some distance into the sheet. As an approximation all movements are assumed to have the same longitudinal stiffness factor of b/6 corresponding to linear distortion along the length.

Only the antisymmetric force reduces the warping displacement, with a consequent reduction in the shear flexibility.

For zero side plate movement,

$$\bar{U}_S = \bar{U}_{S_1} + \bar{U}_{S_2}$$

$$\text{therefore,} \quad \frac{\phi_2}{d} = (\phi_3 + \phi_4)\frac{P_1}{2}$$

$$\text{therefore,} \quad P_1 = \frac{2\phi_2}{d} \Big/ (\phi_3 + \phi_4)$$

Thus the flexibility reduction due to $\frac{P_1}{2}$ is,

$$(2\bar{U}_S{}^1 h + \bar{U}_T{}^1 2b_T)\frac{P_1}{2}$$

$$= \{2h \int_0^{s/2} M_1 M_1 ds + 2b_T \int_0^{s} M_1 M_2 ds\} \frac{\phi_2}{d(\phi_3 + \phi_4)}$$

$$= (2b_T\phi_5 + 2h\phi_3)\frac{\phi_2}{d(\phi_3 + \phi_4)} \quad \text{for a unit fastener force}$$

Comparing with $C_{1.1} \propto 2h\phi_2 + 2b_T\phi_1$

the reduction factor due to edge beam resistance is,

$$r = \frac{(2b_T\phi_5 + 2h\phi_3)}{(2b_T\phi_1 + 2h\phi_2)} \cdot \frac{\phi_2}{\phi_3 + \phi_4}$$

So the flexibility factors K and $\overline{K}$ are assumed to be both modified to the form,

$\overline{K}$ (1 - r) where r is a function of the cross-section shape only.

The actual value of purlin resistance P_1 may be of some importance for deep profiles which may fail by web crippling due to the high compressure forces transferred from the purlin as shown by Baere.(34)

2.9. Effect of Fastening in Intermediate Purlins

In the previous analyses, it has been observed that above a certain length, the shear distortion occurs only in a region of less than 1 metre from the sheet end. For practical sheet lengths of about 8 metres, shallow profiles may span over a number of purlins and to prevent the effects of wind uplift, are often fastened at intermediate points along their length. In order to maintain the uniformity of shear displacement along the sheet length, the trough plate must be constrained to bend as in Figure (2.19) which is mathematically defined by $U_B = 0$ at the intermediate fixings.

Thus the displacement pattern no longer includes a redundant portion in the middle of the sheet consistent with its asymptotic behaviour. Now the trough movement and hence distortion follow a curved path along the sheet. Nevertheless, the great majority of distortion may be expected to occur beyond the penultimate purlin.

The analysis best suited to modification to cope with the fixing in every trough case at intermediate and end purlins is the energy method of assumed displacement functions. As regards the influence of purlin restraint of side plate depression it may be expected that only the end support has any effect and hence any analytical K or $\overline{K}$ value to represent the corrugation distortion will be reduced by an amount independent of the number of intermediate purlins.

At this point it is better to consider each number of intermediate purlins separately up to a total of four. Naturally, one or no middle

support does not affect the deformation pattern, and also it may be expected that the K value for a very large number of intermediate purlins will degenerate to the case where trough line movement is held straight.

2.9.1. Two Intermediate Purlins:

The basic components of energy and deformation are unaltered, except for the number of independent variables defining the displacement pattern.

If $U_B = 0$ at $y = b/6$

then,

$$0 = a_{13} \sin \frac{\pi}{3} + \frac{a_{14}}{2} \cdot \sin \frac{2\pi}{3} + \frac{a_{16}}{4} \cdot \sin \frac{4\pi}{3} + \frac{a_{17}}{5} \cdot \sin \frac{5\pi}{3}$$

or, $$0 = a_{13} + \frac{a_{14}}{2} - \frac{a_{16}}{4} - \frac{a_{17}}{5}$$

thus $$a_{17} = 5a_{13} + \frac{5a_{14}}{2} - \frac{5}{4}a_{16}$$

as a_{17} has already been expressed in terms of a_6 and a_{12} according to

$$a_{17} = \frac{b_T}{b_L} a_6 - \frac{2b_S}{b_L} a_{12}$$

and a_{13}, a_{14} and a_{16} have been given by,

$$a_{16} = - \frac{b_T}{b_L} a_5 - \frac{2b_S}{b_L} a_{11}$$

$$a_{14} = - \frac{b_T}{b_L} a_3 - \frac{2b_S}{b_L} a_9$$

$$a_{13} = - \frac{b_T}{b_L} (a_2 + a_{19}) - a_{23} - \frac{2b_S}{b_L} (a_8 + a_{21})$$

It follows that a_{12} may also be eliminated from the 17 independent variables by combining the equations for a_{13}, a_{14}, a_{16} and a_{17}.

$$a_{12} = -\frac{b_T}{2b_S} a_6 + \frac{5b_T}{2b_S}(a_2 + a_{19}) + \frac{5b_L}{2b_S} \cdot a_{23} + 5(a_8 + a_{21})$$

$$+ \frac{5}{2} \cdot \frac{b_T}{2b_S} a_3 + \frac{5}{2} \cdot a_9 - \frac{5}{4} \frac{b_T}{2b_S} \cdot a_5 - \frac{5}{4} \cdot a_{11}$$

Thus $\bar{a}$, the vector of independent displacements consists of a_1/Δ to a_{11}/Δ except a_7/Δ and a_{18}/Δ to a_{23}/Δ

Minimising the total energy expression gives, as previously,

$$dE_{tot} = 2da(i) \; \Sigma_{j=1}^{23} D(i, j) \; a(j)$$

da_{12} may be eliminated in terms of da_2, da_3, da_5, da_6, da_8, da_9, da_{11}, da_{19}, da_{21} and da_{23}.

Thus 16 equations for the minimized potential energy result, in terms of 23 variables. Again, $\frac{a_{12}}{\Delta}$ may be eliminated giving,

$$(H) \; \bar{a} = B$$

where (H) is a 16 x 16 square symmetric matrix and B is a 16 term column vector.

Solving for the independent variables, and reinsertion into the total energy expression

$$\Sigma_{i=1}^{23} \Sigma_{j=1}^{23} a(i) \; D(i, j) \; a(j) = \frac{\Delta^2}{2C}$$

yields a value for the shear flexibility C which includes both $C_{1.1}$ and

$$C_{1.2} = \frac{(2b_L + 4b_S + 2b_T)}{btG_I}$$

2.9.2. Three Intermediate Purlins

In this case, the middle purlin has no U_B displacement, so the only condition to maintain $U_B = 0$ at the quarter points ($y = b/4$) is,

$$0 = a_{13}.\sin\frac{\pi}{2} + \frac{a_{15}}{3} \cdot \sin\frac{3\pi}{2} + \frac{a_{17}}{5}. \sin\frac{5\pi}{2}$$

$$0 = a_{13} - \frac{a_{15}}{3} + \frac{a_{17}}{5}$$

thus $a_{17} = 5a_{13} - \frac{5}{3}a_{15}$

Again, as a_{17}, a_{15} and a_{13} have already been eliminated consistent with Δ = constant for the no intermediate purlin case,

$$a_{17} = -\frac{b_T}{b_L} a_6 - \frac{2b_S}{b_L} a_{12}$$

$$a_{15} = -\frac{b_T}{b_L} a_4 - \frac{2b_S}{b_L} a_{10}$$

$$a_{13} = -\frac{b_T}{b_L} (a_2 + a_{19}) - a_{23} - \frac{2b_S}{b_L} (a_8 + a_{21})$$

It follows that a_{12} may be removed from the previous 17 independent variables by

$$a_{12} = -\frac{b_T}{2b_S} a_6 + \frac{5b_T}{2b_S} (a_2 + a_{19}) + \frac{5b_L}{2b_S} \cdot a_{23} + 5(a_8 + a_{21})$$

$$- \frac{5}{3} \cdot \frac{b_T}{2b_S} a_4 - \frac{5}{3} a_{10}$$

Similarly da_{12} may be expressed in terms of da_2, da_4, da_6, da_8, da_{10} da_{19}, da_{21} and da_{23}, to give 16 equations for minimum potential energy in 23 variables.

Thus eliminating a_7, a_{12}, a_{13}, a_{14}, a_{15}, a_{16} and a_{17}, the resulting 16 equations in 16 variables may be solved, and on reinsertion into the total energy expression, the total shear flexibility per corrugation may be determined.

In a similar manner to Bryan's original analysis $C_{1.1}$ may be expressed as,

$$C_{1.1} = \frac{0.144ad^4}{Et^3b^3} K \quad \text{where } a = d \text{ in this case}$$

However, K as will be shown later, is no longer constant but rises with b in a similar fashion to the no intermediate purline case.

2.9.3. Four Intermediate Purlins

The displacement of the trough plate is constrained at $y = \frac{b}{10}$ and $y = \frac{3b}{10}$ which gives two additional compatibility conditions, as well as those for $\frac{d\Delta}{dy} = 0$ according to,

$$0 = a_{13} \sin \frac{\pi}{5} + \frac{a_{14}}{2} \sin \frac{2\pi}{5} + \frac{a_{15}}{3} \sin \frac{3\pi}{5} + \frac{a_{16}}{4} \sin \frac{4\pi}{5}$$

$$0 = a_{13} \sin \frac{3\pi}{5} + \frac{a_{14}}{2} \sin \frac{6\pi}{5} + \frac{a_{15}}{3} \sin \frac{9\pi}{5} + \frac{a_{16}}{4} \sin \frac{12\pi}{5}$$

which reduces to,

$$\frac{a_{16}}{4} + a_{13} = 0 \quad \text{and,} \quad a_{15} + \frac{3}{2} a_{14} = 0$$

Thus using,

$$a_{16} = - \frac{b_T}{b_L} a_5 - \frac{2b_S}{b_L} a_{11}$$

$$a_{15} = - \frac{b_T}{b_L} a_4 - \frac{2b_S}{b_L} a_{10}$$

$$a_{14} = - \frac{b_T}{b_L} a_3 - \frac{2b_S}{b_L} a_9$$

$$a_{13} = - \frac{b_T}{b_L} (a_2 + a_{19}) - a_{23} - \frac{2b_S}{b_L} (a_8 + a_{21})$$

It follows that a_{11} and a_{10} may also be eliminated from the 17 independent variables, by

$$a_{11} = -\frac{b_T}{2b_S} a_5 - \frac{4b_T}{2b_S}(a_2 + a_{19}) + \frac{4b_L}{2b_S} a_{23} - 4(a_8 + a_{21})$$

$$a_{10} = -\frac{b_T}{2b_S} a_4 - \frac{3}{2} \cdot \frac{b_T}{2b_S} a_3 - \frac{3}{2} a_9$$

Thus da_{11} and da_{10} may be expressed in terms of the other differentials to give 15 equations for the minimized total potential energy in the 23 variables.

Also a_{10}, and a_{11} may be eliminated to solve for the 15 independent parameters. The flexibility c follows in a similar fashion to the other cases.

It may be expected that four intermediate purlins fastened in every trough will be as many as normally required in practice for manufacturer's sheet lengths. Typically, for a profile depth of 35 mm. spanning 1.8 metres the maximum sheet length would be 9.0 metres.

From statical observations, the theoretical shear flow should have a stepwise increase towards the sheet centre, but must also ensure compatibility between neighbouring shear strains in each bay. The energy method, by maintaining a constant shear displacement satisfies the compatibility requirements but can only approximate the internal rise of shear flow within the sheet length.

As the number of intermediate purlins increases, the solution approaches the case where the trough lines are continuously held straight, which has also been analysed by Libove.[40]

2.10. Sheets Fastened in Intermediate Purlins in Alternate Troughs and in Every Trough at their Ends

This situation is indicated in Fig. (2.20) for the two intermediate purlin case, where the middle trough is free to move unconstrained by the effects of the internal fastenings. Thus, at the intermediate purlin points the movement is the superposition of the previous cases

where fastenings occur in every trough, and an additional concertina action.

As an approximation to the true flexibility, this arrangement could be considered as the mean of fastenings at the ends only, and fastening in every trough at every intermediate purlin.

A theoretical energy method approach, which has not been attempted quantitatively, might be to include an additional Fourier series for the middle trough displacement. Thus the difference between neighbouring trough lateral movements is accommodated by a concertina action which is much less stiff than the profile twisting due to every corrugation fastening. It may be expected, therefore, that quite large relative movements between troughs would occur without much concertina resistance.

Hence, the previous assumption for the shear flexibility may be taken as being reasonably correct for any number of intermediate connections. Thus,

$$K = \frac{K_N + K_1}{2} \qquad \text{and } \overline{K} = \frac{\overline{K}_N + \overline{K}_1}{2}$$

where K_N and K_1 etc., represent the flexibility factors due to N and one intermediate purlin fixings, respectively fastened in every corrugation throughout. For more sparce intermediate connections it is suggested that $K = K_1$.

2.11. Longitudinal Variation of Cross-Section Displacements

2.11.1. Discussion of Energy Method Results

The final displaced shape of top, side and bottom plate movement may be redetermined by combining the relevant Fourier terms times their respective variables as evaluated from minimum total energy principles. End purlin restraint has been omitted.

A typical example of the effect of length on plate bending for

a standard profile is shown in Fig. (2.10). To obtain a dimensionless parametric form each movement is divided by the end top plate displacement ($\bar{U}_T$). For a 1 metre sheet length fastened only at its ends, the rigid plate movement assumption holds, consistent with $U_B = 0$. At 2 metres length, trough and side plate bending is noticeable, and this becomes exaggerated for greater lengths. The asymptotic distortion behaviour is revealed by $U_T = U_B$ and $U_S = 0$ for a wide central portion of the 6 metre sheet length, indicating that there is indeed an internal redundant region which undergoes little or no distortion. Distortion may be seen to be localized within the last metre of the sheet ends.

It appears that crest bending is quite small and that for a given profile, the relative value of top and side plate end movement remains constant independent of length. Bearing this in mind, the ratio of top to side end displacement may be presented as a function of the profile shape for a 1 metre sheet length, as in Fig. (2.12), based on the rigid plate movement assumption.

For most of the profile range, top plate movement dominates the side displacement except for $2b_T/d$ values about 0.5 when both are of similar magnitude. At larger $2b_T/d$ values, as in decking profiles, the side plate movement actually becomes negative, although very small in relation to top plate displacement. It may be expected, therefore, that the 'purlin-prop' reduction flexibility due to side plate restraint will be in rough proportion to the relative value of side to top plate movement.

2.11.2. Comparison with Finite Element Results for any Number of Intermediate Purlins

At a 6 metre sheet length, plate displaced shapes as determined from the energy method in section (2.3) have been plotted for three different profiles under a unit longitudinal shear force. Four cases were considered representing standardly available sheeting, fastened in every trough to one, two, three or four intermediate purlins. For comparison finite element predictions for the longitudinal displaced shapes are indicated.

In Fig. (2.25) for a 35 mm deep roofing profile, the agreement between energy and finite element method displacements for trough and crest movements is acceptable. For side plate movement, however, the one intermediate purlin case does not degenerate quickly to $U_S = 0$ as revealed by the finite element results. Nevertheless, the agreement for actual end movement is very good, which afterall does determine the resultant shear displacement. Energy methods of assumed displacement functions it seems, often give a close a answer to the shear flexibility even though their internal displacements do not accurately follow the actual deformed shape.

It is apparent that for the two, three and four intermediate purlin cases, trough bending is essentially confined to the final bay. However, the internal restraints will tend to disrupt the smooth variation of shear deformation towards the sheet end, by causing local distortion around the intermediate purlins fixings as indicated in Fig. (2.19).

It may be observed from the displaced shapes of Fig. (2.25) that the top plate remains relatively rigid whilst the trough and side plates bend in order to satisfy the compatibility and restraint conditions, as well as minimizing the total internal energy. Agreement between energy and finite element method displacements is good for the two, three and four intermediate purlin cases.

Fig. (2.26) shows the previous profile inverted for decking purposes. Again crest and trough movement agreement is quite good, but side plate movement is not. However, for this case, side plate displacements are much smaller than for the roofing profile.

The final corrugation is only 19mm deep and consequently is distortionally much stiffer. Finite element comparison was only performed for the one (or no) intermediate purlin case and the same basic displaced shapes result as for the previous cases.

The summation of the respective Fourier terms to form the longitudinal displaced shape shows the relative importance of each simusoidal term. This may be tabulated below for a 5 metre sheet length of the 35mm deep profile described in Fig. (2.25) where Δ is the shear displacement parallel to the corrugation for a unit applied force.

Number of Inter Purlins		$\frac{y}{b/2}$	$\sin \frac{2\pi y}{b}$	$\sin \frac{4\pi y}{b}$	$\sin \frac{6\pi y}{b}$	$\sin \frac{8\pi y}{b}$	$\sin \frac{10\pi y}{b}$
1	U_T/Δ	15.9	-1.97	+0.45	+0.02	-0.08	+0.10
	U_S/Δ	21.0	-9.35	+2.90	-0.79	+0.27	-0.14
	U_B/Δ		+7.65	-2.33	+0.59	-0.17	+0.06
2	U_T/Δ	15.0	-1.26	+0.88	+0.04	-0.08	+0.16
	U_S/Δ	20.0	-5.73	+4.81	-0.77	-0.06	-0.13
	U_B/Δ		+4.15	-3.91	+0.56	+0.08	+0.17
3	U_T/Δ	14.1	-0.82	-0.38	-0.16	-0.08	+0.02
	U_S/Δ	18.7	-3.1	+2.6	-2.01	+0.24	+0.15
	U_B/Δ		+1.68	-2.08	+1.56	-0.15	-0.12
4	U_T/Δ	13.4	-0.50	+.009	-0.14	-0.11	+0.11
	U_S/Δ	18.1	-2.00	+1.22	-1.22	+0.86	-0.13
	U_B/Δ		+0.61	-0.91	0.91	-0.61	+. 06

2.12. Comments on the Distortional Flexibility as Determined by the Energy Method

2.12.1. Effect of Profile Shape

The existing theory parameter K, which defines the shear flexibility due to distortion based on rigid plate movement assumptions, will be used as the basis for defining the sheet shear performance. However, it is apparent from section (2.4) that this parameter is not only dependent on sheet length and thickness but also on profile shape.

In Fig. (2.11) the variation of K with length and top plate width is shown for a rectangular profile of depth 30mm omitting 'purlin-prop' effects. For a 1 metre sheet length K rises to a peak at about $\frac{2b_T}{d} = 0.5$ and falls to a trough when $\frac{2b_T}{d} = 0.7$ and then rises steeply. It may be noted that for $\frac{2b_T}{d} = 1$ the distortion behaviour corresponds to a portal frame under lateral load. This variation of the K value reflects the relative magnitude of side to top plate displacement as shown in Fig. (2.12). For longer sheet lengths K increases, but still shows the same basic pattern.

$\bar{K}$, the proposed shear distortion parameter related to the rise of K in the length, also shows the same variation with cross-sectional shape, as in Fig. (2.18). The relationship between shear stiffness (using $\bar{K}$ and profile depth is approximately $(h/d)^{-3/2}$ for rectangular corrugations whereas the corresponding sheet inertia varies roughly as $(h/d)^2$. For folded plate applications which require a high profile depth for buckling restraint and low depth for deflection limitation it is apparent that only a few millimetres change in sheet depth has a marked impact on the relative design importance of these two factors.

Tabulations of the $\bar{K}$ values for a complete range of profile shapes, both including and omitting 'purlin-prop' effects are given in Appendix 2.

2.12.2. Effect of Intermediate Purlins

The greater degree of trough restraint, for intermediate purlin fixings, has the effect of stiffening the shear performance of the sheeting. For short lengths, where trough bending does not contribute to the shear flexibility, the number of intermediate fixings has no effect. As the length increases to about 2 metres, for two intermediate purlins, the K value rises to become linear with increasing sheet length.

Thus the same asymptotic behaviour is observed from the energy method derivation as for the case of simple end attachment. Distortion becomes localised near to the influence of the sheet-purlin fasteners independent of the length. Sheets fastened in intermediate purlins also display this effect, although coupled with the principal end deformation is a local trough bending and distortion around each internal fastener as in Fig. (2.19). As the number of purlins increases so the internal energy must increase, which is consistent with decreasing shear flexibility. Thus if each intermediate purlin contributes its own local deformation then the asymptotic behaviour may again be represented by the proposed $\bar{K}$ parameter, as in Fig. (2.24).

$$\text{where} \quad C_{1.1} = \frac{ad^{2.5}\bar{K}}{Et^{2.5}b^2}$$

If $\bar{K}_1$ is the value due to one intermediate purlin then the $\bar{K}_N$ may approximately be represented by,

$$K_N = \frac{\bar{K}_1}{1 + \alpha (N - 1)}$$

where α represents the contribution of the internal purlins to the distortional energy and roughly equals 0.3.

As shown in Fig. (2.21) the asymptotic behaviour of shear distortion occurs at progressively greater sheet lengths as N increases. Nevertheless, the $\bar{K}$ parameter may still be used in preference to K for practical sheet lengths. The effect of intermediate fixings on $\bar{K}$ may be seen in Fig. (2.23), and it may be observed that as the number increases,

so the reduction in the $\bar{K}$ value, from the simple intermediate purlin case, falls.

Eventually, as the number of internal restraints increases, so the K value will tend to the case where the trough lines are continuously held straight. This is depicted in Figs. (2.31) and (2.32). K rises only gradually showing that side and top plate bending contribute little to the asymptotic shear distortion behaviour. Approximate theoretical reductions in flexibility are for N intermediate purlins.

$N = 2$ - $K_N/K_1 = 0.75$

$N = 3$ - $K_N/K_1 = 0.60$

$N = 4$ - $K_N/K_1 = 0.50$

It should be noted for a given span between purlins of say 2 metres, that the K value remains approximately constant independent of the number of purlins. Thus, the flexibility of practical panels may be more in proportion to b^3 rather than b^2 which perhaps explains why previous tests on full scale diaphragms did not reveal the large increase in the shear flexibility parameter with increasing length.

The convergence of the Fourier series for the intermediate purlin cases appear to be slightly better than for the simple case, as shown in Fig. (2.22). Comparisons of the K values of standard sheets is included in the following sections for both finite element and experimental observations.

$\bar{K}$ parameters for up to four intermediate purlins are given in Appendix 1 for a range of profile geometries. It is assumed that end purlin restraint effects as determined in section (2.8) may be considered separately.

2.13. Comparison of Energy Method Results with Libove and Strehl Methods

Libove studied both the cases of free antisymmetric profile distortion with standard trough fixings, and also the effect of end purlin restraint. Fig. (2.17) shows the good agreement between Libove's

published results and the energy method derivation for four different profiles. Some deviation from the predicted curve is to be expected especially for short lengths where graphical interpolation of the author's small effective stiffness values is difficult. However, the general pattern indicates the linearity of K with increasing length.

The effective shear modulus may be expressed as,

$$\bar{G} = \frac{G}{1 + \frac{2h}{d} + .\frac{d^{2.5}\bar{K}\,G}{t^{1.5}\,bE}}$$

corresponding to a shear flexibility of,

$$C_{1.1} = \frac{ad^{2.5}\bar{K}}{Et^{2.5}b^2}$$

Strehl apparently did not observe the asymptotic behaviour of shear distortion which may be represented by a single dimensionless parameter, $\bar{K}$. However, his derivation gave reasonable agreement for the effective shear stiffness of four published profiles as shown in Fig. (2.28) for lengths of 2, 4 and 6 metres and sheet thickness of 1mm.

2.14. Comparison with Finite Element Results

Four standard profiles were examined by the finite element method outlined in section (2.7), which includes the facility for free antisymmetric end deformation, and also the provision for zero side plate depression due to the end 'purlin-prop' effect. The profiles of Figs. (2.29) to (2.32) cover a range of depths, thicknesses and trough widths, and all behave well compared to the proposed energy method. Generally finite element results are more flexible, except for decking profiles where the low number of cross-sectional elements probably has a stiffening effect.

Experimental results are also indicated which also show reasonable agreement. For one case, the trough lines were held straight by omitting the lateral degree of freedom of the centre trough element. Finite element results (F.E.) are more flexible than the energy method for this very stiff configuration where K remains approximately constant.

'Purlin-prop' reductions in flexibility support the premise that this effect may be considered separately from the free asymmetric deformation.

Intermediate purlin results are shown in Figs. (2.33) and (2.34) for typical shallow and deep profiles. Other theoretical finite element comparisons are given in Fig. (2.36). It is apparent that the experimental and finite element solutions for 2, 3 and 4 intermediate purlin fixings are somewhat more flexible than the corresponding energy method prediction. This is especially true when the number of intermediate purlins is greater than 2 for decking profiles and probably implies that more Fourier terms are required to cope with the severe localization of distortion.

As an approximate observation from the finite element results for roofing profiles ($b_T < b_L$) and decking profiles ($b_T > b_L$), the ratio of K values is,

	decking	roofing	N
$\frac{K_N}{K_1}$	0.80	0.70	2
	0.70	0.60	3
	0.60	0.50	4

where K_N is the value due to fastening the N intermediate purlins.

No finite element tests were performed due to fastening in alternate troughs at the intermediate points and in every trough at the sheet ends.

2.15. Comparison of 'Purlin-Prop' reduction of Flexibility with other Theories

As indicated in the theoretical approach, the simplified idea of a uniform edge beam reduction factor applied to the shear flexibility, independent of sheet length, can only be judged by comparison with more refined theories, notably those due to Libove, Strehl and the finite element method.

Fig. (2.18) shows the distribution of the new effective shear parameter $\bar{K}$ for a range of profile shapes as determined from the energy method. When the purlin prop reduction factor is included it is apparent that this restraint is most effective for profile shapes in the range $0.6 > 2b_T/d > 0.3$. Indeed for a rectangular profile of $2b_T/d = 0.7$ the reduction factor is very small which probably is related to the relative magnitude of side to top plate displacement.

Strehl's comparison of effective shear modulus is tabulated for four profiles, in Fig. (2.28) which indicates the reasonable agreement for the edge beam reduction factor. Libove's values are also plotted for four other profiles over a range of sheet lengths from 1m to 6m. The most important observation is that the reduction factor is essentially constant with length, which is reasonable considering that all the applied forces are at the ends of the sheet. The rise of K with length is due to the localization of end distortion, and it may be expected that the purlin restraint forces also display the same localized effect.

Thus having been justifed by these other theories, the simplified edge reduction shall be used to modify the proposed K parameter to provide a useful design value for the reduced stiffness of corrugated sheeting. Intermediate purlin fixings, it is assumed, are also subject to the same reduction factor due to end purlin restraint. Tabulations of this factor are given in Appendix 2.

2.16. Discussion of Experimental Observations for Every Trough Fastening with No Intermediate Purlins

Test results are shown in Appendix 1. A number of different profile shapes, depths and thicknesses were studied over a range of sheet lengths from 1.1 metres to 6.1 metres. An extra 50mm overhang was included over the normal 1 metre purlin centres to reduce the possibility of local fastener tearing. In order to minimize the effect of seam slip, initially only one sheet width was chosen for testing, but it became apparent that the longitudinal fastenings to rigid rafters held the trough lines straight. As previously discussed, this severely reduces the shear

flexibility and it may also be expected that this extra stiffness is spread some way into the sheet due to the lateral bending rigidity of the purlins.

The experimental and theoretical comparisons are for both the total shear flexibility and the deduced K value parameter, which was derived by subtracting the theoretical minor flexibilities due to slip etc., from the observed total.

$$\text{Hence, } K = \frac{Et^3b^3 C_{1.1}}{0.144\ ad^4}$$

The edge fasteners were consistently set at 300 mm centres and the seam fasteners at 150 mm centres giving a failure load at 6m length of 80 KN.

Bedded in values of fastener slip were used for self-tapping screws and for seam fasteners. The loading range was never applied above 0.3 times the theoretical fastener failure load and the average slop of deflection taken for the flexibility. The minor flexibilities were deduced according to the expressions in Section (1.4.)

In order to observe the actual in situ seam slip during the loading sequence a dial gauge was set up as in Plate (2.4) for the 4.5 metre wide test on profile 10. The results vindicated the use of the reduced bedding in seam stiffness rather than the design value of 0.35 mm/KN in the low load range.

As a more reasonable experimental study, sheet widths of about 1200 mm were used which also had the advantage of limiting premature shear buckling for very long lengths, and a purlin was used for extra support. Of course a single intermediate purlin does not affect the longitudinal deformation.

The theoretical and experimental comparisons for 35 mm deep profile 1 are good, as shown in Fig. (2.31). Two test widths of 7 and 4 corrugations were used, the latter test being proportionally much stiffer due to the longitudinal restraints. In addition the relatively narrow trough width suffered some clamping action by the head of the self-

tapping screw. Profile 2, which is the inverted form of 1 behaved well, although the trough width was to some extent more affected by the rigid side conditions.

Profile 3 was studied for 6 corrugations width and was somewhat stiffer than in theory. Apart from the previous explanations and the possible inaccuracy of the fastener slip no reason could be found for this discrepancy. It is likely that the small deflections were affected by frictional resistance in the test rig. A major problem was that the tolerance in the corner pin connections gave an initial slip which had to be omitted in determining the sheet flexibility. Profile 4 was studied for three sheet widths of 1, 4 and 8 corrugations as in Fig. (2.32), the final width behaving well compared to theory. The single corrugation corresponds to the case of the trough lines being held continuously rigid and the theoretical comparison is also reasonable. It does appear that at least six and possibly eight corrugations are necessary in testing to obtain a consistent shear flexibility.

A smaller profile 19mm deep was studied in both decking (5) and roofing (6) forms. Their performance was also good as revealed in Fig. (2.29) for profile 6.

Profile 7 of 100 mm pitch was specially designed by Dr. J. M. Davies to have optimum proportions in bending for material usage. It's experimental shear performance was considerably more flexible than in theory especially for the 4 metre sheet length. However, it must be borne in mind that the number of Fourier terms used in the energy analysis probably do not accurately model the severe localized end distortion of the very narrow trough width.

Profiles 8 and 9 of 12 corrugations width were tested on a previously designed apparatus of Plate (7.1), and showed good agreement.

Test profile 10 was 4.5 metres wide and 6.6 metres long, which cantilevered by 300 mm each end. The effect of overhanging sheets will be discussed later in Chapter 5.

A number of deeper corrugations were then examined, profiles 11

12 being 45 mm deep and 1200 mm wide and gave very good agreement, which was probably enhanced by the accurate reading of these relatively large shear deflections as shown in Fig. (2.30). Finally a 65 mm deep corrugation studied in decking and roofing forms as profiles 13, and 14 also performed exactly as the theoretical prediction.

The K value comparisons for the four profiles of Figs. (2.29) to (2.32) also indicate the energy method solution with and without the effect of the end 'purlin-prop' reduction in flexibility. Occasional finite element results are given including end purlin effects which are generally more flexible than the energy method predictions.

The overall conclusion from the energy method, finite element and experimental observations is that $\bar{K}$ is a more suitable shear distortion design parameter, consistent with the localization of trough bending. The actual magnitude of $\bar{K}$ is deduced by the slope of the existing K value with length, according to,

$$\bar{K} = \frac{0.144 d^{1.5} K}{t^{0.5} b}$$

is reasonably well defined by the energy method solution. Thus for fastening in every trough with no intermediate purlins, the shear flexibility may be reliably determined by,

$$C_{1.1} = \frac{a d^{2.5} \bar{K}}{E t^{2.5} b^2}$$

where $\bar{K}$ is a tabulated parameter dependent on three geometrical parameters only. Theoretical $\bar{K}$ solutions are given in Appendix 2 for increments of top plate widths $^{2b}T/d = 0.1$ and sheet depths $h/d = 0.1$ with 5^{o} variations in side plate slope to the vertical up to 45^{o}.

2.17. Discussion of Experimental Observations for Every Trough Fastening for up to Four Intermediate Purlins

The test rig purlin spacings of 1 metre required that only sheet lengths of 3 and 6 metres could be experimentally studied fastened in two

intermediate purlins. At the 3m length, profiles 5, 6, 11 and 12 of depths 19mm and 44mm were tested and for comparison the K values were deduced by subtracting the minor flexibilities from the observed total. The flexibility of fixing to intermediate purlins may be expressed as direct ratio of the simple case of fastening at the ends only and together with the experimental results are given in Appendix 1.

It should be noted that the maximum sheet width given for each of the previous tests was used in order to reduce the longitudinal stiffening effect of fixing to rafters. The general observation from the results is that the experimental flexibilities due to fastening in two intermediate purlins are greater than in theory. The approximate theoretical ratio K_N/K_1 for N equals two is 0.65 whereas the experimental value was determined as 0.73. A typical example for profile 6 is shown in Fig. (2.34) also indicating the corresponding finite element results.

For a 6 metre sheet length as used for profiles 10, 13 and 14, the theoretical factor was about 0.7 and the experimental, 0.76. Plate (2.6) shows the 4.5 m wide times 6.6m long test on profile 10 fastened in two intermediate purlins. It has been assumed in the analysis that the intermediate purlin points offer complete restraint to trough movement. However, with all fastener forces there is a corresponding slip and the relatively small trough bending movements may be accommodated to some extent. Thus $U_B = 0$ as in Fig. (2.19) may in practice not exist at the intermediate purlin points.

For three intermediate purlins only a 4.1 metre sheet length could be used and again 5, 6, 11 and 12 were studied. In this case the average value of K_N/K_1 was derived from the energy method analysis to be roughly 0.48. Experimentally the figure was 0.65 although this again may be affected by fastener slip at the intermediate purlins. Profile 5 test results are depicted in Fig. (2.34.)

For four intermediate purlins which were only examined using profiles 11, 12 and for a 5.1 metre sheet length, the theoretical reduction was about 0.4 (Fig. (2.33)) compared to an experimental value of 0.54.

Fastening in alternate trough at the intermediate purlin points and in every corrugation at the ends was examined for profiles 10, 11 and 12. The theoretical K parameter was taken as the average of fastening in every corrugation throughout and the K value of fastening in the end purlins only as in Fig. (2.35). An average reduction factor was 0.8 whereas this was experimentally observed to be 0.9.

The energy method predicts a linear variation of K with sheet length. Due to dimensional limitations the number of intermediate purlins could not be maintained whilst increasing the overall sheet length. However, the agreement between experimental and theoretical results is acceptable, taking into account the practical difficulties in establishing complete restraint at the intermediate purlins.

In a similar fashion to the no intermediate purlin case a new dimensionless parameter $\bar{K}$ may be proposed.

$$C_{1.1} = \frac{ad^{2.5}\,\bar{K}}{Et^{2.5}\,b^{2}}$$

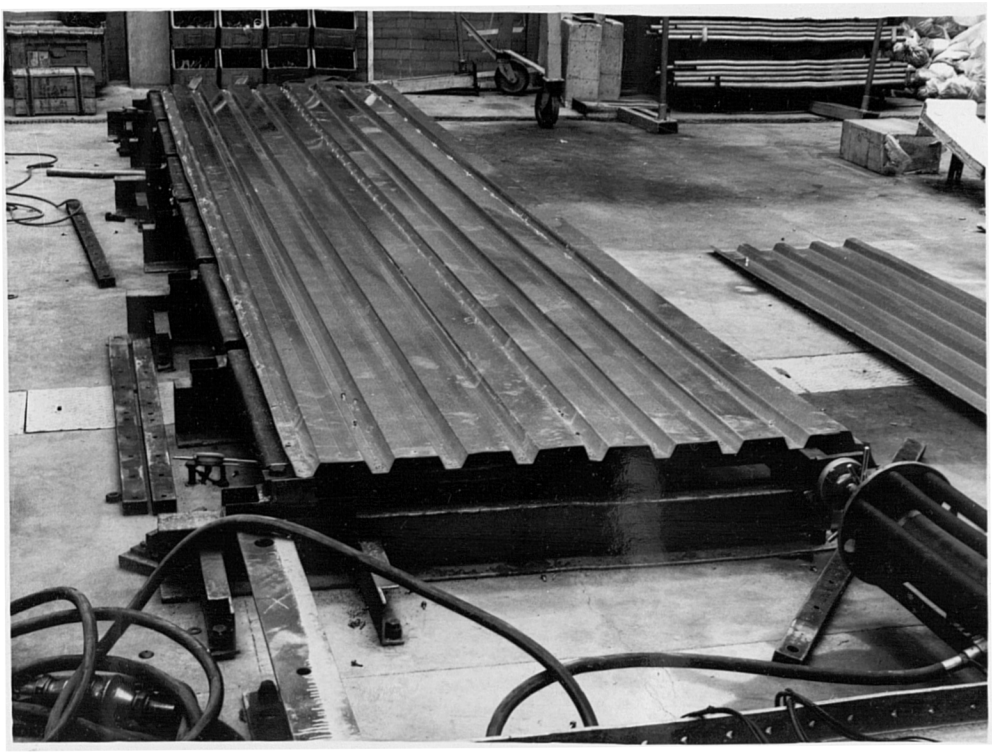

Plate (2.3) Test rig is shown clad with profile 1 fastened to one intermediate purlin

Plate (2.4) Modified test rig is clad with profile 10 fastened in two intermediate purlins. Also shown is the insitu measurement of seam slip by a dial gauge connected to neighbouring sheets

C H A P T E R 3.

THE SHEAR FLEXIBILITY DUE TO DISTORTION OF SHEETS FASTENED IN ALTERNATE OR EVERY THIRD TROUGH

3.1. General Solution

A preliminary diaphragm design would normally be performed on the strength capabilities of a certain number of fasteners usually in every, or alternate or more rarely every third corrugation. However, fasteners separated by a multiple of the corrugation pitch cause distortion of a much more severe kind than the pure twisting form of fastening in every trough.

The force per fastener is assumed to be equally derived from the profile shear flow integrated over half the fastener pitch both in front and behind the discrete connection. For fastenings in every two or three troughs the profile is very flexible laterally, and the effect of this sheet shear flow is to cause compression and extension of the corrugations by trough movement as in Fig. (3.1.).

Considering the forces along one corrugation, there will be tension and compression at each end of the sheet length and it may be expected that the lateral displacement of the trough plate varies linearly between. Hence the in-plane rotation of the individual plates results in longitudinal warping, which is manifested as a shear displacement.

As a simplifying approach the shear flexibility may be considered to be made up of two quite separate modes.

1. For fasteners in every trough the distortion is due to profile twisting as examined in Chapter 2 and this added to,

2. An additional concertina flexibility due to the reapplication of the missing fastener forces. Thus for alternate trough fastenings, the central trough force is considered separately from the rest of the profile shear, in compressing the corrugation. Similarly, for fastenings in every n troughs,

then (n - 1) extra trough forces must be reapplied. In subsequent sections the analytical approach will only be performed for this concertina distortion mode which is by far the major contributor to the total shear flexibility for multiple trough fastenings.

The net force on the ith corrugation from one end for n troughs between fasteners is thus $(\frac{n+1}{2} - i)$, due to a unit force applied at each trough. The ends of the profile will be anti-symmetrically compressed and extended and will contribute to an additional shear warping as in Fig. (3.1.).

Considering the rotation of the left hand trough to be θ_{i-1} and the next trough, θ_i it follows that, from linear plate displacements, the extra shear deflection per trough pitch d is:

$$d\Delta_i = \theta_{i-1}\, d + (\theta_i - \theta_{i-1})\, \frac{d}{2}$$

The compressibility of the profile over a small slice of the sheet length dy due to a unit trough force is:

$$\{\frac{4}{3} b_S + 2b_T\} \frac{h^2}{D} \cdot dy \quad \text{where } D = \frac{Et^3}{12(1 - \nu^2)} \text{ per mm length}$$

For linear plate movements the trough concertina deflection due to a unit end trough force thus becomes.

$$\{\frac{4}{3} b_S + 2b_T\} \frac{h^2 6}{bD} = d_o \frac{6}{bD}$$

where b is the overall length, and b, h, b_S and b_T are defined in Fig. (2.1).

b/6 is the equivalent sheet length to be used in determining end stiffnesses for linearly antisymmetric plate movements.

The longitudinal warping due to the concertina flexibility of the ith profile is:

$$(\theta_i - \theta_{i-1})\, \frac{d}{2} = \frac{6d_o}{bD} (\frac{n+1}{2} - i) \cdot \frac{d}{b}$$

The factor d/b represents conversion from a unit trough force to a unit shear force parrallel to the corrugations.

Using the conditions that $\Delta_1 = 0$, $\theta_o = 0$, $\theta_n = 0$, $\Delta_n = n\Delta$, it follows that the concertina flexibility, Δ, due to fastening every n troughs may be progressively determined.

It is clear that the greater the spacing between fasteners, so the flexibility will rise proportional to roughly n^2. For most practical applications of 150 mm wide profiles, fastenings are never less frequent than every third corrugation and usually alternate troughs fixing is preferred to limit excessive visible distortion.

The final flexibility is determined by superposing the concertina value and the every corrugation fastening flexibility. Bryan[4] has tablulated the K values for multiple trough fastening as determined by linear plate generators according to,

$$C_{1.1} = \frac{0.144ad^4K}{Et^3b^3}$$

where $C_{1.1}$ is the total distortion per panel width, a.

Fig. (3.1) shows a typical case fastened in every third trough. It is apparent that tensile movement causes depression of the side plates which implies that in reality there is some restraint by the end purlin to which the sheet is fastened. This 'purlin-prop' reduction in flexibility will be discussed in section (3.6.).

3.2. Alternate Trough Fastening

For a unit force parrallel to the corrugations the missing fastener for alternate trough fastening is d/b. Hence the net compression and tensile forces at the sheet ends are equally divided between neighbouring profiles.

Assuming linear plate movements the concertina component of shear flexibility, from the expressions of Section (3.1.), is:

$$\Delta = 3\left(\frac{d}{b}\right)^2 \frac{d_o}{D_b}$$

where d_o is the concertina flexibility of the profile due to a unit compressive force. It follows that for

$$d_o = \left(\frac{4}{3} b_S + 2b_T\right) h^2$$

the shear flexibility due to concertina distortion is

$$C_{1.1} = \left(\frac{2}{3} b_S + b_T\right) h^2 \; 72 \; d^2 \; \frac{(1 - \nu^2)}{Et^3 b^3}$$

Using Bryan's expression for the shear flexibility the concertina distortion parameter is

$$K_A = \left\{\frac{b_S}{3} + \frac{b_T}{2}\right\} \frac{h^2}{d^3} \; (1 - \nu^2) \; 100$$

Superimposing the every corrugation K value, (K_E), the total shear flexibility for alternate trough fastening is

$$C_{1.1} = \frac{0.144 \; ad^4 K}{Et^3 b^3} \qquad \text{where } K = K_A + K_E$$

K is a constant for linear plate movements.

This case is depicted in Fig. (3.2(a)). It was concluded from Chapter 2, that for every corrugation fastening, the shear distortion becomes localized towards the sheet extremities due to non-linear plate movements.

In energy method terms this may be explained by the fact that the increase of plate bending energy is such as to reduce the amount of sheet distortion until the total energy becomes a minimum. For alternate trough fastening concertina action is the primary shearing mode rather than distortional twisting, and is a much more flexible form of deformation.

Nevertheless it was experimentally observed that for sheet lengths of above 4 metres, the flexibility and hence the K value did rise above the linear generator theory prediction, which implies that some in-plane plate

bending does occur. In this case plate bending is such as to minimize concertina distortion as shown in Fig. (3.2(b)).

An an analytical technique the energy method of assumed displacement functions will be used to determine the influence of sheet length on the shear flexibility, and finite element tests carried out to check the suitability of the approach.

In a similar fashion to the every trough fastening case, the displaced shapes of the outer and centre trough plates U_{B2} and U_{B1} respectively, may be expressed in terms of truncated Fourier series according to Fig. (3.3). It is assumed that for this concertina mode, all the plate displacements may be described in terms of these two trough movements where the variables a_i try to reduce the amount of internal concertina action (Fig. (3.2(b))).

The sinusoidal terms contribute to the longitudinal plate bending energy and the linear plate movement component is due to a_1

$$U_{B1} = a_1 y + a_2 \frac{b}{2\Pi} \sin \frac{2\Pi y}{b} + a_3 \frac{b}{4\Pi} \sin \frac{4\Pi y}{b} + a_4 \frac{b}{6\Pi} \sin \frac{6\Pi y}{b}$$

$$U_{B2} = a_5 \frac{b}{2\Pi} \sin \frac{2\Pi y}{b} + a_6 \frac{b}{4\Pi} \sin \frac{4\Pi y}{6} + a_7 \frac{b}{6\Pi} \sin \frac{6\Pi y}{b}$$

Top plate displacements resulting from concertina action are assumed to be the same for each corrugation and move according to the average of the neighbouring trough deflections.

$$U_T = \frac{a_1}{2} y + \frac{(a_2 + a_5)}{2} \frac{b}{2\Pi} \sin \frac{2\Pi y}{6} \quad \text{etc}$$

The total internal energy may be evaluated in terms of the concertina distortion and axial strain energies together with an allowance for the torsion of the sides of the corrugation.

For ease of interpretation the different magnitudes of the sinusoidal trough displacements such as a_2 and a_5 may be split up into two modes corresponding to

1. $(\frac{a_2 - a_5}{2})$, which is the concertina action due to equal and opposite sinusoidal trough movements for $U_T = 0$

2. $(\frac{a_2 + a_5}{2})$, which is the component due to equal movements of trough and top plates, as in Fig. (3.3.).

Mode 1 contributes to the concertina energy per corrugation, which is defined by,

$$E_c = k_c \int_0^{b/2} U_c^2$$

where U_c is the concertina action such that,

$$U_c = a_1 y + (a_2 - a_5) \frac{b}{2\pi} \sin \frac{2\pi y}{b} + \text{etc.},$$

k_c is the force required for 1 mm corrugation compression and equals

$$\frac{D}{d_o} = \frac{Et^3}{12(1 - \nu^2).(1.33b_S + 2b_T)h^2}$$

$$E_c = k_c \frac{b^3}{24} a_1^2 + k_c \frac{b^3}{2\pi^2} a_1 \{\frac{a_2 - a_5}{2}\} + k_c \frac{b^3}{4\pi^2} \{\frac{a_2 - a_5}{2}\}^2$$

$$- k_c \frac{b^3}{8\pi^2} \{\frac{a_3 - a_6}{2}\} a_1 + k_c \frac{b^3}{16\pi^2} \{\frac{a_3 - a_6}{2}\}^2 + k_c \frac{b^3}{18\pi^2} \{\frac{a_4 - a_7}{2}\} a_1$$

$$+ \frac{k_c b^3}{36\pi^2} \{\frac{a_4 - a_7}{2}\}^2$$

Due to the concertina trough movement there is a consequent side plate uplift or depression, U_{S1}, given by

$$\frac{U_{S1}}{U_c} = f = \frac{b_L}{4b_S} \{\frac{b_S + b_T}{0.67\, b_S + b_T}\}$$

Mode 2 does not influence the concertina energy as the top and trough plate movements are equal and may be represented as,

$$U_d = \{\frac{a_2 + a_5}{2}\} \frac{b}{2\pi} \sin \frac{2\pi y}{b} + \{\frac{a_3 + a_6}{2}\} \text{ etc.}$$

However, to be consistent with these displacements the side plates must move to maintain compatibility according to,

$$\frac{U_{S2}}{U_d} = \{\frac{b_L + b_T}{2b_S}\}$$

This component of distortion is very similar to the profile twisting of the every trough fastening case and hence the energy associated with displacement U_{S2} is,

$$E_d = \frac{Et^3 \, kd}{12(1 - \nu^2)} \int_o^{b/2} U_{S2}^2 \, dy$$

where $k_d D$ is the side plate force for a 1mm in-plane side plate deflection.

$$1/k_d = \int_o^{S/2} M_1 M_1 \, ds \; . \; (\frac{h}{2b_S})^2$$

Again, t, b_L, b_S, b_T, and h are geometrical properties of the profile and are defined in Fig. (2.1), and M_1 is given in Fig. (2.9).

The distortional displacement U_{S2} will be much smaller than the concertina form U_{S1} and so in general the magnitudes of a_2 and a_3 will be very similar to those of a_5 and a_6 respectively.

The cross-section movements due to fastening in alternate troughs are relatively large and an allowance must necessarily be made of the torsional energy of longitudinal plate twisting.

The bottom, top and side plate rotations are respectively,

$$\theta_B = \frac{f}{b_L} \{a_1 y + (a_2 - a_5) \frac{b}{2\pi} \sin \frac{2\pi y}{b} + (a_3 - a_5) \frac{b}{4\pi} \sin \frac{4\pi y}{b} + \text{etc.}\}$$

$$\pm\{\frac{b_L + b_T}{2b_S \, b_L}\} \{(a_2 + a_5) \frac{b}{4\pi} \sin \frac{2\pi y}{b} + (a_3 + a_6) \frac{b}{8\pi} \sin \frac{4\pi y}{b} \text{ etc}\}$$

$$\theta_T = \{\frac{b_L + b_T}{2b_S\, b_T}\} \{(a_2 + a_5) \frac{b}{4\Pi} \quad \text{etc}\}$$

$$\theta_S = \frac{1}{4b_S} \{a_1 y + (a_2 - a_5) \frac{b}{2\Pi} \quad \text{etc}\}$$

Thus the torsional energy is,

$$E_t = \int_o^{b/2} \frac{2Gt^3}{3} \{(\frac{d\theta_B}{dy})^2 b_L + (\frac{d\theta_T}{dy})^2 b_T + (\frac{d\theta_S}{dy})^2 2b_S\} \, dy$$

$$= \frac{Gt^3 b}{3} \{\frac{f^2}{b_L} + \frac{1}{8b_S}\} . \{a_1^2 + \frac{(a_2 - a_5)^2}{2} + \frac{(a_3 - a_5)^2}{2} + \frac{(a_4 - a_7)^2}{2}\}$$

$$+ \frac{Gt^3 b}{3} \{\frac{1}{b_L} + \frac{1}{b_T}\} (\frac{b_L + b_T}{2b_S})^2 . \{\frac{(a_2 + a_5)^2}{8} + \frac{(a_3 + a_5)^2}{8} + \frac{(a_4 + a_7)^2}{8}\}$$

Owing to the relatively large distortional deflections, the energy caused by shear strain has been neglected. The final energy quantity is the plate axial strain due to the sinusoidal components of trough movement.

Again separating the parameters into two modes as in Fig. (3.3) the axial strain energy may be evaluated by,

$$E_a = \int_o^{b/2} \int_o^{s} \varepsilon_a^2 \, Et \, ds\, dy$$

where ε_a is the axial strain at any section.

Mode 1, due to pure concertina action, gives a top plate axial strain energy of,

$$E_{A1} = \frac{2tE\Pi^2 b_T}{b} (b_L + 2(2f)b_S)^2 \{\frac{(a_2 - a_5)2}{4} + \frac{4(a_3 - a_6)^2}{4} + \frac{9(a_4 - a_7)^2}{4}\}$$

where f derives from the corresponding side plate movement due to corrugation compression.

The side plate axial strain energy is,

$$E_{AS} = \frac{4tE\Pi^2 b_S}{b} (b_L + (2f)b_S)^2 \quad \{ \frac{(a_2 - a_5)^2}{4} + \text{etc} \}$$

The bending energy in the bottom and side plates is,

$$E_{AB} = \frac{2}{3} \cdot \frac{tE\Pi^2}{b} \quad (b_L^3 + 2(2f)^2 b_S^3) \quad \{ \frac{(a_2 - a_5)^2}{4} + \text{etc} \}$$

Mode 2 due to equal movements of top and bottom plates gives top, bottom and side plate bending energies of,

$$E_{A2} = \frac{2}{3} \frac{tE\Pi^2}{b} (b_L^3 + b_T^3 + 2b_S^3 (\frac{b_L + b_T}{2b_S})^2).$$

$$\{\frac{(a_2 + a_5)^2}{4} + \frac{4(a_3 + a_5)^2}{4} + \frac{9(a_4 + a_7)^2}{4} \}$$

An additional side plate axial strain occurs, due to the unequal edge strains across it. As the top and bottom plate movements are equal the centre strain is,

$$\frac{2\Pi}{b} \cdot \sin\frac{2\Pi y}{b} \frac{(b_L - b_T)}{2} \{ \frac{(a_2 + a_5)}{2} + \ldots\ldots$$

Thus $$E_{A1} = \frac{tE\Pi^2 b_S}{b} \quad \frac{(b_L - b_T)^2}{4} \quad \{(a_2 + a_5)^2 \quad \text{etc}$$

Thus the total axial strain energy due to trough bending is,

$$E_a = E_{A1} + E_{AS} + E_{AB} + E_{A2} + E_{AD}$$

The total internal energy, E tot, includes concertina energy, pure distortion, axial strain, and torsion,

$$E_{tot} = E_c + E_d + E_a + E_t$$

The internal work done by a unit applied force parrallel to the corrugations is $\Delta^2/_{2C}$ and hence,

$$\frac{\Delta^2}{2C_{1.1}} = E_{tot} = e(1_1 1)\ a_1^2 + e(1_1 2)\ a_1\ a_2 \ldots\ e(5_1 5)\ a_5^2$$

Expressed in matrix form,

$$\frac{\Delta^2}{2C} = \sum_{i=1}^{5} \sum_{j=1}^{5} a_i \cdot d(i,j).aj$$

where a_i represents the vector of assumed displacement parameters.

d(i,j) are the coefficients of the total energy expression such that,

$$d(i,j) = e(i,j)/2 \quad \text{for } i \neq j$$

and $$d(i,i) = e(i,i)$$

For minimum total potential energy,

$$dE_{tot} = 0$$

taking small increments in each variable, 7 simultaneous equations result where,

$$0 = 2da_i \sum_{j=1}^{7} d(i,j)\ a(j)$$

for i = 1 to 7

However, as for the every corrugation fastening case, it is a necessary condition for compatibility between neighbouring troughs that $\frac{d\Delta}{dy} = 0$. The sinusoidal components of displacement do not contribute to the shear displacement and hence Δ is defined by the rigid movement parameter a_1 where,

$$a_1 \frac{d}{2} = \Delta$$

thus $da_1 = 0$ and the six final equations to solve for the six independent parameters are,

$$\sum_{j=2}^{7} d(i,j).aj = -d(i,1) \frac{2\Delta}{d} \qquad \text{for } i = 2 \text{ to } 7$$

Resubstituting these values of $\frac{a_2}{\Delta}$, up to $\frac{a_7}{\Delta}$ with the total energy expression yields a solution for the shear flexibility due to distortion, $C_{1.1}$.

In a similar fashion to the linear generator theory, the flexibility may be represented by a parameter K_A where,

$$C_{1.1} = \frac{0.144\ ad^4 K_A}{Et^3 b^3}$$

K_A will be constant if solution corresponds to linear tough movement. The final flexibility factor due to fastening in alternate troughs consists of adding this concertina distortion to the torsional form of fastening in every trough as represented by K_E,

Thus the total value is,

$$K = K_A + K_E$$

3.3. Fastening in Intermediate Purlins

As for the case of fastening in every corrugation, intermediate purlin fixings represent an idealized restraint of trough plate movement such that $U_{B2} = 0$.

For any number of intermediate purlins, the concertina action is considered separately from the every trough fixing flexibility. Two internal restraints imply that at $y = b/6$,

$$\frac{a_5}{2} + \frac{a_6}{4} = 0$$

Thus a_6 may be eliminated from the six independent displacements according to $a_6 = -2a_5$.

Three intermediate purlins correspond to zero trough movement at $y = b/4$. Thus,

$$\frac{a_5}{2} - \frac{a_7}{6} = 0$$

Again, a_7 may be removed in the minimization of total energy process by $a_7 = 3a_5$.

Reinsertion of the displacement parameters into the total energy expression yields a solution for the shear flexibility, from which the K_A value may be derived as in Section (3.2.).

However, this only accounts for the concertina distortion. Due to the torsional form of deformation of shear flow around the cross-section which has the same flexibility as every corrugation fastening, an additional K_E value must be added.

It is apparent that the corrugations are fixed to intermediate purlins along one trough and not along the internal trough. As an approximation K_E will be taken as the average of the no and the full intermediate purlin values, which are K_{EO} and K_{EN} respectively.

$$K_E = \frac{K_{EO} + K_{EN}}{2}$$

The total parameter value is thus ,

$$K = K_E + K_A$$

3.4. Effect of Length, Sheet Thickness and Number of Fourier Terms for the Energy Method Derivation

The alternate fastening shear flexibility is at least five times greater than that due to fastening in every trough. This is apparent considering Fig. (3.4) which shows the K value for pure concertina action and the superimposed K value for the every trough fixing case, which combine to give the final alternate trough fastening flexibility parameter.

The concertina action K value is far from being constant with sheet length. For short lengths of about 1 metre there is a stiffening effect due to torsion of the sides of corrugation, and at about 3 metres the K parameter becomes linear with increasing length. This compares with 1.5 metres for the every corrugation fastening case. As previously discussed in Chapter 2 asymptotic behaviour of K indicates that end distortion has become localized rather than based on a linear generator assumption, even for this much more flexible type of concertina deformation.

However, the trough movement can only be modelled accurately for longer sheet lengths by greater numbers of Fourier terms. Fig. (3.5) shows how inclusion of up to $\sin \frac{6\pi y}{b}$ is sufficiently accurate. Each successive term causes the apparent K value to rise until its bending energy is exhausted. Minimization of the internal energy physically takes place by balancing the increase of plate bending against the reduction in concertina distortion.

At a length of 6 metres the displaced trough shapes have been plotted for both roofing and decking profiles at 1kN longitudinal shear force in Figs. (3.6) and (3.7).

It is clear that at about 30 kN longitudinal shear force the trough movement is of the order of 21 mm, which may be considered excessive for insulation fixing. This will be discussed in Section (3.13). The summation of the Fourier terms shows that the displaced shape asymptotes $U_{B1} = U_{B2}$, consistent with no distortion, until the last metre of the sheet length.

The corresponding additional every trough fastening displacements are indicated which again are about one fifth of the more flexible distortion mode. Concertina flexibility increases rapidly with decreasing trough width and greater corrugation depths.

Sheet thickness and corrugation pitch have the same effect as in Chapter 2. Fig. (3.10) reveals the linearity of K and the square root of thickness. Thus a new distortional parameter may be developed according to,

$$\bar{K} = \frac{0.144\ d^{1.5}}{t^{0.5}\ b} K$$

$\bar{K}$ now represents the localised distortion behaviour as for every trough fastening. Again, the complete $\bar{K}$ value for alternate corrugation flexibility, omitting 'purlin-prop' effects is given by,

$$\bar{K} = \bar{K}_A + \bar{K}_E$$

where $\bar{K}_A$ and $\bar{K}_E$ are the corresponding values deduced from concertina and every corrugation fastenings respectively.

Tabulations of $\bar{K}$ unaffected by 'purlin- prop' reduction in flexibility are given in Appendix 2.

3.5. Effect of Intermediate Purlin Fixings

The restraining effect of fastening to intermediate purlins may be seen in Fig. (3.8) for a typical 35 mm deep decking profile. Only the concertina component of the K value for alternate corrugation fastening is considered and it is clear that two intermediate purlins have about 25% increased stiffness compared to the case of end attachment only. Three internal restraints cause about a 50% increase of stiffness.

For short lengths all three cases behave similarly but as the sheet length increases, so gradually the K value rises to become asymptotic to a straight line. This occurs at about 6 and 9 metres for two and

three intermediate purlins respectively which is approaching the limit of practical sheet lengths. It is expected that for four intermediate purlins K will remain roughly constant.

Fig. (3.9) shows the corresponding variation of the proposed $\bar{K}$ value again for concertina action. It is clear that $\bar{K}$ does indeed become constant and is a more suitable design parameter. However, it should be borne in mind that for a 2 metre sheet span between purlins the corresponding K value remains roughly constant whereas $\bar{K}$ falls steeply. The shear stiffness is thus dependent on the cube of the overall sheet length for practical panels with uniform purlin spacing.

Any design expression for increasing numbers of intermediate purlins must introduce the proviso that for short sheet lengths the constant K value, based on rigid plate generators, is a closer approximation to the shear flexibility.

The effect of sheet thickness and corrugation pitch is exactly the same as for the no intermediate purlin case which vindicates the formula for shear flexibility in terms of $\bar{K}$ for longer sheet lengths.

Plate bending displacements are shown for a typical profile in Fig. (3.13), which highlight the smaller degree of trough bending for a 6 metre sheet length fastened in two or three intermediate purlins.

3.6. Edge Beam Reduction Factor Due to Fastening in Alternate Troughs

The accordian-like shear deformation due to multiple trough fastening not only compresses or extends the profile but also lifts or depresses the sides of the corrugation as shown in Fig. (3.15). This free movement is antisymmetric both longitudinally and laterally. In reality, the fixing to rigid members at the sheet ends will disrupt the free deformation by preventing downward motion of the side plates. For alternate trough fastening, edge beam restraint may be represented by forces P_1 and P_2 due to a unit trough force at each end of the sheet.

It has been assumed that deformation occurs by linear plate movements, which will be discussed later. Each end force may be resolved into symmetric and anti-symmetric components of which only the equal and opposite pair contribute to the warping resistance.

As shown in Fig. (3.15(b)), the end displacements due to the anti-symmetric forces $\frac{P_1}{2}$ and $\frac{P_2}{2}$ may be calculated below, and the longitudinal variation of these deflections is linear along the length. Thus referring to Section (3.1), all end displacements such as δ_{11}, δ_{13}, and δ_{33} due to equal and opposite end forces may be derived using an equivalent sheet length of b/6, corresponding to linear plate movements.

The free side plate uplift, V_S, due to a unit trough force may also be calculated using this factor of b/6. Thus the displacement at point i due to an antisymmetric pair of end forces at point j is,

$$\delta_{ij} = \frac{6}{bD} \int_0^s M_i M_j \, ds \qquad \text{where } \frac{Et^3}{12(1-\nu^2)} = D$$

$\int_0^s ds$ implies integration of the cross-section bending moments M_i times M_j around one profile where M_i are evaluated in Fig. (3.16). D is the sheet bending stiffness per mm length.

$$V_S \text{ equals } 0.5\, b_L\, h(b_S + b_T)\, \frac{6}{bD}$$

for a unit trough force generating linear plate movements.

For the symmetric force pairs at each end of the sheet, the problem of selecting an equivalent sheet stiffness in order to calculate the end displacements, is rather more complicated.

In theory, the uplift is constant along the sheet length and consequently the effect of an end force is modified by an equivalent plate length of b/2. However, this does not occur in practice as the sheet-purlin fasteners are only at the end of the sheet and naturally the cross-sectional bending moments due to net upward loading must die away from the influence of the discrete connection.

Fig. (3.15(a)) indicates that the likely region of deformation is close to the fastener and the trough centre line rises due to the uplift force from cross-section deformation. At all sections other than the line of fasteners, the theoretical end displacements δ_{22}, δ_{24} and δ_{44} will decrease, and in fact will decay much more rapidly than the linear plate movements.

Hence as an analytical expedient the equivalent sheet length to be taken for symmetrical end displacements is $\frac{bk}{6}$ in which k is less than unity. This implies that the symmetrical force pair cause proportionately larger end deflections than their corresponding anti-symmetric components.

Edge purlin restraint may be evaluated by considering the compatibility requirements for side plate depression. On the outer plate, the net side plate movement is zero.

$$V_S = \{\delta_{11} + \frac{\delta_{22}}{k}\} \frac{P_1}{2} + \{\delta_{13} + \frac{\delta_{24}}{k}\} \frac{P_2}{2}$$

And the inner side plate,

$$V_S = \{\delta_{13} + \frac{\delta_{24}}{k}\} \frac{P_1}{2} + \{\delta_{33} + \frac{\delta_{44}}{k}\} \frac{P_2}{2}$$

The value arbitarily chosen for k was 0.5, on the basis of finite element comparisons. The reduction in flexibility due to the end restraints P_1 and P_2 may be determined to considering the effect of the anti-symmetric forces. The trough movement is now,

$$\delta = \delta_{oo} + \delta_{10} \frac{P_1}{2} + \delta_{30} \frac{P_2}{2}$$

where δ_{oo} is the unrestrained horizontal trough movement. Hence the flexibility reduction factor which is dependent only on the degree of trough restraint is,

$$r_A = \frac{-\delta_{10} P_1 - \delta_{30} P_2}{\delta_{oo}}$$

and the shear flexibility due to concertina action is $C_{1.1}\ (1 - r_A)$. For some profiles P_1 or P_2 may become negative in the analysis, in which case the appropriate restraint is set to zero and the compatibility condition for $P_2 = 0$ becomes,

$$V_S = (\delta_{11} + \frac{\delta_{22}}{k}) . \frac{P_1}{2}$$

and

$$r_A = \frac{-\delta_{10} P_1}{2\delta_{oo}}$$

Throughout the analysis it has been assumed that the edge beam restraint only affects the concertina component of distortion, which implies that the equivalent torsional form of every trough fastening is free to take place. Thus the final flexibility parameter K is,

$$K = K_A\ (1 - r_A) + K_E$$

where

$$C_{1.1} = \frac{0.144\ ad^4 K}{Et^3\ b^3}$$

In the previous sections it was determined that above a certain length, non-linear trough movement occurs and the deformation becomes localized near to the alternate trough fastenings. This fact does not complicate the effect of 'purlin-prop' reduction in flexibility which is assumed to remain independent of length because the relative longitudinal stiffnesses of each of the applied and restraining forces remains constant. In effect, as all the forces are applied at the same section, their contribution to the shear flexibility may be expected to be just the same for both rigid and non-linear plate movements.

Thus,

$$\bar{K} = \bar{K}_A\ (1 - r_A) + \bar{K}_E$$

where

$$C_{1.1} = \frac{ad^{2.5} K}{Et^{2.5} b^2}$$

It will be shown later in Section (3.8) that r_A does not remain completely constant but for the useful range of sheet lengths is sufficiently accurately determined by the preceding analysis. This reduction factor is largely unaffected by the number of intermediate

purlins.

Tabulations of r_A are indicated in Appendix 2 for a range of profile sizes.

3.7. Testing by Experiment and Finite Elements

The experimental test rig has been described in section (2. 6) and a number of profile sizes were examined ranging from 19 mm to 63 mm depth in lengths from 1 to 6 metres. Of course experimental observations include the effect of end purlin restraint on deformation which cannot be accurately estimated.

In this case the finite element method is of great value as it can easily model local restraints. The principle of setting up a mesh of elements by a data generator is described for the every corrugation case in Section (2. 7). For alternate corrugation fastening, two elements per face were maintained and the longitudinal trough edges were attached to hypothetical axially stiff members which satisfy the axial strain compatibility requirements between corrugations. This whole process was developed by Dr. J. M. Davies and several comparisons were run for the profiles under test with and without the effect of 'purlin-prop' restraint.

Experimental observations and their theoretical energy method comparisons are given in Appendix 1 for both the total flexibility including fastener slip effect and also experimentally deduced K' value. Figs. (3.17) to (3.19) show the corresponding energy method, experimental and finite element K value results for a number of different profiles.

The effect of fastening to intermediate purlins could also be accommodated on the test rig although the one metre pitch of purlin positions, meant that for two intermediate purlins only the 3m and 6m lengths could be examined. Similarly, only a 4m sheet length could be studied for three intermediate purlins.

3.8. Purlin-Prop Reduction Comparison with Finite Elements

The inclusion of the purlin-prop reduction in flexibility is a rather complicated approximation for the energy method in that it is assumed only to affect the concertina deformation component. Torsion of the cross-section similar to the every corrugation fastening flexibility is assumed to be unaffected by purlin restraint. Thus, as in Fig. (3.11), the final reduced K value is obtained by

$$K = K_A (1 - r_A) + K_E$$

This expression also applies for $\bar{K}$ as it is to be expected that r_A remains reasonably constant with length. The effect of the profile shape on $\bar{K}$ for up to three intermediate purlins is shown in Fig. (3.12), which indicates both the ex- and inclusion of 'purlin-prop' reduction in flexibility.

Finite element and energy comparisons are for the K values of three different profiles as shown in Figs. (3.17) to (3.19), together with the corresponding experimental observations. It does appear that the finite element results are consistently about 5% more flexible than the energy method predictions. However, the proposed reduction factor due to purlin deformational restraint does reasonably model the actual decrease in flexibility for most practical sheet lengths.

The rigid plate movement K value coincides with the actual value at about 3 to 4 metres sheet length which was the approximate size of previous test apparatus, perhaps explaining why the increase in flexibility due to alternate trough fastening had never been studied in depth.

Finite element results are somewhat stiffer for short lengths of about 1 metre, and indicate an increase in the flexibility reduction factor. Thereafter, consistent with the localization of end deformation, the factor r_A remains constant irrespective of sheet length.

3.9. Discussion of Experimental Results for No Intermediate Purlins

In total fourteen profiles were studied and the experimental and theoretical comparisons for the shear flexibility and the deduced K values are given in Appendix 2.

35mm deep profiles 1 and 2 are corresponding decking and roofing forms and their experimental, finite element and energy method K values are shown in Figs. (3.18) and (3.19). Two test widths were chosen for each which, similar to the every corrugation fastening case, reveal the restraining effect of fastening to longitudinal members.

Even for a test width of two sheets the experimental solutions are some 20% stiffer compared to theory for the decking profile and 10% stiffer for the roofing profile. An additional factor is the clamping effect of the fasteners, which, especially for narrow trough widths, will stiffen the concertina mode of distortion.

Profiles 3 and 4 also display the same characteristics of the effect of test width. For a 6 metre sheet length, 8 corrugations wide, the observed K value was some 40% more flexible than the corresponding test only four corrugations wide.

A 19mm deep profile was experimentally much stiffer in decking form than in theory, but the roofing value comparison was quite good. Profiles 7, 8 and 9 behaved similarly. The test width was increased to 4.5 metres for 38 mm profile 10 and for the first time the experimental flexibility was slightly higher than its energy method prediction. The greater number of seams may have had an adverse effect, but in general it does appear that trough bending needs a considerable sheet width away from the longitudinal member before it is effectively unrestrained. This explains the apparent stiffness of the previous experimental observations.

Profiles 10 and 11 were 45 mm deep and 8 corrugations wide. Agreement in this case was very good right up to the maximum length of 5 metres.

Similarly, the 65 mm deep profiles 12 and 13 behaved extremely well which was probably enhanced by the relatively easy recording of the large shear deflections of this deep corrugation.

In general, the experimental observations and energy method predictions show reasonable agreement, especially for the deeper profiles. Most tests were somewhat stiffer than in theory, probably due to the prevention of trough bending at the longitudinal members. For longer lengths, where trough bending contributes to a much higher shear flexibility the K value rises approximately linearly with increaseing length.

Thus $\bar{K}$ is a better distortion parameter than K for alternate trough fastening according to,

$$C_{1.1} = \frac{ad^{2.5}\,\bar{K}}{Et^{2.5}b^{2}}$$

However, for sheet lengths below 3 metres the rigid plate movement theory prediction,

$$C_{1.1} = \frac{ad^{4}\,K}{Et^{3}b^{3}} \times 0.144$$

does hold and it is suggested that the maximum value of these two expressions should be taken for the shear flexibility. As a design expression, the formula including $\bar{K}$ is the controlling form and for a given profile shape, $\bar{K}$ should be represented by the bigger of,

$$\bar{K} \text{ and } \frac{0.144d^{1.5}\,K}{t^{0.5}b}$$

Tables of $\bar{K}$ and K for any geometry of profile are given in Appendix 2 .

3.10. Discussion of the Experimental Results for up to Three Intermediate Purlins

Four profiles were examined with fastening to two and three

intermediate purlins. Due to the dimensional limitations of the test rig only one metre purlin centres could be used for three interval restraints which offer a considerable resistance to trough bending.

As previously mentioned, for this number of intermediate purlins at least 6 metre sheet lengths are required to generate the full linearity of K with length. For the shallow corrugation depth of 19 mm as in profiles 5 and 6 the experimental flexibility is about 15% greater than the theoretical prediction for three intermediate purlins with a sheet length of 4 metres. The 45 mm deep profile performs rather better in this respect, although it should be borne in mind that K has risen by only 20% from its rigid movement value.

For two intermediate purlins, studied over three metres length the theoretical and experimental comparisons are good, giving a K value ratio compared to the no internal restraint case, of about 0.8. A single test was performed on a 6 metre sheet length which again showed extremely good agreement.

On the basis of these results, which appear to agree reasonably well with the energy method predictions, the formula in terms of $\bar{K}$ will be taken for the shear flexibility fastened in intermediate purlins. $\bar{K}$ is thus only a function of the profile geometry, the fastening arrangement and the number of intermediate purlins. Tabulations for this parameter are shown in Appendix 2

However, as in Section (3.9), it is suggested for alternate trough fastening that the greater of the flexibility formulae including K and $\bar{K}$ respectively should be used for sheet lengths less than 4 metres.

3.11. Fastening Every Third Corrugation

This case is much more flexible than the previous alternate fastening case and the resulting concertina deflection may be obtained by considering the general formulation of Section (3.1), where Δ is the average displacement per corrugation.

$$d\Delta_1 = 6d_o \frac{d^2}{b^3 D} \quad (1)$$

$$\theta_1 = \frac{12 d_o d}{b^3 D}$$

$$d\Delta_2 = \theta_1 d = \frac{12 d_o d^2}{b^3 D}$$

$$\theta_2 = \theta_1$$

$$d\Delta_3 = \theta_2 d - \frac{6 d^2 d_o}{b^3 D} = \frac{6 d_o d^2}{b^3 D}$$

$$3\Delta = d\Delta_1 + d\Delta_2 + d\Delta_3 = (6 + 12 + 6) \frac{d_o d^2}{b^3 D}$$

Therefore, $\Delta = \frac{4}{3} \cdot \frac{6 d^2}{b^3 D} \cdot d_o$

The equivalent expression for alternate trough fastening is,

$$\Delta = \frac{1}{2} \times \frac{6 d^2}{b^3 D} d_o$$

showing that the increased flexibility is 2.67 times compared to alternate fastening.

For fastening in every fourth trough the shear flexibility would be,

$$\Delta = 2.5 \frac{6 d^2}{b^3 D} d_o$$

which is five times the alternate fastening case.

Consistent with linear plate generators the shear flexibility for every third trough fastening may be represented as,

$$C_{1.1} = \frac{0.144\ ad^4\ K}{Et^3 b^3}$$

where $K = \frac{2}{3} \cdot 1000\ (1 - \nu^2)\ \frac{d_o}{d^3}$ and $d_o = (\frac{4}{3}b_S + 2b_T)\ h^2$

However, this approach makes a number of simplifying assumptions by ignoring the effects of rotation of the central corrugation which not only gives some torsional restraint, but also contributes to a degree of warping in the opposite direction to the main concertina flexibility.

These factors may be calculated by considering Fig. (3.1.). The rotation of the central profile is,

$$\theta = \frac{2}{3}\ V_S/b_L \quad \text{and hence its warping is,}$$

$$\Delta = (V_S^1\ 4b_S + V_T^1 \cdot 2b_T)/b/_2$$

$$= \{(p + b_T)\ 4b_S + 2hb_T\}/b_{/2} \cdot \theta$$

where $\frac{V_S}{d_o} = \frac{(b_S + b_T)\ b_L}{(\frac{4}{3}b_S + 2b_T)h}$, and $\Delta_o \propto \frac{2/3\ d_o d}{b/2}$

The overall warping reduction is half this value after subtracting the opposing twists of the outer corrugations. Thus, the reduction in flexibility compared to concertina action Δ_o alone is,

$$\frac{1}{6}\left\{\frac{(p + b_T)}{d} \cdot \frac{2b_S}{h} + \frac{b_T}{d}\right\} \cdot \frac{(b_S + b_T)}{(\frac{2}{3}b_S + b_T)}$$

This approximately degenerates to,

$$\frac{1}{6}\,\frac{(p + 2b_T)}{d}$$

For decking profiles with $2b_T/d = 0.6$ for example it follows that the flexibility is reduced by about 10%. The torsional increase in stiffness is most noticeable for short sheet lengths but quickly loses its importance for practical sheet spans. At a length of 2 metres for a typical profile, inclusion of torsional effects reduces the flexibility by 15% but this decays to about 4% for a 4 metre length.

To obtain the final flexibility, the distortion due to every corrugation fastening must be added. As for the previous cases, the downward movement caused by profile tension implies that some edge purlin restraint occurs which serves to stiffen the shear deformation.

3.12. Edge Beam restraint for Fastenings in Every Third Trough

The mode of concertina distortion is more complicated than the alternate trough fastening cases. Linear plate movements occur for most sheet lengths and as in Fig. (3.19) end restraints P_1 and P_2 are assumed to prevent downward movement of the corrugation under tension. The free deformation is shown in Fig. (3.1.) and the respective outer and inner side plate movements are $\frac{4}{3}\,V_S$ and $V_S(d + 2b_L)/3b_L$. The internal corrugation is not subject to any force and merely rotates be compatible with the concertina deformation of the neighbouring profiles. V_S represents the side plate uplift for a unit trough force.

The forces P_1 and P_2 may be split up into their respective symmetrical and antisymmetrical components and solution proceeds as for the alternate fastening case. δ_{11}, δ_{13}, and δ_{33} represent the side plate movements caused by the equal and opposite force pairs, and consequently are determined by an effective sheet length of b/6.

$$\delta_{ij} = \frac{6}{bD}\int_0^{3/2S} M_i\, M_j\, ds \qquad D = \frac{Et^3}{12(1 - \nu^2)}$$

$\int_0^{3/2S} ds$ represents integration of the bending moments M_i times M_j over half the pitch between fasteners. The bending moments M_i are defined in Fig. (3.21) and D is the sheet bending stiffness.

Again the symmetrical uplift components of P_1 and P_2 are determined as δ_{22}, δ_{24} and δ_{44} which are then modified by a factor $\frac{1}{k}$, as for alternate corrugation fastening. All displacements other than these uniform uplift values are considered to be linearly varying.

Due to the fact that for symmetrical loading there is a net fastener restraining force a short distance along the trough centre line, the sheet will begin to rise and the net cross-section bending moments will decay rapidly along the sheet length.

Hence, these uplift values will be relatively more flexible than the antisymmetric components by an arbitary factor of 2 (k = 0.5). This was the value which seemed to give good comparison with finite element results for alternate trough fastening and it is assumed that this may be used for the wider pitch of fasteners. So for the outer side plate,

$$\frac{4}{3} V_S = \{\delta_{11} + \frac{\delta_{22}}{k}\} \frac{P_1}{2} + \{\delta_{13} + \frac{\delta_{24}}{k}\} \frac{P_2}{2}$$

and for the inner side plate,

$$\{\frac{d + 2b_L}{3b_L}\} V_S = \{\delta_{13} + \frac{\delta_{24}}{k}\} \frac{P_1}{2} + \{\delta_{33} + \frac{\delta_{44}}{k}\} \frac{P_2}{2}$$

where $V_S = (b_S + b_T)\, b_L h\, \frac{6}{bD}$

The shear deflection is only influenced by the anti-symmetrical forces and hence the relative flexibility is,

$$1 + \frac{P_1}{2} \cdot \frac{\delta_{10}}{\delta_{oo}} + \frac{P_2}{2} \cdot \frac{\delta_{20}}{\delta_{oo}} = 1 - r_T$$

where δ_{oo} is the free concertina deflection and equals,

$$\{\frac{4}{3} b_S + 2b_T \}h^2 \quad \frac{6}{bD}$$

r_T is the flexibility reduction factor for fastening in every third trough and consequently the final K value is,

$$K = K_T (1 - r_T) + K_E$$

Again, it is assumed that only concertina action is restrained by the end purlin and that the free distortion effects may be added separately.

It is considered that the very flexible nature of this deformation is not condusive to localization of shear distortion by trough bending. Thus the formula for shear flexibility using K as a parametric constant shall be used for this fastening arrangement for all sheet lengths.

Tabulations of K are given in the Appendix 2.

3.13. Discussion of Test Results for Every Third Corrugation Fastening

This very flexible mode of fastening was examined for lengths of 3 and 6 metres for the 35 mm deep roofing and decking profiles 1 and 2. The theoretical flexibility, it is assumed, derives mainly from the concertina action which occurs linearly along the sheet length. This is almost three times as much as the alternate trough fastening flexibility and twenty times greater than the flexibility due to fastening in every trough.

The experimental observations show quite good agreement with the theory of Sections (3.11) and (3.12) which includes the reduction factor due to end purlin restraint. The K value and total flexibility comparisons are shown in Appendix 1.

At the 6 metre sheet length, the flexibility was observed to have risen by about 10% above the rigid movement value, but it is expected that this is due to the twisting component similar to fastening in every trough which does rise with length.

At 3 metres, the agreement is quite good, although the decking profile is probably stiffened by the clamping effect of the fasteners.

Thus on the basis of these results, the flexibility due to fastening in every third trough shall be taken as,

$$C_{1.1} = \frac{0.144ad^4}{Et^3 b^3} \quad K$$

K values are constant for each profile shape and are tabulated in Appendix 2 with and without the 'purlin-prop' reduction factor.

3.14. Excessive Deformation due to Concertina Action

For relatively short sheet lengths of less than 4 metres, corrugations fastened in multiples of troughs may suffer considerable deformation before the trough fastener capacity is reached.

If the longitudinal shear flexibility is,

$$C_{1.1} = \frac{0.144\ ad^4}{Et^3 b^3} \quad K$$

then the lateral trough movement per unit fastener force, δ, for alternate fastening is, $C_{1.1} \times (b/d)^2 \times 0.5$

$$\text{Thus,} \quad \delta = \frac{0.072 d^3}{Et^3 b} \quad K$$

For every third trough fastening, the trough deflection per unit fastener force is $C_{1.1} \times (b/d)^2 \times \frac{3}{4} \times \frac{1}{3}$

Alternatively, if sheet length is bigger than 3 metres for alternate trough fastening then,

$$C_{1.1} = \frac{ad^{2.5}\,\bar{K}}{Et^{2.5}b^2}$$

and the lateral trough movement is again $C_{1.1}\,(b/d)^2 \times 0.5$

If the maximum trough fastener force is 6 t kN and χ represents a fraction of this force at the actual working load, then the corresponding trough displacement is,

$$\delta = 0.144\,\left(\frac{d}{t}\right)^2\,\left(\frac{d}{b}\right)\,\frac{K}{E}\,.\,3\chi \quad \text{- linear plate movements}$$

or $$\delta = \left(\frac{d}{t}\right)^{1.5}\,\frac{\bar{K}}{E}.\,3\chi \quad \text{- localised end distortion}$$

The trough movement represents a measure of the visible distortion, but it is likely that the corresponding side plate uplift, V_S, is more important, where,

$$V_S = \frac{b_L}{2h}\,\frac{(b_S + b_T)}{(\frac{2}{3}b_S + b_T)}\,.\delta \quad = f\delta$$

It may be seen that f tends to $\frac{b_L}{2h}$ which means that for very shallow roofing profiles, the side plate uplift may exceed the trough movement. The relative movement between neighbouring crests is $2V_S$.

For a typical set of data,

$d = 150$ mm, $t = 0.7$ mm, $E = 207$ kN/mm^2, $\bar{K} = 1.0$

At $\chi = 1$ $\delta = 46$ mm

This is far in excess of the deformation limit of the profile and it may be necessary to reduce the permissible fastener force in accordance with the value of $\bar{K}$.

Similarly for a typical corrugation fastened in every third trough with data as above plus K = 20 and b = 4 metres,

$$\delta = 0.144 \left(\frac{150}{0.7}\right)^2 \left(\frac{150}{4{,}000}\right) \frac{20}{207} \times 6 \times \frac{1}{4}$$

$$= .36 \text{ mm}$$

It is suggested that, even for long sheets, where the distortion becomes localized towards the panel ends, there should be a serviceability limit of excessive deformation introduced into the fastener capacity. The distortion limit should depend, not only on trough movement, but also on the degree of uplift and depression between crests, which affects the insulation bond.

This will be discussed in Chapter 5 with regard to the stiffening effect of insulation and the corresponding bitumen bond strength.

CHAPTER 4.

THE SHEAR FLEXIBILITY OF SINUSOIDAL CORRUGATIONS

4.1. Theories due to McKenzie and Libove

The first analysis of the shear deformation of a sinusoidally corrugated web attached to flanges at discrete points was performed by McKenzie.[41] He noticed that trough fastening, rather than continuous attachment, resulted in cross-sectional bending deformations which caused a marked reduction in shear stiffness. For the purposes of analysis, the corrugations were considered to be made up of a series of circular arcs fastened to supporting members in every trough.

McKenzie made the important assumptions that shear warping is the result of linear movements of all points of the corrugation along the length and that the boundaries between neighbouring profiles remain rigid. Thus the three strain compatibility conditions, as in Fig. (4.1), at all points are:

$$\frac{du}{dx} = 0 \qquad\qquad \frac{du}{dy} + \frac{dv}{dx} = 0$$

and also for cross-sectional deformation,

$$\frac{dv}{dy} + \frac{w}{R} = 0$$

where R is the radius of the arc, and u, v and w are displacement components.

Hence the total absorbed energy may be evaluated in terms of a cross-sectional function for the out of plane bending displacement w. By applying the calculus of variations for minimum total potential energy, a differential equation solution may be determined whose boundary conditions are controlled by the end attachment.

McKenzie's results are expressed by a relative stiffness compared to the case of continuous attachment which generates pure shear strain.

Libove studied rather more types of end attachment but used effectively the same minimization of total energy principle. The analysis was much more exact in that the generators were permitted to move laterally which introduced longitudinal as well as cross-sectional bending energy.

Deformation is obviously anti-symmetric and it is assumed that no 'purlin-prop' reduction in flexibility occurs for this case of fastening in every trough. The u, v and w deformations were again defined by the above equations except that $\frac{du}{dx} = 0$ to ensure compatibility of longitudinal strains, only at the trough lines.

By establishing a functional form for w and u a differential equation may be developed from the total energy expression by the calculus of variations, similar to the trapezoidal profile analysis of Section (2.3).

Again results may be expressed as a relative stiffness concept. Libove[42] has recently extended this work to 'quasi-sinusoidal' corrugations, according to a sine wave rather than circular arc form. Commercially available sheeting, it appears, is closer to this modified shape and hence some extra refinement is claimed.

However, neither author has carried out experimental observations over a range of sheet lengths to determine the validity of the inherent assumptions. *In addition, only* every trough fastening has been considered which is relative rare in roofing practice due to the very small pitch of troughs for sinusoidal corrugations (150 > d > 75 mm).

An alternative energy method solution will be proposed which can include variations in fastening as well as the possibility of attachment to intermediate purlins.

4.2. Energy Method Solution for Every Trough Attachment

A sinusoidal corrugation may be expected to have considerably better shear distortion performance than a trapezoidal corrugation of the same

height, as cross-section bending is much reduced. The in-plane shear flow passes smoothly around the section and distinct top, side and bottom plate movements cannot be separated.

Any analysis can only be approximate, but an energy method based on assumed displacement functions will provide a reasonable solution provided that the corrugation height is not excessive. Firstly, the cross-sectional distortional energy must be determined in terms of two arbitary parameters U_T and U_B, which define the movement of the crest and trough respectively as in Fig. (4.1).

If a single unit force is applied at the crest then the bending moment M_o which it creates is:

$$M_o = \frac{h}{d} x - \tfrac{1}{2} \cdot Z$$

where Z is the equation of the profile according to,

$$Z = \frac{h}{2} (1 - \cos \frac{2\pi x}{d})$$

h and d are the profile height and pitch respectively, and x is measured from the trough.

Thus, the crest deflection due to a unit crest force per mm length is,

$$\delta = \frac{1}{EI_s} \int_o^{\bar{S}} M_o M_o \, ds \quad \text{where } ds = \sqrt{1 + (\frac{dz}{dx})^2} \, dx$$

and $I_s = t^3/12(1 - \nu^2)$

S is measured around the cross section and hence,

$$ds = \{1 + \tfrac{1}{2} \frac{\pi^2 h^2}{d^2} \sin^2 \frac{2\pi x}{d}\} dx$$

for $h/d < 0.4$, this is a reasonably accurate approximation.

Integration reduces the expression to,

$$\frac{1}{EI_s}\left\{\frac{.022\Pi^2h^2d}{16} + \frac{0.14\Pi^2h^4}{16d}\right\}$$

$$\text{Thus if } \delta = \frac{12(1-\nu^2)\Pi^2h^2d}{16t^3E}\left\{0.14\left(\frac{h}{d}\right)^2 + .022\right\}$$

then the distortion energy is,

$$E_d = \int_0^{b/2} \frac{(U_T - U_B)^2}{\delta} \, dx$$

The longitudinal warping may be approximately evaluated by considering an assumed horizontal displacement around the end profile section, as in Fig. (4.2).

$$U = \frac{\overline{U}_T}{2}\left\{\cos\frac{2\Pi x}{d} + 1\right\}$$

The in-plane displacement is U cos α and the longitudinal warping is,

$$\frac{d\Delta}{ds} = \frac{U\cos\alpha}{b/2}\ ; \quad \text{but } ds = \frac{dx}{\cos\alpha}$$

$$\text{So } \Delta = \frac{2}{b}\int_0^{\overline{S}} U\cos\alpha \, ds$$

where $\overline{S}$ is the complete corrugation perimeter and $\overline{U}_T$ is the end crest movement.

$$\Delta = \frac{4}{b}\int_0^{d/2} \frac{\overline{U}_T}{2}\left(1 - \cos\frac{2\Pi x}{d}\right) dx$$

$$\text{So } \Delta = d/b\ \overline{U}_T$$

Cross-sectional displacements of the form below are asssumed:

$$U_T = a_1 y - \sum_{n=1}^{5} a_{n+1} \frac{b}{2n\Pi} \cdot \sin \frac{2n\pi y}{b}$$

$$U_B = \sum_{n=1}^{5} a_{n+1} \frac{b}{2n\Pi} \sin \frac{2n\Pi y}{b}$$

In order to maintain compatibility between neighbouring trough lines, the shear displacement Δ should remain constant, throughout the sheet length. Thus, $\frac{d\Delta}{dy} = 0$ which requires that $a_1 = b/d\Delta$

The longitudinal displacements consistent with axial strain, ε_a, should also vary sinusoidally over the cross-section, S, as in Fig. (4.2), according to,

$$\varepsilon_a = \bar{\varepsilon}_a \sin \frac{2\Pi S}{\bar{S}}$$

At any section y the maximum cross section axial strain is:

$$\bar{\varepsilon}_a = \frac{\bar{S}}{b} \{a_2 \sin \frac{2\Pi y}{b} + 2a_3 \sin \frac{4\Pi y}{b} + 3a_4 \sin \frac{6\Pi y}{b} , \text{ etc.,}\}$$

Integrating around the section and along the sheet length, the axial strain energy is,

$$E_a = tE \int_0^{\bar{S}} \sin^2 \frac{2\Pi S}{\bar{S}} \int_0^{b/2} (\frac{\bar{S}}{b})^2 \{ a_2^2 \sin^2 \frac{2\Pi y}{b} + 4a_3^2 \sin^2 \frac{4\Pi y}{b} \text{ etc} \} dy$$

$$= \frac{\bar{S}^3 tE}{8b} \{a_2^2 + 4a_3^2 + 9a_4^2 + 16a_5^2 + 25a_6^2 \}$$

where $\bar{S}$ is the corrugation perimeter and approximately equals,

$$d \{1 + \frac{\Pi^2 h^2}{4d^2} - \frac{3}{64} \frac{\Pi^4 h^4}{d^4} \} \qquad \text{for } h/d < 0.4$$

The distortion energy is,

$$E_d = \frac{1}{\delta} \int_0^{b/2} \{a_1 y - 2 \left(a_2 \frac{b}{2\pi} \sin \frac{2\pi y}{b} + a_3 \frac{b}{4\pi} \sin \frac{4\pi y}{b} \text{ etc}\right)\}^2 dy$$

$$E_d = a_1^2 \frac{b^3}{24\delta} + \sum_{n=2}^{6} \{\frac{b^3 a_n^2}{4(n-1)^2 \pi^2 \delta} - (-1)^n \times \frac{a_1 a_n}{2(n-1)^2 \pi^2 \delta}$$

Combining all these energy components but omitting the effects of profile torsion and shear strain gives,

$$E_{Total} = \sum_{i=2}^{6} e(1, i)\ a_1 a_i + \sum_{i=1}^{6} e(i, i)\ a_i^2$$

Minimizing the total internal energy with respect to each variable such that $\frac{dE}{da_1} = 0$, yields,

$$\frac{a_2}{a_1} = \frac{e(1, 2)}{2e(2,2)} \quad \text{and} \quad \frac{a_3}{a_1} = \frac{e(1, 3)}{2e(3, 3)} \quad \text{etc.,}$$

but $a_1 = \frac{b\Delta}{d}$ and $E_{Total} = \frac{\Delta^2}{2C_{1.1}}$

So all the displacement parameters a_i may be expressed in terms of Δ and resubstitution into the total energy expression gives a value for $C_{1.1}$, the flexibility due to distortion.

For linear plate generators corresponding to the solution for a_1 only, the shear flexibility may be written in terms of a dimensionless parameter K, as in the previous chapters, according to,

$$C_{1.1} = \frac{0.144 a d^4 K}{E t^3 b^3}$$

However, the non-linear bending terms are such that they reduce the internal distortion energy with a consequent rise in the shear flexibility. In a similar fashion to trapezoidal sheeting, it may be expected that the K value will rise with length consistent with localized end distortion rather than linear plate movements.

For fastening in every trough at the sheet ends and in alternate troughs at the intermediate purlins, the deformation is obviously only partially restrained at the internal fixings. One trough line is forced to bend between intermediate purlin connections whereas its neighbours are free to distort between the end fastenings without interference from the internal restraints.

Hence the actual shear distortion is somewhere between the extreme cases of fastening at all intermediate purlins points, and attachment at the sheet ends only. The K value, as an approximation, may be taken as the average of the two limiting cases for fastening in alternate troughs internally.

$$K = (K_1 + K_N)/2$$

where K_N and K_1 are the every corrugation fastening values due to attachment in N and 1 intermediate purlins respectively.

4.3. Intermediate Purlin Fixings in Every Corrugation

The Fourier series expression for trough movement may be adjusted to cope with the effect of attachment to intermediate purlins. Lateral displacements are prevented consistent with $U_B = 0$.

For two intermediate purlins, movement is prevented at the third points which implies that,

$$a_2 + a_{3/2} - a_{5/4} - a_{6/5} = 0$$

Eliminating $a_6 = 5a_2 + \frac{5}{2} a_3 - \frac{5}{4} a_5$

then minimizing the total energy, it follows that:

$$\frac{dE}{da_2} = 0, \quad \therefore \{-e(1, 2) - 5e(1, 6)\} a_1 = a_2\{ 2e(2, 2) + 50e(6, 6)\}$$

$$+ 25e(6,6)a_3 - \frac{25}{2} e(6,6)a_5$$

Similar expressions may be derived for,

$$\frac{dE}{da_3} \text{ and } \frac{dE}{da_5} \quad \text{but} \quad \frac{dE}{da_4} = \frac{-e(1,4)}{2e(4,4)}$$

Solving for a_2, a_3 and a_4 consistent with $\frac{dE}{da_i} = 0$, it follows that all the variables may be expressed in terms of a_1. Hence resubstitution into the total energy equation gives a value for $C_{1.1}$.

For three intermediate purlins movement is restrained at the quarter points. It follows that,

$$a_2 - \frac{a_4}{3} + \frac{a_6}{5} = 0$$

Eliminating a_6 and minimizing the total energy,

$$\frac{dE}{da_2} = 0 \text{ gives, } \{ -e(1,2) + 5e(1,6)\} a_1 = a_2\{ 2e(2,2) + 50e(6,6)\} - \frac{50}{3} e(6,6)\, a_4$$

$$\text{and } \frac{dE}{da_4} = 0 \text{ gives, } \{-e(1,4) - \frac{5}{3} e(1,6)\}a_1 = a_2\{-\frac{50}{3} e(6,6)\} + \{2e(4,4) + \frac{50}{9} e(6,6)\} a_4$$

a_3 and a_5 are as in Section (4.2) and hence solving the above two equations yields a_2 and a_4 in terms of Δ. Again reinsertion of these parameters solves for the shear flexibility.

4.4. Effect of Sheet Length, Thickness and Number of Intermediate Purlins

The corrugation displaced shape resulting from minimization of the total internal energy reveals that the distortion becomes localized

towards points of attachment. Fig. (4.5) shows for a 4 metre sheet span fastened only at its ends, how the top and trough plate movements are equal for a great proportion of the sheet length, indicating that the internal region is redundant as regards shear distortion.

Sheet fastened in intermediate purlins also display the same localized end distortion except that around the internal restraints there is an additional distorted region. Thus the total internal energy must be increased and this is consistent with a reduction in the shear flexibility.

As observed for trapezoidal profiles, the K value is initially given by the linear generator theory and is constant. However, as end distortion gains importance so K rises to become proportional to the sheet length. This occurs at about 1 metre for end attachment only and rises to 3 m for the two intermediate purlins. It may be seen from Fig. (4.3) that the K values are extremely influenced by profile height.

Fig. (4.4) shows the linear relationship between K and the square root of sheet thickness. Hence a more reasonable dimensionless parameter $\bar{K}$ may be proposed such that,

$$\bar{K} = \frac{0.144\, d^{1.5}\, K}{t^{0.5}\, b}$$

Hence the shear flexibility due to distortion is,

$$C_{1.1} = \frac{a d^{2.5}\, \bar{K}}{E t^{2.5} b^{2}}$$

$\bar{K}$ values are indicated in Fig. (4.5) for a range of profile depths. $\bar{K}$ is now a design constant for all practical sheet lengths and thicknesses.

4.5. Comparison of Theory with Libove's, McKenzie's and Experimental Results

The linear generator theory due to McKenzie is, compared to the energy method solution in Fig. (4.3). It is clear that even at a length of 1.5 metres there is a considerable discrepancy in the K values due to

non-linear internal movements. Libove's results are also indicated for sheet length up to 4 metres and these do show very good agreement with the proposed theory of Section (4.3).

As expected Libove's comparisons are slightly more flexible but at least the crude assumptions of the energy method approach are vindicated and it may be implied that the intermediate purlin approach is also sufficiently accurate for use. It should be noted that both authors' results were estimated from graphical presentation of effective shear stiffness, and neither was able to develop a controlling parametric equation.

Experimental results are confined to commercially available sheeting being 75 mm in corrugation pitch, 19mm depth and nominally 0.6 mm thickness. Only one sheet length of 3.1m was investigated fastened at its ends and the observed shear flexibility for a 4.2m panel width was 0.11 mm/kN. Subtracting the estimated effects due to seam slip etc., which amounted to 0.07 mm/kN, the experimental $\bar{K}$ value was deduced to be,

$$\bar{K} = \frac{207 \times 0.56^{2.5} \times 3100^2}{75^{2.5} \times 4200} \times 0.04 = 0.090$$

The theoretical $\bar{K}$ value for h/d = 0.25, is 0.079. Thus the energy method approach seems to be reasonably accurate, when compared to this test result, and the existing theories. Design $\bar{K}$ values are tabulated in Fig. (4.5).

It may be noted that the shear flexibility of a sinusoidal profile is considerably less than that of an equivalent 45° sided trapezoidal shape.

4.5. Energy Method Solution for Alternate Trough Attachment

The mechanism of concertina deformation accounts for considerable increase in the shear flexibility. As studied in Chapter 3, the missing trough fastener resistance causes compression and extension of the adjoining profiles. The anti-symmetric behaviour along the sheet

length is consistent with shear warping which may be combined with the flexibility due to every trough attachment to give the total shear distortion.

In a similar fashion to the trapezoidal profile case, non-linear movements may be considered by introducing trough displacements for concertina action of the form,

$$U_{B1} = a_1 \frac{y}{b/2} - a_2 \frac{b}{2\pi} \sin \frac{2\pi y}{b} - a_3 \frac{b}{4\pi} \sin \frac{4\pi y}{b}$$

$$U_{B2} = a_2 \frac{b}{2\pi} \sin \frac{2\pi y}{b} + a_3 \frac{b}{4\pi} \sin \frac{4\pi y}{b}$$

Concertina energy may be deduced by considering the cross-section bending moment $\bar{M}_o$ due to a unit force at the base of the corrugation as in Fig. (4.6), which results in a horizontal deflection, δ

$$\bar{M}_o = \bar{z} \qquad \text{where } \bar{z} = \frac{h}{2} (1 - \cos \frac{2\pi x}{d})$$

thus, $$\delta = \int_o^{\bar{S}} \bar{M}_o \bar{M}_o \, ds \quad \text{and } ds = dx \left(1 + \tfrac{1}{2} \frac{\pi^2 h^2}{d^2} \sin^2 \frac{2\pi x}{b}\right)$$

$\bar{S}$ is the profile perimeter and I_S is $\frac{t^3}{12(1 - \nu^2)}$ per mm length

Thus $\delta = (\frac{h}{2})^2 \frac{1}{EI_S} \int_o^{\bar{S}} (1 - \cos \frac{2\pi x}{d})^2 \, ds = \frac{h^2 d}{8EI_S} \{3 + \frac{5\pi^2 h^2}{8d^2}\}$

The concertina energy per corrugation is,

$$E_d = \frac{1}{\delta} \int_o^{b/2} (U_{B1} - U_{B2})^2 \, dy$$

$$= \frac{1}{\delta} \{ a_1^2 \frac{b^3}{24} - \frac{b^3}{2\pi^2} a_1 a_2 + \frac{b^3}{8\pi^2} a_1 a_3 + \frac{b^3}{4\pi^2} a_2^2 + \frac{b^3}{16\pi^2} a_3^2 \}$$

The axial strain energy due to the sinusoidal distribution of longitudinal movement over each profile perimeter is calculated as in the

every corrugation case. However, the corrugation crest tends to lift or depress in sympathy with the trough movement. Thus the sinusoidal forms of displacement in $(U_{B1} - U_{B2})$ which cause axial strain energy are increased by a factor $(1 + fh/\bar{S})$.

f is the ratio of crest to trough movement and is approximately represented by,

$$f = \frac{\int_0^{\bar{S}} \bar{M}_0 \bar{M}_1 \, ds}{\int_0^{\bar{S}} \bar{M}_0 \bar{M}_0 \, ds} \quad ; \quad \bar{S} \text{ is the profile perimeter}$$

where $\bar{M}_0 = \bar{z}$ and $\bar{M}_1 = x/2$

It follows by integrating over the cross-section that,

$$f = \left\{ \frac{.088 + \frac{\Pi^2 h^2}{d^2} \times .013}{.186 + \frac{\Pi^2 h^2}{d^2} \times .039} \right\}$$

The axial strain around the cross-section is given by,

$$\varepsilon_a = \bar{\varepsilon}_a \sin \Pi S/\bar{S} \quad \text{where } \bar{\varepsilon}_a \text{ is the crest strain.}$$

It follows that the profile strain energy may be derived as for the every corrugation case. However, side plate uplift causes an additional axial strain dependent on fh and hence the total energy is:

$$E_a = \frac{\bar{S}\, {}^3 tE}{2b} \left(1 + \frac{fh}{\bar{S}}\right) (a_2^2 + 4a_3^2)$$

The combined energy terms may be collected together as,

$$\frac{\Delta^2}{2C} = E = e(1, 1)\, a_1^2 + e(1, 2)\, a_1 a_2 + e(1, 3)\, a_1 a_3 + e(2, 2)\, a_2^2 + e(3, 3)\, a_3^2$$

Minimizing with respect to each variable it follows that,

$$\frac{dE}{da_2} = 0 \qquad \text{so } \frac{a_2}{a_1} = \frac{-e(1,2)}{2e(2,2)} \quad \text{etc}$$

As for trapezoidal corrugations only the linear displacement term contributes to the shear deflection, Δ

$$\text{Thus } \Delta = d/b\, a_1 \qquad \text{and } \frac{dE}{da_1} = 0$$

So all the variables a_i may be expressed in terms of Δ and hence reinsertion into the total energy expression yields a value of the shear flexibility due to concertina action.

4.6. Fastening in Alternate Troughs at Intermediate Purlins

Sinusoidal sheets are usually fairly shallow in profile and, therefore, span only a short distance between purlins. Intermediate purlin attachment causes restraint to trough bending such that for two internal fixings.

$$U_{B2} = 0 \text{ at } y = b/6 \text{ and hence } a_2 + a_{3/2} = 0$$

Thus minimizing the total energy with respect to a_2 it follows that,

$$\frac{a_2}{a_1} = \frac{-e(1,2) + 2e(1,3)}{2e(2,2) + 8e(3,3)}$$

Evaluation of the $C_{1.1}$ proceeds as in Section (4.4).

For three intermediate purlins movement is prevented at the quarter points which requires that,

$$a_2 = 0 \qquad a_{3/a_1} = \frac{-e(1,3)}{2e(3,3)}$$

The shear flexibility may be presented as,

$$C_{1.1} = \frac{0.144\ ad^4\ K}{Et^3\ b^3}$$

where K is a constant for rigid plate movement but the non-linear sinusoidal terms will cause K to rise consistent with a reduction in the internal concertina energy.

The final K value is obtained by summing the flexibilities due to the twisting effect of every trough fastening (K_E) and this concertina action (K_A),

$$\text{Thus } K = K_A + K_E$$

For N intermediate purlin fixings K_E is taken as the average of the value for one and N internal restraints. This is because for alternate fastenings, one trough line is constrained by the fasteners whereas the other is not. K_{EN} represents the K_E value for N intermediate purlins,

$$K_E = \frac{(K_{E1} + K_{EN})}{2}$$

4.7. Discussion of Energy Method Results for Alternate Trough Fixing and Comparison with Experiment

Concertina action is an order of magnitude more flexible than the twisting tendency of every trough attachment. Fig. (4.8) shows how the K value remains initially constant but rises at about 3 metres sheet length, to become proportional to increasing length.

For intermediate purlin fixings this increase is delayed and for three internal restraints, does not occur until about 9 metres. As indicated in section (4.5) the final flexibility is the summation of the concertina and twisting effects such that $K = K_A + K_E$. No 'purlin-prop' reduction in flexibility is necessary in this case due to the nature

of the geometry and deformation.

When fastened in alternate troughs to N intermediate purlins K_E is an unknown factor as the internal trough is held only at its ends. As a crude approximation K is taken as the average of extreme cases of fastening to N and no intermediate purlins. Of course, the basic anti-symmetry of deformation is not disrupted by one internal purlin. K_A is much greater than K_E and hence the error of any assumption is reduced.

The rise of K with length is accompanied by an increase of K with the square root of sheet thickness. Hence an alternative parameter may be derived such that,

$$\bar{K} = \frac{0.144\, d^{1.5}\, K}{t^{0.5}\, b}$$

$$\text{Thus } C_{1.1} = \frac{a d^{2.5}\, \bar{K}}{E t^{2.5} b^2}$$

However, practical sheet lengths may not always be consistent with a constant value of $\bar{K}$. It is suggested that a bi-linear relationship ought to be adopted according to the maximum value of,

$$\bar{K} \text{ or } \frac{0.144\, d^{1.5}\, K}{b t^{0.5}}$$

where $\bar{K}$ and K are functions of the profile shape and number of intermediate purlins as in Fig. (4.9). By comparing the corresponding $\bar{K}$ values with those for trapezoidal corrugations it may be seen that sinusoidal profiles are somewhat stiffer.

Experimental results are confined to available profile geometries of 19 mm depth, 75 mm pitch and 0.6 mm thickness. A 3.1m sheet length and 4.15 m width was studied, fastened in alternate corrugations and the observed flexibility was 0.27 mm/kN. Subtracting the minor flexibilities such as seam slip (0.07) yields a shear distortion deflection of 0.20 mm/kN. This corresponds to a $\bar{K}$ value of 0.51 compared to a theoretical value of 0.57.

At a sheet length of 3 metres $\bar{K}$ is reasonably constant. Design $\bar{K}$ values are shown in Fig. (4.9) and on the basis of this single observation, seem to give a close approximation to the actual shear flexibility.

4.8. Multiple Trough Fastenings in Sinusoidal Corrugations

In practice, the relatively shallow pitch of corrugations means that for strength considerations, fixings may be placed at three or even four profile spacings. Referring to section (3. 1) it is apparent that concertina action greatly increases with fastener pitch.

For example, every third trough attachment, based on linear generator theory is 2.67 times more flexible than alternate fixing.

Similarly fastening in every four troughs is 5 times more flexible than alternate attachment. It is likely that the concertina action is so flexible that localized distortion due to trough bending does not take place and that linear movements predominate for most practical sheet lengths.

K values are tabulated in Fig. (4.9) for alternate trough fixings for a range of profile heights and it is suggested that the above multiplication factors may be used for any spacing of trough fastenings.

$$\text{Thus, } C_{1.1} = \frac{0.144\ ad^4\ K}{Et^3b^3}$$

where $K = S\ K_A$

and $S = 2.67$ for every third trough fixing.

$S = 5.0$ for every fourth trough fixing.

K_A refers to the rigid plate movement value for alternate trough attachment.

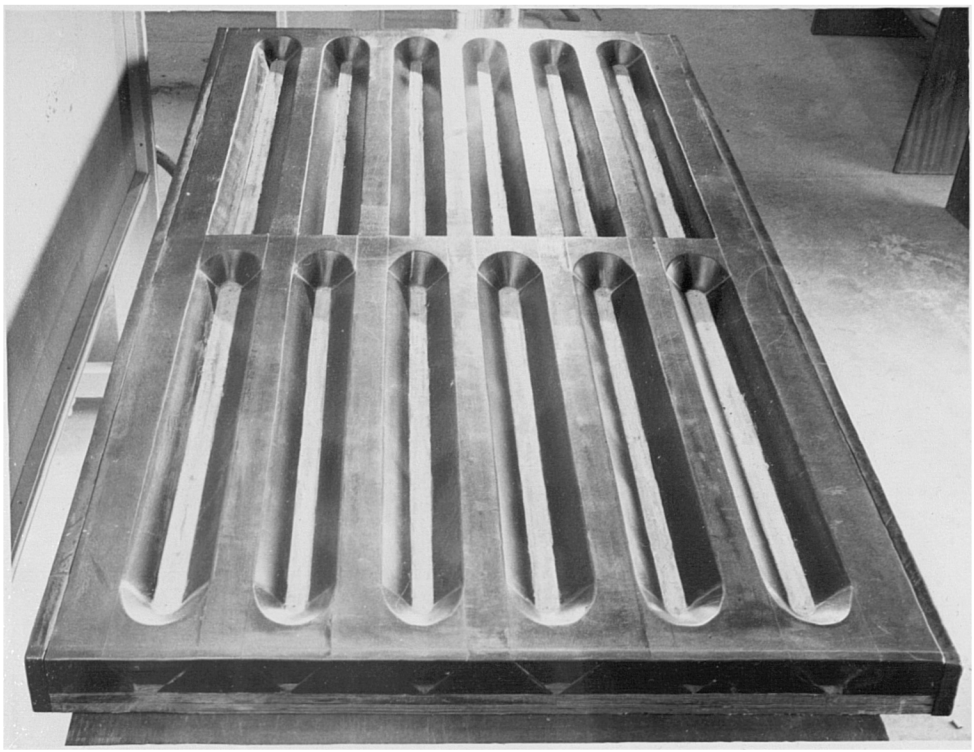

Plate (5.1) Mould made from synthetic material which was used to press closed end sheeting. The insets permit pressing of short lengths

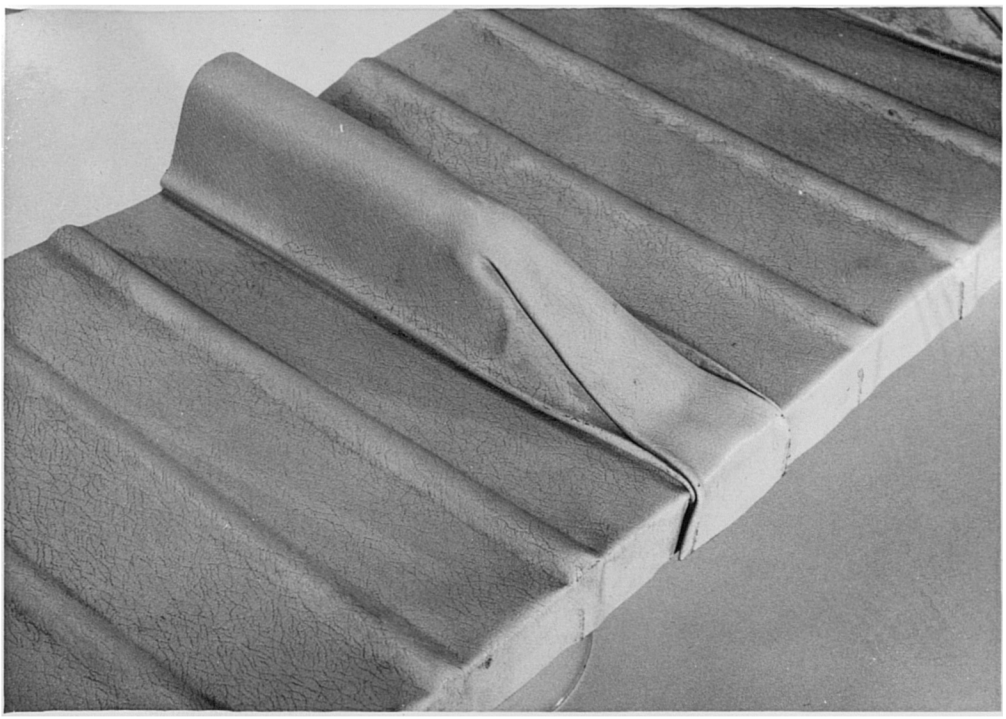

Plate (5.2) Corrugation folded down at its end

CHAPTER 5.

METHODS OF REDUCING SHEAR DISTORTION

The mechanism of shear distortion is very much related to the fastening arrangement. Attachment in every trough results in distortional twisting due to the profile shear flow. However, alternately trough fastened sheets deform in a much more flexible mode due to concertina action caused by compression and extension of neighbouring profiles.

In the following sections, a number of methods of reducing the shear distortion will be discussed for both fastening arrangements.

For every corrugation attachment, the flexibility may be significantly reduced by producing a 'closed-end' profile, or even fastening twice in every trough. Similarly for alternate corrugation attachments, an insulation covering does significantly lessen the concertina action.

The effect of sheet overhangs beyond the outer purlins will be examined with regard to the effective sheet length to be used in the shear distortion formula. In addition, special sheeting with curved overhangs will be studied to evaluate their stiffening effect.

5.1. 'Folded-down' Corrugation Ends

Corrugations fastened in every trough suffer shear distortion due to twisting of the open profile by side and top plate movements. These independent cross-section displacements were initially assumed to vary linearly along the sheet length. However, it was determined in Chapter 2 that the internal distortion is minimized by longitudinal plate bending which results in only local end deformation near to the fasteners.

The analysis of the shear distortion component of flexibility is quite complicated as an assumed Fourier series of plate displacements has to model the asymptotic shear behaviour for all sheet lengths. The local behaviour is consistent with a modified formula for the shear distortion which gives a longitudinal flexibility proportional to $1/(\text{length})^2$.

Clearly for short lengths of less than 2 metres the shear deflection may be sizeable. One method of reducing cross-section distortion, which should have a corresponding influence on the shear flexibility, is to close off the corrugation ends. The flexibility will tend to the case of continuous attachment of all points of the profile, which corresponds to a membrane suffering only from pure shear strain.

Fig. (5.1) shows an example of a 'folded-down' corrugation which can warp to some degree by twisting of the closed end. However, due to the rigid end flange, shear displacement can only occur by compatible trough plate bending. Unlike an open profile, decreasing the sheet length produces a stiffer membrane due to the fact that the trough plate must bend in order to allow shear warping.

A corrugation of this type has been developed for folded plate roof applications and is pressed out of a flat sheet by a dishing process. The actual shape is shown in Plate (11.2) and Fig. (10.6) which indicates the transition from the full profile depth to the end flange. Fastenings in every trough may still be used and the flat end portion also permits a more frequent pitch of attachment.

The shear distortion may again be modelled by expressing the top, side and bottom plate movements (U_T, U_S and U_B) in terms of a truncated Fourier series for each. The displacement variables a_i may be used to establish the total internal energy as in Chapter 2, which is minimized taking into account the boundary conditions at the closed-end.

$$U_T = a_1 y + a_2 \frac{b}{2\pi} \sin \frac{2\pi y}{b}$$

$$U_S = a_3 y + a_4 \frac{b}{2\pi} \sin \frac{2\pi y}{b}$$

$$U_B = a_5 \frac{b}{2\pi} \sin \frac{2\pi y}{b}$$

It was considered that for very short sheet lengths requiring this 'folding-down' process, the number of independent parameters could be kept small. The nature of the 'folded-down' end is that the shear displacement can only occur by corresponding rotations of the top and bottom plates as in Fig. (5.1.). Thus,

$$\frac{\Delta}{d} = \frac{dU_B}{dy} = \frac{dU_T}{dy} \qquad \text{at } y = \frac{b}{2}$$

$$\frac{\Delta}{d} = -a_5 = a_1 - a_2$$

However, as for every trough attachment, it is a necessary condition for compatibility between neighbouring troughs that the shear displacement is constant along the sheet length.

$$\Delta = 2b_L \frac{dU_B}{dy} + 4b_S \frac{dU_S}{dy} + 2b_T \frac{dU_T}{dy}$$

So it follows from $\frac{d\Delta}{dy} = 0$, that,

$$\Delta = 2b_T a_1 + 4b_S a_3$$

$$0 = b_T a_2 + 2b_S a_4 + b_L a_5$$

where $2b_T$, $2b_S$, $2b_L$ are the respective top, side and trough plate widths.

The rotation of the end cross-section occurs as a rigid body and hence there is a relationship between the displacements a_3 and a_1 such that,

$$(b_T + p)\, a_3 = h\, a_1$$

So, $a_3 = g a_1$

All the variables may thus be expressed in terms of Δ according to;

$$a_1 = \frac{\Delta}{k^1} \qquad \text{where } k^1 = \frac{1}{2b_T + g.4b_S}$$

$$a_2 = \Delta\{-\frac{1}{d} + \frac{1}{k^1}\}$$

$$a_3 = \frac{g\Delta}{k^1}$$

$$a_4 = \left(\left\{ \frac{b_T + b_L}{2b_S \cdot d} - \frac{b_T}{2b_S \cdot k^1} \right) \right. \Delta$$

$$a_5 = \frac{-\Delta}{d}$$

As in Section (2.3) the total energy due to distortion bending, torsion, shear strain etc., may be collected as the terms of a symmetrical matrix D(i,j) multiplied by the respective displacement parameters as in Figs. (2.36) and (2.37).

Thus,

$$\frac{\Delta^2}{2C} = E = \sum_{i=1}^{5} \sum_{j=1}^{5} a_i D(i,j)\ a_j$$

The solution for the shear flexibility, C derives directly from this identity without minimization of the energy expression.

As for the previous analyses, the flexibility due to distortion may be represented in terms of a K value such that,

$$C_{1.1} = \frac{0.144\ a\ d^4 K}{E t^3 b^3}$$

K is constant for rigid plate movements of open profiles but in this case the shear flexibility parameter must degenerate zero, corresponding to zero distortion as the sheet length becomes small, due to the fact that shear displacement can only occur by trough bending.

5.2. Discussion of Energy Method and Experimental Results for Folded Down Corrugations

The effect of closing off the profile ends is not the only factor which influences the performance of this type of corrugation. In addition, the trough plate is integral with the end flange which necessitates that, for any shear displacement, the bottom plate is also constrained to bend. Folded down corrugations are best achieved by a pressing operation as outlined in

Section (10.6). A number of companies have tried to fold down the corrugation end after roll forming as in Plate (5.4) and it is expected that this too will show considerable benefit over open profiled sheeting.

The prototype pressed profile of Fig. (5.2.), which has been developed for use in folded plate roofs, shows the increased stiffness to be gained when shear deflection is an important design limitation. Plate displacements indicate the degree of longitudinal bending which must take place even at short sheet lengths. The K value variation with length, when compared to an open profile, reveals that the folded down corrugation is almost seven times stiffer.

Profile shape plays a large part in the shear behaviour as shown in Fig. (5.3), for a rectangular corrugation. At large trough widths the plate bending effects will predominate and for very wide top plate widths, the restriction of end twisting is more important.

Experimental testing of the pressed sheeting as in Plate (11.2) gave good agreement with respect to theory. It should be noted that the curved profile shape was approximated by a trapezoidal form. Using a testing of 2.1 m length and 4.5 m width the shear distortion flexibility was observed to be 0.027 mm/kN after subtraction of the effects of seam and edge slip, cantilever bending and pure shear strain. This corresponds to a K value of 0.13 compared to a theoretical figure of 0.15.

It also appears that alternate trough fastening shows some benefit from the effect of folding down the corrugation end. An experimental K value of only 0.5 was recorded compared to the corresponding value for open profiled sheeting of about 2.5.

This is probably due to the fact that concertina action is restrained by the flanged end until the fastener force builds up and the flat end portion buckles locally.

Thus it appears that pressed corrugations of the closed end type have sizeable advantages over open profiles for all types of fastening arrangements.

5.3. Double Trough Fastened Corrugations

In Section (5.2.) it was observed that one of the major factors which contributed to the increased stiffness of folded down corrugations was the constraint of trough line bending to follow the purlin rotation. This may also be achieved by double fastening the trough plate at its ends. Distortion can now only occur by top plate movement as side plate deflection is completely restrained (Fig. (5.4)).

Again the energy method of assumed displacement functions may be used to cope with these conditions. Using plate displacements of,

$$U_T = a_1 y + a_2 \frac{b}{2\Pi} \sin \frac{2\Pi y}{b}$$

$$U_S = a_3 \frac{b}{2\Pi} \sin \frac{2\Pi y}{b}$$

$$U_B = a_4 \frac{b}{2\Pi} \sin \frac{2\Pi y}{b}$$

The end compatibility requirements are such that,

$$+\frac{\Delta}{d} = +\frac{dU_B}{dy}$$

Similarly, for $\frac{d\Delta}{dy} = 0$ at all points along the sheet length,

$$0 = a_2 b_T + 2a_3 b_S + a_4 b_L$$

and $\Delta = a_1 2b_T$

In this case only four equations may be derived for the end conditions in terms of five unknown parameters. The total internal energy is,

$$E = \frac{\Delta^2}{2C} = \Sigma_{i=1}^{4} \Sigma_{j=1}^{4} a_i D(i,j).a_j$$

where the coefficients of the energy expression may be taken from Fig. (2.36).

If a_2 is considered as an independent variable then $\frac{dE}{da_2} = 0$ corresponds to the minimum internal energy. Reinsertion of the parameters a_i into E after solving for a_2 gives a value for $C_{1.1}$.

5.4. Discussion of Theoretical and Experimental Results for Double Fastened Corrugations

Double fastening in every trough is a very uncommon fastening arrangement but it does have the advantage of raising both the ultimate strength and the shear stiffness for thin sheets. This may be necessary for very long span folded plates utilizing corrugated steel where the shear forces are extremely high.

A very stiff membrane is produced, especially when the trough width is large ($b_L > b_T$). The plate displacements are shown in Fig. (5.5), for the same profile shape of Section (5.2). Trough bending is compatible with the end rotation due to the double fixings and side plate uplift is prevented. This results in a K value of only 0.03 because of the restraint to top plate warping, compared to a normal figure of 1.06 for an open profile with single trough fastenings.

However, the variation with crest width reveals that the greatest benefits are confined to profiles where $b_L > b_T$ for lengths less than 2 metres. Longer spans, it was considered, would not require such additional restraining measures as the shear stiffness is proportional to (length) squared. In addition, the single sinusoidal term only accurately models longitudinal deformation for short spans.

Experimental testing of a 2 metre length of 0.55 mm thick profile 2 (see Appendix 1 for details) was carried out for a panel width of 2.1 metres. The observed shear flexibility gave a deduced K value of 0.10 compared to single fastening value of 0.67. However, the theoretical K value for this 35 mm deep and 105 mm trough width profile was only 0.06. The discrepancy is probably due to the fact that trough end rotation is

less than that of the shear displacement due to slip in the fasteners. Movement is extremely small and is well within the initial fastener clearance.

5.5. Effect of Sheet Overhang Beyond Purlins

The formulae for the shear distortion component of flexibility based on linear plate or alternatively localized sheet deformation take no account of sheets extending beyond the line of purlins. As limits to the actual behaviour, the effective sheet length could be assumed to be the distance between purlins or the actual sheet length. The following section derives an approximate relationship between overhang distance and shear displacement for the case of local end distortion, which is independent of the fastening arrangement.

For corrugations fastened in every trough the end region suffers the most severe distortion. As revealed in Section (2.5) the longitudinal shear flexibility may be evaluated by the considering cross-section performance under a unit fastener force and multiplying by a factor $(d/b^1)^2$ where d is the fastener pitch and b^1 is the distance between outer purlins.

For cases where the sheet length, b, equals b^1 and is bigger than 2 metres, distortion occurs in an approximately parabolic nature over a constant end distance due to local trough bending. At shorter lengths, where rigid plate movements apply, the effect of a sheet overhang ($b > b^1$) is to reduce the shear stiffness of the complete sheeting length from b^3 to $b(b^1)^2$. This is because the lateral stiffness is still proportional to b, but the longitudinal stiffness is divided by the above modification factor, as in Fig. (5.8).

As distortion becomes localized, the effect of any overhang becomes extremely difficult to estimate as the profile is still highly deformed beyond the line of fasteners. However, the interaction of plate bending and cross-section distortion is not unlike the beam on elastic foundations analogy, although the equivalent beam and medium properties are not known.

The lateral fastener force is considered as the disturbing tendency, causing a local deformation which decays along the beam as in Fig. (5.7). The beam on elastic foundation theory[43] may be utilized by considering an overhang distance a^1 where $a^1 = \frac{b - b^1}{2}$. The deflection laterally is,

$$\Delta^1 = \frac{P}{2k} \{ 1 + 3 \cos^2 \lambda a^1 + \sin^2 \lambda a^1 - 2 \sin \lambda a^1 \cos \lambda a^1 \} e^{-\lambda a}$$

where λ is a property of the elastic medium and is given by $\frac{\Pi}{2x_d}$ where x_d is the distorted length for zero overhang. k is the equivalent beam stiffness. However, comparing the deflection Δ^1 to the case where $b = b^1$, gives a ratio of,

$$\frac{\Delta^1}{\Delta^1_o} = \frac{1}{2} \{1 + \cos 2 \frac{\Pi a^1}{2x_d} - \frac{1}{2} \sin \frac{\Pi a^1}{x_d} \}$$

$$= \alpha$$

x_d, the free distorted length, can only be estimated from the profile displaced shapes, but a realistic estimate is about 0.9 m for every trough fastening.

Using the modification formula, the longitudinal shear flexibility becomes,

$$C_{1.1} = \frac{a d^{2.5} \alpha \bar{K}}{E t^{2.5} (b^1)^2}$$

Considering overhangs of a^1 = 100, 200 and 300 mm α becomes respectively 0.90, 0.78, and 0.66.

However, if b^1 = 4m then $(b^1/b)^2$ is respectively 0.90, 0.82 and 0.75, and for b^1 = 6m, $(b^1/b)^2$ is 0.94, 0.88 and 0.82.

It appears that, for overhanging sheets, the shear flexibility is more closely approximated by the overall sheet length rather than the distance between purlins.

Hence as a design formula, the shear flexibility is,

$$C_{1.1} = \frac{ad^{2.5}\bar{K}}{Et^{2.5}b^2}$$

where b is the overall sheet length.

Experimental tests have been carried out on sheeting 6.6. metres long with overhangs of 250 mm at each end. The value of α was determined as 0.72 and $(b^1/b)^2$ is 0.85.

This implies that the actual flexibility should be less than the theory based on the full sheet length. In practice the theoretical and experimental flexibilities were in reasonable agreement which suggests that the real value of α is about 0.85.

However, the analysis is very approximate, not only in assuming an analogous action but also in the fact that a hypothetical distorted wavelength has to be used. Nevertheless, it does seem reasonable for every corrugation fixing, that the complete sheet length ought to be used in design.

For alternate trough fastening the distorted length is of the order of 1.8 metres and the corresponding α factor is reduced. Again for the above data $(b^1/b)^2$ is 0.85 and α is 0.86. Experimental results using the full sheet length of 6.6. metres are reasonably in agreement.

Intermediate purlin attachments should not affect the end distortion pattern where deformation is greatest. So for all fastening arrangements the full sheet length ought to be used to evaluate the distortion flexibility.

5.6. Effect of Insulation Resistance to Deformation

In most practical applications of corrugated sheeting, an insulation and weather proofing layer is bonded onto the sheet surface. The span between profile crests is controlled by the properties of the covering layer, and is usually no more than 75mm. Thus decking profiles ($b_T > b_L$) have covering bonded to their top surface whereas roofing profiles have insulation on the underside.

Decking weather proofing is made up of a number of different layers usually including a single thickness of soft board bonded by bitumen and tar to the sheeting (Fig. (5.11)) and finished with two or more layers of felt.

Shear distortion, as discovered in Chapters 2 and 3, results in cross-sectional movements, which may be considerable for alternate trough fastening. Concertina action, due to successive compression and tension of neighbouring profiles, causes large relative vertical movement of the corrugation crests as in Fig. (5.9).

At a sufficiently great deformation, the insulation layer will break away, unable to contain such a large relative displacement. For subsequent loading the sheet and covering will act independently. Every trough fastening is much stiffer and is generally preferred at the diaphragm extremities to limit distortion.

For concertina deformation, the insulation will behave in three independent modes.

1. Longitudinal warping occurs by rotation of the trough plate which causes a shear displacement between crests. Hence the shear stiffness of the covering is mobilized in the short distance over which it spans.

2. Concertina action causes crest uplift and depression which bends the insulation and this is probably the major contributor to the increased sheet stiffness.

3. The third mode is due to the prevention of crest separation. However, the antisymmetry of deformation implies that this is small.

Lapin[44] found that a 3.6 m sheet span fastened in alternate troughs, was approximately 50% stiffer when the insulation layer was attached. The profile was a decking shape of 35 mm depth and 0.7 mm thickness. The increased stiffness was discovered to be very small for every trough attachment. An important observation was that failure of the sheet-insulation bond occurred at 20 kN rafter force which is less than

50% of the theoretical sheet-purlin fastener capacity. Plate (5.3) shows the insulation just prior to bond tearing.

A theoretical investigation of the stiffening effect of insulation is as follows, assuming that deformation occurs by linear plate displacements. This is a more comprehensive approach than that put forward by Lapin.

The horizontal trough and vertical side plate movements are considered to be ε and V_S respectively.

Thus the trough movement ε per unit concertina force is,

$$\varepsilon = \delta_{00} - 2P_2\,\delta_{10}$$

where $\delta_{00} = 2(\frac{2}{3}b_S + b_T)\,h^2\,\frac{6}{EI_S b}$ and $\delta_{10} = (b_S + b_T)\,b_L\,\frac{h6}{EI_S b}$

P_2 represents the crest force due to insulation bending. δ_{00} and δ_{10} are defined in Fig. (5.11) and correspond to the free trough and side plate movements respectively. I_S is the sheet inertia and $\frac{b}{6}$ is the equivalent lateral stiffness for linear plate movements over the sheet length, b

$$I_S = \frac{t^3}{12(1-\nu)^2} \qquad \text{per mm length}$$

P_2 however, is also compatible with the insulation bending such that,

$$V_S = P_2\,\frac{(P + b_L)^3}{3(EI)_i} = k_i P_2$$

$(EI)_i$ is the insulation bending stiffness per mm length.

$$(EI)_i = \left(\frac{Et^3}{12\,(1-\nu^2)}\right)_i$$

The net side plate uplift is

$$V_S = + \delta_{10} - P_2 \, \delta_{11}$$

where $\delta_{11} = \{2b_S + b_T + \frac{b_L}{3}\} \quad \frac{b_L^2 \, 6}{EI_S \, b}$

However, the net shearing displacement, δ , between neighbouring crests results in an effective insulation resistance P_1 such that,

$$P_1 = G_i t_i \delta = G_i t_i \frac{(4b_S \, V_S + 2b_L \varepsilon)}{b/2} = (a_1 \, V_S + a_2 \, \varepsilon)$$

where G_i and t_i are the insulation shear modulus and thickness respectively.

$$a_1 = G_i t_i \, \frac{8b_S}{b} \qquad a_2 = G_i t_i \, \frac{4b_L}{b}$$

Thus the controlling equations are, for 1kN trough force

$$\varepsilon = \delta_{00} \, (1 - P_1) - 2P_2 \, \delta_{10}$$

$$V_S = \delta_{10} \, (1 - P_1) - P_2 \, \delta_{11}$$

$$V_S = k_i \, P_2$$

$$P_1 = a_1 \, V_S + a_2 \, \varepsilon$$

These may be solved for ε to give,

$$\varepsilon = (\delta_{00} - 2B \, \delta_{10}) \, \{ \frac{1 - A_{11}}{1 - BA_2} \}$$

where $A_1 = (a_1 \delta_{10} + a_2 \, \delta_{00}) / \, (1 + a_1 \delta_{10} + a_2 \delta_{00})$

$$A_2 = (a_1 \delta_{11} + 2a_2 \, \delta_{10}) / \, (1 + a_1 \delta_{10} + a_2 \delta_{10})$$

$$B = \delta_{10} / k_i + \delta_{11}$$

For typical data of,

Insulation: $t_i = 25$ mm, $E_i = 0.1$ kN/mm^2, $G_i = 0.05$ kN/m^2

Sheeting: $t = 0.7$ mm, $E = 207$ kN/mm^2, $b_L = 20$

$2b_S = 30$, $b_T = 55$ $P = 0$

$h = 30$ mm, $b = 3.6$m

$$\beta = \frac{EI_S}{EI_i} = \frac{1}{23} \qquad G_i t_i = 0.05 \times 25 = 1.25 \text{ kN/m}$$

$$\frac{EI_S b}{6} = \frac{207 \times 0.7^3 \times 3.6 \times 10^3}{12 \times 6 \times 0.91} = 3872$$

$$\delta_{00} = 13.50 \times 10^4 \frac{6}{EI_S b} \qquad \delta_{10} = 4.2 \times 10^4 \frac{6}{EI_S b}$$

$$\delta_{11} = 3.67 \times 10^4 \frac{6}{EI_S b} \qquad k = 0.27 \times 10^4 \beta \frac{6}{EI_S b}$$

$$B = 1.142 \qquad a_1 = \frac{1.25 \times 120}{3.6 \times 10^3} = 0.042$$

$$a_2 = \frac{1.25 \times 80}{3.6 \times 10^3} = 0.028$$

Therefore, $A_1 = 0.53$ and $A_2 = 0.41$

The Relative Flexibility is,

$$= \{1 - \frac{2B\delta_{10}}{\delta_{00}}\} \quad \{\frac{1 - A_1}{1 - BA_2}\}$$

$$= \{1 - 1.142 \times \frac{4.20}{13.50} \times 2\} \quad (\frac{1 - 0.53}{1 - 0.41 \times 1.14}) = 0.30 \times 0.88 = 0.26$$

This implies that the insulation both acts in bending and in shear to relieve concertina distortion. The free sheeting has an approximate effective shear modulus of 4.0 and the insulation shear modulus is 1.25 kN/mm. It is, therefore, not unreasonable to assume composite shear action, but it is apparent that the major effect is the

bending property of the insulation. The relatively high stiffness ratio between insulation and sheeting prevents almost all side plate uplift.

However, the figures used for the insulation are only tentative and indeed there are many variations in the stiffness of covering board used in practice. It seems from the above equation for relative flexibility compared to free distortion that there is a 74% increase in stiffness of which the majority is due to concertina restraint by the bending rigidity of the insulation.

The recorded figure[44] of about 50% is reasonably in agreement considering that slip in the bitumen could account for some degree of shear relief. In addition, some side plate movement may be permitted by the compressibility of the board and the elasticity of the bitumen.

5.7. Curved Down Corrugation Overhang Ends

Recently new developments have been made in the techniques for curving corrugated sheeting into fairly tight radii from initially standard straight profiles. This is achieved by indenting the side and trough plates which causes a local crumpling. At each indendation, there is a corresponding rotation of the cross-section which eventually makes up an arc of a circle. Thus long straight sections of roof sheeting may be finished off by end curved pieces which also act as flashings.

Plate (5.4) shows a typical 6.6 m long section under test. Neighbouring sheet overlaps are achieved by a slight difference in radii which in this case is nominally 300 mm.

An additional advantage of using this type of end curving is that it stiffens cross-section distortion considerably for both alternate and every trough fastening cases. This due to the fact that vertical cross-section movements are manifested as sheet shearing displacement at the end of the curved arc. Fig. (5.12) shows how side plate uplift becomes an in-plane displacement, and hence is restrained by this much stiffer shearing mode.

It is likely that alternate trough fastening, involving concertina action, will be considerably restrained by prevention of side plate uplift. The model to represent deformation, is in Fig. (5.13) and the relative flexibility of this case compared to an open profile is,

$$\alpha = 1 - \frac{2\delta_{10}^2}{\delta_{00}\delta_{11}}$$

where $\delta_{00} = \{\frac{4b_S}{3} + 2b_T\} h^2$, $\delta_{10} = (b_S + b_T)\, b_L h$,

$$\delta_{11} = (2b_S + b_T + \frac{b_L}{3})\, b_L^2$$

An experimental study was performed to justify this expression by examining the behaviour of the following profiles where,

$b_L = 38$, $p = 19$, $d = 150$, $h = 38$, $2b_S = 42$, $b_T = 19$ mm

Thus, $\delta_{00} = 9.55 \times 10^4$ $\delta_{10} = 5.78 \times 10^4$ $\delta_{11} = 10.54 \times 10^4$

$$\alpha = 1 - 0.67 = 0.33$$

A table of results is shown on page 128 which indicates that the two thirds increase of stiffness in theory is closely in agreement with the experimental value of 0.63. This restraint of cross-section uplift is very similar to the action of insulation, as discussed in section (5.6).

For every trough fastening the observed increase in stiffness was much less but still quite significant. This again may be theoretically examined by considering that the side plate uplift component of distortion is prevented.

The analysis is rather more complicated, but is achieved using the profile bending moment diagrams of Fig. (2.9) by assuming unknown side plate restraints. For the above profile dimensions α is 0.10, whereas the experimental reduction in flexibility was only 25%.

In practice, therefore, side plate movement is only partially restrained which is not unreasonable as every trough fastening displacements are much smaller than those of concertina action. Consequently, the effect of a stiffening end constraint will be reduced.

The actual mechanism of distortion movement is shown in Fig. (5.12) where relative side plate uplift is accommodated by in-plane trough bending.

In conclusion, the stiffening effect of curving down the corrugation ends is less noticeable for every trough fastening as seen from the table of results below for 4.5m wide and 6.6 m long sheeting.

In practice, alternate trough fastening is greatly stiffened by this end forming method and for most diaphragm applications where applied shear forces require only relatively sparce fixings, the curved end provides a useful benefit. It is suggested that the action may be theoretically modelled by assuming zero side plate movement.

Every trough fixing however, does not conform to such a simplified analysis as end distortion is only partially restrained by the end curving technique.

RESULTS TABLE

Test	C observed mm/kN	$C_{1.2} + C_{2.1} + C_{2.2} + C_{3.1}$ etc	$C_{1.1}$ Deduced	$\bar{K}$ Deduced	$\bar{K}$ Theory	K Curved / K Straight
A -straight	0.38	0.05	0.33	0.75	0.72	
A - curved	0.16	0.05	0.11	0.28		0.37
E -straight	0.13	0.05	0.08	0.20	0.18	
E -curved	0.11	0.05	0.06	0.15		0.75

E - every trough fastening A - alternate trough fastening

DATA: a = 4500 mm b = 6600 mm t = 0.65 mm

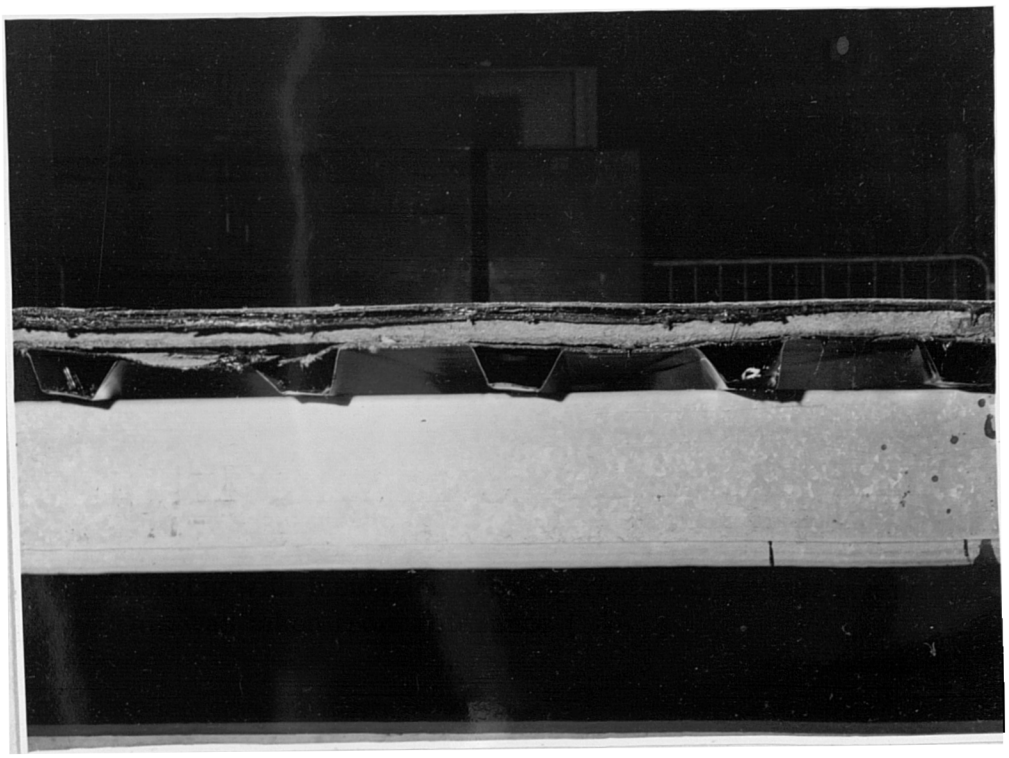

Plate (5.3) Sheeting with insulation showing restraint against concertina uplift. This was taken from reference (44)

Plate (5.4) Sheeting with curved overhangs also reduce concertina action

CHAPTER 6.

OVERLAPPING SHEETS

Practical diaphragms may be of considerable depth, for longer than manufacturers' maximum sheet lengths. Often individual sheets must be overlapped along their length at intermediate purlins to form the full diaphragm span.

Fastening arrangements are not standardized and indeed there are a number of possibilities regarding end and overlap connections. In many roofs sheet-purlin fastenings may be more frequent at the diaphragm perimeter, which makes the analysis of the shear deflection more complex than for the simple fixing arrangements of Chapters 2 and 3.

Unlike a continuous sheet an overlap forms a release, and neighbouring sections distort in an opposite sense with a consequent increase in the warping flexibility, as in Fig. (6.1).

Hence the limits to the complete panel flexibility are underestimated by assuming a continuous sheet, and overestimated by considering that the individual sheets act independently.

Clearly, for deflection reasons it is better to obtain a more realistic value for the overall flexibility especially as the divergence between the two limits is proportional to the square of the number of sheets. In addition, where the design relies on sheet-frame interaction, an over estimate of the sheet's actual flexibility may mean that the panel would attract more force than it is capable of resisting.

In this Chapter, standard diaphragms will be considered where overlapping sheets span across purlins and are fastened in every or alternate troughs. Chapter 7 discusses an alternative arrangement where sheeting spans directly across rafters.

6.1. Overlaps Fastened in Every Corrugation

For rigid plate movements shear warping occurs by anti-symmetric profile distortion at each end of the sheet. At an overlap, cross-section distortions are in opposition and consequently will tend to

interact when attached to a purlin.

The suggested model to represent the restraining effect at a corrugation overlap is shown in Fig. (6.2) where side plate depression is presented, and top plate movement is partially free. These cross-section forces tend to reduce deformation and hence lessen the shear warping.

The effect of profile interaction on the overall shear flexibility may be defined by a factor ε, which depends on the cross-section shape and the fastening arrangement.

For sake of analysis the deformation model is considered at the end cross-section, and it is assumed that these plate movements vary linearly along the sheet length. The profile distortions bear against each other and for sloping sided corrugations the compatibility of movement must be considered as in Fig. (6.2). The restraining forces are assumed to be equal and opposite at each end of the sheet length.

At the left hand side plate, for zero vertical movement,

$$0 = \delta_{40} - X_1 \delta_{44} - X_2 \delta_{22}$$

where $\delta_{ij} = \frac{6}{EI_S b} \int_0^S M_i . M_j \, ds$

X_1 and X_2 are the restraining forces for a unit profile shear flow. M_i are cross-sectional bending movements as defined in Fig. (2.9) and $\int_0^S ds$ represents integration of the moments M_i times M_j around the half cross-section.

I_S is the sheet bending inertia and equals $\frac{t^3}{12(1 - \nu^2)}$

b/6 represents the equivalentlongitudinal stiffness due to the anti-symmetric distortion of rigid plate movements.

For the top plate, the net horizontal movement is,

$$V_T = \delta_{20} - X_1\delta_{42} - X_2\delta_{22}$$

For the right hand side plate the net uplift is,

$$V_S = \delta_{50} - X_1\delta_{45} - X_2\delta_{25}$$

However, V_S and V_T are also related by the compatibility condition.

$$2V_T = V_S \tan\theta$$

where θ is the slope of the side plate. For this final relationship it has been assumed that lapping over a purlin offers extra restraint by preventing side plate depression. This violates the initial compatibility conditions by introducing an extra purlin prop-force in the equations for V_S and V_T. However, as a mathematical necessity to obtain the restraints X_1 and X_2, this force has been ignored, and is introduced merely as a displacement condition for this simplified approach.

The complete bending moment distribution is,

$$M = M_O - X_1M_4 - X_2M_2$$

where M_O is the free profile moment due to a unit shear flow.

The uplift from the edge beam is:

$$V_S = \frac{6}{EI_b} \int_0^S M_S M.ds$$

Hence, the equivalent longitudinal warping due to V_S and V_T is:

$$V_T \cdot \frac{2b_T}{b/2} + V_S \frac{h}{b}$$

The top plate distorts antisymmetrically. However, considering Fig. (6.2), the side plate is only free to lift at one of four points due to interaction of the profiles resting on a purlin. Consequently, the warping due to side plate uplfit is reduced to one quarter of its

free sheet value, which is,

$$\delta_{20} \frac{2b_T}{b/2} + \delta_{40} \frac{2h}{b/2}$$

The relative longitudinal warping compared to the flexibility of completely separate sheets is,

$$\varepsilon = \frac{V_T\ 4b_T + V_S\ h}{\delta_{20}\ 4b_T + \delta_{40}\ 4h}$$

The initial assumption that distortion occurs by linear plate movements is suspect especially for longer sheets where deformation is confined to regions close to the fasteners.

However, the only expression which implied rigid movements was the evaluation of the restraints X_1 and X_2, according to a longitudinal stiffness factor of b/6. For local end distortion this factor will be reduced, but all the terms δ_{ij} are modified by the same amount and hence the restraints may reasonably assumed to be independent of the sheet length for a unit profile shear flow.

This does not seem sc bad an assumption as all the applied and resisting forces are at the end sections. In addition, for local end distortion the shear displacement is constant throughout the sheet length and the expression for longitudinal warping is also determined by the end displacements, V_S and V_T, as above for rigid plate movements.

The factor ε thus represents the effect of profile interaction for all sheet lengths and may be used as a modification factor for the individual sheet flexibility in order to evaluate the flexibility of a number of sheets lapped longitudinally.

Values of ε have been tabulated for every trough fastening in Appendix Table (3.1) and are a function of the profile shape only. It appears that the degree of overlap slip, as reflected in the value of ε, increases with the inclination of the side plate to the vertical. Similarly, the slip rises with top plate width until it reaches a peak at, $\frac{2b_T}{d} = 0.4$, and has a typical value of about 0.5, indicating that the deformational

warping of an individual overlapping sheet is reduced by 50% from its free distortion value.

6.2. Overlapping Sheets Fastened in Alternate Troughs

For every trough fastening relatively small cross-section movements occur at the overlap. Alternately fastened corrugations, however, warp by the more flexible concertina action due to trough movement which causes compression and extension of neighbouring profiles. Interaction may be expected at a very low shear load which soon overcomes the clearance or bad fit between sheets.

The basic action involves opening and closing of the corrugations, and rectangular profiles would interact completely to form a continuous sheet as horizontal trough movement is completely prevented. For sloping sided corrugations, however, discrete points around the profile are likely to interfere. Plate (6.1) and Fig. (6.3(a)) show typical distortion of overlapping sheets.

The suggested model to represent deformation, as in Fig. (6.3(b)) considers that the end cross-section restraints are forces X_1, X_2 and X_3. Top and side plate movement for one corrugation are prevented and X_3 is an inclined force owing to one profile riding over the other.

For zero right hand side plate movement due to a unit trough force,

$$0 = X_1 \delta_{66} + X_2 \delta_{68} + X_3 \sin\theta, \delta_{67} + \delta_{60} (1 - X_3 \cos\theta)$$

And for the right hand top plate restraint,

$$0 = X_1 \delta_{68} + X_2 \delta_{88} + X_3 \sin\theta \, \delta_{78} + \delta_{80}(1 - X_3 \cos\theta)$$

δ_{ij} is the deflection at point i due to a unit force at j, and is given by,

$$\delta_{ij} = \frac{6}{EIb} \int_0^{2S} M_i M_j \, ds$$

where $\int_0^{2S} ds$ represents integration of the bending moments, M_i of Fig. (3.11) around both cross sections. EI is the plate bending stiffness and b/6 is the longitudinal stiffness factor due to linearly varying anti-symmetric distortion over the sheet length, b.

The horizontal trough movement ε_H is,

$$\varepsilon_H = X_1 \delta_{60} + X_2 \delta_{80} + X_3 \sin\theta \, \delta_{70} + \delta_{00} (1 - X_3 \cos\theta)$$

Similarly the vertical movement ε_V of the side plate is,

$$\varepsilon_V = X_1 \delta_{67} + X_2 \delta_{78} + X_3 \sin\theta \, \delta_{77} + \delta_{70} (1 - X_3 \cos\theta)$$

However, ε_H and ε_V are related by the compatibility condition for side plate uplift of one corrugation rising over the other such that,

$$\varepsilon_V \tan\theta = 2\varepsilon_H$$

The attachment of the corrugations to a purlin means that side plate depression is prevented. However, this extra restraining force has been ignored to mathematically derive the overlap forces, and as an approximate allowance, the effect of 'purlin-propping' is only introduced as a displacement condition.

Hence, the forces X_1, X_2 and X_3 may be determined and substituting into the expression for horizontal trough movement, ε_H, yields a value for concertina warping of the overlapped sheets. It is assumed that deformation is completely anti-symmetric at each end of the sheet. Hence warping is simply due to the rotation of each plate taking into account that the right hand top plate movement is prevented.

$$2\Delta^1 = \varepsilon_H \cdot \frac{(2b_L + P)}{b/2} + \frac{\varepsilon_H}{2} \cdot \frac{2b_T}{b/2}$$

However, the free shear displacement between fasteners is,

$$2\Delta = \delta_{00} \frac{(2b_L + 2P)}{b/2} + \frac{\delta_{00}}{2} \frac{2b_T}{b/2} + \frac{\delta_{00}}{2} \cdot \frac{2b_T}{b/2}$$

Consequently the slip value may be determined which represents the ratio of the flexibility of the overlapped profile to that of an individual sheet.

$$\varepsilon = \frac{\Delta^1}{\Delta} = \frac{\varepsilon_H}{\delta_{OO}} \left\{1 - \frac{(b_T + P)}{d}\right\}$$

This overlap factor is strictly only due to concertina action. However, alternate trough fastening flexibility is the sum of the effects of trough movement due to the missing fastener force and also the torsional warping of fastening in every corrugation. In general, concertina action is an order of magnitude greater than the flexibility of fastening in every trough and it may be expected that the factor ε also modifies the overall alternate fastening flexibility, to reasonable accuracy.

Although linear plate movements were required in the analysis, it may be seen that all the displacements δ_{ij} are determined by the same effective stiffness factor of one sixth of the sheet length due to anti-symmetric distortion. However, the restraints X_i are independent of this factor and hence ε, which defines the warping relative to the free sheet value, is independent of the sheet length.

Similarly, ε may be assumed to be unaffected by the mode of internal distortion, whether due to localized trough bending or linear plate movements. Longitudinal warping is constant along the sheet depth, whatever the internal distortion mode, and is determined only by the end displacements.

Thus the slip factor may be used for all sheet lengths and values are tabulated in Appendix Table (3.2) for alternate trough fastening. Rectangular profiles have zero overlap slip, and ε also falls with increasing profile depth. The slip tends to be a maximum for wide trough widths, but is generally smaller than the corresponding values for every trough fastening. Typically $\varepsilon = 0.3$, which means that for an infinite number of similar overlapping sheets, the warping of each individual sheet is reduced by 70% compared to the free distortion value.

For alternate trough fastening, as determined from Chapter 3, distortion occurs by local end deformation for sheet lengths greater than,

roughly,

3 metres for one or no intermediate purlins
6 metres for two intermediate purlins
9 metres for three intermediate purlins

6.3. General Interaction Formula for Overlapping Sheets

The factor ε, as fixed property of the overlap and fastening arrangement may be used to evaluate the flexibility of a number of sheets of different length and shear force. Considering Fig. (6.5) for every trough fastening, the overlap restraining forces are such as to satisfy the plate compatibility conditions for the respective profile shear flows P_1 and P_2.

For the general case of neighbouring corrugations of sufficient length that deformation takes place by local end distortion, the plate displacements are independent of the sheet length. If follows that the net interactive force is, $(P_1 + P_2)/2$.

However, if distortion occurs by rigid plate movements, which is only valid for short sheet lengths, then the top and side plate displacements are dependent on their respective sheet lengths, k_1 and k_2.

Considering equal and opposite forces at each end of a sheet, the equivalent longitudinal stiffness to determine plate movements is b/6. Alternatively, if a force is only applied at one end of the sheet, then the displacements at each end are determined by factors b/4 and b/2 respectively. The warping is consequently reduced by half.

For linear plate movements a 'carry over' factor approach may be used, whereby the joint forces at the discontinuity influence their neighbours. It may be shown that the general interaction equation for the ith joint between sheets of length k_i and k_{i+1} with cross-sectional shear flows P_i and P_{i+1} is,

$$\left\{\frac{P_i}{k_i} + \frac{P_{i+1}}{k_{i+1}}\right\}(1 - \varepsilon) = X_i\left\{\frac{1}{k_i} + \frac{1}{k_{i+1}}\right\}\frac{2}{3} + \frac{X_{i-1}}{3k_i} + \frac{X_{i+1}}{3k_{i+1}}$$

X_i is the hypothetical joint restraining force, and neighbouring joints X_{i-1} and X_{i+1} carry over half of their effect to the ith joint. The left hand term refers to the relative cross-sectional deformation of the overlapping profiles and the right hand term is the effective restraint depending on the overlap slip, ε.

This is a general solution which may be used for any number of overlapping sheets with variable lengths where the shear flows or forces, P_i and P_{i+1} are normal to the corrugations. Hence, the longitudinal warping, W_i, of the ith sheet due to the applied restraining forces is proportional to,

$$W_i = \frac{P_i}{k_i^2} - \frac{X_i + X_{i+1}}{2k_i^2}$$

For a longitudinal shear force Q_i, $P_i k_i = Q_i$.

The corresponding expression for localised sheet end distortion is independent of the sheet length, k_i, and the neighbouring joint forces. Thus,

$$\left\{\frac{P_i + P_{i+1}}{2}\right\}(1 - \varepsilon) = X_i \qquad \text{and } W_i = \frac{P_i}{k_i} - \frac{X_i + X_{i+1}}{2k_i}$$

These mathematically valid formulae will be used to determine the overall flexibility of any number or length of sheets by solving for the effective joint restraints X_i. However, the approach makes the assumption that the vector of profile interaction forces may be represented by a single term. The fastening arrangement and profile shape are only reflected in the value of ε, the overlap slip factor.

6.4. Formulae for a Number of Similar Overlapping Sheets

The general expression for the flexibility of a number of overlapped sheets depends on the deformation pattern of the individual sheets. If the sheet length is sufficiently short that distortion occurs by rigid plate movements, then for profile shear flows of the ith and (i + 1)th overlapping

sheets of magnitude P_i and P_{i+1}, it follows from section (6.3) that,

$$\left\{ \frac{P_i + P_{i+1}}{2} \right\} (1 - \varepsilon) = \frac{2}{3} X_i + \frac{1}{6} X_{i-1} + \frac{1}{6} X_{i+1}$$

where X_i is the joint restraining force between the two sheets and, X_{i-1} and X_{i+1} are the neighbouring joint forces. Σ, the overlap slip, depends only on the fastening arrangement and the profile shape.

The longitudinal warping is proportional to $P_i - \frac{X_i + X_{i+1}}{2}$

Formulae were developed for a number of overlapping sheets based on the rigid plate movement assumption. The warping displacement is constant along the sheet length and the total longitudinal shear force is unity. Considering $C_{1.1}$ to be the flexibility of an individual sheet, the overall longitudinal shear flexibility due to profile interaction has been determined, for N sheets, as

$$\Delta = \frac{C_{1.1}}{8} (1 + 3\varepsilon) \qquad N = 2$$

$$\Delta = \frac{C_{1.1}}{27} \frac{1 + 9\varepsilon}{1 + 0.1\varepsilon} \qquad N = 3$$

$$\Delta = \frac{C_{1.1}}{64} \frac{1 + 18\varepsilon + \varepsilon^2}{1 + 0.75\varepsilon} \qquad N = 4$$

If $\Sigma$is small these expressions degenerate to,

$$\Delta = \frac{C_{1.1}}{N^3} (1 + N^2 \varepsilon)$$

which applies when $C_{1.1}$ is due linear plate movements. This is only true when $0.144 K \frac{d^{1.5}}{bt^{0.5}} > K$ for alternate trough fastening as in Section (3. 2).

For fastening in every third trough ε has not been determined analytically but in this case $C_{1.1}$ would certainly be caused by rigid plate distortion.

The expression for overall shear flexibility, Δ, may be broken down into $C_{1.1}/N^3$ which is the component due to compete sheet continuity and $C_{1.1}/N$ which is the flexibility due to the slip at the overlap.

However, for most sheet lengths, $C_{1.1}$ is determined by local end distortion due to trough bending. In this case the joint restraints are such that,

$$\frac{(P_i + P_{i+1})}{2} \quad (1 - \varepsilon) \quad = \quad X_i$$

The longitudinal warping, Δ, is determined by the end cross-section displacements and is proportional to,

$$P_i - \frac{X_i + X_{i+1}}{2}$$

Again, for an overall imposed longitudinal shear force of unity and constant shear displacement, Δ has been determined in terms of individual sheet flexibility $C_{1.1}$ for N sheets,

$$\Delta = \frac{C_{1.1}}{4} \{1 + \varepsilon\} \qquad N = 2$$

$$\Delta = C_{1.1} \left\{\frac{1 + 3\varepsilon}{11 + \varepsilon}\right\} \qquad N = 3$$

$$\Delta = C_{1.1} \frac{1 + 6\varepsilon + \varepsilon^2}{24 + 8\varepsilon} \qquad N = 4$$

For local end distortion Δ tends to $\frac{C_{1.1}}{N^2}(1 + N\varepsilon)$ although the flexibility is overestimated by this expression. Typically, for N = 4 and $\varepsilon = 0.5$, $\Delta = 0.19\ C_{1.1}$ from the approximate formula and $0.15\ C_{1.1}$ from the exact expression.

Thus for any number N, of equal length sheets, the overall flexibility due to distortion is given by,

$$\frac{C_{1.1}}{N^2}(1 + N\Sigma) \qquad \text{where } C_{1.1} = \frac{ad^{2.5}\,\bar{K}}{Et^{2.5}b^2}$$

Σ is a property of the profile shape and fastening arrangement as tabulated in Appendix Table (3.4). $C_{1.1}$ is the individual sheet flexibility.

6.5. Formulae for Overlapping Sheets of Different Lengths

Considering first two overlapping sheets of lengths in the ratio k to unity, the overall shear flexibility will be first determined for linear plate movements. The overlap factor Σ is considered as an effective slip due to the imposed profile shear flow. Using the controlling equation developed in Section (6.3) for rigid plate distortion,

$$\{\frac{P_1}{k} + P_2\}(1 - \Sigma) = X_1 \{\frac{1}{k} + 1\} \frac{2}{3}$$

where P_1 and P_2 are the profile shear flows for each sheet and X_1 is the joint restraining force.

For a longitudinal shear force of unity,

$$1 = P_1 k + P_2$$

The longitudinal shear warping of each sheet are necessarily equal and so the overall shear displacement is, from Section (6.3).

$$\Delta = \{\frac{P_1}{k^2} - \frac{X_1}{2k^2}\} C_{1.1} = \{P_2 - \frac{X_1}{2}\} C_{1.1}$$

However, the longitudinal shear force is unity and so $P_1 k + P_2 = 1$. Eliminating X_1 gives,

$$\Delta = \frac{1 - 0.75 (1 - \Sigma)}{1 + k^3 + \frac{3}{4} (1 - \Sigma)(k^2 - 1)(k - 1)} \} C_{1.1}$$

where $C_{1.1}$ is the flexibility of the sheet of length unity.

It may be seen that for k = 1 this expression degenerates to $\Delta = \frac{1}{8}(1 + 3)$ which is as in Section (6.4).

However, in general, shear displacements for most practical sheet lengths are caused by local distortion around the fasteners due to trough bending.

In this case for two overlapping sheets of different lengths,

$$\{\frac{P_1 + P_2}{2}\} (1 - \mathcal{E}) = X_1$$

For a longitudinal shear force of unity,

$$P_1 k + P_2 = 1$$

The shear warping of each sheet are equal and so,

$$\Delta = \{\frac{P_1}{k} - \frac{X_1}{2k} \} \; C_{1.1} = \{P_2 - \frac{X_1}{2} \} \; C_{1.1}$$

End displacements are independent of the sheet length and so the longitudinal warping is proportional to 1/k.

Solving these equations gives,

$$\Delta = \{\frac{0.5 + 0.5\mathcal{E}}{1 + k^2 - (1 - \mathcal{E}) \frac{(k - 1)^2}{2}} \} \; C_{1.1}$$

where $C_{1.1}$ is the shear flexibility of the sheet length b.

$$C_{1.1} = \frac{a d^{2.5} \bar{K}}{E t^{2.5} b^2}$$

The sheet lengths are thus b and bk.

For three overlapping sheets where one is of length k times the other two, then it may be shown that,

$$\Delta = \{\frac{\mathcal{E} + 3 (1 - \mathcal{E})^2/16}{2 + k^2 + (1 - \mathcal{E})^2 \frac{k^2}{16} - \frac{(1 - \mathcal{E})}{4} (3k^2 - 2k + 3)} \} \; C_{1.1}$$

$C_{1.1}$ is the flexibility due to local end distortion of the sheet of length b and the total panel depth is thus (2 + k)b.

In many practical cases diaphragm depths are not made up of sheets of exactly the same length. Often a short end section has to be added to a number of complete sheet lengths and the shear flexibility of the diaphragm with be modified.

It is suggested that for one sheet of proportionately differing length, k, from the other N sheets that the overall flexibility due to local end distortion, is given by,

$$\Delta = \frac{C_{1.1}}{(N + k)^2} \{ 1 + (N + k)\mathcal{E} \}$$

where $C_{1.1}$ again is the individual sheet flexibility

The validity of this expression can only be justified by comparisons with the exact derivation above due to local sheet distortion for N = 2 and 3.

Values of F

N = 2 'Exact' $\Delta = F.C_{1.1}$ 'Approximate' $F = \frac{(1 + (N + k)\mathcal{E})}{(N + k)^2}$

Values of

k \ $\mathcal{E}$	1.0	0.5	0.0
1	0.50	0.37	0.25
0.5	0.80	0.60	0.40
0.33	0.90	0.70	0.50

1.0	0.5	0.0
0.75	0.5	0.25
1.11	0.77	0.44
1.32	0.94	0.56

N = 3

k \ $\mathcal{E}$	1.0	0.5	0.0
2	0.17	0.12	0.05
1	0.33	0.22	0.09
0.5	0.44	0.30	0.11
0.33	0.47	0.31	0.13

1.0	0.5	0.0
0.31	0.18	0.06
0.44	0.27	0.11
0.56	0.36	0.16
0.61	0.39	0.18

It may be seen that for a typical value of the overlap slip factor Σ of 0.3 that the approximate formula fives a reasonably close solution to the overall panel flexibility and the accuracy should increase as N increases. Thus the above formula may be used to determine the effect of a single odd sheet of length kb added to N equal sheets of length b.

6.6. Effect of Fastening in Every Corrugation at the Panel Edges and in Alternate Troughs as the Overlaps

Many diaphragm fixing arrangements have evolved through practice to achieve the optimum behaviour for minimum usage of fastenings. In this respect sheets are often attached in every corrugation at the diaphragm edges and in alternate troughs at the intermediate purlins. Sheet overlaps will thus be more sparcely fastened than at the panel extremities, which makes the analysis of the shear flexibility extremely complex.

However, an approximate mathematical treatment may be performed using the property of the overlap slip factor, Σ , and the controlling interaction expression of Section (6.3). For the outer sheet, concertina action is prevented at its open end. However, all the internal joints deform by lateral trough movement and $C_{1.1A}$ is the shear flexibility of an unconnected central sheet due to anti-symmetric concertina action.

Effectively, the outer sheets behave as though twice as long, due to the fact that concertina distortion only occurs at one end and the open end represents the point about which the deformation is anti-symmetric. This is shown in Fig. (6.8) for both cases of local end distortion, and rigid plate movements.

Considering first the most likely distortion mode for sheets longer than 3 metres fastened in alternate troughs, deformation occurs by non-linear trough bending. The every trough fastening flexibility at the free sheet edge will be included later in the analysis.

As the outer sheets are effectively twice as long as the internal sheets, it follows that their shear displacement is defined by k = 2 in

the expression of Section (6.3). In order to maintain anti-symmetry, equal and opposite forces are applied at each end of the equivalent outer sheet length.

For three overlapped sheets, where the respective profile shear flows are P_1 and P_2, the joint restraint is,

$$X_1 = \frac{P_1 + P_2}{2} \cdot (1 - \varepsilon) \qquad \text{where } (2P_1 + P_2)\, b = 1$$

The longitudinal shear displacement for the outer sheet is (k = 2)

$$\Delta = \{\frac{P_1}{2} - \frac{X_1}{2}\} C_{1.1A}$$

and for the internal sheet is, $\{P_2 - X_1\} C_{1.1A}$.

Solving for P_1, P_2 and X_1 it follows that,

$$\Delta = \{\frac{2\varepsilon}{9 + \varepsilon}\} C_{1.1A}$$

For four overlapping sheets fastening in every corrugation at their ends and alternate troughs internally it may be shown that,

$$\Delta = \{\frac{2 + 3\varepsilon}{6(2 + \varepsilon)}\} C_{1.1A}$$

For two overlapping sheets, $\Delta = \varepsilon/4\, C_{1.1A}$.

This theoretical derivation only applies for localized end distortion. If deformation occurs by linear plate movements, then the controlling equation, from Section (6.3), for the outer joint is,

$$\{\frac{P_1}{2} + P_2\}(1 - \varepsilon) = X_1 \cdot \frac{2}{3}\{\frac{1}{2} + 1\} + \frac{X_2}{6} + \frac{X_1}{6}$$

Again P_1 and P_2 are the profile shear flows as in Fig. (6.8). X_1 is the first joint restraint and it is assumed that an imaginary joint force X_1 also exists at the opposite end of the equivalent end sheet length, 2b, in order to maintain anti-symmetry of deformation.

The corresponding expression for rigid plate movement warping is,

$$\Delta = \{\frac{P_1}{4} - \frac{X_1}{4}\} C_{1.1A} = \{P_2 - \frac{X_1 + X_2}{2}\} C_{1.1A} = \cdots\cdots$$

Thus for two and three overlapping sheets the corresponding equations for the overall shear flexibility, where $C_{1.1A}$ is the individual sheet value, are

$$\Delta = \varepsilon/8 \quad C_{1.1A} \qquad -N = 2$$

$$\Delta = \frac{\varepsilon}{6 + 3\varepsilon} \quad C_{1.1A} \qquad -N = 3$$

Approximate formulae have been developed to represent the shear flexibility due to interaction of any number of sheets. This was achieved by assuming that for N sheets all the joint forces are the same, which gives,

$$\Delta = \{\frac{2}{4\varepsilon + N(3 - \varepsilon)}\} C_{1.1A} \qquad \text{- local end distortion}$$

$$\Delta = \{\frac{\varepsilon}{6\varepsilon + N(2 - \varepsilon)}\} C_{1.1A} \qquad \text{- rigid plate movements}$$

The total panel flexibility $C_{1.1}$ is obtained by addition of the individual sheet flexibility due to fastening in every corrugation, $C_{1.1E}$. Thus, for a unit longitudinal shear force,

$$C_{1.1} = \Delta + \frac{C_{1.1_E}}{N}$$

Relative to alternate trough fastening throughout where, for local edge distortion,

$$\Delta = \frac{C_{1.1_A}}{N^2} (1 + N\varepsilon)$$

it follows that the flexibility reduction factor due to fastening in every trough at the sheet perimeter is,

$$r = \frac{2\varepsilon N^2/(1 + N\varepsilon)}{4\varepsilon + N(3 - \varepsilon)}$$

Values of the overall sheet flexibility are listed in Appendix Table (3.4) for a range of ε, which is the profile slip factor due to alternate trough fastening.

Typically r is about 0.4 which indicates that there is a 60% increase in stiffness due to fastening in every corrugation at the sheet ends when sheet overlaps are fastened in alternate troughs.

6.7. Comparison of Theoretical and Experimental Results for Overlaps fastened in Every Trough

Experimental observations, are listed in Appendix Table (1.7) for various numbers of sheet overlaps and profile shapes. Theoretical values of the overlap slip factor, ε, were derived using the analysis of Section (6.1), and the overall flexibility, $C_{1.1}$, was determined using the approximate relationships.

$$C_{1.1} = \frac{C_{1.1_S}}{N^2}(1 + N\varepsilon) \qquad \text{- local end distortion}$$

$$\text{or} \quad C_{1.1} = \frac{C_{1.1_S}}{N^3}(1 + N^2\varepsilon) \qquad \text{- rigid plate movements}$$

An overlap length of 100 mm was used which, it is assumed, is sufficient to generate the full profile interaction.

$C_{1.1_S}$ is the experimentally observed individual sheet flexibility due to every corrugation fastening and is taken from the appropriate value of Appendix Table (1.1). By comparing the overall observed flexibility with those of the theoretical solutions, the mode of overlap interaction may be infered.

For very short sheet lengths of about 1 metre, rigid plate movements occur and at greater lengths local distortion due to trough bending increases the flexibility of the overlapped sheets. In general, individual

sheet lengths of one and two metres were examined in panel depths of up to 6.1 metres. The test data for a given profile is the same as in Appendix Table (1.1).

From the results of Appendix Table (1.7), it may be seen that a typical value of ε is about 0.4, and that the expression due to localized end distortion is reasonably accurate for the longer sheet lengths. It must be noted, however, that some experimental tests were performed for narrow panel widths which seriously restricts trough bending. Hence distortion will effectively behave as though due to linear plate movements independent of the sheet length.

On the basis of these results and the theoretical derivation, the approximate formula above for local sheet distortion may be used with reasonable confidence to model the effect of overlapping sheet flexibility.

6.8. Comparison of Theoretical and Experimental Results for Sheet Overlaps Fastened in Alternate Troughs

This situation is similar to the every trough fastening case, except that a different factor is used to represent the overlap profile slip. A typical value of ε in this case is about 0.3 and the formula for overall sheet flexibility is as in the previous section.

The profile slip factor, ε was derived using the theory of Section (6.3) for alternate trough fastening, and the individual sheet flexibility, for sheet lengths, b, greater than 3 metres, is due to localized sheet distortion where,

$$C_{1.1_S} = \frac{ad^{2.5}\bar{K}}{Et^{2.5}b^2}$$

However, experimental tests, as listed in Appendix Table (1.8), for sheets of length 2 and 1 metres in panel depths of up to 6 metres. In this case, deformation will occur by rigid plate movements such that,

$$\bar{K} = \frac{0.144\ d^{1.5}\ K}{t^{0.5}b}$$

Theoretical results were derived for both cases of linear and local distortion according to the approximate formulae, based on an experimental value for the individual sheet flexibility from table (1.2). Comparing with the observations for a number of sheet overlaps it seems that in general, profile interaction occurs by rigid plate movements.

The experimental flexibilities are usually mid-way between the two limiting theoretical cases, and there are indications that the overall flexibility should tend to the localized distortion theory as the sheet length increases.

As previously mentioned, attachment of the sheets to rafters does inhibit the relatively flexible trough bending of alternately fastened corrugations, which tends to make deformation behave as though due to linear plate movements.

Nevertheless, as an upper bound to the sheet overlap flexibility the formula derived from localized end distortion may be used as a design expression for any number of similarly fastened sheets.

6.9. Results Comparison for Sheets Fastened in Every Trough at their Ends and Alternate Troughs at the Overlaps

The theoretical derivation for the interaction of alternately fastened overlapping sheets, with every trough fastening at the panel extremities has been represented by an approximate formula, as in Section (6.6).

For local end distortion which occurs for sheets longer than 3 metres, the overall panel flexibility may by given by,

$$C_{1.1} = \left\{\frac{2\varepsilon}{4\varepsilon + N(3 - \varepsilon)}\right\} \quad C_{1.1_A} + \frac{C_{1.1_E}}{N}$$

The first term represents the interaction of the sheets at the overlaps, where $C_{1.1_A}$ is the individual sheet flexibility fastened in

alternate troughs. $C_{1.1_E}$ is the sheet flexibility due to every trough fastening and this second term is an approximate allowance for the distortion of the outer sheets. The slip factor ε is due to alternate trough fastening and may be determined from Appendix Table (3.2).

A similar formula has been presented for rigid plate movements. Experimental tests were carried out on the same profiles as the previous two sections and their observations are listed in Appendix Table (1.8). In the above formula the corresponding observed values were used for the every and alternate trough fastening flexibilities.

Comparing the theoretical and experimental results, it may be seen, that for the basic sheet lengths of one and two metres, deformation is more closely represented by linear plate movements. In general, the observations lie between the local and linear distortion cases which indicates that if longer sheet lengths had been used, then the formulation for localised distortion would have been more exact.

It may be seen that the divergence between the two theoretical solutions is relatively small, and hence the above formula may be used as a design expression for the distortion flexibility of this fastening arrangement.

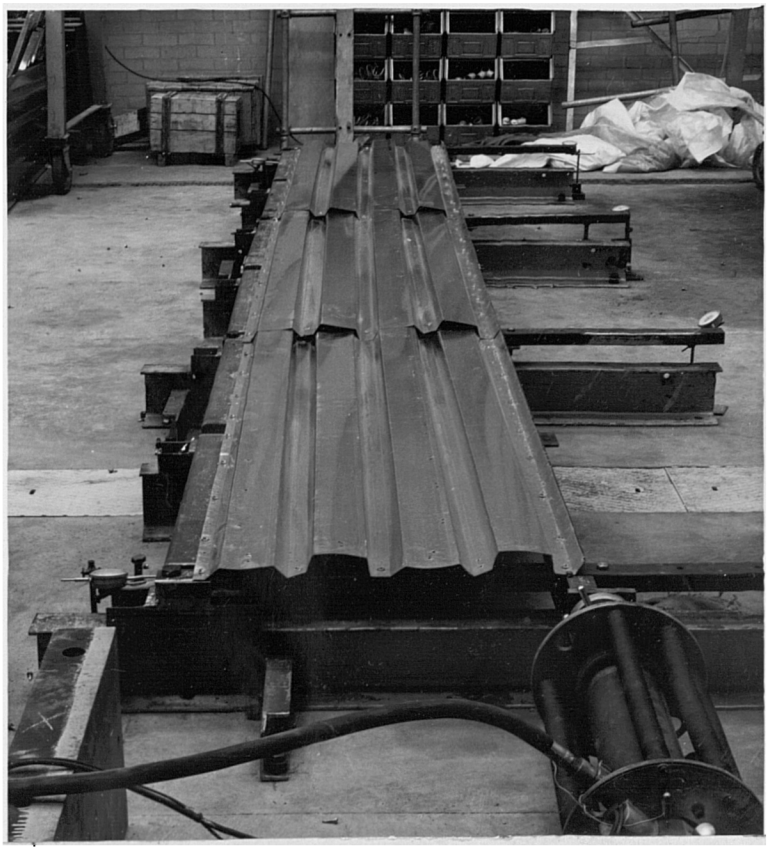

Plate (6.1) Interaction of overlapping sheets fastened in alternate troughs. The concertina action is displayed.

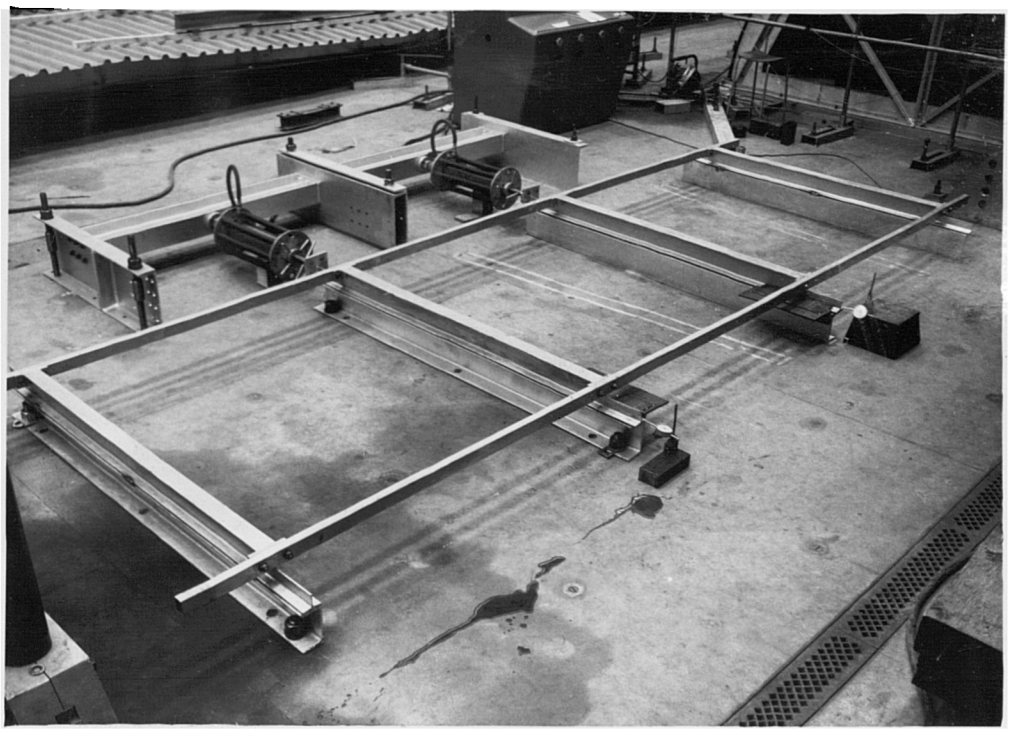

Plate (7.1) Three bay continuous diaphragm test rig

C H A P T E R 7.

CONTINUOUS DIAPHRAGMS

In a continuous diaphragm the sheeting spans perpendicular to the imposed shear force. This form of construction has been used for school buildings and larger framed structures[45] where sheeting spans continuously across rafters, obviating the need for purlins as in Fig. (1.7). The benefits may be considerable especially for stressed skin construction where specific shear connections normally have to be made between purlins and rafters to transfer diaphragm shear forces. For sheets attached directly to rafters, the shear force and resistance are both in the same plane.

In this chapter, the shear displacement of continuous sheets spanning across rafters will be studied. These are less flexible than the corresponding unconnected sheets because of in-plane bending. Similarly overlapping sheets at the rafters also interact to reduce the central shear deflection resulting from profile distortion.

The web of the girder may also be taken into account as regards the diaphragm inertia, although the axial strain in the sheeting is reduced by fastener slip.

7.1. Modified Shear Distortion Flexibility due to Sheets Spanning across a Central Rafter

The shear distortion of an individual diaphragm is due to relative movement of the separate plates of the corrugation. For sheets spanning into different shear fields the cross-section movements not only vary, but also the slope of shear displacement is theoretically discontinuous at the rafter points. In-plane web bending is required to maintain compatibility and the shear deflection is reduced.

The shear flexibility C^1, of a diaphragm between rafters is calculated for a unit force applied along the line of the corrugations and is then multiplied by the orthogonality factor of $(b/a)^2$, where b is the

sheet span and a is the panel width. Thus, as in Fig. (1.5),

$$C^1 = C(\frac{b}{a})^2, \text{ where } C = C_{1.1} + C_{1.2} + C_{2.1} \text{ etc.,}$$

and where $C_{1.1} = \frac{ad^{2.5}\bar{K}}{Et^{2.5}b^2}$

Considering first a simple two bay case where a central force is applied to the sheeting spanning between end restraints, the theoretical shear deflection is linear up to a maximum at the point of loading. However, the web is made up of corrugations spanning continuously over the internal rafter and hence the sheeting must be constrained to bend to maintain slope deflection continuity.

For sheeting fastened in every trough, the plate deformation pattern is shown in Fig. (7.1). As an approximation, the trough lines are all assumed to bend equally in a sinusoidal form over the diaphragm length, 2b, according to,

$$U_B = A_B \sin \frac{\pi Y}{2b}$$

Due to the extra plate bending, it may be expected that the actual shear flexibility will be reduced compared to the theoretical derivation of C^1 above. The following section outlines a possible energy method solution for the central shear displacement, which establishes the basic components of internal energy in terms of chosen plate displacement parameters.

The corrugations will try to distort under the influence of the fastener forces, similar to the behaviour of an unconnected sheet. Consequently, the deformational movements of the corrugation plates at the centre and outer rafters will tend to be in opposite directions, consistent with the applied and resisting forces.

If the respective top and side plate movements are as indicated in Fig. (7.1), then the deflected shapes may also be represented as a sinusoidal form such that,

$$U_T = A_{T_O} + \{ A_B - A_{T_1} - A_{T_O} \} \sin \frac{\Pi y}{2b}$$

$$U_S = A_{S_O} - (A_{S_1} + A_{S_O}) \sin \frac{\Pi y}{2b}$$

where A_{T_O} and A_{S_O} represent the deformation at the outer edge and A_{T_1} and A_{S_1} are the central section movements. Purlin restraint effects on cross-section distortion have been omitted.

The end compatibility condition requires that there is no lateral movement of the fasteners during shearing. Hence for zero axial trough line strain,

$$b_L \frac{dU_B}{dy} + b_T \frac{dU_T}{dy} + 2b_S \frac{dU_S}{dy} = 0$$

$$b_L A_B + b_T \{A_B - A_{T_1} - A_{T_O}\} = 2b_S \{ A_{S_1} + A_{S_O} \}$$

$$A_B (b_L + b_T) = 2b_S (A_{S_1} + A_{S_O}) + b_T (A_{T_1} + A_{T_O})$$

profile geometrical terms, b_L, b_S, b_T, h etc., are shown in Fig. (2.1).

The cross-section distortion energy may be derived from Section (2.3) and is,

$$E_D = 2 \int_0^b C(1, 1)\ U_T^2 + C(1,2)\ U_T U_S + C(1, 3)\ U_T U_B + C(2, 2)\ U_S^2 + C(2, 3)\ U_S U_B + C(3, 3)\ U_B^2\ dy$$

where U_T, U_S and U_B are defined as above.

This distortion energy is approximately equivalent to the behaviour of unconnected sheets which deform by relative linear plate movements.

However, in addition, there are components due to the axial and bending strains absorbed within the sheeting which are a consequence of the shear displacement, A_B.

The bending strain energy of the plates is,

$$E_B = \frac{E\Pi^4 t}{48b^3} \{A_B^2 b_L^3 + (A_{S_1} + A_{S_O})^2 2b_S^3 + b_T^3 (A_B - A_{T_1} - A_{T_O})^2\}$$

However, due to the differing bending strains at either edge of the side plate there is an additional axial strain energy component of magnitude,

$$E_{AS} = \frac{Eb_S t\Pi^4}{32b^3} \{ b_L A_B - b_T (A_B - A_{T_1} - A_{T_O}) \}^2$$

These energy expressions may be collected together as a symmetrical matrix of the form,

$$(A_{T_O}, A_{T_1}, A_{S_O}, A_{S_1}, A_B)\ E(i, j)\ , \begin{Bmatrix} A_{TO} \\ A_{T1} \\ A_{SO} \\ A_{S1} \\ A_B \end{Bmatrix} = E_{Tot} = \frac{A_B^2}{2C}$$

where C is the central deflection due to a unit force. However, A_{S1} may be eliminated in terms of the other parameters by,

$$A_{S1} = \{\frac{b_T + b_L}{2b_S}\} A_B - A_{SO} - \frac{b_T}{2b_S} \cdot (A_{TO} + A_{T1})$$

As in Chapter 2, the total energy may be minimized with respect to the three independent variables, A_{TO}, A_{T1}, and A_{SO} such that,

$$\frac{dE_{Tot}}{dA_{TO}} = 0 \qquad \text{etc}$$

Hence, the three resulting equations may be solved and the parameters determined as direct ratios of the central trough displacement, A_B. The central flexibility C follows from the energy relationship.

For alternate trough fastening of the continuous sheeting, the deformation is rather more complicated as the trough between fasteners is

free to move. As in Chapter 3, this form of attachment causes an extra energy component due to concertina action which occurs by compression and extension of neighbouring profiles.

To obtain an approximate solution for alternate trough fastening of continuous sheeting spanning across rafters, the internal trough line is assumed to deflect as in Fig. (7.2), such that,

$$U_{B1} = A_O + \{ A_B - 2A_O \} \sin \frac{\pi y}{2b}$$

where A_O is the concertina trough movement at the outer and central sections.

The trough, which is attached to the rafters again moves according to,

$$U_{B2} = A_B \sin \frac{\pi y}{2b}$$

The top plate deflects by addition of half this concertina motion to the every corrugation fastening distortion. Thus,

$$U_T = A_{TO} + \frac{A_O}{2} + (A_B - A_{T1} - A_{TO} - A_O) \sin \frac{\pi y}{2b}$$

For end compatibility,

$$b_L \frac{dU_B}{dy} + b_T \frac{dU_T}{dy} + 2b_S \frac{dU_S}{dy} = 0$$

$$b_L A_B + b_T (A_B - A_{T1} - A_{TO}) = 2b_S (A_{S1} + A_{SO}) + A_O \, d/2$$

Again, A_{S1} may be expressed in terms of the other variables.

An additional energy component must be included due to concertina action,

$$E_c = \frac{1}{k} \int_o^b (1 - 2 \sin \frac{\pi y}{2b})^2 \, A_O^2$$

where k is the concertina movement due to a 1 kN trough force and equals,

$$(\tfrac{4}{3} b_S + 2b_T)\, h^2/D \; ; \qquad D = \frac{Et^3}{12(1 - \nu^2)}$$

However, an extra effect of conertina movement is that it modifies the axial strain stored in the sheeting. Lateral movement of the trough does not occur freely as the relative end rotation of neighbouring troughs lines causes a substantial additional strain throughout the corrugation. This is indicated in Fig. (7.2), which shows that concertina movement can only occur by sufficient axial strain absorbed within the sheet length.

The increase in top plate axial strain due to concertina movement, at any section y from one end, is,

$$A_O b_L \left(\frac{\pi}{2b}\right)^2 \sin \frac{\pi y}{2b}$$

However, due to a lateral trough movement A_O there is a corresponding side plate uplift given by,

$$V_S = fA_O \quad \text{where } f = \frac{(b_T + b_S)\, b_L}{(\tfrac{4}{3} b_S + 2b_T)\, h}$$

The top plate axial strain becomes $\left(\frac{\pi}{2b}\right)^2 \sin \frac{\pi y}{2b}\, A_O.(b_L + 2fh)$.

Thus the total axial strain energy in top and side plates is,

$$E_{AT} = Et \frac{\pi}{16b^3}^4 A_O^2 \{ b_T(b_L + 2fh)^2 + 2b_S (b_L + fh)^2 \}$$

Due to side plate displacement V_S, as a consequence of concertina action, there is an extra side plate bending energy component of magnitude,

$$E_{AS} = \frac{Et\pi^4}{24b^3} A_O^2 \, b_S \, f^2 h^2$$

Similarly, the bending energy in the trough plate becomes,

$$E_{BB} = \frac{Et\Pi^4}{96b^3} b_L^3 \quad \{A_B^2 + (A_B - 2A_O)^2\}$$

and the bending energy in the top plate is,

$$E_{BT} = \frac{Et\Pi^4 b_T^3}{48b^3} \quad \{ A_B - A_{T1} - A_{TO} - A_O \}^2$$

Side plate bending and axial strain energy due to A_{S1} and A_{SO} remain unaltered from the previous case.

The total energy components due to distortion, as determined from the every corrugation fastening theory, axial strain and concertina action are collected together as,

$$E_{total} = E_D + E_{AS} + E_{AT} + E_{BS} + E_{BB} + E_{BT} + E_C = \frac{A_B^2}{2C}$$

A_{S1} may bow be eliminated using the compatibility condition,

$$A_{S1} = \frac{(b_L + b_T)}{2b_S} A_B - A_{SO} - \frac{b_T}{2b_S} (A_{TO} + A_{T1}) - A_O \frac{d}{4b_S}$$

Thus differentiating the total energy expression with respect to each independent variable yields four simultaneous equations.

Solving for the displacement parameters in terms of A_B and resubstituting into E_{total} gives a value for C, the central deflection due to a unit force.

In order to evaluate the effect of in-plane bending on the shear flexibility of continuous diaphragms, the central displacement may be expressed relative to the value due to linear plate movements of unconnected sheets.

As the span becomes very large it may be expected that the central shear deflection will decay to the linear plate movement derivation consistent with a negligible internal plate bending energy.

7.2. Discussion of Experimental and Theoretical Observations for Two and Three Bay Continuous Diaphragms

For unconnected sheets spanning perpendicular to the applied shear force and meeting at the rafter points, the shear flexibility of each panel may be evaluated separately. However, when a sheet spans continuously into different shear fields, shear distortion is partially restrained by longitudinal sheet bending. Thus, discontinuities in the shear deflection are smoothed out which results in an increase in the overall diaphragm stiffness.

A simple two bay diaphragm with sheeting spanning across rafters has been examined experimentally for a 3.6 metre long test apparatus as in Fig. (7.4). The shear flexibility will be modified due to sheet continuity and may be expressed as a ratio of the unconnected sheet flexibility. Two profiles were studied, being 35 mm deep decking and roofing shapes, and their theoretical performance as deduced from the approach of Section (7.1), is shown in Figs. (7.5) and (7.6.)

It is apparent that the greater the degree of cross-sectional movements, the greater the restraint against shear deformation. Concertina action, due to alternate trough fastening is very much stiffer than its free sheet flexibility and only decays at about 7 metres sheet length to its linear plate movement prediction.

Every trough fastening flexibility decays at about 4 metres and implies that the in-plane bending is small compared to the shear stiffness of the diaphragm. It should be noted that although the plate displacements are given in a sinusoidal form their sheet distortion flexibility tends to the linear movement solution when the plate bending energy is small.

For sheets spanning across a single internal rafter, experimental observations of the central shear distortion deflections are listed in Appendix Table (1.10) for both profiles. These were deduced by subtracting the simple bending and fastener slip deflections from the measured values. A number of factors could be readily examined including the effect of varying amounts of sheet overlap.

Ideally an overlap ensures complete sheet continuity, but it was observed that only partial joint rigidity could be maintained for both fastening arrangements. It may be seen that the experimental relative flexibilities of the continuous diaphragm compared to unconnected sheeting are considerably less than the theoretical prediction.

The individual sheets, however, do not necessarily deform by linear plate movements. It was concluded from Chapter 2 that for every trough fastening localized end distortion occurs for sheets longer than 1.5 metres. Consequently, the deformation pattern assumed in Section (7.1) is likely to be inadequate to represent the plate displacements of the continuous diaphragm for this fastening arrangement.

For comparison with the experimentally deduced K parameter, two theoretrical K values are listed in Appendix Table (1.10). One was derived for linear plate movements and the other for localized end distortion of unconnected sheets. Examining the results it is apparent that sheets with wide troughs are more stiffened by spanning across the central rafter, which is due to the increase of in-plane bending restraint.

The experimental and theoretical comparisons for the two profiles of Figs. (7.5) and (7.6) only apply for the simple case where the individual sheet flexibility is caused by linear plate movements. For localized end distortion the beam on elastic foundations analogy as in Fig. (7.8) provides an approximate solution to the reduced flexibility.

The trough lines must bend to maintain continuity across the central rafter. The net movement at this point is reduced by one half of its free distortion value, and hence the overall central deflection is 0.75 of the unconnected sheet deflection. Hence this figure of 0.75 is the asymptote of the relative flexibility as the sheet lengths become very large.

The relatively poor comparison between experiment and theory cannot be explained. Nevertheless the consistent increased diaphragm stiffness in practice does indicate that the benefits may be greater than even the theoretical prediction.

No theory has been developed to take account of sheet continuity for multi-framed diaphragms, although for localized sheet distortion, the 3 bay central deflection ideally tends to 0.75 of the free sheet value. Experimental observations for sheeting spanning over three bays were only possible for a diaphragm length of 5.4 metres as summarized in Appendix Table (1.11). The test rig is shown in Plate (7.1).

The reduction in flexibility appears to be less than the two span case, but the three span continuous diaphragm is still significantly stiffer than the unconnected sheet value. The effect of sheet overlaps will be discussed in Section (7.5).

7.3. Inertia of Purlins in Simple Diaphragms

The previous derivations deal with the shear flexibility of sheeting spanning continuously across rafters. This section considers the bending deflection of standard diaphragms which use sheeting spanning over purlins. It is merely included as an introduction to the following section which derives the inertia of a continuous diaphragm by including the contribution of the sheeted web.

In conventional construction, taking account of the contribution of the intermediate purlins to determine the overall diaphragm inertia is important in two respects.

Firstly, the purlins give the diaphragm its bending stiffness and secondly the internal sheet shear flow increases towards the centre of the panel, which is especially important for design of the sheet-seam fasteners. Fig. (7.7(a)) indicates the formulae for beam inertia and maximum shear flow for an odd number, n_p, of purlins. The corresponding expressions for an even number of purlins are derived in Fig. (7.7(b)).

It may be seen that as n_p becomes very large so the beam inertia tends to,

$$I = A\, n_p \, \frac{b^2}{12}$$

where A is the cross-sectional area of each purlin and b is the overall diaphragm depth.

Similarly the maximum sheet shear flow due to a shear force Q is,

$$\frac{3}{2}\frac{Q}{b}$$

The sheet-purlin fasteners mustbe able to transfer their shear force into purlin axial force. Hence the maximum shear flow is at the sheet edge and equals,

$$\frac{Q.bA}{2I}$$

However, this simplified approach makes the assumption for cantilever beams, that the axial strain is linearly varying throughout the diaphragm depth. This implies that the rafter is sufficiently laterally rigid to resist the applied forces from the intermediate purlins. In practice this is unlikely to be so, and it may be that only the outer purlins contribute to the inertia.

7.4. Inertia of Sheets Spanning across Rafters

Profiled sheeting possesses only small axial stiffness perpendicular to the corrugations. For sheets spanning across purlins, uniform purlin axial strain induces no force in the diaphragm and hence the total roof inertia is simply due to the contribution of each purlin, according to a linear variation of strain from the neutral axis (Fig. 7.8 (a)).

However, for sheets spanning across rafters the bending resistance is primarily provided by edge members whose axial strain is transferred in some degree to the body of the diaphragm by the edge fastenings in the longitudinal sheet direction. For completely rigid connections the axial stress attracted to the sheeting is given by the perimeter member strain times Young's modulus. Thus the sheeting will contribute to the overall moment resistance.

For relatively deep diaphragms and light edge members this

additional sheet inertia may be significant. In practice the boundary fixings are relatively sparse and the force spread into the sheets is limited by the inherent load-slip characteristics of the connections. The linear variation of axial strain is also modified by the presence of sheet-seams, which cause a step-wise distribution of strain throughout the roof depth.

In addition to the shear transfer from the longitudinal edges, the sheet-rafter fixings serve to provide a sheet moment connection at the ends of the bay. As an example, for a unit edge member strain, the variation of axial strain in the sheeting is demonstrated in Fig. (7.8(b)) for two continuous sheets which show the effect of longitudinal edge, rafter and seam fastener slip.

Ideally the overall inertia includes the sheeting as though it were a web of a girder and a modification factor may be introduced to account for the effects of fastener slip.

A general formulation of the reduced web inertia as determined by the number of sheets and the fastener characteristics is depicted in Fig. (7.9). Each sheet is subject to the forces transmitted from neighbouring sheets via the seam fasteners, and also the the local rafter connections. This movement is controlled by equilibrium and compatibility requirements which may both be satisfied knowing the load slip parameters for the fixings.

The sheet is strained by forces P_1 and P_2 derived from seam slip, and from a uniform end force P_3 due to the sheet-rafter slip. A rafter connection bending component P_4 may also be introduced. At the outer sheet P_1 depends on the sheet-edge member slip.

The equilibrium condition for the ith sheet is given by,

$$d_i = (4P_1 + 6P_4 + 2P_2 + P_3) \frac{b}{2atE}$$

$$d_{i-1} + S_{i-1} = (P_3 - 4P_2 - 6P_4 - 2P_1) \frac{b}{2atE}$$

where d_i and S_i are defined in Fig. (7.9), and a, b, t and E are the sheets' width, length, thickness and Young's modulus respectively.

The fastener slip characteristics are, for an odd sheet number, N,

$$P_1 = S_i \frac{n_s}{4S_s}$$

$$P_2 = S_{i-1} \frac{n_s}{4S_s}$$

$$P_3 = \left\{ \frac{2(i-1)}{N} - \frac{(d_i + d_{i-1} + S_{i-1})}{2} \right\} \frac{n_e''}{NS}$$

and $$P_4 = \left\{ \frac{1}{N} - \frac{(d_i - d_{i-1} - S_{i-1})}{2} \right\} \frac{n_e''}{6NS}$$

At the outer sheet,

$$P_1 = S_N \frac{n_e'}{4S}$$

where n_s, n_e' and n_e'' are the number of seam, edge, and rafter fixings.

It is assumed that the slip, S_i varies linearly along the sheet length from the centre of the bay and hence the average seam fastener slip is half of the end displacement.

These equations may be combined to eliminate d_i and to solve for the slip of the ith sheet in terms of the (i-1) th unknowns. Thus,

$$S_i = -d_{i-1} \frac{4\left(1 + \frac{k_e''}{2N}\right)}{k_S^*} - S_{i-1} \frac{\left(4 + \frac{2k_e''}{N} + 2k_S\right)}{k_S^*}$$

$$+ (4i - 6) \frac{k_e''}{N^2 k_S^*}$$

At the outer sheet $k_S^* = k_e^1$. At all others $k_S^* = k_S$.

This equation forms the basis of a solution progressing from known values of the (i - 1)th sheet. The initial conditions are obtained by considering the central sheet where,

$$d_i = -d_{i-1} - S_{i-1} \qquad \text{for } i = 1$$

Hence,

$$d_1 \left(1 + \frac{k_e''}{2N}\right) = \frac{3}{4} k_S S_1 + \frac{k_e''}{2N}$$

S_i is taken as an unknown value and consequently all the terms up to $\frac{S_{N+1}}{2}$ and $\frac{d_{N+1}}{2}$ may be determined iteratively.

For unit edge member strain,

$$\frac{d_{N+1}}{2} + \frac{S_{N+1}}{2} = 1$$

Hence substitution yields a solution for S_1 and the rest of the unknown displacements may be determined.

When the number of sheets N is even, the final term in the controlling equation, above reduces to $(4^{i-4}) \frac{k_e''}{N^2 k_S}$ and the initial conditions are,

$$d_0 = -\frac{S_0}{2} \quad \text{and} \quad S_1 = -\frac{(2 + \frac{k_e''}{N} + 2k_S)}{k_S} \cdot S_0$$

S_0 may be considered as an arbitary unknown displacement and consequently all the displacements are expressible in terms of S_0, which is solved by equating to the unit edge strain.

The reduced sheet inertia may be represented by,

$$\frac{S}{d} \frac{t N^3 a^3}{12} \propto \qquad \propto \leq 1$$

where $\frac{S}{d}$ is the profile perimeter to pitch ratio, and

Na is the diaphragm depth

α is a factor due to the effect of fastener slip

The inertia of the ith sheet for an odd number of sheet is,

$$I_i = \int_0^a \{d_{i-1} + S_{i-1} + \frac{x}{a}(d_i - d_{i-1} - S_{i-1})\}\{(i - \frac{3}{2})\, a + x\}\, dx$$

$$\frac{I_i}{a^2} = (d_{i-1} + S_{i-1})\{(i - \frac{3}{2})/2 + \frac{1}{12}\} + d_i\{(i - \frac{3}{2})/2 + \frac{1}{3}\}$$

$$I = 2a^2 \sum_{i=2}^{i=\frac{N+1}{2}} I_i + I_{middle}$$

For unit edge strain,

$$I_o = \frac{N^2}{6} a^2$$

Thus,

$$\alpha = \frac{I}{I_o} = \frac{12}{N^2} \sum_{i=2}^{i=\frac{N+1}{2}} I_i + \frac{1}{N^3} \qquad \text{for N odd}$$

For N even,

$$I_i = \int_0^a \{ d_{i-1} + S_{i-1} + \frac{x}{a}(d_i - d_{i-1} - S_{i-1})\}\{(i-1)\, a + x\}\, dx$$

Thus,

$$\alpha = \frac{12}{N^2} \sum_{i=1}^{i=\frac{N}{2}} I_i \qquad \text{for N even}$$

These two equations for α as expressions for the reduced sheet inertia are functions of a, N, k_s, k_e', and k_e''. The effect of increasing the number of sheets, N, is shown in Fig. (7.10) for 1 metre sheet width, and 4 metre distance between rafters.

is merely included for theoretical comparison. For all other sheet lengths, the interaction formulae due to localized end distortion, apply.

To simplify the analysis, unit rafter forces are considered and the corresponding overlap restraining force X_i reduces the individual sheet flexibility by the ratio $1 - \frac{X_i}{2Q_i}$. This factor applies whether deformation occurs by local end deformation or rigid plate movements.

As an example, for an even number of bays (N = 4), the actual central deflection, Δ, divided by the value due to the free distortion of separate sheets Δ_O, is,

$$\frac{\Delta}{\Delta_O} = \frac{1 - 0.5\ (1 - \varepsilon)}{1} = 0.5 + 0.5\varepsilon$$

Similarly for an odd number of bays (N = 5), the joint fastening forces X_1 and X_2 due to profile interaction are,

$$X_1 = 1.5\ (1 - \varepsilon) \qquad \text{and} \quad X_2 = 0.5\ (1 - \varepsilon)$$

Thus,

$$\frac{\Delta}{\Delta_O} = \left\{\frac{3.0 - 2 \times \frac{1.5}{2}\ (1 - \varepsilon) - \frac{0.5}{2}\ (1 - \varepsilon)}{3.0}\right\} = 0.42 + 0.58\varepsilon$$

The central deflection may be obtained by multiplying by the factors,

$$\Delta_O = \frac{N^2}{8}\ C_{1.1}\ \left(\frac{b}{a}\right)^2 W \quad \text{- N even} \qquad \Delta_O = \frac{(N^2 - 1)}{8}\ C_{1.1}\ \left(\frac{b}{a}\right)^2 W \quad \text{- N odd}$$

where N is the number of overlapping sheets and W is the local rafter force. Values of $\frac{\Delta}{\Delta_O}$ are shown in Fig. (7.13) for various values of N.

For linear plate movements, the solution is more complicated. Typically for N = 5 bays,

$$\left\{\frac{2 + 1}{2}\right\}\ (1 - \varepsilon) = \frac{2}{3} X_1 + \frac{1}{6} X_2 \qquad \text{- joint 1}$$

$$\{\tfrac{1}{2}\}(1 - \varepsilon) = \tfrac{2}{3} X_2 + \tfrac{1}{6} X_1 - \tfrac{1}{6} X_2 \qquad \text{- joint 2}$$

Therefore, $X_1 = 2.18\ (1 - \varepsilon)$ $\qquad X_2 = 0.29\ (1 - \varepsilon)$

Thus,

$$\frac{\Delta}{\Delta_O} = \frac{3 - 2 \times \frac{2.18}{2}(1 - \Sigma) - \frac{0.29}{2}(1 - \varepsilon)}{3} = 0.23 + 0.77\Sigma$$

Approximate formulae have been developed for both the cases of local end distortion and rigid plate movements, which define the relative central deflection due to overlap interaction compared to the free sheet value.

$$\frac{\Delta}{\Delta_O} = \frac{2}{N} + (1 - \frac{2}{N})\Sigma \qquad \text{- local end distortion}$$

$$\frac{\Delta}{\Delta_O} = \frac{1}{N - 1} + \{\frac{N - 2}{N - 1}\}.\varepsilon \qquad \text{- linear plate movements}$$

The maximum error in both these expressions is no more than 10%. Typically for five overlapping sheets with $\Sigma = 0.4$, the central deflection is reduced by 34% from the simple theory where all the sheets are unconnected.

Test results are confined to the example of three overlapping sheets based on a rafter spacing of 1.8 metres. Two profiles were studied as in Fig. (7.5) and (7.6). Their results and comparisons are set out below and are listed more fully in Appendix Table (1.11).

The central deflection formulae are,

$$\Delta = \{0.75 + 0.25\Sigma\}\ C_{1.1}\ (\frac{b}{a})^2 W \qquad \text{- for local end distortion, or}$$

$$\Delta = \{0.5 + 0.5\ \Sigma\}\ C_{1.1}\ (\frac{b}{a})^2 W \qquad \text{- for linear plate movements}$$

The value of the slip overlap factor, Σ, as determined by the analyses of Chapter 6 is dependent both on the profile shape and the

fastening arrangement.

In general the theoretical and experimental values for $\frac{\Delta}{\Delta_o}$, the relative central shear deflection, are very closely in agreement. For every trough fastening the formula due to local plate bending is clearly more applicable than that due to rigid plate movements.

However, for alternate corrugation fastening of the roofing profile, where the troughs are relatively wide, sheet distortion more closely approximates to the rigid plate movement derivation. This is reasonable for a sheet length of 1.8 metres which, as observed from Chapter 3, does not deform by local trough bending until a length of about 3 metres.

Details	Σ Theory	Δ/Δ_o theory		Δ/Δ_o Expt.
		Local	Linear	
A.R.	0.33	0.83	0.67	0.74
E.R.	0.22	0.81	0.61	0.78
A.D.	0.25	0.81	0.63	0.81
E.D.	0.33	0.83	0.67	0.84

A - alternate trough fastening; E - every trough fastening;
R - roofing profile as in Fig. (7.5.); D - decking profiles as in Fig. (7.6)
Local - localized end distortion; Linear - rigid plate distortion.

7.6. Overlapping Sheets with Variations in the Fastening Arrangement

The number of sheet perimeter fasteners often varies in proportion to the applied shear force. In some cases alternate trough rafter fastening is used at the centre of the span and this changes to every trough fastening towards the outside.

Considering just the concertina deformation due to fastening in alternate troughs at (M - 1) rafters, the outer pair of overlapping sheets can only distort along their internal edges. This is depicted in Fig. (7.19). Consequently these outer sheets behave as though they are double the length of the internal spans because of the effective distortion anti-symmetry about the first and Mth rafters.

If shear deformation occurs by local end distortion, which is true for sheet lengths greater than 3 metres, the profile interaction at a sheet overlap is quite independent of its neighbouring joints.

For panel shear forces beginning at Q_1 in the outer panel of alternate fastening and progressing to Q_2 etc., at the neighbouring internal sheets, the overlap *interaction force as given in Section (6.3) is*,

$$X_1 = \left(\frac{Q_1 + Q_2}{2}\right)(1 - \Sigma)$$

where Σ is the profile overlap factor for alternate trough fastening as tabulated in Appendix Table (3.2).

Unlike the previous section, the shear flexibility of the outer sheets is reduced by half and hence the central deflection due to concertina action is,

$$\Delta = \left\{ \frac{Q_1}{2} - \frac{X_1}{2} + Q_2 - \frac{X_1}{2} - \frac{X_2}{2} + Q_3 - \frac{X_2}{2} - \frac{X_3}{2} + \ldots. \right\} C_{1.1A} \left(\frac{b}{a}\right)^2$$

This is consistent with the use of k = 2 in the formula of Section (6.3). $C_{1.1A} \left(\frac{b}{a}\right)^2$ refers to the free sheet flexibility normal to the corrugations when $\left(\frac{b}{a}\right)$ fastened in alternate troughs to rafters. X_i are the joint forces resulting from profile overlap distortion.

If sheet distortion is considered to occur by linear plate movements then the analysis of overlap interaction becomes more involved. In Section (6.3) an interaction formula was developed for one sheet being k times longer than its neighbour. For sheet shear forces Q_1 and Q_2 at the first sheet overlap,

$$\{\frac{Q_1}{k} + Q_2\}\ (1 - \Sigma) = \frac{2X_1}{3}(\frac{1}{k} + 1) + \frac{X_2}{3} + \frac{X_1}{3k}$$

The final term is an imaginary joint force to maintain anti-symmetry of deformation of the outer sheet for which k = 2. The central shear deflection is represented as for the case of localized end distortion.

Theoretical analyses of both deformation modes have been performed. However, as a design formula the roof central shear deflection may be expressed as a ratio of the deflection due to alternate trough fastening completely throughout the M bays. Thus,

$$\Delta_O = \frac{(M^2 - 1)}{8} C_{1.1A} (\frac{b}{a})^2 \text{ - M odd or } \frac{M^2}{8} C_{1.1A} (\frac{b}{a})^2 \text{ - M even}$$

Approximate formulae have been developed to roughly be equivalent to the exact theoretical results of the table of Fig. (7.14) such that,

$$\frac{\Delta}{\Delta_O} = \frac{1}{4M-6} + \{\frac{2M - 4}{2M + 1}\}\Sigma - \quad \text{local end distortion}$$

$$\frac{\Delta}{\Delta_O} = \frac{1}{3M - 2} + \{\frac{M - 2}{M + 3}\}\ \Sigma - \quad \text{linear plate distortion}$$

Over the complete roof diaphragm the central shear deflection per unit rafter force due to profile distortion may be approximately given by,

$$\Delta = C_{1.1E} (\frac{b}{a})^2 \frac{(N^2 - M^2)}{8} + C_{1.1A} (\frac{b}{a})^2 \frac{M^2}{8}\{\frac{1}{4M - 6} + (\frac{2M - 4}{2M + 1})\Sigma\}$$

where $C_{1.1E} (\frac{b}{a})^2$ is the shear distortion flexibility normal to the corrugations for every trough fastening.

$C_{1.1A} (\frac{b}{a})^2$ is the shear distortion flexibility normal to the corrugations for alternate trough fastening.

N is the total number of sheet lengths

M is the number of sheets with alternate trough fastening on one or more edges

Σ is the profile overlap factor for alternate trough fastening.

Plate (8.1) Collection of self tapping screws and a 'monel' pop rivet

Plate (8.2) Apparatus for determining the upstand seam fastener strength and slip characteristics

C H A P T E R 8.

THE SHEAR STRENGTH OF CORRUGATED DIAPHRAGMS

The contribution of the sheet-purlin fasteners to the diaphragm strength will be examined in this chapter. In addition, the provision of roof lights is studied with regard to single or periodic flexible bands within a relatively stiff roof diaphragm. This causes purlin bending stresses and local fastener forces which may limit the overall diaphragm capacity.

8.1. Connections

A shear diaphragm fastened on all four sides relies on the strength of the perimeter connections to transfer its uniform shear flow to reaction framework. Simple expressions have been derived in Chapter (1.3.) for the ultimate diaphragm capacity based on a characteristic edge and seam fastener strengths. Welded diaphragms behave similarly although, the strength per connection is usually so high that local inter-weld buckling problems are a design limitation, as studied by Luttrell[12].

In Britain self drilling screws are the usual means of fixing to perimeter members although bolts and fired pins are suitable provided that their design shear strength and slip values are reliable for stressed skin applications. Seam fasteners again may be self drilling screws or monel 'pop' rivets as shown in Plate (8.1). The individual connection capacity is a function of the sheet thickness, width and clamping action. The latter parameters are properties of the fastener and so, by experimental testing, the strength may be determined as a characteristic load per mm of sheet thickness.

Testing of the fasteners themselves has been the subject of much investigation[46] and at the present time the European Commission on Structural Steelwork Committee 17[47] is preparing recommendations for standardization of connection tests.

A number of failure modes for a fastener in shear are apparent.

(1) fastener shearing,
(2) fastener crushing,
(3) tilting and pull out of fastener,
(4) yield of both sheets,
(5) yield of thinner sheet,
(6) sideways tearing.

Mode (4) generally occurs for seam fasteners which is frequently accompanied by some tilting due to the eccentricity of one sheet thickness. In this case the clamping action of the fastener is important to delay excessive twisting and possible premature pull out. A minimum lateral edge distance of 10 mm is recommended to avoid sideways tearing. Plate (2.2) shows typical seam fastener failure.

Mode (5) is the ideal ductile failure for edge fastenings and the attachment to a thicker member means that the fastener cannot rotate. A simulated diaphragm apparatus is shown in Plate (8.2) which is especially useful for testing upstand seams as well as direct sheet overlaps.

Bryan[4] suggests that ultimate shear strengths of 6 and 2.5 kN per mm sheet thickness should be respectively used as design values for standardly available self drilling screws and seam fasteners, as in Plate (8.1). Their slip values are usually much more variable but Bryan[4] again gives design values of 0.15 and 0.35 mm/kN for edge and seam connections respectively based on the slip at 0.6 times the ultimate load, which is reasonably close to the normal working load.

However, the initial loading cycle is considerably more flexible than subsequent tests due to 'bedding-in', and the reloaded values are only about one third of the above slips. Also, the initial tangent slip, which is generally important for experimental testing, is smaller still.

A typical load-slip curve for a direct overlap seam is shown in Fig. (8.1). The sheet thickness was 0.9 mm and the connection was a 4 mm diameter monel 'pop' rivet. For comparison the same sheet was formed into an upstand which had slightly superior ultimate load characteristics of 2.8 kN/mm sheet thickness (Fig. (8.2)). This is probably due to the fact that an upstand prevents sheet separation and failure must occur by tearing.

In North America button punched seams are widely used in conjunction with welded diaphragms to limit the excessive cost of puddle welding along the sheet connections. This is facilitated by an upstand overlap, as shown in Fig. (8.3), and a special tool indents the steel causing a friction key between the sheets. Preliminary tests indicate that the strength is highly dependent on sheet thickness, t, and distance of the punch from the upstand crest, h.

For closely spaced buttons the number has little importance as failure occurs by bending of the overlap to pass over the indentation. Hence the capacity is proportional to roughly $(\frac{t}{h})^3$. For 0.9 mm thick sheet, a rough strength per button is 1.8 kN although this occurs with very large slip displacements.

Testing has generally been concerned with steel sheets but Bryan[48] has studied connections in aluminium.

Other fastener parameters of importance, although not necessarily for stressed skin applications, are the pull out and pull over strengths for fasteners in axial tension.

8.2. Possible Diaphragm Failure Modes

The strength of a shear diaphragm is not only controlled by the capactity of the connections. Membrane action is responsible for a number of design limitations which are summarized below in rough order of importance.

1. Sheet tearing around fasteners: This will be discussed for general diaphragm applications in the next section. The critical point is usually the outer-sheet purlin fastener which suffers two shear directions.

2. Local shear buckling aroundfastener: This mode often occurs for wide trough widths of thin sheeting where the sheet-purlin fastening causes compressive sheet buckling, as in Plate (9.1). Similarly buckling is possible between seam or shear connector fasteners.

3. Overall shear buckling: The most important parameters are the corrugation depth sheet thickness and distance between purlins for shear buckling. This mode is not critical for most applications, but a check must be made to obtain a considerable safety factor.

4. Excessive deformation: As suggested in Chapter 3, a large degree of corrugation distortion may cause the insulation to break away producing a serviceability design limitation.

5. Lateral deflection: Short diaphragms are very shear flexible and it is possible that the strict horizontal movement limits for buildings could be exceeded. For large scale diaphragms deflection is not usually critical.

6. Other unlikely failure conditions include compression failure of the outer purlin due to diaphragm action.

Of course, the framework beneath the sheeting must be capable of supplying the forces required for equilibrium and the purlin-rafter connections are very important in this respect.

8.3. Indirect Shear Transfer through Purlins

The strength of a seam is ideally simply defined by the number of seam fasteners times their characteristic load. However, this takes no account of the compatibility requirements of purlin movement between neighbouring sheets. Fig. (8.4) shows how, for an infinite number of similar sheets, shear displacement resulting from seam slip causes sheet-purlin discontinuity. Hence for an exact analysis, the induced forces in these edge fasteners must be considered as an effective seam resistance.

For linear purlin movement, the sheet is in equilibrium due to the moment of the applied shear force, the seam resistance and all of the individual sheet-purlin fastener forces about the sheet centre. Davies[17] has derived an expression for the ultimate diaphragm capacity, which is reached when the seam and outer sheet purlin fastener have both failed.

Considering a unit shear force, the consequent seam slip per bay has been expressed by Davies,[17] as,

$$\Delta = \frac{1}{\frac{n_s}{S_s} + g_1 \frac{n_p}{2S}}$$

where n_s and n_p are the number of seam fasteners and purlins respectively.

S_s and S are the seam and sheet-purlin slips respectively.

g_1 refers to the effect of the number of sheet purlin fasteners, n.

If n becomes very large then g_1 will tend to $\frac{n}{6}$.

A table of g_1 is shown in Fig. (8.10), which is influenced by whether the fastenings are in the sheet crests (roofing) or troughs(decking).

It is clear that the purlin will be indirectly subject to lateral forces which depend on the relative amount of shear force transferred through the seams. However, purlins are usually laterally very weak as they are primarily designed for their bending strength spanning between rafters. Davies[17] inclues a provision for parabolic purlin movements, over the panel width, a, which modifies the parameter g_1. Thus the amount of shear force effectively attracted to the purlins will be reduced.

He suggests that the dividing line between these two displacement modes is the relative flexibility of purlin bending(EI) and the effective shear modulus for the sheeting (G^1) according to,

$$\eta = \frac{a^3 G^1 b}{EI} \quad 8 \times 10^3 < \eta < 4 \times 10^5$$

For η below 8000 a linear purlin displacement should be used and in the above range parabolic movements apply. If η is greater than 4×10^5 an effective sheet width based on a parabolic force system is necessary, given by the value of a at $\eta = 4 \times 10^5$.

Davies has carried out extensive finite element analyses of complete diaphragms to arrive at this conclusion, and by observing the resulting

purlin movements over a range of panel sizes has obtained the above empirical relationships.

He also has derived a similar expression for the slip of the sheet - shear connector fasteners, of number n_{sc}. If the perimeter fixings are all of the same type and have slip, S, then the edge slip is,

$$\Delta = \frac{S}{n_{sc} + n_p g_1}$$

The case of sheeting fastened on two sides only, as studied by Bryan, corresponds to $n_{sc} = 0$ and,

$$\Delta \text{ tends to } \frac{6S}{n.n_p} \quad \text{for linear purlin movements}$$

The seam fastener capacity, Q_S, can only be achieved by tearing of the sheet-purlin fasteners which pass through the overlap. Ideally,

$$Q_S = n_s F_s + n_p F_p$$

where F_s, and F_p are the characteristic strengths of the seam and sheet-purlin fasteners respectively.

However, there is some additional benefit in that the rest of the sheet-purlin fasteners are contributing to the overall strength by causing the purlins to absorb some of the applied shear force. A load-seam slip graph will be bilinear corresponding to the combined action of seam and sheet-purlin fasteners. When the seam fasteners initally fail due to their higher slip value and lower capacity, the sheet acts as though fastened only along the purlins until the outer fastener also fails. Complete collapse occurs as the internal sheet-purlin fastener tear with little addition to the shear load.

The seams fail at a shear load of,

$$Q_1 = F_s \frac{S_s}{\Delta} \quad \text{where } \Delta = \frac{1}{\frac{n_s}{S_s} + \frac{g_1}{2}\frac{n_p}{S}}$$

The end sheet-purlin fastener then fails at an additional shear load Q_2, where,

$$Q_2 = (\delta F_p)\frac{2S}{\Delta} \qquad \text{where } \Delta = \frac{1}{\frac{g_1}{2}\frac{n_p}{S}}$$

However, at the point of initial seam failure the sheet purlin fastener force is,

$$F_{p1} = \frac{\Delta Q_1}{2S} = F_s \cdot \frac{S_s}{2S}$$

Thus, $\delta F_p = F_p - F_{p1}$

where δF_p is the additional sheet-purlin fastener capacity.

The total diaphragm seam strength is thus,

$$Q_S = Q_1 + Q_2 = F_s\left(n_s + \frac{g_1}{2}n_p\frac{S_s}{S}\right) + \left(F_p - F_s\frac{S_s}{2S}\right) g_1 n_p$$

$$= F_s n_s + F_p g_1 n_p$$

which tends to $F_s n_s + \frac{F_p\, n\, n_p}{6}$ as $n \to \infty$

This represents failure of the seam and the outer sheet-purlin fastener. Complete collapse will occur by tearing of the internal purlin fasteners but this may be neglected due to the large shear displacements that are required.

Davies [17] has derived a rather different expression not based on the elastic-plastic failure curve, where the shear stiffness gradually decreases. Using the initial slip relationship throughout for Δ, it follows that,

$$Q_S = \frac{(n_s F_s + n_p F_p)}{\Delta}\,\Delta_1$$

where Δ_1 assumes that the end-sheet purlin fastener and the seam fasteners act like two parallel springs in distributing the applied shear force between themselves. Thus,

$$Q_S = (n_s F_s + n_p F_p) \frac{\left(\frac{n_s}{S_s} + \frac{g_1 n_p}{2S}\right)}{\left(\frac{n_s}{S_s} + \frac{n_p}{2S}\right)}$$

This formula will give an underestimate to the diaphragm capacity compared to the previous derivation on page 177.

Strictly the above expression only applies for decking profiles where seams are in the corrugation troughs. For seams in the corrugation crests,

$$Q_S = (n_s + g_1 \frac{S_s}{S}) F_s$$

Actually, seam failure must also involve tearing of the outer sheet-purlin fastener even though these are separated from the line of seam fasteners.

Expressions may also be derived for the sheet-shear connector strength by replacing n_s and S_s by n_{sc} and $2S_{sc}$ respectively.

The term g_1 is an important factor for indirect shear transfer in diaphragms where shear connectors may not be used. In this case, the total applied shear is passed via the sheet-purlin fasteners as a transverse purlin shear force.

Not only are purlins laterally weak inbending but also free to twist, which is a factor not previously accounted for in finite element or alternative analyses. In the following section a differential equation form will be developed for the contribution of the purlins to the seam slip and diaphragm strength.

8.4. Effect of Laterally Weak Purlins

Indirect shear transfer through purlins implies, that for rigid purlin movement, the shear force must gradually build up in the sheeting toward the centre of the panel. Similarly the applied shear force is completely absorbed by the lateral bending rigidity of the purlins and the sheet-purlin fasteners spread the load back into the diaphragm. Thus the sheet shear force at any section x from one end is,

$$Q_S = \frac{6Q}{a^2} (a - x) x$$

corresponding to a parabolic shear force distribution depending on the distance x from the end of the panel width a.

The central shear force is $\frac{3}{2}Q$, where Q is the applied shear.

However, for a complete analysis of indirect shear transfer, the properties of the purlin must be considered corresponding to,

EI - lateral bending stiffness and
GJ - torsional stiffness

The general purlin displacements are shown in Fig. (8.4) where,

V_E and V_O are respectively the top flange and centroid movements. V_S is the shear shear displacement.

A differential equation solution will be proposed which takes account of purlin bending and torsion in establishing the seam slip.

Considering an element of a purlin where q is local loading, the bending equilibrium equation is,

$$q = n_p EI \frac{d^4 V_O}{dx^4}$$

where n_p is the number of purlins

The simplified torsion equation, omitting warping effects is,

$$q = -n_p GJ \frac{d^2\phi}{dx^2}$$

where $\phi = \frac{V_E - V_O}{\frac{h}{2}}$, and $\frac{h}{2}$ is the depth of the shear centre from the top flange.

The sheet-purlin fastener slip is,

$$q = \frac{n_p . n_e}{S} (V_S - V_E)$$

where S is their characteristic slip and n_e is the number of fasteners per mm of purlin length. It is assumed that the individual fasteners behave as a uniform elastic medium.

Finally the sheet shear equilibrium equation is,

$$q = \frac{1}{C} \frac{d^2 V_S}{dx^2}$$

where C is the panel shear flexibility per mm width. Combining these four equations and eliminating V_E and V_S gives,

$$\frac{S}{n_e} \frac{d^6 V_O}{dx^6} - \left[n_p C + \frac{h^2}{4GJ} \right] \frac{d^4 V_O}{dx^4} + \frac{1}{EI} \frac{d^2 V_O}{dx^2} = 0$$

The solution of this differential equation is given by,

$$V_O = \sum_{j=1}^{4} A_j e^{\lambda_j x} + A_5 x + A_6$$

where λj are the roots of,

$$\lambda^4 - 2x_1 \lambda^2 + x_2^2$$

For imaginary roots, such that $x_2^2 > x_1^2$, the solution is,

$$V_O = A \sin h\, a_1 x \cos a_2 x + B \cos h\, a_1 x \sin a_2 x + Cx$$

where x is defined from the centre of the diaphragm or sheet and observes the antisymmetry requirements,

$$a_1 = \sqrt{\frac{x_1 + x_2}{2}} \qquad a_2 = \sqrt{\frac{-x_1 + x_2}{2}}$$

where $x_1 = \{n_p C + \frac{h^2}{4GJ}\} / \frac{2S}{n_e}$; $x_2 = \sqrt{\frac{n_e}{EIS}}$

According to the relationships,

$$\frac{d^2V_S}{dx^2} = n_p EIC \frac{d^4V_O}{dx^4} \quad \text{and} \quad \frac{d^2V_E}{dx^2} = \frac{d^2V_O}{dx^2} - \frac{EIh^2}{4GJ} \cdot \frac{d^4V_O}{dx^4}$$

It follows that V_S and V_E must also be represented by the same differential form, but with constants A^1, B^1 and A^{11}, B^{11} respectively replacing A, B, such that,

$$A^1 = n_p CEI \{x_1 A + y B\} \qquad \text{where } y = \sqrt{x_2^2 - x_1^2}$$

$$B^1 = n_p CEI \{-yA + x_i B\}$$

$$A^{11} = A - \frac{EIh^2}{4GJ} \{x_1 A + y B\}$$

$$B^{11} = B - \frac{EIh^2}{4GJ} \{-yA + x_1 B\}$$

All the linear terms in x must equal the sheet flexibility C, due to the fact that, if the sheet shear force is unity,

$$1 = \frac{1}{C} \frac{dV_S}{dx} - n_p EI \frac{d^3V_O}{dx^3}$$

An alternative displaced shape is possible for real roots ($x_2^2 < x_1^2$) which occurs when GJ is very small.

$$V_O = A_r \sin h\, a_1^1 x + B_r \sin h\, a_2^1 x + Cx$$

where $a_1^1 = \sqrt{x_1 + \sqrt{x_1^2 + x_2^2}}$

$a_2^1 = \sqrt{x_1 - \sqrt{x_1^2 - x_2^2}}$

Similarly,

$$V_S = A_r^1 \sin h\, a_1^1 x + E_r^1 \sin h\, a_2^1 x + Cx$$

and $V_E = A_r^{11} \ldots\ldots + E_r^{11} \ldots\ldots + Cx$

where $A_r^1 = n_p\, C\, EI\, (a_1^1)^2\, A_r$

$E_r^1 = n_p\, C\, EI\, (a_2^1)^2\, E_r$

$A_r^{11} = \{1 - \frac{EIh^2}{4GJ}\, (a_1^1)^2\}\, A_r$

$E_r^{11} = \{1 - \frac{EIh^2}{4GJ}\, (a_2^1)^2\}\, E_r$

It is a necessary condition for similarity between neighbouring sheets that,

$\frac{d^2V_O}{dx^2} = O$ at $x = \frac{a}{2}$ where a is the panel width.

Hence, $B = b_a A$

where $b_a = \frac{-x_1\ sh.cs + y\ \ ch.sn}{x_1\ ch.sn + y\ \ sh.cs}$ for imaginary roots

$sh = \sin h\, \frac{a_1 a}{2}$ $\qquad$ $sn = \sin \frac{a_2 a}{2}$

$ch = \cos h\, \frac{a_1 a}{2}$ $\qquad$ $cs = \cos \frac{a_2 a}{2}$

alternatively, $b_a = -\left\{\frac{a_1^1}{a_2^1}\right\}^2 \frac{\sin h\, \frac{a_1^1 a}{2}}{\sin h\, \frac{a_2^1 a}{2}}$ for real roots

The final condition, to determine the constant A or A_r, is the shear force at the seam. The total shear force absorbed into the purlin is determined by taking moments about the centre of the panel for the effect of all the sheet-purlin fastener slips. Thus an equivalent shear resistance is,

$$F = \frac{2}{a} \int_0^{a/2} (V_E - V_S) . x . \frac{n_e n_p}{s} \, . \, dx$$

On integration, for imaginary roots, this becomes,

$$F = \frac{2n_e n_p}{as} \left\{ \frac{a}{2} . \frac{ch.cs}{a_{12}} (a_1\bar{A} - a_2\bar{B}) + \frac{a}{2} \, . \, \frac{sh.sn}{a_{12}} (a_2\bar{A} + a_1\bar{B}) \right\}$$

$$+\frac{ch.sn}{a_{12}^2} (2a_1 a_2\bar{A} + (a_2^2 - a_1^2)\bar{B}) + \frac{sh.cs}{a_{12}^2} ((a_2^2 - a_1^2)\bar{A} + 2a_1a_2\bar{B})$$

where $a_{12} = a_1^2 + a_2^2$

$\bar{A} = A^{II} - A^1$ and $\bar{B} = B^{II} - B^1$

Similarly for real roots

$$F = \frac{2n_e n_p}{as} \left\{ \bar{A}\left\{\frac{a}{2a_1'} . ch_1' - \frac{1}{a_1'^2} . sh_1'\right\} + \bar{B}\left\{ \frac{a}{2a_2'} . ch_2' - \frac{1}{a_2'^2} . sh_2'\right\} \right.$$

where $\bar{A} = A_r^{II} - A_r^1$ and $\bar{B} = B_r^{II} - B_r^1$; $ch_1' = \cosh \frac{a_1'a}{2}$; $sh_2' = \sin h \frac{a_2'a}{2}$ etc.

So the total seam equilibrium equation is given by,

$$1 = \frac{n_s}{S_s} \Delta + F$$

the end shear displacement, Δ, between seams is such that,

$$\frac{\Delta}{2} = A \{sh.cs + b_a \, ch.sn \}$$

or $$\frac{\Delta}{2} = A_r \{\sin h\, a_1 \frac{l}{2} \frac{a}{2} + b_a \sin h\, a_2 \frac{l}{2} \frac{a}{2}\}$$

Thus,

$$\Delta = \frac{1}{\frac{n_s}{S_s} + g\, n_{ps} \frac{n}{}} \quad \text{where } n = n_e.a$$

g is a factor reflecting the influence of purlin bending. For rigid movements $g = \frac{1}{12}$ and as non linearity increases so g will gradually fall. It should be noted that Davies' factor g_1 is equivalent to 2ng, where n is the total number of sheet-purlin fasteners in the panel width.

The factor g is a function of EI, $\frac{GJ}{h^2}$, a, C and $\frac{n_e}{S}$ but is unaffected by the number of seam fasteners.

An alternative form for the influence of sheet-purlin fastenings on seam slip is an effective width concept as represented by,

$$a_{eff} = a.12g$$

a_{eff} is thus an effective diaphragm width for localized linear purlin movements, characterized by a redundant internal portion of $(a - a_{eff})$.

Hence, the diaphragm capacity from section (8.3), is given by,

$$Q_S = F_S n_s + 2F_p\, g.n_p.n$$

8.5. Discussion of Theoretical Results for Diaphragm Strength

The differential equation solution of the previous section has been expressed in computer form as in Appendix (5.2) in order to determine the factor g which represents the proportion of shear force attracted to the purlins due to sheet or panel shearing. Output is restricted to the displaced shapes V_E, V_O and V_S at eight points from the centre of the diaphragm, in addition to values of g, and the effective sheet width.

A factor of importance is the resultant sheet shear force which, for linear purlin movements, rises parabolically towards the diaphragm centre when added to the shear transferred directly via the seams. For localized purlin deformation, the maximum shear force is lower, but rises initially more steeply as in Fig. (8.4).

The proposed analysis may be applied to the equilibrium of complete diaphragms as well as a single sheet. Indeed once the parameter g has been determined for a given purlin and fastening arrangement, then this may be used to evaluate the diaphragm design strength for any width or number of seam fasteners. For the longitudinal edge capacity, the seam fastener properties are replaced by those of the sheet- shear connectors and the effect of the internal seams may be superimposed later by a local analysis.

However, for very wide panels, most practical purlins will suffer considerable local bending as implied in Fig. (8.7). For a lateral inertia of 5×10^5 mm^4 corresponding to two 3 mm thick, 100 mm wide purlins, it is clear that even the most torsionally stiff members decay to a constant effective panel width.

The influence of sheet width for an infinitely torsionally stiff purlin is depicted in Fig. (8.5) and the purlin displacement V_O again indicates that the end deformation remains constant for increasing panel width. If the torsional stiffness is reduced to realistic proportions, the displacements of the purlin top flange (V_E) and centroid (V_O) are clearly much different, consistent with cross-sectional twisting rather than lateral bending. As in Fig. (8.6), V_O tends to remain linear whilst V_E follows the shear displacement between sheets.

A summary of the purlin performance is shown in Fig. (8.8) for the relative sheet displacement Δ, when the number of seam fasteners is zero, corresponding to indirect shear transfer. The panel width, it is assumed is large enough so that local purlin deformation takes place. Thus Δ is independent of the sheet width and in this case is related to g by,

$$g = \frac{S}{\Delta n} \qquad \text{and} \qquad a_{eff} = 12.g.a$$

Fig. (8.8) may be used as a design chart for both the end slip Δ without shear connectors and also indirectly gives a value for g, which may be used in the expression for overall diaphragm strength or seam slip.

For n_p, number of purlins, n_s and S_s, number and slip of the seam fasteners, the actual seam slip will be,

$$\frac{1}{\frac{n_s}{S_s} + g.n_p.\frac{n}{s}}$$

Similarly, for seam and sheet purlin fastener capacities F_s and F_p respectively the overall diaphragm strength may be expressed as,

$$Q_S = F_S.n_s + 2F_p.n.n_p.g$$

The variation of Δ, and hence g, shows how the purlin behaviour asymptotes the two limits of zero bending and zero torsion for every and alternate trough fastenings. Sheet shear flexibility has relatively little importance compared to fastener slip. Fig. (8.9) reveals how increasing the flexibility, C, reduces the effective sheet width. However, typical values of C are less than 0.0001 mm/kN/mm sheet width, below which C has little effect on a_{eff}.

In conclusion, for standard sheet widths of less than 1 metre, the concept of linear purlin movements is reasonable. However, for complete diaphragms, relying on the indirect transfer of rafter shear via purlins, an allowance must be made for the effect of purlin bending and twisting as given by the factor g.

For most practical purlin sizes the equivalent panel width acting in indirect shear transfer is certainly less than 2 metres which suggests that the overall diaphragm strength is constant and is independent of the panel width.

Member torsion cannot be ignored as it severly reduces the value of g which nominally equals 1/12 for linear purlin movements. Davies' factor g_1 is determined by taking the influence of the discrete fasteners,

whereas g assumes that the fasteners form a uniform medium. By consulting Fig. (8.10) it may be seen that g always underestimates the contribution of the sheet-purlin fasteners and hence represents a safe design formula.

Non-linear purlin movements can only be approximated by quadratic displacements and the complex interaction of purlin, sheet and fastener properties means that no single parameter can be used to determine the point at which rigid purlin displacements break down. Hence the factor g_1 must be considered inaccurate for large scale diaphragms without shear connectors.

The alternative parameter g which takes into account member torsion, bending, fastener slip and sheet flexibility is a much more realistic value for practical diaphragms in determining strength and slip. However, further work is required to estimate the effect of discrete fastenings compared to a uniform fastener medium.

By adjusting the boundary conditions this differential equation approach may be used to evaluate the effect of rafter forces supplying a *transverse force to the roof diaphragm via* the lateral rigidity of the purlins.

Local purlin bending and twisting will exist around the rafter as in Fig. (8.12), due to the eccentricity of applied force and sheeting resistance when shear connectors are not used.

8.6. Comparison of Differential Equation and Finite Element Results for Diaphragm Strength

The equilibrium of both individual sheets and overall diaphragm are controlled by the same equation which includes the parameter g to account for the influence of sheet-purlin fastenings on the shear capacity.

Davies [49] has performed a number of finite element studies of the shear deformation of plate girders using corrugated webs, and can model individual sheets and their fastenings. He has varied the sheet width, and member inertia to ascertain the effect of fold line bending on the seam slip. Results are expressed in terms of sheet-member fastener

forces and their comparison with the corresponding differential equation solutions are indicated in Fig. (8.11).

Member torsion has been ignored, which is correct of folded plate roofs where the fold line acts in conjunction with two neighbouring girders. However, for normal diaphragms it is likely that purlin twisting will reduce g and the effective sheet width.

For two purlins each of inertia 1.54×10^5 mm^4, the effect of increasing sheet width is to maintain a roughly constant region of member deformation of 0.8 m compared to the maximum width of 3.34 m. When the inertia is increased to a very large value of 9.2×10^6 mm^4, the effective sheet width only rises to 1.6 metres indicating that a reduced width concept will apply for most realistic panel sizes.

The seam slip displacement comparisons were made for the penultimate folded plate roof sheet as displayed in reference (49) which is connected to its neighbours by 22 seam fasteners.

The agreement between the theoretical and finite element results is good especially for the more gross purlin bending cases. Fold line displaced shapes show that linear member movements break down for widths greater than 1 metre, even for this relatively rigid example of zero torsion. It may be concluded that the parameter g, as developed in Section (8.4) is on reasonably exact design value for sheet slip and hence overall diaphragm capacity.

8.7. Holes in Diaphragms

Within the broad limits of suitable roof diaphragms there are many practical deviations from that of a simple shear membrane. Quite apart from the non-homogeneity of the medium due to discrete sheet lengths, and variations in the fastening arrangement, provision is usually made for roof lights, generally in some sort of pattern.

Indeed, the poor distribution of a given area of roof lighting may be a serious design limitation to the shear capacity of the roof diaphragm.

The design of the openings themselves is also a major factor. Ideally, the most suitable roof lights span between neighbouring purlins and the unsupported longitudinal sheet edges are attached to a stiffening member. In order to transfer the sheet shear force, the same number of seam connectors are used in the reduced diaphragm depth as in the complete depth and it is assumed that the shear force normally passing through the hole area, is spread uniformly over the rest of the seam.

However, with some roof lights, conditions may not be so favourable for smoothing the shear transfer across an opening. For example, a simple hole cut in a sheet is subject to severe local distortion by the unresisted profile shear flow.

If all these practical difficulties are ignored in order to obtain the overall diaphragm performance, then an opening may ideally be represented as a local increase in the shear flexibility of the diaphragm depth. Thus, a single roof light or periodic distribution of openings may be theoretically modelled by a flexible band with an overall stiffer medium.

However, in some cases the removed sheeting may be replaced by a roof light frame of the same shear stiffness.

As previously discussed in Chapter (2.3), the distortional component of shear deflection dominates in all but the largest and most lightly seam fastened diaphragms. This flexibility is highly dependent on the length and continuity of the individual sheets. For example, halving a sheet length quadruples its shear flexibility, and hence the shear deflection of the reduced diaphragm depth may easily be an order of magnitude greater than its neighbouring sheet.

The relative flexibility of the reduced to the complete diaphragm depth is given by $b_o^2 / \sum_{i=1}^{N} b_i^2$ where b_i is the depth of the individual sheeted lengths between openings as in Fig. (8.12), and b_o is the complete diaphragm depth. Each length of sheet attracts shear force in rough proportion to the square of its length and hence the flexibility of the reduced diaphragm depth is defined by the reciprocal of the sum of the sheet stiffnesses.

Laterally weak purlins are constrained to follow the deflected shape of the sheeting and their bending stresses are relieved by cross-sectional twisting and slip of the fasteners. Thus, the purlin to sheet fasteners are subjected not only to the global transfer of shear but also the effects of purlin stiffness around a diaphragm opening. A proportion of the diaphragm shear force is hence taken by lateral bending of the purlins and the induced flange stresses may be very large. In addition, the shear forces in the seams in and around the hole are subject to some variation from the simple applied shear force.

For most general applications, two cases may be readily examined being a discrete flexible band within a stiffer medium corresponding to a single opening and a periodic distribution of flexible bands. The parameters of most importance are the properties of the purlin, number and slip characteristics of the sheet-member fasteners, and the flexibilities of the complete and reduced diaphragm depths.

A differential equation solution assumes that the influence of the discrete fasteners may be spread out to form a uniform medium upon which the purlin is free to bend and twist.

Considering an element of a purlin as in Fig. (8.13) its equations of equilibrium may be defined simply as,

$$q = n_p EI \frac{d^4 V_O}{dx^4}$$

and $q = - n_p GJ \frac{d^2\phi}{dx^2} + n_p ECw \frac{d^4\phi}{dx^4}$ where q is the local fastener force/mm

EI and GJ are respectively the purlins bending torsional stiffness. The sheet-purlin fastener load-slip relationship is,

$$q = \frac{n_e n_p}{S} (V_S - V_E)$$

where n_e is the number of sheet-purlin fasteners per mm.

S is the slip in mm per fastener force in kN

n_p is the number of purlins.

The sheet shear equation is,

$$q = + \frac{1}{C} \frac{d^2 V_S}{dx^2}$$

where V_O and V_E are the purlins centroid and top edge movement, respectively. V_S is the sheet displacement.

$$\text{Also, } V_E - V_O = \phi \frac{h}{2}$$

For ease of analysis, it has been assumed that the restraint due to warping term, Cw, may be omitted, although it is appreciated that for wide, torsionally weak sections there will be flange stresses generated which resist the pure St. venant twisting. $\frac{h}{2}$ represents the distance from the top flange to the purlin shear centre.

Reduction of the above equations to a single differential equation for each section yields,

$$\frac{S}{n_e} \frac{d^6 V_O}{dx^6} - \{ n_p C_i + \frac{\left(\frac{h}{2}\right)^2}{GJ} \} \frac{d^4 V_O}{dx^4} + \frac{1}{EI} \frac{d^2 V_O}{dx^2} = 0$$

where x is defined as from the centre of the opening. The factor n_p is due to the number of purlins and modifies C_i which is the flexibility of either the stiff, or the flexible region, where $C_2 > C_1$.

The solution of this differential equation depends on whether the roots are real or imaginary, and on the inherent anti-symmetry of the deformation. Also, for a single roof opening, the local purlin bending must decay to zero away from the flexible region. Assuming a solution of the *form*,

$$V_O = \sum_{i=1}^{4} A_i e^{\lambda i x} + Bx + C,$$

the displacement parameters may be adjusted according to the two cases below.

case (1): A single flexible band in a diaphragm as displayed in Fig. (8.14). The solution for an opening width a, is,

$$V_o = e^{-b_1 x^1} \{ A \sin b_2 x^1 + B \cos b_2 x^1 \} + Fx^1 + \Delta$$

for the stiffer portion which observes the decay requirement for $x^1 = \infty$, where $x^1 = x - \frac{a}{2}$. Δ is the displacement to the cente of the opening. $V_o = C \sin h\, a_1 x \cos a_2 x + D \cos h\, a_1 x \sin a_2 x + Gx$ for the flexible region which is antisymmetric about $x = 0$.

$$a_1 = \sqrt{\frac{x_1 + x_2}{2}} \qquad \text{where } x_2 = \sqrt{\frac{n_e}{EIS}}$$

$$a_2 = \sqrt{\frac{-x_1 + x_2}{2}} \qquad x_1 = \sqrt{n_p C_2 + \sqrt{\frac{h^2}{4GJ}} \Big/ \frac{2S}{n_e}}$$

$$b_1 = \sqrt{\frac{x_3 + x_2}{2}} \qquad x_2 = \sqrt{n_p C_1 + \sqrt{\frac{h^2}{4GJ}} \Big/ \frac{2S}{n_e}}$$

$$b_2 = \sqrt{\frac{-x_3 + x_2}{2}}$$

C_1 and C_2 are the corresponding shear flexibilities of the stiff and flexible portions respectively. The roots in this case are imaginary, such that $x_2^2 > x_1^2$ and $x_2^2 > x_3^2$. If both set of roots are real (x_1^2 or $x_3^2 > x_2^2$) then,

$$V_o = A_r e^{-b_1^1 x^1} + B_r e^{-b_2^1 x^1} + F_r x^1 + \Delta$$

for the stiffer protion and,

$$V_o = C_r \sin h\, a_1^1 x + D_r \sin h\, a_2^1 x + G_r x$$

for the flexible section which again observe the decay and anti-symmetry requirements.

$$a_1^1 = \sqrt{x_1 + \sqrt{x_1^2 - x_2^2}} \qquad b_1^1 = \sqrt{x_3 + \sqrt{x_3^2 - x_2^2}}$$

$$a_2^1 = \sqrt{x_1 - \sqrt{x_1^2 - x_2^2}} \qquad b_2^1 = \sqrt{x_3 - \sqrt{x_3^2 - x_2^2}}$$

If $x_2^2 > x_3^2$ and $x_1^2 > x_2^2$ then the appropriate imaginary and real forms must be combined for the complete displaced shape of V_O given by terms in A, B, C_r and D_r.

The sheet movement is given by,

$$\frac{d^2V_S}{dx^2} = n_p C_i EI \frac{d^4V_O}{dx^4}$$

and the purlin top flange movement is,

$$\frac{d^2V_E}{dx^2} = \frac{d^2V_O}{dx^2} - \frac{EIh^2}{4GJ} \frac{d^4V_O}{dx^4}$$

By implication V_S and V_E have the same basic form as V_O with merely different displacement constants replacing the unknowns A, A_r, B, B_r, C etc. These new parameters are summarized on page 195 and may be expressed in terms of the above constants.

The joint compatibility conditions are such that equality of, V_O, $\frac{dV_O}{dx}$, $\frac{d^2V_O}{dx^2}$ and $\frac{d^3V_O}{dx^3}$ must be maintained at the boundary between the flexible and stiff regions $(x = \frac{a}{2})$. In addition, if a unit shear force is applied, then,

$$- n_p EI \frac{d^3V_O}{dx^3} + \frac{1}{C_i} \frac{dV_S}{dx} = 1$$

Therefore $F = F^1 = C_1$

and $G = G^1 = C_2$

Also, $EI \frac{d^4V_O}{dx^4} = \frac{S}{n_e} (V_S - V_E)$

and $- (\frac{dV_e}{dx} - \frac{dV_O}{dx}) \frac{4GJ}{h^2} = EI \frac{d^3V_O}{dx^3}$

Hence, all the linear terms in x such as F, G, F_r and G_r must reduce to their respective sheet shear flexibilities for the above equations to hold.

As a final condition V_S is made equal at the boundary for both sections implying that no slip occurs in that seam. It is assumed that the effects of seam slip may be superimposed as these movements are small compared to the deformation of the purlin.

The five conditions may be solved to evaluate the resultant displacement, Δ, at the centre of the hole, depending on the roots of the controlling differential equation. Each boundary condition may be represented as a row of a matrix as in Figs. (8.25) and (8.26) and the parameters A, B, C, D, and Δ may be solved in terms of the unit applied shear force and the sheet flexibilities. Different solutions exist for both the real and imaginary root cases, and if the condition exists where the roots are real for the stiff region and imaginary for the flexible region, then the relevant columns in each matrix must be combined. The displacement parameter A_r, B_r, C_r and D_r apply when the roots of the differential equation are real.

After solving for these parameters, the net shear force in the sheet may be redetermined by,

$$\frac{dV_S}{C_i dx} = 1 + n_p EI \frac{d^3 V_O}{dx^3}$$

For the case of an isolated hole it may be expected that the purlin members reduce the seam shear forces around the opening.

An important design parameter is the tearing force induced in the sheet-purlin fasteners local to the hole. The maximum force is given by,

$$\frac{V_S - V_E}{S}$$

The purlin bending stresses may be significant and are represented as,

$$\sigma = E\frac{w}{2} \cdot \frac{d^2 V_E}{dx^2}$$

where w is the overall member width.

A number of factors detract from the validity of this analysis. The main sources of error are likely to be,

1. The assumption that the discrete fasteners may be spread out to form a uniform flexible medium.

2. The omission of warping restraint of purlin twisting.

3. The restriction of free twisting of the member due to attachment of the top flange to the sheeting.

All these factors will effectively add to the torsional stiffness of purlin movement and raise the relative lateral bending to twisting tendency.

Consequently, the analysis may be expected to underestimate effects such as purlin lateral bending stress but overestimate deflection.

Displacements of the purlin and sheeting for a single opening depending on the nature of the roots of the controlling differential equation.

(1) Roots Imaginary

For the flexible section comprising the hole,

$$V_O = C \sin h\, a_1 x \cos a_2 x + D \cos h\, a_1 x \sin a_2 x + C_2 x$$

$$V_S = C^1 \sin h\, a_1 x \cos a_2 x + D^1 \cos h\, a_1 x \sin a_2 x + C_2 x$$

$$V_E = C^{11} \sin h\, a_1 x \cos a_2 x + D^{11} \cos h\, a_1 x \sin a_2 x + C_2 x$$

$$C^1 = n_p C_2 EI \{ x_1 C + y_1 D \}$$

$$D^1 = n_p C_2 EI \{ -y_1 C + x_1 D \}$$

where $y_1 = \sqrt{x_2^2 - x_1^2}$

$$C^{11} = C - \frac{EIh^2}{4GJ} \quad \{x_1 C + y_1 D\}$$

$$D^{11} = D - \frac{EIh^2}{4GJ} \quad \{- y_1 C + x_1 D\}$$

For the stiffer medium,

$$V_O = Ae^{-b_1 x^1} \sin b_2 x^1 + Be^{-b_1 x_1} \cos b_2 x^1 + C_1 x^1 + \Delta$$

where $x^1 = x - \frac{a}{2}$

$$V_S = A^1 e^{-b_1 x^1} \sin b_2 x^1 + E^1 e^{-b_1 x^1} \cos b_2 x^1 + C_1 x^1 + \Delta$$

$$V_E = A^{11} e^{-b_1 x^1} \sin b_2 x^1 + E^{11} e^{-b_1 x^1} \cos b_2 x^1 + C_1 x^1 + \Delta$$

A^1, E^1, A^{11}, B^{11} have the same form as C^1, D^1, C^{11}, D^{11} respectively, above except that x_3 replaces x_1 according to the difference in sheet flexibility and C_1 replaces C_2.

(2) Roots Real

For the flexible region,

$$V_O = C_r \sin h\, a_1{}^1 x + D_r \sin h\, a_2{}^1 x + C_2 x$$

$$V_S = C^1_r \sin h\, a_1{}^1 x + D_r{}^1 \sin h\, a_2{}^1 x + C_2 x$$

$$V_E = C^{11}{}_r \sin h\, a_1{}^1 x + D_r{}^{11} \sin h\, a_2{}^1 x + C_2 x$$

where $C_r{}^1 = n_p C_2\, EI\, (a_1{}^1)^2\, C_r$

$$D_1{}^1 = n_p C_2\, EI\, (a_2{}^1)^2\, D_r$$

$$C^{11}{}_r = (1 - \frac{EIh^2}{4GJ} (a_1{}^1)^2)\, C_r$$

$$D^{11}{}_r = (1 - \frac{EIh^2}{4GJ} (a_2{}^1)^2)\, D_r$$

For the stiffer medium,

$$V_O = A^1_r e^{-b_1 x} + B_r e^{-b_2 x} + C_1 x + \Delta$$

$$V_S = A^1_r e^{-b_1 x} + B_r{}^1 e^{-b_2 x} + C_1 x + \Delta$$

$$V_E = A^{11}_r e^{-b_1 x} + B_r{}^{11} e^{-b_2 x} + C_1 x + \Delta$$

where A^1_r, B^1_r, A^{11}_r, B^{11}_r have the same form as $C_r{}^1$, $D_r{}^1$ etc., except that $a_1{}^1$, and $a_2{}^1$ are replaced by $b_1{}^1$ and $b_2{}^1$ and C_2 by C_1. The same form of A^1, $A_r{}^1$, $A_r{}^{11}$, A^{11}, B^1, etc., exist for a periodic distribution of openings.

Case (2).

A periodic distribution of flexible bands within a stiffer medium corresponding to a uniform pitch of openings as in Fig. (8.15).

The solution of the differential equation for imaginary roots ($x_1{}^2$ and $x_3{}^2 < x_2{}^2$), is,

$$V_O = C \sin h\, a_1 x.\ \cos a_2 x + D \cos h\, a_1 x.\ \sin a_2 x + Gx$$

for the flexible protion, where x is measured from the centre of the opening and for the stiffer region, which again must observe anti-symmetry,

$$V_O = A \sin h\, a_1 x^1.\ \cos a_2 x^1 + B \cos h\, a_1 x^1.\ \sin a_2 x^1 + Fx + \Delta$$

where $x^1 = \frac{a+b}{2} - x$

is the net displacement between neighbouring points of anti-symmetry and a and b represent the respective widths of the flexible and stiff regions.

a_1, a_2, b_1, b_2 are the roots of the controlling differential equation and are unaltered from case (1).

If the both sets of roots are real (x_1^2 and $x_3^2 > x_2^2$) then,

$V_O = C_r \sin h\, a_1^1 x + D_r \sin h\, a_2^1 x + G_r x$ for the flexible section

$V_O = A_r \sin h\, b_1^1 x^1 + B_r \sin h\, b_2^1 x^1 + F_r x^1 + \Delta$ for the stiff section

where $x^1 = \frac{a+b}{2} - x$

a_1^1, a_2^1, b_1^1, b_2^1 are the same as case (1).

The boundary conditions for a uniform applied shear force reduce the constants G and G_r to C_2, and F and F_r to C_1, which are the corresponding sheet flexibilities of each region.

Again, purlin movement compatibility must be ensured at the joint between the two regions and hence four equations may be written in matrix form for, V_O, $\frac{dV_O}{dx}$, $\frac{d^2V_O}{dx^2}$, and $\frac{d^3V_O}{dx^3}$

Together with a final equation for continuity of sheet displacement, V_S, the matrices of Figs. (8.27) and (8.28) may be solved for the displacement parameters depending on the nature of the differential equation roots. V_S and V_E have the same form as V_O and the displacement constants are modified to give C^1, D^1, A^{11}, E^{11}, etc., as for the simple opening case.

If the roots of the flexible region are real and those of the stiff region imaginary, then the relevant columns of each matrix may be combined to solve for A, B, C_r, D_r and Δ.

8.8. Discussion of Differential Equation Results for Openings in Diaphragms

On redetermining the net sheet shear force as given by $\frac{1}{C_i}\frac{dV_S}{dx}$ where C_i corresponds the sheet shear flexibility at the section under consideration, the expected distribution is shown in Fig. (8.16). For a periodic pitch of openings the shear force variation must have peaks or troughs at the points of anti-symmetry. In the more flexible sheeted region, C_2, the purlins will absorb some of the applied shear, corresponding

to the transfer of force via the edge fasteners.

The purlins are, in effect, smoothing the shear displacement around the opening and the degree of force attraction is very much related to the ratio of purlin to sheet flexibility, C_2. As determined in the analysis of indirect shear transfer via purlins, the torsional stiffness parameter, J is perhaps more important than the lateral bending stiffness, I, due to the eccentricity of sheet force from the centroid of relatively flexible purlins, $(\frac{h}{2})$. Fig. (8.17) shows, for a single opening in an infinitely wide medium, how the purlin movements are influenced by I and J. In this case the 2 metre wide region representing the opening is roughly consistent with the flexibility of a 4 metre long sheet fastened in every corrugation.

It is clear that, for realistic proportions of J/h^2, the purlin top flange and centroid movements are widely differing, which suggests member twisting rather than bending.

Considering the case of periodic openings at a 2 metre pitch with very high shear flexibility, the purlin displacements at the approximate practical limits of J/h^2 are indicated in Fig. (8.18). Again, purlin twisting seems to be a more flexible mode than lateral bending.

The central displacement for a unit applied shear force is reduced considerably indicating that the purlins are attracting a significant proportion of the sheet hsear around the opening.

Ideally, the periodic and isolated hole solutions should degenerate to the same solution for a very wide pitch of openings. This is considered in Fig. (8.19), for hole widths of 1 metre at 3.6 metre spacing and it is apparent that the two purlin displaced shapes are reasonably close.

However, displacements are relatively unimportant compared to their related sheet-purlin fastener forces and purlin bending stresses. Due to the relatively high sheet shear stiffness in practice, the purlins tend to follow the displaced shape around the opening and the consequent lateral bending is only relieved by fastener slip and member torsion. The The maximum purlin stress, σ, at the boundary between the flexible and stiff regions rises with opening width until it is constant at about 1.5

metres. The computer analysis of Section (8.7) was performed for a purlin width of 100 mm and hence the extreme bending stress must be modified by w/100 as in Fig. (8.19), where w is the total member width.

Fastening in alternate troughs tends to reduce the maximum bending stress as the degree of fastener slip increases. Similarly the maximum sheet-purlin fastener force rises with both I and J as in Fig. (8.20). The variation of purlin bending stress with opening flexibility, C_2, and purlin inertia, I, is shown in Fig. (8.22), for zero twisting.

The analysis of both isolated and periodic openings has been written as a computer program and a listing is shown in Appendix (5.3). Output is restricted to purlin displacements, the maximum purlin bending stress and sheet-purlin fastener force, as well as the sheet shear force at certain critical points.

The number of variables are too great for design charts and only typical results have been presented.

8.9. Comparison of Differential Equation and Finite Element Results

To assess the accuracy of the differential equation solution of Section (8.7), for single or periodic holes in a diaphragm, a typical practical shear panel was examined by the finite element method. The geometrical arrangement is detailed in Fig. (8.23) which shows how the sheet seam and purlin fasteners may be modelled by equivalent springs.

A panel of 5.4 metres depth and 4.5 metres width was chosen, with a central 0.9 m wide opening spanning between the two intermediate purlins. For fastening in alternate troughs a typical profile $\bar{K}$ value may be used to evaluate the shear flexibilities of the stiff and flexible regions as .00013 and .00058 mm/kN/mm respectively. The four purlins were each of lateral inertia 5×10^5 mm^4, and the torsional stiffness was necessarily infinite for this two dimensional analysis.

The cantilever panel was subject to a unit shear force and the finite element solution performed to ascertain the purlin displaced shape,

local bending stress, and the induced sheet-purlin fastener forces. Geometrical and member data was fed in for both line and plate elements, as well as for the fastener springs. Dr. J. M. Davies developed this finite element program to deal with general diaphragm arrangements.

The differential equation solution was performed for a periodic pitch of openings based on points of anti-symmetry at the diaphragm edge and the centre of the panel. Thus a and b equal 0.9 and 3.6 metres respectively. Purlin displacements are shown in Fig. (8.23) indicating the observations from the finite element (FE) and differential equation (D.E.) solutions for $J = \infty$.

It is clear that the central displacements agree reasonably well, the F.E. and D.E. results being 0.50 and 0.47 mm respectively compared to a simple shear deflection of 0.51 mm. For comparison a typical torsional value of $J/h^2 = 0.5$ was also studied.

An interesting result from the F.E. analysis is the end rafter bending due to the axial forces transferred from the intermediate purlins. Even though the lateral inertia is substantial ($10^7 mm^4$) there is considerable degeneration in the linear axial strain assumption between the outer purlins. In fact, at the fixed end the intermediate purlins do not seem to contribute to the diaphragm inertia. This is worth extra investigation as some of the flexibility factors listed in Chapter (1.4) are influenced by the number of purlins.

The distribution of purlin bending stress is also shown and has a maximum (F.E.) value of 4.1 N/mm^2. Similarly the sheet-purlin forces are indicated although the finite element observations are also influenced by the local sheet slip effects. However, taking an approximate mean the maximum edge force is 0.09 kN compared to 0.18 kN from the D.E. solution.

Again it should be noted that the differential equation will always overestimate the sheet-purlin connection forces as it assumes a uniform fastener medium for solution, yet takes the worst displacement at the boundary between the stiff and flexible regions to evaluate the resulting slip. The seam fastener forces tend to be less than unity and correspond to 0.89 and 0.92 kN for the F.E. and D.E. solutions respectively.

In conclusion, openings in diaphragms constrain purlins to follow the resulting shear displacement with consequent high local purlin and fastener forces. The differential equation solution presented in Section (8.6) seems to give a reasonable solution for the displaced shapes and local stresses and is left in computational form in Appendix (5.3).

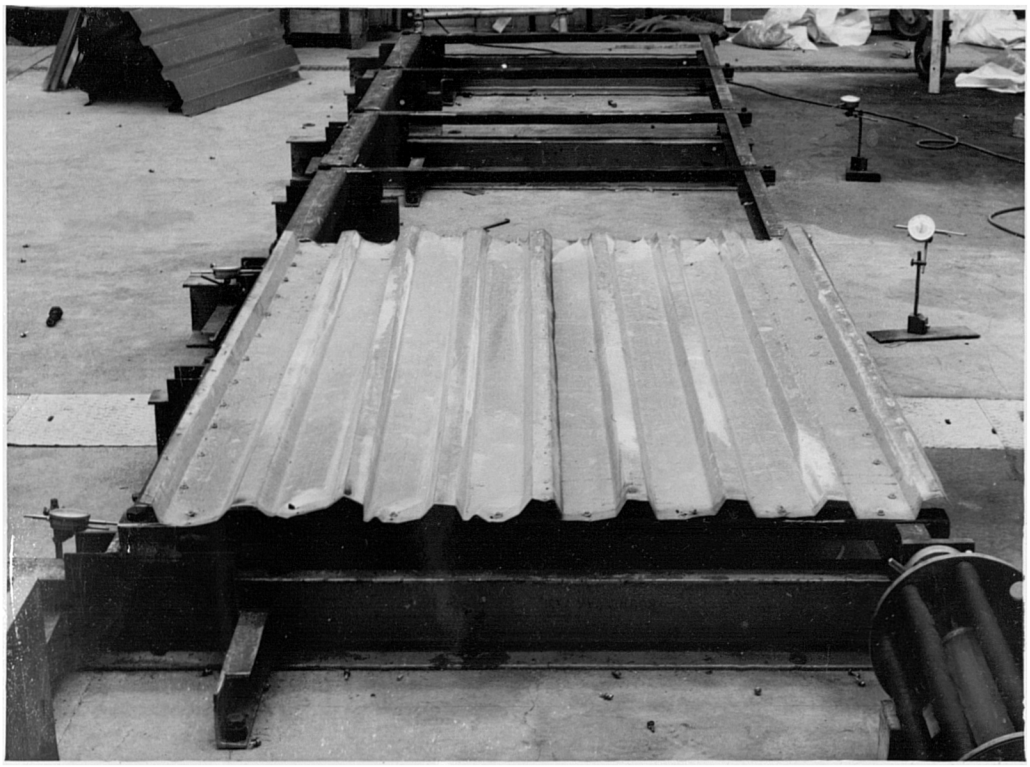

Plate (9.1) Local buckling around trough fasteners

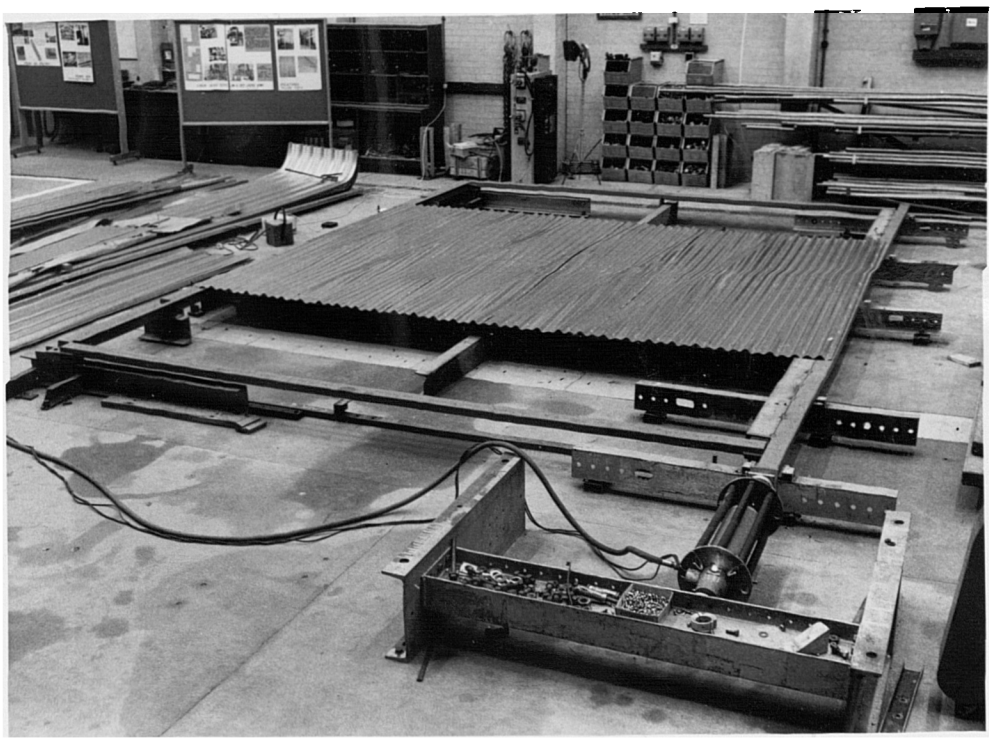

Plate (9.2) Buckling wave passes through every fourth trough fastenings at the intermediate purlin for sinusoidal corrugations

CHAPTER 9.

SHEAR BUCKLING OF CORRUGATED SHEETING

9.1. Review of Theoretical Investigations for Flat Diaphragms

Relatively little research effort has been expanded over the years into the shear buckling problems associated with orthotropic plates, compared to other plate buckling theory. The first exact solution for shear buckling of an infinitely long isotropic plate was provided by Southwell [50] in 1924, who developed the governing differential equation giving a solution for the critical shear stress of,

$$\tau_{cr} = k_s \frac{\pi^2 D}{tb^2}$$

where D is the plate bending stiffness $Et^3/12(1 - \nu^2)$

t is the sheet thickness

b is the plate width

k_s is 5.35 for a simply supported plate.

Stowell [51], in 1943, considered the effect of elastic restraints against edge rotation and later authors such as Budianski [52] studied variations in the boundary conditions of isotropic plates. The buckling of plates under combined stress systems including shear was investigated by Batdorf [53], who developed an interaction formula for shear and compressive stress.

Using the fact that k_s increases as the panel width to length ratio $(\frac{a}{b})$ decreases, isotropic plates may be strengthened by dividing the panel up by means of transverse stiffeners. This was first studied by Crate [54] in 1948.

The shear buckling of orthotropic plates was initially examined by Bergmann and Reissner [55] who considered an infinitely long plate with zero bending stiffness in that direction. A similar analysis was later presented which derived the critical shear flow, Q_{cr} as,

$$\frac{Q_{cr}\, b^2}{4\,(Dx\, Dy^3)^{1/4}} = \begin{cases} 8.3 & \text{simply supported edges} \\ 15.3 & \text{clamped edges} \end{cases}$$

where Dx and Dy are the minor and major bending stiffnesses respectively.

Seydel [56] presented a general method of solution allowing for elastic rotational restraint at the panel edges. The first direct application to corrugated sheeting was made by Peterson and Card [57] who gave buckling criteria for long clamped corrugated webs with complete restraint against warping along the edges.

Recently, Hlavacek [58] has studied the shear instability of orthropic panels by using an energy method approach based on an assumed buckling wave shape. This was later refined by Easley and McFarland [59] who used a wave defined, as in Fig. (9.1), by,

$$w = A \sin \frac{\pi}{\ell}(x - ky) \sin \frac{\pi y}{b}$$

k is the buckling wave slope to the major bending direction
ℓ is the wave pitch and b is the panel length
x and y are the axes directions.

This relationship strictly only applies for an infinitely wide plate, as it violates some of the lateral boundary conditions for finite dimensions. However, the acuteness of the buckling wave k, for highly orthotropic plates, means that for panel widths greater than 2b, no increase in the critical shear load will be observed.

The solution proceeds by a Ritz technique of establishing the total energy due to the two directions of bending energy, and torsional energy. This is equal to the work done by the uniform shear stress in creating the wave. The total energy is expressible in terms of the wave pitch and inclination which are independent variables. Thus by differentiation with respect to each, the minimized energy expressions may be used to develop an equation for the critical shear buckling load.

For the buckling load (kN/mm) they [59] obtained,

$$Q_{cr} = Dy \frac{\Pi^2}{b^2} \left\{ \frac{\ell^2}{2kb^2} + 3k + \frac{k^3 b^2}{2\ell^2} \right\} + Dx \frac{\Pi^2}{2k\ell^2}$$

where k is the smallest root of,

$$8Dy^2 k^8 + \frac{27}{4} Dy.Dxy\, k^6 + (11\, DxDy - \frac{11}{4} Dxy^2) k^4 + (\frac{Dxy^3}{4Dy} - 3\, Dx\, Dxy)\, k^2$$

$$+ (\frac{Dxy^2\, Dx}{4Dy} - Dx^2) = 0$$

where Dy and Dx are again the orthogonal bending stiffnesses and Dxy is the torsional stiffness.

However, for Dy >> Dx and Dy >> Dxy, Easley[20] showed that this reduces to,

$$k = (\frac{Dx}{11Dy})^{1/4} \quad \text{and also} \quad \ell = b\, (\frac{Dx}{Dy})^{1/4}$$

If $\gamma = \frac{Dy}{Dx}$ it follows that, $Q_{cr} = \frac{36\, Dx^{1/4}\, Dy^{3/4}}{b^2}$

Hlavacek[58] assumed that $\ell = kb$ which gives a corresponding critical shear load per mm, Q_{cr}, of some 14% greater than above

Diaphragm shear buckling has not been studied experimentally to any great extent due to the fact that the points of support, such as purlins, are usually sufficiently close that failure of the connections occurs before the buckling load can be reached. This will undoubtably be the case for folded plate roofs, as will be discussed in Chapter 10, shear buckling is an important design limitation.

It should be noted that Reissners'[55] equivalent formula for Q_{cr} has a constant term of 33. However, from experimental observations and theory, Easley showed there is some post buckling strength which does raise the buckling load, and hence the above formula is sufficiently accurate for design use. Plate (12.1) shows a typical shear buckling failure of highly orthotropic sheeting.

9.2. Special Notes on the Shear Buckling Formula

The simplified formula for the critical shear load of orthotropic sheeting is given as,

$$Q_{cr} = \frac{36}{b^2} \; Dx^{1/4} \; Dy^{3/4}$$

Dx and Dy may be expressed in terms of the dimensional properties of the corrugation according to,

$$Dx = \frac{d}{s} \cdot \frac{Et^3}{12(1 - \nu^2)} \quad \text{and} \quad Dy = E\bar{D}t$$

where s/d is the profile perimeter to pitch ratio and $\bar{D}$ is the profile inertia for a 1mm thick sheet. E is Young's modulus, t is the sheet thickness, and ν is Poisson's ratio.

$$\text{So,} \quad Q_{cr} = \frac{19Et^{3/2} \; \bar{D}^{3/4}}{b^2 \left(\frac{s}{d}\right)^{1/4}}$$

Two practical observations may be made from this equation in cases where a diaphragm is subject to high shear and normal loading typical of folded plate roofs using corrugated steel. A whole range of possible sections and sheet thicknesses exists and it is not apparent which criteria control the optimization of the buckling load.[60]

For symmetrical profiles where the top and bottom plate widths are equal, the relevant parameters may be combined for constant material volume, V, and section modulus, Z, such that,

$$V = st \qquad Z = \frac{2\bar{D}t}{h}$$

$$\text{Thus} \quad Q_{cr} = \frac{11}{b^2} (VZ)^{3/4} \; d^{1/4} \; \frac{h^{3/4}}{s}$$

where h is the profile depth.

If V, Z and d are kept constant then,

$$Q_{cr} \propto \frac{h^{3/4}}{s}$$

The section which maximizes the buckling load must maximize the depth and minimize the corrugation perimeter.

Fig. (9.2) shows the gain in buckling load for various side slopes of corrugation of the same section modulus and material volume as a rectangular profile 1 mm thick and 30 mm deep. It is clear that a triangular profile would tend to be most suitable from buckling considerations.

The second observation refers to the possible design problem where the shear buckling load of the sheeting is above the capacity of the diaphragm designed on simple bending alone. In this case it is debatable whether to increase the sheet depth or thickness. Considering a rectangular profile, it follows that by increasing the sheet thickness, dt, the gain in buckling load dQ, is,

$$\frac{dQ}{Q} = \frac{3}{2} \cdot \frac{1}{t} \cdot \frac{dV}{(2h + d)} = \frac{3}{2} \frac{dV}{V}$$

A similar expression may be derived by taking a small increment, dh, in the profile depth. For all practical values of $\frac{h}{d}$, it may be shown that it is more beneficial to increase the profile depth than sheet thickness to raise the shear buckling load.

The formula for Q_{cr} only applies for a uniform orthotropic medium. Local buckling around the fasteners in relatively wide trough plates is a severe design limitation. This has been observed for 100 mm wide trough plates using self tapping screws in 0.6 mm thick sheet, and occurred at 3.7 kN fastener force. A typical local buckling failure is illustrated in Plate (9.1).

In recent years, many innovations have been made in wall panels which use flat panels periodically stiffened, as in fig. (9.3). Clearly, shear buckling may occur by a combination of local inter-stiffener buckling and overall failure, which can only be merely approximated by theory. Profiles, themselves, may have sufficiently wide troughs that failure occurs across only one or two corrugations, which consequently have a lower average Dy value than that assumed in the evaluation of Q_{cr}. Hence care must be taken in the use of the buckling formula, especially with regard to the equivalent orthotropic medium.

9.3. Effect of Periodic Intermediate Purlin Fasteners

The simple theory for the shear buckling of corrugated diaphragms has been developed by assuming that the buckling wave is made up of sinusoidal curves of pitch b and ℓ in the y and x directions respectively, as in Fig. (9.1).

For highly orthotropic sheeting the wave is at a small angle to the major bending stiffness direction which may be as low as 5^{o} and hence the practical boundary conditions may influence the buckling wave. The fastener spacing may also be close to the pitch of the x direction sine wave.

Diaphragms usually consist of a number of purlins with sheeting spanning between. Fastenings are often relatively sparce at the internal purlins compared to the perimeter members, and may be as far apart as 450 or 600 mm.

Shear buckling is ideally confined to each bay separately, but the above conditions are suitable for a wave to pass between the internal attachments, over the full diaphragm depth. This may severely reduce the buckling capacity as determined from Easley's formula.[20] However, the theoretical analysis of a buckle passing between the intermediate purlin fixings is only a special case of the energy method where, for (n-1) intermediate purlins (n > 2).

ℓ - the wave pitch equals p', the internal fastener pitch
k - the wave inclination equals n.mp/b where m is an integer
b - is the overall panel length

$$Q_{cr} = Dx \frac{\pi^2}{b^2} \left\{ \left(\frac{1}{2mn} + 3mn + \frac{(mn)^3}{2} \right) \frac{p'}{b} \cdot \frac{Dy}{Dx} + \frac{1}{2mn} \cdot \left(\frac{b}{p'} \right)^3 \right\}$$

Easley's equivalent formula for this case is,

$$Q_{cr} = \frac{36n^2}{b^2} Dy^{3/4} Dx^{1/4}$$

Again Dy and Dx are the major and minor bending stiffnesses respectively. Q_{cr} is in units kN/mm length. Easley's formula may be expressed in terms of a buckling parameter X, where,

$$X = 36n^2 \gamma^{3/4} \quad ; \qquad \gamma = \frac{Dy}{Dx}$$

$$Q_{cr} = X \frac{Dx}{b^2}$$

Corresponding values for the two intermediate purlin case are shown in Fig. (9.8), where m is chosen to minimize the buckling capacity. The controlling parameters are γ and p/b.

However, for one intermediate purlin the slope of the buckling wave, k, is a variable as it is not confined by the pitch of the internal fastenings.

$$\frac{dQ_{cr}}{dk} = 0; \quad \text{So,} \quad Dy \left\{ -\frac{g^2}{2k^2} + 3 + \frac{3k^2}{2g^2} \right\} - \frac{Dx}{2k^2 g^2} = 0$$

where g = p/b. Solving for k/g gives,

$$\frac{k^2}{g^2} = -1 + \sqrt{\frac{4}{3} + \frac{1}{3} \cdot (\gamma g^4 - 1)} \quad = \alpha^2$$

Reinsertion into Q_{cr} gives,

$$Q_{cr} = \frac{\pi^2 Dx}{b^2} \left\{ \alpha g \left\{ \frac{1}{2\alpha^2} + 3 + \frac{\alpha^2}{2} \right\} \gamma + \frac{1}{2\alpha g^3} \right\}$$

This represents the minimum value of the buckling load, for values of p/b and γ as shown in Fig. (9.7).

It should be noted that this theory is an over-simplification, as the buckling wave must be free to rise and depress equally. However, due to the intermediate purlins this condition is violated and only uplift can occur. Hence, this derivation is a lower bound to the buckling capacity.

A number of experimental tests were performed on various diaphragm configurations to justify this theory and the buckling load (kN/mm) is expressed in terms of the parameter X. The experimental and theoretical

comparisons for attachment to intermediate purlins are discussed in Section (9.5).

9.4. Effect of Sparce Perimeter Attachments

The simple buckling theory requires that all points on the perimeter act as though simply supported. However, for fasteners at relatively wide spacing, there is a possibility that a cylindrical shape buckle could form between the edge attachments. This has been experimentally observed, as in Plate (9.4). Fig. (9.6) shows how the length and inclination of the buckling wave are determined by the pitch of the fasteners.

This mode of failure is very possible for highly orthotropic sheeting where fasteners are in alternate or every third trough. To obtain a realistic estimate of the shear buckling capacity the deformation is assumed to occur in the usual sinusoidal mode, but an additional end uplift component is included. This is because the corrugation is free to rise at the end purlins but must depress on a sinusoidal curve, with zero end movement.

Analytically, the wave form is represented by two equations.

$$W_1 = A \sin \frac{\Pi y}{b} \cdot \sin \frac{\Pi}{p} (x - ky)$$

$$W_2 = \frac{A}{2} (1 - \sin \frac{\Pi y}{b}) \quad (1 - \cos \frac{2\Pi}{p'} (x - ky))$$

W_1 is the overall sine wave, and W_2 is an additional uplift such that $(W_1 + W_2)$ is of constant magnitude along the cylindrical buckle shape. W_2 is fixed-ended in the x direction, as shown in Fig. (9.6), which is due to the clamping effect of the fasteners.

The total internal energy is the sum of the orthogonal bending components and is equated to the work done by the shear flow. Due to the combination of waves the average energy is determined by,

$$W = \frac{(W_1 + W_2)^2}{2} + \frac{W_1^2}{2} = W_1^2 + W_1 W_2 + \frac{W_2^2}{2}$$

The longitudinal bending energy is,

$$\frac{Dy}{2} \int_0^b \int_0^p \frac{d^2w}{dy^2} \, dy.dx$$

which may be evaluated to give,

$$\{ \frac{k^4}{g^4} . 0.25 + \frac{k^2}{g^2} . 0.47 + 0.07 \} \quad Dy \, A^2 \frac{pb}{8} . \frac{\pi^4}{b^4}$$

The lateral bending energy is,

$$\frac{Dx}{2} \int_0^b \int_0^{p'} \frac{d^2w}{dx^2} \, dy.dx$$

$$= A^2 bp' \frac{\pi^4}{b^4 g^4} = 0.27 \quad \text{where } g = \frac{p'}{b} \text{ and m is an integer}$$

The work done by the shear flow Q_{cr} is,

$$Q_{cr} \cdot \int_0^b \int_0^{p'} \frac{dw_1}{dx} \cdot \frac{dw_1}{dy} + \frac{1}{2} \frac{dw_2}{dx} \frac{dw_1}{dy} + \frac{1}{2} \frac{dw_2}{dx} \cdot \frac{dw_2}{dy} + \frac{1}{2} \frac{dw_1}{dx} \frac{dw_2}{dy} \cdot dx \, dy$$

$$= Q_{cr} A^2 . bp . \frac{\pi^2}{b^2} . \frac{k}{g^2} \cdot 0.37$$

Solving for Q_{cr} gives,

$$X = \pi^2 g^2 / k \left\{ \gamma \{ 0.67 (\frac{k}{g})^4 + 1.27 (\frac{k}{g})^2 + 0.19 \} + \frac{0.73}{g^4} \right\}$$

where $Q_{cr} = \frac{X \, Dx}{b^2}$

If $k = m . \frac{p'}{b}$, then

$$X = \gamma \frac{p'}{b} \{ 6.6 \, m^3 + 12.5m + \frac{1.9}{m} \} + (\frac{b}{p})^3 . \frac{7.2}{m}$$

Usually m = 1 and so,

$$X = \gamma \cdot \left(\frac{p'}{b}\right) 21.3 + \left(\frac{b}{p}\right)^3 \cdot 7.2$$

If there are (n - 1) intermediate purlins then,

$$X = \gamma \cdot \frac{p'}{b} \{6.6\ (m)^3 + 12.5\ (m) + 1.9/(m)\} + \left(\frac{b}{p'}\right)^3 \cdot 7.2/(m)$$

where m is an integer to give the lowest value of X.

Again usually m = 1, and so, for 1 intermediate purlin,

$$X = \gamma \left(\frac{p'}{b}\right) 80 + \left(\frac{b}{p}\right)^3 \cdot 3.6$$

for 2 intermediate purlins,

$$X = \gamma\left(\frac{p'}{b}\right) 216 + \left(\frac{b}{p'}\right)^3 \cdot 2.4$$

Both these equations give a buckling load considerably less than the accepted formula where,

$$X = 36\ n^2\ \gamma^{3/4} \quad \text{and} \quad Q_{cr} = X\ Dx/b^2$$

Theoretical curves are shown in Figs. (9.9) and (9.10) for two cases of no and two intermediate purlins. For end attachment only, it is clear that length to fastener pitch ratios of 10 would fail at about 30% less than the above formula. This is an extremely likely situation in practice typically for a 3 metre long sheet, fastened in alternate troughs.

The family of curves for the two intermediate purlin case are very similar to those of Section (9.3) where fastenings are widely spaced only at the internal connections. It may be infered that the end conditions have a rapidly decreasing effect as the number of purlins increases, and, that the buckling load is more controlled by the purlin spacing and internal fastener pitch than end uplift.

9.5. Discussion of Theoretical and Experimental Results for Shear Buckling

For simple diaphragms, fastened in every trough around their perimeter,

the critical shear buckling load is sufficiently accurately given by,

$$Q_{cr} = \frac{36}{b^2} Dy^{3/4} . Dx^{1/4} \qquad (kN/mm)$$

where,

$$Dx = \frac{Et^3}{12(1 - \nu^2)} . \frac{d}{s} \qquad \text{and } Dy = \frac{\overline{E}Dt}{}$$

as defined in Section (9.2).

Experimental results are given in Appendix Table (1.12) which show that, in general, the actual shear capacity is within 5% of the theoretical value. If the panel width becomes less than the sheet length some strengthening may be observed, due to the fact that the rafters interfere with the free formation of the buckling wave. This is noticeable for less orthotropic sheeting.

The theory assumes that the corrugation may be hypothetically represented by an orthotropic medium. Thus for a given profile shape, the buckling load should be independent of whether the sheeting is used in its correct or inverted form. In addition, vertical loading should not affect the performance of the diaphragm. Both these statements were experimentally verified.

A range of $\gamma (= \frac{Dy}{Dx})$ values were examined, ranging from 2×10^3 to 12×10^3 kNmm. For diaphragms involving sheets spanning across a number of intermediate purlins, a considerable reduction in the theoretical buckling load was apparent. In theory a buckling wave will form in each sheet between purlins, independently of the neighbouring spans. Thus the above buckling formula will be increased by a factor n^2 where (n - 1) is the number of intermediate purlins.

For example, attachment to a single internal purlin ought to increase the buckling capacity of a sheet length b by four times. However, as outlined in Section (9.3), with sparce intermediate purlin fixings, it is possible for a buckling wave to pass between the internal connections and to span over the full diaphragm depth. The critical buckling load may be

expressed as,

$$Q_{cr} = X \frac{Dx}{b^2}$$

The variation of this buckling parameter, X, is shown in Figs. (9.7) and (9.8) for one and two intermediate purlins for a range of values of b/p, where p is the pitch of the internal fasteners. It is clear that for practical values of b/p, there is a considerable reduction in the shear buckling load. The experimental results are above this lower bound prediction, which assumes that the intermediate purlins do not prevent depression of the buckling wave. This extra restraint to the formation of a wave over the complete panel depth will raise the buckling capacity.

In general, the observed failure loads seem to be roughly mid-way between the upper and lower bounds defined by $X = 36\ n^2\ \gamma^{3/4}$ and the proposed theoretical curves. Nevertheless, in most cases the experimental results were about 30% less than simple theory. An aluminium diaphragm was also tested which showed the same behaviour. Plates (9.2) and (9.3) show typical failures.

Another limitation to the buckling load is the possibility of a cylindrical buckle, rather than a sine wave, forming over the diaphragm depth due to periodic perimeter fixings. An approximate energy method solution has been outlined in the previous section. Plate (9.4) shows how uplift has occured uniformly along the sheet depth with slope and wave length determined by the pitch of the perimeter fasteners.

Simple theory reductions of about 20% were observed for this case, for no intermediate purlin. In addition, tests were also performed with intermediate purlins attachments, which also appeared to give lower results than the more frequent perimeter fastening cases.

In every case of intermediate purlin attachment the failure load was less than the simple formulation. However, the recorded buckling capacities did agree remarkably well with the energy method approach of Section (9.3) considering the approximate nature of the assumed buckling wave.

Typically a b/p ratio equal to 10n, where (n + 1) is the number of purlins seems to be the most critical case, which corresponds to a 3m span between purlins with alternate trough fastening.

As a conclusion from the experimental and theoretical investigation, many practical diaphragms fail below the simple shear buckling formulation.

It may be suggested as a reasonably safe design value for diaphragms with intermediate purlins or sparce perimeter fixings, that the design buckling capacity should be no more than 50% of the value based on the simple formula for sheet buckling between neighbouring purlins. However, for single span panels fastened in every trough, Easley's shear buckling formula may be used with confidence. This is used as a design equation for folded plate roofs utilizing corrugated steel where the actual sheet capacity is often a critical factor.

9.6. Shear Buckling of Hyperbolic Paraboloid Shells

Hypar shells have pleasing architectural properties and due to their double curvature, uniform out of plate loading may be transmitted as in-plane stresses. Another advantage is that the surface may be constructed from straight line generators which are twisted relative to each other along their length. This corrugated sheeting is ideally suited for these types of membranes both from a practical and theoretical viewpoint.[61]

The surface is defined by a rise of unit c over panel widths a and b, and hence,

$$z = c \frac{xy}{ab}$$

which produces an in-plane shear flow of $\frac{abq}{2C}$, where q is the normal loading per unit area.

A hyperbolic paraboloid shell is subject to a uniform shear stress and thus its inplane deflection and shear buckling properties will be very similar to those discussed for flat diaphragms.

The effect of the curved surface will raise the shear buckling capacity above that predicted by,

$$Q_{cr} = \frac{36\ Dx^{1/4}\ Dy^{3/4}}{b^2}$$

where b is the span of the sheeting.

Hypars have only recently been studied theoretically and experimentally, and in 1970 a huge 70 metre cantilever module structure[22] was built for American Airlines in San Francisco. Although essentially a folded plate form of design, the sheeting spanning between the fold lines was warped along its length to give added buckling strength.

Gergely[62] has made model studies, and proposed a finite element analysis[63] which takes into account sheet instability. However, his most useful contribution was the adaptation of Easley's shear buckling theory to this doubly curved shell[23]. Nevertheless, he was unable to develop an equation showing the advantages of a hyper curvature over the capacity of a flat sheet. The subsequent analysis follows Gergerly's approach but goes one step further by deriving a controlling equation for the shear buckling strength of a hyperbolic paraboloid shell, utilizing single span corrugated sheeting.

The buckling wave is again defined by,

$$W = A \sin \frac{\Pi y}{b} \sin \frac{\Pi}{\ell} (x - ky)$$

where ℓ and k are the pitch and the slope of the wave respectively, as in Fig. (9.11).

Due to the curvature of the surface an out of plane movement, w, creates a shear strain given by,

$$2W \frac{d^2 z}{dxdy} = \frac{2C}{ab} \cdot w$$

Thus the total energy due to the formation of the buckling equation not only includes the orthogonal bending stiffnesses, but also an additional component due to the absorbed shear strain of magnitude.

$$\frac{1}{2}\int_0^b \int_0^\ell 4.Gt.\ w^2\ \left(\frac{C}{ab}\right)^2\ dx\ dy$$

where Gt is the shear stiffness of the sheeting. This does not include sheet distortion, which can only occur when the shear strain is constant. Gergerly[23] used the effective shear stiffness which is in error.

Thus equating to the work done by the shear flow Q.

$$Q = \frac{\Pi^2}{b^2}\left\{\frac{Dx}{2kg^2} + Dy\left(\frac{g^2}{2k} + \frac{k^3}{2g^2} + 3k\right) + 2\left(\frac{cb}{a}\right)^2 \frac{Gt}{\pi^4} \cdot \frac{g^2}{k}\right\}$$

where $g = \frac{\ell}{b}$

To obtain the critical shear flow, Q_{cr}, the expression in terms of k and g must be minimized. Hence,

$$\frac{dQ}{dk} = 0 \text{ and } \frac{dQ}{dg} = 0$$

$$\text{If } \bar{G} = \left(\frac{cb^2}{a}\right) \cdot \frac{Gt}{\Pi^4}$$

Eliminating the term in Dx it follows that,

$$4\bar{G} = Dy\left\{\frac{2k^4}{g^4} + \frac{3k^2}{g^2} - 1\right\}$$

$$\frac{k^2}{g^2} = -0.75 + \sqrt{1.06 + 2\,\bar{G}/Dy} \quad = \alpha^2$$

As Gt tends to zero, so k/g = 0.53, which is correct for a flat sheet.

Similarly, substituting α^2 into $\frac{dQ}{dk} = 0$, it may be shown that,

$$\gamma = \frac{Dy}{Dx} = \frac{1}{g^4\{-1 - 4\,\bar{G}/Dy + 3\alpha^4 + 6\alpha^2\}}$$

Again if $\bar{G} = 0$ $\quad \frac{Dy}{Dx} = \frac{1}{g^4}$ which is true for a flat sheet.

Insertion into the formula for Q gives,

$$Q_{cr} = \frac{\pi^2 Dx}{b^2} \cdot g \quad \{ \frac{1}{2\alpha g^4} + \gamma\{\frac{1}{2\alpha} + \frac{\alpha^3}{2} + 3\alpha + \frac{2}{\alpha}\frac{\bar{G}}{Dy} \}\}$$

$$= 36\ Dx^{1/4}\ \frac{Dy^{3/4}}{b^2} \cdot \frac{0.32}{\alpha}\{ 1 + 4\ \bar{G}/Dy + 3\alpha^2 \}^{0.75}$$

Thus the gain in the critical buckling load is given by this second term in brackets where,

$$\alpha = \sqrt{- 0.75 + \sqrt{1.06 + 2\ \bar{G}/Dy}}$$

For a rectangular profile of height, h,

Dy tends to $\frac{th^2E}{4}$ and Gt is $\frac{Et}{2.6}$, which consequently gives $\frac{\bar{G}}{Dy}$ in proportion to $(\frac{c}{h})^2$.

Fig. (9.11) shows the variation of the $\frac{\bar{G}}{Dy}$ parameter in terms of the factor F where,

$$Q = \frac{36}{b^2} Dx^{1/4}\ Dy^{3/4} \cdot F \qquad kN/mm$$

When $\frac{\bar{G}}{Dy}$ equals about 2, the buckling capacity is almost doubled. For large values of corner uplfit, c, the factor F rises in proportion to roughly (c/h).

For experimental comparison Gergerly[62] listed the failure load of a single skin hypar of dimensions 1.8 m square and 0.36 m corner uplfit, as 3.35 kN/m^2.

This corresponds to an inplane shear flow of,

$$q = \frac{abw}{2C} = \frac{1.8^2 \times 3.35}{2 \times 355} = 0.015\ kN/mm$$

The corrugation data, for a sheet thickness of 0.4 mm, is,

Dy = 1180 kNmm; $\qquad$ Dx = 0.85 kNmm

$$\frac{\bar{G}}{Dy} = \left(\frac{cb}{a}\right)^2 \frac{Gt}{\Pi^4 Dy} = \frac{360^2 \times 80 \times 0.4}{\Pi^4 \times 1180} = 36.0$$

$$\alpha = \sqrt{-0.75 + \sqrt{1.06 + 36.0}} = 2.30$$

$$F = \frac{0.32}{2.30} \{1 + 4 \times 36.0 + 3 \times 2.30^2\}^{3/4} = 6.28$$

$$Q = \frac{36 \times 0.85^{0.25} \times 1180^{0.75}}{1800^2} \times 6.28 = 0.013 \text{ kN/mm}$$

This is reasonably in agreement and the extra strength in practice is probably due to restraint at the panel edges.

The assumed buckling wave concept may be applied to any curved surface, providing that the in-plane shear flow is uniform. Cylindrical shells, where corrugations span around the surface, deform by an additional in-plane shear strain due to normal displacements. Thus the total energy not only includes the simple orthogonal bending energies but also requires an additional component due to the effect of curvature.

This is illustrated in Fig. (9.12). However, due to the very flexible nature of the sheeting perpendicular to the corrugations, any shear strain generated due to buckling displacements is partly relieved by lateral inplane movement. Abdel-Sayed[24] has studied the shear buckling performance of cylindrical shells by solution of the controlling differential equations in terms of Fourier series.

Plate (9.3) Buckling wave passes through alternate trough fastenings at two intermediate purlins

Plate (9.4) Buckling between alternate trough perimeter fasteners

C H A P T E R 1 0.

FOLDED PLATE ROOFS

10.1. THE FOLDED PLATE CONCEPT

Folded plates may be defined as structures which rely on the mutual support of a number of laterally flexible flat surfaces, to transfer loading into in-plane forces. The changes of geometry are termed fold lines.

Prismatic folded plate structures are the classical form of construction which have been developed with the use of reinforced concrete. The name 'hipped' connotes folded plate construction when applied to roofs and other forms have been used for box beams and grainbins. Plates meeting at a shallow angle may be pieced together to form cylindrical shells.

Fig. (10.1) shows the various geometrical arrangements of hipped roof ranging from the simple prismatic shape to a warped hyper form. Circular folded plates are a pleasant architectural form supported only on perimeter columns and an inner compression ring. This construction has been used for a large arena in Madison, Wisconsin, U.S.A. (64)

The basic structural action is one where applied loads are resolved into two components, one perpendicular and one parallel to the plate surface. Normal loads cause slab action which spread the out of plane forces back to the fold lines and the net fold reactions are resolved parallel to the plate surfaces.

This in-plane loading is then transmitted longitudinally to the supports by plate action. The free movement of the fold lines means that for continuous slab action, moments are generated at the fold lines similar to a beam on elastic supports. Any analysis must also provide for compatibility of both stress and deflection at the fold lines.

During the 1950's and 1960's a considerable amount of work was carried out on concrete hipped roofs to account for the effect of continuous slab action.

The first design of concrete folded plates was suggested by Winter and Pei[65] in 1947. This was followed by Craemar[66] and later Gaafar[67] in 1954 who proposed the most clear method of analysis. The lateral bending is considered in two steps - firstly moment distribution for unyielding supports and then applying unknown displacements at each joint to find the resulting in-plane plate forces. The longitudinal action must produce displacements which are compatible with the transverse action.

A number of authors such as Thadani,[68] Ketchum[69] and Simpson[70] followed this approach and Traum[71] in 1959 summarized the iterative - corrective techniques, and the exact slope deflection methods. He also proposed the method of particular loading. Baer[72] designed a steel folded plate roof with inplane trusses.

In 1961 Shapiro[73] performed an insitu load test on a 14 metre steel folded plate roof using double skin corrugated sheeting of 1.1 mm thickness and obtained a safety factor of 3.

Nilson[74] at Cornell University initiated a study of the use of corrugated diaphragms in folded plate construction, and a number of companies began to market the standard materials for design. The first problems were met between responsibility for design and supply of materials, as from this time onwards the roofing contractor had to ensure the safety of the whole building.

With the advent of computers, Scordelis[75] in 1961 proposed a matrix method of analysis and also performed some model tests. Yitzaki[76] in 1962 used Traum's method by which he first considers the fold lines to be spatially fixed and calculates the resultant in-plane forces. Consequently, the longitudinal plate deflections may be determined using the theorem of three shears as outlined by Born[77]. To remain in this deflected shape certain unknown fold line forces have been generated. By the method of particular loads each force system may be applied in turn until the out of balance reactions are set to zero, consistent with a modified deflected shape.

Meek[78] also presented a matrix derivation in terms of the slab and plate actions and Fialkow[79] developed an energy method solution.

In 1963 the American Society of Civil Engineers summarized all the previously presented analyses. Following the simplified methods for long span folded plates, a number of authors turned their attention to short spans where slab action occurs in two directions. Notably Goble,[80] Setharamalu,[81] De Fries,[82] Lee[83] and Reiss[84] developed stiffness approaches of general application.

Powell[85] compared all the existing theories in 1965 which marked the end of the 'hand' method of analysis. Beaufait[86] studied continuous folded plates over a number of supports and Farmer[87] developed a non-linear approach. Mast[88] claimed to have presented an 'exact' analysis in 1967 and Johnson[89] began a theoretical and experimental study of non-prismatic folded plates. Lee[90] analysed the effect of the support conditions and in 1969, Cheung[91] introduced the finite strip method.

Meanwhile steel folded plates had gradually been not only researched but also constructed in increasing numbers from the early 1960's. A number of articles describe their inherent simplicity, for all forms of application such as halls, banks,[92] and gymnasia with spans generally ranging from 10 to 30 metres.[93]

Conferences in cold formed structures highlighted the increasing economies of using steel rather than concrete especially with a double skin construction which is also the finished underside of the roof. The lower flat sheet, spot welded to profiled sheeting, is perforated to improve its acoustic properties.

An advantage in the design of all steel folded plates is that the fold line joints are effectively pinned laterally which obviates the need for complex analysis. Up to now almost 80 folded plates have been constructed in regions where the snow loads are very high. In recent years the high cost of in-situ welding have reduced the material economies and it was for this reason that it was decided to build a prototype folded plate roof using mechanical fixings at Salford University. Following the work of Thompson[21] and Davies[94] the basic data for using open profiled sheeting are known and a full scale test demonstrates that the design criteria may be extrapolated accurately.

Hyperbolic paraboloids using corrugated sheeting received world-wide notice with the construction of 70 metre cantilevered Jumbo Jet modules in San Franscisco in 1970, saving 40% by weight over conventional designs.[22]

Shoeller et al[95] in 1972 proposed a finite element technique for steel folded plates which could be applied to all shapes of roof.

At the present time the American Iron and Steel Association is compiling a design manual for folded plate construction using welded steel decking.

The erection of steel folded plates has generally been a modification of that used for concrete, by shoring under the fold lines. However, construction at ground level and lifting into position, as revealed by the Jumbo Jet aircraft hangars, does have advantages.

In Europe, steel folded plate construction has only been used in one or two cases, notably for an 18m hall in Nantes, France. A building of interest utilizing a form of folded plate resistance has been developed for nursery school units in Surrey, England by M.A.C.E.*[96]. In this case the building is 11 metres square with a central roof light supported on an inner compression ring. The walls provide local support for an outer tension ring and folded plate action occurs by tranferring in-plane loads back to corner diagonal members.

10.2. Folded Plate Analysis as Applied to Concrete Roofs

The problem of lateral bending continuity around the fold lines makes the analysis of concrete folded plates very difficult. As previously discussed a considerable number of authors have proposed theories for the effect of fold line bending moments, some based on matrix techniques, others on energy solutions, and still more on iterative methods.

A simplifying assumption is that the length to width of the plates is sufficiently large, so that each act as longitudinal girders without

* Metropolitan Architects Consortium for Education

any deep beam effects, and have an approximately sinusoidal deflected shape.

In general, the analyses take the following form, whereby the in-plane forces are a function of their own displacements as well as the applied loading. Three distinct parts may be described corresponding to the lateral and longitudinal actions which are complexly inter-related.

1. For the imposed loading on each plate, the inplane component is separated, and the roof shape spread out to form a continuous beam where supports exist at all the fold lines. The normal loading causes joint reactions as determined by the joint bending moments resulting from an analysis of the beam. Thus the net support reactions are separated vectorially according to the actual roof geometry and are combined with the previous in-plane loading. The total is given as a resultant applied load w_i in the direction of each of the plates.

2. The second part of the analysis refers to the effect of in-plane joint displacements δ_i on the cross-sectional bending moments and are assumed to occur sinusoidally along the roof length. Each displacement δ_i of the i th plate is an unknown, but according to the Williot diagram of Fig. (10.3) the out of plane displacements V_{i1} and V_{i2} at each end of the plate may be determined in terms of δ_i.

Thus the fold line bending moments are functions of δ_i and θ_i, the joint rotation, according to,

$$\begin{bmatrix} M_{i1} \\ M_{i2} \end{bmatrix} = 1/D \begin{bmatrix} 6/d_i^2, & 4/d_i, & 2/d_i \\ 6/d_i^2, & 2/d_i, & 4/d_i \end{bmatrix} \begin{bmatrix} V_{i1} - V_{i2} \\ \theta_i \\ \theta_{i-1} \end{bmatrix}$$

The rotations of the fold lines, θ_i may be then eliminated. Hence, the cross-sectional bending moments cause fold line forces which again may be separated vectorially into in-plane components. Consequently, the effective uniform in-plane force of the ith plate may be given as,

$$W_i^1 = W_i + 2/\Pi \ (a_{i1}\delta_1 + a_{i2}\delta_2 + a_{in}\delta_{in})$$

where the factor $2/\Pi$ represents the modification of a sinusoidal form of loading, resulting from the joint displacements, to a uniform loading. The constants a_{ij} reflect the influence of the in-plane displacement of the jth plate on the effective loading of the ith plate.

3. The effective in-plane loading W_i^1 causes a central bending moment given by,

$$M_i = W_i^1 L^2/8$$

which is assumed to decay sinusoidally.

Consistent with this bending moment is a linear stress variation of maximum value,

$$\sigma_{oi} = \frac{6M_i}{td_i^2}$$

However, at neighbouring joints there is a consequent incompatibility of axial strain. This is relieved by longitudinal shears T_i giving a net stress distribution of,

$$\sigma_i = \sigma_{oi} + \frac{2}{3} T_i + \frac{1}{3} T_{i-1}$$

$$\sigma_{i-1} = -\sigma_{oi} - \frac{1}{3} T_i - \frac{2}{3} T_{i-1}$$

Solving for each plate, yields simultaneous equations in T_i and thus the final stress distribution may be determined in terms of θ_{oi}, etc.

The in-plane deflection is now controlled by the stress difference across a given plate and is represented as,

$$\delta_i = \frac{\{\sigma_i - \sigma_{i-1}\}}{Ed_i} \left(\frac{L}{\Pi}\right)^2$$

But σ_i is a function of W_i^1 which is in turn dependent on the loading W_i, and the joint displacements, δ_i. Thus for n plates, n equations may be solved for each of the in-plane displacements in terms of the applied loading. The cross-sectional bending moments may be recalculated.

The edge beams are usually designed to be torsionally stiff so that the final joint rotation does not cause large outward displacements. It has also been assumed that the internal plates are very thin, so that torsional effects have been neglected.

10.3. Folded Plate Roof Design using Corrugated Steel Sheeting

The basic behaviour of a folded plate is to resolve out of plane forces into in-plane components which are resisted by longitudinal beam action. This is a very simple concept when applied to corrugated sheeting spanning between fold line members.

For a saw tooth roof design, a typical internal bay acts like a girder spanning between end frames. Bending resistance is provided by the fold line members to which the sheets are attached and the sheets themselves, act as an inclined web. Thus, the corrugated sheeting must transfer the complete roof shear force to the end gables. (Fig. (10.2)).

According to folded plate action, the sheeting serves to spread local forces back to the fold lines, which resolve the net resultants vectorially into in-plane loading. Hence the corrugated sheeting acts in its two most stiff modes - shear and bending, and relies on the strength of the connections.

A simplifying advantage of using corrugated sheeting is that there is little lateral rotational continuity at the fold lines which means that the sheet span merely acts in simple bending. The roof action is thus internally statically determinate and the fold line deflections do not influence the internal force system, which is not true for concrete folded plates.

As with all beam deflections, both axial strain and shear components are included. The in-plane deflections of the neighbouring plates are added according to the Williot principle of Fig. (10.2) whereby out of plane movements are assumed to be completely flexible.

The shear deflection of corrugated sheeting has been studied in Chapter 2 when fastened in every corrugation. It is considered that this should be the usual fastening mode whatever the roof length due to the relatively short sheet span which greatly increases the shear distortion component of deflection. For smaller roof lengths, alternate fastening may be used towards the centre of the span if the deflection limitation permits.

For the case of variable fastening along the roof lengths with relatively stiff fold members, some reduction from the simple theory is possible and this will be discussed in Section (11.3). Similarly holes in folded plate roofs are theoretically possible in the region of zero shear force, and this is examined in Section (11.1).

For vertical imposed loading the separation into in-plane forces is depicted in Fig. (10.2) for a typical folded plate roof. It may be seen that at the outer plate, an edge beam is required to absorb the local out of plane forces.

Wind loading, which may be represented as a horizontal eaves force, is split vectorially into in-plane components and the edge beam suffers an uplift force which implies that the compression chord is laterally unsupported.

All the internal fold members are completely restrained from

instability which means that, neglecting local buckling of the member, the full axial stress may be generated.

The axial stress pattern itself can only be determined by studying the folded plates acting in combination. A simplifying approach is to assume half the fold area acting with each plate, but for variable in-plane loads and fold area sizes, this is a very crude assumption.

The exact solution is outlined in Fig. (10.4) where the ith plate is subjected to in-plane loading W_i and has fold areas A_i and A_{i+1}. Its inertia may be determined by a simple expression and hence the $(i + 1)$th fold line stress is controlled by the superposition of the axial stresses due to the bending of neighbouring plates. It should be noted that the section modulus for the $(i + 1)$th fold of the ith plate is $A_{i+1}\ d_i$ where d_i is the plate width.

Consequently, the bending stress resultants may be determined at all fold lines, and the bending deflections are dependent on the stress difference across a plate. The deflection of the ith plate may be given by the expression of Fig. (10.4) showing the effect of loading of the neighbouring plates, which is represented as a modification factor applied to the simple bending deflection.

Corrugated sheeting must have sufficient strength in its connections to withstand the maximum shear force. Davies[96] has produced expressions for the capacity of seams and end gable fasteners. However, the usual maximum capability is determined by the strength of the sheet-fold fasteners which are themselves controlled by the corrugation pitch and the sheet thickness.

In addition the shear buckling capacity represents a severe design limitation, and in this respect, Easley's formula[20] gives a reliable figure for the buckling load of highly orthotropic sheeting. A decision table for design of a typical folded plate roof is shown below.

1. Is the clear span between end frame less than 25 metres? If not, a folded plate roof using mechanical fixings is likely to be unsuitable.

2. Choose pitch of columns between 3 and 5 metres.

3. Choose a roof slope between 20^{o} and 45^{o} remembering that structural efficiency increases with roof angle.

4. Knowing the column pitch and roof slope design the roof sheeting to span between fold lines.

5. At the design roof span, split the loading into in-plane components and evaluate the maximum shear force and central bending moment which fixes the required fold line area.

6. For fastenings in every trough evaluate the ultimate strengh of the connections reduced by the safety factor. If this is too low then the sheet thickness and/or roof slope must be increased. The required number of seam fasteners can also be determined.

7. Knowing the sheeting profile and thickness, the shear buckling capacity can be evaluated. If this is too small increase the sheet depth or reduce the column spacing.

8. The design information may now be used to evaluate the central roof deflection which includes the pure bending. Shear distortion and fastener slip components. An appropriate deflection limit may be selected and if this is exceeded, the fold area may be increased. Otherwise the sheet thickness and/or column spacing must be increased.

10.4. Formulae for Steel Folded Plate Roof Design

For two or more bays subject to a uniform vertical loading the internal plates are the most important consideration in design. However, the edge conditions are likely to be the most critical for wind loading.

As previously discussed each plate acts as a longitudinal girder

and has the same failure criteria of bending, shear and deflection.

Each of these factors has been studied for flat diaphragms and design formulae merely represent an extrapolation to uniform in-plane loading conditions.

Thus after vectoral separation of fold line reactions into in-plane components, the following steps in the analysis are required.

1. The fold line area is determined by simple bending conditions and the girder section modulus is,

$$Ab = \frac{qL^2}{8\sigma}$$

where σ is the full yield stress.

q is the in-plane loading and equals $\frac{wB}{2 \sin \theta'}$

where w is the vertical loading, B is the column spacing and θ', the roof slope.

For each plate A represents only half the total fold area and for unequal fold lines A is modified to,

$$A = \frac{2A_1A_2}{A_1 + A_2}$$

A_1 and A_2 are also half the fold line area at each flange of the plate, which may be the case where some effective area reduction is necessary for the compression chord.

As indicated in Section (10.2), this is only an approximate approach for the axial stress distribution over the complete roof.

2. The shear strength of a typical panel is controlled by the seam capacity, the end gable fastener strength and the sheet-fold strength.

The end shear force reaction is given by,

$$Q = \frac{wBLF}{4 \sin \theta}$$

where F is the safety factor.

As in Chapter (8) the design seam strength for seams in the corrugation troughs is given by,

$$Q_S = \frac{(n_s F_s + 2F_p)\ (\frac{ns}{S_s} + \frac{1}{s} g_1)}{(\frac{n_s}{S_s} + \frac{1}{S})} \times (\frac{nsh}{nsh-2})$$

where n_s is the number of seam fasteners

S_s, s are the slip of the seam and edge fasteners respectively

nsh is the number of sheets in one span

F_s, F_p are the ultimate strengths of the seam and perimeter fasteners respectively

g_1 is a factor dependent on the number of sheet-fold fasteners - see Chapter (8).

For seams in the corrugation crests, this formula becomes,

$$Q_S = (n_s + g_1\ S_{s/s})\ F_s \cdot (\frac{nsh}{nsh-2})$$

Similarly the strength of the sheet-end frame fasteners is,

$$Q_{sc} = (n_{sc} - 2 + 2g_1)\ Fp$$

where n_{sc} is the number of end gable fasteners.

It is assumed that the same fasteners are used for the sheet-fold and sheet-gable connections.

The strength of the sheet-fold fasteners is simply $\frac{b}{p}.F_p$ where b is the sheet length along the slope and p is the fastener pitch.

3. The shear deflection of the folded plate roof is determined by the components due to fastener slip, pure shear strain and shear distortion as determined in Chapter 2.

The in-plane shear distortion deflection is given by,

$$d_{1.1} = \frac{d^{2.5}\overline{K}}{Et^{2.5}\,b^2} \cdot q \cdot \frac{L^2}{8} \quad \text{where } q = \frac{wB}{2 \sin \theta'}$$

and d is the trough pitch, t is the sheet thickness, and E Young's modulus.

The panel pure shear strain deflection is,

$$d_{1.2} = \frac{(1 + \nu)\ (1 + 2h/d)}{Etb}\ q\,\frac{L^2}{4}$$

ν is poisson's ratio and (1 + 2h/d) represents the corrugation perimeter to pitch ratio.

Sheet-fold line slip is given by,

$$d_{2.1} = \frac{sp\ q\ L^2}{4b^2}$$

Seam slip, for a constant number of seam fasteners along the length is,

$$d_{2.2} = \frac{(nsh - 2)}{\left(\frac{n_s}{S_s} + \frac{gl}{S}\right)}\ \frac{qL}{8}$$

In many cases n_s will vary linearly with the applied shear force

and so $d_{2.2}$ will be doubled. Thompson[21] studied a step wise variation of seam fastenings but it is suggested that the worst case, as above, is selected.

The sheet-end gable slip is,

$$d_{2.3} = \frac{qL.S}{2(n_{sc} - 2 + 2g_1)}$$ where n_{sc} are the number of sheet-end gable fasteners. Hence the total panel shear deflection is $d_{1.1} + d_{1.2} + d_{2.1} + d_{2.2} + d_{2.3}$.

The axial strain in the fold lines contributes an additional bending deflection given by,

$$d_{1.3} = \frac{qL^4}{38.4\ EAb^2}$$

A is the half the fold line area which is again represented by $\frac{2A_1 A_2}{A_1 + A_2}$ for unequal fold areas.

The total panel deflection is modified by the factor $(1/\sin\ \theta)$ to give the vertical fold line movement as shown in Fig. (10.2).

4. The shear buckling capacity has been reliably determined by Easley and McFarland[20] as,

$$Q = \frac{36\ D_x^{1/4} D_y^{3/4}}{b}$$

where $D_x = \frac{t^3 E}{12(1 - \nu^2)} (1 + 2h/d)$

$$D_y = \frac{\bar{D}t}{d} E$$

where D_y and D_x are the sheets' major and minor bending stiffnesses respectively. $\bar{D}$ represents the cross-sectional inertia of one corrugation, not including the sheet thickness. The European Design Recommendations[47]

suggest that, due to the sudden nature of buckling, an extra 25%. reserve of safety should be used for this mode of failure.

5. The sheeting itself must simply be designed to span between fold lines, with the appropriate effective width reductions in bending. This is covered in the Metal Roof Deck Associations Manual.(98)

10.5. Prototype Folded Plate Roof Design

It was decided to test the folded plate design philosophy using corrugated sheeting by constructing a three bay roof of 21.6 metres length. The roof was selected to comply with a 3.6 metre square module size as used by the S.E.A.C.* and C.L.A.S.P.* building systems and had a total width of 10.8 metres. The clear distance between end frame represents the approximate maximum permissible span for chosen roof slope of 35^{o}.

Structural performance increases as the tangent of roof angle, as will be discussed later, and a balance had to be sought between aesthetics and material useage for such a small pitch of bays.

It is clear that, although the roof is statically determinate, many of the design factors such as buckling strength and roof deflection are highly influenced by the choice of column spacing, profile depth and thickness. For large roof spans it may be that only a narrow band of permissible geometrical arrangements is feasible.

This particular folded plate roof design of 21.6 m span and 3.6m column centres could have utilized 35 mm deep ordinary corrugated sheeting of 0.9 mm thickness. This would have satisfied the fastener strength and shear buckling requirements but the central deflection, due mainly to the distortion of the open profile, would be much greater.

It was for this reason that a closed end profile was developed which has shear stiffness approaching that of a flat sheet. In addition, by pressing rather than rolling the corrugation from the originally 1.0 mm

* South East Architects Collaboration

* Consortium of Local Authorities Special Projects

thick material, the profile perimeter to pitch ratio is equivalent to that of a 0.8 mm sheet, without reducing the trough thickness which controls the fastener tearing strength. The small reduction in crest thickness only slightly influences the simple bending and shear buckling strengths.

The chosen profile shape is shown in Fig. (10.6) and is 32 mm deep. Section (10.6) outlines the pressing operation and the shear flexibility derivation is developed in Chapter 5.1. Detailed design calculations follow in Appendix 3 and by using this pressed sheeting, central deflections are limited to about 56 mm at the working load of 1.2 KN/m^2.

The required fold line area is determined from the simple bending relationships and in order to fasten the sheets easily to the fold, a 5 mm thick cold pressed channel section was used as in Fig. (10.22). The compression member was checked for width reduction of the relatively thin section due to local buckling according to B.S.449 addendum No. 1.

Overall compression buckling of the fold member is prevented by the shear stiffness of the sheeting transferred via the fasteners, which implies that the full yield stress may be used in design.

The lower fold member also serves as a gutter with suitable pre-cambering of the roof, and slope run off is facilitated by the flat ends of the pressed sheeting.

Sheet shear force is transferred directly to the end frames, the outward component of thrust being relieved by a tie bar. The vertical force from neighbouring bays is thus passed to columns which need only be designed for axial stress.

It is important that the axial strain in the fold line members is not transferred as a bending moment to the relatively light columns. For this reason a suitably large clearance was used for the bolted connections between end frame and fold lines.

Rectangular hollow sections were used for all the end frame members, being,

101 x 101 x 6.3 mm thick for the columns
101 x 51 x 3.2 mm thick for the gable and tie members.

The folded plate concept hehaves well for internal changes of roof slope, but at the outer span, one edge will remain unsupported. In the prototype design local forces are accommodated by a vertical edge beam which again utilized the corrugated sheeting as a shear web.

Another suitable method for providing local edge support is to use periodic columns and to rely on the bending strength of the fold member. This has an additional advantage in that normally side sheets require side rails and posts for fixing. In some cases in U.S.A. an upstand side beam has been used tied back to the nearest apex member which also provides stability against lateral buckling of the edge beam.

Detailed drawings for the general layout and end frame connections are shown in Figs (10.24) to (10.27).

It should be noted that the internal roof slopes attract twice the force of the external slopes for uniform vertical loading. For wind loading, however, the horizontal eaves force is split up as in-plane components into the edge beam and outer slope.

The edge beam must also be checked for lateral instability even though its compression flange is restrained. It was for this reason that a torsionally stiff rectangular hollow section was used for the lower chord. An approximate analysis is shown in Section (11.3).

The net horizontal wind force is passed as compression force in the tie bar to end bracings. Similarly longitudinal wind forces are passed by the roof diaphragm to the eaves and then to corner braces.

Column end frame connections used a bolted gusset arrangement which facilitated the erection procedure by allowing free sliding of the roof during the lifting operation which is described in Section (10.7). For extra strength at the very high testloads the joint was welded.

The ultimate load, as previously indicated, is controlled by the connection strengths, the buckling capacity, sheet bending strength, and deflection limitations. The seam fastener strength was derived by Davies,[94] and the buckling capacity by Easley.[20] Central deflection includes the experimentally derived shear distortion component for the folded down corrugation ends.

It should be noted that the fold line members were over designed so that failure should occur by a mode associated with the sheeting. The lowest design safety factor was for seam failure, followed by sheet fold fasteners tearing, and shear buckling. An accepted seam fastener strength of 2.5 KN/mm sheet thickness was taken for the tearing of the pop rivets, although it was expected the failure might occur at a higher value due to the superior performance of an upstand seam compared to a direct overlap. The corresponding strength of self tapping screws is 6kN/mm sheet thickness.

The folded plate idea as applied to corrugated steel and cold formed members is very efficient in that each component is subjected to its most ideal form of loading. Even the columns need only be slender in order to resist axial force alone. Material wastage occurs only at the extremities of the fold lines where axial stress is low, and it may be that in prefabrication, thinner sections could be used in this region. Edge fasteners need to be in every corrugation for deflection limitation but seam fastenings may vary in proportion to the applied shear force as studied by Thompson.[97]

The performance of the closed profile sheeting was studied in individual shear panel tests and also by a 21.6 metre long plate test which shall be described in Chapter (11.4).

10.6. Design of Specially Pressed Sheeting

The main design criterion for the roof sheeting was simply to provide the required section modulus to span 2.1 metres between fold lines for a 150 mm trough pitch. However, an open profile is free to distort

and warp under shear and it was observed that by closing off the sheet ends, the shear stiffness could be raised dramatically. It was for this reason that it was decided to produce a corrugation with the full depth at the centre for bending rigidity, decreasing to a flat portion at the sheet ends.

Some companies have tried to fold down the corrugation ends after roll-forming, but for this application a pressing operation using a mould was prefered.

Preliminary tests were carried out on a small scale wooden former (1m x 0.6m) in which the corrugations were hollowed out. It should be borne in mind that the full profile depth is produced by elongation rather than bending of the metal, as very little material is drawn in from the sides during the pressing operation. The profile shape has thus to be designed with very shallow sides (45°) in order to keep within the elongation capacity of the metal. The final chosen profile is shown in Fig.(10.9). A number of different grades of metal were tested from ordinary mild steel to extra deep drawing quality and it appeared that any material with an elongation to failure greater than 30% would be suitable. The end transition had to be sufficiently smooth to allow the material to gradually elongate without wrinkling.

The pressing operation, itself was carried out at Hawker Siddeley Aviation Company Limited of Greengate, Manchester, and used their high capacity rubber press of maximum table size 1.2 x 2.4 m. The technique of pressing is to push the female former into a solid bed of rubber which moulds itself within the corrugation indentations. Thus the sheet of metal lying across the form is first gripped as it meets the rubber and then the required profile depth is drawn as the table is pushed further and further inwards. It was clear after the first trial operations, that the quality of the metal was less important than the pressure build up on the sheet. Both low and high elongation metals failed if the pressure was applied too quickly.

Eventually a pressure of 1,000 tonnes/metre^2 was selected for the full scale production. The metal chosen was a special drawing quality

steel of yield stress 160 N/mm^2 and elongation to failure of 50%. A total of 190 sheets were supplied by the Product Development Centre of British Steel Corporation, Shotton, Clwyd. The stress-strain relationship of this sheeting and a typical mild steel curve is shown in Fig. (10.28).

A special mould was constructed for the full scale sheet of dimensions 2150 x 1050 mm. This was somewhat in excess of the sheet size (2110 x 900), but it allowed the curved edge resulting from the slight drawing in, to the trimmed. The mould was made from a very hard synthetic material called 'delaron' which does not split during pressing process. Again the corrugations were hollowed into the material, as shown in Plate (5.1).

During the production run which maintained about 20 sheets per hour rate, a mild steel sheet was inserted and behaved exactly the same as the better elongation material. The measured cross sectional extensions and reduced thicknesses for the two sheets are shown in Fig. (10.9). Lines were etched on the flat sheets and the separation of each pair was measured after pressing Coupon tensile tests were also performed on samples of the sheeting to determine this elongation capaicty at failure.

By comparing the actual profile shape and the mould dimensions it is clear that some elastic rebound takes place and that the depth is almost 10% less than the mould depth.

The method of seam fastening posed some problems in that one sheet could not be easily lapped over another. This was not such a disadvantage as it is difficult to ensure a secure placing of fastener by a direct overlap. Hence, it was decided to develop an upstand trough seam inclined at 30° to the vertical which allowed placement of a 'monel' pop rivet without interfering with the neighbouring corrugation. A punch rather than drill could be used which speeds up the whole fixing operation. The seam may later be sealed for watertightness.

An additional advantage as discussed in Chapter 8 is that the upstand has slight superior shear capacity characteristics compared to a direct overlap. The sheet longitudinal edges were trimmed and each end

folded upwards in a single operation, at a rate of 50 sheets per hour.

The load-slip characteristics for a segment cut out of the actual sheeting upstand seam is shown in Fig. (10.29). Two 'pop' rivets were placed in the same fashion as on the prototype roof and at the same spacing. The ultimate strength was observed to be 2.6 kN compared to the accepted design value of 2.4 kN (2.5 kN/mm sheet thickness). However, the special drawing quality steel stress-strain curve has different characteristics to mild steel which have been the basis of previous fastener tests.

Finally, for the longitudinal edge beam a shorter length of sheet had to be pressed which was achieved by inserting a section within the full scale mould to produce the folded down end. This may be seen in plate (5.1). The edge beam depth was 1m and this also had to be designed as a longitudinal beam.

10.7. Erection of Prototype Folded Plate Roof

The stressed skin nature of the folded plate roof concept requires that the surface be continuous to spread the self weight of the roof back to the end frames. Thus during construction the complete roof structure must be supported on temporary framework.

In the U.S.A. where a considerable number of welded deck folded plate roofs have been built, construction takes place at the final roof height on scaffolding. However, the erection of the 70 metre cantilever hyperbolic paraboloid modules in San Fransisco proved that a more viable system is to set out the roof geometry on the ground and lift a complete unit into place by jacking against the columns. (22)

Thus it was decided to build the prototype folded plate structure which was in some degree novel in design, by a relatively untried erection method. The whole roof would be built at ground level and jacked in stages on the end columns to the full height.

Firstly the end columns and frames were set out. Then four triangular wooden trestles were positioned at 4.3 m centres along each span and the fold line channel members lifted into their respective positions by a small stacker truck. The folds were each one third of the full span which meant that after welding for continuity, the most highly stressed region would not coincide with the weld position. The weight of each section was suitable for lifting by four men.

After the full roof compliment of fold line members had been placed as shown in Plate (10.1) and their extremities attached by bolts to the end frames, the centre of the span was raised to provide a 200 mm camber. It was estimated that 100 mm would be needed for rainfall runoff (1:100) and that another 100mm would be lost due to the elastic sag and also the effects of testing to collapse which results in considerable permanent deformation.

It should be borne in mind that although the roof was to be tested to failure, the more catastrophic forms such as column buckling and fold line yield were designed against, so that the building could be revised as a storage area after replacing the damaged sheets.

Cambering was achieved by a hand operated jack applied under each frame in turn. The main roof sheets were now attached, the end frame member width allowing a maximum of 200 mm total deviation in overall sheet span. Edge fastenings were 5.5 mm diameter Teks 4 self drilling and tapping screws which are suitable for the 5 mm thick fold members, and have a nominal ultimate strength of 6kN/mm sheet thickness. Plate (8.1) typical screw fasteners, which could be placed by a hand drill.

Seam fastenings were 4 mm diameter Tucker 'pop'-rivets which were attached through an upstand seam as shown in Fig. (10.9). The preparatory holes were punched and the fasteners placed by an air gun. This method was extremely fast, some 300 fixings per hour being achieved. However, cat-ladders were necessary to avoid damaging the sheets during fastening. The upstand seam could also be sealed after fixing.

At this stage only the roof sheets were attached, and the attachment of edge beam was left until the final roof height had been reached. Thus

the eaves were longitudinally unsupported, and the wooden erection trestles had to be designed to resist the local inward component of self weight thrust. The total roof weight was 0.22 kN/m^2.

Lifting took place at the end frames by eight hand operated jacks which each had a maximum stroke of 300 mm. This jacking had to be carried out in stages which required fixing the end frame at each new height. This was achieved by predrilling the columns at 250 mm centres and locating a 12 mm diameter rod through the gusset plates which were bolted to the end frames. Special 'knees' were fabricated which could be reset at each new position to support the jack, and thus the roof raising operation could take place on a 'lift-reset-lift' pattern as in Plate (10.2). The complete lift took four men, operating two jacks each , about six hours.

During the entire erection process each line of columns was stiffened by external bracing. At the final height, all the connections were bolted down and the actual wind bracing positioned. Before the temporary erection trestles could be removed the edge beam had to be fixed. Firstly, the lower rectangular hollow section chord was lifted into place at the required 1 metre depth from the eaves and bolted to the corner columns. Straps held the flexible member along its length until the side sheets could be attached.

The wooden trestles could then be removed and for a system building are probably reusable. The loading system was then positioned and the total applied weight prior to testing was determined to be 0.45 kN/m^2. The roof camber settlement was observed to be of the order of 15 mm at this stage.

It should be noted that the weight of the loading system approximately equals the allowance for dead weight of 0.25 kN/m^2. Hence the jack force represents only the theoretical imposed load.

10.8. Design of Loading System

Due to imposed vertical loading, the equivalent collapse force, uniformly distributed, is 2.2 kN/m^2. After removing an allowance for the

dead weight of roof, the required total jacking force becomes about 450 kN.

The choice of the number of jacks needed for testing was influenced by the amount required for roof erection (eight). It was decided that nine 80 kN capacity jacks with a 300 mm movement would be suitable for both operations. The overall layout of the jacking points is shown in Fig. (10.7).

A hydraulic pump was specially purchased for the task of remotely loading the roof and was linked via four three way connections and considerable lengths of high pressure hose

The roof loading points had to be sufficiently close to minimize the risk of premature local sheet bending. For this reason the sheeting was chosen to be slightly thicker than necessary, but more importantly, it was considered from preliminary tests, that loading points ought to be based on a 0.9 metre square grid.

Thus 72 wooden trestles as shown in Plate (10.3) were necessary to distribute the applied load, each having four pads which rested in the corrugation troughs. To equally simulate the bending and end shear effects of a uniform out of plane loading, the point loads were set at the quarter positions on each sheet span. The applied force is vertical and to prevent these wooden trestles sliding down the slope, angle strips were fastened across neighbouring corrugation crests. Their resistance at roof failure needed to be about 0.9 kN each.

The load per point at roof failure was about 1.6kN and for each trestle a rod had to be passed through a hole in the roof sheeting to the first layer of spreader beams. The loading jacks were each associated with eight rods and hence three types of simply supported spreader beams were necessary to transfer the applied force by the 'tree' arrangement of Fig. (10.7). It should be noted that failure of one part of this system during testing meant complete collapse of the 'tree'.

Each element was designed as a beam reaching 150 N/mm^2 at the theoretical roof failure load. Channel sections were used throughout,

generally back to back to allow a rod to pass between, and where appropriate, web stiffners were used. The jack reaction members were arranged to prevent lateral buckling of the long thin jack compression, and four ground points spread the force into the slab base.

As the first part of the construction operation, a 225 mm thick reinforced concrete base had been laid. The reinforcement consisted of a lower 300 mm square grid of 12mm diameter bars and an upper 150 mm square grid of 6 mm mesh. Thus the load per rawlbolt of 12kN, it was felt, would be spread out into the slab without local uplift.

To account for the roof camber, the 19mm and 22mm diameter rods connecting the individual beams had to have a screwed portion at each end of 75 mm. In total 108 separate steel members, 72 trestles, and 192 rods were required for the complete loading system.

To simulate side wind loading five 3.5 metre high frames were constructed as shown in Plate (C.4) and positioned along one side. A steel wire was attached to the eaves and passed over a roller to a hanger upon which 55 kg weights were hung. The overturning moment had to be resisted by rawlbolts fastened to the slab.

In fact, the applied load is opposite to actual wind conditions but for this type of roof, the load direction is elastically reversible.

10.9. Testing Procedure:

The elastic performance of the folded plate roof was studied under working imposed and eaves wind loads of 1.2 kN/m^2 and 0.78 kN/m respectively. Each test was initially loaded, unloaded and then reloaded to determine the effect of fastener slip on the elastic response.

For the imposed vertical loading, the sag in the roof due to the self weight and the spreader system was estimated as 15mm by measurement from the initial roof camber of 200 mm. However, the theoretical deflection due to 0.45 kN/m^2 should have been 20mm. It should be noted that the design dead weight due to insulation almost exactly equals the spreader

system equivalent uniform loading.

Increments of loading were taken up to the working load, and it was noticed that on unloading, some residual deflection remained. Reloading merely retraced the unloading line. Some outward movement of the bottom chord of the edge beam was apparent due to the rotation continuity of the sheeting at the eaves which twists the relatively flexible side beam.

The central and outer bays were then separately loaded to show the spread of deflection laterally. In all tests vertical readings were to be recorded at all centre section points and at the centre apex quarter span points.

For wind loading the same sequence of loading un- and reloading was applied in six increments by application of approximately 55kg weights.

An optical level and suspended tapes were used to measure the changes in vertical movement. Lateral displacements at the edge beam were recorded by a theodolite sighted on to horizontal scales.

10.10. Discussion of Experimental Results

The elastic test results for uniform vertical loading are shown in Fig. (10.9). The central apex deflection is plotted to demonstrate the overall roof performance. It is clear that the structure stiffens by about 20% on reloading which is totaly due to the 'bedding-in' of the perimeter and seam fasteners. This reloaded flexibility reappears in all subsequent tests.

Fig. (10.10) shows the vertical load-deflection plot for the edge beam and the quarter points of the central apex. At the working load the central deflection is only 35mm (L/620), and the dead weight settlement was measured to be an additional 15mm (theoretical 20mm). The complete cross-sectional displacements due to 0.75 kN/m^2 are shown in Fig. (10.11) which shows the decay of deformation towards the outside of the roof. This is because of the change of plate loading and fold line areas, which causes fold line stresses as determined in Fig. (10.5). The beam type

deflections are caused wholly by the fold line axial strain and these may be added for each plate to give net vertical deflections according to the Williot diagram principle.

The axial strain component of deflection together with the shear deflection is shown in Fig. (10.13) and their summation closely approximates the initial loading deflection curve. It should be noted that if open profiled sheeting had been used together with more realistic fold member sizes then the total deflection would have been roughly 70% greater.

The theoretical shear deflection includes an allowance for the seam and edge fastener slip of 0.35 mm/kN and 0.15 mm/kN respectively. Fig. (10.28) shows that on reloading these become about 0.12 and 0.05 mm/kN respectively. Hence theoretical results for the total reloaded deflection may be calculated as in Fig. (10.11) for test 2 showing the influence of fastener slip and the good agreement with the observed deflections.

In addition, the centre and outer bays were separately loaded, and their theoretical comparisons, for initial fastener slip, are indicated.

For the wind loading, applied at the eaves, the behaviour is about 30% stiffer on initial loading and about 40% stiffer on reloading, compared to theory (Fig. (10.12)). The most noticeable discrepancy is in the edge beam uplift which is somewhat lower than in theory. In practice, the stiffness of the fold members probably has a significant effect. The five loading points may also not sufficiently accurately represent a uniform lateral distribution, and of course frictional resistance of the suspended weights on the tunner bearing may have some importance. Lateral deflection was measured as 16 mm and the outward end column sway was approximately 1mm.

The test to failure under imposed load was carried out before a large audience on 13th July 1976, and to monitor the roof performance a running plot was made of the central apex deflection (Fig. (10.15)).

Severe non-linearity first became apparent at 2.0 kN/m^2 and at this stage the loading increments were reduced. Seam failure occurred at

2.3 kN/m^2 which compares well with the failure theoretical load of 2.2 kN/m^2 corresponding to a seam fastener strength of 2.5 kN/mm sheet thickness. Preliminary tests indicated that the upstand seam had slightly superior load bearing characteristics of 2.6 kN and this gives better agreement.

The other failure modes, as seen from the design calculations, have a higher safety factor. The actual failure seam was at the end of the internal bay and occurred by ductile tearing of the 22 seam fasteners. By extrapolating the elastic response and subtracting from the deflection just prior to collapse, it may be seen that the total magnitude of seam tearing is about 25 mm. The experimental load-deflection curve is initially about 20% stiffer than in theory.

Fig. (10.16) also shows how, by comparing the pure elastic deflection with the actual roof displacement at failures, the area of likely failure is apparent. By studying the apex quarter point movements it is clear that one side is some 10% greater than the other which is precisely where failure occurs.

Failure represents almost twice the working load and vindicates the design philosophy.[99,100]

During the testing operation, the large seam displacements caused local bending, and twisting of the neighbouring fold members at failure as shown in Plate (10.6) which was exacerbated by the surge of the stored energy in the jack and spreader systems as the load decreased.

Replacement of the damaged members has not yet been carried out, but it is suggested that the folds could be locally supported and cut off before rewelding, and positioning of new sheets. The loss in camber of the undamaged portion was only 75 of the initial 200 mm.

10.11. Limits of Viability of Folded Plate Roofs

The structural action of folded plate roofs utilizing corrugated steel sheeting has been discussed in Section (10.3). It is clear that

the longitudinal action is essentially that of a plate girder spanning between end frames. Hence, for each geometrical configuration there will be a definite span to depth ratio above which folded plate action is likely to be unsuitable. In the U.S.A. where double skin sheets are used, the web becomes extremely stiff, and welded perimeter fixings to relatively thick gauge steel will raise the permissible spans greatly.

However, in Britain, mechanical fixings to standard gauge open profiled sheeting are the only generally available materials for folded plate construction. The failure criteria may be divided up into:

1. Properties of the sheeting for simple bending, shear distortion, and shear buckling requirements

2. Properties of the connections for strength and slip requirements

3. Properties of the fold lines for bending resistance and deflection limitation.

To determine the limits of viability, the most important design parameter must first be considered, which is the tearing strength of the perimeter fixings. It is assumed that the trough pitch of corrugations is 150 mm and that this only accommodates one self-drilling screw of shear capacity 6 kN/mm sheet thickness.

The chosen parameters which determine the limits of roof span, L (metres), are:

B - spacing of columns m
θ' - roof slope
t - sheet thickness, mm,
h - profile height, mm

It should be noted that Young's modulus (E) is 210 kN/mm^2
Roof loading (w) equals 1.2 kN/m^2
The deflection limit is L/360

The corrugation is a standard shape with 75 mm trough width and 15^{o} side slope. Hence its shear distortion property $\overline{K}$ may be determined as a function of h.

The in-plane force component, R is resolved vectorially and the end shear force in kN is,

$$\frac{RL}{2} = \frac{wBL}{4 \sin \theta'}$$

The sheet length in metres is

$$b = \frac{B}{2 \cos \theta'}$$

therefore the shear flow $\frac{RL}{2b}$

$$= \frac{wL}{2 \tan \theta'}$$

Thus $\frac{6t}{F} = \frac{wL}{2 \tan \theta'} \times 0.15$ where F = safety factor = 1.75

The maximum span is $L_S = 46 \tan \theta' . \frac{t}{w} = 38t \tan\theta'$ and is independent of B.

For bending strength the fold area may be evaluated by considering the central bending moment $RL^2/8$ and the section modulus Ab where A is half the fold area.

Thus $A = \frac{wL^2 \times 10^3}{8 \tan \theta' . \sigma}$, again independent of B

σ is the permissible axial fold line stress (= 150 N/mm^2).

The bending deflection due to beam action is given by,

$$\Delta_b = \frac{10}{384} \cdot \frac{RL^4}{EAb^2} \times \frac{1}{\sin \theta'}$$

where the factor $(\sin \theta')^{-1}$ represents the translation from in-plane to vertical deflection.

Thus, after insertion of A, and R,

$$\Delta_b = \frac{5}{12} \cdot \frac{\sigma L^2 \cot \theta'}{EB} \times 10^3 \quad \text{mm}$$

The shear distortion deflection is,

$$\Delta_d = \frac{150^{2.5} . \bar{K}}{Et^{2.5} b^2} \quad \frac{RL^2}{8} \times \frac{1}{\sin \theta'}$$

$$= \frac{150^{2.5} \bar{K} wL^2 . \cot^2 \theta'}{Et^{2.5} B \times 10^3 \times 4} \text{ mm}$$

It is assumed that the minor sources of shear flexibility such as seam slip may be neglected, which is in some way accounted for by the relatively severe deflection limitation. The loading w for deflection only includes the live load component of 0.75 kN/m^2. Thus, the maximum span for deflection limitation is,

$$\Delta_d + \Delta_b = \frac{L}{360}$$

So $$\frac{1}{360} = \frac{L}{B} \cot \theta' \{0.30 \times \frac{0.75}{1.2} + \frac{0.25 \bar{K}}{t^{2.5}} \cot \theta'\}$$

therefore, $$L_d = \frac{10^3 \times B \tan \theta}{360 \{0.19 + 0.25 \bar{K} \frac{\cot \theta'}{t^{2.5}}\}}$$

$$= \frac{2.78 B \tan \theta'}{(0.19 + \bar{K} \frac{\cot \theta'}{t^{2.5}} \times 0.25)}$$

However, $\bar{K}$ is a property of the sheeting given in Fig. (10.7) which has a single parameter h. If profile heights of 20, 30, 40 and 50 mm are considered, then the corresponding $\bar{K}$ values are .067, .133, .194 and .246.

The profile shape also determines the sheet bending and shear buckling strengths. For simple bending it is assumed that no effective width reduction need be applied to the compression plate, which is merely a crude simplifying assumption.

The neutral axis is given by,

$$\bar{x} = \frac{(76 - 0.53\,h)\,h + 1.04\,h^2}{150 + 1.55\,h}$$

The sheet inertia is thus,

$$D = 76\ \bar{x}^2 + (76 - 0.53\,h)\ (h - \bar{x})^2 + 2.08\,\frac{h^3}{12} + (\frac{h}{2} - \bar{x})^2 \times 2.08\,h$$

The sheeting merely spans between fold lines and hence,

$$\frac{wb^2}{8}\cos^2\theta = \frac{\sigma}{150} \cdot \frac{Dt}{(h - \bar{x})}$$

$$\text{therefore, } B_b = \sqrt{\frac{Dt}{(h - \bar{x})}\ .025}$$

The shear buckling capacity is determined by the minor and major sheet bending stiffnesses, D_x and D_y respectively,

$$D_y = \frac{DtE}{150} \quad \text{per mm}$$

$$D_x = \frac{t^3 E}{12(1-\nu^2)}\ (1 - .01\,h)$$

According to Easley's formula for shear buckling,

$$\frac{RL}{2} = \frac{36\ D_y^{3/4}\ D_x^{1/4}}{b.F} \quad \text{where F = safety factor of 1.75}$$

$$\frac{wBL}{4 \sin\theta'} = 36\ (\frac{Dt}{150})^{3/4}\ (\frac{t^3}{11}\ (1 - .01\,h))^{1/4}\ \frac{207 \times 2 \cos\theta'}{B \times 1.75}$$

$$L_B = 0.36 \frac{D^{3/4} t^{3/2}}{B^2} (1 - .0025 h) \cos \theta' . \sin \theta'$$

It should be noted that $D \propto h^2$ and hence the permissible span due to buckling L_B is proportional to,

$$L_B \propto \frac{h^{3/2} t^{3/2}}{B^2} . \sin 2 \theta'$$

The design criteria outlined are the shear strength of the connections, the deflection limitation, the shear buckling capabilities and the sheet bending strength. The maximum permissible roof span is determined only by four geometrical properties, - B, θ', h, and t.

For folded down corrugations it is suggested that $\bar{K}/5$ ought to be taken for the corresponding shear distortion parameter.

Thus L as a function of B and h may be plotted for various t and h as in Fig. (10.18). An envelope of the four limits may be drawn and it is apparent that the maximum covered area L times B is generally determined by the coincidence of the fastener and buckling strength lines. However, the European Code of Practice does indicate that shear buckling failure should have an extra 25% reserve of safety. It may consequently mean that the fastener tearing capacity is not the primary limitation.

When fastener strength is the main criterion Fig. (10.20) shows the effect of sheet thickness and roof slope. Great spans are possible for 45 degree slopes, of the order of 35 metres. At any roof length the required fold line area may be calculated in Fig. (10.21).

It may be seen that for the prototype test structure of column spacing 3.6 metres, the failure modes and deflection limit are very close for open profiled sheeting. Closed end sheeting greatly reduces the central deflection.

It is assumed that the number of seams fasteners is adjusted so that failure occurs simultaneously with the tearing of the sheet-fold fastener.

Some reduction in roof load is possible for slopes bigger than 30^{o} but it is assumed for simplicity that 1.2 kN/m^2 represents the total dead and imposed load for all roof angles.

10.12. Comparison with Portal Frame Construction

The prototype test folded plate roof utilizes cold formed fold line members of sufficient cross-sectional area for bending strength, and corrugated sheeting spanning between. For comparison with conventional construction, (Fig. (10.23) indicates the approximate weights of steel required for both folded plate and portal frame buildings of size 20 metres x 10 metres.

The same sheeting would be used for each although the folded plate requires 0.8 mm thick steel for the fastener strength based on a 3.3 metre column spacing as determined from Fig. (10.19). Conventional sheeting, it is assumed is 0.7 mm thick.

Portal frames span 10 metres although the roof structural dimension is 20 metres. A number of simplifications have been made in the design and cost comparison is only for the roof portion and not the completed building. The portals are at 5m spacing.

The calculated steel saving is about 33% in this case and as a casual observation, the cost of the fold members is about that of the purlins. On the debit side for folded plate construction, more fasteners are required and construction time might be greater. In addition, the longitudinal edges, it is assumed are supported by perimeter sheeting posts.

On the credit side, the end frames allow side sheets to be attached, as sheeting rails and posts are normally required for portal framed buildings. A main advantage is that there is no need for roof wind bracing in folded plate construction.

It should be noted that for square buildings the material savings are even greater.

For a 10 m x 10 m square building the fold line weight reduces to 465 kg. Lighter end frames can be used (647 kg), as well as 0.7 mm thick sheeting.

Three portal frames are required which, reduces their weight to 1953 kg, and the ratio of steel costs is now only 0.57.

For a 20 m x 20 m roof the folded plate concept really becomes structurally very efficient. Its cost merely varies linearly with increasing width as the structural span remains unaltered (4406 kg). However, a portal frame spanning 20 metres requires almost double the weight of steel per metre. (356 x 174 x 45 kg/m R.S.J.).

The frame weight soars to 6210 kg and the purlin weight is 2112 hg making a total of 8322 kg. The ratio of weights of steel is now only 0.53.

Thus, the optimum folded plate plan shape is where there are a large number of repeating bays with a span of about 20 metres and it may be expected that this saves in excess of 40% by weight of steel over conventional construction.

However, balanced against this obvious material advantage must be determined the lack of roof lighting (mid. span only), the difficulties in erection, and the increased number of fastenings.

The cost advantage can only be maintained by prefabrication of longitudinal panels and a standard erection technique whereby complete sections may be fastened at ground level and lifted into place. Detailing and weather proofing must also be devised to suit folded plate construction.

10.13. Design Summary for Folded Plate Roof Using Open Profiled Sheeting

Data: Span, L = 21.6 metres
Bay width B=3.6 m
Profile depth, h>35 mm; $\bar{K}$ = 0.17

Sheet thickness, t 0.9 mm (actual 0.85 mm)
Loading, 1.2 kN/m^2 at working load (0.75 kN/m^2 imposed)
Roof slope, $\theta = 35^o$
Safety factor, F on fasteners = 1.75
Sheet span, b = 2.1 m
Young's modulus E = 207 kN/mm^2

The design is carried out according to section (10.4) using the notation previously stated.

The in-plane loading $q = \frac{wB}{2 \sin \theta} = 3.76$ kN/m

Area of fold line is $A = \frac{qL^2}{8\sigma b} = 700$ mm^2

where $\sigma = 150$ N/mm^2

Total fold area is $2A = 1400$ mm^2

Fastener Strengths: End seam

Decking profile $n_s = 24$, $S_s = 0.35$ mm/kN, $S = 0.15$ mm/kN, $g_1 = 1.56$ (see table 8.10) $n_{sh} = 24$

F_s - individual seam fastener capacity = 2.5 x 0.85 = 2.13 kN

F_p - individual fold fastener capacity = 6.0 x 0.85 = 5.10 kN

$$Q_s = (n_s F_s + 2F_p) \frac{(\frac{n_s}{S_s} + \frac{g_1}{s})}{(\frac{n_s}{S_s} + \frac{1}{s})} \{\frac{n_{sh}}{n_{sh} - 2}\} = 74 \text{ kN}$$

Q_s represents the equivalent end frame reaction which should be bigger than $3.76.\frac{L}{2}.F$ where F = 1.75

= 71 kN

Roofing profile; $n_s = 30$ $g_1 = 0.97$ (see table 8.10)

$$Q_s = (n_s + g_1 S_s/s) F_s \left\{\frac{n_{sh}}{n_{sh} - 2}\right\} = 74 \text{ kN}$$

Sheet-fold fasteners: d = 150 mm

$$Q_F = \frac{b}{d} F_p = 71 \text{ kN}$$

Sheet-end frame fasteners are of the same pitch as the sheet-fold fasteners (150 mm).

Deflections: At imposed loading of 0.75 kN/m^2

$q = 2.35$ kN/m

Distortion: $d_{1.1} = \frac{d^{2.5}\overline{K}}{Et^{2.5} b^2} \cdot \frac{qL^2}{8} = 10.6$ mm

Shear strain: $d_{1.2} = \frac{(1 + \nu)(1 + 2h/d)}{Etb} \frac{qL^2}{4} = 1.3$ mm

Sheet fold slip: $d_{2.1} = \frac{sdq L^2}{4b^2} = 1.5$ mm

Seam slip: $d_{2.2} = \frac{(n_{sh} - 1)}{2} \left\{\frac{s S_s}{n_s S + g_1 S_s}\right\} \frac{qL}{2} = 4.0$ mm

for a linear variation in seam strength.

Sheet-end frame slip: $d_{2.3} = \frac{sqL}{2(n_{sc} - 2 + 2g_1)} = 0.2$ mm

Simple bending deflection: $d_{1.3} = \frac{10}{384} \cdot \frac{qL^4}{EAb^2} = 20.8$ mm

Total in-plane shear deflection = 17.6 mm

Therefore, total in-plane deflection = 38.4 mm

Vertical deflection of fold line = $38.4/\sin 35^{\circ}$ = 67 mm
= L/322

Shear buckling capacity

Corrugation data, d = 150 mm, $2b_T$ = 47, $2b_L$ = 76, h = 35mm

$$D_y = \frac{\bar{D}}{d} tE = 260E \qquad D_x = \frac{t^3 E}{12(1-\nu^2)} \frac{1}{(1 + 2h/d)} = 0.38E$$

$$Q_{cr} = \frac{36 D_y^{3/4} D_x^{1/4}}{b} = 101 \text{ kN}$$

$$Q = \frac{wbL}{4 \sin \theta} F = 71 \text{ kN}$$

So shear buckling is not critical.

Summary of design requirements for roof of 35° slope, 21.6 m span and 3.6 m column spacing.

1. 35mm deep corrugations of 150 mm trough pitch and 0.9 mm thickness. The sheet width is 900 mm and the length 2100 mm.

2. Sheet-fold line fasteners in every trough with self drilling screws; 5.5 mm diameter (ultimate strength 6kN/mm sheet thickness).

3. For decking profiles, with a trough overlap seam, 24, 4 mm diameter 'pop rivet' seam fasteners at 85 mm centres (ultimate strength 2.5 kN/mm sheet thickness) are required in the final seams. For roofing profiles with a crest overlap, 30 seam fasteners are necessary at 70 mm centres. A linear variation of seam fastenings is possible towards the centre of the roof span down to a suggested minimum of six.

4. 14 sheet-end frame fasteners similar to 2 are required at 150 mm spacing.

5. The minimum fold line total area is 1400 mm^2. It is suggested that the thickness should be 4 mm giving a fold perimeter of 350 mm which is sufficient to allow sheet attachment without much width reduction of the compression member.

Failure should occur by seam or sheet-fold fastener tearing at a roof load of 2.1 kN/m^2 which includes the self weight of fold lines and sheeting totalling 0.14 kN/m^2.

Roughly 8 self drillings screws are required per square metre and also 8 seam fasteners per sq. m. of roof plan area.

Plate (10.1) Sheeting between fold lines in operation. The fold lines are held in position by wooden trestles which are set to the correct roof camber

Plate (10.2) Jacking of the roof in stages from moveable knees. External bracing was temporarily attached

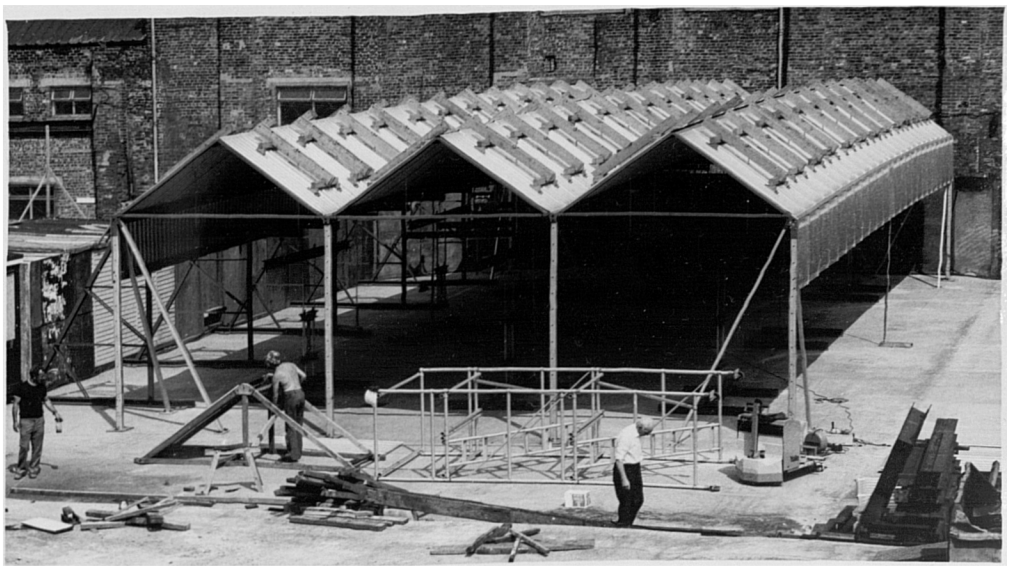

Plate (10.3) Roof ready for testing with side sheeting and loading system attached

Plate (10.4) Side wind loading system connected to eaves fold line member

Plate (10.5) Failure occurred by seam tearing of the central bay. This caused excessive twisting of the adjoining fold line members

Plate (10.6) View along the valley member towards end failure. Also shown are the angle pieces which prevented sliding of the loading trestles

CHAPTER 11.

SPECIAL PROBLEMS RELATED TO FOLDED PLATE ROOFS

This chapter deals with some factors not normally considered in the idealized behaviour of folded plate roofs. Firstly, the most important practical problem is the provision of roof lights in the sheeting skin. The initial investigation concerns the likelihood of strut buckling of the fold line in compression where there is only partial restraint from the sheeting on either side of the gap. This is followed by a more exact analysis which includes the shear flexibility of the sheeting to determine the fold line pre-buckling response to local loads and axial forces.

Variations in the sheet-purlin fastening arrangement along the roof span may be encountered and often the fold line members are sufficiently shear rigid to smooth out the change in shear flexibility. The central roof deflection may be quite substantially reduced and a finite difference method has been developed to take account of this effect.

Problems exist also at the plate extremities where, in some designs, an edge beam is required to absorb local forces. For a down-stand edge beam the bottom chord will usually be in tension, but even so it is free to buckle sideways and an approximate expression has been developed for lateral instability of this very long thin girder.

11.1. Holes in Folded Plates

A serious disadvantage in the design of corrugated steel folded plates is that their surface must be complete for longitudinal transfer of shear to end supports. This does not seem to have unduely concerned the designers of existing roofs who offset this inability with glazed sides between the end columns.

However, for industrial buildings requiring completely covered walls, roof lights are necessary. In theory, the low shear force at the

centre of the span should obviate the need for a load carrying membrane. Roof lights may be designed to span between fold line members, and the central sheets ideally can be removed. In general, however, some shear resistance must be introduced to account for the effects of uneven roof loading.

A low central shear field is a very useful property of beam action under uniform loading, although in this region the relatively weak fold line members are subject not only to local bending forces but also to the effect of the extremely high axial forces. Their combination may cause local fastener failure, additional fold line bending stresses, excessive deflection or even buckling of the fold line.

It is assumed that the free edge of the sheeting bordering the roof light is stiffened in some way to prevent buckling between fold lines due to the high sheet-fold fastener force.

The first analysis concerns the critical buckling load of the fold line in compression spanning across the opening. Failure will occur ideally by buckling as an encastré member, although in practice tearing of the sheet fold fasteners will occur as in Fig. (11.1).

In this analysis, sheet shearing is neglected and it is assumed that the effect of the discrete fastener forces is to provide a uniform elastic medium upon which the fold line is free to bend.

For the portion of the fold line affected by the restraining stiffness of the fasteners, the following differential equation holds, where v is the vertical displacement of the fold line.

$$EI \frac{d^4v}{dx^4} + P\frac{d^2v}{dx^2} + \frac{2n}{S}\sin^2\theta' v = 0$$

I is the fold line inertia about a horizontal axis and E is Young's modulus.

P is the fold line compressive force

$\sin^2\theta'$ represents the component of fastener stiffness vertically for a roof slope θ'.

n is the number of fasteners per mm, and
S their characteristic slip.

Due to the effect of a local fold line vertical uniform loading, q_f, the centre portion has a differential equation of the form,

$$EI \frac{d^4v}{dx^4} + p\frac{d^2v}{dx^2} = q_f$$

Considering $\frac{2n}{S} . \sin^2\theta'$ to be represented by k the solution of the first equation is given by,

$$v = \sum_{i=1}^{4} A_i e^{\lambda_i x}$$

where λ_i has four values given by,

$$\lambda_i = \pm \sqrt{\frac{-p}{2EI} \pm i\sqrt{\frac{k}{EI} - \left(\frac{p}{2EI}\right)^2}}$$

However, if x is defined as outwards fromthe centre of the hole then v must decay as x tends to infinity,

So $V = \{A \sin M_1 (x - a) + B \cos M_1 (x - a)\} e^{-M_2 (x - a)}$

(a is half the hole width)

where $M_1 = \sqrt{\beta^2 + \frac{p}{4EI}}$

and $M_2 = \sqrt{\beta^2 - \frac{p}{4EI}}$

and $\beta^2 = \frac{1}{2}\sqrt{\frac{k}{EI}}$

The second differential equation has a rather different solution,

$$V = \frac{q_f}{2p} x^2 + C \cos M_3 x + D \qquad \text{where } M_3 = \sqrt{\frac{p}{EI}}$$

This observes the necessary symmetry of deformation about $x = 0$. The first and last terms in V refer to the particular integral of solution.

The four unknown of the solutions require four geometrical boundary conditions at the edge of the opening such that, V, $\frac{dv}{dx}$, and $\frac{d^2v}{dx^2}$ are continuous.

An additional condition is that the applied loading, $2q_f.a$ equals the total fastener resistance along the fold lines.

For equality of displacement v

$$B = \frac{q_f}{2p} a^2 + C \cos M_3 a + D$$

Similarly for $\frac{dv}{dx}$

$$-M_2 B + M_1 A = \frac{q_f}{p}.a - C M_3 \sin M_3 a$$

And for $\frac{d^2v}{dx^2}$

$$(M_2^2 - M_1^2) B - 2M_1 M_2 A = \frac{q_f}{p} - C M_3^2 \cos M_3 a$$

Solving for B and A in terms of C

$$B = C \left\{ \frac{M_3^2 \cos M_3 a + 2M_2 M_3 \sin M_3 a}{M_2^2 + M_1^2} \right\} - \frac{q_f}{p} \frac{(2M_2 a + 1)}{(M_1^2 + M_2^2)}$$

$$A = C\left\{\frac{M_3^2 M_2 \cos M_3 a + M_3 \sin M_3 a\,(M_2^2 - M_1^2)}{M_1(M_1^2 + M_2^2)}\right\}$$

$$- \frac{q_f}{p}\ \frac{\{(M_2^2 - M_1^2)\,a + M_2\}}{M_1(M_1^2 + M_2^2)}$$

The final condition concerns the equality of applied and resisting forces.

$$\text{So}\quad q_f a = \int_0^{\infty} (A \sin M_1 x + B \cos M_1 x)\, e^{-M_2 x} \cdot k$$

$$\frac{q_f a}{k} = \frac{M_2 \cdot B}{M_1^2 + M_2^2} + \frac{M_1}{M_1^2 + M_2^2} \cdot A$$

Thus inserting A and B and solving for C.

$$C = \frac{(\ \ldots\ldots\ldots\ldots\ )\, q_{f/p}}{2M_2 M_3^2 \cos M_3 a + M_3\,(3M_2^2 - M_1^2) \sin M_3 a}$$

At the critical buckling load C will tend to infinity and thus the denominator will become to zero.

Knowing the parameters M_1, M_2 and M_3 in terms of P, EI and k, the denominator may be rearranged to give,

$$M_3 = \frac{-(3M_2^2 - M_1^2)}{2M_2} \tan M_3 a$$

$$\text{So}\qquad \frac{P}{EI} = \frac{(2\beta^2 - P/EI)^2}{4(\beta^2 - P/4EI)} \tan^2 M_3 a$$

If the Euler load for an encastré strut is given by,

$$P_E = \frac{\Pi^2 EI}{a^2}$$

which is consistent with complete end fixity at the edges of the opening, then,

$$\pi^2 \frac{P}{PE} = \frac{(2\beta^2 a^2 - \pi^2 P/PE)^2}{4\beta^2 a^2 - \pi^2 P/PE)} \tan^2 \pi\sqrt{\frac{P}{PE}}$$

Solving for P/PE this becomes,

$$\frac{P}{PE} = \frac{2\beta^2 a^2}{\pi^2} \{1 + \sqrt{\frac{1}{1 + \tan^2 \sqrt{P/PE}\ \pi}}\ \}$$

So $$\frac{P}{PE} = \frac{1}{\pi^2}\sqrt{\frac{a^4 k}{EI}}\ \{1 + \cos \pi\sqrt{\frac{P}{PE}}\ \} = \text{ß}\ \{1 + \cos \pi\sqrt{\frac{P}{PE}}\ \}$$

where $k = \frac{2n}{S} \sin^2 \theta$

It is a well known solution for a strut continuously supported on an elastic medium, (43)

$$P_{crit} = 2\sqrt{kEI}$$

It may be seen that as P_E becomes very large consistent with a tending to zero

$$\cos \pi\sqrt{\frac{P}{PE}} \to 1 \qquad \text{and} \quad PE = \frac{\pi^2 EI}{a^2}$$

and hence the equation does degenerate to the above case a typical solution for a practical folded plate is as follows:

If $I = 5 \times 10^5$ mm^4, $E = 200$ kN/mm^2, $a = 1000$ mm

$n = 1/150$ mm^{-1}, $S = 0.15$ mm/kN, $\sin \theta' = \frac{1}{2}$

$$\text{ß} = \frac{1}{\pi^2}\sqrt{\frac{ka^4}{EI}} = \frac{1}{9.9}\sqrt{\frac{10^{12} \times 2}{4 \times 5 \times 10^2 \times 2 \times 10^5 \times 22.5}} = 1.5$$

For a span L of roof and 2a hole width.

$$P = \frac{wL^2}{4 \cot \theta} \quad ; \quad P_E = \pi^2 . \frac{EI}{a^2}$$

Typically, L = 20 m; $\cot \theta' = 2$; $I = 5 \times 10^5$ mm^4

$w = 2$ kN/m^2 overall u.d.l.

So $$\frac{P}{PE} \cdot \frac{100}{1000} = 0.10$$

For $\aleph = 1.5$ the critical value of P/PE is 0.18.

$\aleph$	$P_{crit}/_{PE}$	Effective length
50	0.65	1.2 a
20	0.58	1.3 a
10	0.43	1.5 a
5	0.35	1.7 a
2	0.22	2.1 a
1	0.14	2.7 a
0.5	0.08	3.5 a
0.1	0.02	7 a

$$P_E = \frac{\pi^2 EI}{a^2}$$

$$\aleph = \frac{1}{\pi} 2 \sqrt{\frac{ka^4}{EI}}$$

$$k = \frac{2n}{S} \sin^2 \theta'$$

hole width = 2a

The above table represents the iterative solutions for P/PE knowing a value for $\aleph$ which represents the ratio of the fastener stiffness to the effective lateral stiffness of the fold member spanning across the opening.

Of course, the analysis can only be approximate in that it neglects imperfections, roof camber and other effects which tend to reduce the practical buckling load. This obviously requires future research, but at least it does give an indication of the likely opening widths based on a suitably high safety factor.

For the example indicated, it seems that a hole width of less than 2 metres in a 20 metre span would be flexible. As a safe design approximation the total applied load on the roof light may be assumed to be absorbed by the last fastener on each side of the opening. Thus the maximum opening span is given by,

$2F_p \sin\theta' > \frac{wBa}{2}$ where B is the bay width. F_p is the fastener strength.

Typically B = 4m, $w = 2kN/m^2$, $F_p = 4kN$, $\sin\theta' = \frac{1}{2}$ and so the maximum value of a is 1m, corresponding to a 2m hole width.

11.2. General Approach for Holes in Folded Plates

The previous analysis of strut like buckling of the fold lines is an upper bound to the failure load. Prior to this, severe bending moments and sheet-fold line fastener forces may be generated due to the combined effect of the local loading and axial force.

A modified analysis takes into account the shear flexibility of the sheeting as well as the effect of axial force on the deflection of the fold line.

The equilibrium equation for member bending is:

$$q = + EId^4 \frac{V_E}{dx^4} + P \frac{d^2V_E}{dx^2}$$

where V_E is the movement of the fold line
q is the local vertical force per mm
P is the compressive axial force

For sheet shearing:

$$q = \frac{d^2V_S}{dx^2} \cdot \frac{1}{C} \cdot 2\sin^2\theta' = \frac{d^2V_S}{dx^2} \cdot \frac{1}{C}$$

For fastener slip:

$$q = (V_E - V_S)\frac{n}{S} \cdot 2\sin^2\theta' = k(V_E - V_S)$$

where V_S is the vertical sheet movement and C is the in-plane sheet shear flexibility. As in Section (11.1) the factor $2\sin^2\theta$ is the modification from an in-plane to a vertical fastener or sheet stiffness due to two plates meeting at an angle $2\theta'$.

By solving these three equations for the sheeted portion it follows that:

$$\frac{d^6V_E}{dx^6} \cdot \frac{1}{k} + \frac{d^4V_E}{dx^4}\left\{+\frac{P}{k.EI} - C\right\} + \frac{(1 - CP)}{EI}\frac{d^2V_E}{dx^2} = 0$$

The internal unsupported fold line deflects according to:

$$EI\frac{d^4V_E}{dx^4} + P\frac{d^2V_E}{dx^2} = q_f'$$

where q_f is the local vertical uniform loading on the fold line.

As previously, the solution for the sheeted part, which must decay as x tends to infinity away from the centre of the opening, is:

$$V_E = e^{-M_2(x - a)}\{A\sin M_1(x - a) + B\cos M_1(x - a)\}$$

Again a is the half hole width.

Using the fact that:

$$\frac{d^2V_S}{dx^2} = C\,EI\frac{d^4V_E}{dx^4} + C\,P\frac{d^2V_E}{dx^2}$$

V_S must also be represented by a similar form.

$$V_S = e^{-M_2(x-a)} \{A^1 \sin M_1 (x-a) + B^1 \cos M_1 (x-a)\}$$

Using $x_1 = \frac{1}{2} (Ck - P/EI)$ and $x_2 = \sqrt{\frac{k}{EI} (1 - CP)}$

$$M_1 = \sqrt{\frac{-x_1 + x_2}{2}} \qquad M_2 = \sqrt{\frac{x_1 + x_2}{2}}$$

Consequently, A^1 and B^1 are related to A and B by equating terms in cos and sin according to:

$$(M_2^2 - M_1^2) B^1 - 2M_1M_2 A^1 = \{C EI (M_2^4 - 6M_1^2 M_2^2 + M_2^4)$$

$$+ CP(M_2^2 - M_1^2) \}B + \{CEI(-4M_2^3 M_1 + 4M_1^3 M_2) - 2M_1M_2 CP \}A$$

and $$(M_2^2 - M_1^2) A^1 + 2M_1 M_2 B^1 = \{CEI (M_1^4 - 6M_1^2 M_2^2 + M_2^4)$$

$$+ CP(M_2^2 - M_1^2) \} A + \{CEI (4M_2^3 M_1 - 4M_1^3 M_2) + 2M_1M_2 CP \} B$$

Thus $A^1 = AA.A + AB.B$

and $B^1 = BA.A + BB.B$

The solution for the internal portion is again:

$$V_E = \frac{q_f}{2P} x^2 + D \cos M_3 x + E$$

which is consistent with the symmetry about $x = 0$ where $M_3 = \sqrt{\frac{P}{EI}}$

Solving for A, B, D and F requires boundary conditions such that V_E, $\frac{dV_E}{dx}$ and $\frac{d^2V_E}{dx}$ are equal for each differential form at $x = a$,

which is the edge of the opening, as in Section (12.1).

An additional relationship is that the sum of all sheet-fastener forces equals the applied load on the opening. Thus,

$$\frac{q_f a}{k} = \int_0^{\infty} (V_E - V_S)\, dx$$

$$\frac{q_f a}{k} = \frac{M_1}{M_1^2 + M_2^2} \{ A - A^1 \} + \frac{M_2}{M_1^2 + M_2^2} \{B - B^1\}$$

where k is the equivalent vertical fastener stiffness.

Hence, A, B, D and F may be solved in terms of q_f and P as in Section (11.1). The bending stress at the centre of the hole is an important design factor and is given by:

$$\sigma = y \frac{d^2 V_E}{dx^2}$$

where y is the distance from the neutral axis of the fold line section.

$$\text{Thus } \sigma = y \{\frac{q_f}{P} - M_3^2 D \}$$

The central deflection is (D + F) and the maximum fastener force is:

$$\frac{(B - B^1)}{S} \sin \theta'$$

where S is the characteristic fastener slip and θ' is the roof slope.

A copy of the program developed for this general hole in folded plate solution is given in Appendix5

As a typical example, the program has been run for a folded plate panel suffering an in-plane load of q_f =1kN/m as shown in Fig. (11.2(a)). The hole width (2a) was selected as 1.5 metres and the influence

of the axial compressive force on the central deflection is indicated for a realistic fold line inertia of 10^5 mm^4. It should be noted that the theoretical buckling load for $\bar{z} = 3.8$ in this case, is about 110 kN (see Section 11.1) and the Euler buckling load for an equivalent fixed ended strut is 355 kN. In this case fastening is locally in every corrugation and the effect of fold line inertia and hole width on the central deflection is also shown in Fig. (11.2(b)).

For zero axial force it may be expected that the displacements behave linearly with the applied loading q_f. However, when axial force is included the deflections and stresses become non-linear due to the eccentric effects of compressive loading. Thus for higher values of q_f, so a given axial force will have an increasing effect.

The local fastener forces around the hole are depicted in Fig. (11.3(a)) for alternate and every trough fastenings. The assumption that the discrete fastener restraints may be spread out to form a uniform elastic medium will tend to over-estimate the outer fastener force where the displacement is largest.

Naturally the degree of sheet-fold line fastening has a marked effect on the local fastener forces around the hole.

As a design parameter, the fold line bending stress is probably most valuable and this is shown in Fig. ((11.3 (b)) for a hypothetical 100 mm deep member. For a general member the stress at any distance y from the neutral axis is $\sigma \cdot y/50$. It is clear that quite large additional stresses are generated of the order of 40 N/mm^2 for a 2 metre hole width.

11.3. Lateral Instability of Edge Beams

The extremities of a folded plate roof span are worthy of special notice. In concrete roofs the edge plate is usually sufficiently torsionally stiff so that the penultimate fold line transverse moment does not cause large outward twisting movement.

For corrugated steel folded plates with effectively pinned joints,

the problem is more one of the possibility of lateral buckling of the very slender edge beam spanning between end frames. Unlike the internal joints the final fold line member is unsupported. The bottom chord of a downstand beam will be in tension for vertical loading (Fig. (10.2)) but in compression for leeward wind suction.

This lateral instability chord is free to move sideways. Two modes of failure are apparent and the actual buckling load is a function of the two, providing that rotational continuity can be maintained at the lower chord.

1. Where the edge beam acts as a rigid member developing the full torsional resistance of the fold lines.

2. The bottom chord does not twist, and lateral movement occurs by web bending of the edge beam.

For the prototype roof design the lower chord was selected as a 100 x 50 rectangular hollow section which increases the torsionally rigidity.

Assuming that the edge beam rotation is:

$$\theta = \bar{\theta} \sin \frac{\Pi y}{L}$$

The bending energy of the bottom chord is:

$$E_b = \int_0^{L/2} EI \left(\frac{d^2\theta}{dx^2}\right)^2 h^2 \, dx = EI \frac{\Pi^4}{4L^3} h^2 \bar{\theta}^2$$

where I is the lateral inertia of the lower chord
h is the edge beam depth
L is the span between lateral restraints

The torsional energy is:

$$E_T = \int_0^{L/2} GJ \left(\frac{d\theta}{dx}\right)^2 dx = GJ \left(\frac{\Pi}{4L}\right)^2 \bar{\theta}^2$$

where J is the lower chord torsional stiffness.

Work done by axial stresses where $\sigma = \bar{\sigma} \sin \frac{\Pi y}{L}$ and the axial shortening at any point is:

$$\frac{h^2}{2} \left(\frac{d\theta}{dx}\right)^2$$

$$E_A = \bar{\sigma} \frac{Ah^2}{L^2} \Pi^2 \int_0^{L/2} \cos^2 \frac{\Pi y}{L} \sin \frac{\Pi y}{L} \, dy$$

$$= \frac{\bar{\sigma} A}{3} h^2 . \frac{\Pi}{L} \cdot \bar{\theta}^2$$

where A is the lower chord area and.

σ is the central axial compressive stress

$$\bar{\sigma} Ah = \frac{wL^2}{8}$$

w is the in-plane loading producing compression in the final chord.

Work done by the imposed loading, w is:

$$E_L = wh \frac{\bar{\theta}^2}{2} \int_0^L \sin^2 \frac{\Pi y}{L} \, dy$$

Case (1) $$= \frac{wLh}{4} \cdot \bar{\theta}^2$$

(a) For unsupported tension chord $E_L - E_A = E_T + E_B$

(b) For unsupported compression chord $E_L + E_A = E_T + E_B$

This gives:

$$w = \frac{\Pi^2 h}{F L^2} \left\{ \frac{\Pi^2 EI}{L^2} + \frac{GJ}{h^2} \right\}$$

for the case where F = 1.52 for case (b) and F = 0, 48 for (a)

It should be noted that if no special provision is made for sheet-end fold rotational continuity, then J tends to zero.

Case (2): If the lower chord remains torsionally rigid and the sheeted web has moment continuity at the lower chord by periodic double fastenings as in Fig. (11.8), an additional energy component results.

The sheet bending energy over the complete length is:

$$E_S = \int_0^{L/2} 3\frac{EI_S}{h}\bar{\theta}^2 \sin^2\frac{\Pi y}{L}\, dy$$

where I_S is the sheet inertia per mm width.

This gives a corresponding expression of:

$$w = \frac{\Pi^2 h}{FL^2}\{\frac{\Pi^2 EI}{L^2} + \frac{3EI_S L^2}{\Pi^2 h^3}\}$$

where again F = 1.52 for the compression chord and 0.48 for the tension chord.

However, these two cases represent only upper bounds to the instability mode which will occur by partial web bending and fold line torsion providing there is no relative rotation between the sheeting and final chord member.

$$w = \frac{\Pi^2 h}{FL^2}\{E_B + \frac{E_S E_T}{E_S + E_T}\}$$

where:
$$E_S = \frac{3EI_S L^2}{\Pi^2 h^3}, \quad E_T = \frac{GJ}{h^2} \text{ and } E_B = \frac{\Pi^2 EI}{L^2}$$

F = 0.48 or 1.52 as above.

For the actual roof data of:

$I = 0.47 \times 10^6$ mm^4; $J = 1.1 \times 10^6$ mm^4, $L = 21.6$ m
$h = 1$ m. $I_S = 150$ mm^4/mm

$$E_S = \frac{3 \times 200 \times 150 \times 21.6^2}{\pi^2 \times 10^3} \qquad E_T = 80 \times 1.1 = 88$$

$$E_B = \frac{\pi^2 \times 200 \times 0.47}{21.6^2} = 2 \qquad \frac{E_S E_T}{E_S + E_T} = 86$$

$$w = \frac{\pi^2 \times 88}{F \times 21.6^2} = 1.22 \text{ kN/m uplift or } 3.86 \text{ kN/m downward}$$

Actual imposed working loads for the prototype test building of Chapter 10 are respectively about 0.5 and 1.1 kN/m.

11.4. Variations in Sheet Flexibility along the Roof Length

In relatively short span folded plates, where fastenings in every corrugation to standard sheet thicknesses have sufficient reserve of safety, the fixing pattern may be changed towards the centre of the roof. Alternate ocrrugation fastening, however, is much more flexible and this will result in a considerable increase in the roof deflection. The rapid change in shear flexibility causes local bending of the fold members which, therefore, absorb some of the panel shear force.

It may be expected, that the fold line members, which are relatively wide to facilitate attachment of the sheets, will provide a shear stiffening effect. The central deflection may thus be reduced to some degree.

A theoretical investigation was initiated by the method of finite differences which allowed an abrupt change in the sheet flexibility to be accommodated easily. The roof panel is split up along its length

into segments which each behave according to a predetermined differential equation.

It is assumed that fastener slip effects are small compared to the large shear deformations which are present in folded plates.

For a shear force Q_i on an element the differential equation of equilibrium is:

$$- EI \frac{d^3V}{dx^3} + \frac{1}{C_i} \cdot \frac{dV}{dx} = Q_i$$

This implies that the applied shear force is split between the sheeting, of flexibility C_i, and the fold line of bending stiffness EI.

For two plates of slope θ to the horizontal meeting each other, this equation is modified to cope with a vertical movement V of the fold line, rather than an in-plane displacement as in Fig. (11.1). Thus,

$$-2EI \frac{d^3V}{dx^3} + \frac{dV}{dx} \cdot \frac{2 \sin^2\theta'}{C_i} = \bar{Q}_i$$

C_i is the individual sheet flexibility and $2 \sin^2 \theta$ represents modification to an equivalent vertical flexibility.

I now is the inertia of an individual fold line about a horizontal axis.

$$\bar{Q}_i = \frac{Q_i + Q_{i-1}}{2} \qquad \text{-average force per element}$$

θ_i now represents the vertical roof shear force per bay and varies linearly along the span from a maximum value of Q_o, which equals the total applied load on half the span times one bay width. If the element width is dj then the i_{th} shear force according to Fig. (11.4) is:

$$Q_i = Q_o - \sum_{j=1}^{i} dj \frac{Q_o}{L/2}$$

But $V_3\, x(2,\ 3) + V_2\, x(2,\ 2) + V_1\, x(1,\ 0) = \bar{Q}_2$

and so V_3 is also a function of V_1.

In general, if,

$$V_i = A(i) + B(i)\ V_1$$

then,

$$V_{i+1} = V_1 \left\{ \frac{-x(i,\ i)}{x(i,\ i+1)}\ A(i) - \frac{x(i,\ i-1)}{x(i,\ i+1)}\ A(i-1) - \frac{x(i,\ i-2)}{x(i,\ i+1)}\ A\ (i-2) \right\}$$

$$\left\{ + \frac{\bar{Q}_i}{x(i,\ i+1)} - \frac{x(i,\ i)}{x(i,\ i+1)}\ B(i) \text{ etc.,} \right\}$$

At the centre of the span, the deformations are purely symmetric. If the centre displacement is V_M, then $V_{M+1} = V_{M-1}$, etc.

Finally, the last equation of equilibrium is,

$$V_{M+1} \cdot x(M,\ M+1) + V_M x(M,\ M) \text{ etc.,} = \bar{Q}_M$$

but all the displacements are known in terms of V_1 and hence the absolute value of V_1 may be determined. Reinsertion into the general equation for V_i, yields the displaced shape of the fold line.

The general nature of this approach means that the sheet flexibility may be changed for a selected number of elements, as may the individual element widths.

It should be noted that as an approximation, $\bar{C}$ includes all the sheet flexibility components rather than just distortion and shear strain.

The equivalent vertical element flexibility may be redefined by:

$$\bar{C}_i = \frac{C_i}{2 \sin^2 \theta},$$

The differentials $\frac{dV}{dx}$ and $\frac{d^3V}{dx^3}$ may be represented by:

$$\frac{dV_i}{dx} = \frac{V_i - V_{i-1}}{d_i}$$

$$\frac{d^3V_i}{dx^3} = \left\{ \frac{V_{i+1}}{d_{i+1}} - V_i \left\{ \frac{2}{d_i} + \frac{1}{d_{i+1}} \right\} + V_{i-1} \left\{ \frac{2}{d_{i-1}} + \frac{1}{d_i} \right\} - \frac{V_{i-2}}{d_{i-1}} \right\} \frac{1}{d_i^2}$$

The total finite difference form may be collected together to give, for element i

$$V_{i+1} \cdot x(i, i+1) + V_i \cdot x(i, i) + V_{i-1} \cdot x(i, i-1)$$

$$+ V_{i-2} \cdot x(i, i-2) = \bar{Q}_i$$

where x(i, i) represents typically,

$$\frac{2EI}{d_i^2} \left\{ + \frac{2}{d_i} + \frac{1}{d_{i+1}} \right\} + \frac{1}{C_i} \cdot \frac{1}{d_i}$$

The initial conditions are determined by the free end fixity which observes anti-symmetric deformation. Therefore,

$$V_o = 0; \quad V_{-1} = -V_1; \quad V_{-2} = -V_2, \text{ etc.},$$

$$V_2 \cdot x(1, 2) + V_1 (x(1, 1) - x(1, -1) = \bar{Q}_1$$

Thus assuming V_1 to be an unknown,

$$V_2 = A + BV_1$$

A number of typical folded plate examples were analysed using this method which coincided with experimental plate test data. The comparisons of theoretical and experimental results for a number of individual plate tests are described in the next Chapter.

Plate (11.1) Plate girder test showing buckling failure of open profiled sheeting under uniform in plane load

Plate (11.2) Seam failure of pressed sheeting in equivalent plate girder

CHAPTER 12

EXPERIMENTAL TESTING OF CORRUGATED WEB GIRDERS

12.1. Tests on Pressed Sheeting and Standard Open Profile

Folded plate roof action may be simulated by flat plate tests under uniform in-plane loading. Thompson[21] has carried out a number of tests on horizontal plate girders of 18 metre length but suffered from having too few loading points. Consequently, the modes of failure were associated mainly with local deformation.

To examine the deflection and strength of folded plate roofs it was decided to construct a 21.6 metre corrugated web girder of the same span as the prototype building of Chapter 10. The plate depth of 2.1 metres was also the same as the roof sheet span and so the deflection and failure load may be directly related to a practical folded plate structure.

The flanges of the plate girder were rectangular sections of szie 100 x 50 x 3.2 mm thick, and the sheet ends were fastened to channel sections which were bolted to a solid floor. To prevent lateral buckling of the flanges, runners were provided in the middle of the span at 2 metre spacings, and the in-plane load was provided by nine jacks separated into eighteen points uniformly along the length.

A view of the test rig is shown in Plate (12.2) and is clad with the pressed sheeting actually used for the prototype folded plate roof. Deflections were measured at the centre and quarter points along the span as well as at the ends.

In addition, a range of tests was performed on a 35mm deep roofing profile to determine the effect of variable fastening along the sheet length and also to study the occurence of the failure modes such as fastener tearing and shear buckling.

The test data for the pressed sheeting is,

A Fold line area 940 mm^2

b	Sheet length	2.1 m
L	Plate span	21.6 m
t	Sheet thickness	0.97 mm
n_s	Number of seam fasteners on end seam is 24 and this varies linearly along the length	
S_s	Reloaded slip value per seam fastener is 0.07 mm/kN	
S	Reloaded slip value per edge fastener is 0.03 mm/kN	
F_s	Seam fastener strength	2.43 kN
F_p	Edge fastener strength	5.82 kN
E	Young's modulus 207 kN/mm^2	
d	Trough pitch 150 mm	

The bending deflection at a distance x from one end due to an in-plane load w, is,

$$d_{1.3} = \frac{2wL^4}{AEb^2} \cdot \{ \frac{-y^3}{12} + \frac{y^4}{24} + \frac{y}{24} \} \qquad y = \frac{x}{L}$$

The shear distortion component is,

$$d_{1.1} = \frac{d^{2.5}\,\bar{K}}{Et^{2.5}\,b^2} \cdot \frac{wL^2}{8}$$

$\bar{K}$ for a 'folded-down' corrugation is much reduced from the open profile value, and has been experimentally determined as 0.020 for this 2.1 metre sheet fastened in every corrugation.

The minor factors due to seam slip, pure shear strain etc., have been determined from the expressions of section (10. 4)

The observed and theoretical deflection comparisons are shown for $w = 1$ kN/m on page 284 and are in good agreement. It is clear that the bending deflection is by far the biggest contributor to the total. The complete load-deflection plot to failure is shown in Fig. (12.1).

The alternative test data for the open profiles sheeting is,

I	Fold line lateral inertia	1.19 x 10^6 mm^2

b	Sheet span	2.05 metres
t	Sheet thickness	0.57 mm
F_s	Strength per seam fastener	1.43 kN
F_p	Strength per edge fastener	3.42 kN
n_s	Number of seam fasteners on the end seam equals 33 and this varies linearly along the length	
d	Trough pitch	178 mm

$\bar{K}$ for the various fastening details have been theoretically determined and experimentally verified as,

0.022	for double trough fastened sheets
0.110	for every trough fastening
0.747	for alternate fastening
0.066	for double fastening and every trough fastenings, alternately (approximate)

The theoretical component deflections are also given on page for w = 1 kN/m for a number of different fastening arrangements, which are summarised below. The figures in brackets represent the fastening distance.

Test 1	Every (5.4 m), Alternate (5.4 m)
Test 2	Every/double (4.1 m), Every (5.1 m), Alternate (1.6 m)
Test 3	Double (5.4 m), Every (5.4 m)

The load-deflection curves for each test are given in Figs. (12.2) to (12.4).

12.2. Discussion of Deflection Comparisons

It is apparent from all the load deflection graphs for the four tests that initially the movements at all points are stiffer than in the mid load range. This is due to the bearing of the flanges of the beam on the runners which provide the lateral buckling restraint. In addition the test rig was constructed in the open which meant that over

a period of weeks there was an unavoidable increase in the frictional resistance.

Nevertheless, the deflection per kN at about half the failure load was measured for comparison with the theoretical deflection. On page 284 the tabulations assume that all the shear force is absorbed by the corrugated web.

For the closed profile the total shear deflection is only about 20% of the bending deflection which reaffirms that this corrugation is indeed extremely stiff. In the actual prototype roof the fold line areas are some 25% greater but if the plate test movement is reduced by the extra beam inertia and multiplied by $(\sin 35^{o})^{-1}$, then the predicted deflection for a load of 0.75 kN/m^2 is 25 mm. The corresponding recorded deflection during the roof test on reloading was 28 mm.

This correlation does indicate that the main frictional resistance is only of an initial nature, and hence the observed deflections may be taken as being reasonably accurate.

The deflections for the open profiles often differ considerably from the simple theory. However, this may be accounted for by including the effect of fold line inertia which implies that some of the shear force is taken by the fold lines where the web is very flexible.

Below the load-deflection plot for each test, the theoretical shear displacements along the sheet length are indicated. For the appropriate data, the finite difference analysis of section (11.4) has been performed and the corresponding solutions are superimposed.

Test 1 is for a typical fastening arrangement of equal regions of every and alternate trough attachment. In this case the observed central deflection is some 30% less than its simple theory prediction. The quarter point deflections, however, are reasonable and this indicates that some central flange restraint does occur. The finite difference comparison agrees well with the observed deflection as in Fig. (12.2).

Test 2 is a rather more complex form of fastening but it again highlights the flange stiffening of a relatively narrow flexible band.

The observed deflection is about 25% less than in theory but again the finite difference analysis presents a reasonably close approximation.

Test 3 represents a much stiffer web where the shear deformation is less than that due to flange axial strain. Double trough fastening, studied in Section (5. 3) almost eliminates shear distortion and as expected the flange bending stiffness makes little difference to the theoretical deflection.

The observed shear deflections were obtained by subtracting the theoretical bending deflection from the measured total. It should be borne in mind that the shear deflection of Test 1 is almost 5 times the bending deflection, indicating the importance of accurate quantification of the distortional flexibility.

Test 4 on the pressed sheeting shows good agreement between the observed and theoretical deflections which are some 50% stiffer than the previous test 3, for the open profiled sheeting of roughly the same proportions.

12.3. Corrugated Web Beam Test Results

TEST 1: Open Profile - (Fig. 12.2).
Points 1 and 2 are mid and quarter span readings respectively. All deflections are mm per 1 kN/m distributed load.

Point	Observed Deflection	Bending Deflection	Distortion Deflection	Shear Strain Slip etc	Total Shear Deflection	Theoretical Deflection
2	13.2	4.5	9.5	1.2	10.7	15.2
1	26.6	6.5	29.5	1.8	30.3	37.8

TEST 2: Open Profile - (Fig. 12.3)

Point	Observed Deflection	Bending Deflection	Distortion Deflection	Shear Strain Slip etc	Total Shear Deflection	Theoretical Deflection
2	9.6	4.5	6.8	1.1	7.3	12.2
1	13.7	6.5	11.6	1.7	11.3	18.8

TEST 3: Open Profile - (Fig. 12.4)

Point	Observed Deflection	Bending Deflection	Distortion Deflection	Shear Strain Slip etc	Total Shear Deflection	Theoretical Deflection
2	7.2	4.5	2.0	0.8	2.8	7.3
1	10.8	6.5	4.8	1.2	6.0	12.5

TEST 4: Pressed Sheeting with Folded down Ends - (Fig. 12.1)

Point	Observed Deflection mm	Bending Deflection	Distortion Deflection	Shear Strain Slip etc	Total Shear Deflection	Theoretical Deflection
2	5.5	4.5	0.4	0.6	1.0	5.5
1	7.2	6.5	0.5	0.9	1.4	7.9

NOTE: The theoretical deflection does not include the flange lateral bending stiffness.

12.4. Comparison of the Failure Loads with Theory

Each test will be considered in turn and the theoretical failure loads are indicated for each of the observed collapse modes. The contribution of fastener slip to the central deflection is quite small and severe non-linearity in the load deflection plot is really only noticeable for the large tearing deformations just prior to collapse.

Test 1: Sheet-flange fastener failure occurred at the boundary between the alternate and every trough fastening regions. This was observed at an equivalent end shear of 41 kN.

The theoretical end shear capacity at this point is,

$$\frac{10.8}{5.4} \times 3.42 \times \frac{2050}{300} = 46 \text{ kN}$$

Failure was probably exacerbated by the closeness of the jack loading point of 4.6 kN.

Test 2: Failure occurred by seam tearing at 49 kN. The theoretical end failure shear, according to Section (10.3), for roofing profiles where fastenings are along the corrugation crest, is,

$$Q = \left\{ \frac{n_{sh}}{n_{sh} - 2} \left\{ n_s + g_1 \frac{S_s}{S} \right\} F_s \right\}$$

where $n_{sh} = 30$ $g_1 = 0.8$

$$Q = 1.07 \times 34.8 \times 1.43 = 53 \text{ kN}$$

Test 3: For this test an extra five seam fasteners were introduced and failure occurred by global shear buckling at a load of 54 kN.

The theoretical failure load in this case is 51 kN which was determined according to Easley's formula

$$Q_{crit} = \frac{36\, D_x^{1/4} D_y^{3/4}}{b}$$

where $D_y = (143\ mm^4/mm) \cdot E$ $\quad D_x = \frac{0.57^3}{12\,(1 - \nu^2)} \times \frac{E}{1.24} = .013\ E$

Test 4: In this case the pressed sheeting was used with folded down ends, and failure occurred in three stages. Firstly, due to the flat portion of sheeting around the sheet-fold fasteners, local buckling was noticed at about 90% of the actual collapse load. Secondly, slight shear buckling was noticed at about 95% and finally failure of the end seam occured at an end shear of 94kN.

Local buckling cannot be estimated although the fastenings are still able to carry additional load. The theoretical shear buckling load, as above, for,

$$D_y = 174\ E \qquad D_x = \frac{150}{171} \cdot \frac{0.97^3 E}{12\,(1 - 0.25^2)} = 0.071E$$

is $Q_{crit} = 89.5$ kN

The seam failure load for an upstand seam, where edge fastenings lie on either side, constitutes a decking profile for analysis sake. Therefore,

$$Q = \frac{(n_{sh})}{(n_{sh} - 2)} \cdot \frac{\left(\frac{n_s}{S_s} + \frac{n_p g_1}{2S}\right)}{\left(\frac{n_s}{S_s} + \frac{n_p}{2S}\right)} \{2F_p + n_s F_s\}$$

where $n_{sh} = 24$, $g_1 = 1.56$, $n_p = 2$

$$Q = 1.09 \times 1.10 \times (2 \times 5.82 + 24 \times 2.43) = 84\ kN$$

However, the upstand seam has been shown to have slightly superior load carrying characteristics of 2.7 kN/mm sheet thickness and in this case,

$$Q = 1.09 \times 1.10 \times (2 \times 5.82 + 24 \times 2.62) = 89 \text{ kN}$$

The discrepancy of 5 kN between observed and theoretical failure is probably due to frictional resistance of the runners. For the actual prototype roof test 22 rather than 24 seam fasteners were used in order to ensure that failure occurs by seam tearing.

C H A P T E R 1 3

CONCLUSIONS TO THESIS

13.1. Summary of Main Observations

The purpose of this thesis has been to present approximate analyses for the behaviour of corrugated sheeting in shear. This includes the in-plane deflection and the strength of the connections, as well as the shear buckling capacity of the profile spanning between purlins. In many cases the diaphragm strength is controlled by local effects such as deformation around an opening.

More emphasis has been placed on deriving approximate design formulae for the basic components of flexibility and strength, which may be verified by experimental and more accurate theoretical observations. Chapters 2 to 7 deal with the shear displacement of diaphragms. Chapters 8 and 9 consider the strength of the sheeting and connections, and Chapters 10, 11 and 12 apply the design information to folded plate roofs utilizing corrugated sheeting.

The main conclusions are listed below in points, to be followed by design examples.

1. A new formula has been developed for the shear flexibility of corrugated sheeting for fastening in every or alternate troughs. This also takes into account fastening to intermediate purlins. Profile distortion, due to the eccentricity of fastener resistance, accounts for the majority of the in-plane deflection and it has been found that deformation is localized near to the sheet ends rather than being linearly varying along the sheet length. Hence the flexibility due to distortion, parallel to the corrugations is,

$$C_{1.1} = \frac{a d^{2.5} \bar{K}}{E t^{2.5} b^2}$$

where $\bar{K}$ is a dimensionless parameter depending on the profile shape and fastening arrangement only, as tabulated in Appendix 2. The parameters are defined in Section (1.4).

A considerable range of profile shapes and sheet lengths were experimentally studied to verify this design formula. However, for sheets fastened in every third trough or for short lengths of alternate trough fastening, distortion may be more accurately treated by assuming linear plate movements. For these cases $\bar{K}$ is taken as the greater of the tabulated value or,

$$\bar{K} = \frac{0.144\ d^{1.5}\ K}{t^{0.5}\ b}$$

All the factors $\bar{K}$ and K are reduced by the influence of end attachment to purlins which restricts free anti-symmetric profile distortion. Sinusoidal profiles distort in a similar fashion and their corresponding parameters are shown in Fig. (4.1).

For sheets overhanging beyond the outer purlins, the complete sheet length should be used in the distortion design formula. Insulation attachment reduces the deformation of alternately fastened corrugations, but this relies on the bitumen bond, and can only be justified by experimental varification.

2. Sheets often have to be overlapped along their length to form the full diaphragm depth. To establish the overall panel flexibility, an overlap slip factor Σ may be used. Where deformation occurs by local distortion, consistent with the use of $\bar{K}$ in the individual sheet flexibility formula, $C_{1.1}$, the complete diaphragm flexibility is,

$$\frac{C_{1.1}}{N^2}\ (1 + N\Sigma)$$

A different formula exists for linear plate movements. These relationships apply for uniform fastening throughout, but a corresponding expression has been developed for every trough fastening at the sheet ends and alternate fastening at the overlaps as in Chapter (6.6.).

3. Diaphragms need not necessarily comprise sheets attached to purlins. For sheets spanning normal to the applied shear force across rafters the distortion shear flexibility is modified to,

$$C_{1.1}\ \left(\frac{b}{a}\right)^2$$

Due to the variation of shear force across rafters continuous sheeting can only shear deflect differentially by in-plane bending, which does contribute to an increase in the shear stiffness. Sheets normally have to be overlapped at the rafters and the central deflection is reduced by profile distortion interaction. For shear flexibility caused by local plate deformation, the central deflection for N overlapping sheets is approximately,

$$C_{1.1} \left(\frac{b}{a}\right)^2 \frac{N^2}{8} \left\{\frac{2}{N} + \left(1 - \frac{2}{N}\right)\varepsilon\right\}$$

Corresponding formulae have been developed for linear plate movements and variations in fastening arrangement. The inertia of the continuous diaphragm beam may also be increased by including the web of the girder multiplied by a reduction factor due to fastener slip.

4. Diaphragm strength is usually controlled by the capacity of the seam connections. However, in order that the seams may slip during failure, the strength of the sheet purlin fasteners is mobilized, which is transfered via the lateral rigidity of the purlins. A new formula has been developed for the seam flexibility and strength which takes account of the lateral bending and torsional stiffness of the purlins in terms of a factor g.

The seam slip is,

$$C_{2.2} = \frac{1}{\frac{n_s}{S_s} + g.n.\frac{n_p}{S}}$$

g is ideally 1/12 for linear purlin movements, and the parameters are defined in Section (8.4). g may be determined from Fig. (8.8) for the various purlin properties, which is related to the effective width of sheet-purlin fastening acting with the seam.

The ultimate seam strength may be given by,

$$Q_S = F_S n_s + 2.g.n.n_p F_p$$

This formula gives a more realistic estimate for diaphragm strength, especially for the case of indirect shear transfer where shear- connectors

are not used. In general, most panels broader than 3 metres require an effective sheet width approach which implies that the longitudinal edge capacity is independent of increasing diaphragm width.

Openings in diaphragms cause locally high sheet-purlin fastener forces and purlin lateral bending stresses, which may be determined using the computer program of Appendix (5), as derived from the solution of the controlling differential equation.

6. Shear buckling between purlins is not normally a design criterion, but it has been experimentally and theoretically shown that buckling is highly influenced by the pitch of the purlin fastenings. For sheeting of single span, b, fastened in every trough the shear buckling load (kN/mm) is reliably given by,

$$Q_{cr} = \frac{36}{b^2} Dx^{1/4} Dy^{3/4}$$

However, for lightly fastened intermediate purlins, there is a liklihood that a buckling wave can pass along the full diaphragm depth rather than between the points of support. As a suggested design formula for multispan sheeting, of overall length b, the design capacity should be no more than $0.5\ Q_{cr}$.

For edge fasteners in alternate or third troughs, the capacity is also reduced.

7. Folded plate roofs using corrugated sheeting spanning between fold lines may be designed as a girder, according to the fastener strength, shear buckling and deflection criteria of the previous sections.

Some additional problems have been studied such as the effect of variations in the shear flexibility which are smoothed by the stiffness of the fold lines. Holes in folded plates are an important design problem. Ideally, the central sheets may be removed and the fold lines checked for compression buckling taking into account the elastic restraint of the sheet-fold fasteners.

A number of panels of 21.6 metre span were studied experimentally and varified the design formulae. The central shear deflection may be reduced by using corrugations which have closed ends and a prototype pressed sheet was developed which was observed to be seven times stiffer than the corresponding open profile.

A full scale folded plate roof was constructed which deflected and failed almost exactly as according to theory. At the working vertical uniform load of 0.75 kN/mm^2, the central movement was only 36 mm, and seam failure occurred at a load of 2.3 kN/m^2 which corresponded to a maximum panel shear of 78 kN. A summary of the design is shown in Appendix 4.

A number of typical calculations for the flexiblity and strength of practical diaphragms follow.

13.2. Design Examples

Flexibility design examples for profiles with a trough pitch of 150 mm, sheet thickness of 0.7 mm and Young's modulus of 207 kN/mm^2.

1. 1 sheet 4.5 metres long, fastened in every trough to two intermediate purlins . ($\bar{K} = 0.2$). The distortion flexibility is:

$$C_{1.1} = \frac{150^{2.5}\ \bar{K}}{0.7^{2.5} \times 4500^2 \times 207} = .000032 \text{ mm/kN/mm;}$$

$\bar{G}$ = 8.8 kN/mm^2 - effective shear modulus

2. 1 sheet 4.5 metres long fastened in alternate troughs to two intermediate purlins, $\bar{K} = 1.0$, K = 16

Choose greater of $\bar{K}$ or $\frac{0.144 \times d^{1.5} K}{t^{0.5} b} = 1.12$

$$C_{1.1} = \frac{150^{2.5} \times 1.12}{0.7^{2.5} \times 4500^2 \times 207} = .00018 \text{ mm/kN/mm;}$$

$\bar{G}$ = 1.8 kN/mm^2

3. 3 overlapped sheets each of 4.5 m length as in 1, fastened in every trough throughout ($\mathfrak{E}$ = 0.3). The overall flexibility is,

$$\frac{C_{1.1}}{n^2}(1 + n\mathfrak{E}) = \frac{.000032}{3^2}(1 + 0.3 \times 3) = .0000068;$$

$$\bar{G} = 13.1$$

The flexibility of unconnected sheets is .000011 mm/kN/mm and for continuous sheeting is .0000036 mm/kN/mm.

4. 3 overlapped sheets each of 4.5 m length as in 2, fastened in alternate troughs throughout ($\mathfrak{E}$ = 0.2). The overall flexibility is,

$$\frac{C_{1.1}}{n^3}(1 + n^2\mathfrak{E}) = \frac{.00018}{3}(1 + 0.2 \times 3^2) = .000019;$$

$$\bar{G} = 5.3$$

It should be noted that the deformation of the individual sheets in this case corresponds to linear plate movements, consistent with the use of K rather than $\bar{K}$. The overall flexibility is expressed by this modified form.

5. 3 overlapped sheets each of 4.5 m length as in 2, fastened in every trough at the diaphragm ends and in alternate troughs at the overlaps ($\mathfrak{E}$ = 0.2, N = 3).

$$C_{1.1} = .00018 \times \frac{\mathfrak{E}}{6\mathfrak{E} + N(2 - \mathfrak{E})} + \frac{.000032}{N} = .000015:$$

$$\bar{G} = 6.4$$

This formula is given in Appendix Table (3.4) and applies to linear plate movements. An alternative expression has been developed for localized end distortion.

6. 1 sheet, 7.5 metres long, fastened in every trough at its ends and in alternate troughs at 4 intermediate purlins.

$\bar{K}$ for 4 intermediate purlins is 0.2
$\bar{K}$ for no intermediate purlins is 0.08
This case corresponds to the average of the above values.

$$C_{1.1} = \frac{150^{2.5} \times 0.14}{0.7^{2.5} \times 7500^2 \times 207} = .0000081;$$

$$\bar{G} = 17.6$$

7. Three overlapping sheets in a six bay continuous diaphragm of 18 m length as in Fig. (13.1). Fastening is in every corrugation at the diaphragm edges and in alternate troughs internally.

The flexibility of the individual sheets spanning 6 m perpendicular to the applied shear force is, ($\bar{K} = 1$)

$$\frac{a\bar{K}d^{2.5}}{Et^{2.5}b^2}\left(\frac{b^2}{a^2}\right) = \frac{150^{2.5}}{207 \times 0.7^{2.5} \times 6000} = 0.54 \text{ mm/kN}$$

The central deflection is the superposition of two cases. Firstly due to the overlapping sheets, fastened in alternate troughs as in Fig. (7.14).

$$\delta_2 = 0.54 \frac{M^2}{8}\left\{\frac{1}{4M-6} + \frac{2M-4}{2M+1}\Sigma\right\} \times 2$$

For M = 3, $\Sigma = 0.2$; therefore, $\delta_2 = 0.28$ mm/kN rafter force.

Due to the deflection of the centre of the sheet between overlaps, $\delta_1 = 0.54$ mm/kN.

Therefore, the total central deflection due to shear distortion is 0.82 mm/kN rafter force.

For alternate trough fastening throughout, the central deflection would be,

$$\Delta = 0.54 \times \{ \frac{2}{M} + (1 - \frac{2}{M})\Sigma \} \times 2 + 0.54 = 1.33 \text{ mm/kN}$$

8. The diaphragm with a central opening as in Fig. (8.23) is part of a 4 bay beam of 18 metre span. Fig. (13.2) shows the general layout with shear connectors only at the outer rafters. Using the differential equation solutions of Fig. (8.24), the local forces induced around the opening may be used to evaluate the diaphragm capacity for realistic purlin sizes.

The maximum sheet-purlin fastener force is 0.09 kN and this may be combined with the local force from seam slip (0.09 kN) and the perpendicular simple shear component (0.06 kN) to give a resultant of 0.19 kN/kN shear force. If the sheet-purlin fastener capacity (Fp) is 4 kN then the maximum rafter force is 4/(1.5 x 0.19) = 14.0 kN.

For indirect shear force from the rafter to the purlins the induced sheet-purlin fastener force is determined using a value for g based on a typical effective sheet width of 1.5 metres. Thus,

$$g = \frac{1}{12} \cdot \frac{a_{eff}}{a} = \frac{1}{36}$$

For four purlins as in Fig. (13.2) the diaphragm capacity, determined by the extreme sheet-purlin fastener force is,

$Q = 2g.n.np\ Fp$ where n = number of sheet-purlin fasteners (= 16)
= 14.2 kN rafter force

Thus failure will occur in the sheet purlin fasteners almost simultaneously around the opening and at the rafter, corresponding to a maximum shear force of 21 kN.

The distortional flexibility of the panel is 0.5 mm/kN. Other factors such as the fastener slip, axial strain, etc., amount to 0.55mm/kN. Hence the total central deflection per unit rafter force is 2.1mm/kN.

REFERENCES

1. INNES, P. et al — "Fasteners for Light Gauge Steel Construction", Thin Walled Steel Structures (book).

2. BRYAN, E. R. and EL DAKHAKHNI, W. M. — "Shear in Thin Plates with Flexible Edge Members", Proc. American Soc. of Civil Engineers, J. Struct. Div. August 1964.

3. NILSON, A. H. — "Shear Diaphragms in Light Gauge Steel" Proc. American Soc. of Civil Engineers, J. Struct. Div., November 1960.

4. BRYAN, E. R. — "The Stressed Skin Design of Steel Buildings", Constrado Monograph (book).

5. MILLER, C. J. — "Analysis of Multi-Storey Frames with Light Gauge Steel Panel Infills", Res. Rep. No. 349, Dept. of Struct. Engrg. Cornell University, August 1972.

6. NILSON, A. H. — "Testing a Light Gauge Steel Hyperbolic Paraboloid Shell", Proc. American Soc. of Civil Engineers, J. Struct. Div. October 1962.

7. EL-ATROUZY, M. N. and ABDEL-SAYED, G. — "Shell Roofs and Grain Bins made of Corrugated Steel Sheets", Proc. 2nd Speciality Conf. on Cold Formed Steel Structures, Rolla Missouri, October 1973.

8. LUTTRELL, L. D. — "Screw Connected Shear Diaphragms", Proc. 2nd. Spec. Conf. on Cold Formed Steel Structures, Rolla Missouri, October 1973.

9. DAVIES, J. M. — "The Plastic Collapse of Framed Structures Clad with Corrugated Steel Sheeting", Proc. Inst. of Civil Engineers, March 1973.

10. ERRERA, S. J. et al — "Columns and Beams Braced by Diaphragm", Proc. American Soc. of Civil Engineers, J. Struct. Div. February, 1967.

11. TARLTON, D. L. "Diaphragm Action", Design in Cold Formed Steel, Solid Mech. Div. University of Waterloo, Ontario, 1974.

12. LUTTRELL, L. D. "Light Gauge Steel Shear Diaphragms", Civ. Eng. Dept. Report, West Virginia University, 1965.

13. Canadian Sheet Steel Building Institute "Diaphragm Action of Cellular Steel Floor and Roof Deck Construction", December 1972.

14. BRYAN, E. R. and EL DAKHAKHNI, W. M. "Behaviour of Sheeted Portal Frame Sheds: Theory and Experiments", Proc. Inst. of Civil Engrs. December, 1964.

15. NILSON, A. H. "Analysis of Light Gauge Shear Panels", Proc. 2nd Spec. Conf. on Cold Formed Steel Structs., Rolla Missouri, October 1973.

16. LAWRENCE, S. J. and SVED, G. "A Finite Element Analysis of Clad Structures", Conf. on Metal Structures Research and its Applications, Sydney 1972.

17. DAVIES, J. M. "Calculation of Steel Diaphragm Behaviour", Proc. Am. Soc. of Civil Engrs. Struct. Div. July 1976.

18. SEDEN, M. R. "The Stiffening of Light Cladding on Steel Structures", PhD, University of Salford, 1975.

19. ELLIFRITT, D. S. and LUTTRELL, L. R. "Strength and Stiffness of Steel Deck Subjected to In-Plane Loading", Rep. No. 2011, Dept. of Civil Engineering, West Virginia University, 1970.

20. EASLEY, J. T. "Buckling Formulas for Corrugated Metal Shear Diaphragms", Proc. American Soc. of Civil Engrs. J. Struct. Div. July, 1975.

21. THOMPSON, F. "The design Development of Light Gauge Steel Folded Plate Structures", MSc Thesis, University of Salford, 1974.

22. THORNTON, C. H. and TOMASETTI, R. L. "Hangar Features Stressed Skin Hypers", Civil Engrg. ASCE, November 1970.

23. GERGELY, P. "Stability of Thin Steel Hyperbolic Paraboloid Roofs", Inst. Am. of Bridge and Struct. Eng. North Congress, May, 1972.

24. ABDEL SAYED, G. "Critical Shear Loading of Curved Panels of Corrugated Sheets", Proc. American Soc. of Civil Engrs. J. Eng. Mech. December, 1970.

25. YOUNG, J. G. "The Analysis of Corrugated Cylindrical Shell Roofs", PhD Thesis, University of Salford, 1976.

26. HLAVACEK, V. "The Effect of Support Conditions on the Stiffness of Corrugated Sheets Subject to Shear", ACTA Technica Csov No. 2, 1972.

27. BRYAN, E. R. and JACKSON, P. "The Shear Behaviour of Corrugated Steel Sheeting", Symposium on Thin Walled Steel Structures", University of Swansea, September 1967.

28. ROTHWELL, A. "The Shear Stiffness of Flat Sided Corrugated Webs", Aero Quarterly, August 1968.

29. BRYAN, E. R. and EL DAKHAKHNI, W. M. "Shear Flexibility and Strength of Corrugated Decks", Proc. American Soc. of Civil Engrs. J. Struct. Div. Nov. 1968.

30. HORNE, M. R. and RASLAN, R. A. S. "An Energy Solution to the Shear Deformation of Corrugated Plates, Publ. Int. Assoc. of Bridge and Structural Eng. 31 - I, 1971.

31. HORNE, M. R. and RASLAN, R. A. S. "A Finite Difference approach to Corrugated Shear Panels", Publ. IABSE 31 - I, 1971.

32. LIBOVE, C. and LIN, C. "Theoretical Study of Corrugated Plates: Shearing of a Trapezoidally Corrugated Plate with Trough Lines Permitted to Curve", Dept. of Mech. and Aero. Eng. Syracuse University, Rep. No. MAE 1833 - T2, June 1970.

33. STREHL, C. "Berechnung Regelmassig Periodisch Anfgebauter Faltwerksquerschnitte unter Schubbelastung am Beispeil des Trapezbleches", Technische Hochschule Darmstadt, 1975.

34. BAERE, W. "Skivverkan Av Trapetsprofilerad Plat", Stalbyggnad, Kungliga Tekniska Hogsholan, Stockholm, 1975.

35. TING, R. "Structural Behaviour of Light Gauge Shear Diaphragm", PhD thesis, University of Pittsburg 1973.

36. FALKENBERG, J.C. Discussion of Ref. 29, above. Proc. Am. Soc. of Civil Engrs. Jnl. Struct. Div. June 1969.

37. DAVIES, J. M. and LAWSON, R. M. "The Shear Flexibility of Corrugated Steel Sheeting", Third International Spec. Conf. on Cold Formed Steel Structures University of Missouri - Rolla, Nov., 1975.

38. LAWSON, R. M. "The Flexibility of Practical Shear Diaphragms", University of Salford Report, 75/69, September 1975.

39. HSIAO, C. and LIBOVE, C. "Theoretical Study of Corrugated Plates with Discrete Attachments to a Rigid Flange", Dept. of Mech. and Aero Eng. Syracuse Univ. Rep. No. MAE 1833 - T3, July 1971.

40. LIN, C. and LIBOVE, C. "Shearing of a Trapezoidally Corrugated Plate with Trough Lines held Straight", Dept. of Mech. and Aero Eng. Syracuse Univ. Rep. No. MAE, 1833 - T1, May 1970.

41. McKENZIE, K. I. "The Shear Stiffness of a Corrugated Web", Aero. Res. Council R. and M. 3342, 1963.

42. WU L. H. and LIBOVE, C. "Shearing of a Corrugated Plate with Curvilinear Corrugations", Dept. of Mech. and Aero. Eng. Syracuse Univ. Rep. No. MAE 1833 - T4, January 1972.

43. HETENYI, M. "Beams on Elastic Foundations", University of Michigan Press, (book).

44. JAPIN, D. "Behaviour of Insulated Metal Decking under Shear Load", MSc Thesis University of Salford, November 1974.

45. BRYAN, E. R. "Stressed Skin Roof Decks for SEAC and CLASP Building Systems", Constrado March, 1973.

46. FRACZEK, J. "Mechanical Connections in Cold Formed Steel", Cornell University Res. Rep. No. 359, Sept. 1975.

47. European Convention for Constructional Steel Work Committee 17, "Stressed Skin Design", Draft May 1975.

48. BRYAN, E. R. "Aluminium Diaphragms", Civil Engineering February, 1974.

49. DAVIES, J. M. "Light Gauge Steel Folded Plate Roofs", University of Salford Report, 75/58, Jan. 1975.

50. SOUTHWELL, R. V. and SKAN, S. W. "On the Stability under Shearing Forces of a Flat Elastic Strip", Proc. Roy. Soc. A. Vol 105, May 1924.

51. STOWELL, E. T. "Critical Shear Stress of an Infinitely Long Flate Plate with Equal Restraints against Rotation Along the Parrallel Edges", NACA Report 3K12, 1943.

52. BUDIANSKI, B. and CONNOR, R. W. "Buckling Stresses of Clamped Rectangular Flat Plates in Shear", NACA TN 1559, 1948.

53. BATDORF, S. B. and STEIN, M "Critical Combinations of Shear and Direct Stress for Simply Supported Rectangular Flat Plates", NACA TN 1223 1947.

54. CRATE, H. and LO, H. "Effect of Longitudinal Stiffeners on the Buckling Load of Long Flat Plates in Shear" NACA TN 1589, 1948.

55. BERGMANN, S and REISSNER, H. "Neuere Probleme ans der Flugzeugstatik" Zeitschrift Flugtech und Motorluftsch, Vol. 20, 1929.

56. SEYDEL, E. "The Critical Shear Load of Rectangular Plates", NACA TN 705, 1933.

57. PETERSON, J. and CARD, M. "Investigation of the Buckling Strength of Corrugated Webs in Shear", NASA TN D 42[illegible] 1960.

58. HLAVACEK, V. "Shear Instability of Orthotropic Panels" Acta Technica Csov No. 1, 1968.

59. EASLEY, J. and McFARLAND "Buckling of Light Gauge Corrugated Metal Shear Diaphragms", Proc. Am. Soc. of Civil Engrs. Struct. Div. July, 1969.

60. LAWSON, R. M. Discussion of reference 20, Proc. Am. Soc. of Civil Engineers, Struct Div. May, 1976.

61. GRAHAM, H. T. "New Way to Build a Shell", Architectural Record, March 1962.

62. GERGELY, P. and WINTER, G. "Experimental Investigation of Thin Steel Hyperbolic Paraboloid Structures", Proc. Am. Soc. of Civil Engrs. Struct. Div. October 1972.

63. BANAVALKAR, P. V. and GERGELY, P. "Analysis of Thin Steel Hyperbolic Paraboloid Shells", Proc. Am. Soc. of Civil Engrs. Struct. Div. November 1972.

64. "Folded Plate Roof Design", H. H. Roberstson Company, Pittsburg, Pa USA, 1967.

65. WINTER, G. and PEI, M. "Hipped Plate Construction", Journal of American Concrete Institute, January 1947.

66. CRAEMER, H. "Design of Prismatic Shells", Jn. Am. Concrete Inst. February 1953.

67. GAAFAR, I. "Hipped Plates", Trans. Am. Soc. Civ. Engrs., 1954.

68. THADANI, B. N. "The Analysis of Hipped Plate Structures by Influence Coefficients", Indian Concrete Journal, April, 1957.

69. KETCHUM, M. S. "Design and Construction of Folded Plate System", Jn. Am. Concrete Inst. January 1955.

70. SIMPSON, H. "Design of Folded plate Roofs", Proc. Am. Soc. of Civ. Engrs. Struct. Div. January 1958.

71. TRAUM, E. "Design of Folded Plate", Proc. Am. Soc. of Civ. Engrs. Struct. Div. October 1959.

72. BAER, O. "Steel Frame Folded Plate Roof", Proc. Am. Soc. of Civ. Engrs. Struct. Div. June 1961.

73. SHAPIRO, D. "Load Test on Folded Plate Roof", Eng. News Record, July 1961.

74. NILSON, A. H. "Folded Plate Structures of Light Gauge Steel", Proc. Am. soc. of civ. engrs. Struct. Div. October 1961.

75. SCORDELIS, A. C. "Matrix Formulation of Folded Plates", Trans. Am. Soc. of Civ. Engrs. II 1961.

76. YITZAKI, D. and REISS, M. "Analysis of Folded Plates", Proc. Am. Soc. of Civ. Engrs. Struct. Div. October 1962.

77. BORN, J. "Hipped Plate Structures", (book), Crosby Lockwood, London, 1962.

78. MEEK, J. L. "Matrix Derivation of Folded Plate Roof", Proc. Am. Soc. of Civ. Engrs. June 1963.

79. FIALKOW, M. N. "Folded Plate Analysis by Minimum Energy Principle", Proc. Am. Soc. of Civ. Engrs. Struct. Div. June 1962.

80. GOBLE, G. G. "Analysis of Folded plate Structures", Proc. Am. Soc. of Civ. Engrs. Struct. Div. December 1964.

81. SETHARAMULU, K. "Analysis of Short Span Folded Plates", Proc. Am. Soc. of Civ. Engrs. June 1964.

82. DEFRIES, A. and SCORDELIS, A. "Direct Stiffness Solution of Folded Plate", Proc. Am. Soc. of Civ. Engrs. Struct. Div. August 1964.

83. LEE, S. PULMANO, V. A. and LIN, T. J. "Ribless Folded Plates", Proc. Am. Soc. of Civ. Engrs. Struct. Div. February 1965.

84. REISS, M. and YITZAKI, M. "Analysis of Short Folded Plates", Proc. Am. Soc. of Civ. Engrs. Struct. Div. October 1965.

85. POWELL, G. H. "Comparison of Simplified Theories for Folded Plates", Proc. Am. Soc. of Civ. Engrs. Struct. Div. December 1965.

86. BEAUFAIT, F. W. "Analysis of Continuous Folded Plate Surface", Proc. Am. Soc. of Civ. Engrs. Struct. Div. December 1965.

87. FARMER, L. E. and BREEN, J. E. "Non-Linear Solution for Folded Plate Structures", Proc. Am. Soc. of Civ. Engrs. Struct. Div. April 1966.

88. MAST, P. E. "New Method for Exact Analysis of Folded Plates", Proc. Am. Soc. of Civ. Engrs. Struct. Div., April 1967.

89. JOHNSON, C. D. and LEE, T. "Experimental Study of Non-Prismatic Folded Plates", Proc. Am. Soc. of Civ. Engrs. Struct. Div., June 1968.

90. LEE, T. and VOS, R. G. "Multiple Folded Plates with Various End Conditions", Proc. Am. Soc. of Civ. Engrs. Struct. Div. July 1968.

91. CHEUNG, Y. K. "Folded Plate by Strip Method", Proc. Am. Soc. of Civ. Engrs. Struct. Div. December 1969.

92. "Folded Plate Tops New School", Building Construction 1965.

93. SHOGREN, V. E. "Folded Steel Plate Roof For a Suburban Branch Bank", American Iron and Steel Co. Journal, January 1964.

94. DAVIES, J. M. "Light Gauge Steel Folded Plate Roofs" The Structural Engineer, May 1976.

95. SCHOELLER, W. C. et al "Cold Formed Folded Plate Structures", First Speciality Conference on Cold Formed Steel Structures Missouri - Rolla, November 1971.

96. DAVIES, J. M., LAWSON, R. M. and YOUNG, J. G. "Calculated and Observed Behaviour of Steel Folded Plate of a Nursery School", Performance of Building Structures, Glasgow University, 1976.

97. DAVIES, J. M. and THOMPSON, F. "Light Gauge Steel Folded Plate Construction" Int. Assn. of Bridge and Struct. Eng. Memoires 36 - II 1976.

98. "Light Gauge Metal Roof Decks", Metal Roof Deck Association, 1970.

99. "Big Break for Folded Plate Roofs", Contract Journal July 1976.

100. "Roof Failure Proves Theory", New Civil Engineer, 22nd July 1976.

THE FLEXIBILITY AND STRENGTH OF CORRUGATED DIAPHRAGMS AND FOLDED PLATES

VOLUME 2.

A Thesis Submitted for
the Degree of
DOCTOR OF PHILOSOPHY

by

Robert Mark Lawson, B.Sc., A.C.G.I.

Department of Civil Engineering,
University of Salford

September 1976

PAGE

NUMBERING

AS ORIGINAL

VOLUME 2

C O N T E N T S

LIST OF FIGURES

FIGURES

APPENDIX 1

Experimental Test Results

APPENDIX 2

Design Data for Corrugated Sheeting Flexibility

APPENDIX 3

Sheet Overlap Design Data

APPENDIX 4

Folded Plate Roof Design

APPENDIX 5

Computer Programs

LIST OF FIGURES

CHAPTER 1.

1. A typical roof diaphragm
2. Equilibrium of sheet and members
3. A practical diaphragm arrangement
4. Diaphragm restraint of frame sway
5. Sheet flexibilities in normal directions
6. Flexibilities due to fastener slip
7. Complete lateral stability of roof provided by the sheeting
8. Spread of pitched roof portal frame under normal load
9. Forms of frameless structure - folded plate roof
10. Hyperbolic paraboloid
11. Cylindrical shell

CHAPTER 2.

1. Shear distortion for every trough fixing
2. Warping due to plate movements
3. Cross-sectional bending moments
4. Superposition of Fourier terms
5. Asymptotic behaviour of shear distortion
6. Standard test rig
7. Finite element representation
8. Edge beam restraint due to every trough fixing
9. Summary of cross-sectional bending moments
10. Profile displacements along sheet length
11. Effect of profile shape and sheet length on K parameter
12. End cross-section displacements
13, 14. Variation of K parameter with number of Fourier terms
15. Effect of pitch and thickness
16. Variation of K with sheet thickness
17. Purlin prop reduction of K value
18. Effect of profile shape on $\bar{K}$ parameter

19. Trough movement restrained at two intermediate purlins

20. Fastening in every trough at the ends and in alternate troughs at the intermediate purlins

21. Effect of increasing number of intermediate purlins

22. Effect of increasing number of Fourier terms, for above

23. Effect of profile shape and number of intermediate purlins on $\bar{K}$

24. Variation of $\bar{K}$ with sheet length.

25, 26, 27. Profile displacements for up to four intermediate purlins

28. Comparison of effective shear modulus with Strehl's results

29, 30, 31, 32. Experimental, energy method and finite element K value comparisons

33, 34, 35. As above for intermediate purlin attachments

36. 37, 38. Comparison between finite element and energy methods

CHAPTER 3.

1. Fastening in a multiple of troughs

2. Alternate trough fastening

3. Superposition of Fourier terms

4. Variation of K value with length

5. Effect of number of Fourier terms

6, 7. Trough displaced shapes

8. Effect of number of intermediate purlins

9. Variation of $\bar{K}$ parameter with length

10. Effect of sheet thickness

11. Effect of trough pitch

12. Effect of fastening to an end purlin

13. Effect of profile shape on $\bar{K}$ parameter

14. Trough displaced shapes for 2 and 3 intermediate purlins

15. Purlin-prop reduction in flexibility

16. Bending moments used in alternate trough fastening analyses

17, 18. 19. Experimental energy method and finite element comparisons

20. Purlin-prop reduction in flexibility for every third trough fixing

21. Bending moments used in every third trough fixing analyses

CHAPTER 4.

1. Sinusoidal corrugation geometry
2. Energy method displacements
3. Effect of profile, length and number of intermediate purlins on K value
4. Effect of sheet thickness
5. Displaced shapes of sinusoidal profiles
6. Alternate trough fastening displacements
7. Effect of thickness for alternate trough fixing
8. Effect of profile, length and number of intermediate purlins for alternate trough fastening

CHAPTER 5.

1. Shear deformation of a 'closed-end' corrugation
2. Cross-section displacements
3. Comparison of open and 'closed' profiles
4. Shear deformation of a double fastened corrugation
5. Cross-section displacements
6. Comparison with a profile fastened in every trough
7. Effect of sheets extending beyond purlins
8. As above, for rigid plate movements
9. Effect of insulation covering
10. Composite shear action
11. Insulation bending
12. Curved end sheeting - every trough attachment
13. As above, for alternate trough fixing

CHAPTER 6.

1. Overlapping corrugations
2. Model for every trough fastening
3. Model for alternate trough fastening
4. Longitudinal warping
5. Unequal sheet lengths

6. General interaction expression for rigid plate movements
7. As above, for localized end distortion
8. Variations in fastening arrangement

CHAPTER 7.

1. Continuous diaphragm displacements for every trough fixing
2. As above, for alternate trough attachment
3. Plate displacements
4. Test apparatus for 2 and 3 bay diaphragms
5, 6. Modified shear flexibility
7. Inertia of purlins
8. Contribution of sheet to beam inertia
9. General formularion for sheet inertia
10. Sheet displacements in web
11. Overlapping sheets
12. Beam on elastic foundations analogy
13. Formulae for central deflection
14. Variations in the fastening arrangement

CHAPTER 8.

1. Overlap seam performance
2. Upstand seam performance
3. Performance of button punched seams
4. Indirect shear transfer
5, 6. Purlin displacements
7. Effective sheet widths
8. Variation with bending and torsional stiffnesses
9. Influence of sheet flexibility
10. Tabulation of g_1 parameter
11. Comparison of differential equation with finite element results

12. Holes in diaphragms; simple shear deflection
13. Isolated opening in diaphragm
14. Periodic openings in diaphragm
15. Shear force variation
16. Purlin displacements for single opening
17. Purlin displacements for periodic openings
18. Comparison of periodic and isolated hole solutions
19. Maximum purlin bending stress variation
20. Maximum sheet-purlin fastener force variation
21. Effect of parameters on purlin bending
22. Finite element representation of shear panel with opening
23. Finite element results and theoretical comparisons
24, 25, 26, 27. Matrices for single and periodic opening solutions

CHAPTER 9.

1. Shear buckling of corrugated sheeting
2. Buckling of various profile shapes
3. Derivations from uniform or the tropic medium
4. Buckling between intermediate purlin fasteners
5. As above, for three bays
6. Possibility of uplift between sparce perimeter fasteners
7, 8. Curves for buckling between intermediate purlin fasteners
9, 10. Curves for buckling between perimeter fasteners
11. Shear buckling of hypar shells
12. Shear buckling of cylindrical shells

CHAPTER 10.

1. Forms of folded plate roofs
2. Resolution of forces and deflection
3. Concrete folded plate roof theory
4. Axial stress and deflection in folded plates
5. Axial stresses in prototype folded plate roof
6. Pressed sheeting

7, 8. Vertical loading system

9, 10. Elastic tests on folded plate roof

11. Centre section deflections

12. Wind load deflections

13. Bending and shear deflections for uniform loading

14. Bending and shear deflections for wind loading

15. Test to failure

16. Centre section deflections prior to collapse

17, 18.
19.

20. Maximum folded plate roof span

21. Fold area at a given span and inclination

22. Typical section through folded plate roof bay

23. Weight of steel comparison for folded plate and portal frame

24, 25, Folded plate roof details
26, 27.

28. Stress-strain curve for steel used in sheeting

29. Load-slip curve for upstand seam

CHAPTER 11.

1. Holes in folded plate roofs

2. Fold line deflections

3. Local fastener forces and fold line stresses

4. Variations in fold line fastening

5. Lateral instability of edge beam

CHAPTER 12.

1. Equivalent beam test for pressed sheeting

2, 3, Equivalent beam tests for open profiled sheeting
4.

CHAPTER 13.

1. Design examples for profiled sheeting

A TYPICAL ROOF DIAPHRAGM

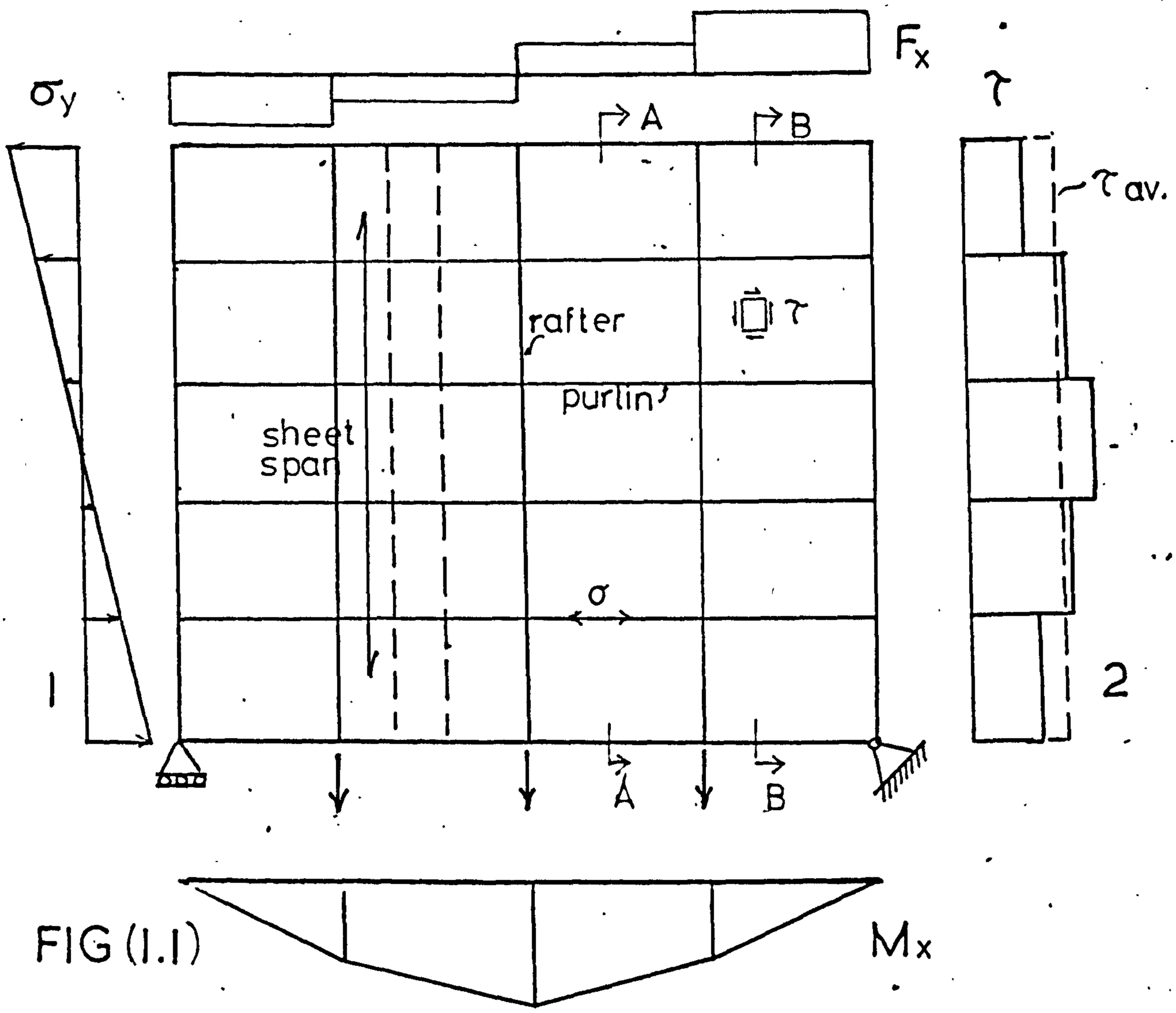

FIG (1.1)

1. PURLIN STRESS , σ_y, FOR BENDING MOMENT, M_x, AT A-A
2. SHEET SHEAR STRESS, τ ; AT SECTION B-B. FOR SHEAR FORCE, F_x

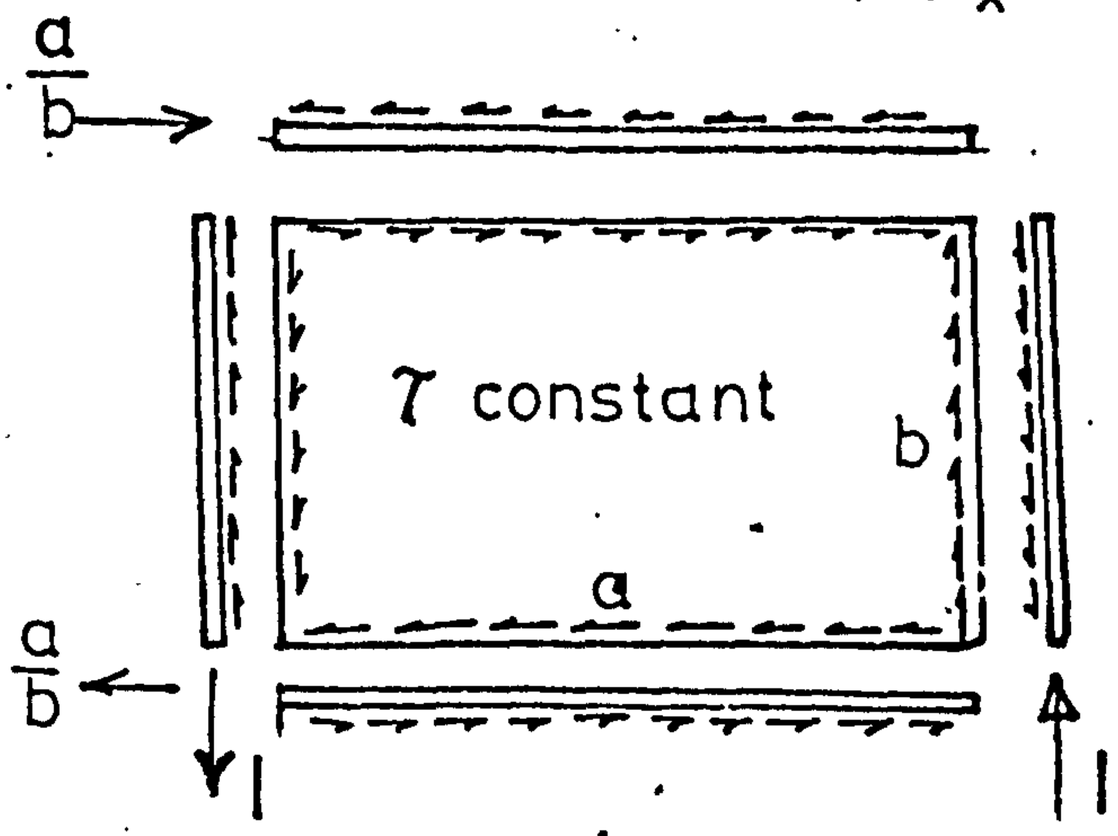

FIG(1.2(a))

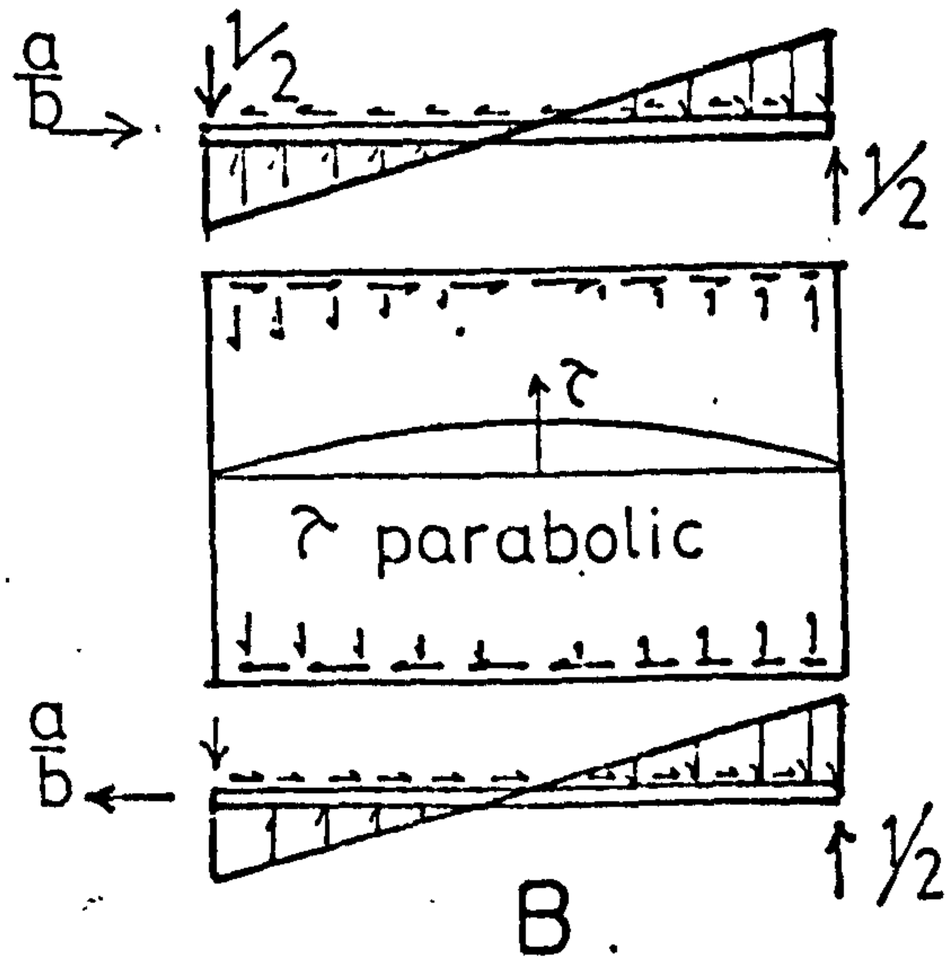

FIG 1.2(b)

SHEETS FASTENED ON (A) 4 SIDES
(B) 2 SIDES

EQUILIBRIUM OF SHEET AND MEMBERS

A PRACTICAL DIAPHRAGM ARRANGEMENT

WITH SHEET CONNECTIONS ON ALL FOUR SIDES

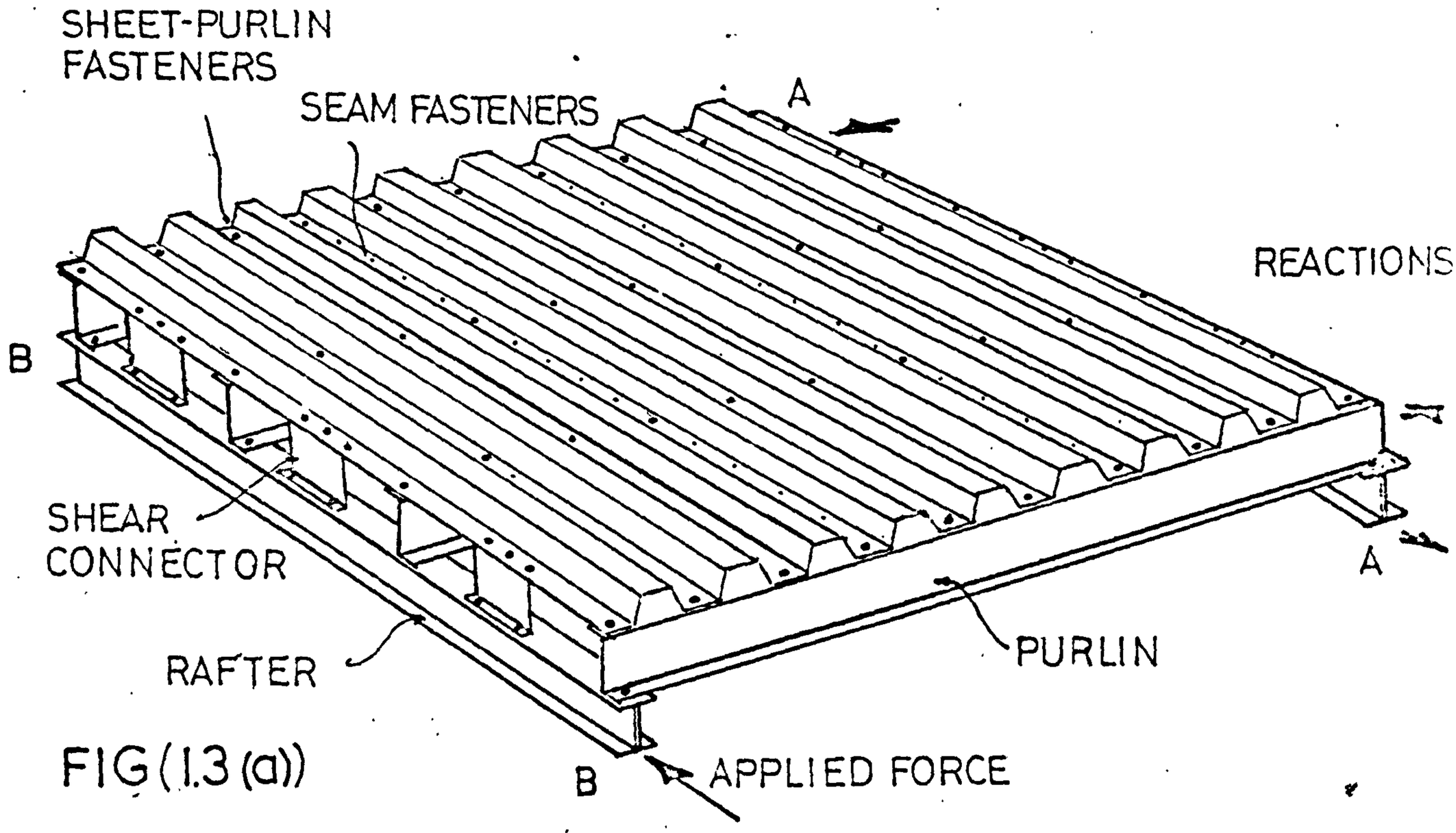

FIG (1.3 (a))

ABOVE DIAPHRAGM AS PART OF A ROOF

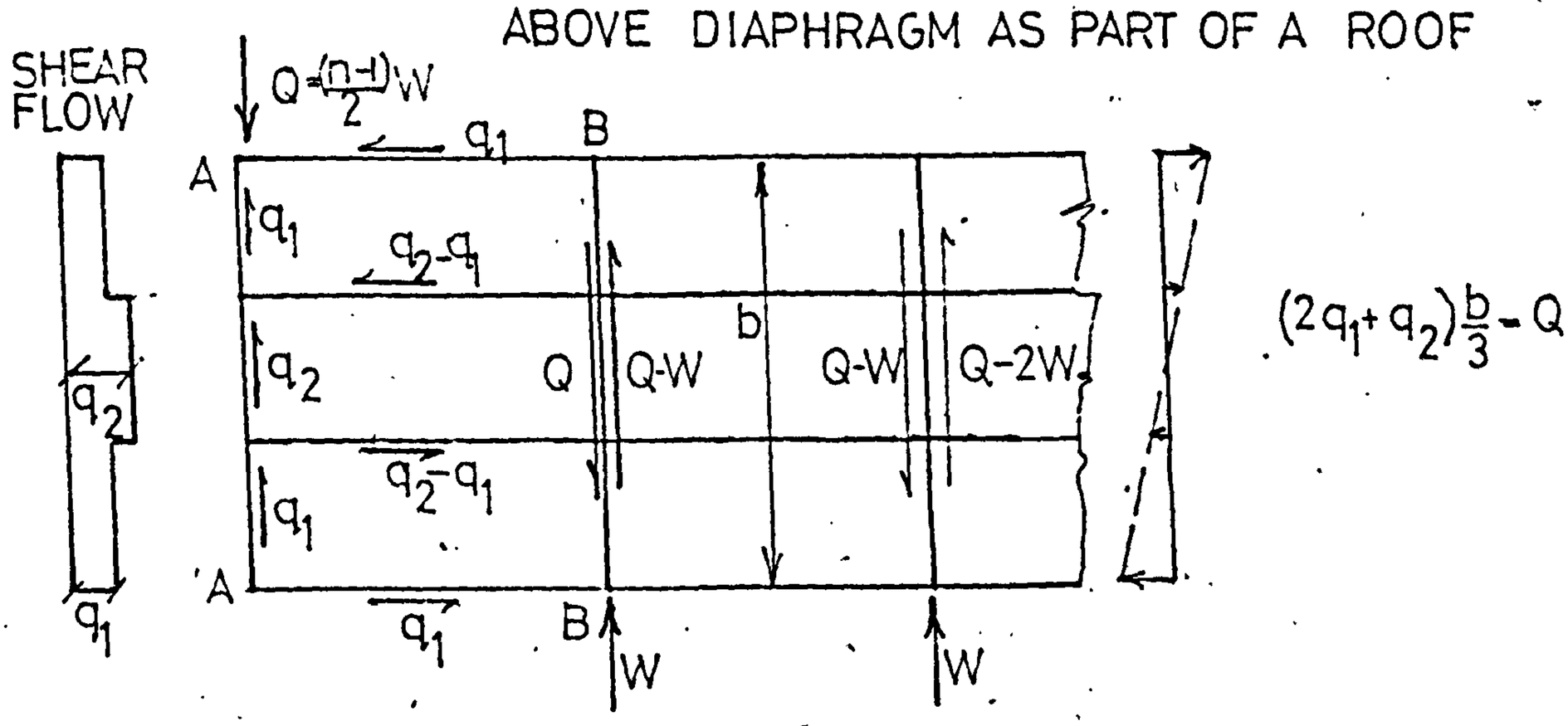

THEORETICAL DISTRIBUTION OF FASTENER FORCES IN END ROOF BAY, BASED ON LINEAR AXIAL STRAIN

FIG (1.3(b))

DIAPHRAGM RESTRAINT OF FRAME SWAY

FRAME 1 ; $K\delta_1 = 1 - \frac{\delta_1}{C} + \frac{\delta_2 - \delta_1}{C}$

FRAME 2 ; $K\delta_2 = 1 - \frac{2}{C}(\delta_2 - \delta_1)$

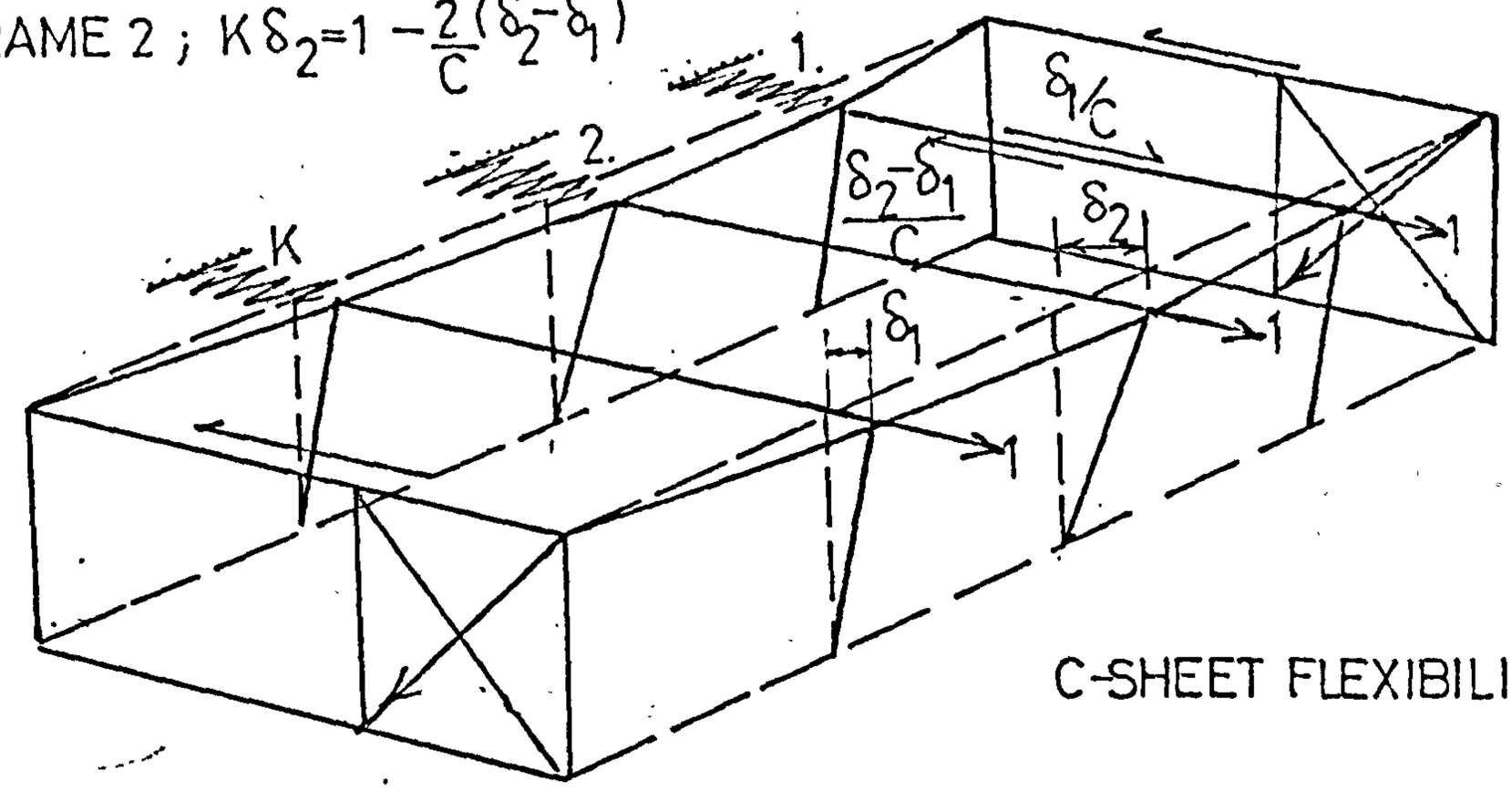

FIG(1.4) K-FRAME STIFFNESS REPRESENTED BY SPRING

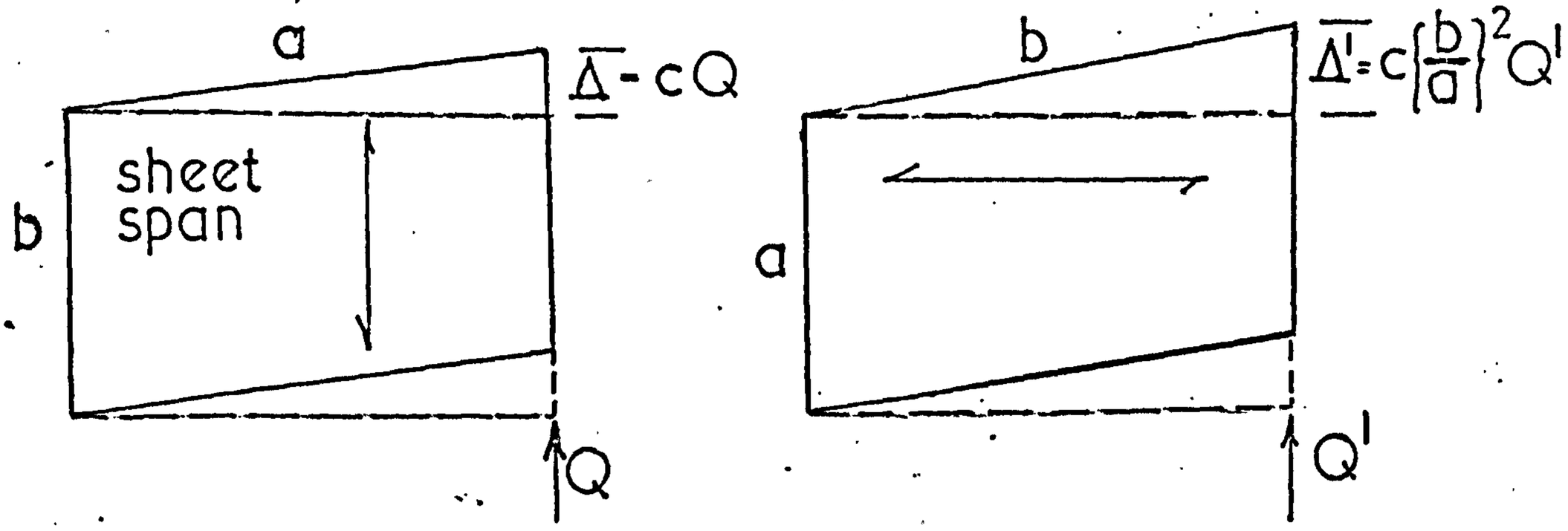

FIG(1.5) SHEAR FLEXIBILITIES IN EACH DIRECTION

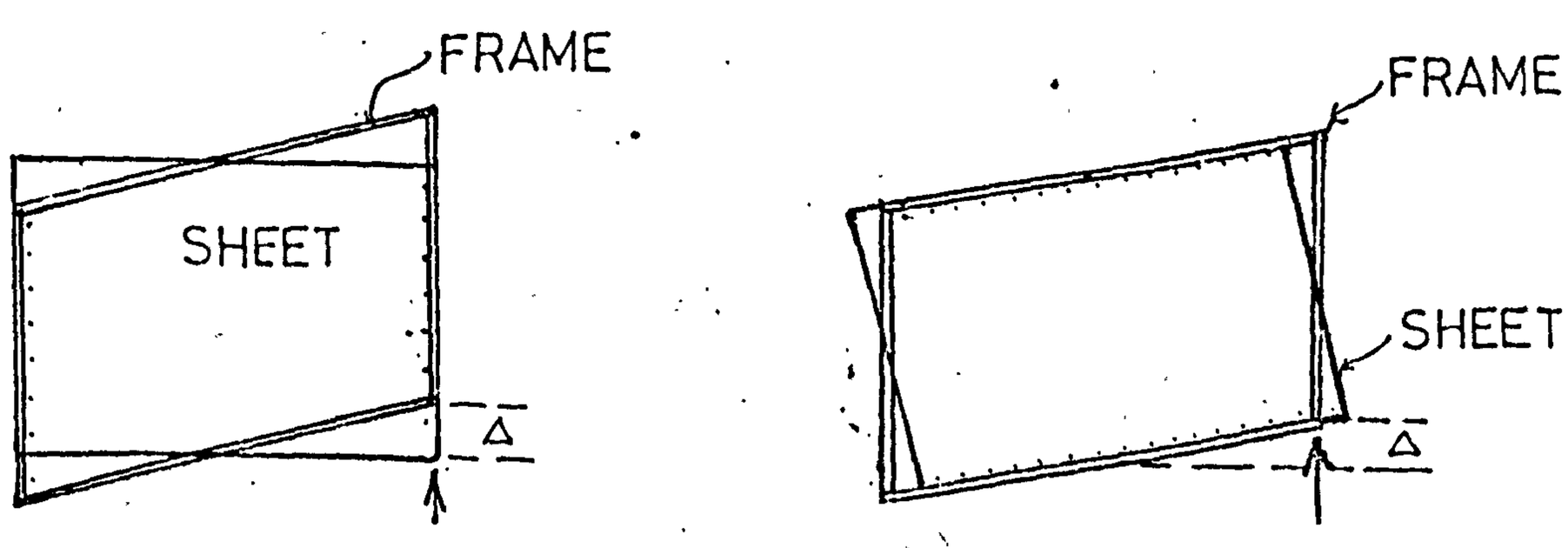

FLEXIBILITIES DUE TO FASTENER SLIP IN EACH DIRECTION

FIG(1.6)

COMPLETE LATERAL STABILITY OF ROOF PROVIDED BY THE SHEETING —
pin jointed frame

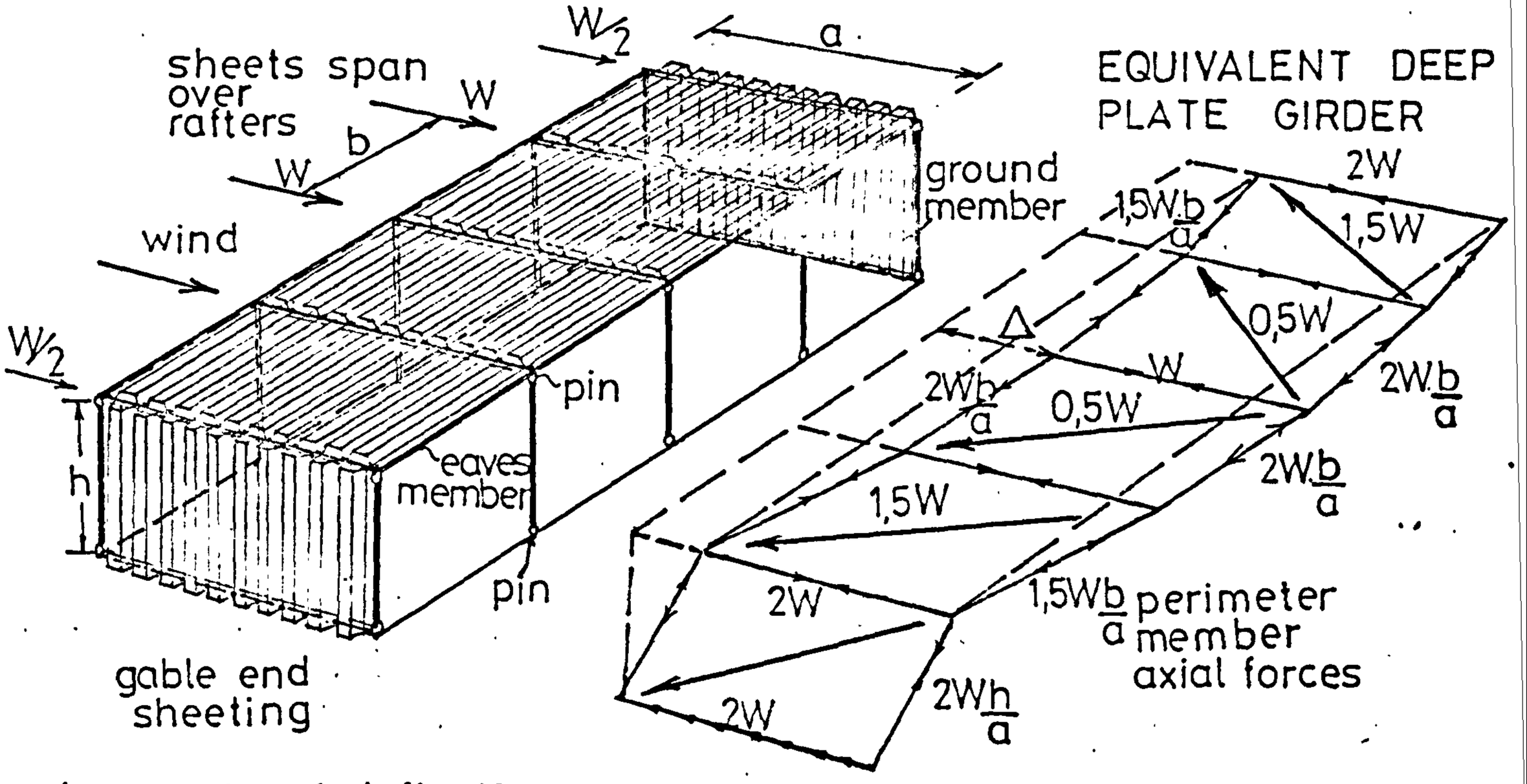

gable end sheeting

Δ central roof deflection

DIAPHRAGM SHEAR FORCES

FIG(1.7)

SPREAD OF PITCHED ROOF PORTAL. FRAME UNDER NORMAL LOADING

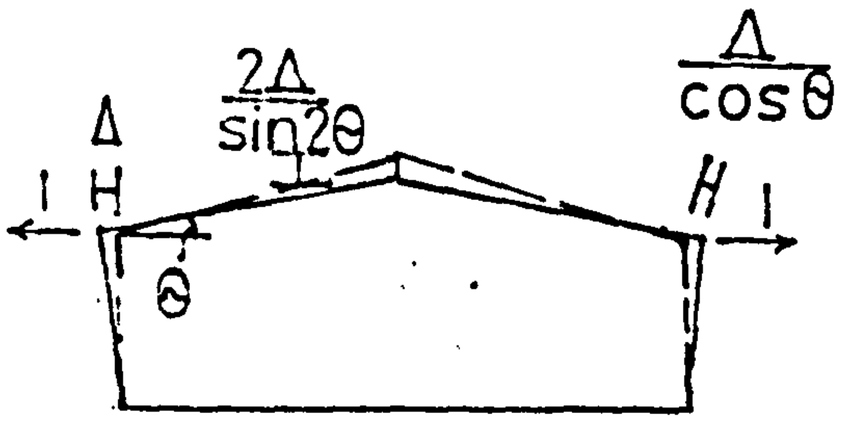

Δ, frame flexibility

inclined plate girder

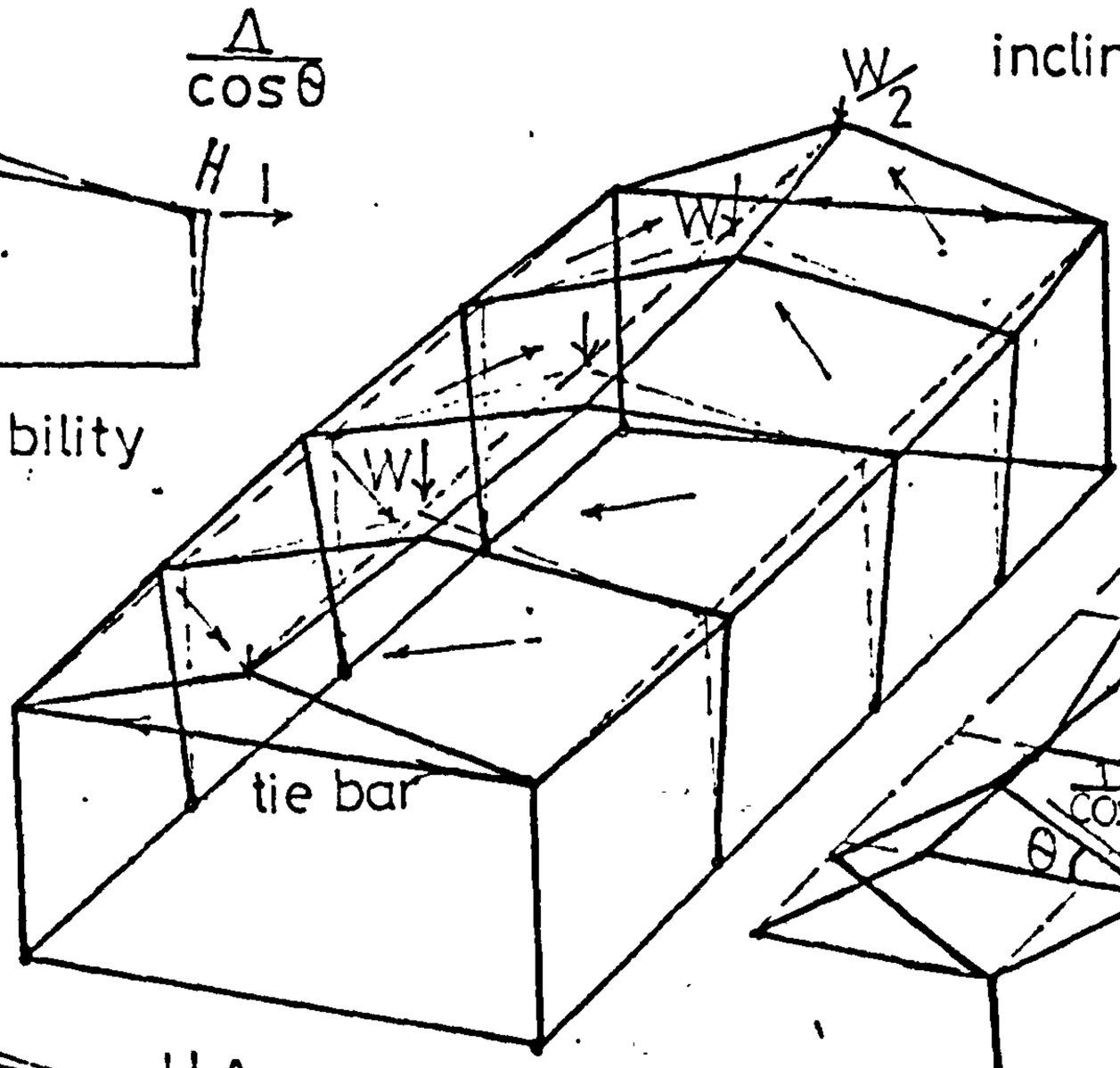

in-plane sheet flexibility, C

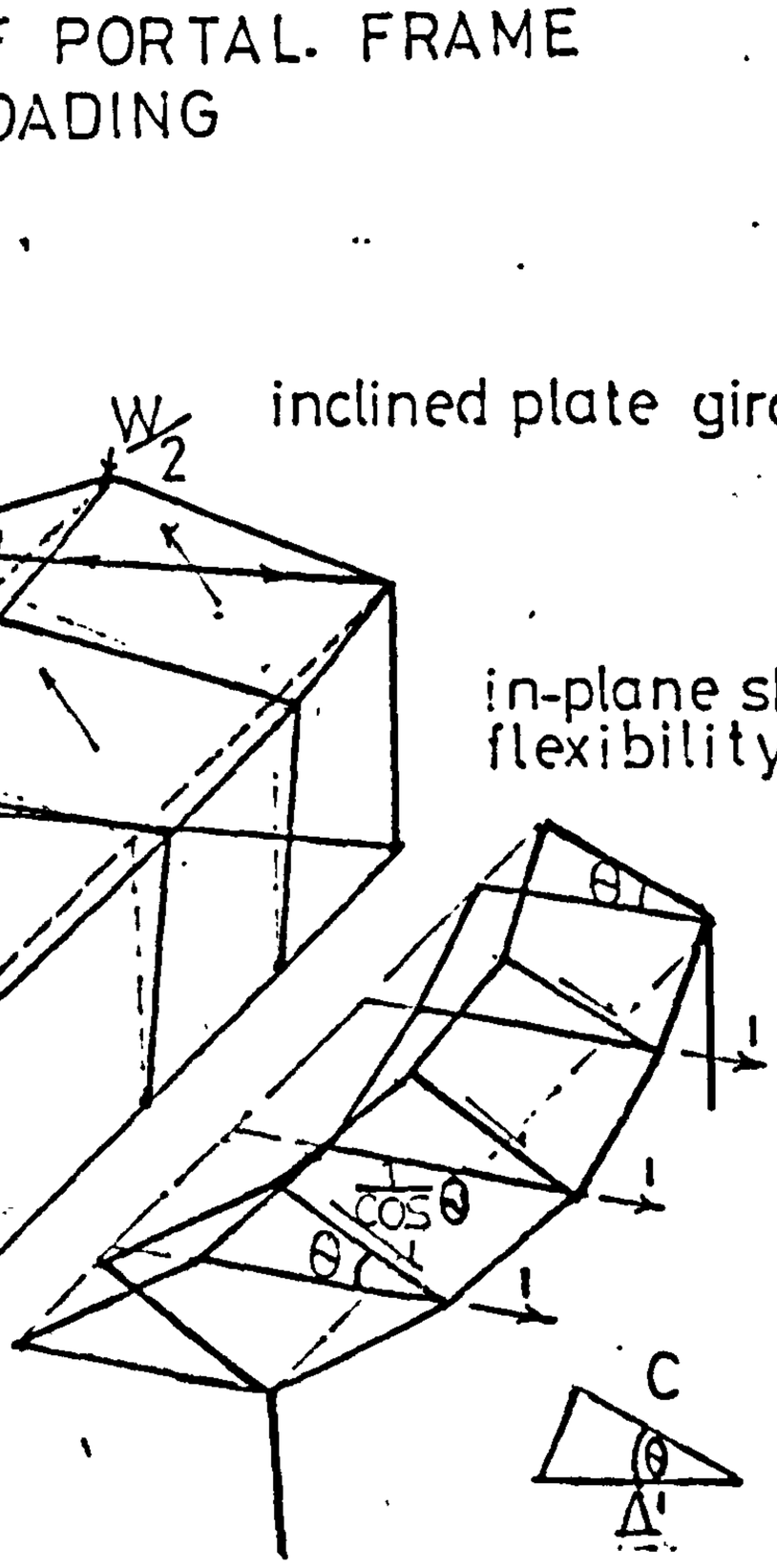

Δ_o-free spread

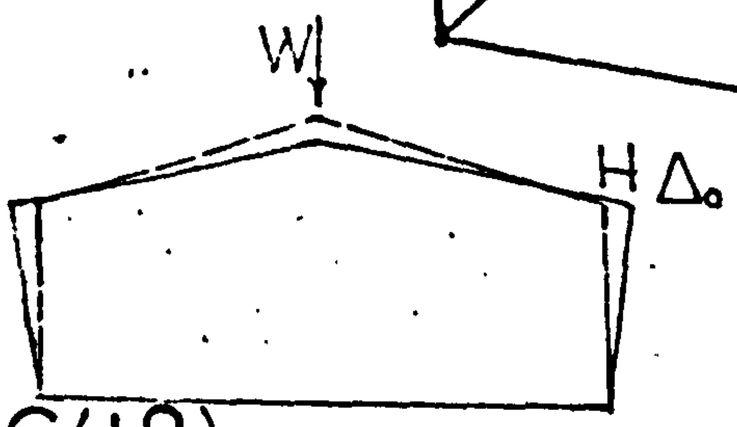

Δ', equivalent horizontal diaphragm flexibility = $C/\cos^2\theta$

FIG(1.8)

FORMS OF FRAMELESS STRUCTURE

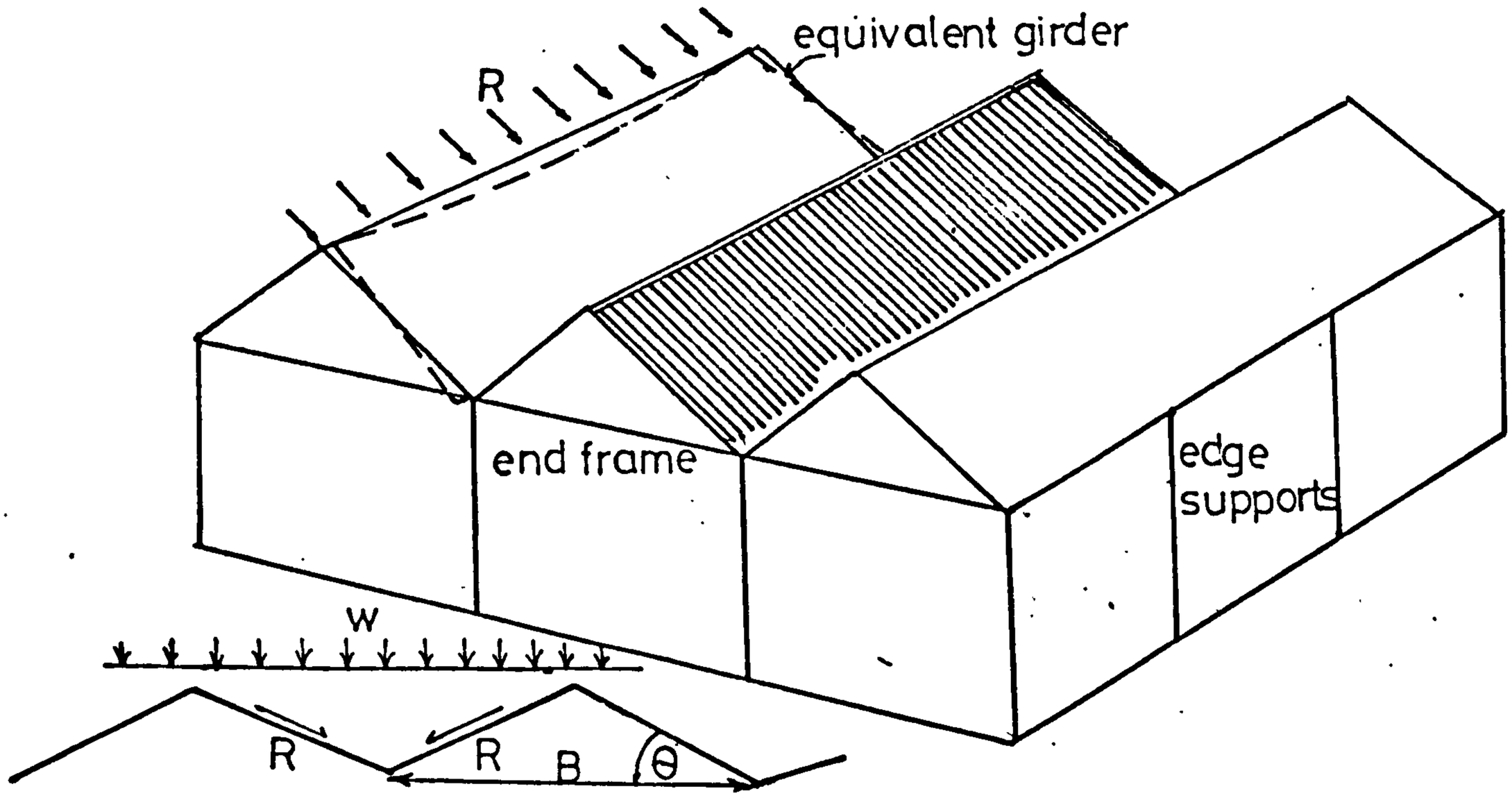

$R = \frac{wB}{2\sin\theta}$

resolution into in plane forces

FOLDED PLATE ROOF

FIG 1.9

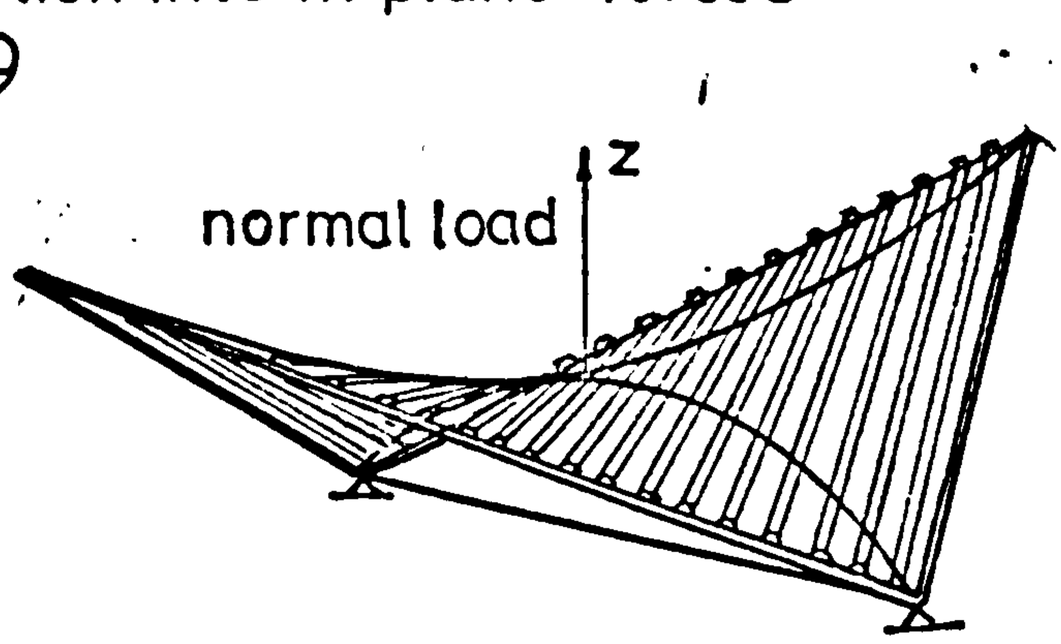

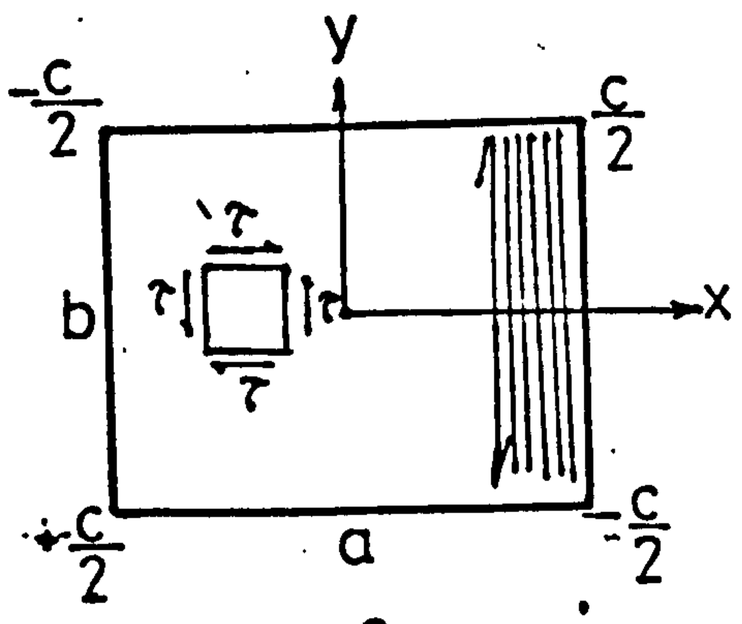

$z = 2c\frac{xy}{ab}$

HYPERBOLIC PARABOLOID

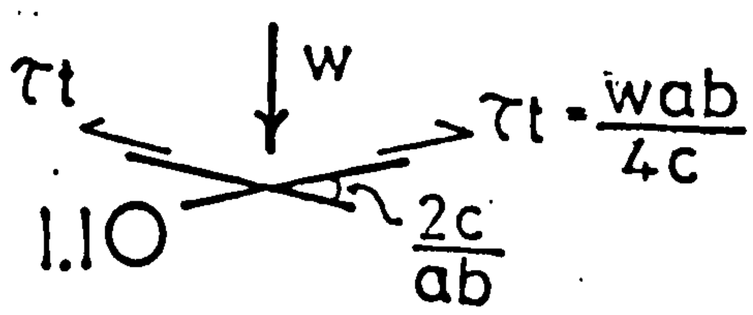

FIG 1.10

CYLINDRICAL SHELL

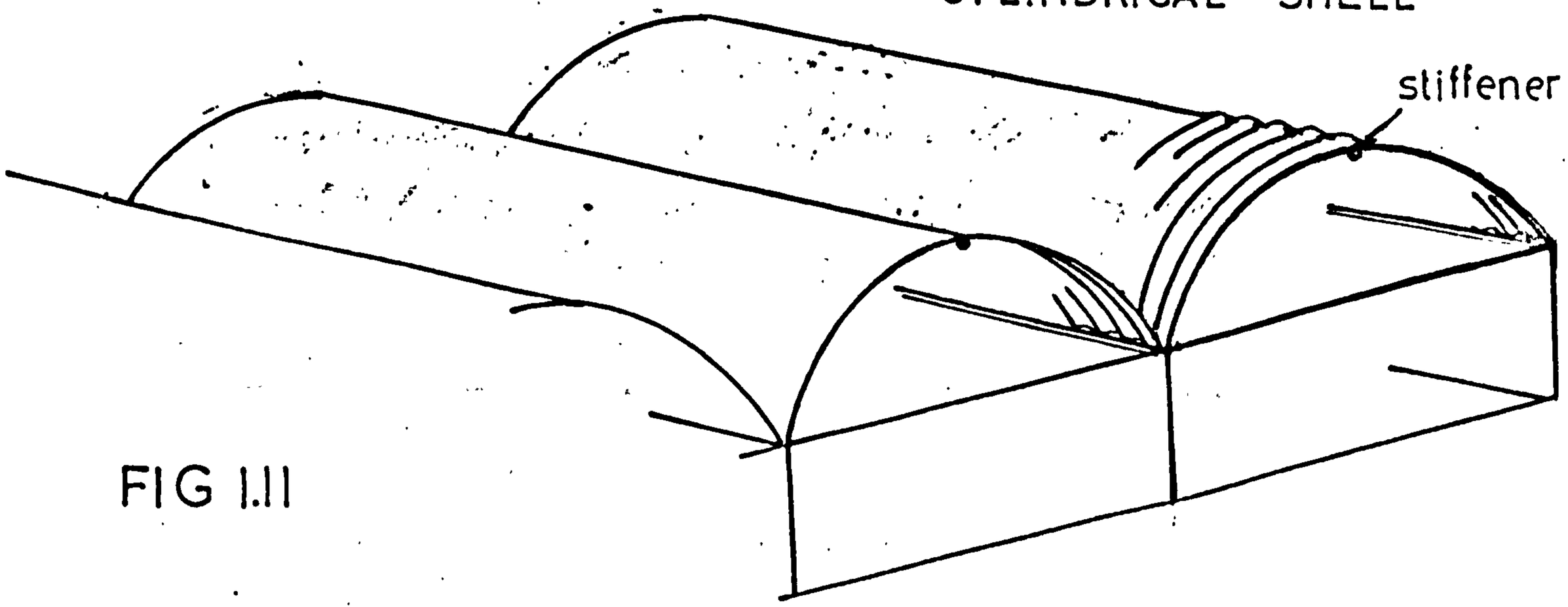

FIG 1.11

PROFILE DIMENSIONS

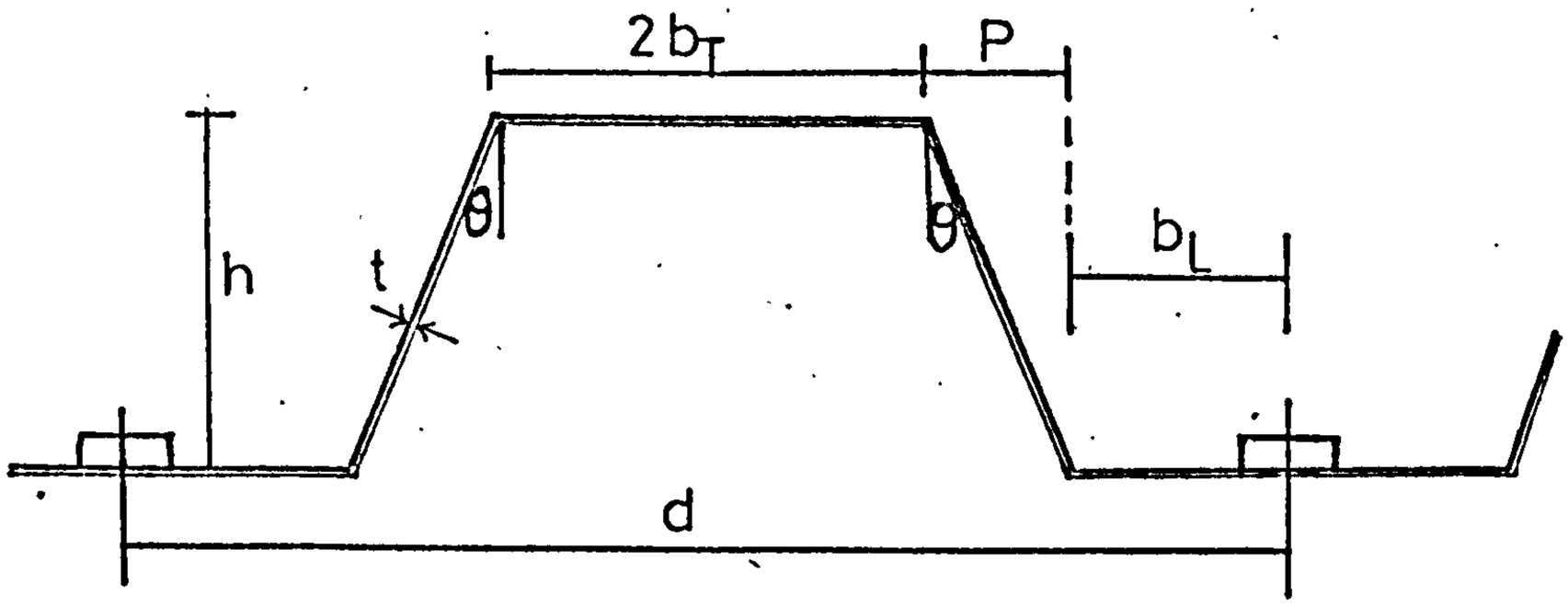

FIG (2.1(a))

SHEAR DISTORTION FOR EVERY TROUGH FIXING

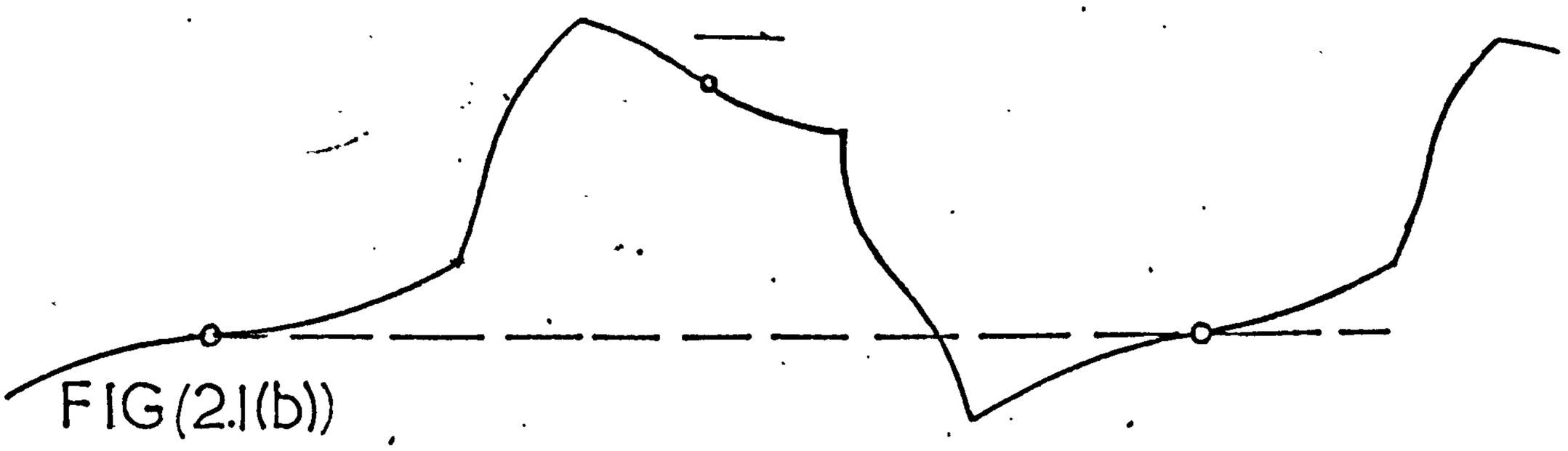

FIG (2.1(b))

FREE DEFORMATION, SHOWING POINTS OF INFLEXION.

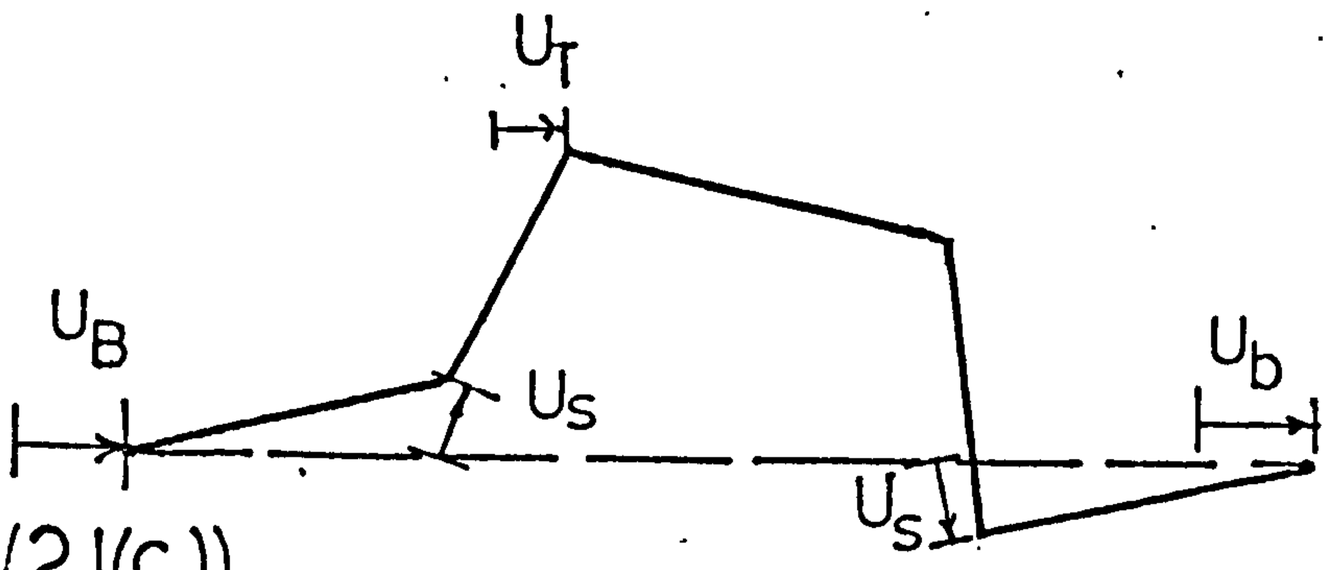

FIG (2.1(c))

CROSS-SECTION DISPLACEMENTS

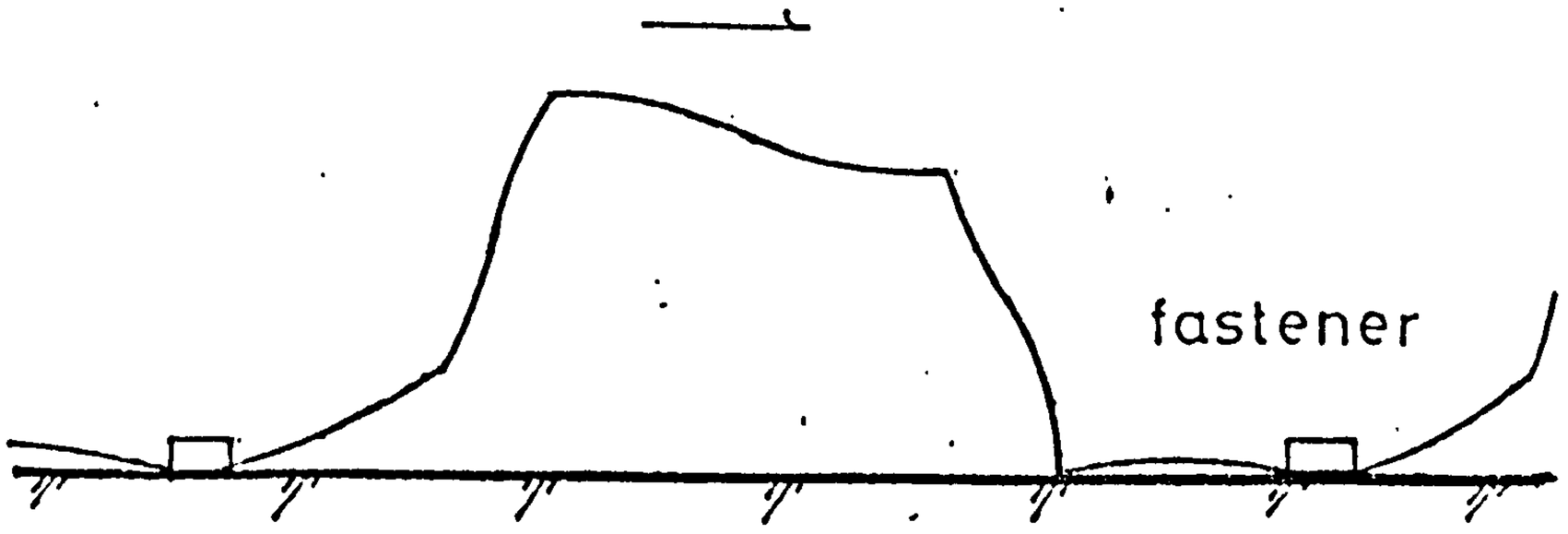

REAL SITUATION - END PURLIN RESTRAINT

FIG (2.1(d))

WARPING DUE TO RIGID PLATE MOVEMENTS

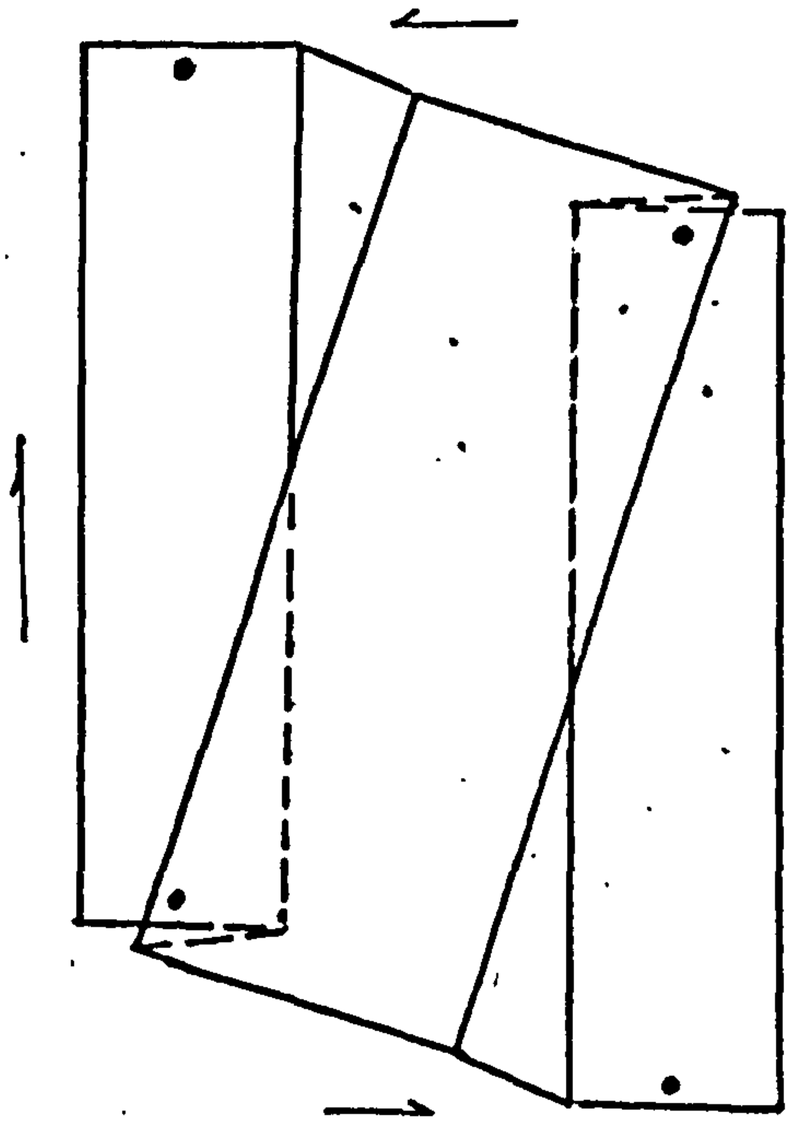

EVERY TROUGH FASTENING

FIG (2.2(a))

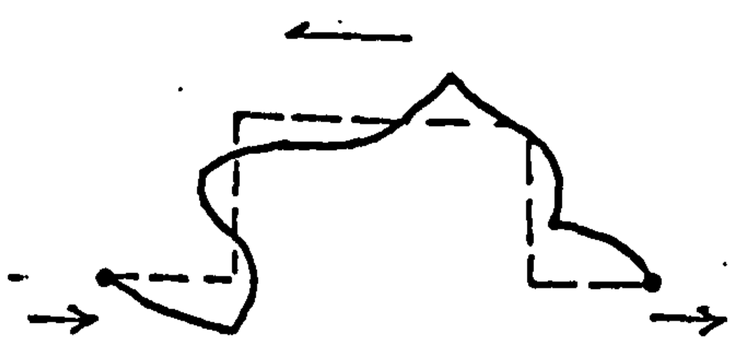

CROSS-SECTION DISTORTION

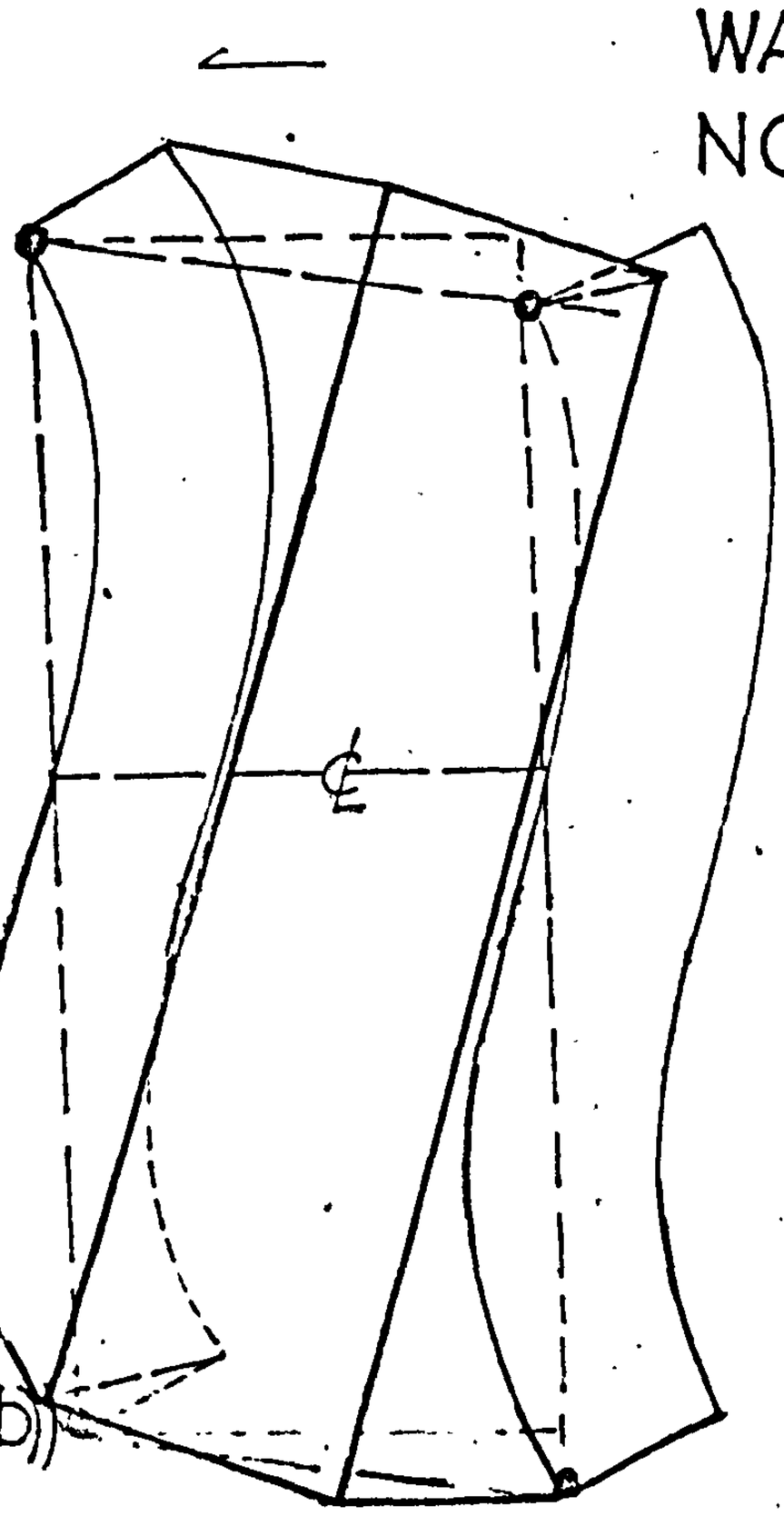

WARPING DUE TO NON-LINEAR TROUGH MOVEMENT

FIG(2.2(b))

CROSS-SECTIONAL BENDING MOMENTS

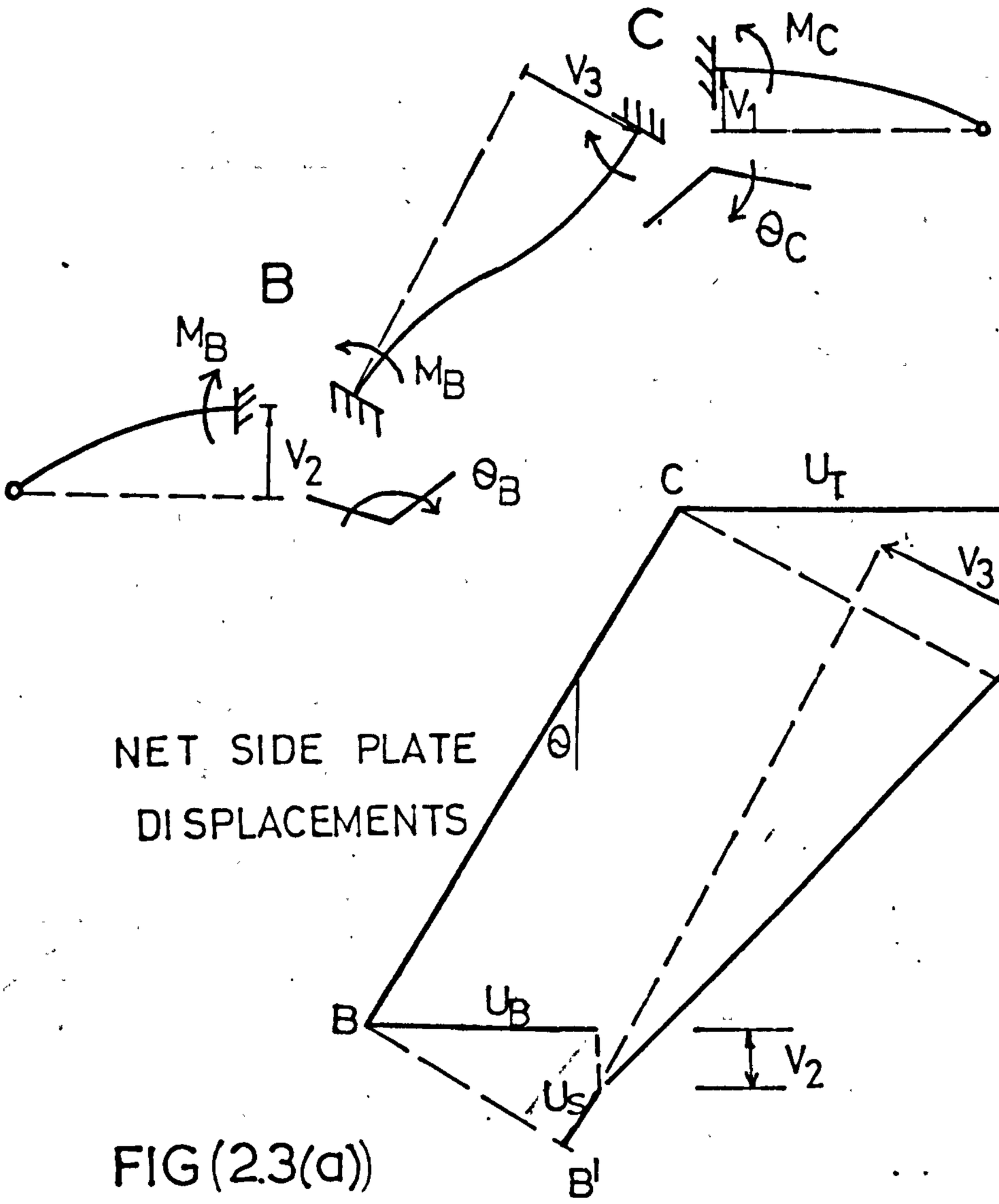

NET SIDE PLATE DISPLACEMENTS

FIG (2.3(a))

EQUILIBRIUM OF SIDE PLATE

$$\frac{dP}{dy} = Q_B - Q_T$$

$$\frac{dF_S}{dy} = q_T + q_B$$

$$\frac{dM_S}{dy} = +F_S$$

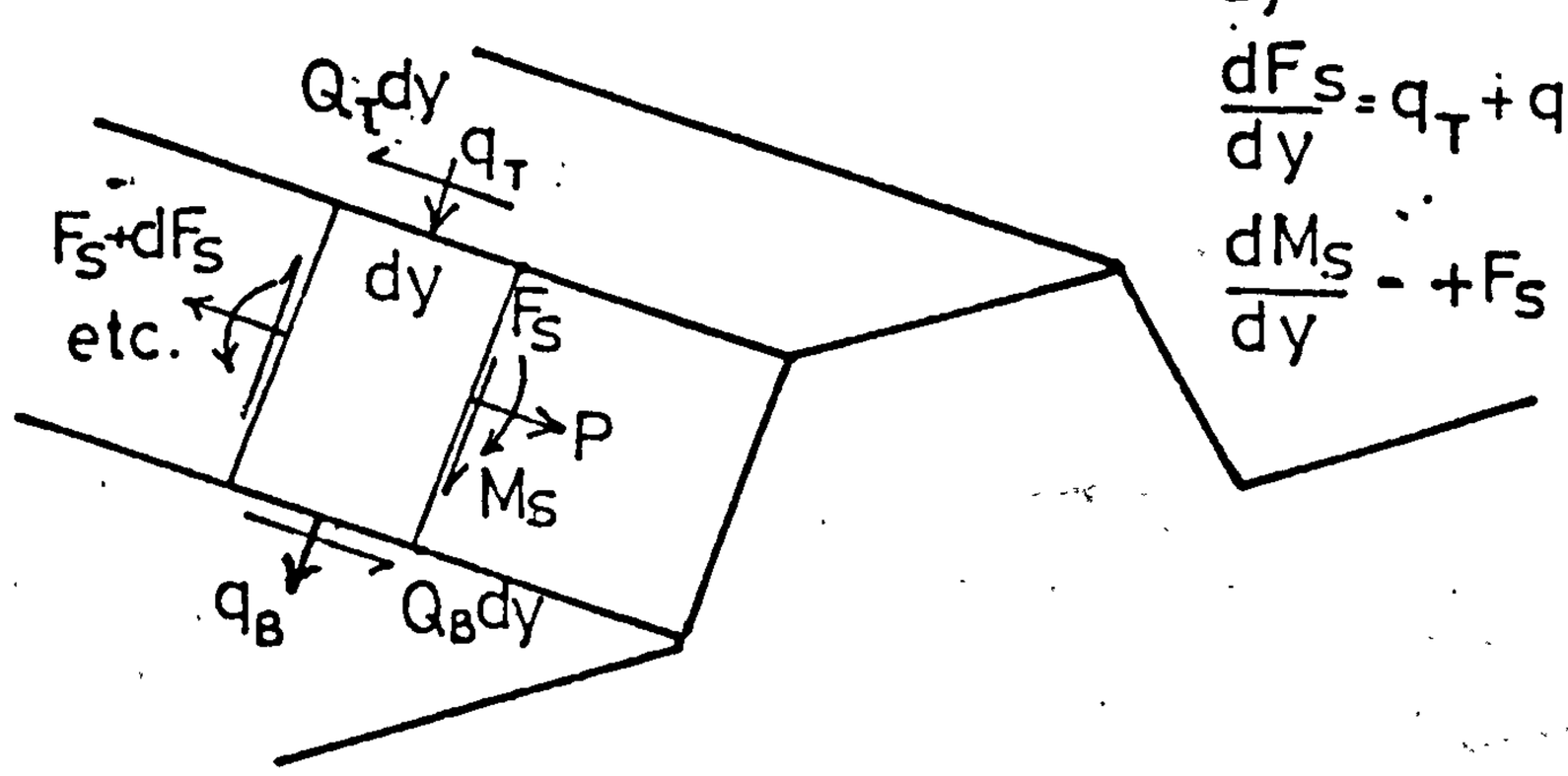

FIG (2.3(b))

SUPERPOSITION OF FOURIER TERMS

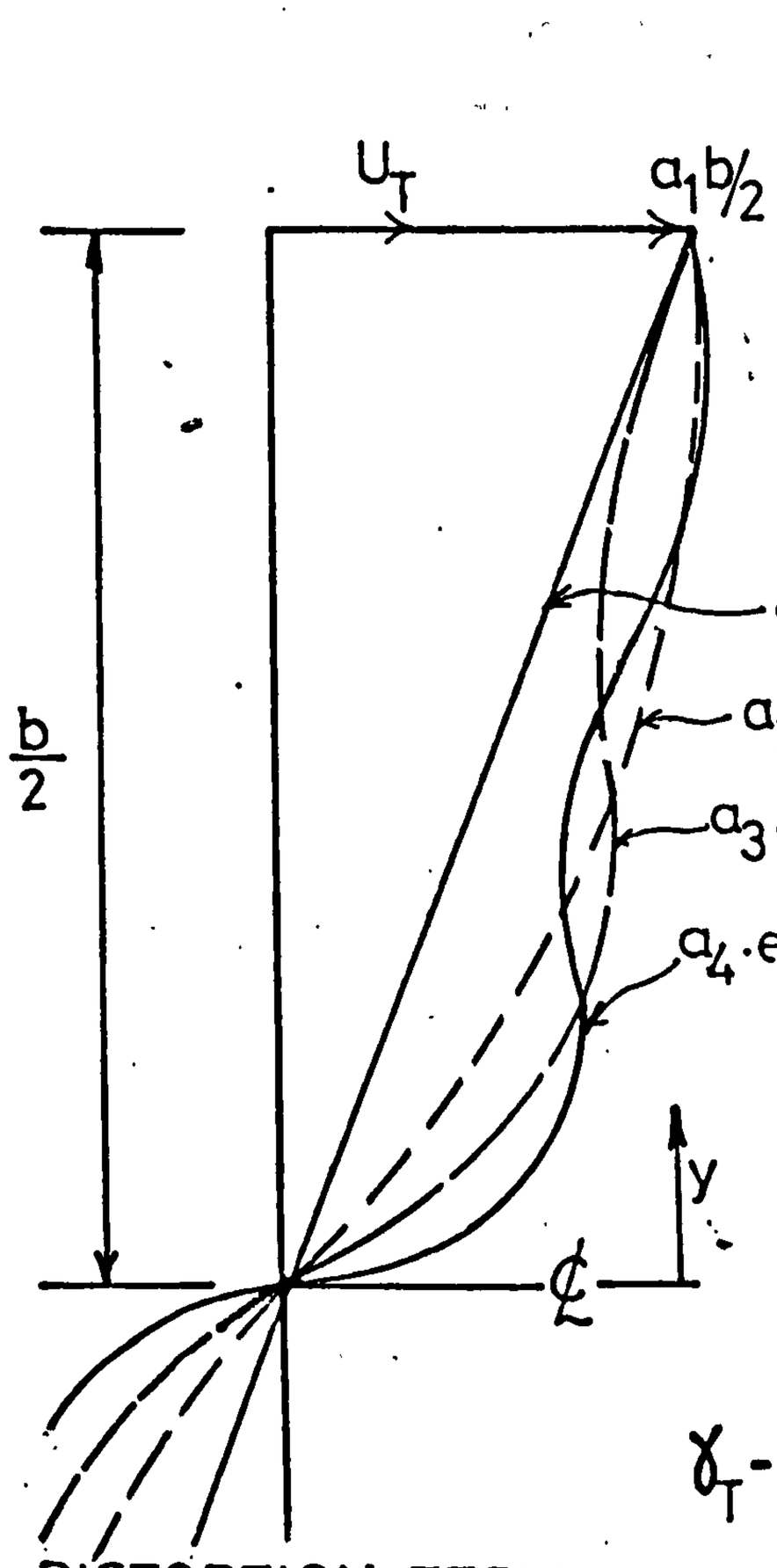

$$U_T - a_1 y + \sum_{n=1}^{\infty} a_{n+1} \cdot \frac{b}{2\pi n} \cdot \sin\frac{2\pi n y}{b}$$

DISTORTION TERMS FOR TOP PLATE

FIG (2.4(a))

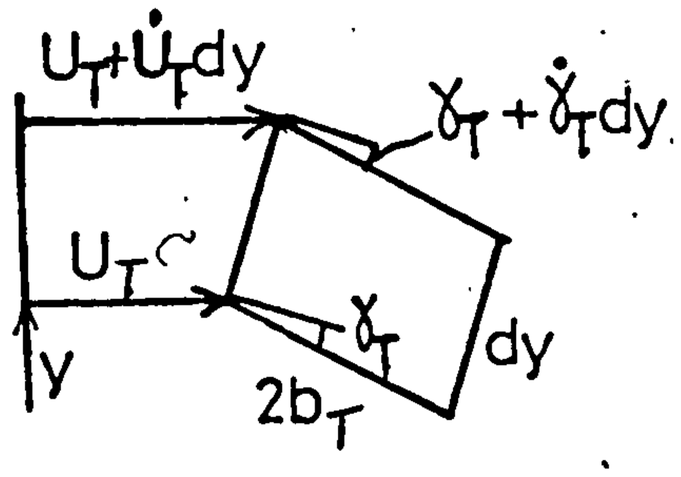

$$\gamma_T - \gamma_1 + \gamma_2 \cos\frac{2\pi y}{b}$$

SHEAR STRAIN TERMS

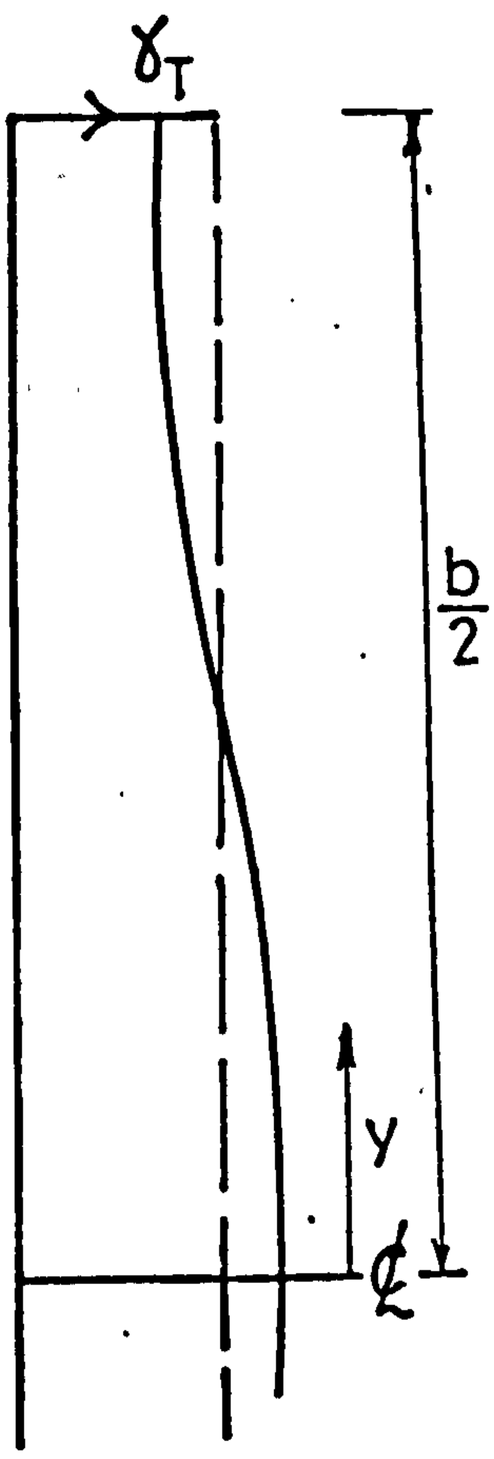

AXIAL STRAIN IN SIDE PLATE CONSISTENT WITH $\frac{d\Delta}{dy} = 0$

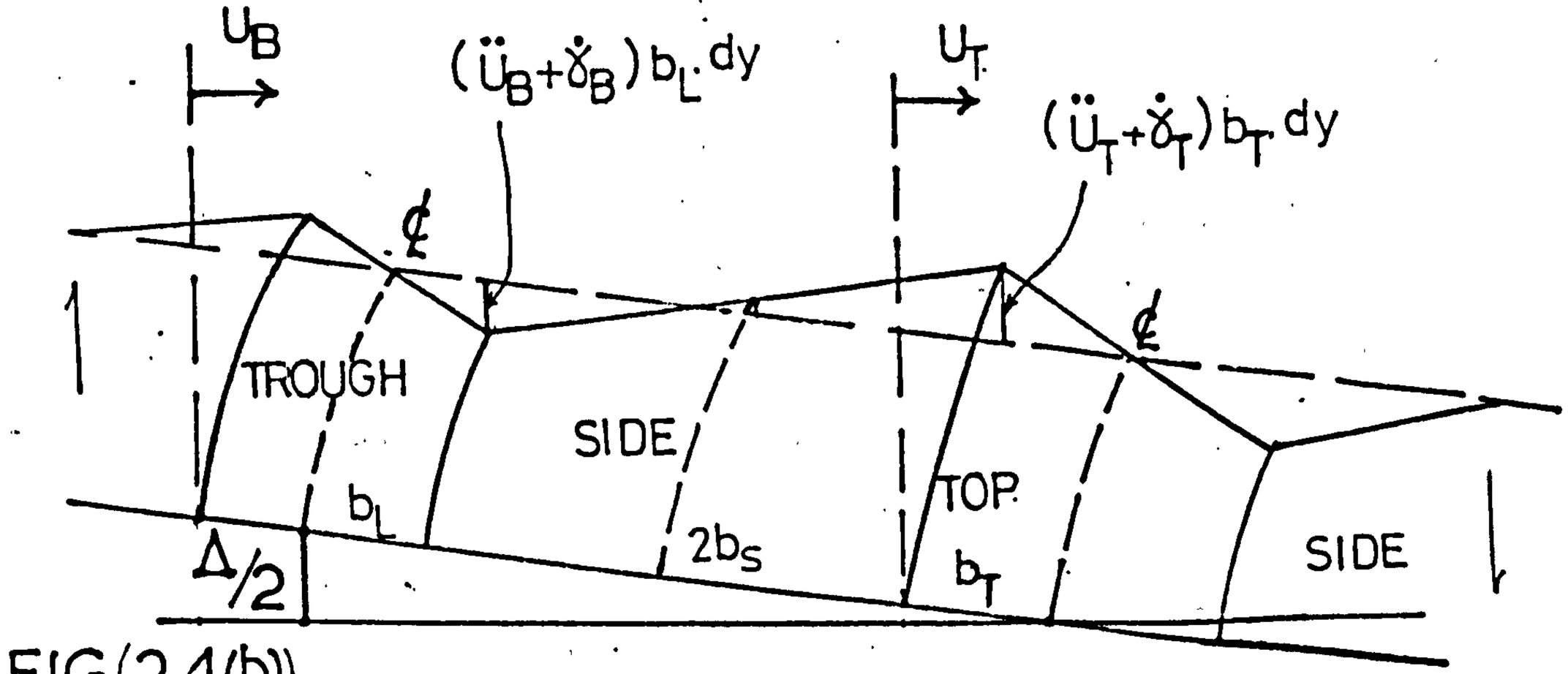

FIG (2.4(b))

ASYMPTOTIC BEHAVIOUR OF SHEAR DISTORTION

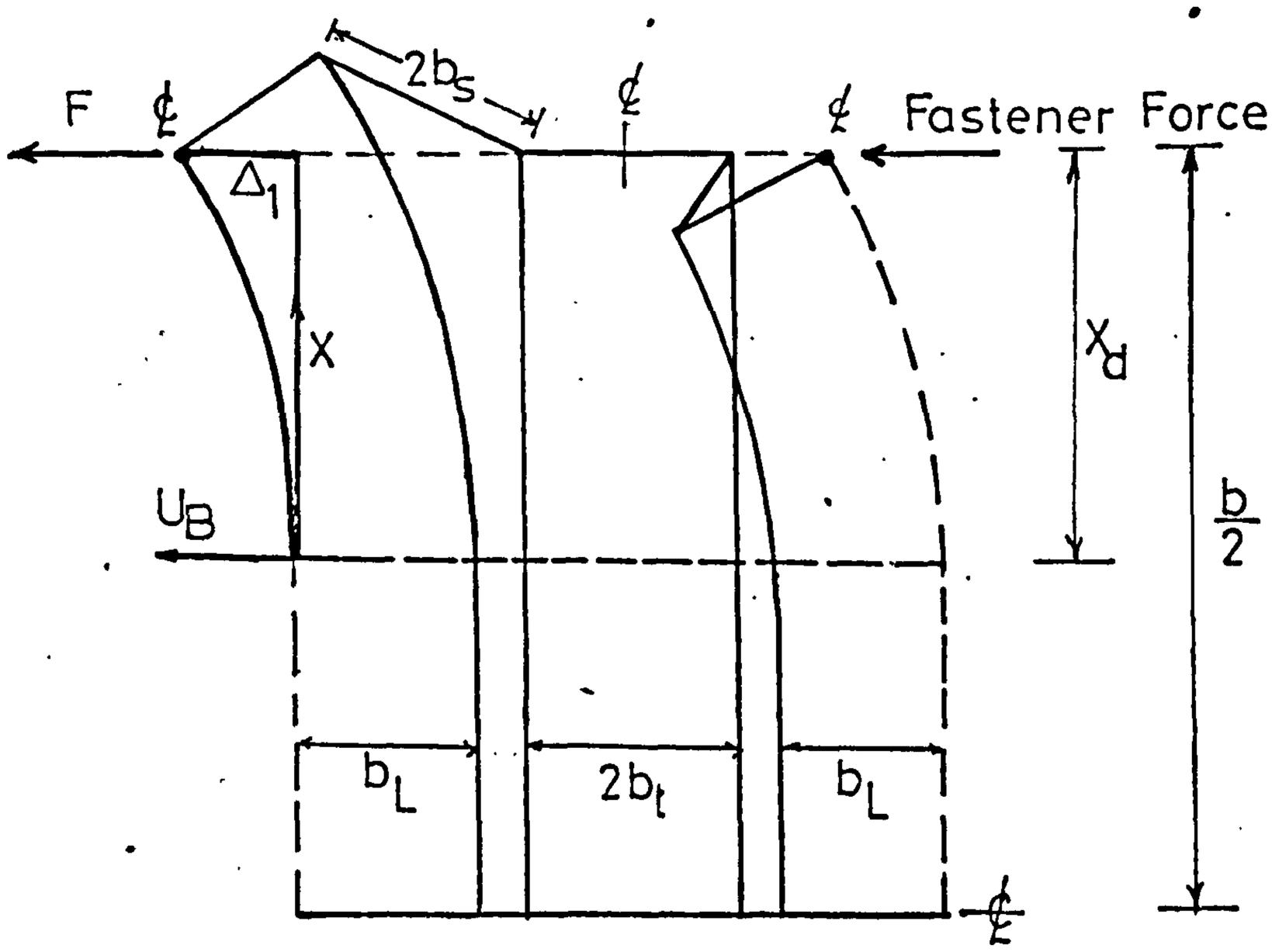

$$U_B = \left\{\frac{X}{X_d}\right\}^2 \cdot \Delta_1 \qquad \delta_{shear} = \Delta_1 \left\{\frac{a}{b}\right\}^2$$

LOCALIZED DISTORTION LENGTH, X_d, INDEPENDENT OF b

FIG(2.5)

$$\delta_{shear} = \delta_1 - \delta_2 - \frac{a}{b}(\delta_3 + \delta_4)$$

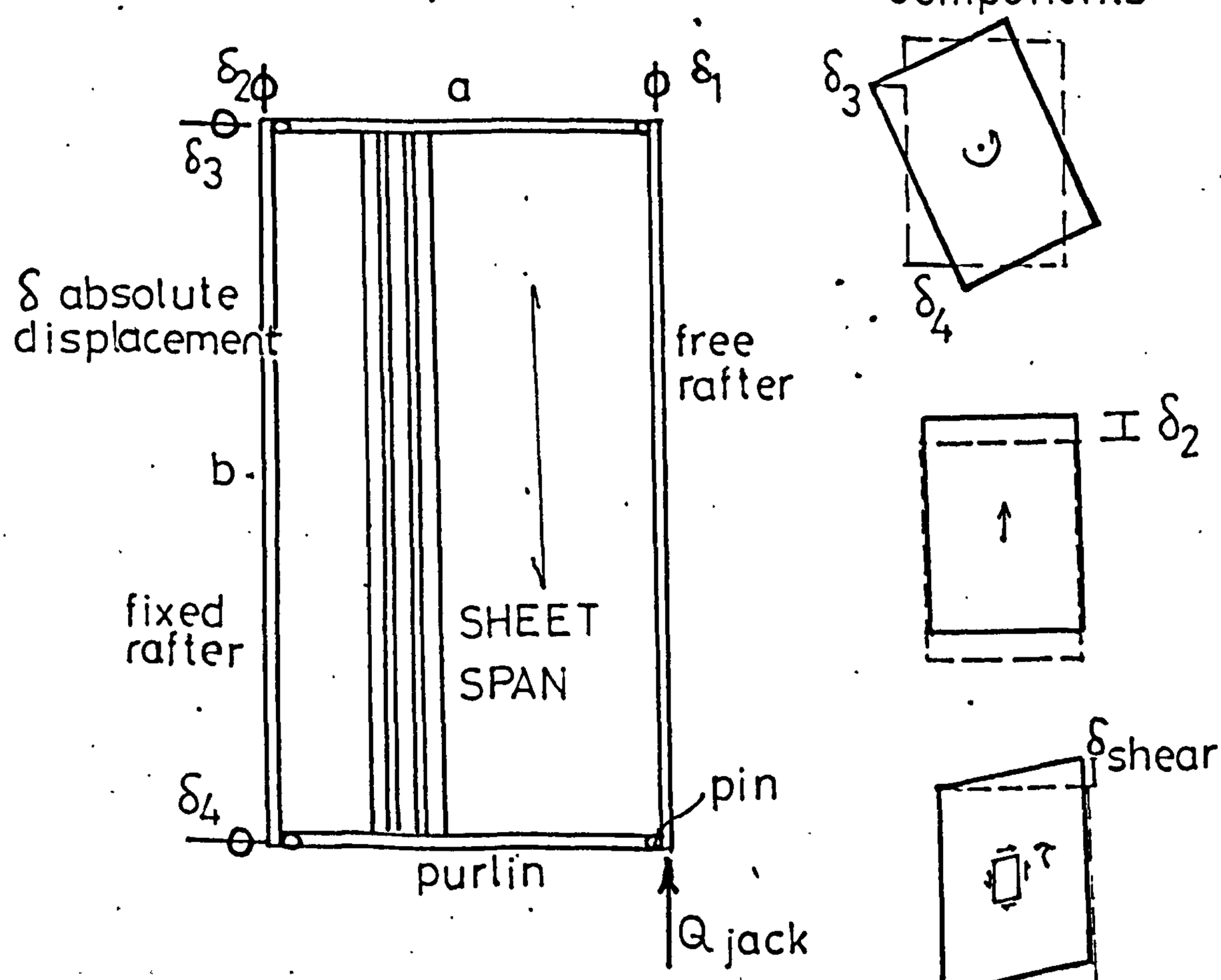

STANDARD TEST RIG

FIG(2.6)

FINITE ELEMENT REPRESENTATION OF A CORRUGATION FASTENED IN EVERY TROUGH

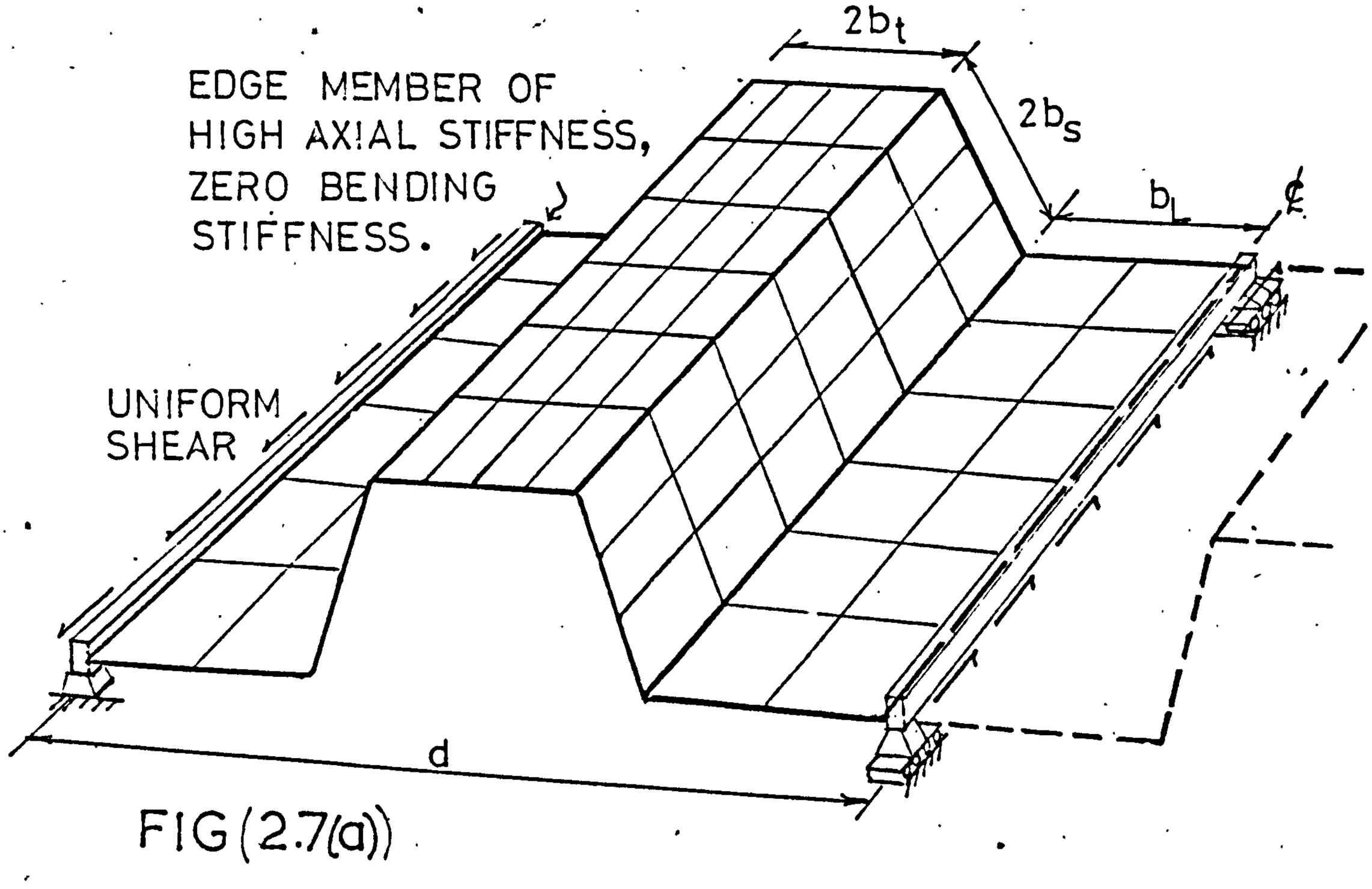

FIG (2.7(a))

CONVERGENCE. TESTS FOR ELEMENTS

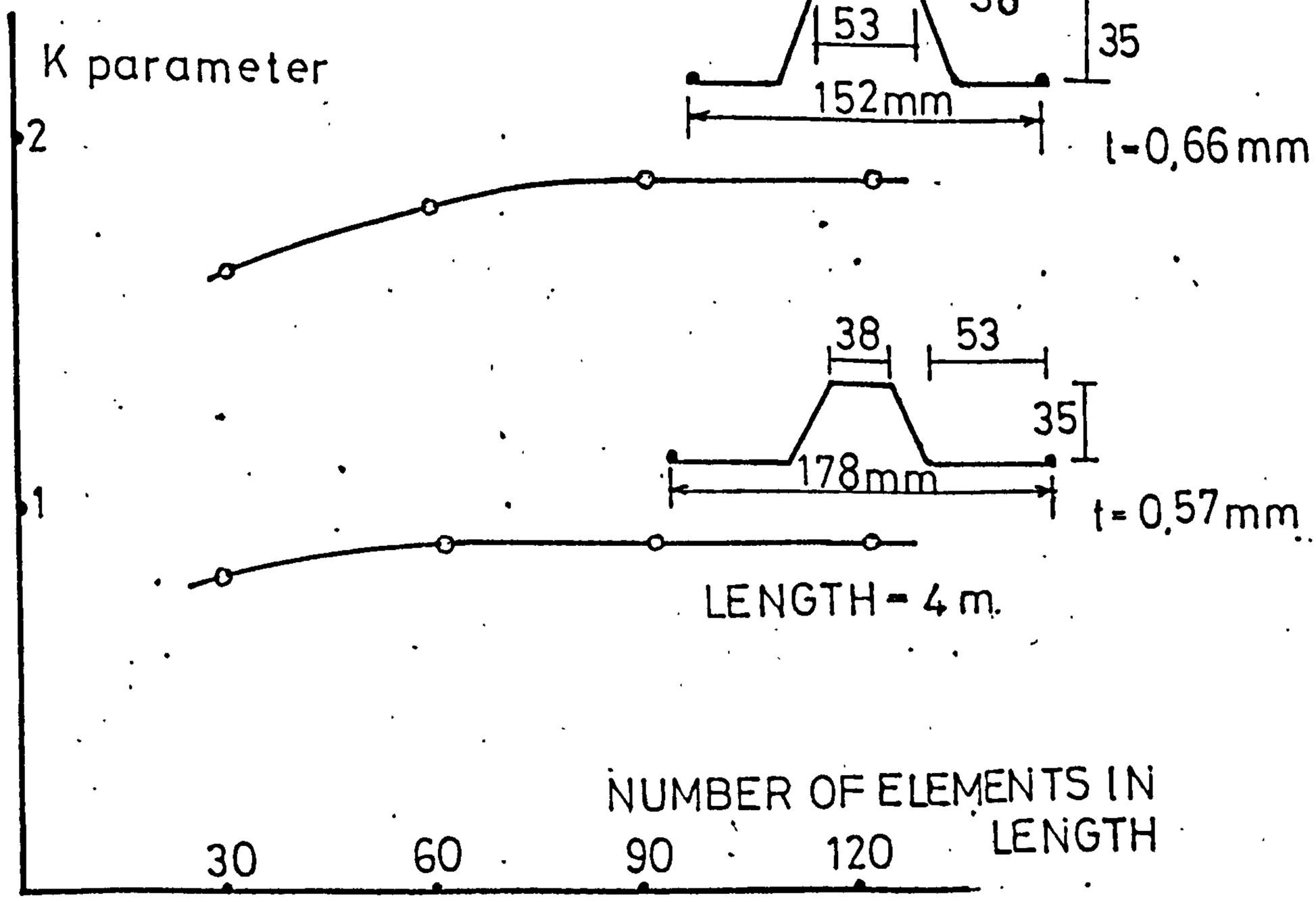

FIG (2.7(b))

EDGE BEAM RESTRAINT DUE TO EVERY TROUGH FASTENING

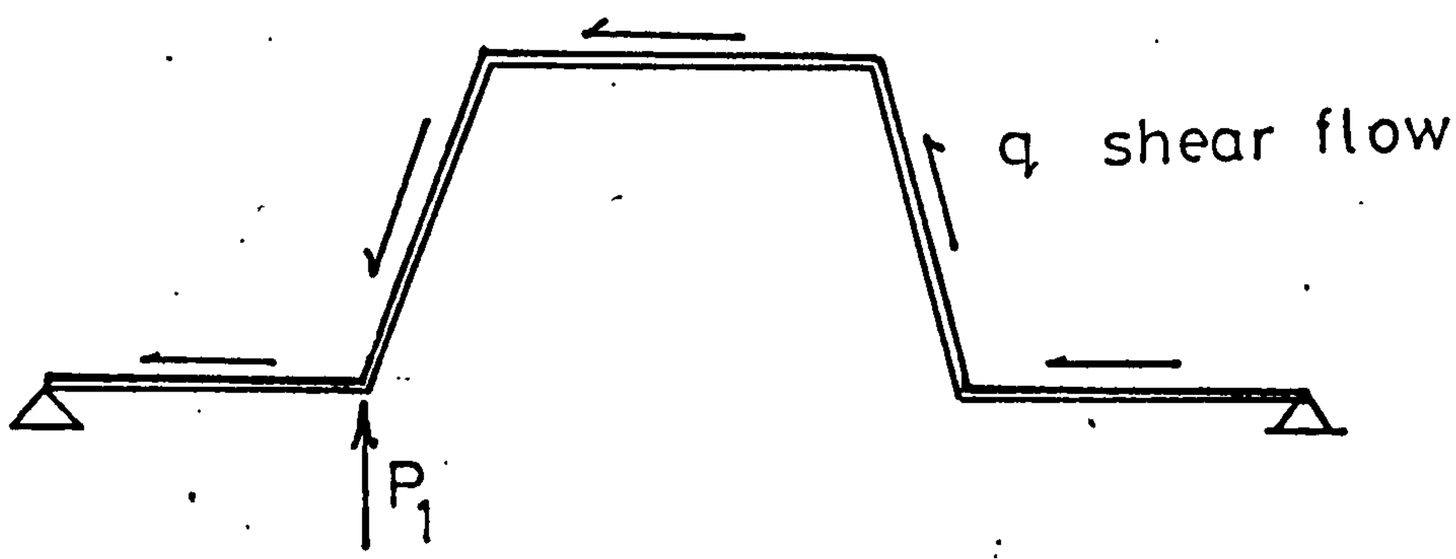

FIG(2.8(a))

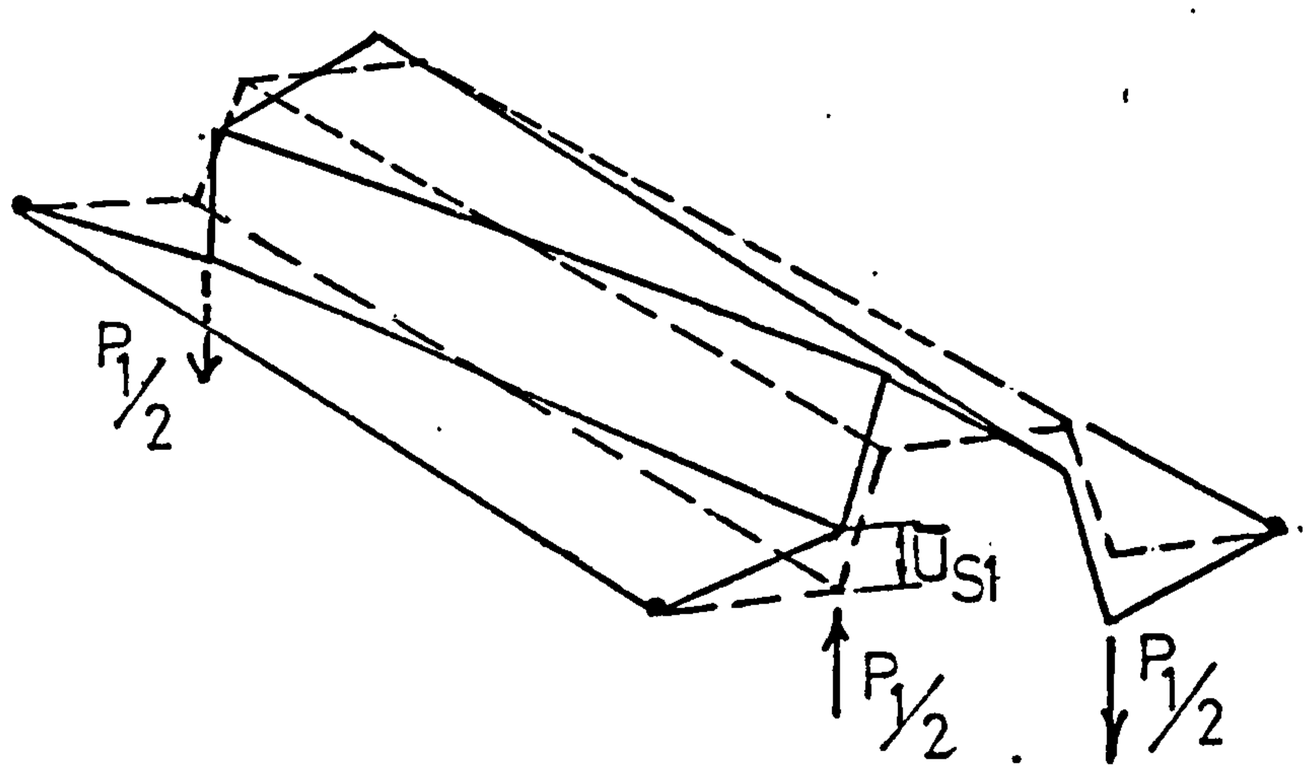

ANTISYMMETRIC END FORCES CAUSING UPLIFT. $\bar{U}_{S1}$

FIG(2.8(b))

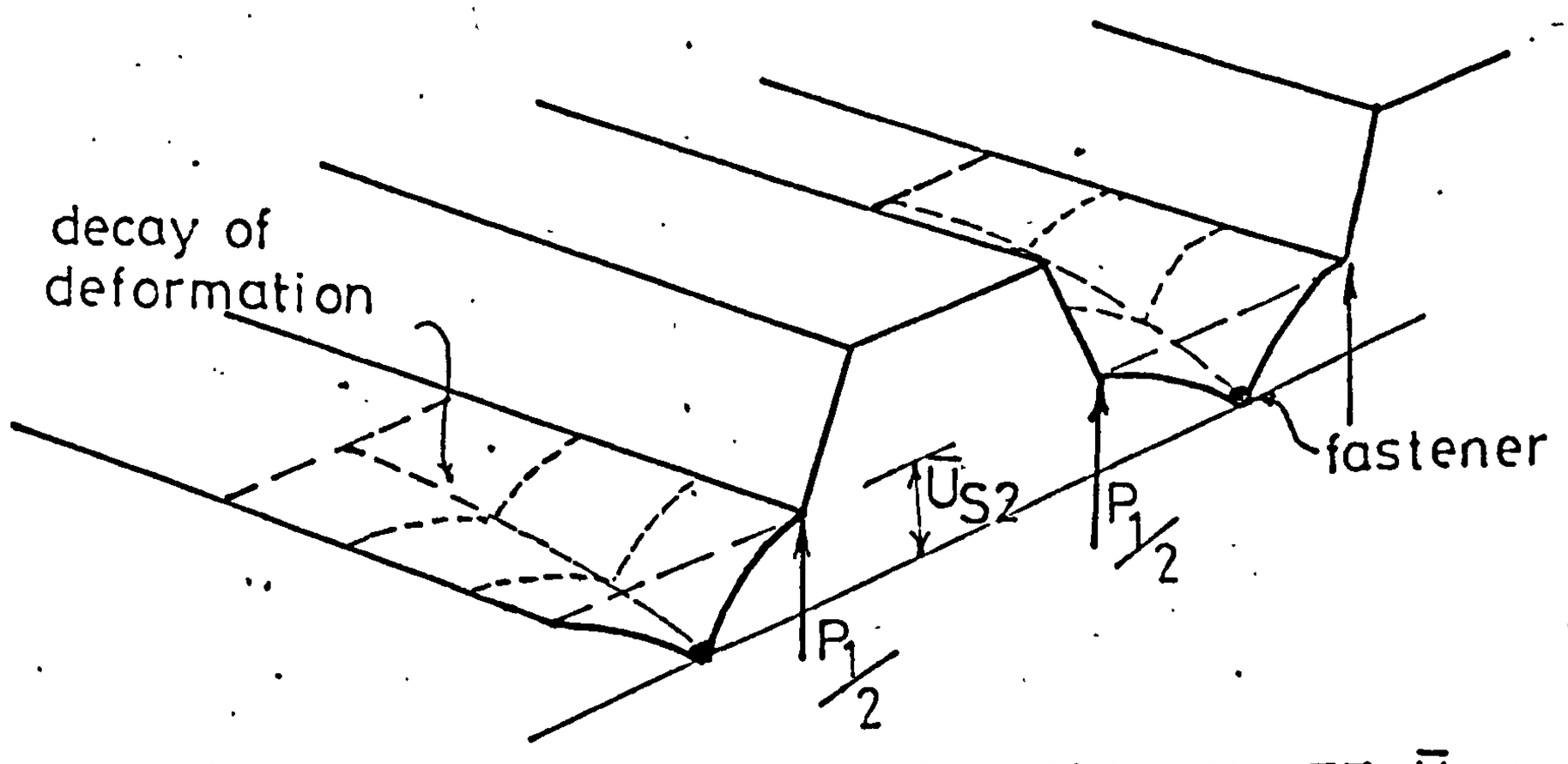

SYMMETRIC COMPONENTS AND UPLIFT $\bar{U}_{S2}$.

FIG(2.8(c))

SUMMARY OF BENDING MOMENT DIAGRAMS USED IN EVERY TROUGH FIXING ANALYSES

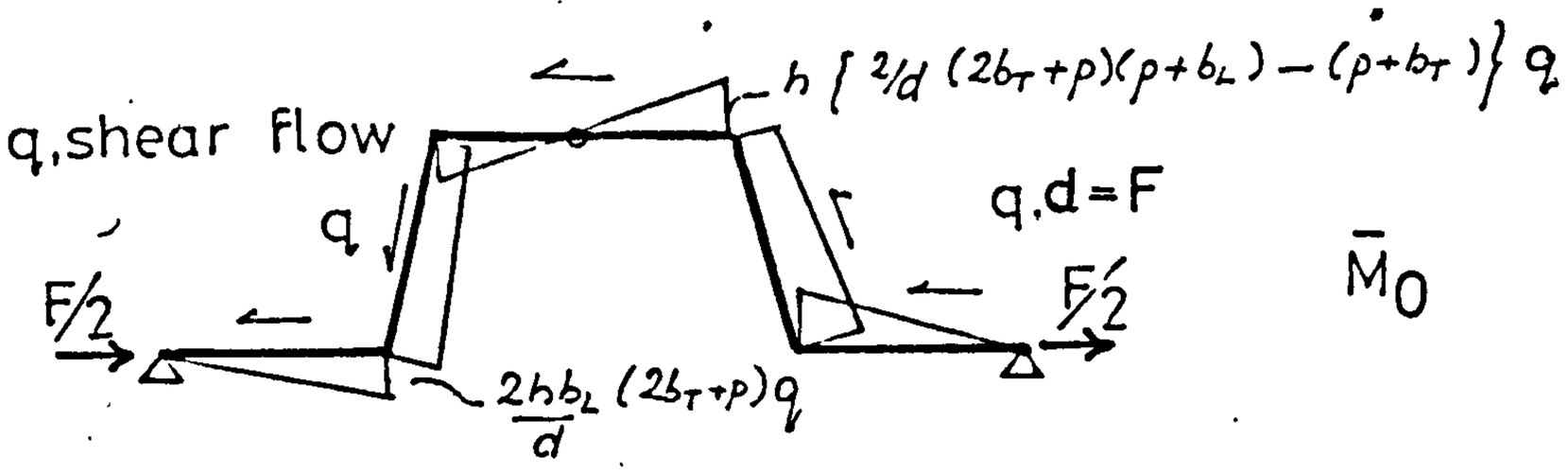

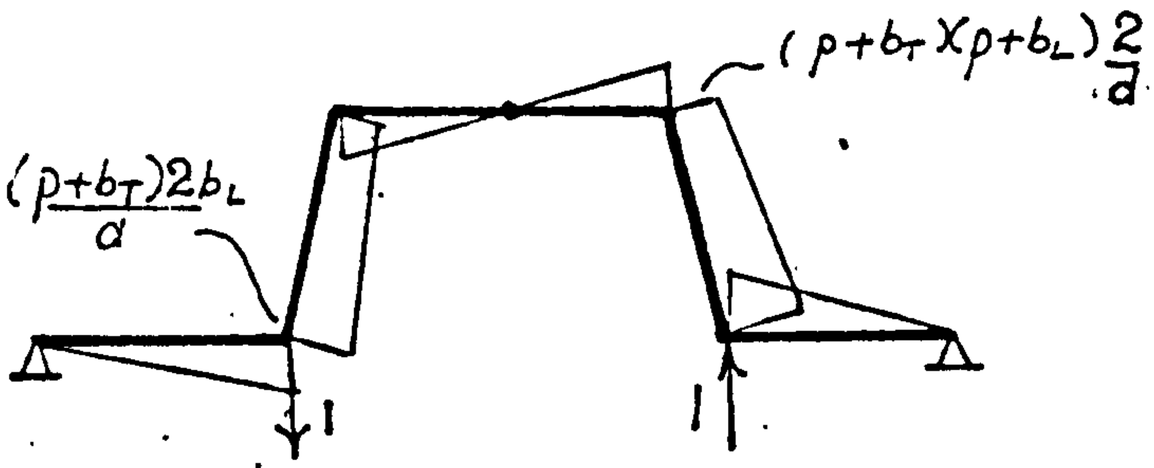

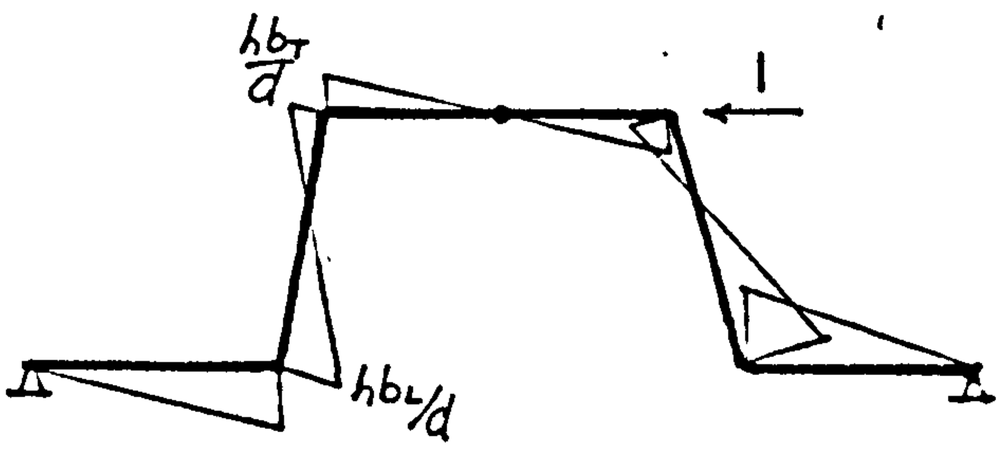

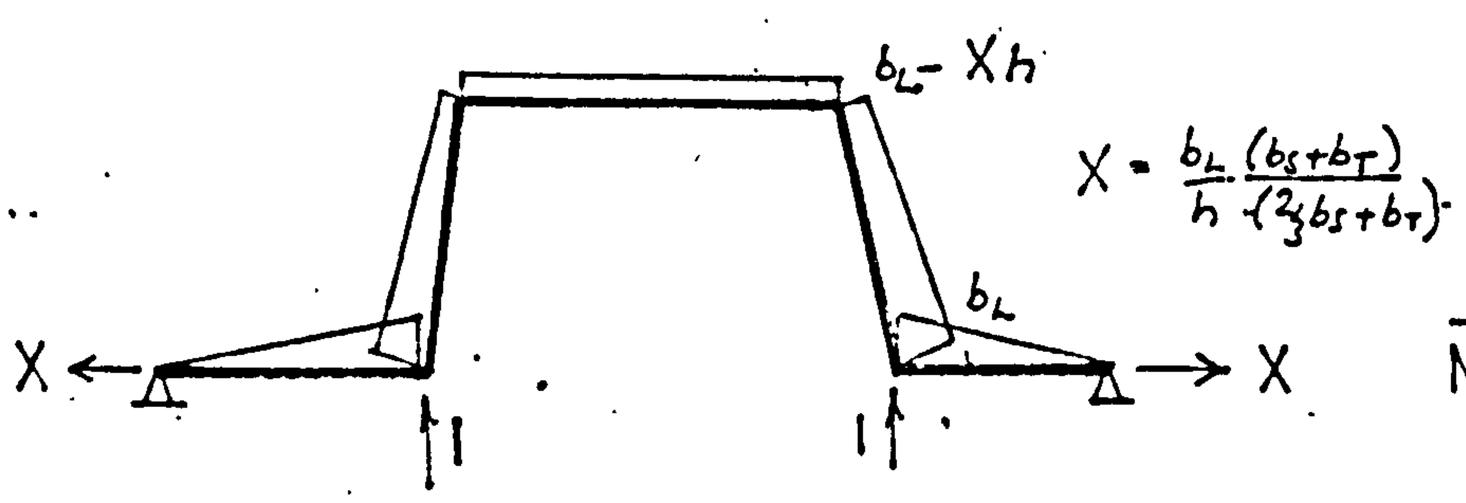

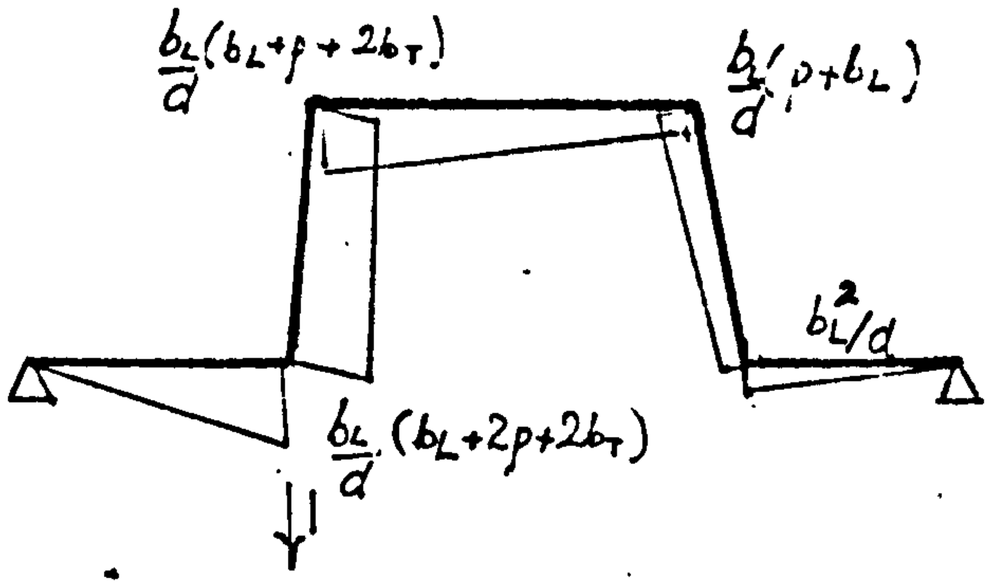

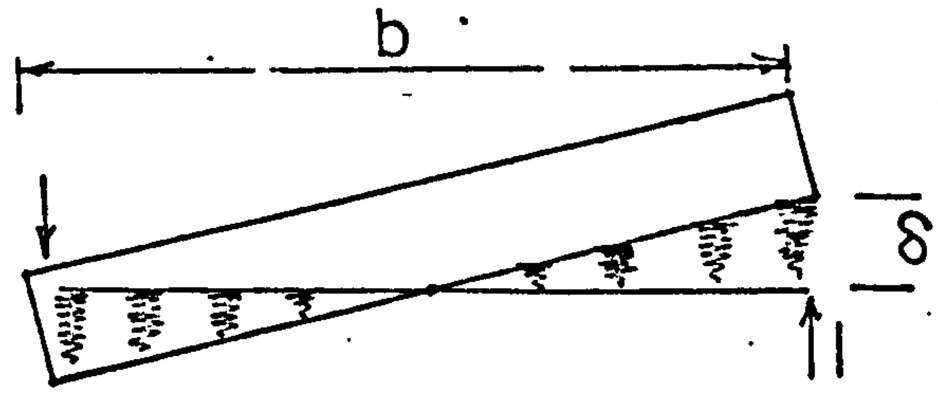

$b/6$ IS EQUIVALENT LONGITUDINAL STIFFNESS

FIG (2.9)

PROFILE DISPLACEMENTS—

VARIATION WITH SHEET LENGTH FOR EVERY TROUGH FASTENING

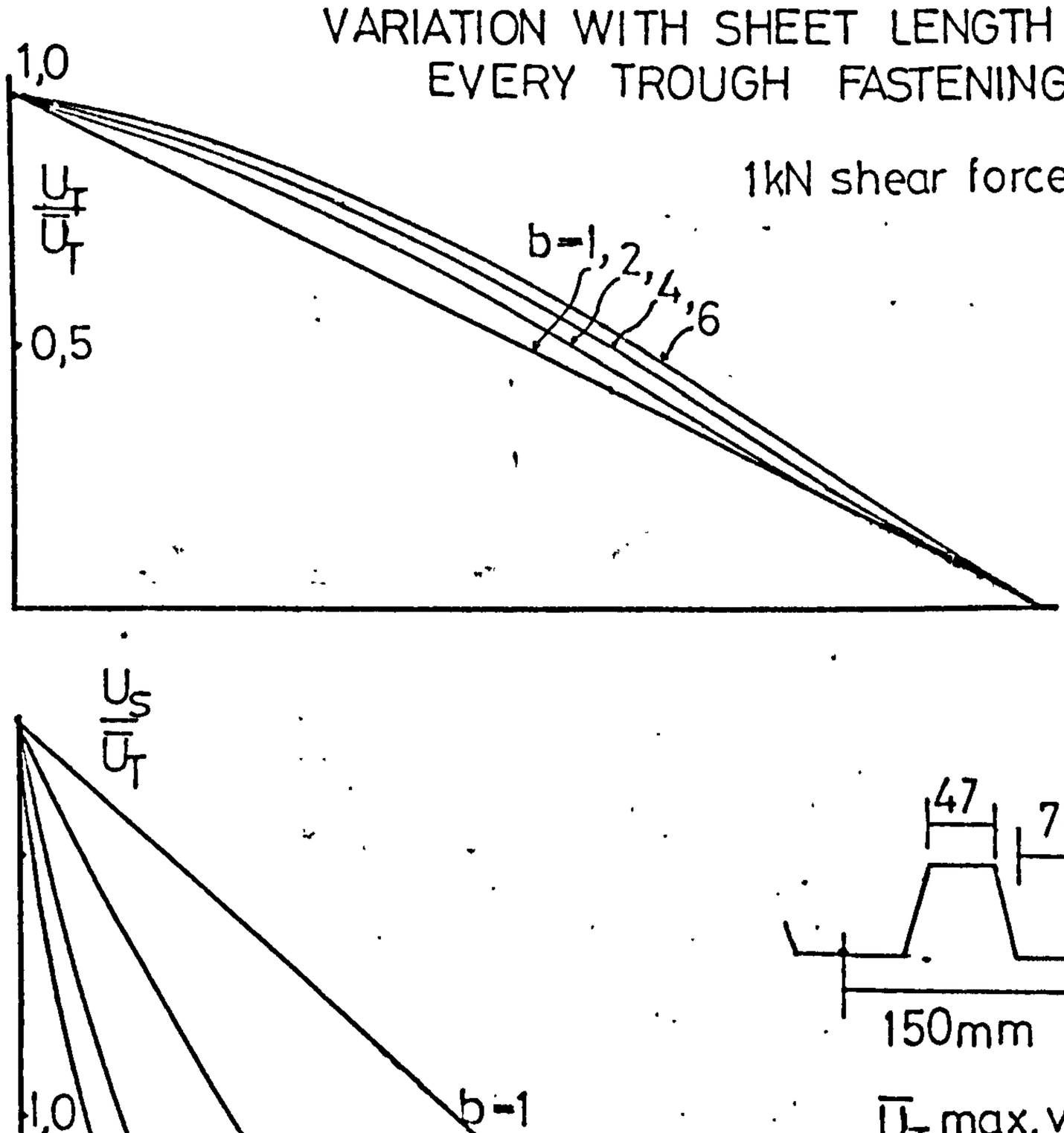

$\bar{U}_T$ max. value of U_T

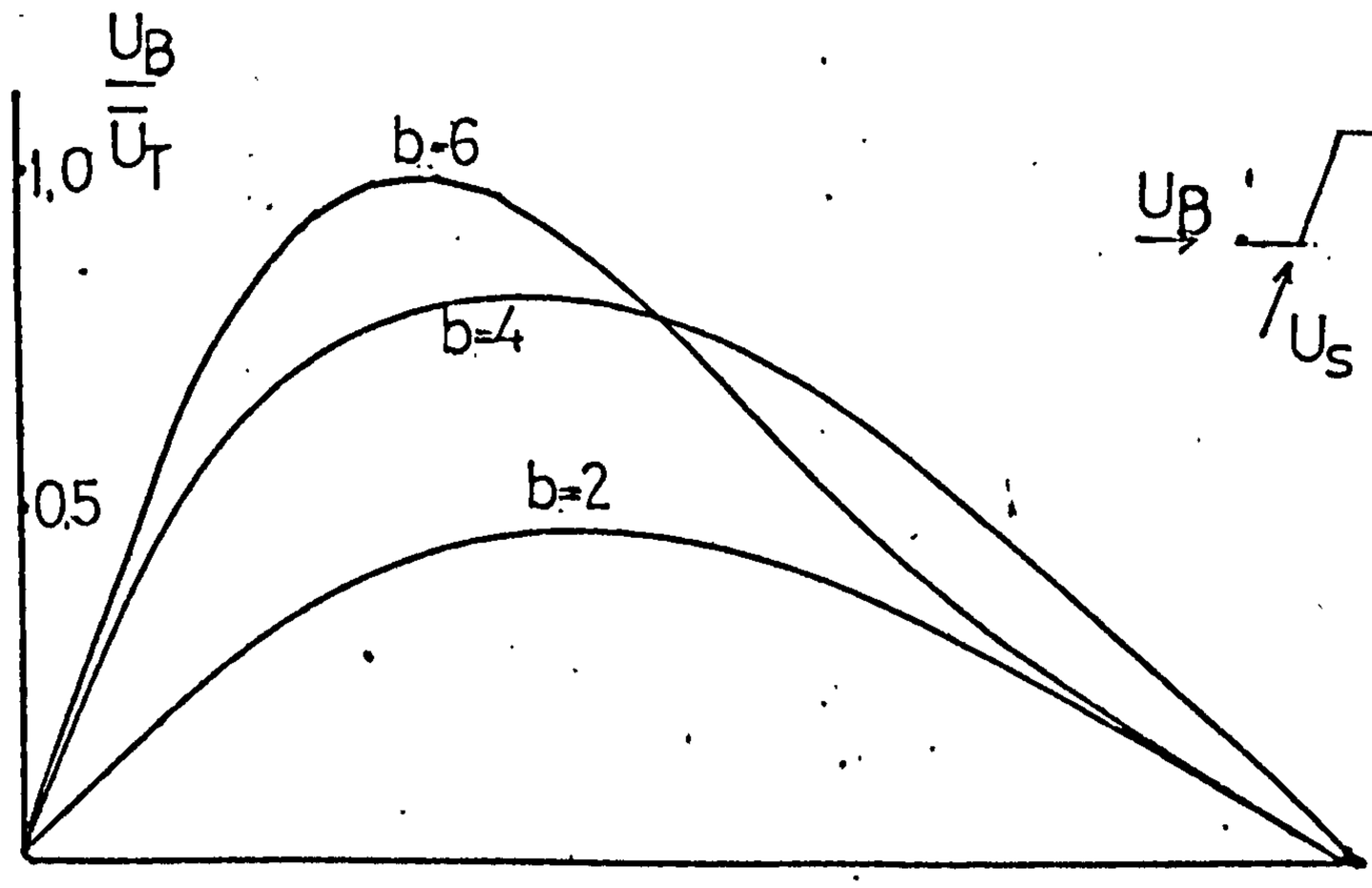

FIG (2.10(c))

EFFECT OF PROFILE SHAPE AND SHEET LENGTH ON K PARAMETER

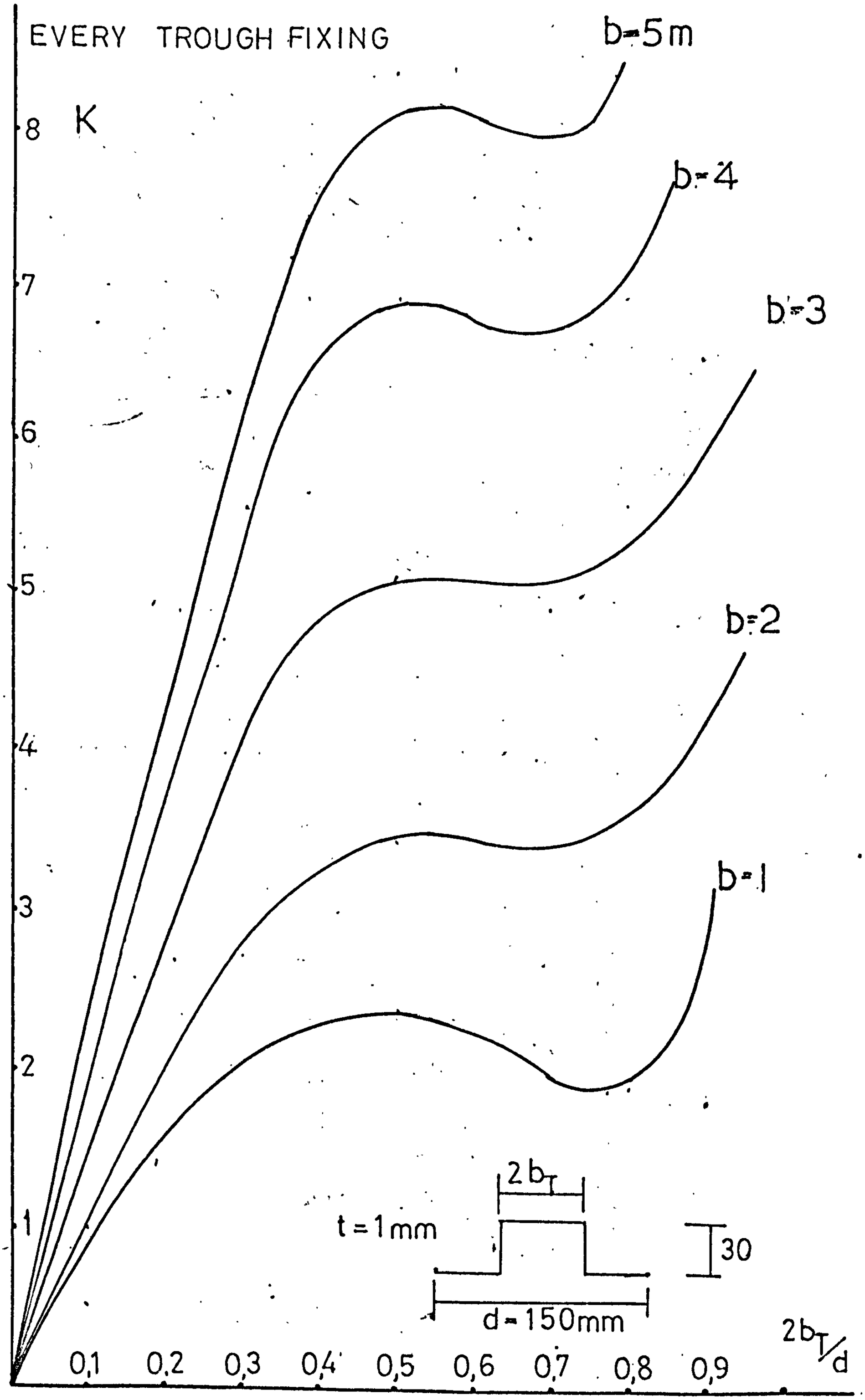

FIG(2.11)

END CROSS-SECTION DISPLACEMENTS

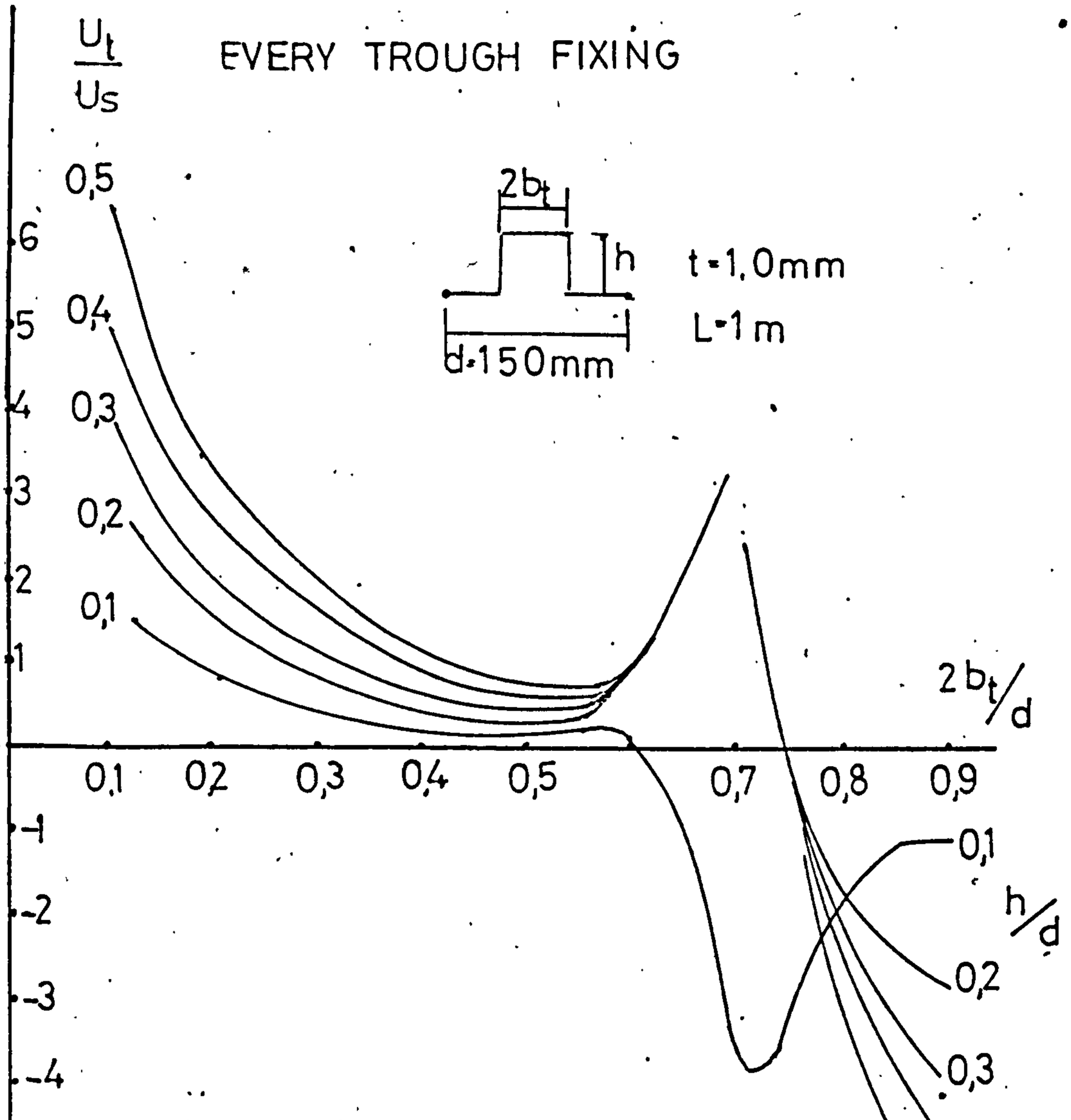

FIG(2.12(a))

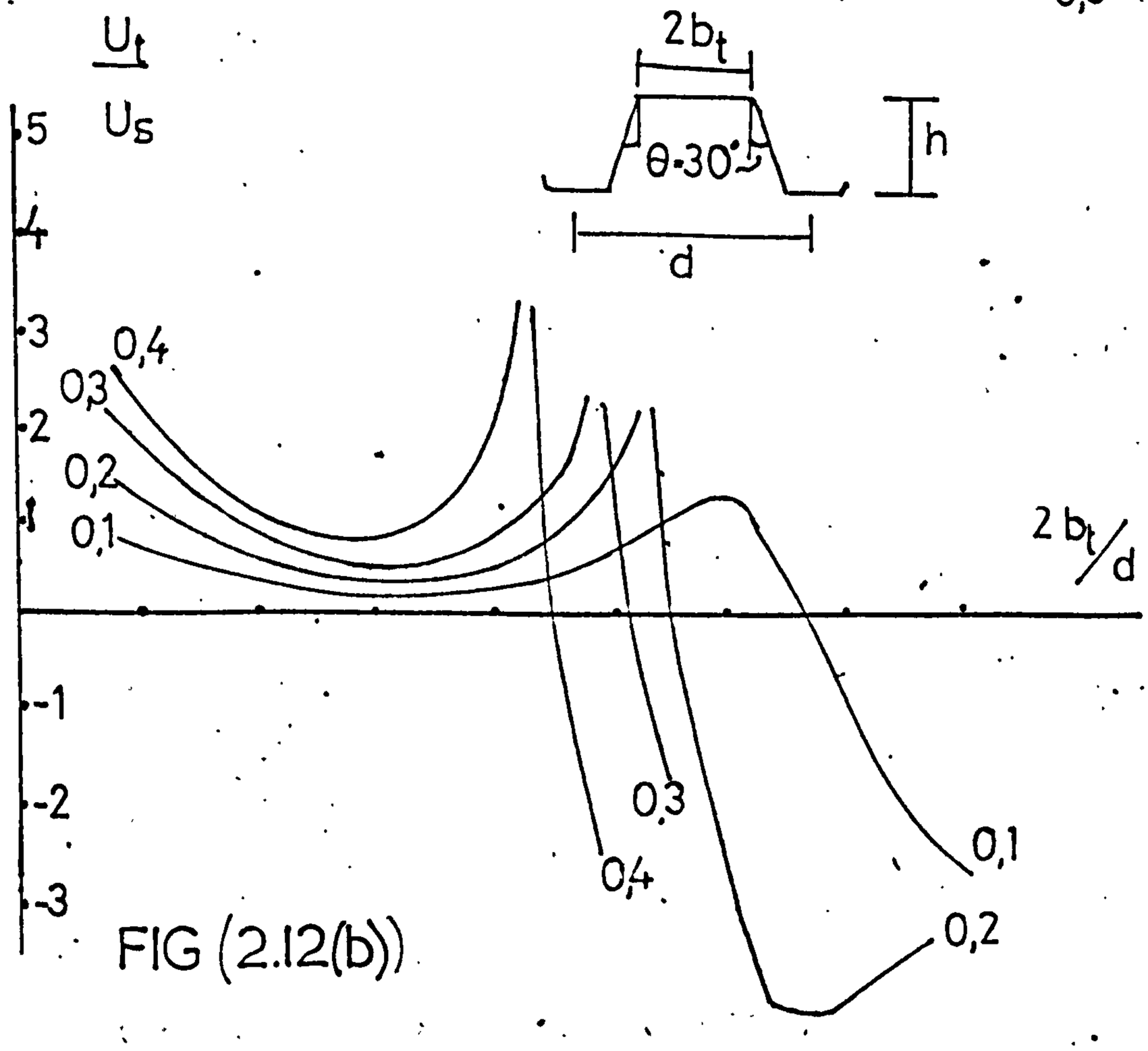

FIG (2.12(b))

VARIATION OF K PARAMETER WITH NUMBER OF FOURIER TERMS

EVERY TROUGH FIXING

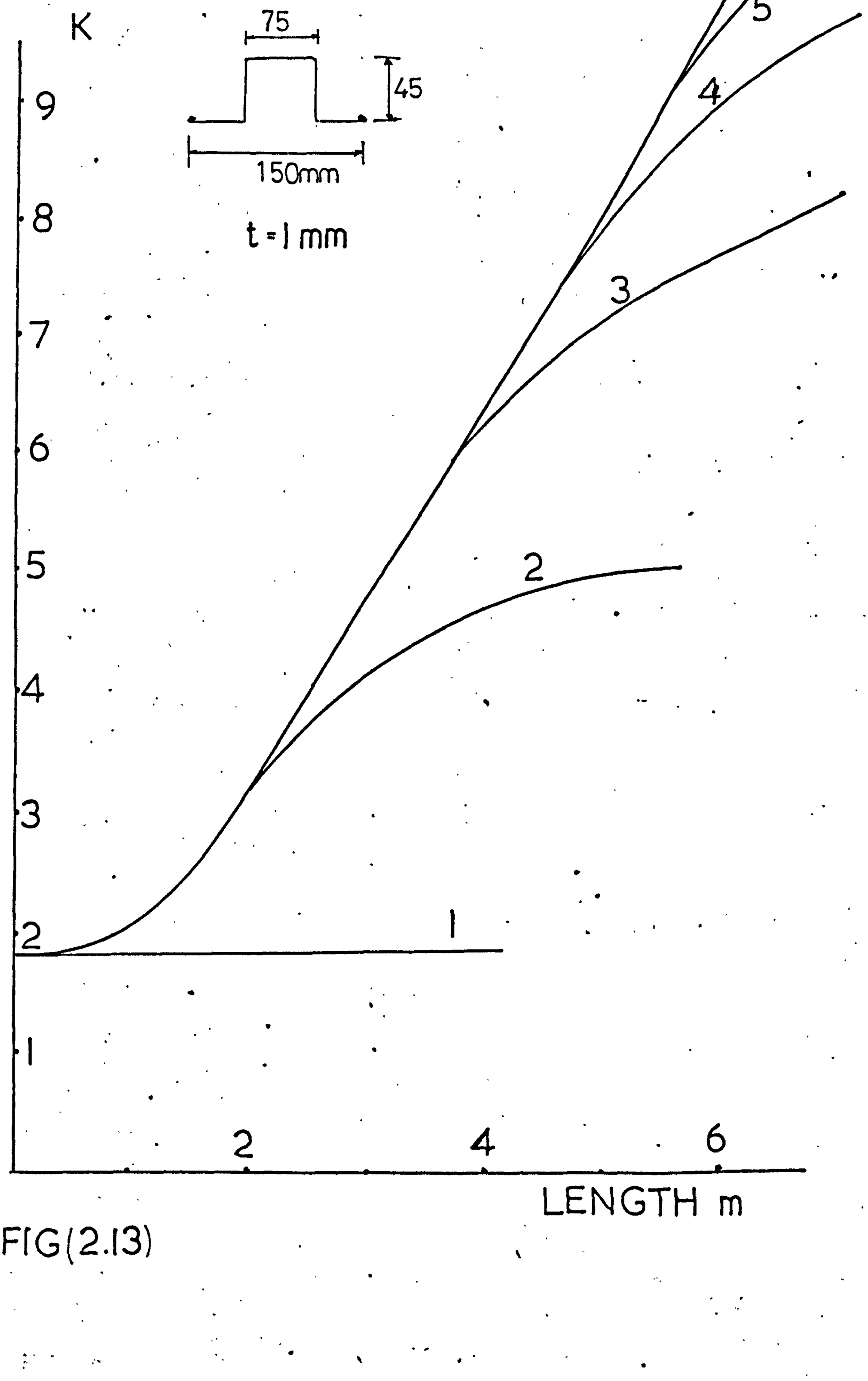

FIG(2.13)

EFFECT OF NUMBER OF FOURIER TERMS

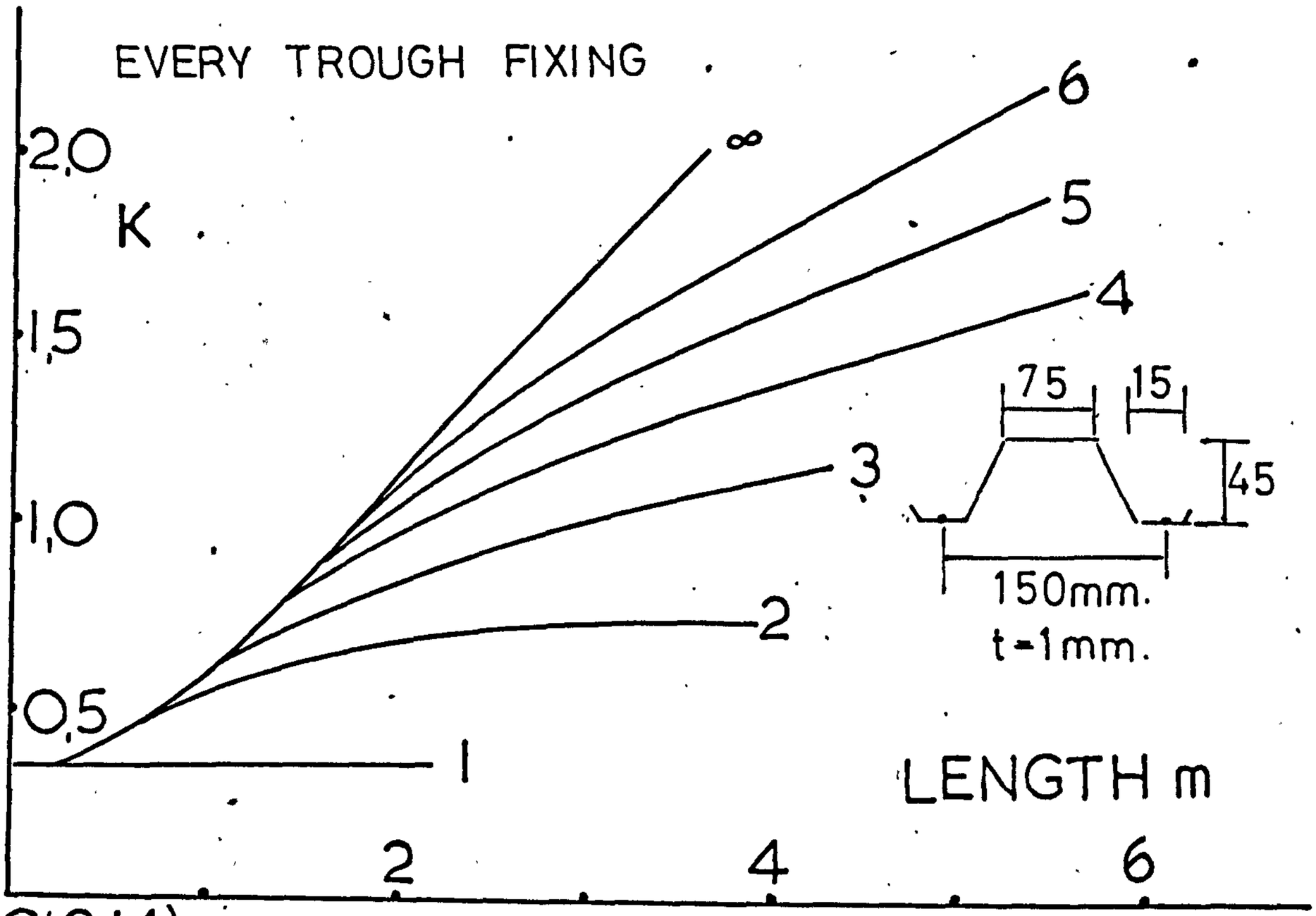

FIG(2.14)

EFFECT OF PITCH AND THICKNESS

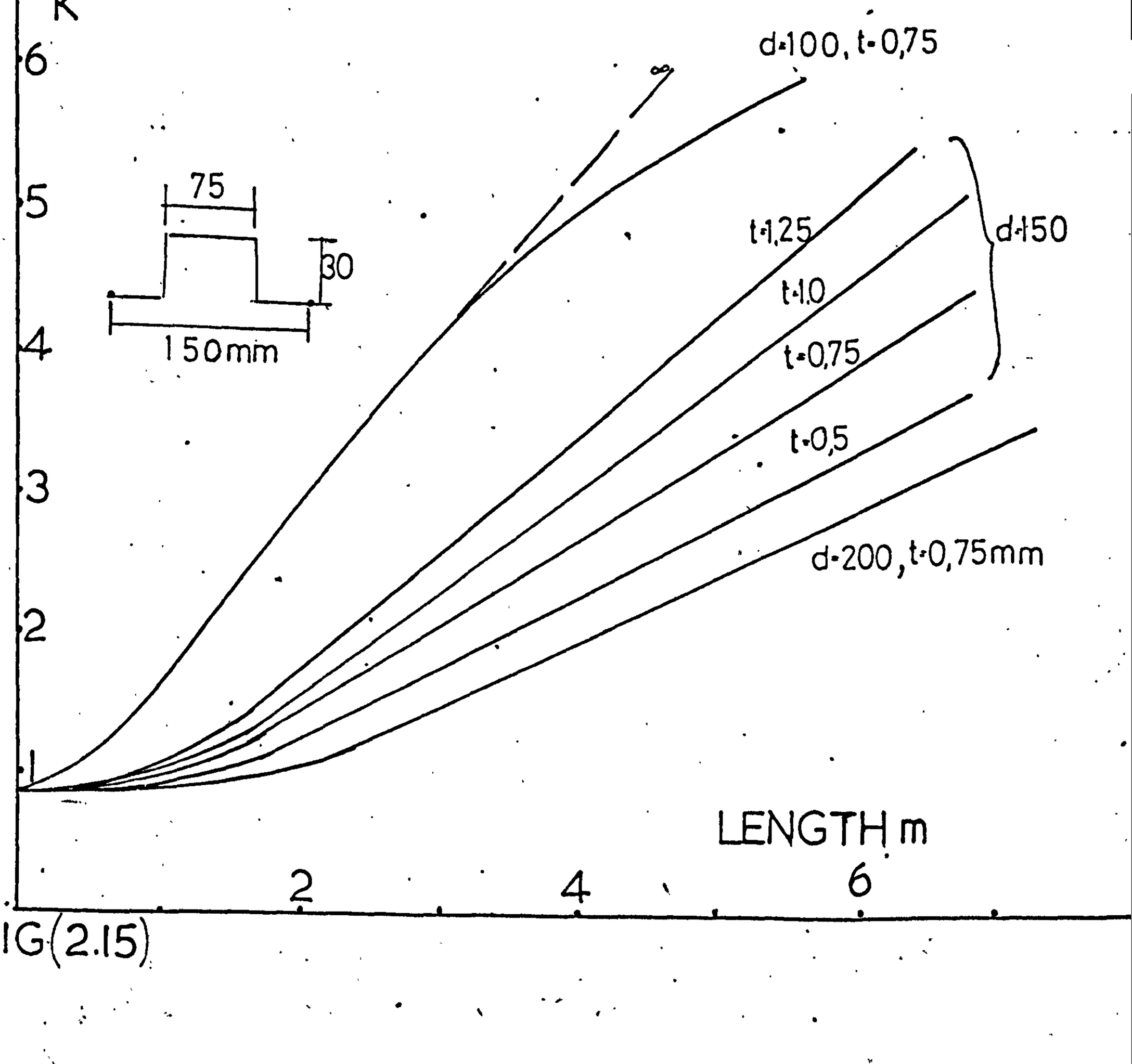

FIG(2.15)

VARIATION OF K PARAMETER WITH SHEET THICKNESS

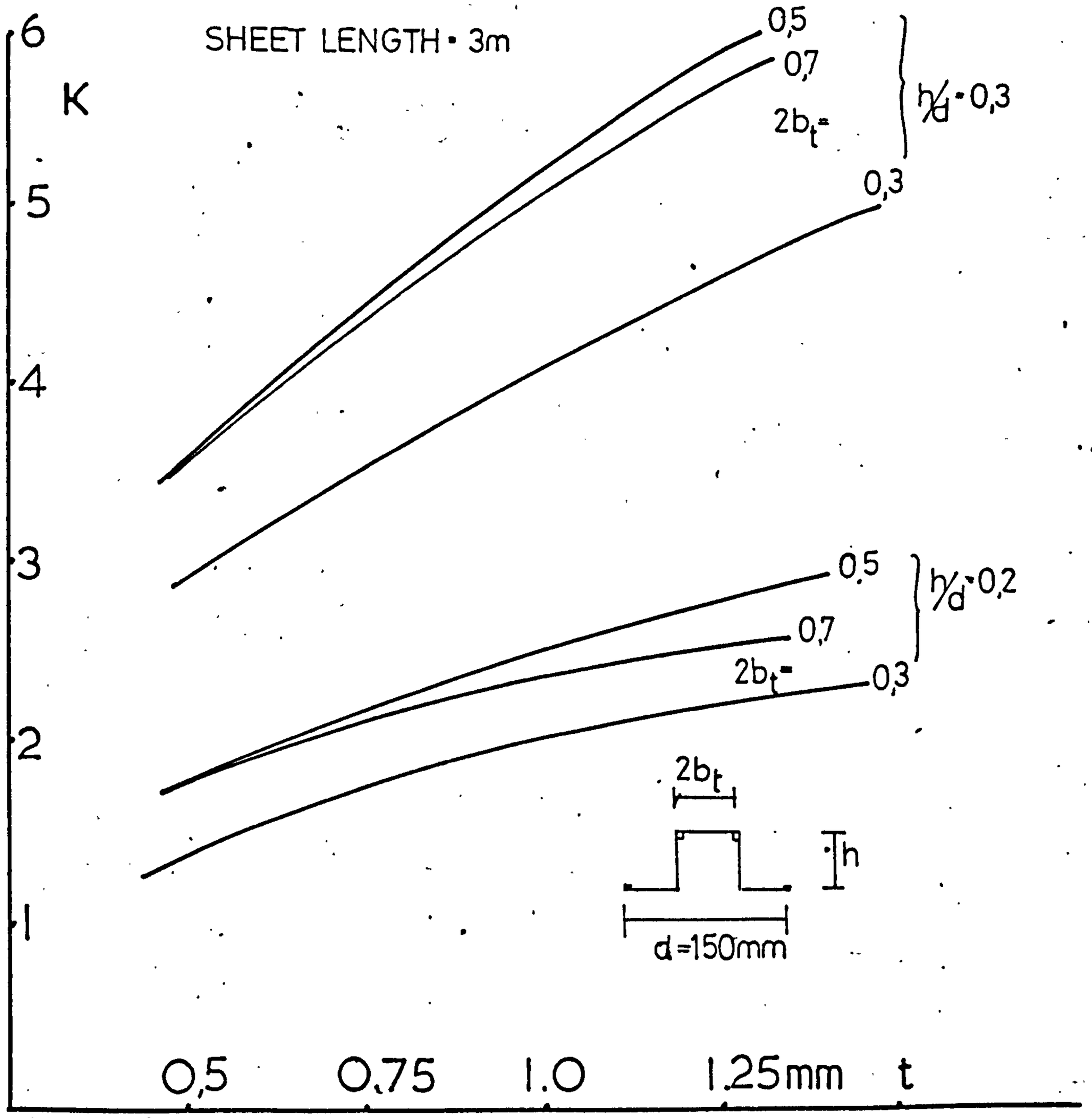

FIG(2.16(a))

EVERY TROUGH FIXING

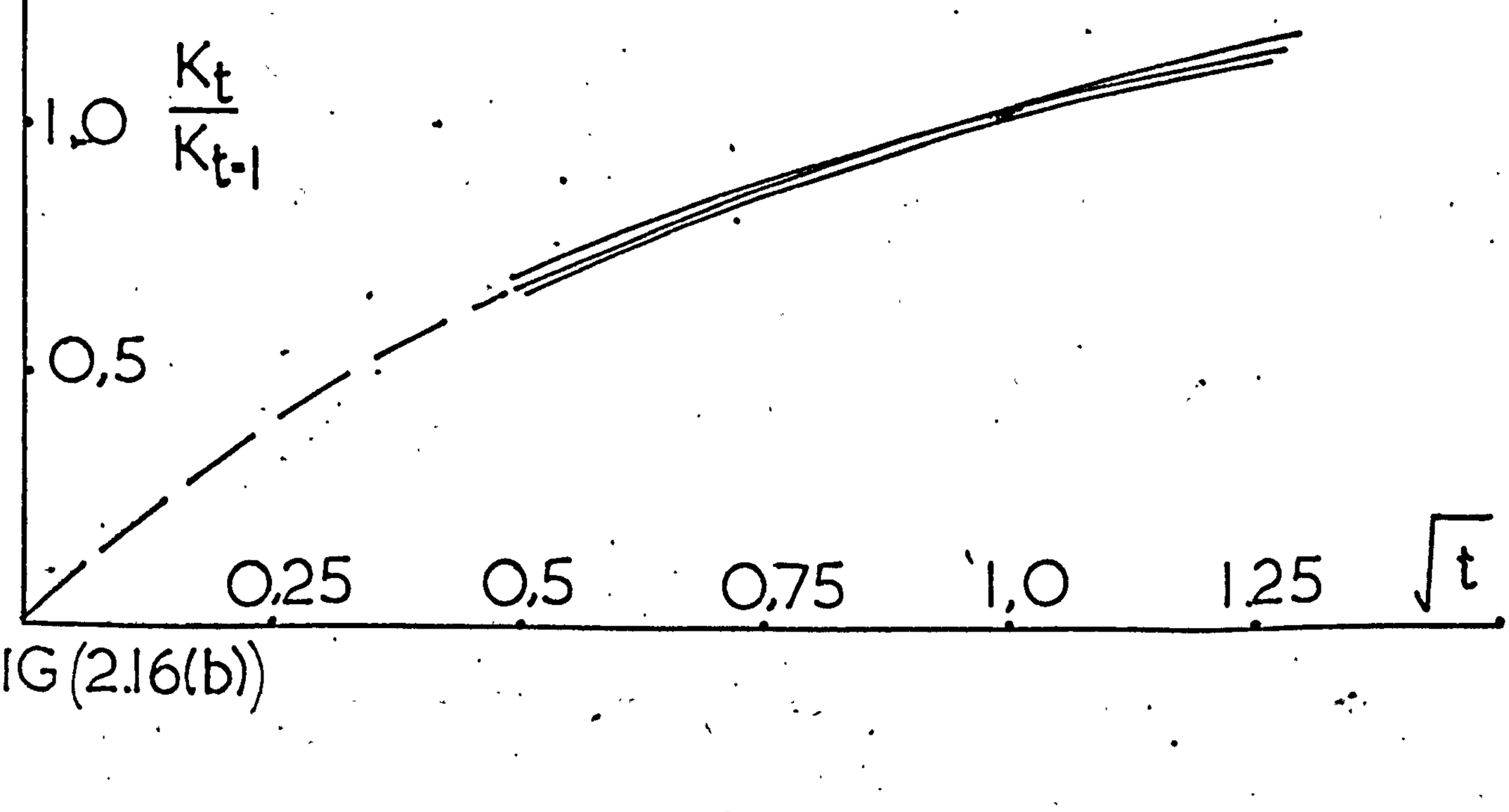

FIG (2.16(b))

'PURLIN PROP' REDUCTION OF K VALUE.

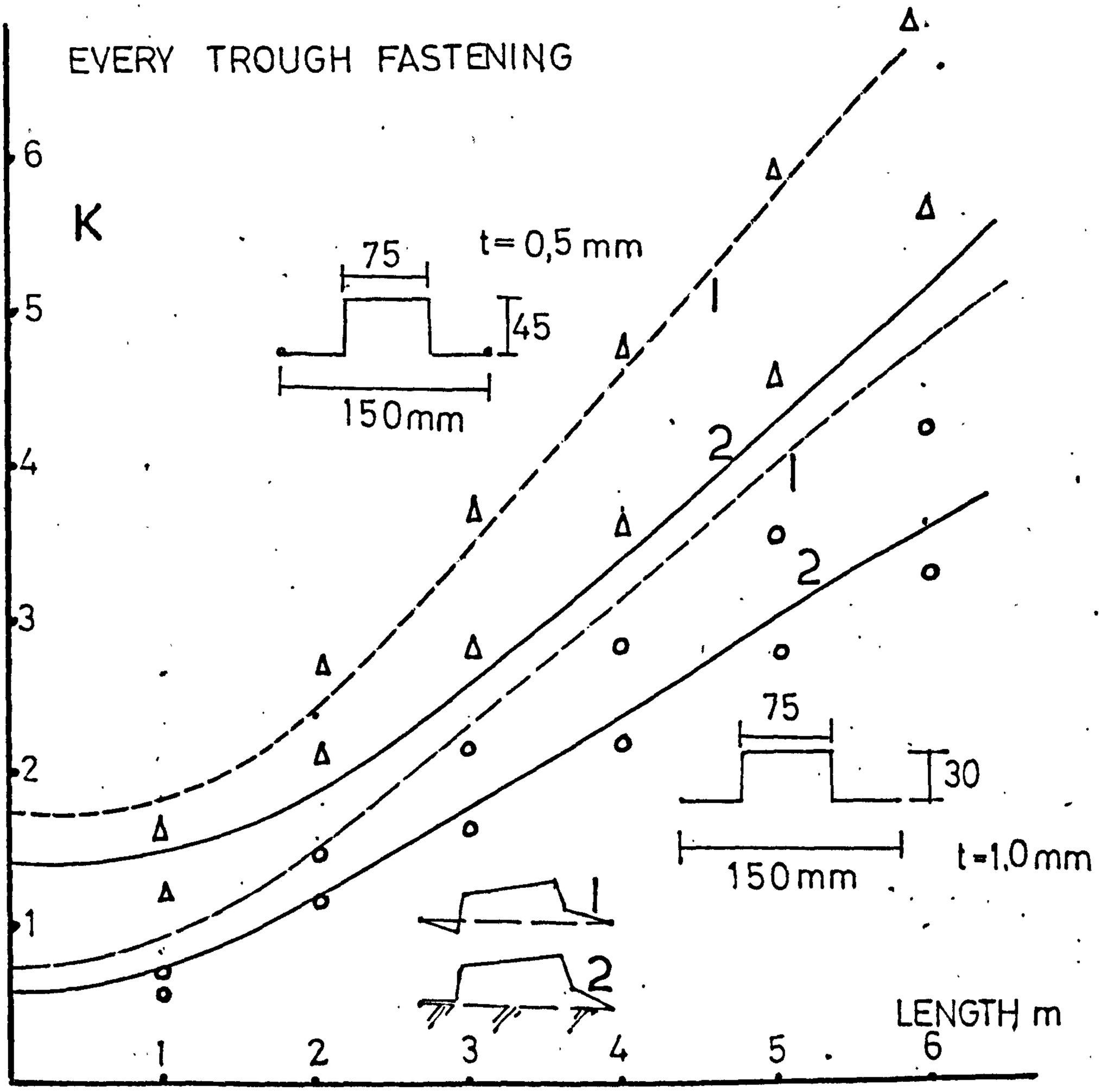

FIG(2.17(a))

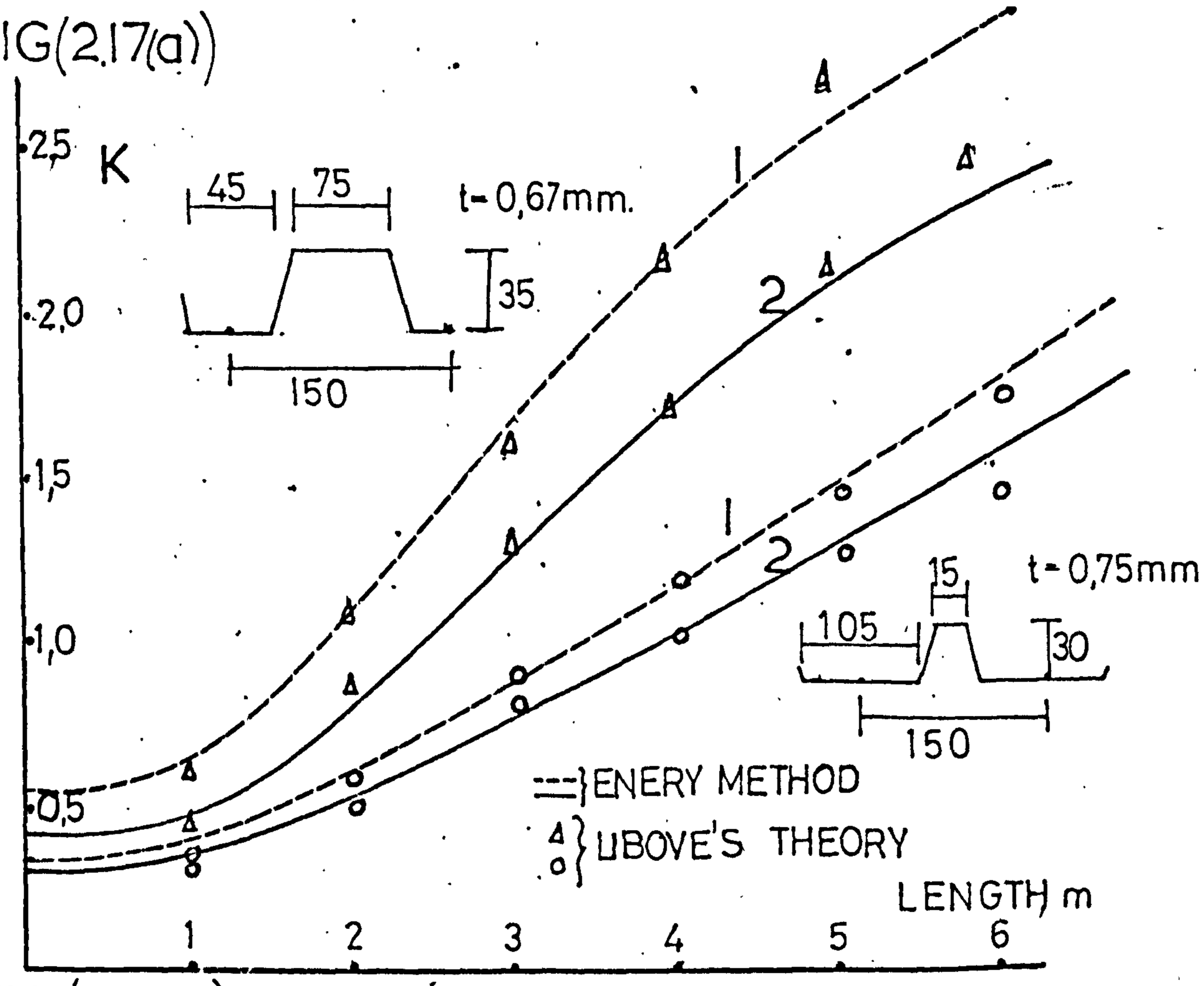

FIG (2.17(b))

EFFECT OF PROFILE SHAPE ON $\bar{K}$ PARAMETER

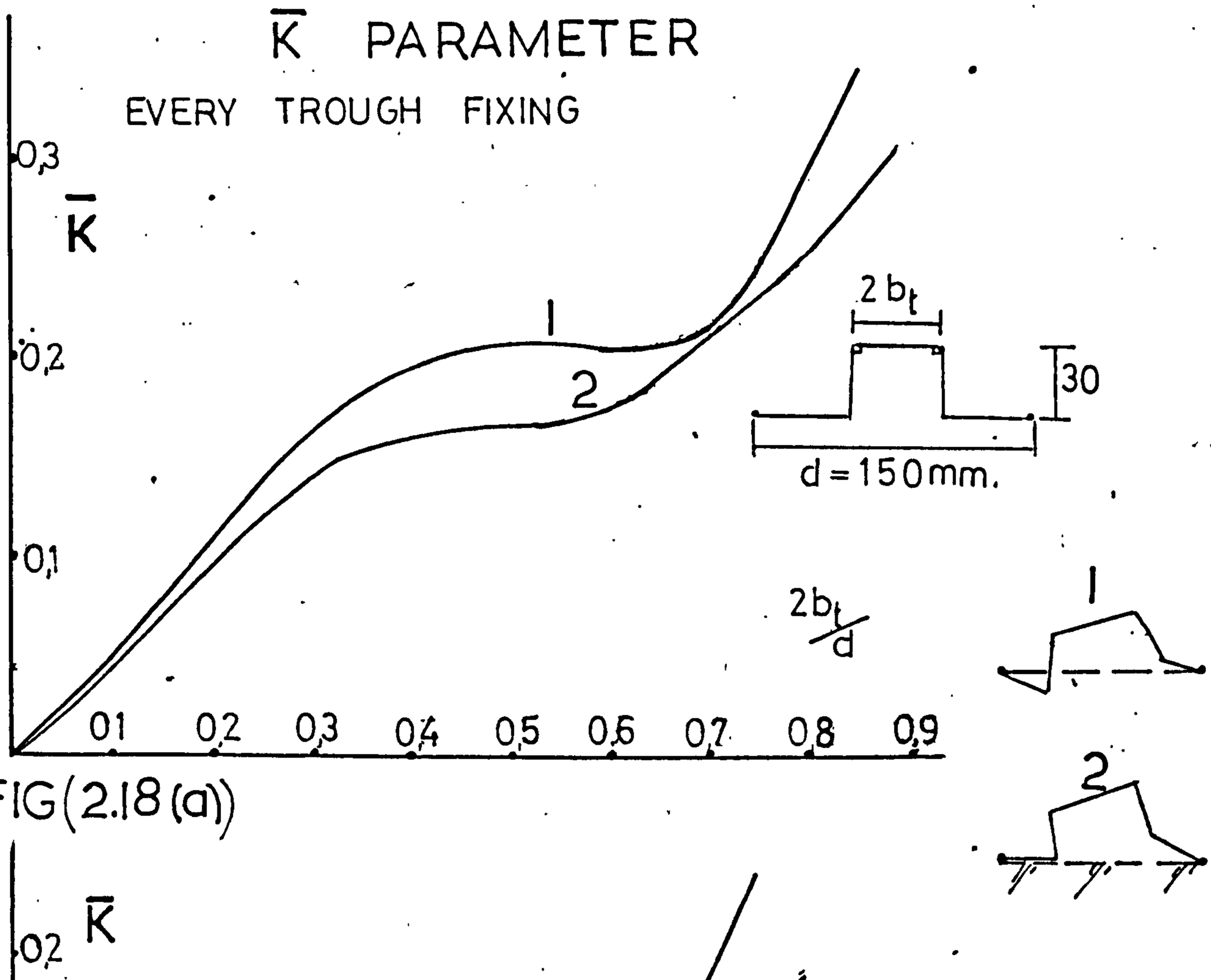

FIG (2.18 (a))

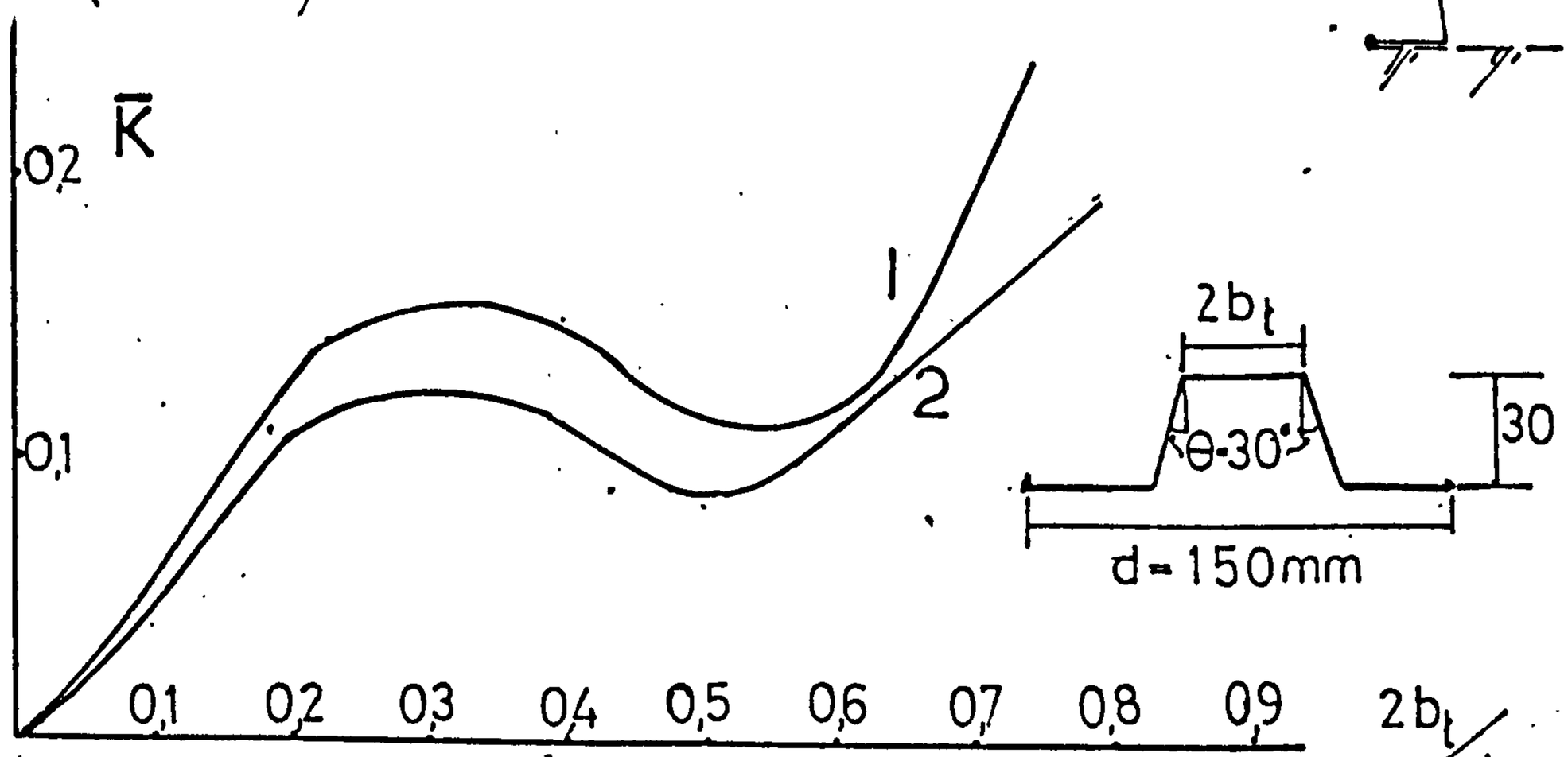

FIG (2.18(b))

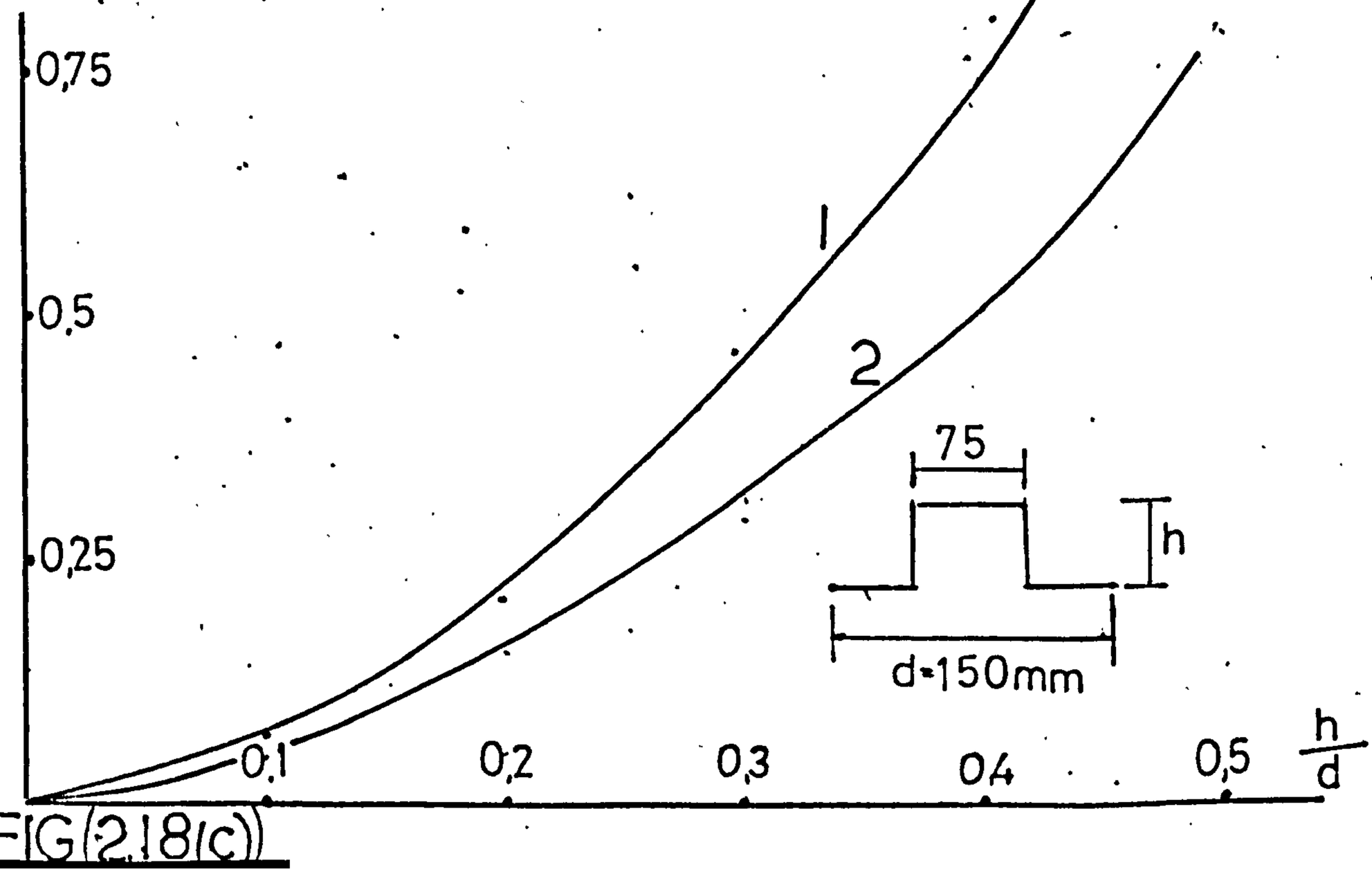

FIG (2.18(c))

TROUGH MOVEMENT RESTRAINED AT TWO INTERMEDIATE PURLINS

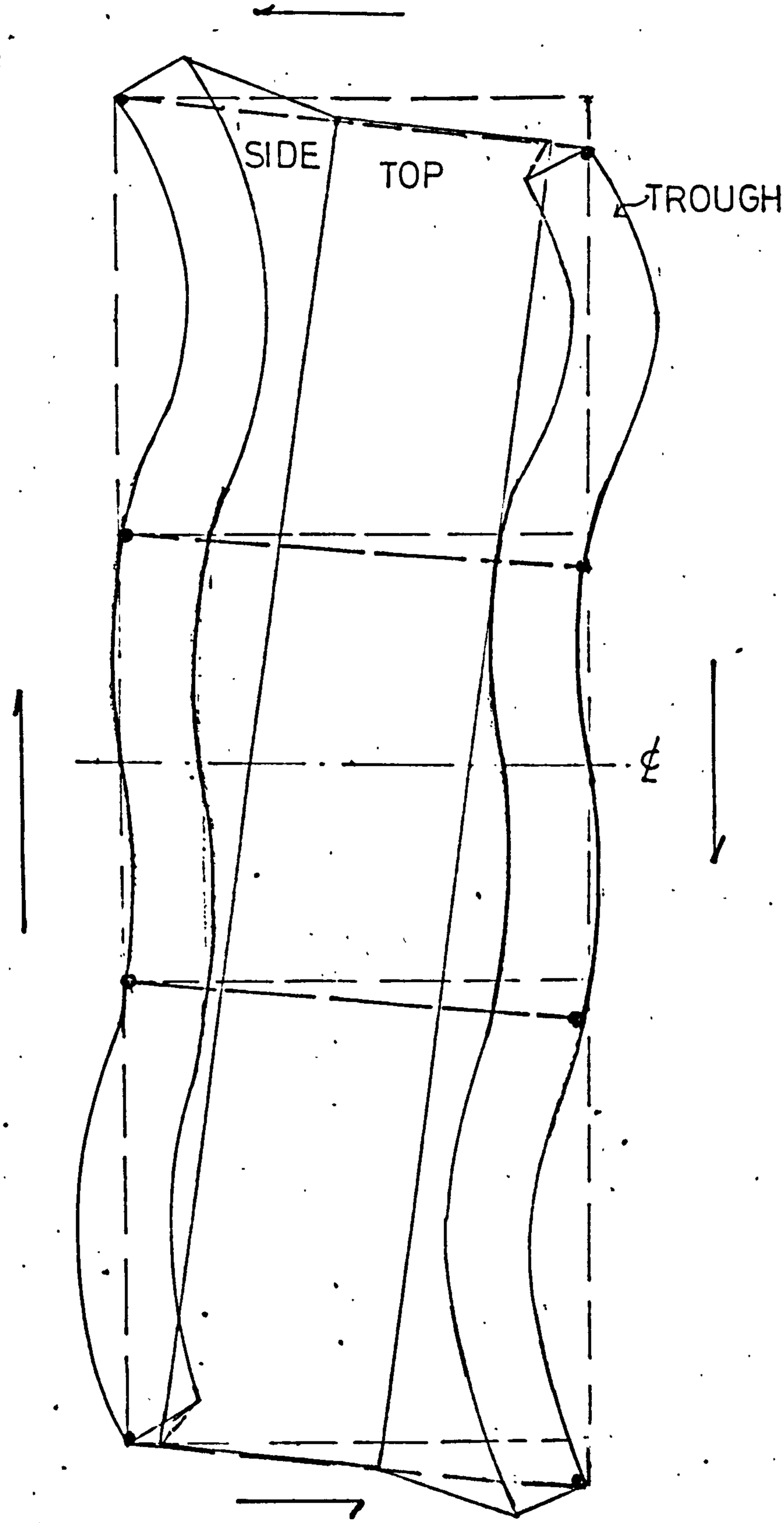

EVERY TROUGH FIXING

FIG (2.19)

FASTENING IN EVERY TROUGH AT THE ENDS AND IN ALTERNATE TROUGHS AT INTERMEDIATE PURLINS

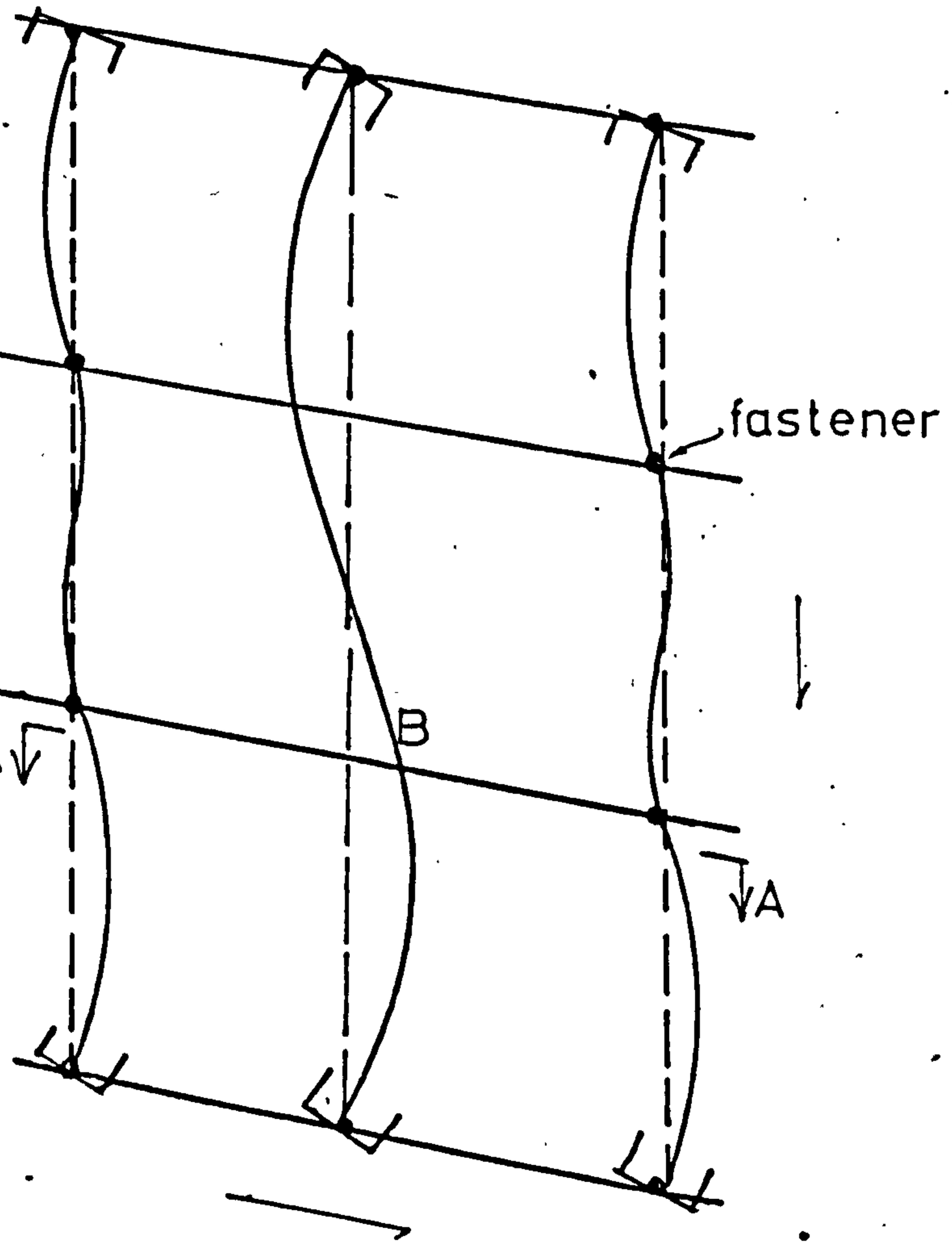

SECTION AA MOVEMENT IS SUM OF 1&2

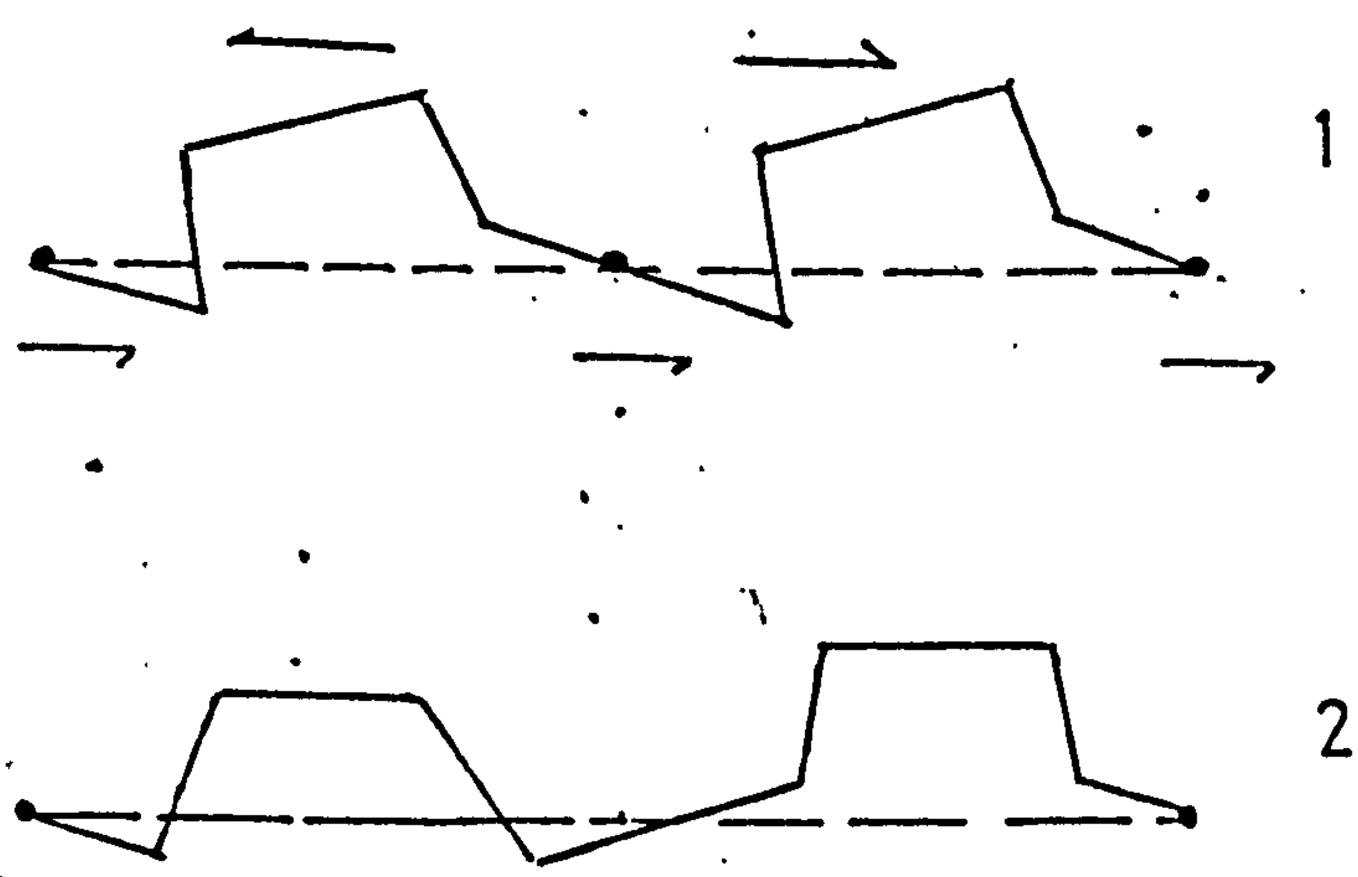

ADDITIONAL FREEDOM DUE TO REMOVAL OF FASTENER B

FIG (2.20)

EFFECT OF INCREASING NUMBER OF INTERMEDIATE PURLINS, N

—EVERY TROUGH FIXING

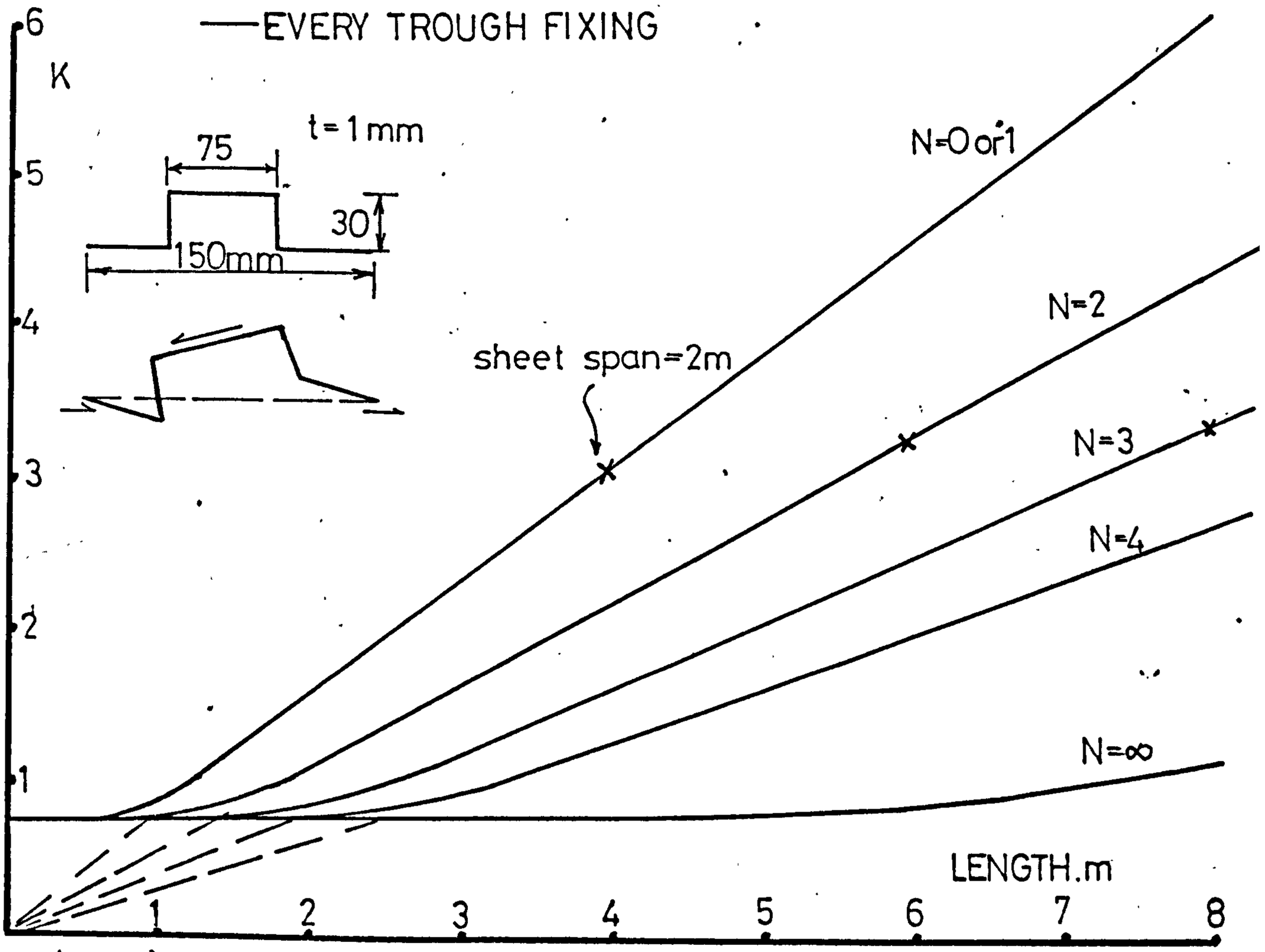

FIG(2.21)

INCREASING THE NUMBER OF FOURIER TERMS

—2 INTERMEDIATE PURLINS

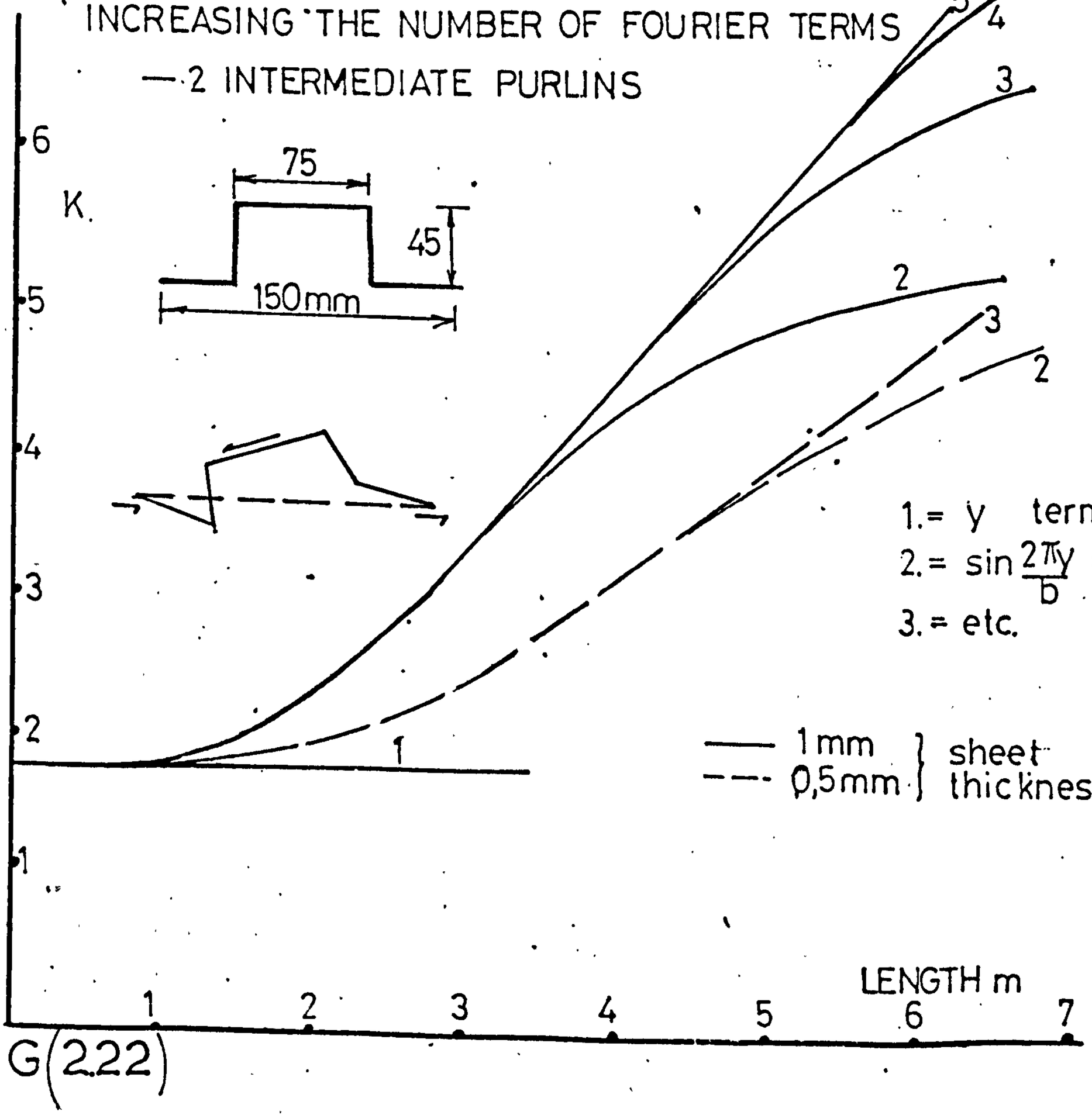

FIG(2.22)

EFFECT OF PROFILE SHAPE AND NUMBER OF INTERMEDIATE PURLINS ON $\bar{K}$ PARAMETER

—EVERY TROUGH FIXING

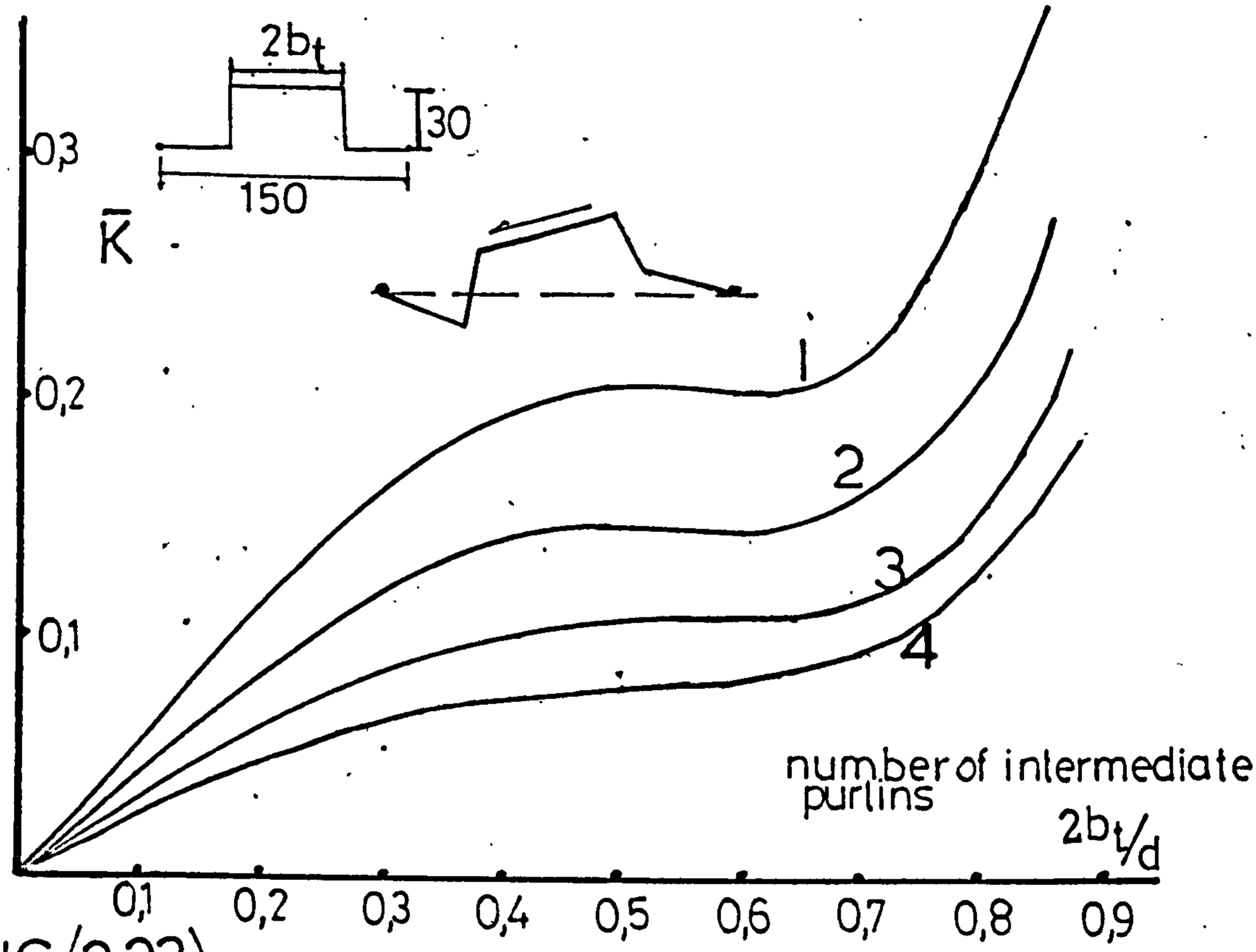

FIG(2.23)

VARIATION OF $\bar{K}$ WITH LENGTH

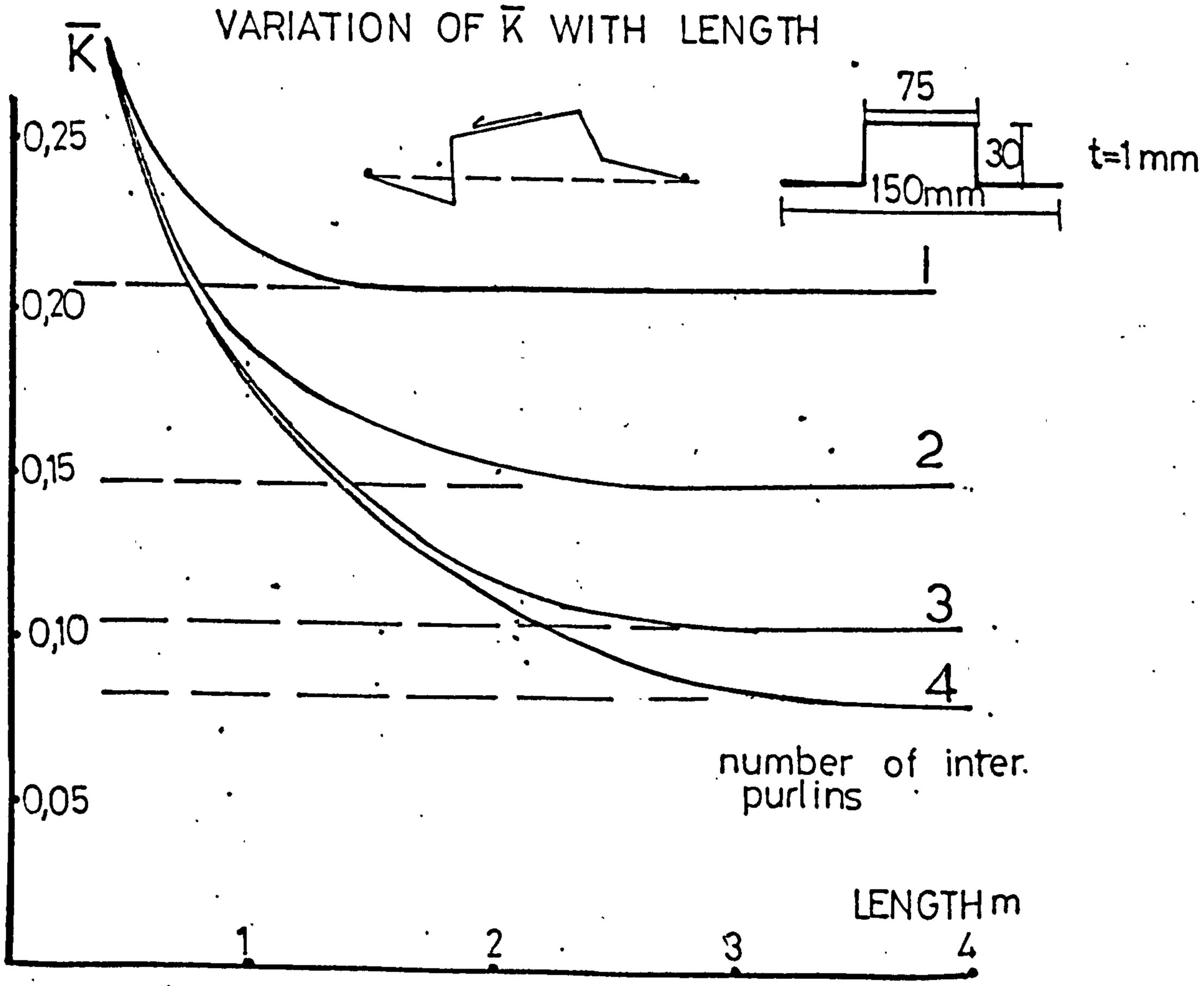

FIG(2.24)

EVERY TROUGH FIXING —
1,2,3,4 INTERMEDIATE PURLINS

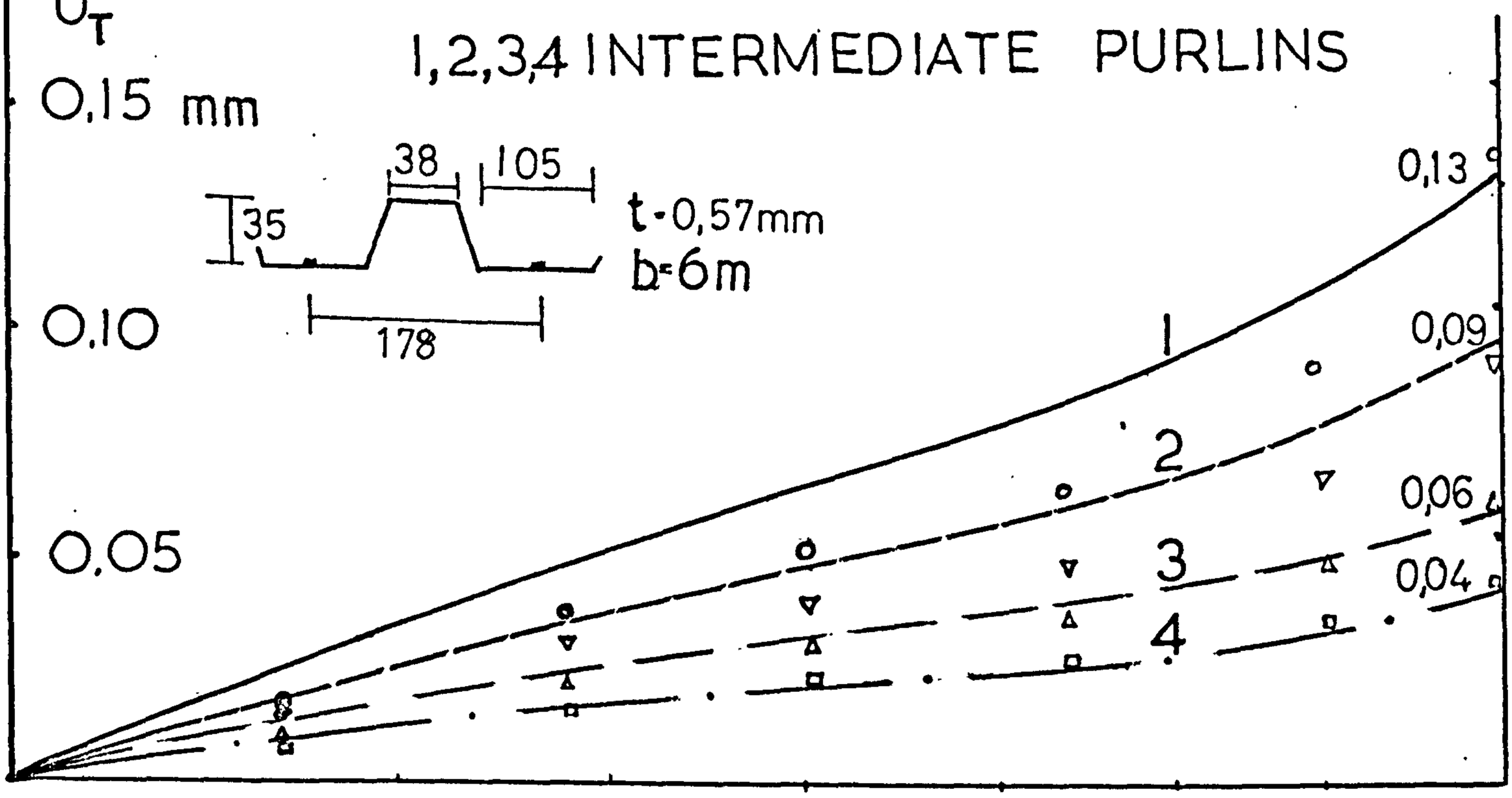

PROFILE DISPLACEMENTS –

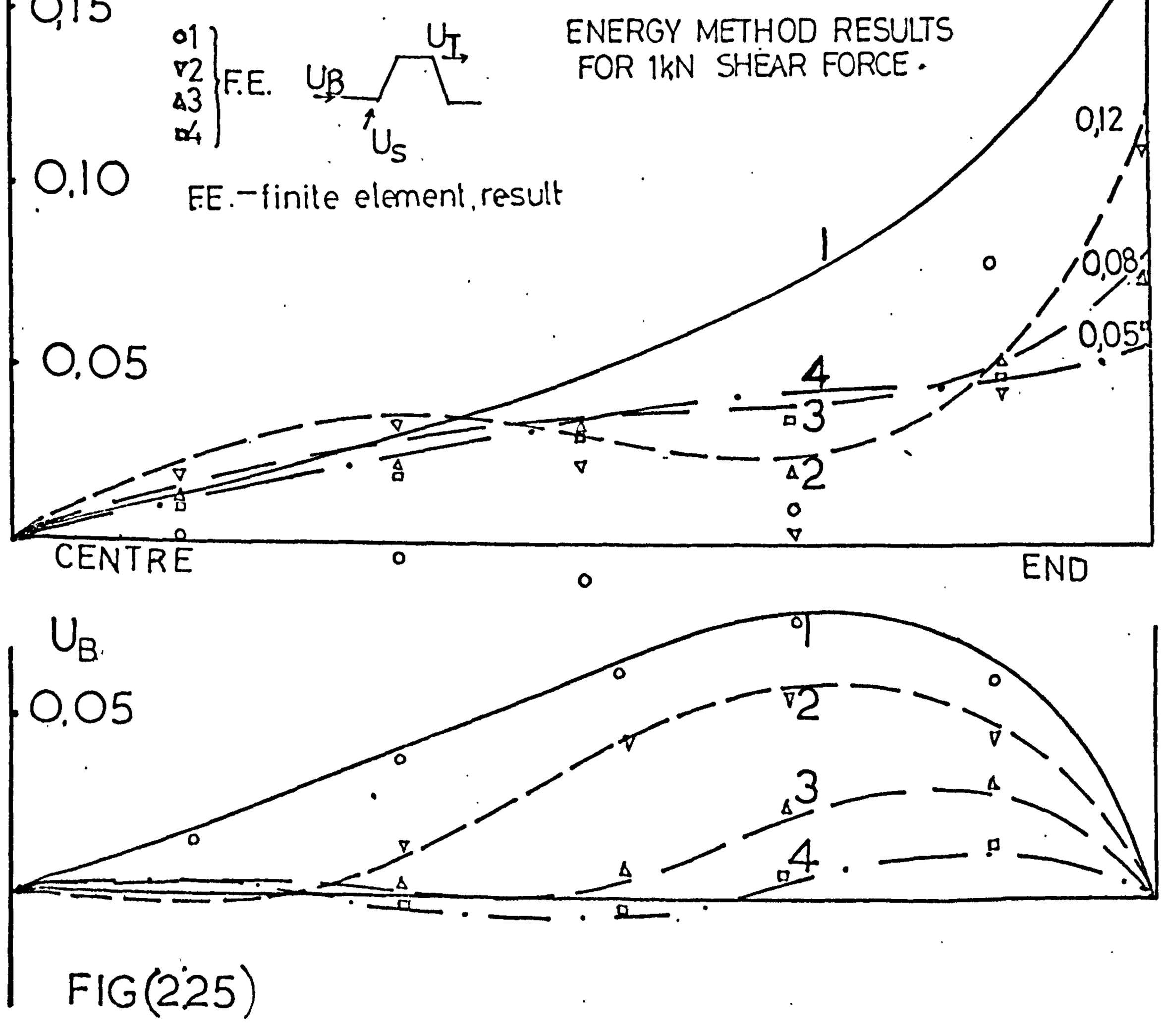

FIG(225)

EVERY TROUGH FIXING —
1,2,3,4 INTERMEDIATE PURLINS

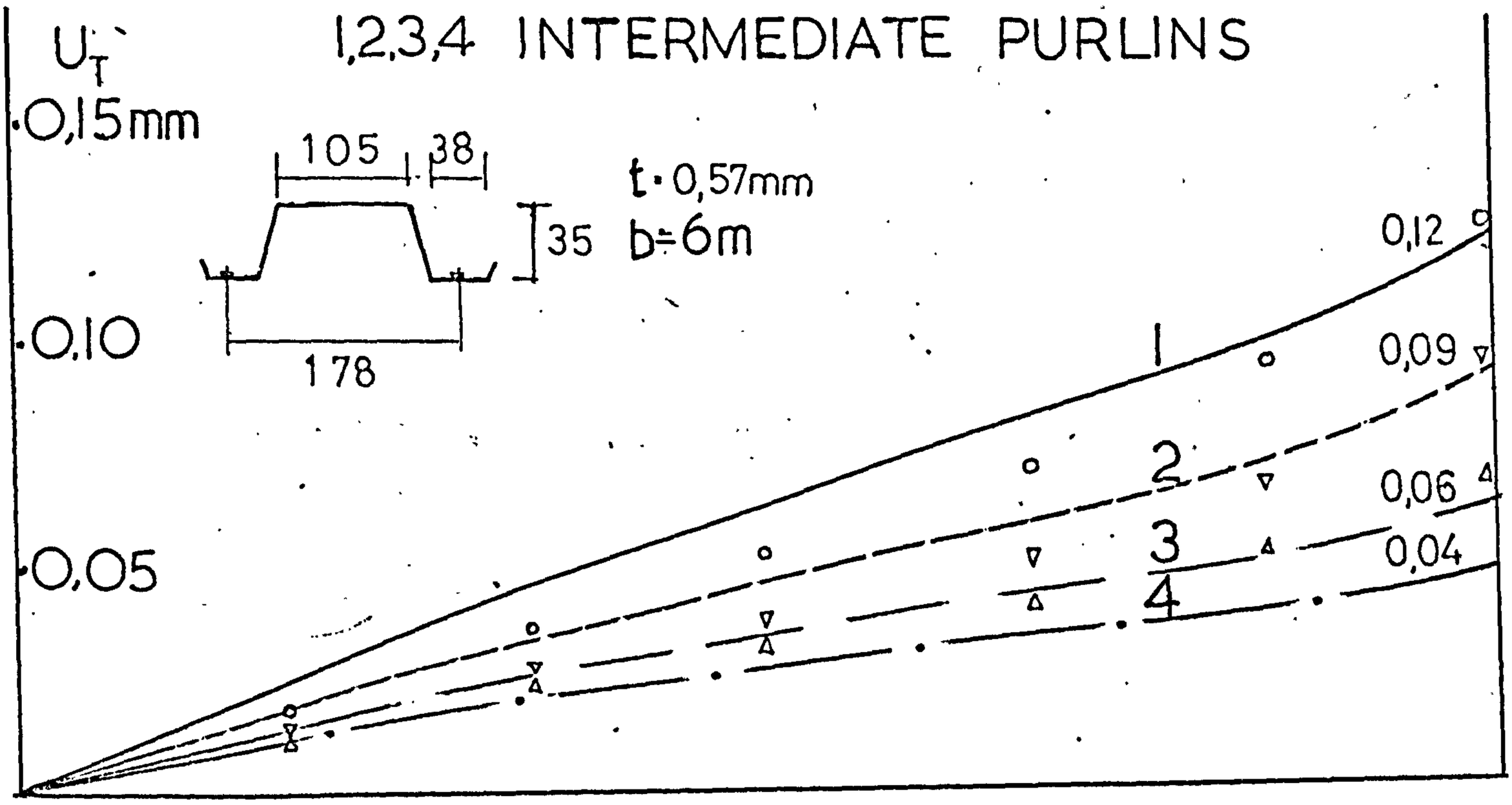

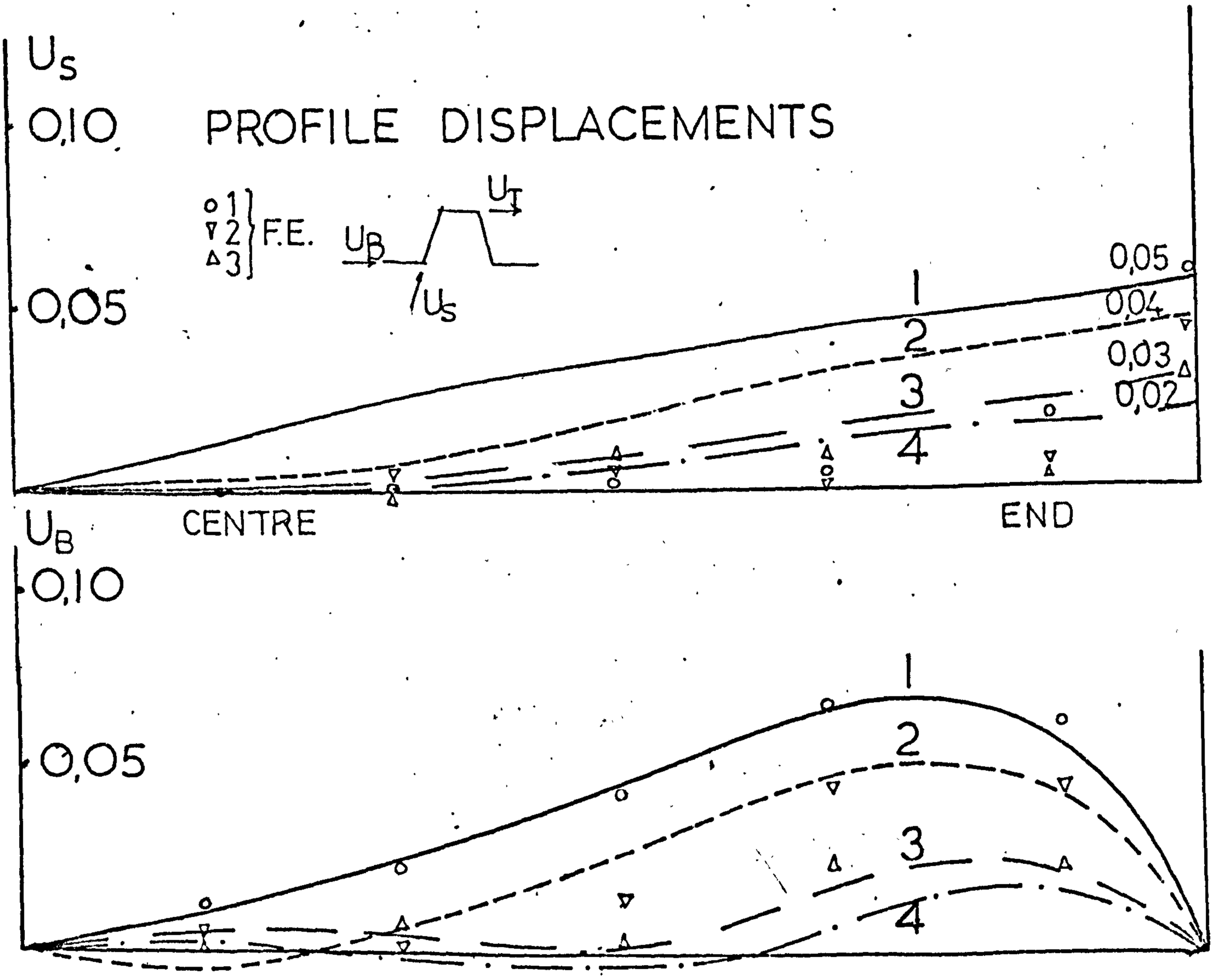

FIG(2.26)

EVERY TROUGH FIXING –
1,2,3,4 INTERMEDIATE PURLINS

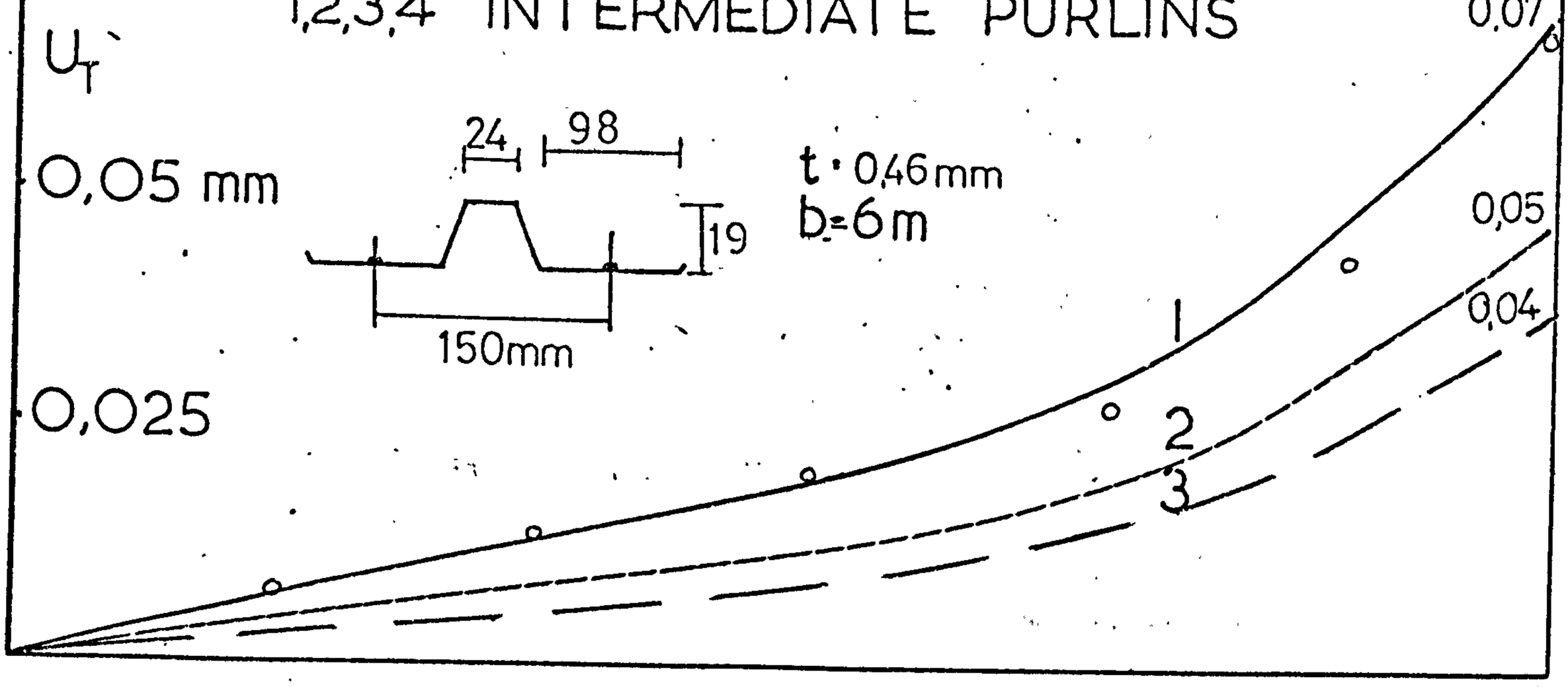

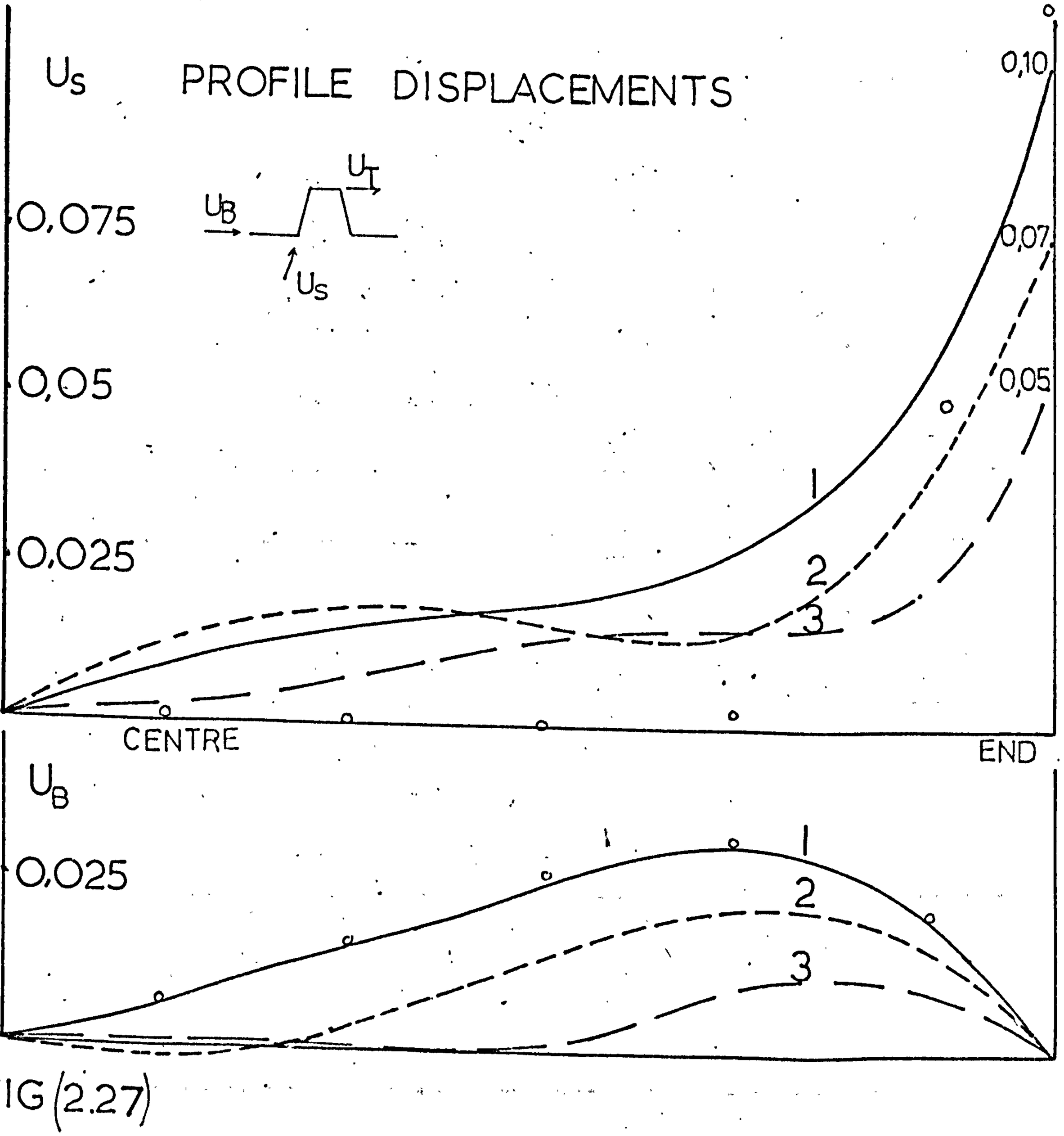

FIG (2.27)

COMPARISON OF EFFECTIVE SHEAR MODULUS WITH STREHL'S RESULTS

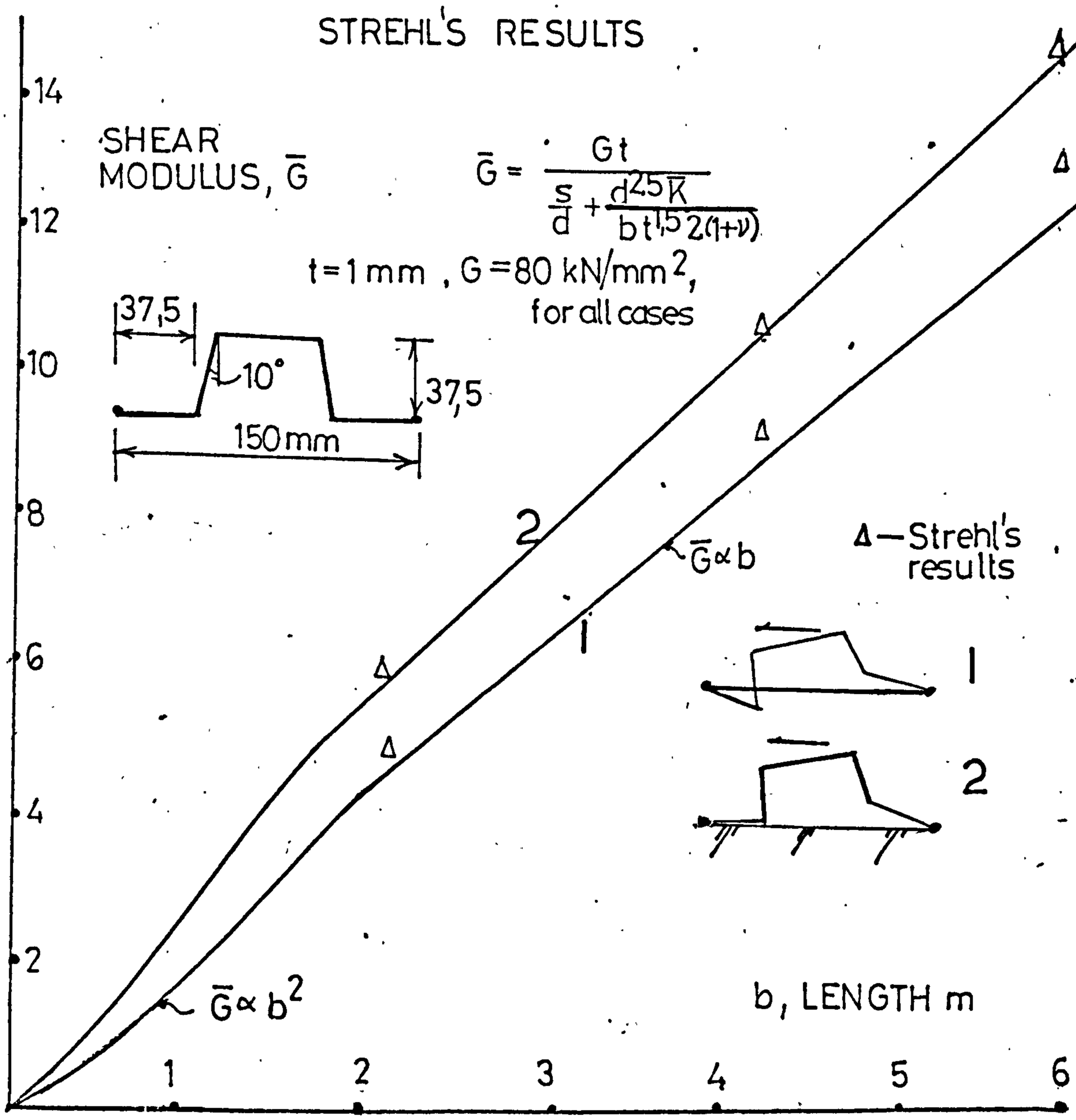

1 ENERGY METHOD — FREE DEFORMATION

2 INCLUDING 'PURLIN-PROP' RESTRAINT.

PROFILE	LENGTH m	EFFECTIVE SHEAR MODULUS BY, 'ENERGY' 1	'ENERGY' 2	'STREHL' 1	'STREHL' 2
89, 27, 79, 183mm	6	5,6	6,8	6,0	7,0
	4	3,9	4,8	4,0	4,8
	2	2,0	2,5	2,0	2,5
58, 45, 85, 166	6	3,4	4,1	3,3	4,3
	4	2,4	2,8	2,4	3,0
	2	1,3	1,4	1,4	1,6
145, 9, 39, 195	6	7,6	8,0	7,0	7,0
	4	5,3	5,6	5,0	5,0
	2	2,8	3,0	2,6	2,6

FIG (2,28)

ENERGY METHOD COMPARISONS—
EVERY TROUGH FIXING

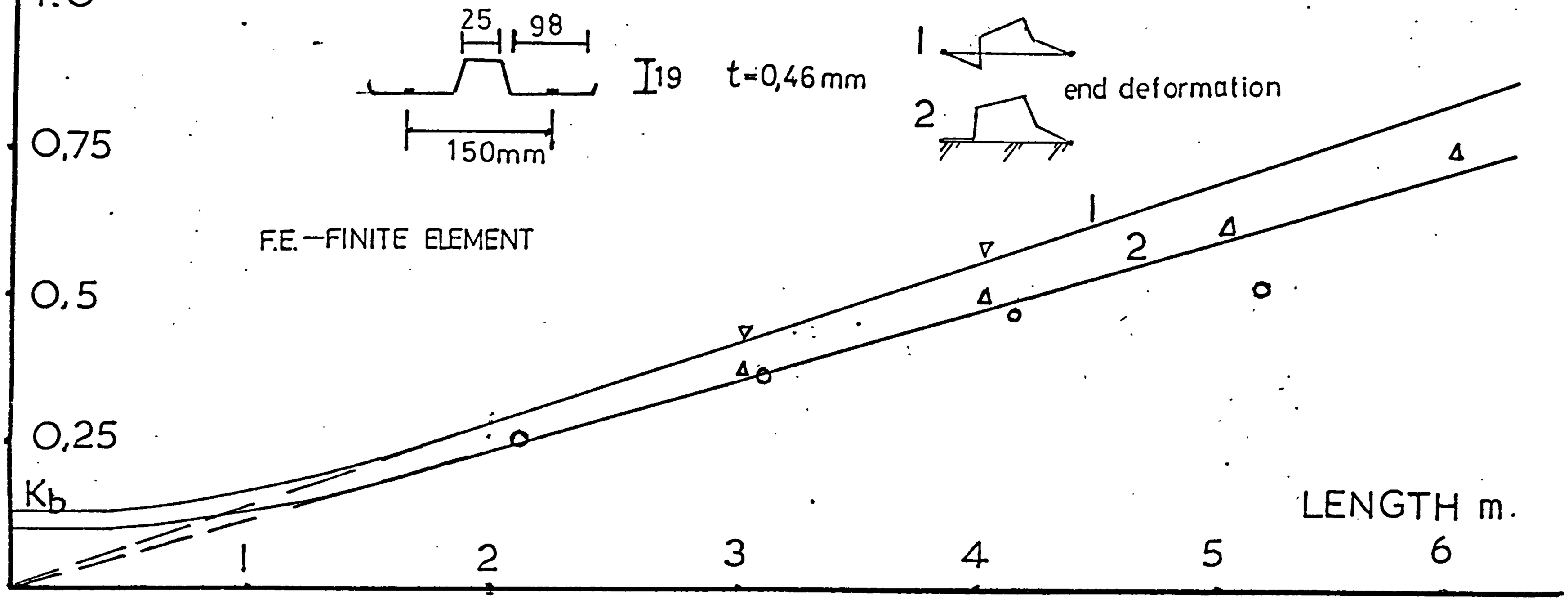

FIG(2.29)

EVERY TROUGH FIXING

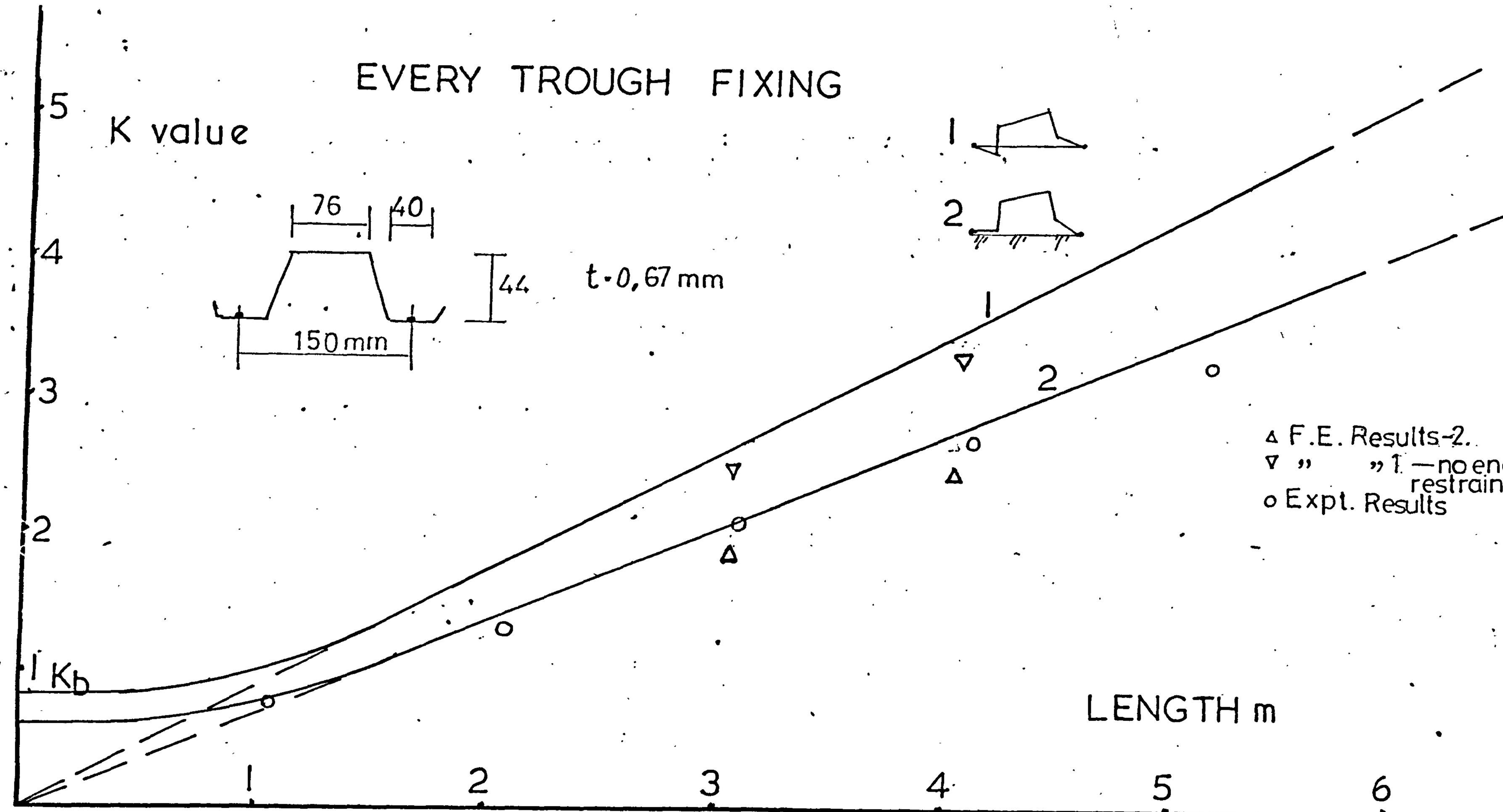

FIG (2.30)

EVERY TROUGH FIXING

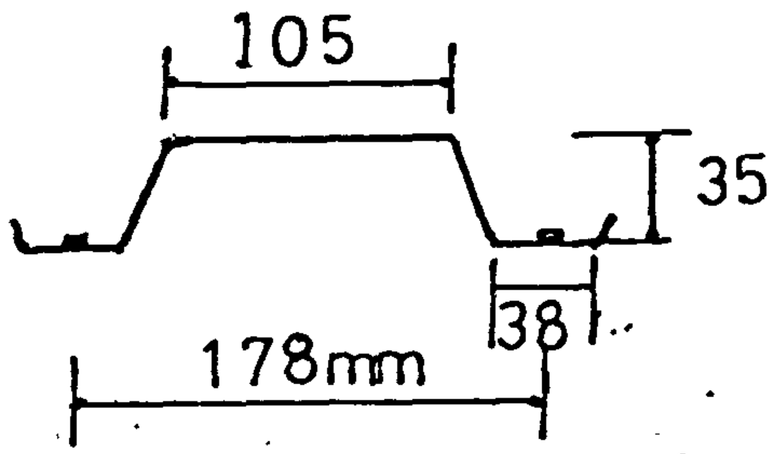

t=0,57 mm

FIG(2.31)

EVERY TROUGH FIXING

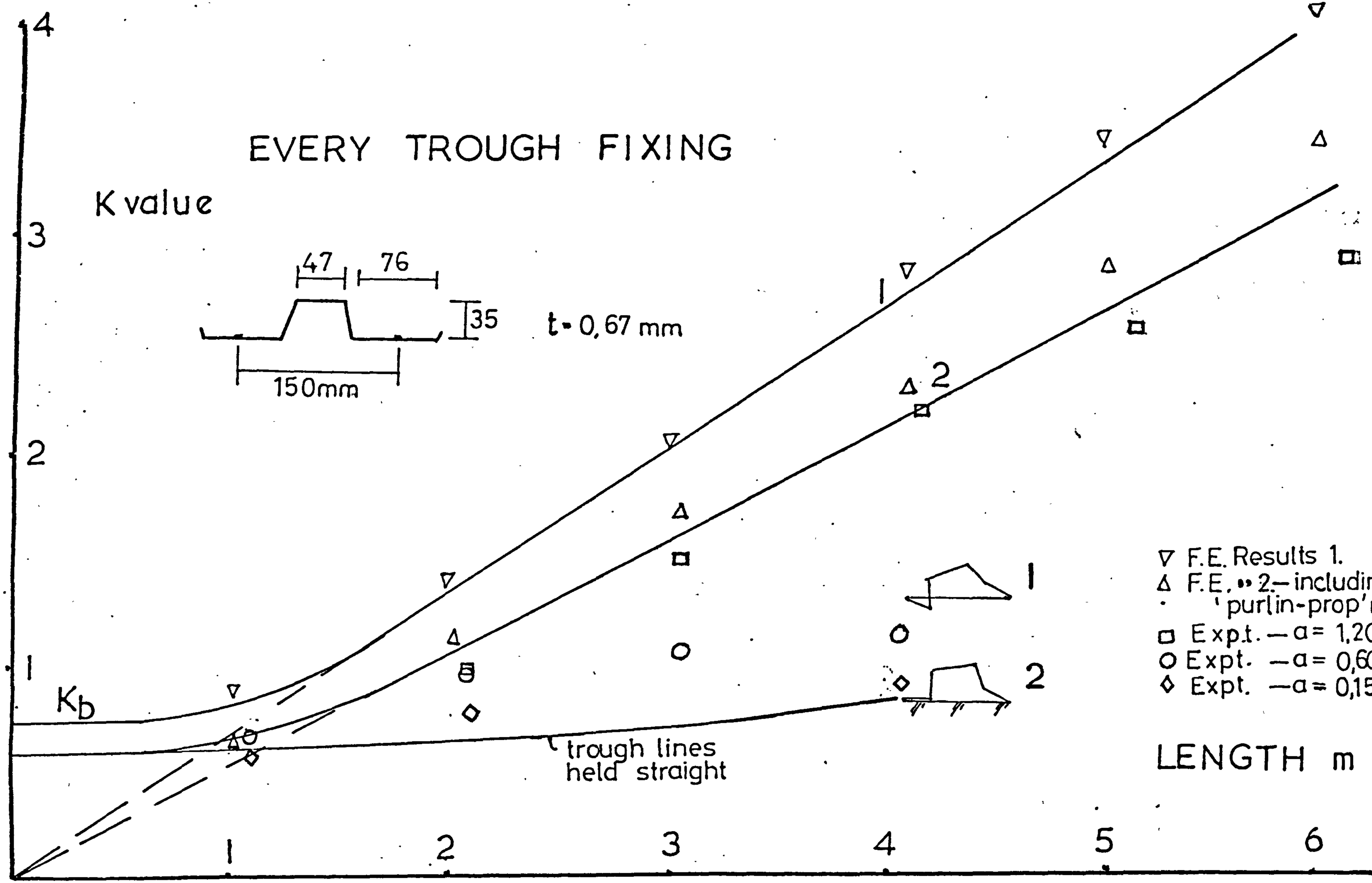

FIG(2.32)

INTERMEDIATE PURLINS
—EVERY TROUGH FIXING

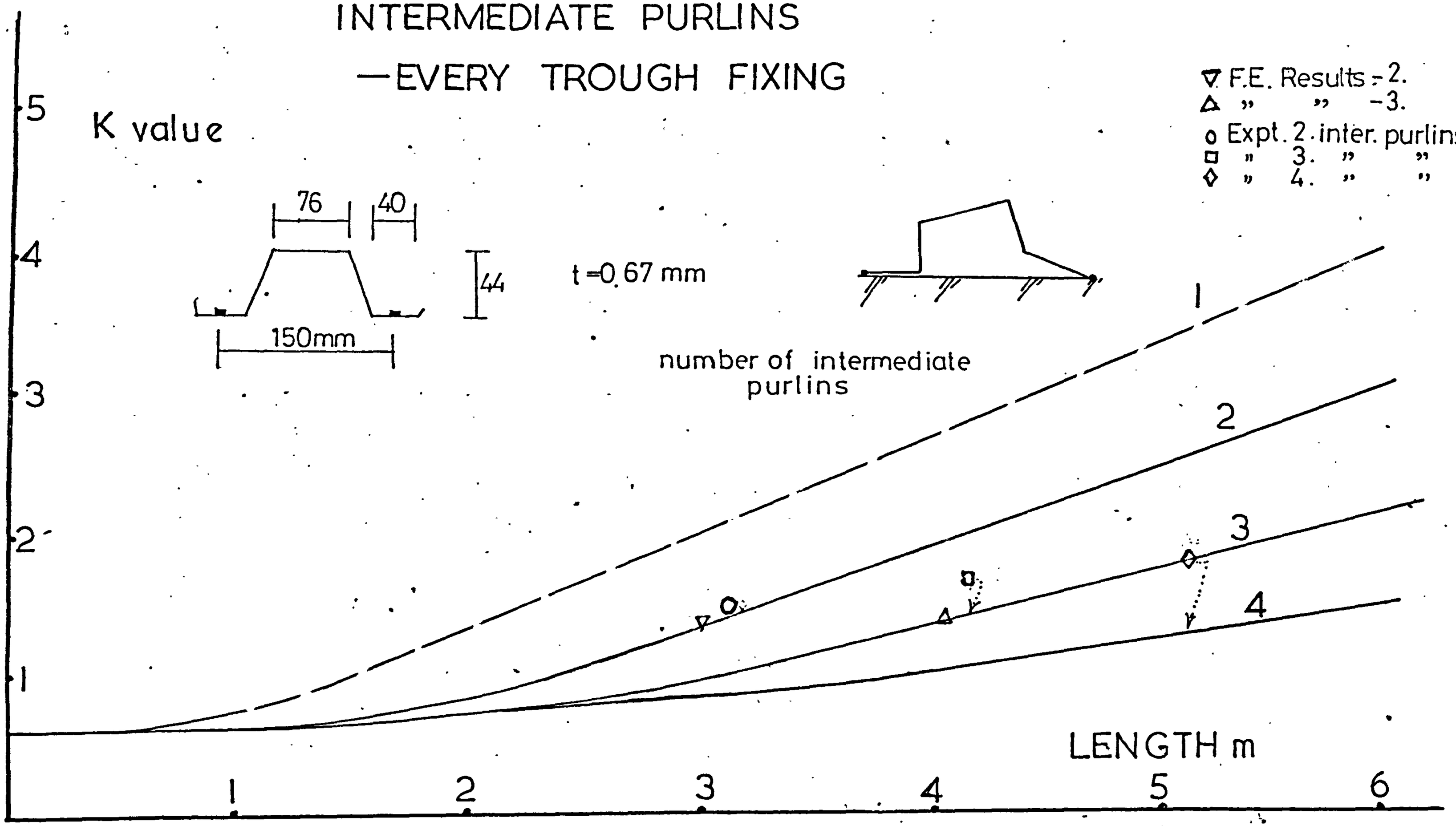

FIG (2.33)

INTERMEDIATE PURLINS — EVERY TROUGH FIXING

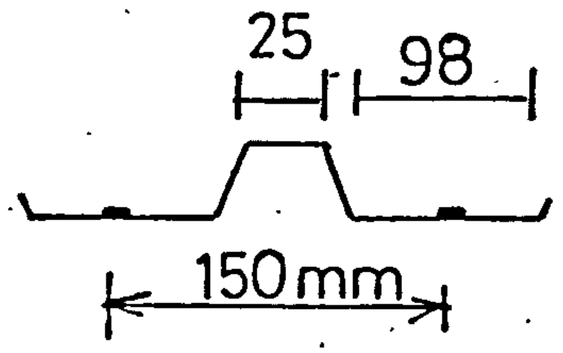

19. t = 0,46 mm

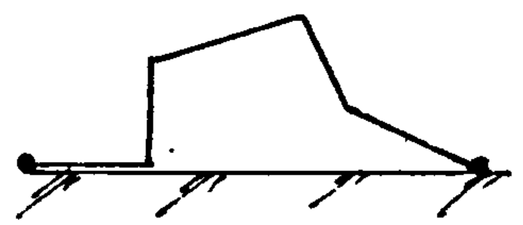

△ F.E. 2 inter. purlins
▽ " 3 " "
◇ " 4 " "
○ Expt. 2. " "
□ " 3. " "

K value

0,8

0,6

0,4

0,2

'purlin-prop' reduction in flexibility included

1

2

3

4

— number of intermediate purlins

LENGTH m

1 2 3 4 5 6

FIG (234)

INTERMEDIATE PURLINS

— EVERY TROUGH FIXING AT ENDS, ALTERNATE TROUGHS INTERNALLY

o — Expt. Result – 2 inter purlins
□ — " " – 3 " "

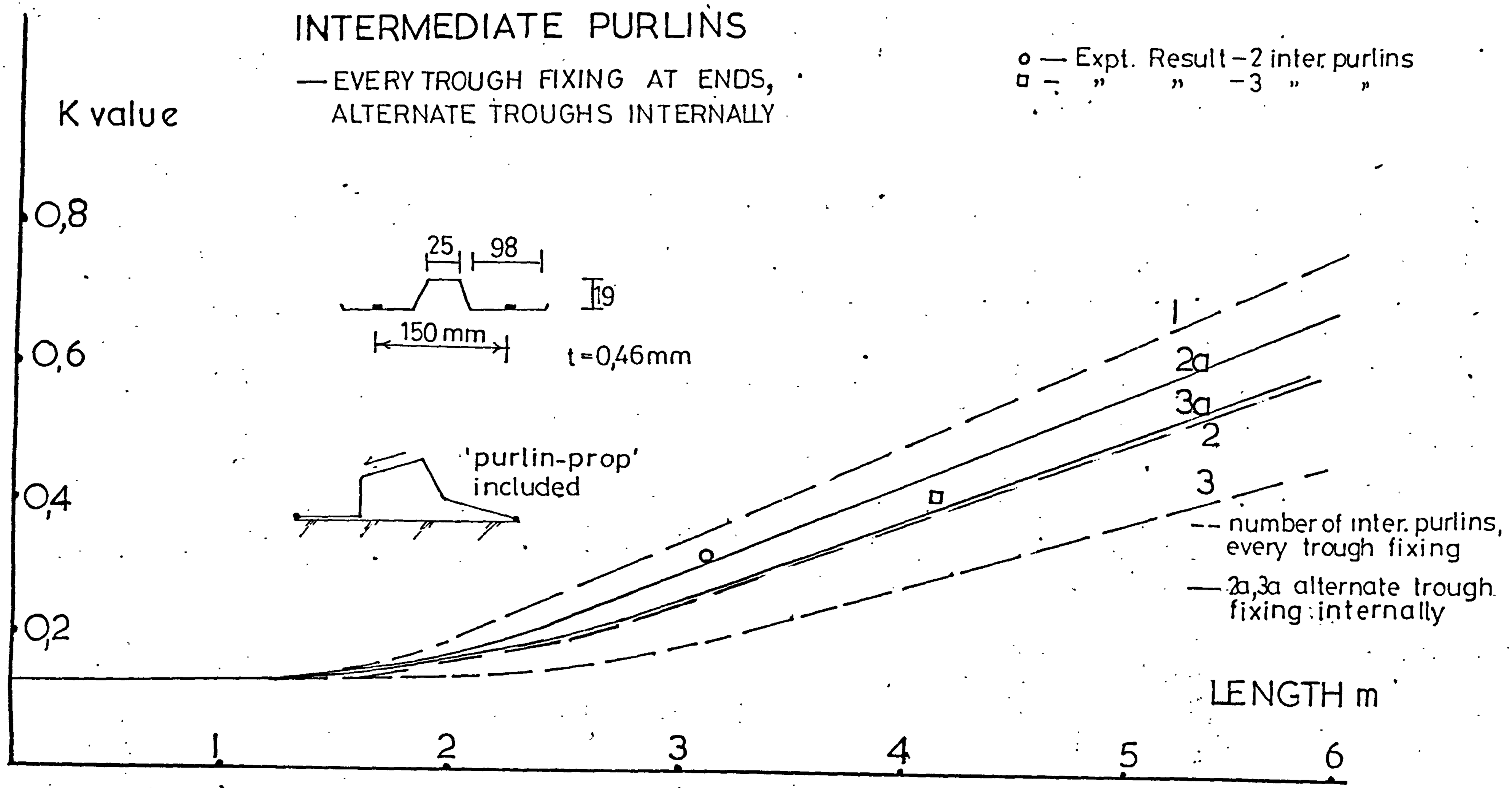

FIG (2.35)

1	2	3	4	5	6	7	8	
$C(1,1)\frac{b^3}{12} + \frac{G_1}{2b_S}$	$C(1,1)\frac{b^3}{4\pi^2}$	$-C(1,1)\frac{b^3}{16\pi^2}$	$C(1,1)\frac{b^3}{36\pi^2}$	$-C(1,1)\frac{b^3}{64\pi^2}$	$C(1,1)\frac{b^3}{100\pi^2}$	$C(1,2)\frac{b^3}{24}$	$C(1,2)\frac{b^3}{8\pi^2}$	1
$Y_A = \frac{8}{3}E_t\pi^4/b^3$ $Y_B = E_t\pi^4 b_S/4b^3$	$\left[C(1,1)\frac{b}{2} + b_T^2(b_T Y_A + Y_B)\right] \times F_1^2 + G_1/4b_S$					$C(1,2)\frac{b^3}{8\pi^2}$	$C(1,2)\frac{b^3}{16\pi^2}$	2
	$G_1 = G_t b/3$ $F_1 = \frac{b}{2\pi}$; $F_2 = \frac{b}{4\pi}$ $F_3 = \frac{b}{6\pi}$; $F_4 = \frac{b}{8\pi}$; $F_5 = \frac{b}{10\pi}$	$\left[C(1,1)\frac{b}{2} + 16b_T^2 \cdot (Y_A b_T + Y_B)\right]F_2^2 + \frac{G_1}{4b_S}$				$-C(1,2)\frac{b^3}{32\pi^2}$		3
			$\left[C(1,1)\frac{b}{2} + 81b_T^2 \cdot (Y_A b_T + Y_B)\right]F_3^2 + \frac{G_1}{4b_S}$			$C(1,2)\frac{b^3}{72\pi^2}$		4
				$\left[C(1,1)\frac{b}{2} + 256b_T^2 \cdot (Y_A b_T + Y_B)\right]F_4^2 + \frac{G_1}{4b_S}$		$-C(1,2)\frac{b^3}{128\pi^2}$		5
					$\left[C(1,1)\frac{b}{2} + 625b_T^2 \cdot (Y_A b_T + Y_B)\right]F_5^2 + \frac{G_1}{4b_S}$	$C(1,2)\frac{b^3}{200\pi^2}$		6
						$C(2,2)\frac{b^3}{12} + G_1\left(\frac{1}{b_L} + \frac{1}{b_T}\right)$	$C(2,2)\frac{b^3}{4\pi^2}$	7
							$\left[C(2,2)\frac{b}{2} + Y_A \cdot 2b_S^3\right] \cdot F_1^2 + \frac{G_1}{2}\left\{\frac{1}{b_L} + \frac{1}{b_T}\right\}$	8
						$\left[C(2,2)\frac{b}{2} + 162b_S^3 Y_A\right] \cdot F_3^2 + \frac{G_1}{2}\left(\frac{1}{b_L} + \frac{1}{b_T}\right)$		9
					$\left[C(2,2)\frac{b}{2} + 312 Y_A b_S^3\right] \cdot F_4^2 + \frac{G_1}{2}\left(\frac{1}{b_L} + \frac{1}{b_T}\right)$			10
				$\left[C(2,2)\frac{b}{2} + 1250 Y_A \cdot b_S^3\right]F_5^2 + \frac{G_1}{2}\left(\frac{1}{b_L} + \frac{1}{b_T}\right)$				11
$C(2,3)\frac{b^3}{400\pi^2}$								12
	$C(2,3)\frac{b^3}{256\pi^2}$							13
		$C(2,3)\frac{b^3}{144\pi^2}$						14
			$C(2,3)\frac{b^3}{64\pi^2}$					15
								16
								17

17	16	15	14	13	12	11	10	9
$\left[C(3,3) + 625b_L^2 \cdot (Y_A b_L + Y_B)\right]F_5^2 + \frac{G_1}{4b_S}$								17
	$\left[C(3,3)\frac{b}{2} + 156b_L^2 \cdot (Y_A b_L + Y_B)\right]F_4^2 + \frac{G_1}{4b_S}$							16
		$\left[C(3,3)\frac{b}{2} + 81b_L^3 \cdot (Y_A b_L + Y_B)\right]F_3^2 + \frac{G_1}{4b_S}$						15
			$\left[C(3,3)\frac{b}{2} + 16b_L^2 \cdot (Y_A b_L + Y_B)\right]F_2^2 + \frac{G_1}{4b_S}$					14
				$\left[C(3,3)\frac{b}{2} + b_L^2 \cdot (Y_A b_L + Y_B)\right]F_1^2 + \frac{G_1}{4b_S}$				13
					$\left[C(2,2)\frac{b}{2} + 1250 Y_A \cdot b_S^3\right]F_5^2 + \frac{G_1}{2}\left(\frac{1}{b_L} + \frac{1}{b_T}\right)$			12
						$\left[C(2,2)\frac{b}{2} + 312 Y_A b_S^3\right] \cdot F_4^2 + \frac{G_1}{2}\left(\frac{1}{b_L} + \frac{1}{b_T}\right)$		11
							$\left[C(2,2)\frac{b}{2} + 162b_S^3 Y_A\right] \cdot F_3^2 + \frac{G_1}{2}\left(\frac{1}{b_L} + \frac{1}{b_T}\right)$	10
								9

$$\frac{\Delta^2}{2c} = \sum_{i=1}^{23}\sum_{j=1}^{23} a_i \cdot \mathcal{V}(i,j) \cdot a_j$$

$\mathcal{V}(i,j)$ symmetrical

$$U_T = a_1 y + \sum_{n=1}^{5} \frac{b}{2n\pi} \sin\frac{2n\pi}{b} \cdot a_{n+1}$$

$$U_S = a_7 y + \sum_{n=1}^{5} \frac{b}{2n\pi} \sin\frac{2n\pi}{b} \cdot a_{n+7}$$

$$U_B = \sum_{n=1}^{5} \frac{b}{2n\pi} \sin\frac{2n\pi}{b} \cdot a_{n+12}$$

FIG (2.36) EVERY TROUGH FIXING ANALYSIS : TERMS IN ENERGY MATRIX D(I,J)

	9	10	11	12	13	14	15	16	17
1	$-C(1,2)\frac{b^3}{32\pi^2}$	$C(1,2)\frac{b^3}{72\pi^2}$	$-C(1,2)\frac{b^3}{128\pi^2}$	$C(1,2)\frac{b^3}{200\pi^2}$	$C(1,3)\frac{b^3}{8\pi^2}$	$-C(1,3)\frac{b^3}{32\pi^2}$	$C(1,3)\frac{b^3}{72\pi^2}$	$-C(1,3)\frac{b^3}{128\pi^2}$	$C(1,3)\frac{b^3}{200\pi^2}$
2					$\{C(1,3)\frac{b}{2} - 2b_L b_T Y_B\} \cdot \frac{F_1^2}{2} - G_1/4b_S$				
3	$C(1,2)\frac{b^3}{64\pi^2}$					$\{C(1,3)\frac{b}{2} - 32 b_L b_T Y_B\} \cdot F_{2/2}^2 - G_1/4b_S$			
4		$C(1,2)\frac{b^3}{144\pi^2}$					$\{C(1,3)\frac{b}{2} - 162 b_L b_T Y_B\} \cdot F_{3/2}^2 - G_1/4b_S$		
5			$C(1,2)\frac{b^3}{256\pi^2}$					$\{C(1,3)\frac{b}{2} - 512 b_L b_T Y_B\} \cdot F_{4/2}^2 - G_1/4b_S$	
6				$C(1,2)\frac{b^3}{400\pi^2}$					$\{C(1,3)\frac{b}{2} - 1250 b_L b_T Y_B\} \cdot F_{5/2}^2 - G_1/4b_S$
7	$-C(2,2)\frac{b^3}{16\pi^2}$	$C(2,2)\frac{b^3}{36\pi^2}$	$-C(2,2)\frac{b^3}{64\pi^2}$	$C(2,2)\frac{b^3}{100\pi^2}$	$C(2,3)\frac{b^3}{8\pi^2}$	$-C(2,3)\frac{b^3}{32\pi^2}$	$C(2,3)\frac{b^3}{72\pi^2}$	$-C(2,3)\frac{b^3}{128\pi^2}$	$C(2,3)\frac{b^3}{200\pi^2}$
8					$C(2,3)\frac{b^3}{16\pi^2}$				

$Y_A = 8/3 E t \pi^4/b^3$ $\quad G_1 = G t^3 b/3$ $\quad F_3 = b/6\pi$ $\quad \mathcal{D}(i,j)$ symmetrical.

$Y_B = E t \pi^4 b_S/4b^3$ $\quad F_1 = b/2\pi$ $\quad F_4 = b/8\pi$

$F_2 = b/4\pi$ $\quad F_5 = b/10\pi$

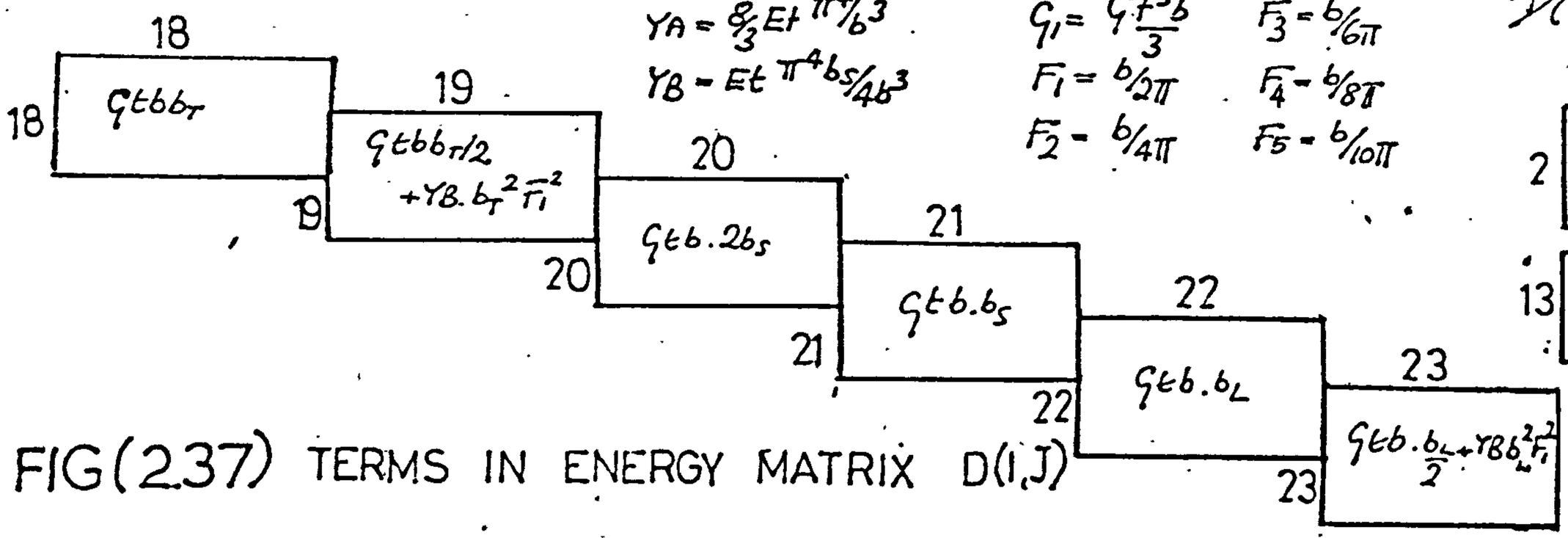

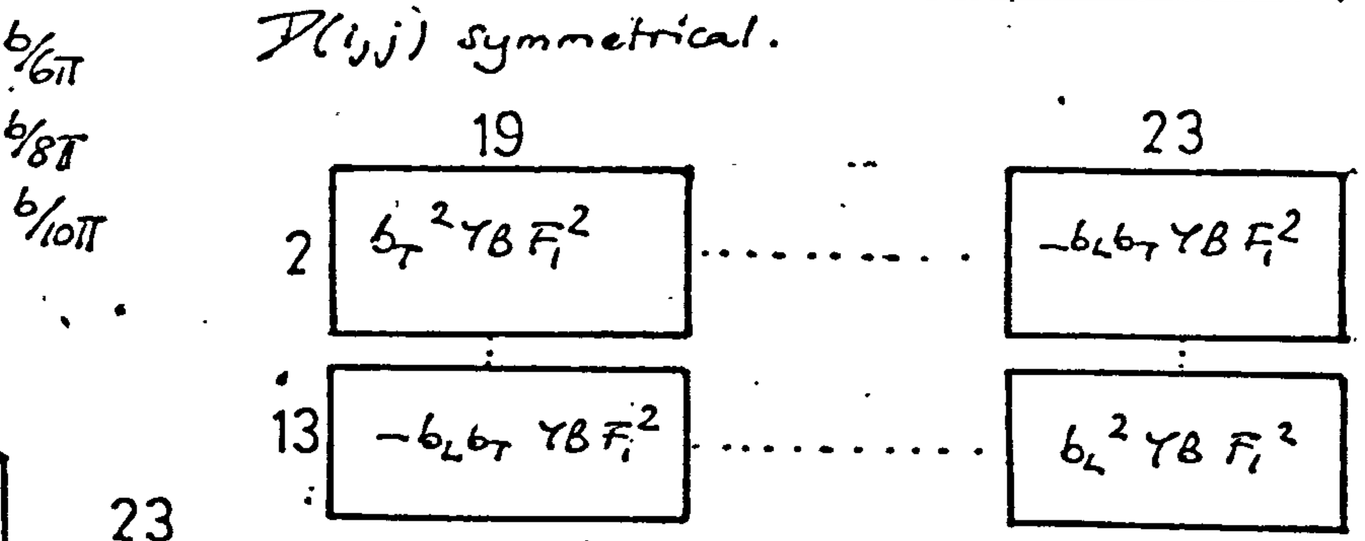

$\gamma_T = a_{18} + a_{19} \cos \frac{2\pi y}{b}$

$\gamma_S = a_{20} + a_{21} \cos \frac{2\pi y}{b}$

$\gamma_B = a_{22} + a_{23} \cos \frac{2\pi y}{b}$

FIG(2.37) TERMS IN ENERGY MATRIX D(I,J)

$$\frac{\Delta^2}{2c} = \sum_{i=1}^{23} \sum_{j=1}^{23} a_i \mathcal{D}(i,j) . a_j$$

FINITE ELEMENT COMPARISONS FOR UP TO FOUR INTERMEDIATE PURLINS FOR EVERY TROUGH ATTACHMENT

Profile	No. of inter purlins	Length m	K Finite Element	K Energy Method
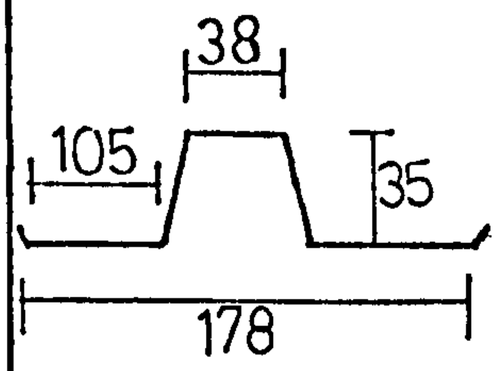	1	6	1.70	1.76
	2		1.27	1.22
	3		0.93	0.83
	4		0.83	0.65
	3	4.8	0.70	0.66
	2	3.6	0.68	0.69
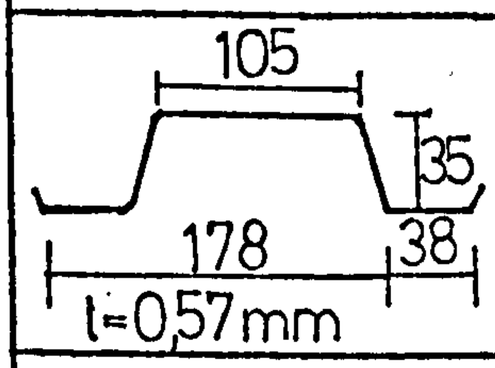	3	4.8	0.82	0.69
	2	3.6	0.76	0.78
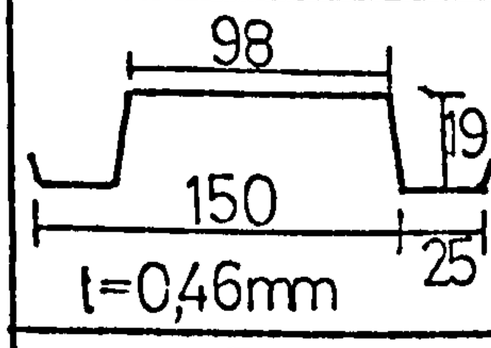	3	4	0.45	0.32
	2	3	0.40	0.40
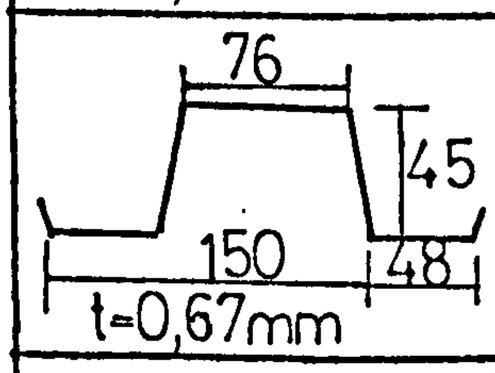	3	4	1.73	1.65
	2	3	1.65	1.74
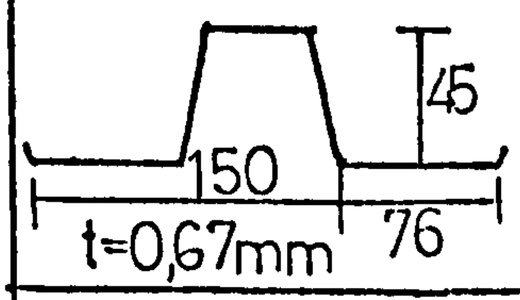	3	4	1.84	1.83
	2	3	1.89	1.79
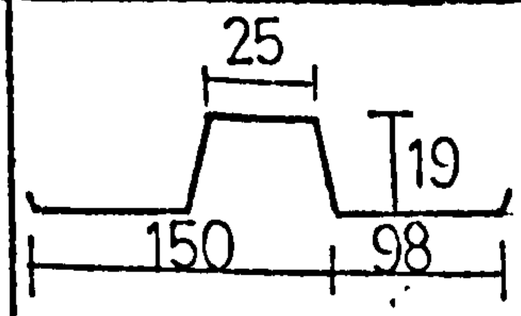	4	5	0.29	0.28
	3	4	0.27	0.28
	2	3	0.29	0.27

K does not include purlin restraint

FIG (2.38)

FASTENING IN MULTIPLE OF TROUGHS

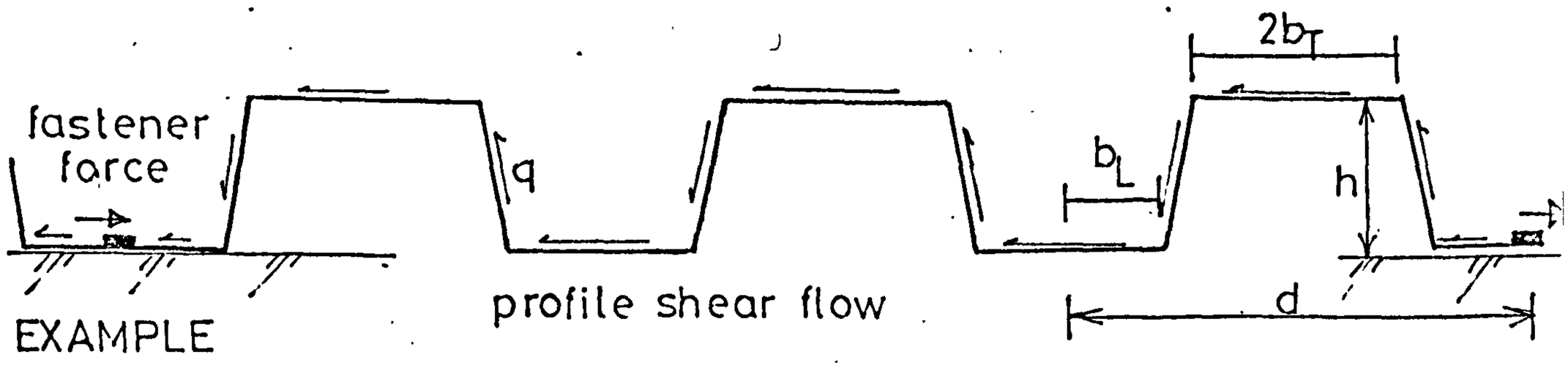

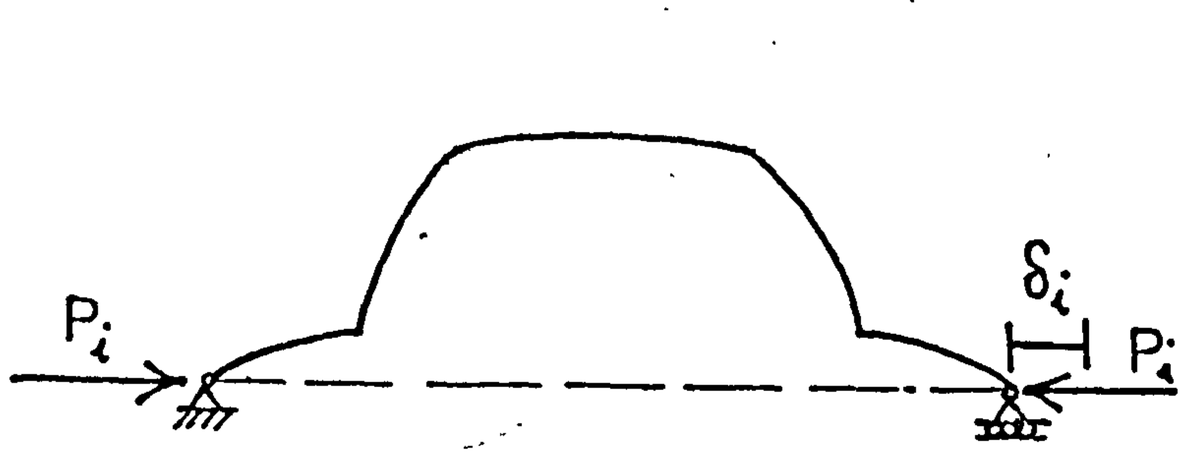

COMPRESSIVE FORCE ON i th CORRUGATION AND SHEAR WARPING DUE TO CONCERTINA EFFECT

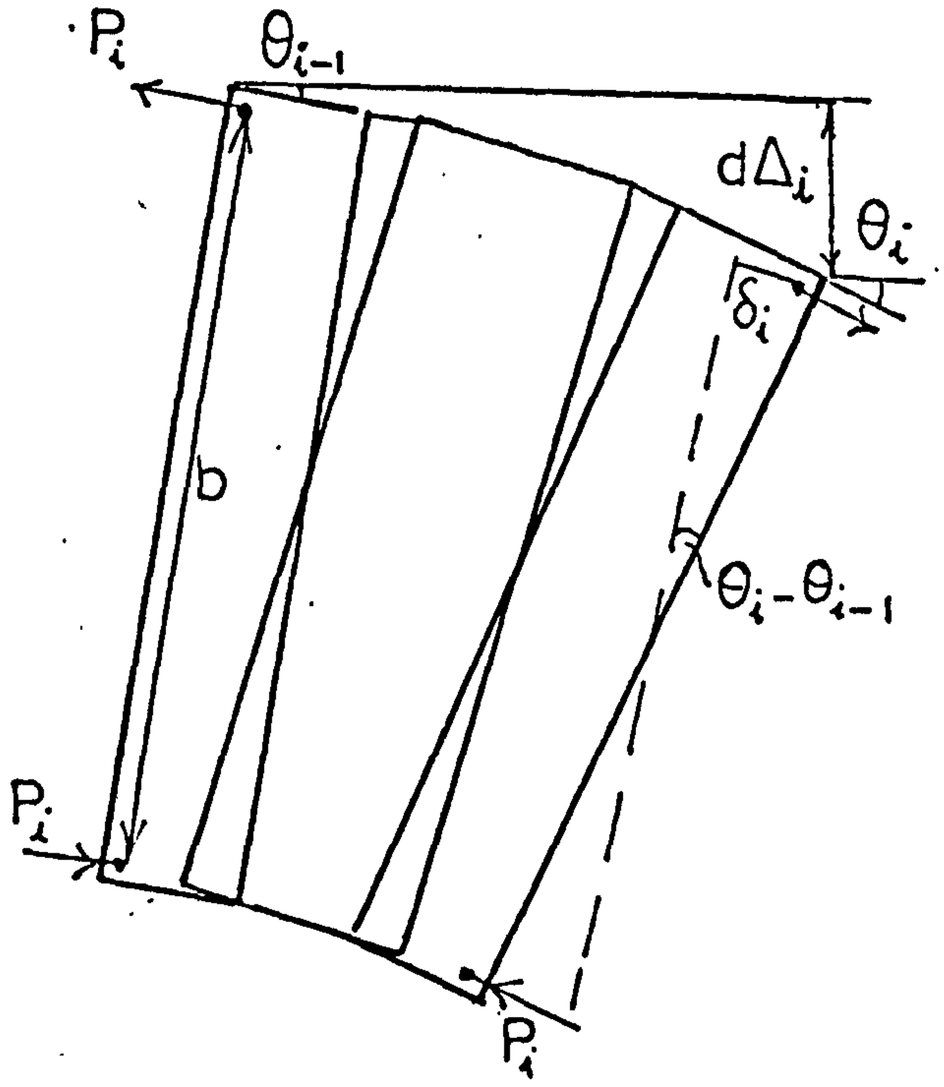

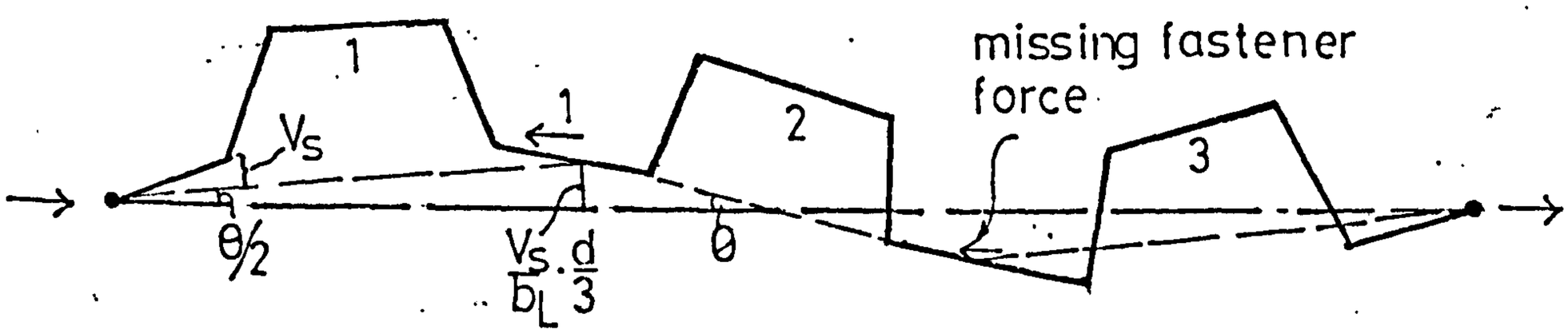

CONCERTINA FOR FASTENING IN EVERY THIRD TROUGH

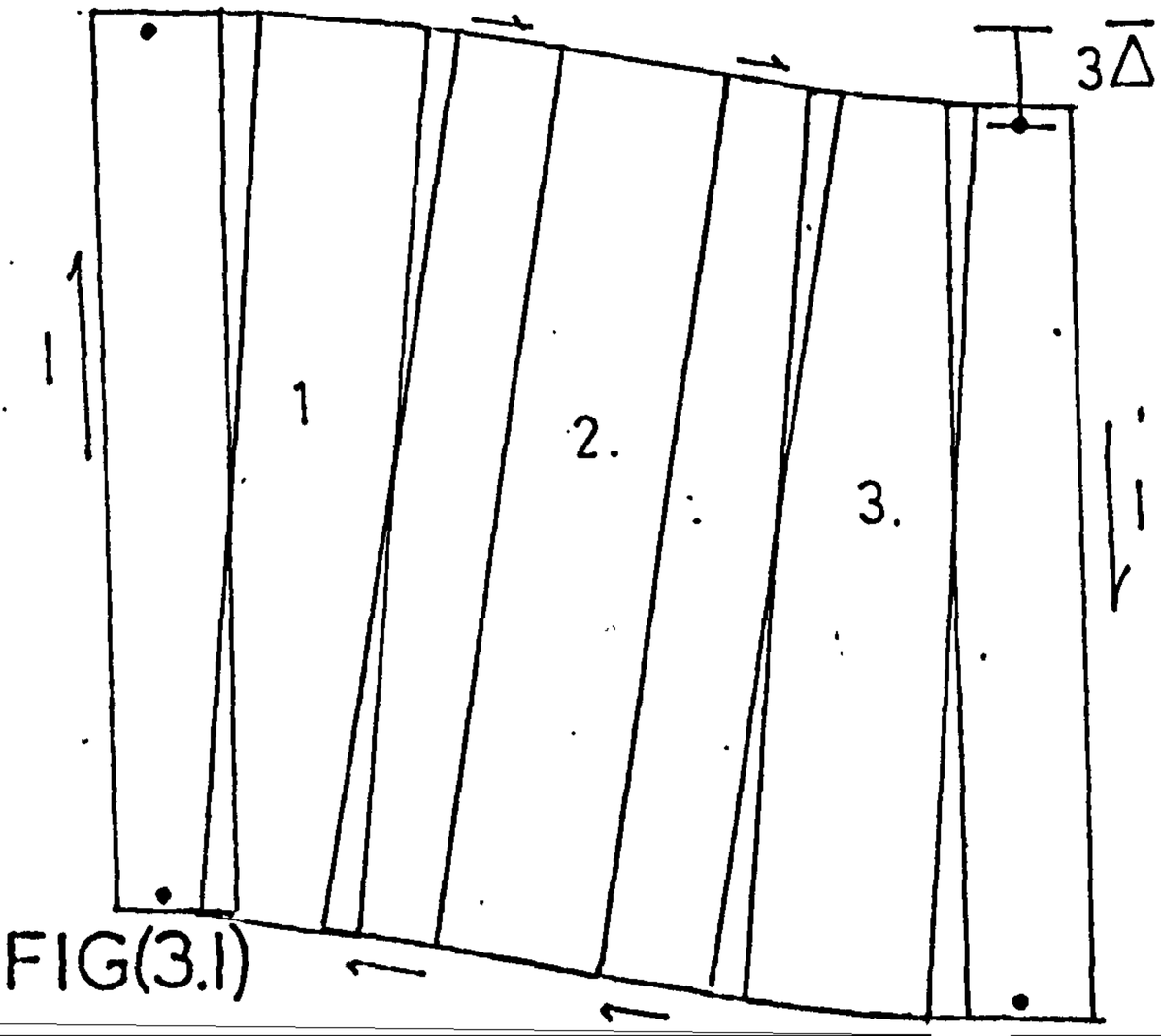

LONGITUDINAL WARPING

— central profile undistorted

$\bar{\Delta}$ — average flexibility per corrugation.

FIG(3.1)

ALTERNATE TROUGH FASTENING

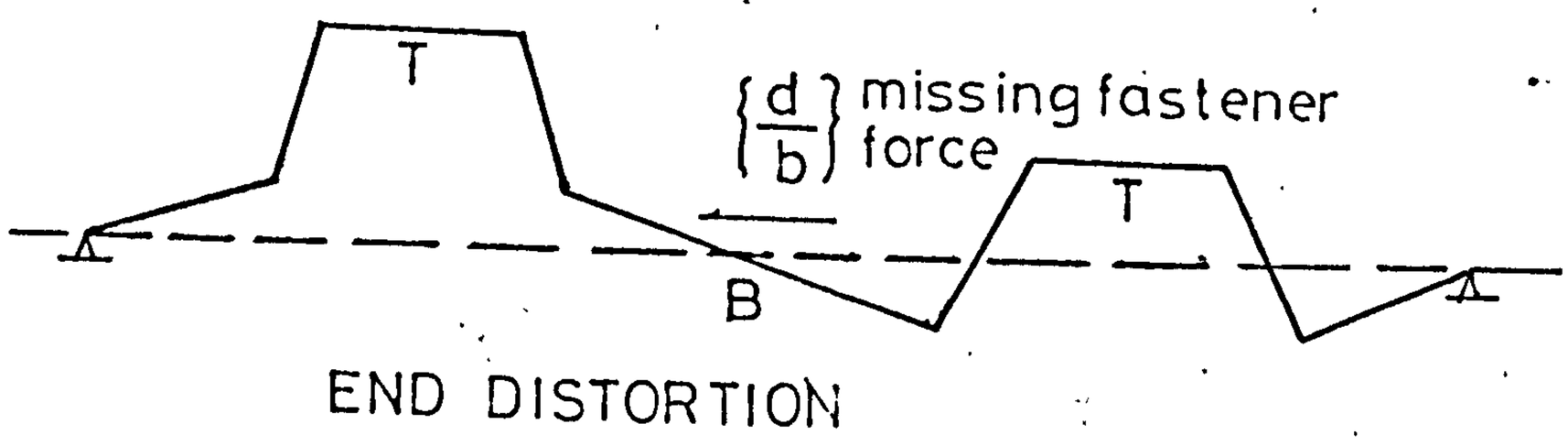

END DISTORTION

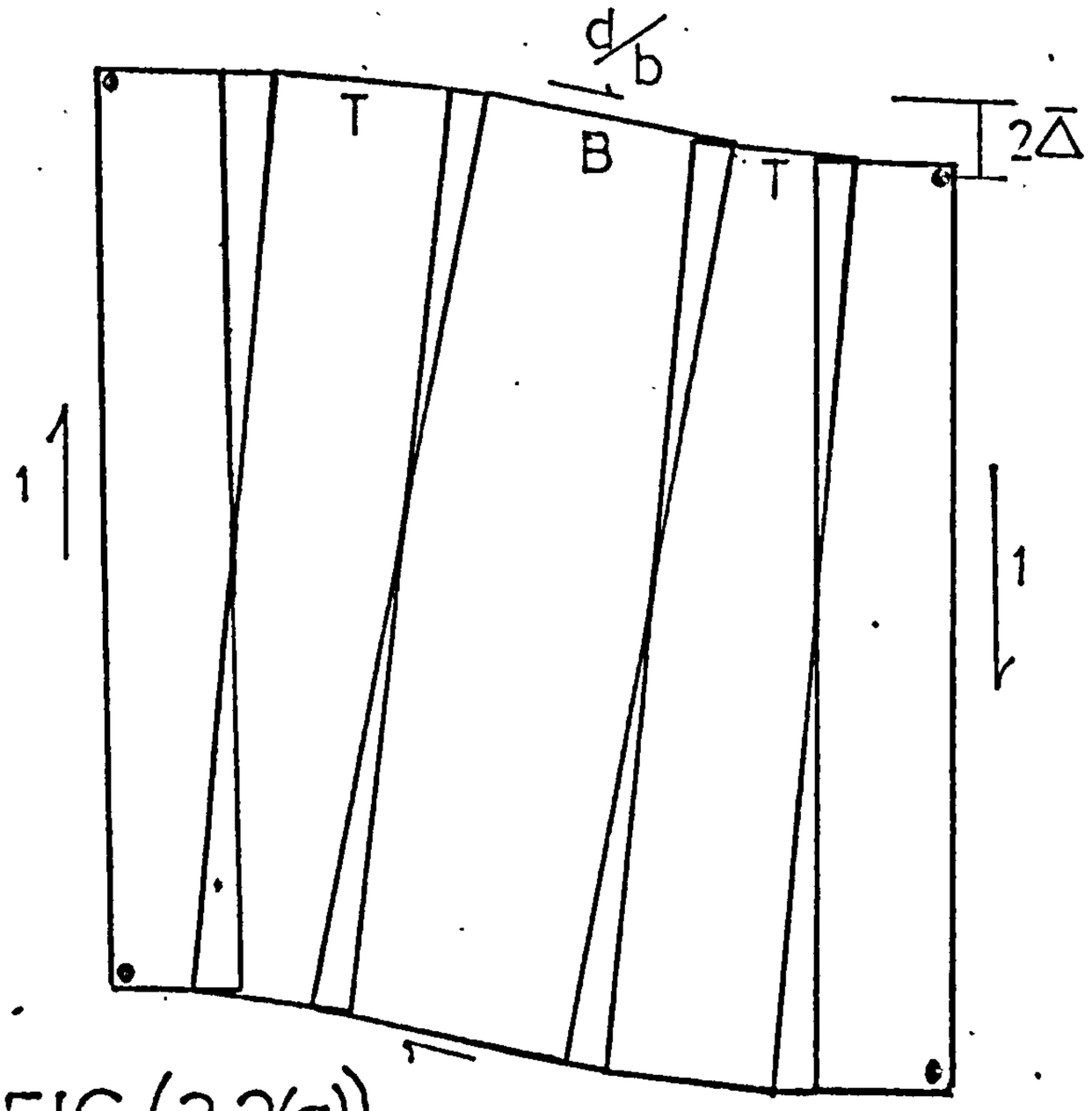

FIG (3.2(a))

RIGID PLATE MOVEMENTS

—concertina effect

1kN longitudinal shear force

$\bar{\Delta}$—shear displacement per corrugatation

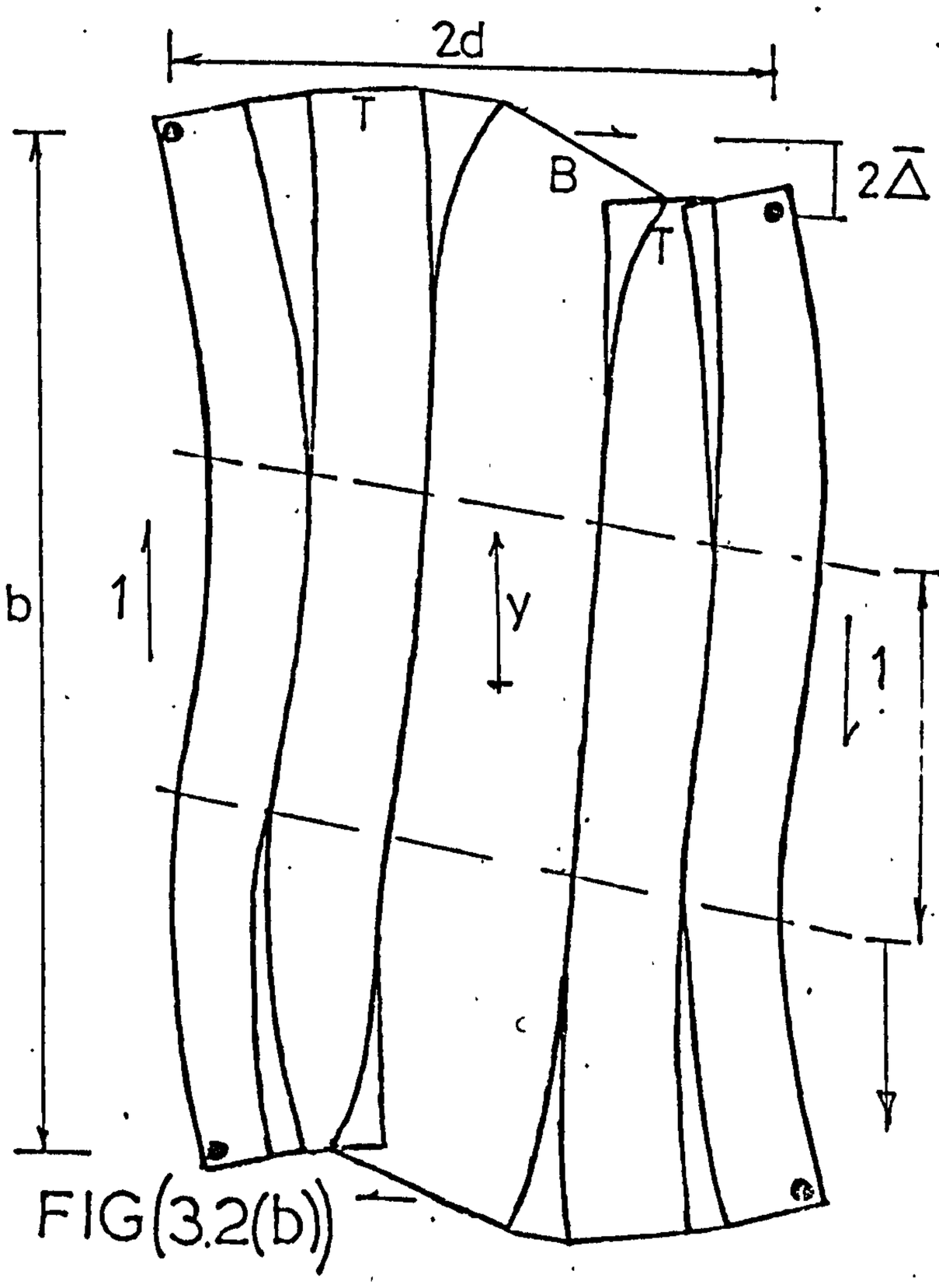

FIG(3.2(b))

PLATE BENDING

—asymptotic behaviour

$\bar{\Delta}$—constant with y

$\frac{d\Delta}{dy}=0$

ALTERNATE TROUGH FASTENING

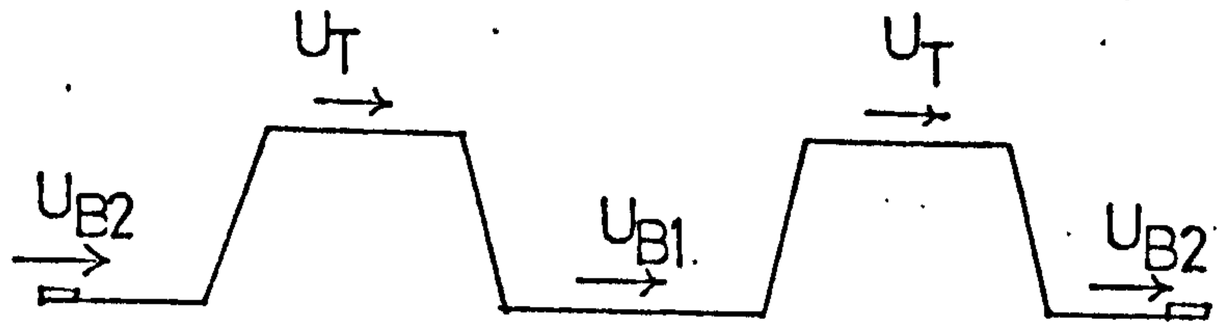

CROSS-SECTION DISPLACEMENTS

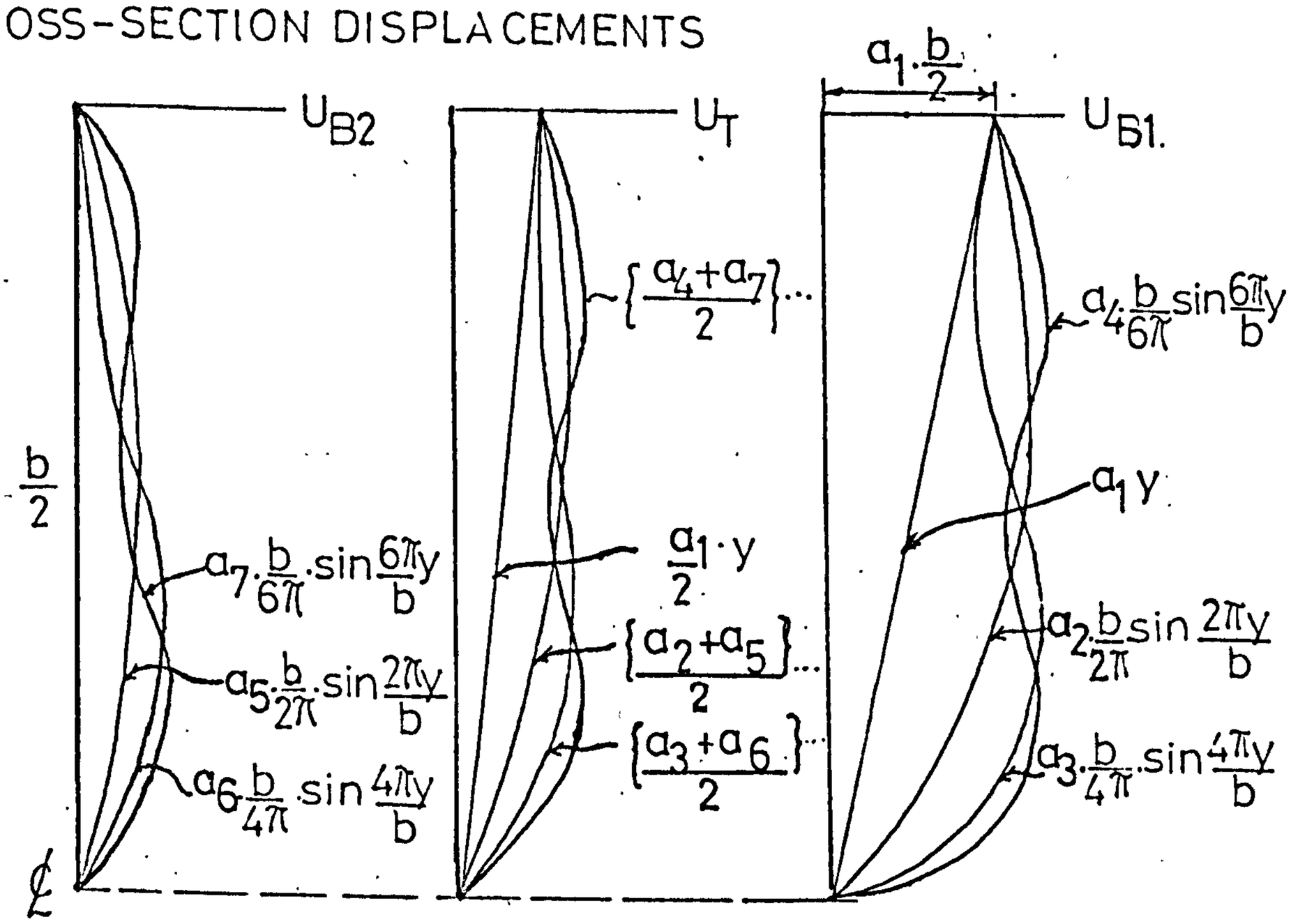

SUPERPOSITION OF FOURIER TERMS

SIDE PLATE UPLIFT

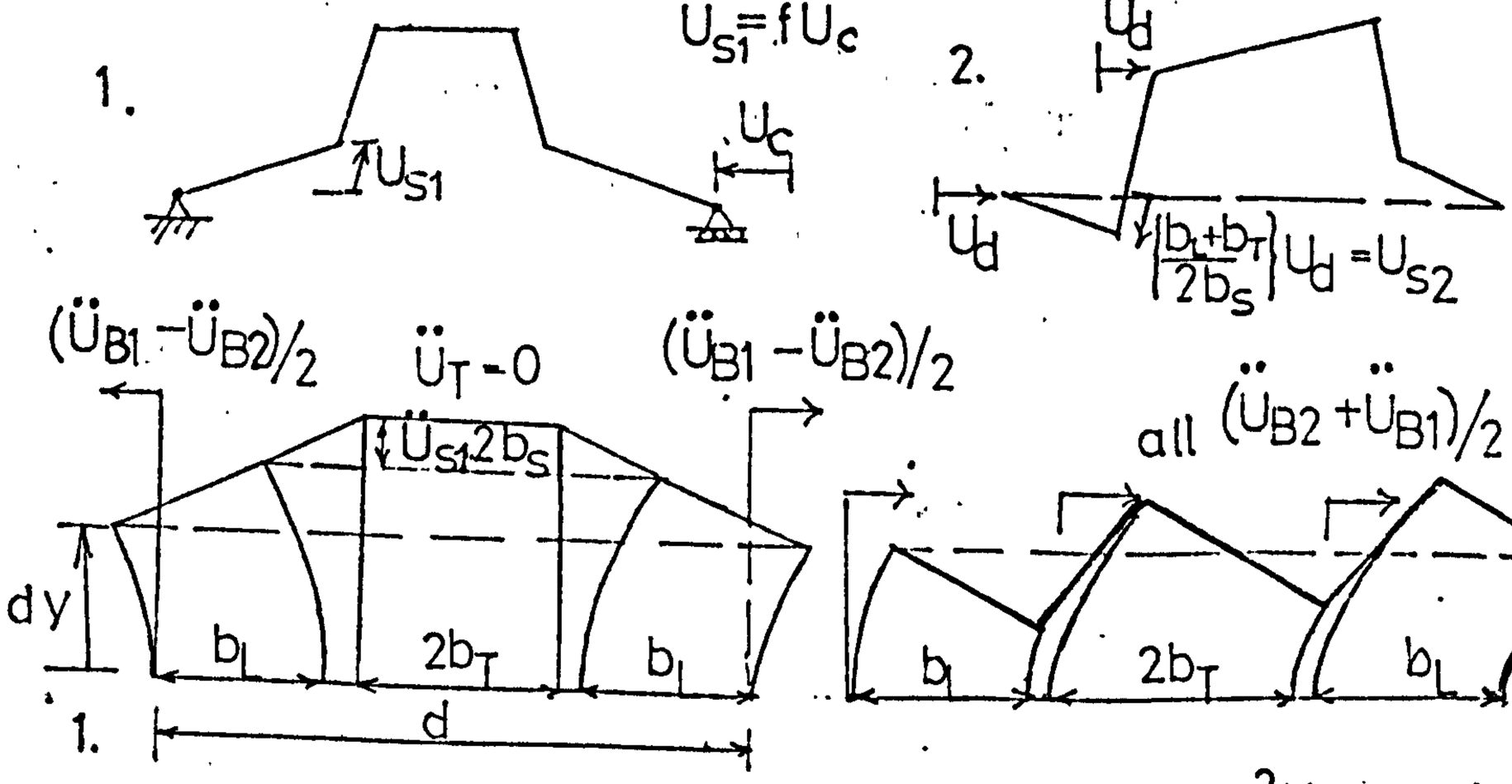

MOVEMENTS SPLIT INTO 2 MODES $\left\{\frac{d^2 U_{B1}}{dy^2} = \ddot{U}_{B1}\right\}$ etc.

— showing axial strain due to each

$$\ddot{U}_{S1} = f\{\ddot{U}_{B2} - \ddot{U}_{B1}\} \quad ; \ddot{U}_{S2} = \left\{\frac{b_L + b_T}{2b_S}\right\}\left\{\frac{\ddot{U}_{B1} + \ddot{U}_{B2}}{2}\right\}$$

FIG (3.3)

ALTERNATE TROUGH FASTENING

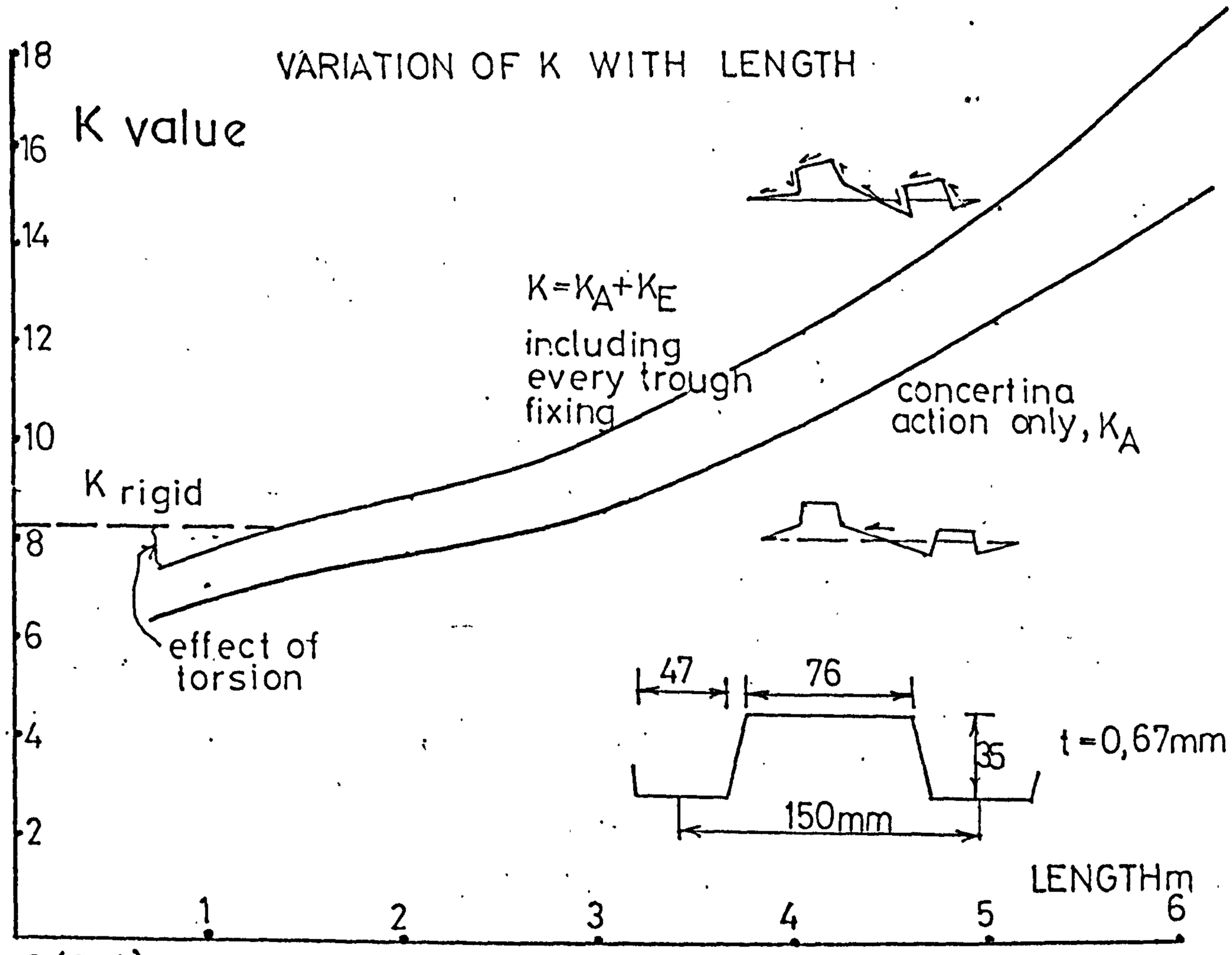

FIG(3.4)

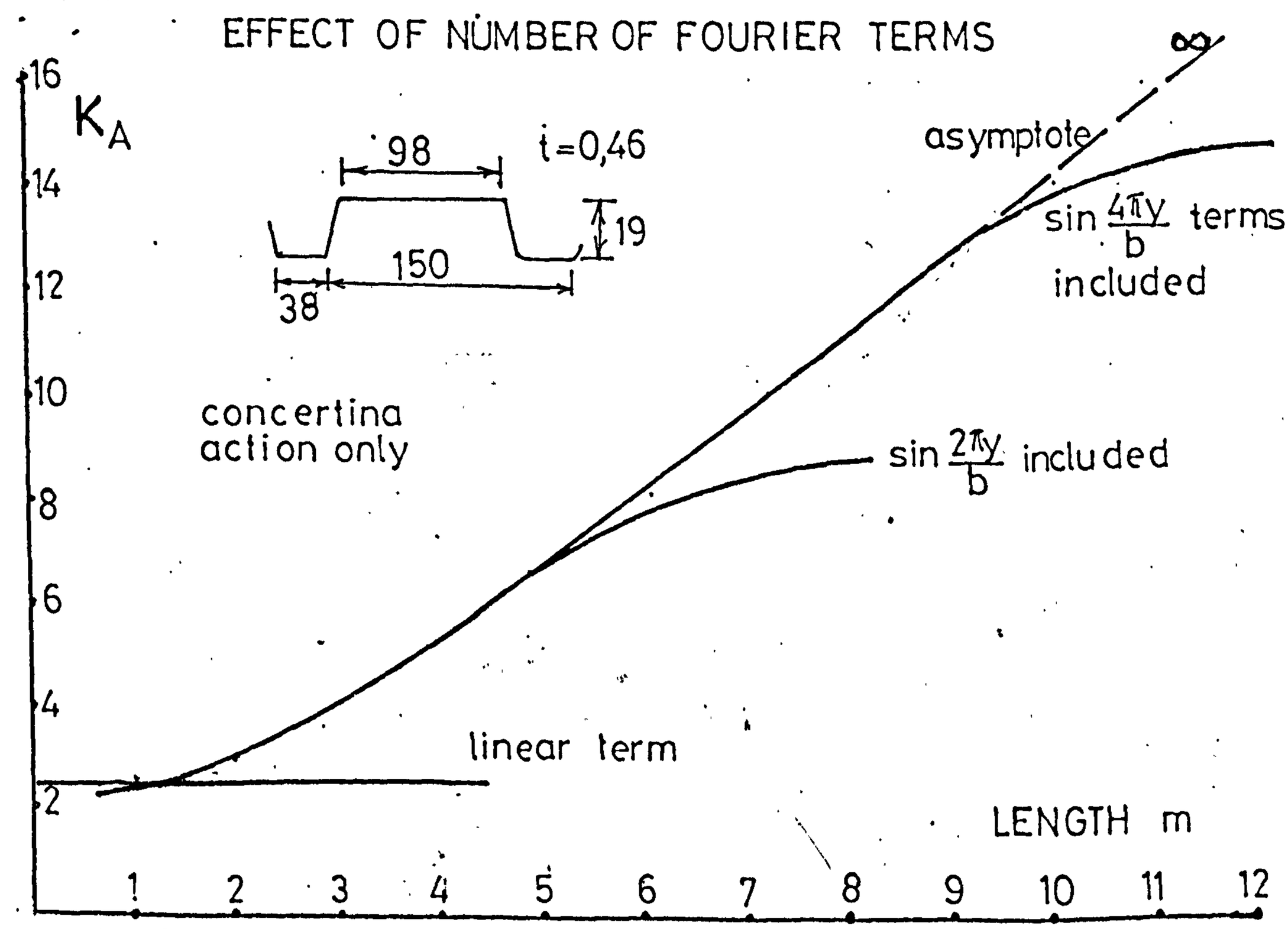

FIG(3.5)

ALTERNATE TROUGH FASTENING

DISPLACED SHAPES OF TROUGHS

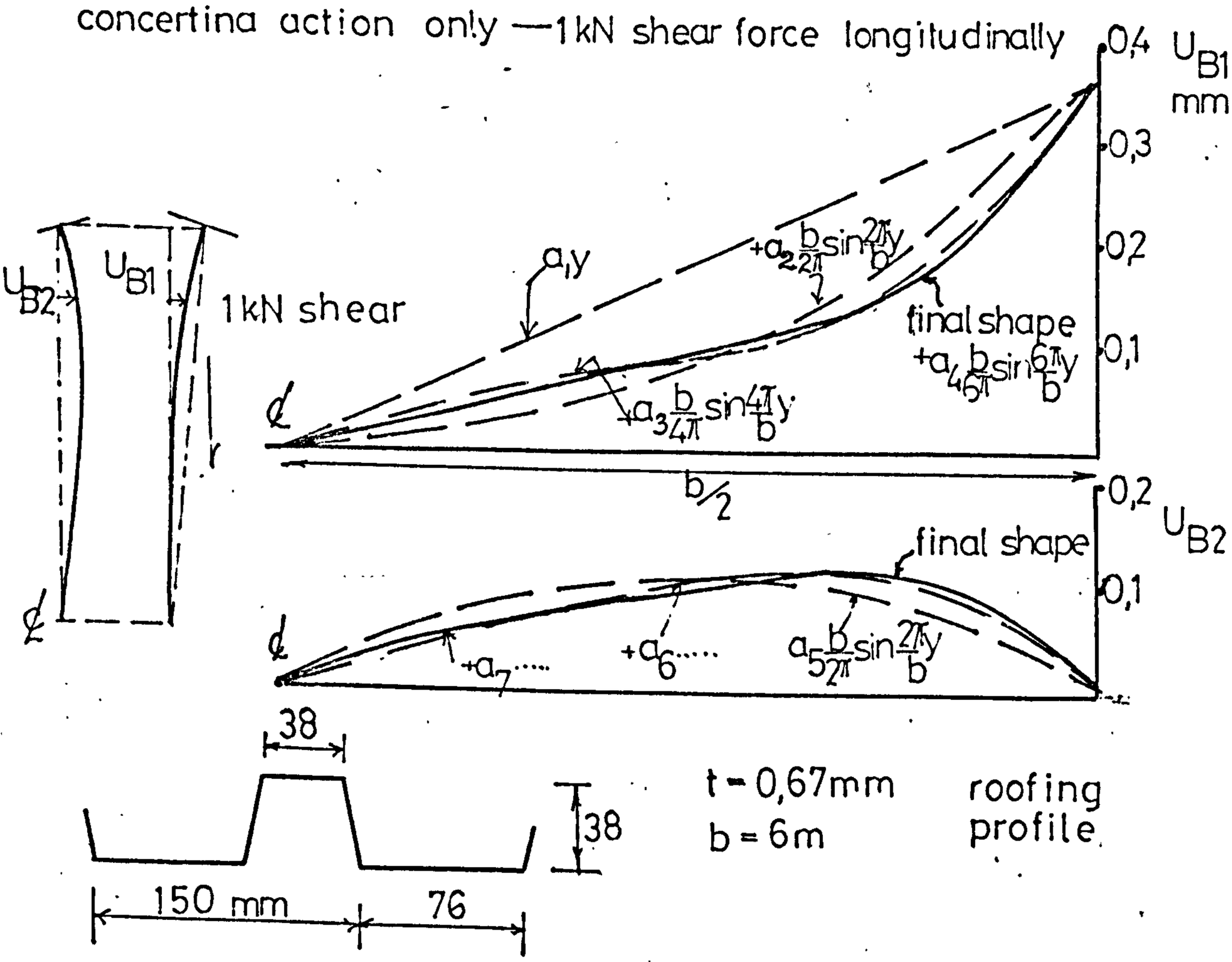

COMBINING CONCERTINA AND EVERY TROUGH FASTENING DEFLECTIONS

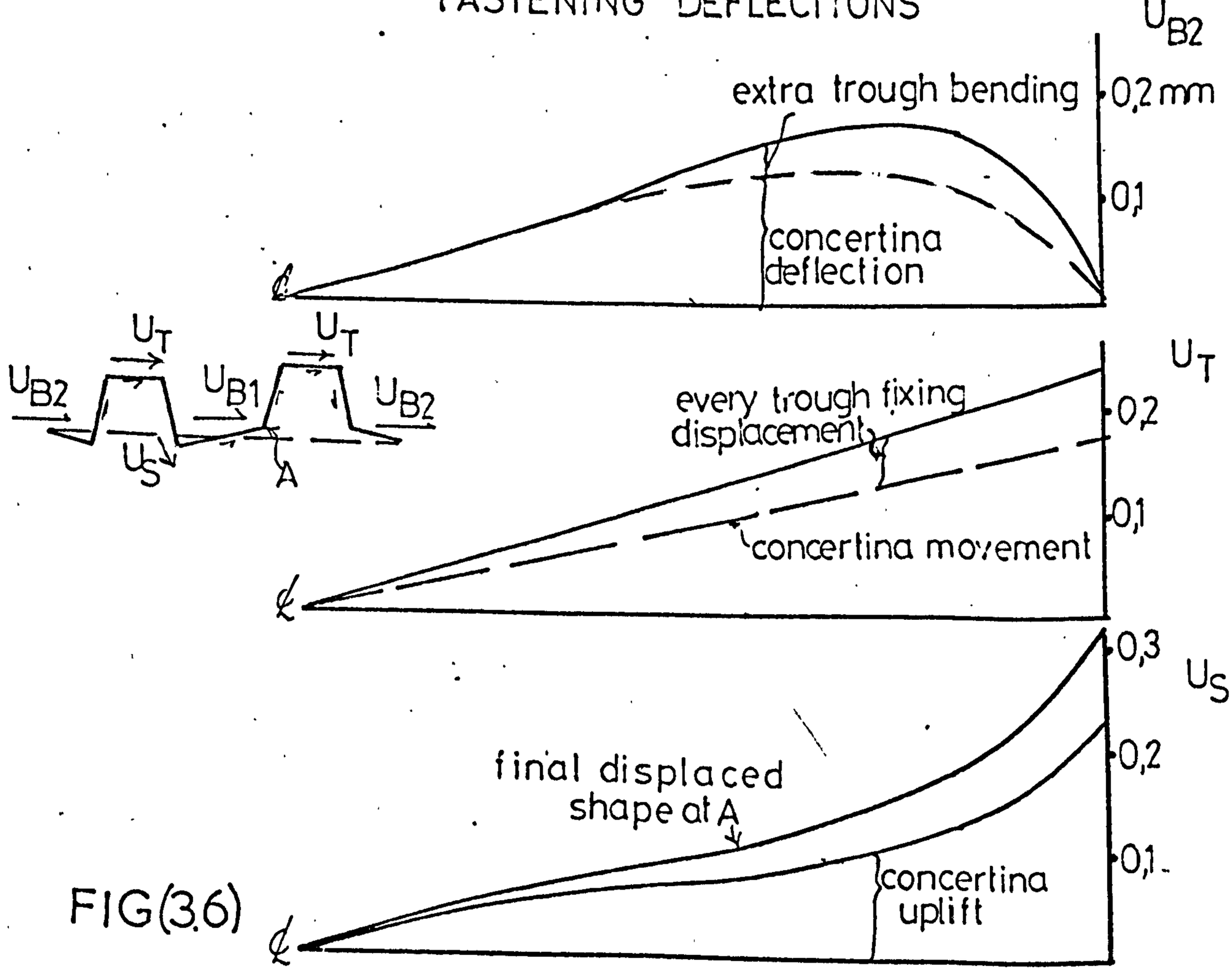

FIG(3.6)

ALTERNATE TROUGH FASTENING

DISPLACED SHAPES ALONG LENGTH

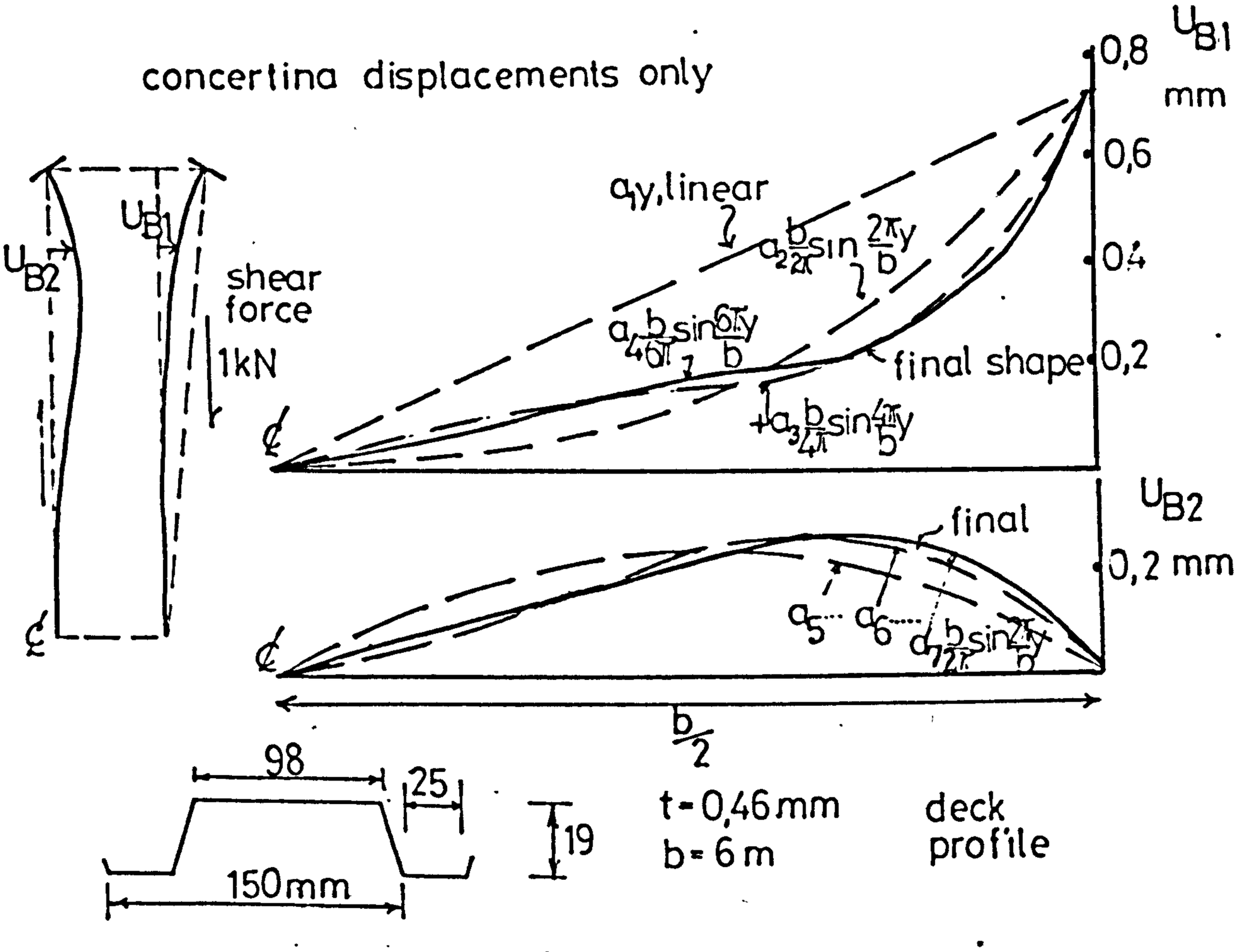

DISPLACEMENTS COMBINED WITH EVERY TROUGH FASTENING CASE

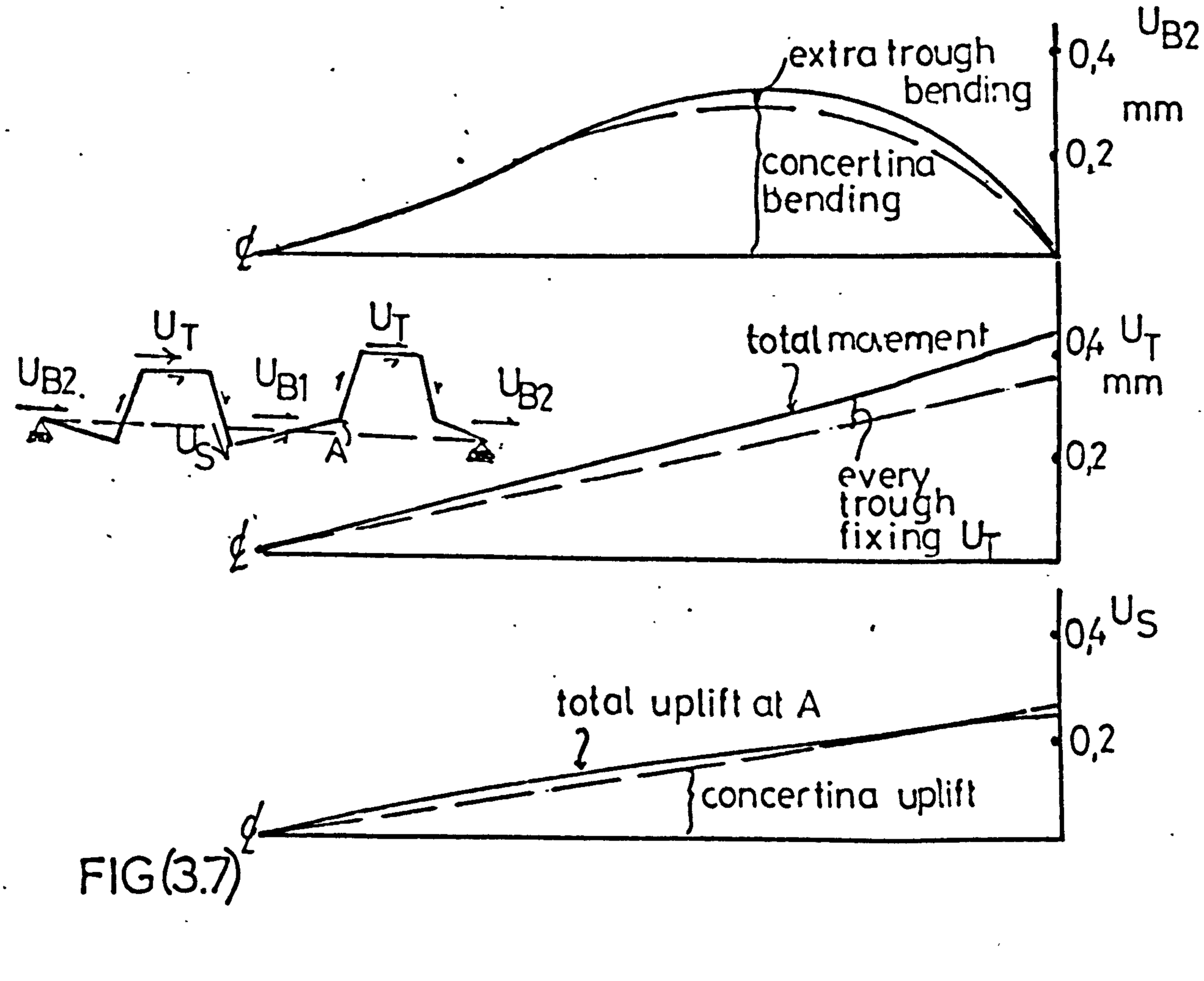

FIG(3.7)

ALTERNATE TROUGH FASTENING

—EFFECT OF LENGTH AND NUMBER OF INTERMEDIATE PURLINS, N

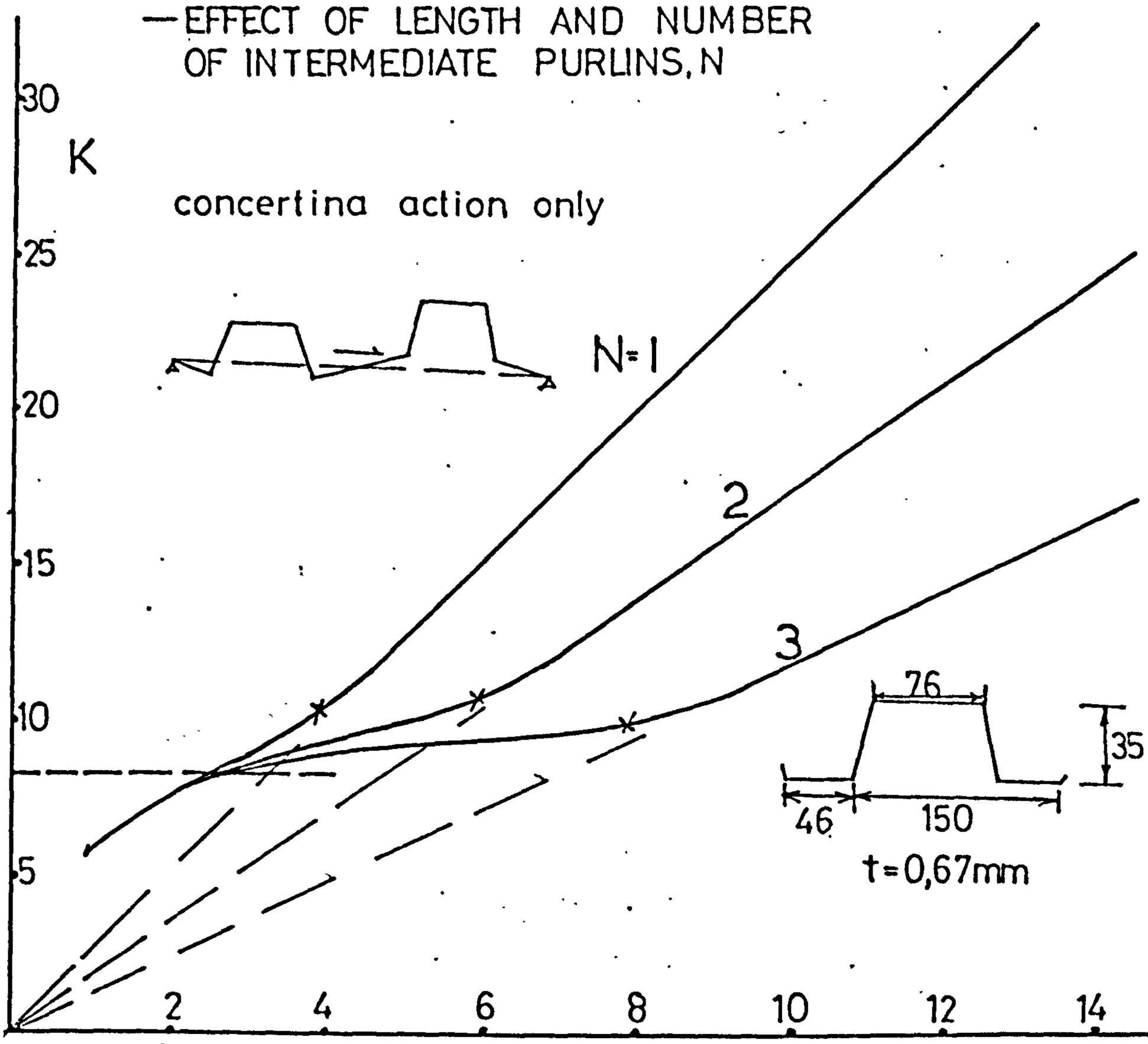

FIG (3,8)

VARIATION OF NEW $\bar{K}$ PARAMETER

—data as above

$$\bar{K} = K \frac{0{,}144\, d^{1,5}}{t^{0.5} b}$$

x—value for sheet span of 2m

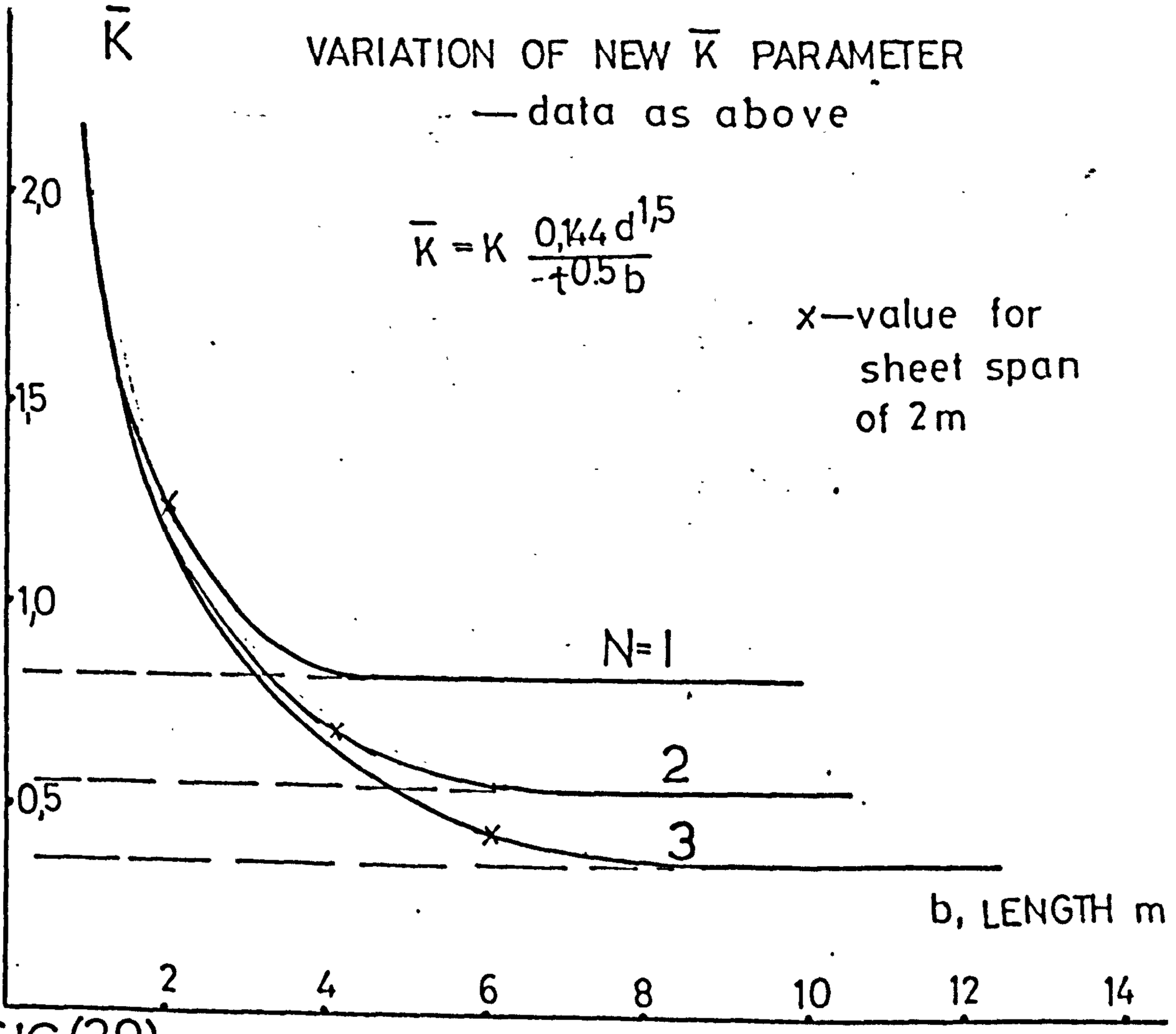

FIG (3.9)

ALTERNATE TROUGH FASTENING

EFFECT OF SHEET THICKNESS AND TROUGH PITCH

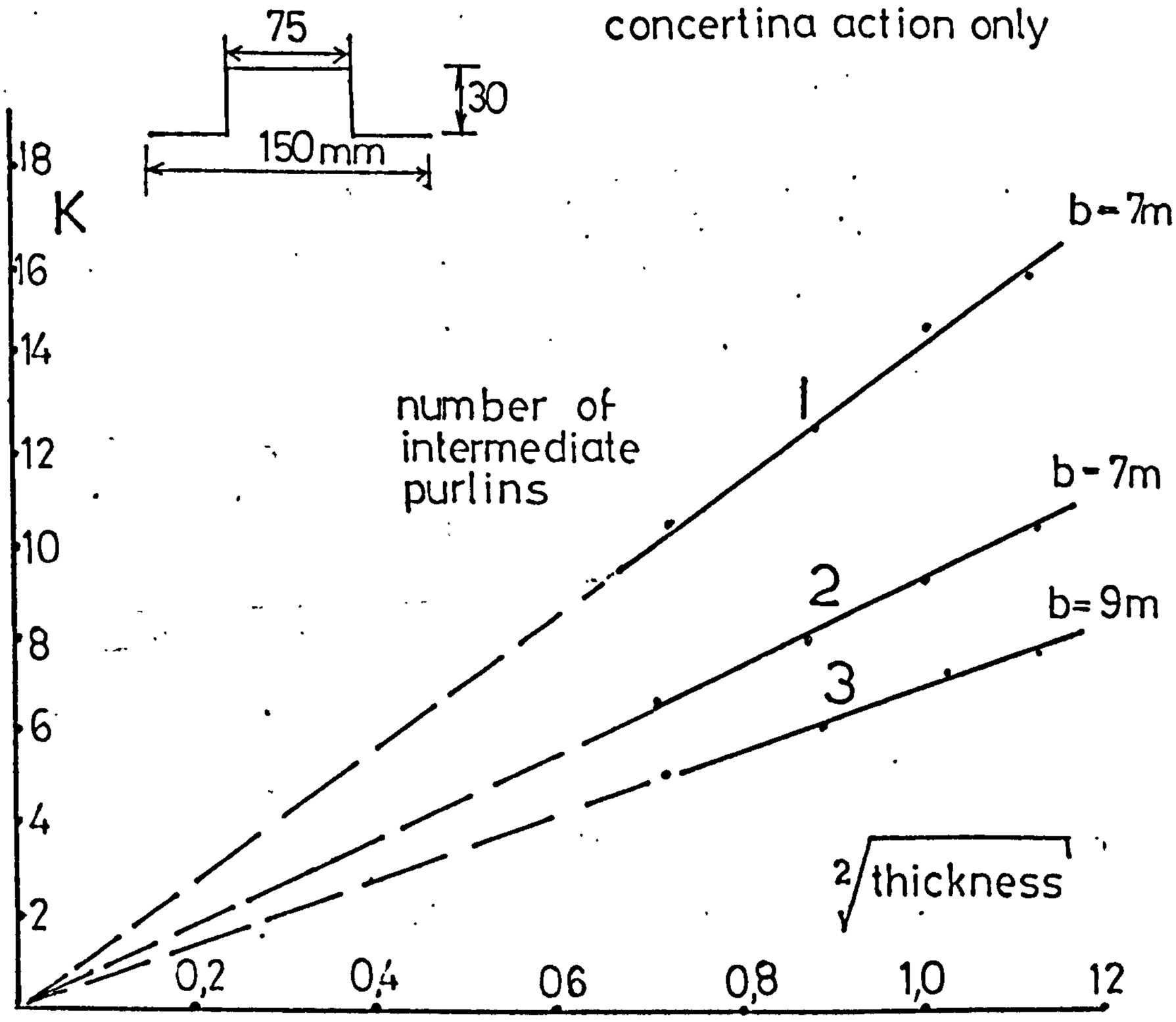

FIG(3.10)

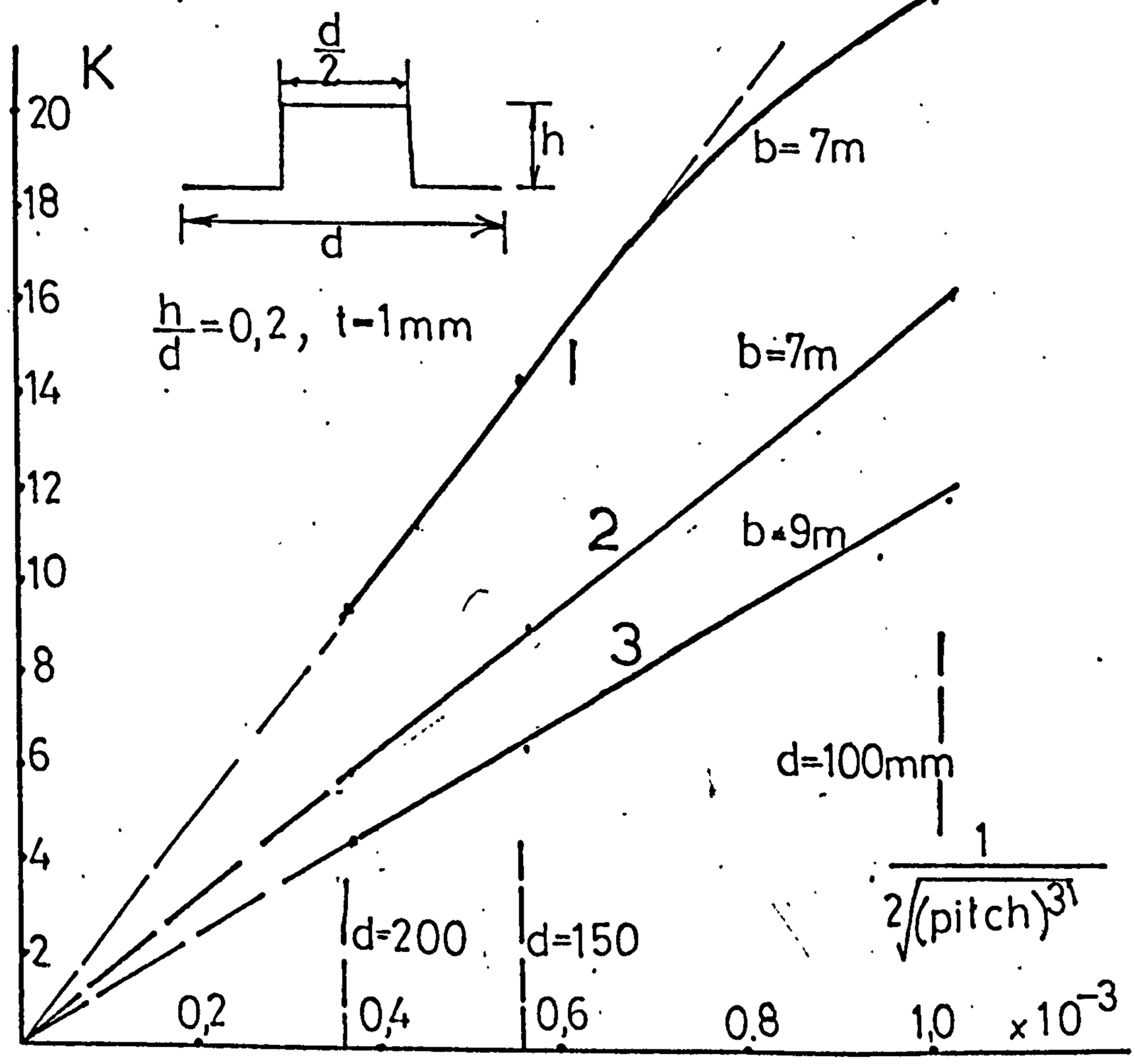

FIG (3.11)

ALTERNATE CORRUGATION FASTENING

—EFFECT OF FASTENING TO END PURLIN

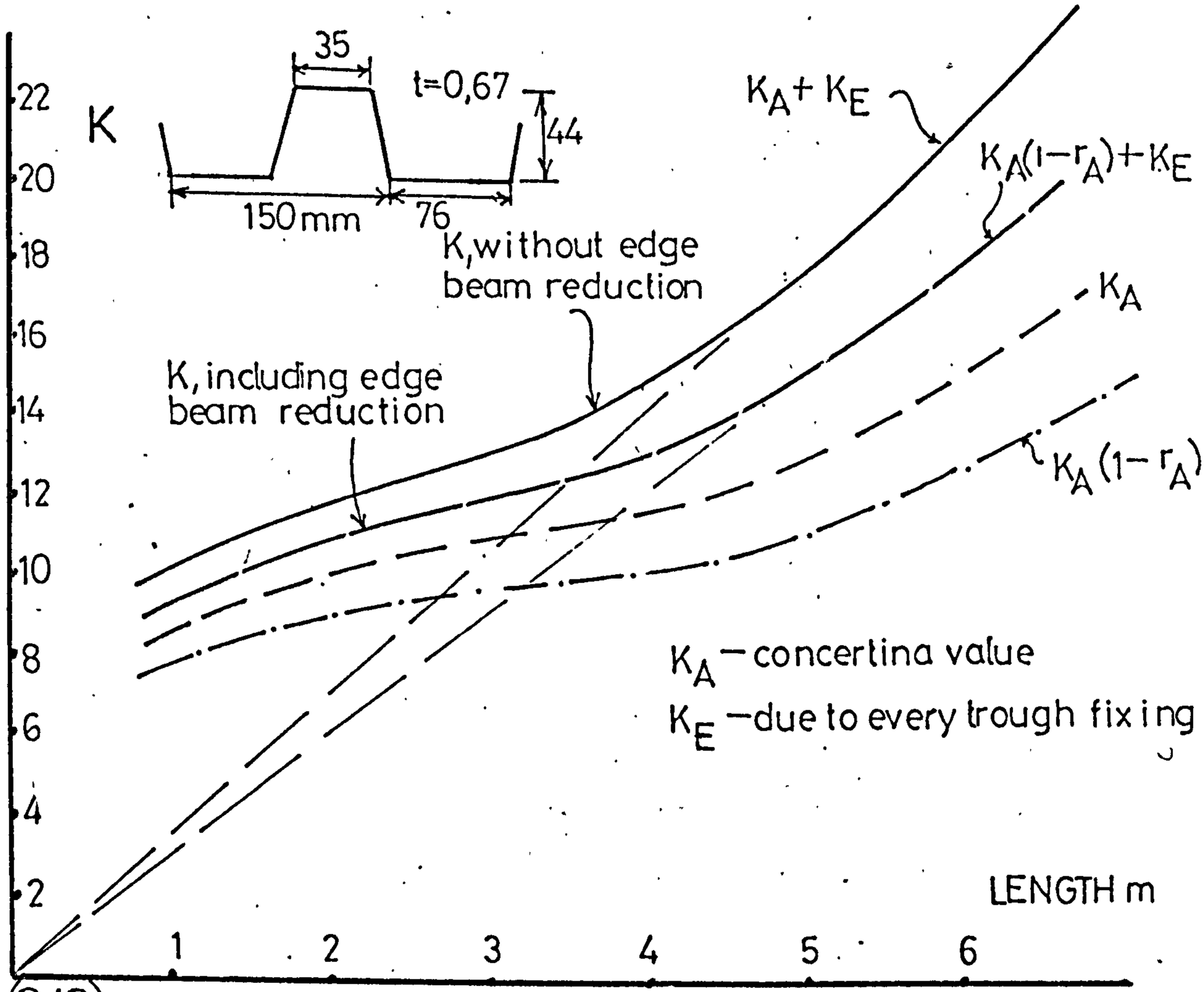

FIG(3.12) EFFECT OF PROFILE SHAPE ON NEW $\bar{K}$ PARAMETER

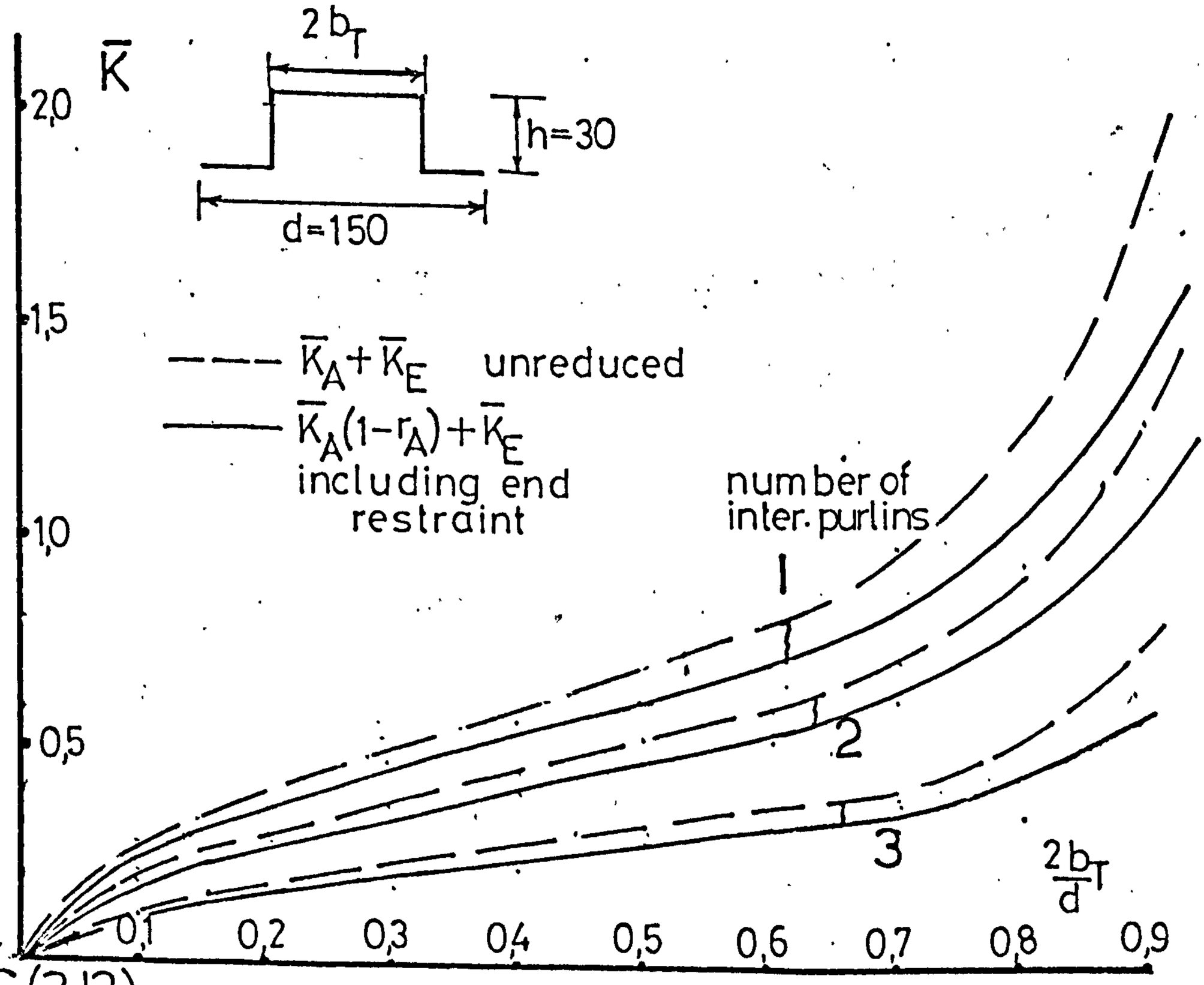

FIG(3.13)

ALTERNATE TROUGH FASTENING

DISPLACED SHAPES FOR 2,3 INTERMEDIATE PURLINS

concertina action only

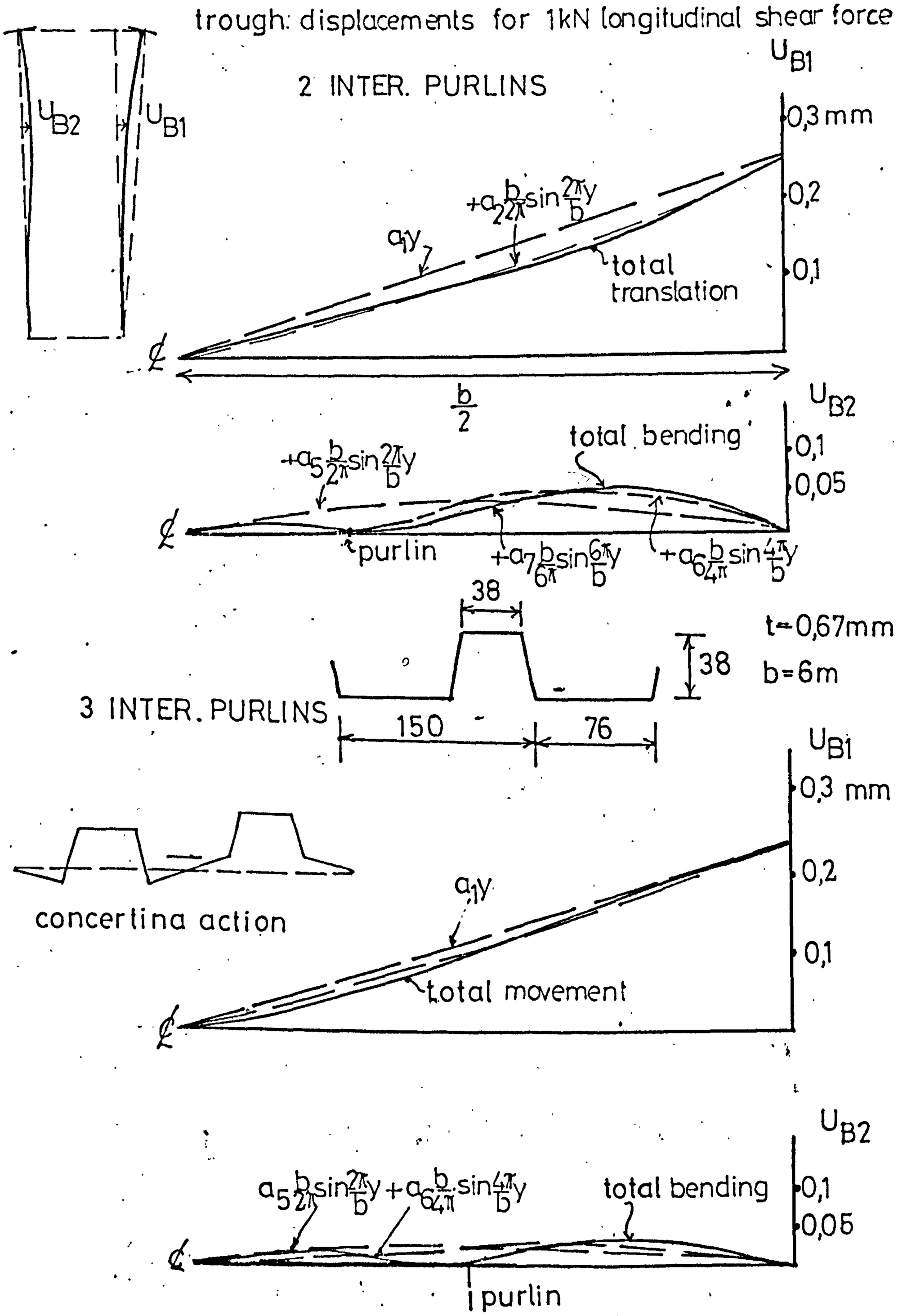

FIG (3.14)

PURLIN PROP REDUCTION IN FLEXIBILITY

—ALTERNATE TROUGH FASTENING

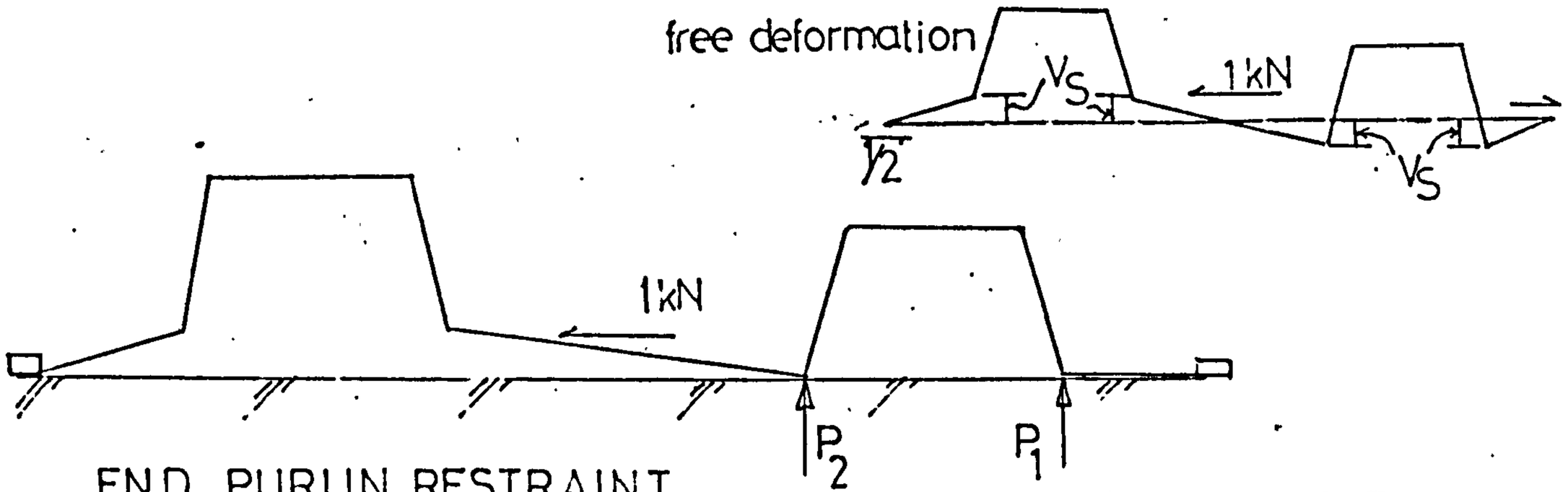

END PURLIN RESTRAINT

antisymmetrical forces P_1, P_2 are split into two components

TYPICAL FORM OF SYMMETRICAL END UPLIFT

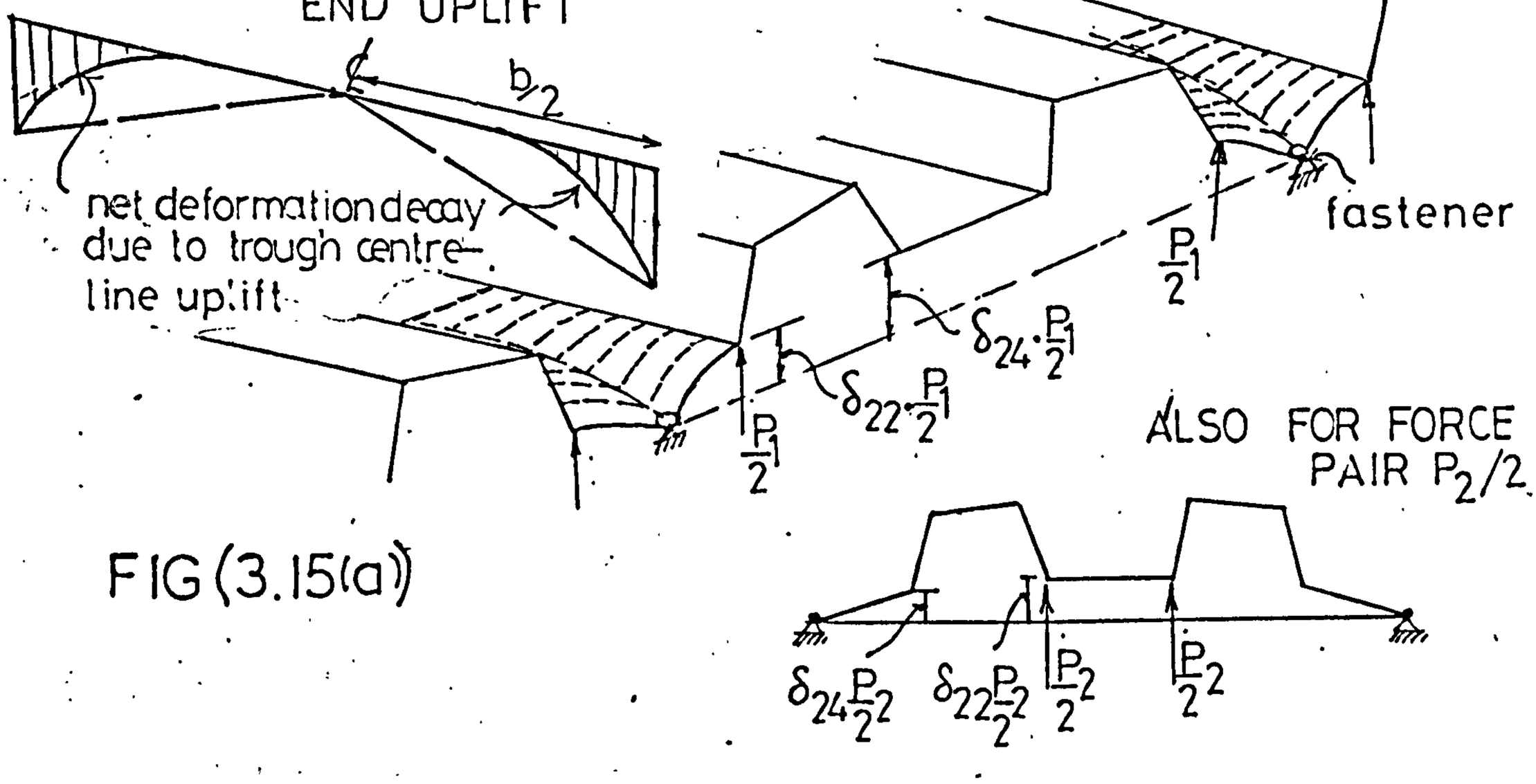

FIG (3.15(a))

ANTISYMMETRICAL END UPLIFT —linear plate movements

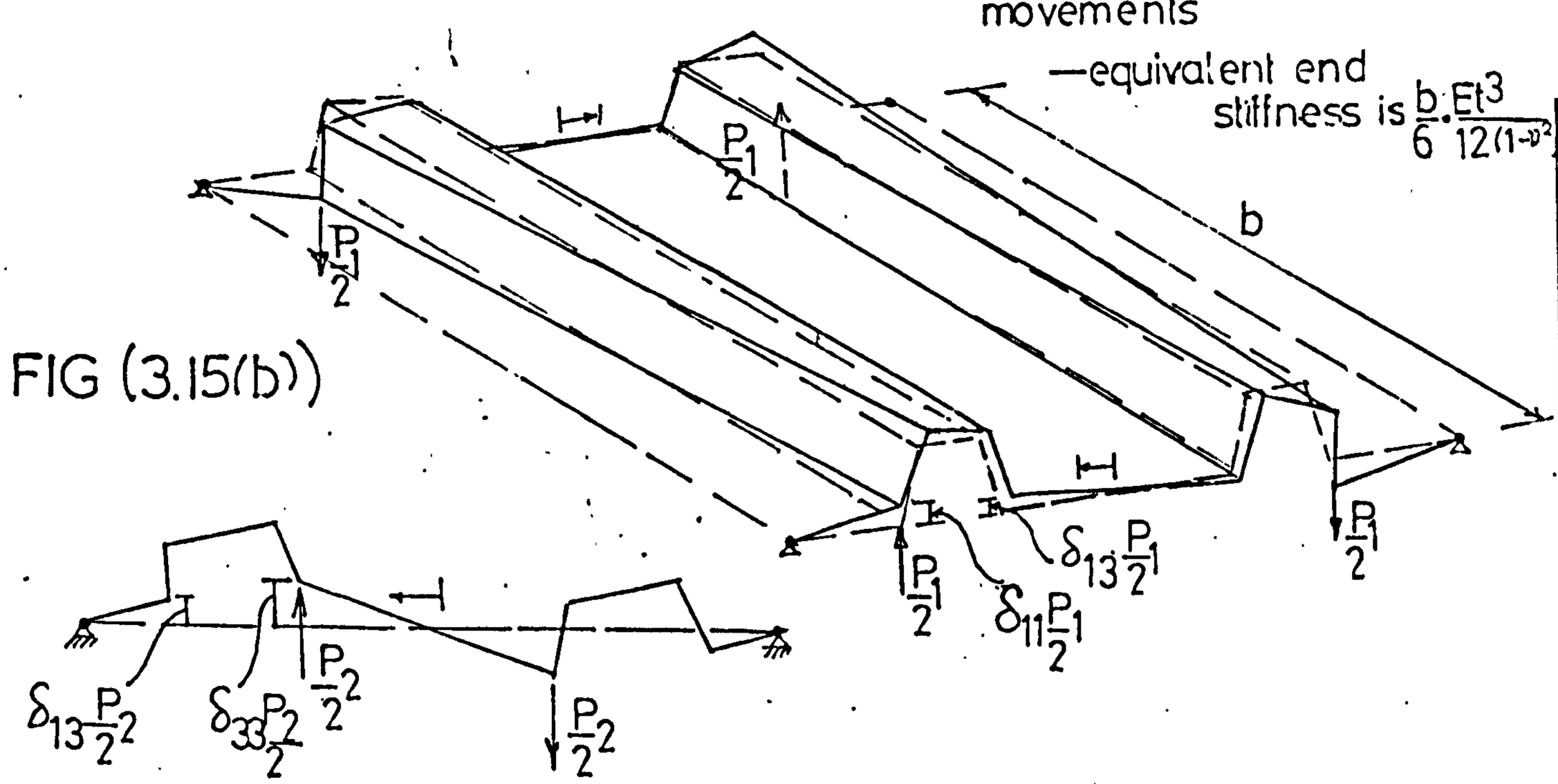

FIG (3.15(b))

BENDING MOMENTS USED IN ALTERNATE TROUGH FIXING ANALYSES

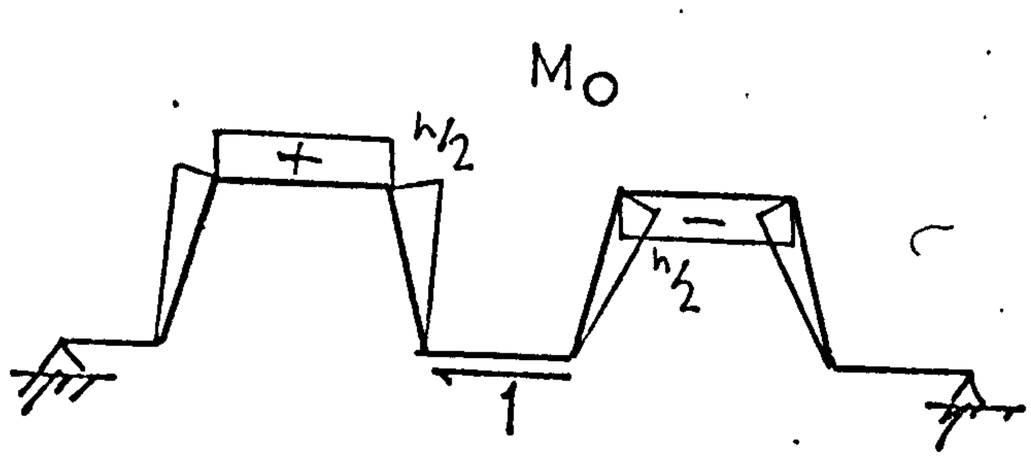

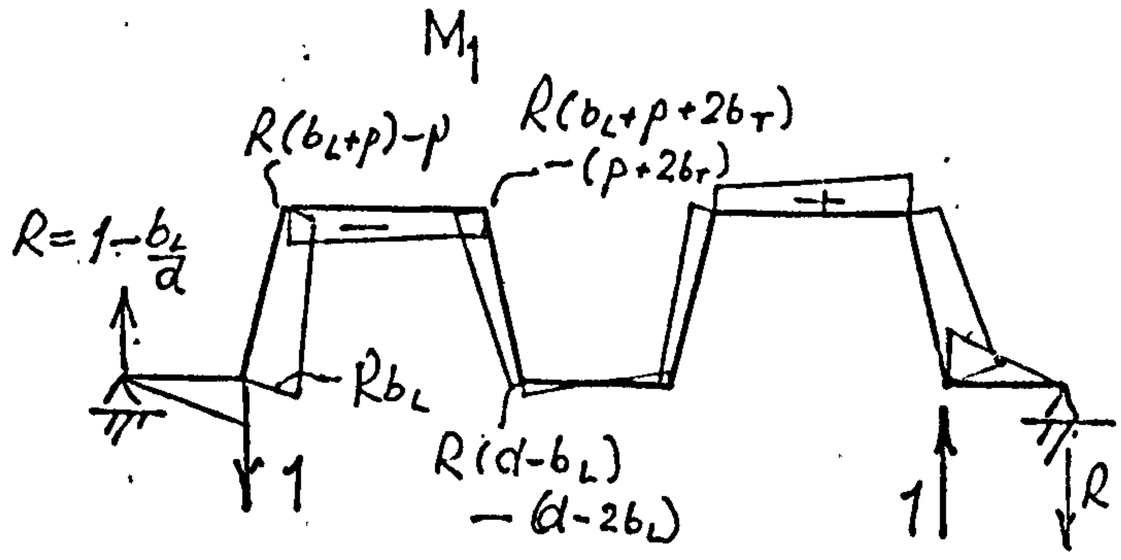

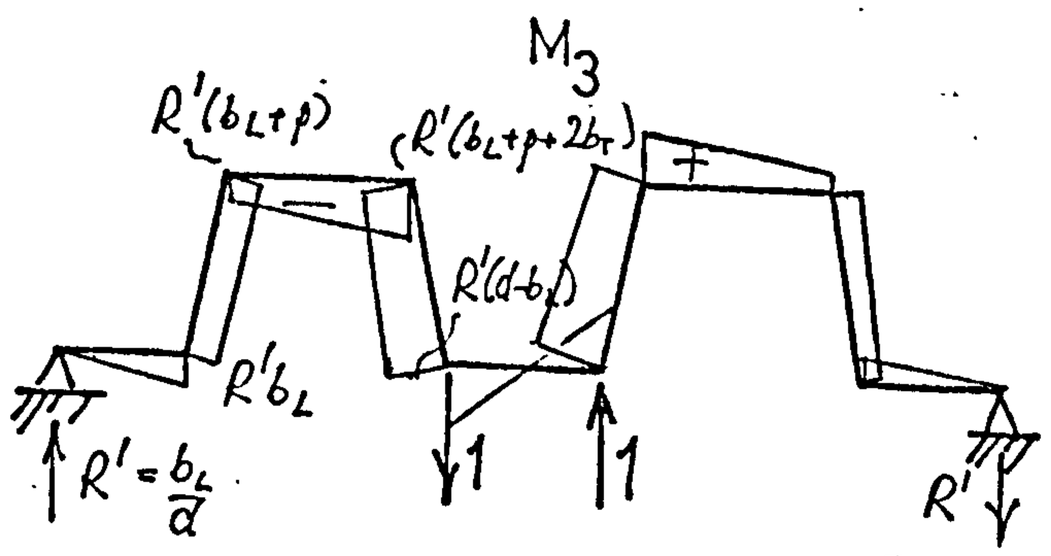

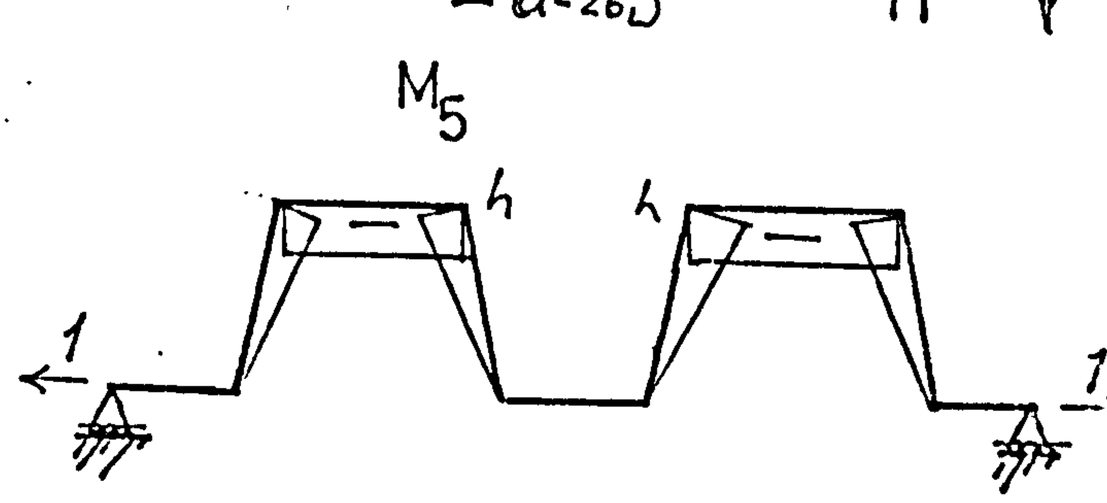

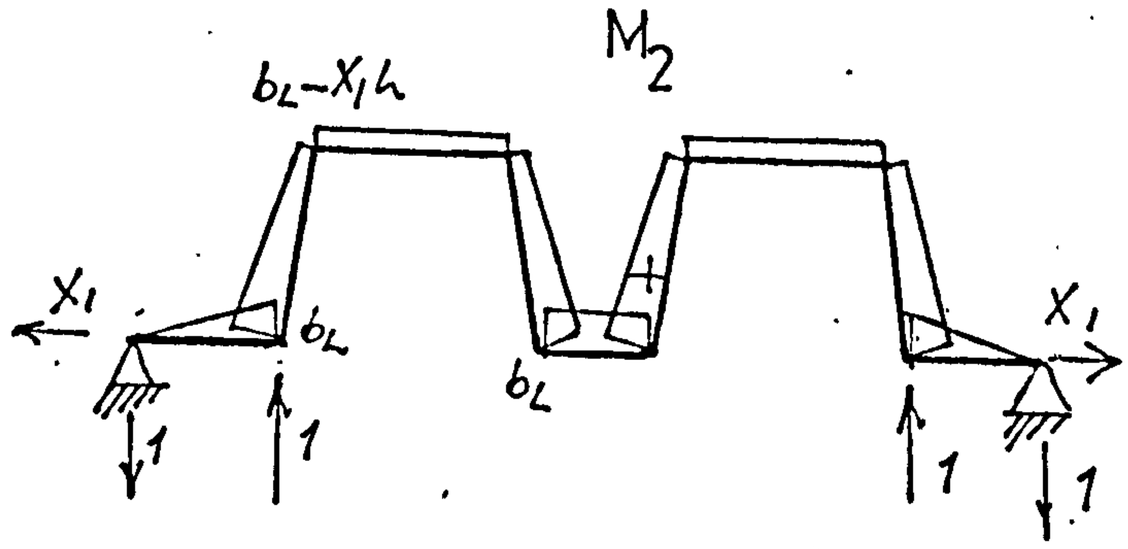

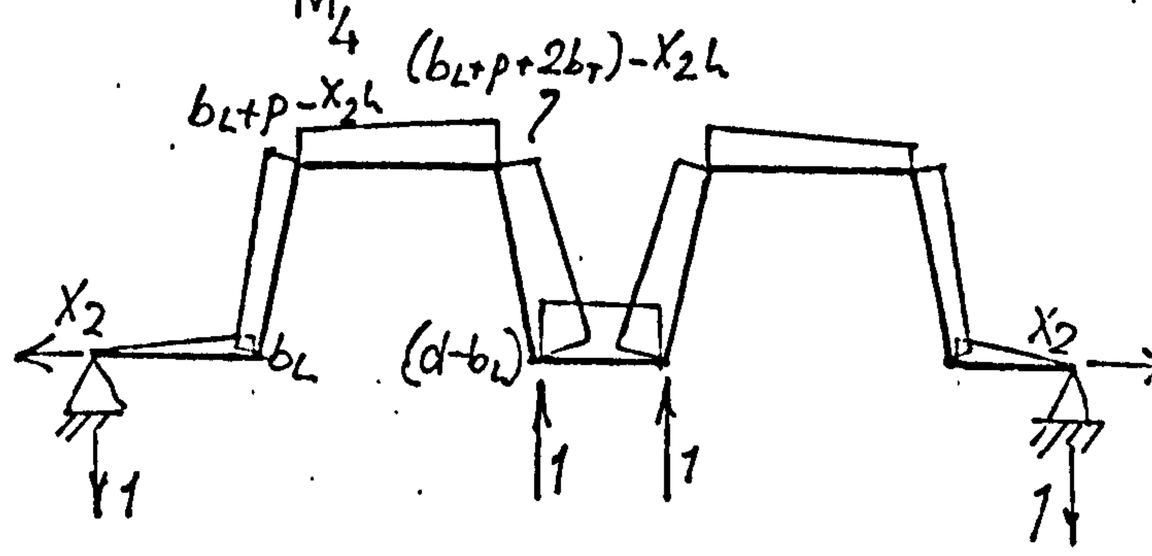

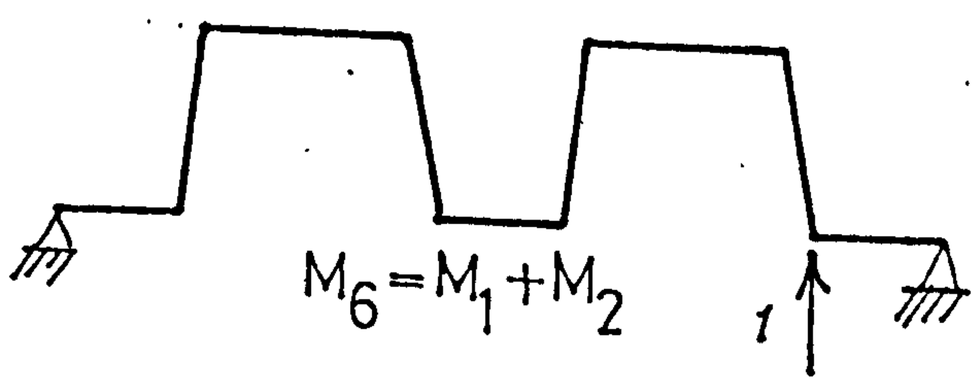

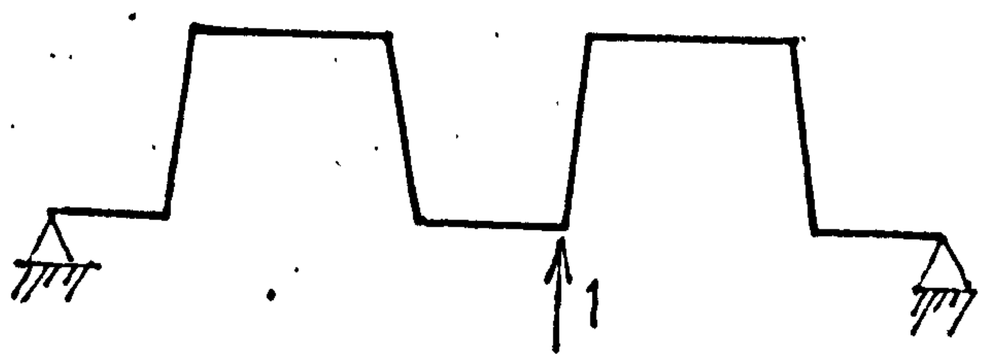

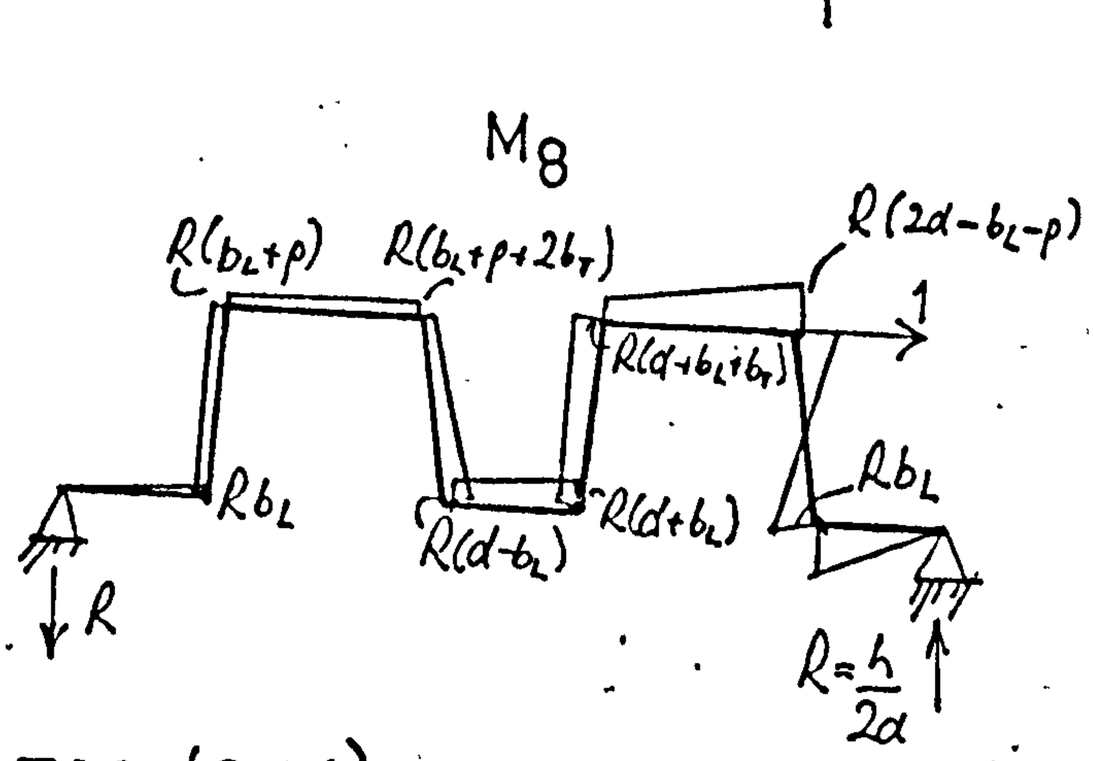

FIG (3.16)

ENERGY METHOD COMPARISONS—
ALTERNATE TROUGH FIXINGS

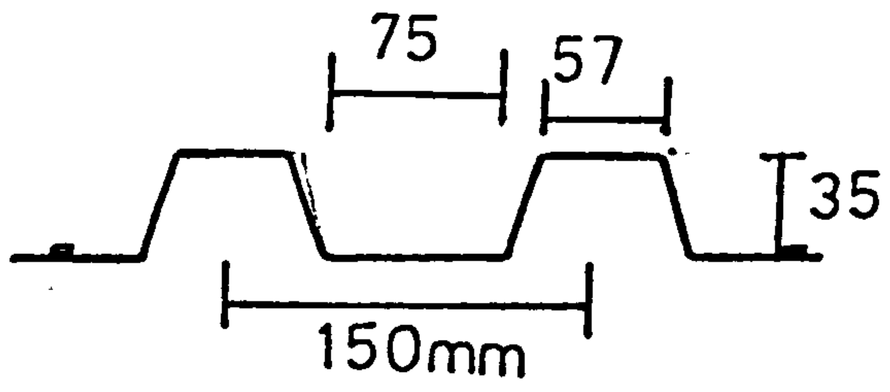

t = 0,67 mm

K value

K_b —rigid plate value

F.E.-FINITE ELEMENT RESULT

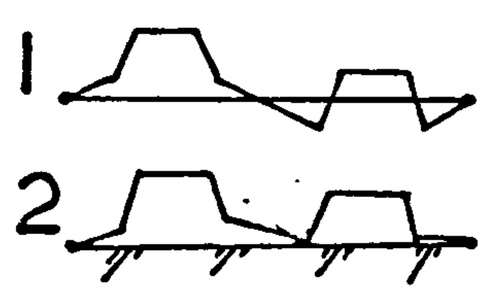

1. ▽ F.E. Result—no end restraint
2. △ F.E. Result—actual " "
○ Expt.—test width 1200 mm
□ Expt.— " " 600 "

LENGTH m

FIG(3.17)

ALTERNATE TROUGH FIXINGS

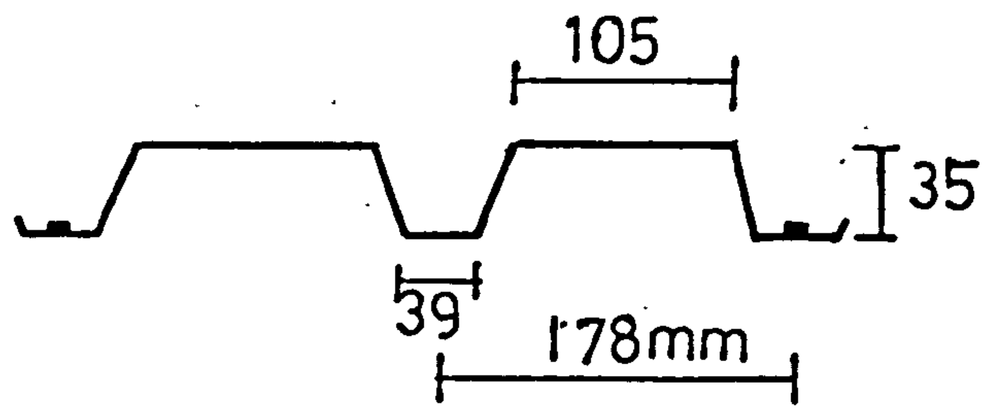

t-0,57mm

K value

K_b — rigid plate value

14
12
10
8
6
4
2

1 2 3 4 5 6

LENGTH m

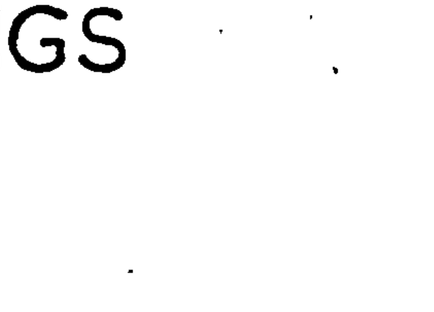

1. ▽ F.E. Result—no end restraint
2. △ F.E. Result—actual " "
○ Expt.—test width 1250mm
□ Expt.— " " 700 "

FIG(3.18)

ALTERNATE TROUGH FIXINGS

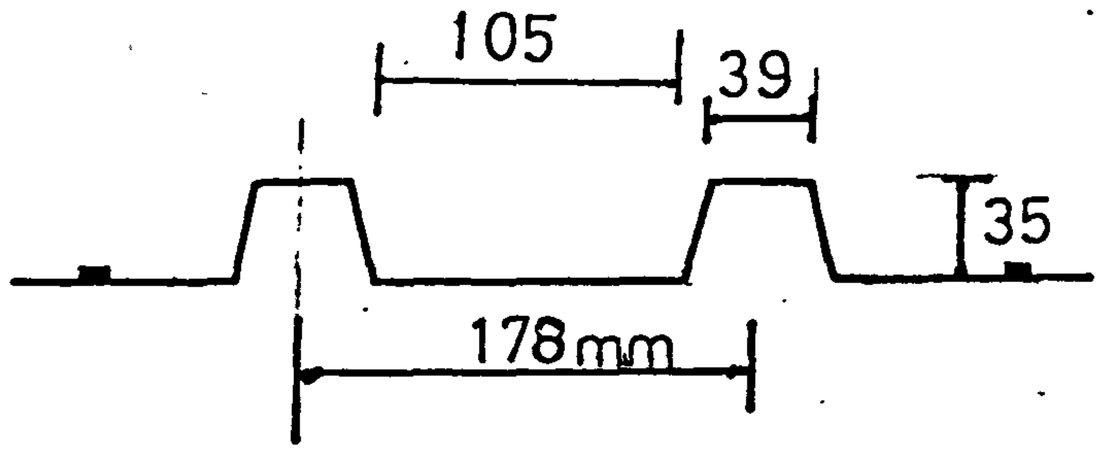

t - 0,57mm

K value

8
7
6
5
4
3
2
1

K_b — rigid plate value

1 2 3 4 5 6

LENGTH m

1. ▽ F.E. Result — no end restraint
2. △ F.E. Result — actual " "
○ Expt. — test width 1250 mm
□ Expt. — " " 350mm

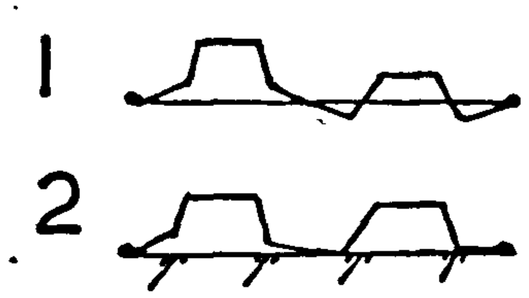

FIG (3.19)

FASTENING EVERY THIRD TROUGH

—PURLIN PROP REDUCTION IN FLEXIBILITY

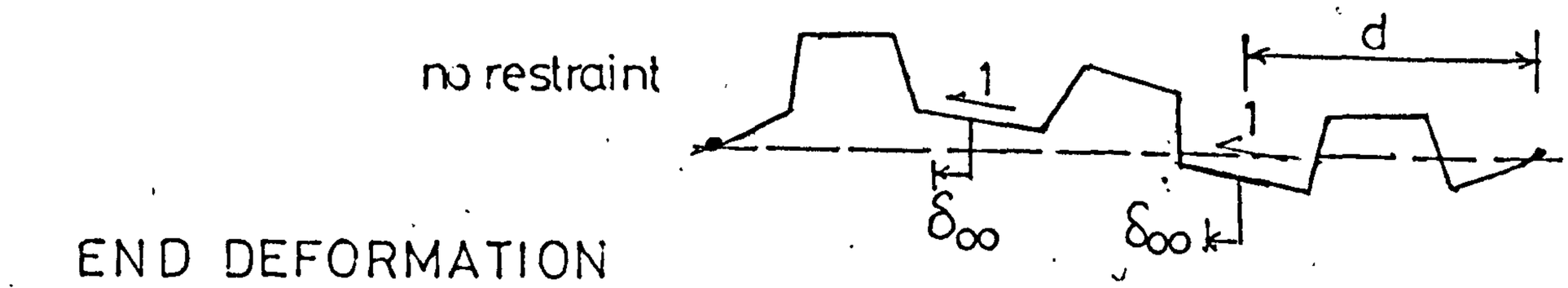

END DEFORMATION

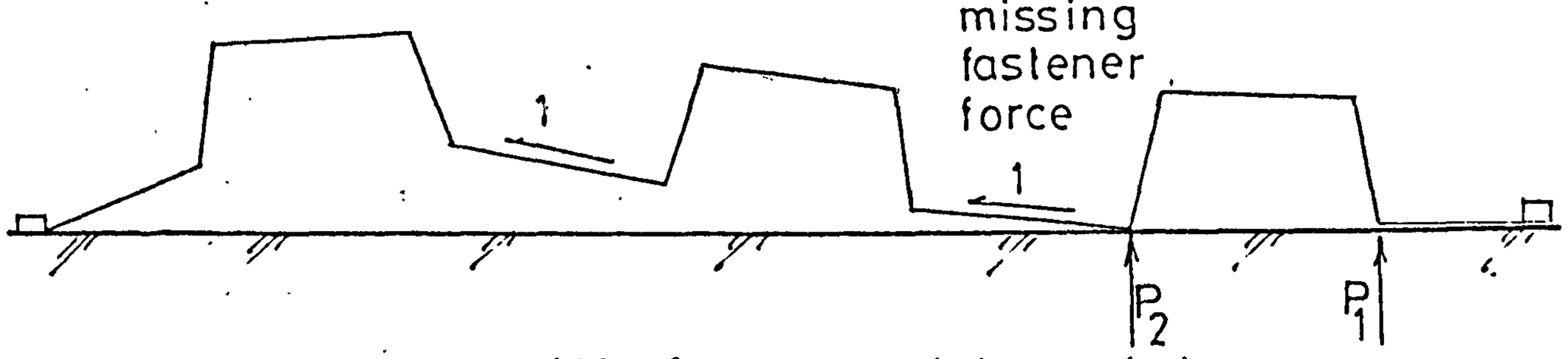

uplift forces per kN trough force

SYMMETRICAL END FORCES APPLIED

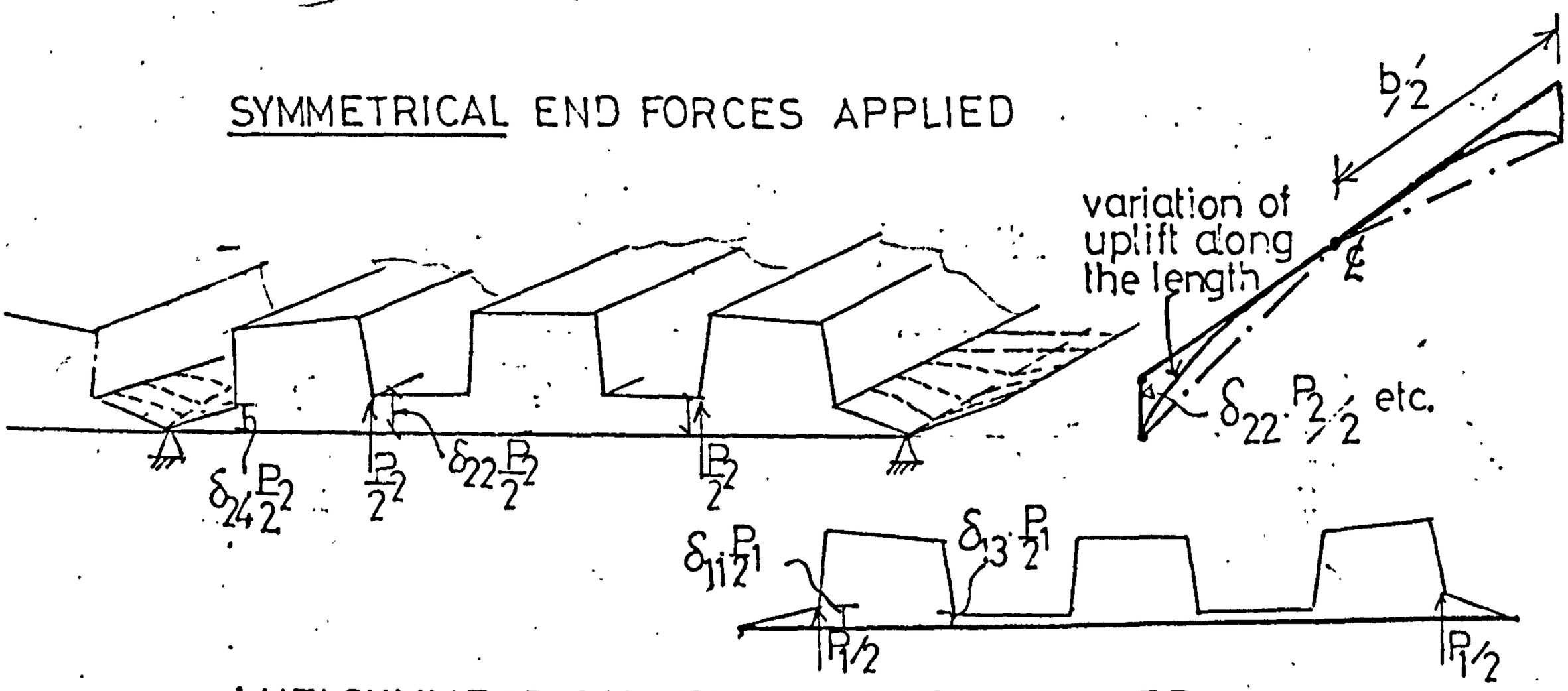

ANTISYMMETRICAL END FORCES APPLIED

linear plate movements

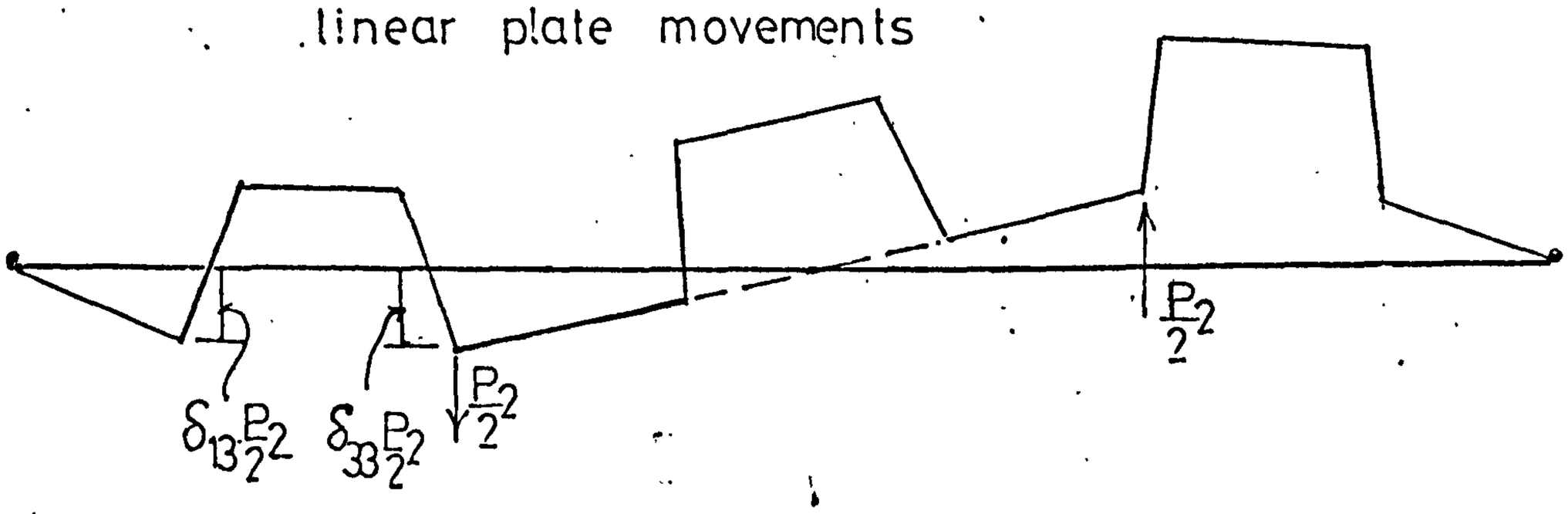

—ALSO FOR FORCE PAIR OF $P_1/2$

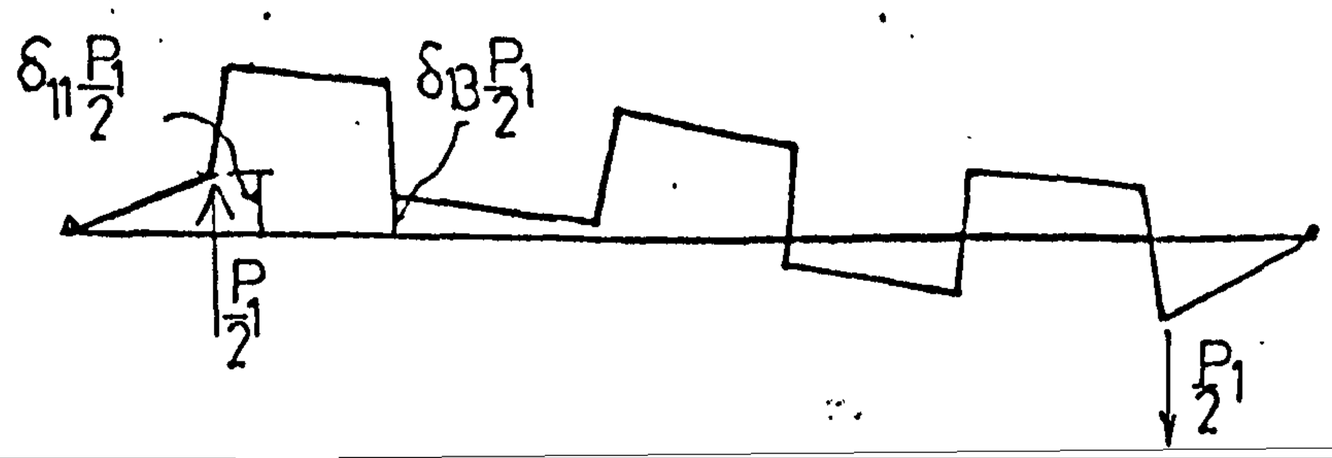

FIG (3.20)

BENDING MOMENTS USED IN EVERY THIRD TROUGH FIXING ANALYSES

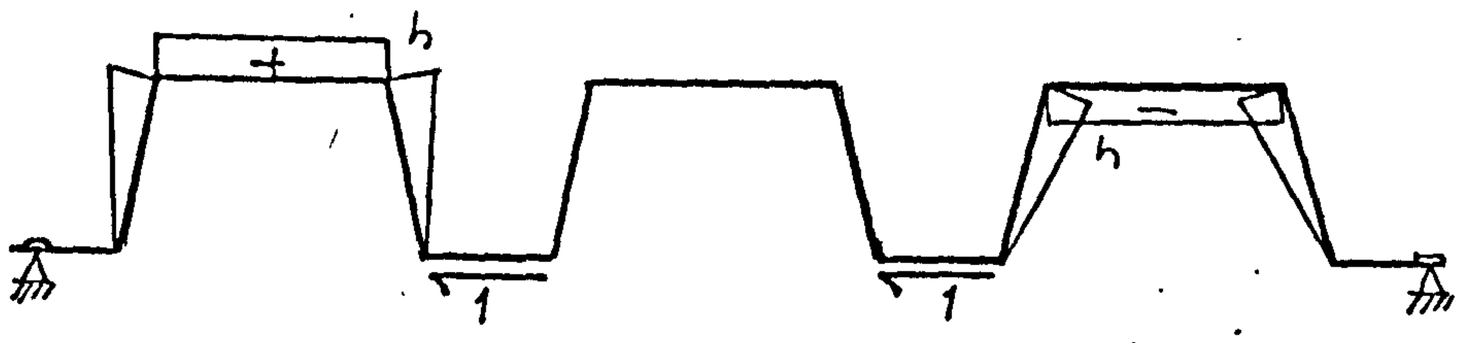

M_0

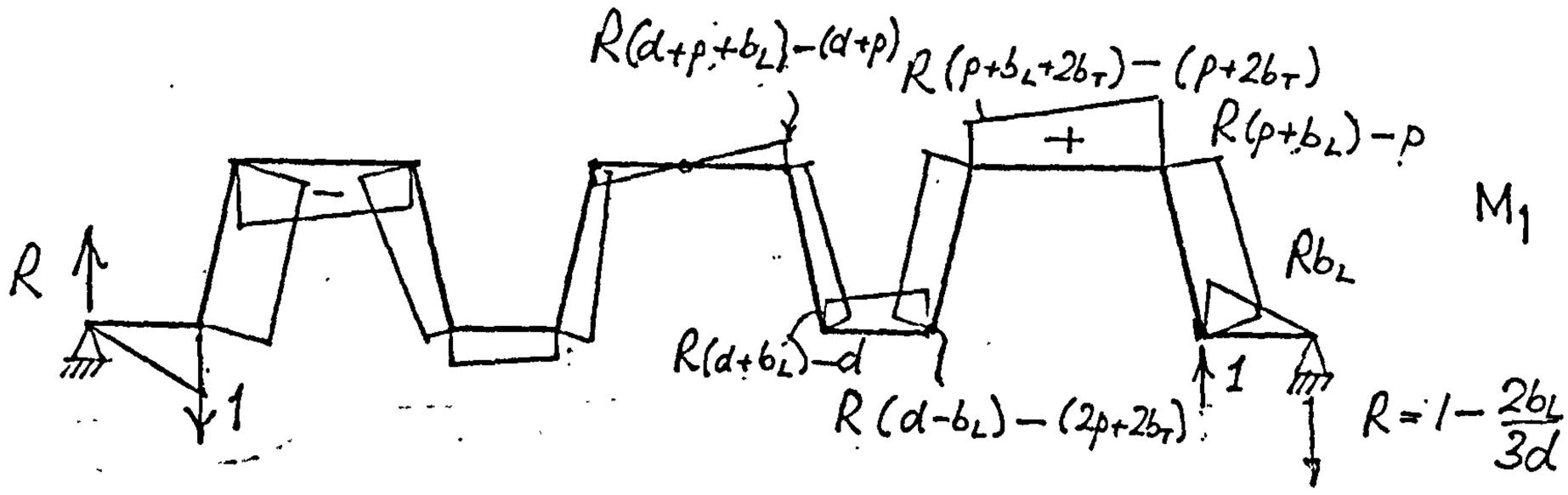

M_1

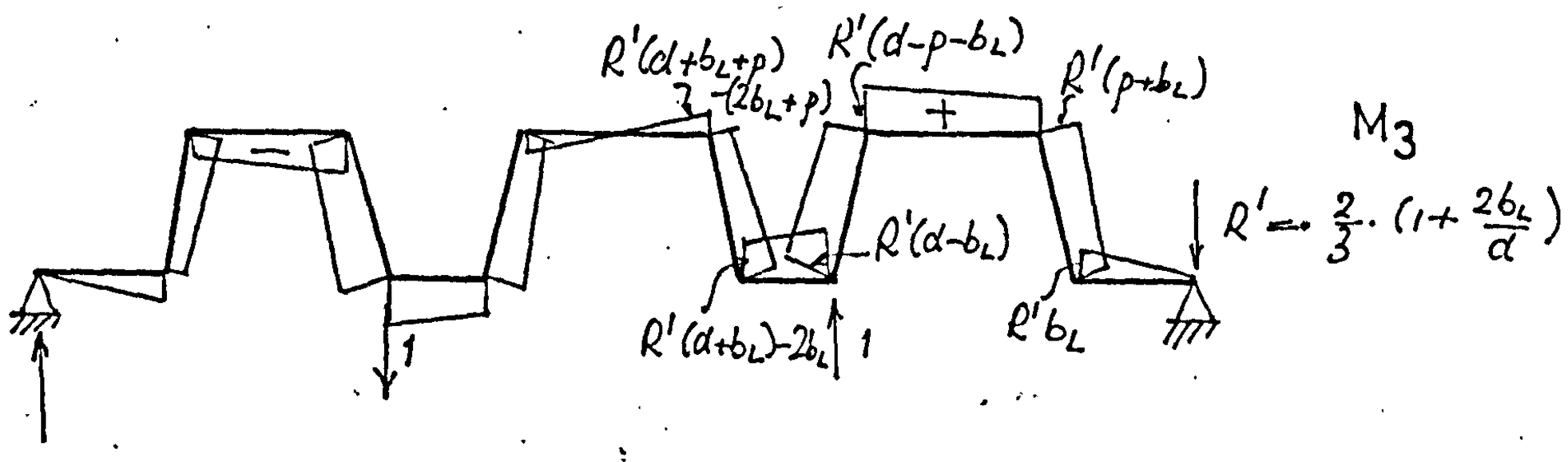

M_3

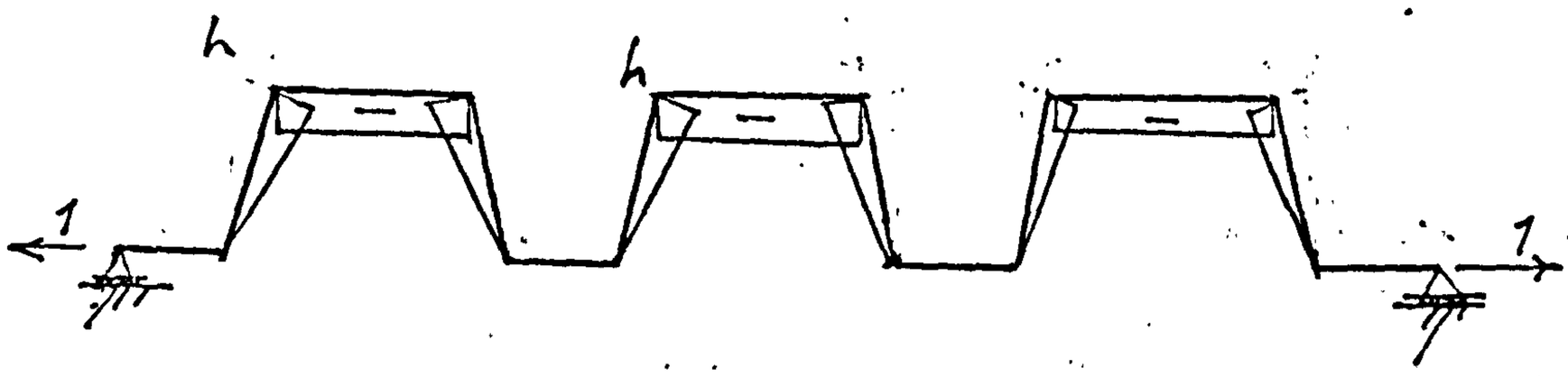

M_5

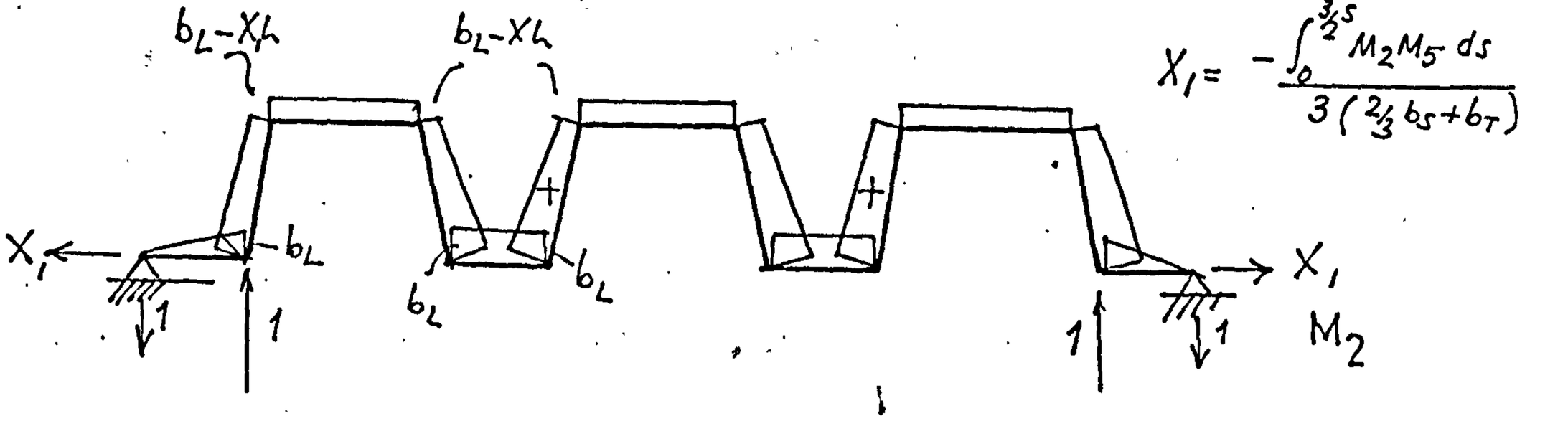

M_2

$$X_1 = -\frac{\int_0^{\frac{3}{2}s} M_2 M_5 \, ds}{3\left(\frac{2}{3}b_S + b_T\right)}$$

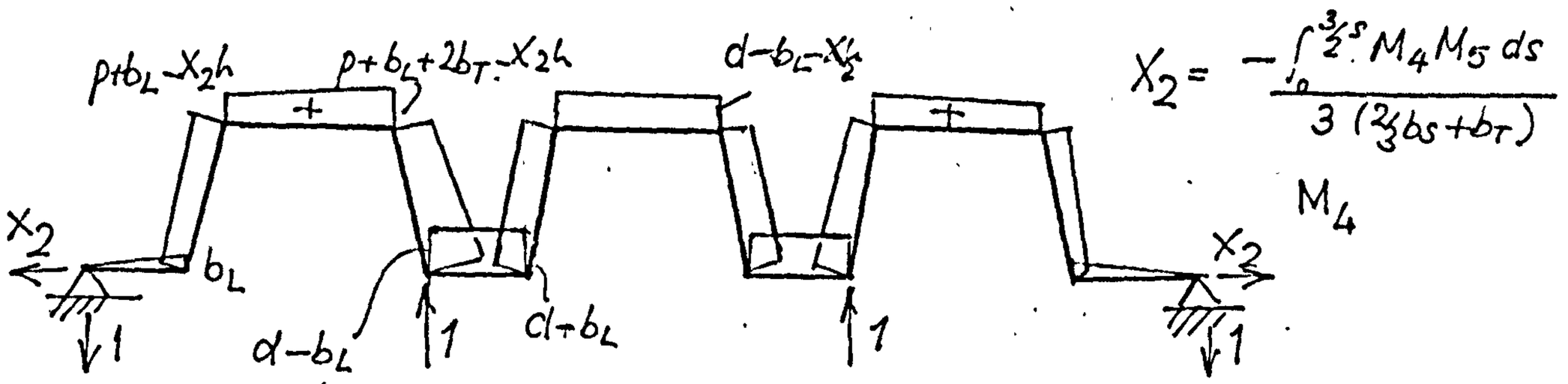

M_4

$$X_2 = -\frac{\int_0^{\frac{3}{2}s} M_4 M_5 \, ds}{3\left(\frac{2}{3}b_S + b_T\right)}$$

FIG (3.21)

SINUSOIDAL CORRUGATIONS
— GEOMETRY IN McKENZIE'S ANALYSIS

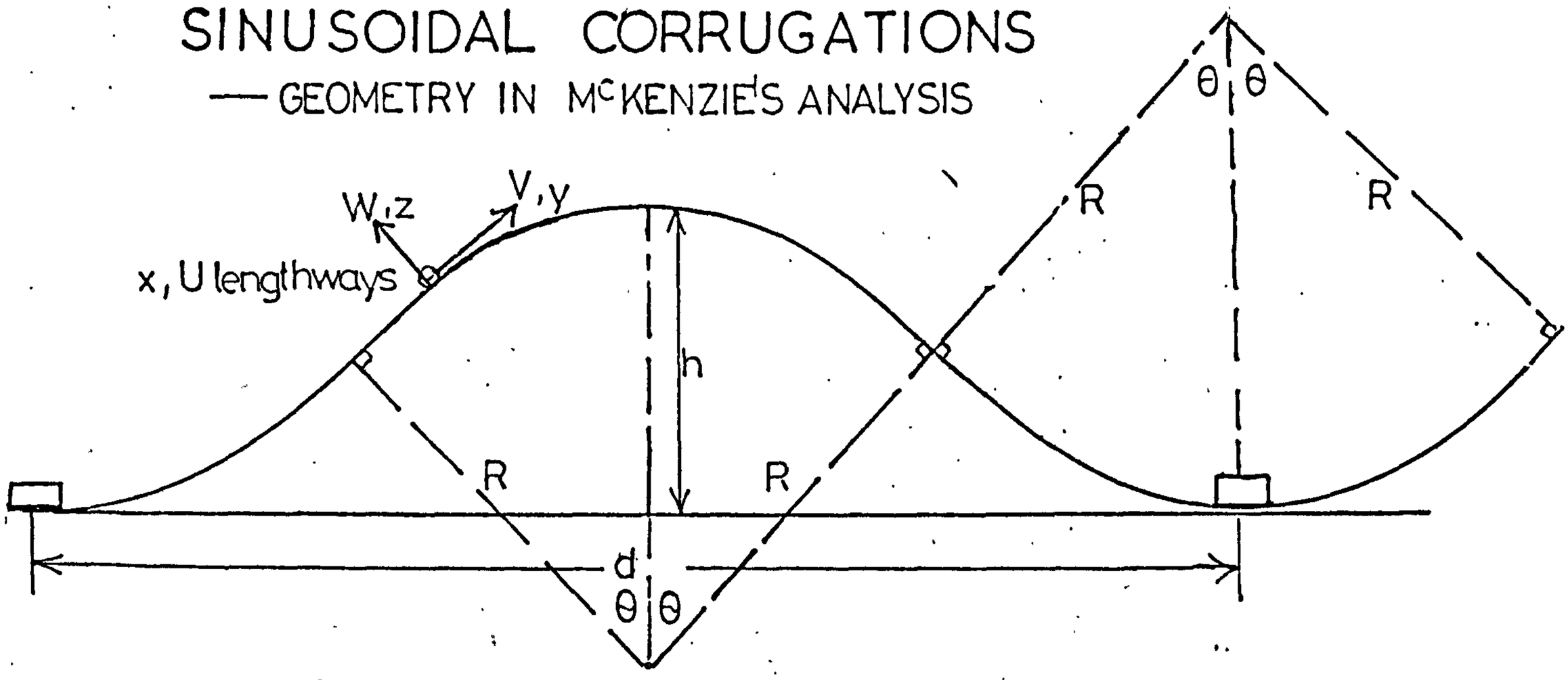

$h = 2R(1-\cos\theta)$; $d = 4R\sin\theta$

EVERY TROUGH FIXING

FIG (4.1)

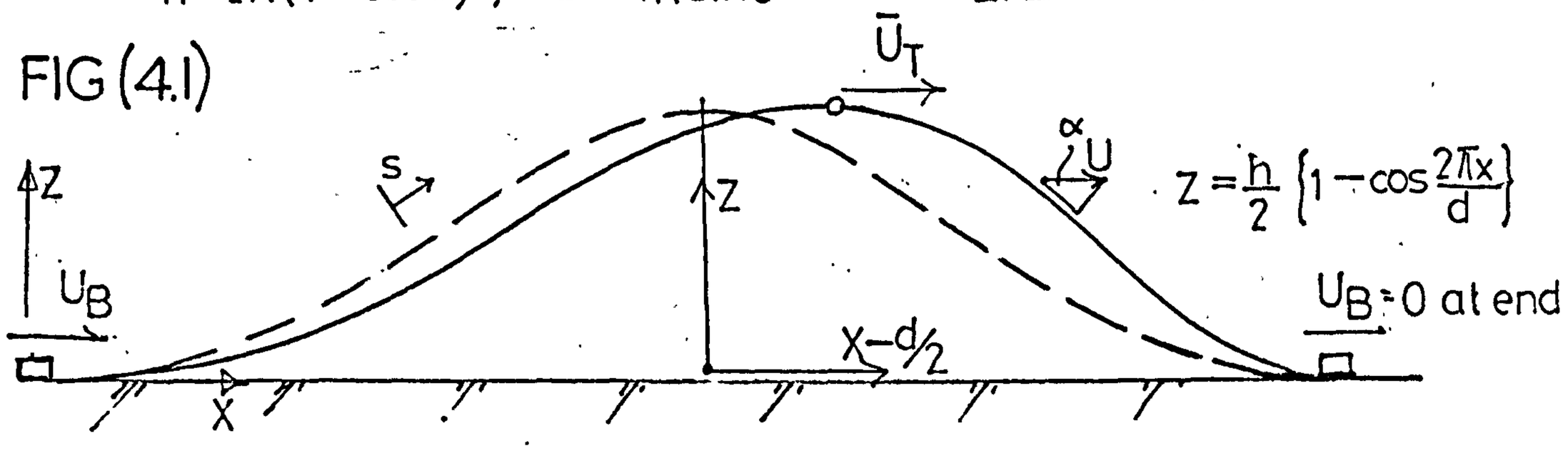

ENERGY METHOD SOLUTION FOR SHEAR FLEXIBILITY

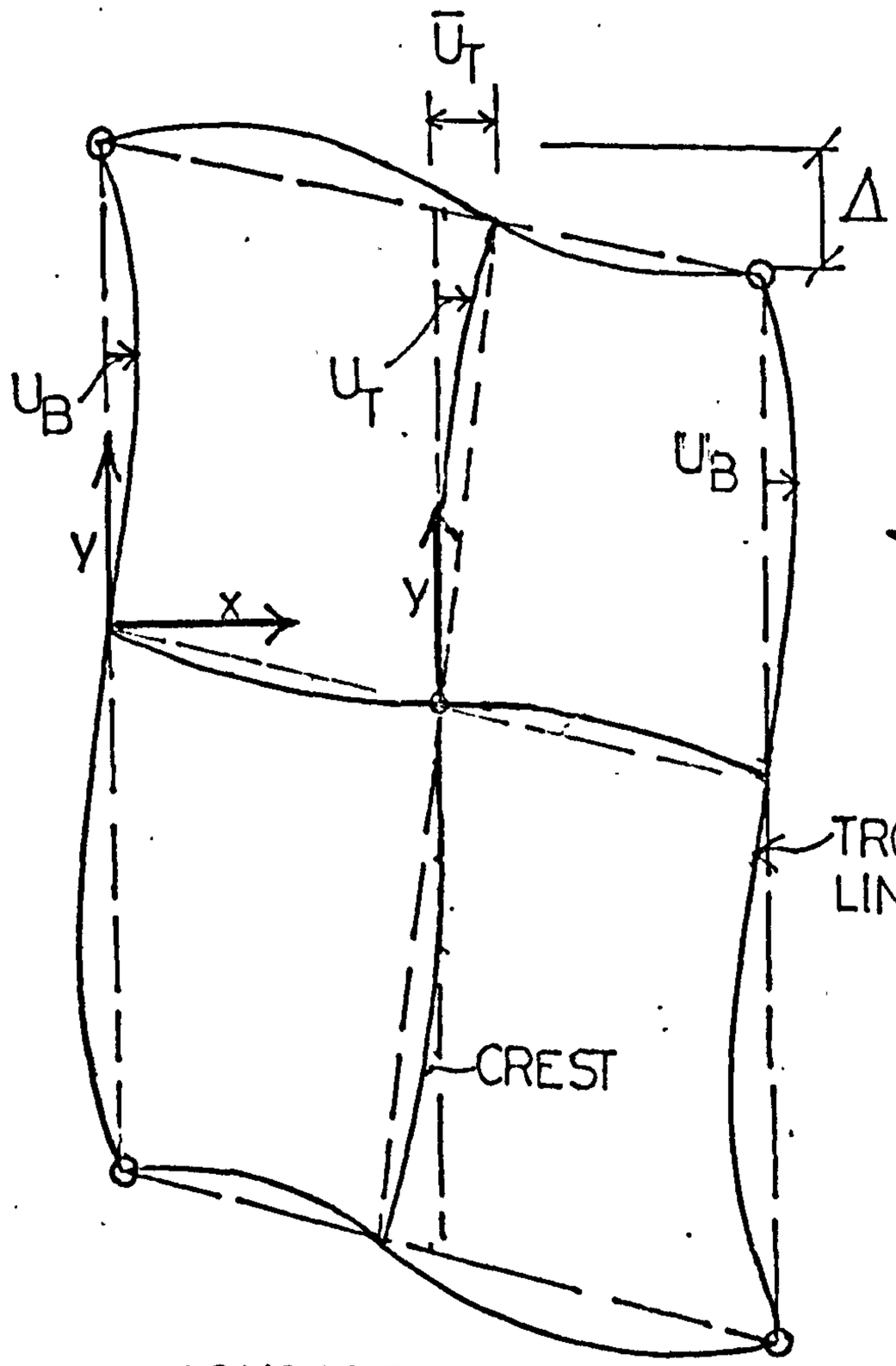

LONGITUDINAL DISPLACEMENTS

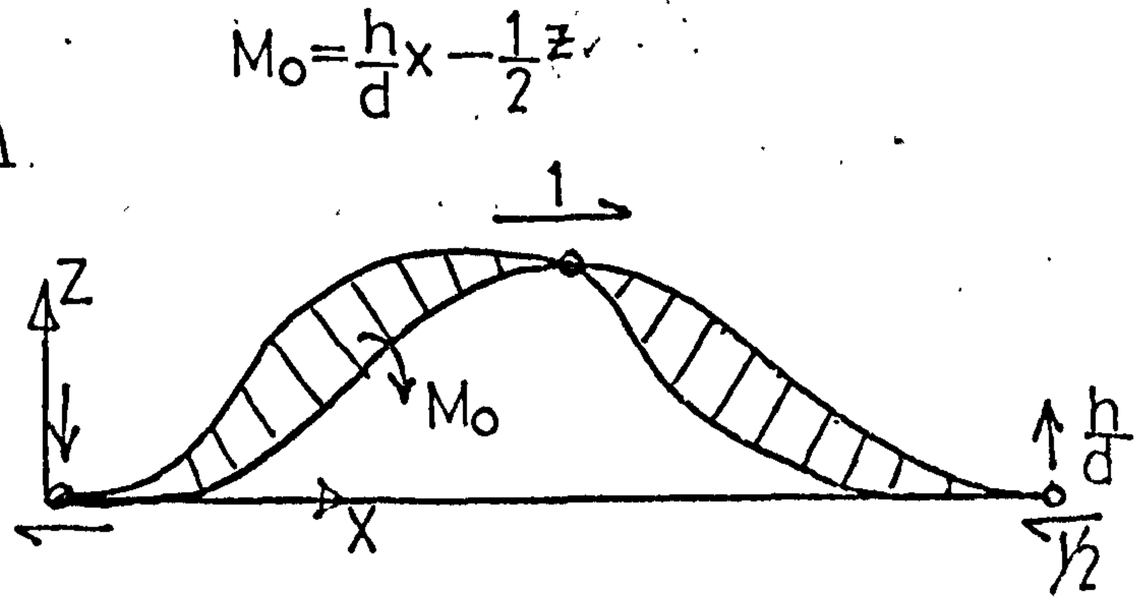

BENDING MOMENT DUE TO DISPLACEMENT $(U_T - U_B)$

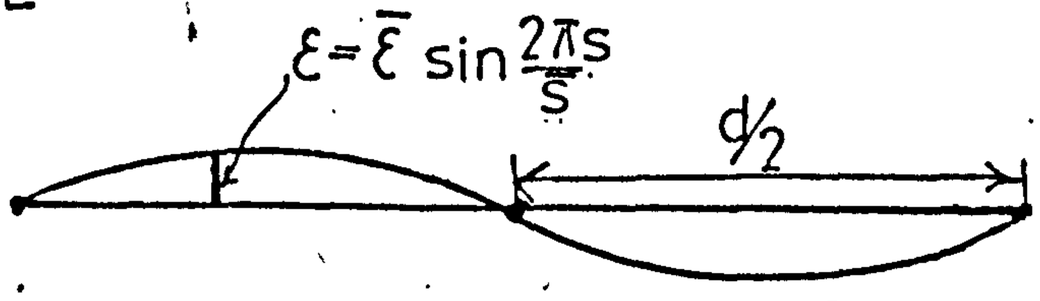

ε, AXIAL STRAIN DUE TO $\frac{d^2U_T}{dy^2}$ etc

$\bar{s}$ — profile perimeter

FIG (4.2)

EFFECT OF PROFILE, LENGTH, AND NUMBER OF INTERMEDIATE PURLINS ON K VALUE

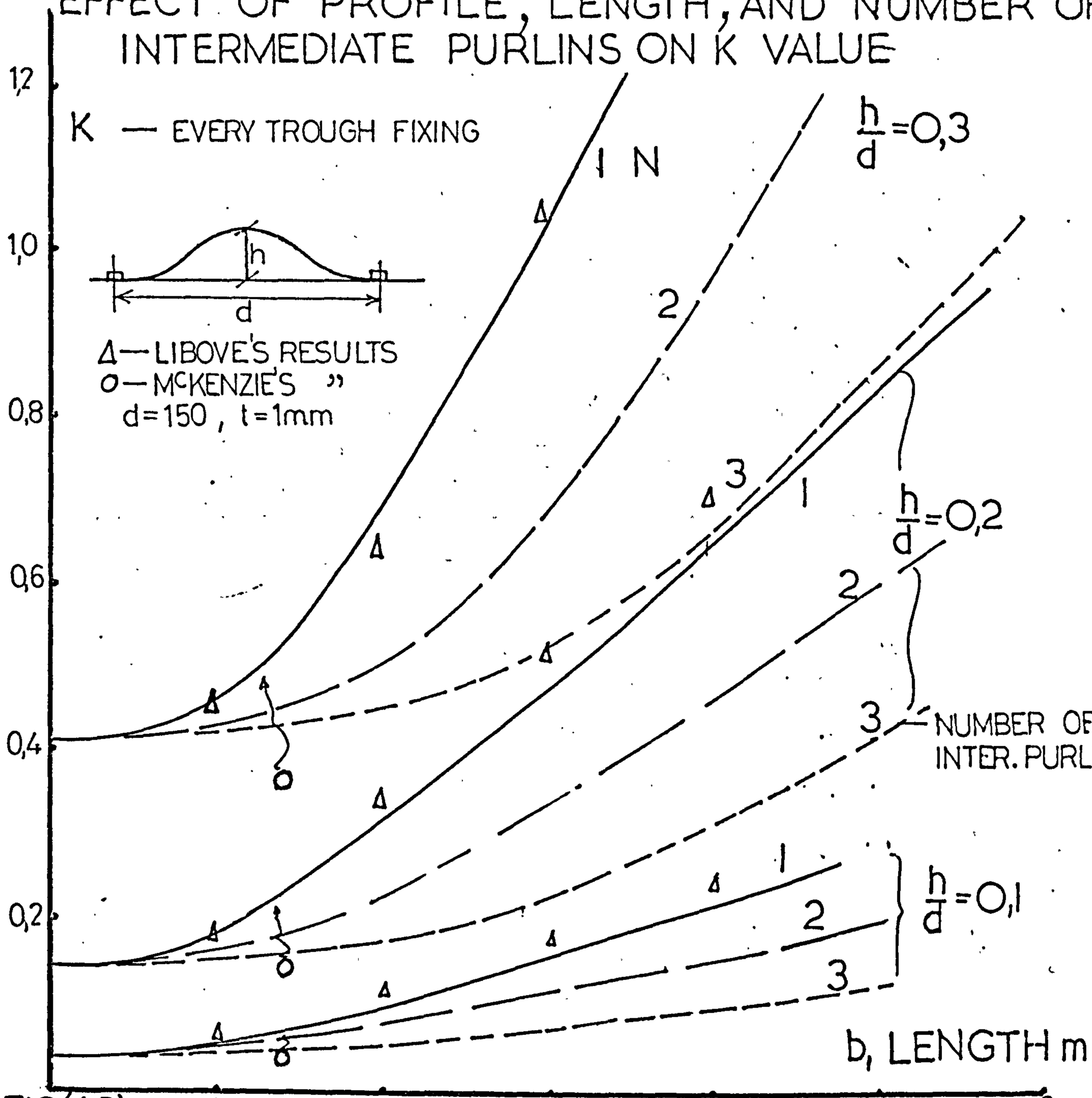

FIG(4.3)

EFFECT OF SHEET THICKNESS ON K VALUE

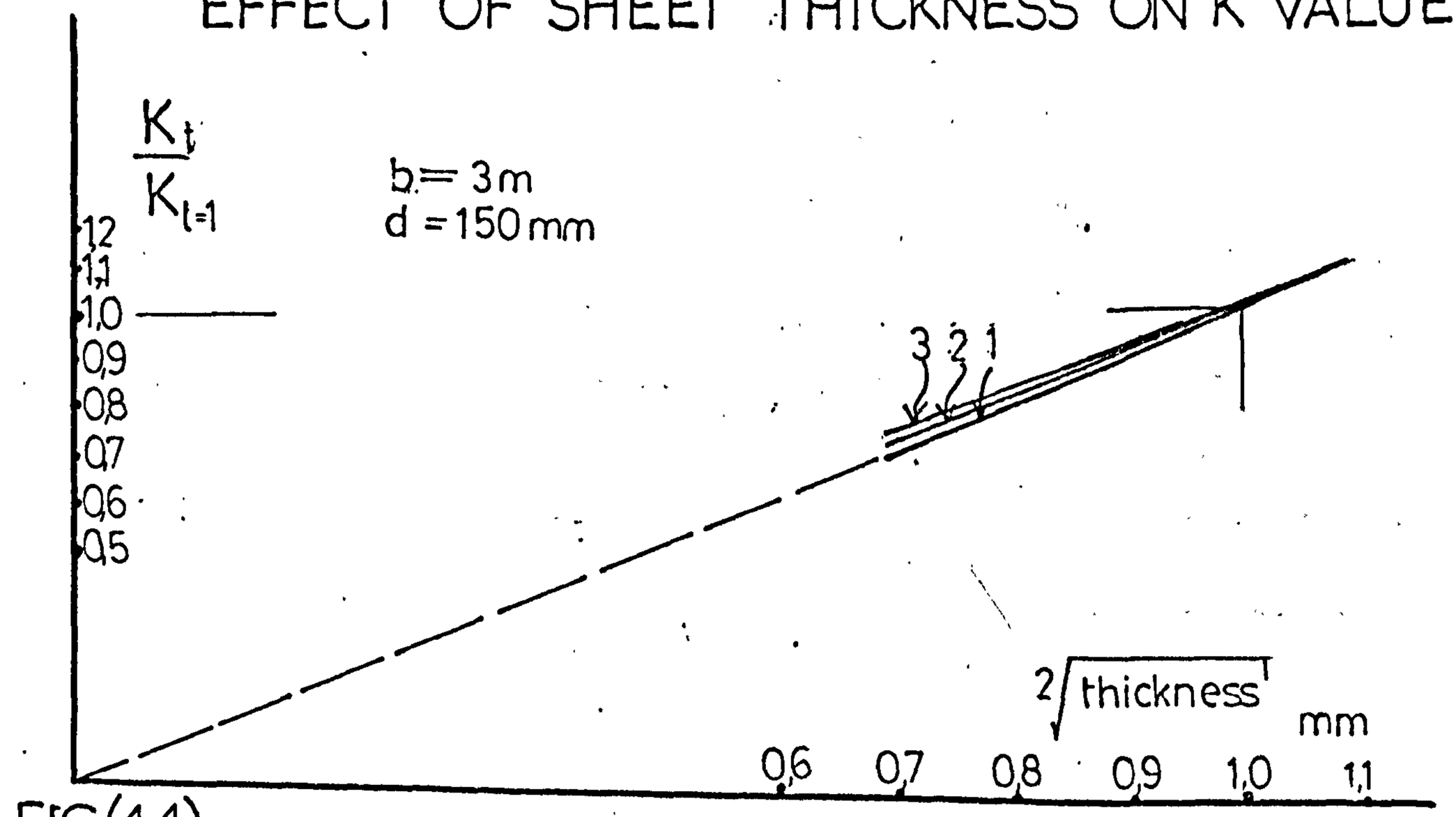

FIG(4.4)

DISPLACED SHAPE OF SINUSOIDAL PROFILES

1kN SHEAR — EVERY TROUGH FIXING

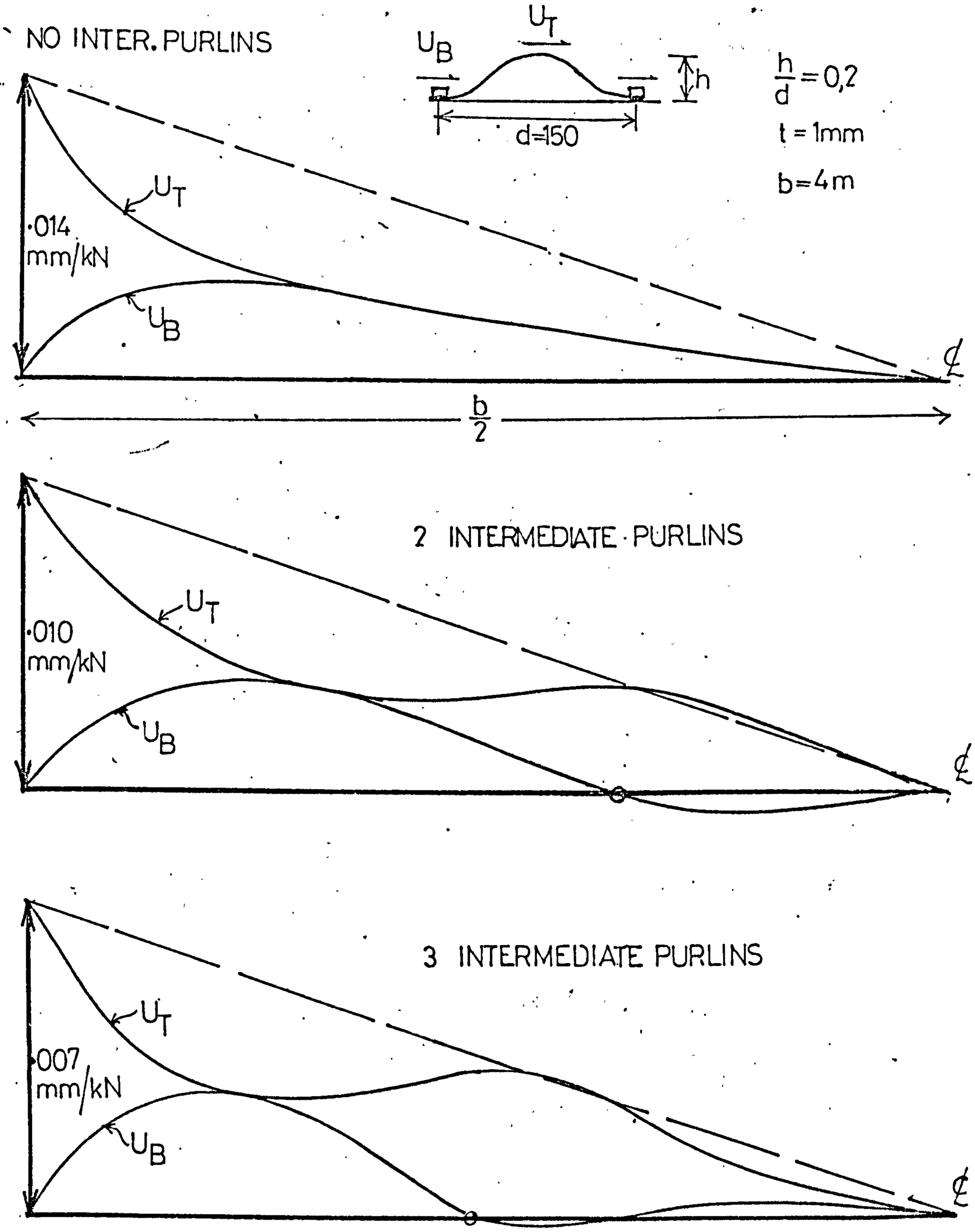

$\bar{K}$ VALUES DEPENDING ON NUMBER OF INTERMEDIATE PURLINS, N

N \ h/d	0.1	0,2	0,25	0,3	0,4
0, 1	·017	·052	·079	·112	·204
2	·011	·035	·051	·070	·124
3	·009	·023	·034	·050	·098

FIG(4.5)

ALTERNATE TROUGH FASTENING—SINUSOIDAL CORRUGATIONS —CONCERTINA ACTION, δ

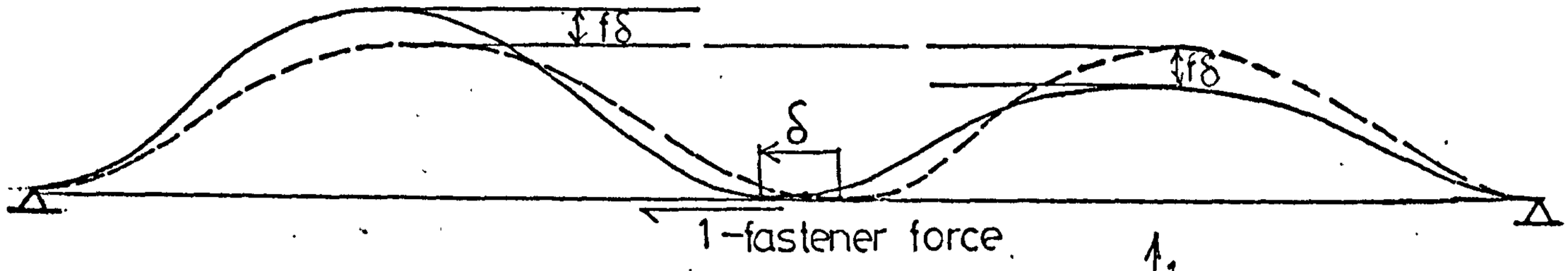

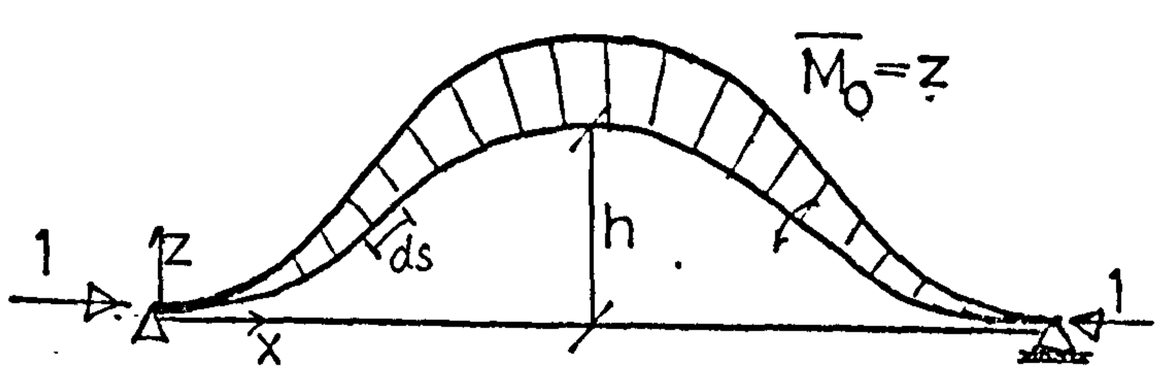

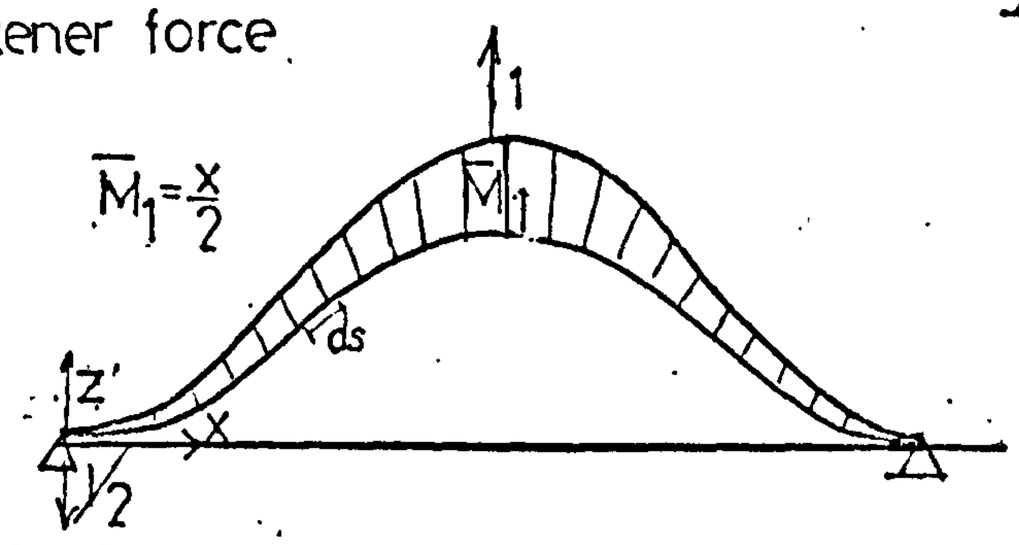

BENDING MOMENTS DUE TO CONCERTINA ACTION

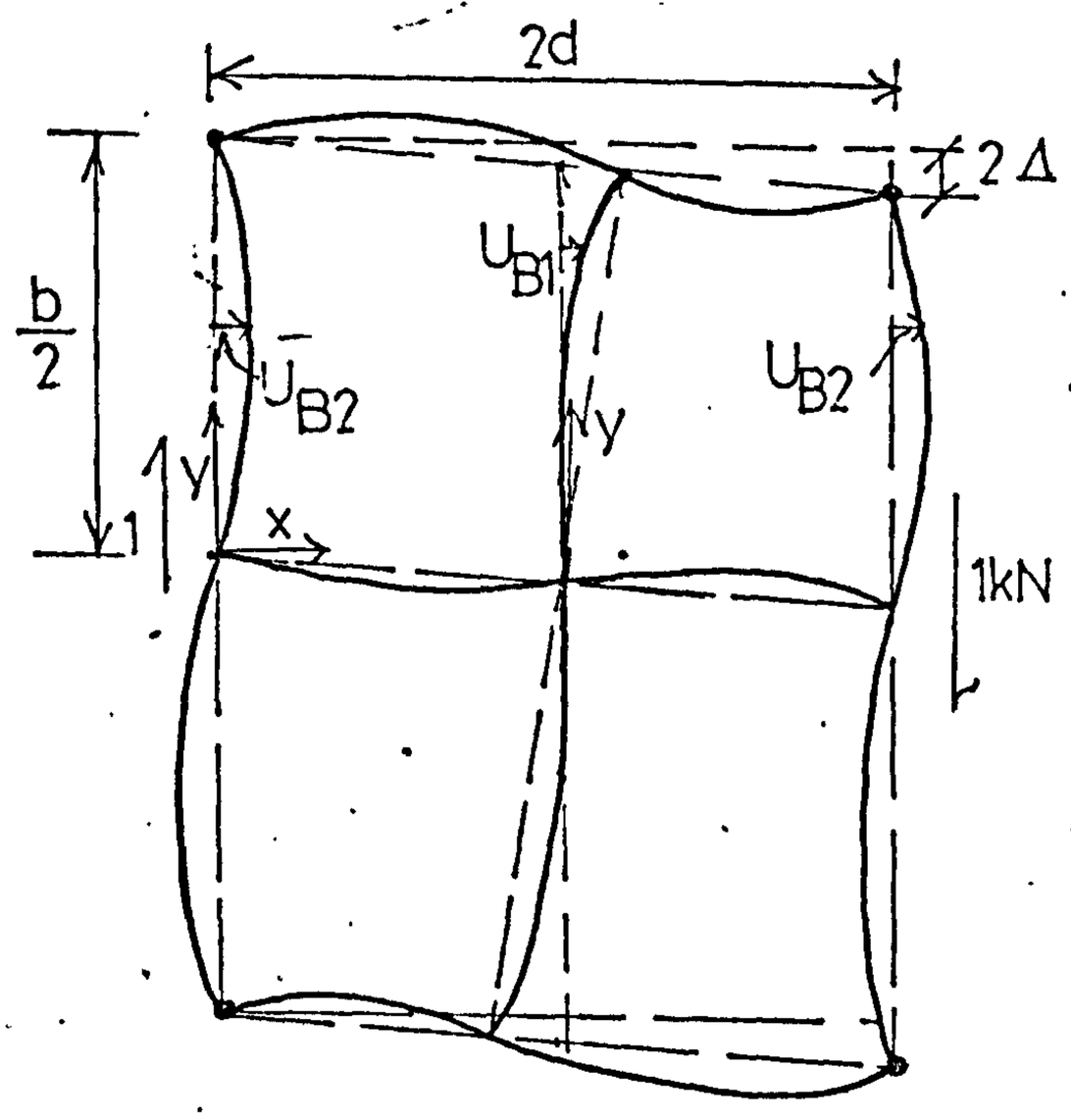

TROUGH DISPLACEMENTS

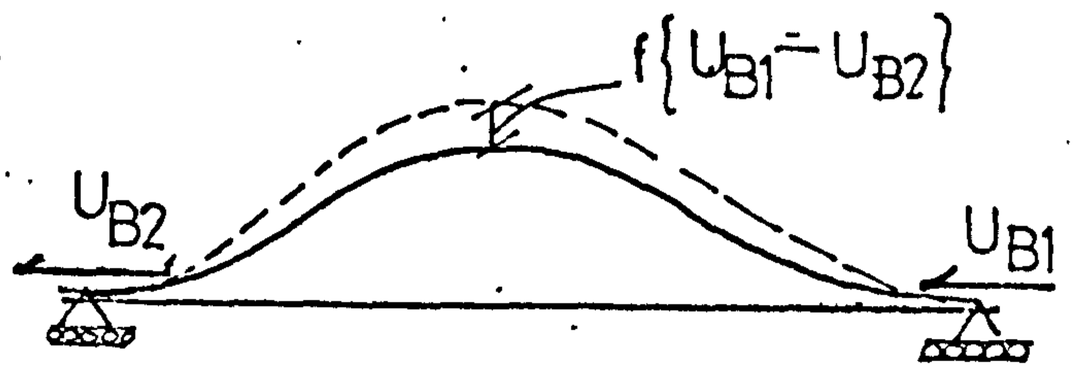

CREST UPLIFT, f

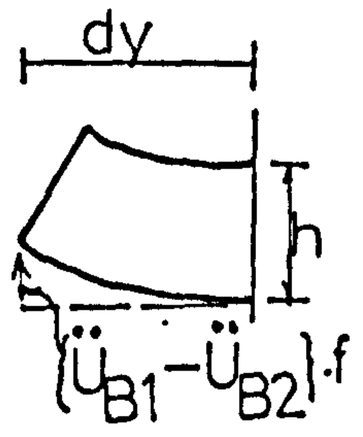

$\bar{s}$ — profile perimeter

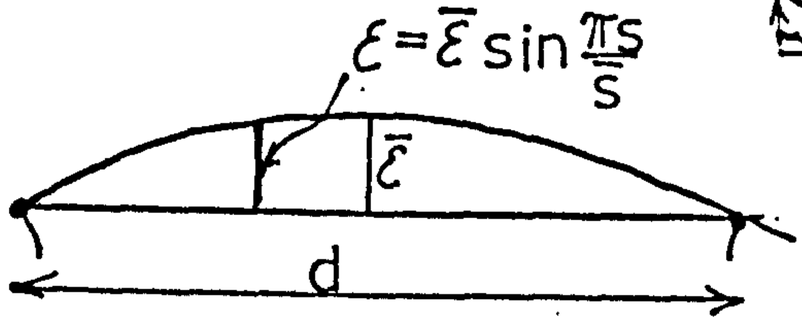

ε, AXIAL STRAIN DUE TO $\frac{d^2}{dy^2}\{U_{B1} - U_{B2}\} \times (\bar{s} + fh)$

FIG(4.6)

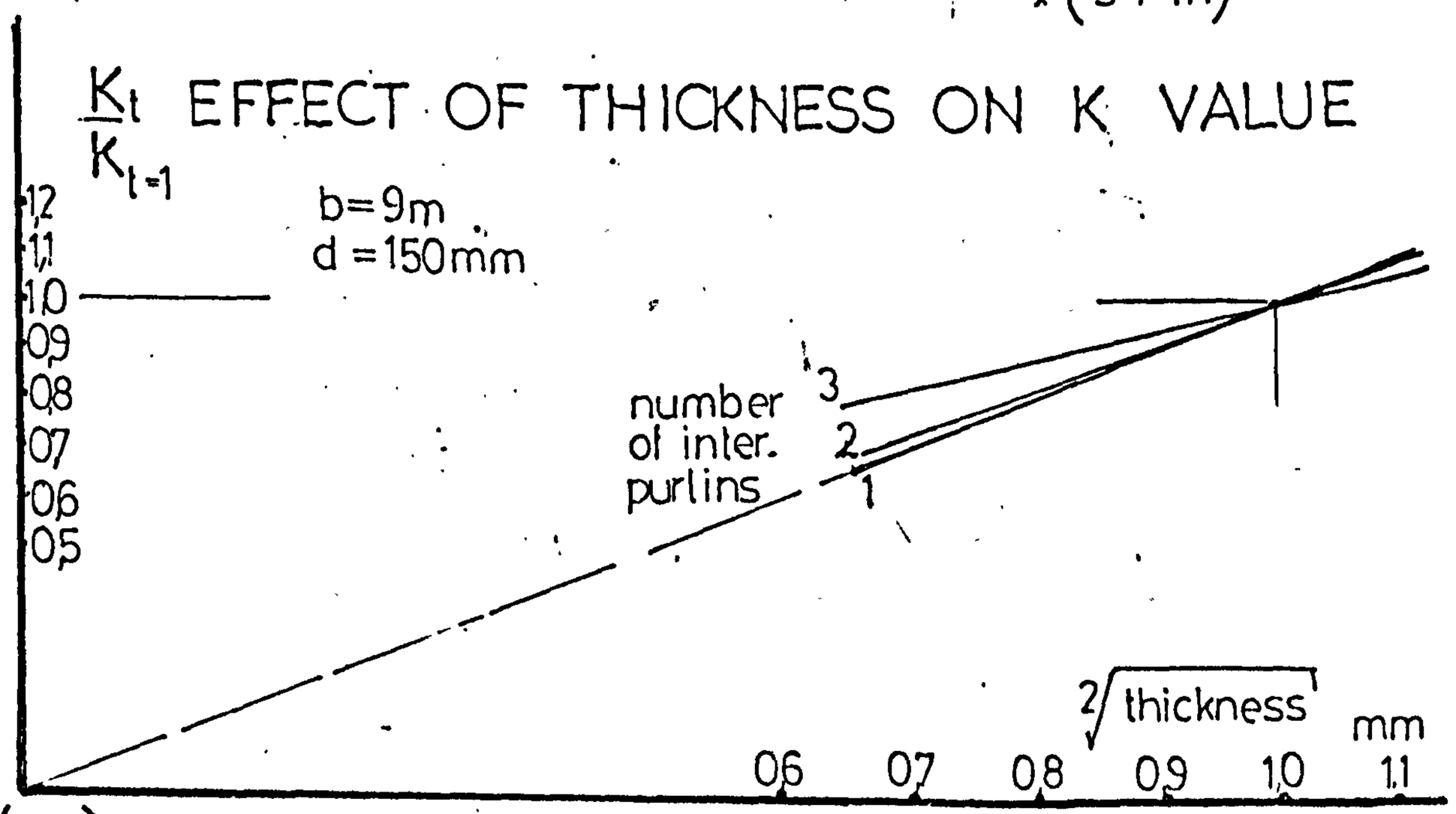

FIG (4.7)

EFFECT OF PROFILE, LENGTH, AND NUMBER OF INTERMEDIATE PURLINS ON K VALUE

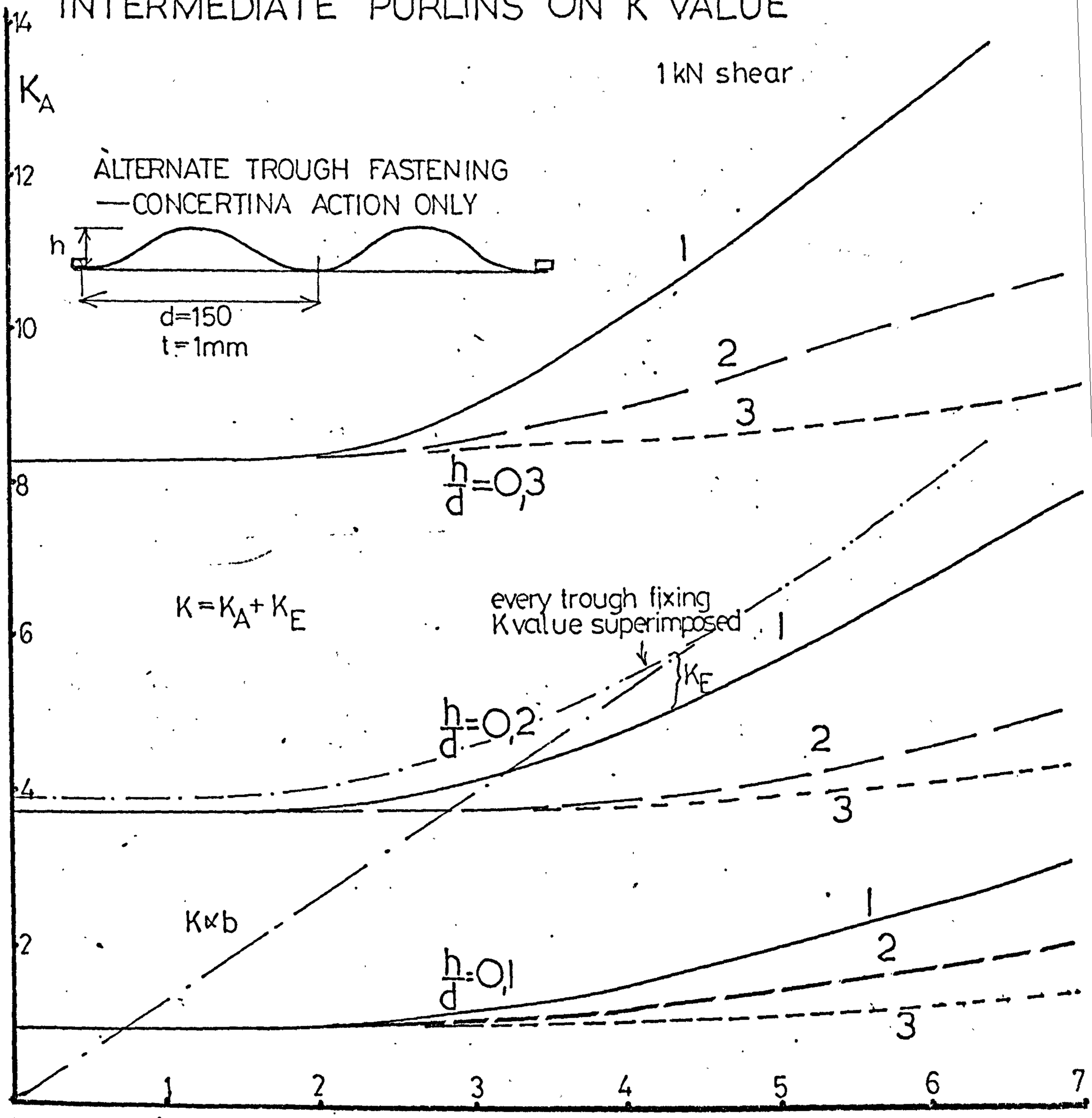

FIG(4.8)

ALTERNATE TROUGH FIXING. $\bar{K}$ VALUES. N—NUMBER OF INTERMEDIATE PURLINS

$$C_{1,1} = \frac{a d^{2.5} \bar{K}}{E t^{2.5} b^2}$$

choose greater of $\bar{K}$ or

$$\frac{0{,}144\, d^{1,5} K}{b . t^{0,5}}$$

N \ h/d	0,1	0,2	0,25	0,3	0,4
0,1	·134	·409	·566	·755	1,25
2	·092	·266	·386	·545	·982
3	·051	·159	·229	·338	·569

ALTERNATE TROUGH FIXING K VALUES

h/d	0,1	0,2	0,25	0,3	0,4
K	1,02	3,43	5,82	8,95	18,29

FIG(4.9)

SHEAR DEFORMATION OF A 'CLOSED-END' CORRUGATION

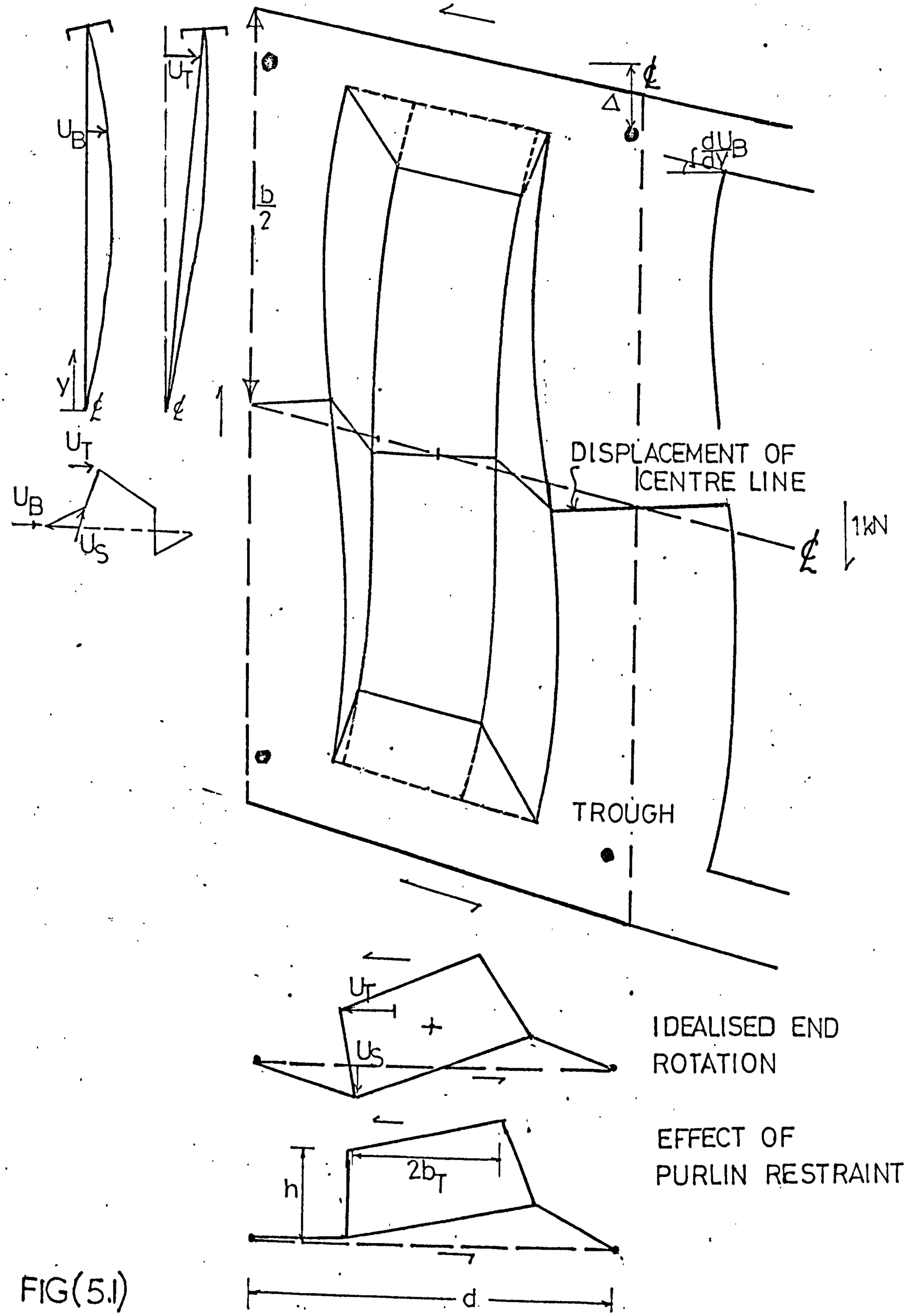

FIG(5.1)

FOLDED DOWN CORRUGATION

—— PROTOTYPE PRESSED SHEETING t = 0,95mm

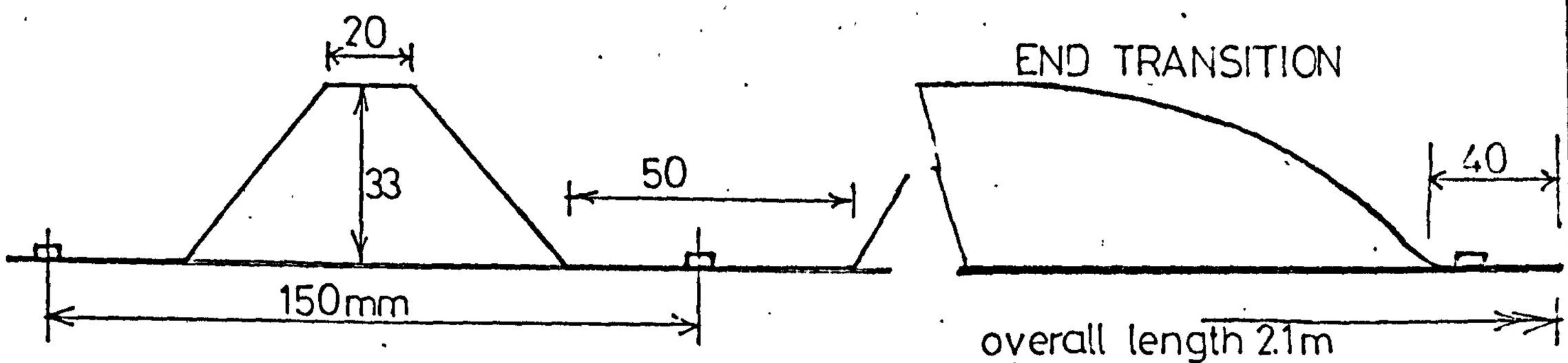

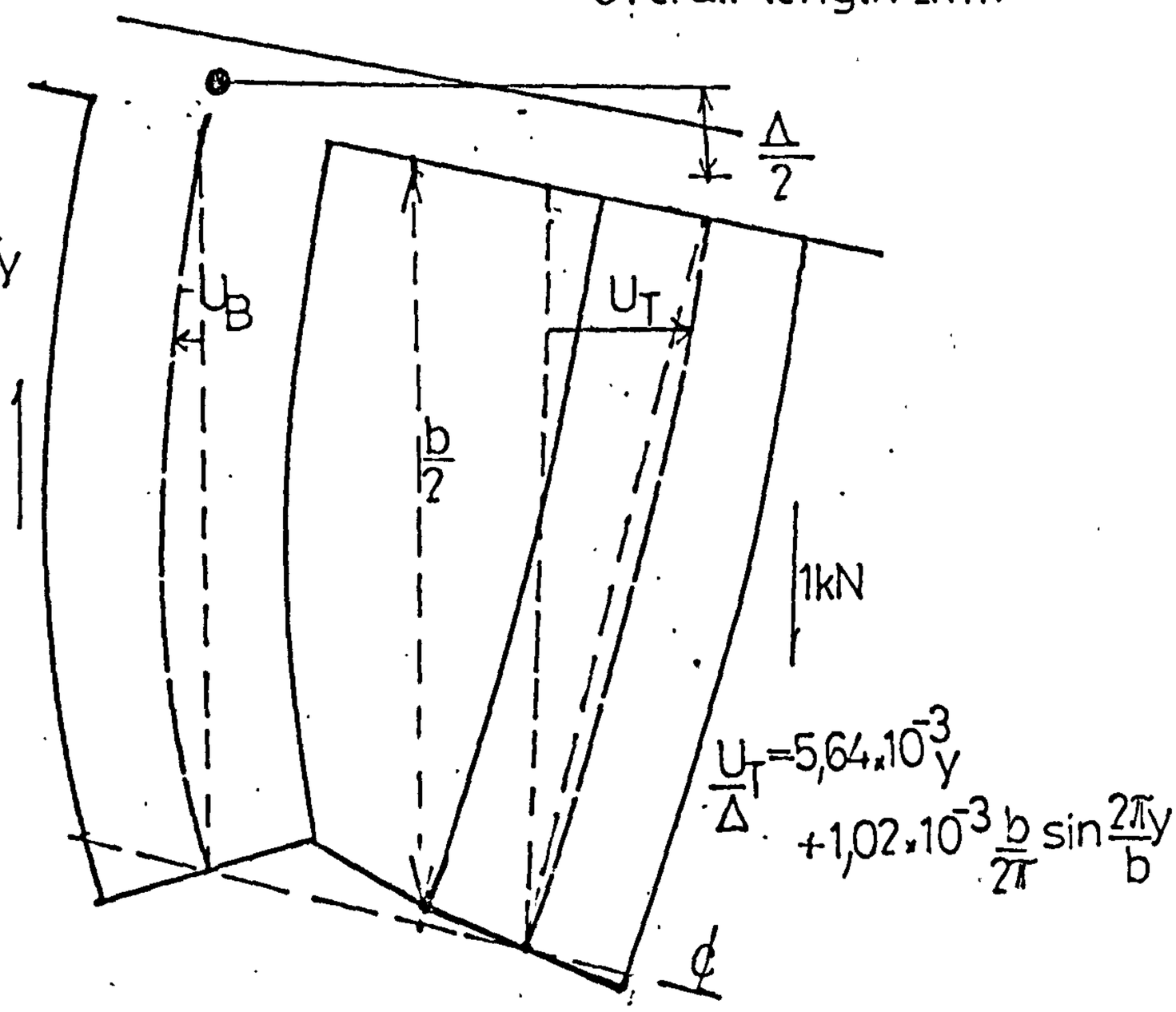

FIG(5.2)

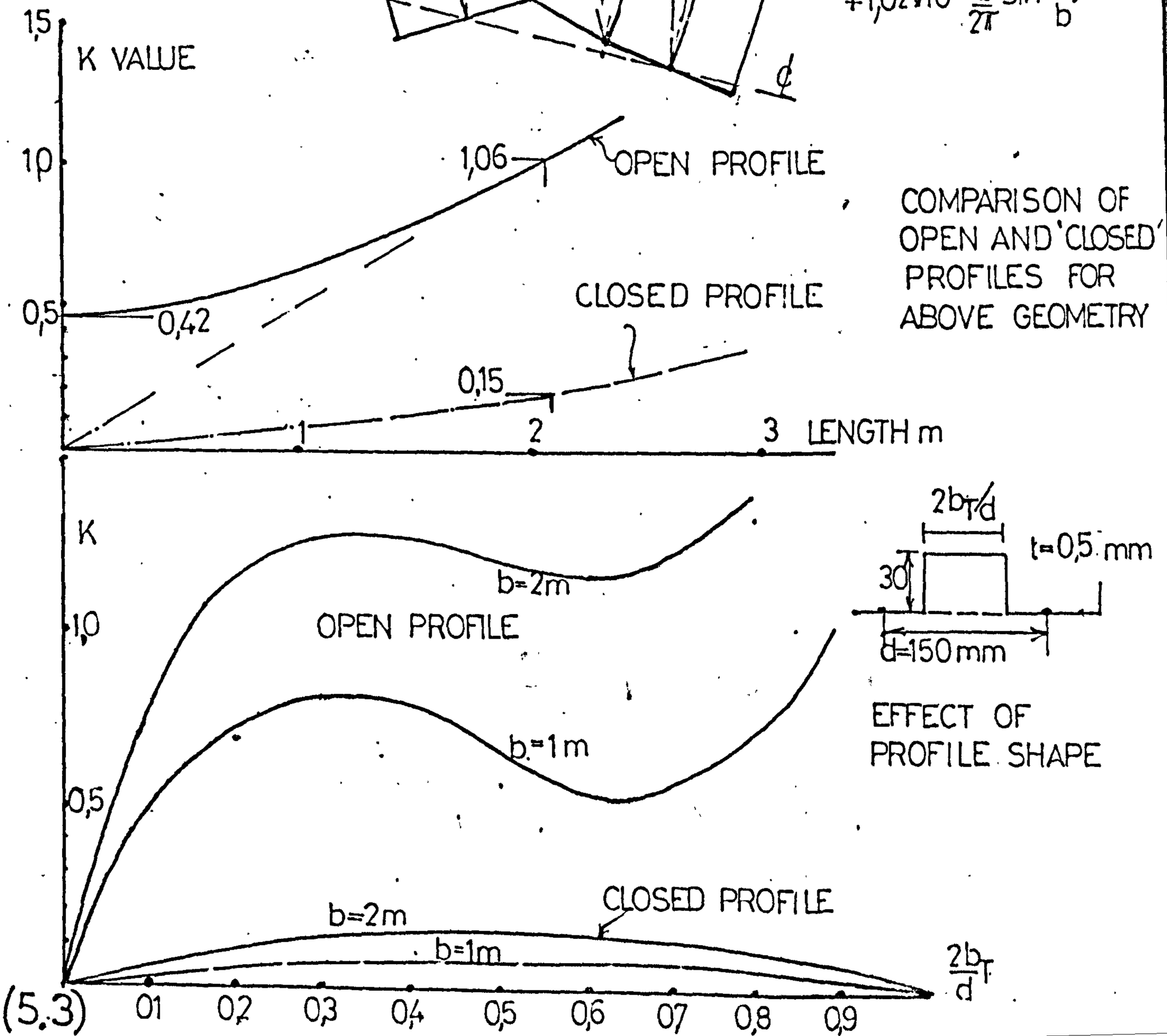

FIG(5.3)

SHEAR DEFORMATION OF A DOUBLE-FASTENED CORRUGATION

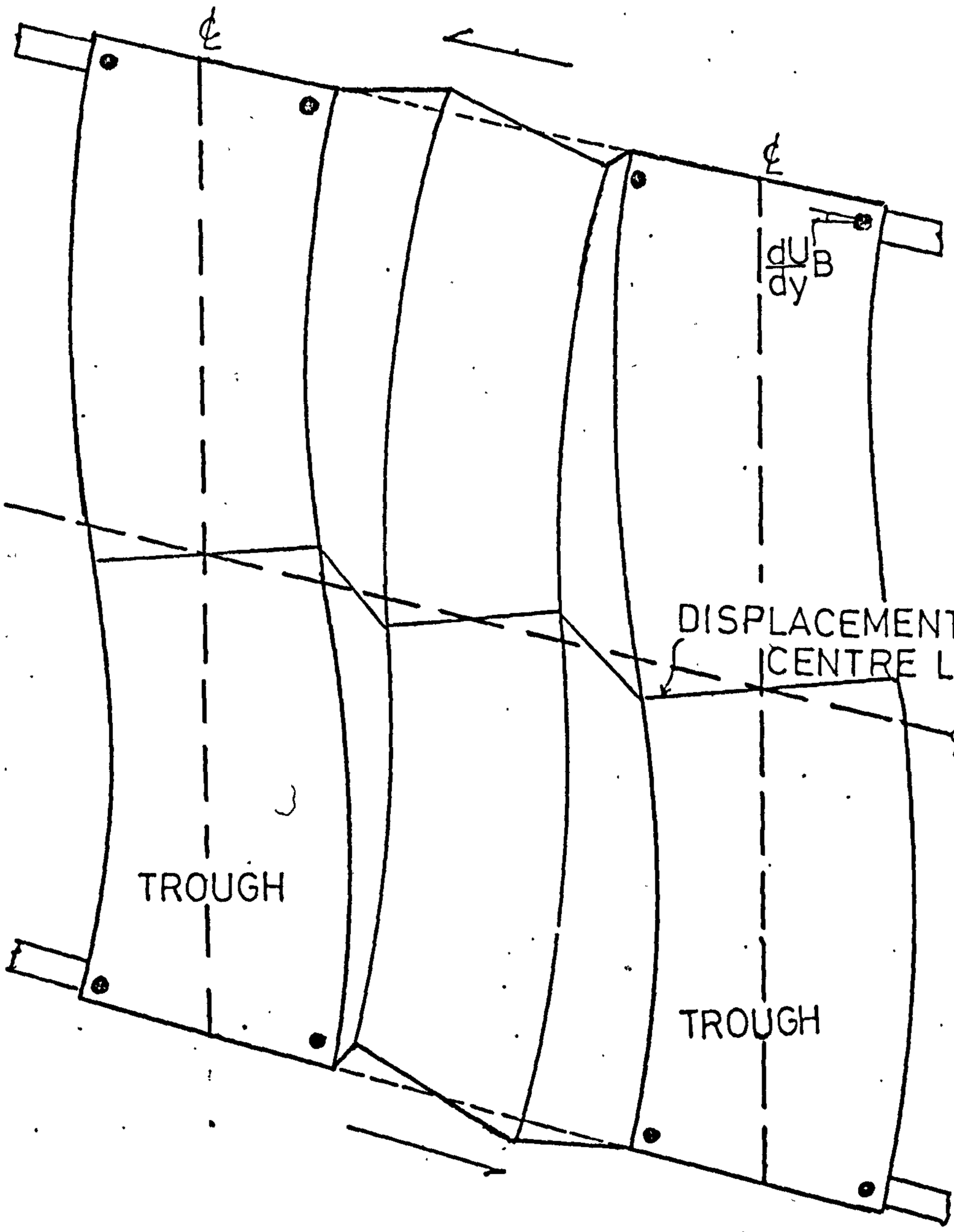

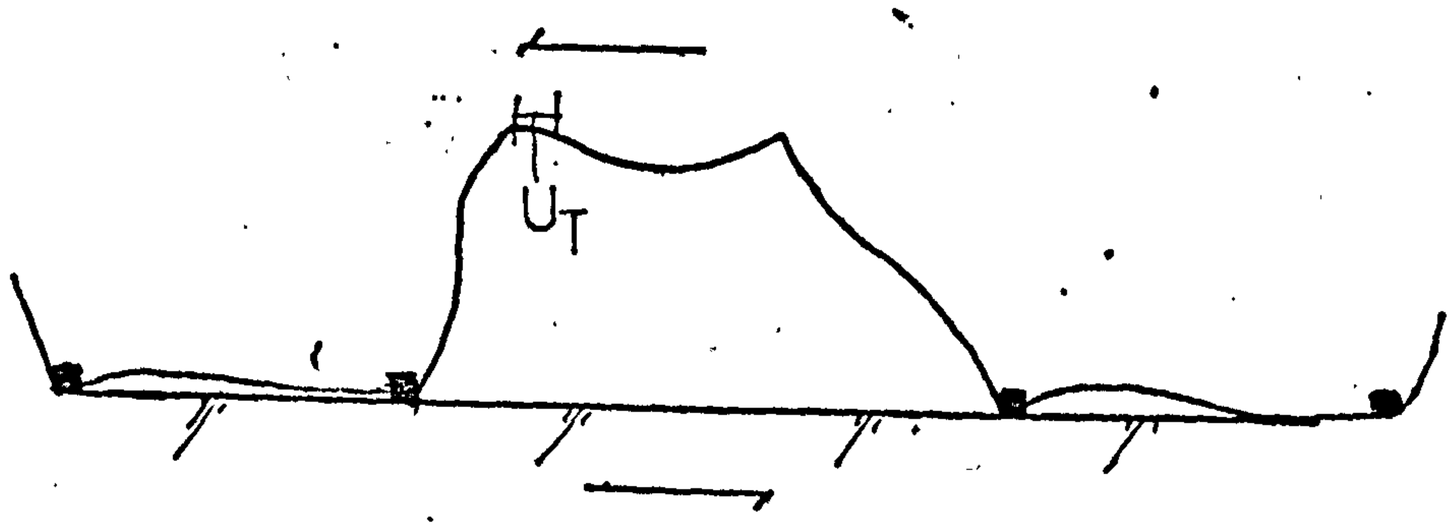

END DISTORTION

FIG(5.4)

DOUBLE – FASTENED CORRUGATION

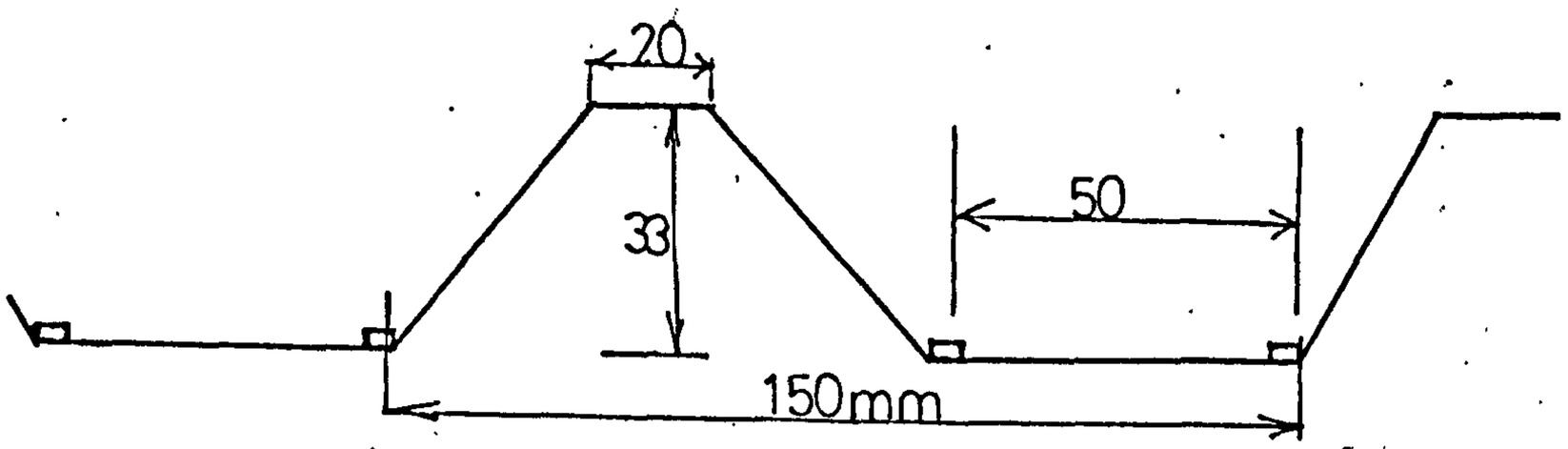

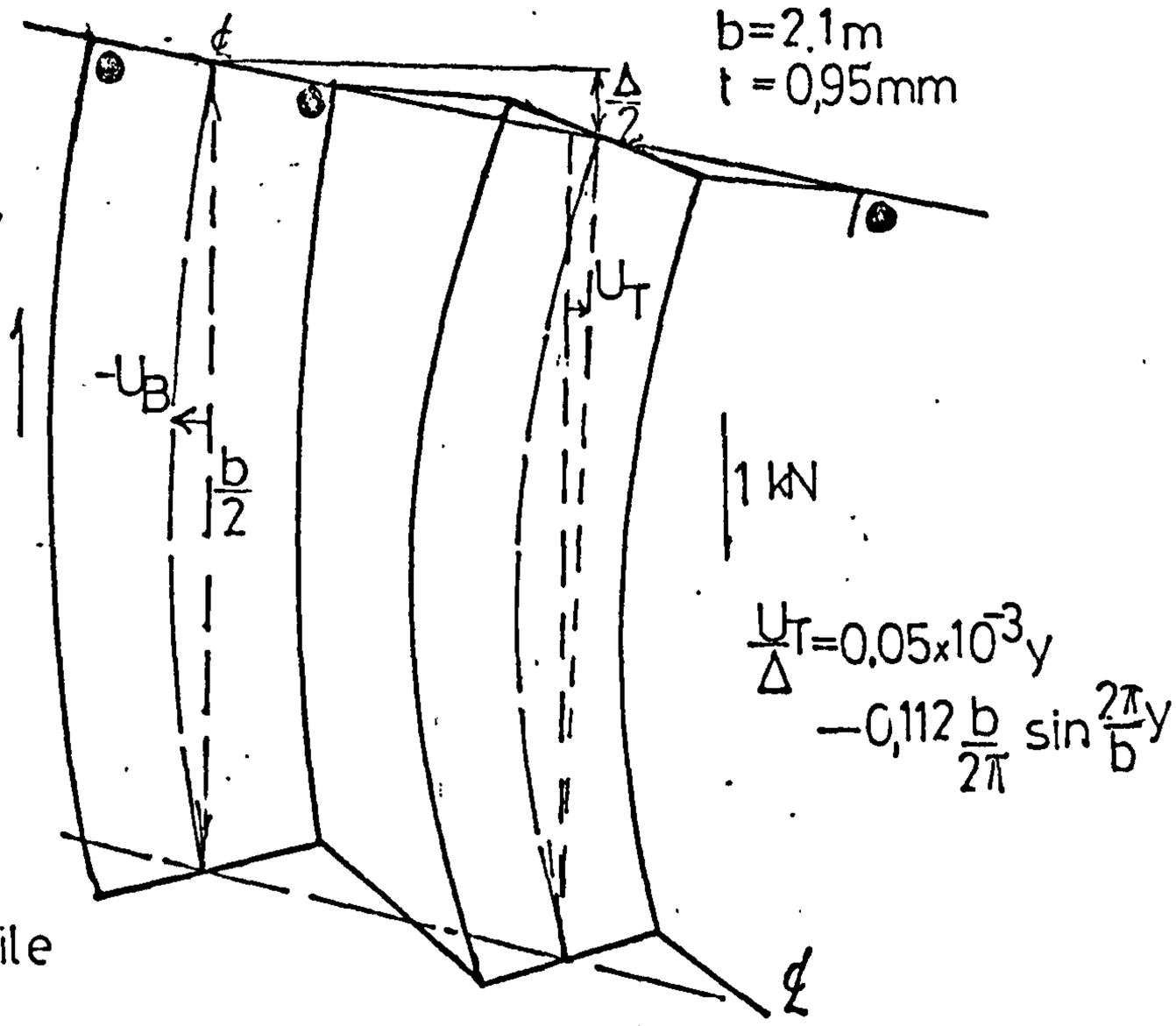

CROSS-SECTION DISPLACEMENTS

FIG(5,5)

K = 0,03
– cf 1,06 – open profile

EFFECT OF PROFILE SHAPE ON K VALUE FOR DOUBLE TROUGH FASTENED CORRUGATIONS

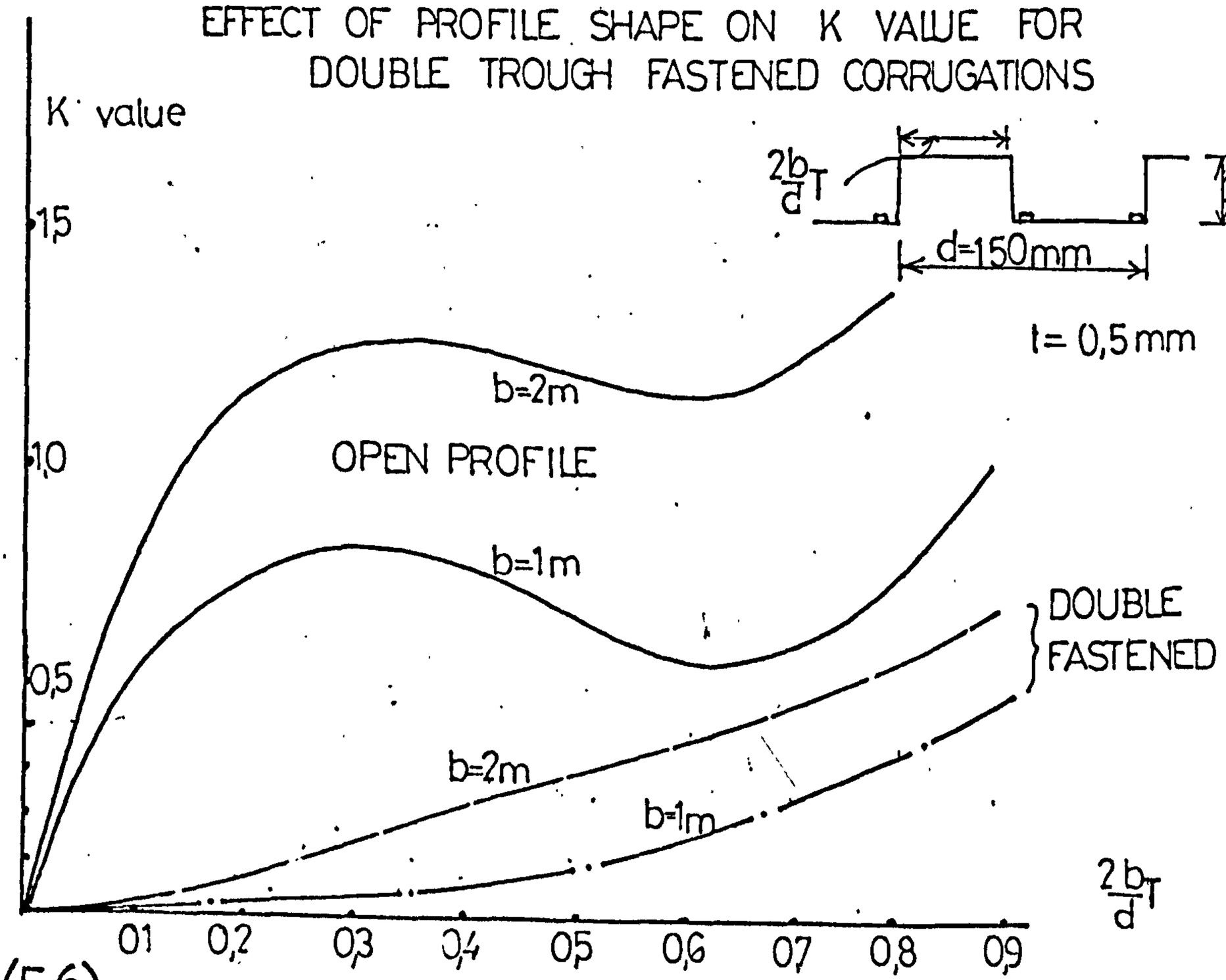

FIG(5.6)

EFFECT OF SHEET EXTENDING BEYOND PURLINS

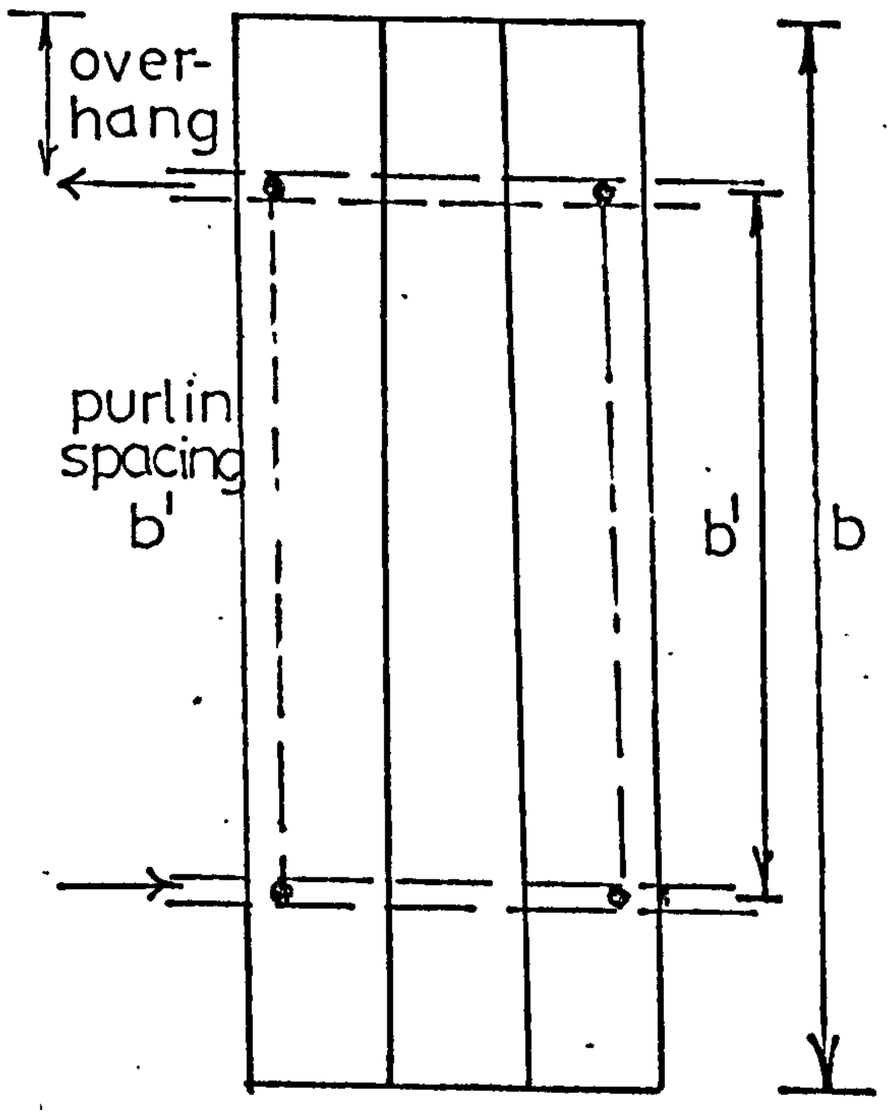

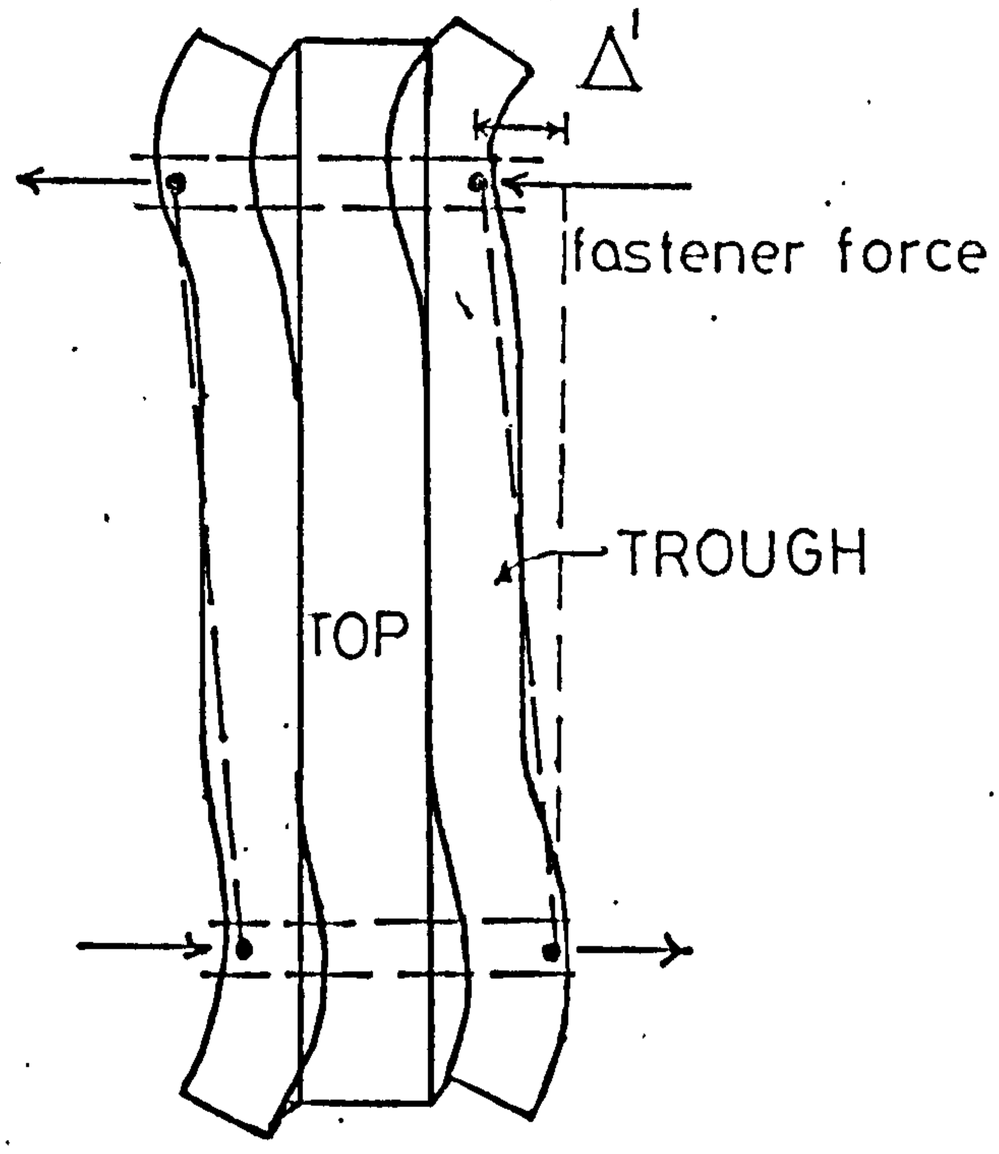

LOCALIZED END DISTORTION

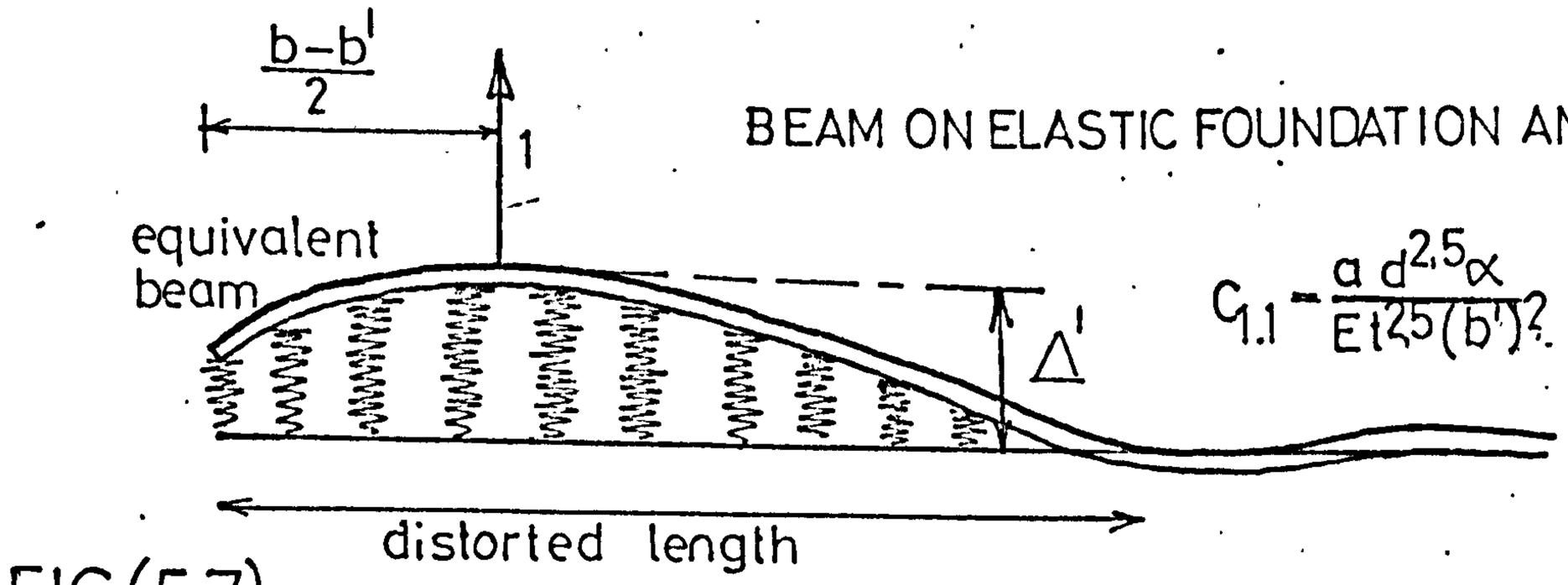

$$C_{1.1} = \frac{a\, d^{2.5} \alpha}{E t^{2.5} (b')^2}$$

BEAM ON ELASTIC FOUNDATION ANALOGY

FIG(5.7)

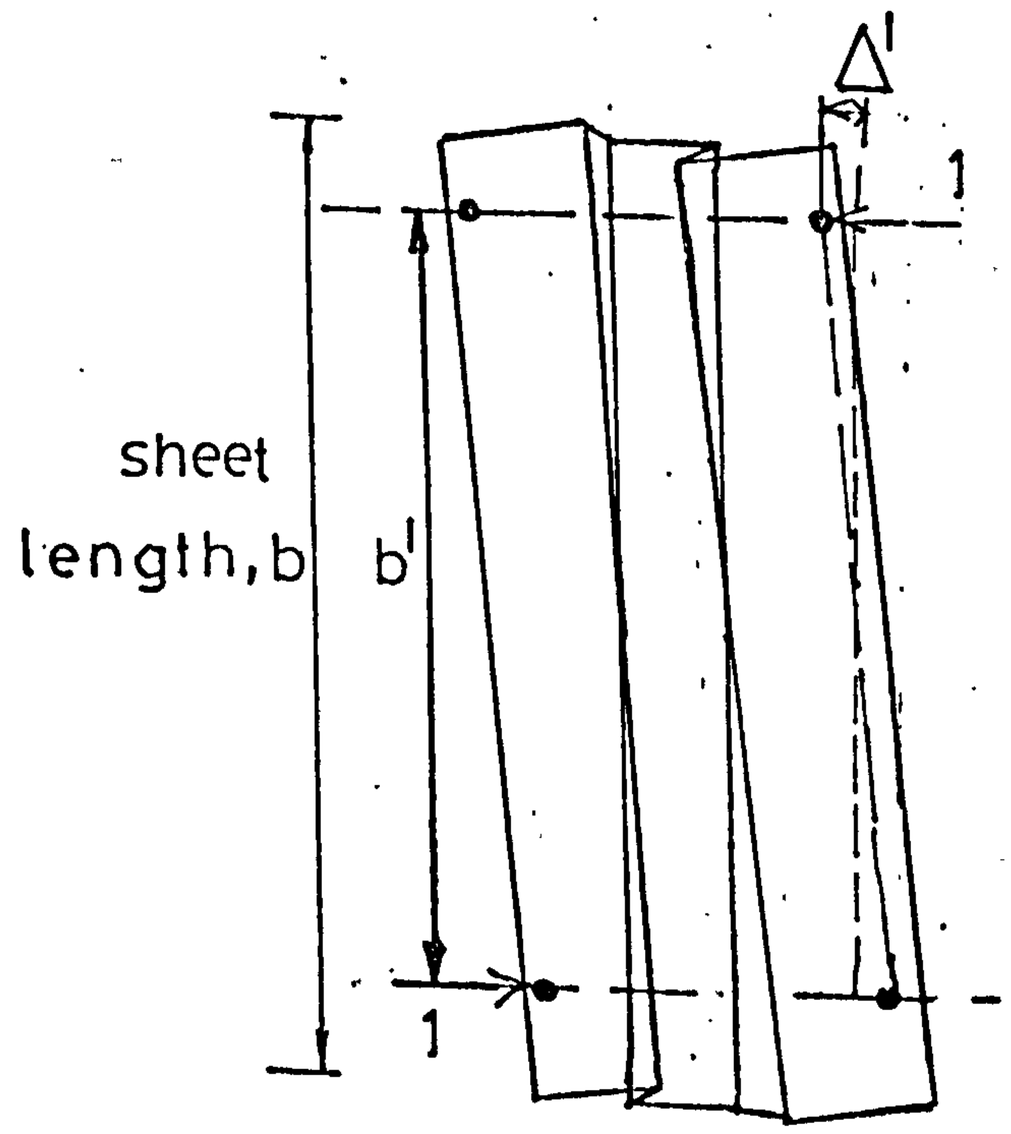

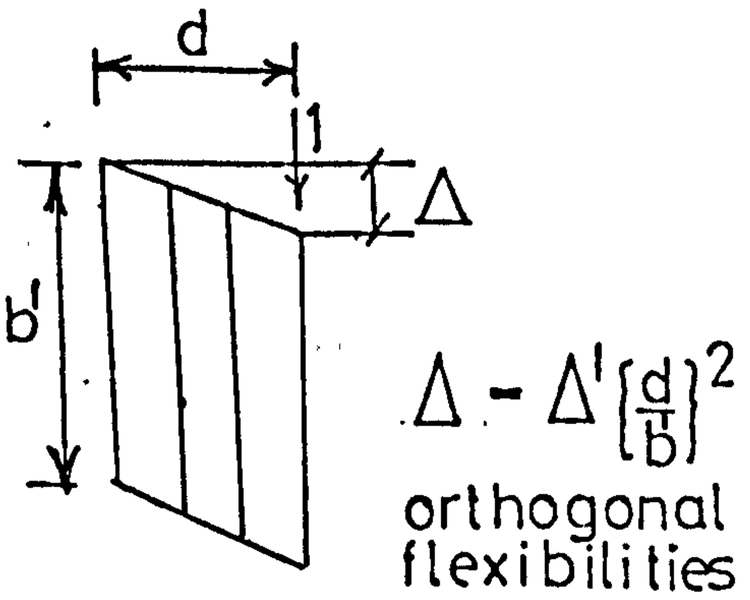

$$\Delta = \Delta' \left[\frac{d}{b}\right]^2$$

orthogonal
flexibilities

RIGID PLATE MOVEMENTS

$$C_{1.1} = \frac{0{,}144 . a . d^4 . K}{E\, t^3\, b (b')^2}$$

FIG(5,8)

EFFECT OF INSULATION COVERING

—ALTERNATE TROUGH FIXING

MODES OF RESISTANCE

1.

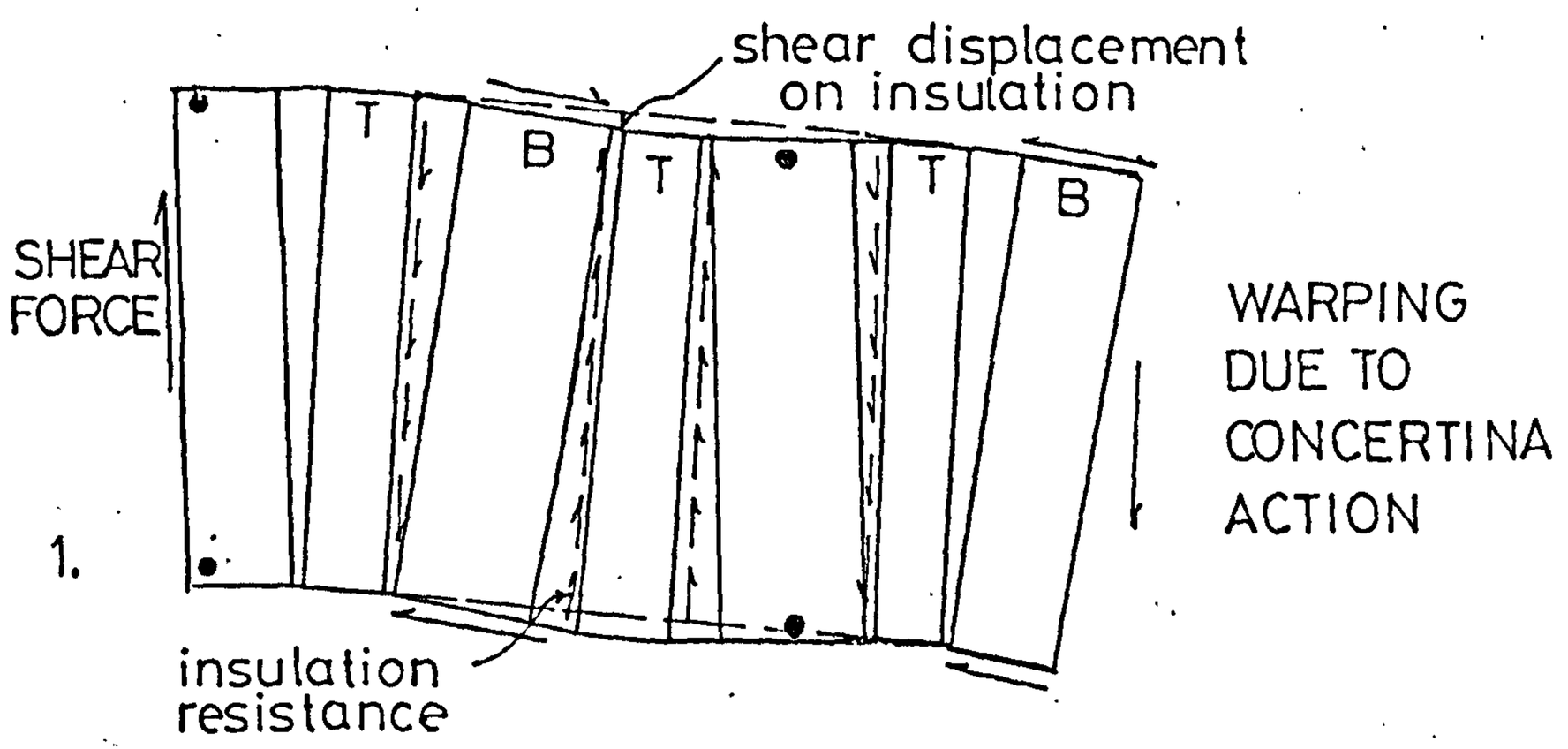

2.

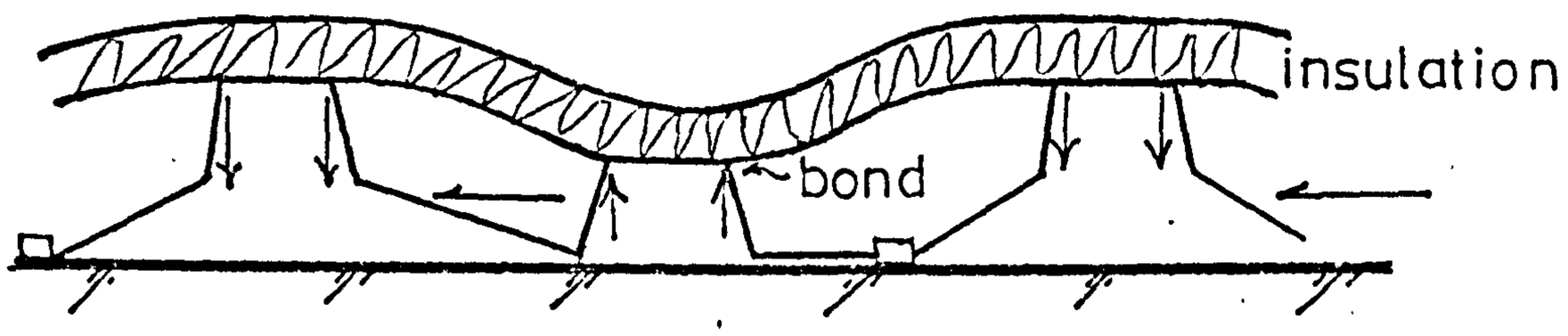

END MOVEMENTS—INSULATION BENDING

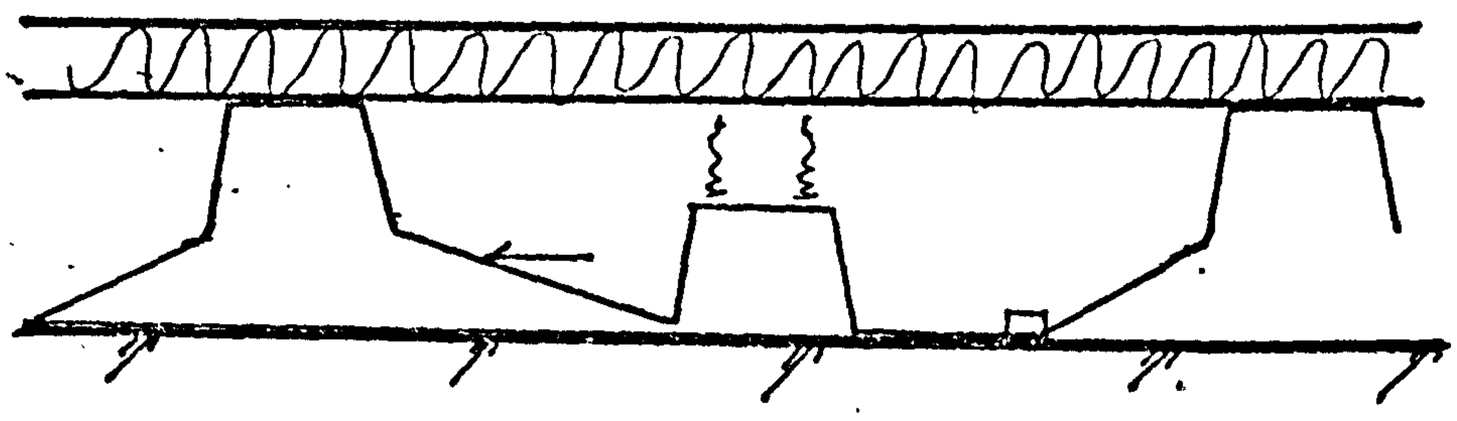

EXCESSIVE DEFORMATION — BOND BROKEN

3.

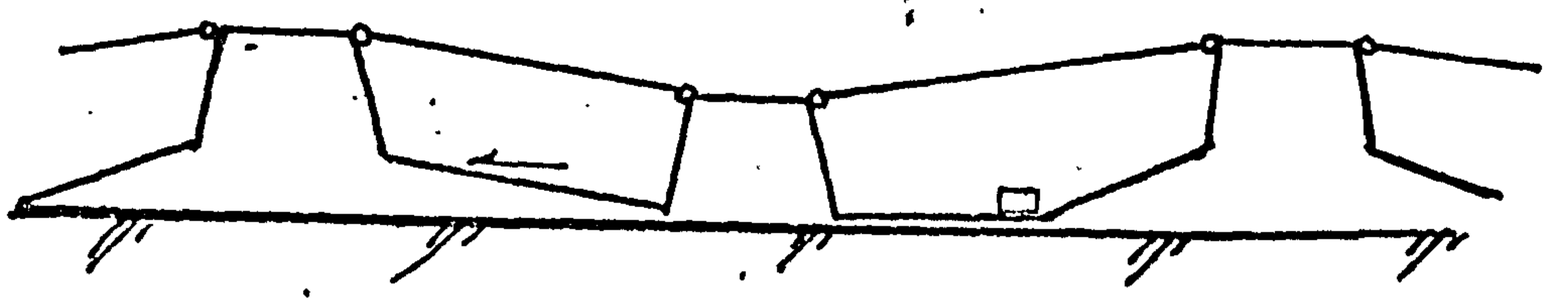

INSULATION PREVENTS CREST SEPARATION

FIG (5.9)

EFFECT OF INSULATION COVERING

1. SHEAR OF INSULATION BETWEEN CRESTS

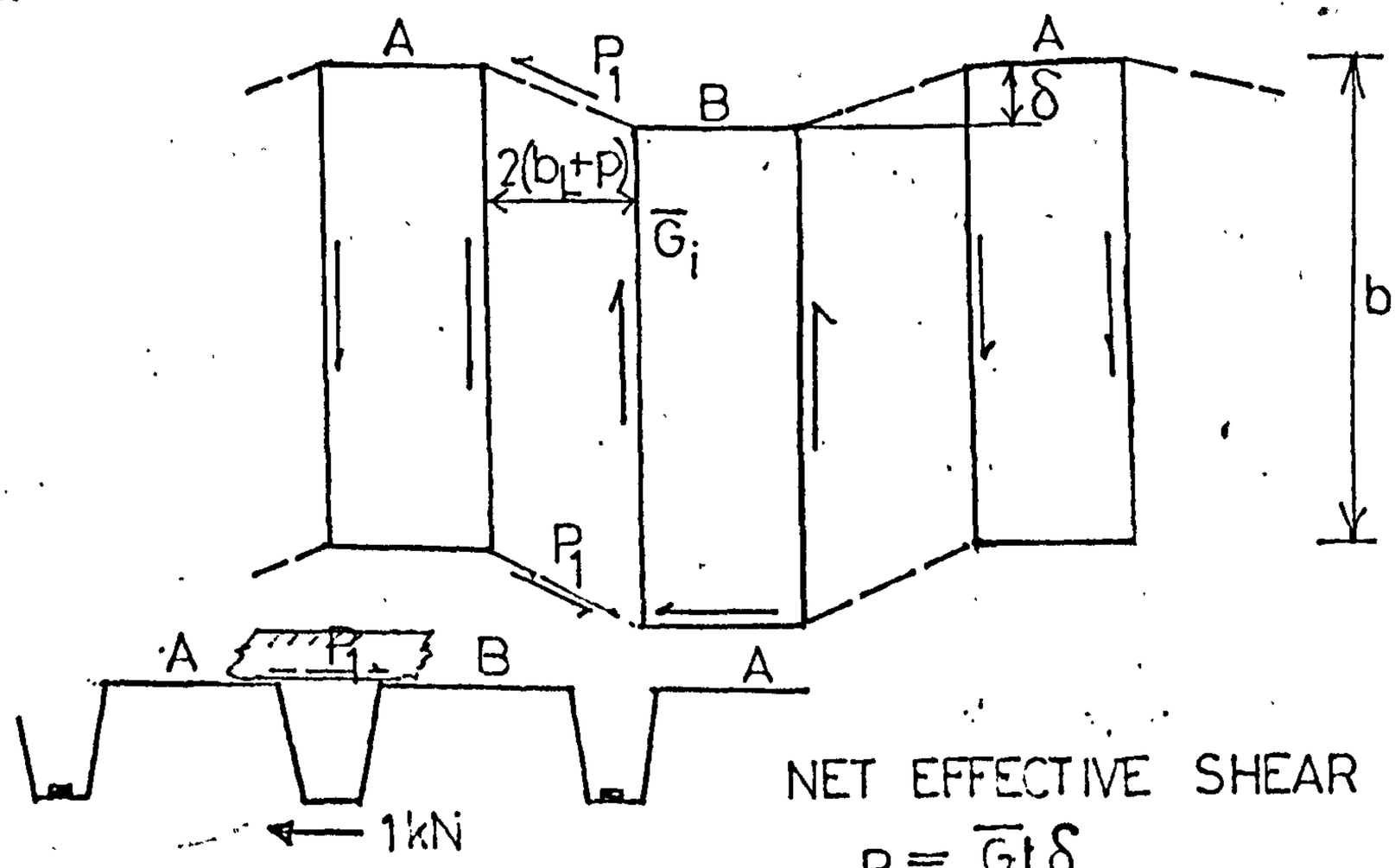

COMPOSITE ACTION

NET EFFECTIVE SHEAR FORCE $= (1 - P_1)$

$P_1 = \bar{G}_i t \delta$

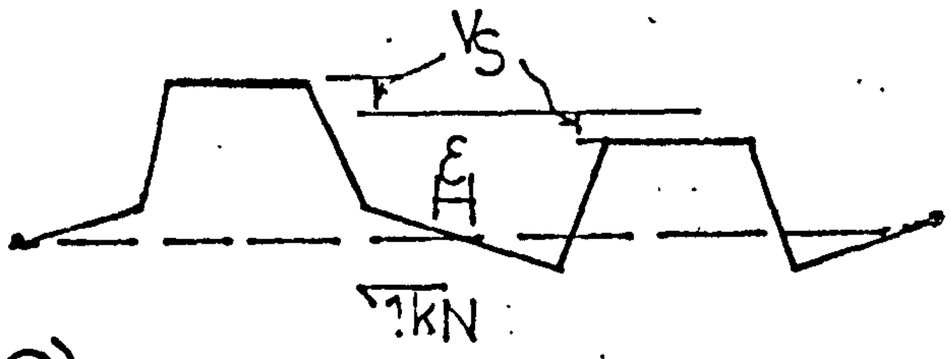

FINAL DISPLACEMENTS

V_S and ε $\therefore$ $\delta = \dfrac{(4 b_s V_s + 2 b_L \varepsilon)}{b/2}$

FIG (5.10)

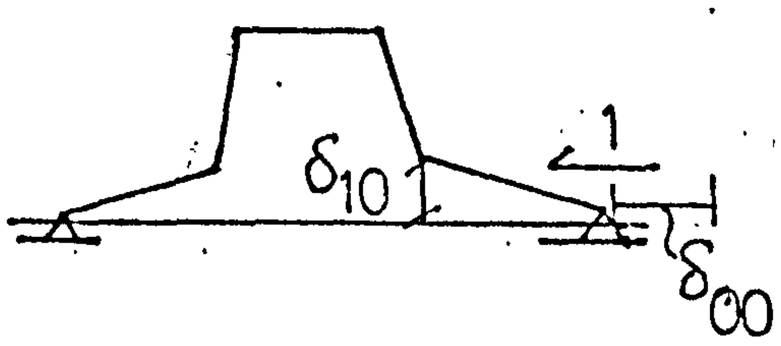

FREE DEFORMATION

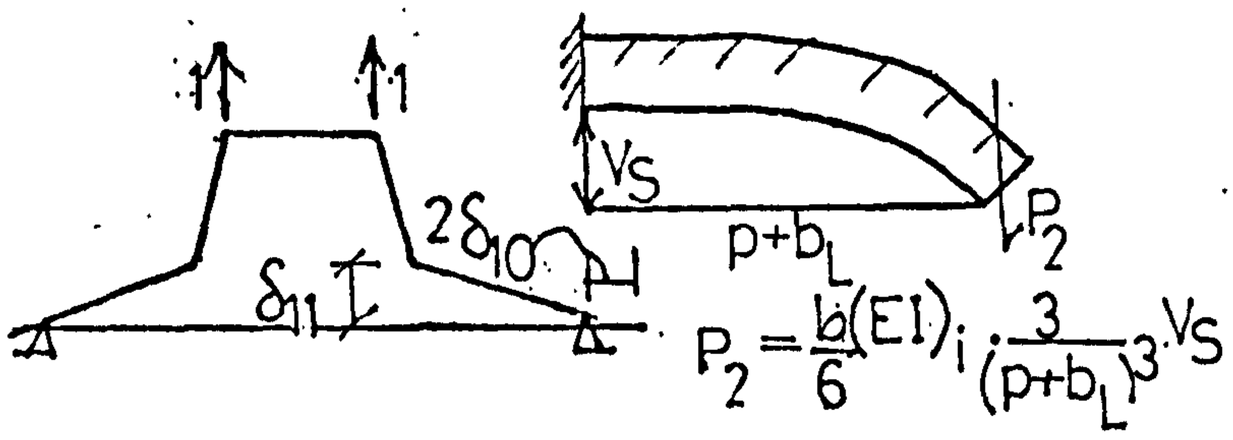

$P_2 = \dfrac{b}{6}(EI)_i \cdot \dfrac{3}{(p+b_L)^3} V_S$

2. EFFECT OF INSULATION BENDING

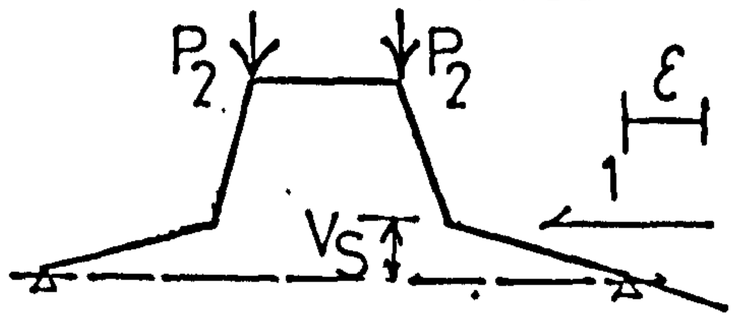

LAYERS OF INSULATION

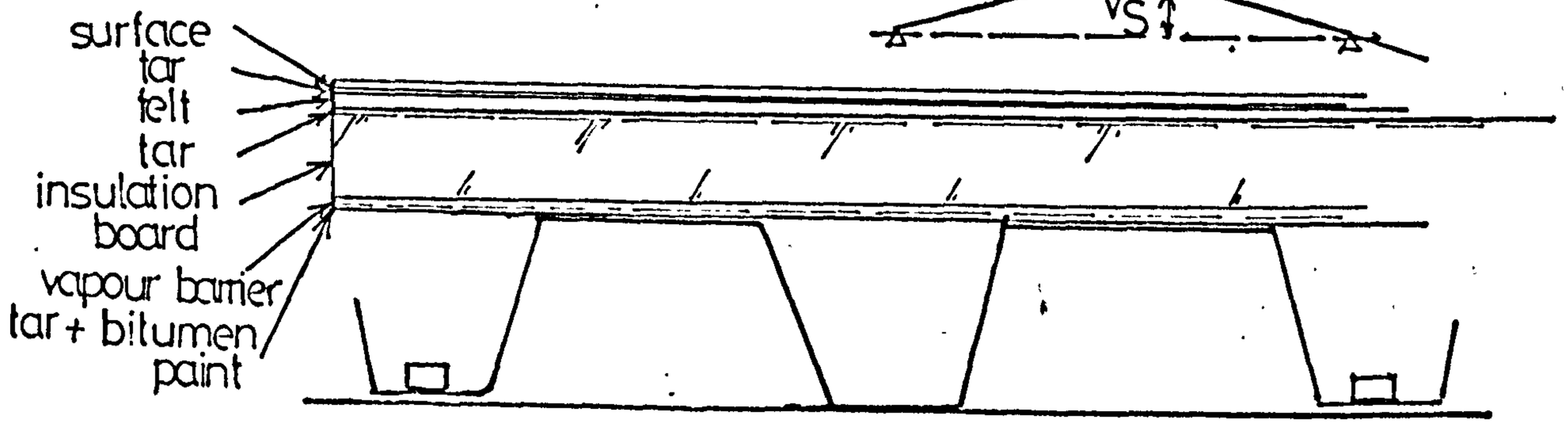

FIG (5.11)

INFINITELY STIFF INSULATION

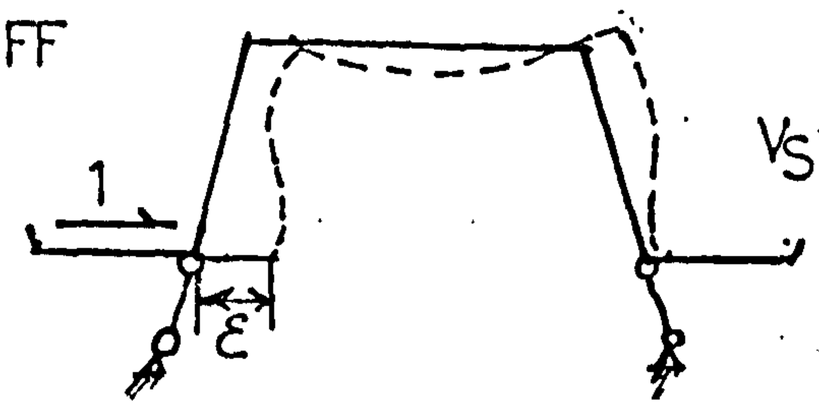

MAXIMUM INSULATION RESISTANCE

METHODS OF REDUCING DISTORTION

— CURVED END SHEETING

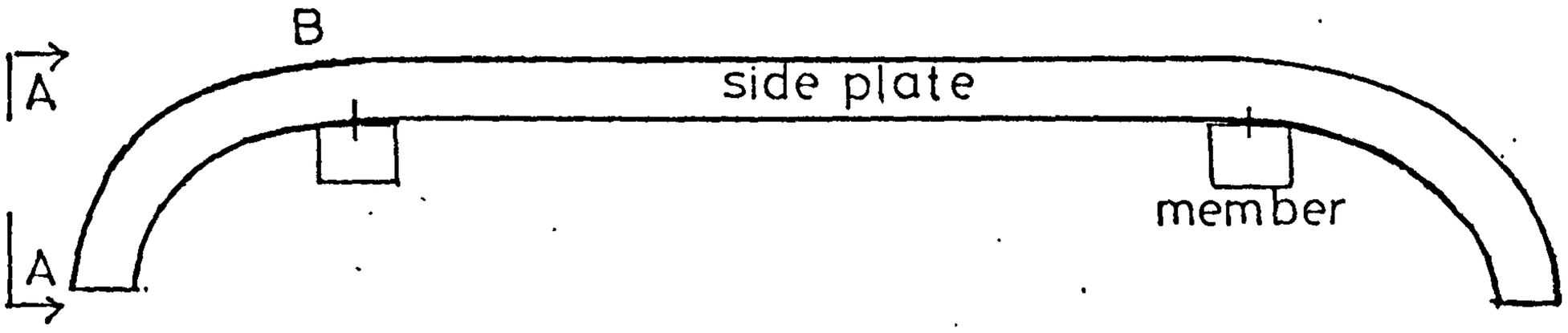

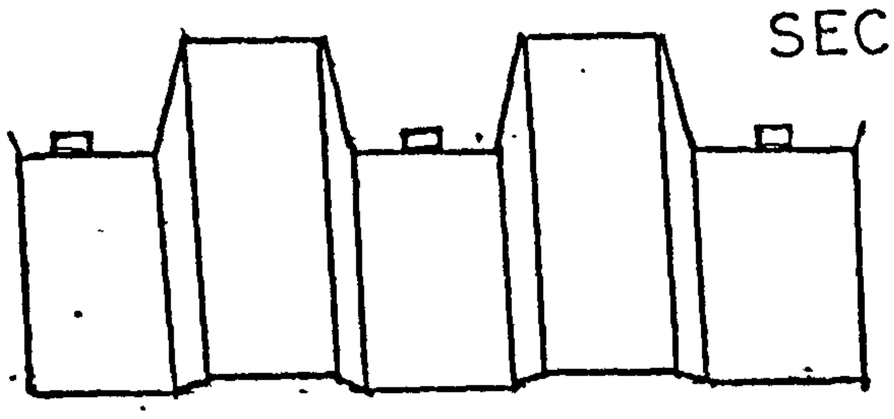

every trough fixing

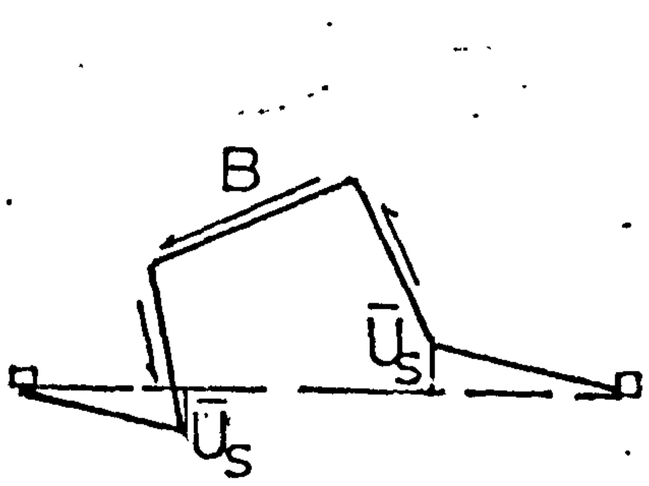

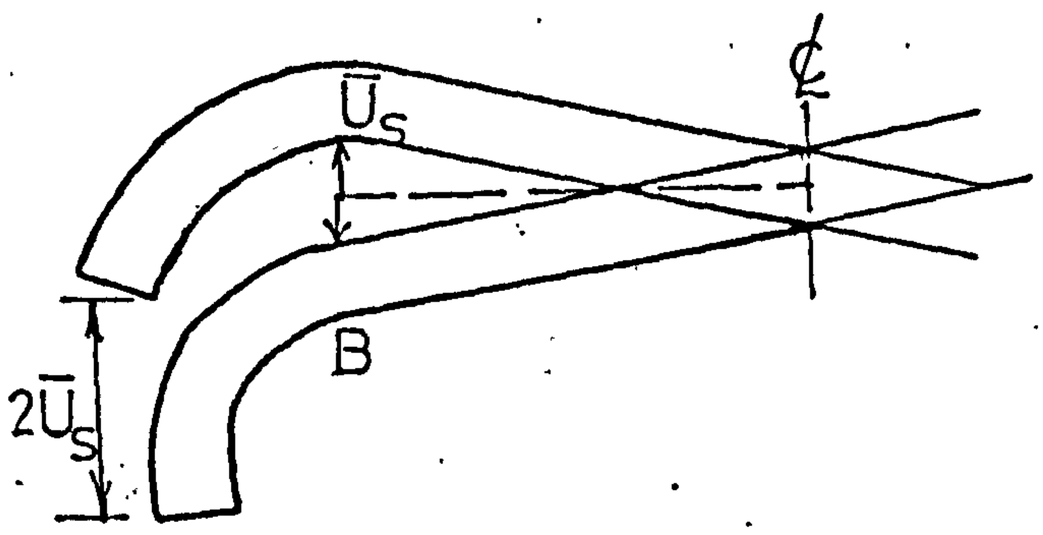

FREE DEFORMATION OF SIDE PLATE AT B

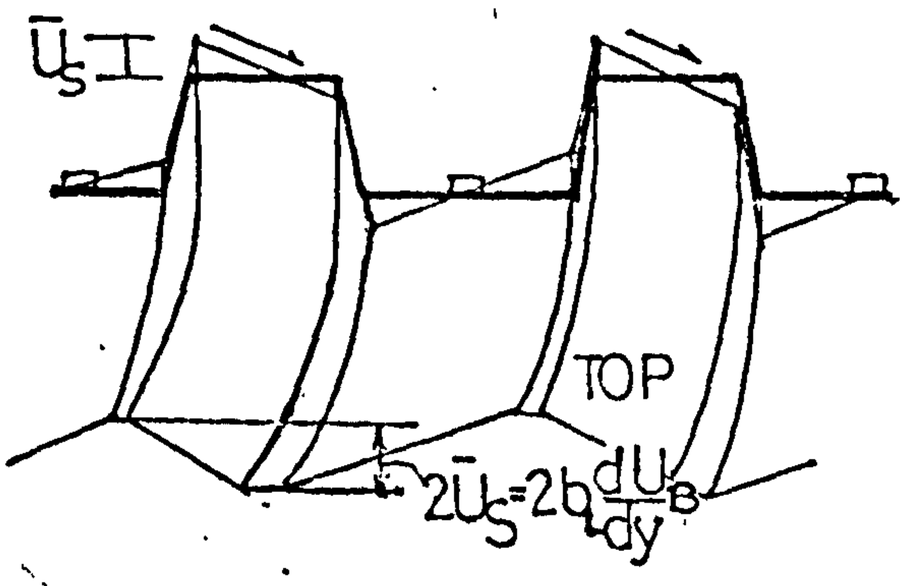

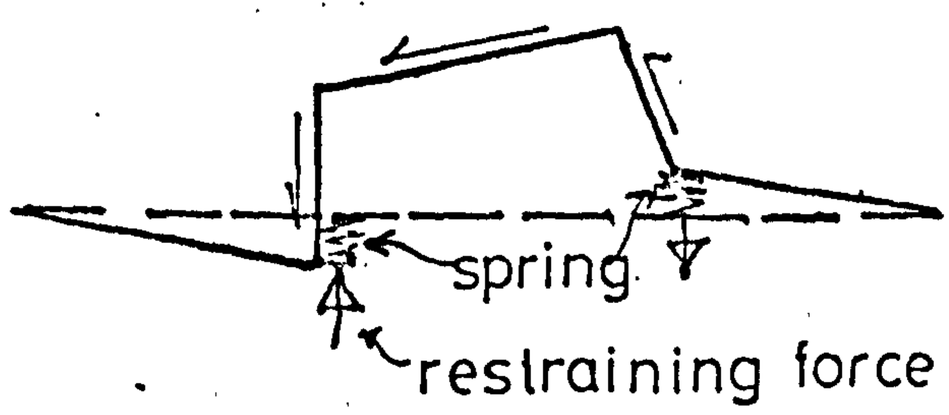

EQUIVALENT SPRING RESISTING SIDE PLATE MOVEMENT

FIG(5.12) END MOVEMENT ON SECTION AA TO ACCOMMODATE UPLIFT AT B

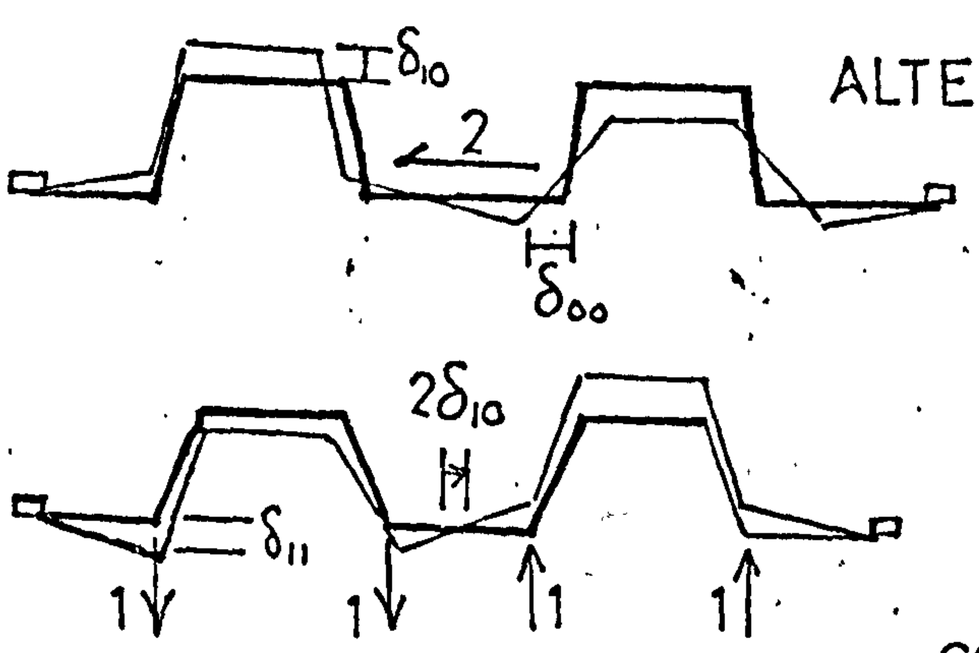

ALTERNATE TROUGH FIXING

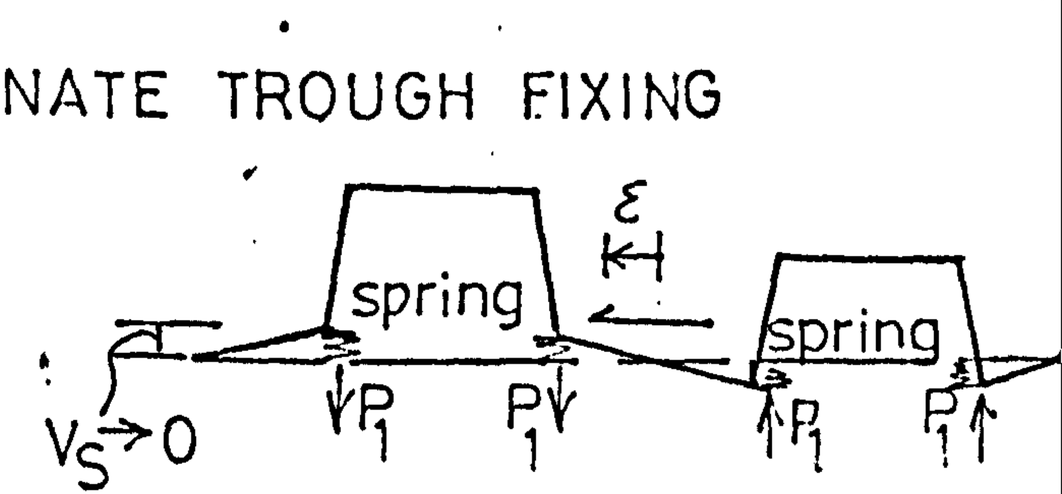

UPLIFT RESISTANCE

CONCERTINA MOVEMENT ONLY

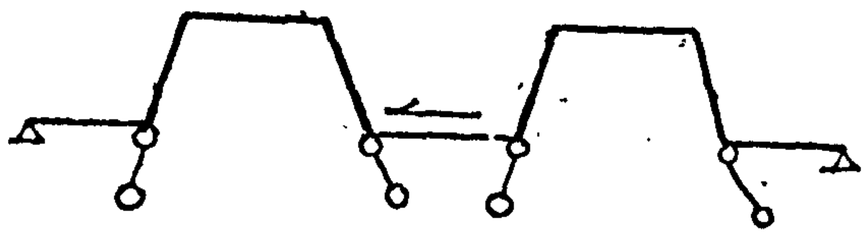

MODEL OF RESTRAINT

FIG(5.13)

OVERLAPPING CORRUGATIONS

—EVERY TROUGH FIXING THROUGHOUT

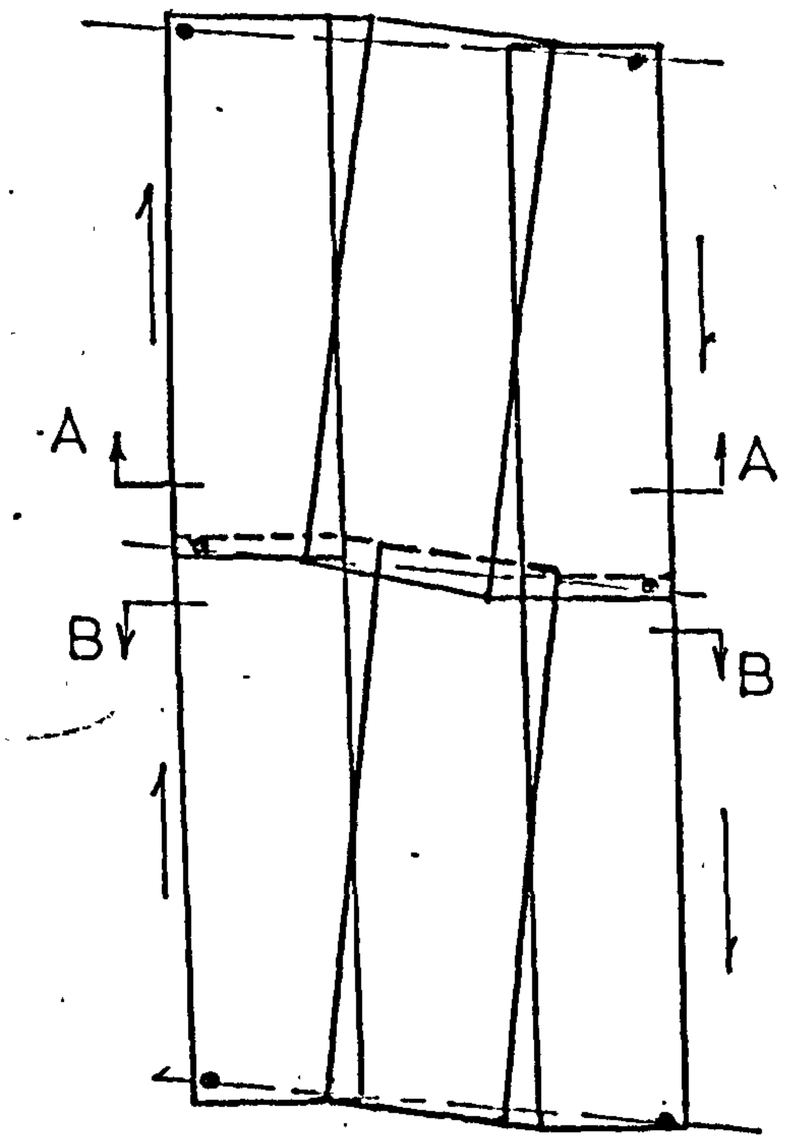

free movement of corrugations

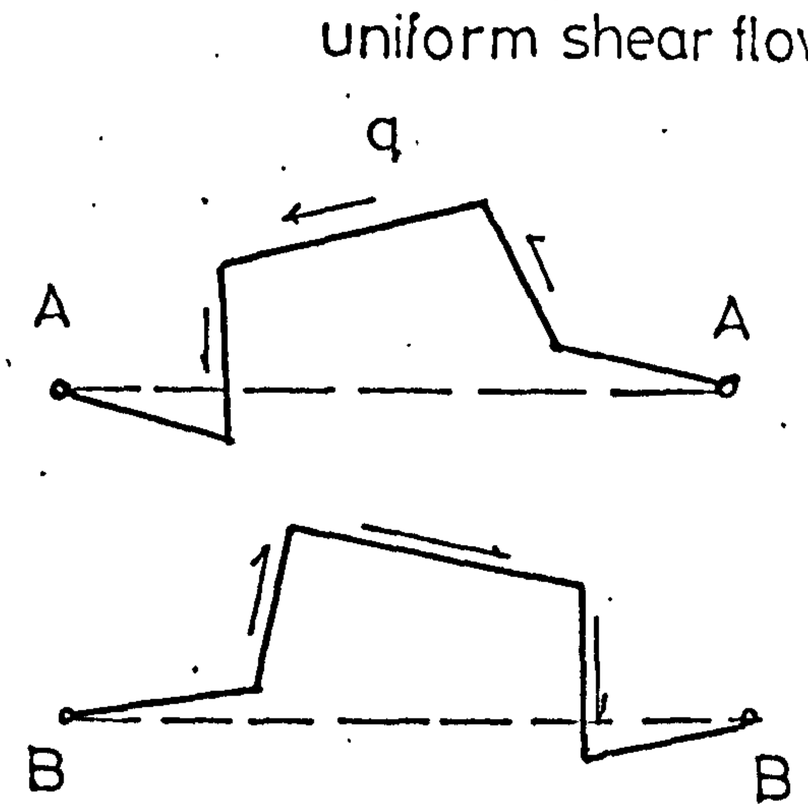

opposite distortions
at the overlap

FIG(6.1)

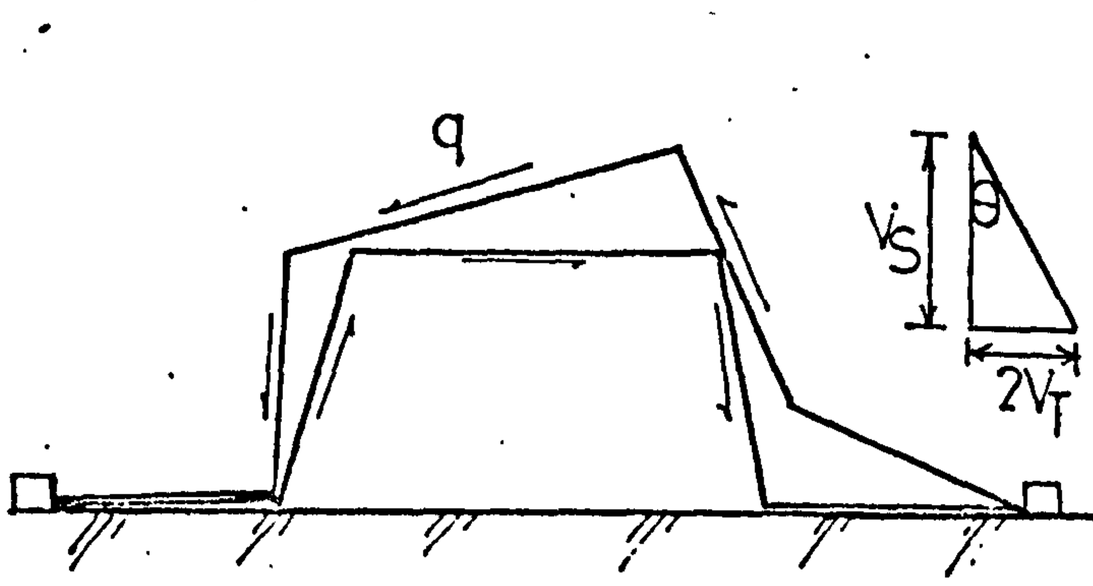

INTERACTION OF CORRUGATIONS
LAPPING OVER A PURLIN

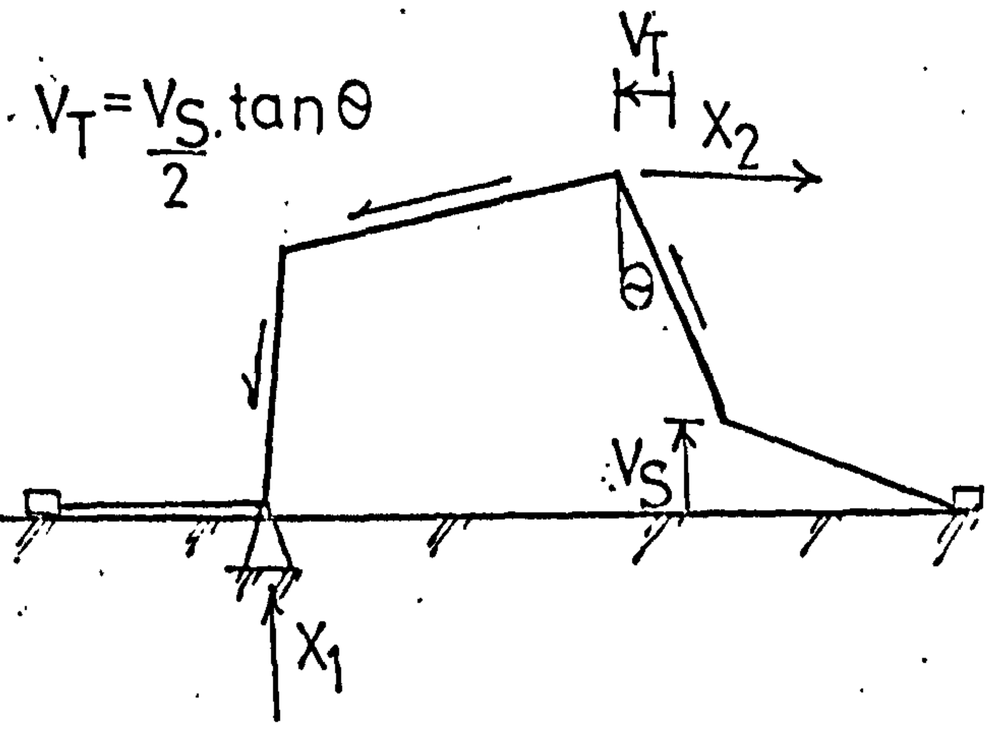

DEFORMATION MODEL.

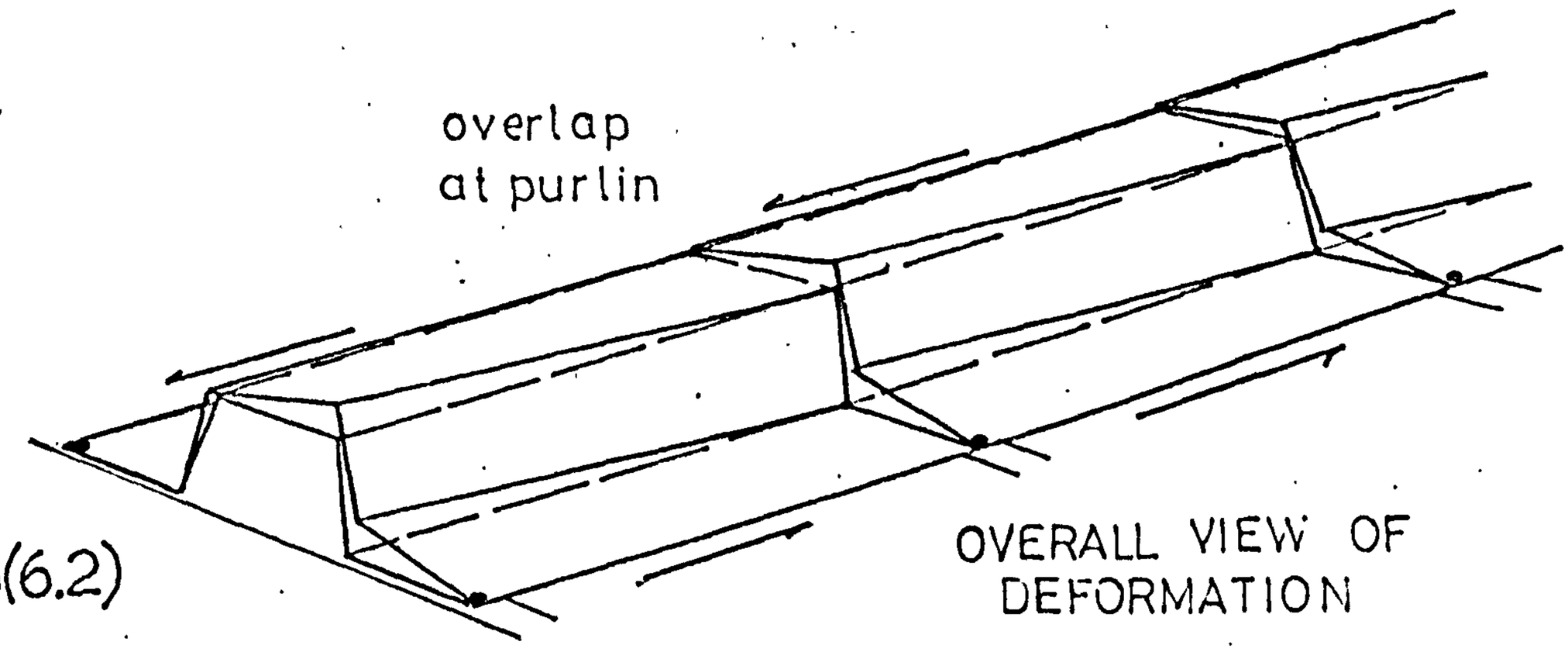

FIG(6.2)

OVERALL VIEW OF
DEFORMATION

OVERLAPPING CORRUGATIONS

—ALTERNATE TROUGH FIXING THROUGHOUT

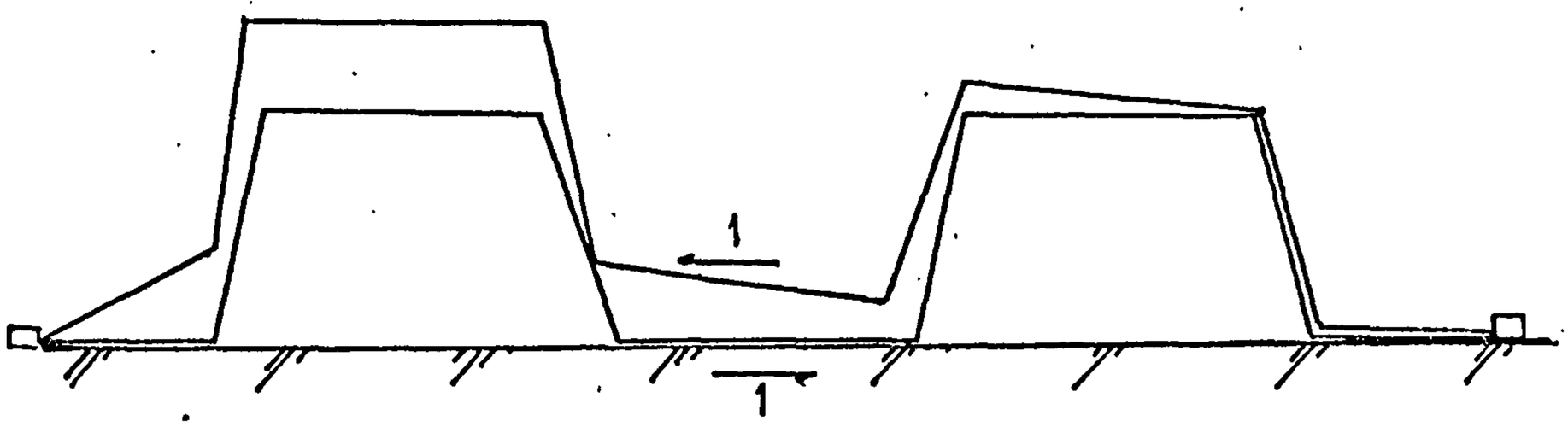

FIG(6.3(a))CONCERTINA MOVEMENT INTERACTION OVER PURLIN

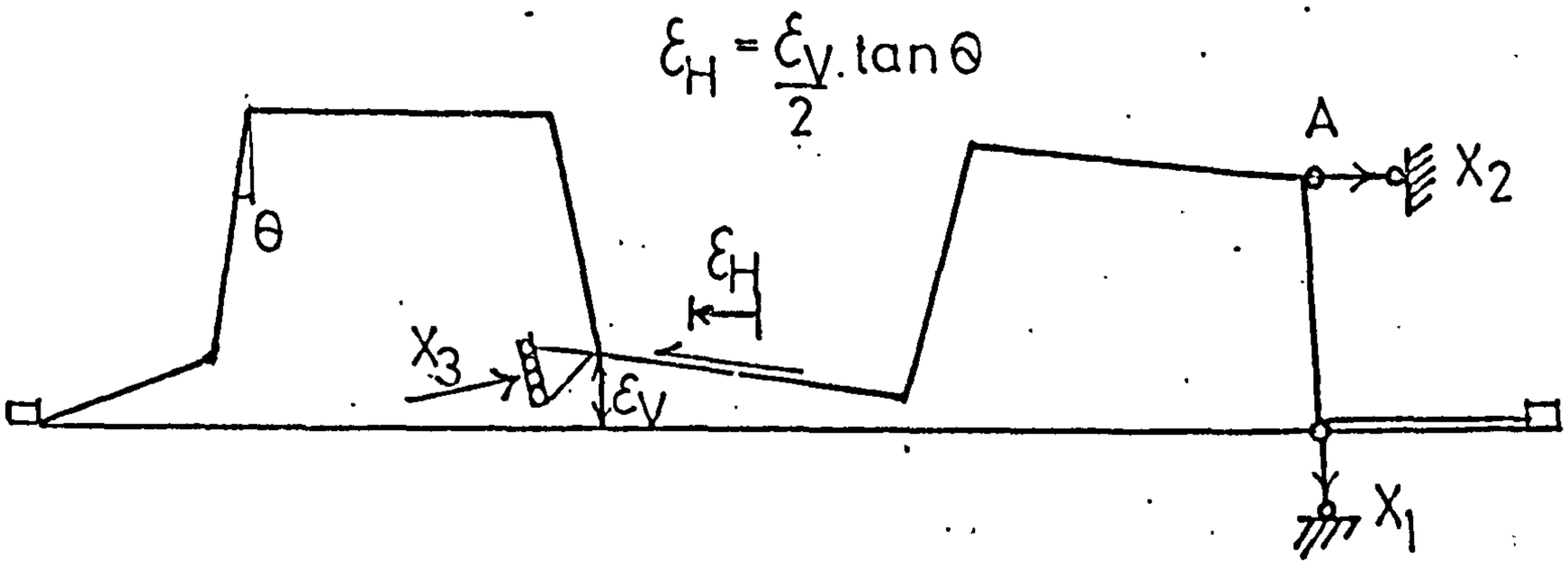

FIG(6.3(b)) MODEL TO REPRESENT DEFORMATION

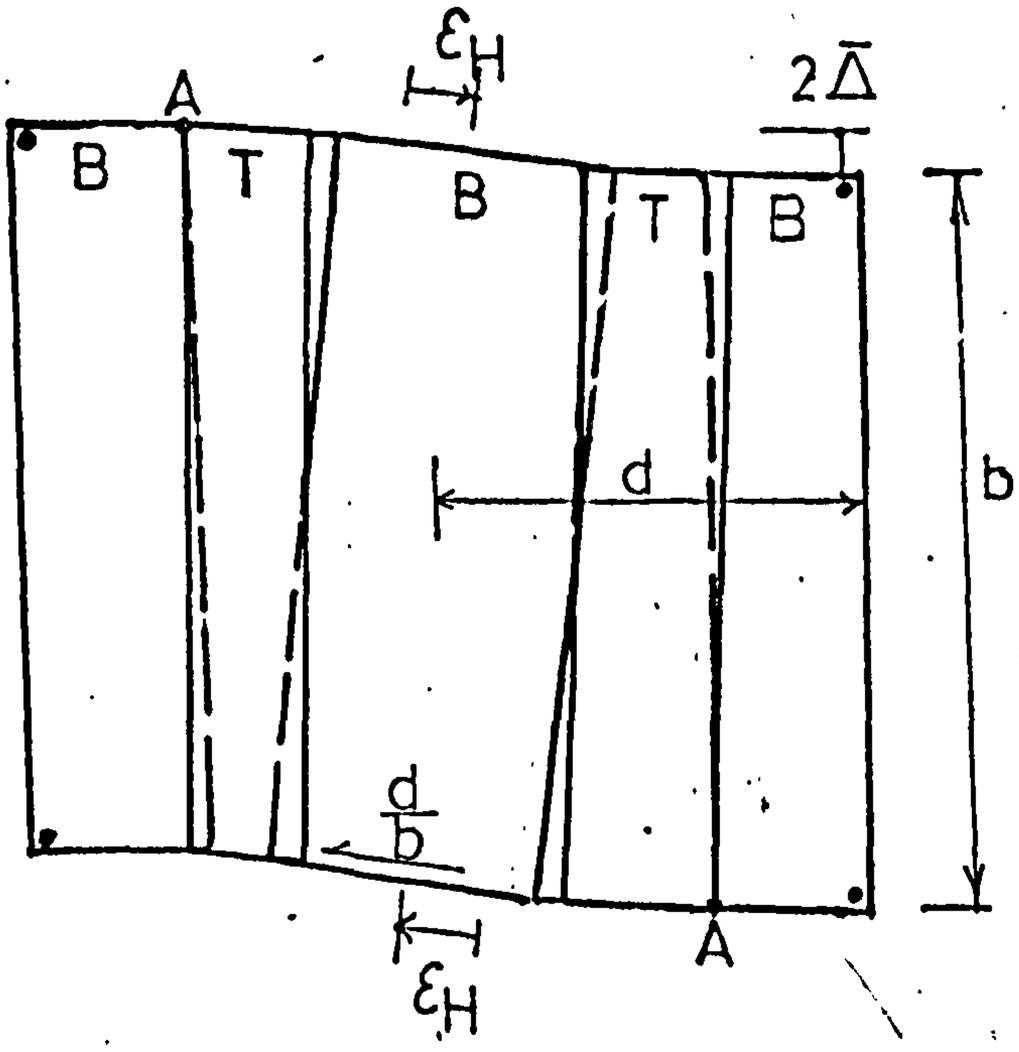

$$\bar{\Delta} = \varepsilon_H \frac{d}{b}\left(1 - \frac{b+D}{d+D}\right)$$

rigid plate movements

FIG(6.4) LONGITUDINAL WARPING SHOWING CONCERTINA RESTRAINT AT A

OVERLAPPING SHEETS

—RIGID PLATE MOVEMENTS

UNEQUAL SHEET LENGTHS

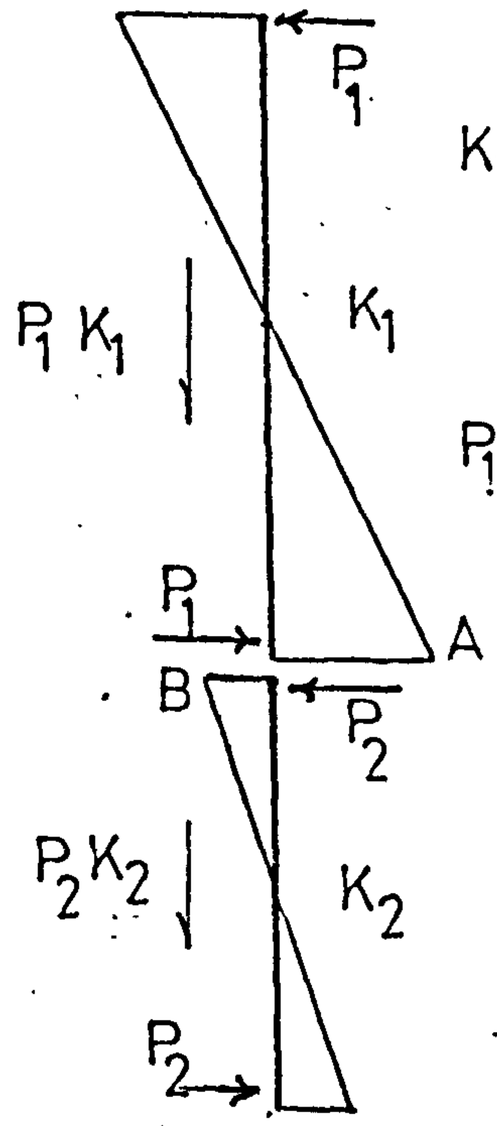

TOP PLATE MOVEMENT

FIG(6.5)

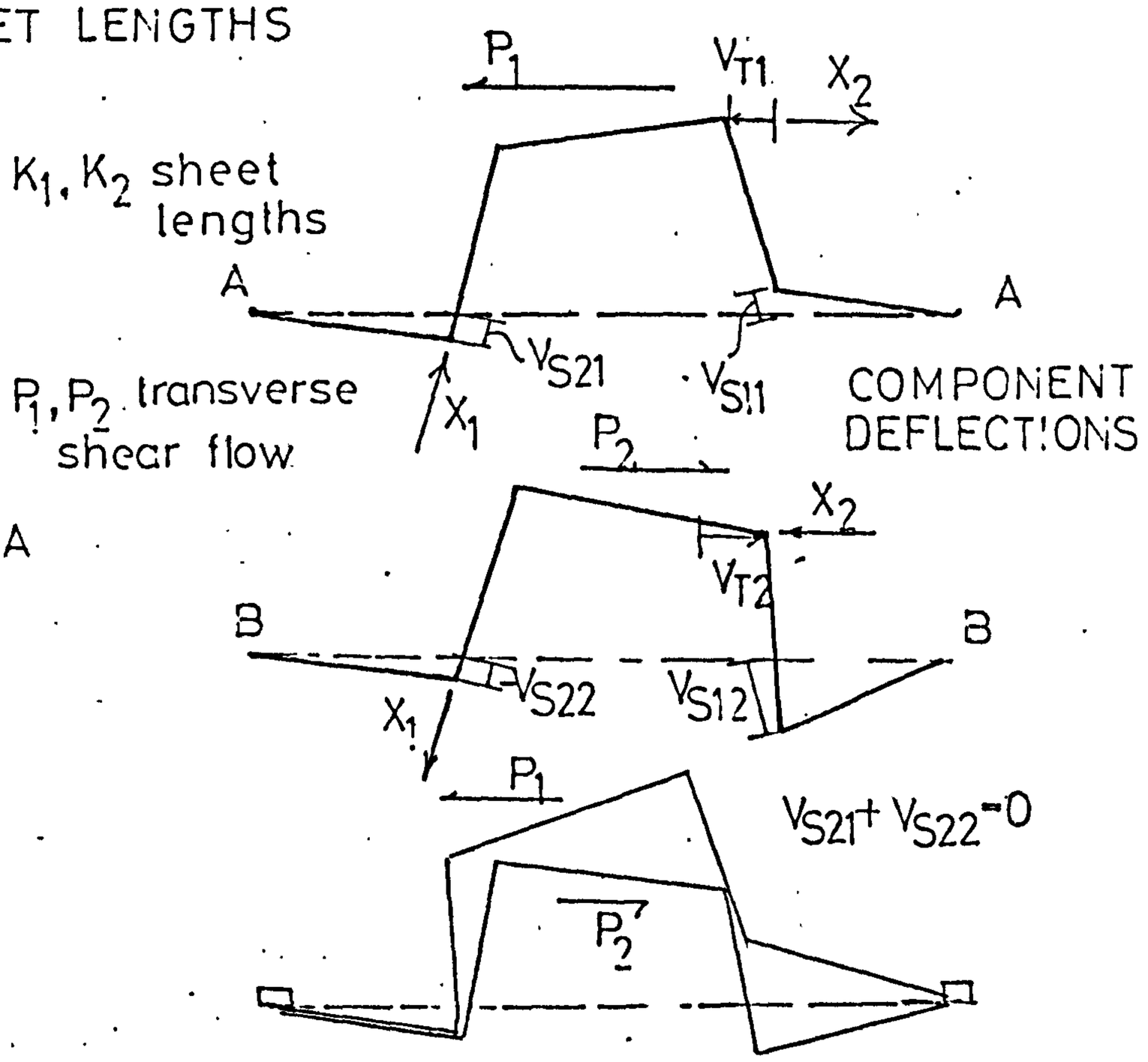

NET INTERACTION—IGNORING PURLIN RESTRAINT

GENERAL EXPRESSION

—any number or length of sheet

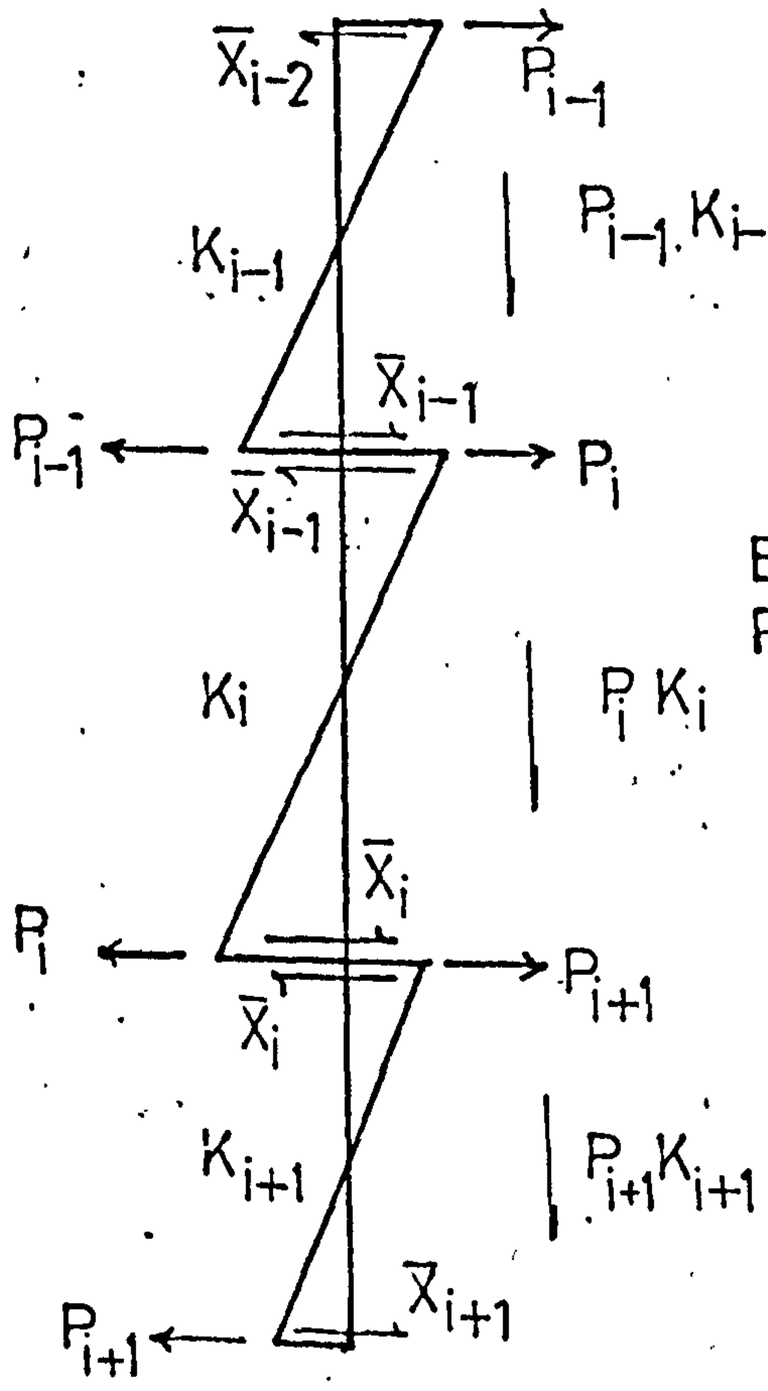

FIG(6.6)

K_i — sheet length

P_iK_i — longitudinal shear force

$\bar{X}_i$ — equivalent restraint

EQUIVALENT TOP PLATE DISPLACEMENTS

Δ_o — shear displacement

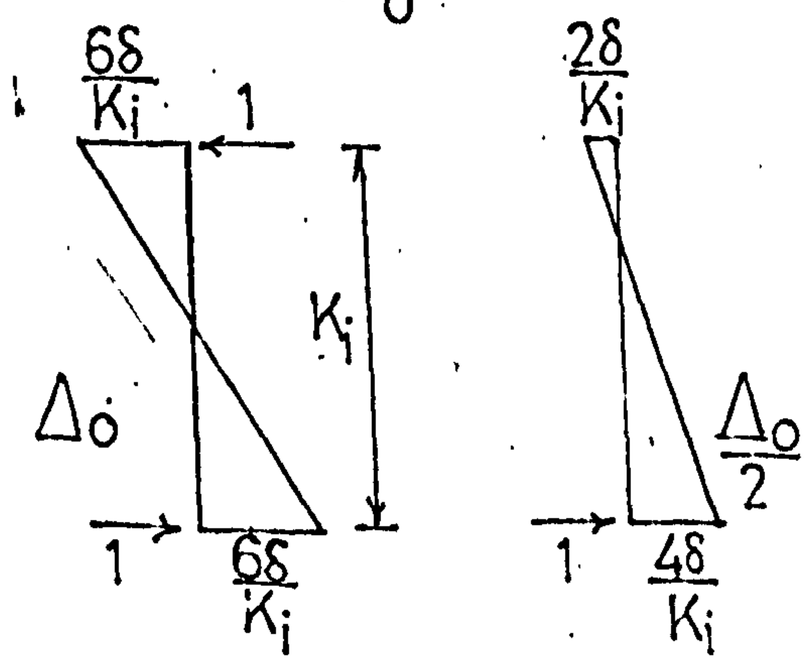

EFFECT OF FORCE AT ONE END ONLY

OVERLAPPING SHEETS

— LOCALIZED END DISTORTION

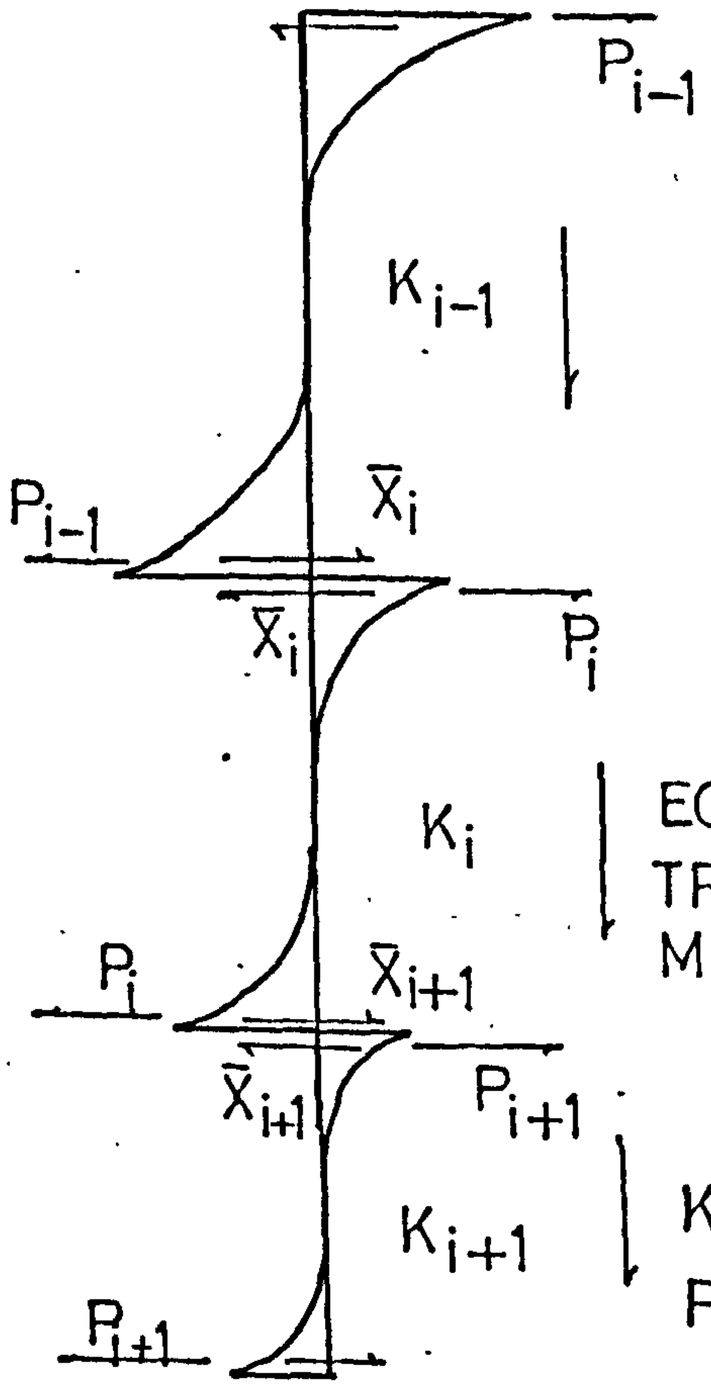

FIG(6.7)

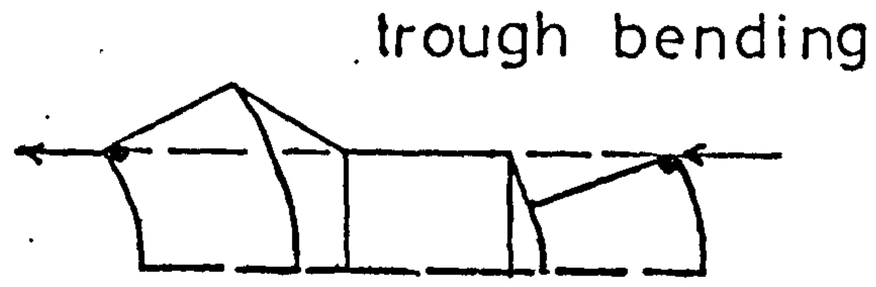

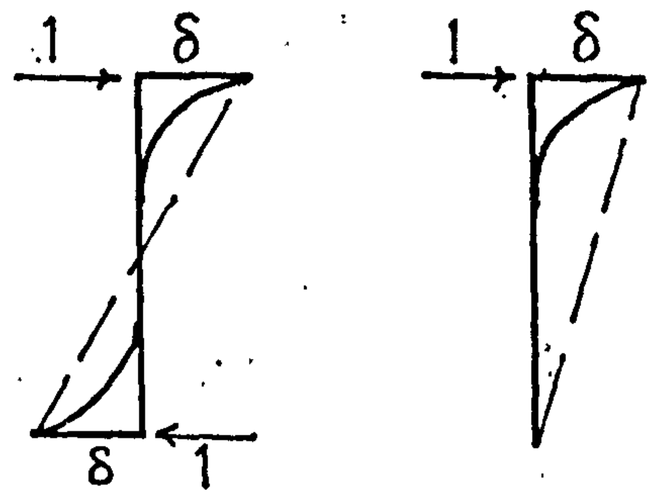

EFFECT OF FORCE AT ONE END

VARIATION IN FASTENING ARRANGEMENT

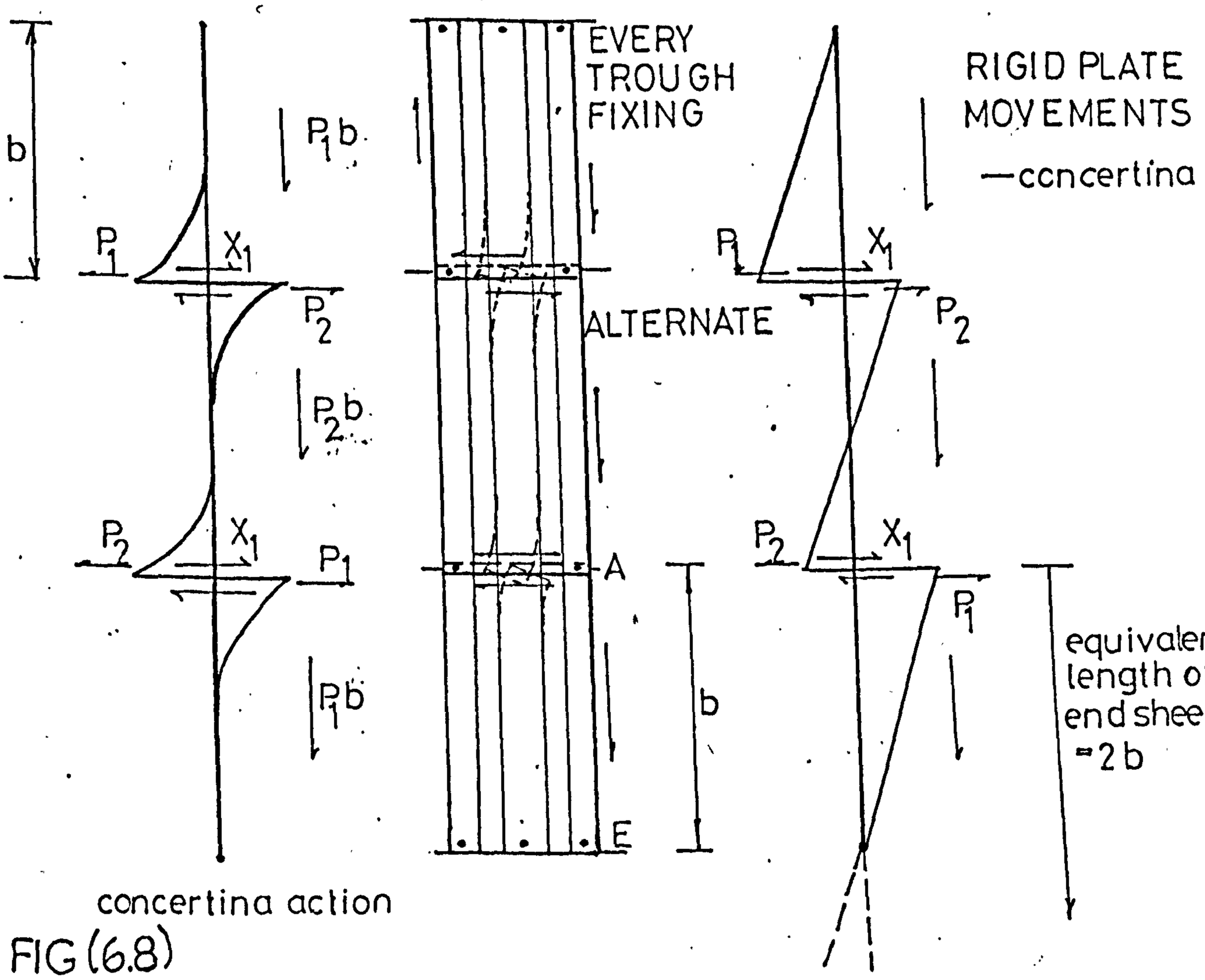

FIG (6.8)

CONTINUOUS DIAPHRAGM—WEB BENDING

—EVERY TROUGH FIXING

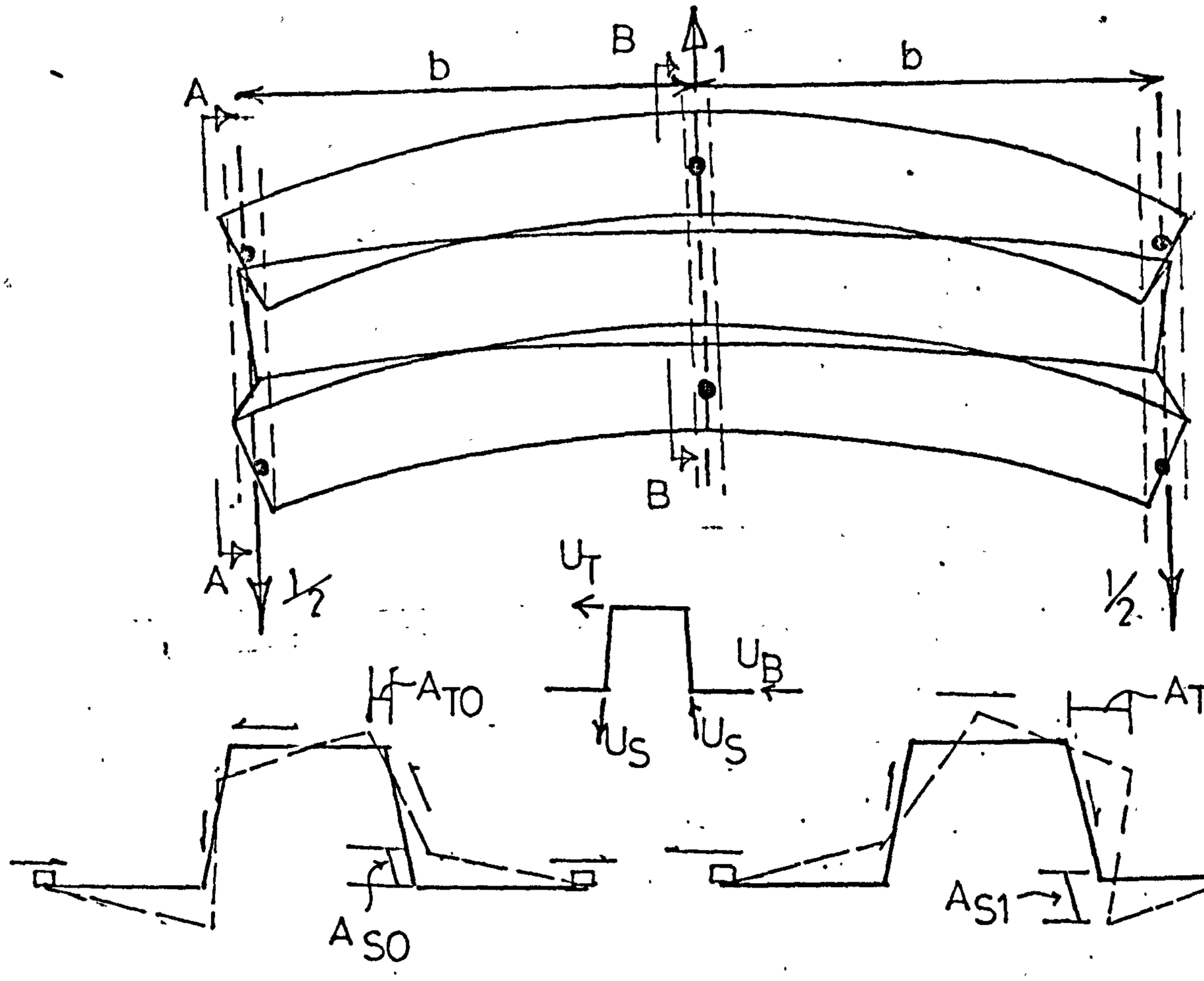

END SECTION AA

CENTRE SECTION BB

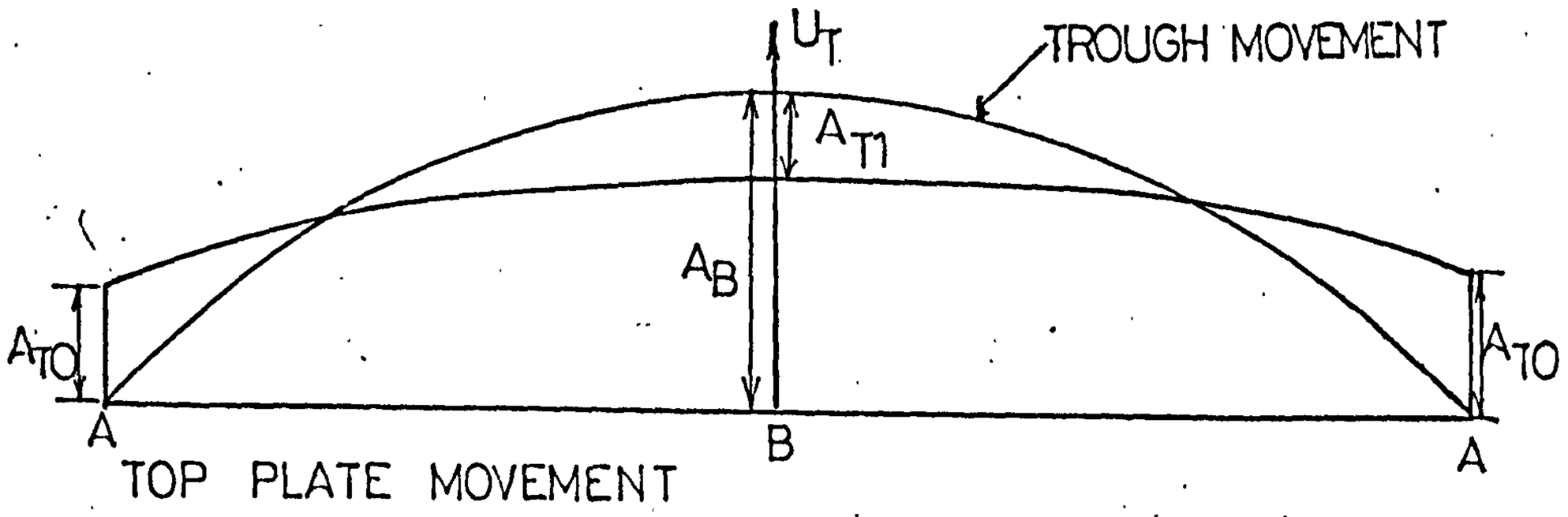

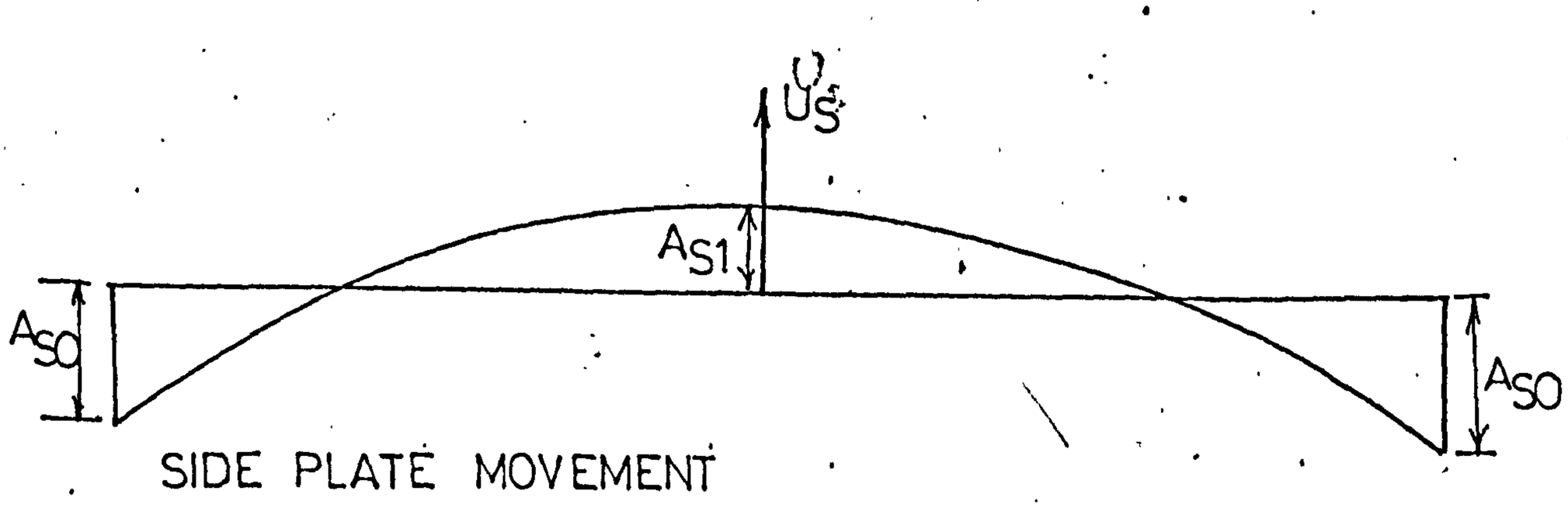

FIG(7.1)

CONTINUOUS DIAPHRAGM–ALTERNATE TROUGH FIXING

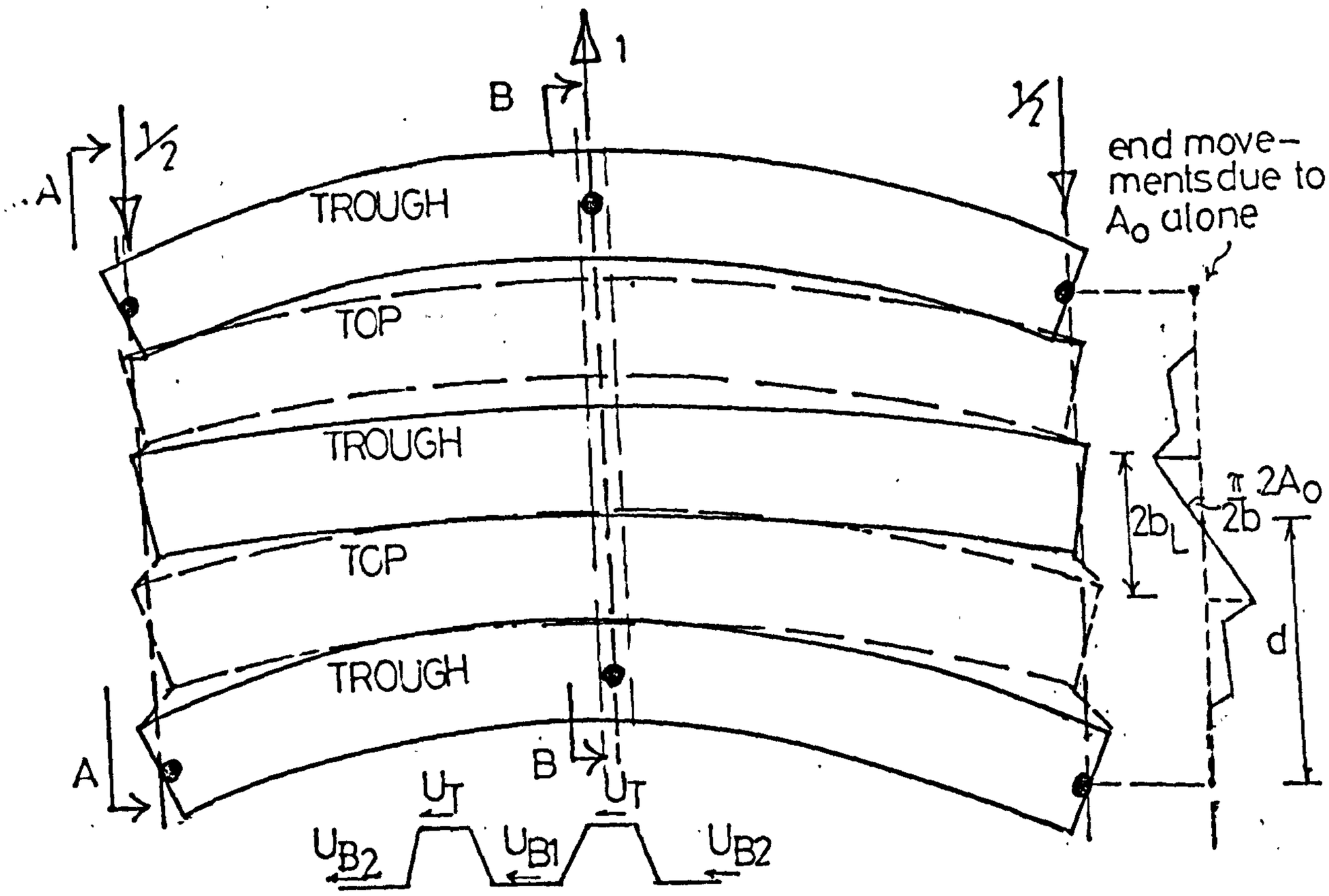

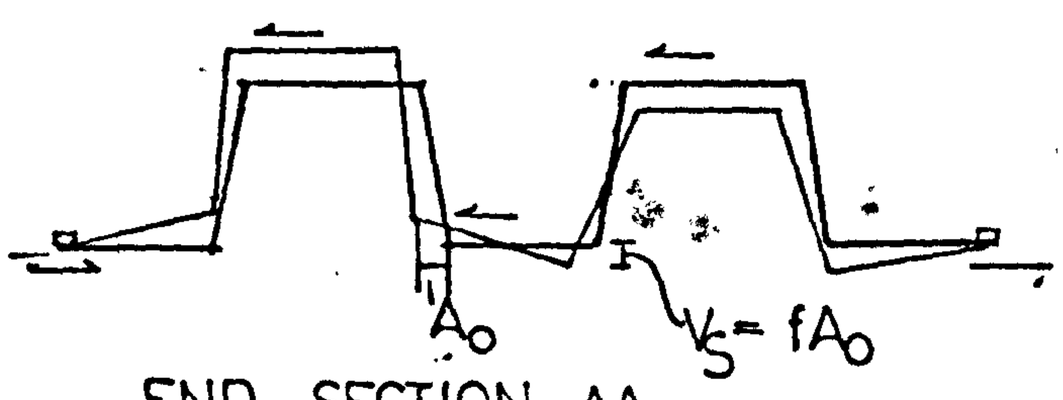

END SECTION AA

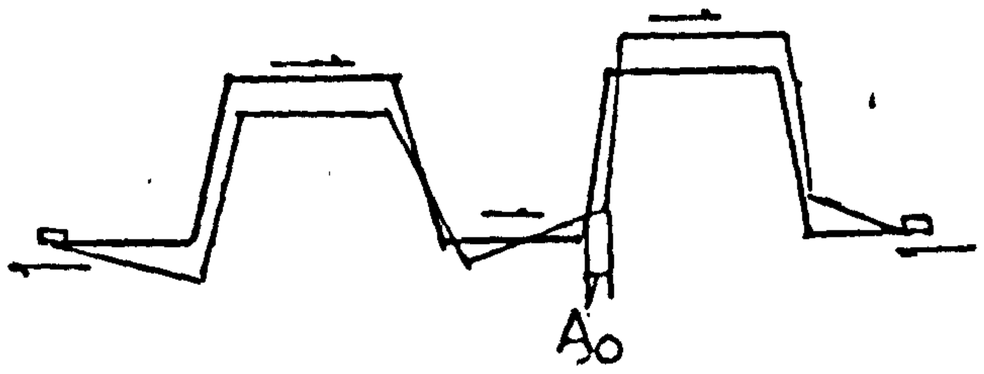

CENTRE SECTION BB

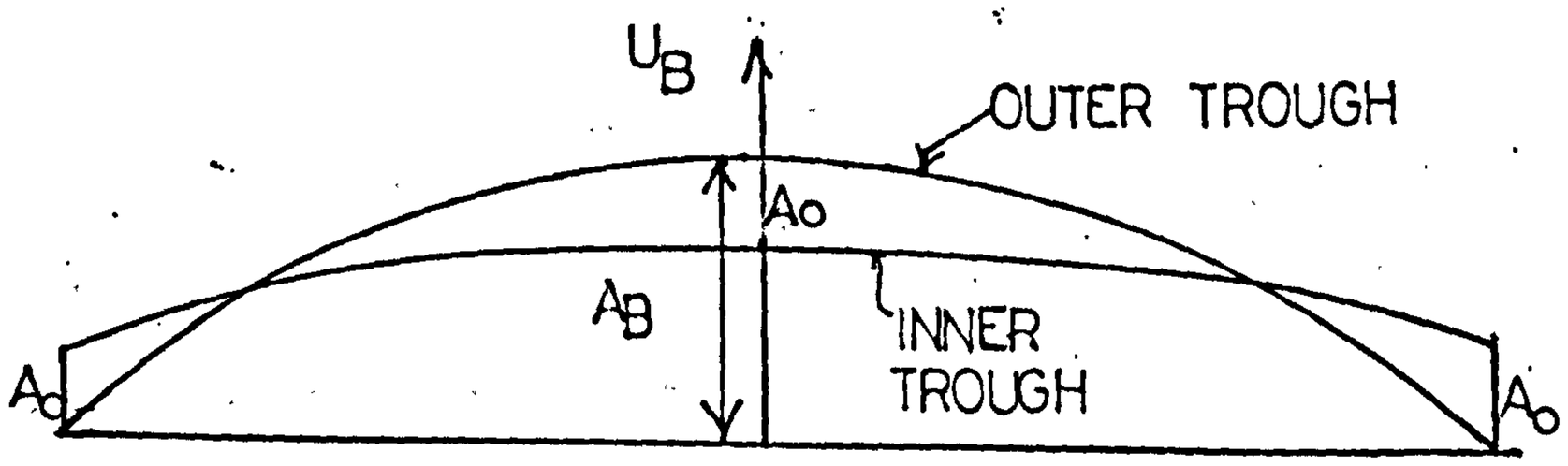

TROUGH CONCERTINA MOVEMENT

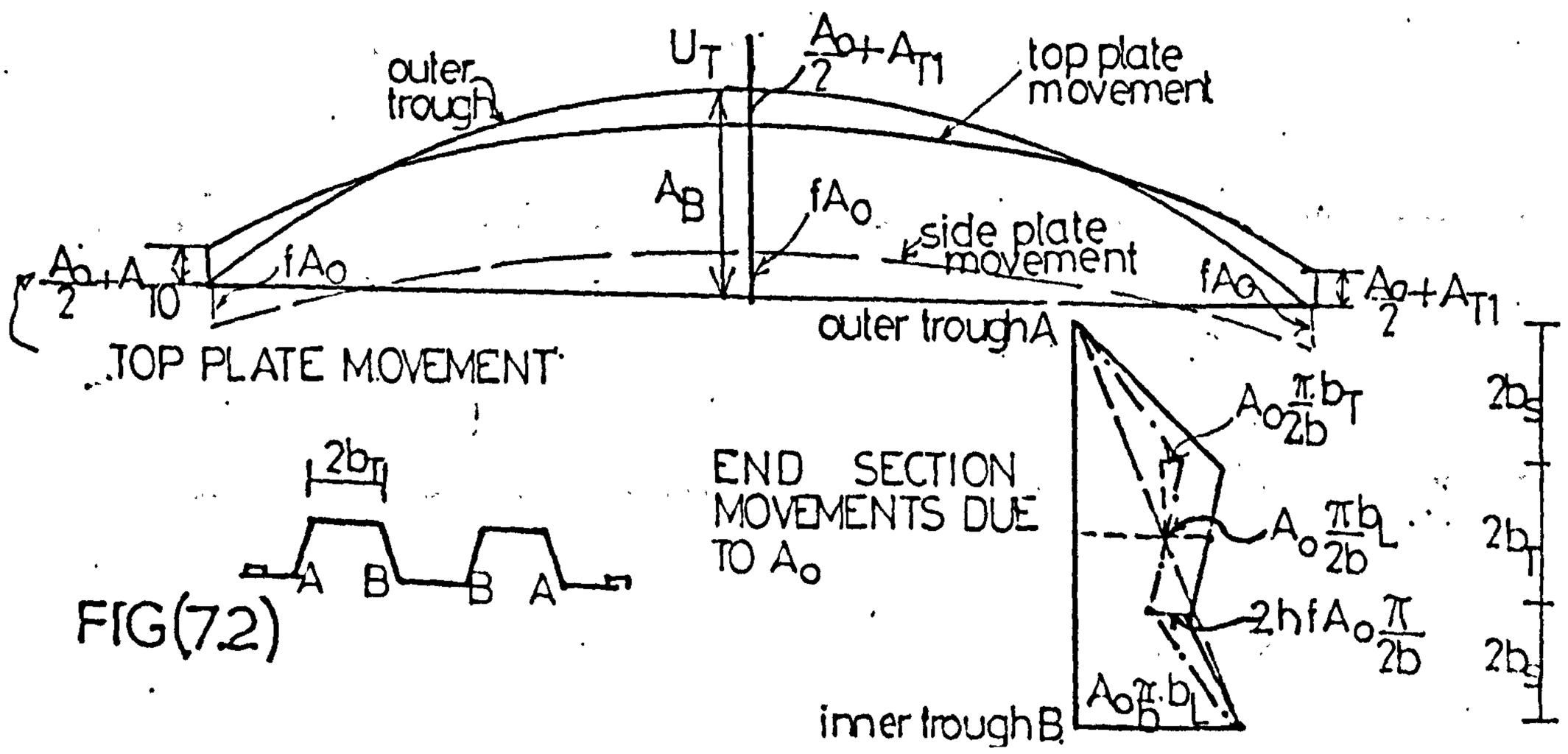

FIG(7.2)

END SECTION MOVEMENTS DUE TO A_o

CONTINUOUS DIAPHRAGM — PLATE DEFLECTIONS FOR A_B=1mm

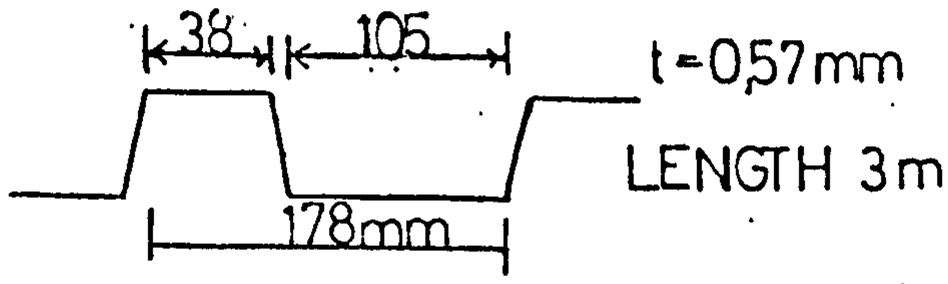

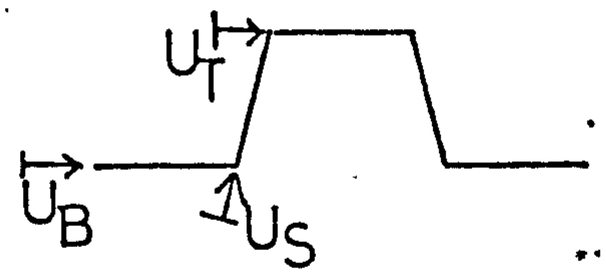

EVERY TROUGH FIXING

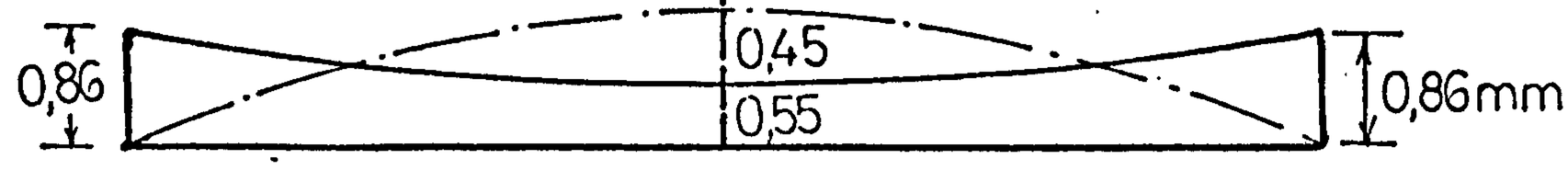

TOP PLATE MOVEMENT

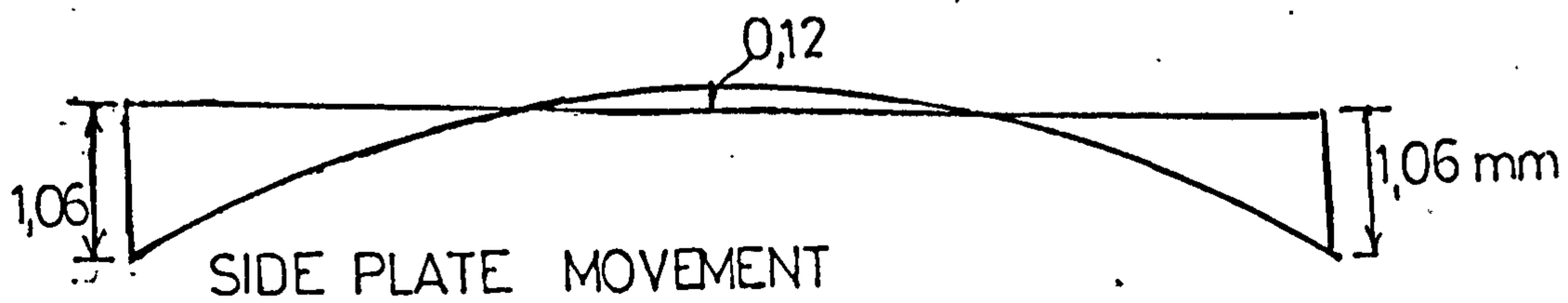

SIDE PLATE MOVEMENT

ALTERNATE TROUGH FIXING

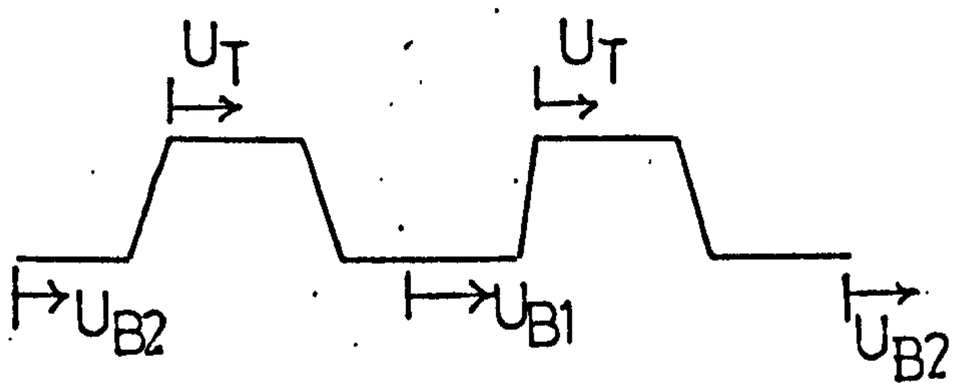

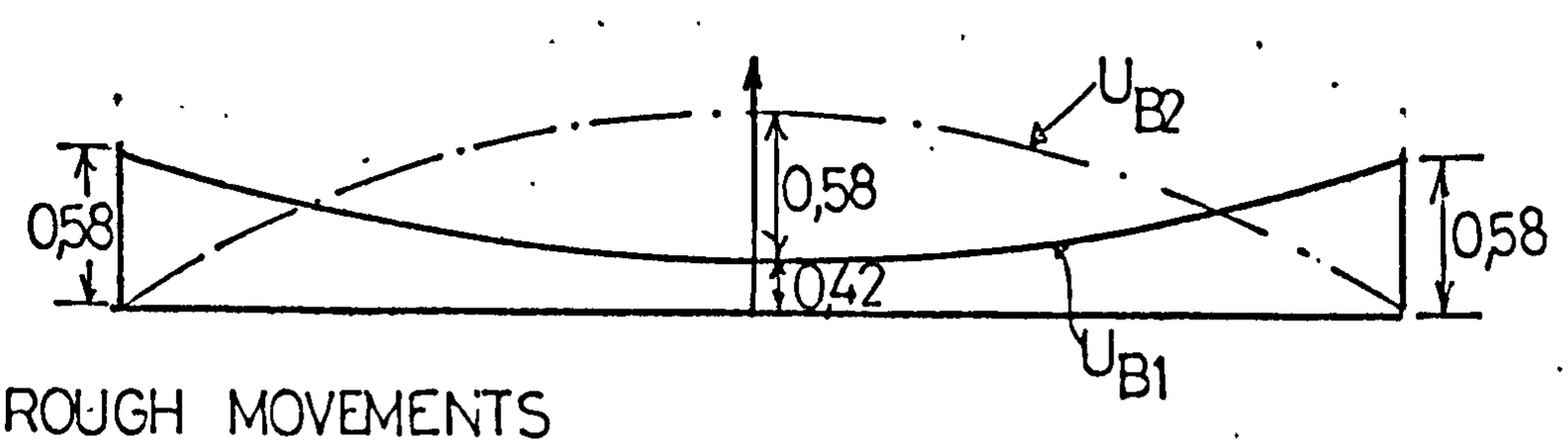

TROUGH MOVEMENTS

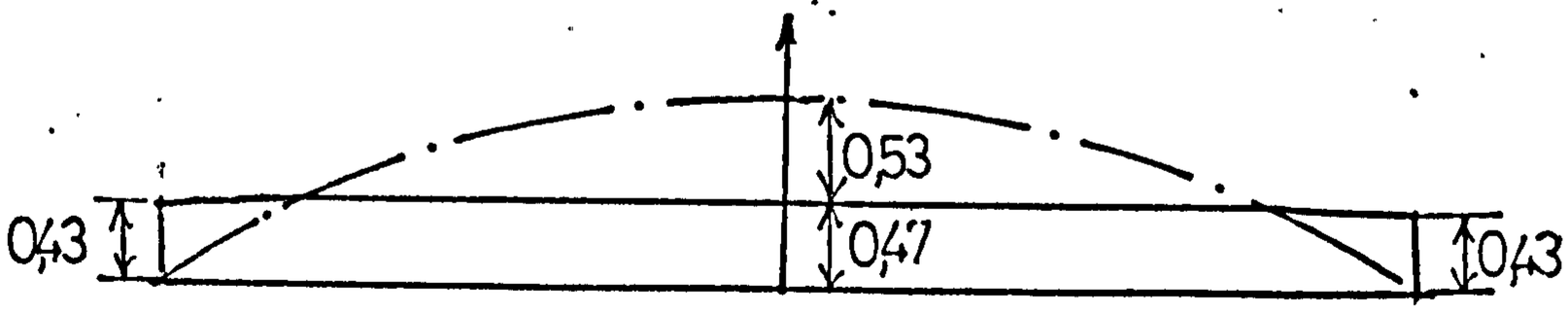

TOP PLATE MOVEMENTS

FIG (7.3)

TEST APPARATUS FOR 2 AND 3 BAY DIAPHRAGMS

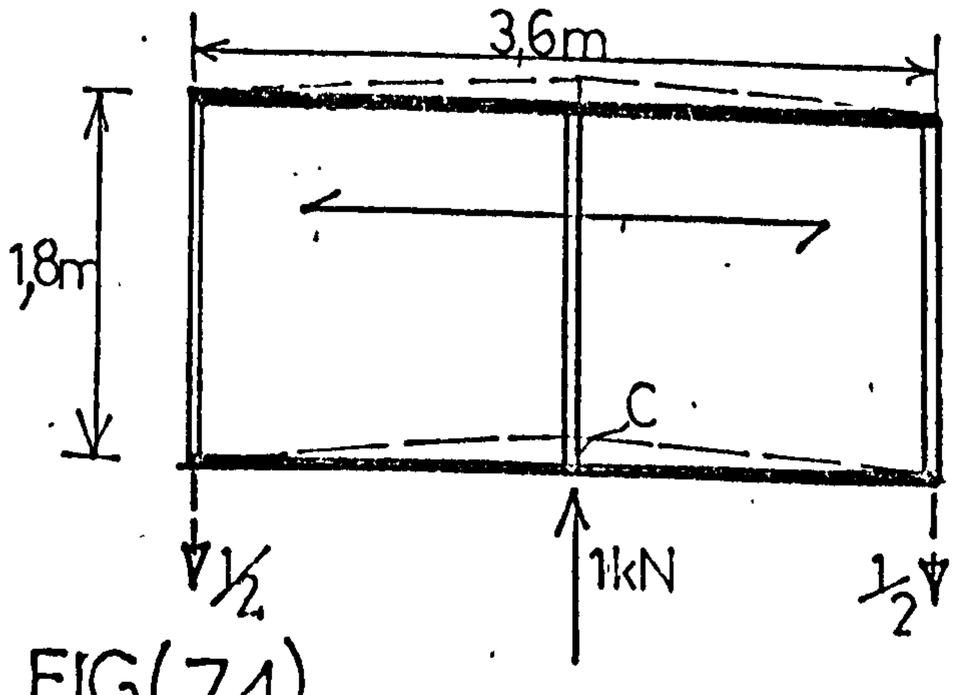

FIG(7.4)

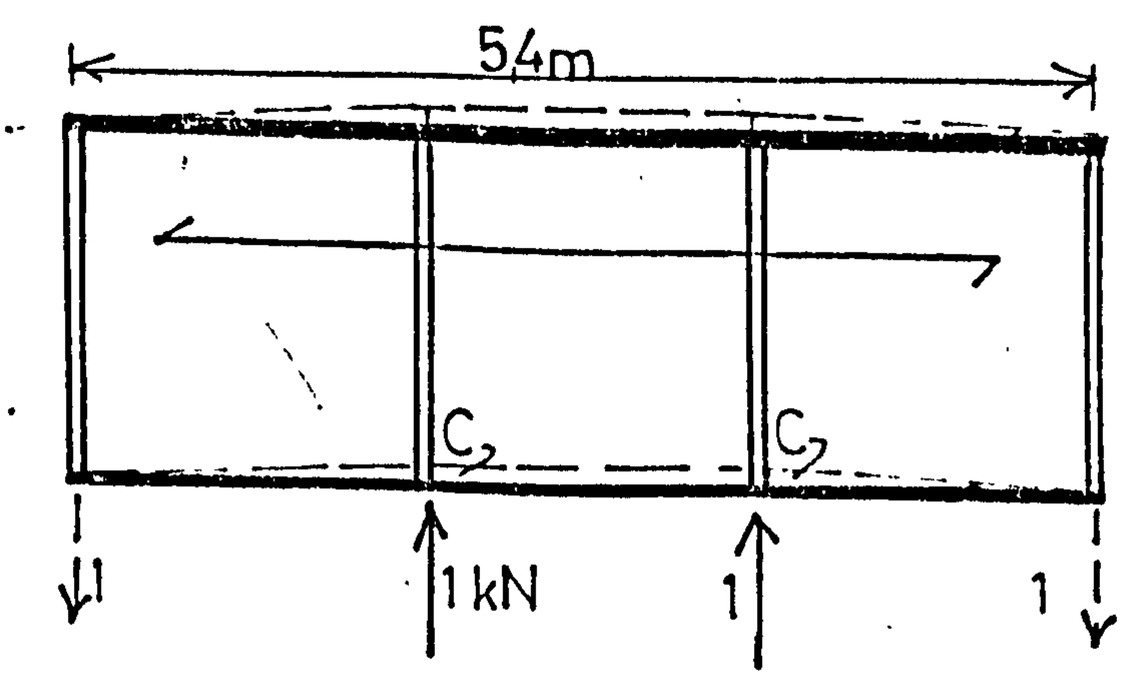

CONTINUOUS DIAPHRAGM —

MODIFIED SHEAR FLEXIBILITY RELATIVE TO LINEAR PLATE MOVEMENT DISTORTION

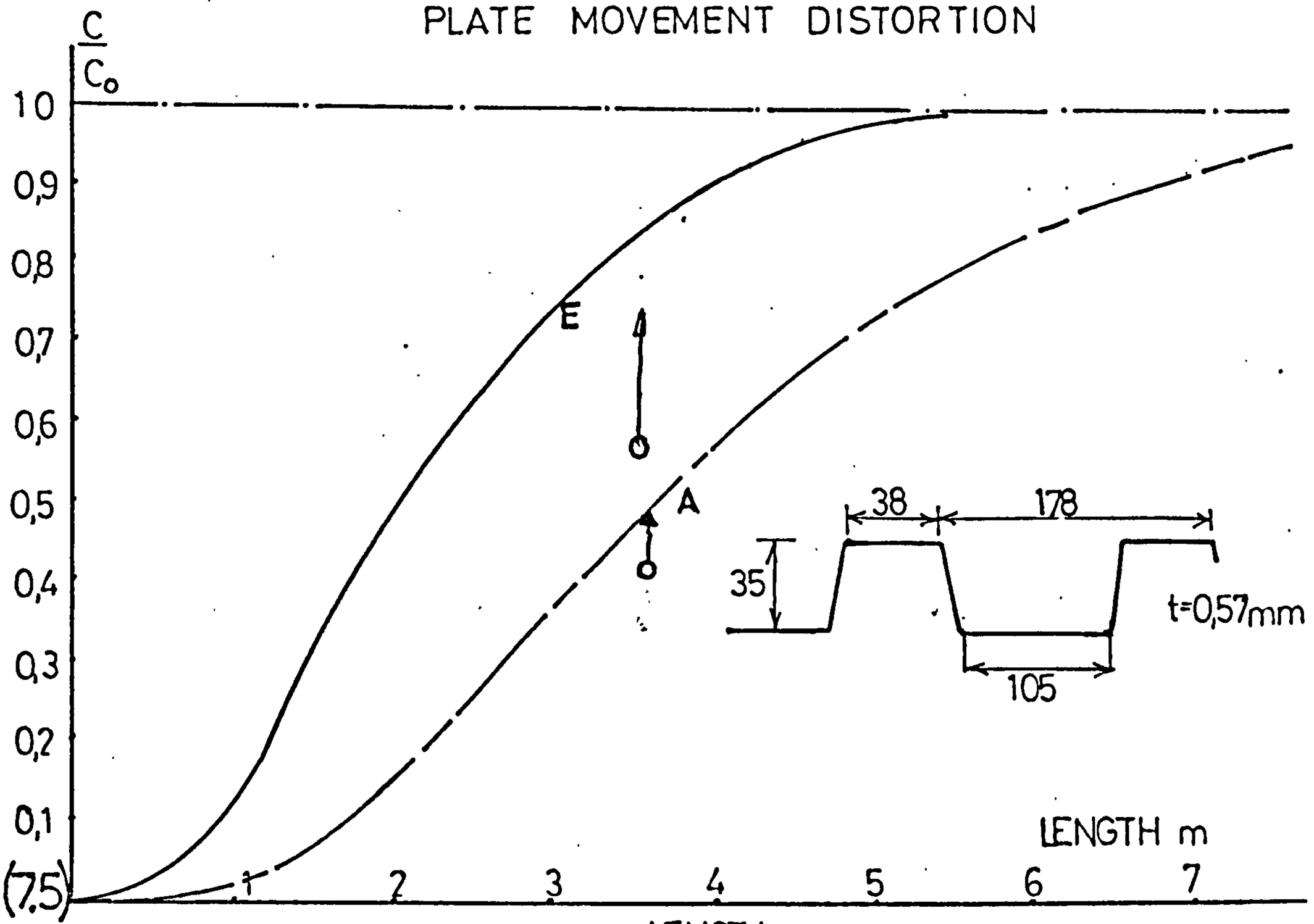

FIG(7.5)

E—every trough fixing
A—alternate " "
C--continuous sheeting flexiblity
C_o—unconnected " "
o —experimental point

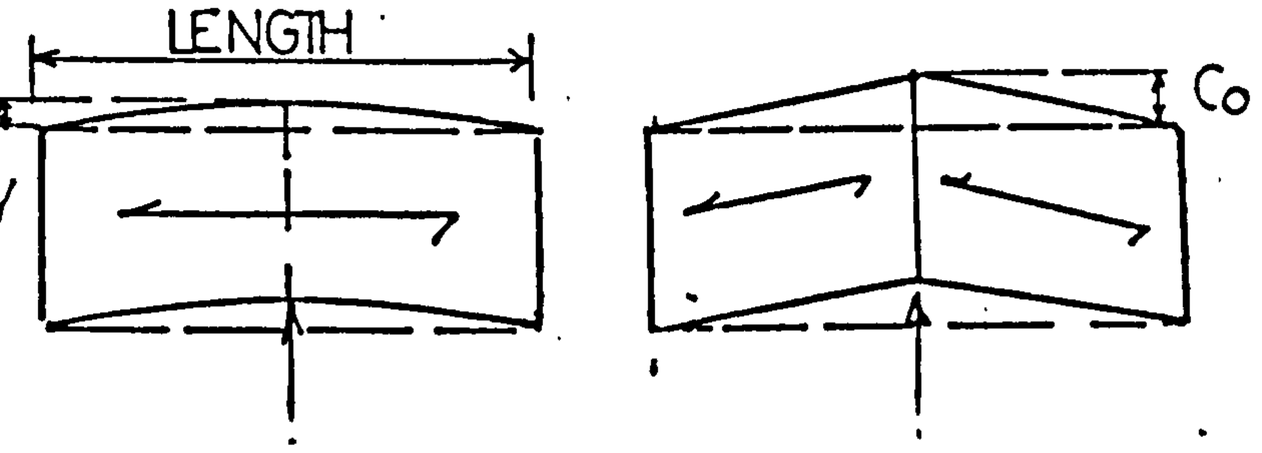

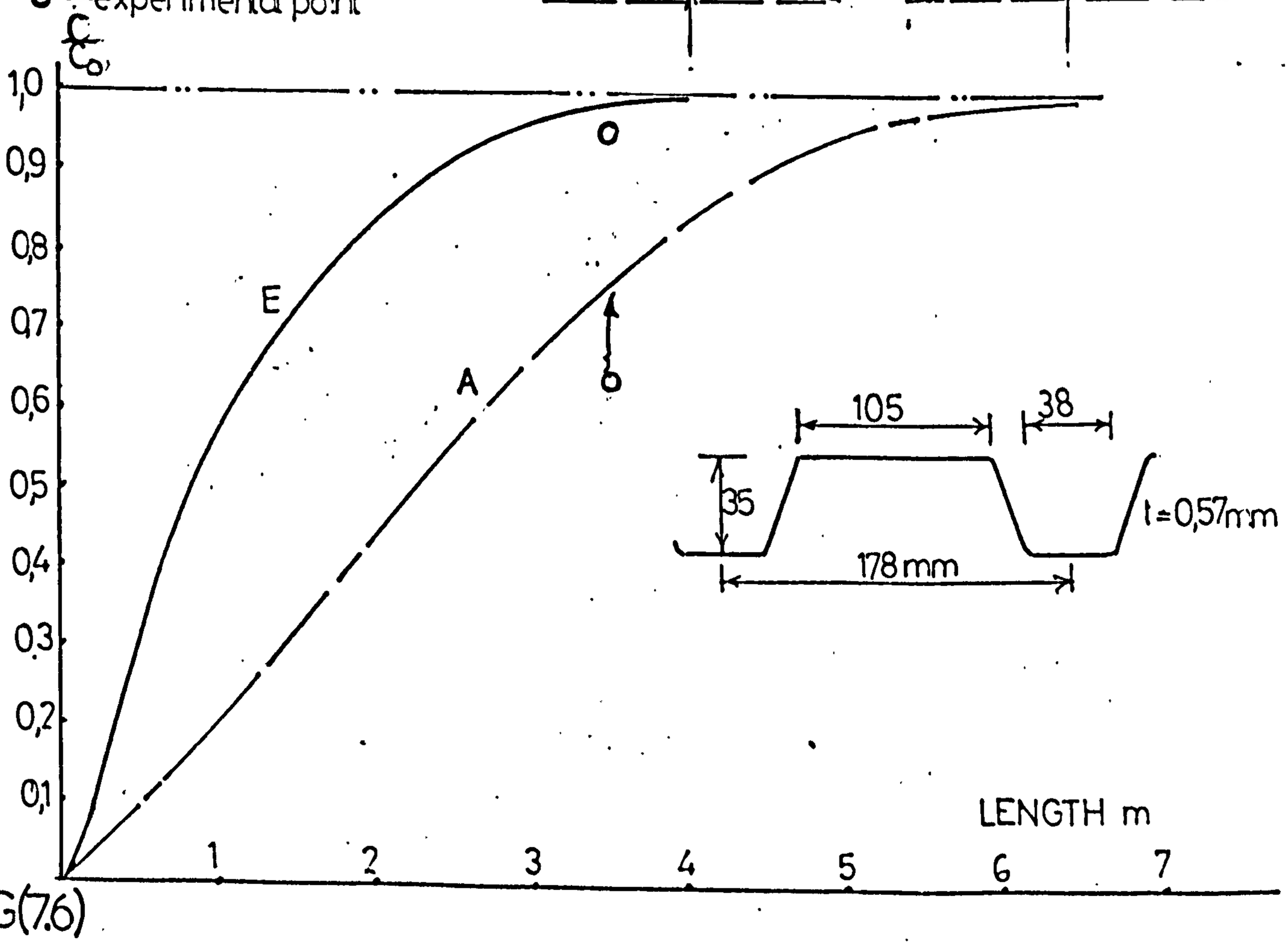

FIG(7.6)

INERTIA OF PURLINS

—AND DIAPHRAGM SHEAR FLOW

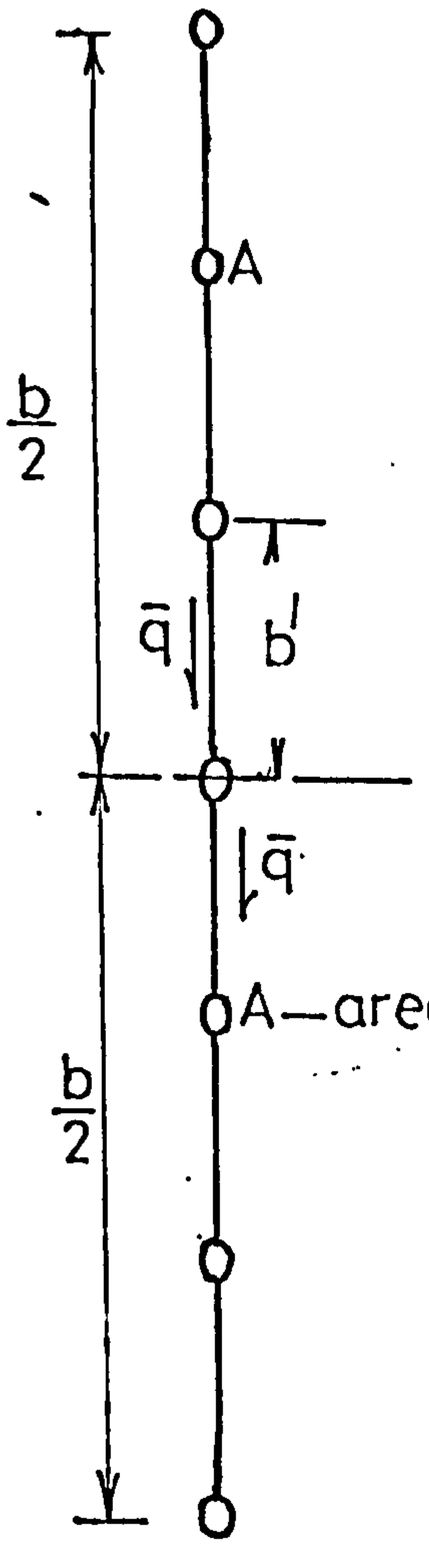

FIG (7.7 (a))

n_p — number of purlins

n_p odd ; $I = 2A(b')^2 \sum_{r=1}^{N} r^2$; $N = \frac{(n_p-1)}{2}$

$$I = 2.\frac{N}{6}.\{N+1\}.\{2N+1\}.A.(b')^2 \quad ; \quad b = (n_p-1).b'$$

$$I = \frac{A\,b^2}{12}\ \frac{(n_p+1).n_p}{(n_p-1)}$$

for unit shear force — max. shear flow

$$\bar{q} = \frac{\sum_{r=1}^{N} r.Ab'}{I} = \frac{N}{2}.(N+1).\frac{Ab'}{I}$$

$$= \frac{3}{2}.\frac{(n_p-1)}{n_p.b}$$

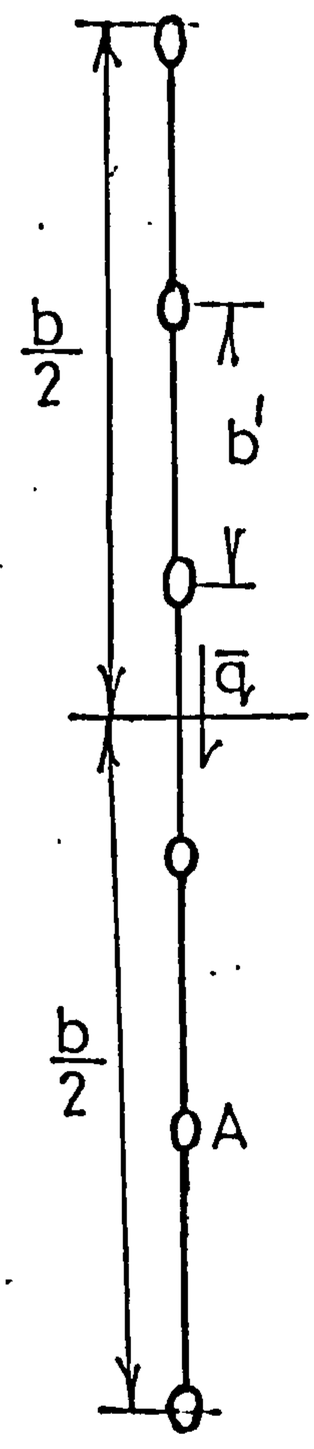

FIG (7.7(b))

n_p even ; $I = 2A(b')^2 \sum_{r=1}^{N} (r-0,5)^2$; $N = \frac{n_p}{2}$

$$I = \frac{Ab^2}{12}.\ \frac{(n_p+1)\,n_p}{(n_p-1)} \quad ; \quad b = (n_p-1).b'$$

max shear flow.

$$\bar{q} = \sum_{r=1}^{N} (r-0,5)\frac{Ab'}{I}$$

$$= \frac{n_p^2 Ab'}{8I} = \frac{3}{2}.\frac{n_p}{(n_p+1)}$$

if $n_p \longrightarrow$ large

$$I = A.n_p.\frac{b^2}{12}$$

$$\bar{q} = \frac{3}{2}\frac{Q}{b}$$

Q —shear force

CONTINUOUS DIAPHRAGM

—CONTRIBUTION OF SHEET TO BEAM INERTIA

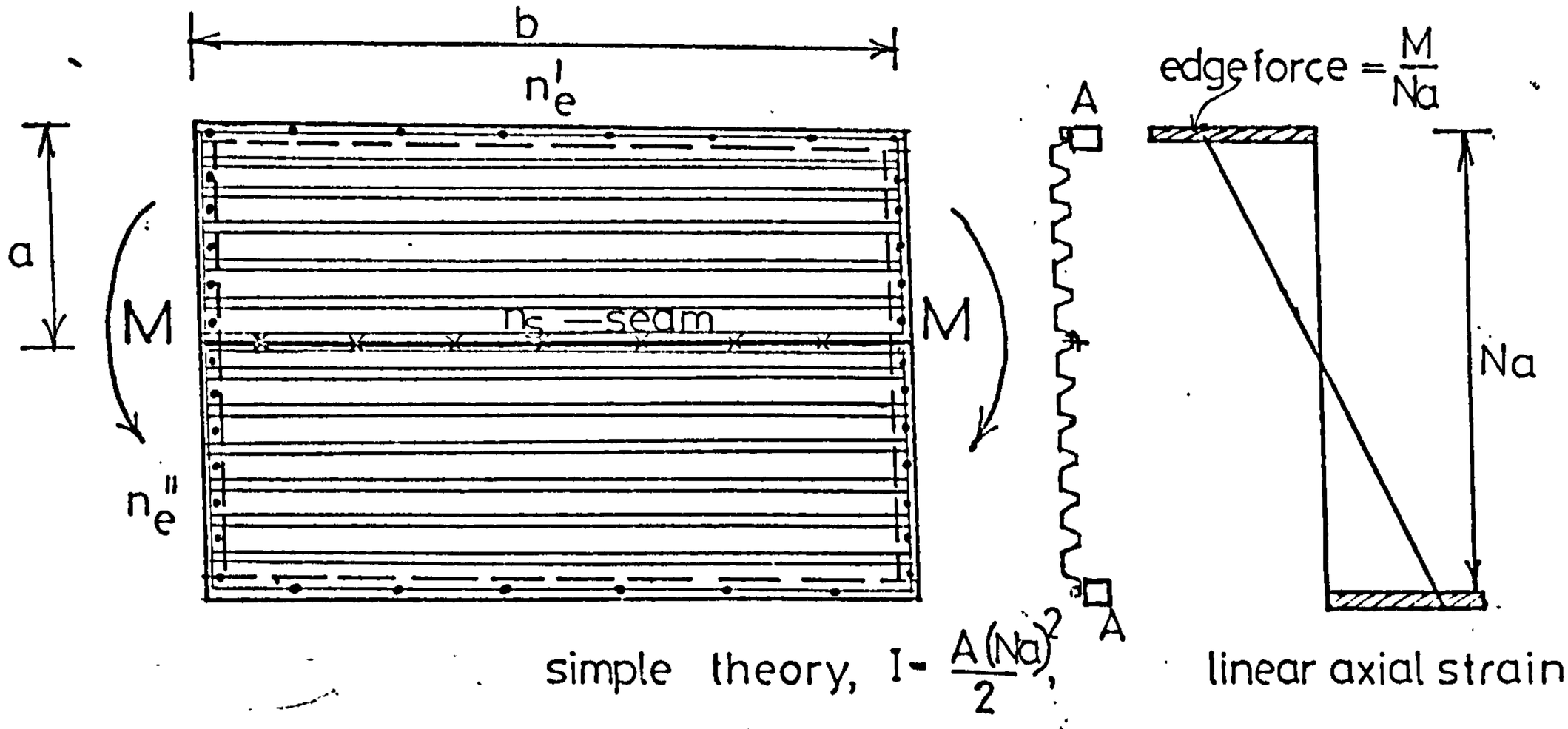

simple theory, $I = \frac{A(Na)^2}{2}$,

linear axial strain

n'_e — number of edge fasteners
n''_e — number of rafter fasteners
n_s — number of seam fasteners
N — number of sheets

FIG(7.8(a))

REAL SITUATION

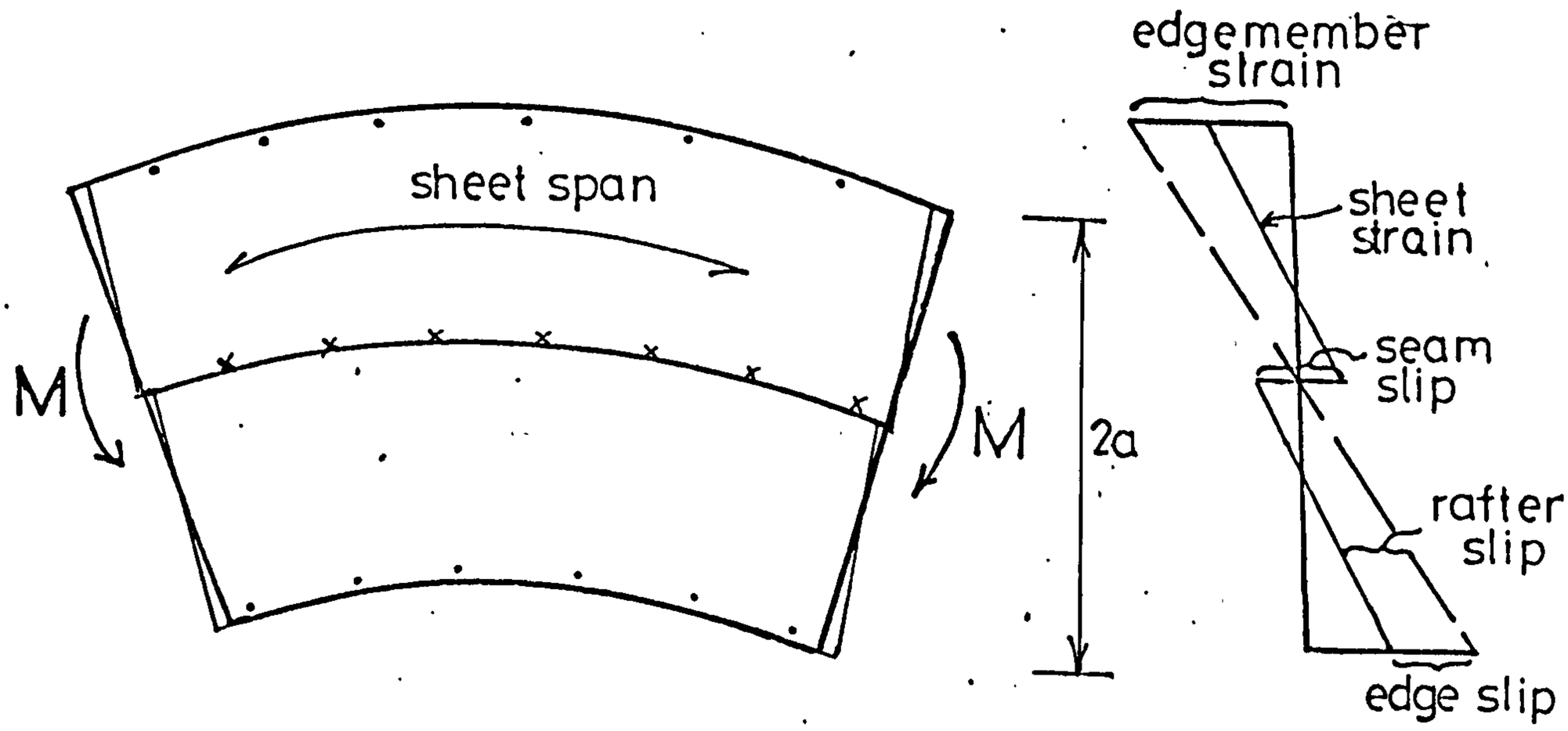

AXIAL STRAIN TRANSMITTED TO BOTH BEAM AND SHEET

NET SHEET STRAIN

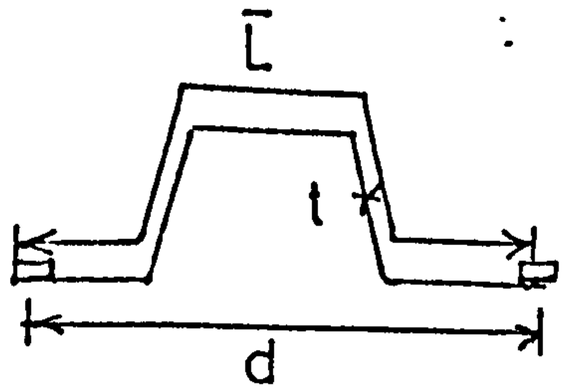

FIG(7.8(b))

$\therefore$ SHEET INERTIA = $t\frac{\bar{L}}{d}\frac{(Na)^3}{12}\alpha$

α — reduction factor

GENERAL FORMULATION — SHEET INERTIA

ODD SHEET NUMBER, N

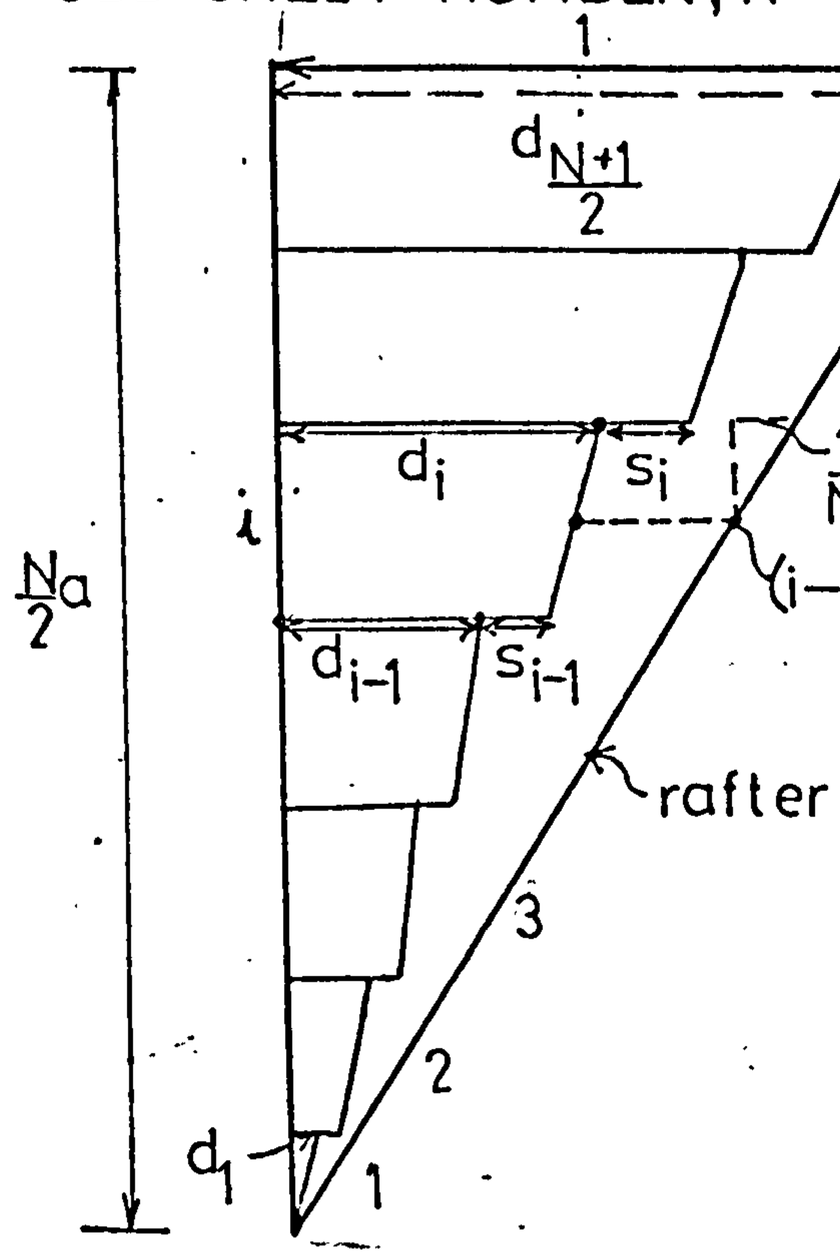

NET SHEET STRAIN

FIG(7.9(a))

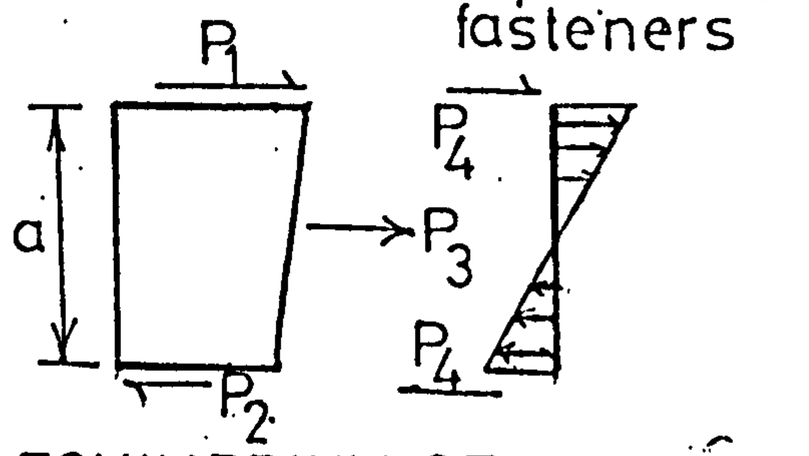

EQUILIBRIUM OF ELEMENT

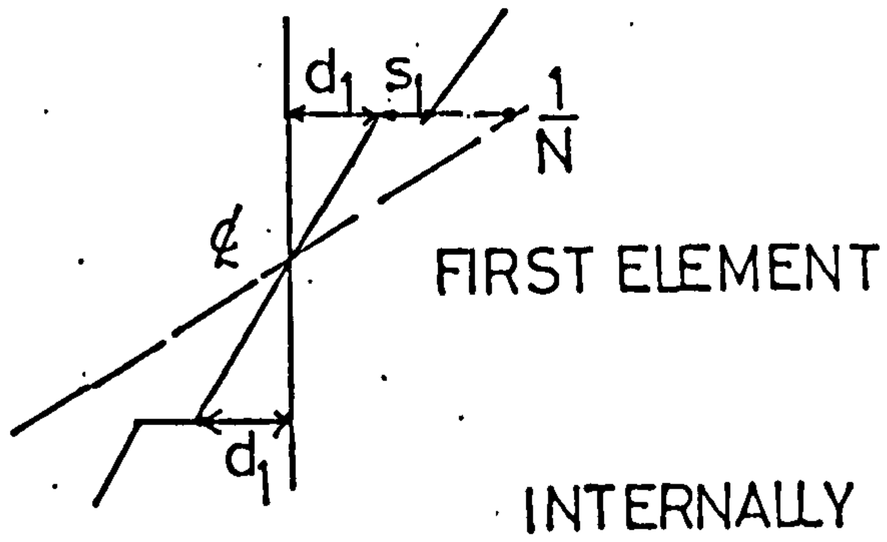

FIRST ELEMENT

INTERNALLY

$P_1 = s_i k_s$

$P_2 = s_{i-1} k_s$

$P_3 = \left\{\frac{2(i-1)}{N} - \frac{(d_i + d_{i-1} + s_{i-1})}{2}\right\}\frac{k_e''}{N}$

N, odd

$P_4 = \left\{\frac{1}{N} - \frac{(d_i - d_{i-1} - s_{i-1})}{2}\right\}\frac{k_e''}{6N}$

$P_3 = \left\{\frac{(2i-1)}{N} - \text{etc} \cdots\right\}\frac{k_e''}{N}$

N, even

EVEN SHEET NUMBER, N

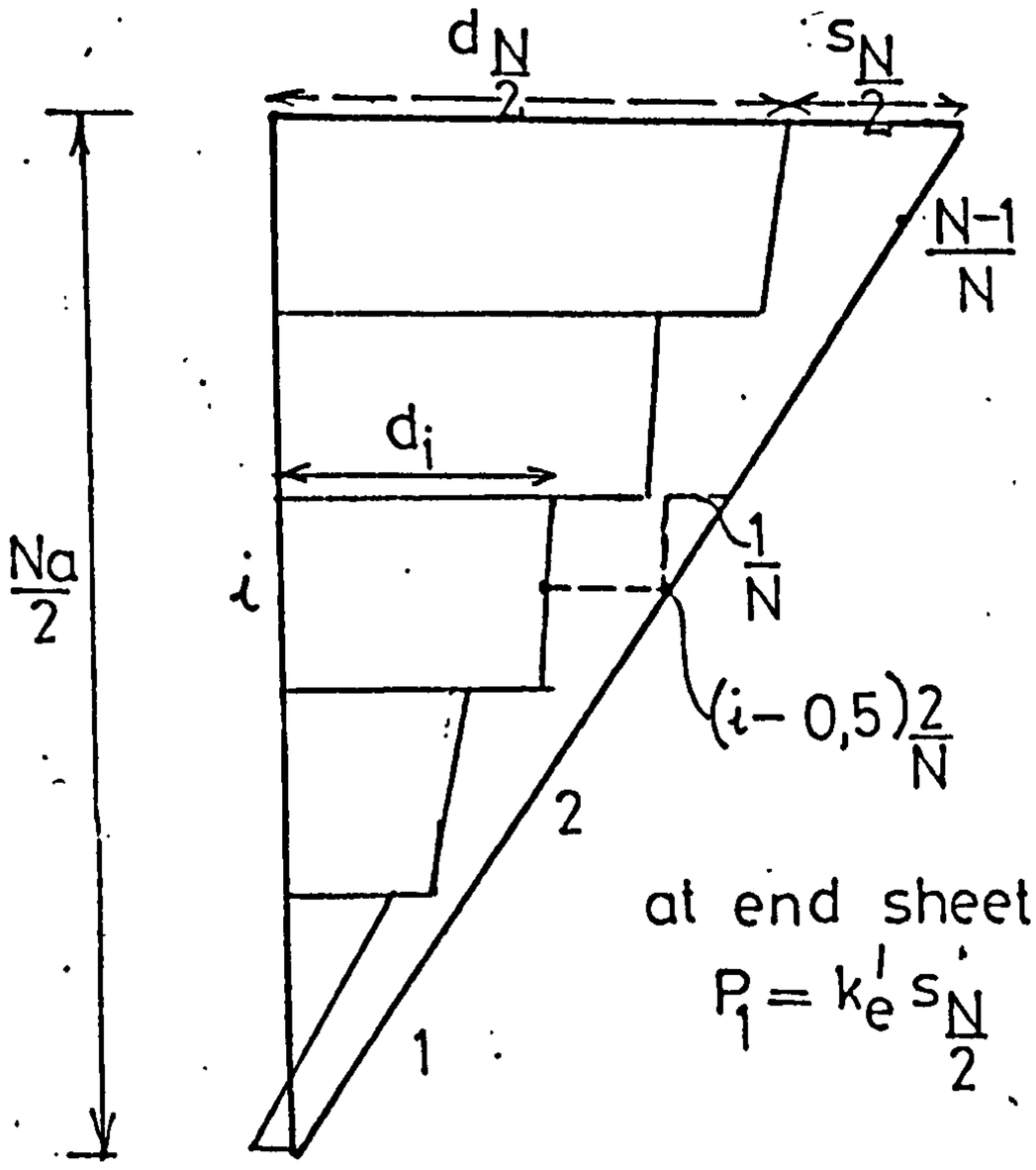

at end sheet,

$P_1 = k_e' s_{\frac{N}{2}}$

FASTENER SLIP FACTORS

k_s, k_e', k_e''

FIG (7.9(b))

FIRST ELEMENT

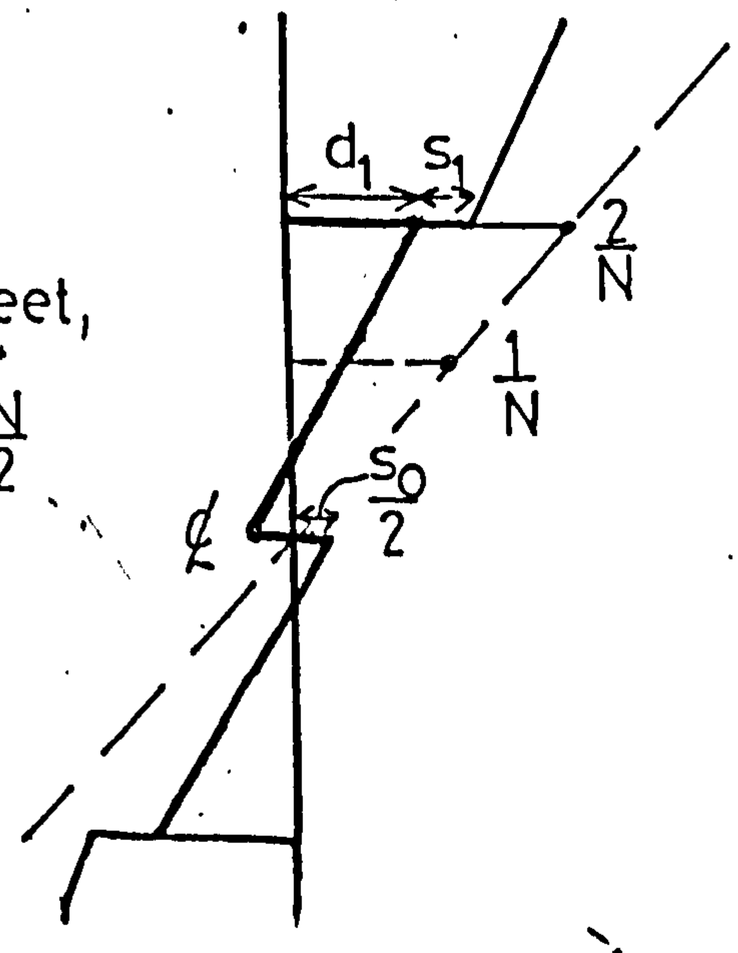

REDUCED SHEET INERTIA

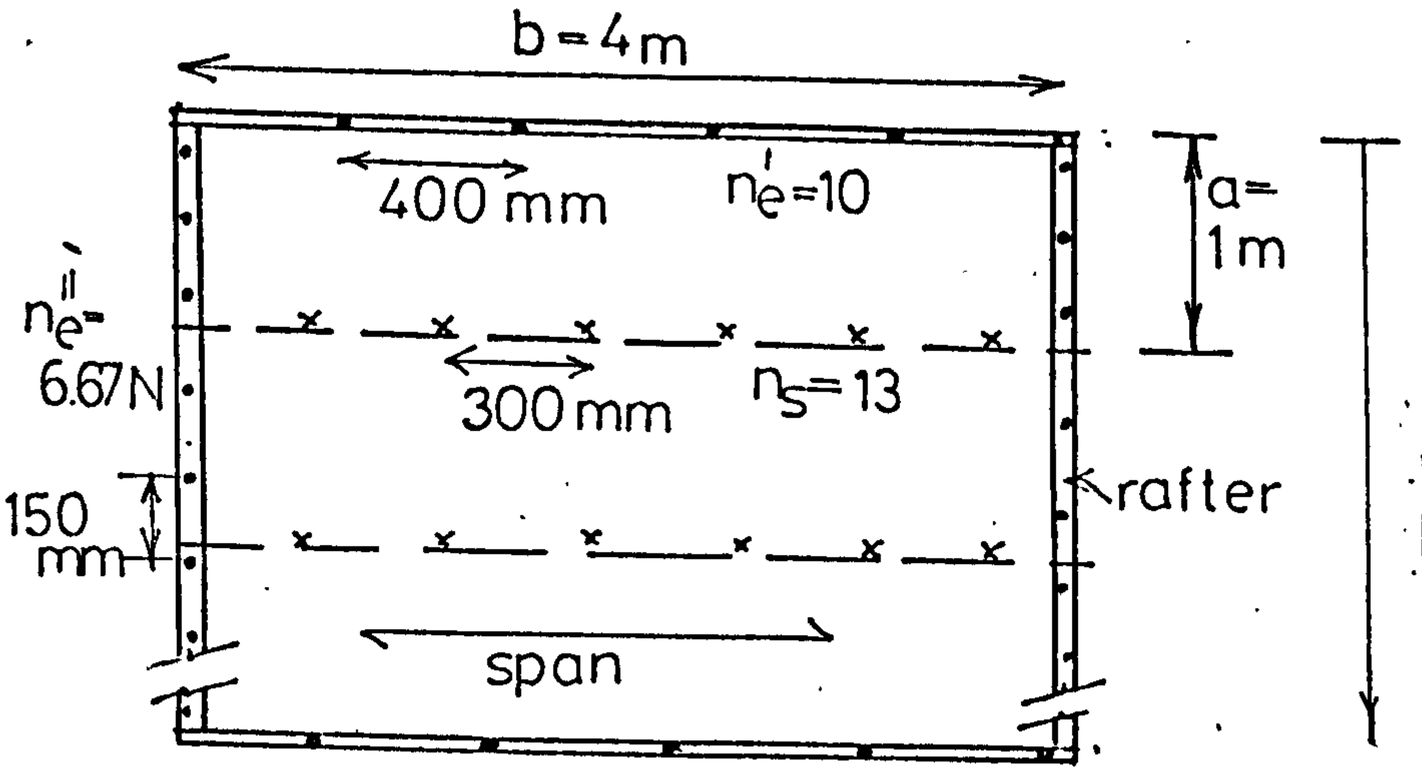

DATA :

$$k'_e = \frac{b}{a} \cdot \frac{n'_e}{s_e E t}$$

$$k_s = \frac{b}{a} \cdot \frac{n_s}{s_s E t}$$

$$k''_e = \frac{b}{a} \cdot \frac{n''_e}{s_e E t}$$

s_e= 0,15 mm/kN/mm
s_s= 0,35 ,,

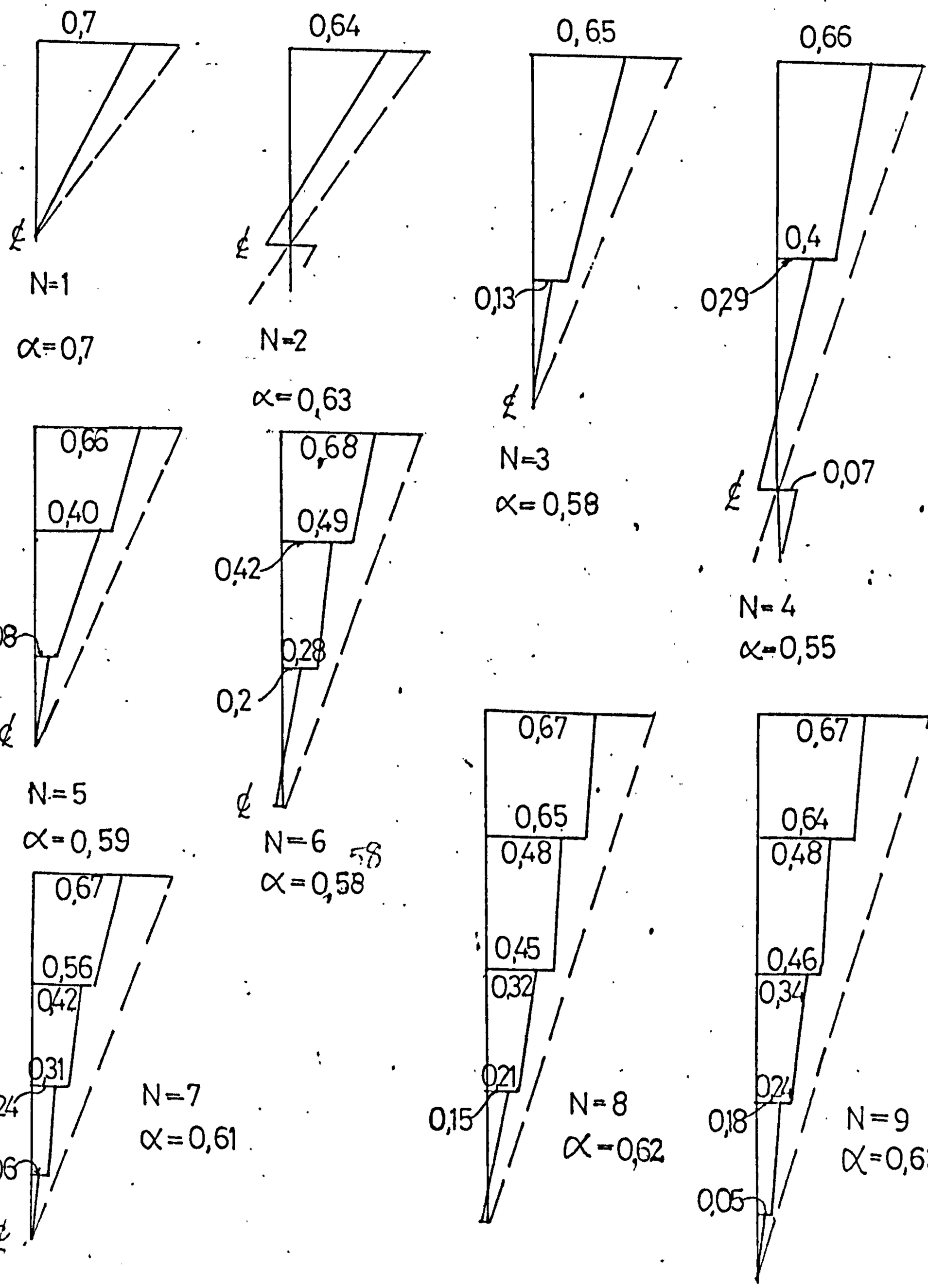

FIG(7.10)

CONTINUOUS DIAPHRAGM — MULTI BAYS

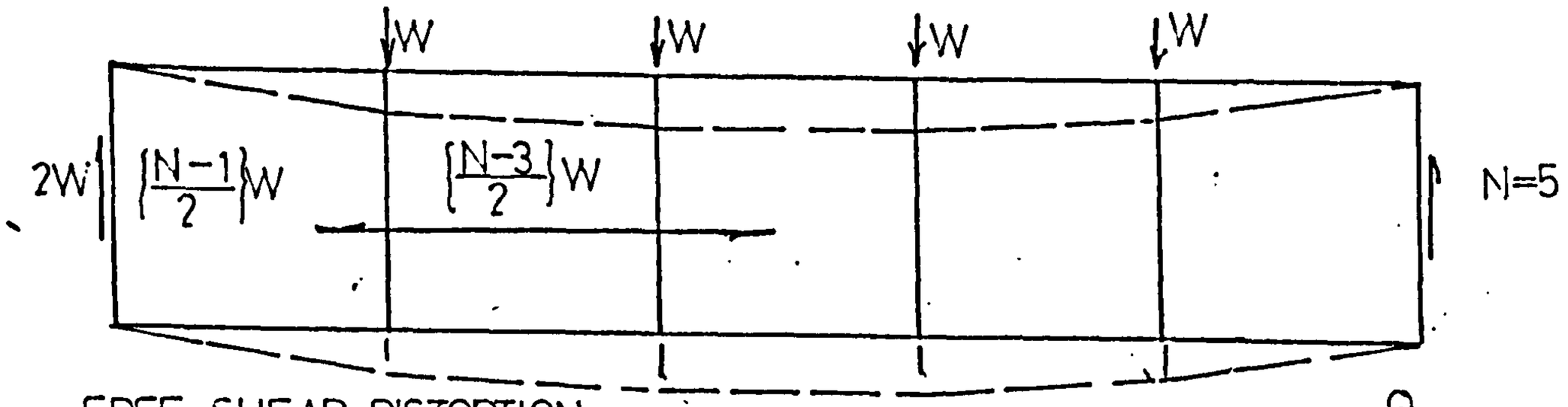

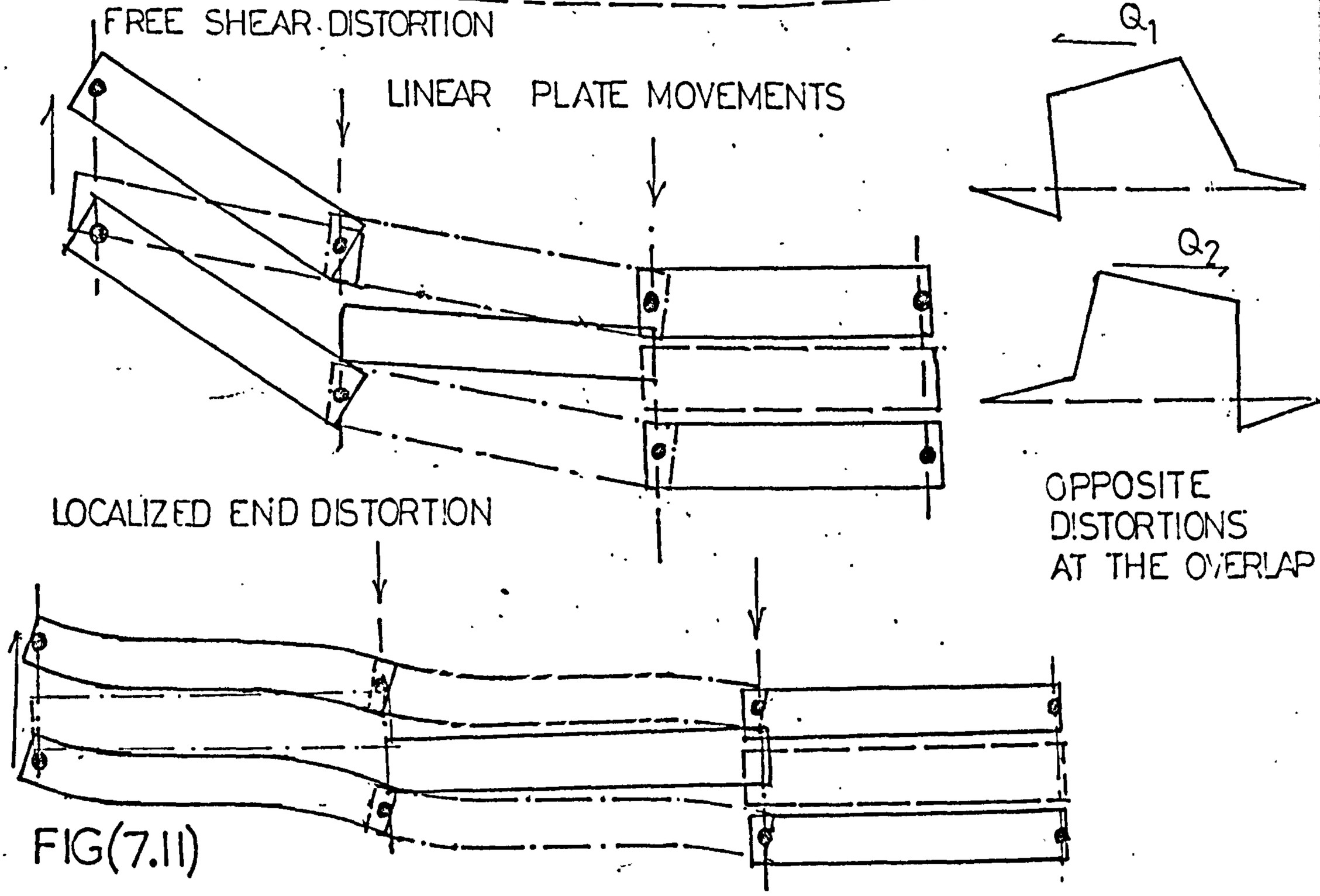

FIG(7.11)

2 BAY CONTINUOUS SHEET — TROUGH BENDING

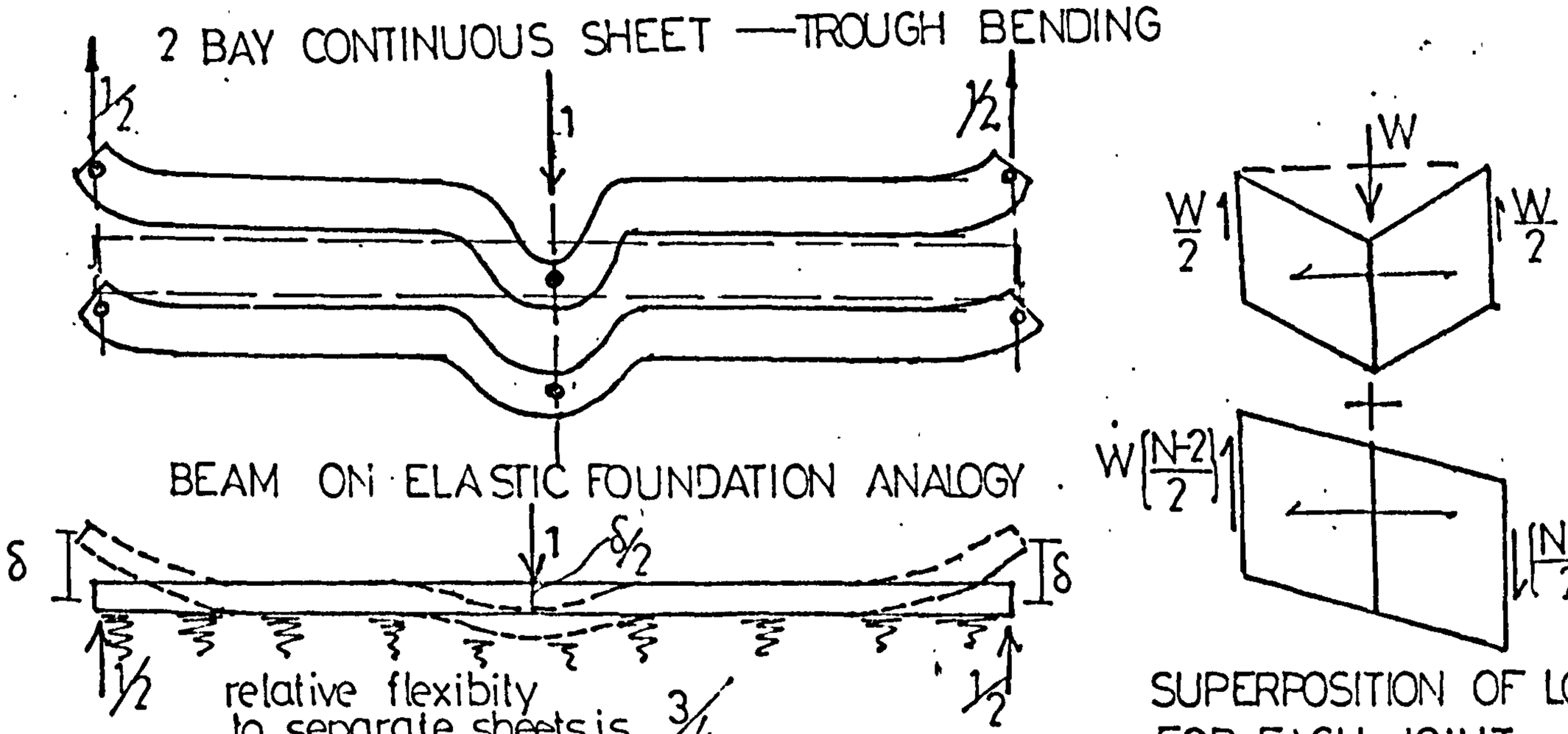

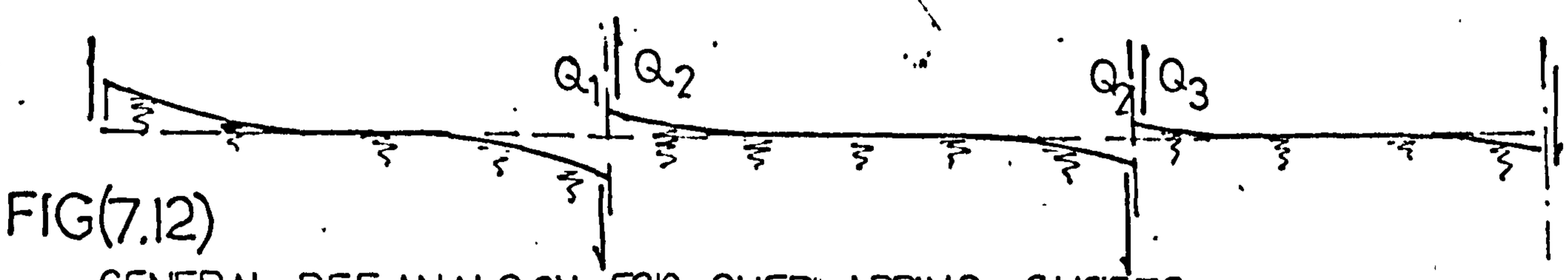

FIG(7.12)

GENERAL B.E.F. ANALOGY FOR OVERLAPPING SHEETS

CONTINUOUS DIAPHRAGM — OVERLAPPING SHEETS

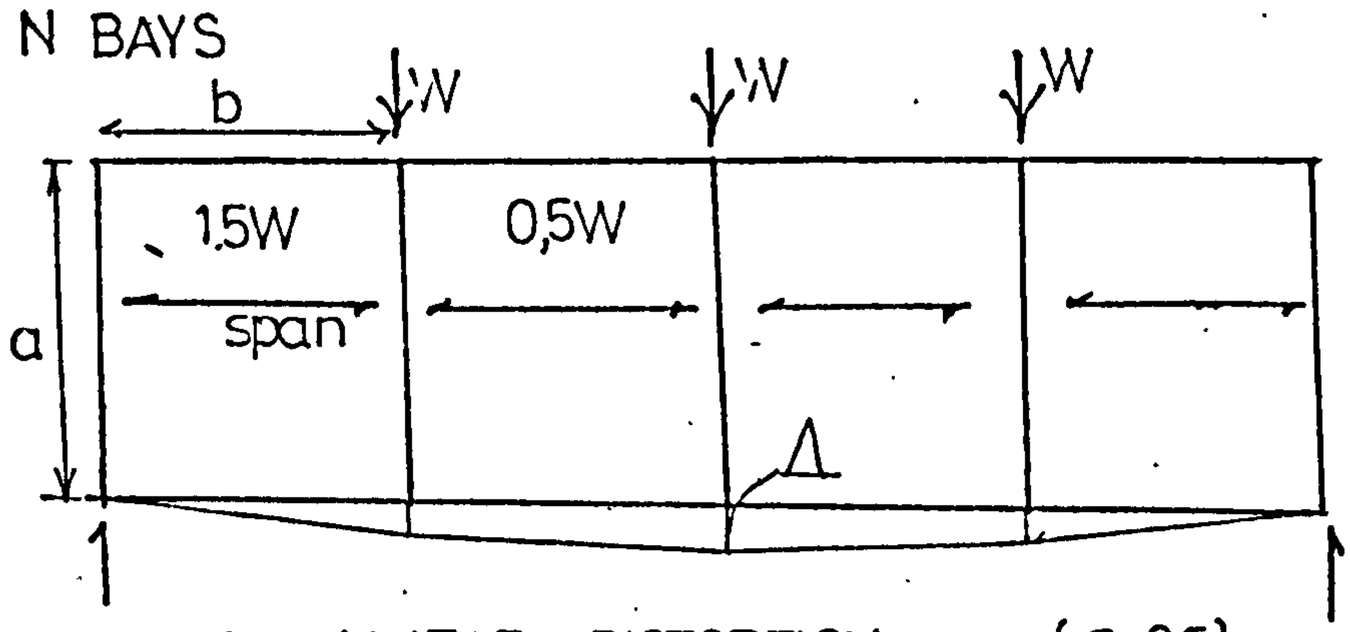

N-EVEN; LINEAR DISTORTION $X_1 = \left\{\frac{1.5+0.5}{2}\right\}(1-\varepsilon)$

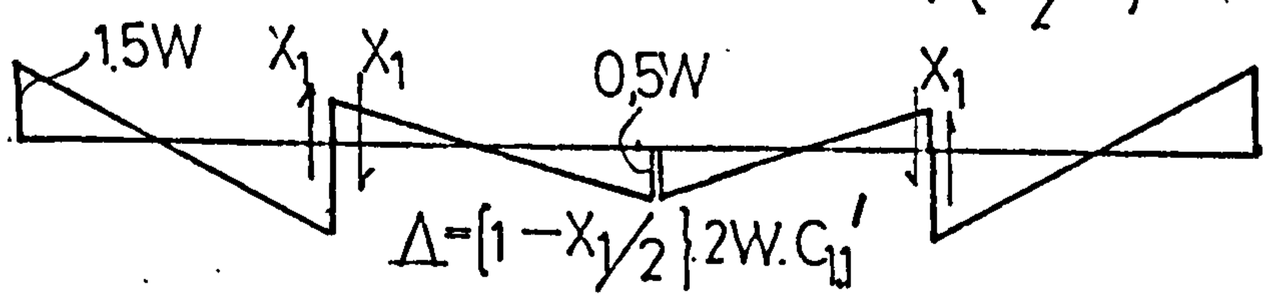

$\Delta = \{1 - X_1/2\}\, 2W.C_{1,1}'$

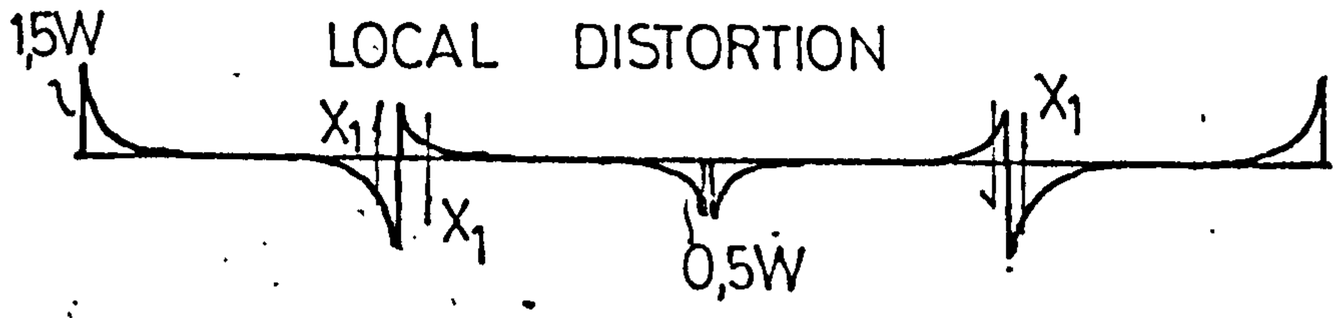

N—ODD LINEAR DISTORTION

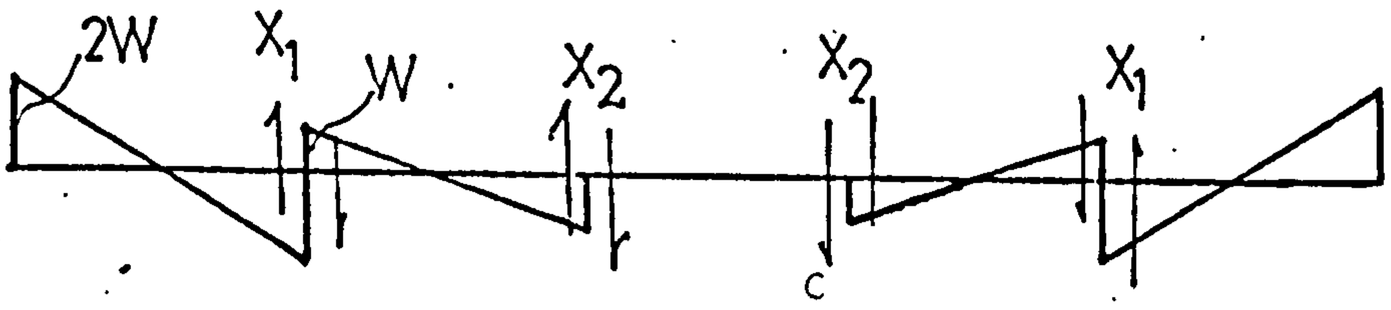

LOCAL DISTORTION

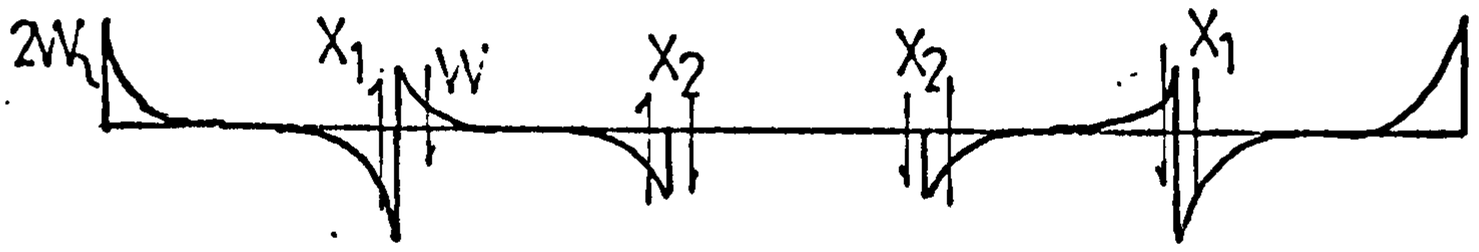

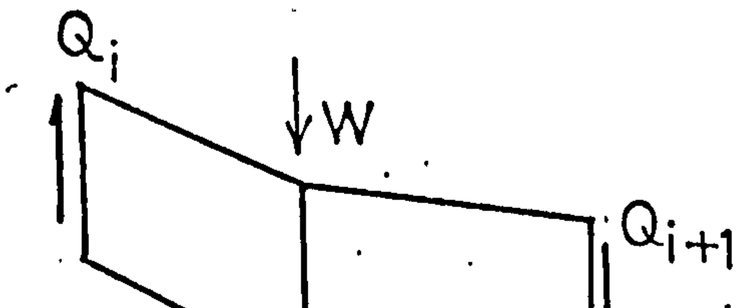

$C_{1,1}' = C_{1,1}\left\{\frac{b}{a}\right\}^2$ — sheet distortion flexibility

FREE CENTRAL DEFLECTION

$\Delta_o \doteq \left\{\frac{N^2-1}{8}\right\} C_{1,1}' W$

relative deflection = $\frac{\Delta}{\Delta_o}$

RELATIVE DEFLECTION $\frac{\Delta}{\Delta_o} = \frac{2}{N} + \left(1 - \frac{2}{N}\right)\varepsilon$ — approximate formula for local end distortion (flexible)

$\frac{\Delta}{\Delta_o} = \frac{1}{N-1} + \left\{\frac{N-2}{N-1}\right\}\varepsilon$ — approx formula for rigid movements

ε — overlap factor <1

N	relative deflection		approx. formula	
	flexible	rigid	flexible	rigid
3	0,75+0,25ε	0,5+0,5ε	0,67+0,33ε	0.5+0.5ε
4	0,5+0,5ε	0,25+0,75ε	0.5+0,5ε	0,33+0,67ε
5	0,42+0,58ε	0,23+077ε	0,4+0,6ε	0,25+0,75ε
6	0,33+0,67ε	0,2+0,8ε	0,33+0,67ε	0,2+0,8ε
7	0,29+0,71ε	0,18+0,82ε	0,29+0,71ε	0,17+0,83ε
8	0,25+0,75ε	0,15+0,85ε	0,25+0,75ε	0,14+0,86ε
9	0,21+0,79ε	0,16+0,84ε	0,22+0,78ε	0,13+0,87ε

FIG(7.13)

CONTINUOUS DIAPHRAGM — OVERLAPPING SHEETS

WITH VARIATIONS IN THE FASTENING ARRANGEMENT

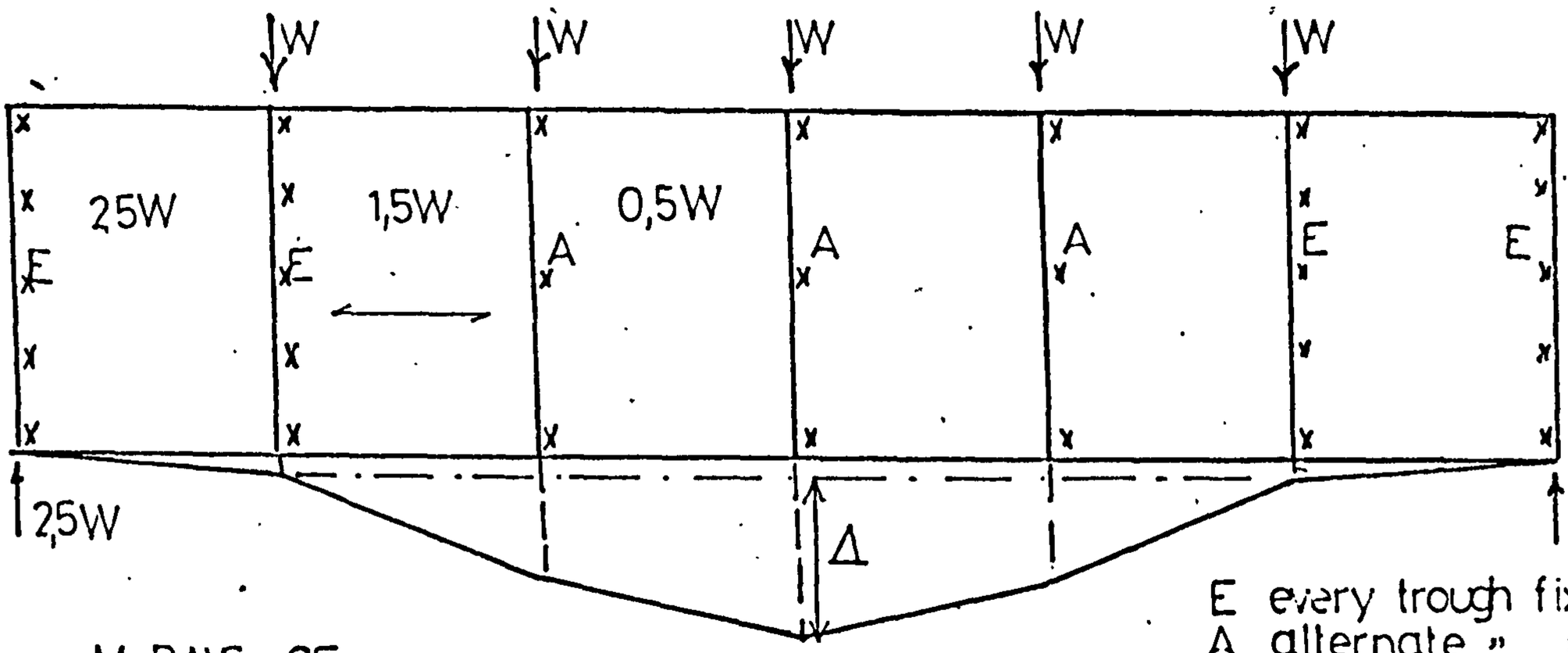

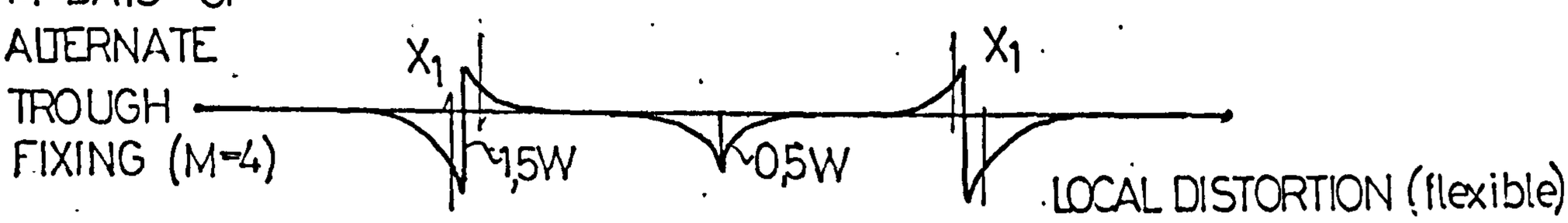

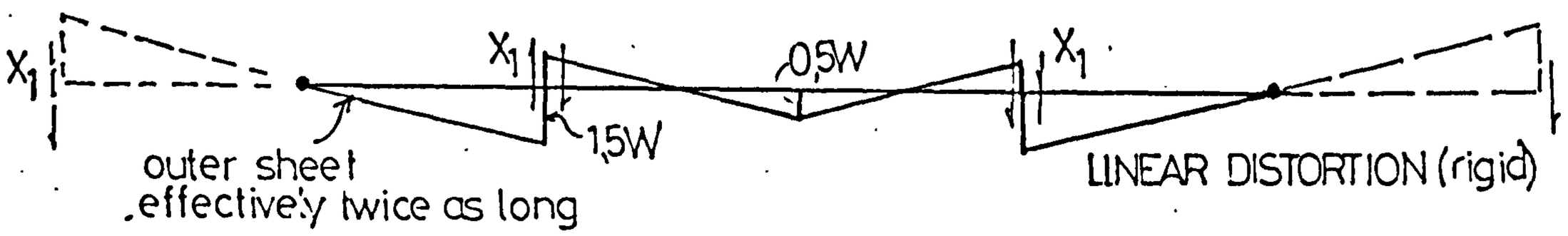

DEFORMATION PATTERN DUE TO ALTERNATE TROUGH FIXING

Δ_o — free centrd deflection for alternate trough fastening over M bays is $\left\{\frac{M^2-1}{8}\right\} C_{11A} \left[\frac{b}{a}\right]^2 W$

$\frac{\Delta}{\Delta_o} = \frac{1}{(4M-6)} + \left\{\frac{2M-4}{2M+1}\right\}\varepsilon$ — local end distortion

$\frac{\Delta}{\Delta_o} = \frac{1}{(3M-2)} + \left\{\frac{M-2}{M+3}\right\}\varepsilon$ — linear distortion

approximate formulae for relative defln.

ε — overlap factor due to alternate trough fixing

M	relative deflection		approx. formula	
	flexible	rigid	flexible	rigid
2	0,5	0,25	0,5	0,25
3	0,25+0,25ε	0,10 +0,15ε	0,17+ 0,28ε	0,14+ 0,16ε
4	0,13+0,50ε	0,10 +0,33ε	0,10 +0,45ε	0,10 +0,29ε
5	0,08 +0,58ε	0,09+0,40ε	0,07+0,52ε	0,09 + 0,38ε
6	0,06+0,67ε	0,07 +0,51ε	0,06 +0,61ε	0,05 +0,46ε
7	0,04+0,71ε	0,08+0,55ε	0,05 +0,79ε	0,05 + 0,50ε
8	0,03+0,75ε	0,04 +0,62ε	0,04 +0,82ε	0,05 + 0,55ε

FIG (7.14)

SEAM FASTENER PERFORMANCE

'MONEL' POP-RIVET — 4 mm diameter

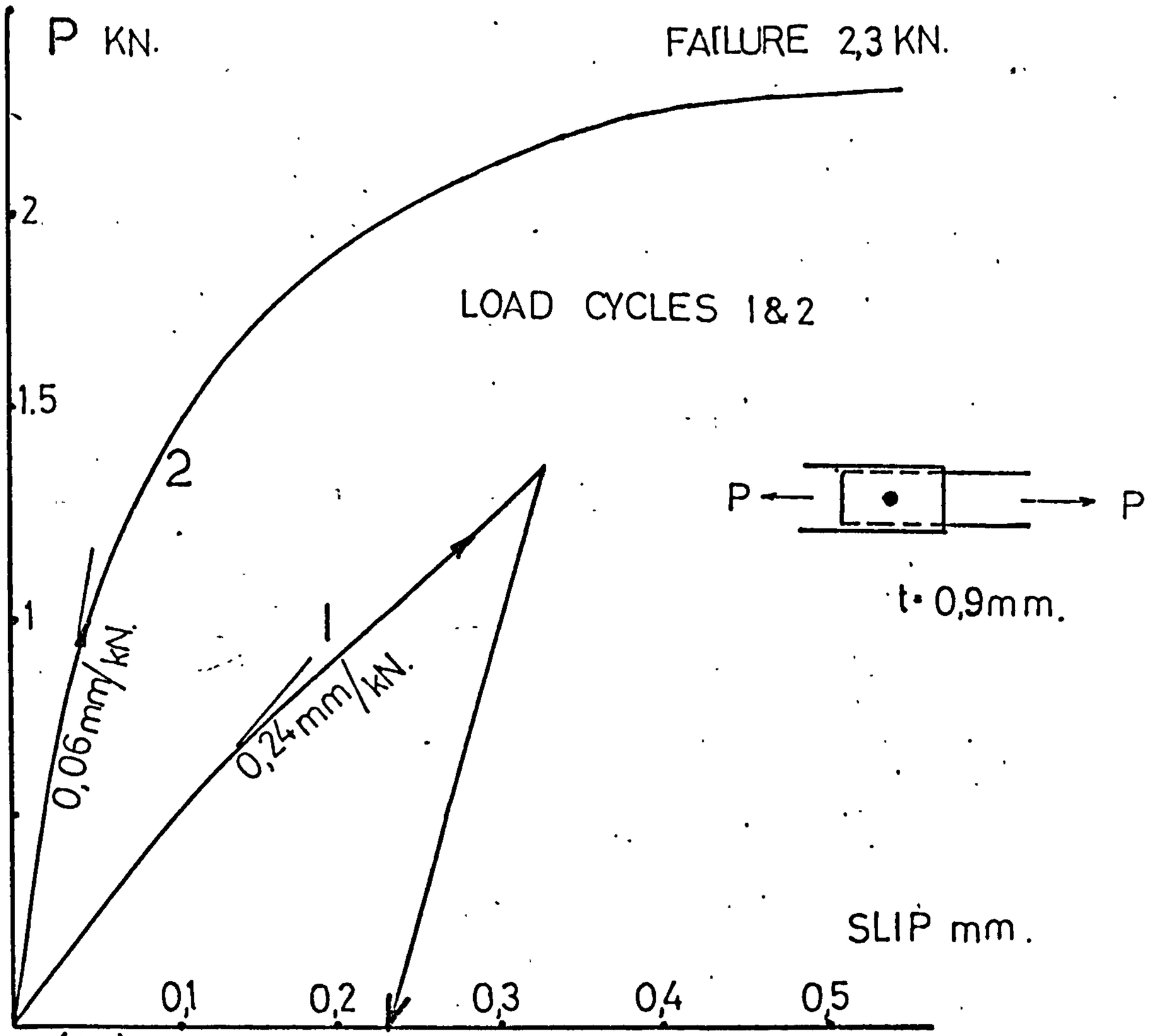

FIG(8.1)

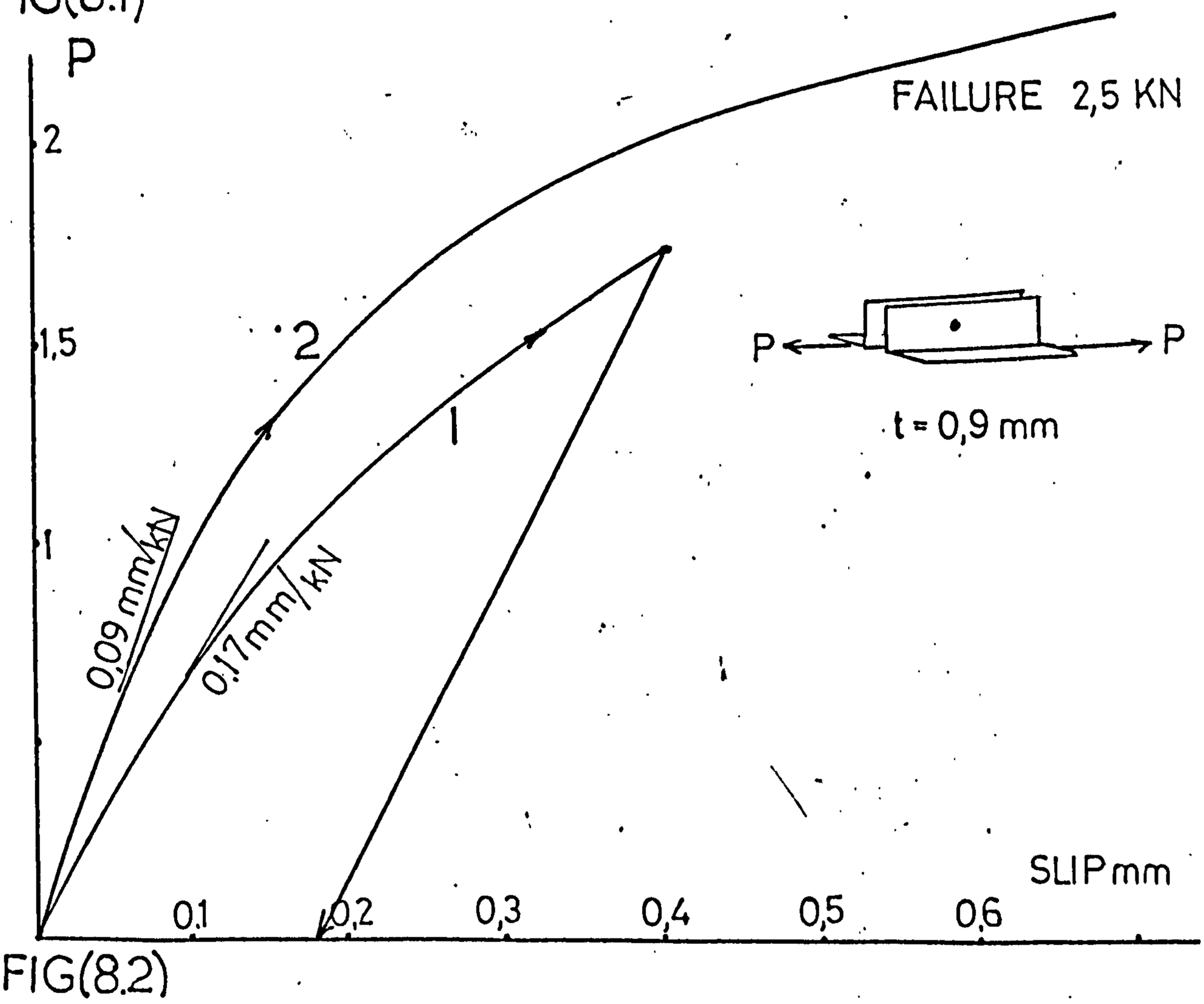

FIG(8.2)

PERFORMANCE OF BUTTON-PUNCH SEAMS

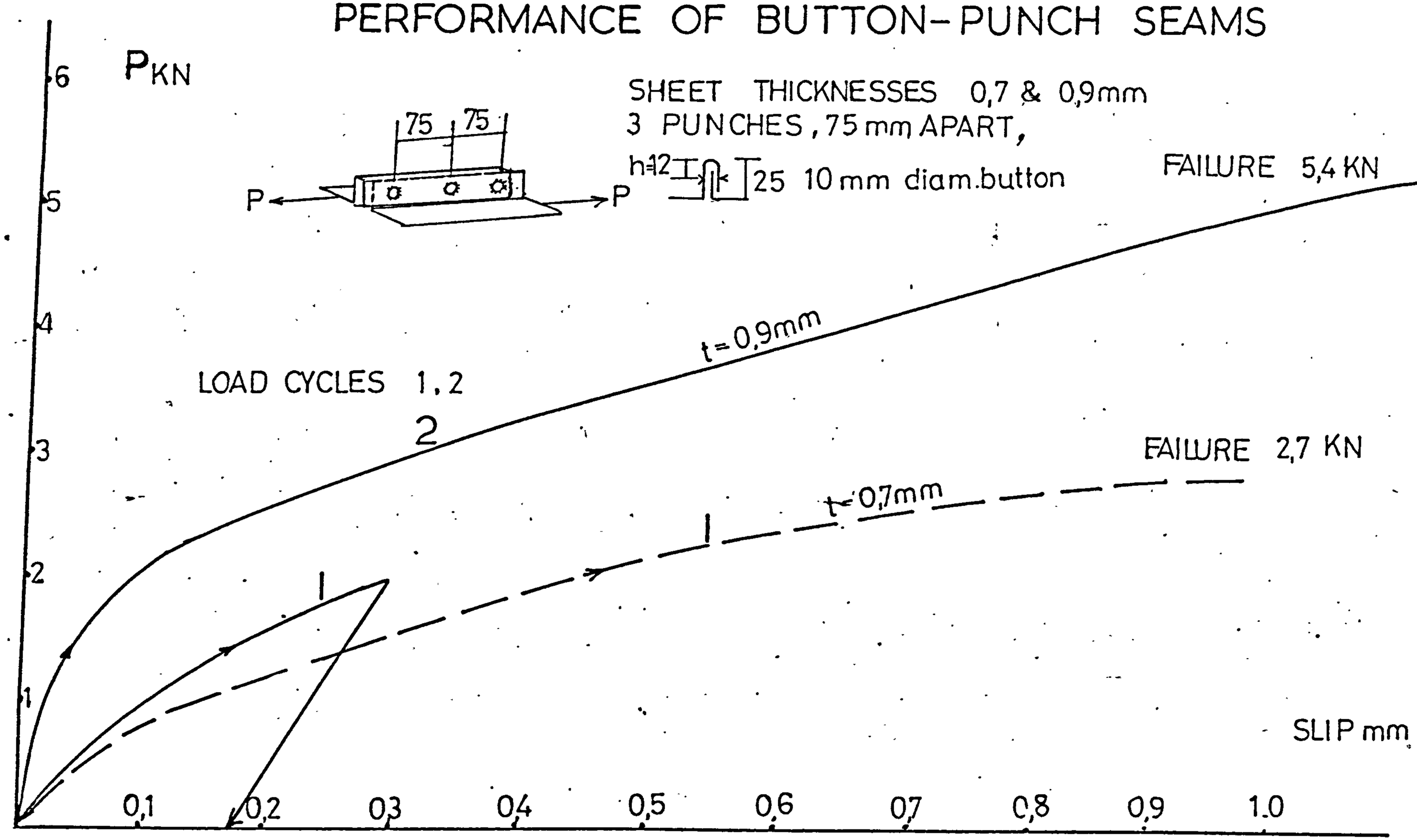

FIG(8.3)

INDIRECT SHEAR TRANSFER

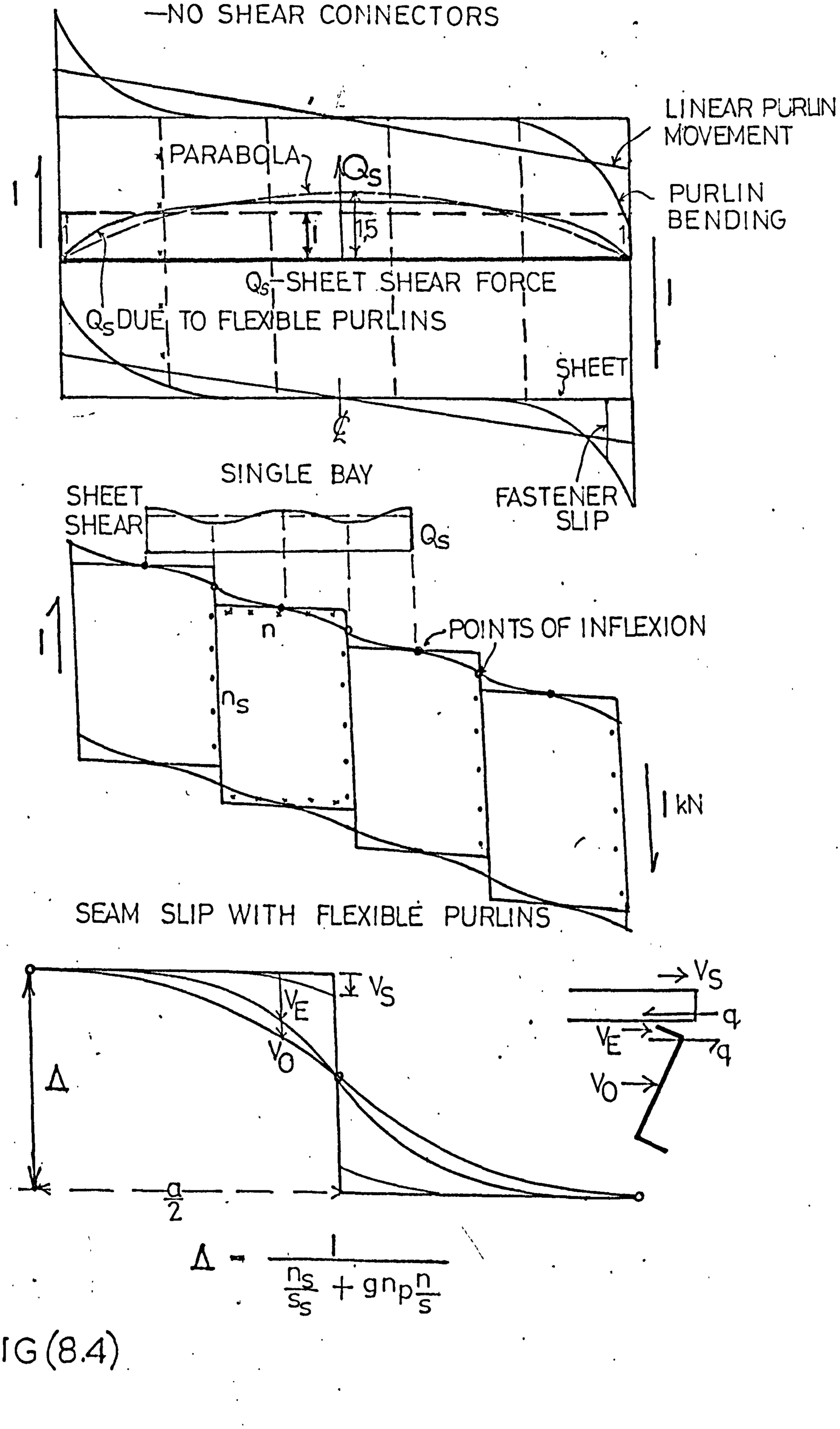

$$\Delta = \frac{1}{\frac{n_s}{s_s} + g n_p \frac{n}{s}}$$

FIG (8.4)

INDIRECT SHEAR TRANSFER–EFFECTIVE SHEET WIDTH

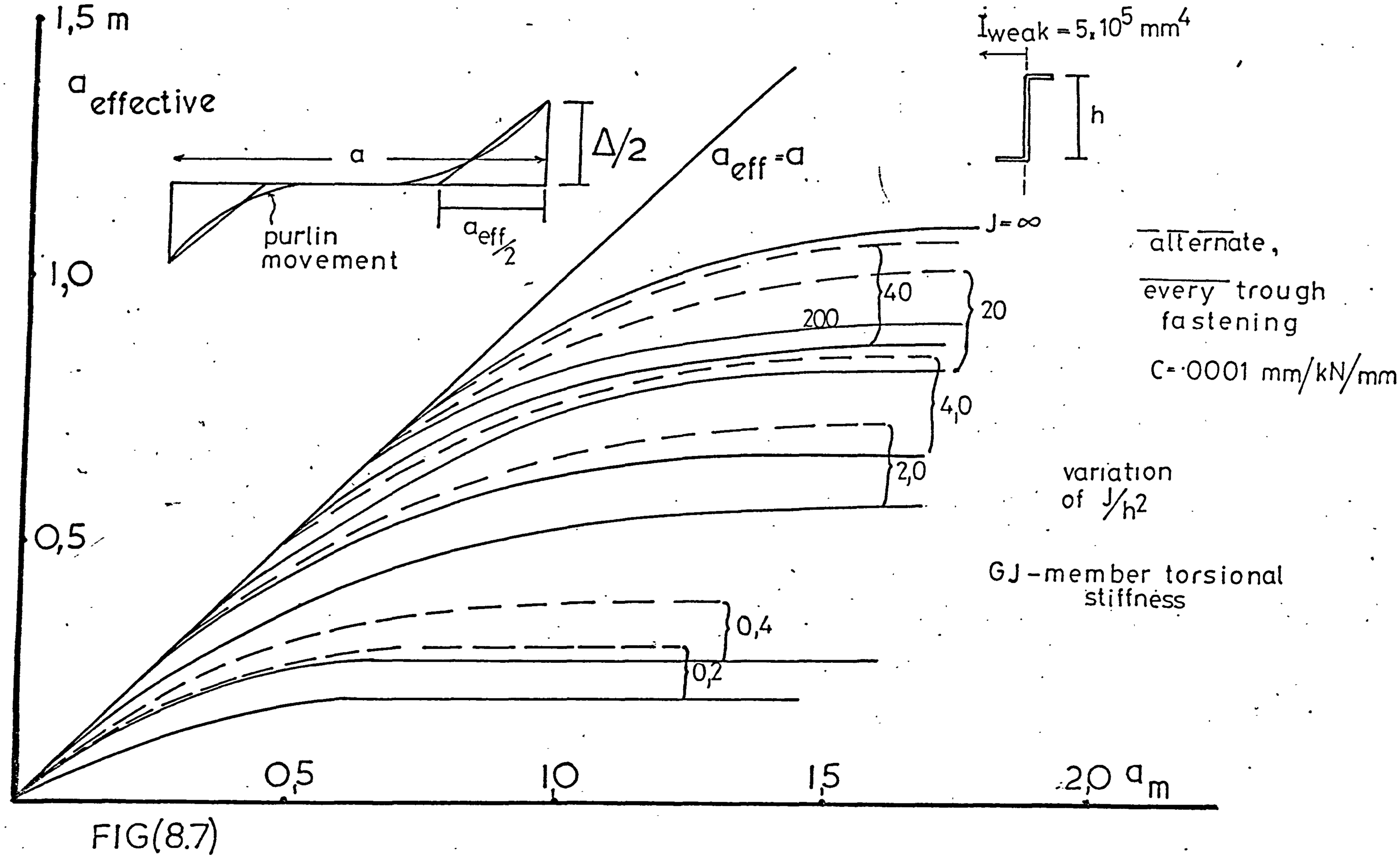

FIG(8.7)

INDIRECT SHEAR TRANSFER

PURLIN DISPLACED SHAPES

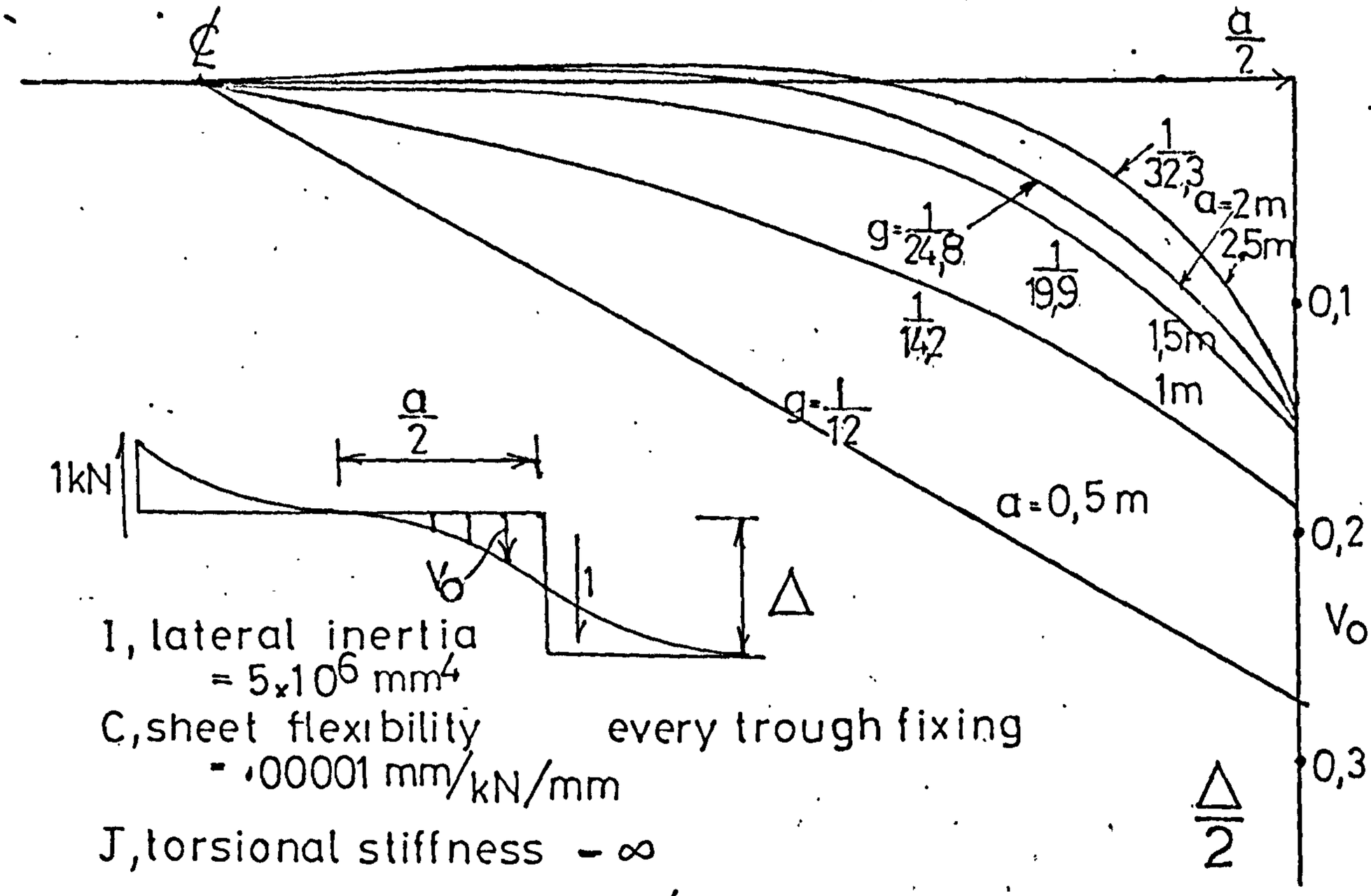

I, lateral inertia
$= 5 \times 10^6\ mm^4$

C, sheet flexibility every trough fixing
$= \cdot 00001\ mm/kN/mm$

J, torsional stiffness $= \infty$

$n_p = 1$; $n_s = 0$; $s = 0{,}15\ mm/kN$; $n = \frac{a}{150}$

FIG(8.5)

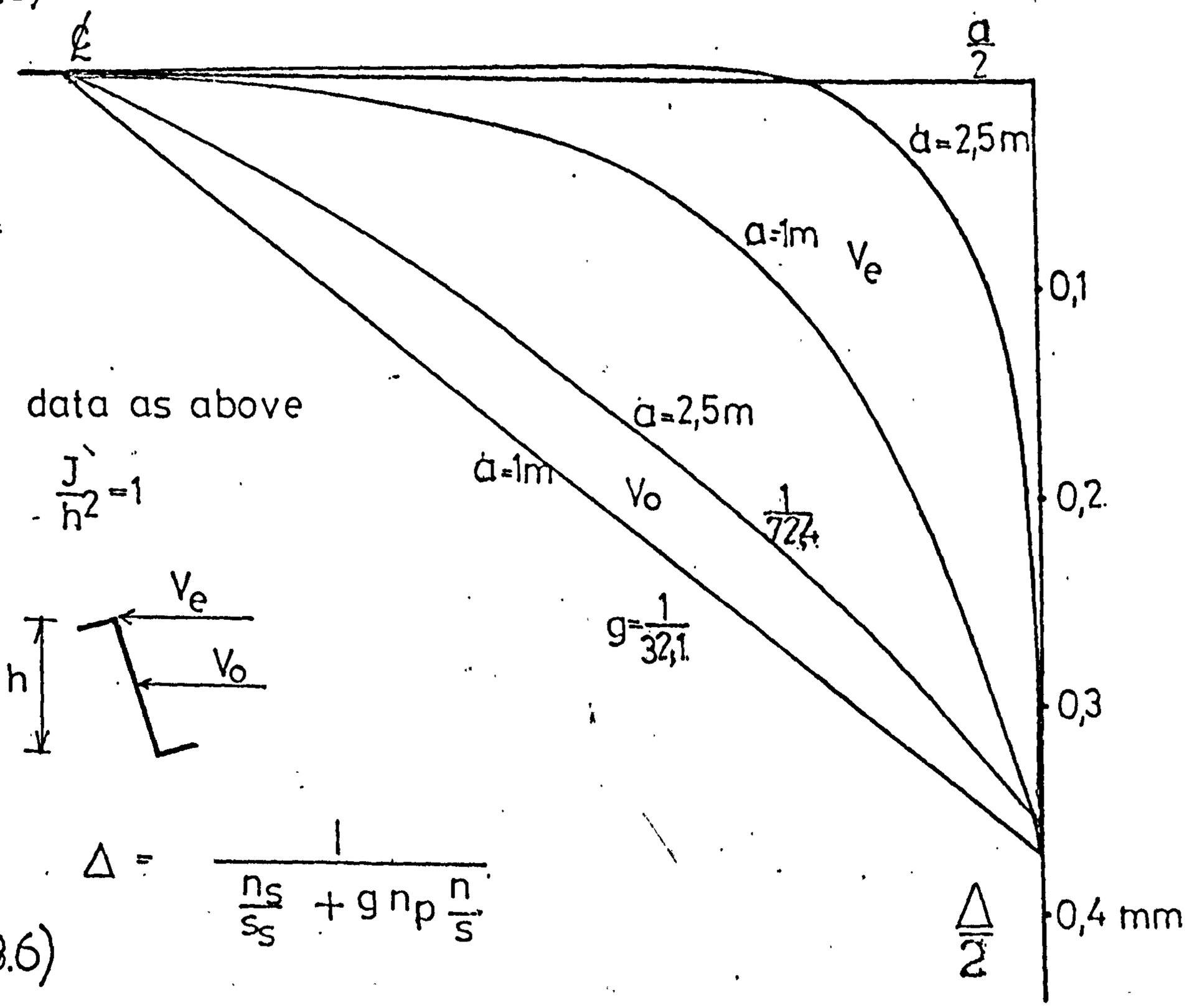

data as above

$\frac{J}{h^2} = 1$

$$\Delta = \frac{1}{\frac{n_s}{s_s} + g\, n_p \frac{n}{s}}$$

FIG(8.6)

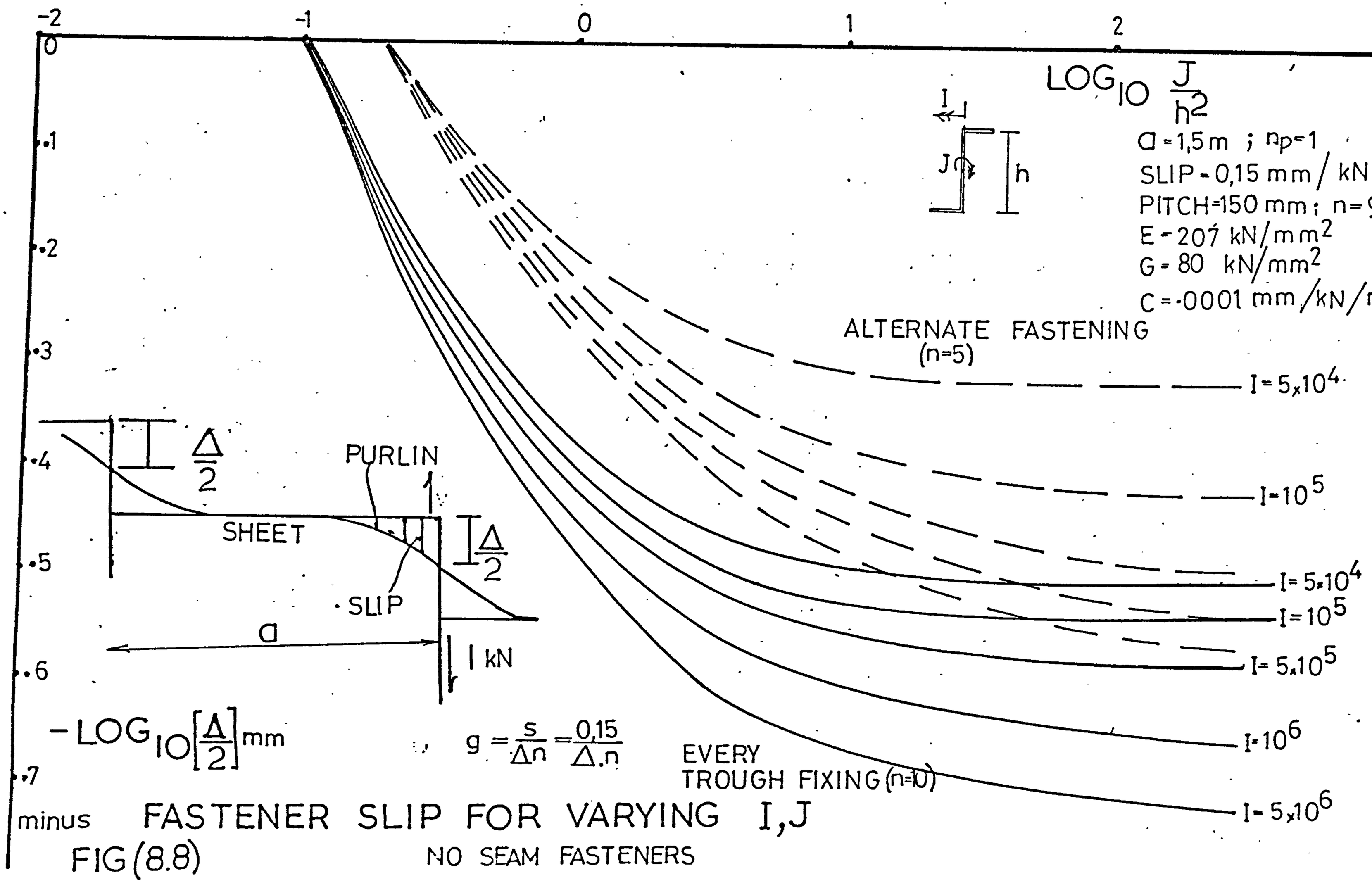

minus FASTENER SLIP FOR VARYING I, J

NO SEAM FASTENERS

FIG (8.8)

INFLUENCE OF SHEET FLEXIBILITY, C ON EFFECTIVE SHEET WIDTHS

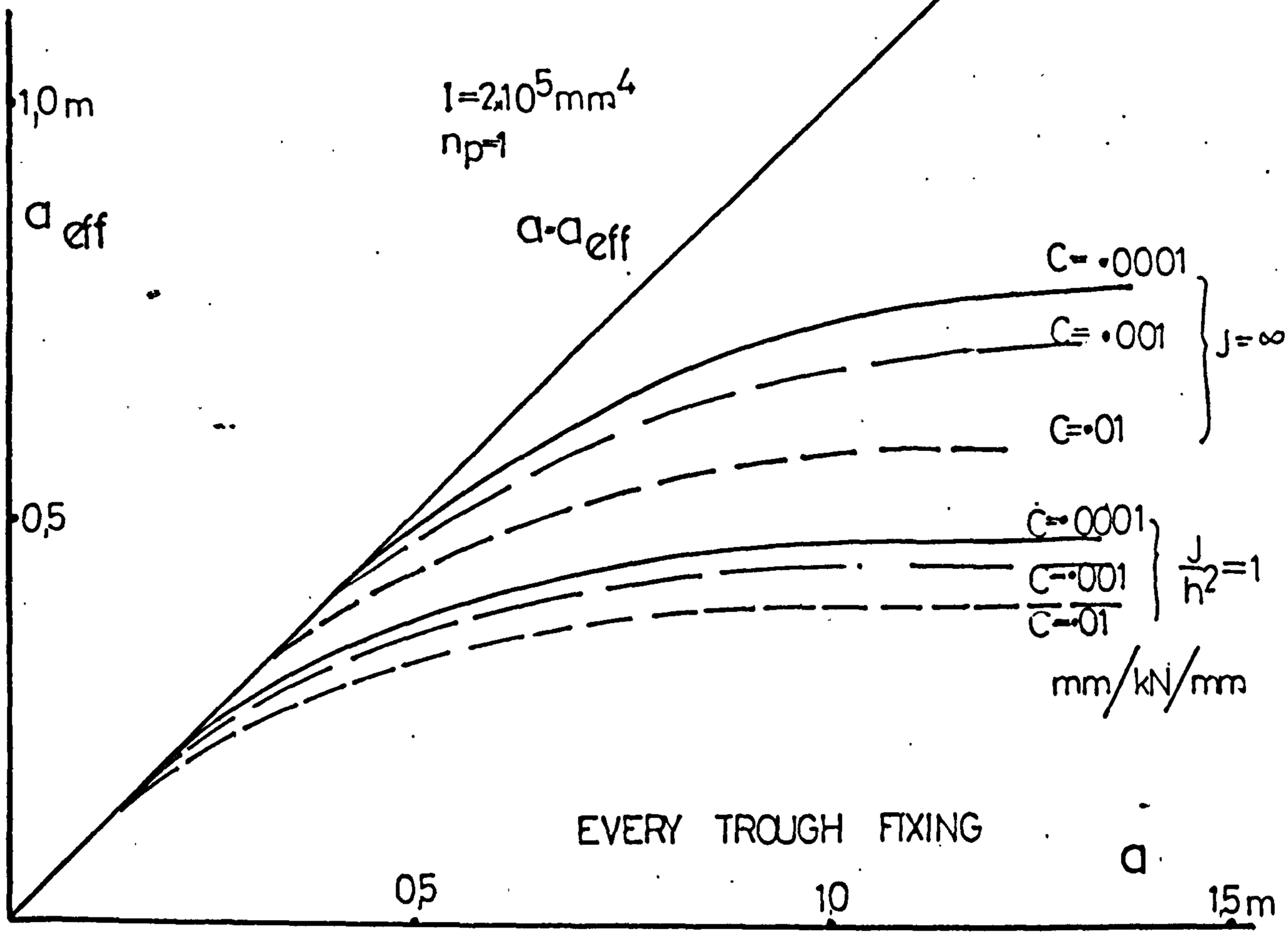

FIG (8.9)

TABULATION OF g_j FOR EFFECT OF PURLIN FASTENINGS ON SEAM SLIP — REF(94).

$$\Delta = \sqrt{\frac{n_s}{s_s} + \frac{g_1 n_p}{2 s}}$$

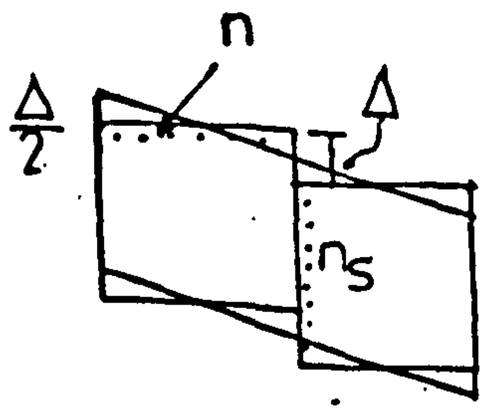

no of sheet purlin fixings n	decking ($b_l < b_T$)		roofing ($b_l > b_T$)	
	linear	quadratic	linear	quad.
2	1,00	1,00	0,25	0,13
3	1,00	1,00	0,44	0,30
4	1,11	1,04	0,63	0,44
5	1,25	1,13	0,80	0,58
6	1,40	1,22	0,97	0,71
7	1,56	1,33	1,14	0,84
8	1,71	1,45	1,31	0,97
9	1,88	1,56	1,48	1,10
10	2,04	1,68	1,65	1,23
11	2,20	1,80	1,82	1,35
12	2,36	1,92	1,99	1,48

$g_1 \rightarrow \frac{n}{12}$ (linear)

FIG (8.10)

COMPARISON OF DIFFERENTIAL EQUATION WITH FINITE ELEMENT RESULTS — REF(49)

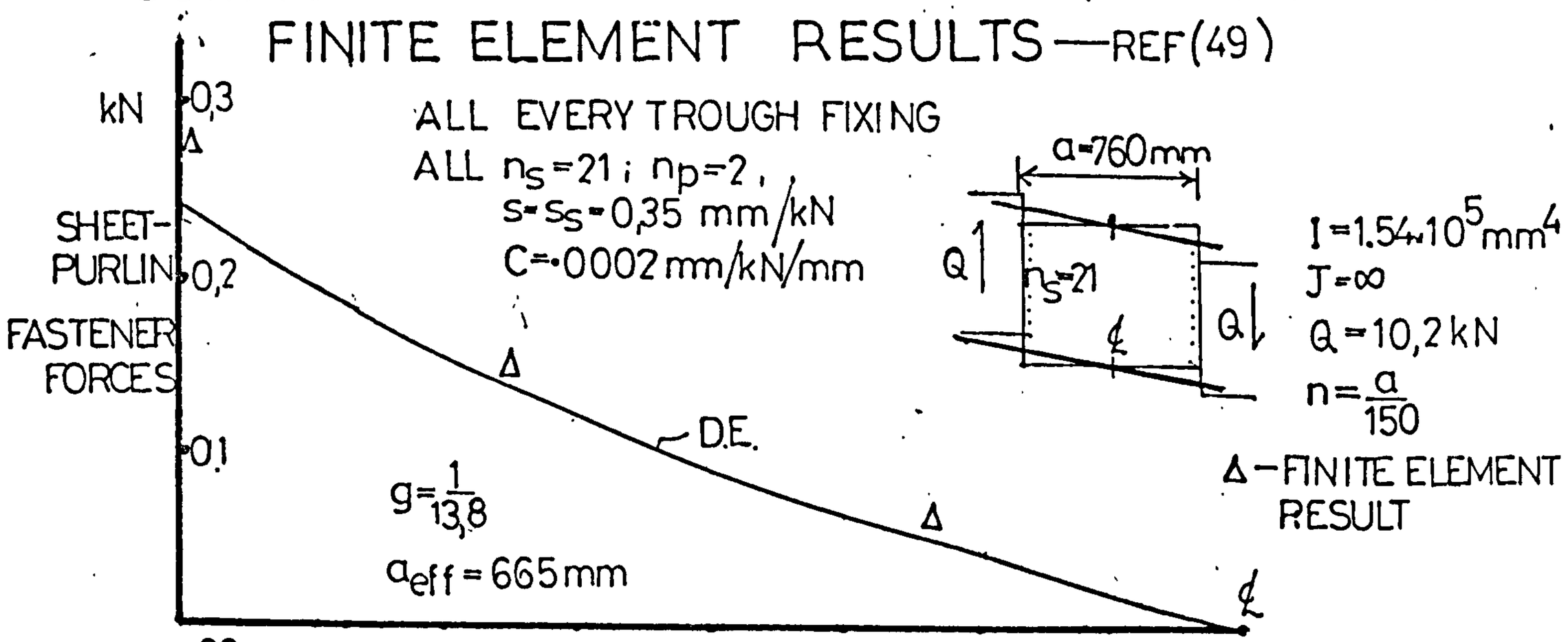

FIG(8.11)

LOCAL DEFORMATION AROUND RAFTER

—NO SHEAR CONNECTORS

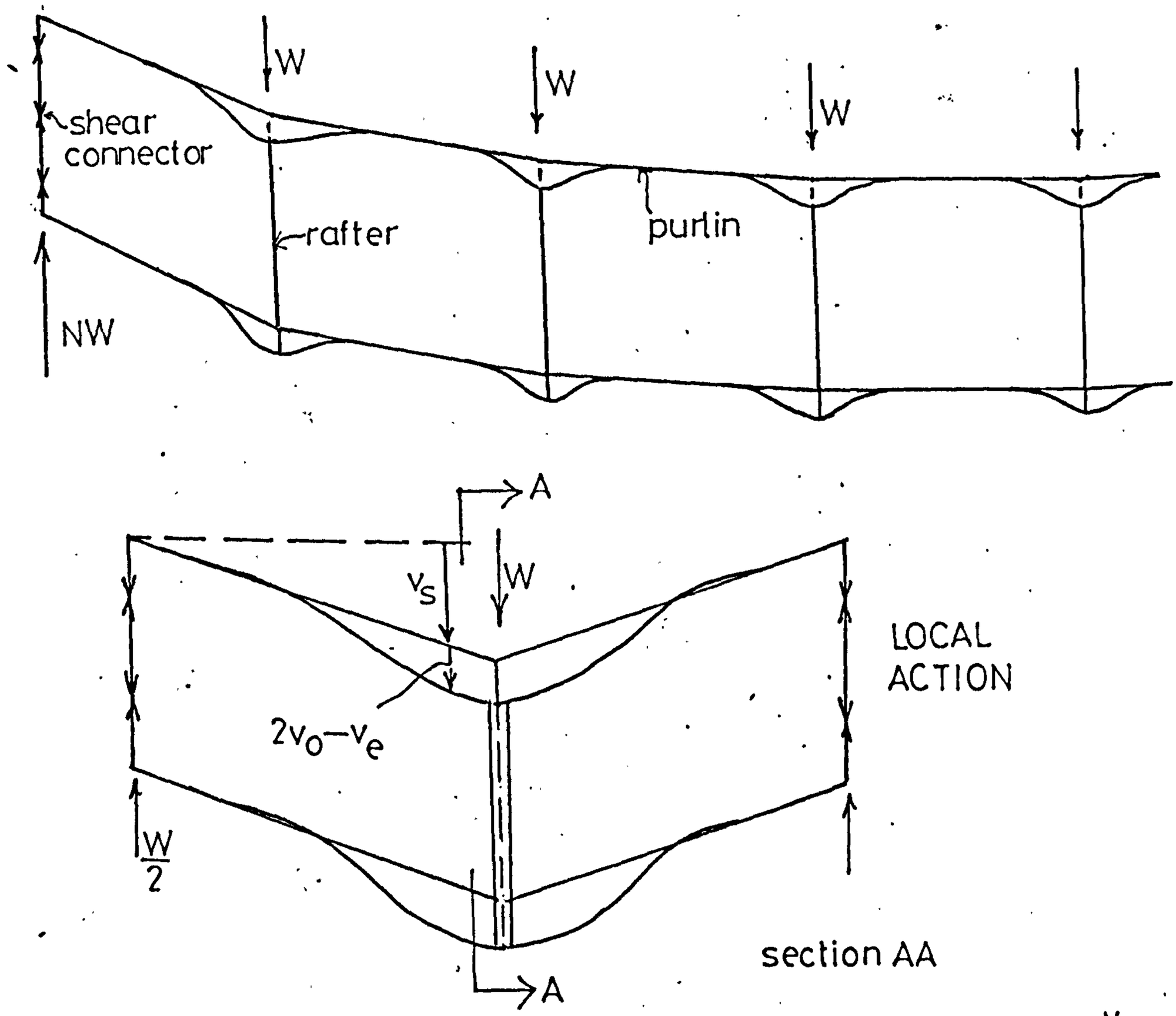

FIG(8.12)

HOLES IN DIAPHRAGMS —SIMPLE SHEAR DEFLECTION

C—flexibility

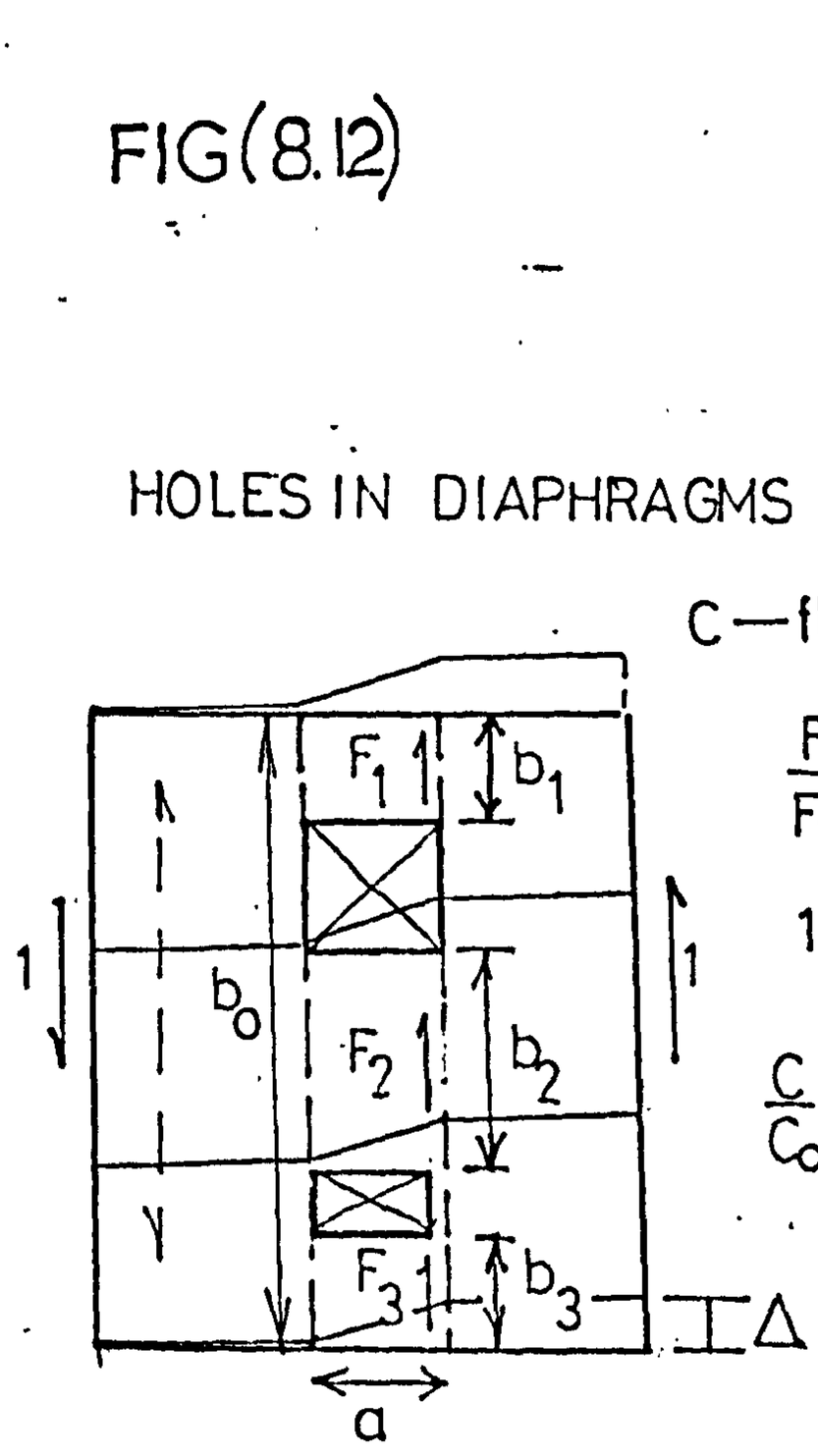

FIG(8.13)

$$\frac{F_1}{F_2} = \frac{C_2}{C_1} \simeq \left[\frac{b_1}{b_2}\right]^2$$

$$1 = F_1 + F_2 + F_3 \propto \sum b_i^2$$

$$\frac{C}{C_o} = \frac{b_o^2}{\sum b_i^2}$$

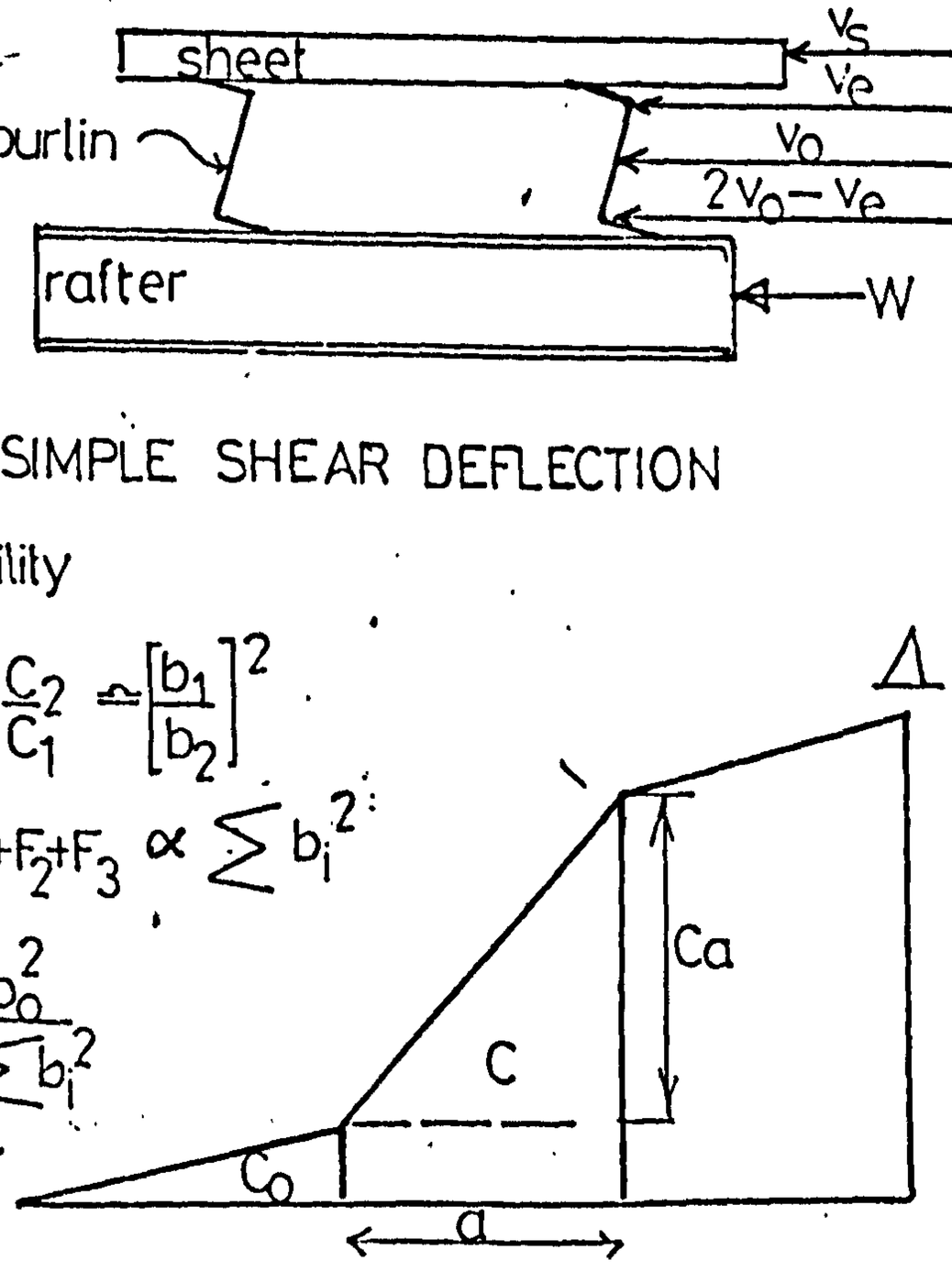

OPENINGS IN DIAPHRAGMS

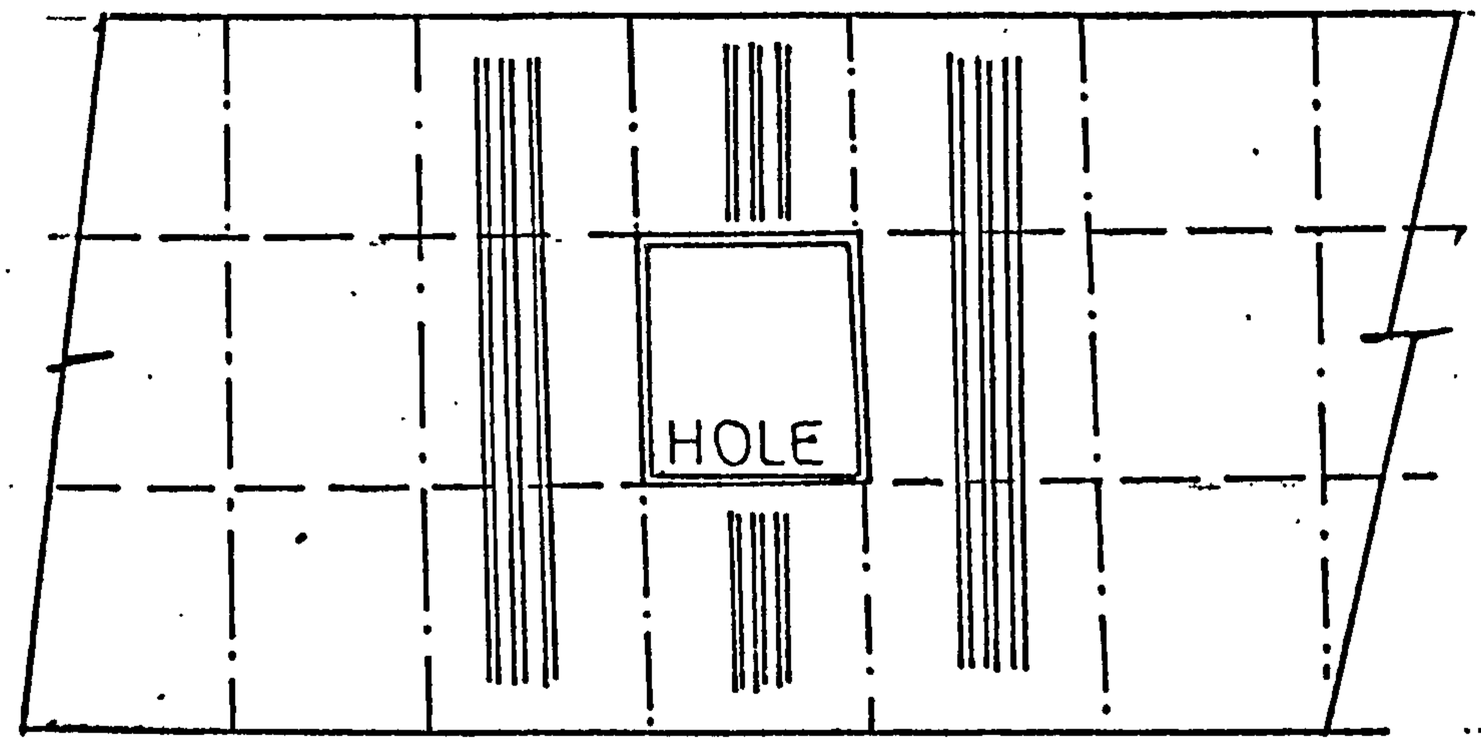

CASE OF A SINGLE FLEXIBLE SECTION, C2
IN A STIFFER DIAPHRAGM, C1

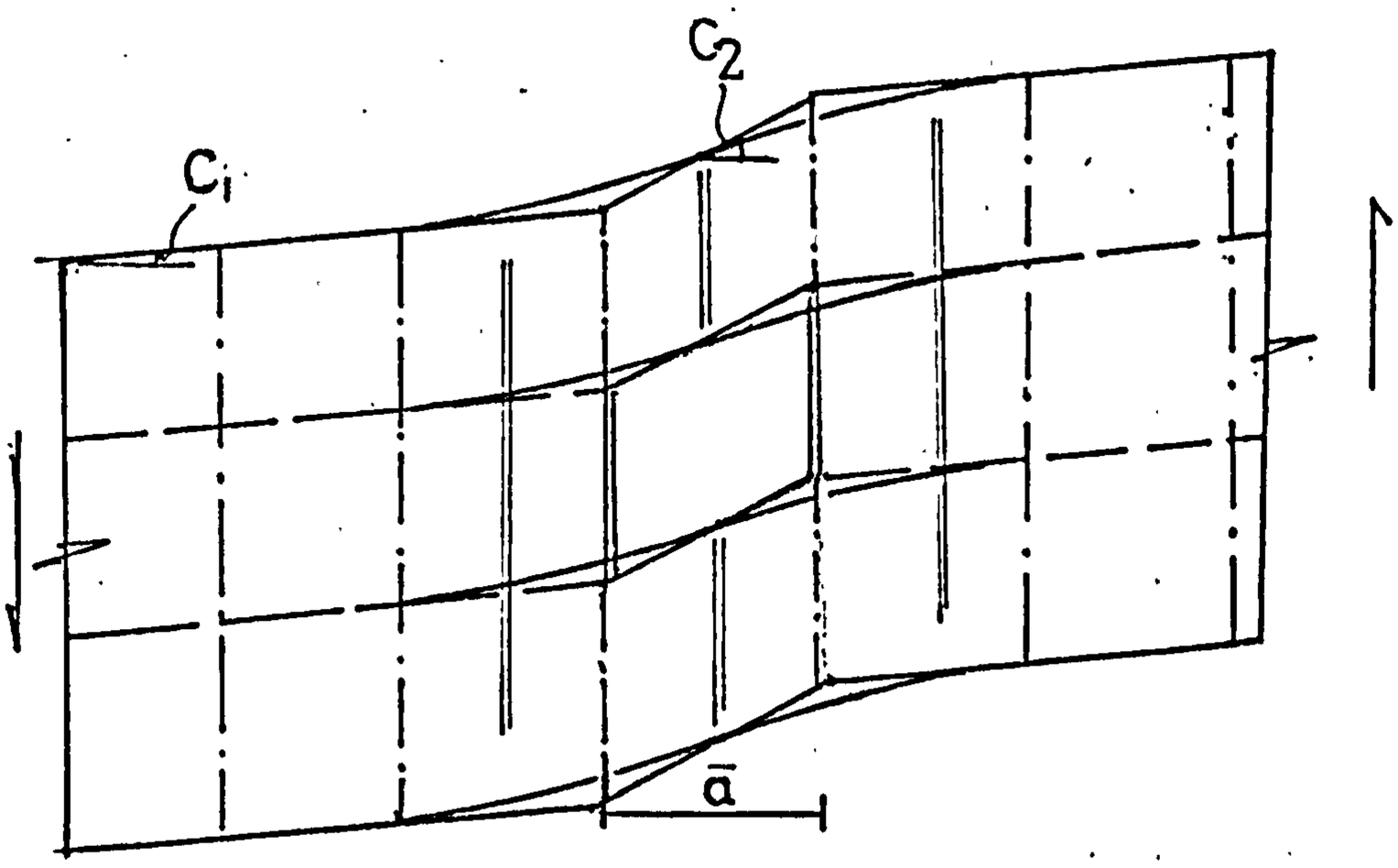

BENDING OF PURLINS AROUND OPENING

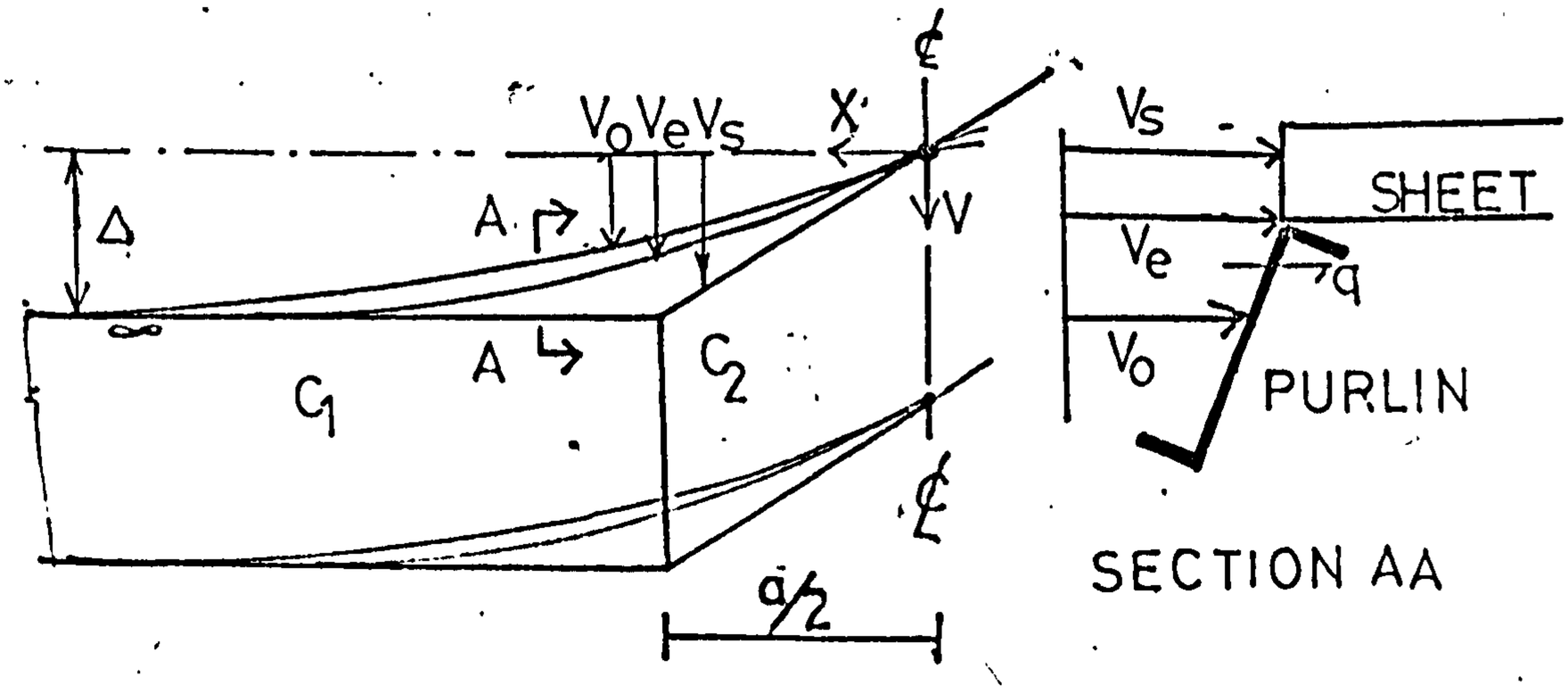

DISPLACEMENT COMPONENTS

FIG(8.14)

OPENINGS IN DIAPHRAGMS

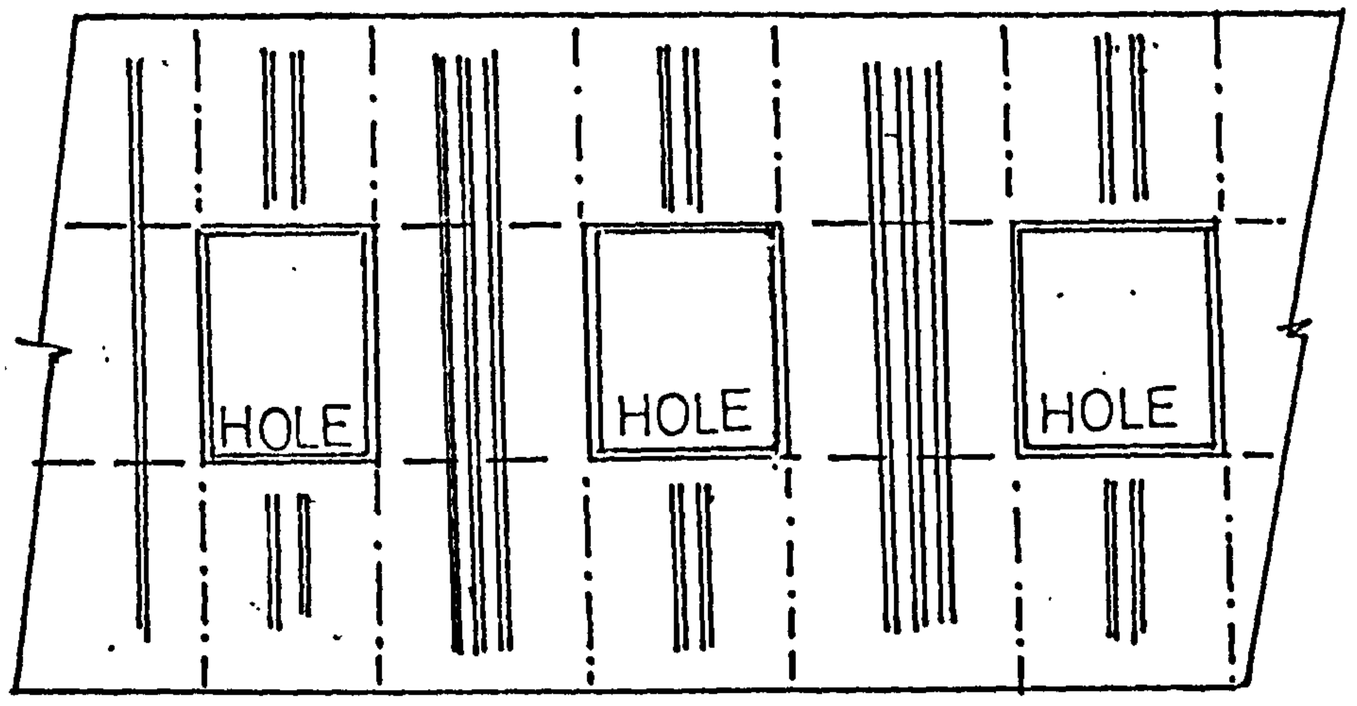

CASE OF PERIODIC FLEXIBLE SECTIONS, C2
WITHIN A STIFFER DIAPHRAGM, C1

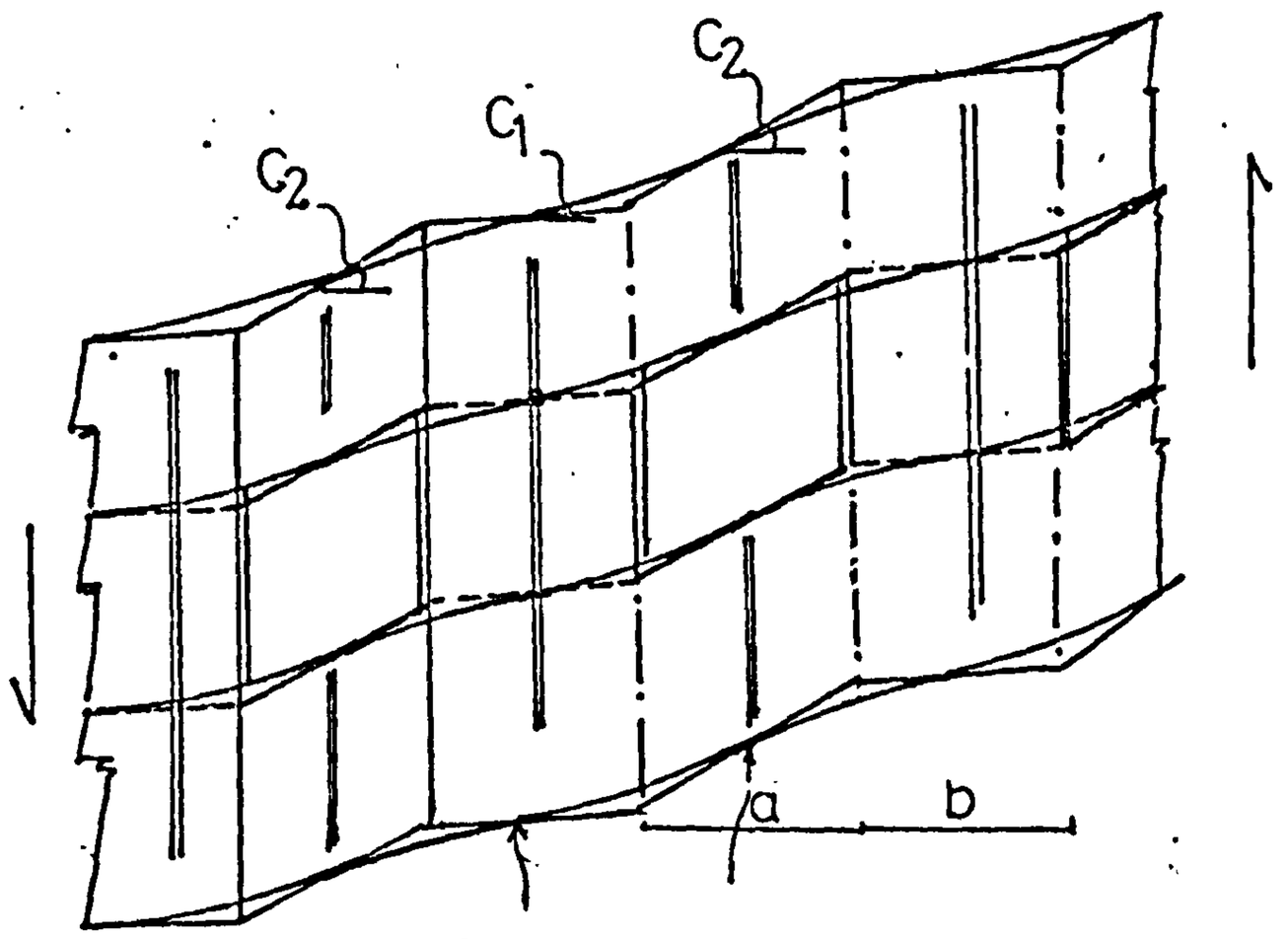

POINTS OF ANTISYMMETRY

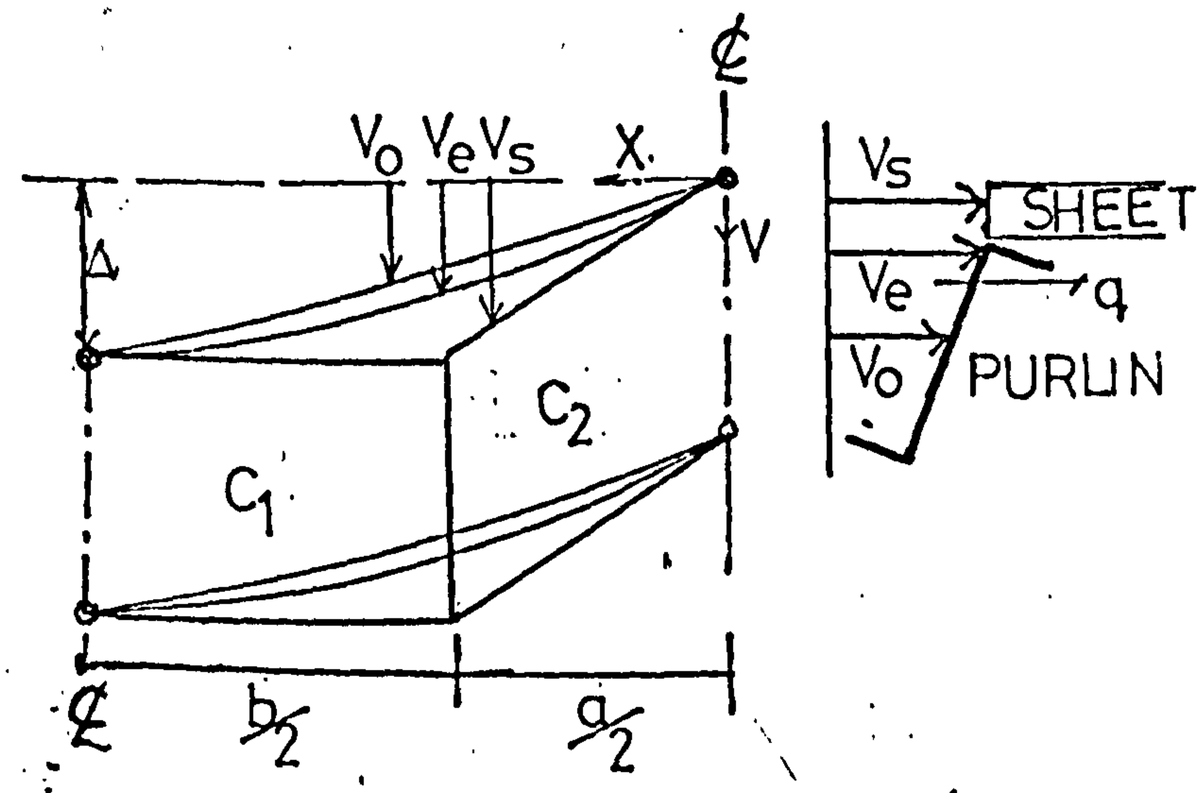

DISPLACEMENT COMPONENTS

FIG(8.15)

HOLES IN DIAPHRAGMS

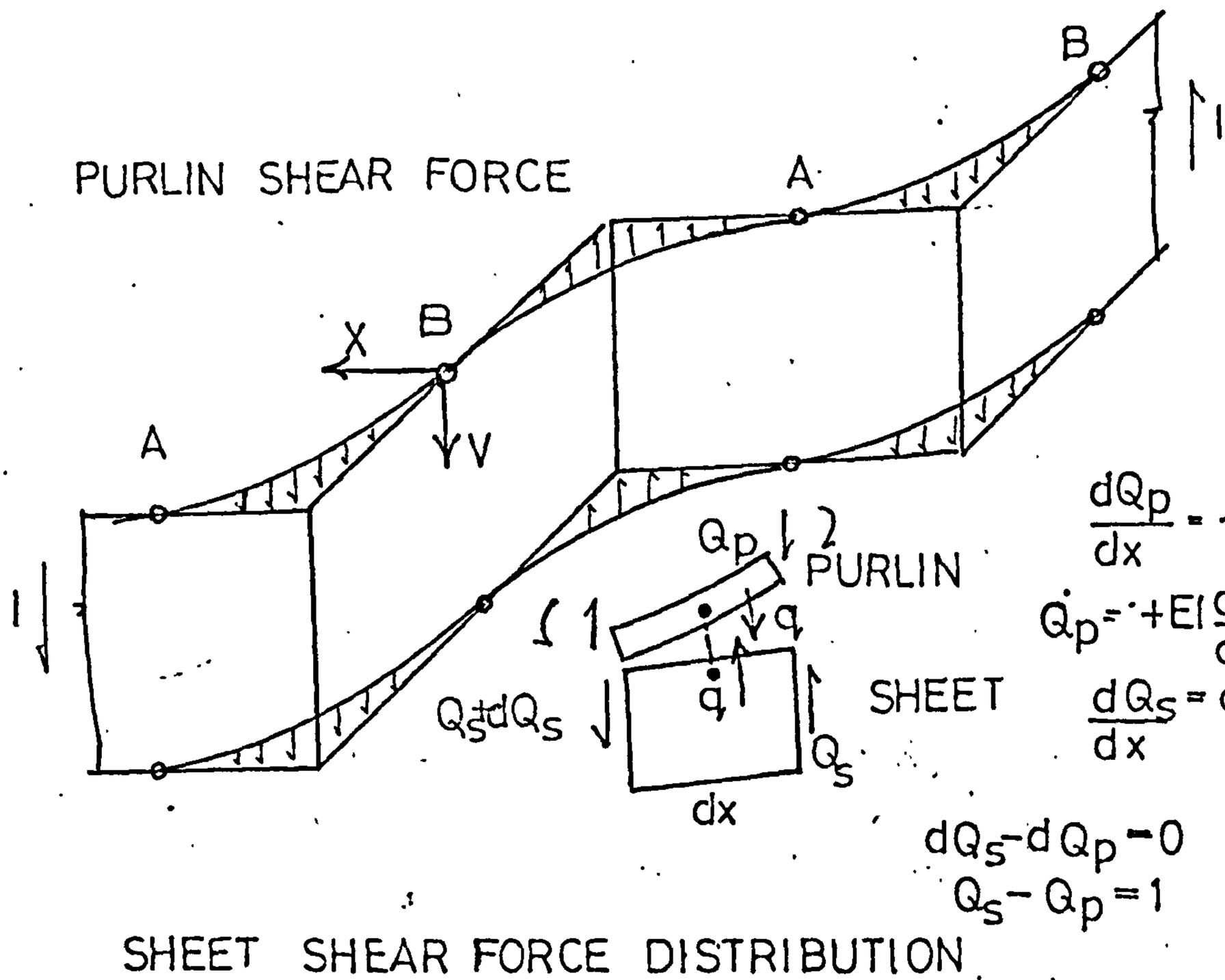

SHEET SHEAR FORCE DISTRIBUTION

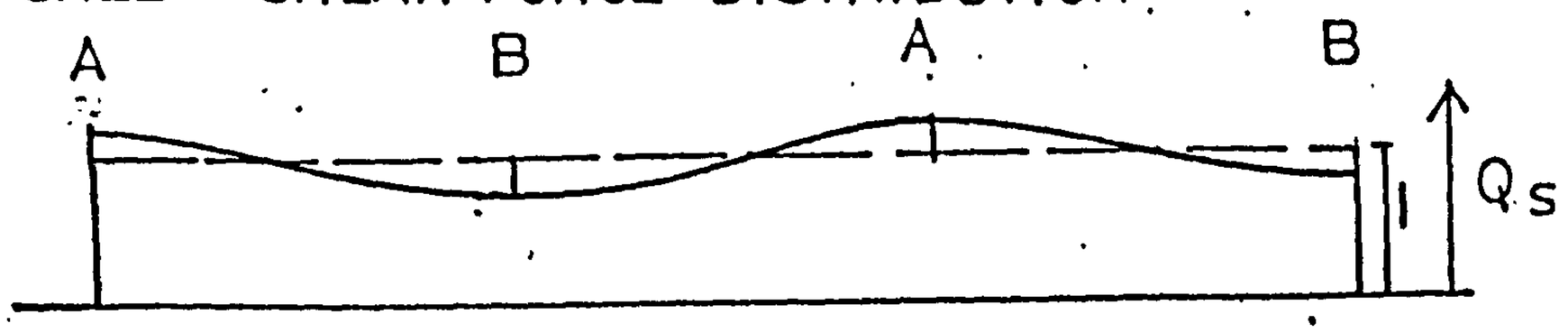

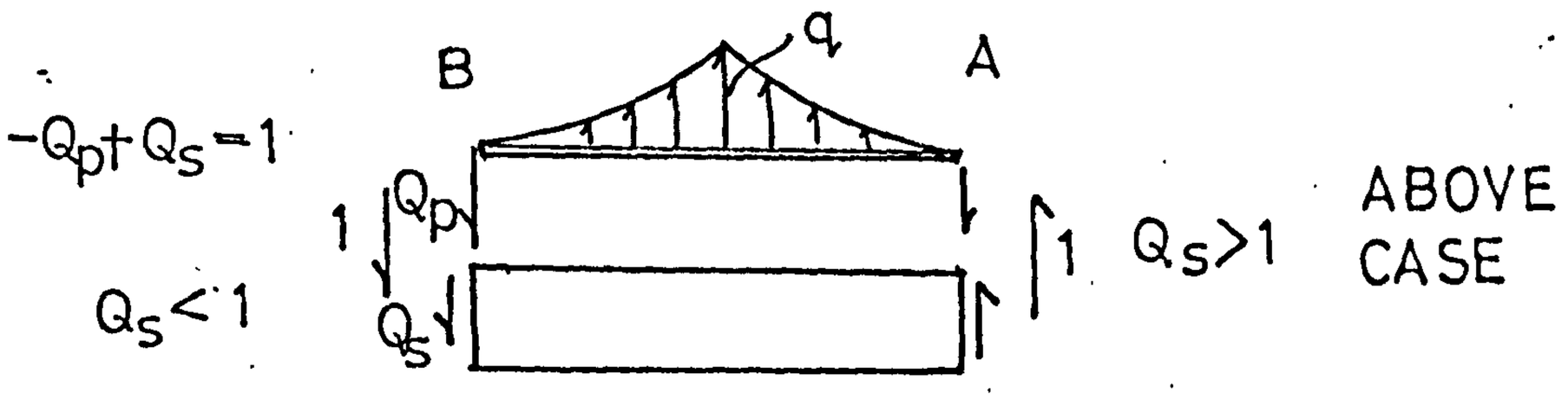

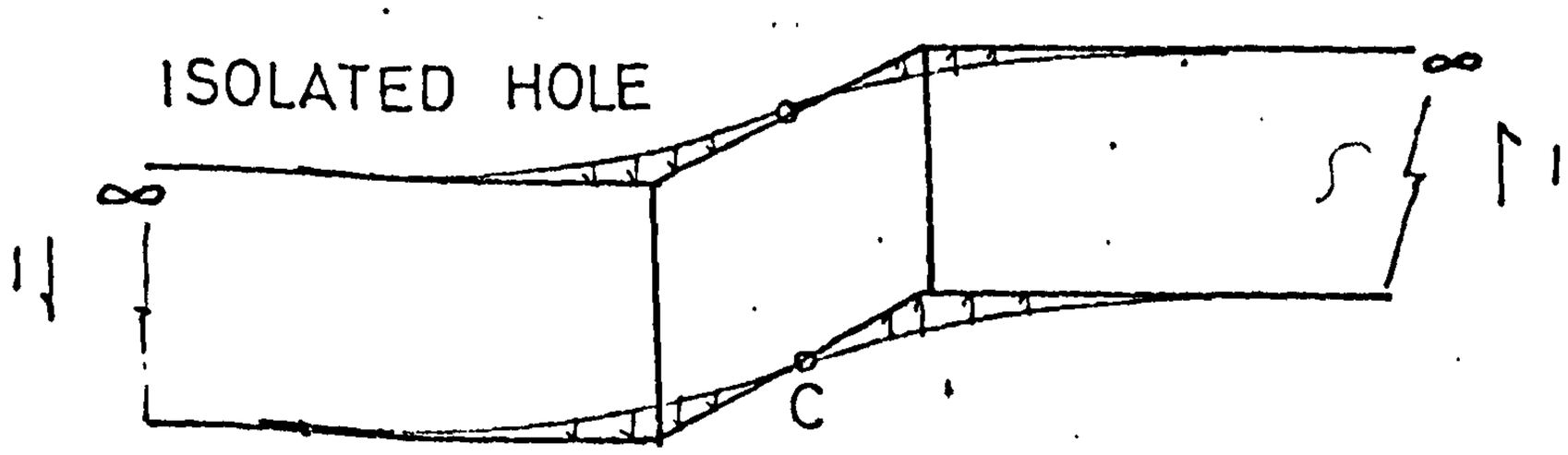

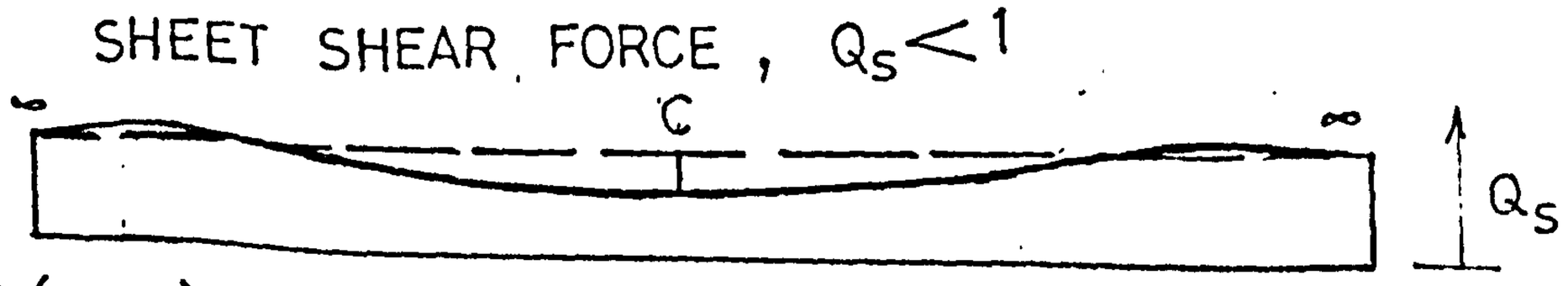

FIG(8.16)

SINGLE DIAPHRAGM OPENING (a=2m)

— PURLIN DISPLACEMENTS FOR 1 kN SHEAR .

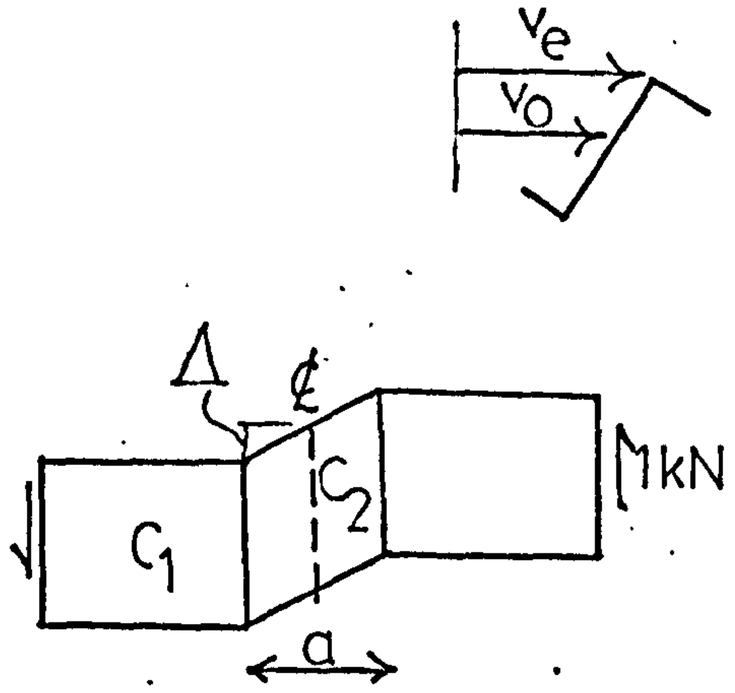

$I = 5 \cdot 10^5 mm^4$
$C_2 = \cdot 0001$ mm/kN/mm
$C_1 = \cdot 00001$ "
$n_p = 2$ purlins
$s = 0{,}15$ mm/kN every trough fixing

FIG(8.17)

PERIODIC DIAPHRAGM OPENINGS (a=b=2m)

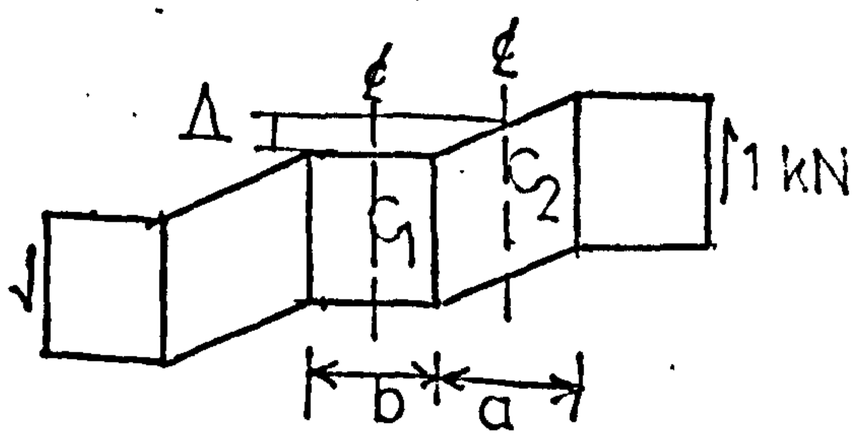

data as above
except $C_2 = 001$ mm/kN/mm

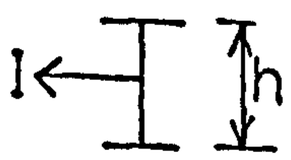

FIG(8.18)

COMPARISON OF PERIODIC AND ISOLATED HOLE SOLUTIONS

— PURLIN DISPLACEMENTS

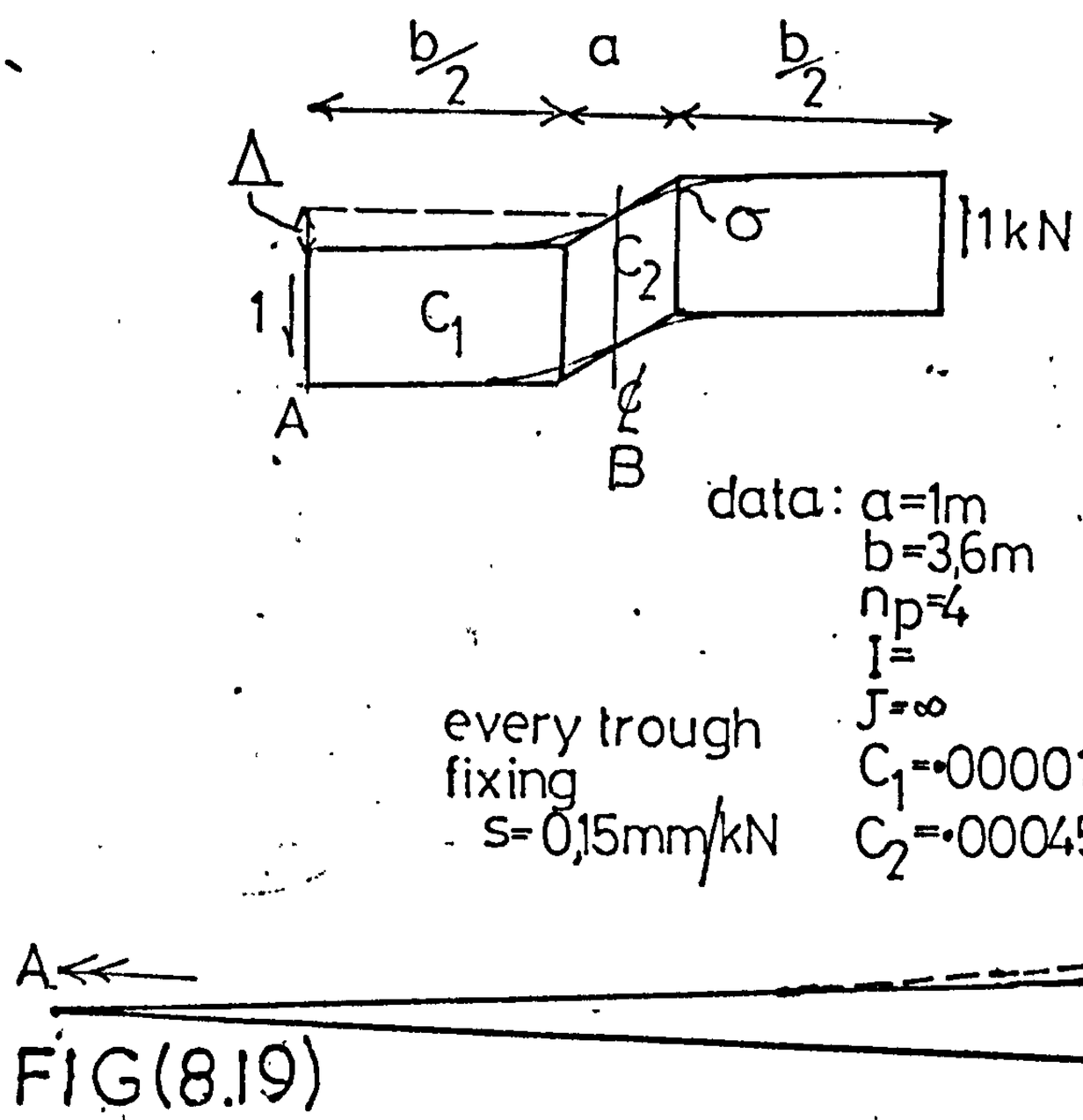

FIG(8.19)

MAX. PURLIN BENDING STRESS DEPENDING ON HOLE WIDTH

— isolated hole case C_2=·0005 , I=5.10^5

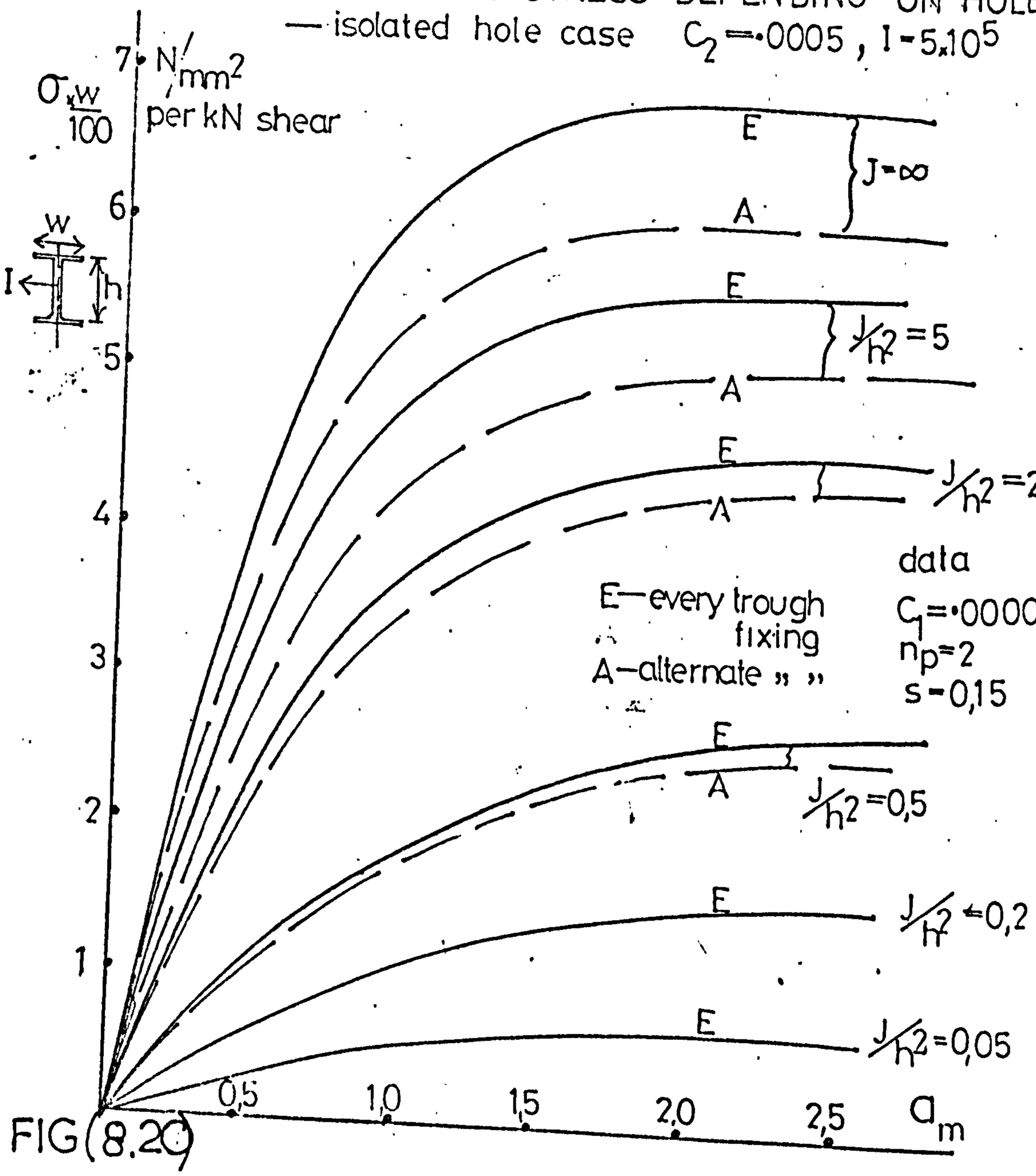

FIG(8.20)

VARIATION OF EDGE FASTENER FORCES

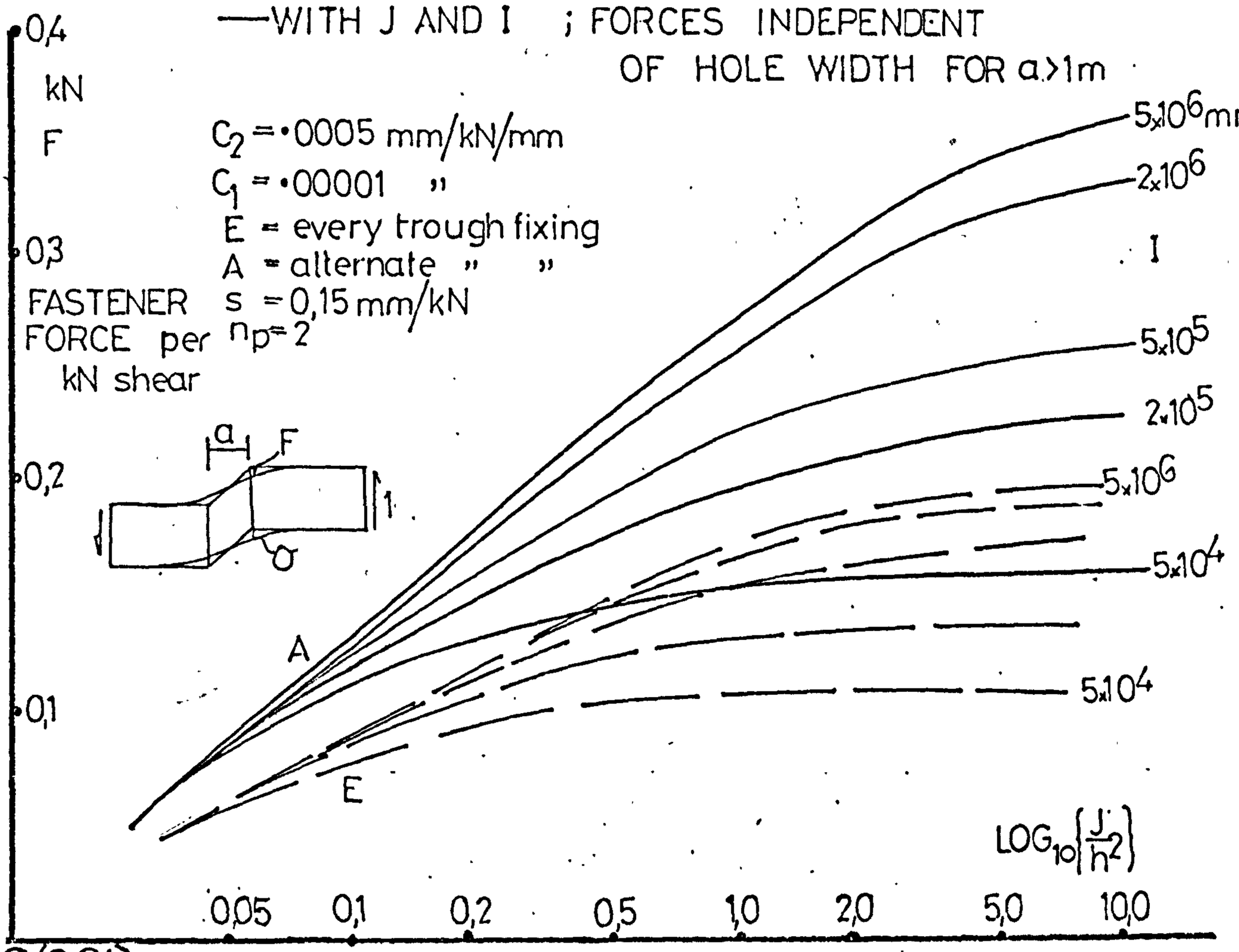

FIG(8.21)

VARIATION OF PURLIN BENDING STRESS

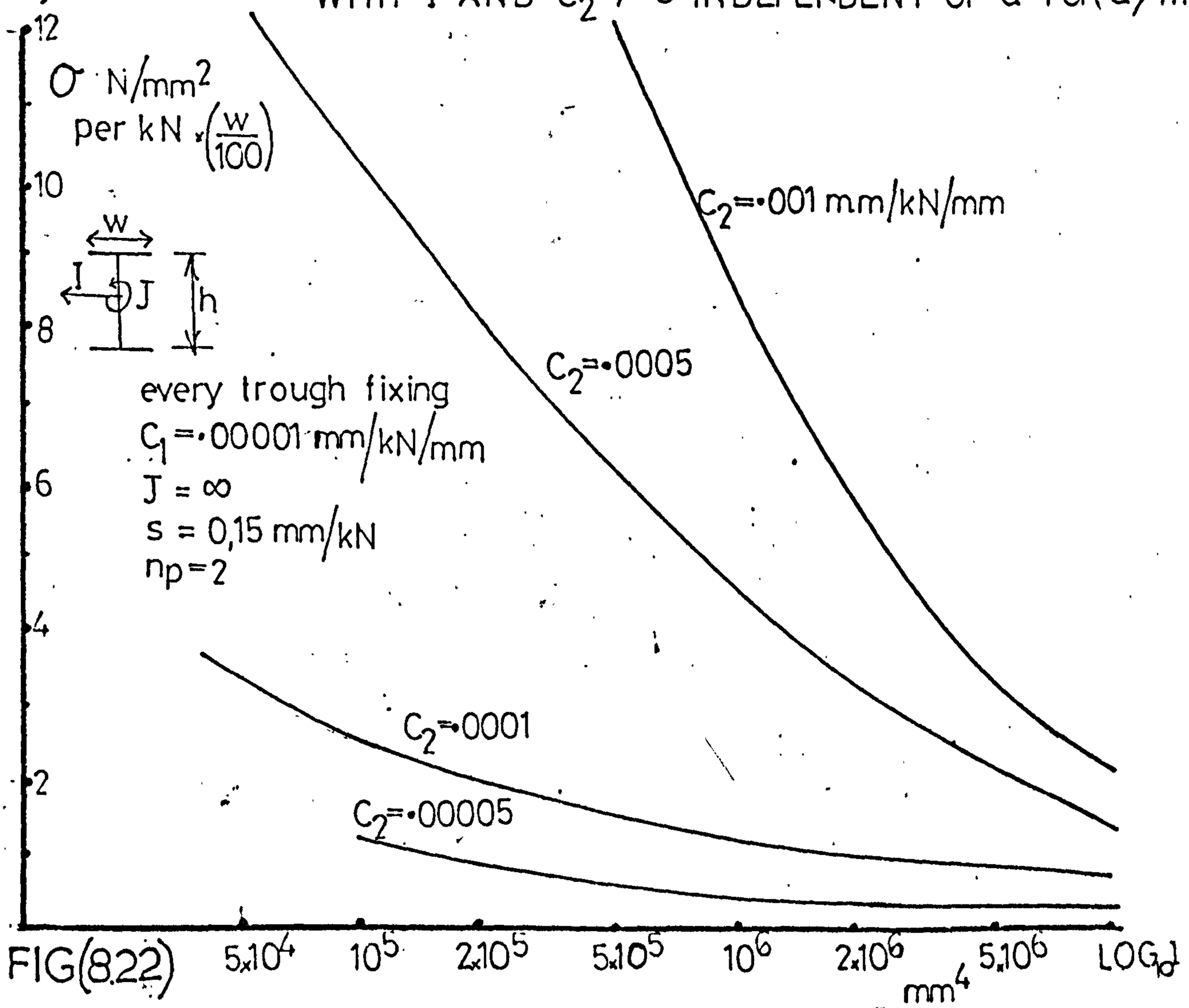

FIG(8.22)

FINITE ELEMENT REPRESENTATION OF A SHEAR PANEL WITH AN OPENING

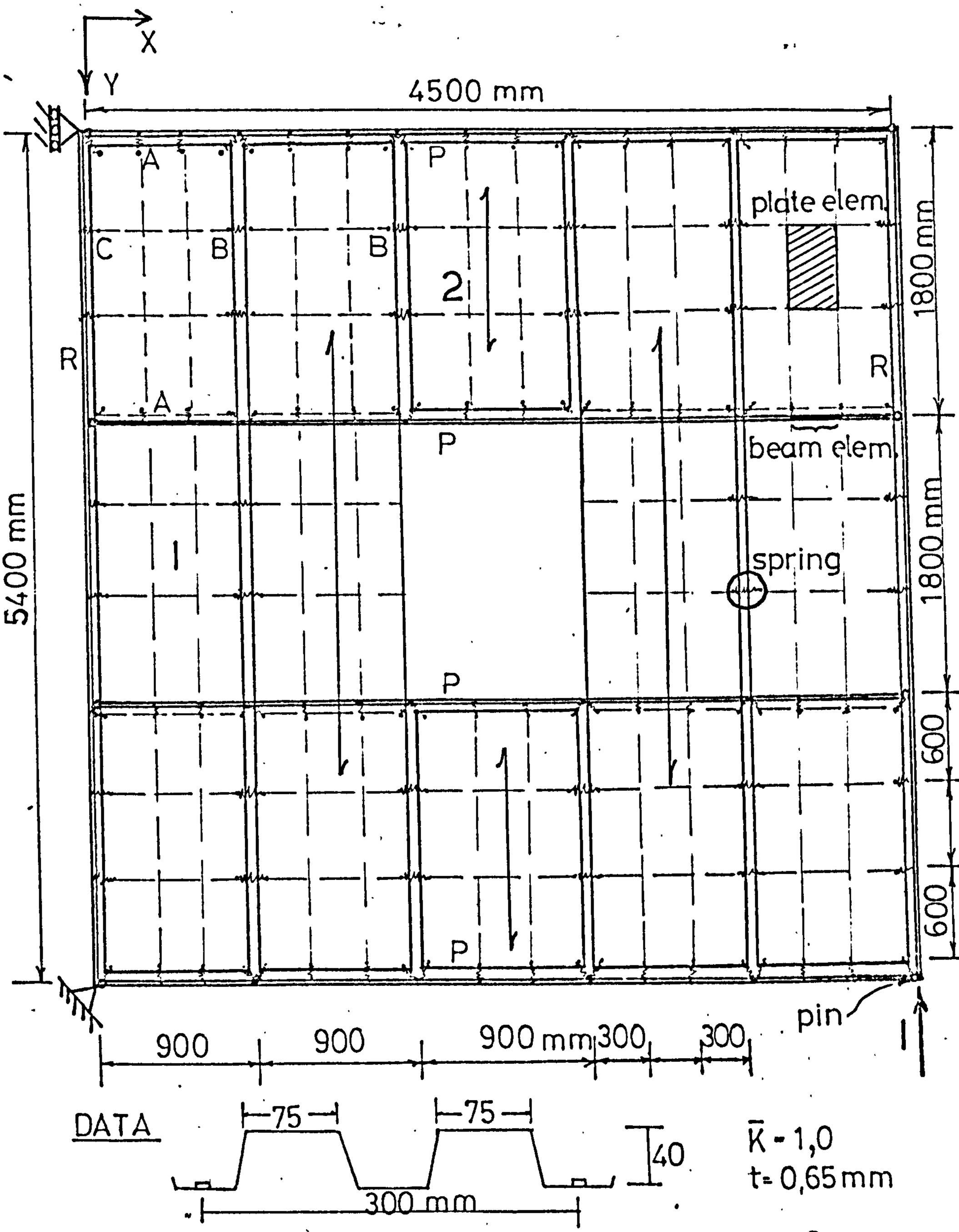

$$G_{eff} = \frac{G}{\frac{G\, d^{2,5}\, \bar{K}}{E\, t^{1,5}\, b} + 1 + \frac{2h}{d}}$$

= 2,04 kN/mm² for plate 1
= 0,68 " " " 2

FASTENERS; type A 0,15 mm/kN
type B 0,09 mm/kN (4 seam fast.)
type C 0,075 " (2 edge fast.)

PURLIN ; area 500 mm² ; inertia 5.10^5 mm⁴

RAFTER ; area 5000 mm² ; inertia 10^7 mm⁴ (lateral)

FIG(8.23)

HOLES IN DIAPHRAGMS – FINITE ELEMENT RESULTS AND THEORETICAL COMPARISONS – FIG (8.23)

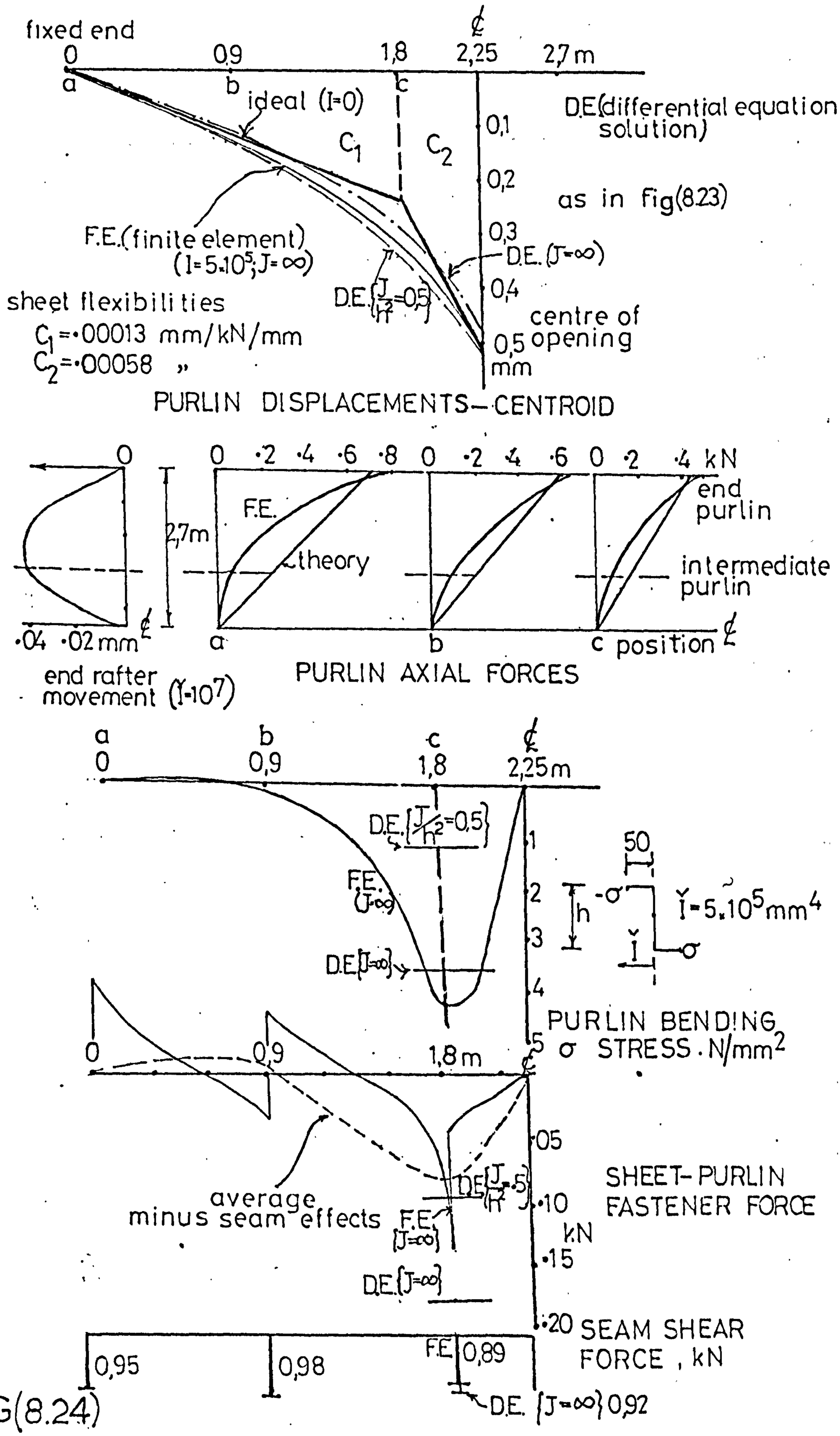

FIG (8.24)

SINGLE OPENING - IMAGINARY ROOTS

$$
\begin{bmatrix}
0 & 1 & -SH1.CA2 & -CH1.SA2 & 1 \\
b_2 & b_1 & -v_1 & -v_2 & 0 \\
-2b_1b_2 & b_1^2-b_2^2 & -(a_1^2-a_2^2)SH1.CA2 + 2a_1a_2CH1.SA2 & -2a_1a_2SH1.CA2 - (a_1^2-a_2^2)CH1.SA2 & 0 \\
x_3b_2+y_2b_1 & y_2b_2-x_3b_1 & -(x_1v_1-y_1v_2) & -(y_1v_1+x_1v_2) & 0 \\
-C_1.EI.y_2 & C_1.EI.x_3 & -C_2.EI.(x_1SH1.CA2 - y_1CH1.SA2) & -C_2.EI.(y_1SH1.CA2 + x_1.CH1.SA2) & 1
\end{bmatrix}
\cdot
\begin{bmatrix} A \\ B \\ C \\ D \\ \Delta \end{bmatrix}
=
\begin{bmatrix} C_2\frac{a}{2} \\ C_2-C_1 \\ 0 \\ 0 \\ C_2\frac{a}{2} \end{bmatrix}
\begin{matrix} \text{DUE TO,} \\ V_o \\ \frac{dV_o}{dx} \\ \frac{d^2V_o}{dx^2} \\ \frac{d^3V_o}{dx^3} \\ V_s \end{matrix}
$$

WHERE, $CH1 = COSH(a_1 a/2)$, $SA1 = SIN(a_2 a/2)$, $v_1 = -a_2 SH1.SA2 + a_1 CH1.CA2$, $y_1 = \sqrt{x_2^2 - x_1^2}$

$SH1 = SINH(a_1 a/2)$, $CA2 = COS(a_2 a/2)$, $v_2 = a_2 CH1.CA2 + a_1 SH1.SA2$, $y_2 = \sqrt{x_2^2 - x_3^2}$

FIG(8.25)

SINGLE OPENING — REAL ROOTS

$$\begin{bmatrix} 1 & 1 & -SH1 & -SH2 & 1 \\ -b_1' & -b_2' & -a_1'.CH1 & -a_2'.CH2 & 0 \\ (b_1')^2 & (b_2')^2 & -(a_1')^2 SH1 & -(a_2')^2.SH2 & 0 \\ -(b_1')^3 & -(b_2')^3 & -(a_1')^3.CH1 & -(a_2')^3.CH2 & 0 \\ C_1.EI(b_1')^2 & C_1.EI.(b_2')^2 & -C_2.EI(a_1')^2.SH2 & -C_2.EI.(a_2')^2.SH2 & 1 \end{bmatrix} \cdot \begin{bmatrix} A_r \\ B_r \\ C_r \\ D_r \\ \Delta \end{bmatrix} = \begin{bmatrix} C_2.\frac{a}{2} \\ C_2-C_1 \\ 0 \\ 0 \\ C_2.\frac{a}{2} \end{bmatrix}$$

DUE TO, V_o, $\frac{dV_o}{dx}$, $\frac{d^2V_o}{dx^2}$, $\frac{d^3V_o}{dx^3}$, V_s

WHERE, $CH1 = COSH(a_1'a/2)$, $CH2 = COSH(a_2'a/2)$

$SH1 = SINH(a_1'a/2)$, $SH2 = SINH(a_2'a/2)$

FIG(8.26)

PERIODIC OPENINGS – IMAGINARY ROOTS

$$
\begin{bmatrix}
SK1.CB2 & , & CK1.SB2 & , & , & , \\
-u_1 & , & -u_2 & , & , & , \\
(b_1^2-b_2^2)SK1.CB2 - 2b_1b_2CK1.SB2 & , & 2b_1b_2.SK1.CB2 + (b_1^2-b_2^2).CK1.SB2 & , & \text{AS FOR SINGLE OPENING CASE} & \\
-(x_3u_1-y_2u_2) & , & -(y_2u_1+x_3u_2) & , & , & , \\
EI.C_1.(x_3.SK1.CB2 - y_2.CK1.SB2) & , & EI.C_1.(y_2SK1.CB2 + x_3CK1.SB2) & , & , & ,
\end{bmatrix}
\cdot
\begin{bmatrix} A \\ B \\ C \\ D \\ \Delta \end{bmatrix}
=
\begin{bmatrix} C_2a/2 + C_1b/2 \\ C2-C1 \\ 0 \\ 0 \\ C_2a/2 + C_1b/2 \end{bmatrix}
\begin{matrix} \text{DUE TO,} \\ V_o \\ \frac{dV_o}{dx} \\ \frac{d^2V_o}{dx^2} \\ \frac{d^3V_o}{dx^3} \\ V_s \end{matrix}
$$

WHERE, $CK1=COSH(b_1b/2)$, $SK1=SINH(b_1b/2)$, $u_1=-b_2SK1.SB2+b_1CK1.CB2$, $y_2=\sqrt{x_2^2-x_3^2}$

$CB2=COS(b_2b/2)$, $SB2=SIN(b_2b/2)$, $u_2=b_2CK1.CB2+b_1SK1.SB2$

FIG (8.27)

PERIODIC OPENINGS – REAL ROOTS

$$\begin{bmatrix} -SK1 & , & -SK2 & , & , & , \\ b_1' CK1 & , & b_2' CK2 & , & , & , \\ (b_1')^2 SK1 & , & (b_2')^2 . SK2 & , & \text{AS FOR SINGLE} & \\ & & & & \text{OPENING CASE} & \\ (b_1')^3 . CK1 & , & (b_2')^3 CK2 & , & , & , \\ -C_1 EI . (b_1')^2 . SK1 & , & -C_2 . EI . (b_2')^2 . SK2 & , & , & , \end{bmatrix} \cdot \begin{bmatrix} A_r \\ B_r \\ C_r \\ D_r \\ \Delta \end{bmatrix} = \begin{bmatrix} C_2 a/2 + C_1 b/2 \\ C_2 - C_1 \\ 0 \\ 0 \\ C_2 a/2 + C_1 b/2 \end{bmatrix}$$

DUE TO,

V_o

$\frac{dV_o}{dx}$

$\frac{d^2V_o}{dx^2}$

$\frac{d^3V_o}{dx^3}$

V_s

WHERE $CK1 = COSH\ (b_1' b/2)$, $CK2 = COSH\ (b_2' b/2)$

$SK1 = SINH\ (b_1' b/2)$, $SK2 = SINH\ (b_2' b/2)$

FIG (8.28)

SHEAR BUCKLING OF CORRUGATED SHEETING

INFINITELY WIDE PANEL — BUCKLING WAVES

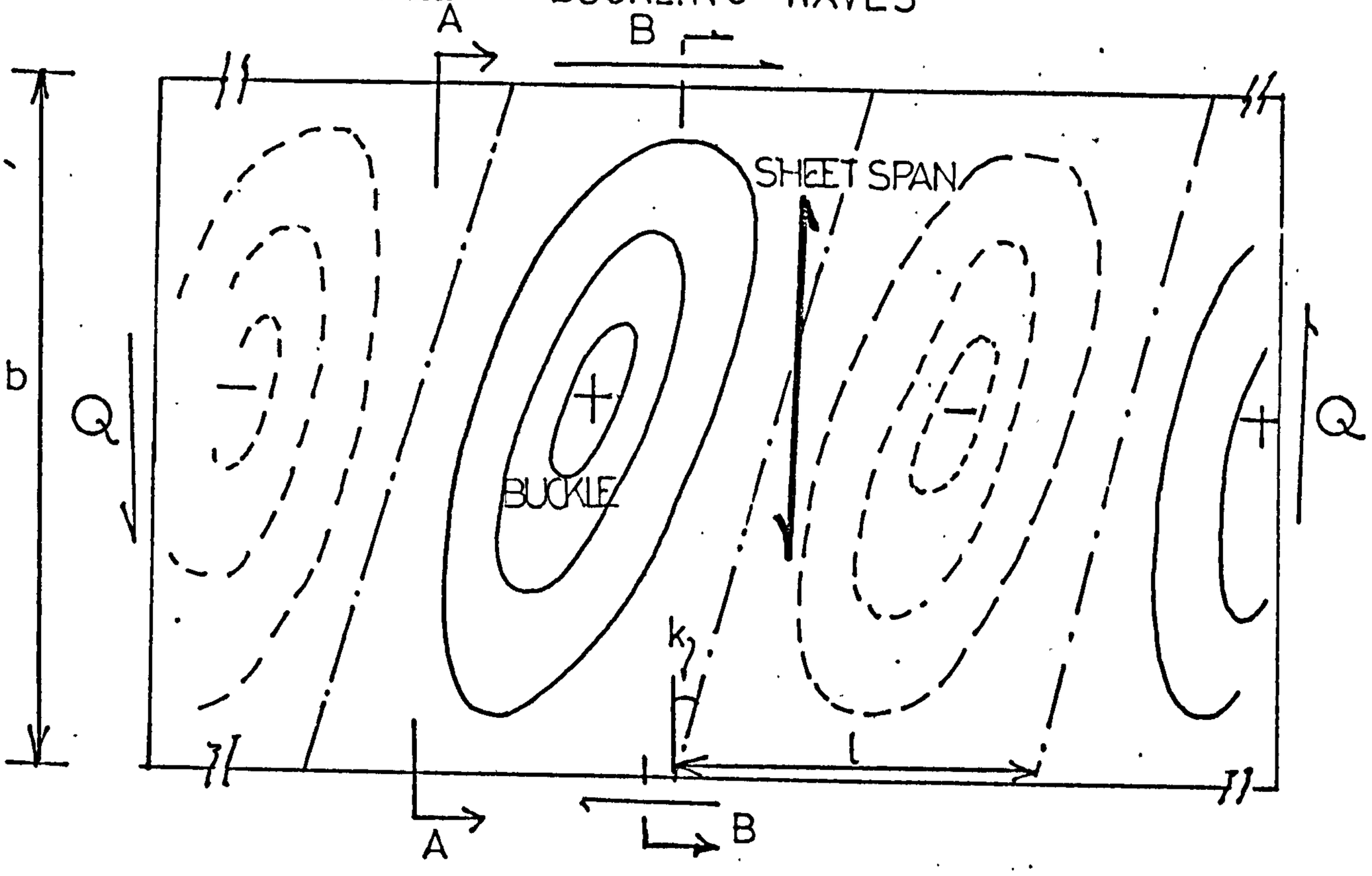

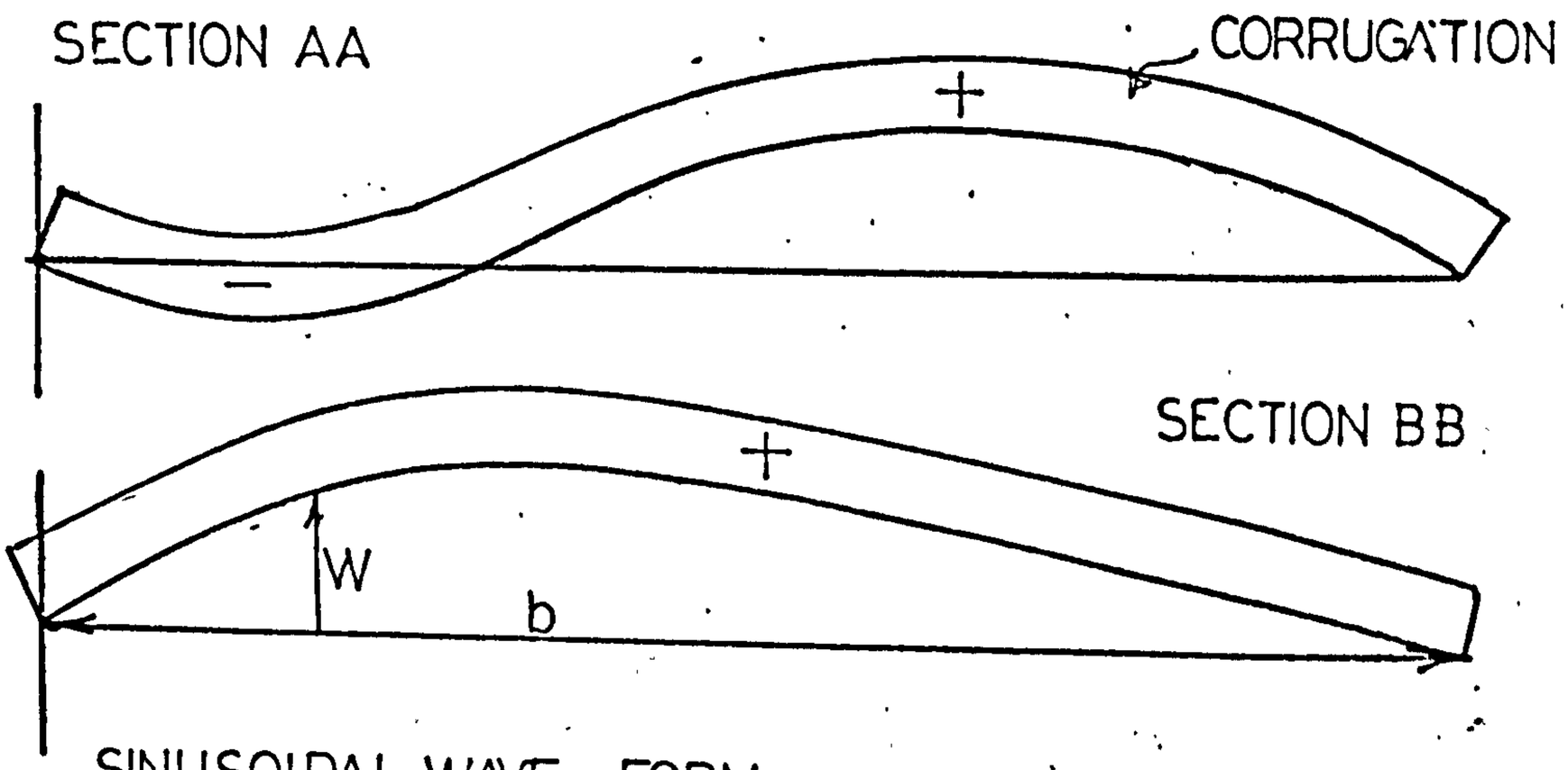

SINUSOIDAL WAVE FORM

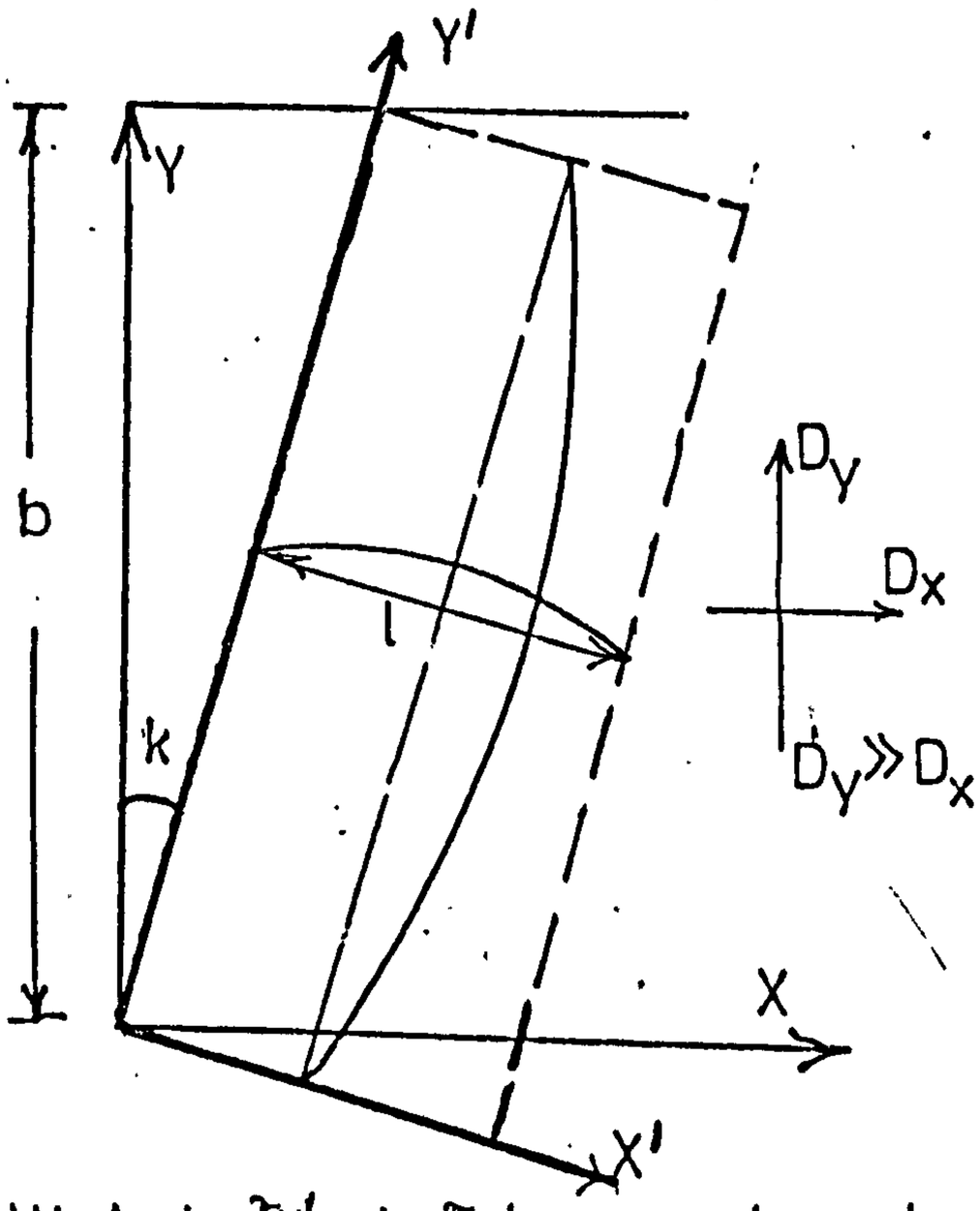

FIG (9.1)

$$W = A \sin \frac{\pi x'}{l} \cdot \sin \frac{\pi y'}{b}$$

$y' \triangleq y$; $x' \triangleq x - ky$

SHEAR STRAIN DUE TO BENDING DISPLACEMENT, W

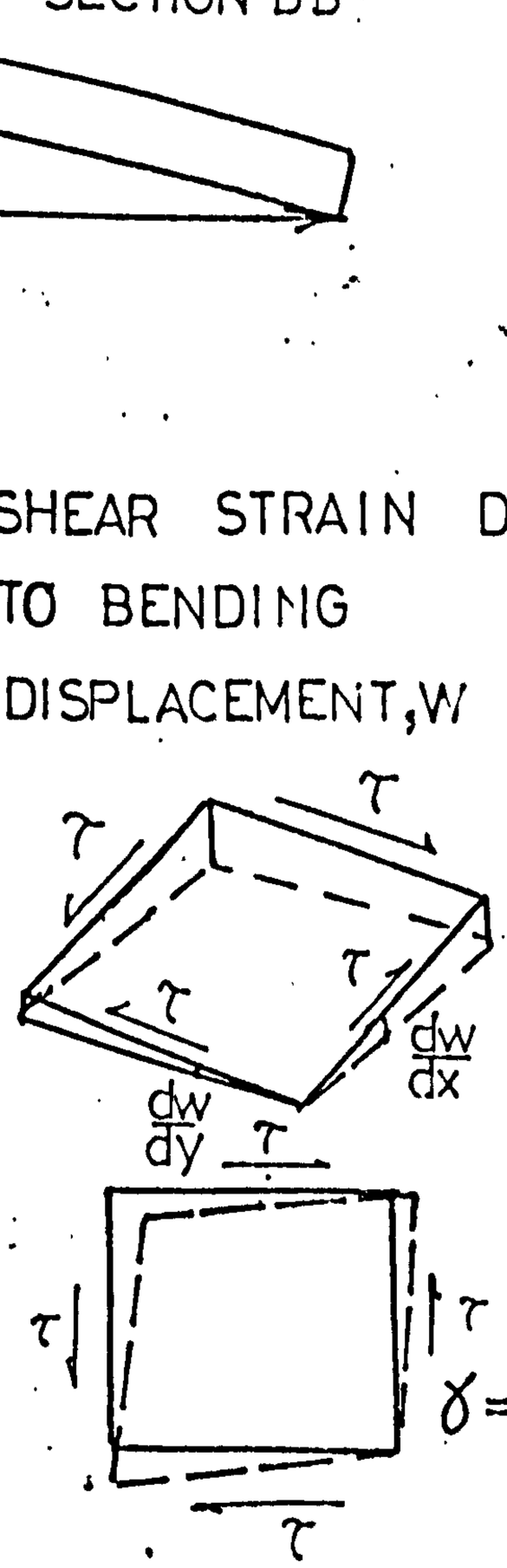

BUCKLING OF VARIOUS PROFILE SHAPES

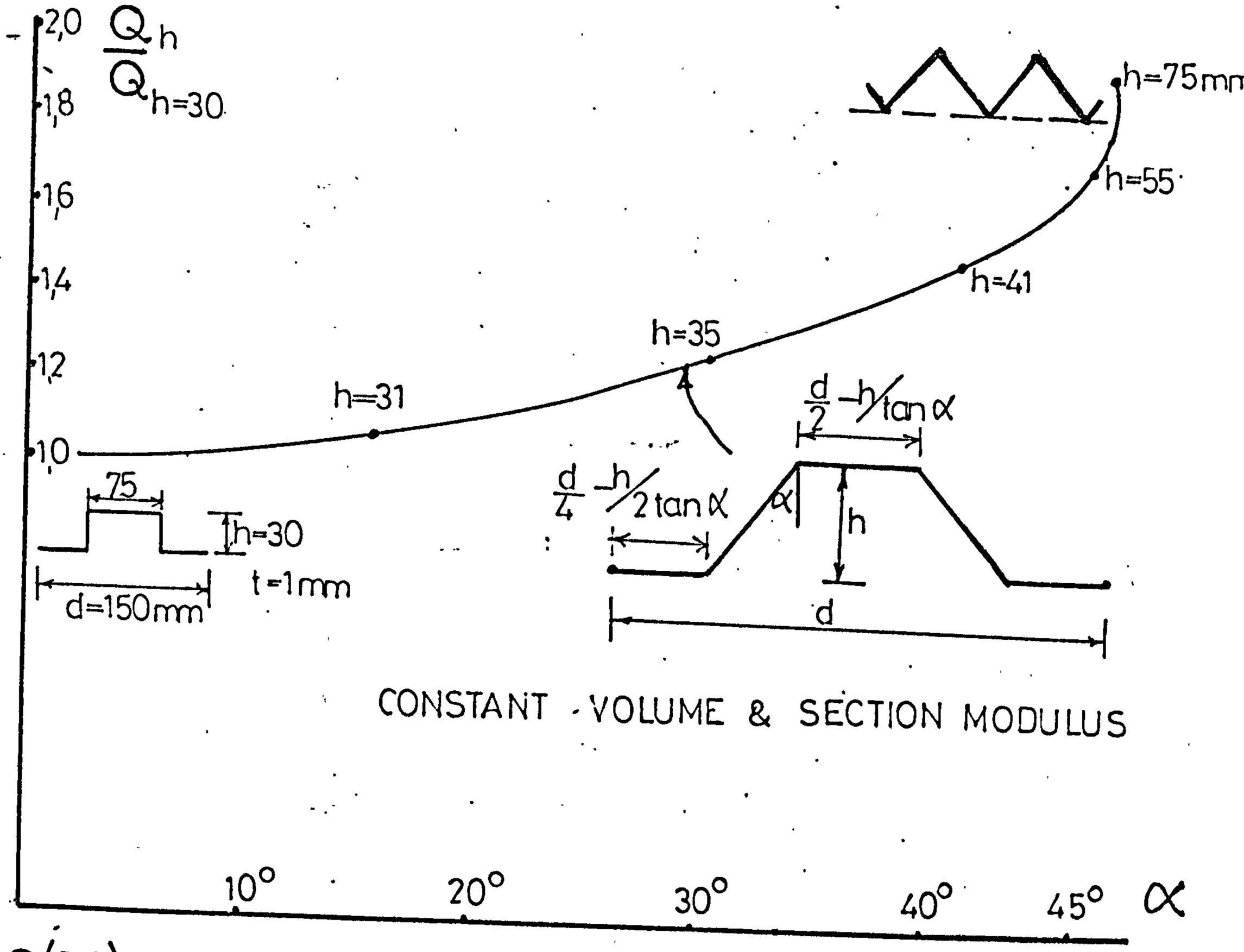

CONSTANT - VOLUME & SECTION MODULUS

FIG(9.2) VARIATION OF BUCKLING LOAD WITH SIDE PLATE SLOPE

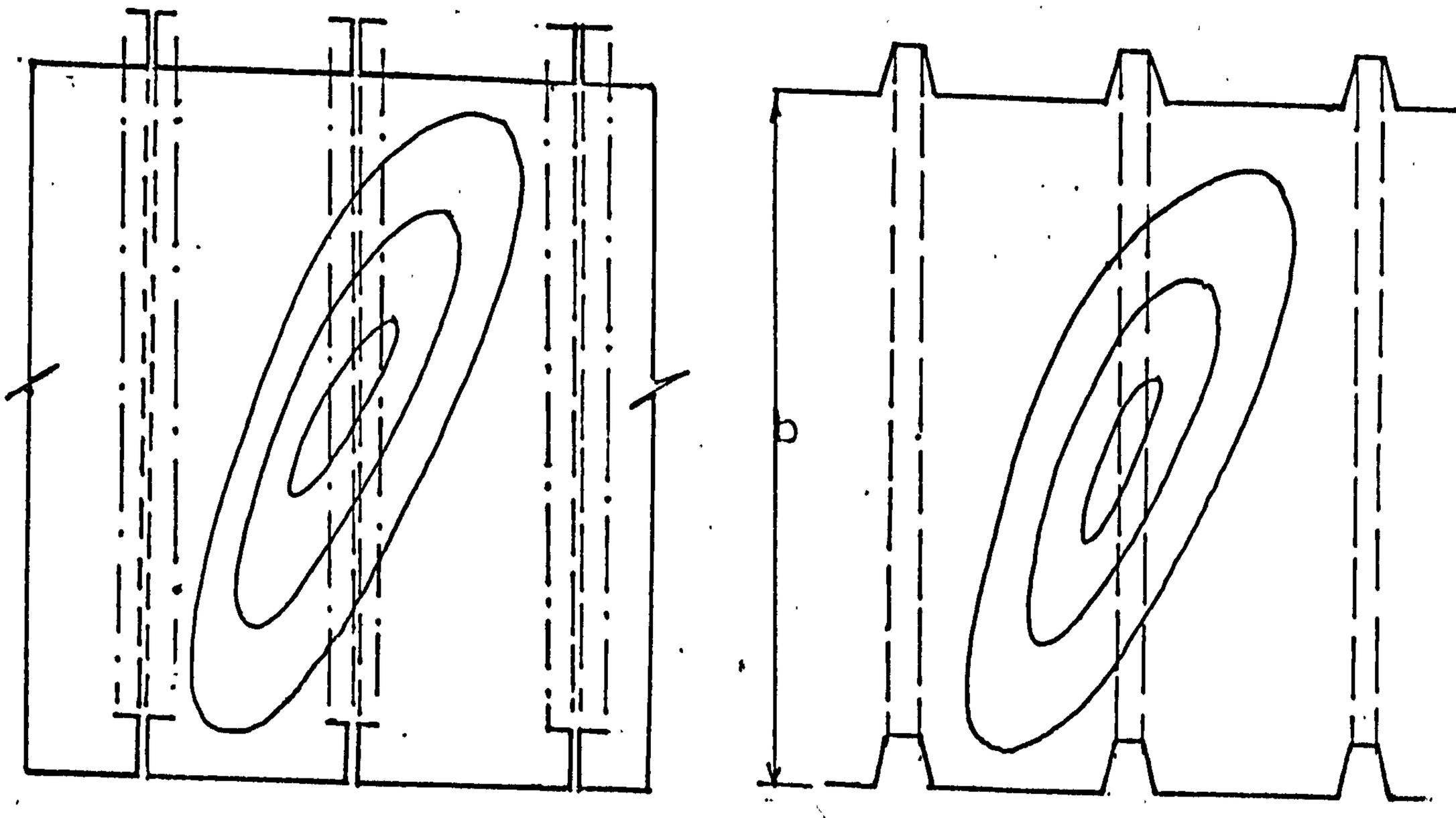

FIG(9.3) DEVIATIONS IN THE UNIFORM ORTHOTROPIC MEDIUM DUE TO STIFFENERS OR WIDE TROUGHS

LIMITATIONS OF SHEAR BUCKLING FORMULA

BUCKLING BETWEEN INTERMEDIATE PURLIN FASTENERS

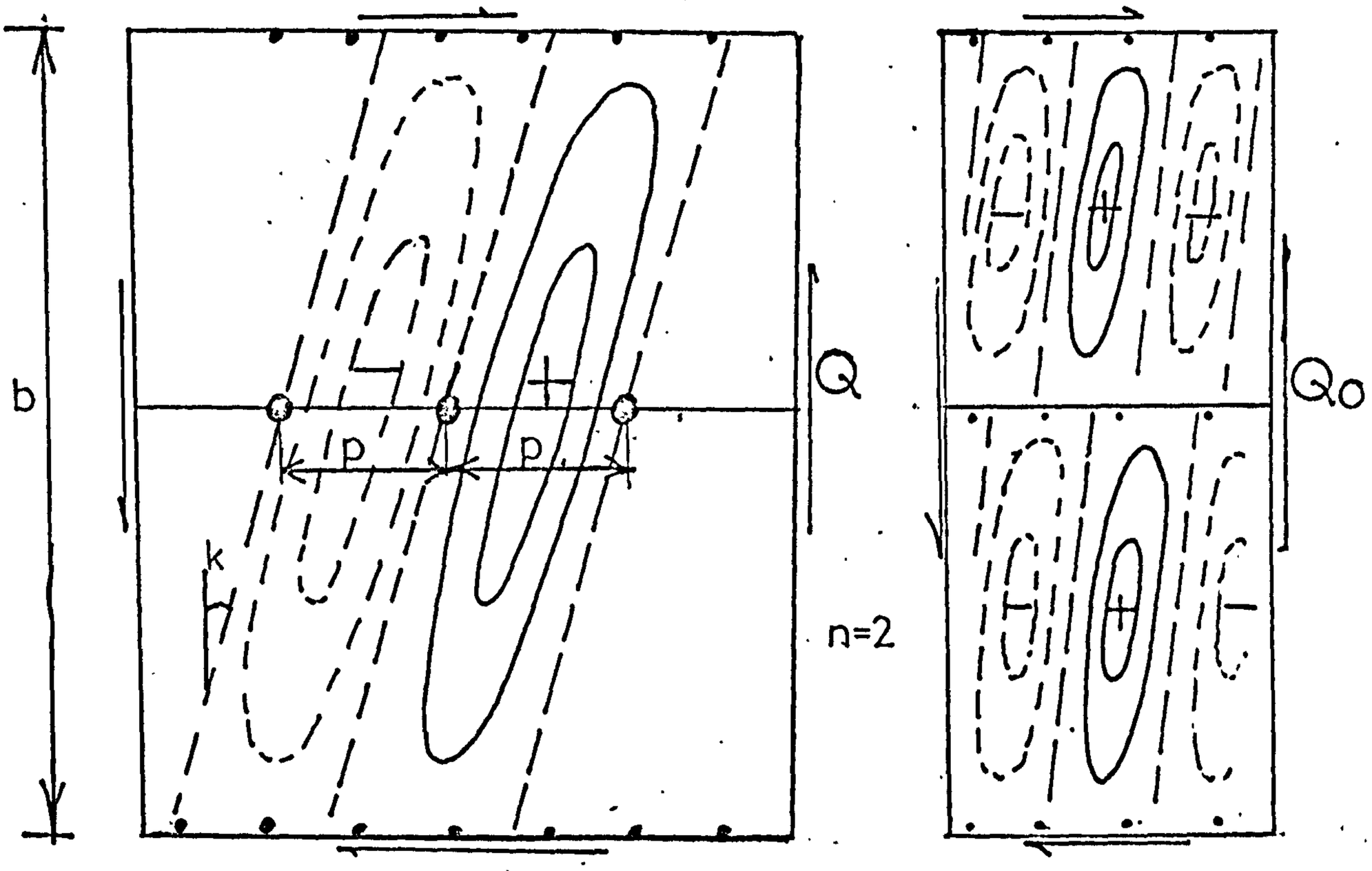

TWO BAYS — WAVE SLOPE IS VARIABLE

Q — shear flow (kN/mm)

INDEPENDENT SHEET BUCKLING, $Q_o = 36n^2 \frac{D_x^{1/4} D_y^{3/4}}{b^2}$

FIG (9.4)

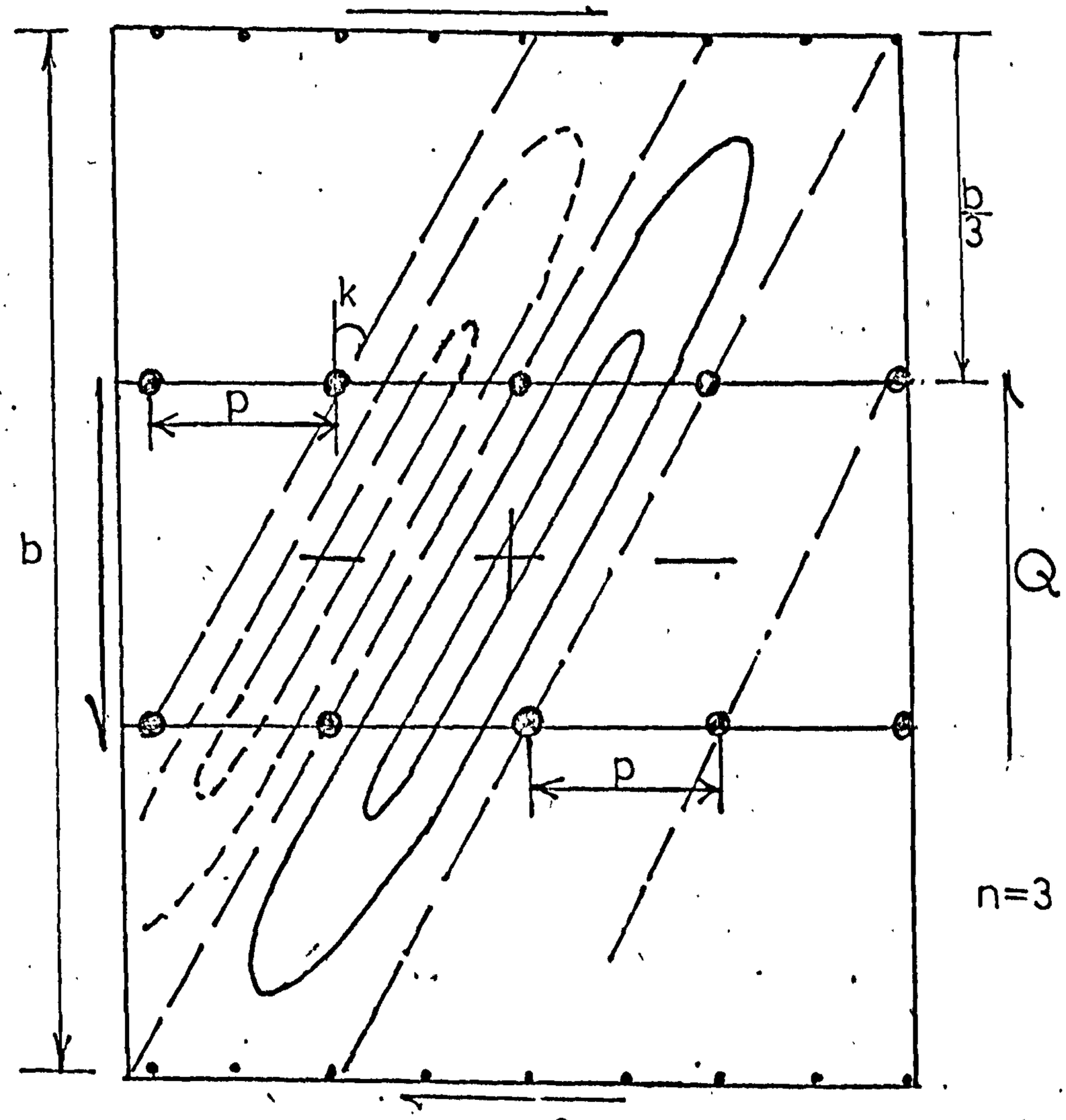

THREE BAYS — WAVE SLOPE IS $\frac{3p}{b}.m.$ — m integer

FIG (9.5)

LIMITATIONS OF SHEAR BUCKLING FORMULA

POSSIBILITY OF UPLIFT BETWEEN SPARCE FASTENINGS

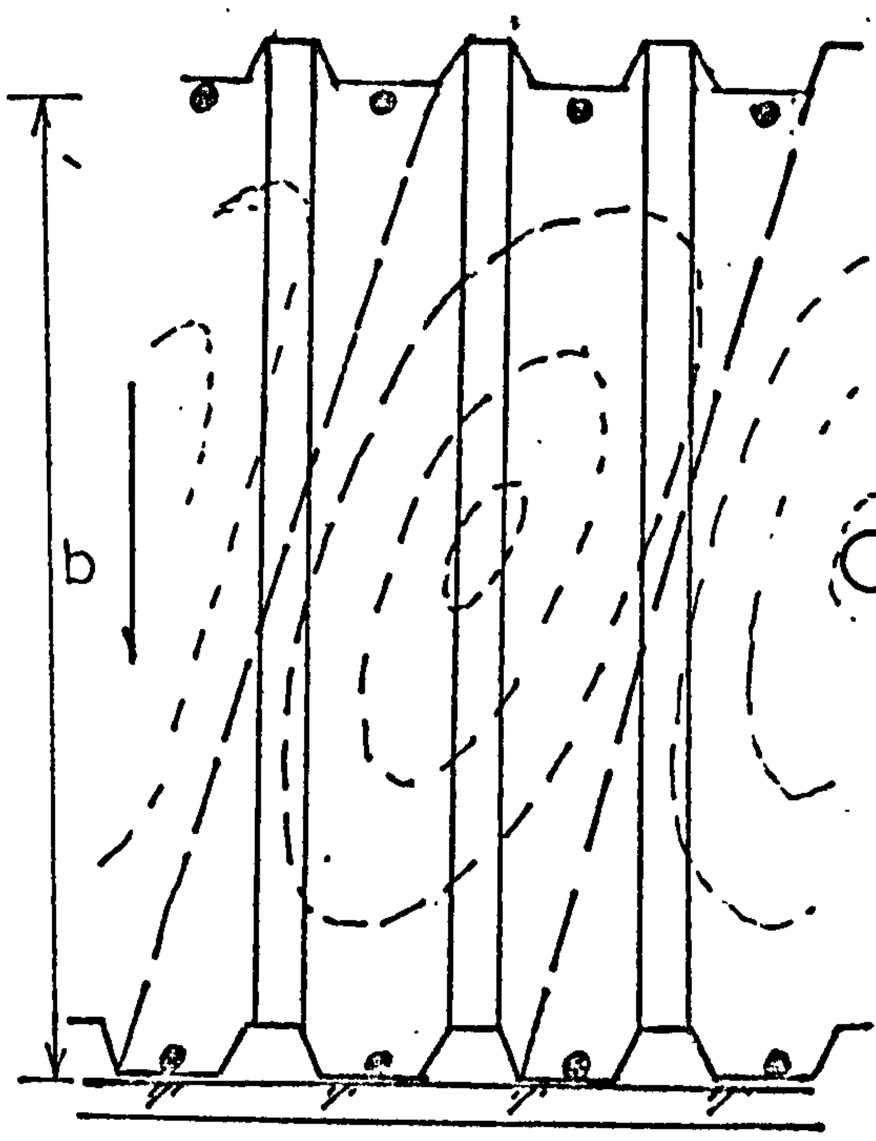

EVERY TROUGH FIXING

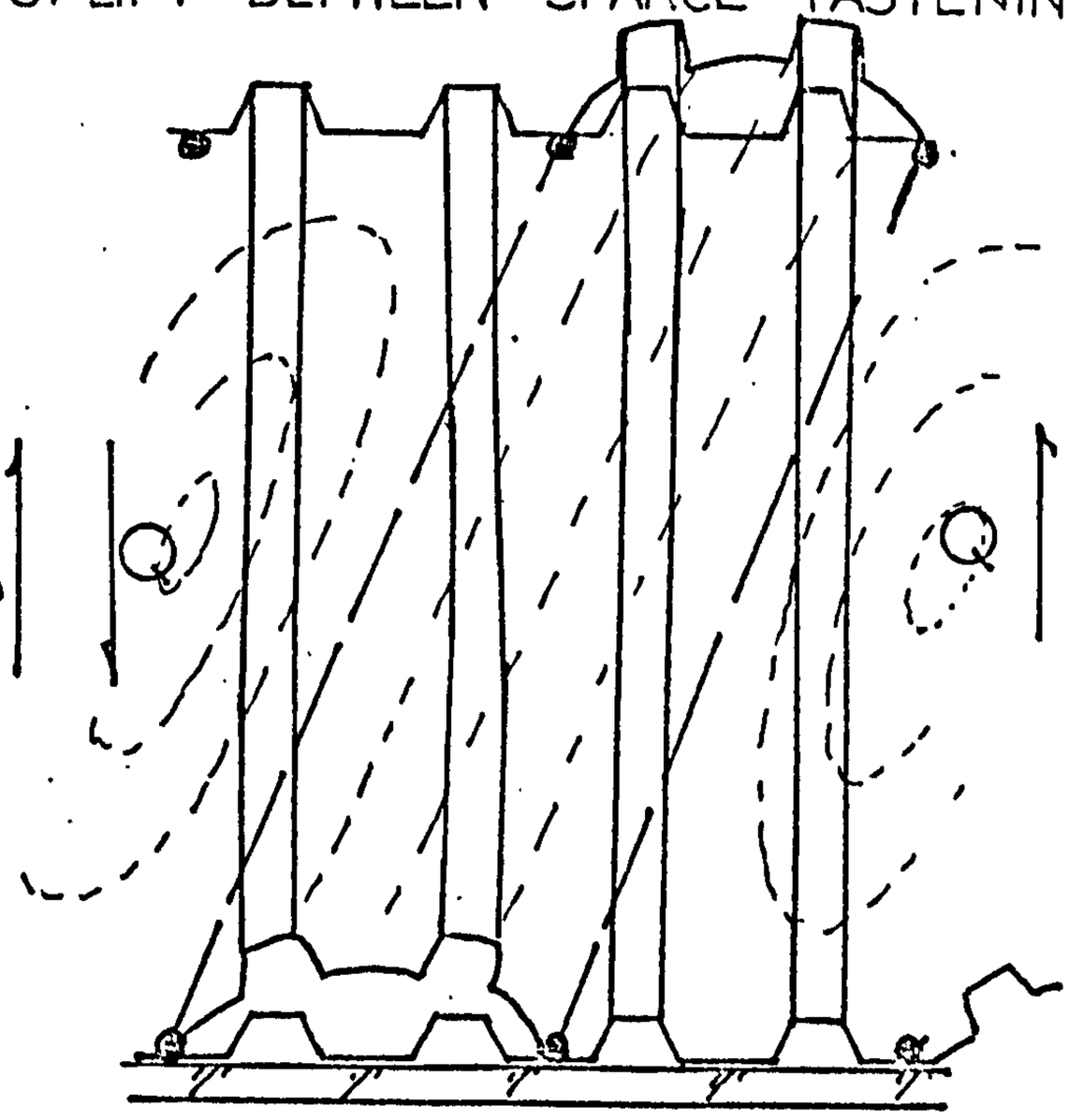

ALTERNATE TROUGH FIXING

ASSUMED BUCKLE DISPLACEMENTS

FIG (9.6)

BUCKLING BETWEEN INTERMEDIATE PURLIN FASTENERS

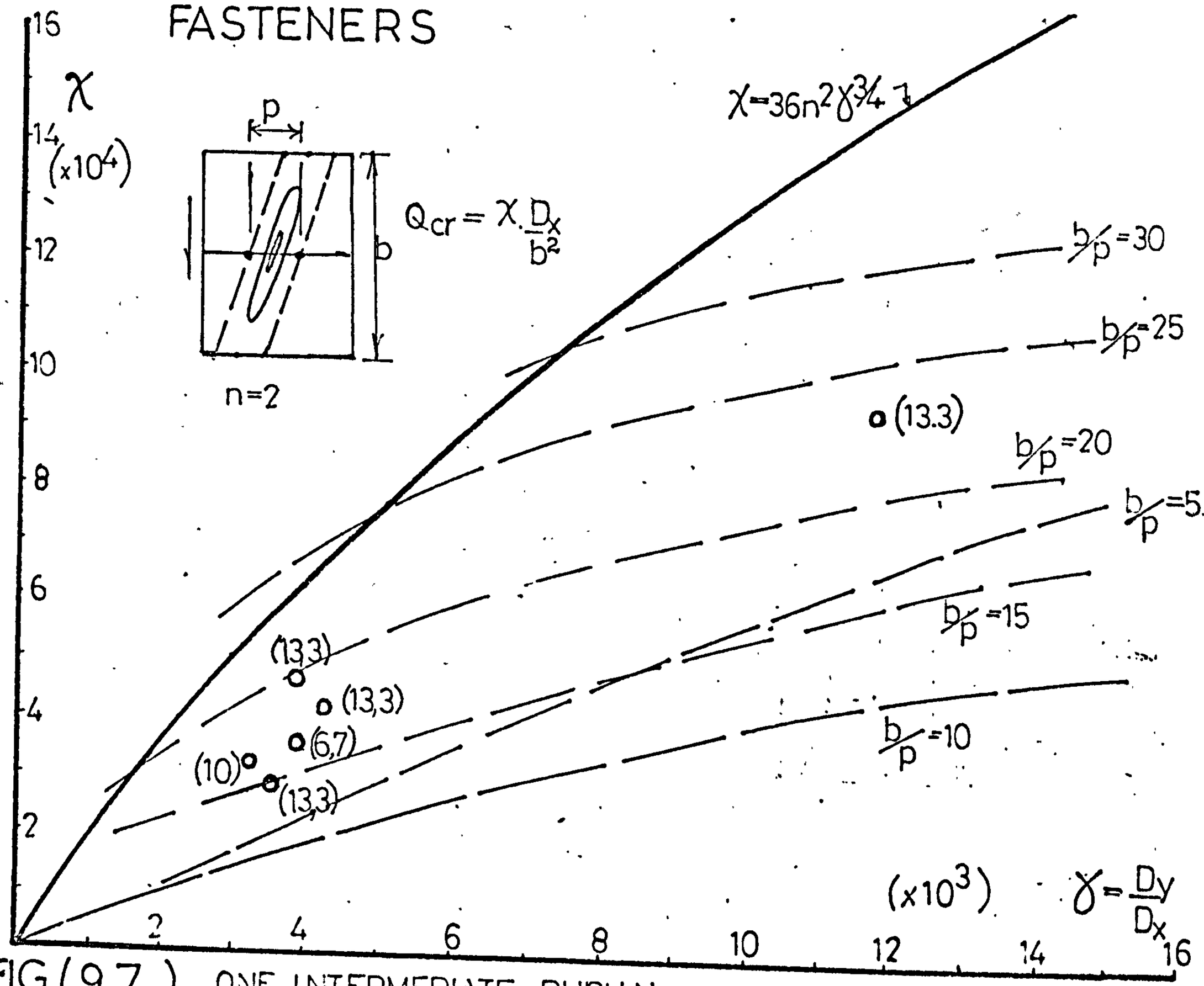

FIG (9.7) ONE INTERMEDIATE PURLIN

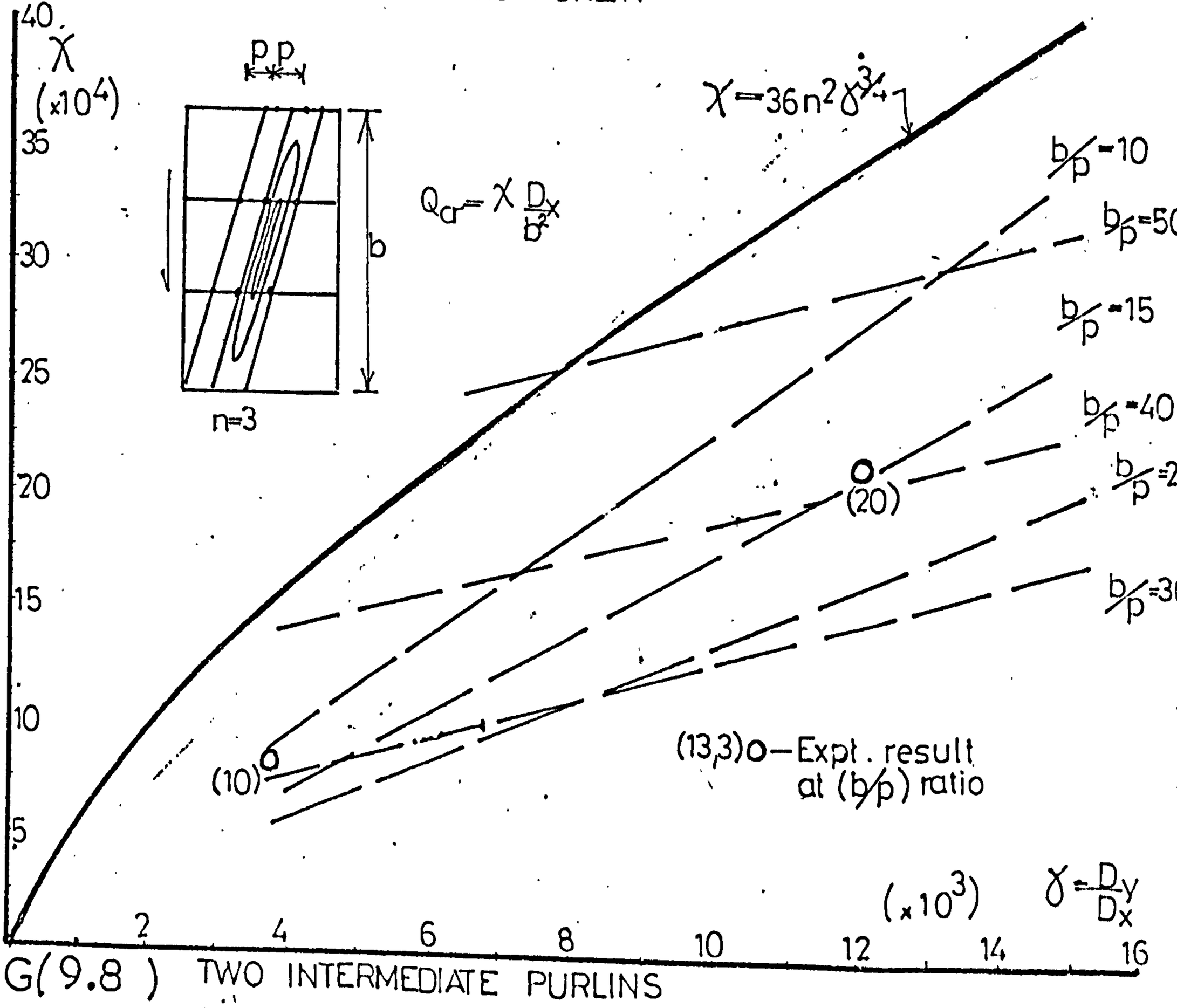

FIG(9.8) TWO INTERMEDIATE PURLINS

BUCKLING BETWEEN PERIMETER FASTENERS

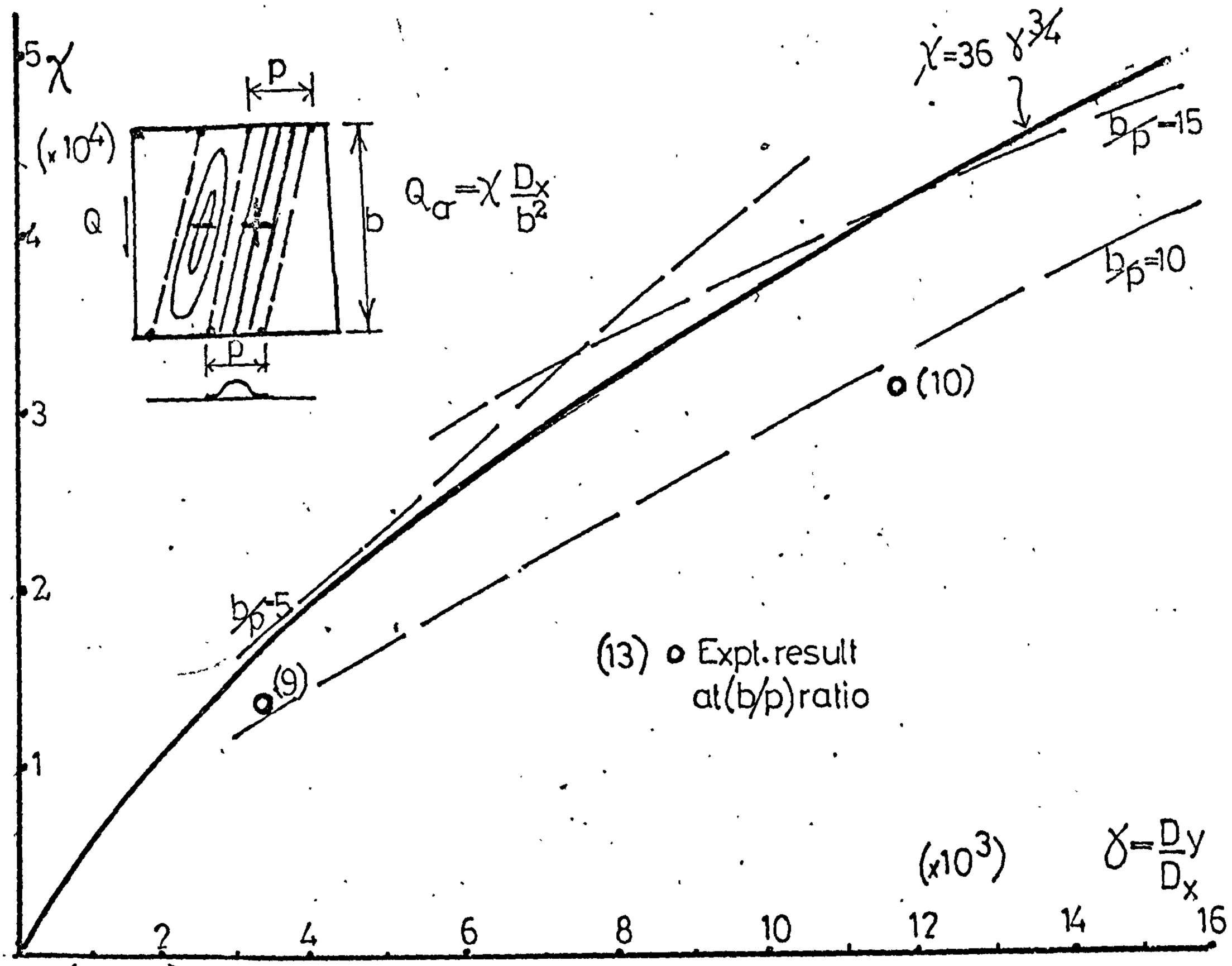

FIG(9.9) NO INTERMEDIATE PURLINS

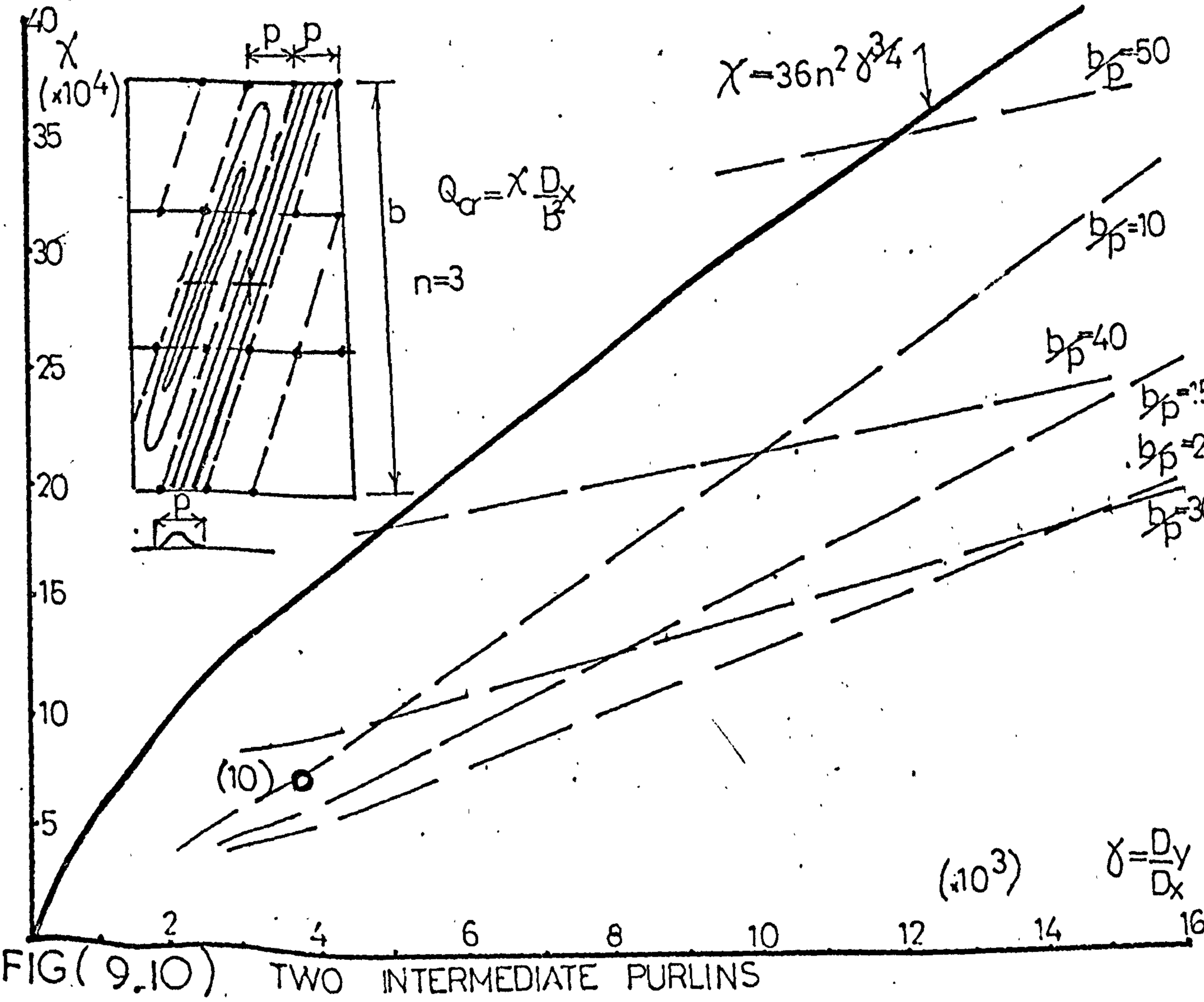

FIG(9.10) TWO INTERMEDIATE PURLINS

SHEAR BUCKLING OF HYPAR SHELLS

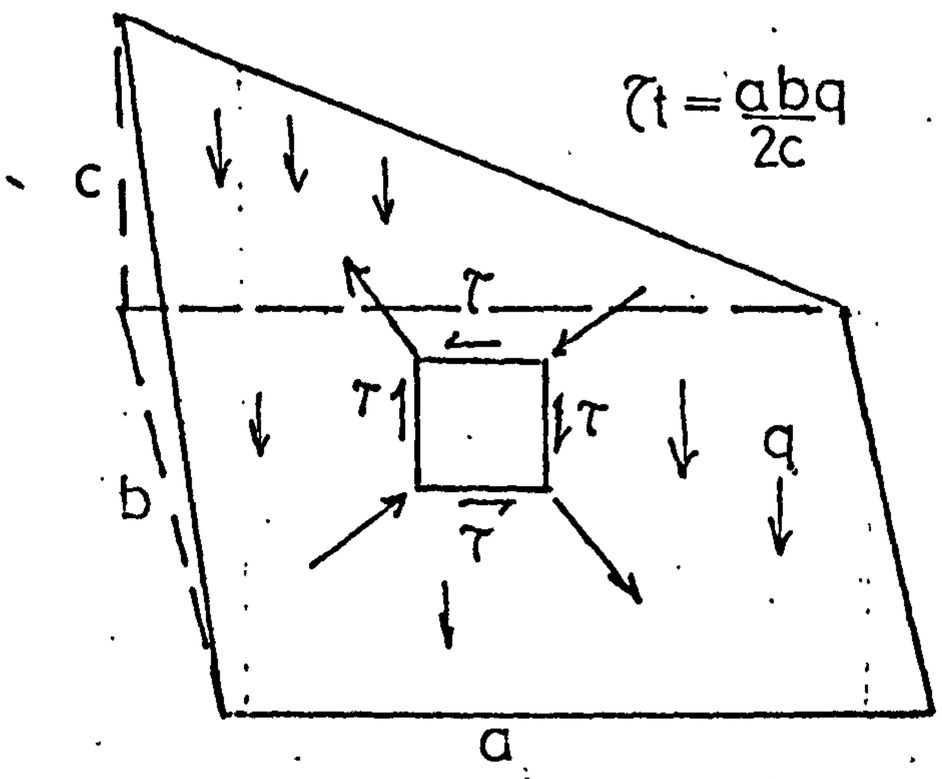

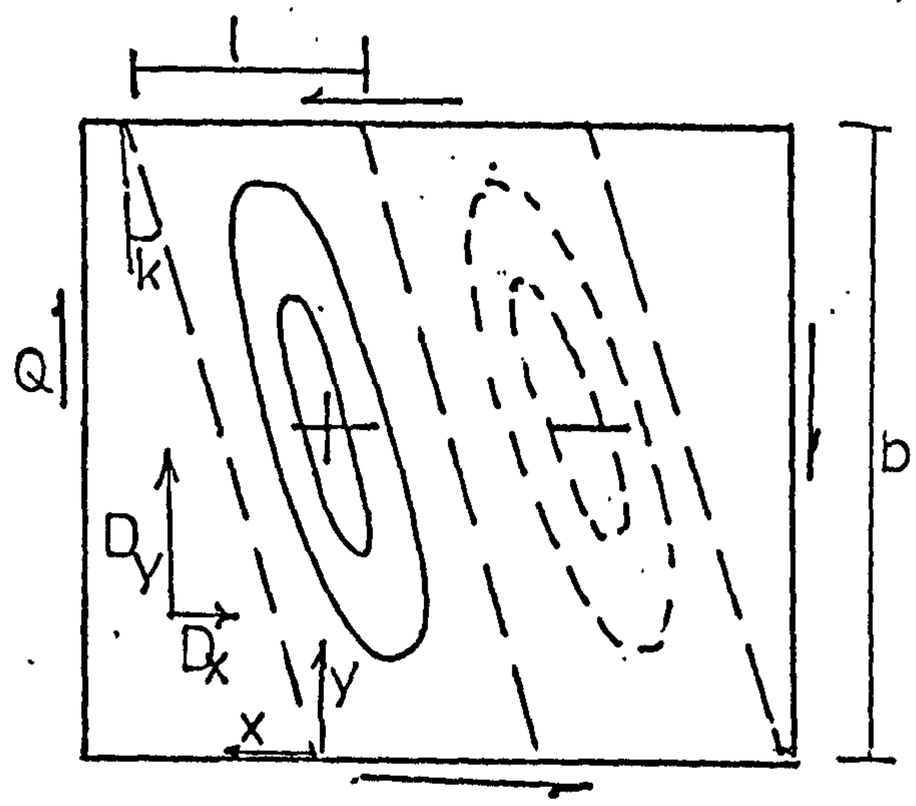

$$Q_{cr} = \frac{36}{b^2} D_x^{1/4} D_y^{3/4} . F \qquad D_y \gg D_x$$

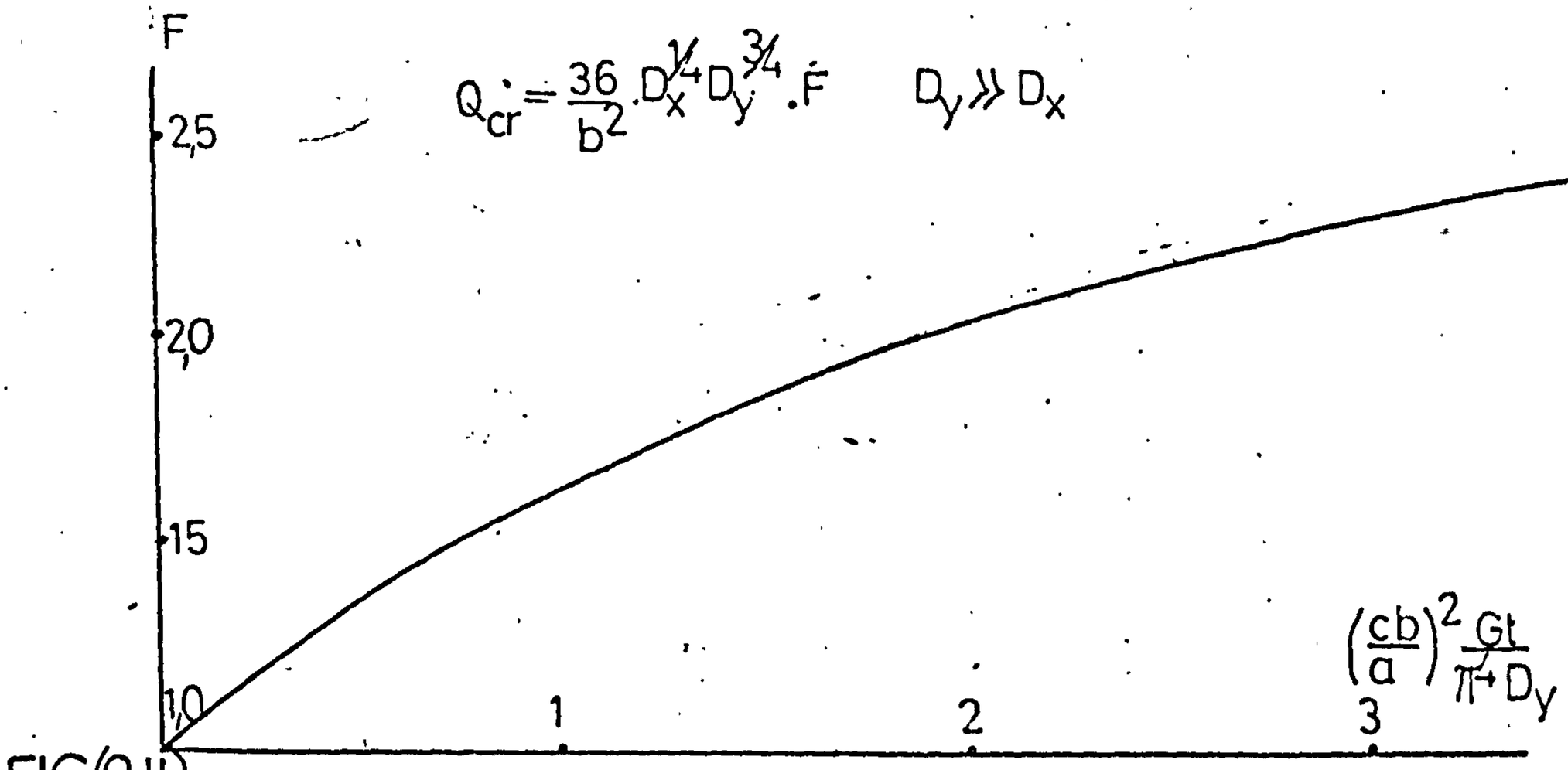

FIG(9.11)

SHEAR BUCKLING OF CYLINDRICAL SHELLS

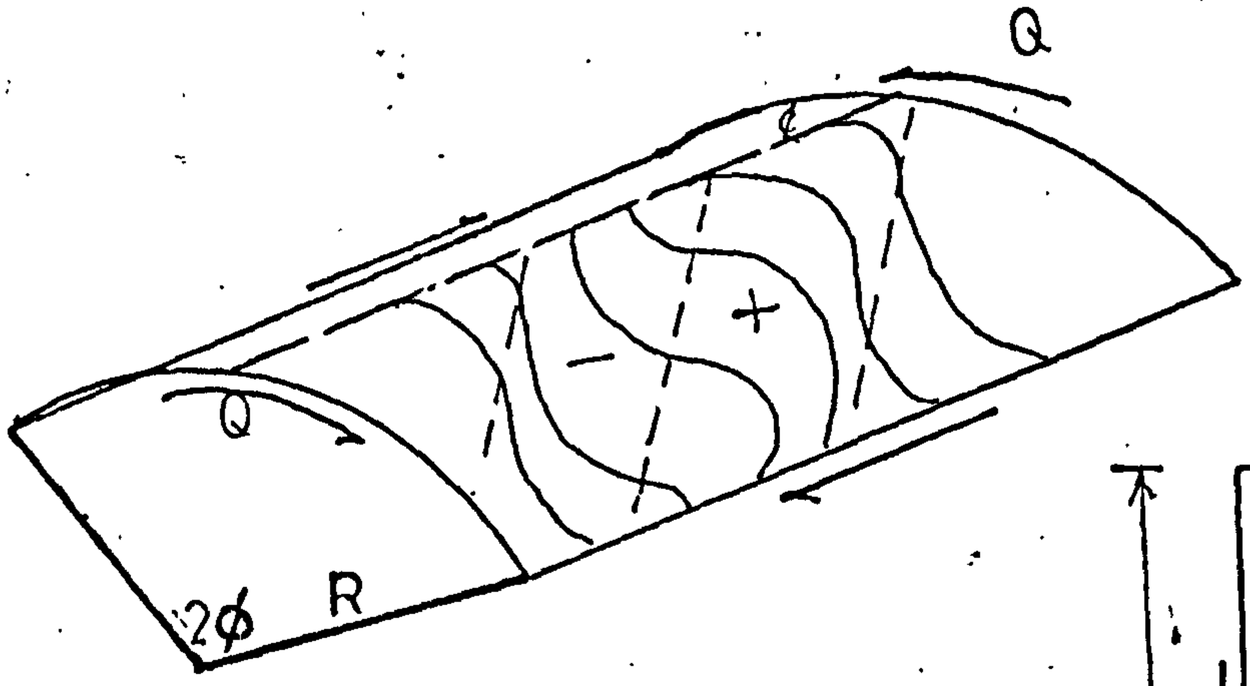

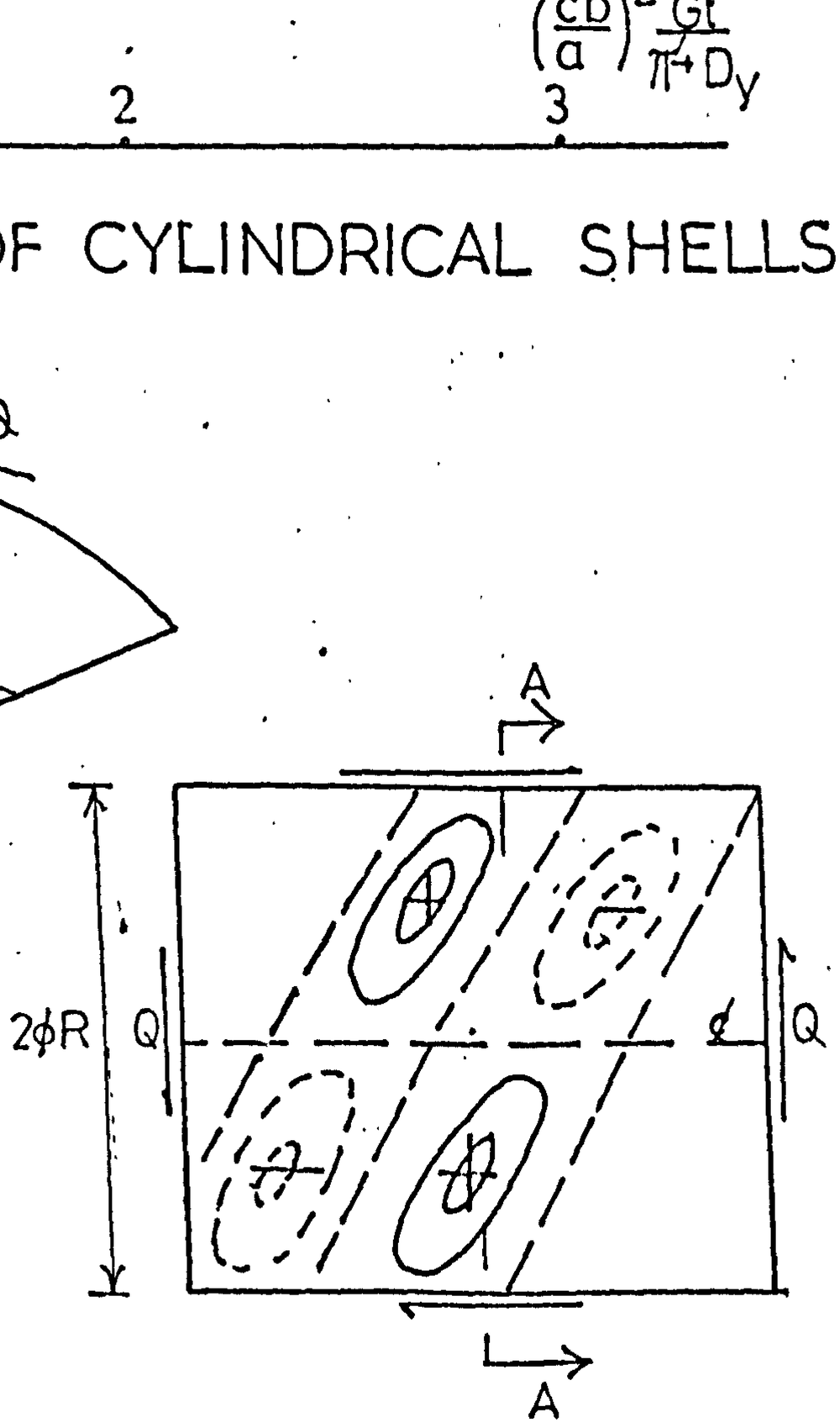

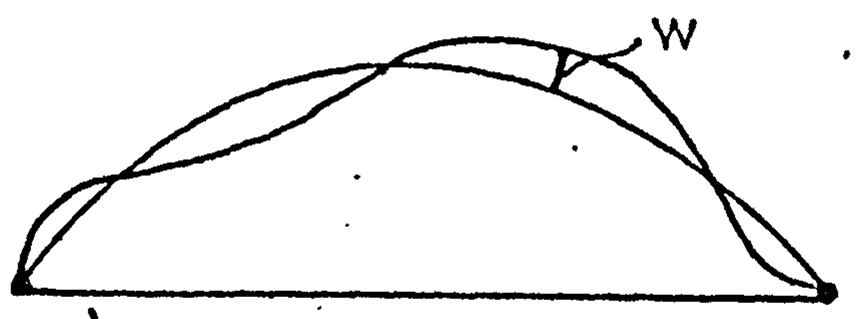

FIG (9.12) SECTION AA

FORMS OF FOLDED PLATE ROOFS

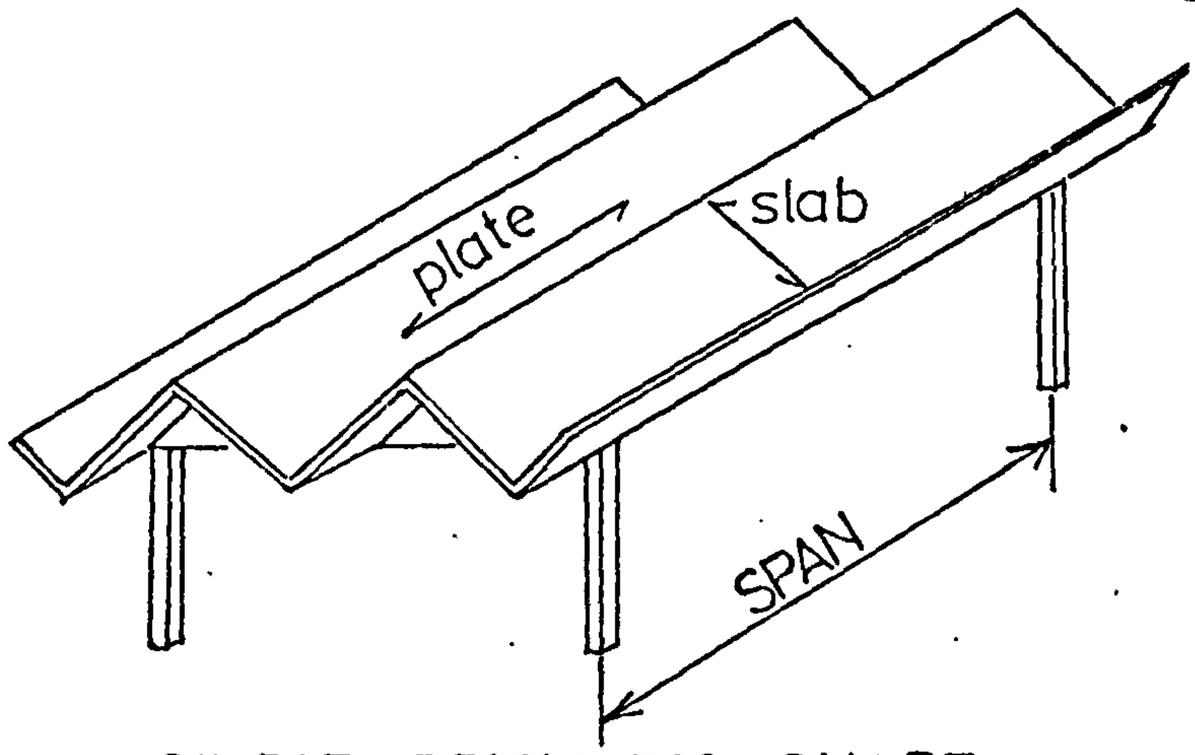

SIMPLE PRISMATIC SHAPE

NORTH LIGHT ROOF

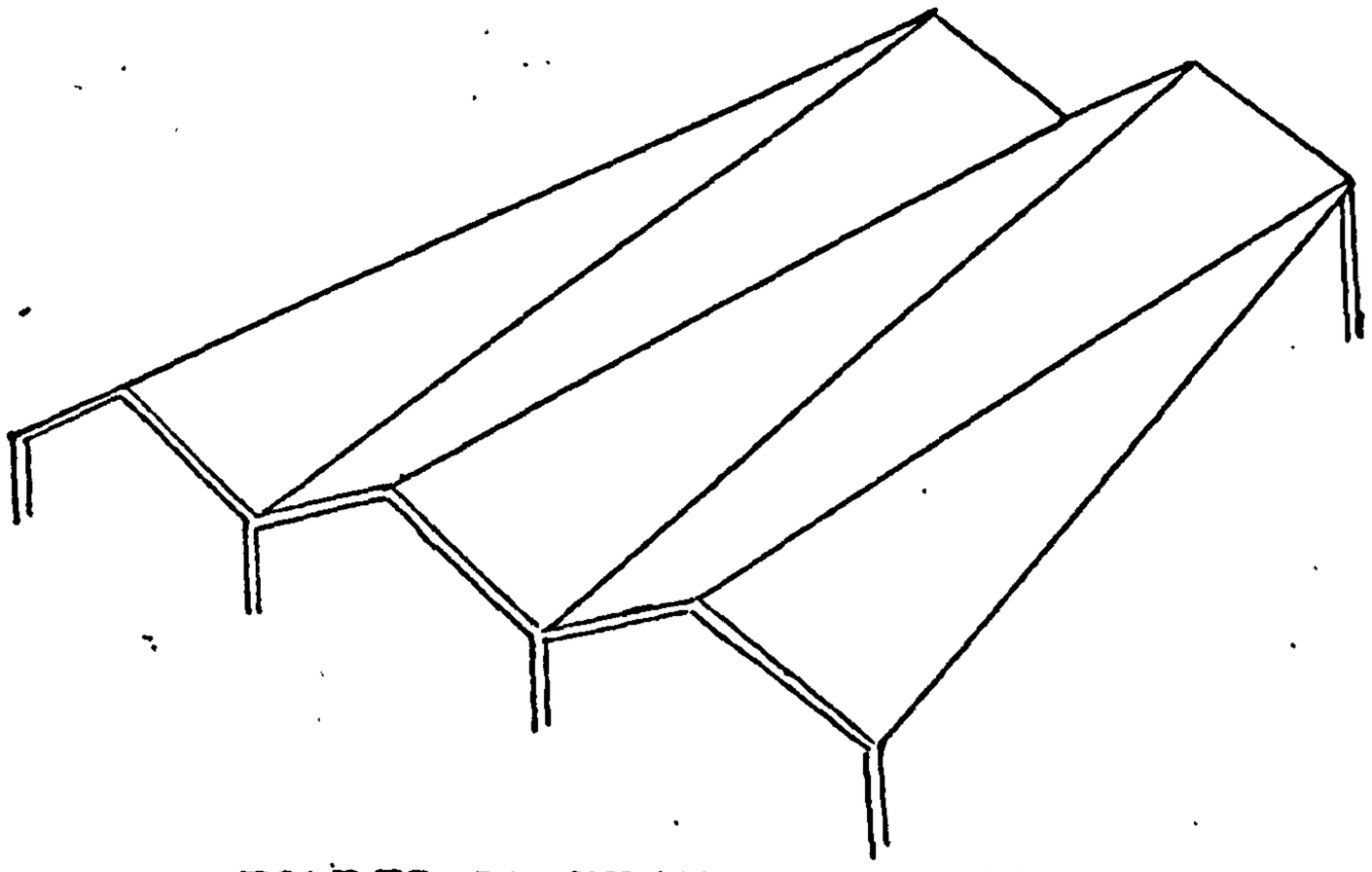

FOLDED PLATE WARPED INTO HYPAR SHAPE

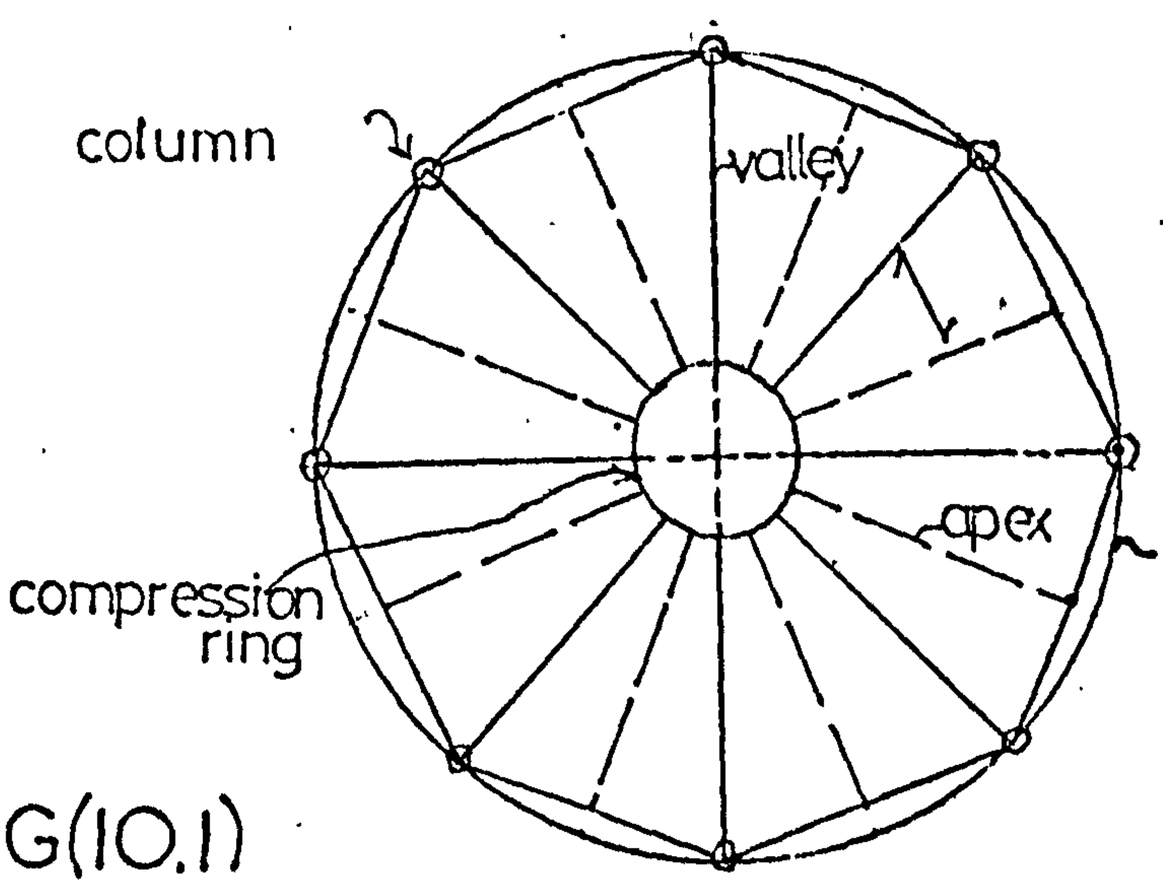

CIRCULAR FOLDED PLATE ROOF

FIG(10.1)

FOLDED PLATE ROOF – RESOLUTION OF FORCES AND DEFLECTION

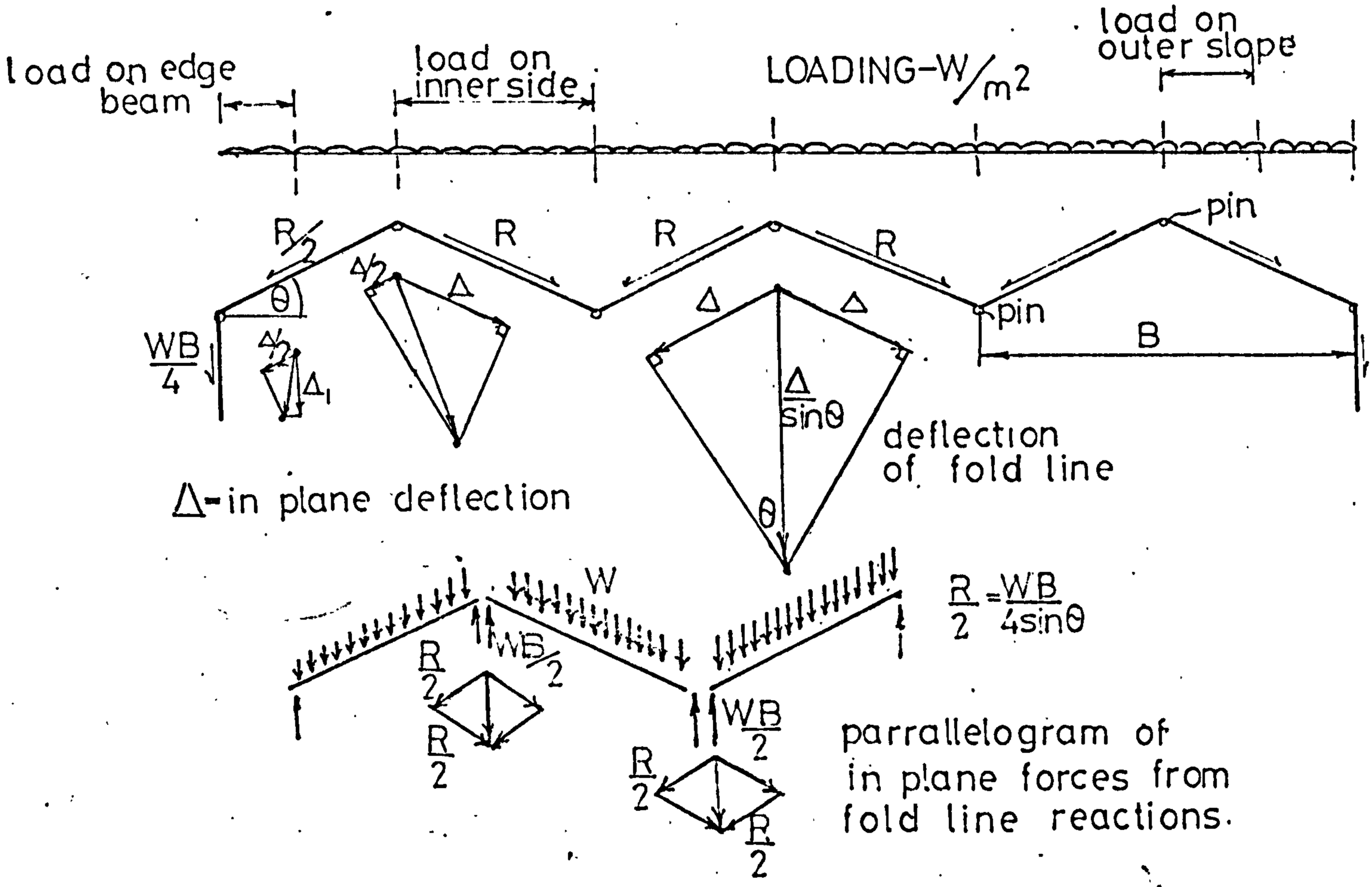

BEAM ACTION

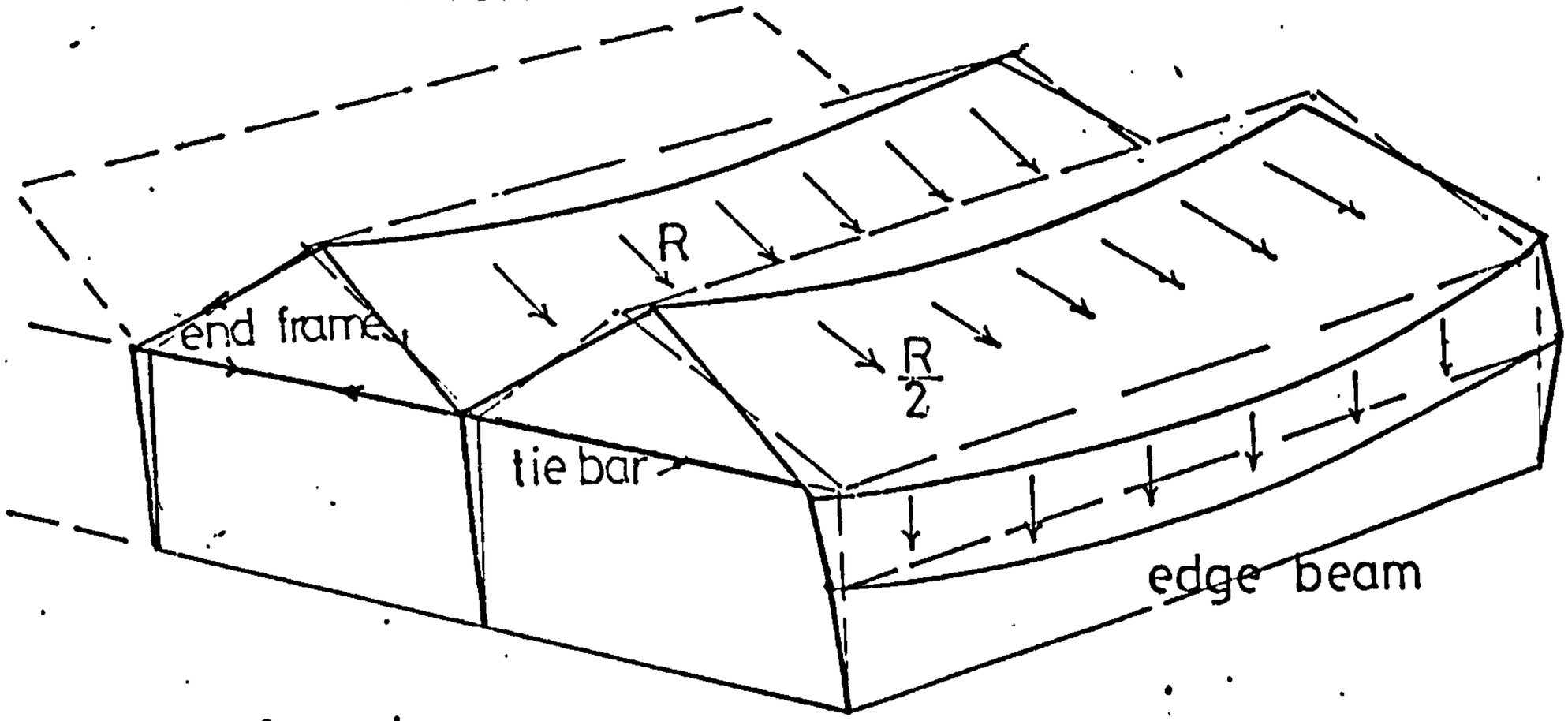

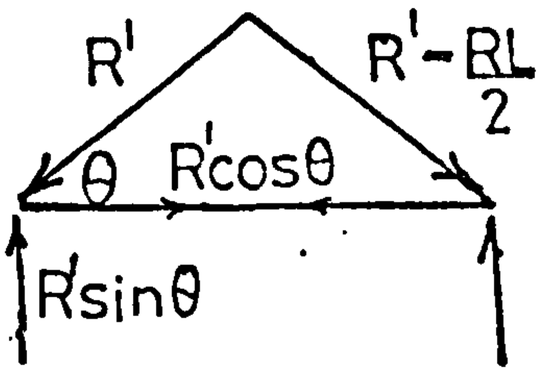

INCLINED BEAMS

fold area $2A_1$

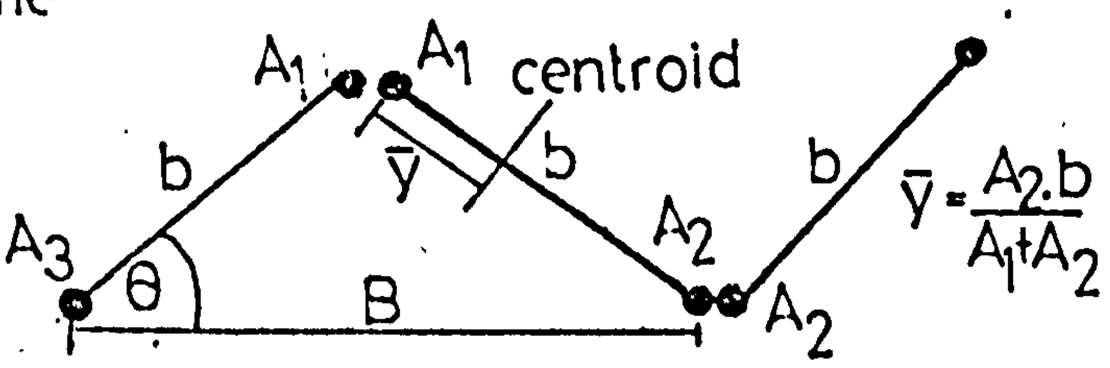

beam inertia $= \frac{A_1 A_2}{A_1 + A_2} . b^2$

FOLD AXIAL FORCE $= 2 . \frac{RL^2}{8I} . A_1 . \bar{y} = \frac{RL^2}{4b} = \frac{WL^2}{4} . \cot\theta$

FIG(10.2)

FOLDED PLATE ROOF— WIND LOADING

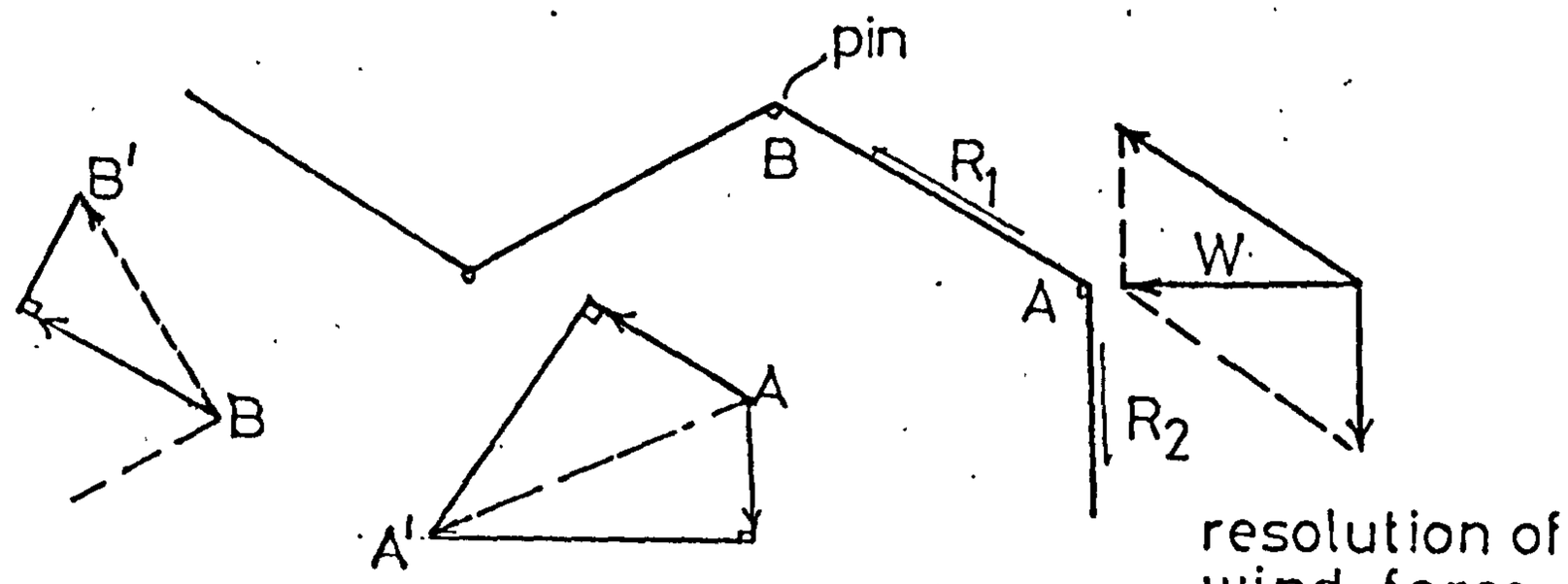

CONCRETE FOLDED PLATE ROOF THEORY

TRANSVERSE BENDING —3BAY CASE

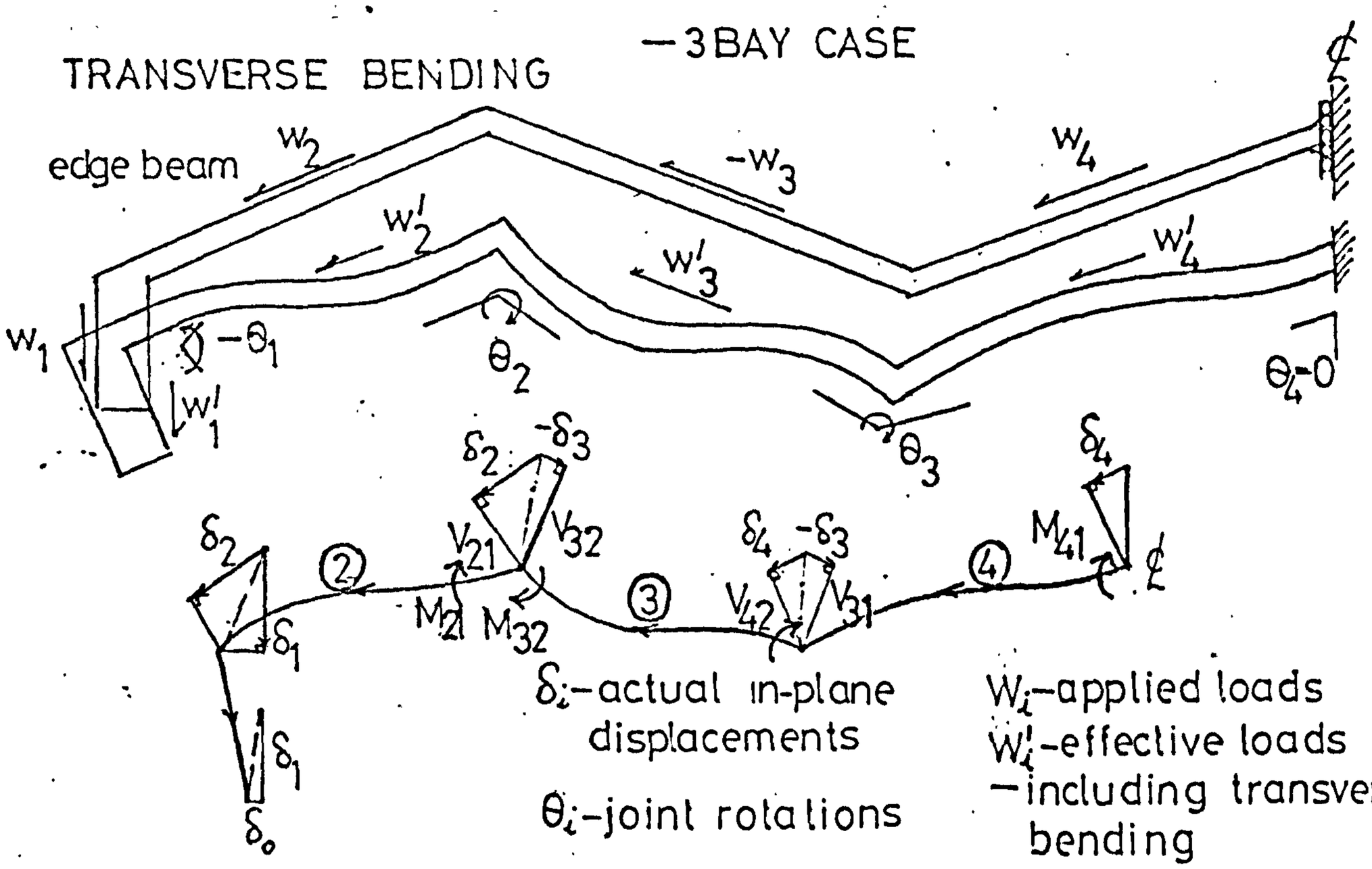

δ_i–actual in-plane displacements

θ_i–joint rotations

W_i–applied loads

W_i'–effective loads –including transverse bending

LONGITUDINAL STRESSES

assume $\delta_i = \delta_i^{max} \sin \frac{\pi}{L} y$

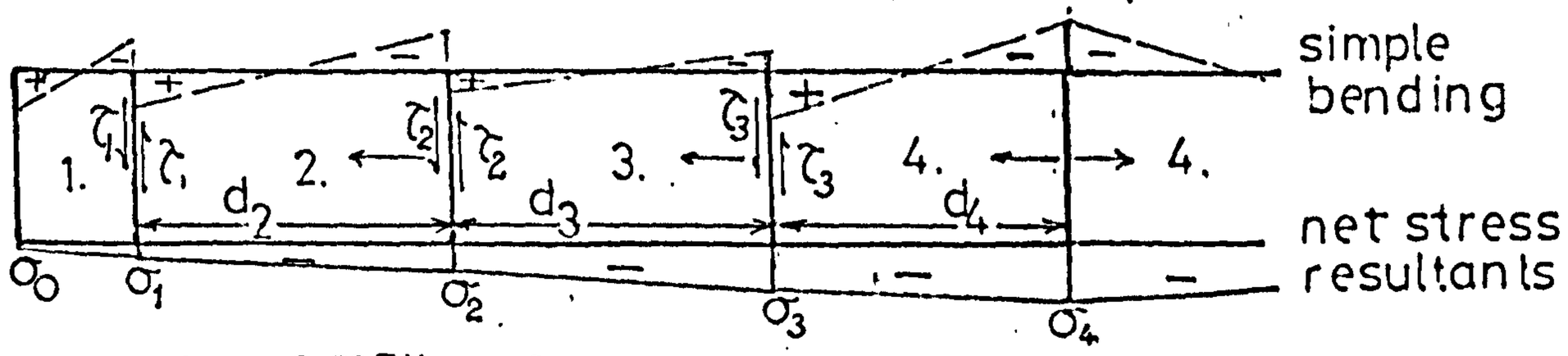

$$\tau_i = \tau_i^{max} \cos \frac{\pi y}{L}$$

$$\overline{M}_i = w_i' \cdot \frac{L^2}{8} \cdot \sin \frac{\pi y}{L}$$

$$\delta_i = \frac{(\sigma_{i-1} - \sigma_i)}{E\, d_i} \left\{\frac{L}{\pi}\right\}^2$$

τ_i–edge shear flow

$\overline{M}_i$–plate moment(τ_i=0)

σ_i–actual joint stress

d_i–plate width

L –roof length

FIG(10.3)

AXIAL STRESS AND DEFLECTION IN FOLDED PLATES

—— GENERAL FORMULATION FOR NO TRANSVERSE BENDING

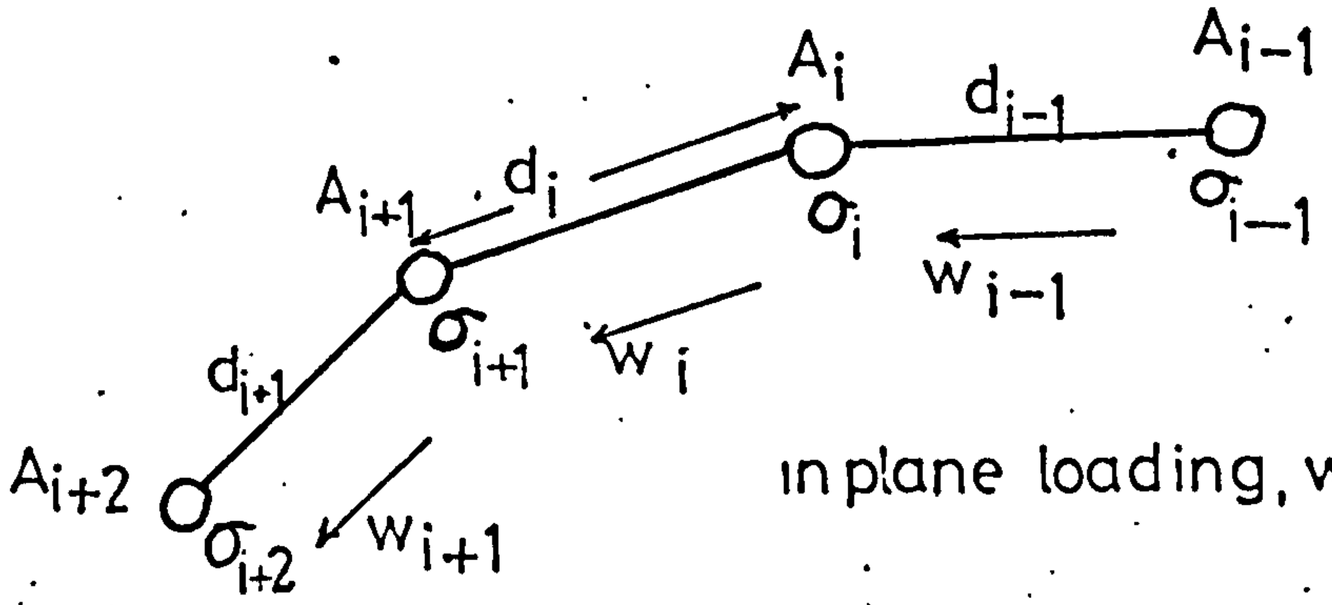

in plane loading, w_i

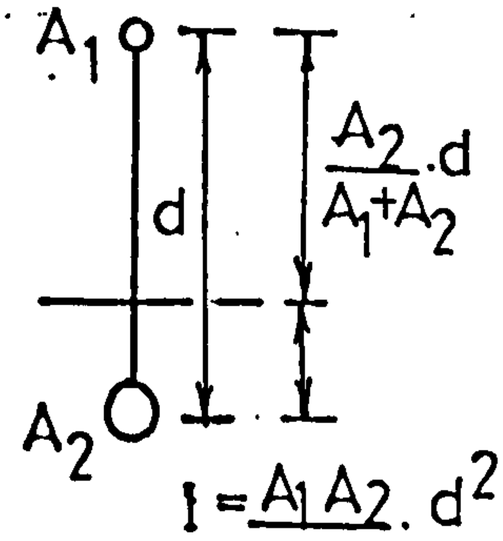

$$I = \frac{A_1 A_2 \cdot d^2}{A_1 + A_2}$$

ith FOLD LINE TOTAL AREA, A_i
" " " AXIAL STRESS, σ_i

$$\sigma_i = \left\{ -\frac{w_{i-1}}{A_i \cdot d_{i-1}} + \frac{w_i}{A_i \cdot d_i} \right\} \frac{L^2}{8} \qquad \text{compression +}$$

$$\sigma_{i+1} = \left\{ -\frac{w_i}{A_{i+1} \cdot d_i} + \frac{w_{i+1}}{A_{i+1} \cdot d_{i+1}} \right\} \cdot \frac{L^2}{8}$$

INPLANE DEFLECTION δ_i

simple theory $\delta_i = \frac{5 w_i L^4}{384 E I_i}$

where $I_i = \frac{A_i A_{i+1}}{A_i + A_{i+1}} d_i^2$

but,

$$\delta_i = \frac{5}{48} \cdot \frac{L^2}{E} \left\{ \frac{\sigma_i - \sigma_{i+1}}{d_i} \right\}$$

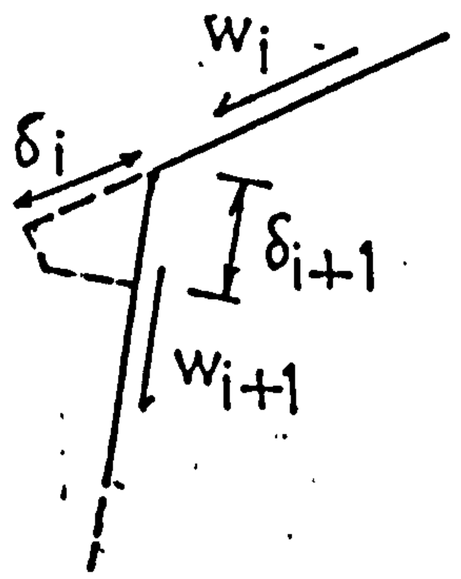

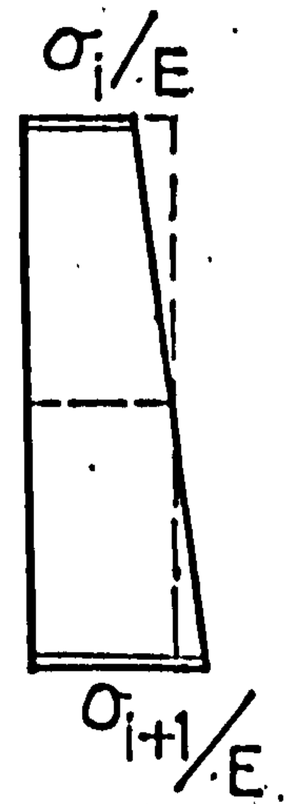

axial strain

$$\delta_i = \frac{5}{384} \frac{L^4}{E d_i^2} \cdot \left\{ +\frac{w_i}{A_i} + \frac{w_i}{A_{i+1}} - \frac{w_{i+1}}{A_{i+1}} \cdot \frac{d_i}{d_{i+1}} - \frac{w_{i-1}}{A_i} \cdot \frac{d_i}{d_{i-1}} \right\}$$

$$\delta_i = \frac{5}{384} \cdot \frac{L^4 w_i}{E I_i} \left\{ 1 - \frac{d_i}{w_i} \frac{\left(\frac{w_{i+1}}{A_{i+1} \cdot d_{i+1}} + \frac{w_{i-1}}{A_i \cdot d_{i-1}} \right)}{\left(\frac{1}{A_i} + \frac{1}{A_{i+1}} \right)} \right\}$$

$\therefore \quad \delta_i = \delta_{simple}$ (1-modification factor)

FIG (10.4)

AXIAL STRESSES IN PROTOTYPE FOLDED PLATE ROOF

— VERTICAL LOADING AT 1,2 kN/m²

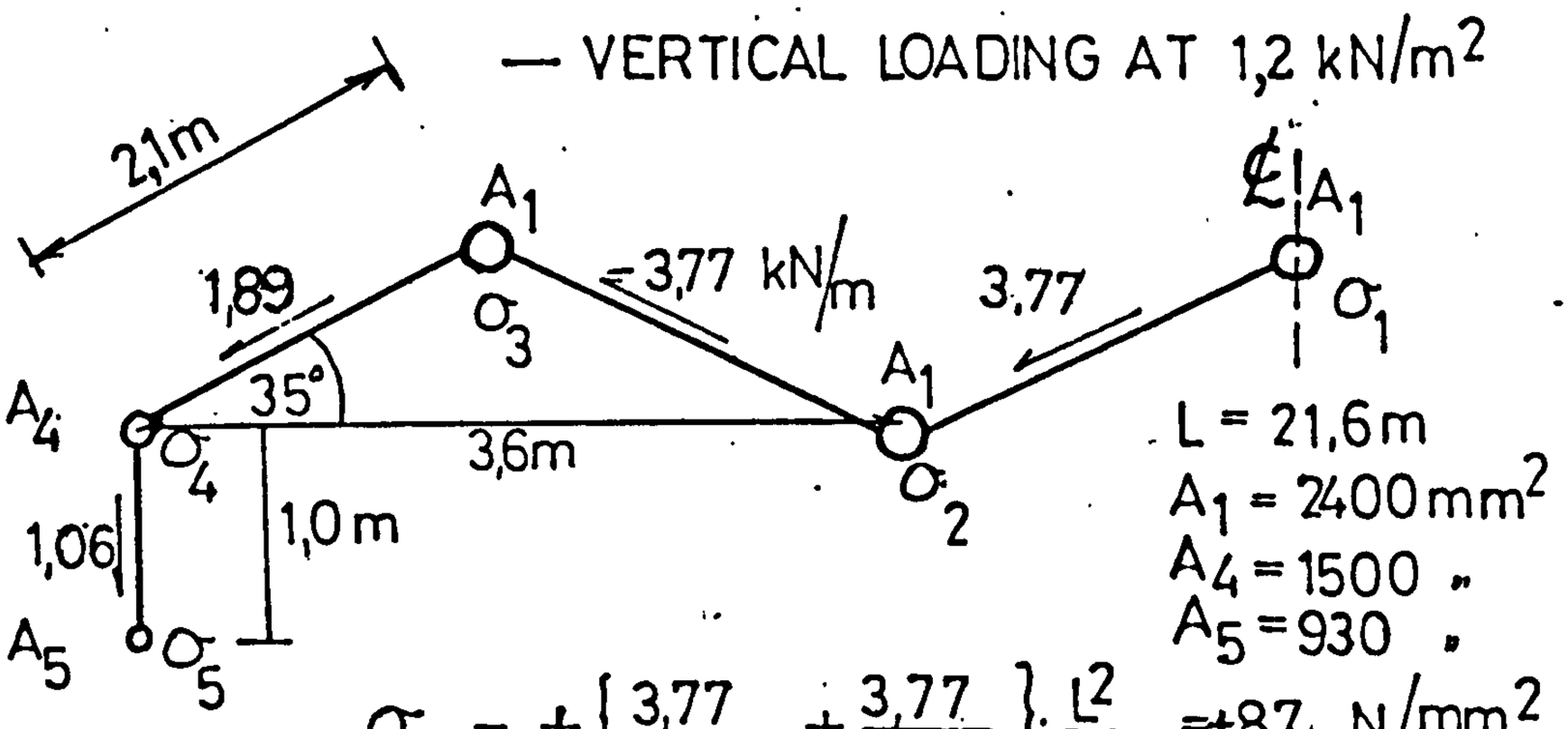

L = 21,6 m
A_1 = 2400 mm²
A_4 = 1500 "
A_5 = 930 "

$$\sigma_1 = +\left\{\frac{3,77}{2,4\times2,1} + \frac{3,77}{2,4\times2,1}\right\}\cdot\frac{L^2}{8} = +87 \text{ N/mm}^2$$

$\sigma_2 = -87$ N/mm² (+ve compression)

$$\sigma_3 = +\left\{\frac{3,77}{2,4\times2,1} + \frac{1,89}{2,4\times2,1}\right\}\frac{L^2}{8} = +66 \text{ N/mm}^2$$

$$\sigma_4 = +\left\{\frac{1,06}{1,5\times1,0} - \frac{1,89}{1,5\times2,1}\right\}\frac{L^2}{8} = +6 \text{ N/mm}^2$$

$$\sigma_5 = -\left\{\frac{1,06}{0,93\times1,0}\right\}\frac{L^2}{8} = -66 \text{ N/mm}^2$$

WIND LOADING DURING TEST

$$\sigma_1 = \left\{\frac{0,54}{0,93\times1,0}\right\}\frac{L^2}{8} = 34 \text{ N/mm}^2$$

$$\sigma_2 = -\left\{\frac{0,54}{1,5\times1,0} + \frac{0,95}{1,5\times2,1}\right\}\frac{L^2}{8} = -38 \text{ N/mm}^2$$

$$\sigma_3 = \left\{\frac{0,95}{2,1\times1,5}\right\}\frac{L^2}{8} = 17 \text{ N/mm}^2$$

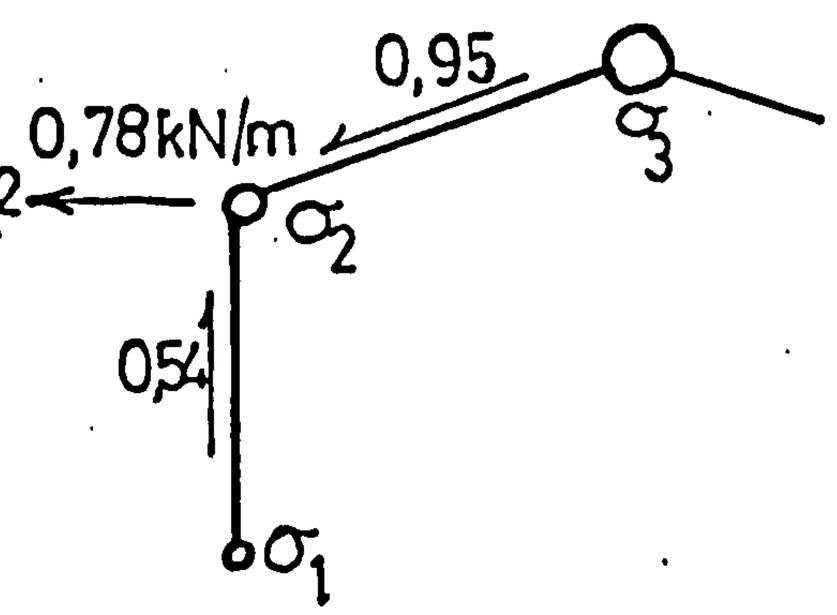

IN PLANE BENDING DEFLECTION OF FOLDED PLATE ROOF

using $\delta_i = \frac{5}{48}\frac{L^2}{E}\left\{\frac{\sigma_i - \sigma_{i+1}}{d_i}\right\}$

δ_V — vertical joint movement

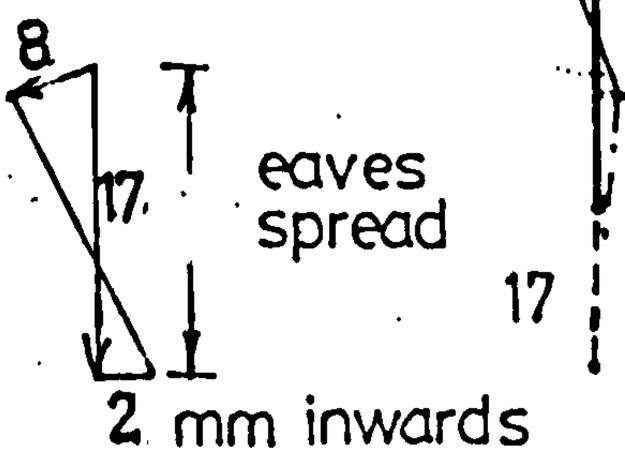

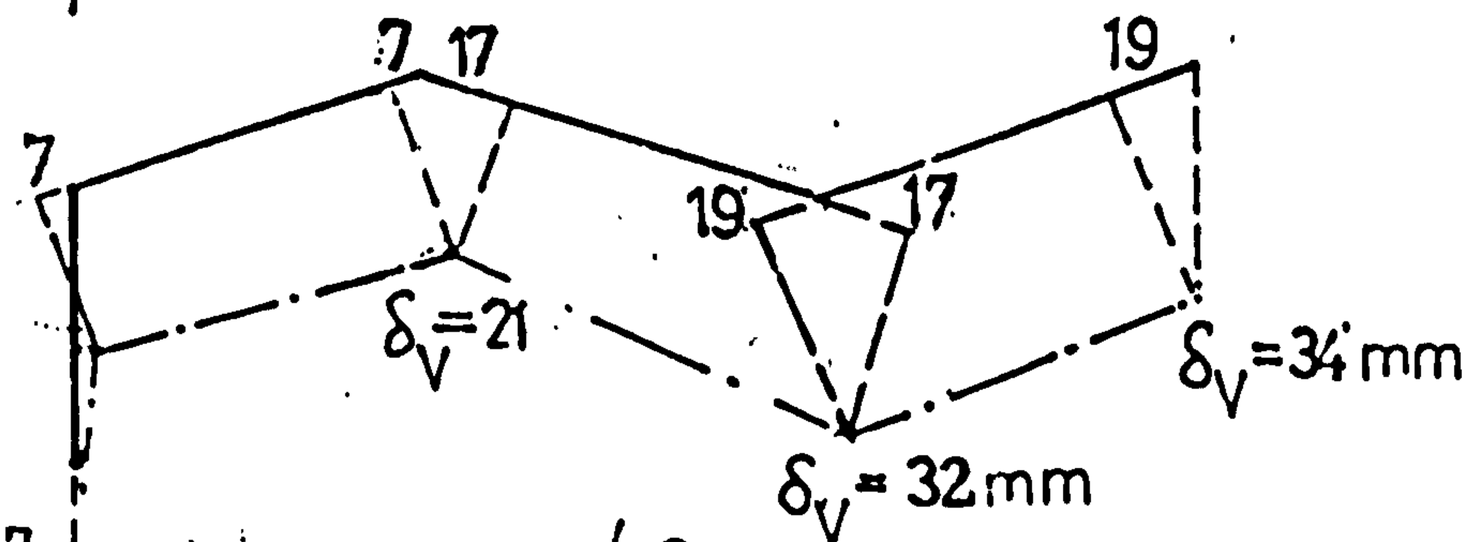

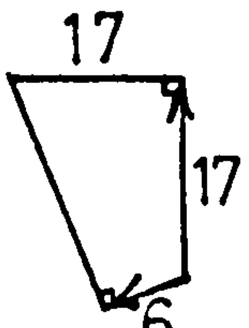

eaves
spread
17mm outwards

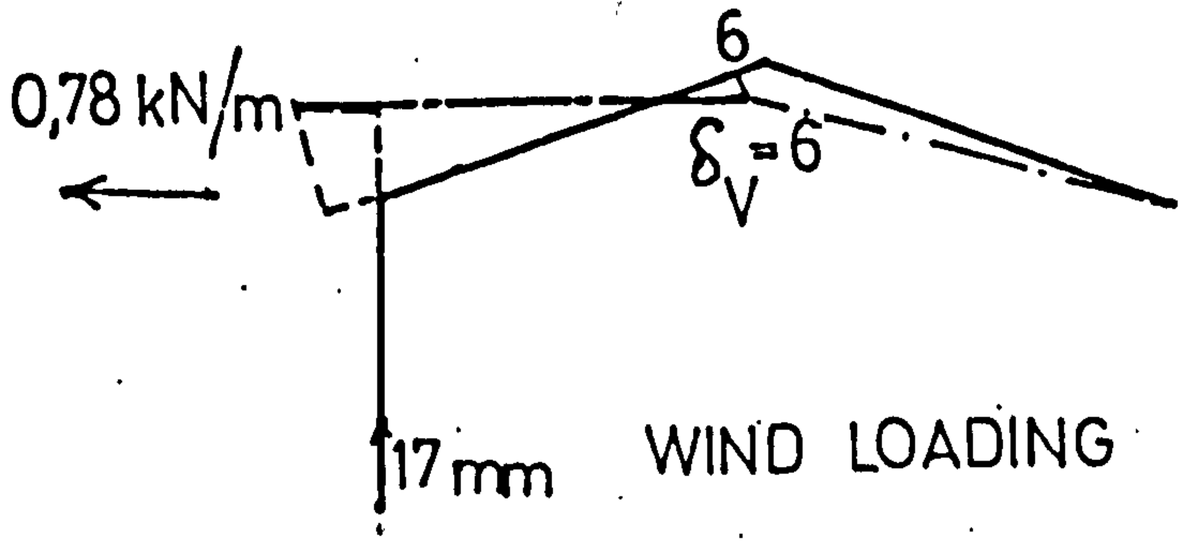

FIG(10.5)

FOLDED PLATE ROOF — PRESSED SHEETING

REDUCED SHEET THICKNESSES (originally 1mm – 0,05 galv.)

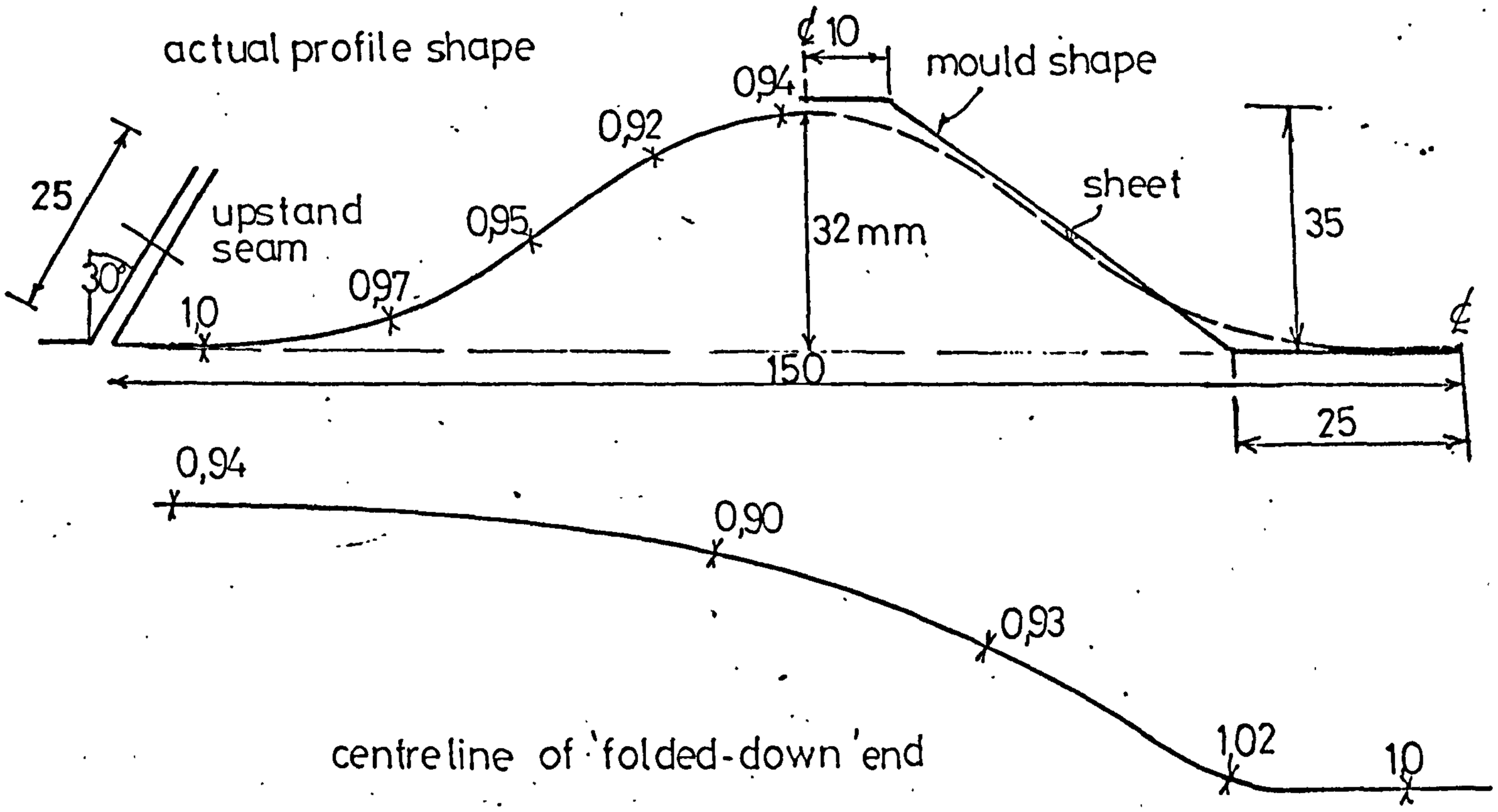

EXTENSIONS AROUND PROFILE — deep drawing steel
failure elongation 50%

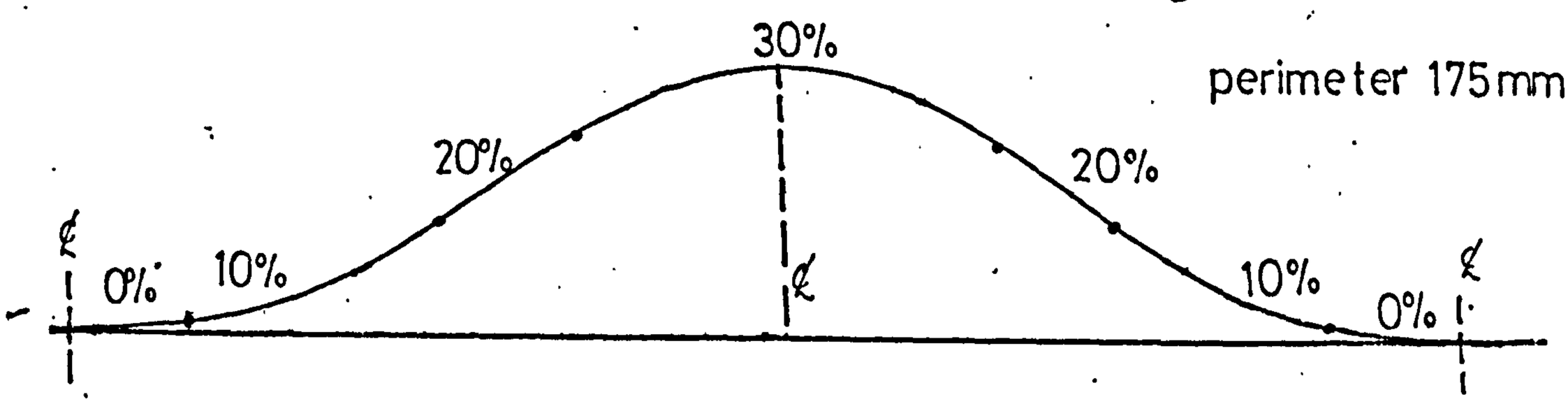

EXTENSIONS AROUND PROFILE — mild. steel

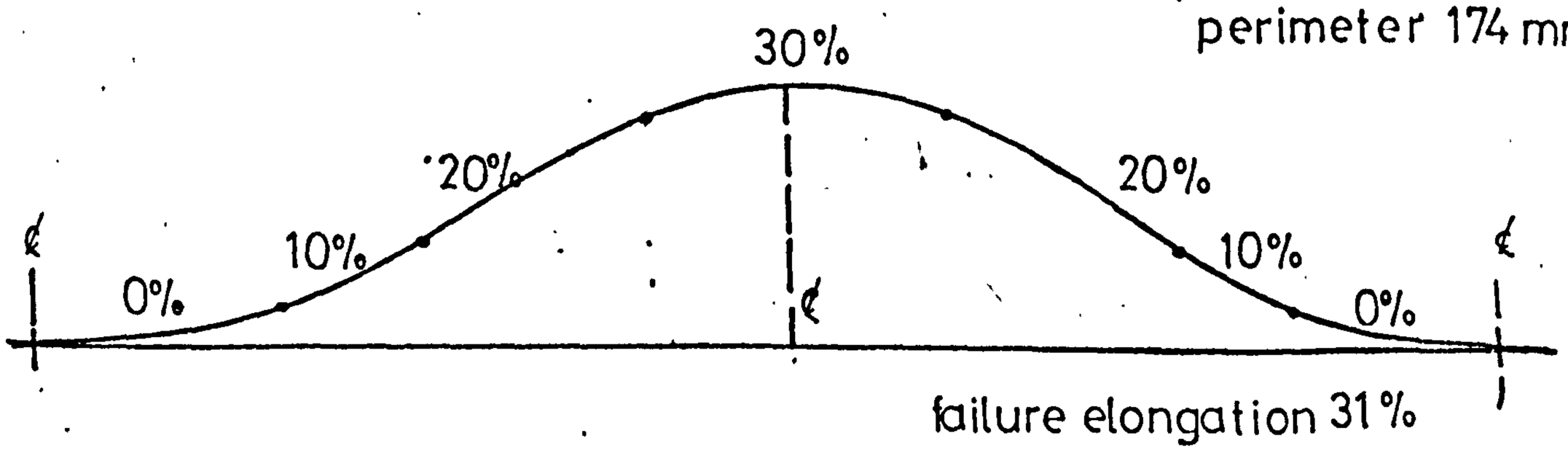

FIG(10.6)

VERTICAL LOADING SYSTEM FOR ROOF TESTS

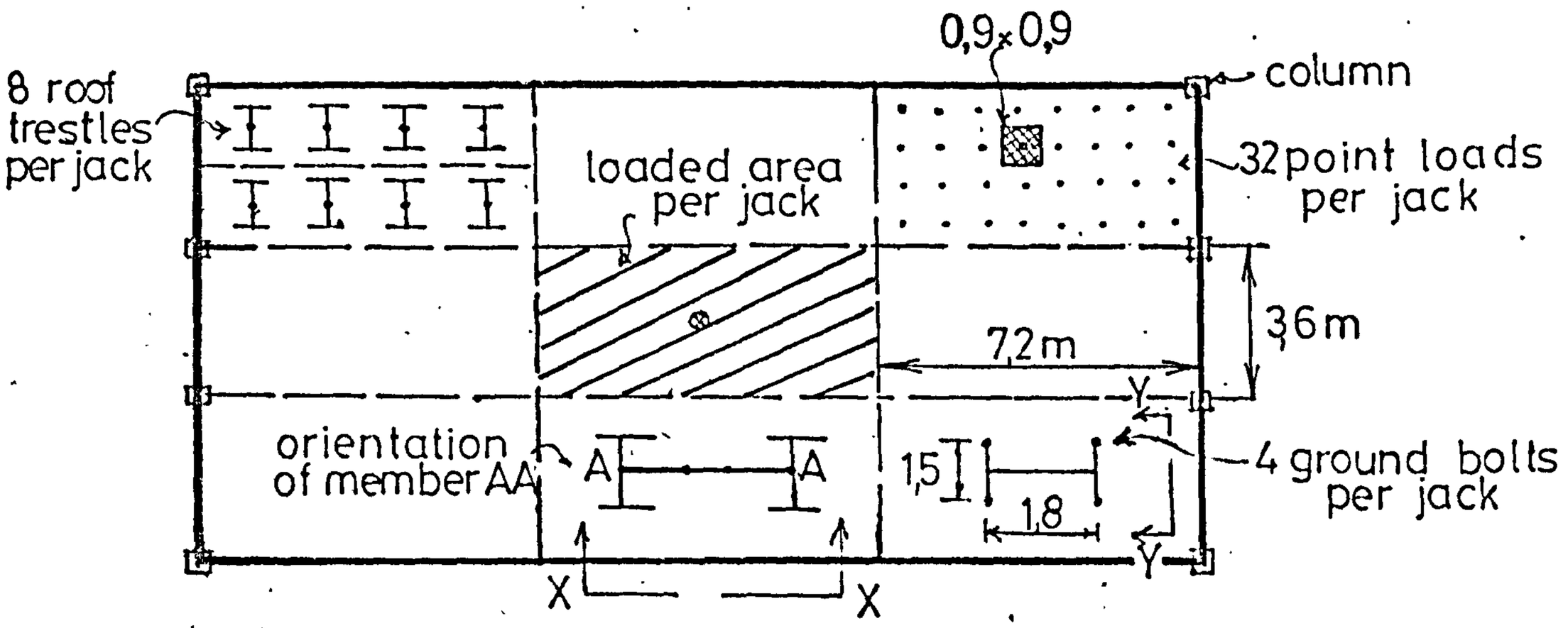

ROOF LOADED BY NINE JACKS

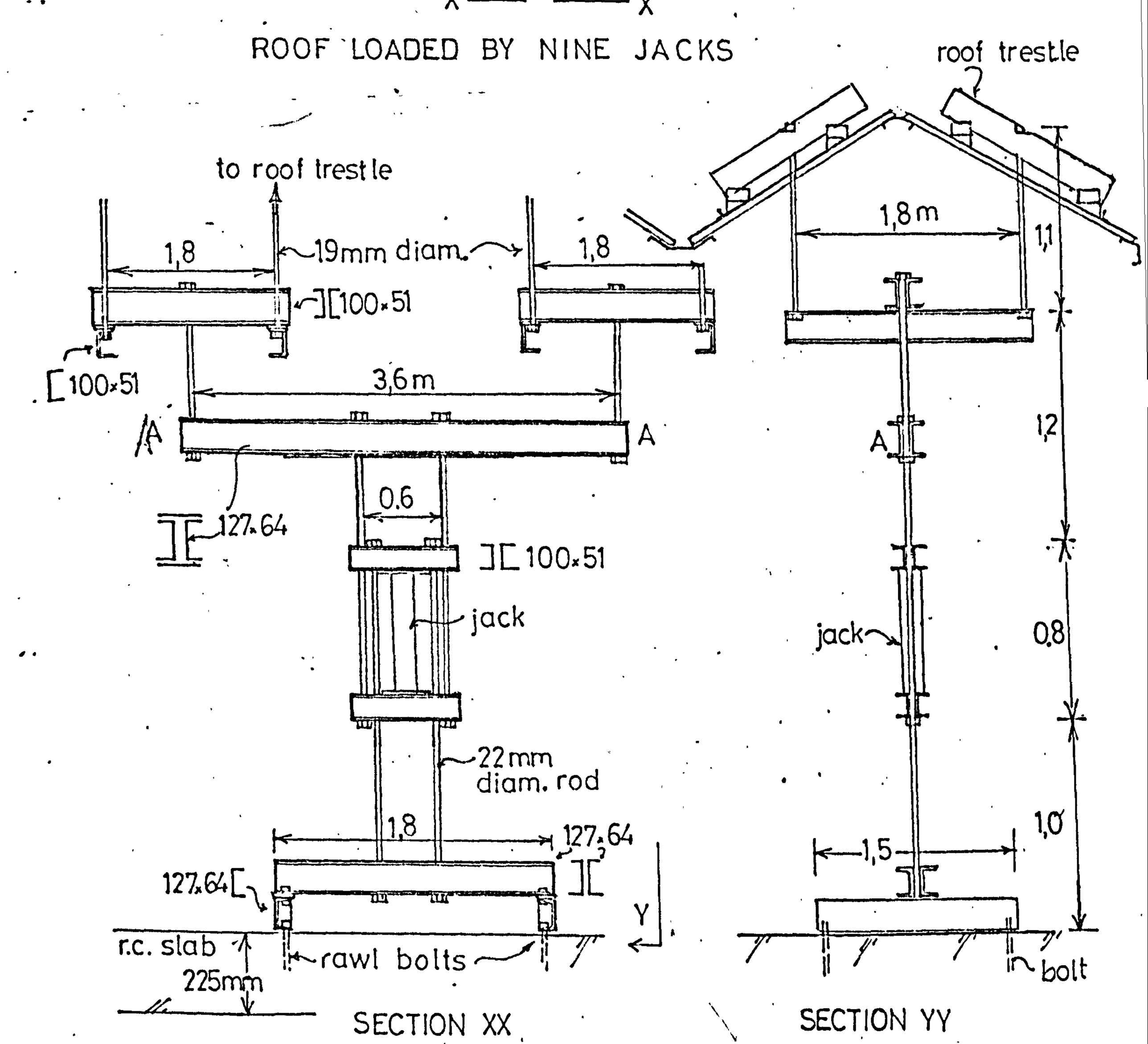

SECTIONS THROUGH ROOF LOADING 'TREE' SYSTEM

FIG(10.7)

VERTICAL LOADING SYSTEM — CONTINUED

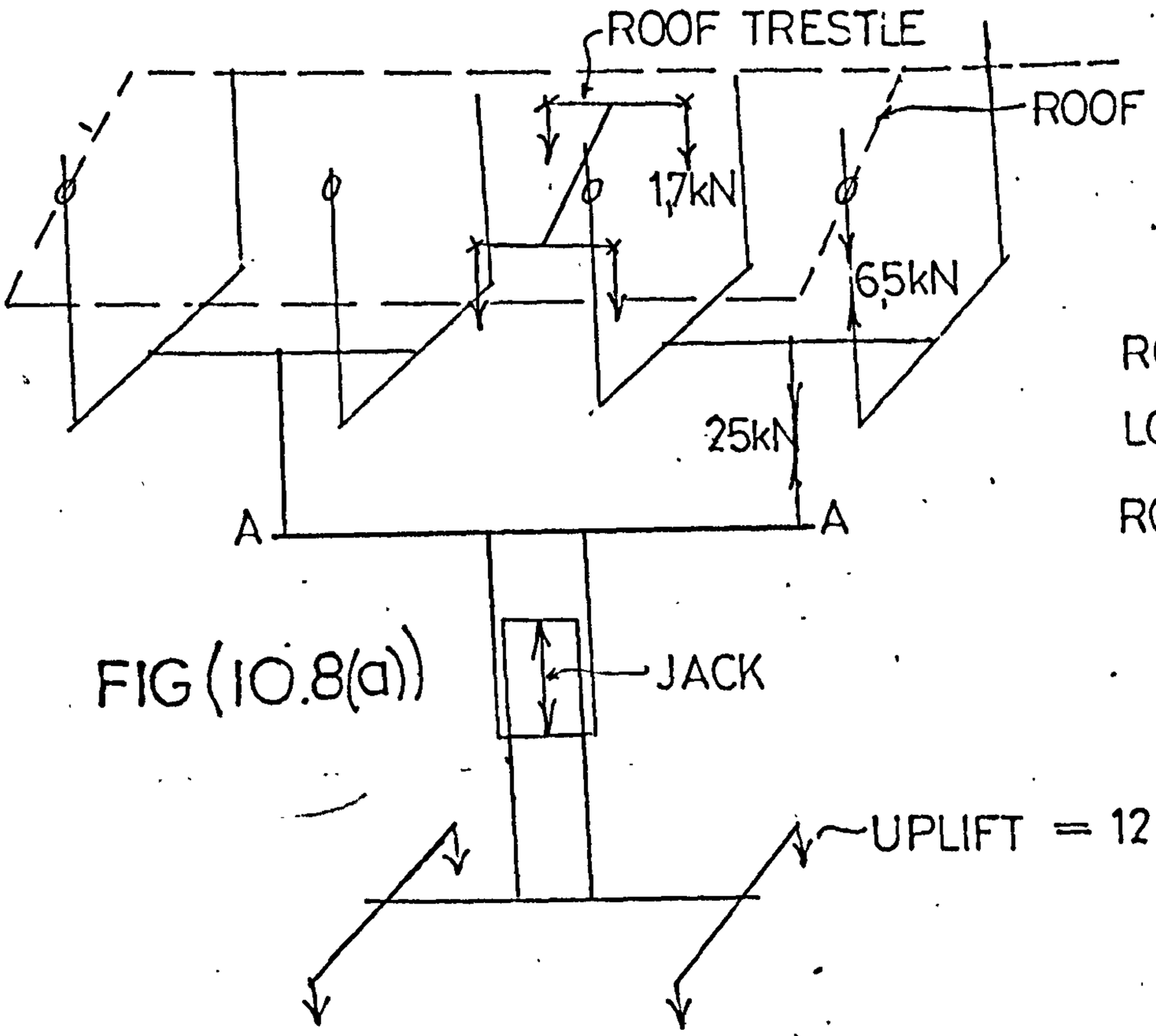

ROOF WEIGHT = 0,22 kN/m²
LOADING SYSTEM = 0,23 "
ROOF FAILURE = 2,3 kN/m²

NET JACK FORCE = 1,85×3,6×7
= 48 kN

FIG (10.8(a))

FORCES IN 'TREE' LOADING SYSTEM AT FAILURE OF ROOF

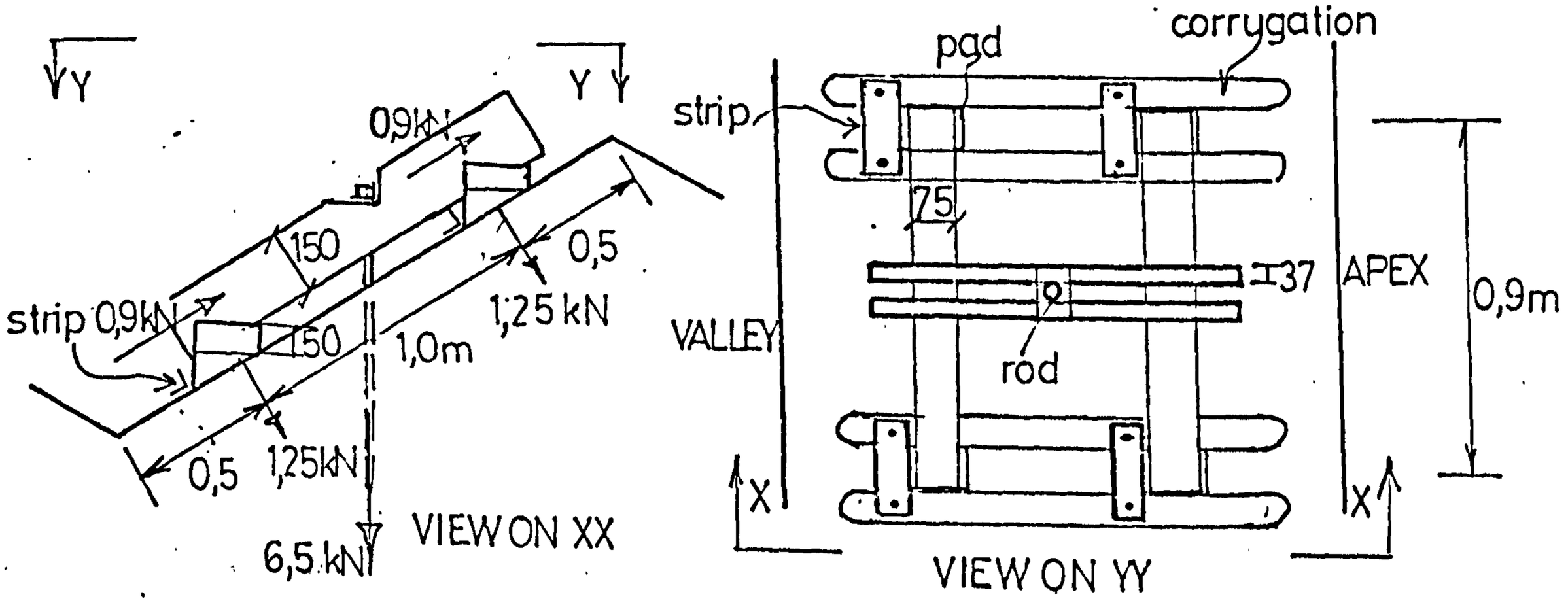

WOOD ROOF LOADING TRESTLE — AT 1,8 m SPACING

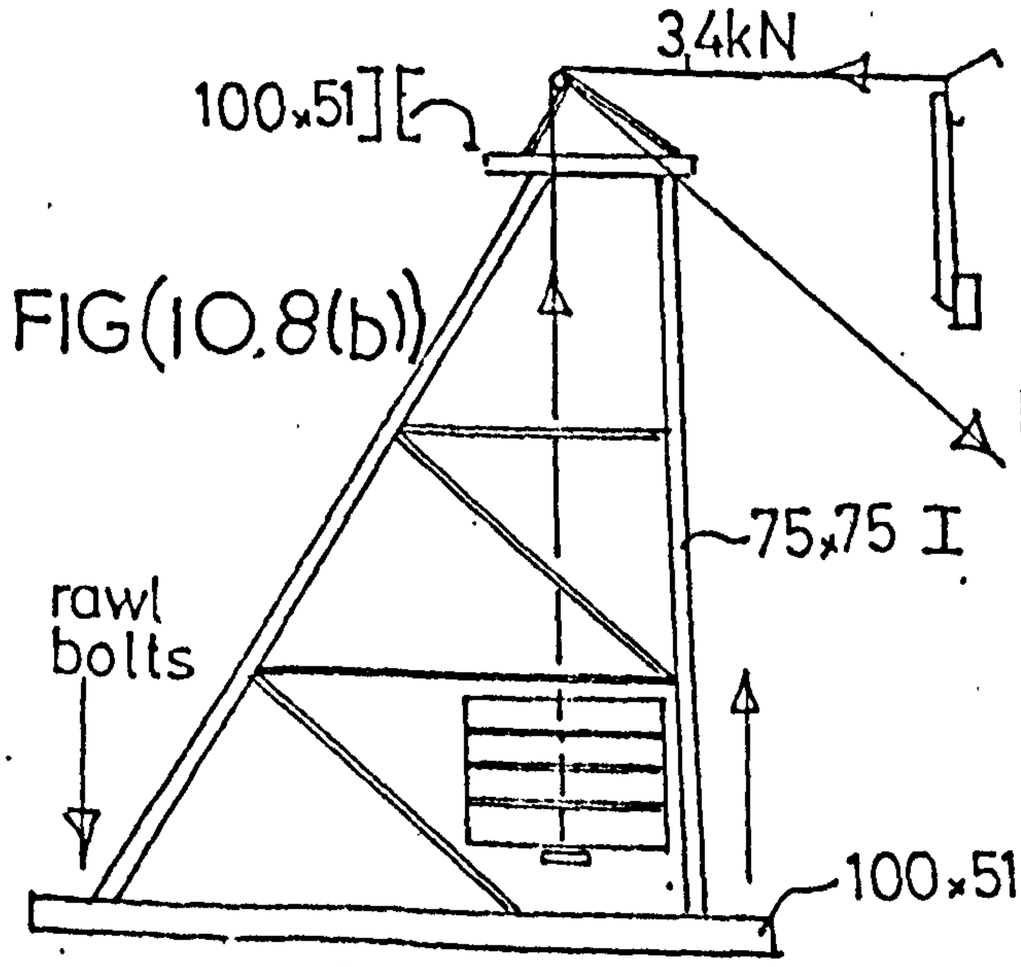

EAVES TENSILE FORCE

5 FRAMES
AT 4,3 m SPACING

NET THRUST AT W.L. = 4,8 kN.

HORIZONTAL WIND
FORCE SIMULATION

FIG (10.8(b))

ELASTIC TESTS ON FOLDED-PLATE ROOF

— UNIFORM LOADING OVER COMPLETE ROOF

CENTRAL APEX DEFLECTION

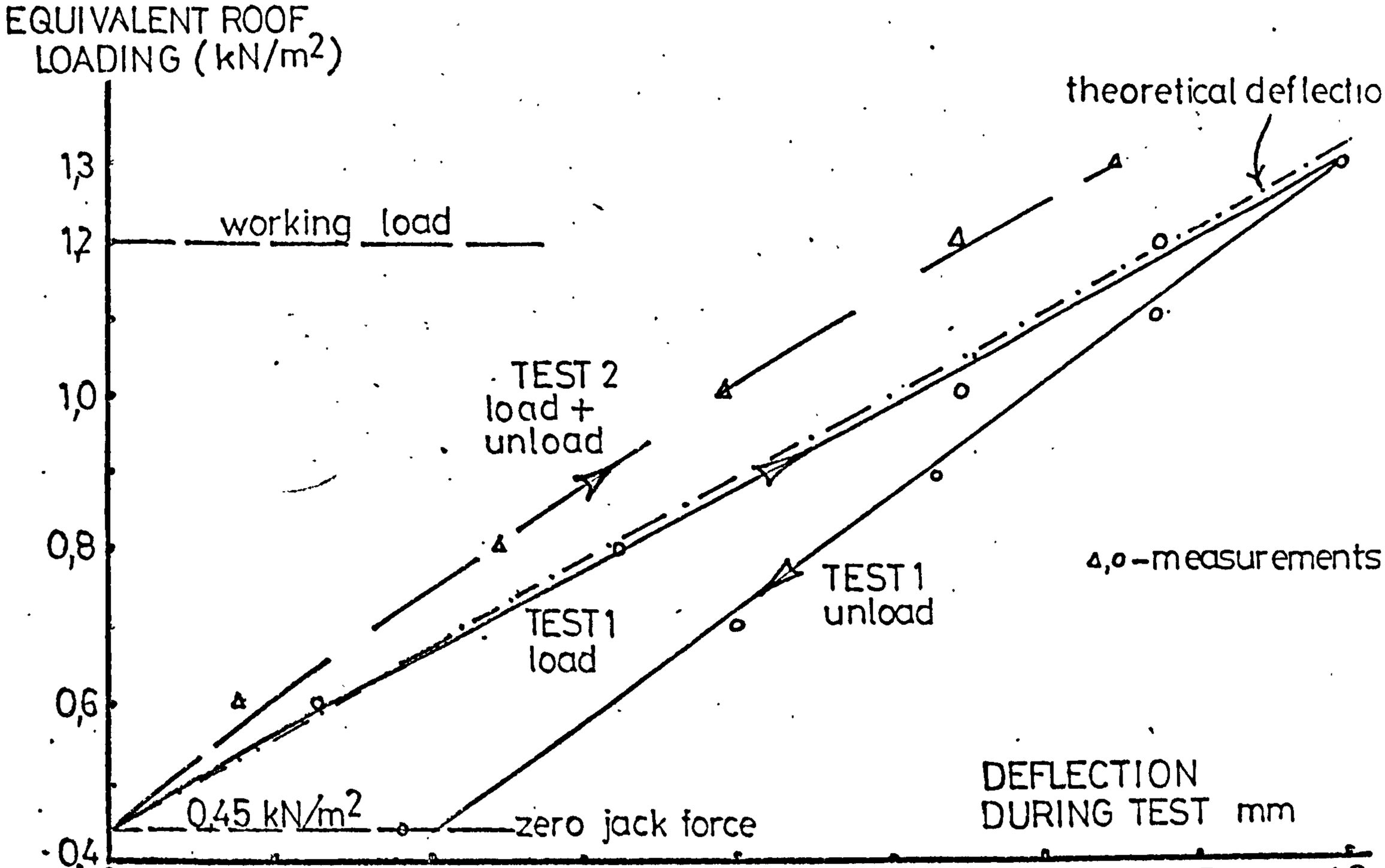

FIG (10.9)

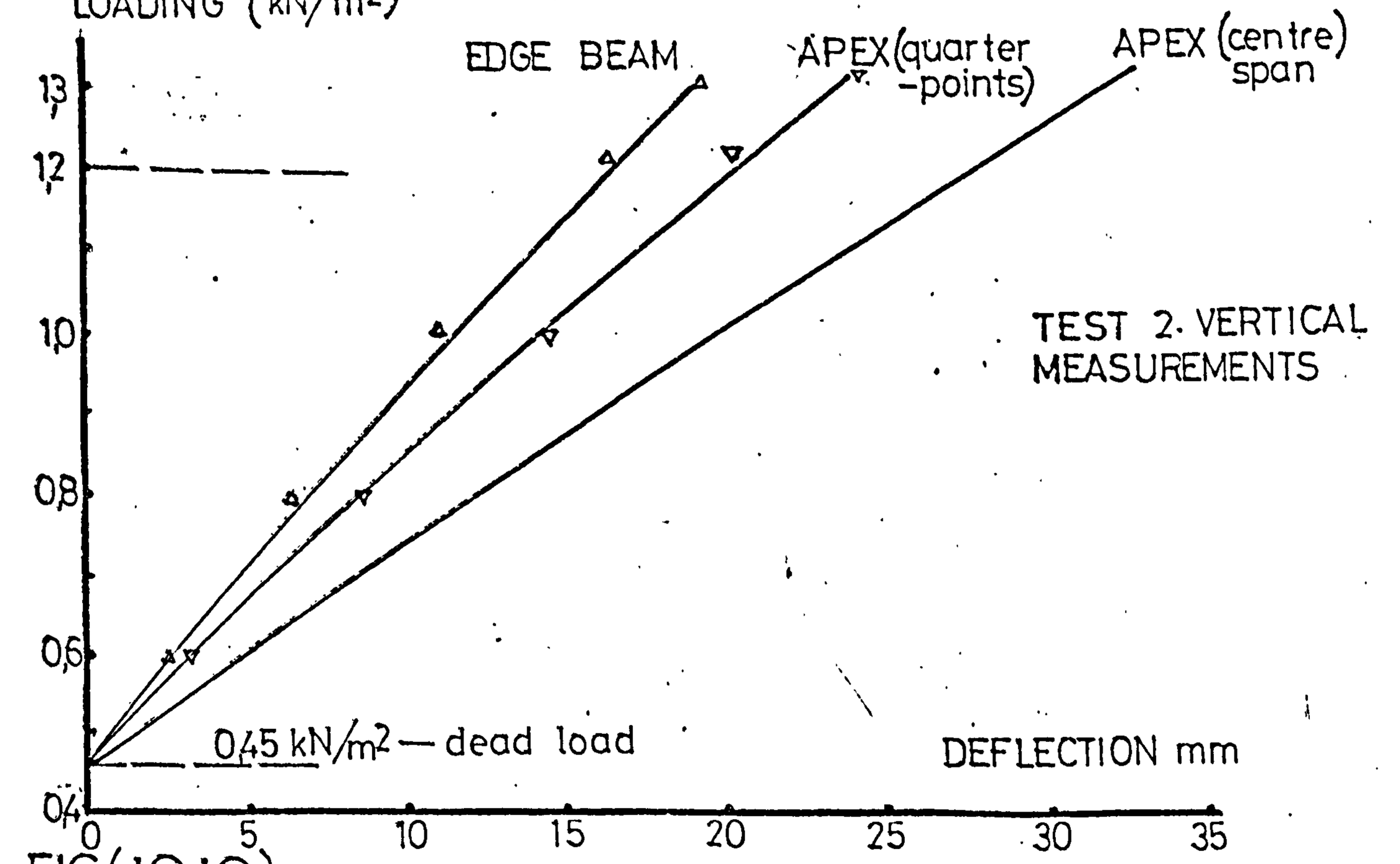

FIG (10.10)

ELASTIC TESTS ON FOLDED-PLATE ROOF

—CENTRE SECTION DEFLECTIONS AT WORKING LOAD (mm)

JACK LOADING – 1,2 minus 0,45 equals 0,75 kN/m²

—theoretical design values in brackets; initial slip values used

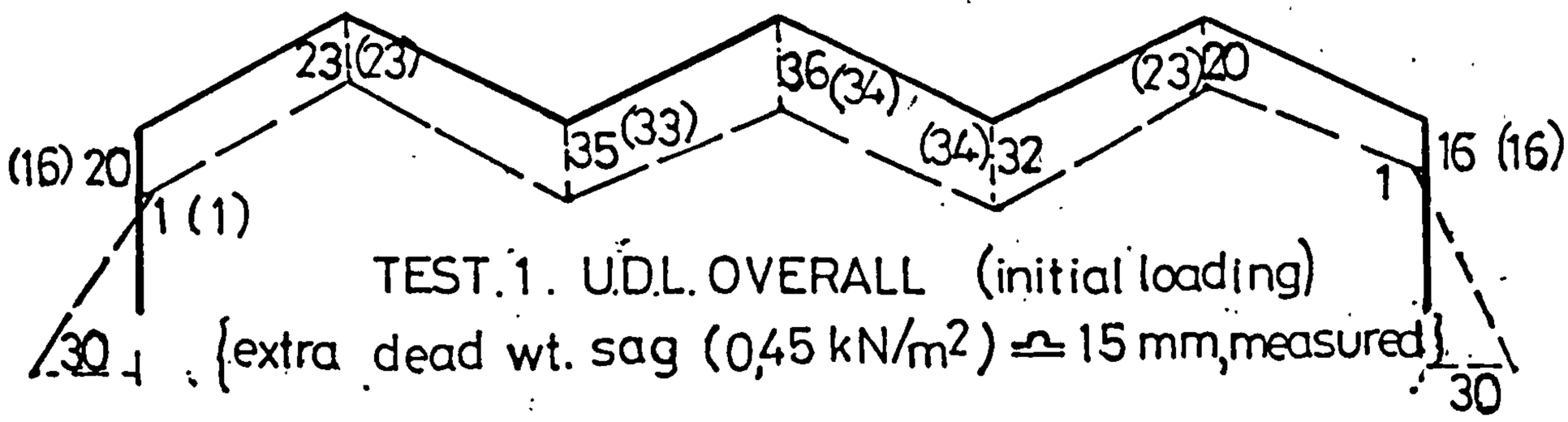

TEST. 1. U.D.L. OVERALL (initial loading)

{extra dead wt. sag (0,45 kN/m²) ≙ 15 mm, measured}

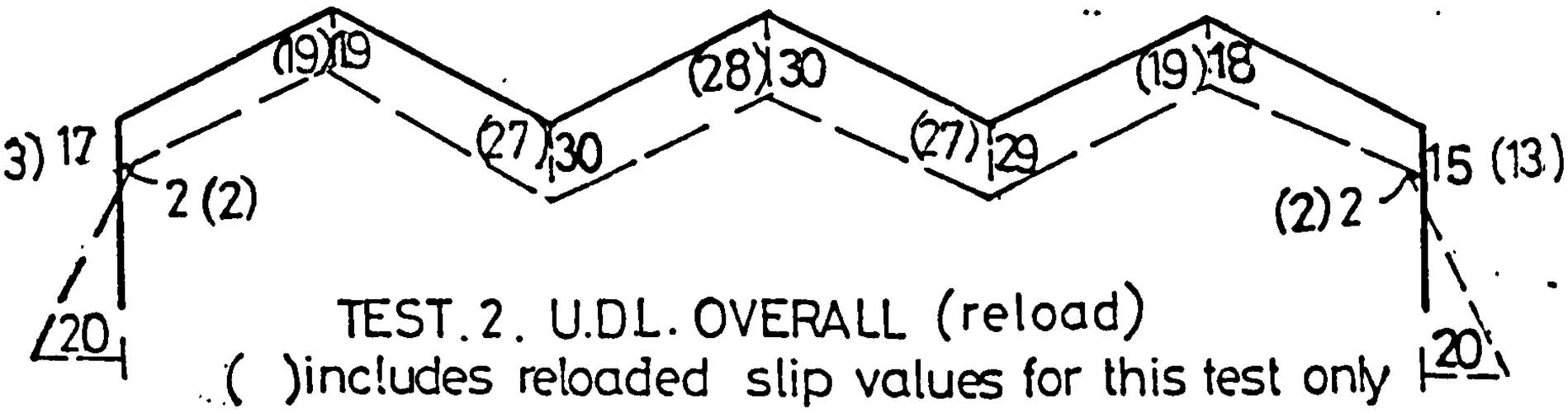

TEST. 2. U.D.L. OVERALL (reload)

( )includes reloaded slip values for this test only

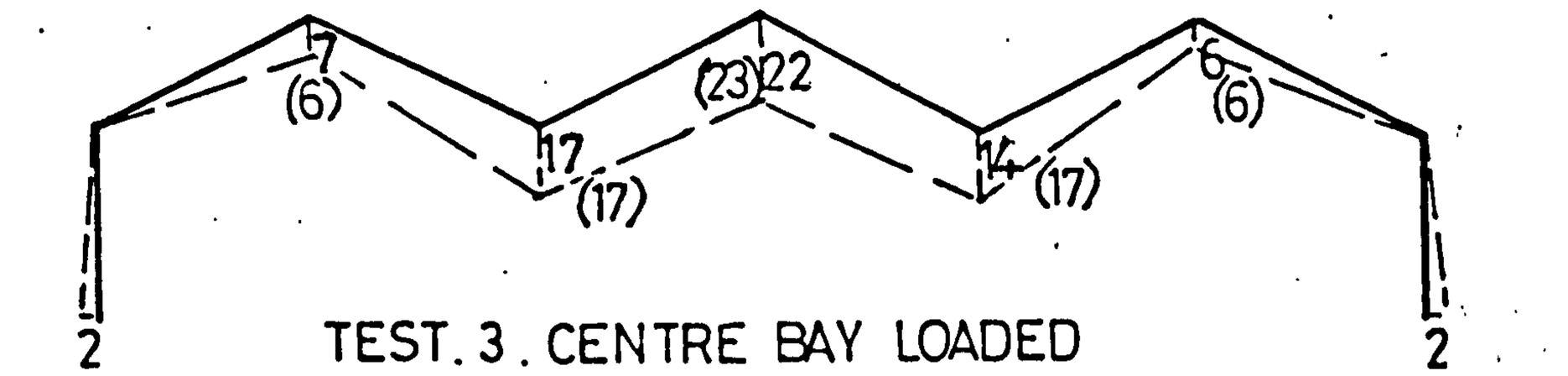

TEST. 3. CENTRE BAY LOADED

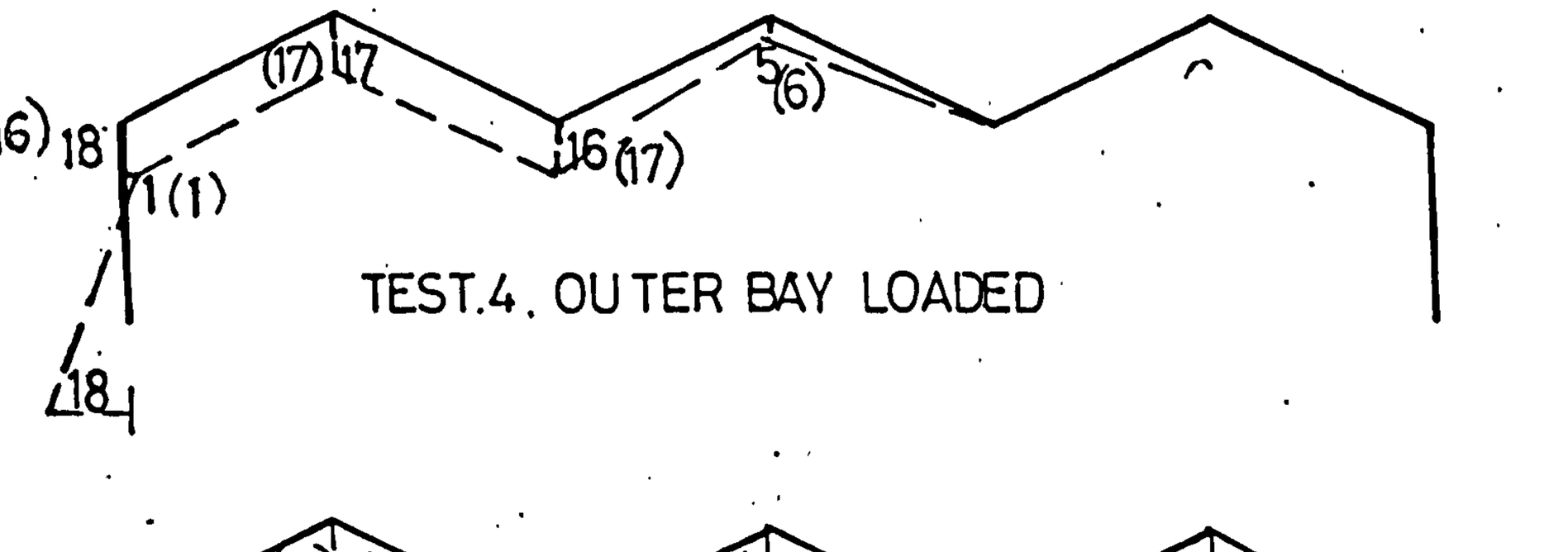

TEST. 4. OUTER BAY LOADED

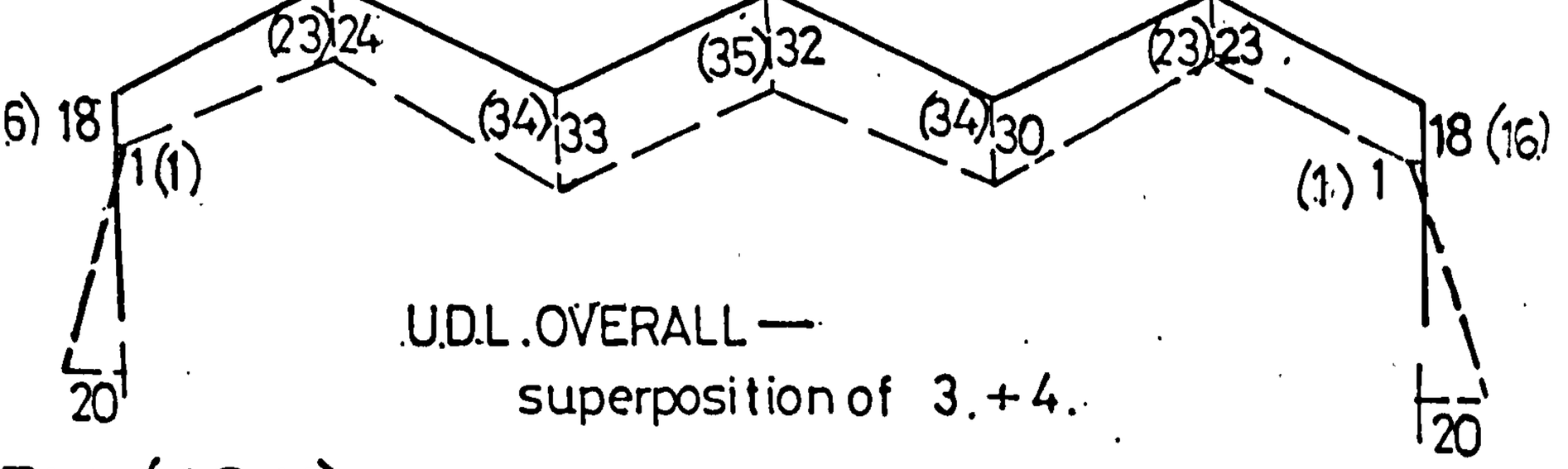

U.D.L. OVERALL —

superposition of 3. + 4.

FIG (10.11)

ELASTIC TESTS ON FOLDED PLATE ROOF

WIND LOADING — TENSILE FORCE APPLIED AT EAVES

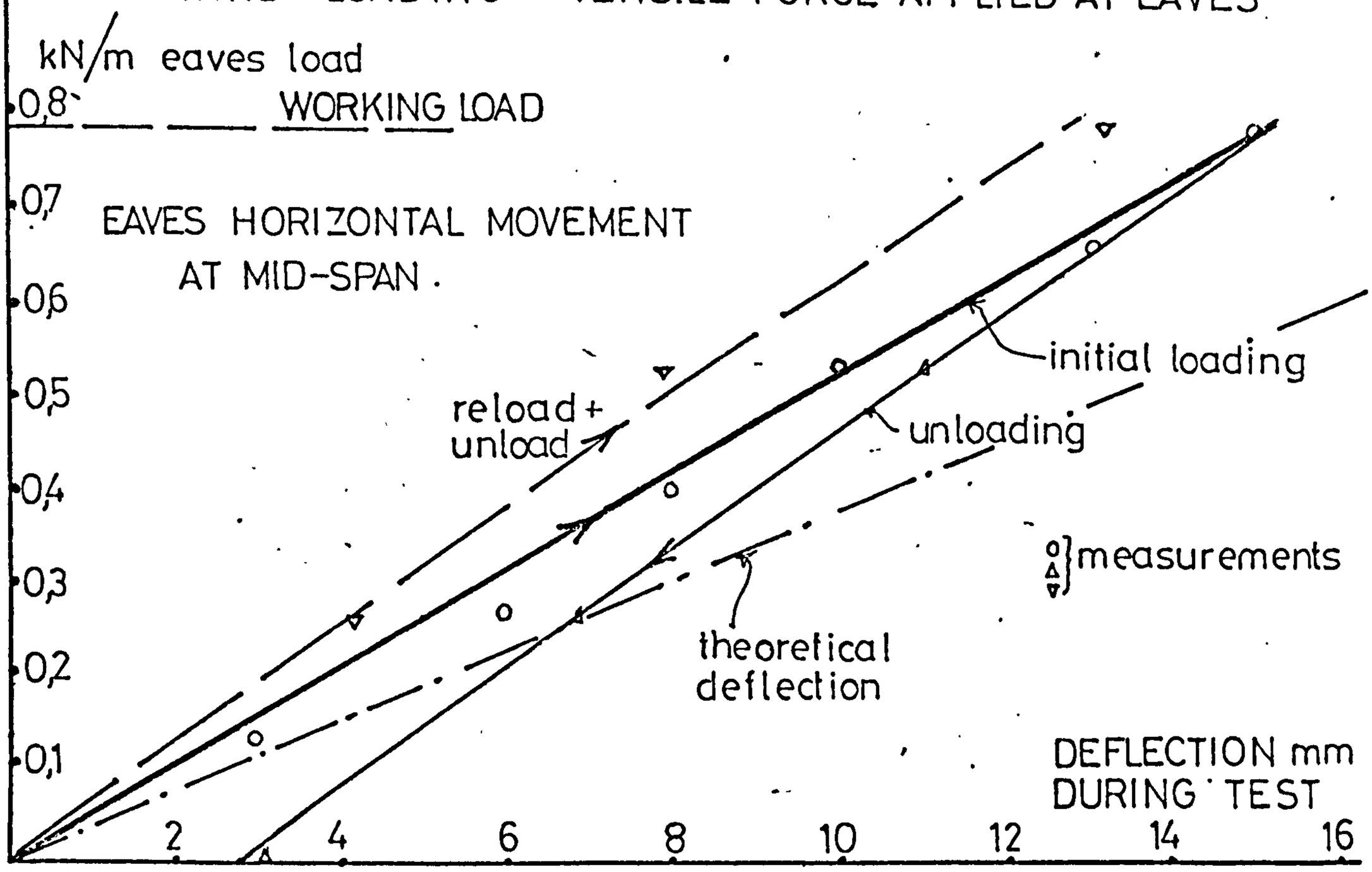

CENTRE SECTION DISPLACEMENTS AT WORKING LOAD —minus column sway

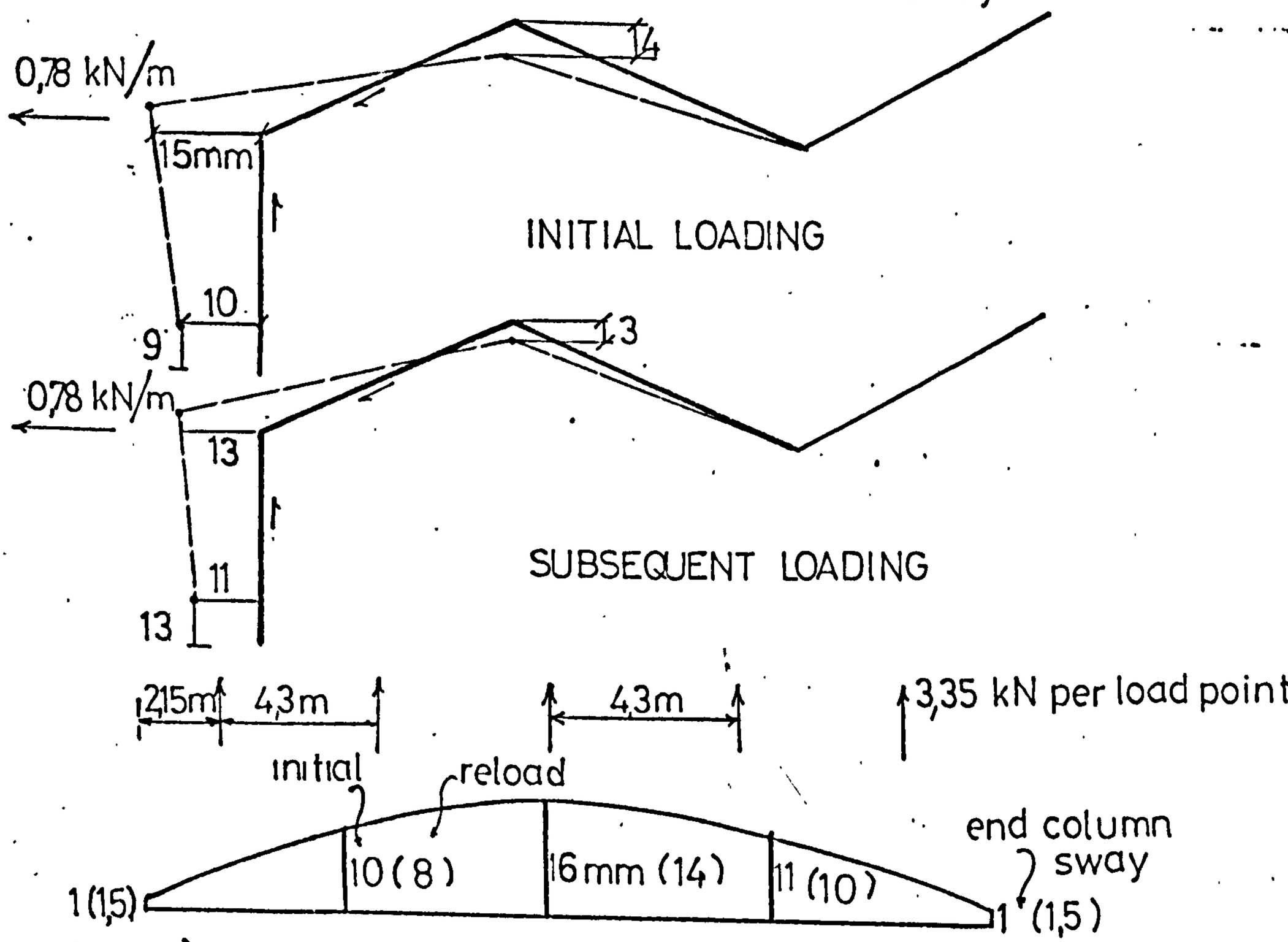

FIG(10.12) MOVEMENT ALONG EAVES

THEORETICAL CENTRE SECTION DEFLECTIONS

0,75 kN/m² UNIFORM VERTICAL LOADING { UP TO WORKING LOAD / FROM DEAD LOAD }

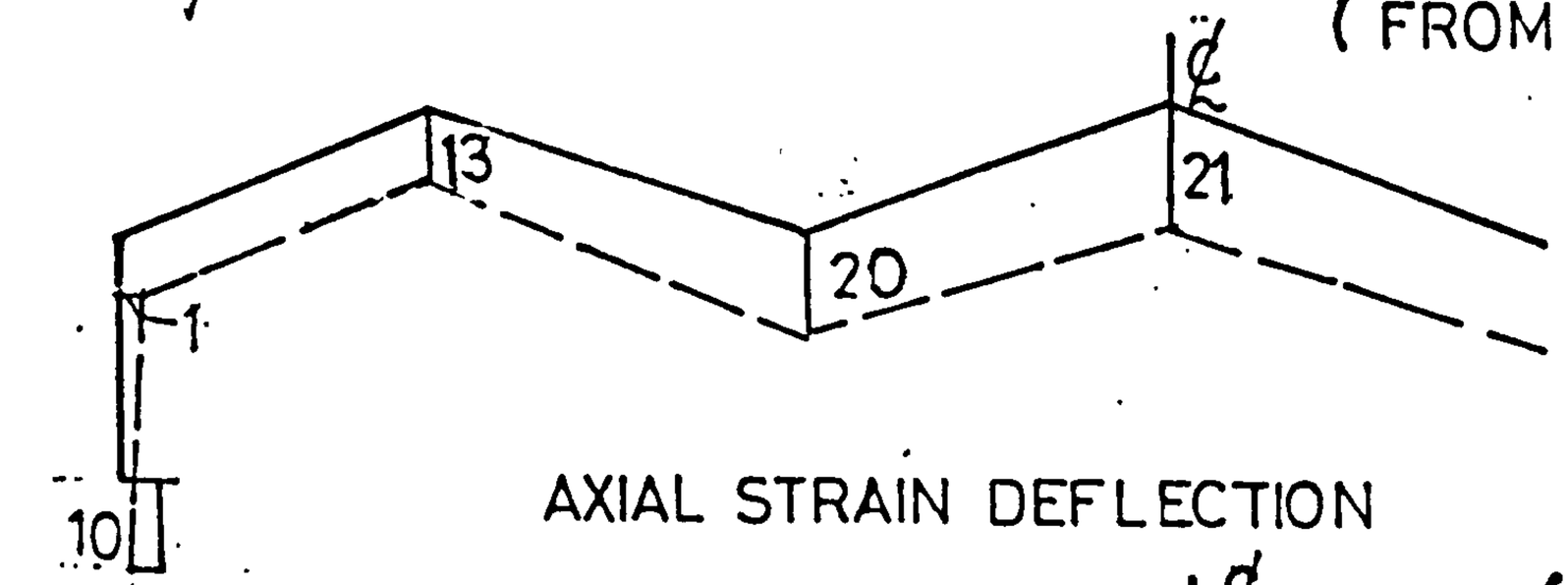

AXIAL STRAIN DEFLECTION

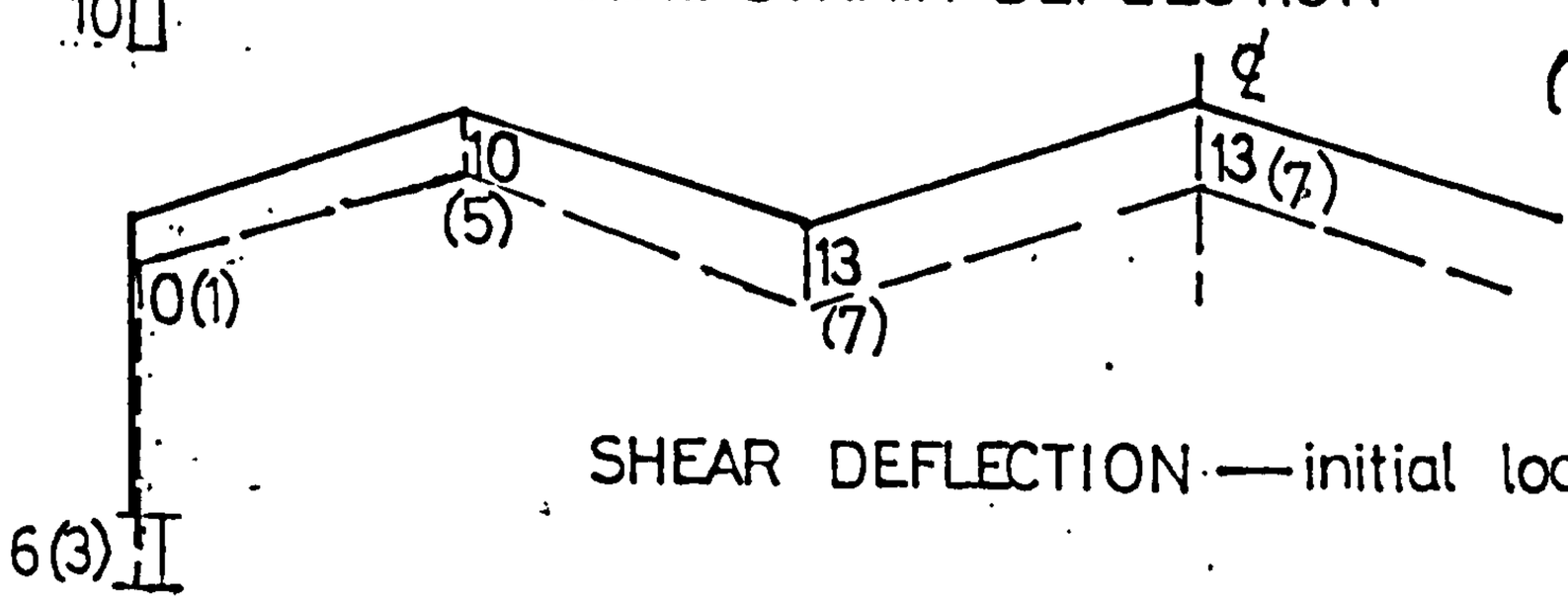

( ) figures include reload slip values

SHEAR DEFLECTION — initial loading

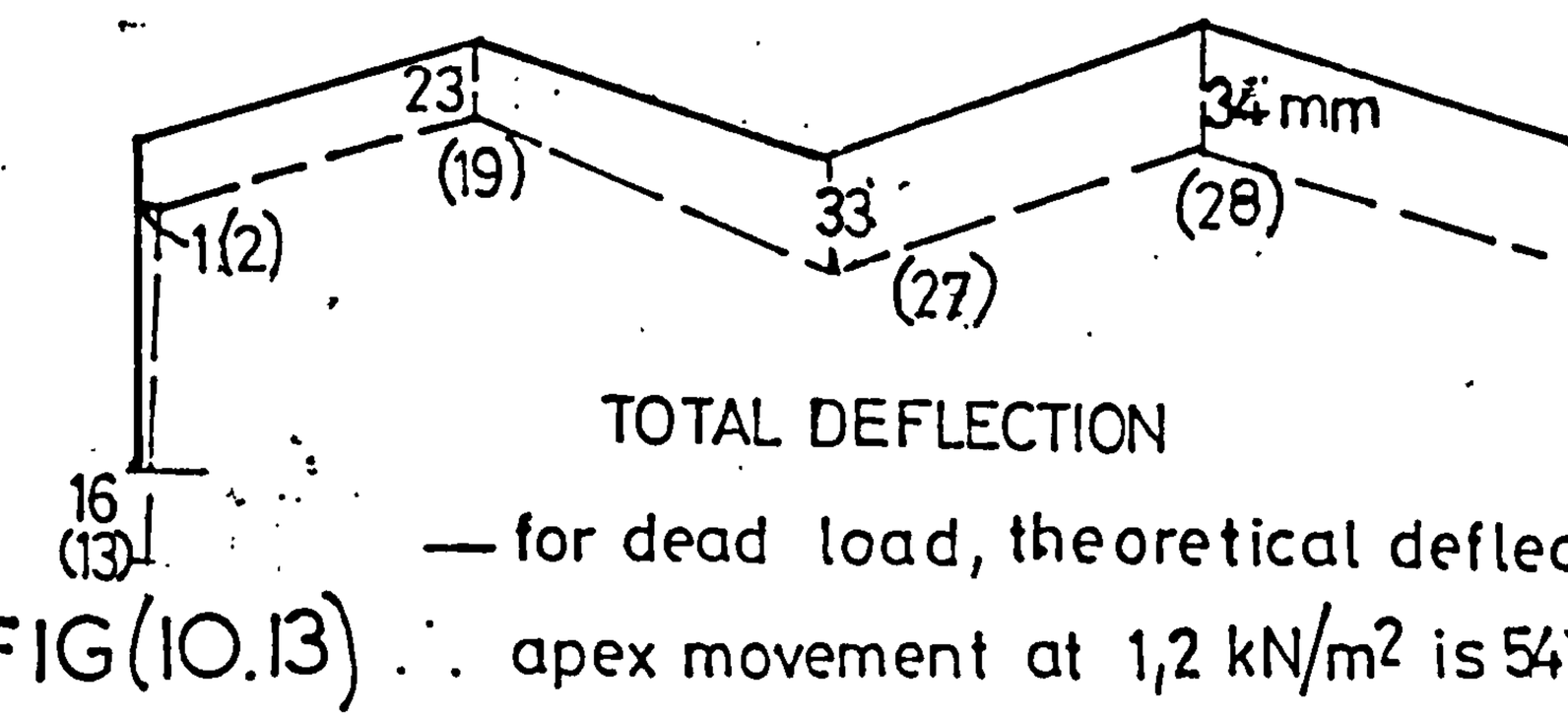

due to imposed load of 0,75 kN/m²

34 mm = L/635

TOTAL DEFLECTION

— for dead load, theoretical deflection = 20mm ,

FIG (10.13) ∴ apex movement at 1,2 kN/m² is 54 mm (L/400)

0,78 kN/m WIND WORKING LOAD AT EAVES

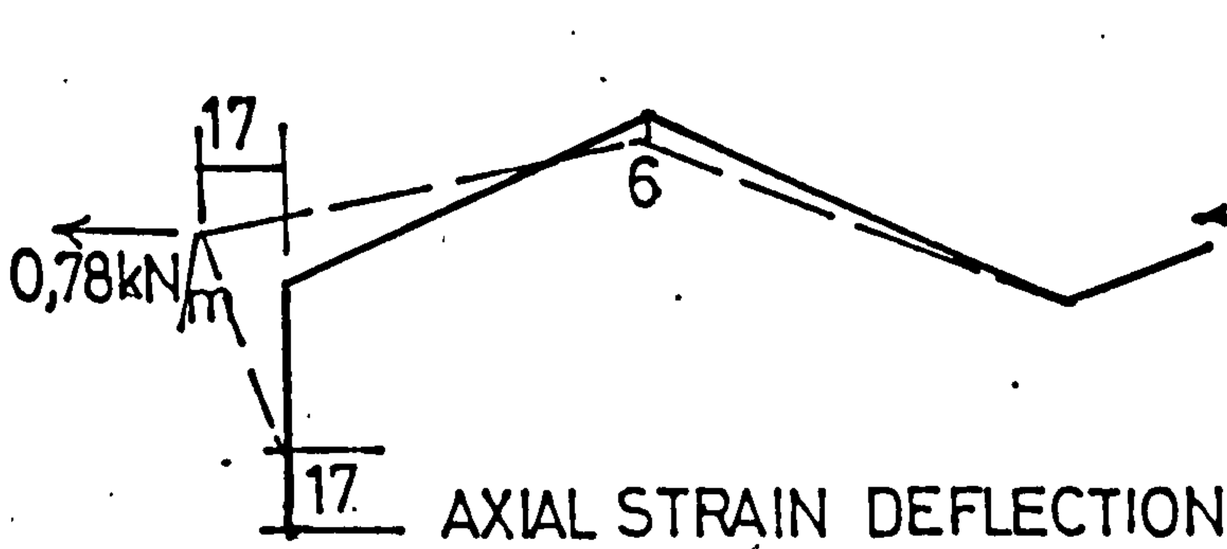

AXIAL STRAIN DEFLECTION

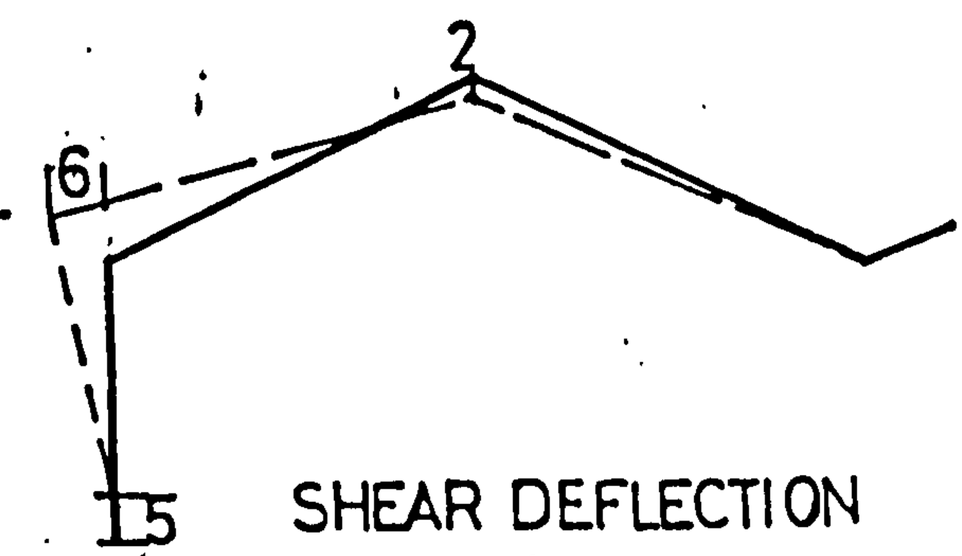

SHEAR DEFLECTION

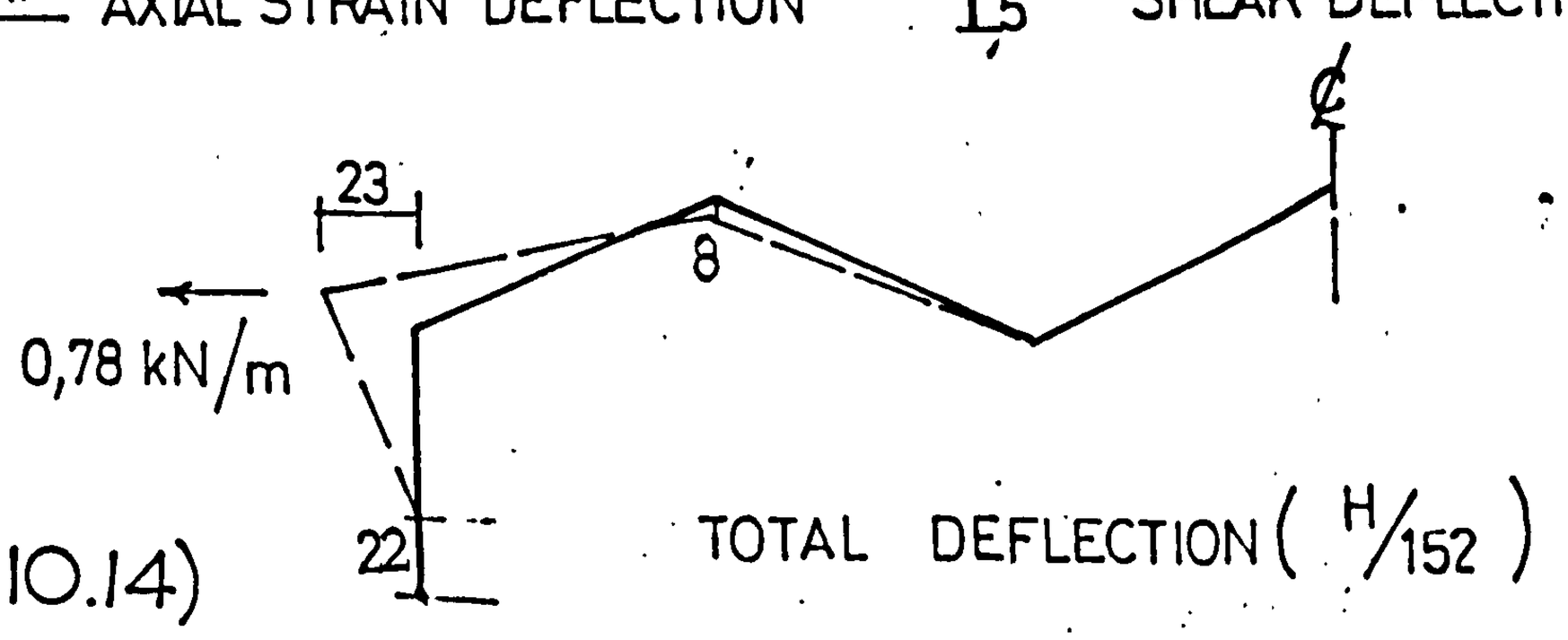

FIG (10.14)

TOTAL DEFLECTION (H/152)

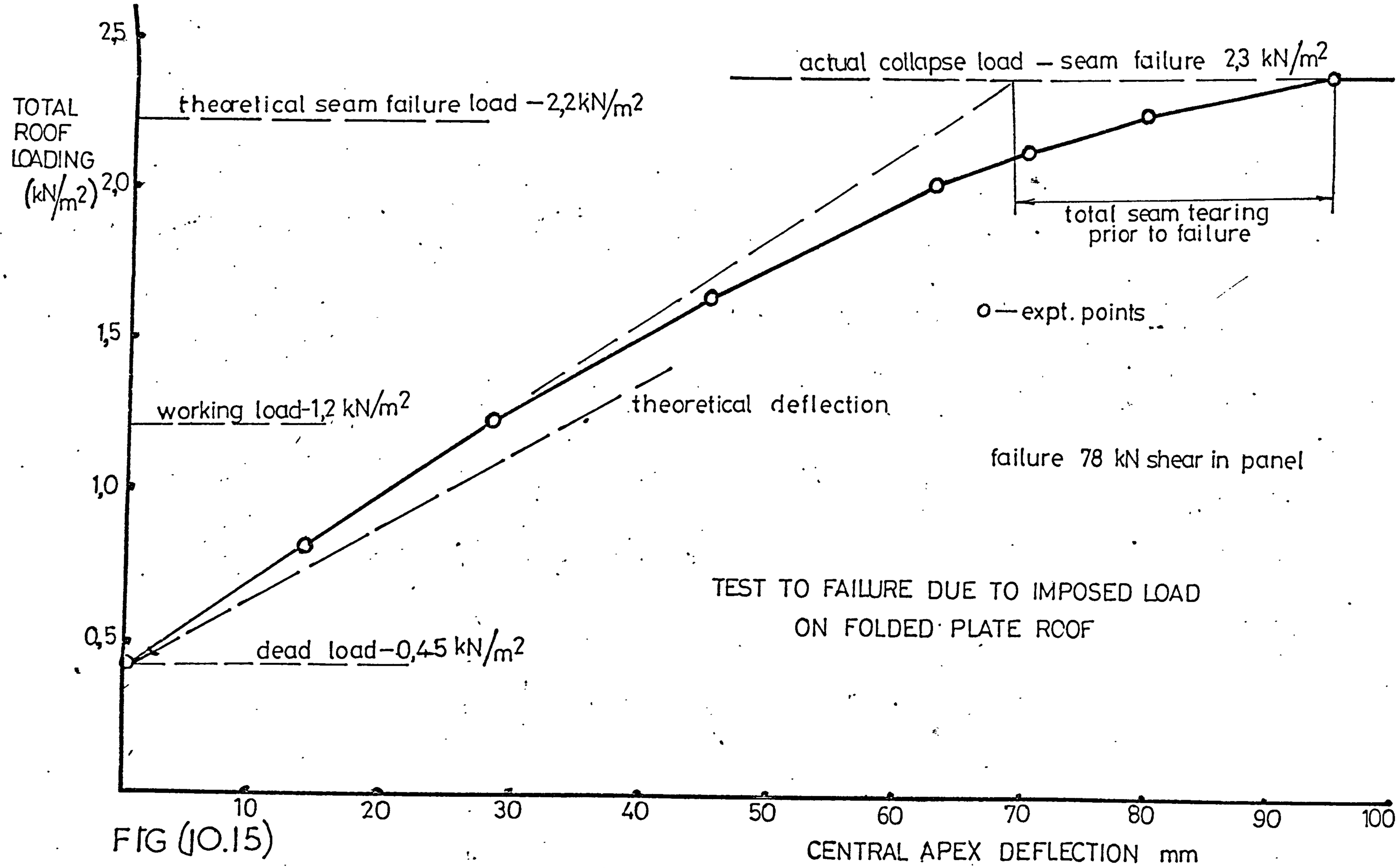

TEST TO FAILURE DUE TO IMPOSED LOAD ON FOLDED PLATE ROOF

FIG (10.15)

TEST TO FAILURE ON FOLDED PLATE ROOF

CENTRE SECTION DEFLECTIONS JUST PRIOR TO COLLAPSE (mm)

LOADING 2,3 minus 0,45 equals 1,85 kN/m²

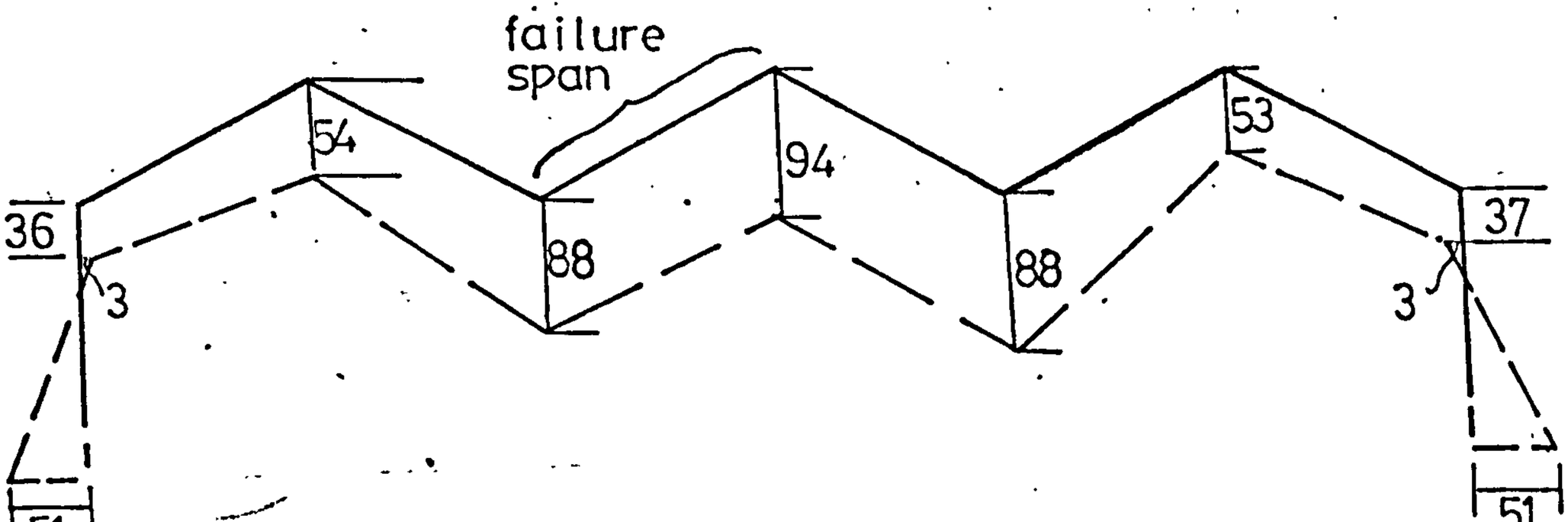

CENTRE APEX DEFLECTION ALONG LENGTH (mm)

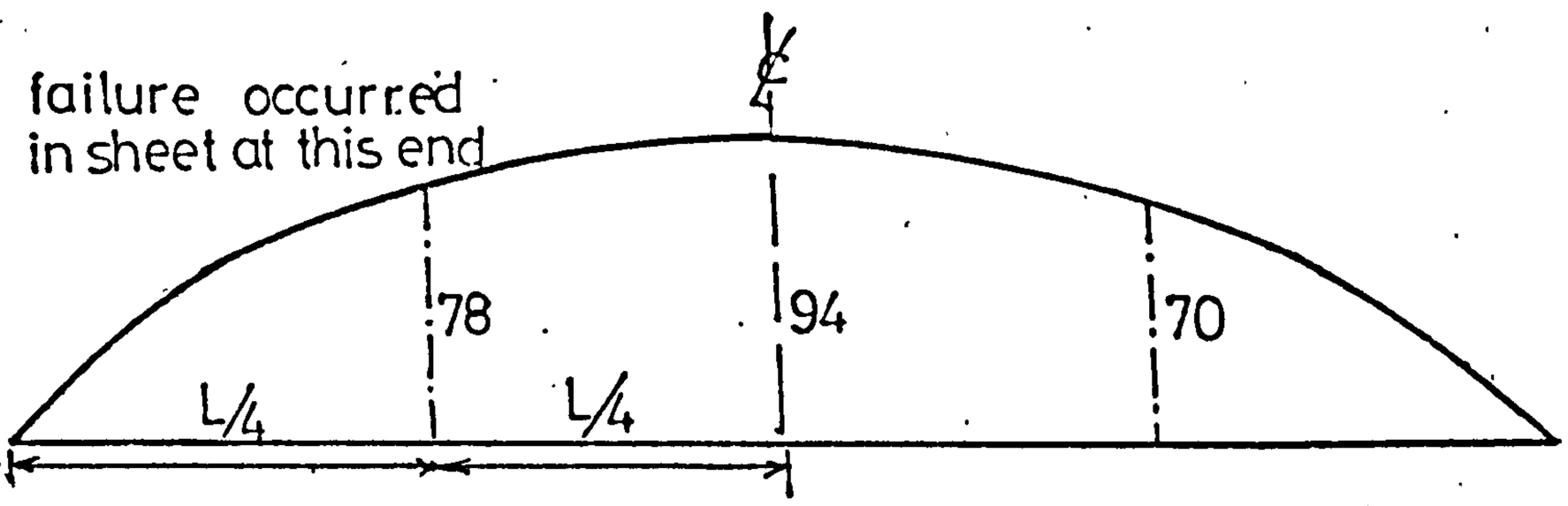

EXTRAPOLATION OF ELASTIC DEFLECTIONS (mm) OF TEST 2. (0,75) TO 1,85 kN/m². — CENTRE SPAN

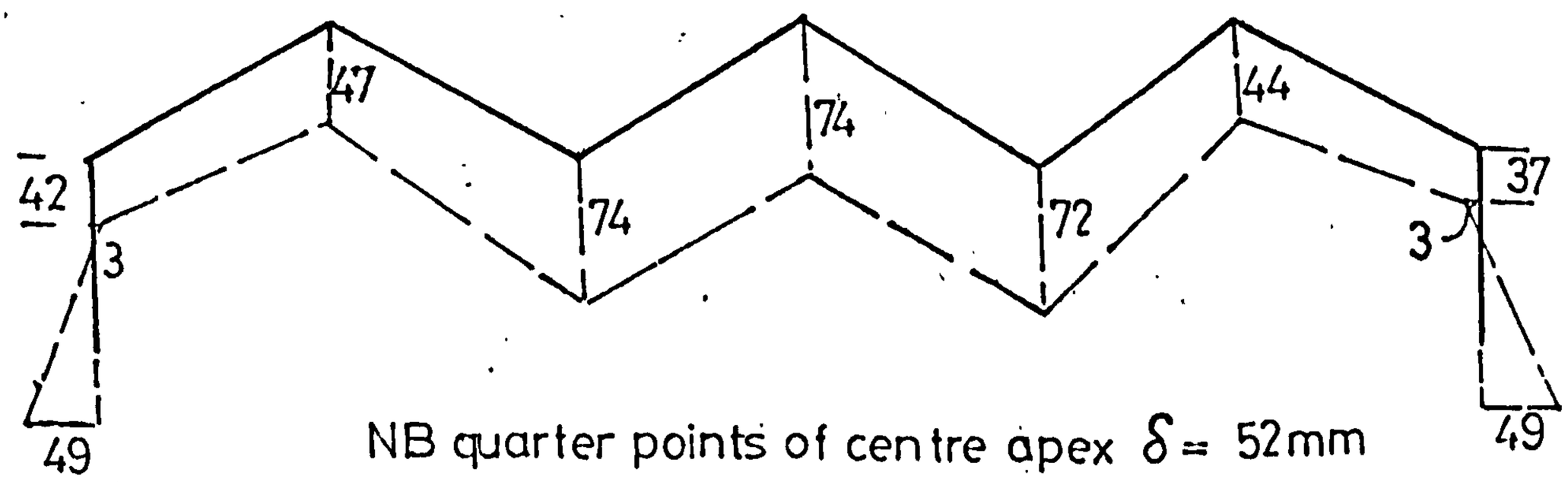

NB quarter points of centre apex δ = 52mm

FIG (10.16)

VIABILITY OF FOLDED PLATE ROOFS

$L < 38.\tan\theta.t$ —— shear strength 1.

$L < \dfrac{2{,}78.B.\tan\theta}{\left(0{,}19 + \dfrac{\bar{K}\cot\theta}{t^{2.5}}.0{,}25\right)}$ —deflection 2.

$L < \dfrac{0{,}18\bar{D}^{0{,}75}.t^{1{,}5}.(1 - 0025h).\sin 2\theta}{B^2}$ —— buckling 3.

$B \leq \sqrt[2]{\dfrac{\bar{D}t}{h-\bar{x}} \times 0{,}025}$ —— sheet bending 4.

LOADING $= 1{,}2\ kN/m^2$

STANDARD PROFILE

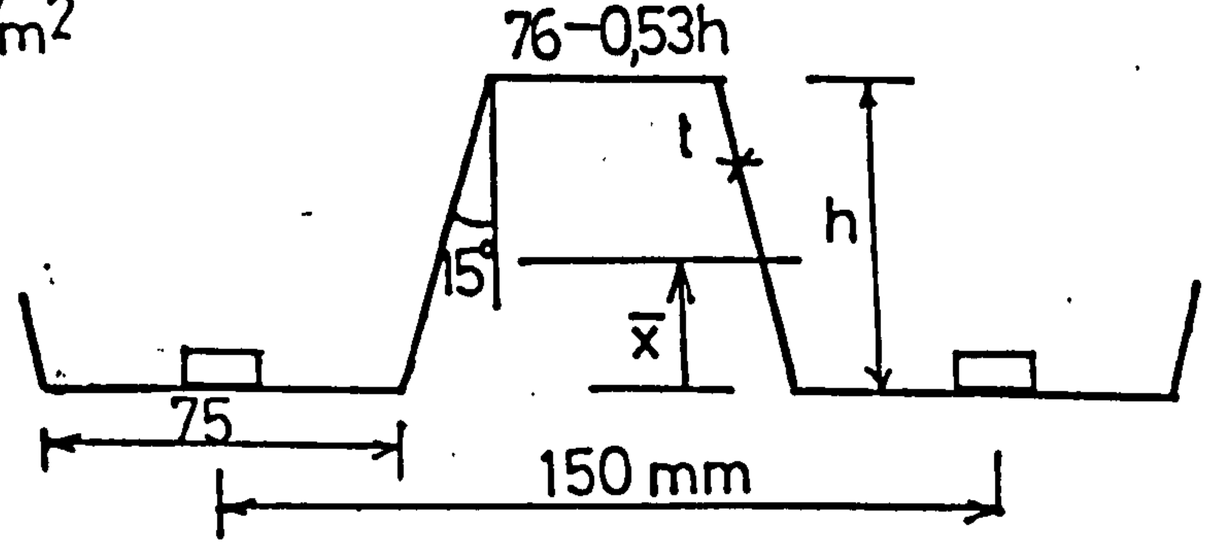

h mm	$\bar{K}$	$\bar{x}$ mm	$\bar{D}$ mm^4
20	•067	9,5	$1{,}43 \times 10^4$
30	•133	13,9	$3{,}51 \times 10^4$
40	•194	18,0	$6{,}26 \times 10^4$
50	•246	22,4	$9{,}82 \times 10^4$

DATA :

MIN. FOLD AREA(mm^2) $= 2L^2\cot\theta$

[NOTE: L,B — metres
h,t — mm]

ENVELOPE OF FAILURE CURVES —given θ,h,t

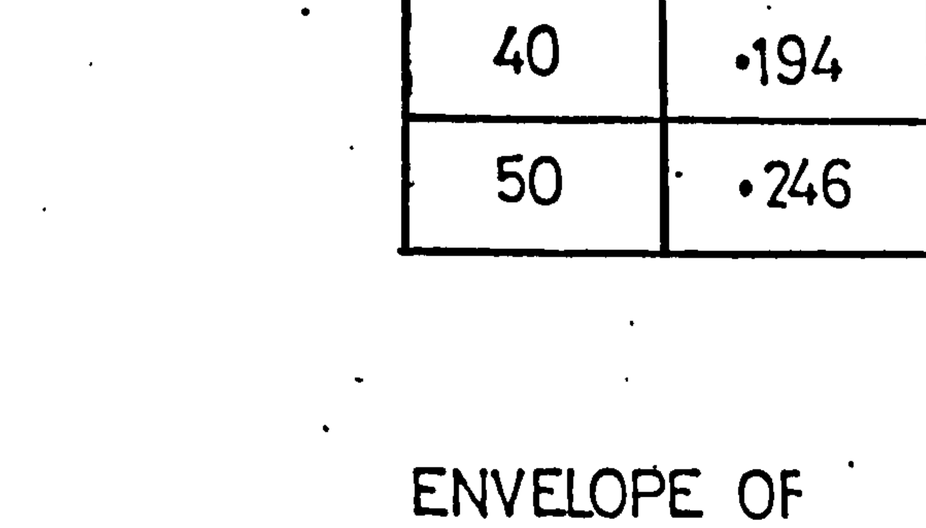

FIG(10.17)

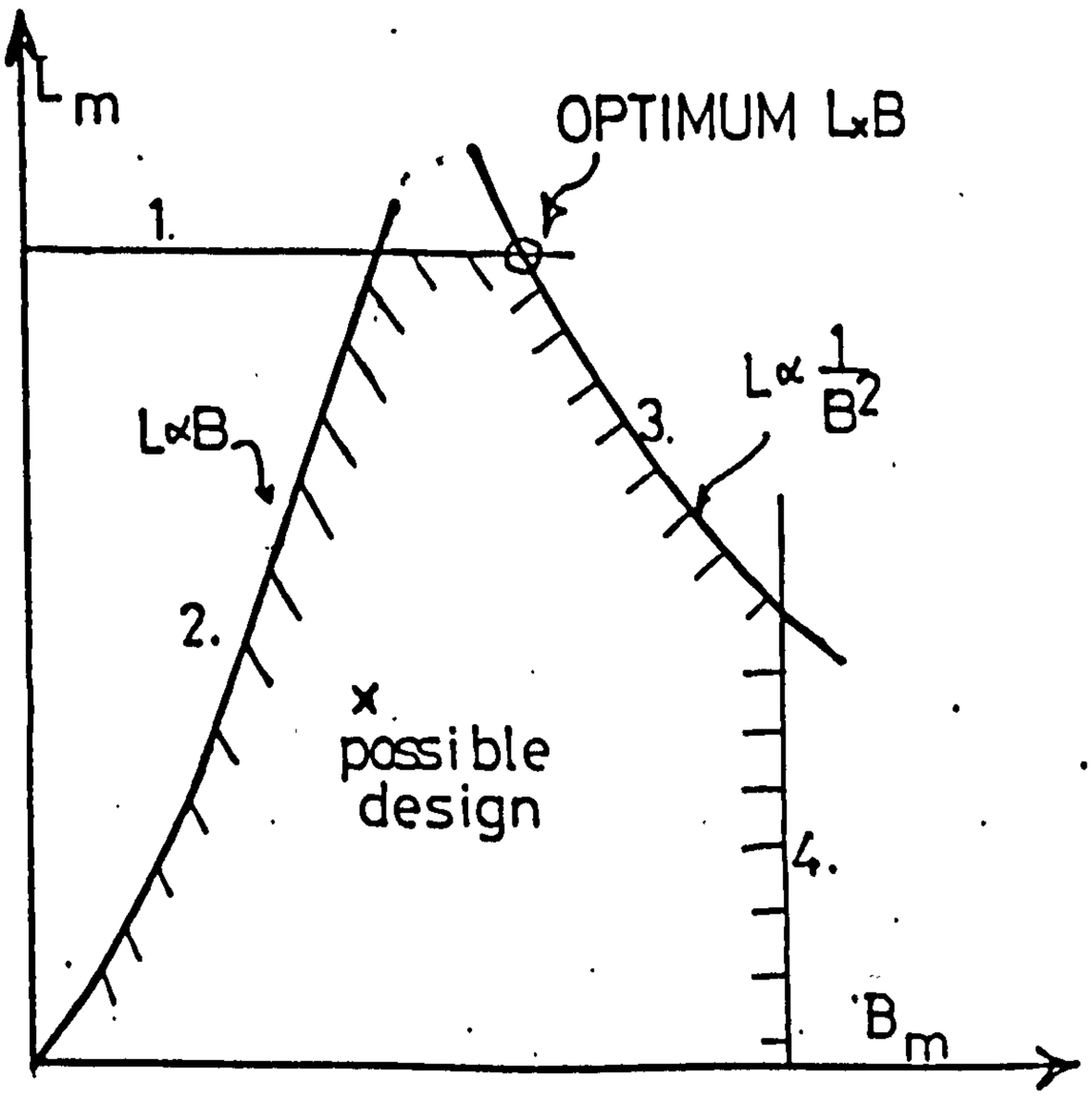

FOLDED PLATE ROOF DESIGN

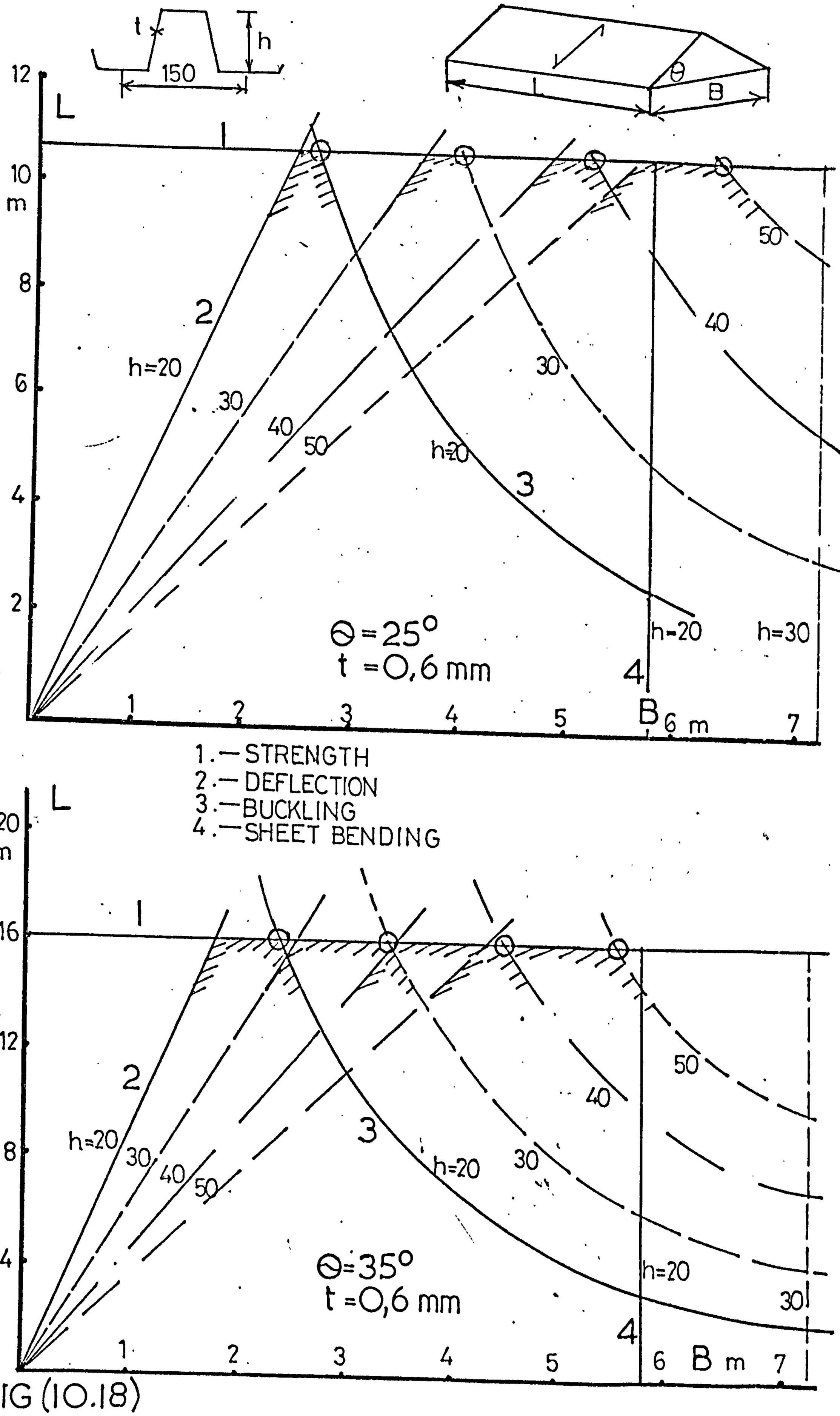

FIG (10.18)

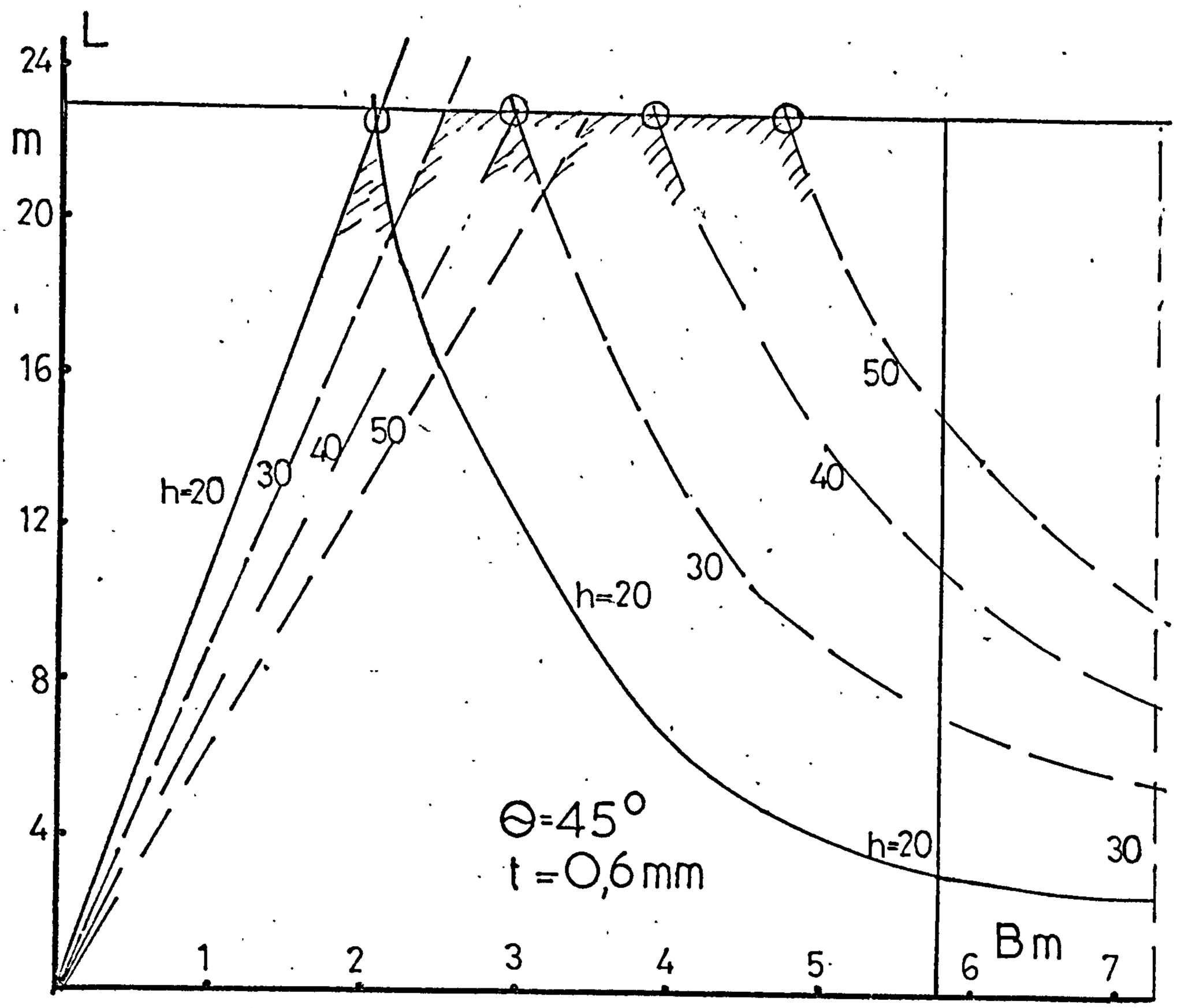
L
m
24
20
16
12
8
4
h=20
30
40
50
Θ=45°
t =0,6 mm
1
2
3
4
5
6
7
Bm
L
m
24
20
16
12
8
4
h=20
30
40
50
Θ=35°
t -0,9 mm
1
2
3
4
5
6
7
8
9
Bm

FIG (10.19)

MAXIMUM POSSIBLE SPANS FOR FOLDED PLATE ROOFS

—INFLUENCE OF SLOPE, THICKNESS

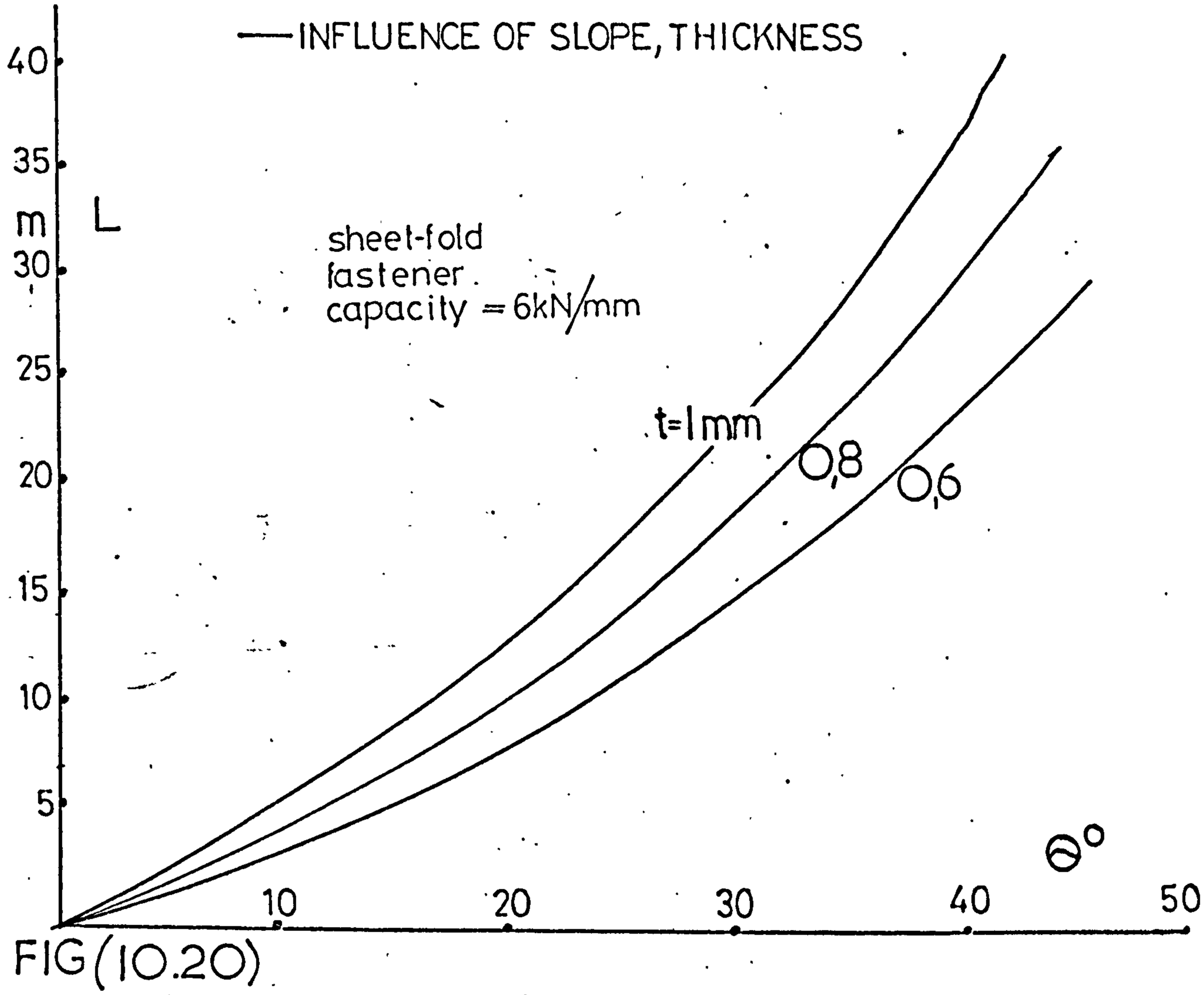

FIG (10.20)

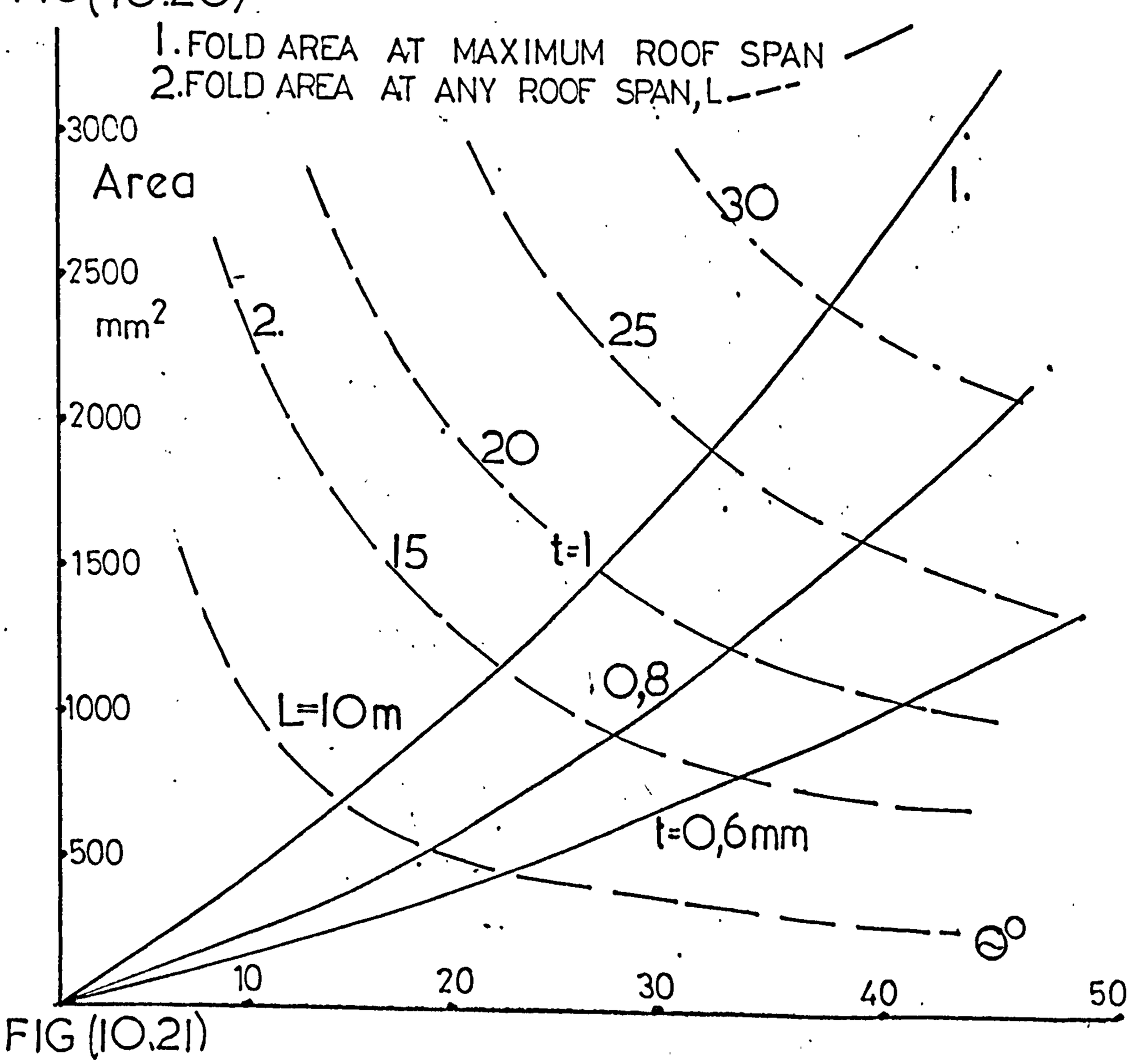

FIG (10.21)

TYPICAL SECTION THROUGH FOLDED PLATE ROOF BAY

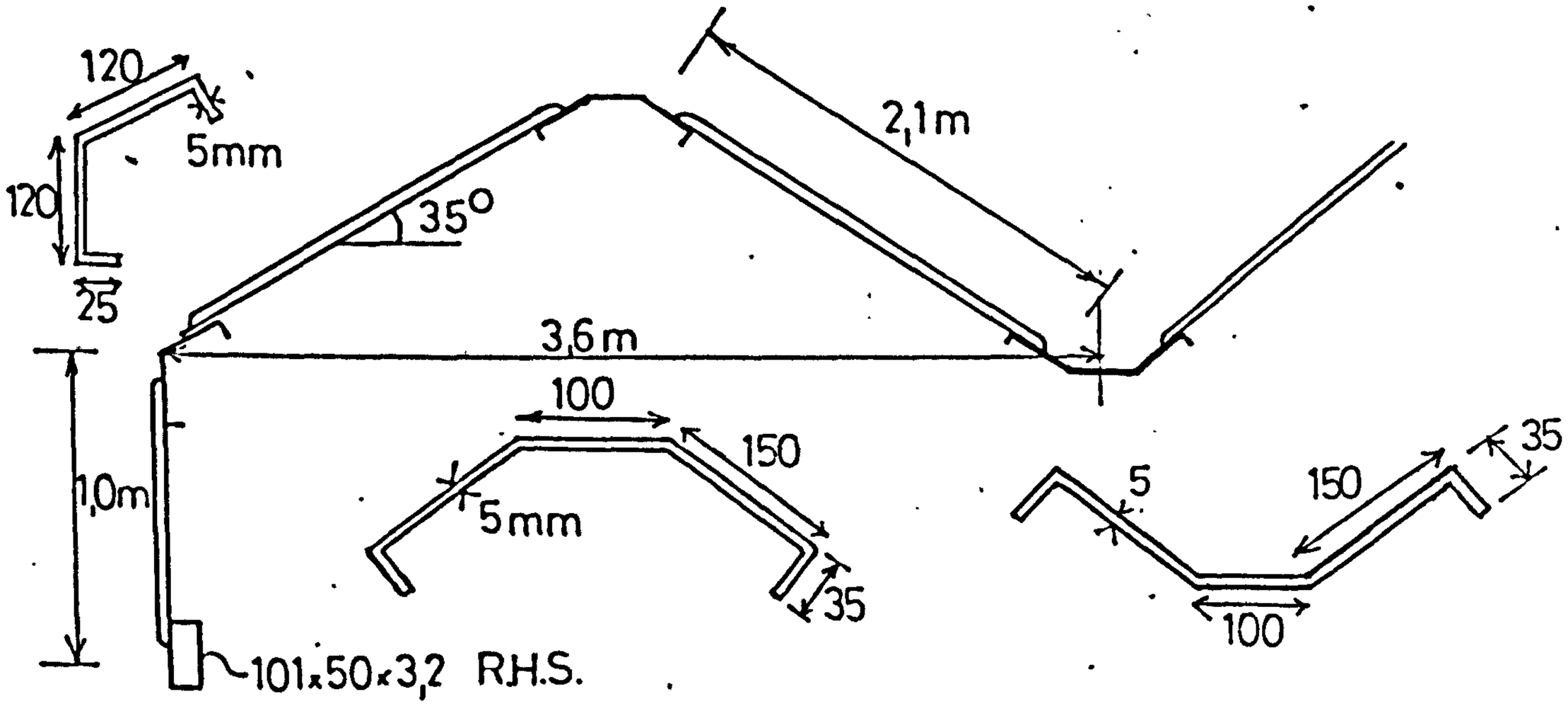

FIG (10.22)

WEIGHT OF STEEL COMPARISON FOR 20x10 m FOLDED PLATE ROOF AND PORTAL FRAME

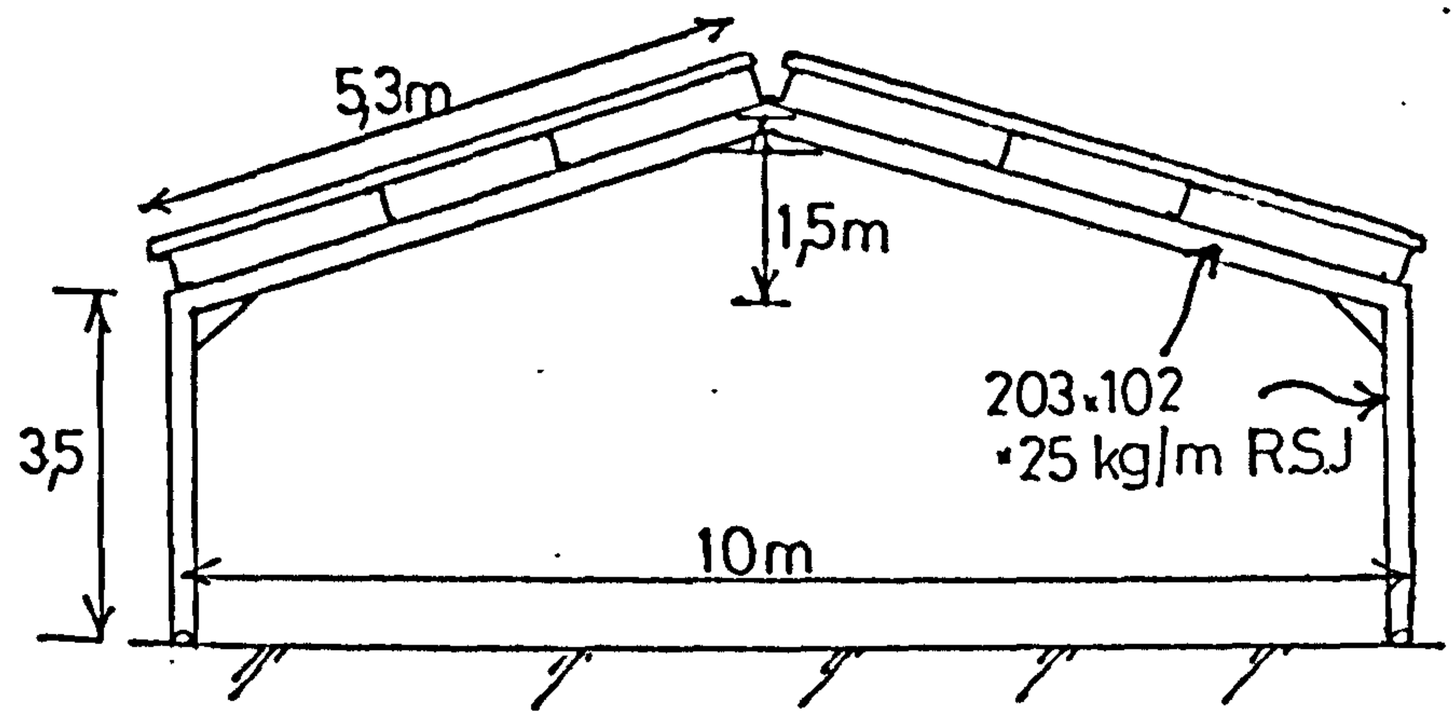

5 FRAMES
AT 5m SPACING

PURLINS

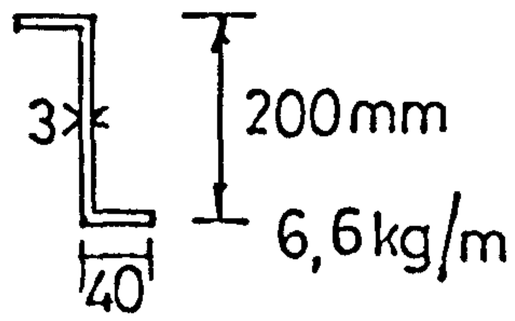

DATA: TOTAL FRAME WEIGHT = 5x17,6x25 = 2200 kg
TOTAL PURLIN AREA = 8x20x6,6 = 1056 kg
3256 kg

FOLDED PLATE θ = 35° ; COLUMNS @ 3,3 m SPACING

FOLD AREA REQUIRED = 1200 mm²

TOTAL FOLD LINE WEIGHT = 6x20x9,3 kg/m = 1116 kg

8 COLUMNS 100x100x6,3 (19,8 kg/m) = 554 kg
6 END FRAMES 100x50x3,2 RHS. = 375
929 kg

0,1 mm EXTRA SHEET THICKNESS (0,8 mm) = 158 kg
TOTAL = 2203 kg

∴ COST IN STEEL — 67 %

FIG (10.23)

Length of fold line
21.498 m

FOLDED PLATE ROOF DETAILS

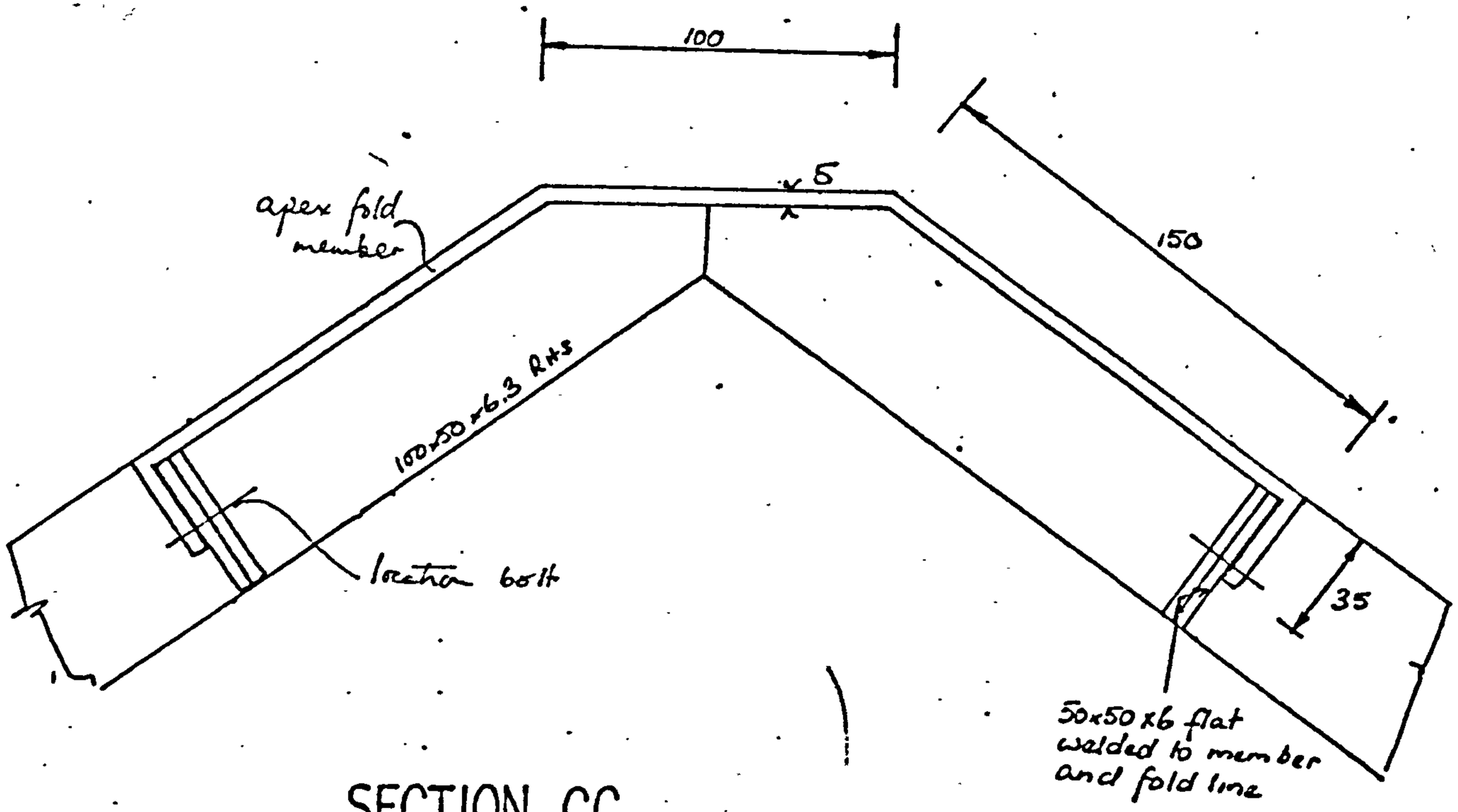

SECTION CC

FIG (10.24)

Scale 1cm : 2cm.

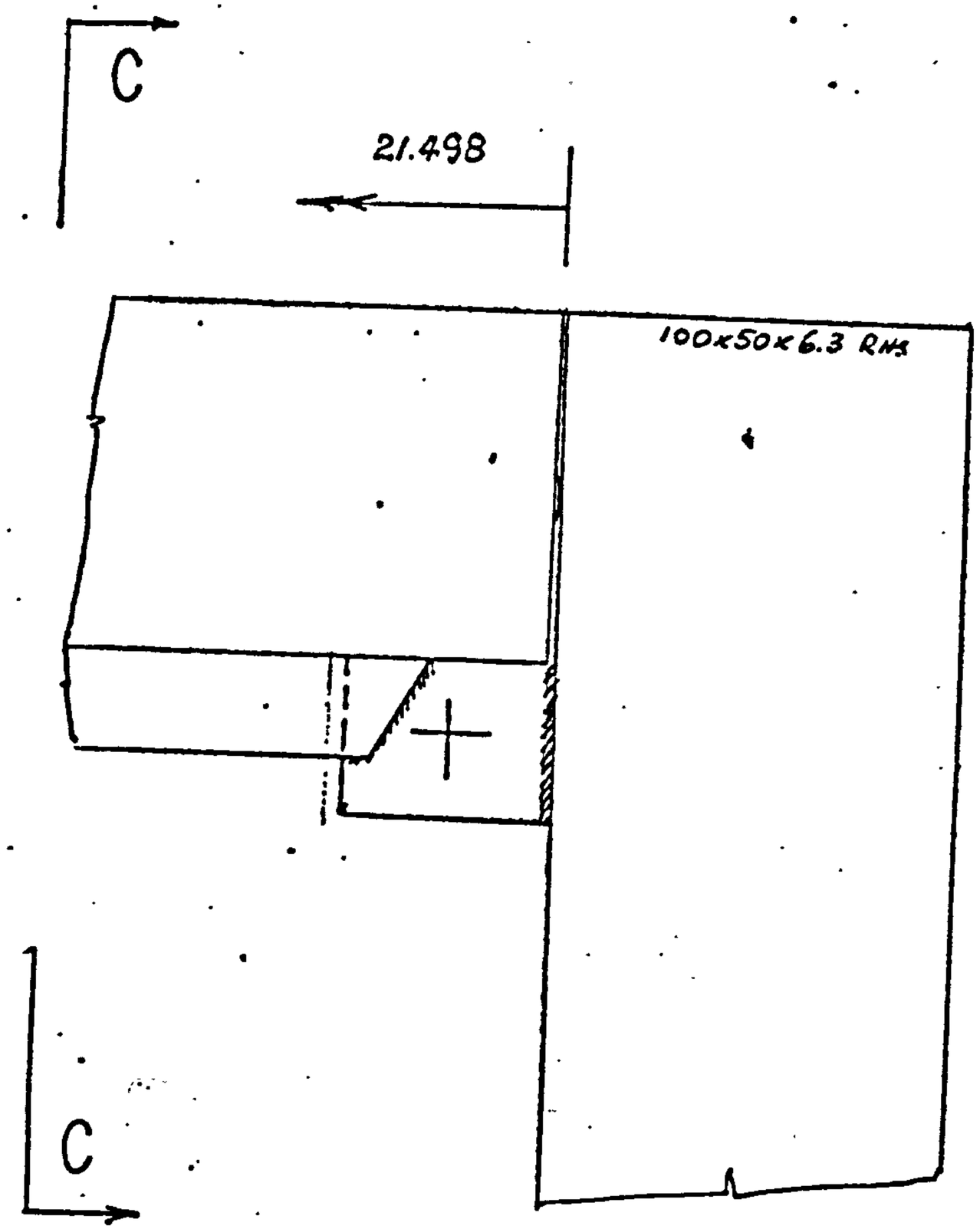

All dimensions in

APEX DETAIL

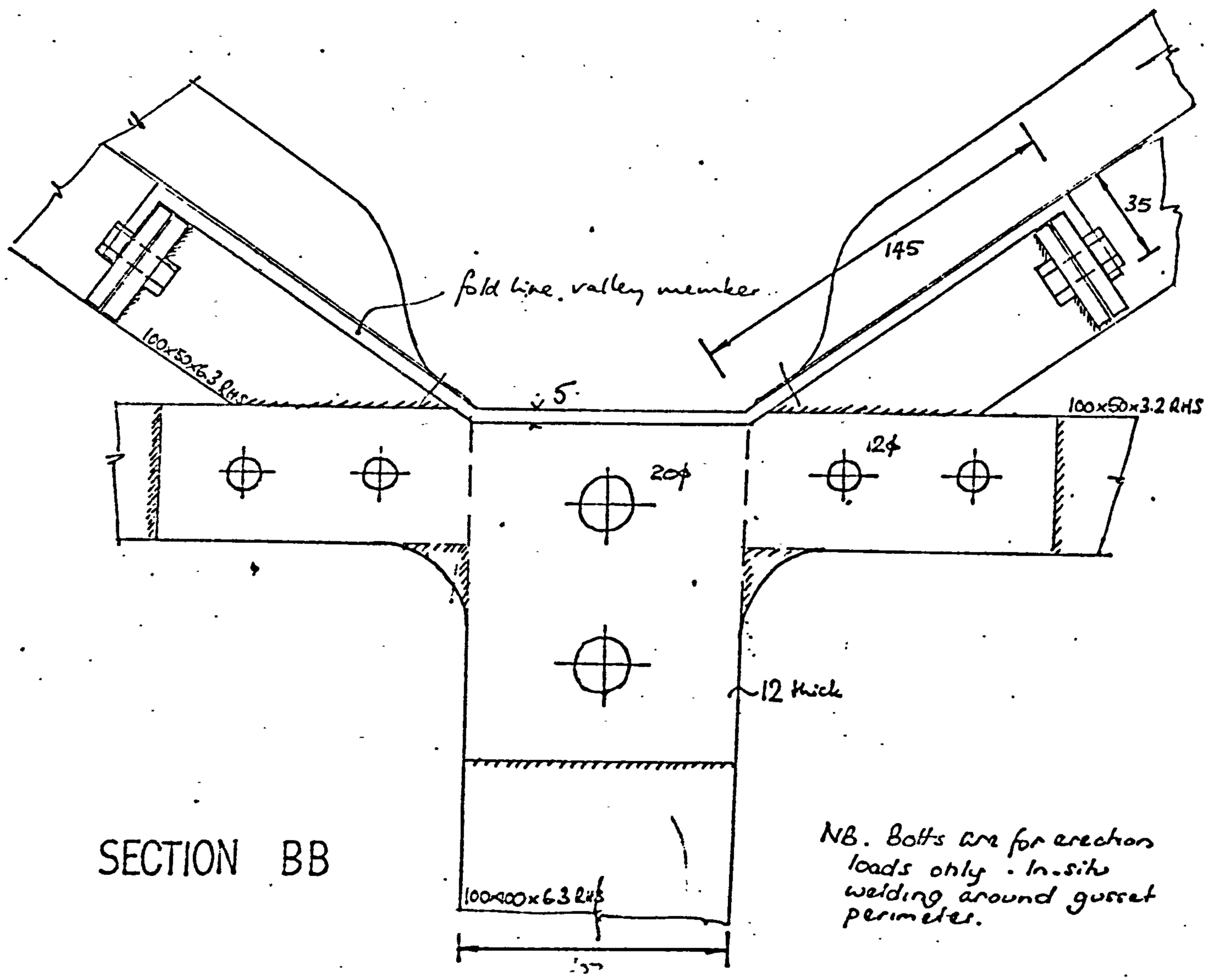

SECTION BB

NB. Bolts are for erection loads only. In-situ welding around gusset perimeters.

Scale 1cm : 2cm.

FIG (10.25)

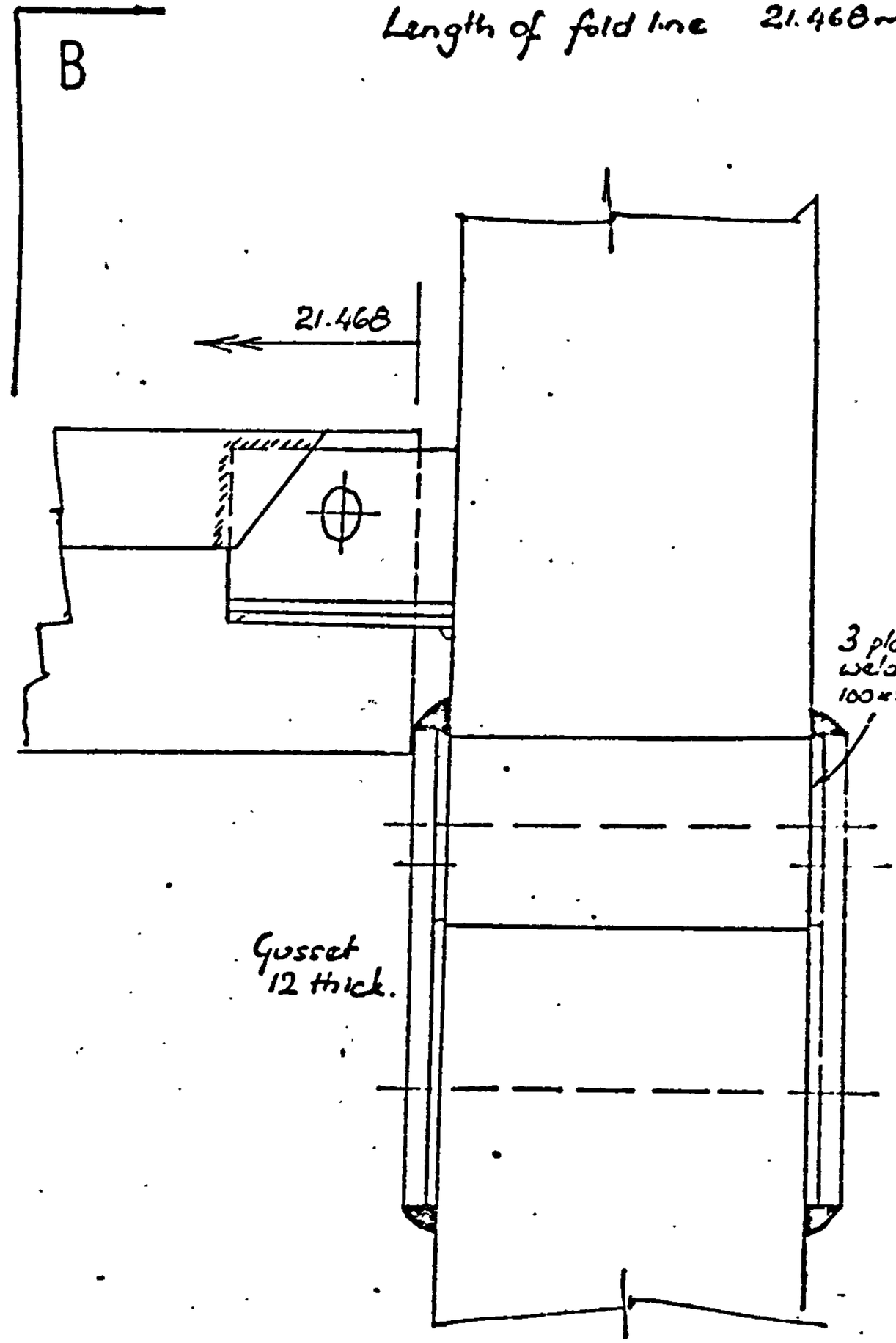

All dimensions mm

MIDDLE COLUMN

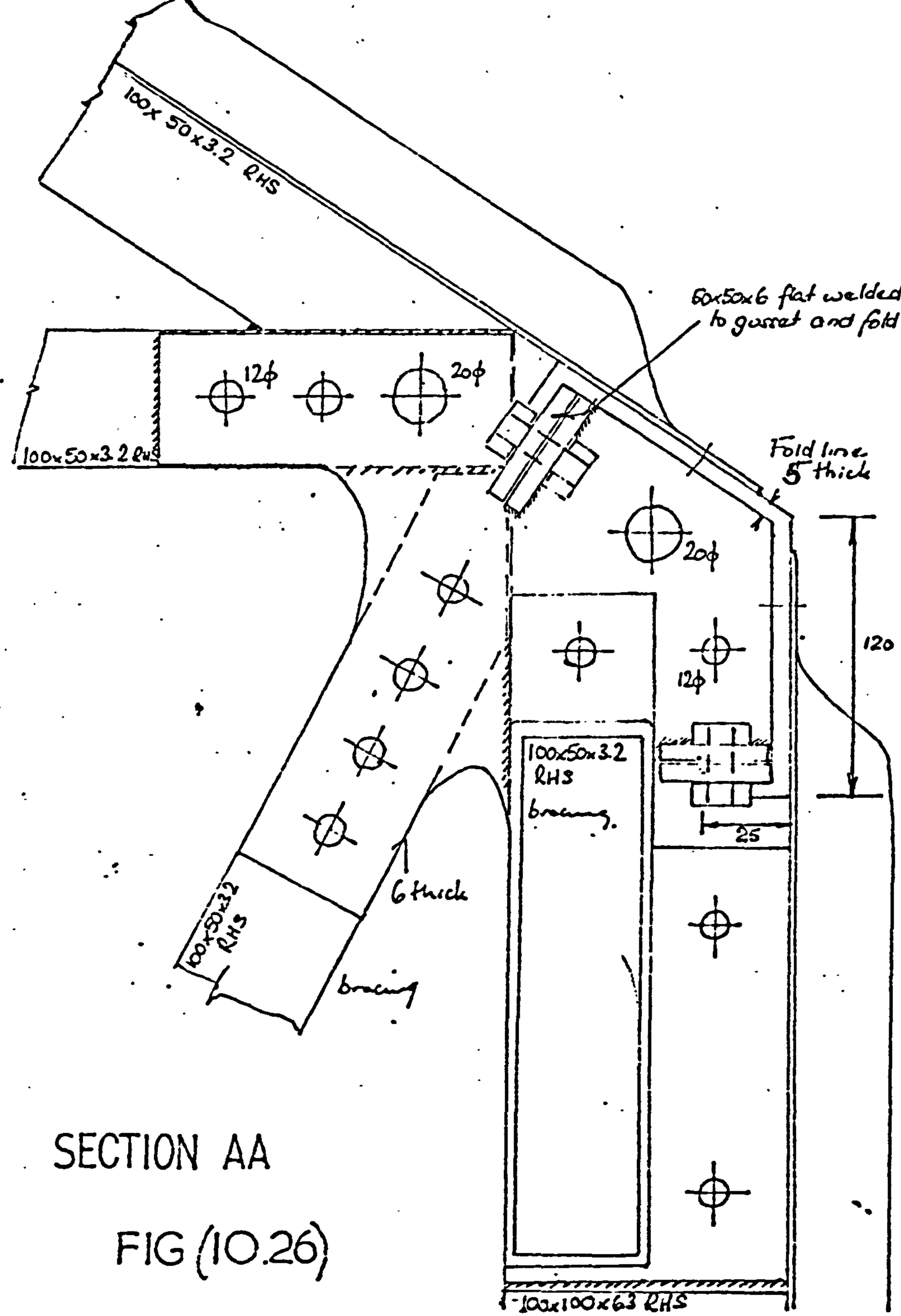

SECTION AA

FIG (10.26)

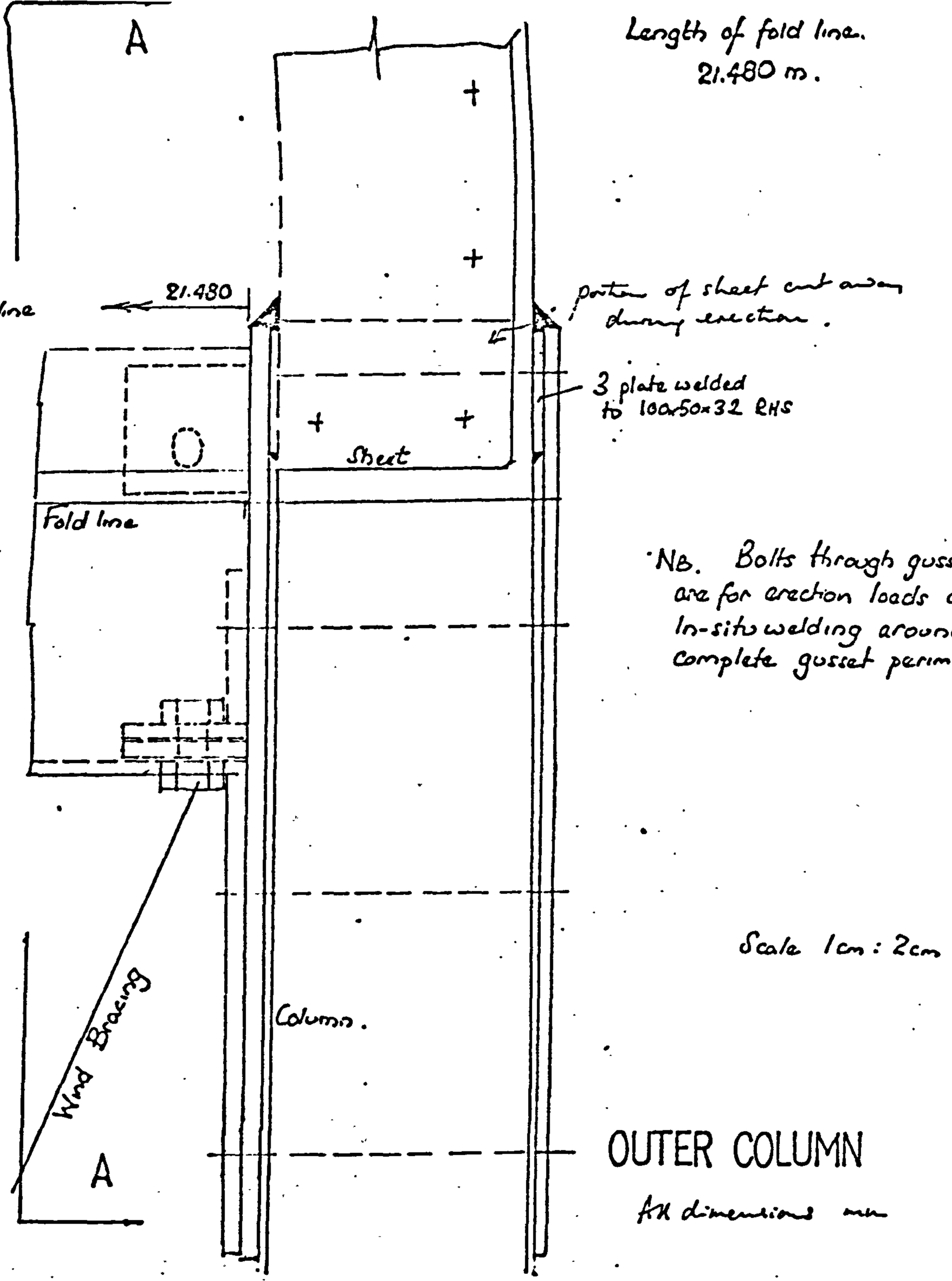

NB. Bolts through gusset are for erection loads only. In-situ welding around complete gusset perimeter

Scale 1cm : 2cm

OUTER COLUMN

All dimensions mm

ERECTION OF FOLDED PLATE ROOF

All dimensions in

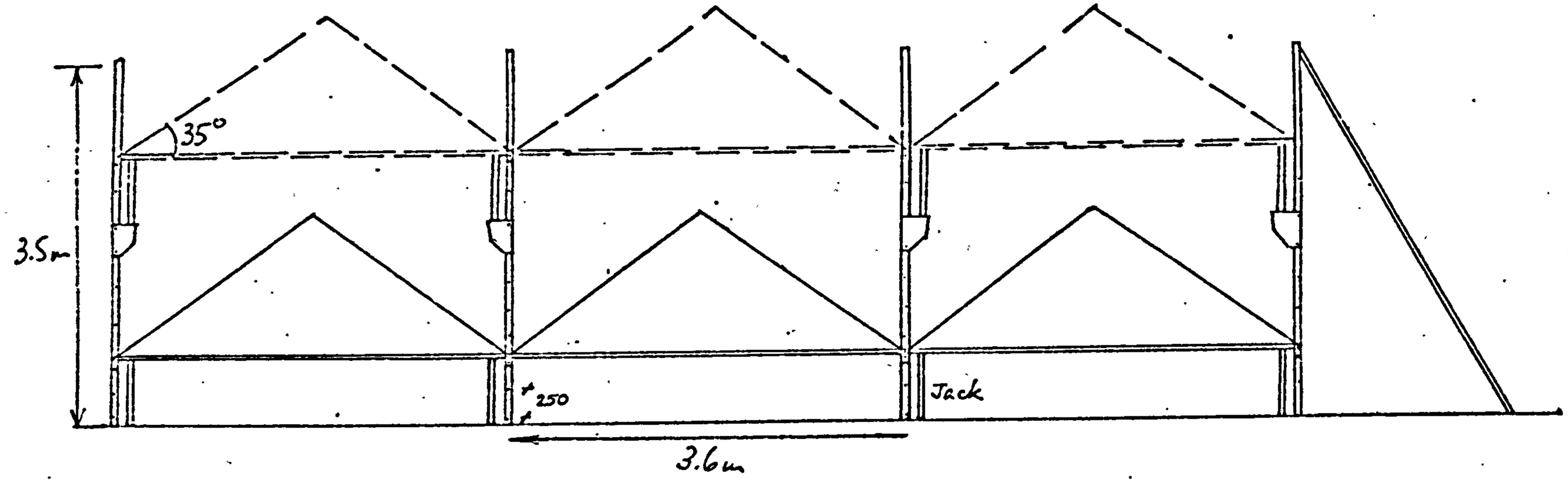

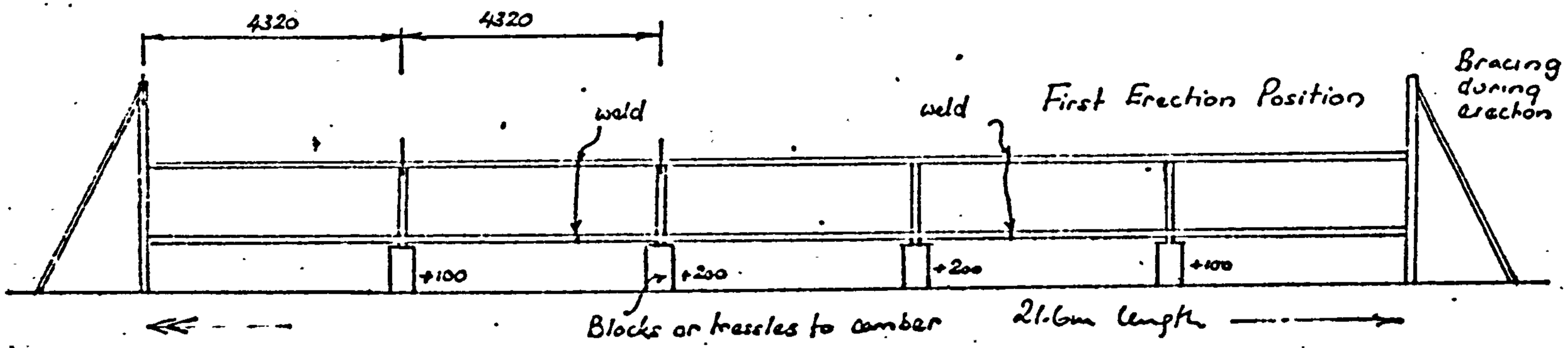

DETAIL B

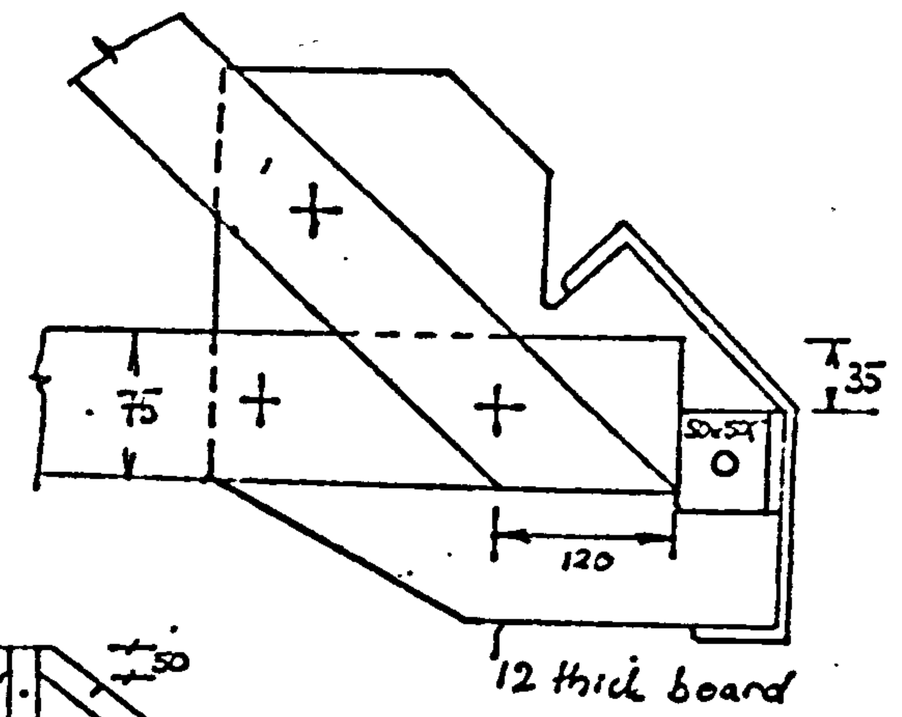

DETAIL A

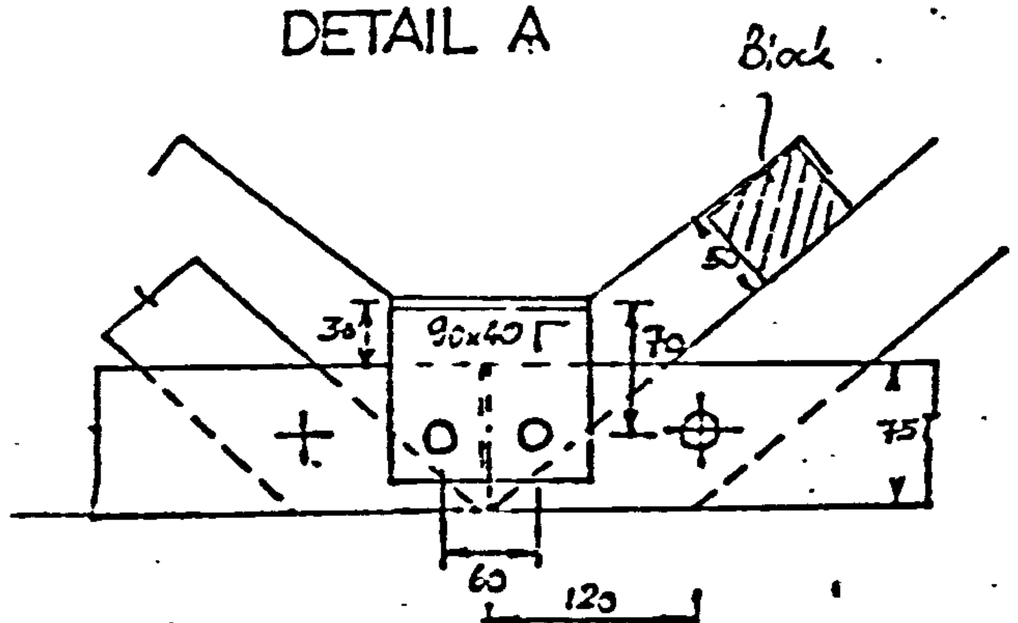

Erection trestles.

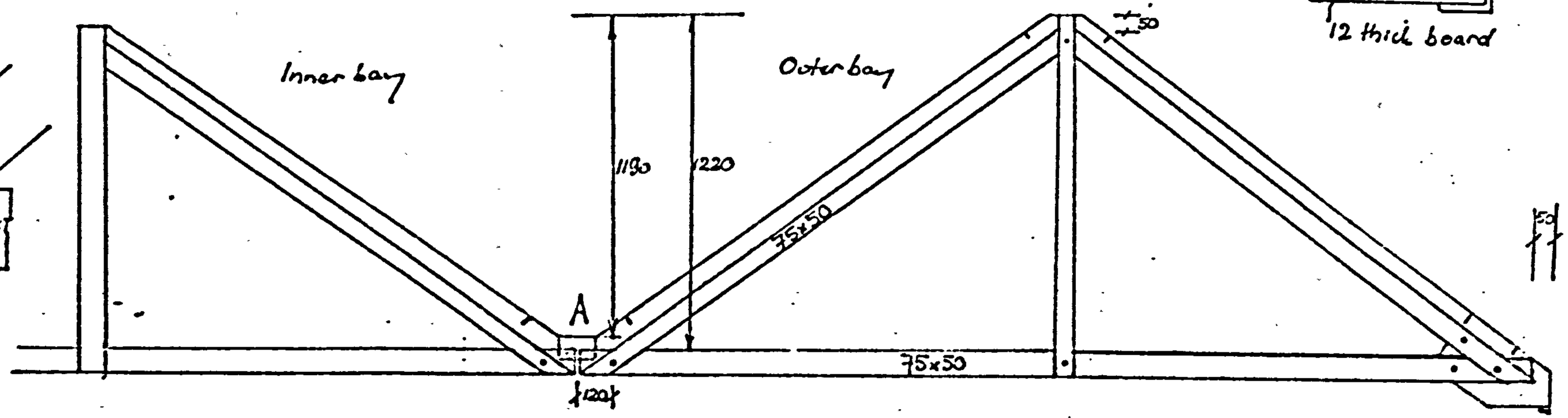

FIG (10.27)

STRESS-STRAIN CURVES FOR STEEL USED IN FOLDED PLATE ROOF SHEETING, AND MILD STEEL (M.S.)

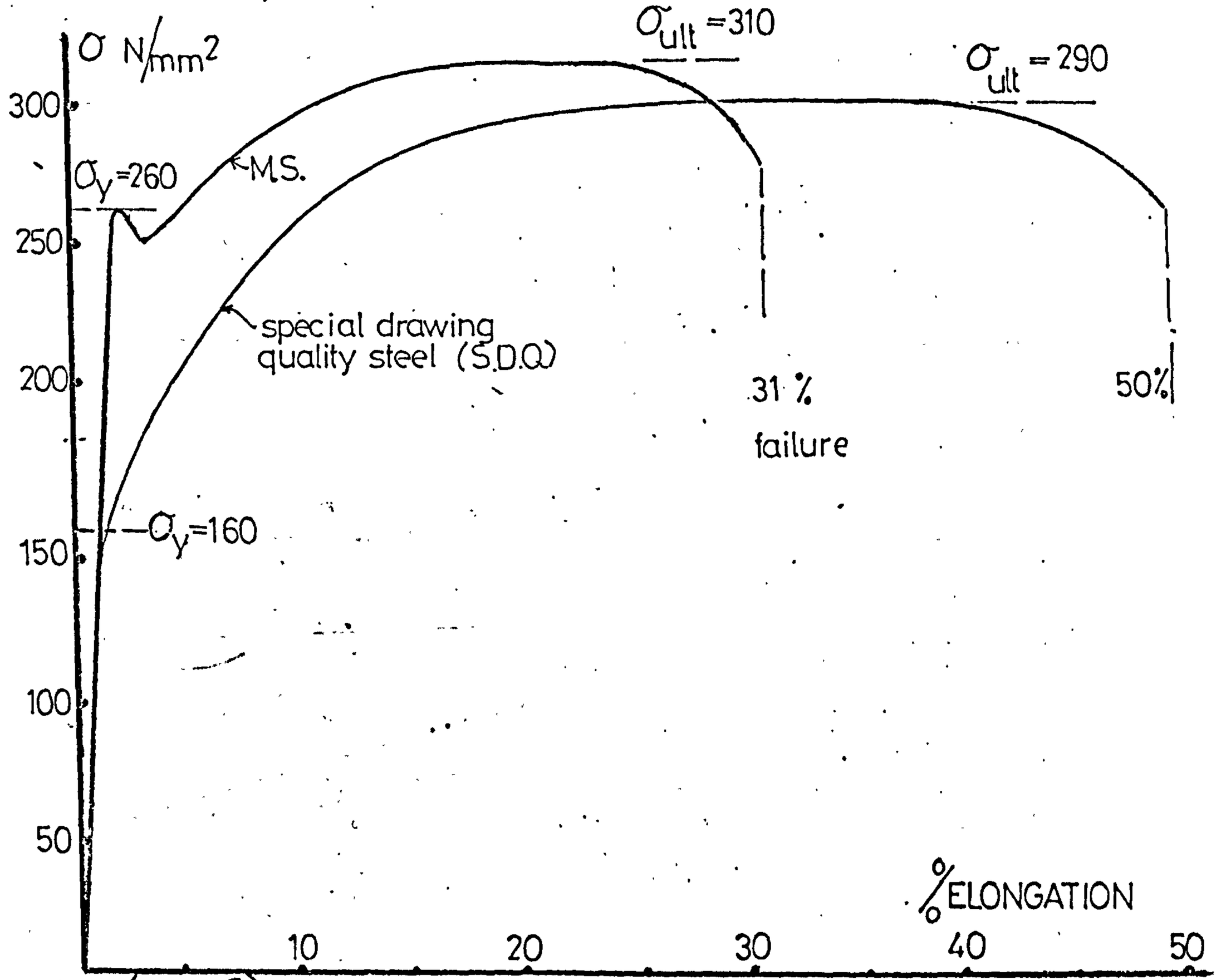

FIG (10.28)

TYPICAL LOAD—SLIP CURVE FOR UPSTAND SEAM IN S.D.Q. SHEET

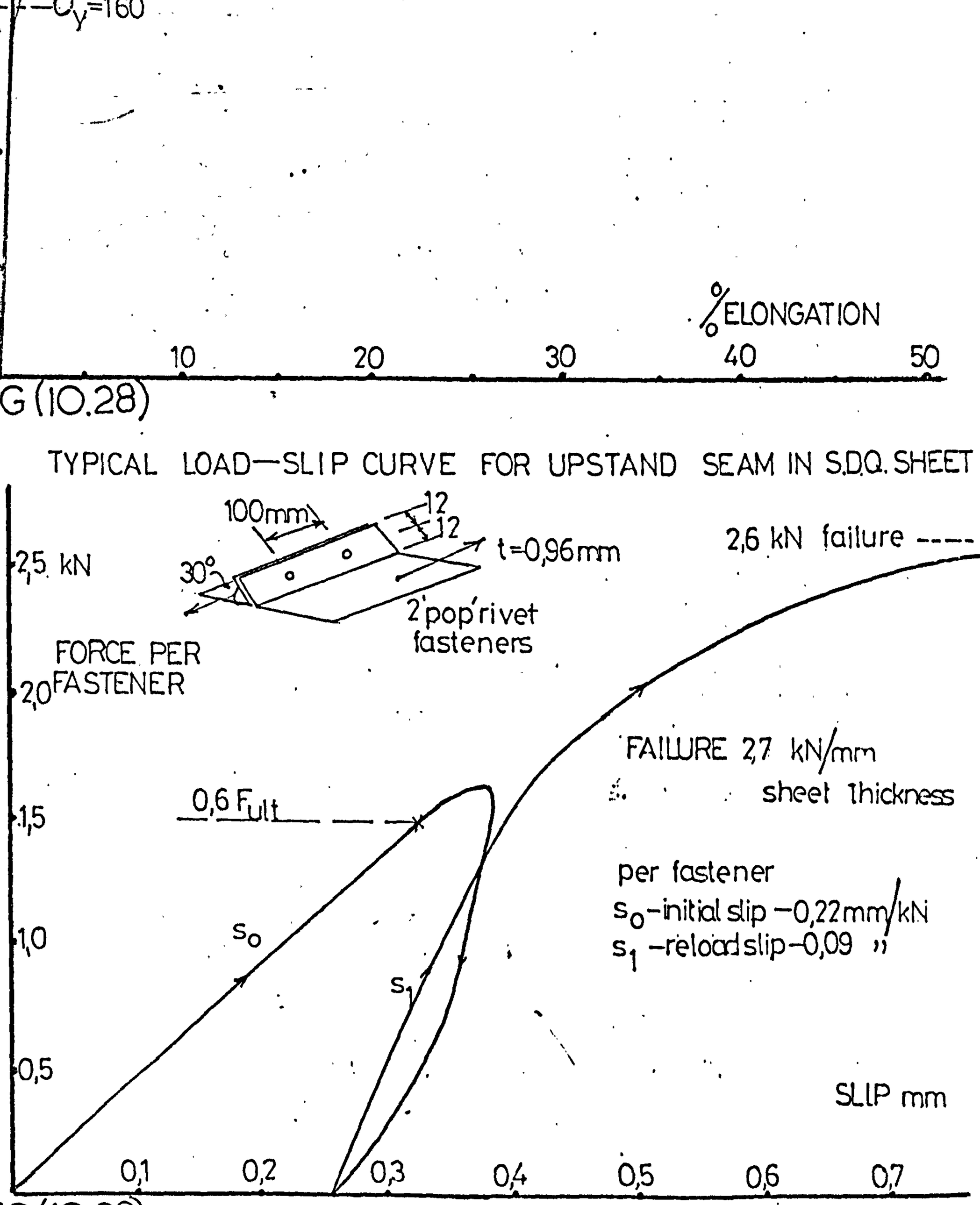

FIG (10.29)

HOLES IN FOLDED PLATE ROOFS

BUCKLING OF FOLD LINES IN COMPRESSION

HOLE IN CENTRE SPAN

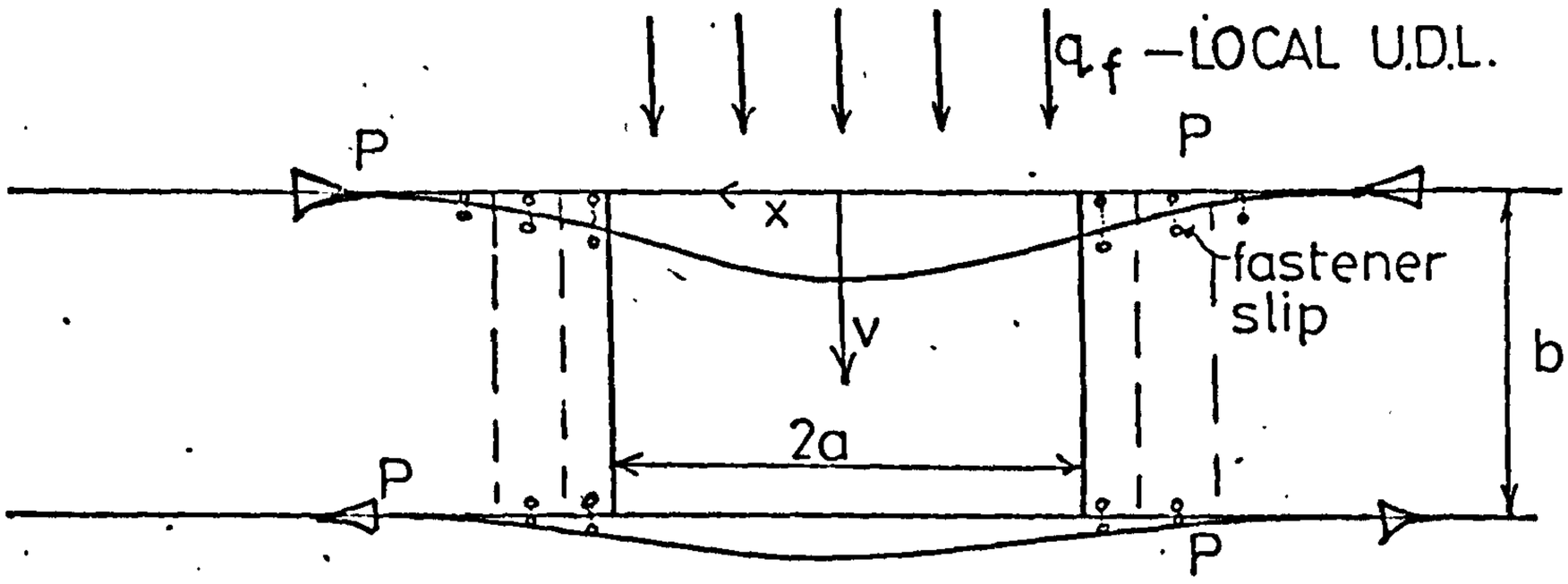

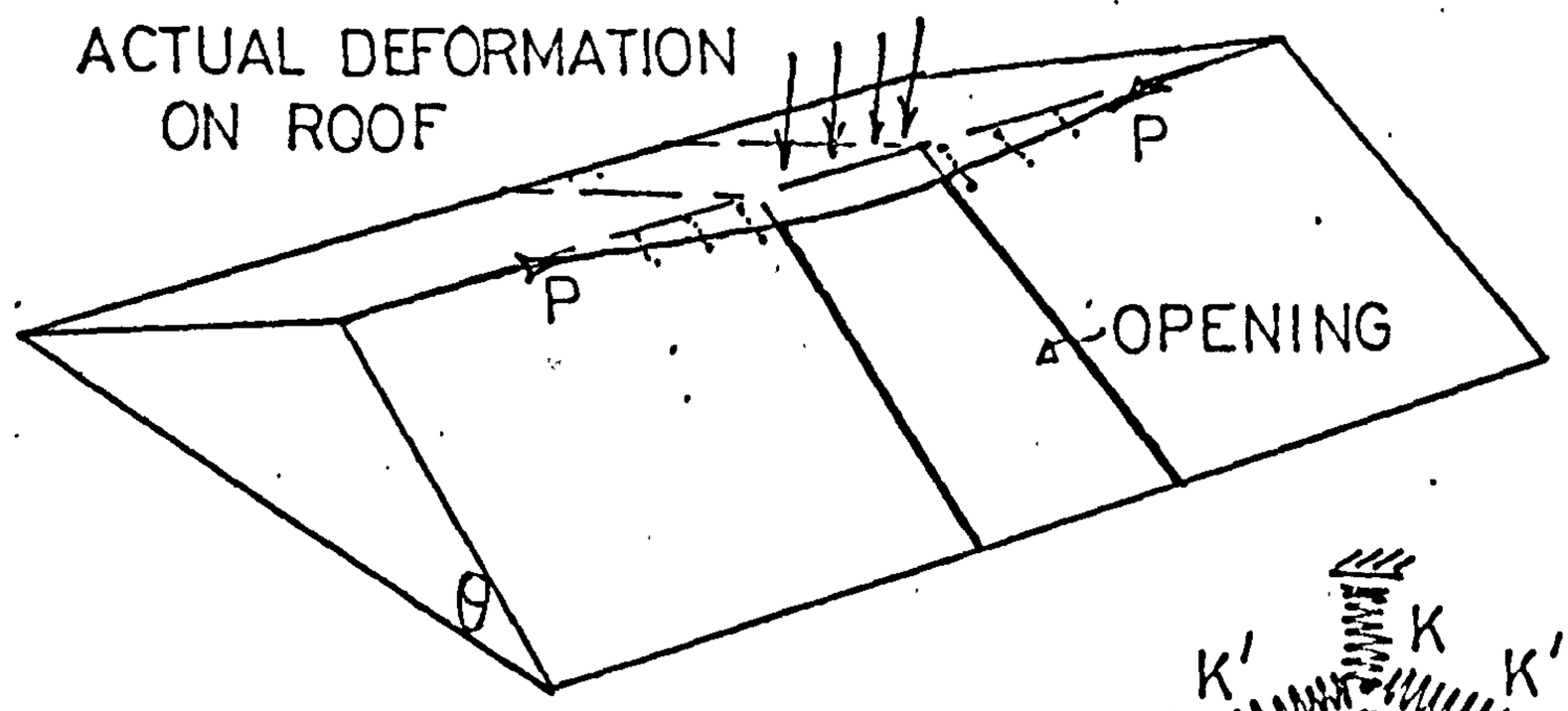

MODIFICATION FOR FASTENER STIFFNESS VERTICALLY,

$$K = 2K' \sin^2\theta$$

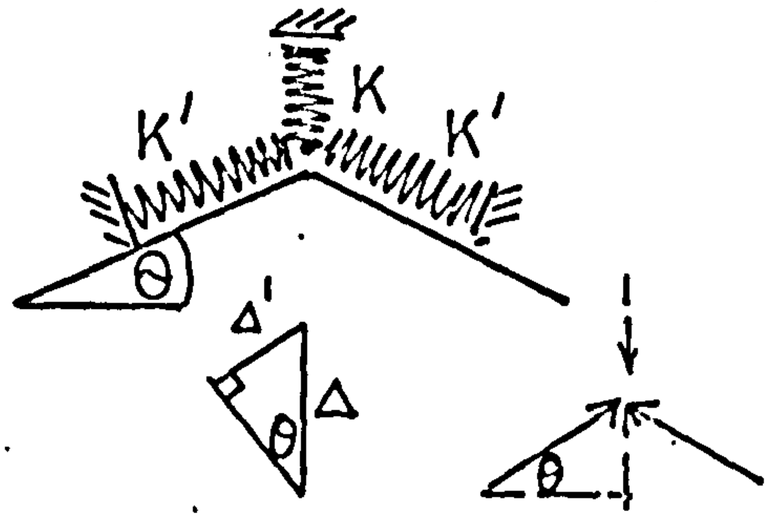

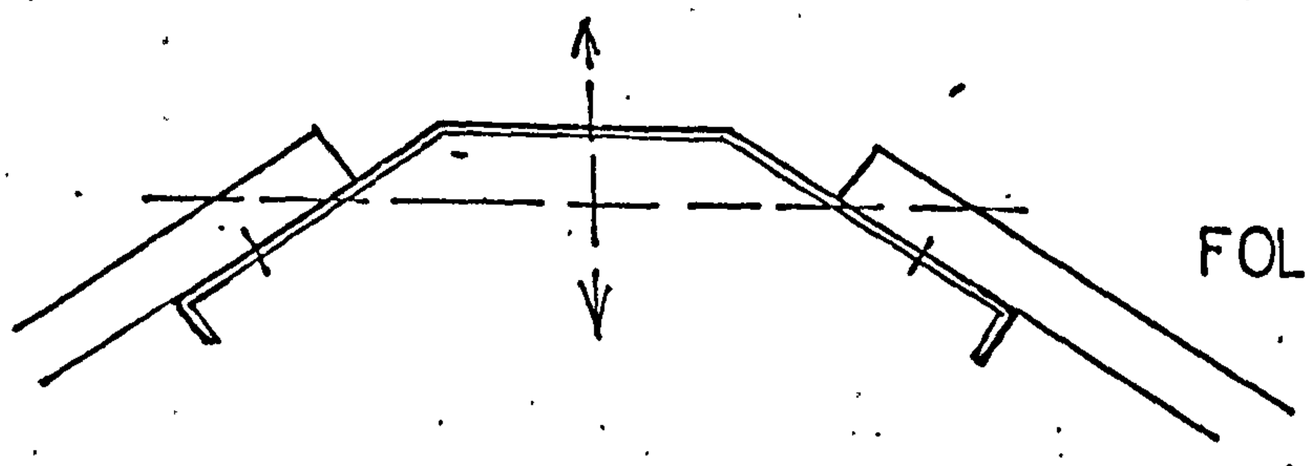

FOLD LINE MOVES VERTICALLY

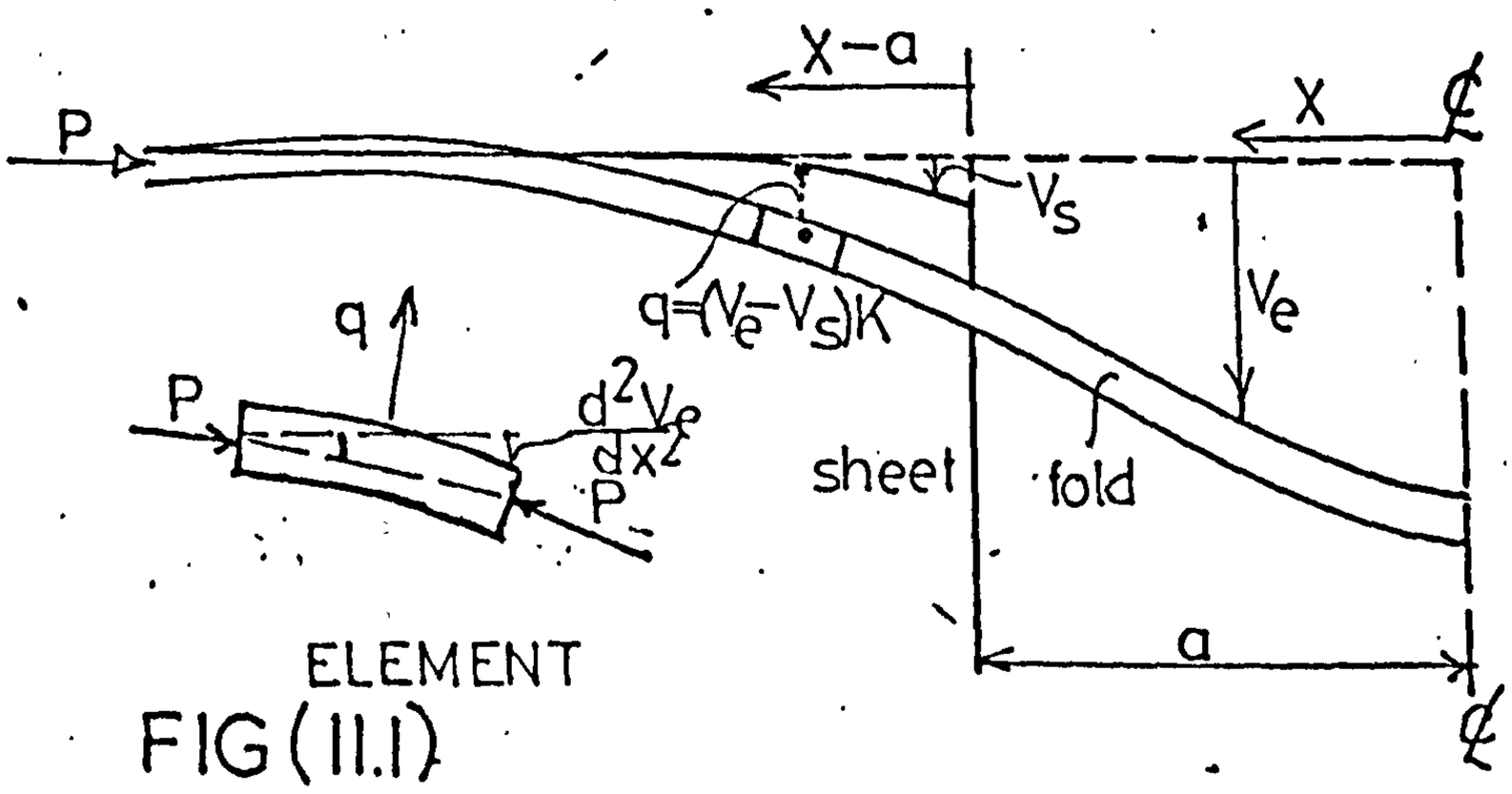

ELASTIC RESPONSE

V_s – sheet shear

V_e – fold movement

FIG (11.1)

HOLES IN FOLDED PLATE ROOFS

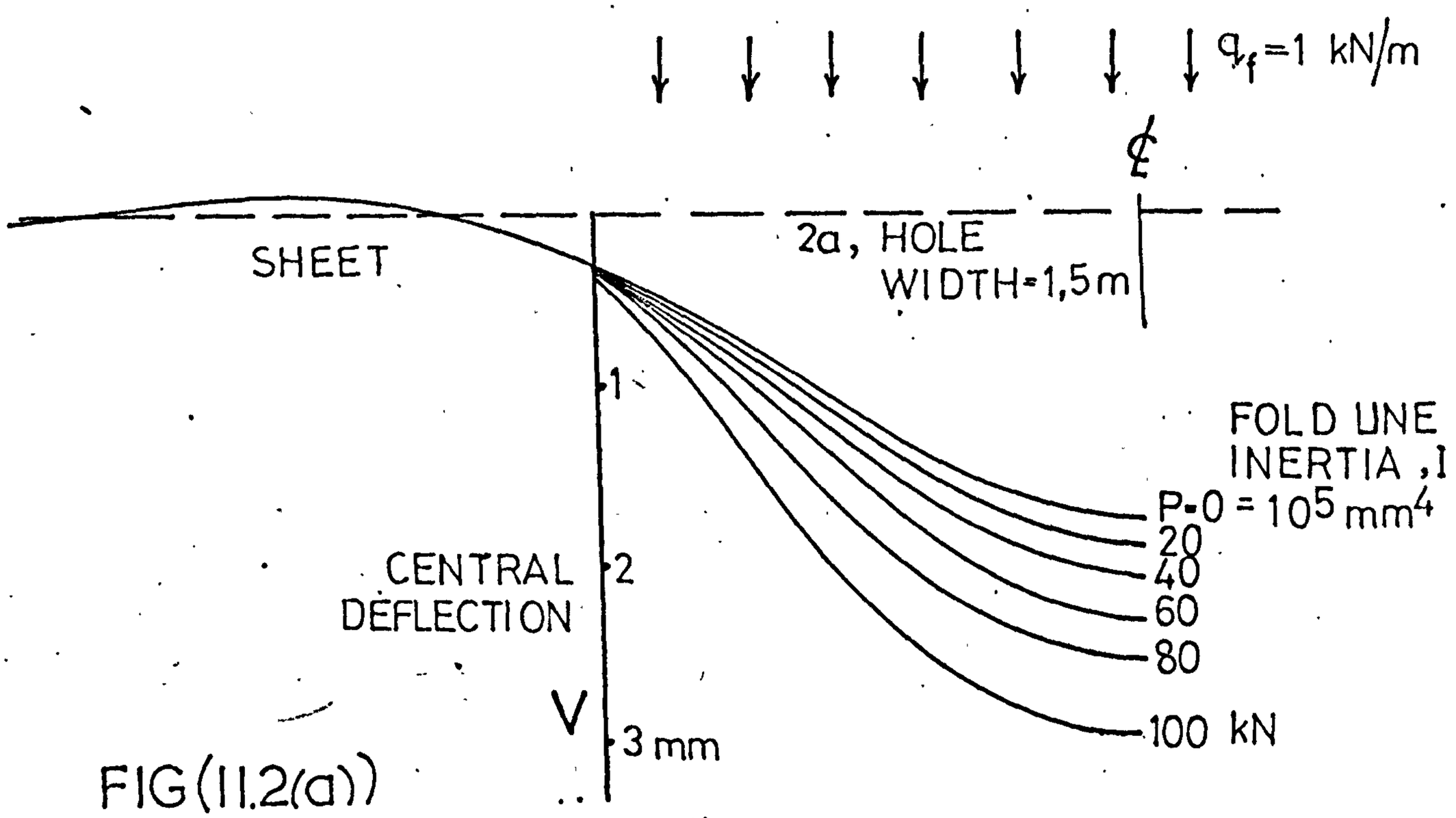

FIG(11.2(a))

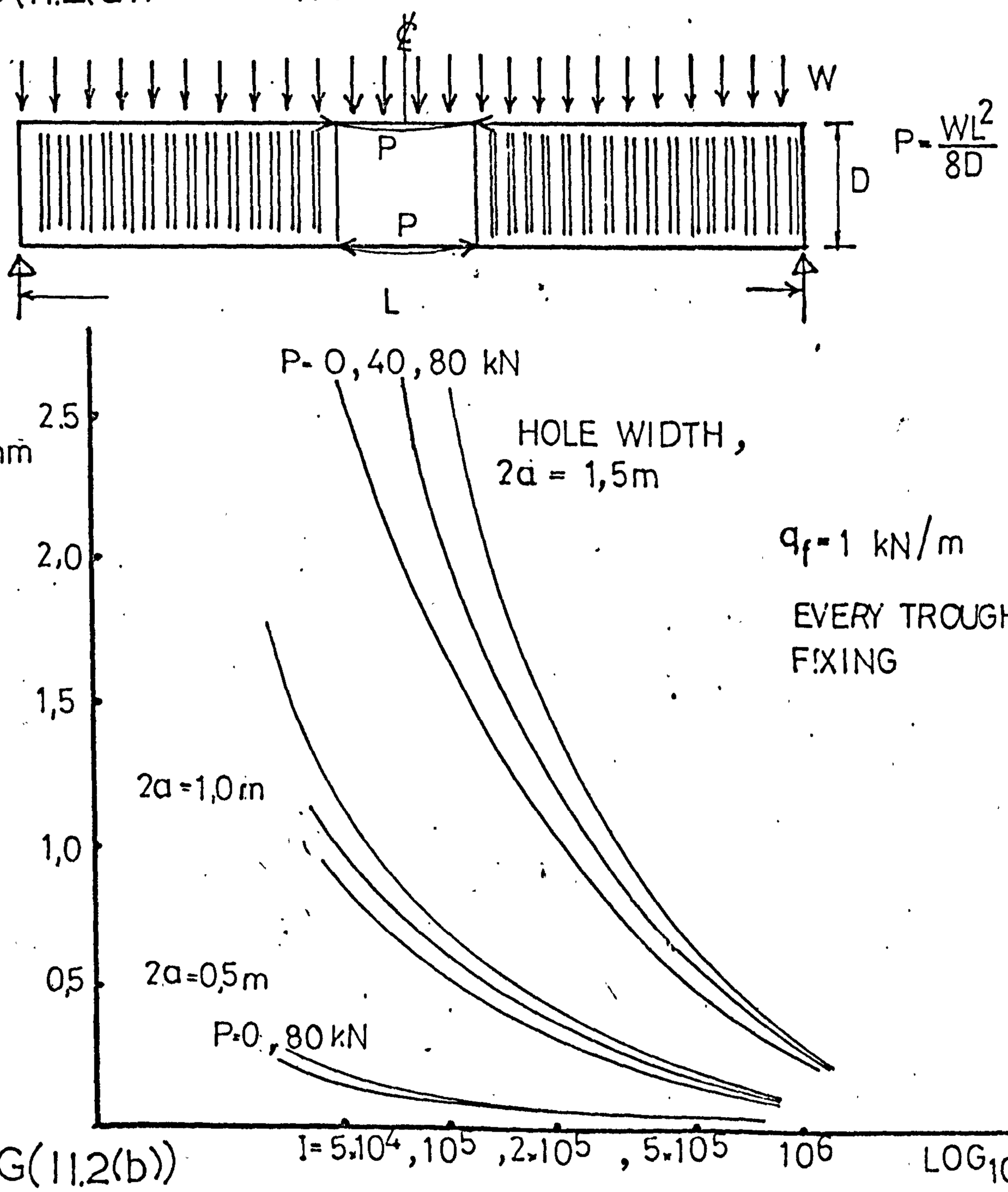

FIG(11.2(b))

LOCAL FASTENING FORCES AROUND A HOLE

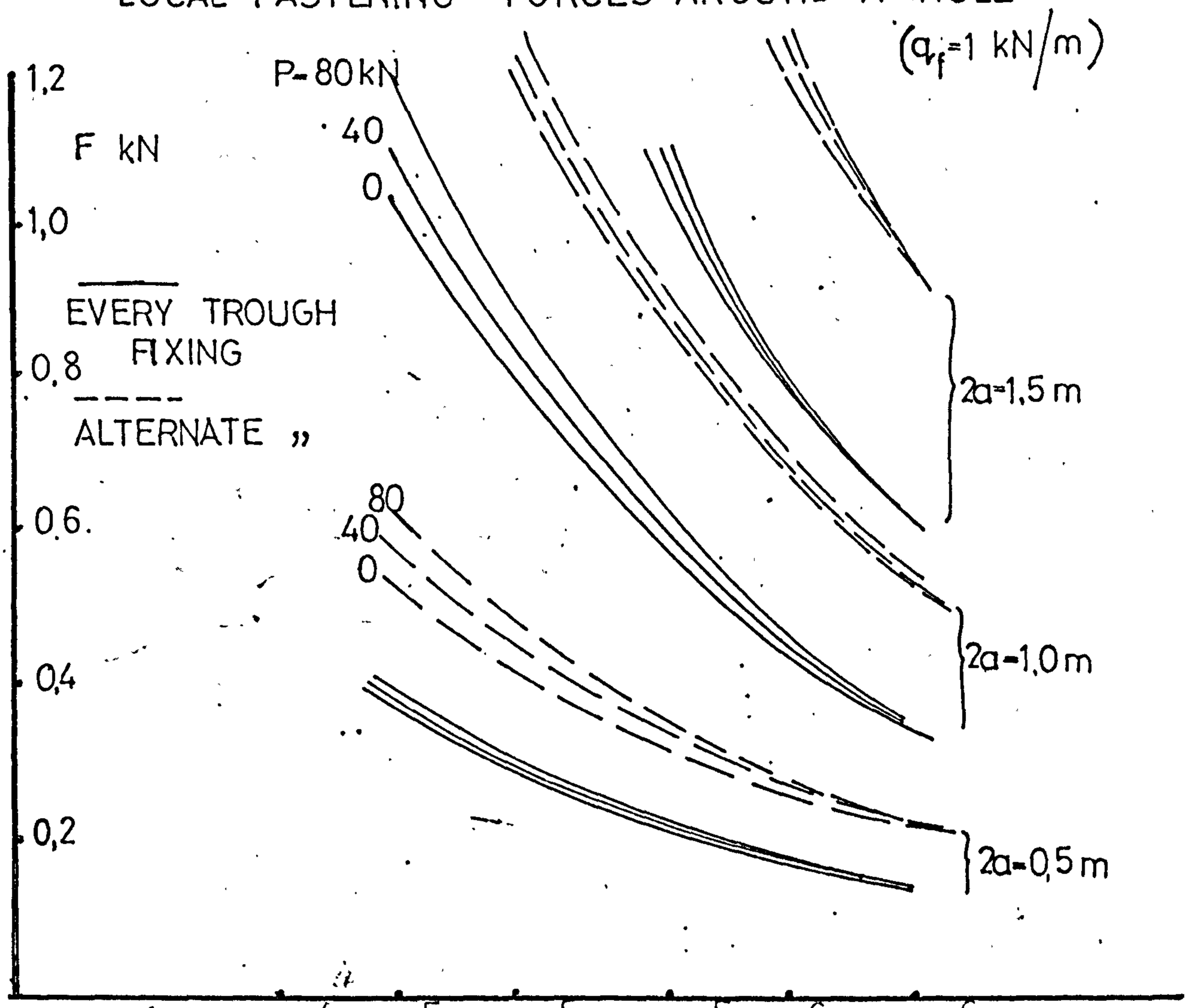

FIG(11.3(a))

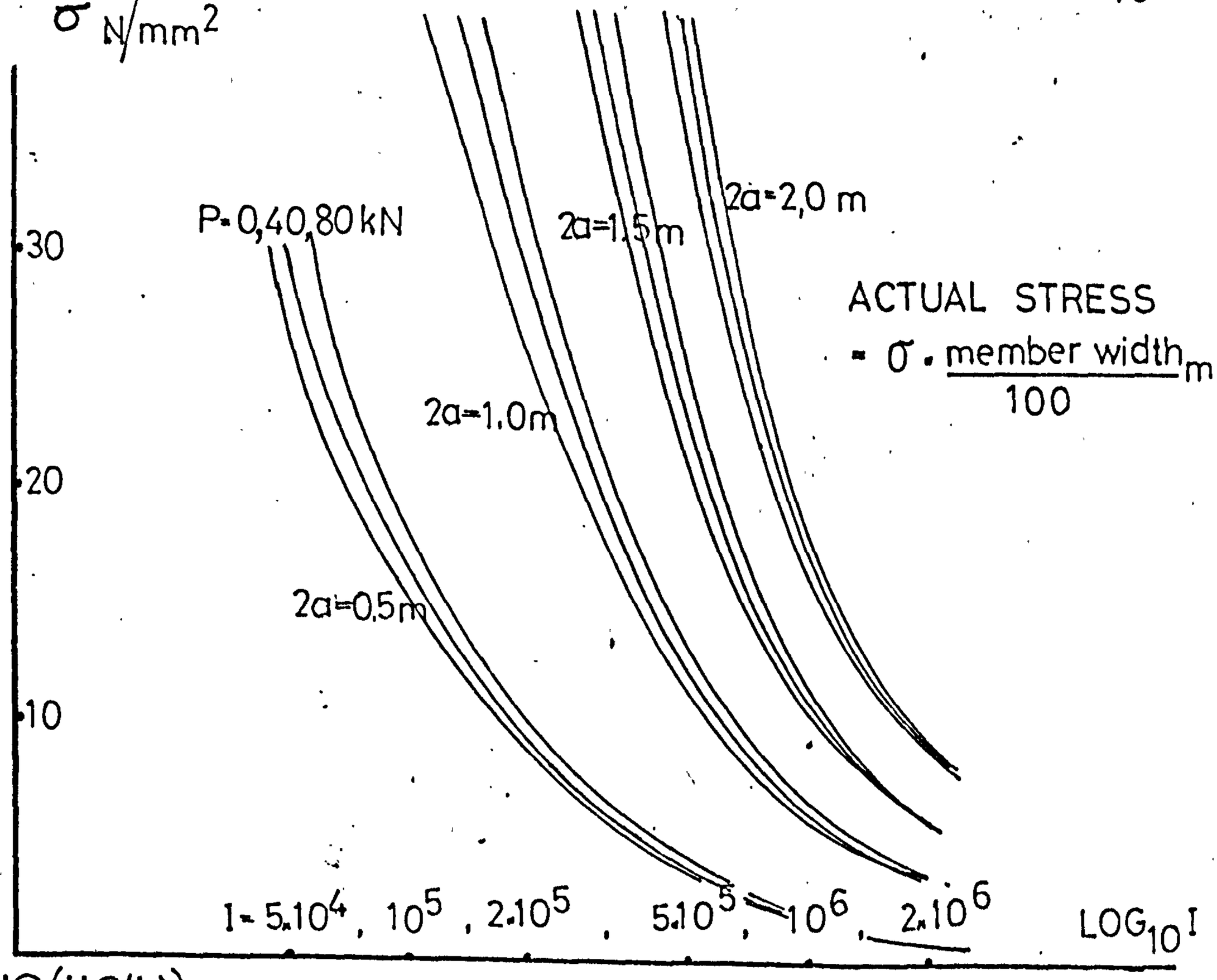

FIG(11.3(b)) FOLD LINE BENDING STRESS

FOLDED PLATE ROOF—VARIATIONS IN FASTENING

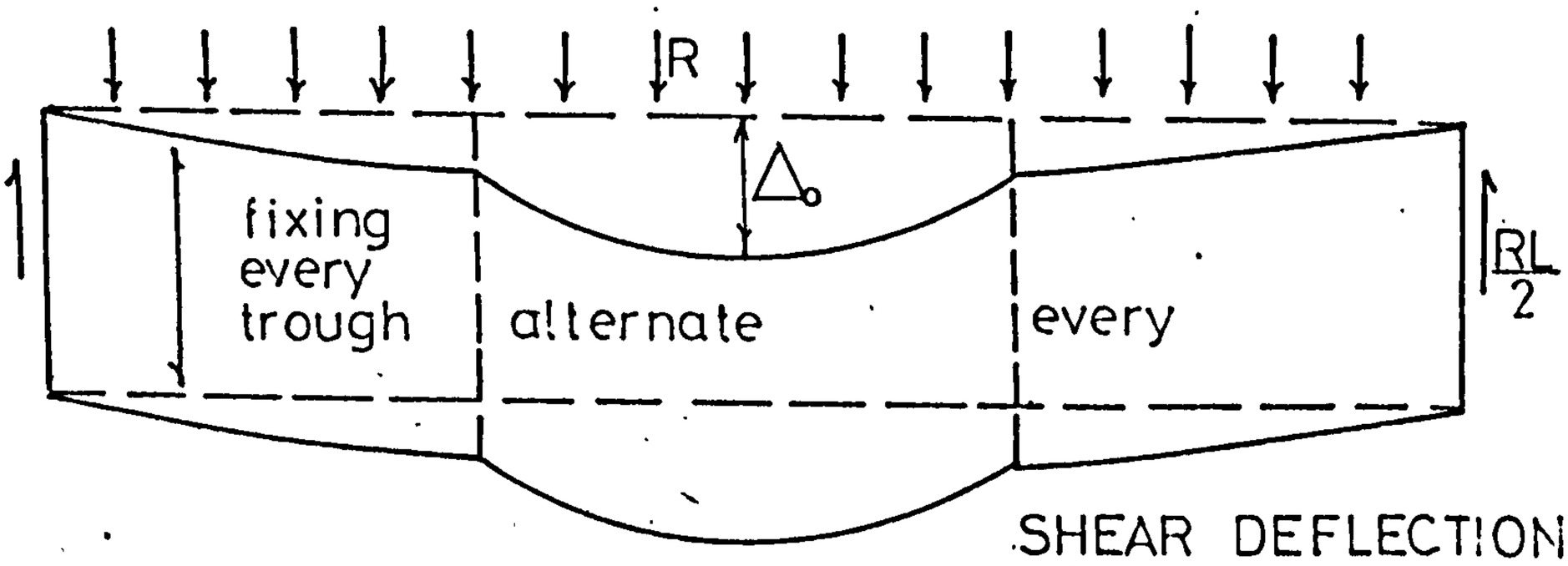

FINITE DIFFERENCE REPRESENTATION

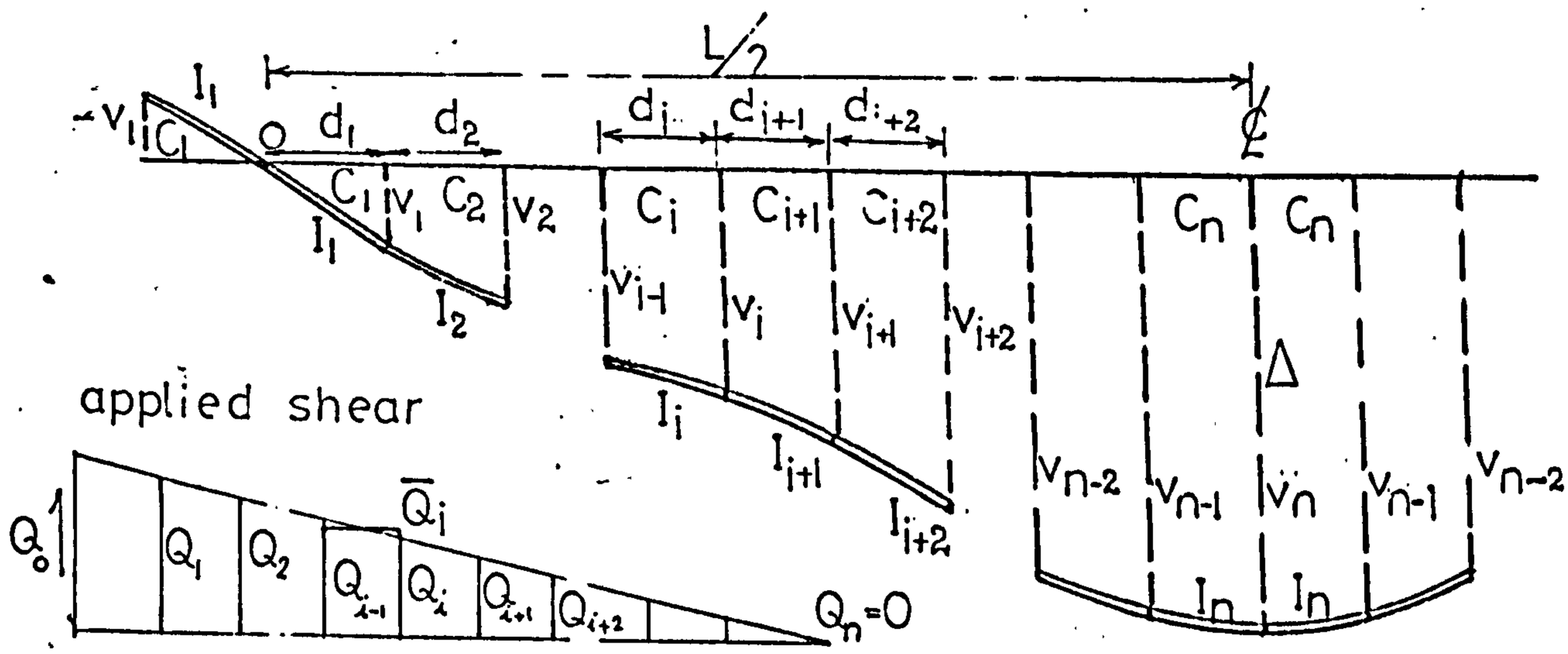

$$Q_i = Q_o - \sum_{j=1}^{i} d_j \frac{Q_o}{L/2}$$

$$\bar{Q}_i = \frac{Q_i + Q_{i-1}}{2}$$

v_i – shear displacement,
I_i – fold inertia,
C_i – sheet flexibility

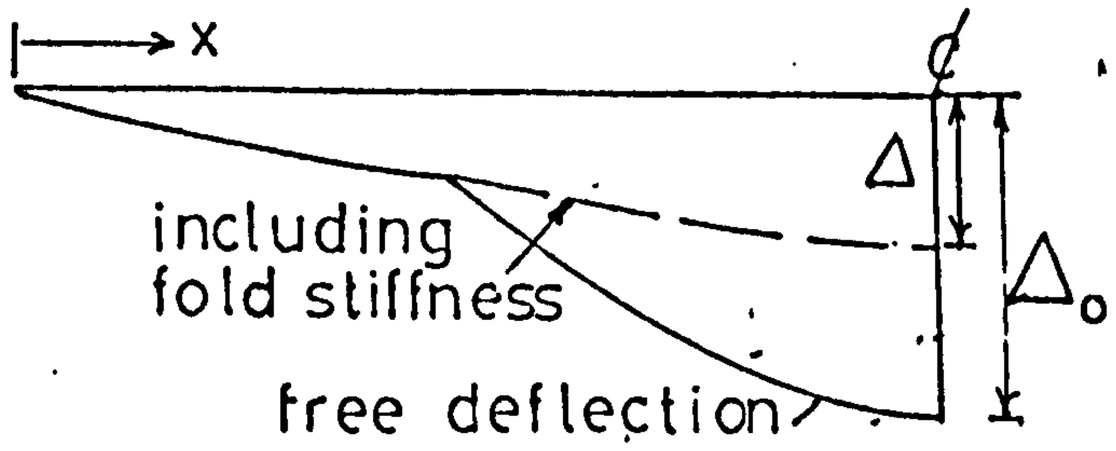

DIFFERENTIAL EQUATION

$$-EI_i \frac{d^3v}{dx^3} + \frac{dv}{dx} \cdot \frac{1}{C_i} = \bar{Q}_i$$

FIG(11.4)

LATERAL INSTABILITY OF EDGE BEAM

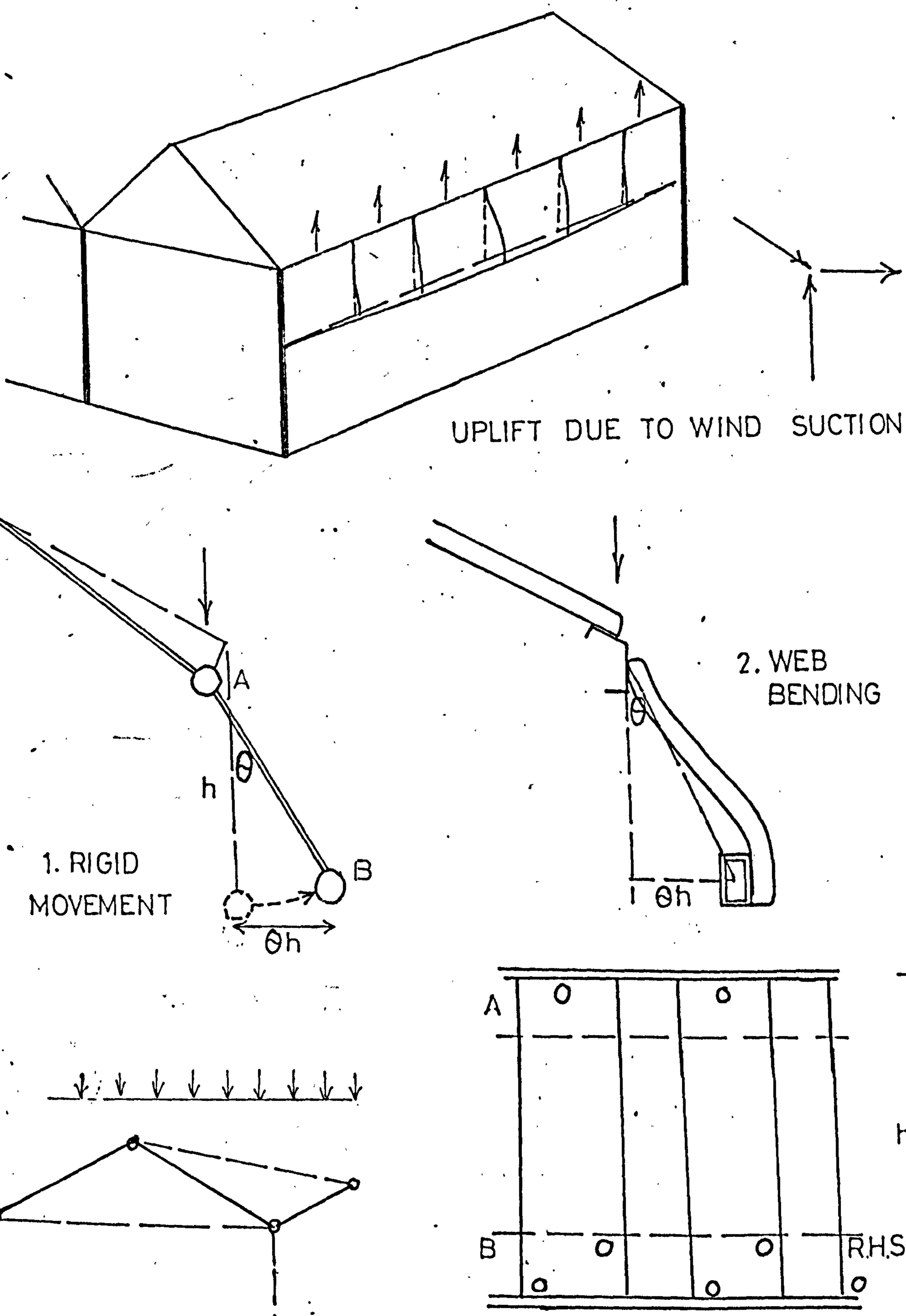

UPSTAND EDGE BEAM MUST BE TIED BACK

FASTENINGS ON LOWER CHORD FOR ROTATION CONTINUITY

FIG (11.5)

FOLDED PLATE ROOF TESTS

— EQUIVALENT BEAM

TEST WITH 'PRESSED-OUT' SHEETS.

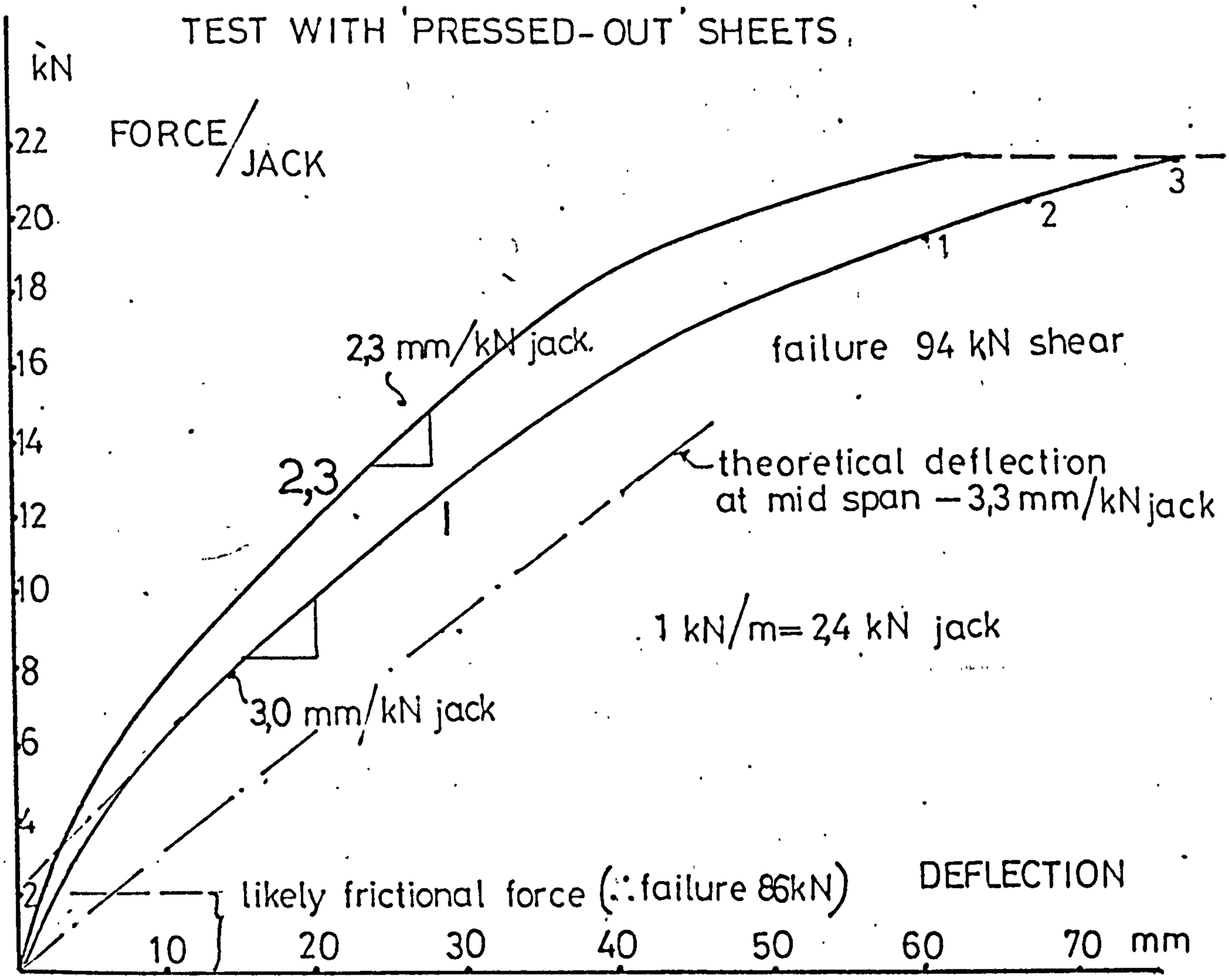

EVERY TROUGH FIXING

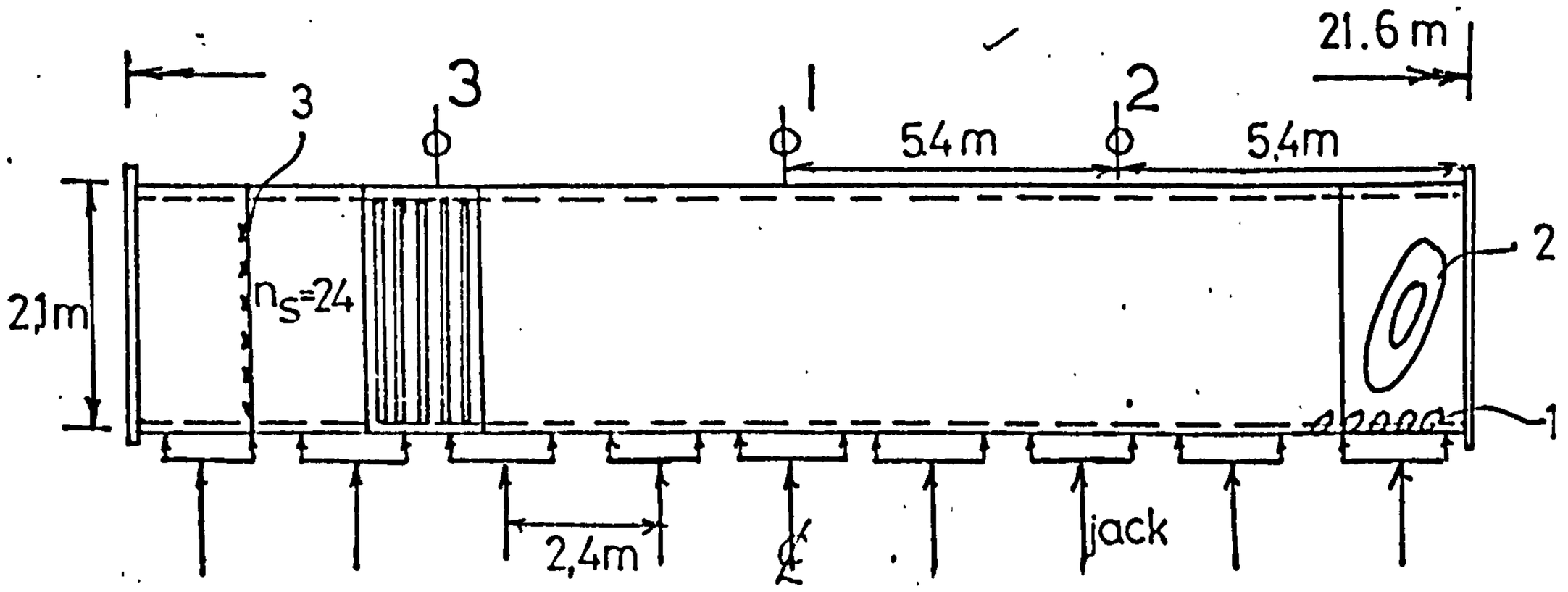

1. LOCAL BUCKLING
2. SHEAR BUCKLE — theory 19.8 kN/jack (89 kN)
3 SEAM FAILURE — theory 18.6 kN/jack (84kN)

FIG (12.1)

FOLDED PLATE ROOF TESTS

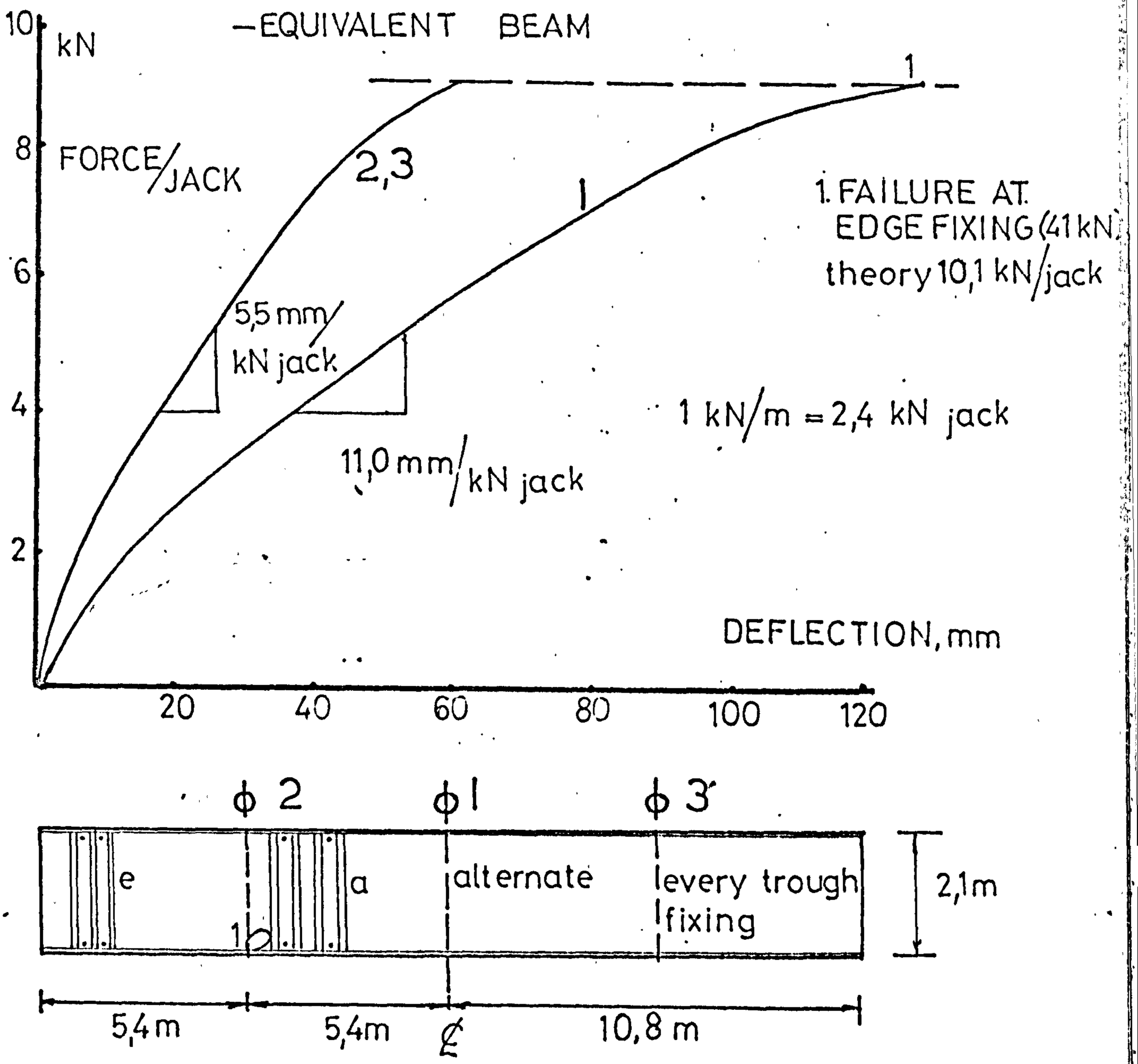

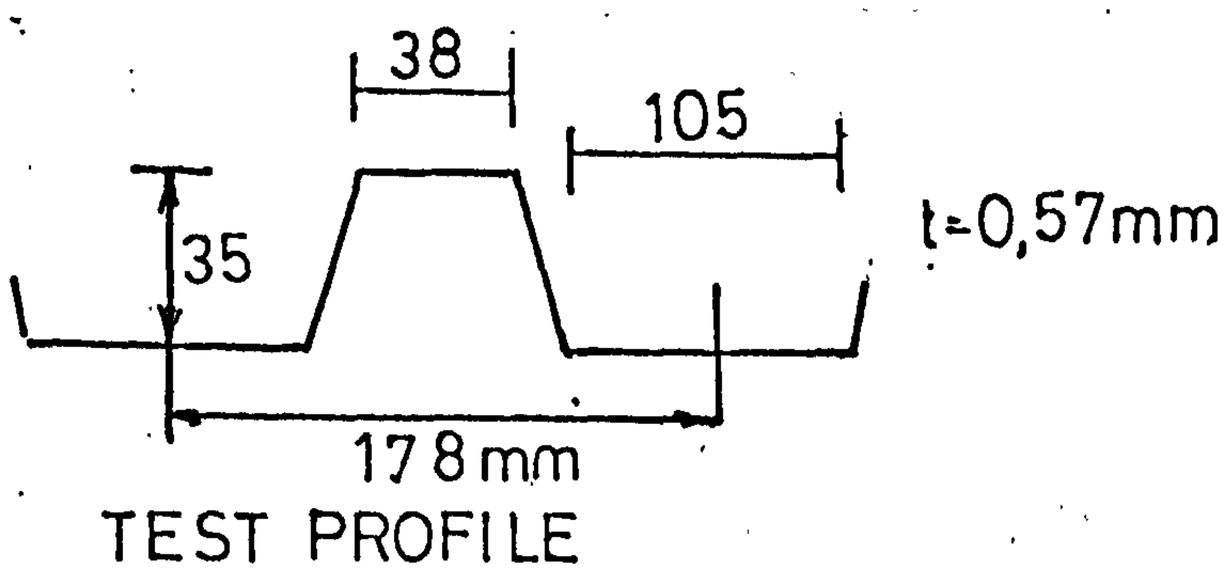

FIG(12.2)

FOLDED PLATE ROOF TESTS

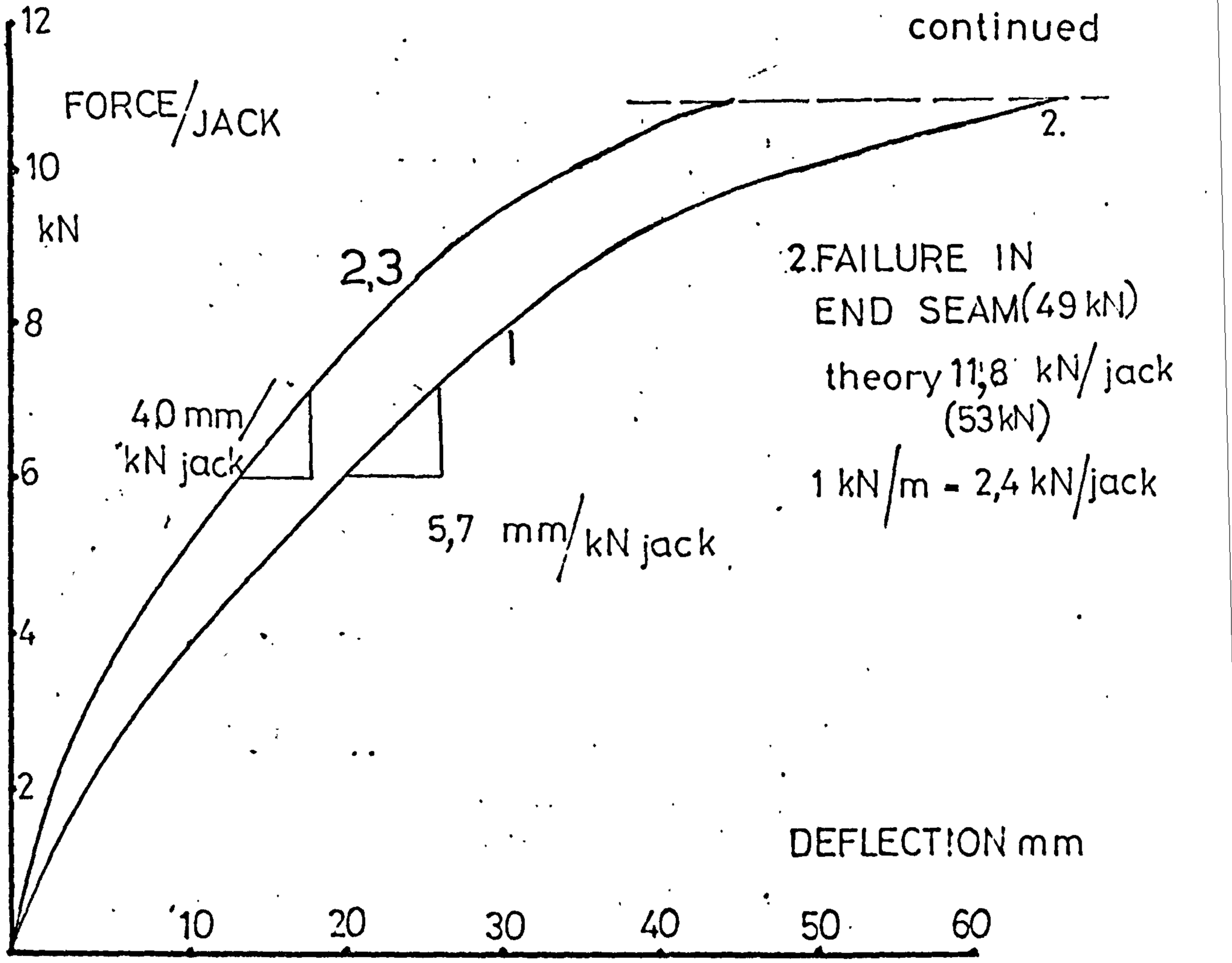

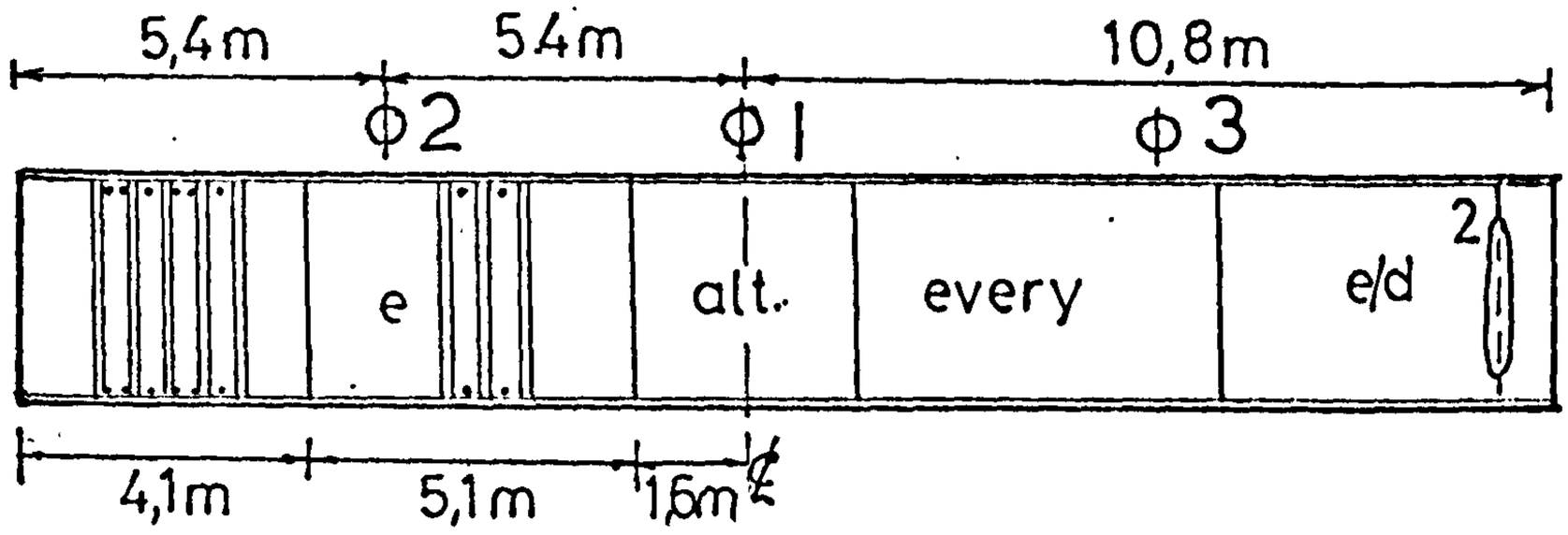

e/d — every and double trough fixings alternately

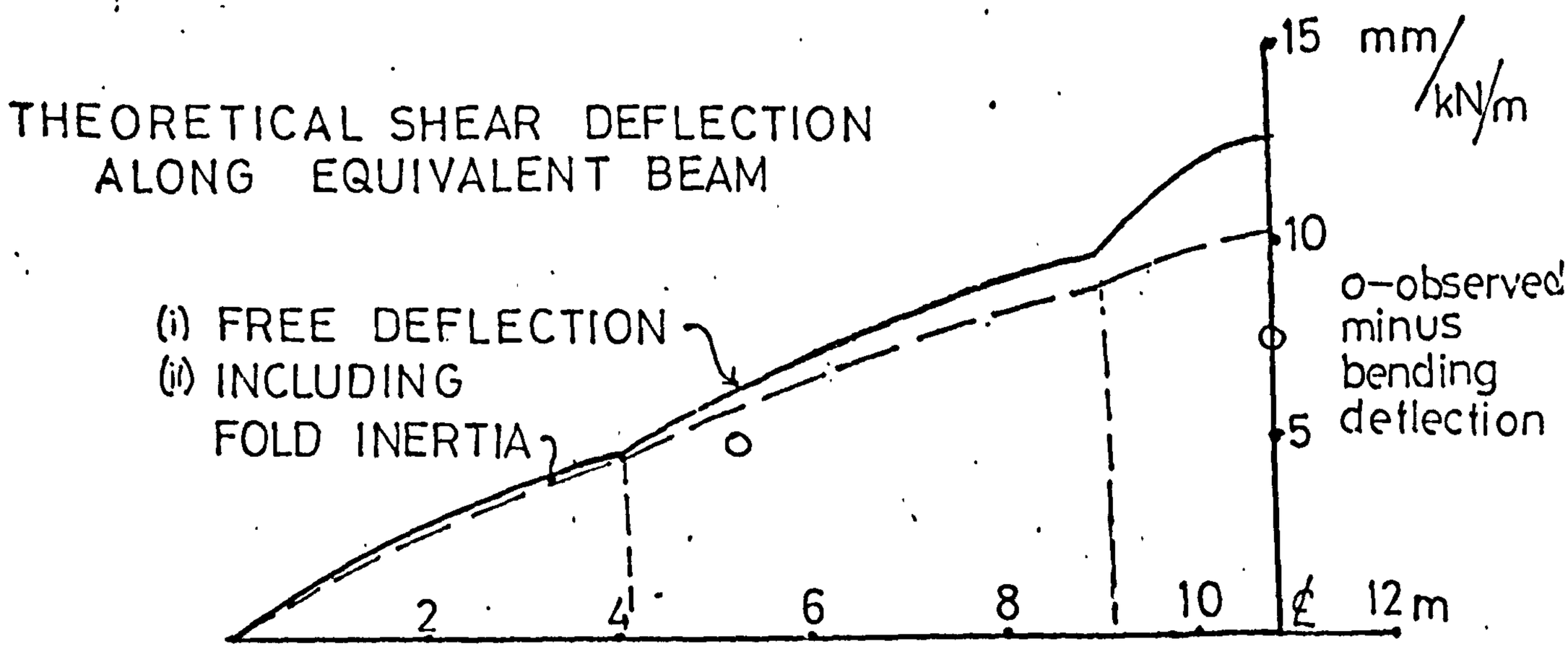

FIG(123)

FOLDED PLATE ROOF TESTS

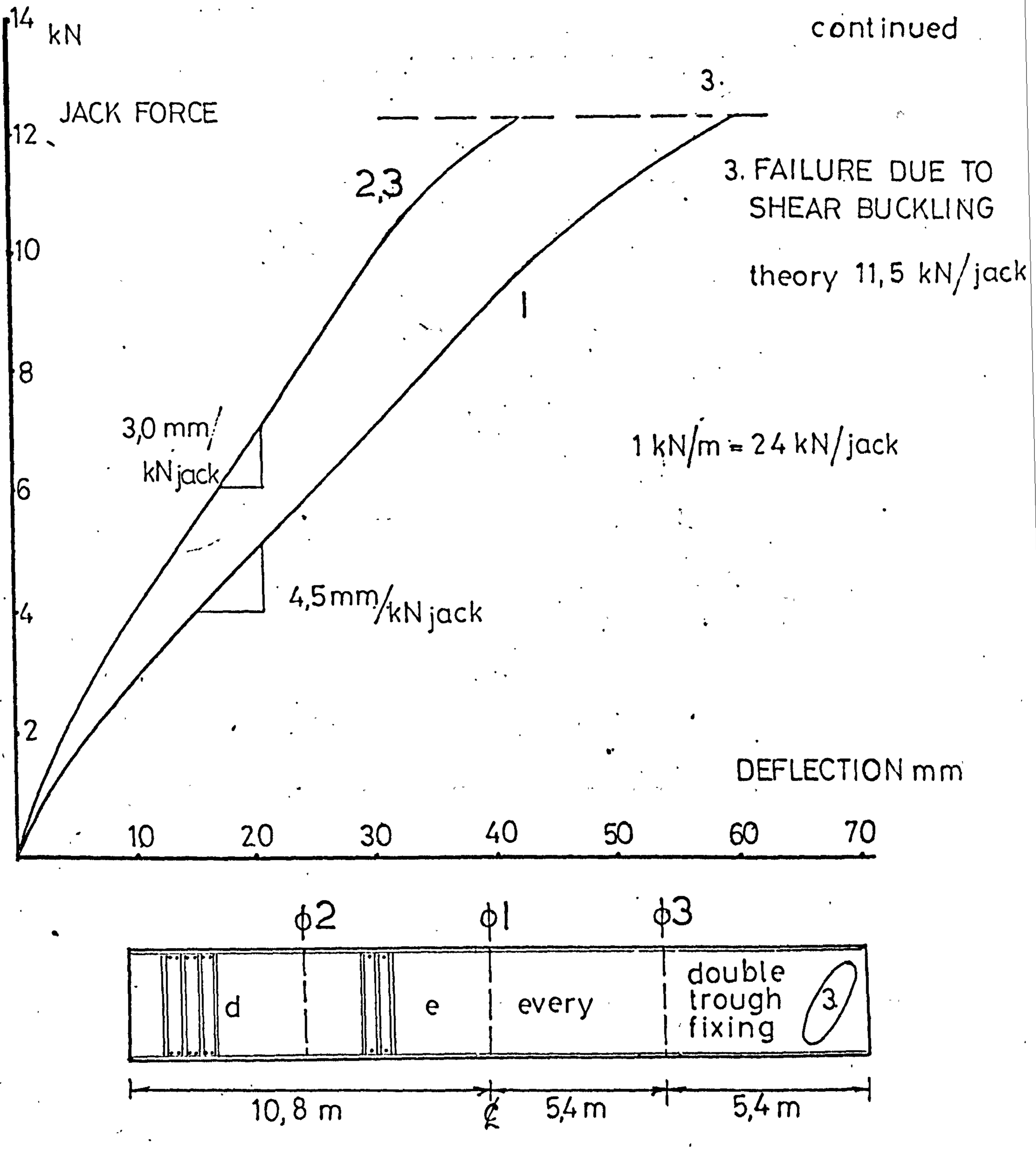

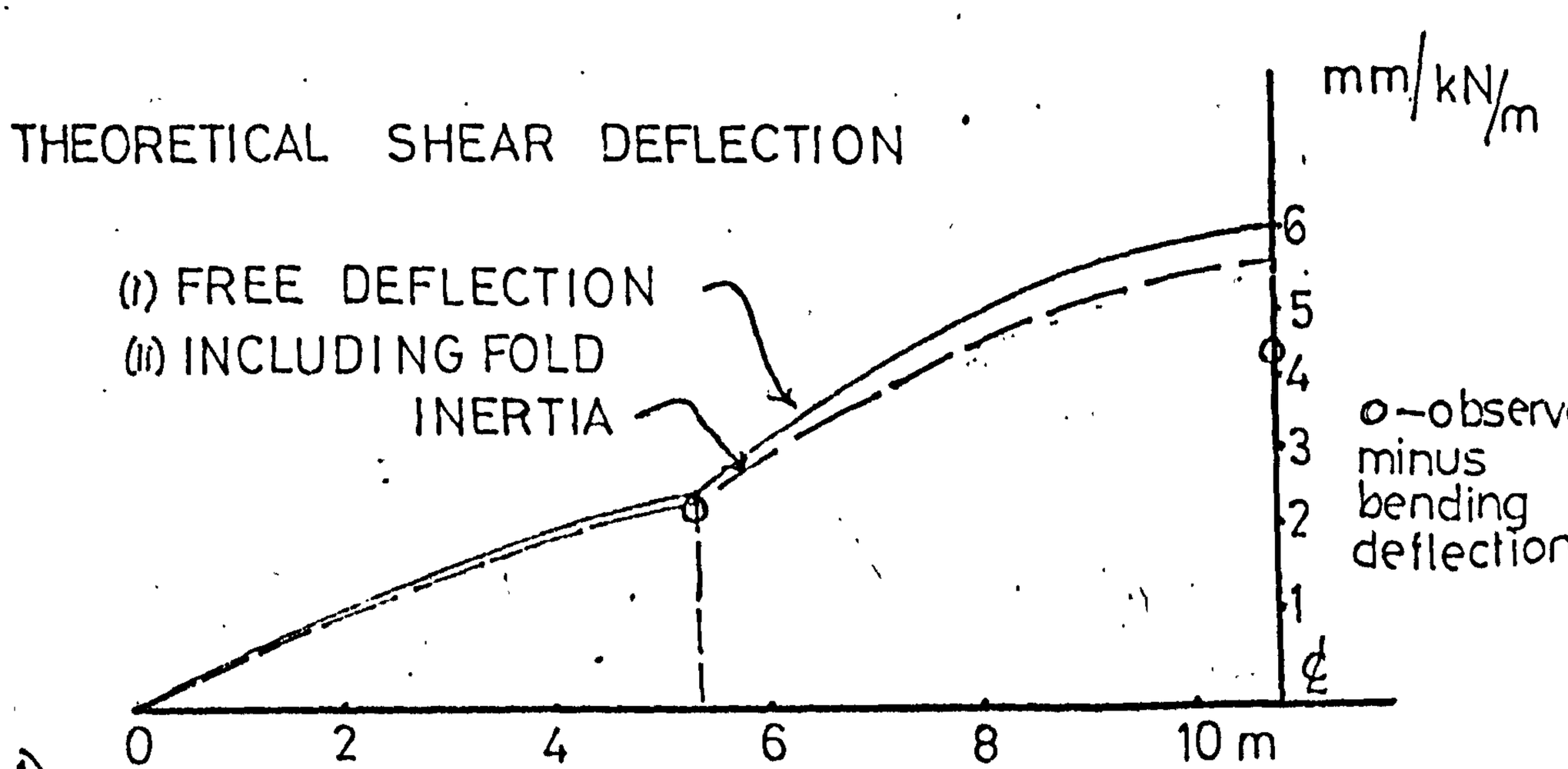

FIG(12.4)

DESIGN EXAMPLES FOR PROFILED SHEETING

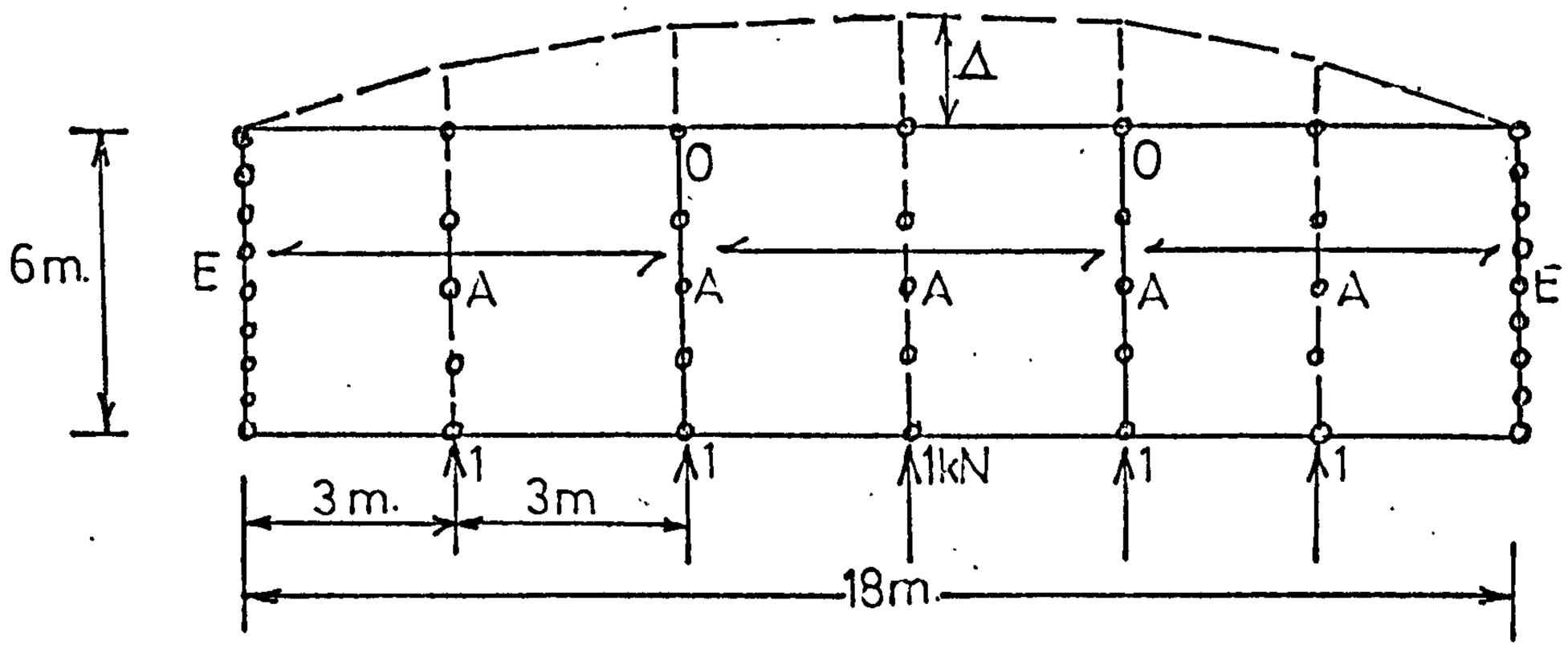

O— overlap; E—every trough fixing
A—alternate " "

superposition of $\delta_1 + \delta_2 = \Delta$

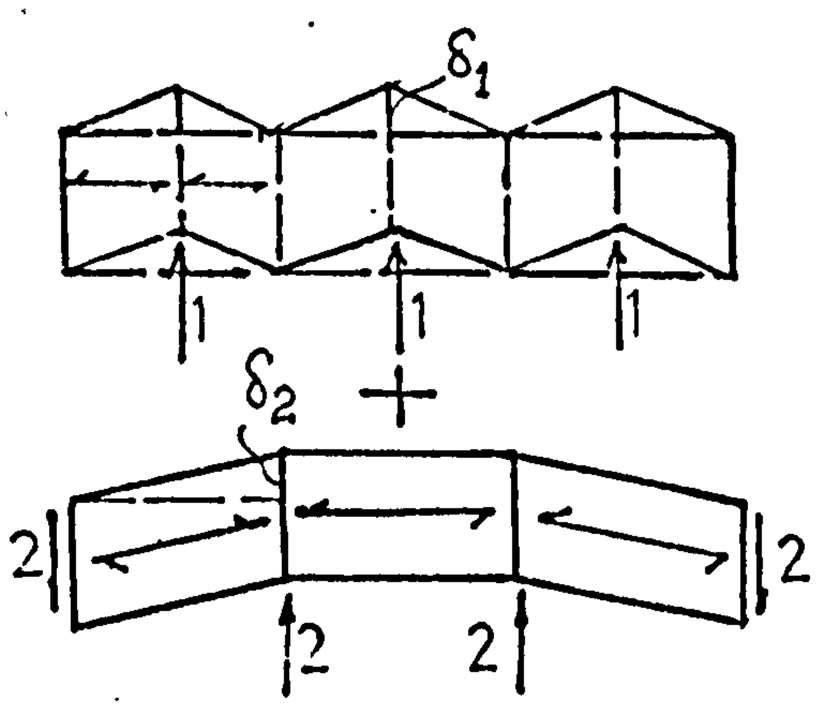

FIG(13.1) DEFLECTION OF TYPICAL CONTINUOUS DIAPHRAGM

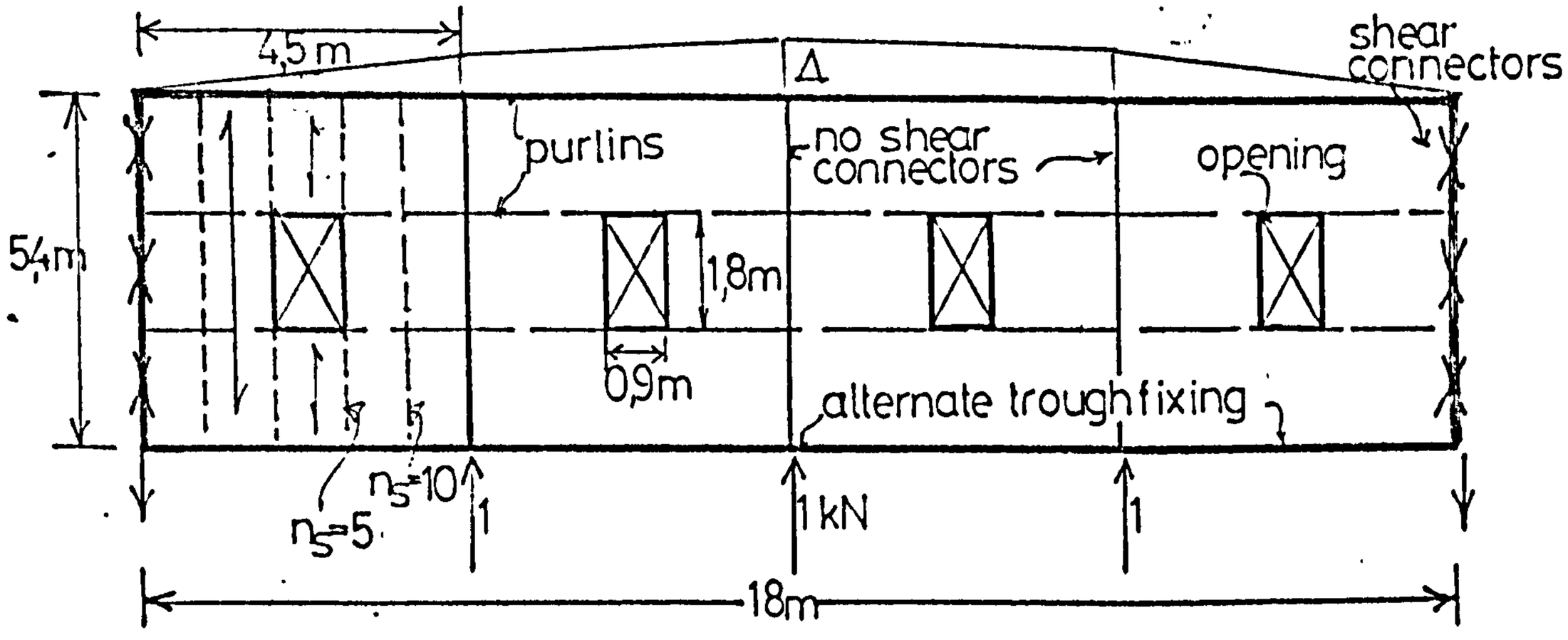

SHEET–PURLIN FASTENER FORCES AROUND OPENING:

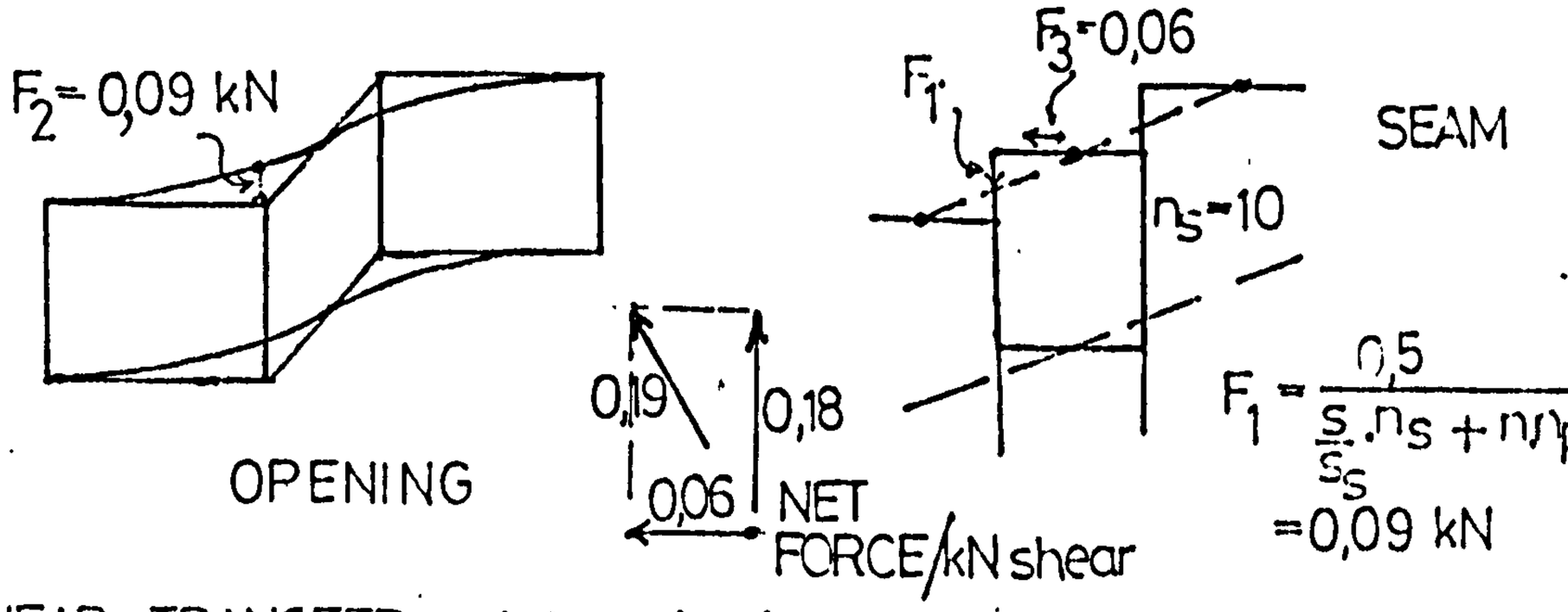

INDIRECT SHEAR TRANSFER —internal rafter

$$F_1 = \frac{0,5}{n.n_p.g} = \frac{0,5}{n_p.\frac{a_{eff}}{a}.\frac{n}{12}} \; ; \; \begin{matrix} a_{eff}=1,5m \\ n=16 \end{matrix} \; ; \; F_1 = \frac{0,5}{4,5.\frac{16}{12}} = 0,28 \text{ kN/kN rafter force}$$

FIG (13.2) DIAPHRAGM WITH OPENINGS —FIGS(8.23);(8.24)

APPENDIX 1. EXPERIMENTAL RESULTS

Table (1.1) Every corrugation fastening tests

(1.2) Alternate corrugation fastening tests

(1.3) Every corrugation fastening to intermediate purlins

(1.4) Every trough fastening at the sheet ends and alternate troughs at the intermediate purlins

(1.5) Alternate trough fastening to intermediate purlins

(1.6) Every third trough fastening tests

(1.7) Sheet overlaps fastened in every trough

(1.8) Sheet overlaps fastened in alternate troughs

(1.9) Sheets fastened in every trough at their ends and in alternate troughs at the overlaps

(1.10) Two bay continuous diaphragm tests

(1.11) Three bay continuous diaphragm tests

(1.12) Shear buckling of one bay diaphragms

(1.13) Shear buckling through intermediate purlins

TEST RESULTS FOR EVERY CORRUGATION FASTENING

Profile	Length m	Observed Flexibility	$C_{1.2}+C_{2.1}+C_{2.2}$ etc	K theory	$C_{1.1}$ theory mm/kN	Theoretical Flexibility	Experimental K value
1. 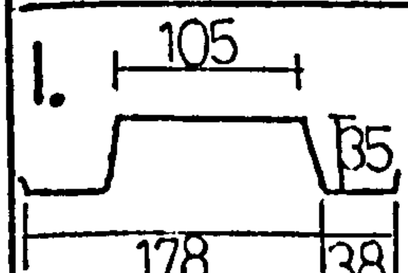 t = 0.57mm a = 1250mm	6.1	0.038	0.011	1.58	0.030	0.041	1.42
	5.1	0.055	0.014	1.43	0.049	0.063	1.20
	4.1	0.084	0.017	1.20	0.081	0.098	1.00
	3.1	0.141	0.027	0.91	0.142	0.163	0.77
As above a = 700mm	3.1	0.069	0.012	0.91	0.079	0.091	0.66
	2.1	0.130	0.018	0.61	0.167	0.185	0.41
	1.1	0.720	0.036	0.32	0.812	0.848	0.27
2. 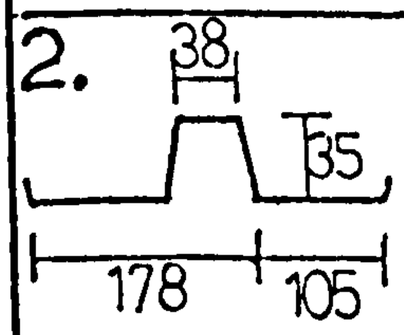 t = 0.57mm a = 1250mm	6.1	0.036	0.011	1.50	0.028	0.039	1.34
	5.1	0.052	0.014	1.25	0.043	0.057	1.10
	4.1	0.073	0.017	1.00	0.067	0.084	0.84
	3.1	0.121	0.021	0.75	0.115	0.136	0.65
As above a = 350mm	3.1	0.030	0.009	0.75	0.032	0.041	0.49
	2.1	0.052	0.013	0.50	0.068	0.081	0.29
	1.1	0.357	0.027	0.39	0.494	0.521	0.26

TABLE (1.1)

TEST RESULTS FOR EVERY CORRUGATION FASTENING

Profile	Length m	Observed Flexibility	$C_{1.2}+C_{2.1}+C_{2.2}$ etc	K theory	$C_{1.1}$ theory mm/kN	Theoretical Flexibility	Experimental K value
3. 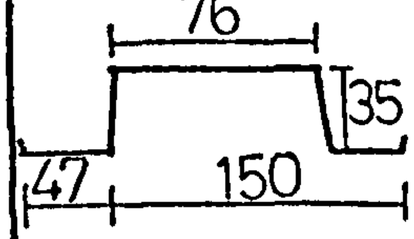 a = 900mm t = 0.67mm	6.1	0.013	0.0066	2.76	0.013	0.020	1.57
	5.1	0.020	0.0080	2.39	0.019	0.027	1.51
	4.1	0.029	0.010	1.94	0.029	0.039	1.27
	3.1	0.055	0.013	1.46	0.051	0.064	1.20
	2.1	0.14	0.020	0.97	0.129	0.149	0.90
	1.1	0.50	0.040	0.49	0.384	0.424	0.59
4. 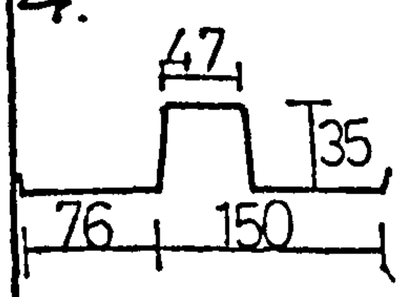 a = 600mm t = 0.67mm	6.1	0.0085	0.005	3.09	0.0095	0.0145	1.14
	4.1	0.019	0.008	2.09	0.021	0.029	1.02
	3.1	0.033	0.010	1.57	0.037	0.047	0.98
	2.1	0.085	0.015	1.03	0.078	0.093	0.92
	1.1	0.35	0.031	0.63	0.33	0.361	0.61
As above a = 1200mm	6.1	0.028	0.012	3.09	0.018	0.030	2.74
	5.1	0.039	0.014	2.59	0.027	0.041	2.40
	4.1	0.060	0.018	2.09	0.042	0.060	2.09
	3.1	0.092	0.024	1.57	0.073	0.095	1.46
	2.1	0.170	0.036	1.03	0.149	0.185	0.93
As above a = 150mm	6.1	0.0036	0.003	3.09	0.0023	0.0053	0.81
	4.1	0.0078	0.006	2.09	0.0052	0.0112	0.72
	2.1	0.019	0.009	1.03	0.019	0.028	0.54

TABLE (1.1) (Continued)

TEST RESULTS FOR EVERY CORRUGATION FASTENING

Profile	Length m	Observed Flexibility	$C_{1.2}+C_{2.1}+C_{2.2}$ etc	K theory	$C_{1.1}$ theory mm/kN	Theoretical Flexibility	Experimental K value
5. 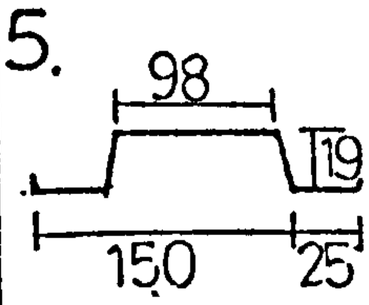 t = 0.46mm a = 1050mm	5.1	0.028	0.009	0.76	0.021	0.030	0.69
	4.1	0.050	0.012	0.67	0.036	0.048	0.70
	3.1	0.094	0.016	0.57	0.071	0.087	0.62
	2.1	0.150	0.023	0.41	0.165	0.188	0.32
6. 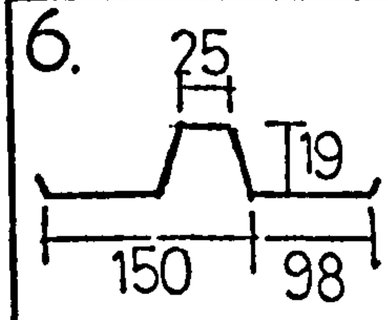 t = 0.46mm a = 1050mm	5.1	0.022	0.009	0.61	0.017	0.026	0.47
	4.1	0.035	0.012	0.50	0.027	0.039	0.43
	3.1	0.060	0.076	0.37	0.046	0.062	0.35
	2.1	0.120	0.023	0.25	0.100	0.123	0.25
7. 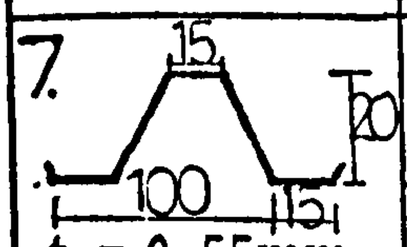 t = 0.55mm a = 1000mm	4.1	0.018	0.012	0.533	0.003	0.015	1.06
	2.1	0.050	0.023	0.311	0.014	0.037	0.60
8. 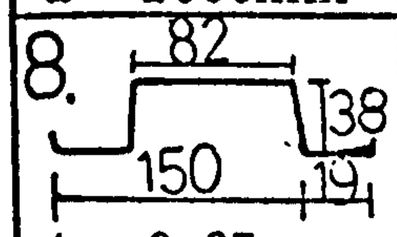 t = 0.67mm a = 1800mm	4.1	0.065	0.016	1.49	0.045	0.061	1.62
	2.1	0.261	0.031	0.94	0.211	0.242	1.03
9. 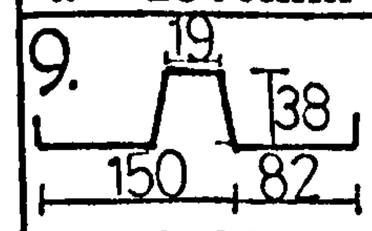 t = 0.67mm a = 1800mm	4.1	0.076	0.016	1.64	0.050	0.066	1.96
	2.1	0.284	0.031	0.81	0.245	0.276	0.84
10. 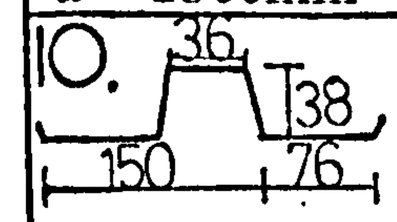 t = 0.65mm a = 4500mm	6.6	0.130	0.045	3.29	0.076	0.121	3.67

TABLE (1.1) (Continued)

TEST RESULTS FOR EVERY CORRUGATION FASTENING

Profile	Length m	Observed Flexibility	$C_{1.2}+C_{2.1}+C_{2.2}$ etc	K theory	$C_{1.1}$ theory mm/kN	Theoretical Flexibility	Experimental K value
11. 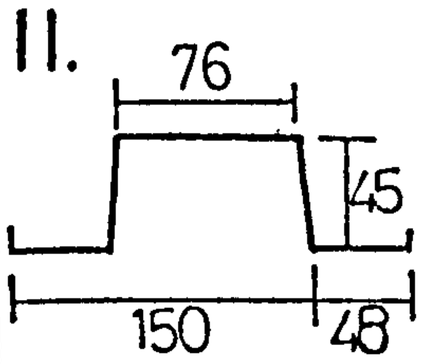 t = 0.67mm a = 1200mm	5.1	0.041	0.010	3.37	0.035	0.045	2.98
	4.1	0.066	0.014	2.71	0.054	0.068	2.61
	3.1	0.120	0.018	2.03	0.103	0.121	2.01
	2.1	0.210	0.027	1.35	0.200	0.227	1.22
	1.1	0.86	0.054	0.71	0.739	0.793	0.77
12. 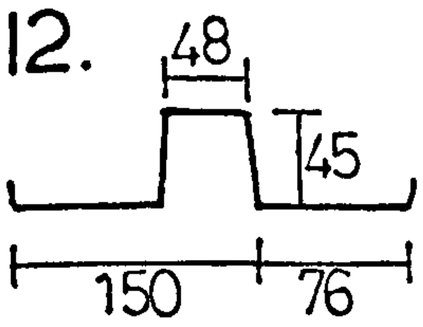 t = 0.67mm a = 1200mm	5.1	0.051	0.010	3.75	0.039	0.049	3.94
	4.1	0.075	0.014	3.01	0.058	0.072	3.16
	3.1	0.130	0.018	2.25	0.106	0.124	2.33
	2.1	0.290	0.027	1.48	0.256	0.283	1.49
	1.1	1.06	0.054	1.04	1.00	1.054	1.10
13. 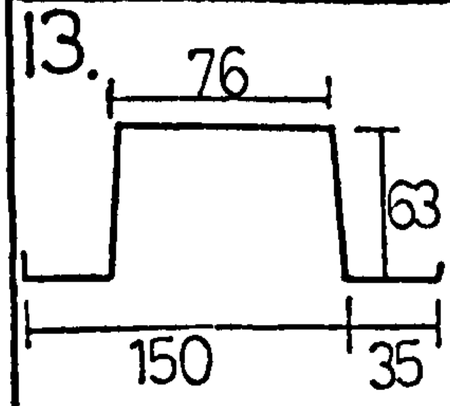 t = 0.67mm a = 1200mm	6.1	0.036	0.009	4.81	0.029	0.038	4.47
	5.1	0.051	0.011	4.16	0.042	0.053	3.96
	4.1	0.075	0.075	3.35	0.067	0.082	3.00
	3.1	0.140	0.019	2.49	0.128	0.147	2.35
	2.1	0.300	0.029	1.65	0.247	0.276	1.78
14. 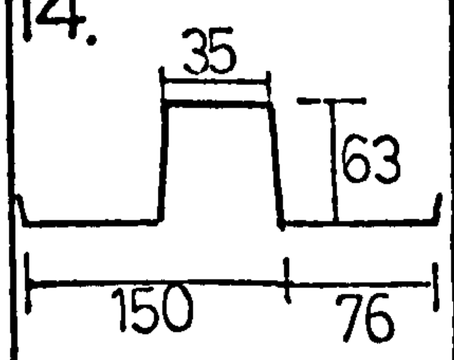 t = 0.67mm a = 1200mm	6.1	0.042	0.009	5.71	0.035	0.044	5.38
	5.1	0.060	0.011	4.77	0.050	0.061	4.67
	4.1	0.093	0.015	3.87	0.077	0.092	3.87
	3.1	0.170	0.019	2.82	0.131	0.150	3.25
	2.1	0.340	0.029	1.96	0.293	0.322	2.06

TABLE (1.1) (Continued)

TEST RESULTS FOR ALTERNATE CORRUGATION FASTENING

Profile	Length m	Observed Flexibility	$C_{1.2}+C_{2.1}+C_{2.2}$ etc	K theory	$C_{1.1}$ theory mm/kN	Theoretical Flexibility	Experimental K value
1. 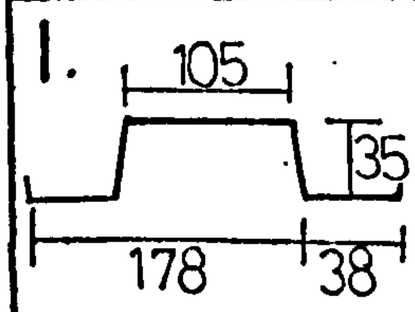 a = 1250mm	6.1	0.195	0.011	11.2	0.224	0.235	9.20
	5.1	0.268	0.014	9.4	0.321	0.335	7.44
	4.1	0.451	0.017	7.8	0.514	0.531	6.59
	3.1	0.820	0.021	6.7	1.02	1.04	5.42
As above a = 700mm	3.1	0.475	0.012	6.7	0.572	0.584	5.32
	2.1	1.19	0.018	5.9	1.62	1.64	4.33
	1.1	7.84	0.036	5.4	10.3	10.34	4.14
2. 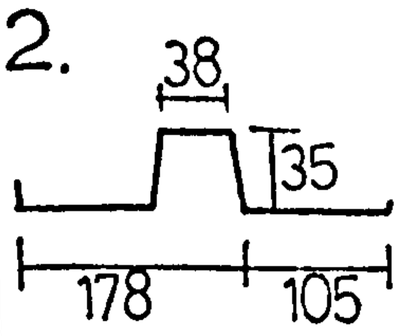 a = 1250mm	6.1	0.121	0.011	5.8	0.116	0.127	5.50
	5.1	0.164	0.014	4.9	0.168	0.182	4.38
	4.1	0.275	0.017	4.3	0.283	0.300	3.80
	3.1	0.505	0.021	3.7	0.564	0.585	3.20
As above a = 350mm	3.1	0.130	0.009	3.7	0.158	0.167	2.83
	2.1	0.386	0.013	3.4	0.467	0.480	2.72
	1.1	1.86	0.027	3.1	2.96	2.99	1.92

TABLE (1.2)

TEST RESULTS FOR ALTERNATE CORRUGATION FASTENING

Profile	Length m	Observed Flexibility	$C_{1.2}+C_{2.2}+C_{2.1}$ etc	K theory	$C_{1.1}$ theory mm/kN	Theoretical Flexibility	Experimental K value
3. 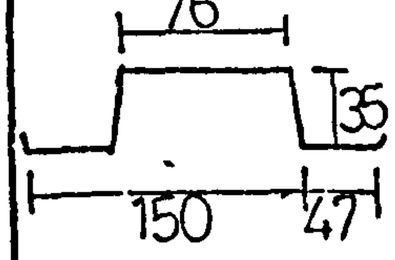 a = 900mm	6.1	0.064	0.007	16.20	0.074	0.083	12.5
	5.1	0.103	0.008	13.51	0.106	0.114	12.0
	4.1	0.18	0.010	11.03	0.167	0.177	11.2
	3.1	0.33	0.013	9.19	0.322	0.335	9.1
	2.1	0.93	0.020	7.98	0.900	0.920	8.01
	1.1	5.6	0.040	6.99	5.51	5.54	7.06
4. 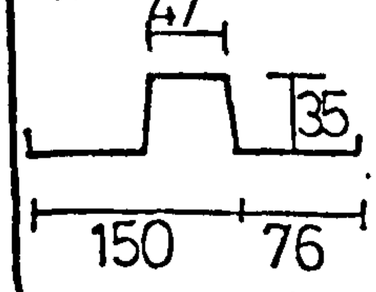 a = 600mm	6.1	0.032	0.005	13.29	0.042	0.047	8.55
	4.1	0.087	0.008	9.16	0.093	0.101	7.78
	3.1	0.19	0.010	7.70	0.182	0.192	7.61
	2.1	0.52	0.015	6.65	0.505	0.520	6.52
	1.1	2.8	0.031	5.87	3.10	3.13	5.30
As above a = 1200mm	6.1	0.085	0.012	13.29	0.081	0.093	12.00
	5.1	0.12	0.014	11.07	0.115	0.129	10.17
	4.1	0.22	0.018	9.16	0.184	0.202	8.24
	3.1	0.37	0.024	7.70	0.358	0.382	7.75
	2.1	1.07	0.036	6.65	0.994	1.03	6.90

TABLE (1.2) (Continued)

TEST RESULTS FOR ALTERNATE CORRUGATION FASTENING

Profile	Length m	Observed Flexibility	$C_{1.2}+C_{2.1}+C_{2.2}$ etc	K theory	$C_{1.1}$ theory mm/kN	Theoretical Flexibility	Experimental K value
5. 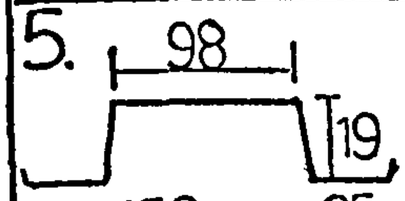 a = 1050mm	5.1	0.162	0.009	7.34	0.205	0.214	5.48
	4.1	0.29	0.012	5.90	0.318	0.340	5.16
	3.1	0.50	0.016	4.46	0.556	0.572	3.82
	2.1	1.02	0.023	3.40	1.36	1.38	2.5
6. 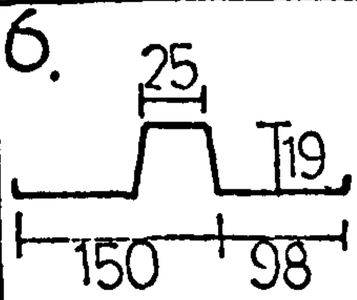 a = 1050mm	5.1	0.071	0.009	2.52	0.070	0.079	2.23
	4.1	0.11	0.012	2.01	0.108	0.120	1.82
	3.1	0.20	0.016	1.57	0.195	0.211	1.45
	2.1	0.55	0.023	1.29	0.517	0.540	1.31
7. 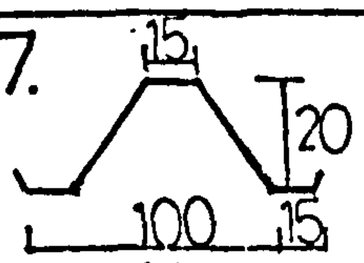 a = 1000mm	2.1	1.00	0.023	5.46	1.13	1.15	4.73
	4.1	0.08	0.012	12.02	0.073	0.085	11.2
8. 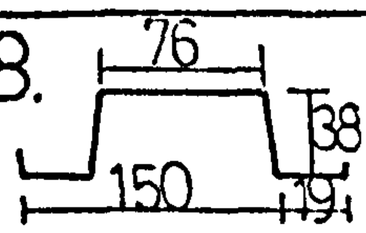 a = 1800mm	2.1	2.42	0.031	10.22	2.30	2.61	9.37
	4.1	0.50	0.016	17.12	0.512	0.53	16.1
9. 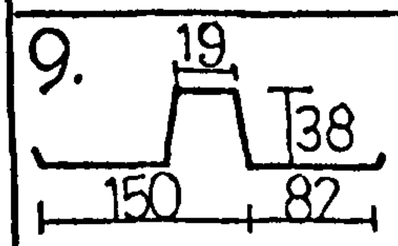 a = 1800mm	2.1	1.02	0.03	4.86	1.09	1.12	4.41
	4.1	0.23	0.016	6.64	0.201	0.22	6.97
10. 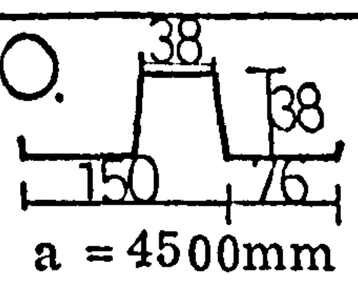 a = 4500mm	6.6	0.377	0.045	13.55	0.311	0.356	14.46

TABLE (1.2) (Continued)

TEST RESULTS FOR ALTERNATE CORRUGATION FASTENING

Profile	Length m	Observed Flexibility	$C_{1.2}+C_{2.1}+C_{2.2}$ etc	K theory	$C_{1.1}$ theory mm/kN	Theoretical Flexibility	Experimental K value
11. 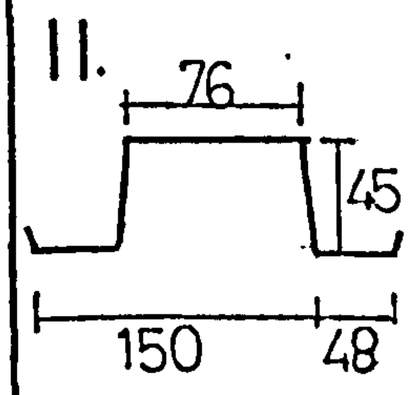 a = 1200mm t = 0.67mm	5.1	0.20	0.010	19.46	0.203	0.213	18.49
	4.1	0.34	0.014	16.35	0.328	0.342	16.88
	3.1	0.70	0.018	14.20	0.66	0.68	14.60
	2.1	2.02	0.027	12.83	1.92	1.95	13.36
	1.1	9.01	0.054	11.52	11.9	11.95	8.71
12. 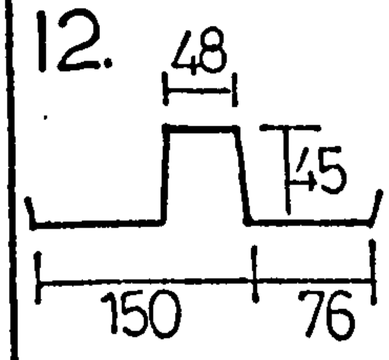 a = 1200mm t = 0.67mm	5.1	0.16	0.010	14.85	0.155	0.165	14.37
	4.1	0.32	0.014	12.76	0.321	0.355	12.36
	3.1	0.56	0.018	11.24	0.522	0.540	11.60
	2.1	1.62	0.027	10.10	1.51	1.54	10.71
	1.1	7.52	0.054	9.22	9.59	9.63	6.73
13. 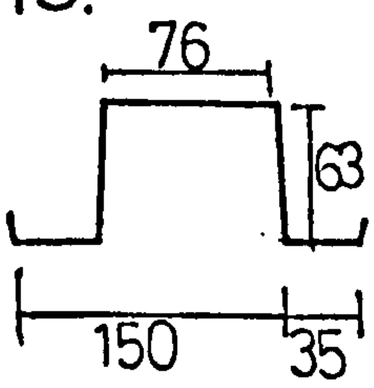 a = 1200mm t = 0.67mm	6.1	0.23	0.009	37.5	0.228	0.237	37.5
	5.1	0.37	0.011	32.6	0.340	0.351	33.3
	4.1	0.64	0.015	29.0	0.583	0.598	31.0
	3.1	1.18	0.019	25.2	1.17	1.19	25.0
	2.1	3.23	0.029	24.3	3.63	3.66	21.4
14. 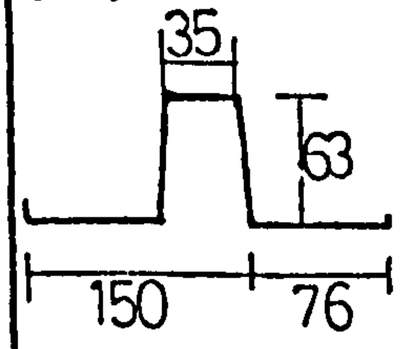 a = 1200mm t = 0.67mm	6.1	0.18	0.009	25.7	0.157	0.166	27.3
	5.1	0.26	0.011	23.0	0.242	0.251	24.0
	4.1	0.47	0.015	21.0	0.421	0.44	22.5
	3.1	0.95	0.019	19.6	0.910	0.930	20.1
	2.1	2.61	0.029	18.4	2.75	2.78	17.2

TABLE (1.2) (Continued)

TEST RESULTS FOR EVERY CORRUGATION FASTENING - INTERMEDIATE PURLIN EFFECTS

Profile	No. of inter. purlins	Length m	Obs. Flex. mm/kN	$C_{1.2}$ + $C_{2.1}$	K theory	$C_{1.1}$ theory	Theor. flex.	Theor. reduc-tion	Expt. reduc-tion
5. 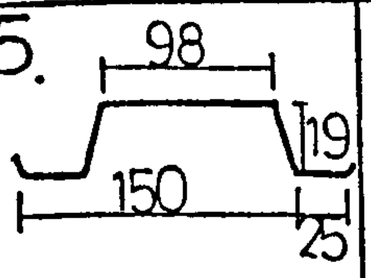	3	4.1	0.038	0.012	0.299	0.016	0.028	0.45	0.68
	2	3.1	0.075	0.016	0.387	0.048	0.062	0.68	0.73
6. 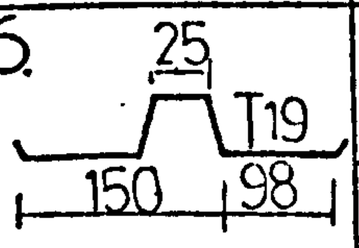	3	4.1	0.027	0.012	0.241	0.013	0.025	0.49	0.66
	2	3.1	0.048	0.016	0.244	0.030	0.046	0.66	0.73
14 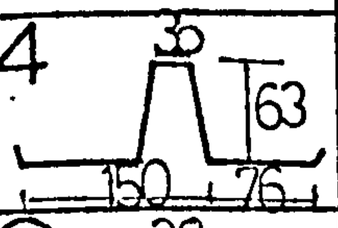	2	6.1	0.032	0.009	3.86	0.023	0.032	0.68	0.70
10. 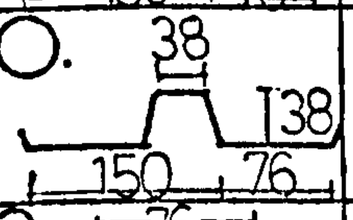	2	6.6	0.115	0.045	2.36	0.052	0.092	0.72	0.82
13. 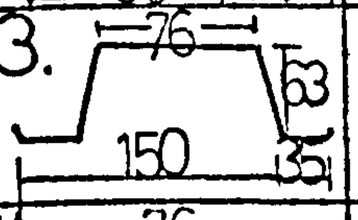	2	6.1	0.029	0.009	3.58	0.022	0.031	0.74	0.74
11. 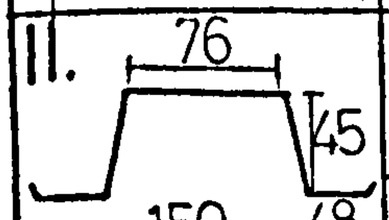	3	4.1	0.048	0.015	1.29	0.026	0.041	0.48	0.63
	2	3.1	0.090	0.019	1.37	0.064	0.083	0.67	0.71
	4	5.1	0.026	0.010	1.27	0.014	0.024	0.38	0.52
12. 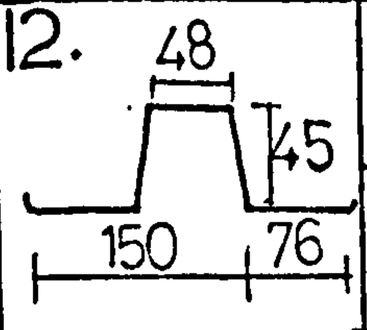	3	4.1	0.055	0.015	1.38	0.028	0.043	0.46	0.65
	2	3.1	0.10	0.019	1.42	0.066	0.085	0.63	0.73
	4	5.1	0.033	0.010	1.36	0.015	0.025	0.38	0.56

TABLE (1.3)

TEST RESULTS FOR EVERY CORRUGATION FASTENING AT ENDS AND IN ALTERNATE TROUGHS AT INTERMEDIATE PURLINS

6. 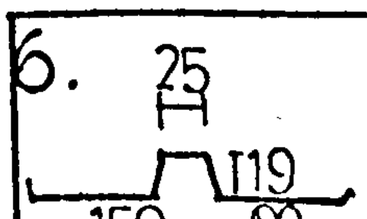	3	4.1	0.031	0.012	0.37	0.620	0.032	0.74	0.83
	2	3.1	0.055	0.016	0.31	0.038	0.052	0.84	0.90
10. 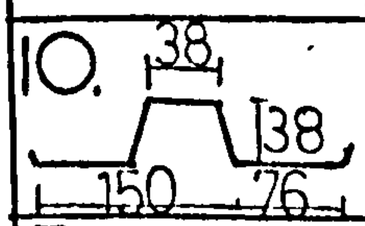	2	6.6	0.125	0.045	2.82	0.062	0.107	0.86	0.94
5. 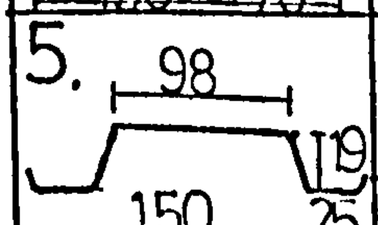	3	4.1	0.042	0.012	0.48	0.025	0.037	0.73	0.83
	2	3.1	0.086	0.016	0.47	0.059	0.075	0.82	0.89

TABLE (1.4)

TEST RESULTS FOR ALTERNATE CORRUGATION FASTENING - INTERMEDIATE PURLIN EFFECTS

Profile	No of inter purlins	Length m	Obs. Flex. mm/kN	$C_{1.2}+C_{2.1}+\ldots$	K theory	$C_{1.1}$ theory	Theor. Flex.	Theor. Reduc-tion	Expt. Reduc-tion
5. 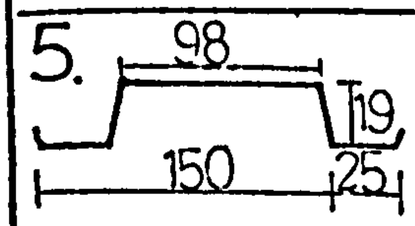	3	4.1	0.19	0.012	2.74	0.148	0.160	0.46	0.54
a = 1050mm	2	3.1	0.36	0.016	2.84	0.350	0.37	0.64	0.73
6. 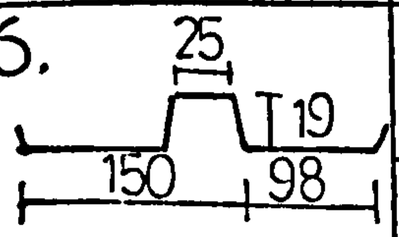	3	4.1	0.087	0.012	1.27	0.068	0.080	0.63	0.75
a = 1050mm	2	3.1	0.16	0.016	1.24	0.154	0.170	0.79	0.83
10. 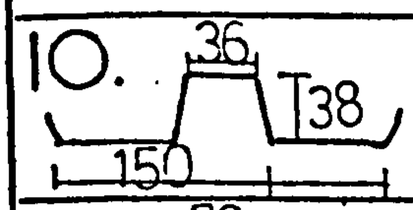	2	6.6	0.26	0.045	9.80	0.225	0.270	0.72	0.67
11. 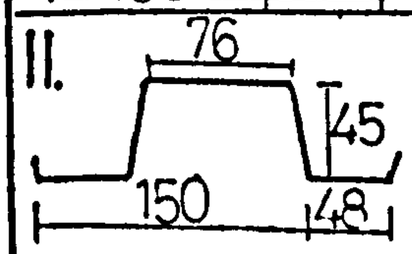	3	4.1	0.31	0.014	14.1	0.283	0.302	0.86	0.91
a = 1200mm	2	3.1	0.62	0.018	12.8	0.590	0.611	0.90	0.88

TABLE (1.5)

TEST RESULTS FOR EVERY THIRD TROUGH FASTENING

Profile	Length m	Obs. Flex. mm/kN	$C_{1.2}+C_{2.1}+\ldots$	K theory	$C_{1.1}$ theory	Theor. Flex.	Expt. K value
2. 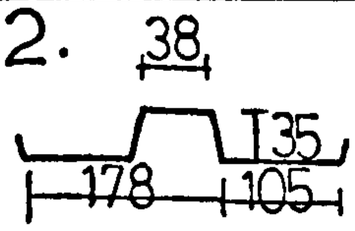	3.1	1.34	0.021	8.2	1.52	1.54	8.7
a = 1250mm	6.1	0.22	0.011	8.2	0.20	0.21	10.6
1. 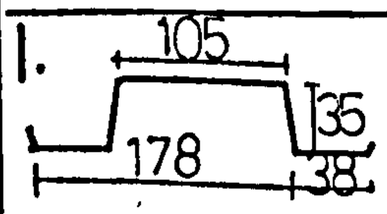	3.1	2.31	0.021	17.5	2.66	2.68	15.2
a = 1250mm	6.1	0.39	0.011	17.5	0.35	0.36	19.0

TABLE (1.6)

Experimental and theoretical reductions refer to K_N/K_1

where K_N is the K value for N intermediate purlins

and K_1 is the K value from Table (1.1) or (1.2)

This applies for Tables (1.3) to (1.5)

EFFECT OF OVERLAPPING SHEETS - EVERY CORRUGATION FASTENING

Profile	Length m	No. of overlaps	Observed flexibility mm/kN	$C_{1.2}+C_{2.1}+C_{2.2}$ etc	$\mathcal{E}$ theory	Individual $C_{1.1}$	Total C	
							Rigid	Flexible
1. 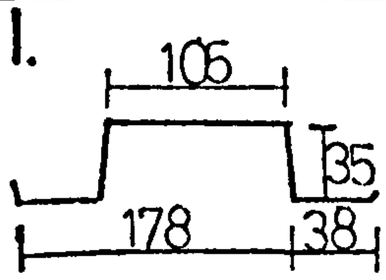 a = 700mm	6.1	1	0.025	0.006	0.33	0.043	0.017	0.020
	4.1	1	0.038	0.009	0.33	0.100	0.034	0.043
	6.1	2	0.022	0.006	0.33	0.100	0.023	0.029
	2.1	1	0.23	0.018	0.33	0.680	0.19	0.24
	4.1	3	0.07	0.009	0.33	0.680	0.072	0.084
	6.1	5	0.04	0.006	0.33	0.680	0.043	0.060
2. 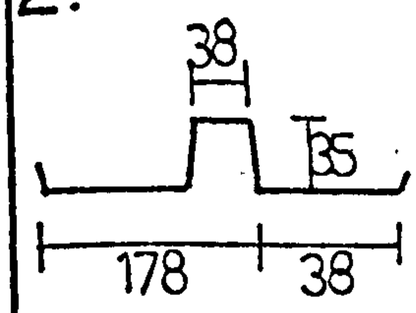 a = 350mm	6.1	1	0.013	0.006	0.22	0.019	0.010	0.012
	4.1	1	0.019	0.009	0.22	0.039	0.017	0.020
	6.1	2	0.010	0.006	0.22	0.039	0.010	0.015
	2.1	1	0.083	0.018	0.22	0.330	0.087	0.120
	4.1	3	0.029	0.009	0.22	0.330	0.033	0.048
	6.1	5	0.017	0.006	0.22	0.330	0.019	0.027
3. 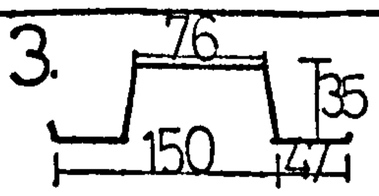 a = 900mm	4.1	1	0.050	0.010	0.47	0.12	0.048	0.055
	6.1	2	0.031	0.007	0.47	0.12	0.030	0.042
7. 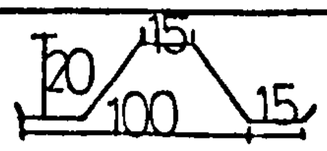 a = 1000mm	4.1	1	0.030	0.012	0.66	0.027	0.022	0.024
4. 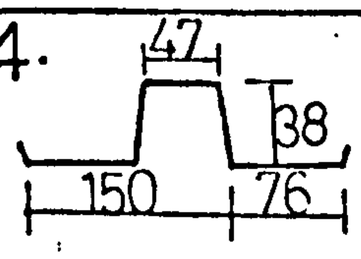 a = 600mm	4.1	1	0.032	0.010	0.37	0.07	0.029	0.034
	6.1	2	0.024	0.007	0.37	0.07	0.018	0.024

TABLE(1.7)

EFFECT OF OVERLAPPING SHEETS - EVERY CORRUGATION FIXING

Profile	Length m	No. of overlaps	Observed flexibility mm/kN	$C_{1.2}+C_{2.1}+C_{2.2}$ etc	$\mathcal{E}$ theory	Individual $C_{1.1}$	Total C	
							Rigid	Flexible
11. 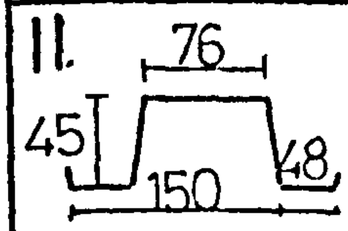 a =1200mm	4.1	1	0.060	0.012	0.45	0.183	0.055	0.065
	6.1	2	0.032	0.007	0.45	0.183	0.031	0.048
12. 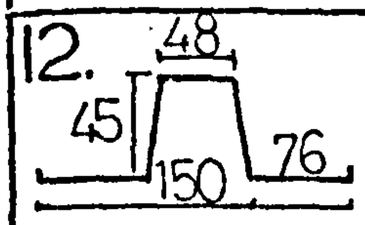 a = 1200mm	4.1	1	0.080	0.012	0.30	0.260	0.059	0.086
	6.1	2	0.038	0.007	0.30	0.260	0.034	0.057
13. 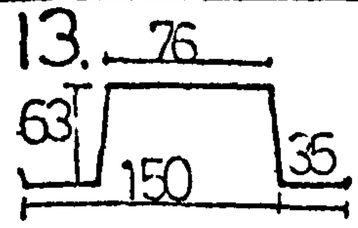 a = 1200mm	4.1	1	0.080	0.012	0.10	0.270	0.045	0.074
	6.1	2	0.050	0.007	0.10	0.270	0.022	0.049
14. 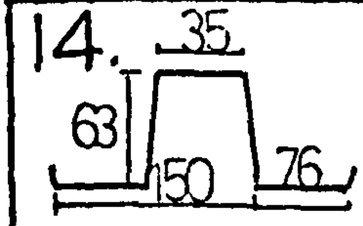 a = 1200mm	4.1	1	0.090	0.012	0.15	0.310	0.054	0.088
	6.1	2	0.052	0.007	0.15	0.310	0.026	0.062
5. 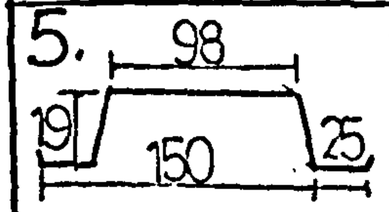 a = 1050mm	4.1	1	0.041	0.012	0.17	0.127	0.025	0.038
6. 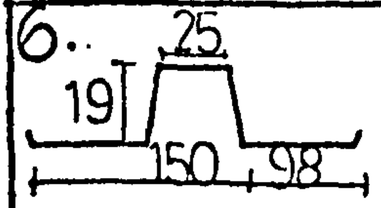 a = 1050mm	4.1	1	0.027	0.012	0.29	0.097	0.023	0.031

C_{RIGID} is the flexibility deduced from table (3.3)due to rigid plate movements

$$\simeq \frac{C_{1.1}}{n^3}(1+n^2\mathcal{E}) + (C_{1.2}+C_{2.1}+\ldots.)$$

$C_{FLEXIBLE}$ is the flexibility due to localised end distortion

$$\simeq \frac{C_{1.1}}{n^2}(1+n\mathcal{E}) + (C_{1.2}+C_{2.1}+\ldots.)$$

$C_{1.1}$ is the measured individual sheet flexibility due to fastening in every trough throughout

TABLE (1.7) (Continued)

EFFECT OF OVERLAPPING SHEETS - ALTERNATE CORRUGATION FIXING

Profile	Length m	No. of overlaps	Observed flexibility mm/kN	$C_{1.2}+C_{2.1}+C_{2.2}$ etc	$\mathcal{E}$ theory	Individual $C_{1.1}$	Total C	
							Rigid	Flexible
1. 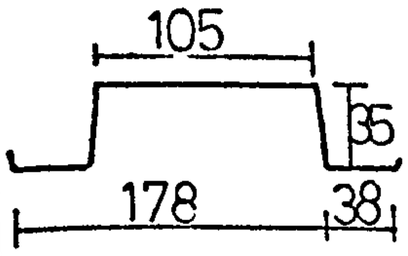 a = 700mm	6.1	1	0.12	0.006	0.25	0.463	0.108	0.151
	4.1	1	0.26	0.009	0.25	1.06	0.242	0.342
	6.1	2	0.15	0.006	0.25	1.06	0.128	0.240
	2.1	1	1.7	0.018	0.25	6.00	1.33	1.90
	4.1	3	0.55	0.009	0.25	6.00	0.483	0.585
	6.1	5	0.35	0.006	0.25	6.00	0.310	0.425
2. 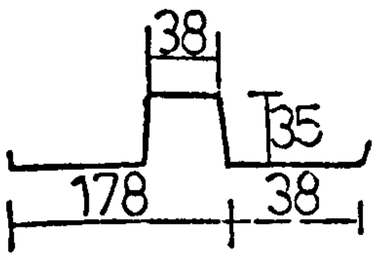 a = 350mm	6.1	1	0.041	0.006	0.33	0.121	0.036	0.045
	4.1	1	0.091	0.009	0.33	0.373	0.102	0.131
	6.1	2	0.054	0.006	0.33	0.373	0.058	0.093
	2.1	1	0.52	0.018	0.33	1.83	0.48	0.62
	4.1	3	0.19	0.009	0.33	1.83	0.173	0.210
	6.1	5	0.10	0.006	0.33	1.83	0.115	0.151
3 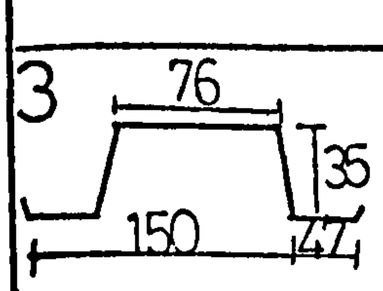 a = 900mm	4.1	1	0.25	0.010	0.11	0.93	0.169	0.265
	6.1	2	0.18	0.007	0.11	0.93	0.073	0.174
4 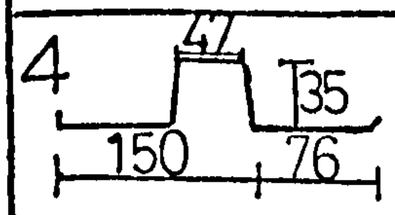 a = 600mm	4.1	1	0.15	0.010	0.12	0.50	0.095	0.150
	6.1	2	0.075	0.007	0.12	0.50	0.044	0.099
7. 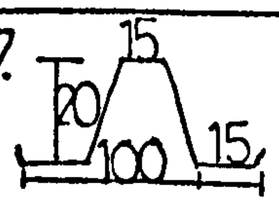 a = 100mm	4.1	1	0.42	0.009	0.84	0.98	0.44	0.47

TABLE (1.8)

EFFECT OF OVERLAPS - ALTERNATE CORRUGATION FIXING

Profile	Length m	No. of overlaps	Observed flexibility mm/kN	$C_{1.2}+C_{2.1}+C_{2.2}$ etc	$\mathcal{E}$ theory	Individual $C_{1.1}$	Total C	
							Rigid	Flexible
11. 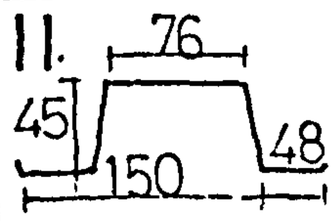 a = 1200mm	6.1	2	0.24	0.007	0.08	1.97	0.13	0.34
	4.1	1	0.52	0.012	0.08	1.97	0.31	0.55
12. 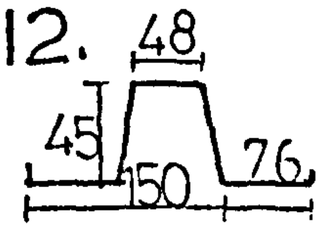 a = 1200mm	6.1	2	0.20	0.007	0.09	1.57	0.12	0.27
	4.1	1	0.38	0.012	0.09	1.57	0.25	0.44
13 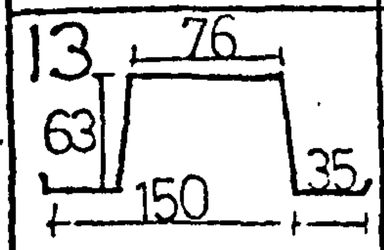 a = 1200mm	6.1	2	0.35	0.007	0.04	3.2	0.15	0.57
	4.1	1	0.80	0.012	0.04	3.2	0.42	0.84
14. 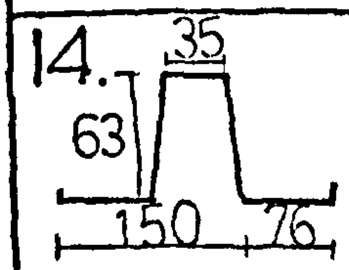 a = 1200mm	6.1	2	0.30	0.007	0.05	2.6	0.14	0.41
	4.1	1	0.60	0.012	0.05	2.6	0.35	0.68
5. 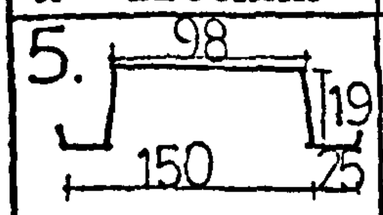 a = 1050mm	4.1	1	0.34	0.007	0.57	1.00	0.34	0.39
6. 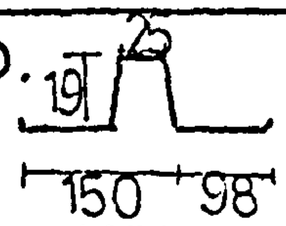 a = 1050mm	4.1	1	0.16	0.012	0.64	0.52	0.17	0.22

C_{RIGID} is the flexibility deduced from table(3.3) due to rigid plate movements

$$\simeq \frac{C_{1.1}}{n^3}\ (1+n^2\mathcal{E}\ ) + (C_{1.2} + C_{2.1} + \ldots.)$$

$C_{FLEXIBLE}$ is the flexibility due to localised end distortion

$$\simeq \frac{C_{1.1}}{n^2}\ (1+n\,\mathcal{E}\ ) + (C_{1.2} + C_{2.1} + \ldots.)$$

$C_{1.1}$ is the measured individual sheet flexibility due to fastening in alternate troughs throughout

EFFECT OF OVERLAPPING SHEETS - EVERY CORRUGATION FIXING AT ENDS, ALTERNATE AT THE OVERLAPS

Profile	Length m	No. of overlaps	Observed flexibility mm/kN	$C_{1.2}+C_{2.1}+C_{2.2}$ etc	$\mathcal{E}$ theory	Individual $C_{1.1}$	Total C	
							Rigid	Flexible
1 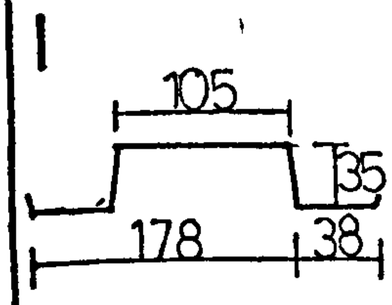 a = 700mm	6.1	2	0.075	0.006	0.25	1.08	0.087	0.103
	4.1	1	0.120	0.009	0.25	1.08	0.117	0.150
	6.1	5	0.24	0.006	0.25	6.00	0.246	0.344
	4.1	3	0.31	0.009	0.25	6.00	0.306	0.376
2. 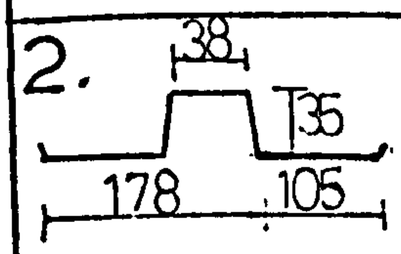 a = 350mm	6.1	5	0.10	0.004	0.33	1.86	0.126	0.167
	4.1	3	0.13	0.007	0.33	1.86	0.131	0.170
3. 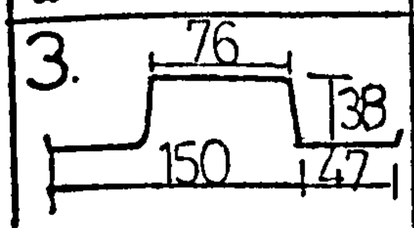 a = 900mm	6.1	2	0.063	0.007	0.11	0.93	0.066	0.077
	4.1	1	0.084	0.010	0.11	0.93	0.088	0.097
4. 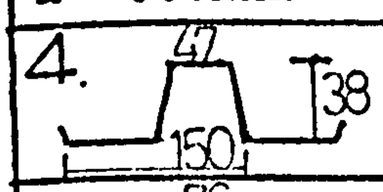 	6.1	2	0.041	0.007	0.12	0.50	0.040	0.052
11. 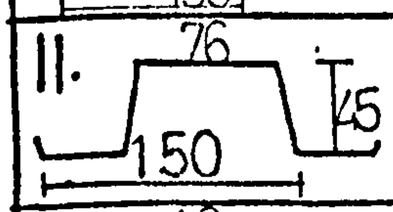 	6.1	2	0.11	0.007	0.08	1.97	0.090	0.116
12. 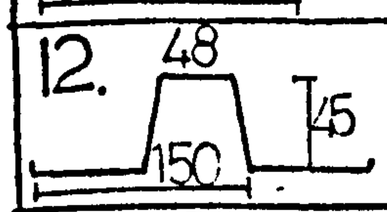 	6.1	2	0.10	0.007	0.09	1.57	0.107	0.118
13. 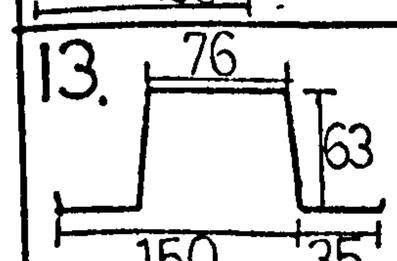 	6.1	2	0.12	0.007	0.04	3.17	0.128	0.138
	4.1	1	0.20	0.012	0.04	3.17	0.174	0.194
14. 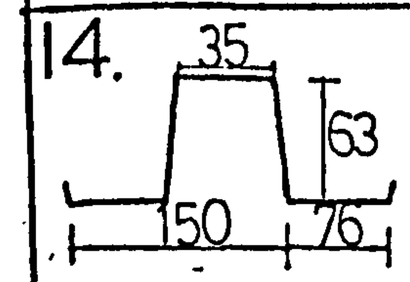 	6.1	2	0.13	0.007	0.05	2.57	0.083	0.088
	4.1	1	0.19	0.012	0.05	2.57	0.110	0.136
5. 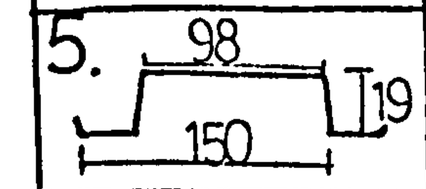 	4.1	1	0.19	0.007	0.57	1.00	0.152	0.221
6. 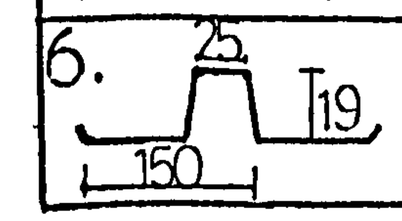 	4.1	1	0.097	0.012	0.64	0.63	0.105	0.162

TABLE (1.9)

C_{Total} is the value deduced from Table (3.4)

TEST RESULTS FOR TWO BAY TEST OF CONTINUOUS DIAPHRAGM

Description of test	Observed Flexibility	$C_{1.2}+C_{2.1}+C_{2.2}$ etc	$C_{1.1}$ mm/kN	K_{expt}	K_{rigid}	K_{free}
A.D.C.	1.60	0.02	1.58	3.00	5.4	5.8
A.D.O.(150)	2.02	0.02	2.00	3.80	5.4	5.8
A.D.O.(50)	2.24	0.02	2.20	4.18	5.4	5.8
A.D.O.(0)	2.61	0.02	2.59	4.92	5.4	5.8
E.D.C.	0.18	0.02	0.16	0.30	0.32	0.53
E.D.O.(150)	0.19	0.02	0.17	0.32	0.32	0.53
E.D.O.(50)	0.21	0.02	0.19	0.36	0.32	0.53
E.D.O.(0)	0.25	0.02	0.23	0.44	0.32	0.53
A.R.C.	0.58	0.02	0.56	1.06	3.1	3.3
A.R.O.(150)	0.72	0.02	0.70	1.33	3.1	3.3
A.R.O.(50)	0.86	0.02	0.84	1.60	3.1	3.3
A.R.O.(0)	1.40	0.02	1.38	2.63	3.1	3.3
E.R.C.	0.12	0.02	0.10	0.19	0.35	0.47
E.R.C.(150)	0.13	0.02	0.11	0.21	0.35	0.47
E.R.C.(50)	0.16	0.02	0.14	0.27	0.35	0.47
E.R.O.(0)	0.25	0.02	0.23	0.44	0.35	0.47

KEY as for Table (1.11)

Frame flexibility 15mm/kN

TABLE (1.10)

TEST RESULTS FOR THREE BAY TEST OF CONTINUOUS DIAPHRAGM

Description of test	Observed flexibility	$C_{1.2}+C_{2.1}+C_{2.2}$ etc	$C_{1.1}$ mm/kN	$K_{expt.}$	K_{rigid}	K_{free}
A.D.C.	3.40	0.04	3.36	3.20	5.4	5.8
A.D.O. (150)	4.20	0.04	4.16	3.95	5.4	5.8
A.D.O. (0)	5.22	0.04	5.18	4.02	5.4	5.8
E.D.C.	0.37	0.04	0.33	0.31	0.32	0.53
E.D.O. (150)	0.42	0.04	0.38	0.36	0.32	0.53
E.D.O. (0)	0.50	0.04	0.46	0.44	0.32	0.53
A.R.C.	1.68	0.04	1.64	1.56	3.1	3.3
A.R.O. (150)	2.10	0.04	2.06	1.94	3.1	3.3
A.R.O. (0)	2.80	0.04	2.76	2.62	3.1	3.3
E.R.C.	0.30	0.04	0.26	0.25	0.35	0.47
E.R.O. (150)	0.39	0.04	0.35	0.33	0.35	0.47
E.R.O. (0)	0.50	0.04	0.46	0.44	0.35	0.47

Key: K_{rigid} - K value due to linear plate movements

K_{free} - K value due to free localized end distortion

A - alternate trough fastening

E - every trough fastening

D - decking profile of Fig (7.6)

R - roofing profile of Fig (7.5)

C - continuous sheeting across rafters

O(150) - sheeting overlapped by 150mm

O(0) - unconnected sheet overlap

Frame flexibility 30mm/kN

TABLE (1.11)

EXPERIMENTAL RESULTS FOR THE SHEAR BUCKLING OF CORRUGATED SHEETING - SIMPLE DIAPHRAGM TESTS

Profile	Fastening	Length b m	D_y $\times 10^3$	D_x	γ $\times 10^3$	Theoretical Failure $Q_{cr}.b$ kN	Observed buckling load kN
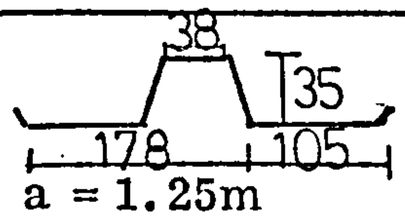 a = 1.25m t = 0.57mm	D	2.0	30.6	2.60	11.75	53	50
As above, with 0.75kN/m^2 u.d.l.	D	2.0	30.6	2.60	11.75	53	49
As above a = 1.25m	D	3.0	30.6	2.60	11.75	36	39
As above	E	2.0	Local buckling next to fastener			53	42
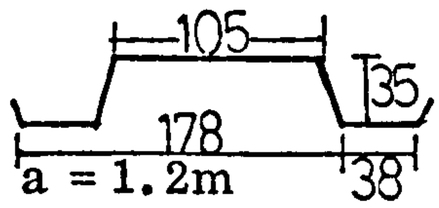 a = 1.2m t = 0.57mm	E	2.0	30.6	2.60	11.75	53	52
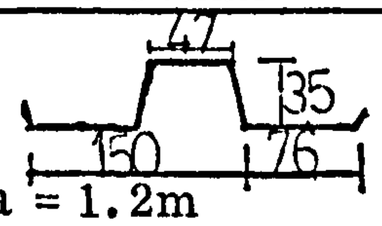 a = 1.2m t = 0.67mm	E	2.0	42.4	3.95	10.73	75	71
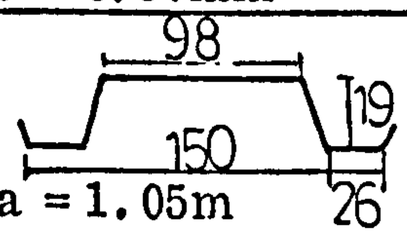 a = 1.05m t = 0.46mm	E	2.0	6.0	1.53	3.92	13	12
As above	E	3.0	6.0	1.53	3.92	9	10
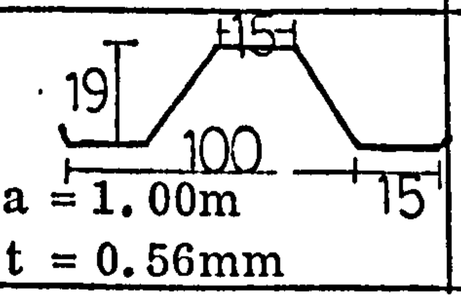 a = 1.00m t = 0.56mm	E	2.0	6.2	3.02	2.05	17	21

$$Q_{cr} = 36\, D_x^{1/4}\, D_y^{3/4}\, \frac{1}{b^2}$$

D - double fasteners per trough

E - every trough fastening

TABLE (1.12)

EXPERIMENTAL RESULTS FOR THE SHEAR BUCKLING OF CORRUGATED SHEETING - N INTERMEDIATE PURLINS

Profile	N	Fastening	Length b m	γ x10^3	Theoretical Failure $Q_{cr}.b$	Observed Failure kN	Expt. Ratio	b/p'
5. 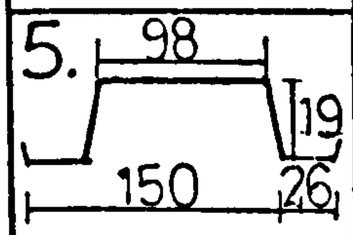	1	EE	2.0	3.92	52	42	0.81	13.3
a = 1.05m	1	EA	2.0	3.92	52	35	0.67	6.7
t = 0.46mm	2	AA	3.0	3.92	78	45	0.58	10.0
	2	EA	3.0	3.92	78	50	0.64	10.0
15. 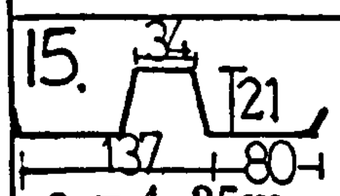 a = 4.35m t = 0.56mm	1	AA	4.0	4.05	49	40	0.81	13.3
2. 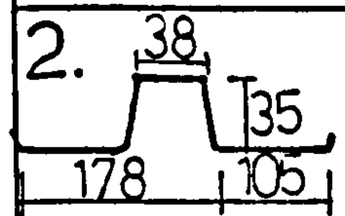 a = 4.35m t = 0.56mm	2	EA	6.0	11.75	159	106	0.67	20.0
	1	EA	4.0	11.75	106	75	0.70	13.3
	0	A	3.0	11.75	36	26	0.72	10.0
16. 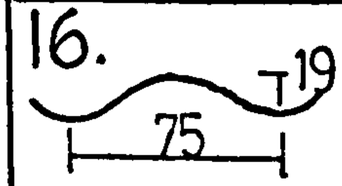 a = 4.15m t = 0.57mm	1	AF	3.0	3.25	72	49	0.68	10.0
7 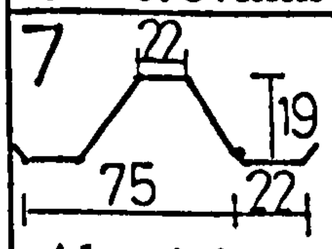 Aluminium a = 1.0m t = 0.56mm	1	ET	3.0	3.44	22	13	0.59	13.3
	0	T	2.0	3.44	8,5	7	0.82	8.7

Fastening:

EE - every corrugation throughout

EA - every at the ends, alternate internally

AA - alternate throughout

AF - alternate, at ends, every fourth trough internally

ET - every at ends, every third trough internally

A - alternate fastening at ends

T - every third trough fastening

b/p' - sheet length/fastener pitch

internally

TABLE (1.13)

APPENDIX 2. TABULATIONS OF THE FLEXIBILITY FACTORS $\bar{K}$ AND K

Table (2.1) $\bar{K}$ values for every trough fastening at 5^{o} side slope intervals

(2.2) $\bar{K}$ values for every trough fastening with two intermediate purlins

(2.3) $\bar{K}$ values for every trough fastening with three intermediate purlins

(2.4) $\bar{K}$ values for every trough fastening with four intermediate purlins

(2.5) $\bar{K}$ values for every trough fastening, excluding 'purlin-propping' effects, at 15^{o} side slope intervals

(2.6) $\bar{K}$ values, as above, for two intermediate purlins

(2.7) $\bar{K}$ values, as above, for three intermediate purlins

(2.8) $\bar{K}$ values, as above, for four intermediate purlins

(2.9) Values of the 'purlin-prop' reduction factor for every trough fastening

(2.10) $\bar{K}$ values for alternate trough fastening at 5^{o} side slope intervals

(2.11) $\bar{K}$ values for alternate trough fastening with two intermediate purlins

(2.12) $\bar{K}$ values for alternate trough fastening with three intermediate purlins

(2.13) $\bar{K}$ values for alternate trough fastening, excluding 'purlin-propping' effects, at 15^{o} side slope intervals

(2.14) $\bar{K}$ values, as above, for two intermediate purlins

(2.15) $\bar{K}$ values, as above, for three intermediate purlins

(2.16) Values of the 'purlin-prop' reduction factor for alternate trough fastening

(2.17) K values for alternate trough fastening including 'purlin-prop' reduction factor

(2.18) K values for every third trough fastening

(2.19) K values for every third trough fastening, excluding 'purlin-propping' effects

The shear flexibility due to distortion is given by

$$C_{1.1} = \frac{a\, d^{2.5}\, \bar{K}}{E\, t^{2.5}\, b^{2}} \quad \text{mm/kN}$$

where b is the sheet length, mm

t is the sheet thickness, mm

a is the panel width, mm

d is the profile pitch

E is Young's modulus, kN/mm^2

$\bar{K}$ is determined according to the above tables.

For alternate trough fastening $\bar{K}$ is taken as the greater of

$$\bar{K} \quad \text{and} \quad \frac{0.144\, d^{1.5}\, K}{t^{0.5}\, b}$$

For every third trough fastening, $\bar{K} = \frac{0.144\, d^{1.5}\, K}{t^{0.5}\, b}$

$\bar{K}$ VALUES FOR EVERY TROUGH FIXING

ONE OR NO INTERMEDIATE PURLINS; INCLUDING END RESTRAINT

h/d \ 2bT/d	0.1	0.2	0.3	0.4	0.5	0.6	0.7	0.8	0.9	
0.1	.013	.030	.044	.050	.048	.047	.053	.061	.089	θ=0°
0.2	.044	.101	.145	.165	.165	.171	.203	.256	.323	
0.3	.090	.208	.298	.336	.332	.343	.423	.516	.711	
0.4	.157	.350	.491	.560	.554	.568	.689	.877	1.24	
0.5	.227	.522	.735	.832	.828	.843	1.03	1.30	1.92	
	.014	.032	.044	.049	.047	.046	.057	.061	.092	
	.050	.102	.144	.155	.155	.163	.189	.246	.328	
	.113	.206	.288	.310	.320	.326	.391	.506	.860	θ=5°
	.180	.359	.459	.509	.503	.525	.609	.922	1.56	
	.315	.533	.711	.759	.746	.797	.917	1.43	2.58	
	.015	.033	.045	.047	.045	.045	.049	.061	.095	
	.057	.103	.143	.145	.146	.155	.177	.232	.533	
	.130	.204	.277	.291	.305	.311	.364	.490		θ=10°
	.209	.369	.422	.455	.432	.503	.544	.960		
	.401	.544	.659	.663	.639	.688	.797	1.49		
	.016	.033	.045	.046	.043	.045	.047	.061	.097	
	.065	.104	.141	.133	.135	.145	.165	.217		
	.147	.201	.261	.257	.248	.290	.323	.472		θ=15°
	.236	.379	.389	.390	.376	.463	.572			
	.421	.556	.537	.509	.459	.622	.737			
	.017	.033	.044	.044	.041	.042	.046	.063	.105	
	.070	.107	.134	.124	.124	.132	.151	.245		
	.161	.226	.248	.234	.231	.232	.344			θ=20°
	.274	.359	.371	.354	.302	.294	.520			
	.424	.521	.490	.408	.305	.431				

TABLE (2.1)

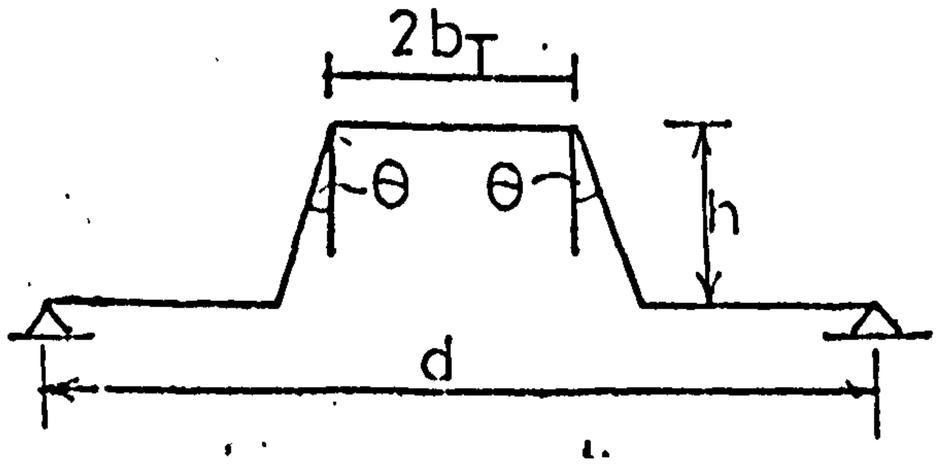

$\frac{2b_T}{d}$ / h/d	0.1	0.2	0.3	0.4	0.5	0.6	0.7	0.8	0.9
0.1	·018	·034	·043	·043	·038	·039	·045	·065	·115
0.2	·076	·110	·127	·117	·113	·120	·145	·303	
0.3	·170	·201	·222	·206	·201	·186	·481		
0.4	·282	·340	·305	·288	·206	·355			
0.5	·430	·424	·360	·250	·276				

θ=25°

·020	·034	·042	·041	·035	·035	·044	·068	
·082	·113	·121	·109	·098	·107	·149		
·176	·205	·193	·159	·155	·181			
·271	·275	·219	·169	·166				
·331	·281	·159	·122					

θ-30°

·021	·034	·041	·039	·032	·033	·042	·076	
·085	·110	·111	·106	·082	·111	·184		
·159	·168	·164	·108	·079	·135			
·246	·211	·109	·080					
·230	·169							

θ-35°

·022	·035	·040	·036	·028	·031	·035		
·087	·164	·092	·083	·065	·093			
·157	·146	·110	·055					
·168	·092	·034						
·063								

θ·40°

·024	·035	·039	·032	·026	·029	·049		
·089	·093	·081	·066	·038				
·128	·091	·056						
·059								

θ·45°

$\bar{K}$ VALUES FOR EVERY TROUGH FIXING

TWO INTERMEDIATE PURLINS ; INCLUDING END RESTRAINT

$\theta = 0°$

h/d \ 2bT/d	0.1	0.2	0.3	0.4	0.5	0.6	0.7	0.8	0.9
0.1	·011	·024	·034	·038	·038	·038	·042	·048	·095
0.2	·035	·078	·103	·118	·120	·129	·147	·156	·234
0.3	·064	·136	·192	·221	·228	·257	·289	·351	·470
0.4	·103	·224	·313	·355	·357	·385	·469	·600	·833
0.5	·150	·349	·492	·536	·537	·574	·705	·901	1.25

$\theta = 5°$

·012	·025	·034	·037	·037	·038	·040	·048	·092
·039	·076	·103	·112	·112	·124	·140	·157	·264
·078	·141	·189	·210	·216	·238	·274	·328	·638
·123	·239	·303	·327	·338	·376	·448	·555	1.11
·203	·368	·462	·471	·482	·523	·639	·856	1.89

$\theta = 10°$

·013	·025	·033	·036	·035	·035	·038	·047	·089
·044	·079	·102	·109	·107	·120	·130	·158	·338
·091	·149	·186	·195	·201	·225	·247	·315	
·156	·242	·290	·302	·316	·358	·386	·422	
·240	·365	·420	·428	·443	·483	·553		

$\theta = 15°$

·014	·025	·033	·035	·033	·033	·037	·046	·080
·050	·081	·101	·103	·099	·116	·120	·160	
·103	·154	·184	·185	·181	·210	·225	·335	
·176	·243	·273	·271	·270	·320	·377		
·265	·350	·371	·352	·385	·429	·493		

$\theta = 20°$

·014	·026	·033	·035	·031	·034	·036	·056	·128
·052	·081	·096	·097	·092	·096	·111	·267	
·110	·151	·174	·169	·170	·168	·226		
·180	·235	·257	·258	·233	·201	·357		
·270	·327	·339	·320	·228	·299			

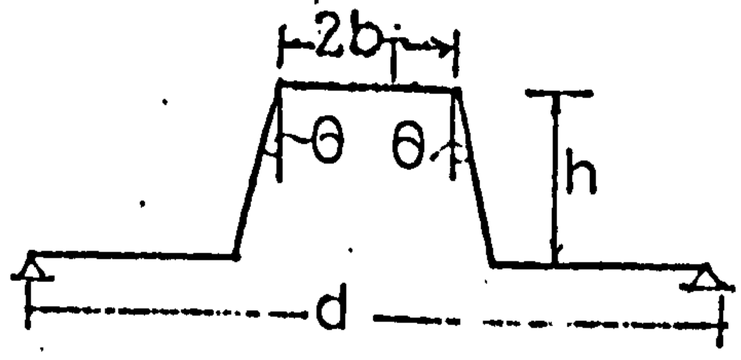

TABLE (2.2)

h/d \ $2b_T/d$	0.1	0.2	0.3	0.4	0.5	0.6	0.7	0.8	0.9
0.1	·014	·027	·032	·034	·029	·031	·035	·067	·121
0.2	·056	·082	·092	·093	·083	·082	·110	·306	
0.3	·117	·149	·158	·158	·147	·133	·277		
0.4	·182	·219	·220	·213	·146	·221			
0.5	·257	·300	·267	·184	·199				

θ·25°

·014	·028	·032	·034	·028	·028	·035	·090	
·061	·082	·088	·071	·073	·080	·112		
·123	·145	·141	·114	·115	·138			
·186	·174	·162	·124	·120				
·229	·202	·120	·090					

θ·30°

·016	·028	·031	·032	·027	·026	·035	·075	
·061	·077	·079	·071	·062	·073	·162		
·112	·120	·119	·088	·059	·119			
·139	·133	·066	·056					
·188	·089							

θ·35°

·018	·029	·030	·029	·026	·024	·035	·066	
·062	·070	·070	·062	·051	·071			
·105	·091	·079	·072					
·108	·068	·029						
·033								

θ40°

·020	·029	·029	·026	·026	·021	·035		
·064	·068	·056	·053	·048				
·092	·066	·044						
·041								

θ45°

$\bar{K}$ VALUES FOR EVERY TROUGH FIXING

THREE INTERMEDIATE PURLINS ; INCLUDING END RESTRAINT

$\theta = 0°$

h/d \ $2b_T$/d	0.1	0.2	0.3	0.4	0.5	0.6	0.7	0.8	0.9
0.1	.010	.021	.027	.028	.027	.029	.031	.032	.043
0.2	.028	.052	.071	.085	.085	.090	.105	.113	.151
0.3	.049	.103	.144	.159	.156	.186	.210	.248	.316
0.4	.081	.190	.261	.280	.262	.263	.332	.432	.603
0.5	.126	.318	.438	.460	.414	.391	.478	.659	.950

$\theta = 5°$

.011	.022	.026	.027	.025	.028	.030	.032	.043
.031	.054	.071	.082	.081	.086	.097	.108	.148
.049	.101	.139	.155	.154	.182	.200	.221	.320
.079	.181	.261	.266	.264	.280	.302	.377	.729
.123	.289	.417	.438	.424	.415	.430	.545	.962

$\theta = 10°$

.012	.022	.026	.027	.025	.025	.029	.032	.045
.034	.056	.071	.079	.077	.082	.088	.106	.193
.064	.111	.133	.137	.137	.155	.171	.205	
.121	.191	.220	.210	.211	.242	.277	.363	
.201	.306	.333	.307	.294	.341	.405	.670	

$\theta = 15°$

.013	.022	.026	.027	.025	.023	.028	.032	.046
.038	.057	.071	.072	.073	.076	.086	.102	
.074	.110	.127	.126	.128	.145	.153	.209	
.134	.183	.193	.182	.185	.224	.238		
.213	.280	.269	.239	.253	.299	.349		

$\theta = 20°$

.013	.022	.026	.026	.024	.022	.026	.033	.054
.042	.058	.069	.072	.067	.068	.074	.131	
.081	.108	.120	.116	.117	.118	.149	.206	
.131	.167	.178	.168	.149	.138	.156		
.205	.237	.224	.205	.185	.205			

TABLE (2.3)

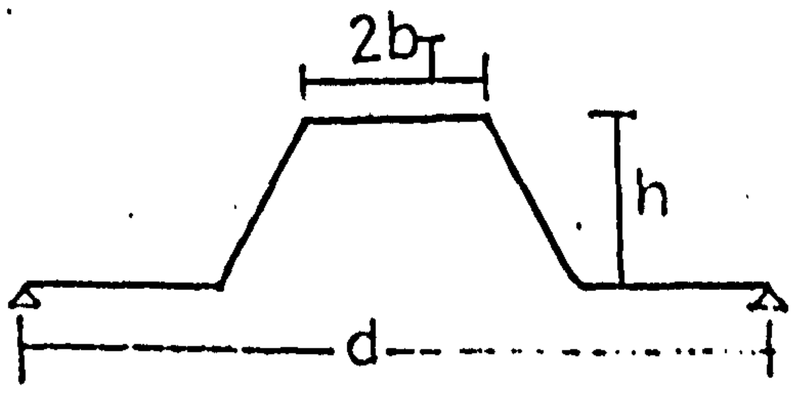

$\frac{2b_T}{d}$ / h/d	0.1	0.2	0.3	0.4	0.5	0.6	0.7	0.8	0.9
0.1	·014	·022	·025	·025	·023	·021	·025	·034	·058
0.2	·044	·059	·067	·067	·060	·059	·076	·086	
0.3	·083	·104	·109	·102	·100	·089	·159		
0.4	·133	·151	·148	·118	·098				
0.5	·182	·150	·118	·099					

θ=25°

·014	·022	·025	·025	·021	·021	·024	·036	
·046	·059	·064	·062	·051	·055	·070		
·086	·100	·097	·081	·077	·083			
·127	·138	·109	·083	·075				
·155	·140	·077	·069					

θ=30°

·017	·022	·024	·024	·020	·020	·025	·046	
·047	·056	·058	·051	·050	·053	·102		
·078	·084	·084	·073	·060	·089			
·097	·105	·059	·046					
·135	·069							

θ=35°

·020	·022	·023	·023	·019	·019	·026		
·048	·053	·052	·041	·040	·055			
·078	·084	·064	·053					
·087	·055	·024						
·028								

θ=40°

·023	·022	·022	·022	·018	·018	·026		
·048	·057	·041	·030	·033				
·060	·046	·025						
·036								

θ=45°

$\bar{K}$ VALUES FOR EVERY TROUGH FIXING

FOUR INTERMEDIATE PURLINS; INCLUDING END RESTRAINT

h/d \ 2bT/d	0.1	0.2	0.3	0.4	0.5	0.6	0.7	0.8	0.9	
0.1	·009	·017	·023	·025	·025	·026	·029	·030	·036	
0.2	·022	·042	·059	·064	·064	·068	·085	·096	·119	
0.3	·042	·094	·128	·136	·126	·122	·159	·207	·273	θ=0°
0.4	·073	·176	·244	·257	·229	·213	·250	·353	·573	
0.5	·120	·302	·422	·439	·386	·345	·385	·542	·843	

·010	·017	·023	·025	·025	·025	·028	·029	·037	
·025	·043	·058	·061	·061	·067	·087	·092	·142	
·048	·094	·120	·122	·118	·123	·150	·197	·307	θ·5°
·083	·171	·221	·216	·199	·202	·236	·379	·593	
·142	·288	·372	·346	·318	·279	·348	·584	1·03	

·011	·018	·022	·024	·025	·024	·027	·029	·038	
·028	·044	·057	·059	·059	·066	·078	·087	·159	
·055	·093	·112	·106	·107	·120	·142	·186		θ·10°
·093	·168	·191	·187	·169	·192	·226	·322		
·183	·279	·307	·258	·234	·264	·358			

·011	·018	·022	·024	·025	·023	·025	·028	·039	
032	·046	·055	·056	·056	·064	·074	·081		
·063	·093	·102	·096	·094	·118	·135	·171.		θ·15°
·106	·163	·164	·142	·136	·184	·214			
·199	·252	·232	·185	·186	·258	·323			

·011	·018	·022	·023	·023	·022	·024	·029	·045	
·032	·046	·053	·054	·053	·060	·067	·089		
·065	·087	·091	·087	·086	·097	·127			θ·20°
·105	·143	·148	·122	·118	·126	·191			
·186	·202	·182	·147	·135	·159				

TABLE (2.4)

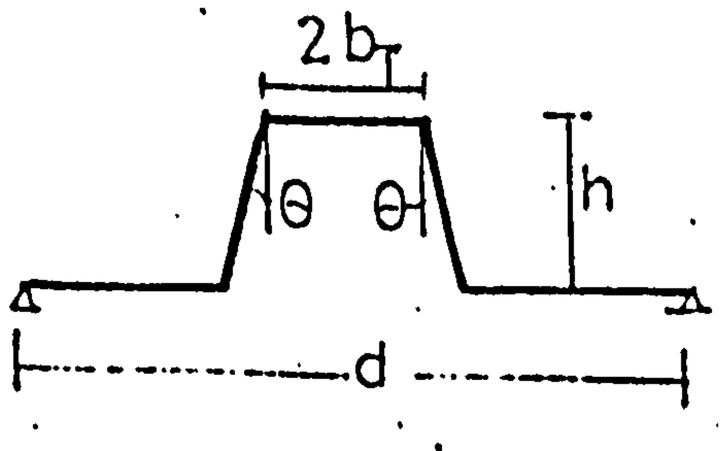

h/d \ $2b_T/d$	0.1	0.2	0.3	0.4	0.5	0.6	0.7	0.8	0.9
0.1	.011	.018	.022	.022	.021	.021	.023	.030	.056
0.2	.032	.045	.051	.051	.050	.055	.062	.126	
0.3	.067	.082	.082	.077	.078	.070	.139		
0.4	.103	.123	.112	.095	.088	.079			
0.5	.155	.151	.131	.104	.106				

$\theta = 25°$

.011	.017	.022	.021	.020	.020	.023	.031	
.032	.045	.049	.047	.045	.050	.057		
.069	.076	.073	.065	.076	.071			
.103	.100	.084	.076	.068				
.120	.104	.069	.053					

$\theta = 30°$

.012	.018	.021	.020	.019	.019	.020	.039	
.034	.044	.044	.040	.042	.042	.076		
.063	.069	.073	.066	.048	.079			
.076	.078	.055	.041					
.098	.049							

$\theta = 35°$

.013	.019	.020	.019	.018	.018	.017		
.036	.042	.039	.035	.035	.046			
.057	.062	.050	.038					
.063	.046	.018						
.023								

$\theta = 40°$

.015	.019	.020	.018	.016	.017	.014		
.038	.040	.035	.027	.028				
.052	.041	.021						
.025								

$\theta = 45°$

$\bar{K}$ VALUES FOR EVERY TROUGH FIXING

ONE OR NO INTERMEDIATE PURLINS ; NO 'PURLIN-PROP' RESTRAINT (r_E)

$\theta = 0°$

h/d \ 2bT/d	0.1	0.2	0.3	0.4	0.5	0.6	0.7	0.8	0.9
0.1	.013	.032	.049	.059	.059	.053	.053	.082	.194
0.2	.044	.106	.163	.199	.206	.196	.203	.291	.622
0.3	.090	.219	.335	.410	.426	.404	.423	.614	1.27
0.4	.151	.368	.564	.692	.719	.676	.698	1.02	2.14
0.5	.227	.550	.844	1.04	1.09	1.02	1.03	1.49	3.20

$\theta = 15°$

.017	.035	.049	.056	.053	.049	.048	.091	.243
.068	.124	.166	.182	.171	.153	.178	.350	
.159	.265	.337	.354	.318	.296	.387	.858	
.297	.457	.554	.548	.470	.463	.693		
.481	.695	.799	.738	.612	.655	1.17		

$\theta = 30°$

.021	.038	.049	.049	.041	.033	.049	1.26	
.091	.136	.159	.150	.117	.110	.204		
.209	.270	.282	.224	.164	.220			
.353	.390	.343	.194	.203				
.487	.461	.230	.144					

$\theta = 45°$

.027	.041	.073	.043	.032	.029	.058		
.109	.127	.115	.068	.054				
.189	.149	.048						
.089								

TABLE (2.5)

$\overline{K}$ VALUES FOR EVERY TROUGH FIXING

TWO INTERMEDIATE PURLINS ; NO 'PURLIN-PROP' RESTRAINT

$\theta = 0.0°$

h/d \ $2b_T/d$	0.1	0.2	0.3	0.4	0.5	0.6	0.7	0.8	0.9
0.1	·011	·026	·038	·045	·046	·042	·042	·064	·149
0.2	·035	·077	·116	·142	·150	·144	·147	·205	·457
0.3	·065	·145	·218	·271	·292	·289	·304	·418	·854
0.4	·103	·238	·360	·438	·463	·459	·493	·698	1.38
0.5	·151	·372	·566	·670	·680	·653	·705	1.04	2.08

$\theta = 15°$

·014	·028	·038	·043	·041	·035	·039	·072	·183
·052	·090	·120	·133	·125	·112	·129	·259	
·111	·178	·230	·257	·232	·214	·265	·610	
·193	·293	·365	·382	·345	·330	·456		
·305	·438	·516	·513	·453	·452	·752		

$\theta = 30°$

·018	·030	·038	·040	·035	·029	·039	·089	
·068	·098	·115	·109	·087	·080	·159		
·147	·191	·202	·164	·114	·170			
·245	·286	·253	·143	·146				
·337	·332	·173	·116					

$\theta = 45°$

·022	·032	·037	·034	·026	·024	·047		
·079	·093	·084	·053	·043				
·135	·110	·038						
·068								

TABLE (2.6)

$\bar{K}$ VALUES FOR EVERY TROUGH FIXING

THREE INTERMEDIATE PURLINS ; NO 'PURLIN-PROP' RESTRAINT

$\theta = 0°$

h/d \ $2b_T/d$	0.1	0.2	0.3	0.4	0.5	0.6	0.7	0.8	0.9
0.1	·010	·022	·030	·035	·035	·032	·031	·044	·094
0.2	·028	·056	·082	·099	·106	·103	·105	·140	·290
0.3	·050	·110	·164	·194	·202	·195	·200	·295	·575
0.4	·081	·199	·300	·346	·339	·312	·332	·503	1.06
0.5	·128	·332	·503	·576	·546	·472	·478	·757	1.59

$\theta = 15°$

·013	·023	·030	·034	·031	·027	·028	·048	·110
·039	·063	·084	·095	·091	·100	·106	·164	
·080	·127	·159	·170	·160	·147	·181	·380	
·147	·220	·257	·256	·231	·224	·322		
·241	·343	·372	·341	·298	·315	·554		

$\theta = 30°$

·015	·024	·030	·031	·026	·022	·027	·056	
·050	·070	·083	·080	·061	·055	·099		
·102	·131	·141	·113	·077	·107			
·168	·195	·173	·095	·092				
·228	·230	·111	·057					

$\theta = 45°$

·028	·026	·029	·026	·020	·018	·032		
·059	·069	·061	·047	·033				
·089	·076	·030						
·049								

TABLE(2.7)

$\bar{K}$ VALUES FOR EVERY TROUGH FIXING

FOUR INTERMEDIATE PURLINS ; 'NO PURLIN-PROP' RESTRAINT

$\theta = 0°$

h/d \ $2b_T/d$	0.1	0.2	0.3	0.4	0.5	0.6	0.7	0.8	0.9
0.1	·009	·018	·025	·029	.031	·029	·029	·039	·079
0.2	·023	:046	·066	·078	..080	·079	·087	·119	·230
0.3	·043	·099	·145	·167	·162	·148	·159	·247	·487
0.4	·074	·187	·280	·318	·298	·253	·254	·411	·885
0.5	·121	·321	·485	·549	·506	·411	·385	·623	1·43

$\theta = 15°$

·011	·019	·025	·029	·028	·025	·026	·042	·099
·034	·051	·066	·072	·071	·068	·077	·131	
:068	·108	·130	·130	·120	·120	·159	·311	
·131	·196	·219	·200	·170	·184	·291		
·229	·315	·323	·268	·219	·274	·513		

$\theta = 30°$

·013	·021	·026	·027	·025	·021	·025	·050	
·039	·054	·063	·064	·054	·050	·081		
·082	·101	·106	·091	·070	·091			
·135	·147	·132	·087	·083				
·177	·171	·100	·062					

$\theta = 45°$

·016	·022	·025	·024	·019	·017	·029		
·046	·054	·052	·036	·028				
·077	·067	·027						
·046								

TABLE (2.8)

EDGE BEAM REDUCTION FACTOR

— EVERY TROUGH FASTENING (r_E)

$\theta = 0°$

$\frac{2b_r}{d}$ / h/d	0.1	0.2	0.3	0.4	0.5	0.6	0.7	0.8	0.9
0.1	.01	.04	.10	.15	.18	.10	.00	.25	.54
0.2	.01	.05	.11	.17	.20	.13	.00	.19	.48
0.3	.01	.06	.12	.18	.22	.15	.00	.16	.44
0.4	.01	.06	.13	.19	.23	.16	.01	.14	.42
0.5	.01	.06	.13	.20	.24	.17	.01	.13	.41

$\theta = 15°$

.02	.06	.12	.18	.19	.08	.03	.33	.61
.04	.10	.16	.22	.21	.05	.07	.38	
.07	.13	.21	.26	.22	.02	.15	.45	
.09	.17	.25	.29	.20	.00	.26		
.13	.20	.28	.31	.15	.05	.37		

$\theta = 30°$

.04	.09	.15	.21	.19	.04	.09	.39	
.09	.16	.23	.27	.16	.00	.29		
.16	.24	.31	.29	.01	.22			
.24	.32	.34	.13	.18				
.32	.39	.31	.15					

$\theta = 45°$

.07	.13	.19	.24	.18	.00	.19	.	
.18	.26	.32	.25	.00				
.32	.39	.25						
.45								

TABLE(2.9)

$\overline{K}$ VALUES FOR ALTERNATE TROUGH FIXING

ONE OR NO INTERMEDIATE PURLINS; INCLUDING END RESTRAINT.

$\theta = 0°$

h/d \ $2b_T/d$	0.1	0.2	0.3	0.4	0.5	0.6	0.7	0.8	0.9
0.1	0.076	0.120	0.161	0.196	0.223	0.249	0.293	0.388	0.617
0.2	0.257	0.375	0.494	0.597	0.680	0.767	0.905	1.20	1.93
0.3	0.507	0.745	0.974	1.17	1.33	1.47	1.72	2.30	2.77
0.4	0.893	1.19	1.66	1.98	2.22	2.43	2.78	3.66	5.07
0.5	1.47	2.06	2.62	3.09	3.43	3.69	4.13	5.30	8.77

$\theta = 5°$

0.078	0.122	0.162	0.196	0.223	0.250	0.297	0.399	0.643
0.262	0.383	0.502	0.602	0.686	0.779	0.939	1.30	2.31
0.533	0.771	1.04	1.18	1.34	1.51	1.87	2.72	3.55
0.962	1.29	1.70	1.99	2.23	2.49	3.05	4.50	8.35
1.62	2.26	2.81	3.26	3.63	4.07	5.20	8.71	12.91

$\theta = 10°$

0.080	0.124	0.163	0.197	0.224	0.252	0.303	0.417	0.697
0.275	0.400	0.514	0.611	0.695	0.795	0.983	1.42	2.89
0.578	0.813	1.12	1.20	1.36	1.56	2.02	3.15	
1.03	1.40	1.74	2.00	2.24	2.64	3.49	6.12	
1.88	2.48	3.03	3.46	3.86	4.57	6.50	14.54	

$\theta = 15°$

0.082	0.125	0.164	0.197	0.224	0.254	0.309	0.429	0.736
0.287	0.412	0.524	0.619	0.706	0.720	1.01	1.63	
0.613	0.842	1.11	1.22	1.41	1.69	2.40	4.15	
1.11	1.44	1.77	2.04	2.38	3.12	5.60		
1.91	2.45	2.94	3.36	4.01	6.22	9.22		

$\theta = 20°$

0.084	0.127	0.164	0.197	0.224	0.256	0.316	0.458	0.788
0.302	0.424	0.534	0.627	0.714	0.843	1.13	1.98	
0.656	0.879	1.11	1.25	1.44	1.82	2.85		
1.17	1.53	1.83	2.08	2.52	3.59	8.75		
1.94	2.43	2.84	3.27	4.28	8.30			

TABLE (2.10)

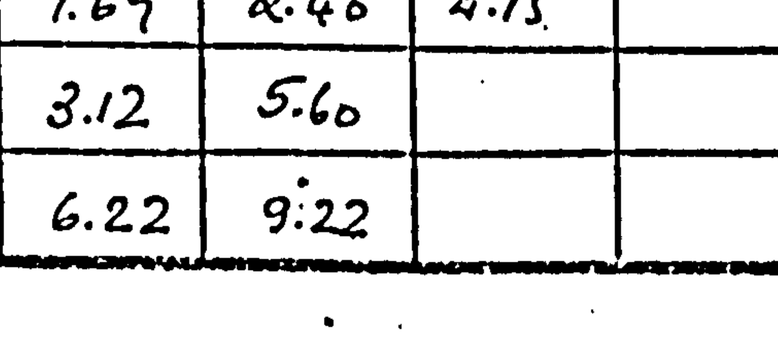

h/d \ 2br/d	0.1	0.2	0.3	0.4	0.5	0.6	0.7	0.8	0.9
0.1	0.086	0.130	0.167	0.198	0.223	0.256	0324	0.486	0.815
0.2	0.317	0.437	0.543	0.634	0.727	0.883	1.27	2.52	
0.3	0.600	0.915	1.11	1.29	1.54	2.12	4.50		
0.4	1.26	1.60	1.90	2.25	3.01	6.27			
0.5	2.06	2.61	3.03	392	7.7-1				

θ=25°

0.092	0.132	0.168	0.198	0.223	0.258	0.333	0.575	
0.331	0.449	0.554	0.644	0.747	0.951	1.65		
0.681	0.955	1.16	1.38	1.90	2.42			
1.35	1.69	2.06	333	4.91				
2.28	3.15	5.01	8.01					

θ=30°

0.096	0.134	0.169	0.198	0.223	0.262	0.351	0.566	
0.347	0.463	0.564	0656	0.777	1.09	2.09		
0.787	1.00	1.21	1.47	2.23				
1.46	1.85	2.39	4.43					
2.57	366	8.73						

θ=35°

0.096	0.136	0.167	0.199	0.224	0.266	0.381	0.631	
0.362	0.473	0.559	0.682	0.891	1.37			
0.834	1.65	2.00	4.02					
1.62	2.23	4.59						
4.06								

θ=40°

0.098	0.138	0.166	0.196	0.227	0.279	0.409		
0.385	0.493	0.593	0.710	1.01				
0.925	1.15	1.62						
2.19								

θ=45°

$\bar{K}$ VALUES FOR ALTERNATE TROUGH FIXING

TWO INTERMEDIATE PURLINS; INCLUDING END RESTRAINT

h/d \ $2b_T/d$	0.1	0.2	0.3	0.4	0.5	0.6	0.7	0.8	0.9	
0.1	0.053	0.091	0.125	0.153	0.173	0.188	0.209	0.257	0.379	
0.2	0.215	0.326	0.432	0.522	0.599	0.664	0.779	0.956	1.39	
0.3	0.437	0.637	0.830	1.00	1.14	1.29	1.51	1.97	2.95	θ=0°
0.4	0.700	1.02	1.33	1.59	1.80	2.01	2.36	3.15	4.99	
0.5	1.05	1.57	1.98	2.35	2.63	2.88	3.34	4.47	7.38	
0.1	0.054	0.092	0.126	0.153	0.172	0.186	0.208	0.260	0.391	
0.2	0.225	0.337	0.440	0.528	0.599	0.669	0.778	0.991	1.51	
0.3	0.471	0.673	0.863	1.03	1.17	1.33	1.60	2.15	3.40	θ=5°
0.4	0.778	1.09	1.39	1.64	1.85	2.10	2.62	3.73	6.27	
0.5	1.19	1.65	2.07	2.41	2.68	3.03	3.83	5.80	10.30	
0.1	0.055	0.093	0.126	0.152	0.170	0.184	0.208	0.263	0.406	
0.2	0.236	0.348	0.449	0.533	0.602	0.674	0.792	1.03	1.67	
0.3	0.509	0.709	0.895	1.06	1.20	1.38	1.70	2.37		θ=10°
0.4	0.861	1.17	1.46	1.70	1.93	2.27	2.99	4.48		
0.5	1.33	1.78	2.17	2.49	2.81	3.40	4.79	7.72		
0.1	0.057	0.094	0.127	0.151	0.169	0.182	0.207	0.268	0.422	
0.2	0.247	0.358	0.456	0.538	0.604	0.679	0.810	1.09		
0.3	0.546	0.746	0.928	1.08	1.22	1.44	1.84	2.65		θ=15°
0.4	0.947	1.25	1.53	1.77	2.04	2.52	3.62			
0.5	1.49	1.91	2.29	2.63	3.10	4.14	6.31			
0.1	0.058	0.096	0.128	0.152	0.168	0.181	0.208	0.274	0.440	
0.2	0.260	0.369	0.464	0.542	0.606	0.685	0.834	1.16		
0.3	0.587	0.784	0.961	1.11	1.27	1.52	2.02			θ=20°
0.4	1.04	1.34	1.61	1.87	2.21	2.94	4.12			
0.5	1.65	2.07	2.46	2.88	3.69	5.41				

TABLE (2.11)

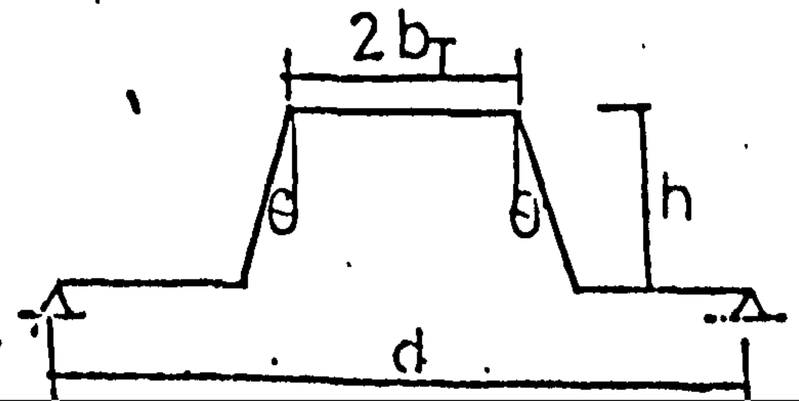

θ 25°

2bT/d \ h/d	0.1	0.2	0.3	0.4	0.5	0.6	0.7	0.8	0.9
0.1	0.061	0.097	0.128	0.151	0.166	0.180	0.209	0.282	0.449
0.2	0.273	0.380	0.473	0.546	0.608	0.694	0.868	1.26	
0.3	0.630	0.823	0.996	1.14	1.32	1.64	2.23		
0.4	1.14	1.44	1.71	2.00	2.49	3.43			
0.5	1.85	2.27	2.72	3.39	4.80				

θ 30°

0.063	0.099	0.129	0.150	0.164	0.179	0.210	0.291	
0.288	0.392	0.481	0.549	0.610	0.707	0.916		
0.678	0.866	1.03	1.18	1.39	1.79			
1.26	1.55	1.84	2.21	2.93				
2.09	2.59	3.19	4.37					

θ 35°

0.066	0.101	0.130	0.150	0.163	0.178	0.214	0.304	
0.304	0.405	0.488	0.557	0.612	0.731	0.987		
0.730	0.912	1.07	1.22	1.50				
1.39	1.70	2.01	2.58					
2.46	3.05	3.83						

θ 40°

0.069	0.103	0.131	0.150	0.161	0.177	0.219	0.320	
0.323	0.419	0.500	0.551	0.621	0.771			
0.790	0.963	1.10	1.30					
1.57	1.87	2.31						
2.98								

θ 45°

0.073	0.107	0.132	0.149	0.159	0.177	0.226	0.153	
0.345	0.434	0.501	0.551	0.642	0.650			
0.859	1.02	1.16	1.32					
1.78	2.03							

$\bar{K}$ VALUES FOR ALTERNATE TROUGH FIXING

THREE INTERMEDIATE PURLINS; INCLUDING END RESTRAINT

$\theta = 0°$

h/d \ 2bT/d	0.1	0.2	0.3	0.4	0.5	0.6	0.7	0.8	0.9
0.1	0.024	0.057	0.074	0.091	0.097	0.096	0.096	0.114	0.192
0.2	0.104	0.201	0.288	0.354	0.390	0.399	0.402	0.448	0.671
0.3	0.260	0.476	0.665	0.805	0.887	0.919	0.941	1.04	1.45
0.4	0.512	0.880	1.20	1.44	1.58	1.65	1.71	1.89	2.58
0.5	0.865	1.40	1.87	2.23	2.45	2.58	2.71	3.02	4.08

$\theta = 5°$

0.026	0.052	0.075	0.090	0.095	0.093	0.093	0.114	0.202
0.118	0.213	0.295	0.353	0.382	0.384	0.387	0.441	0.737
0.308	0.524	0.687	0.808	0.868	0.880	0.893	1.01	1.63
0.621	0.964	1.25	1.45	1.55	1.59	1.64	1.84	2.95
1.06	1.55	1.96	2.26	2.41	2.49	2.59	2.97	4.84

$\theta = 10°$

0.028	0.054	0.076	0.090	0.094	0.091	0.091	0.115	0.211
0.133	0.225	0.302	0.354	0.373	0.368	0.368	0.441	0.841
0.383	0.525	0.702	0.808	0.845	0.837	0.838	1.00	
0.730	1.04	1.29	1.45	1.50	1.50	1.50	1.83	
1.24	1.69	2.04	2.27	2.35	2.35	2.37	3.03	

$\theta = 15°$

0.030	0.056	0.077	0.090	0.093	0.088	0.089	0.117	0.223
0.150	0.238	0.310	0.354	0.364	0.351	0.351	0.453	
0.409	0.586	0.725	0806	0.812	0.782	0.780	1.06	
0.831	1.11	1.33	1.44	1.44	1.36	1.36		
1.42	1.87	2.11	2.25	2.22	2.03	2.16		

$\theta = 20°$

0.033	0.058	0.078	0.090	0.091	0.086	0.088	0.120	0.231
0.167	0.251	0.317	0.354	0.354	0.332	0.337	0.484	
0.456	0.621	0.742	0.797	0.774	0.709	0.738		
1.02	1.30	1.52	1.60	1.57	1.33	1.21		
1.59	1.94	2.15	2.16	1.86	1.66			

TABLE (2.12)

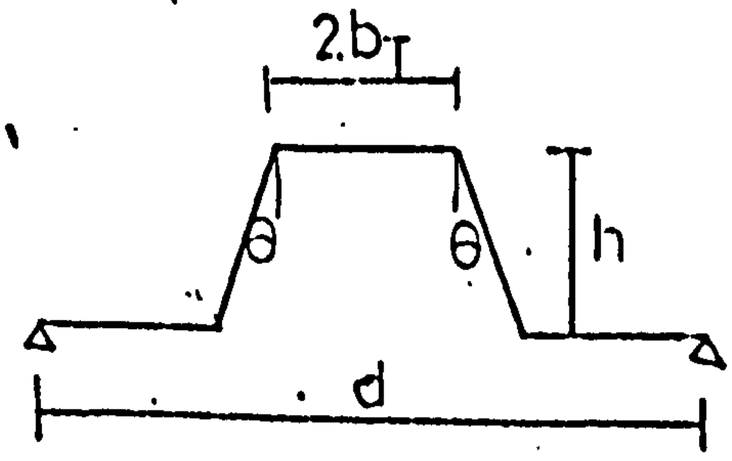

h/d \ 2bT/d	0.1	0.2	0.3	0.4	0.5	0.6	0.7	0.8	0.9
0.1	0.036	0.061	0.081	0.091	0.090	0.084	0.087	0.124	0.168
0.2	0.185	0.265	0.325	0.352	0.340	0.311	0.328	0.448	
0.3	0.502	0.653	0.756	0.778	0.710	0.625	0.736		
0.4	1.02	1.24	1.37	1.32	1.08	1.01			
0.5	1.74	2.03	2.12	1.79	1.34				

θ=25°

0.039	0.064	0.082	0.091	0.089	0.083	0.087	0.130	
0.202	0.278	0.332	0.248	0.323	0.290	0.331		
0.545	0.682	0.761	0.735	0.614	0.562			
1.10	1.29	1.32	1.09	0.821				
1.89	2.08	1.76	1.10					

θ=30°

0.042	0.067	0.084	0.092	0.088	0.081	0.087	0.137	
0.220	0.298	0.338	0.340	0.300	0.268	0.319		
0.586	0.708	0.747	0.650	0.493				
1.17	1.30	1.13	0.71					
1.99	1.76	0.804						

θ=35°

0.046	0.070	0.086	0.092	0.087	0.079	0.087	0.140	
0.237	0.305	0.340	0.325	0.270	0.252			
0.623	0.719	0.690	0.499					
1.21	1.16	0.609						
1.71								

θ=40°

0.050	0.074	0.089	0.093	0.086	0.079	0.090	0.099	
0.255	0.315	0.336	0.300	0.220	0.107			
0.650	0.693	0.536	0.251					
1.13	0.411							

θ=45°

$\bar{K}$ VALUES FOR ALTERNATE TROUGH FIXING

ONE OR NO INTERMEDIATE PURLINS ;EXCLUDING END RESTRAINT

$\theta = 0^\circ$

h/d \ 2br/d	0.1	0.2	0.3	0.4	0.5	0.6	0.7	0.8	0.9
0.1	0.080	0.128	0.174	0.214	0.249	0.284	0.340	0.454	0.716
0.2	0.269	0.403	0.535	0.653	0.757	0.868	1.06	1.38	2.23
0.3	0.549	0.807	1.06	1.17	1.21	1.65	1.97	2.64	4.33
0.4	0.977	1.40	1.87	2.18	2.46	2.72	3.17	4.18	6.89
0.5	1.63	2.26	2.86	3.41	3.83	4.16	4.71	6.04	9.90

$\theta = 15^\circ$

0.087	0.134	0.178	0.217	0.252	0.296	0.361	0.513	0.863
0.309	0.445	0.572	0.685	0.795	0.940	1.22	1.91	
0.669	0.962	1.14	1.36	1.58	1.93	2.69	5.16	
1.12	1.64	1.97	2.29	2.62	3.38	5.29		
2.01	2.59	3.10	3.53	4.12	5.60	11.50		

$\theta = 30^\circ$

0.093	0.141	0.183	0.220	0.254	0.301	0.398	0.616	
0.357	0.490	0.612	0.726	0.862	1.11	1.83		
0.809	0.955	1.29	1.55	2.02	3.53			
1.49	1.90	2.34	3.10	5.93				
2.53	3.22	4.35	9.71					

$\theta = 45^\circ$

0.104	0.148	0.213	0.221	0.260	0.329	0.488		
0.421	0.547	0.673	0.830	1.69				
1.03	1.34	1.95						
2.57								

TABLE(2.13)

$\bar{K}$ VALUES FOR ALTERNATE TROUGH FIXING

TWO INTERMEDIATE PURLINS; NOT INCLUDING END RESTRAINT

$\theta = 0^\circ$

h/d \ 2br/d	0.1	0.2	0.3	0.4	0.5	0.6	0.7	0.8	0.9
0.1	0.055	0.097	0.134	0.167	0.192	0.213	0.241	0.297	0.427
0.2	0.230	0.352	0.468	0.573	0.663	0.752	0.878	1.10	1.58
0.3	0.474	0.690	0.904	1.10	1.27	1.45	1.73	2.26	3.36
0.4	0.766	1.11	1.45	1.75	2.00	2.27	2.70	3.61	5.66
0.5	1.16	1.67	2.16	2.59	2.92	3.24	3.80	5.10	8.34

$\theta = 15^\circ$

0.060	0.100	0.136	0.166	0.189	0.209	0.241	0.310	0.472
0.265	0.387	0.499	0.597	0.682	0.782	0.945	1.26	
0.593	0.813	1.02	1.21	1.40	1.67	2.16	3.07	
1.04	1.38	1.70	1.99	2.34	2.94	4.12		
1.63	2.12	2.56	2.98	3.58	4.84	7.41		

$\theta = 30^\circ$

0.066	0.106	0.140	0.167	0.186	0.206	0.246	0.335	
0.310	0.428	0.532	0.619	0.704	0.836	1.08		
0.743	0.959	1.16	1.35	1.63	2.13			
1.40	1.75	2.11	2.60	3.49				
2.36	2.95	3.74	5.18					

$\theta = 45^\circ$

0.077	0.114	0.145	0.168	0.183	0.208	0.264		
0.376	0.482	0.568	0.642	0.763				
0.969	1.17	1.38						
2.09								

TABLE(2.14)

$\bar{K}$ VALUES FOR ALTERNATE TROUGH FIXING

THREE INTERMEDIATE PURLINS; NOT INCLUDING END RESTRAINT

$\theta = 0°$

h/d \ $2b_T/d$	0.1	0.2	0.3	0.4	0.5	0.6	0.7	0.8	0.9
0.1	0.025	0.053	0.078	0.097	0.105	0.106	0.106	0.125	0.204
0.2	0.109	0.213	0.310	0.383	0.427	0.443	0.451	0.497	0.719
0.3	0.280	0513	0.720	0.880	0.980	1.03	1.06	1.16	1.57
0.4	0.557	0.957	1.31	1.58	1.76	1.86	1.94	2.12	2.79
0.5	0.950	1.53	2.05	2.45	2.73	2.90	3.08	3.40	4.42

$\theta = 15°$

0.031	0.059	0.081	0.096	0.100	0.098	0.100	0.128	0.234
0.159	0.255	0.334	0.387	0.404	0.395	0.396	0.497	
0.441	0.637	0.795	0.894	0.919	0.889	0.881	1.16	
0.910	1.22	1.47	1.62	1.64	1.56	1.54		
1.56	2.01	2.36	2.55	2.54	2.33	2.42		

$\theta = 30°$

0.041	0.068	0.087	0.098	0.098	0.093	0.098	0.140	
0.216	0.301	0.364	0.387	0.366	0.332	0.370		
0.596	0.753	0.850	0.837	0.711	0.643			
1.22	1.45	1.57	1.26	0.956				
2.14	2.38	2.06	1.89					

$\theta = 45°$

0.053	0.078	0.096	0.102	0.096	0.089	0.100		
0.277	0.347	0.377	0.343	0.269				
0.730	0.758	0.693						
1.33								

TABLE (2.15)

EDGE BEAM REDUCTION FACTOR (r_A)

—CONCERTINA COMPONENT OF ALTERNATE TROUGH FASTENING FLEXIBILITY

$\theta = 0°$

h/d \ $\frac{2b_T}{d}$	0.1	0.2	0.3	0.4	0.5	0.6	0.7	0.8	0.9
0.1	0.06	0.08	0.10	0.12	0.14	0.15	0.16	0.18	0.19
0.2	0.08	0.10	0.11	0.13	0.14	0.15	0.16	0.17	0.18
0.3	0.09	0.10	0.11	0.13	0.14	0.15	0.16	0.17	0.18
0.4	0.10	0.11	0.12	0.13	0.14	0.15	0.16	0.17	0.17
0.5	0.11	0.12	0.13	0.14	0.14	0.15	0.16	0.16	0.17

$\theta = 15°$

0.06	0.09	0.11	0.12	0.14	0.16	0.17	0.18	0.19
0.07	0.10	0.12	0.13	0.15	0.16	0.17	0.18	
0.10	0.12	0.13	0.14	0.15	0.16	0.17	0.18	
0.11	0.12	0.13	0.14	0.15	0.16	0.17		
0.12	0.13	0.14	0.15	0.16	0.16	0.17		

$\theta = 30°$

0.07	0.09	0.11	0.13	0.15	0.16	0.18	0.19	
0.09	0.11	0.13	0.14	0.16	0.17	0.18		
0.12	0.13	0.14	0.15	0.16	0.18			
0.13	0.14	0.15	0.16	0.17				
0.14	0.15	0.16	0.16					

$\theta = 45°$

0.08	0.10	0.12	0.14	0.15	0.17	0.18		
0.11	0.13	0.14	0.16	0.17				
0.14	0.15	0.16						
0.15								

TABLE(2.16)

K VALUES FOR ALTERNATE TROUGH FIXING

ANY NUMBER OF INTERMEDIATE PURLINS ;
INCLUDING 'PURLIN-PROP' REDUCTION FACTOR.

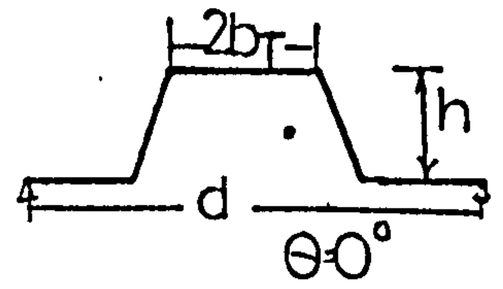

h/d \ 2bT/d	0.1	0.2	0.3	0.4	0.5	0.6	0.7	0.8	0.9
0.1	0.43	0.71	1.07	1.17	1.41	1.70	1.84	2.04	2.46
0.2	2.35	3.50	4.82	5.53	6.25	6.79	7.66	8.50	10.2
0.3	6.62	9.21	11.4	14.1	15.7	17.4	18.7	21.3	25.5
0.4	14.7	18.9	24.3	27.4	30.8	33.1	35.7	40.0	48.5
0.5	26.1	34.2	41.8	47.5	52.8	55.1	595	67.2	81.6

θ=15°

0.44	0.72	1.02	1.19	1.39	1.68	1.80	2.01	2.47
2.55	3.62	4.80	5.37	6.15	6.59	7.65	8.60	
7.08	9.90	11.4	13.1	14.8	16.2	18.9	22.6	
15.3	19.6	22.9	25.5	28.4	30.6	36.1		
27.6	34.3	39.6	43.5	46.8	51.9	62.0		

θ=30°

0.48	0.77	0.99	1.14	1.29	1.53	1.79	2.08	
2.61	3.60	4.40	5.13	5.78	6.63	8.01		
7.56	9.68	11.3	12.9	14.5	16.9			
15.8	19.1	21.8	24.6	28.1				
27.8	32.7	36.6	42.5					

θ=45°

0.52	0.76	0.99	1.13	1.29	1.53	1.83		
2.88	3.70	4.44	5.10	5.96				
7.74	9.35	11.1						
16.1								

TABLE (2.17)

K VALUES FOR EVERY THIRD TROUGH FIXING

ANY NUMBER OF INTERMEDIATE PURLINS ;
INCLUDING 'PURLIN-PROP' REDUCTION FACTOR.

θ=0°

h/d \ 2br/d	0.1	0.2	0.3	0.4	0.5	0.6	0.7	0.8	0.9
0.1	0.86	1.59	2.17	2.77	3.36	4.05	4.63	5.46	6.42
0.2	4.92	7.52	9.84	12.3	15.3	17.6	20.2	23.4	20.9
0.3	13.9	19.8	26.2	31.5	37.4	43.0	48.4	53.2	63.9
0.4	30.4	41.9	52.6	63.1	72.2	82.5	96.0	106.0	125.0
0.5	56.2	73.3	88.1	107.0	130.0	142.0	159.0	182.0	202.0

TABLE (2.18)

θ=30°

0.92	1.62	2.21	2.79	3.39	4.09	4.76	5.60	
6.25	8.02	10.9	12.8	15.7	17.4	20.2		
16.8	21.9	27.4	32.3	37.8	43.6			
35.6	44.8	54.7	63.8	73.9				
64.8	79.2	91.3	107.0					

'PURLIN-PROP' REDUCTION FACTOR — (r_T)

EVERY THIRD TROUGH FASTENING

θ=0°

0.1	0.22	0.19	0.17	0.16	0.14	0.12	0.11	0.09	0.07
0.2	0.23	0.20	0.18	0.16	0.15	0.13	0.12	0.10	0.09
0.3	0.23	0.21	0.18	0.17	0.15	0.14	0.12	0.11	0.10
0.4	0.24	0.21	0.19	0.17	0.16	0.14	0.13	0.12	0.11
0.5	0.24	0.22	0.20	0.18	0.16	0.15	0.14	0.13	0.12

θ=30°

0.22	0.19	0.16	0.15	0.13	0.11	0.10	0.08	
0.21	0.18	0.16	0.15	0.13	0.12	0.10		
0.21	0.19	0.17	0.15	0.14	0.13			
0.21	0.19	0.17	0.16	0.15				
0.22	0.20	0.18	0.17					

TABLE (2.19)

APPENDIX 3. SHEET OVERLAP DESIGN DATA

Table (3.1) $\mathcal{E}$ values for every trough fastening

(3.2) $\mathcal{E}$ values for alternate trough fastening

(3.3) Overall panel flexibility for any number of sheet overlaps

(3.4) Overall panel flexibility for every trough fastening at the sheet ends and alternate trough fastening at the overlaps

Design formulae for shear distortion flexibility:

1. N overlapping sheets, parallel to the applied shear force

$$C_{1.1} = \frac{C_{1.1_s}}{N^2} (1 + N\mathcal{E})$$

where $C_{1.1_s}$ is the individual sheet distortion flexibility

2. N overlapping sheets, where fastenings are in every trough at the sheet ends and alternate troughs at the overlaps.

$$C_{1.1} = C_{1.1_A} \left\{ \frac{2\mathcal{E}}{3N + (4 - N)\mathcal{E}} \right\} + \frac{C_{1.1_E}}{N}$$

$C_{1.1_A}$ - individual sheet flexibility fastened in alternate troughs

$C_{1.1_A}$ - individual sheet flexibility fastened in every trough

3. N overlapping sheets spanning perpendicular to the applied shear force, with overlaps at the rafters

The central shear deflection per unit rafter force, is

$$\Delta = \left[\frac{2}{N} + \left(1 - \frac{2}{N}\right)\mathcal{E} \right] \cdot \frac{N^2}{8} \cdot C_{1.1_s} \cdot \left(\frac{b}{a}\right)^2$$

$C_{1.1_s} \left(\frac{b}{a}\right)^2$ is the panel flexibility perpendicular to the corrugations.

OVERLAP SLIP FACTOR, $\mathcal{E}$, FOR FASTENING IN EVERY TROUGH

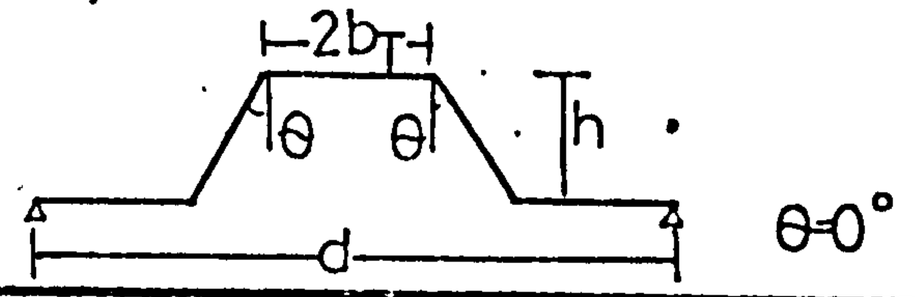

θ=0°

h/d \ 2bT/d	0.1	0.2	0.3	0.4	0.5	0.6	0.7	0.8	0.9
0.1	0.04	0.07	0.12	0.19	0.25	0.25	0.14	0.03	0.00
0.2	0.04	0.08	0.13	0.20	0.26	0.26	0.16	0.03	0.00
0.3	0.05	0.09	0.14	0.21	0.27	0.27	0.17	0.04	0.00
0.4	0.06	0.10	0.15	0.22	0.28	0.28	0.18	0.04	0.00
0.5	0.06	0.10	0.15	0.22	0.28	0.28	0.19	0.05	0.00

θ=15°

0.04	0.14	0.33	0.52	0.57	0.49	0.21	0.03	0.00
0.04	0.12	0.25	0.40	0.50	0.37	0.12	0.07	
0.04	0.12	0.25	0.38	0.43	0.30	0.05	0.00	
0.04	0.12	0.26	0.39	0.42	0.20	0.02		
0.04	0.13	0.29	0.41	0.39	0.10	0.00		

θ=30°

0.07	0.37	0.69	0.84	0.80	0.54	0.15	0.01	
0.05	0.23	0.50	0.61	0.55	0.21	0.01		
0.05	0.24	0.49	0.55	0.31	0.01			
0.06	0.31	0.52	0.43	0.07				
0.09	0.44	0.51	0.01					

θ=45°

0.15	1.00	1.00	0.99	0.83	0.36	0.04		
0.11	0.44	0.67	0.63	0.16				
0.20	0.56	0.44						
0.50								

TABLE(3.1)

OVERLAP SLIP FACTOR, $\mathcal{E}$, FOR FASTENING IN ALTERNATE TROUGHS.

$\theta = 0°$

h/d \ 2br/d	0.1	0.2	0.3	0.4	0.5	0.6	0.7	0.8	0.9
0.1									
0.2									
0.3			All values are 0.0						
0.4									
0.5									

$\theta = 15°$

0.47	0.38	0.33	0.29	0.27	0.25	0.23	0.20	0.18
0.19	0.15	0.13	0.11	0.10	0.09	0.09	0.08	
0.09	0.08	0.07	0.06	0.05	0.05	0.04	0.04	
0.05	0.04	0.04	0.04	0.03	0.03	0.03		
0.04	0.03	0.03	0.02	0.02	0.02	0.02		

$\theta = 30°$

0.69	0.62	0.58	0.56	0.55	0.54	0.53	0.52	
0.43	0.38	0.35	0.33	0.31	0.30	0.28		
0.27	0.24	0.22	0.20	0.19	0.18			
0.17	0.16	0.14	0.13	0.12				
0.12	0.11	0.10	0.09					

$\theta = 45°$

0.78	0.75	0.74	0.73	0.73	0.72	0.70		
0.77	0.65	0.60	0.58	0.56				
0.56	0.54	0.52						
0.44								

TABLE(3.2)

TABLE OF FACTORS FOR OVERLAPPING SHEETS

Flexibility Formulae	$\mathcal{E}$=0.0	0.2	0.4	0.6	0.8	1.0	
$\frac{C_{1.1}}{n^3}(1+n^2\mathcal{E})$	0.125	0.225	0.325	0.425	0.525	0.625	RA
$\frac{C_{1.1}}{8}(1+3\mathcal{E})$	0.125	0.200	0.275	0.350	0.425	0.500	RE n=2
$\frac{C_{1.1}}{n^2}(1+n\mathcal{E})$	0.250	0.350	0.450	0.550	0.650	0.750	FA
$\frac{C_{1.1}}{4}(1+\mathcal{E})$	0.250	0.300	0.350	0.400	0.450	0.500	FE
$\frac{C_{1.1}}{n^3}(1+n^2\mathcal{E})$	0.037	0.104	0.170	0.237	0.303	0.370	RA
$C_{1.1}\left\{\frac{1+9\mathcal{E}}{27+3\mathcal{E}}\right\}$	0.037	0.101	0.163	0.222	0.278	0.330	RE n=3
$\frac{C_{1.1}}{n^2}(1+n\mathcal{E})$	0.111	0.178	0.244	0.311	0.378	0.444	FA
$C_{1.1}\left\{\frac{1+3\mathcal{E}}{7+2\mathcal{E}}\right\}$	0.142	0.216	0.250	0.341	0.395	0.444	FE
$\frac{C_{1.1}}{n^3}(1+n^2\mathcal{E})$	0.016	0.066	0.116	0.166	0.216	0.266	RA
$C_{1.1}\frac{(1+18\mathcal{E}+9\mathcal{E}^2)}{64+48\mathcal{E}}$	0.016	0.068	0.108	0.162	0.196	0.250	RE n=4
$\frac{C_{1.1}}{n^2}(1+n\mathcal{E})$	0.063	0.113	0.163	0.212	0.263	0.313	FA
$C_{1.1}\frac{1+6\mathcal{E}+\mathcal{E}^2}{8(3+\mathcal{E})}$	0.041	0.086	0.131	0.182	0.211	0.250	FE
$\frac{C_{1.1}}{n^3}(1+n^2\mathcal{E})$	0.008	0.048	0.088	0.128	0.168	0.208	RA n=5
$\frac{C_{1.1}}{n}(1+n\mathcal{E})$	0.040	0.080	0.120	0.160	0.200	0.240	FA
$\frac{C_{1.1}}{n^3}(1+n^2\mathcal{E})$	0.005	0.038	0.071	0.105	0.138	0.171	RA n=6
$\frac{C_{1.1}}{n^2}(1+n\mathcal{E})$	0.028	0.061	0.094	0.128	0.161	0.194	FA

n - number of sheets

$\mathcal{E}$ - overlap factor

$C_{1.1}$ - individual sheet flexibility

R - rigid plate movements

F - localized end distortion

A - approximate formula

E - exact expression

TABLE (3.3)

TABLE OF FACTORS FOR OVERLAPPING SHEETS WITH EVERY CORRUGATION FASTENING AT THE ENDS AND ALTERNATE FASTENING AT THE INTERMEDIATE PURLINS

Overall shear flexibility formulae	$\mathcal{E} = 0.0$	0.2	0.4	0.6	0.8	1.0	
$C_{1.1_A}\ \mathcal{E}/_8$	0.0	0.03	0.05	0.08	0.10	0.13	R
$C_{1.1_A}\ \mathcal{E}/_4$	0.0	0.05	0.10	0.15	0.20	0.15	n=2 F
$C_{1.1_A}\left\{\mathcal{E}/_{(6+3\mathcal{E})}\right\}$	0.0	0.03	0.06	0.08	0.10	0.11	R
$C_{1.1_A}\left\{2\mathcal{E}/_{(9+\mathcal{E})}\right\}$	0.0	0.04	0.09	0.13	0.16	0.20	n=3 F
$C_{1.1_A}\left\{\mathcal{E}/_{(8+2\mathcal{E})}\right\}$	0.0	0.02	0.05	0.07	0.08	0.10	R
$C_{1.1_A}\left\{\mathcal{E}/_6\right\}$	0.0	0.03	0.07	0.10	0.13	0.17	n=4 F
$C_{1.1_A}\left\{\mathcal{E}/_{(10+\mathcal{E})}\right\}$	0.0	0.02	0.04	0.06	0.07	0.09	R
$C_{1.1_A}\left\{2\mathcal{E}/_{(15-\mathcal{E})}\right\}$	0.0	0.03	0.06	0.08	0.10	0.14	n=5 F
$r = \dfrac{\mathcal{E}n^3/(1+n^2\mathcal{E})}{6\mathcal{E}+n(2-\mathcal{E})}$	0.0	0.39	0.43	0.42	0.40	0.38	R
$r = \dfrac{2\mathcal{E}n^2/(1+n\mathcal{E})}{4\mathcal{E}+n(3-\mathcal{E})}$	0.0	0.27	0.43	0.47	0.49	0.54	n=4 (example) F

$C_{1.1_A}$ - individual sheet flexibility fastened in alternate troughs

$C_{1.1_E}$ - individual sheet flexibility fastened in every trough

n - number of sheets

R - rigid plate movements F - localized end distortion

$\mathcal{E}$ - overlap factor for alternate trough fastening

r - reduction factor compared to alternate trough fastening throughout

General formulae for any number of sheets:

$$C_{1.1} = \frac{2\mathcal{E}\ C_{1.1_A}}{4\mathcal{E}+n(3-\mathcal{E})} + \frac{C_{1.1_E}}{n} \quad \text{or} \quad C_{1.1} = \frac{\mathcal{E}.\ C_{1.1_A}}{6\mathcal{E}+n(2-\mathcal{E})} + \frac{C_{1.1_E}}{n}$$

for localized end distortion or rigid plate movements respectively

TABLE (3.4)

FOLDED PLATE ROOF DESIGN —APPENDIX 4

Summary

Layout

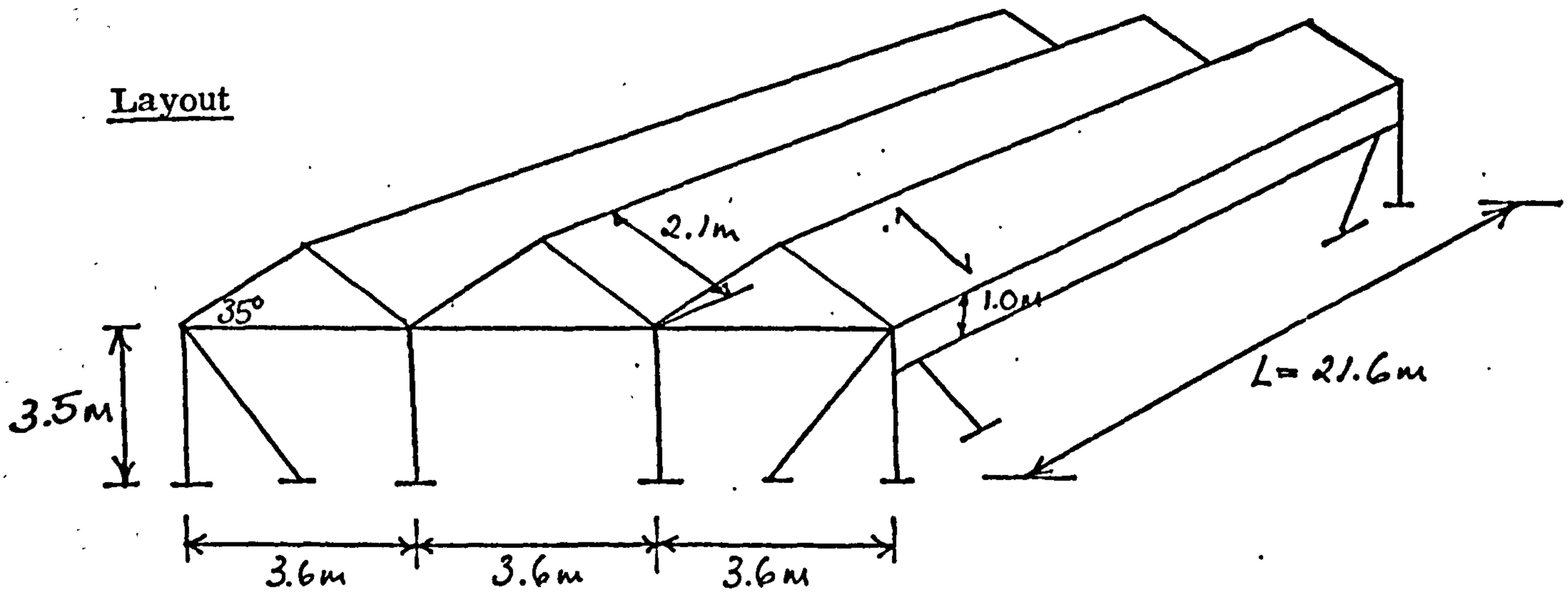

Loading

Snow Load	0.75 kN/m^2	
Insulation	0.23 kN/m^2	- same as loading system
Self weight	0.22 kN/m^2	
Total	1.2 kN/m^2	

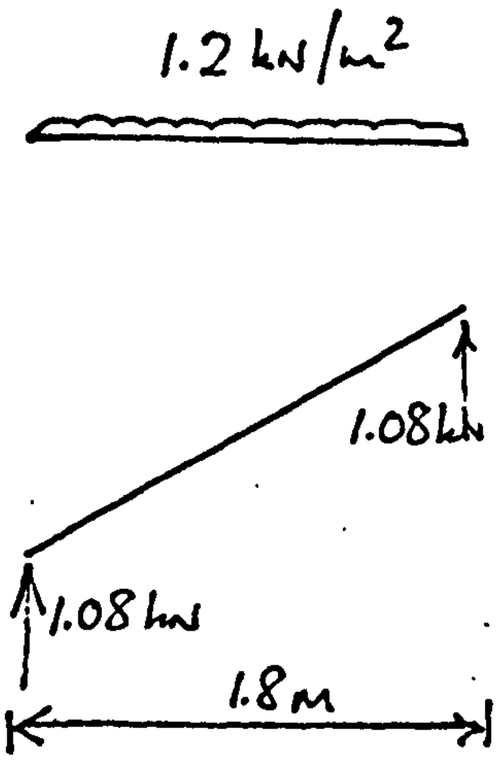

For design bending stress in sheet of 150 N/mm^2,

Required section modulus is

$$Z = \frac{(1.2\times10^3 \times 1.8) \times 1800}{8 \times 150} = 3.24 \times 10^3 \text{ mm}^3$$

In fact, pressed sheeting of Fig (10.6) has properties $I = 174 \times 10^3$ mm^4/mm

$Z = 9.27 \times 10^3$ mm^3/mm

$\therefore$ Actual stress = 53 N/mm^2

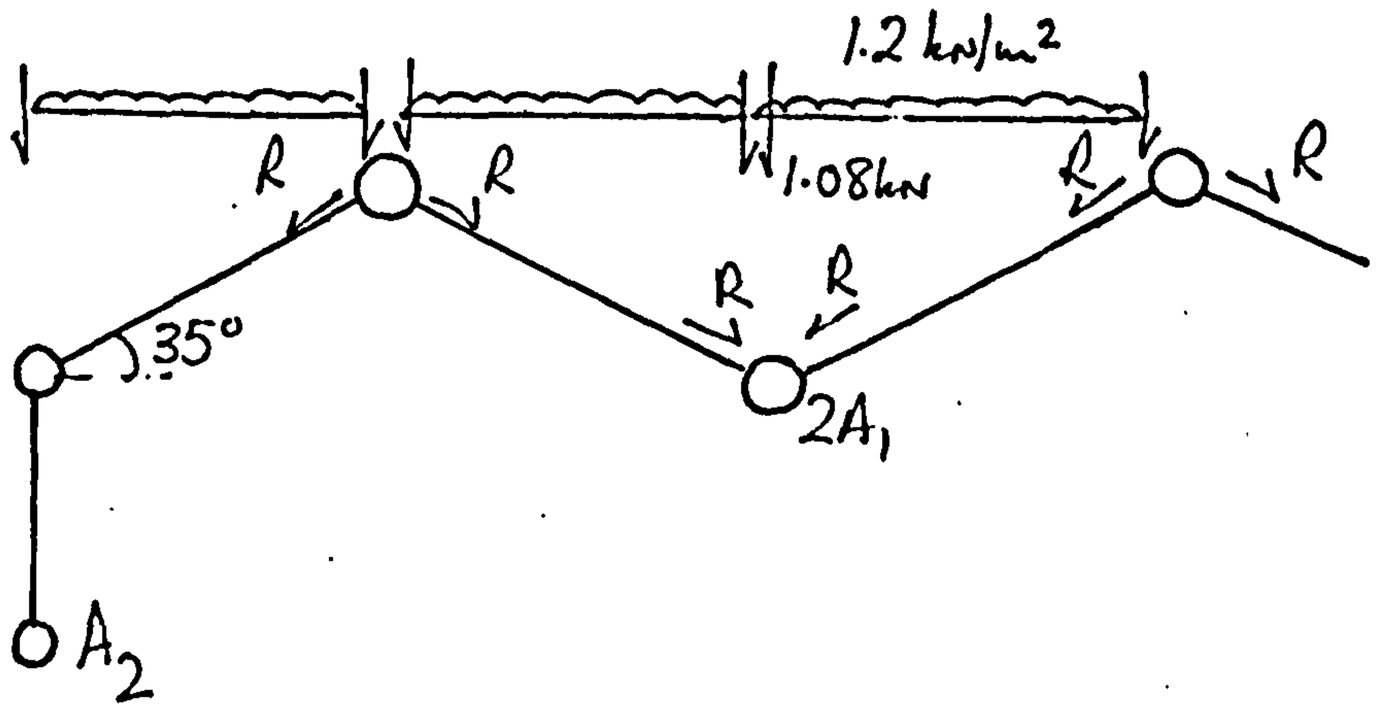

Axial stress in fold line members:

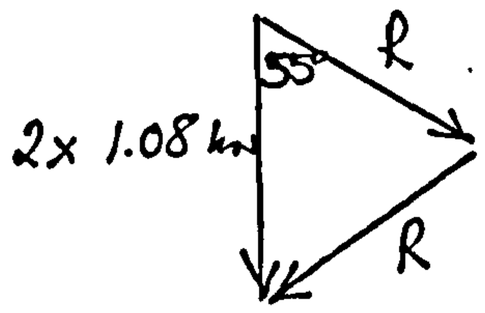

$2R = 3.78$ kN/m

Section modulus of inclined girder $= A_1 \times 2100$ mm^3

$$2R = 2 \times 1.08/\sin 35^\circ$$

$$\therefore \quad \frac{3.78 \times 21.6^2 \times 10^6}{8 \times 150} = A_1 \times 2100; \quad A_1 = 700 \text{ mm}^2$$

Fold line area required for stress of 150 N/mm^2 is $2A_1 = 1400$ mm^2

Chosen fold line area is 2400 mm^2 $\quad \therefore$ stress is 88 N/mm^2

(The fold line is continuously supported)

Fold lines for edge member:

$$\frac{1.08 \times 21.6^2 \times 10^6}{8 \times 150} = A_2 \times 1000 : \quad A_2 = 420 \text{ mm}^2$$

Chosen fold line is 100 x 50 x 3.2 RHS which has area 950 mm^2

From section (11.3) lateral buckling occurs at 3.8 kN/m

<u>End frame members</u>

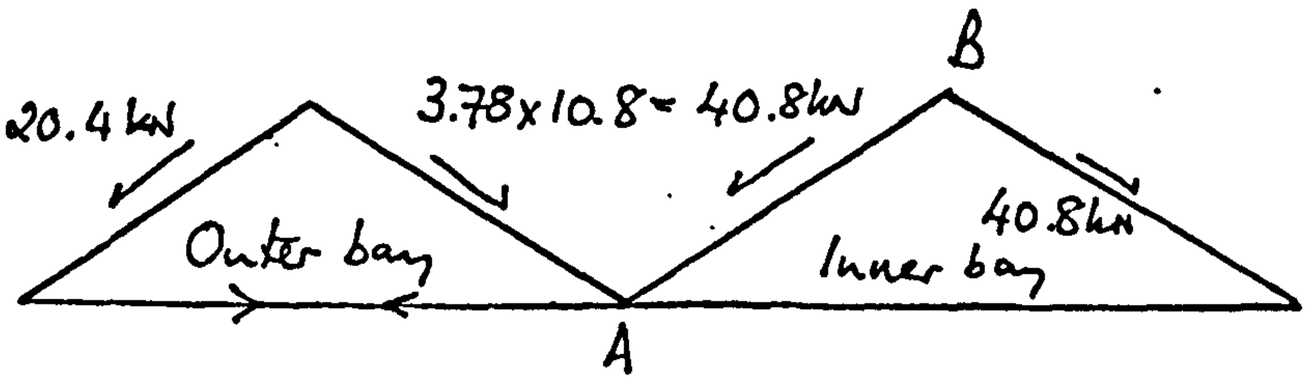

<u>All members -</u>

<u>100 x 50 x 3.2 RHS</u>

Member AB. Axial stress $= \frac{40.8 \times 10^3}{950} = 43$ N/mm^2

If AB acts as a strut $l/r_y = \frac{2200}{20.7} = 106$; $\therefore$ permissible $= 73$ N/mm^2

Member AC. Axial stress $= \frac{33 \times 10^3}{950} = 35$ N/mm^2

Columns - interior, assume load eccentricity of 100 mm from face of column with half column load

Axial force = $40.8 \sin 35^{o} = 23.4$ kN

Bending moment = $23.4 \times 10^{3} (100 + 50) = 3510 \times 10^{3}$ Nmm

$l/r_y = \frac{3500}{38.1} = 93$ Column - 100 x 100 x 6.3 RHS

$\therefore \quad p_c = 87 \text{ N/mm}^2 ; \quad p_{bc} = 165 \text{ N/mm}^2$

Axial stress = $\frac{23.4 \times 10^3}{2340} = 10 \text{ N/mm}^2$; Bending stress = $\frac{3510}{68.2}$

$= 52 \text{ N/mm}^2$

$\therefore \quad \frac{10}{87} + \frac{52}{165} = 0.12 + 0.31 = 0.54 < 1$

Sheet Strength - thickness 0.97 mm

Maximum shear stress is $\frac{40.8 \times 10^3}{2100 \times 0.97} = 20 \text{ N/mm}^2$

Combined stress with bending is $\frac{1}{2} (53) + \frac{1}{2} \sqrt{53^2 + 4 \times 20^2}$

$= 59 \text{ N/mm}^2$

Shear buckling strength $Q = 36 D_x^{1/4} D_y^{3/4} \frac{1}{b}$ kN

$D_y = E.174 \text{ mm}^4/\text{mm}; \quad D_x = \frac{150}{171} \cdot \frac{0.97^3 E}{12(1-0.25^2)}$

$= 0.71 \text{ mm}^4/\text{mm}$

$\therefore \quad Q_{crit} = \frac{36 \times 0.71^{1/4} \times 174^{3/4} \times 210}{2100} = 89.5 \text{ kN}$

Load factor against shear buckling is $\frac{89.5}{40.8} = 2.2$

Strength of sheeting fasteners

Sheet - fold line fasteners:- Each has capacity $6 \times 0.97 = 5.82$ kN

The actual force/fastener is $\frac{wpL}{2b} = \frac{40.8 \times 150}{2100} = 2.91$ kN

where $\frac{wL}{2} = 40.8$ kN; $p = 150$ mm; $b = 2100$ mm

$\therefore$ Load factor is $\frac{5.82}{2.91} = 1.99$

Seam fasteners: Using the formula of section (10.4), the seam failure force is

$$\left\{\frac{n_{sh}}{n_{sh}-2}\right\} \cdot \left[\frac{\frac{n_s}{s_s} + \frac{g_1}{s}}{\frac{n_s}{s_s} + \frac{1}{s}}\right] \cdot (n_s F_s + 2F_p)$$

where $g_1 = 1.56$ for 7 sheet-purlin fasteners, as in Fig (8.10);

$n_{sh} = 24$; $s_s = 0.35$ mm/kN; $s = 0.15$ mm/kN

F_s, Seam fastener capacity is $2.5 \times 0.97 = 2.43$ kN; $n_s = 22$

Failure force is $\frac{24}{22}\left\{\frac{22/0.35 + 1.56/0.15}{22/0.35 + 1/0.15}\right\}(2.43) = 75.0$ kN

Load factor is $\frac{75.0}{40.8} = 1.84$

Sheet-gable fasteners; failure force for $n_{sc} = 14$

$$(n_{sc}+2)\left\{\frac{\frac{n_{sc}}{s_{sc}} + \frac{2g_1}{s}}{\frac{n_{sc}}{s_{sc}} + \frac{2}{s}}\right\} \cdot F_p = \frac{14 + 2 \times 1.56}{14 + 2} \quad 5.82 \times 16 = 99.6 \text{ kN}$$

Load factor is $\frac{99.6}{40.8} = 2.44$

Note. same fasteners used as for fold lines

$\therefore$ $s_{sc} = s = 0.15$ mm/kN

$\therefore$ Critical roof loading is $1.84 \times 1.2 = 2.2$ kN/m^2

Roof deflection - using formulae of section (10.4)

Shear distortion: $$d_{1.1} = \frac{\bar{K} d^{2.5}}{E t^{2.5} b^2} \cdot \frac{wL^2}{8}$$

$\bar{K}$ for closed profile from section (12.1) is 0.019

(For a similar open profile, this would be 0.14)

For 1.2 kN/m^2 loading, the in plane component is 3.78 kN/m

$$d_{1.1} = \frac{0.019 \times 150^{2.5} \times 3.78 \times 21.6^2 \times 10^3}{207 \times 0.97^{2.5} \times 2100^2 \times 8} = 1.4 \text{ mm}$$

Shear strain: $$d_{1.2} = (1 + \nu)(1 + {}^{2h}/_{d}) \frac{wL^2}{4Etb}$$

$$d_{1.2} = 1.25 \times 1.2 \times 3.78 \times 21.6^2 / (4 \times 207 \times 0.97 \times 2100)$$

$$= 1.6\text{m}$$

Axial strain in flanges:

$$d_{1.3} = \frac{wL^4}{38.4 \times E \times A \times b^2}$$ - A fold line area = 1200 mm^2

$$= \frac{3.78 \times 21.6^4 \times 10^9}{38.4 \times 210 \times 1200 \times 2100^2} = 19.3 \text{ mm}$$

Sheet-flange fasteners:

$$d_{2.1} = \frac{spwL^2}{4b^2} = \frac{0.15 \times 150 \times 3.78 \times 21.6^2 \times 10^3}{4 \times 2100^2} = 2.3 \text{ mm}$$

Seam fasteners: no of seam fasteners varies with the shear force

$$d_{2.2} = \frac{2.\frac{wL}{4}\left\{\frac{n_{sh}}{2} - 1\right\}}{\left\{\frac{n_s}{s_s} + \frac{g_1}{s}\right\}} = \frac{3.78 \times 21.6 \times 11}{2\ \frac{22}{0.35} + \frac{1.56}{0.15}} = 6.1 \text{ mm}$$

Sheet/gable fasteners:

$$d_{2.3} = \frac{wL/2}{\left\{\frac{n_{sc}}{s_{sc}} + \frac{2g_1}{s}\right\}} = \frac{3.78 \times 10.8}{\left\{\frac{14}{0.15} + \frac{2x1.56}{0.15}\right\}} = 0.4 \text{ mm}$$

Total deflection in plane of roof slope is

$$1.4 + 1.6 + 19.3 + 2.3 + 6.1 + 0.4 = 31.1 \text{ mm}$$

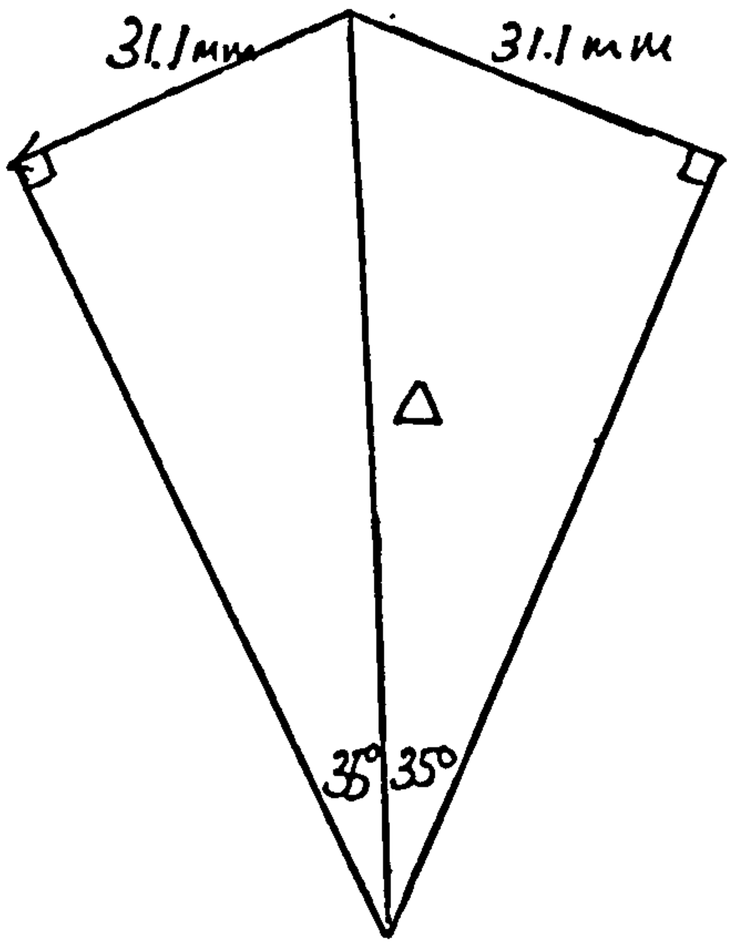

$$\Delta = 31.1/\sin 35^\circ = 54.2 \text{ mm}$$

If an open profile had been used together with smaller fold line area (150 N/mm^2 at failure), then in-plane deflection is

$$10.5 + 1.6 + 33.1 + 2.3 + 6.1 + 0.4$$
$$= 54.0 \text{ mm}$$

$$\therefore \quad \Delta = 54/\sin 35^\circ = 94.1 \text{ mm}$$

Eaves deflection : Vertical deflection of edge beam in isolation from rest of roof is 47.6 mm

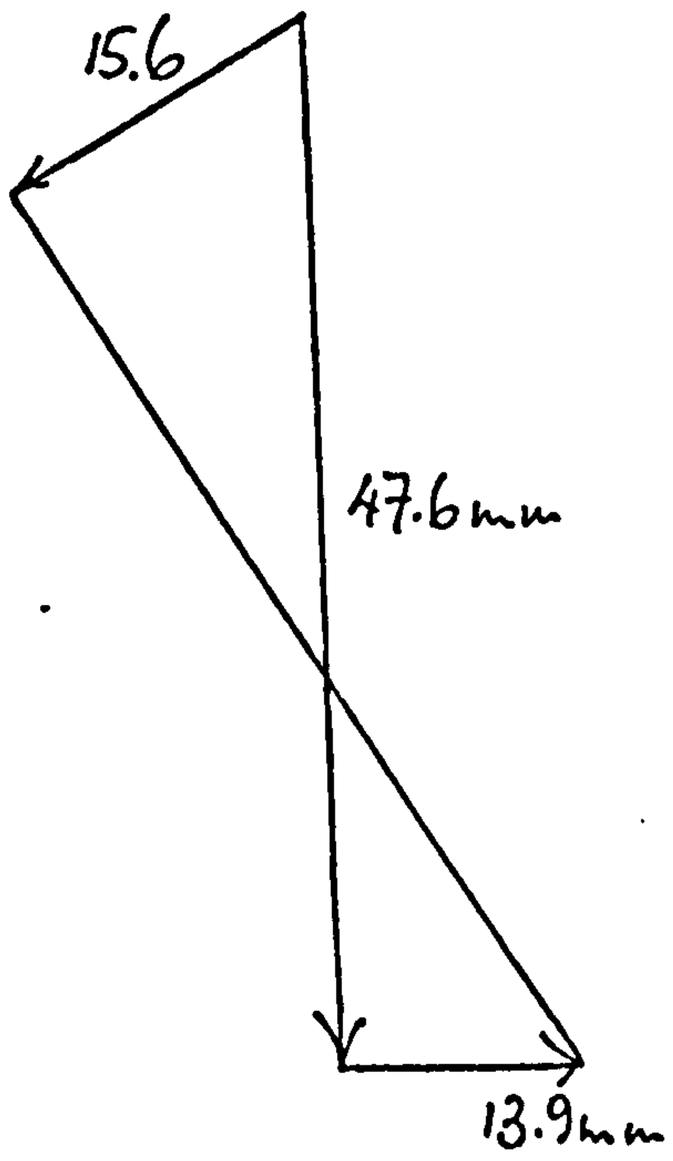

As the outer plate is only subject to half the shear force the central deflection is $31.1/2$ mm.

Thus the inward component is

13.9 mm

This simplified folded plate deflection analysis ignores the true axial strain in the fold lines. The actual deflected shape is shown in Fig (10.11).

APPENDIX 5. COMPUTER PROGRAMS

(5.1) General solution for shear distortion flexibility of every and alternate trough fastened sheets for up to four intermediate purlin attachments as in chapters 2 and 3. The flexibility is output in terms of the $\bar{K}$ parameter

(5.2) Strength of diaphragms due to seam or sheet-shear connector failure. Output is in terms of a factor g such that the seam slip is

$$C_{2.2} = \frac{1}{\left\{\frac{n_s}{s_s} + n_p \cdot \frac{n}{s} \cdot g\right\}}$$

All the terms are defined in section (8.4).

Similarly the diaphragm strength is $\left\{n_s F_s + 2g\, n_p . n . F_p\right\}$

(5.3) Diaphragm openings, as in section (8.7). Both isolated and periodic pitches of flexible bands may be studied and output includes local fastener forces and purlin bending stresses.

(5.4) Holes in folded plate roof solution with regard to critical fold line buckling, and fastener tearing as in section (11.2).

(5.5) Variations in folded plate stiffness due to changes in the sheet-fold line fastening arrangement as developed in section (11.4).

SHEAR FLEXIBILITY OF PROFILED SHEETING

```
      PROGRAM FRED(INPUT,OUTPUT,TAPE1=INPUT,TAPE2=OUTPUT)
      REAL L
      DIMENSION F(17,23),D(23,23),X(289),U(289),Y(17)
      DIMENSION FA(17),FB(17),Z(24)
      DIMENSION FC(17),FD(17),DD(23)
      DIMENSION A(3),B(3),C(3,3),AA(3,3),BB(3,3),AB(3,3)
      DIMENSION AKHAR(7),AKHAKK(7),E(7,7),W(9)
      DIMENSION DT(8),DS(8),DB(8),UB1(8),UB2(8)
   88 READ(1,100) BL,BT,P,H,T,EY,AL
  100 FORMAT(7F8.0)
      WRITE(2,101) BL,BT,P,H,T,EY,AL
  101 FORMAT(7E15.6//)
      IF(BL.EQ.0.0.OR.P) GOTO 51
      ALA=2.0*(BL+BT+P)
      BS=0.5*SQRT(H*H+P*P)
      DO 62 I=1,23
      DO 61 J=1,23
      D(I,J)=0.0
   61 CONTINUE
   62 CONTINUE
      X4=EY*T**3/(12.0*P.91)
      N=0
      X5=BS**2*((2.0+BL/BS)*(2.0+BT/BS)-1.0)/3.0
      X10=2.0*BS/H*((2.0*BS+BL)/BT-BS/BL)
      X8=2.0*BS/H*((2.0*BS+BT)/BL-BS/BT)
      X6=BS/H*(3.0+BT/BS+P/(2.0*BS)*((2.0*BS+BT)/BL+BS/BT))
      X7=P/(2.0*H)*((2.0*BS+BT)/BL-BS/BT)
      X9=BS/H*(3.0+BL/BS+P/(2.0*BS)*((2.0*BS+BL)/BT+BS/BL))
      X11=P/(2.0*H)*((2.0*BS+BL)/BT-BS/BL)
      A(1)=X4/X5*(X7-X6)
      A(2)=X4/X5*X8
      A(3)=X4/X5*(+X6+X7)
      B(1)=X4/X5*(+X9+X11)
      B(2)=+X4/X5*X10
      B(3)=X4/X5*(+X11-X9)
      DO 12 I=1,3
      AB(I,I)=A(I)*B(I)
      DO11 J=1,3
      AI=1.0
      IF(I.NE.J)GOTO30
      GOTO31
   30 AI=2.0
      AB(I,J)=A(I)*B(J)+A(J)*B(I)
   31 AA(I,J)=A(I)*A(J)*AI
      BB(I,J)=B(I)*B(J)*AI
      CCO=1.0/(3.0*X4)
      C(I,J)=CCO*((BL+2.0*BS)*AA(I,J)+(BT+2.0*BS)*BB(I,J)
     1+2.0*BS*AB(I,J))
   11 CONTINUE
   12 CONTINUE
      YA=EY*3.14**4/AL**3*2.67*T
      FAL=AL/6.28
      YB=EY*T*3.14**4*BS/AL**3*4.0
      FALLL=AL/18.84
      G=EY/2.6
      GG=0.33*G*T**3*AL*(H/(2.0*BS))**2.
      D(1,15)=C(1,1)*AL**2/9.42*FALLL
```

Input data

t – sheet thickness, mm
b_L – half trough width, mm
b_T – half top plate width, mm
p – $h \cdot \tan^{-1}\theta$, mm
h – profile depth, mm
E_Y – Young's modulus kgf/mm²
A_L – sheet length, mm.

Profile:

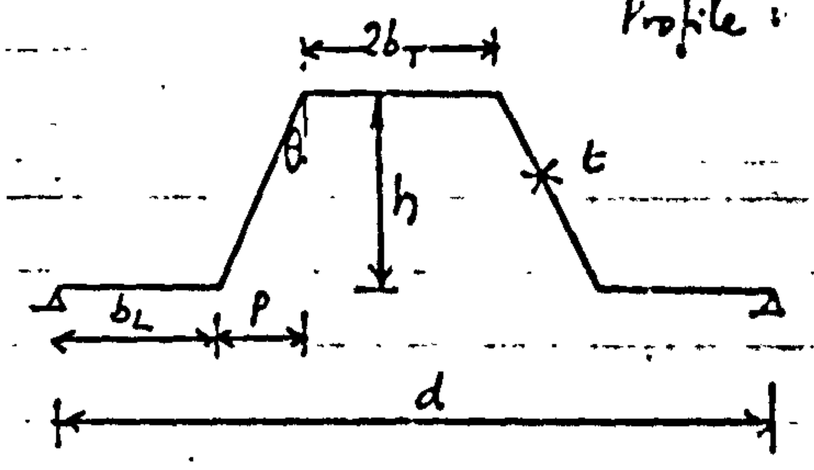


```
      D(1,16)=C(1,2)*AL**2/18.84*FALLL
      D(1,17)=C(1,3)*AL**2/18.84*FALLL
      D(3,15)=C(1,2)*AL**2/18.84*FALLL
      D(3,16)=C(2,2)*AL**2/9.42*FALLL
      D(3,17)=C(2,3)*AL**2/18.84*FALLL
      D(15,15)=(C(1,1)*AL/2.0+81.0*(YB*BT**2+YA*BT**3))*FALLL**2
     1+P.25/BS*GG
      D(16,16)=(C(2,2)*AL/2.0+162.0*BS**3*YA)*FALLL**2
     1+GG*(H.5/BT+0.5/BL)
      D(17,17)=(C(3,3)*AL/2.0+81.0*(YB*BL**2+YA*BL**3))*FALLL**2
     1+P.25/BS*GG
      D(15,16)=C(1,2)*AL/2.0*FALLL**2
      D(15,17)=(C(1,3)*AL/2.0-162.0*BL*BT*YB)*FALLL**2
     1-0.5/HS*GG
      D(16,17)=C(2,3)*AL/2.0*FALLL**2
      D(1,1)=C(1,1)*AL**3/12.0+GG/(2.0*BS)
      D(1,2)=C(1,1)*AL**2/3.14*FAL
      D(1,4)=C(1,2)*AL**2/6.28*FAL
      D(1,5)=C(1,3)*AL**2/6.28*FAL
      D(2,2)=C(1,1)*AL/2.0+YA*BT**3+YB*BT**2
      D(2,2)=D(2,2)*FAL**2+0.25/HS*GG
      D(2,4)=C(1,2)*AL/2.0*FAL**2
      D(2,5)=C(1,3)*AL/2.0-2.0*BT*BL*YB
      D(2,5)=D(2,5)*FAL**2-0.5/HS*GG
      D(4,4)=C(2,2)*AL/2.0+YA*2.0*HS**3
      D(4,4)=D(4,4)*FAL**2+GG*(0.5/BL+0.5/BT)
      D(4,5)=C(2,3)*AL/2.0*FAL**2
      D(5,5)=C(3,3)*AL/2.0+YA*BL**3+YB*HL**2
      D(5,5)=D(5,5)*FAL**2+0.25/BS*GG
      FALL=AL/12.56
      D(1,6)=-C(1,1)*AL**2/6.28*FALL
      D(1,7)=-C(1,2)*AL**2/12.56*FALL
      D(1,8)=-C(1,3)*AL**2/12.56*FALL
```

Terms in energy matrix for energy trough flattening

```
      D(1,1)=C(1,2)*AL**3/12.,0
      D(3,8)=-C(2,1)*AL**2/12.,5*FALL
      D(3,7)=-C(2,2)*AL**2/6.,28*FALL
      D(3,6)=-C(1,2)*AL**2/12.,5*FALL
   95 D(3,5)=C(2,3)*AL**2/6.,28*FAL
      D(3,4)=C(2,2)*AL**2/3.14*FAL
      D(2,3)=C(1,2)*AL**2/6.,28*FAL
      D(3,3)=C(2,2)*AL**3/12.,0+GG*(1./BT+1.,0/BL)
      D(9,9)=G*T*AL*BT
  100 D(10,10)=G*T*AL*BT/2.,0+YB*BT**2*FAL**2
      D(10,14)=-2.,0*BL*BT*YB*FAL**2
      D(11,11)=G*T*AL*2.,0*BS
      D(12,12)=G*T*AL*BS
      D(13,13)=G*T*AL*BL
  105 D(14,14)=G*T*AL*BI/2.,0+YB*BL**2*FAL**2
      D(6,6)=(C(1,1)*AL/2.,0+16.,0*(YB*BT**2+YA*BT**3))*FALL**2
     1+0.25/BS*GG
      D(6,7)=C(1,2)*AL/2.,0*FALL**2
      D(6,8)=(C(1,3)*AL/2.,0-32.,0*BT*BL*YB)*FALL**2
  110 1-0.5/BS*GG
      D(7,7)=(C(2,2)*AL/2.,0+32.,0*BS**3*YA)*FALL**2
     1+GG*(0.5/BT+0.5/BL)
      D(7,8)=C(2,3)*AL/2.,0*FALL**2
      D(8,8)=(C(3,3)*AL/2.,0+(YA*BL**3+YB*BL**2)*16.,0)*FALL**2

  115 1+GG*0.25/BS
      D(5,14)=YB*2.,0*BL**2 *FAL**2
      D(5,10)=-YB*2.,0*BT*BL*FAL**2
      D(2,14)=-YB*2.,0*BT*BL*FAL**2
      D(10,14)=-YB*2.,0*BT*BL*FAL**2
  120 D(2,10)=YB*2.,0*BT**2*FAL**2
      FL=AL/(8.,0*3.14)
      D(18,18)=(C(1,1)*AL/2.,0+4.,0**4*(YB*BT**2+YA*BT**3))*FL**2
     1+0.25/BS*GG
      D(19,19)=(C(2,2)*AL/2.,0+2.,0*4.,0**4*BS**3*YA)*FL**2
  125 1+GG*(0.5/BT+0.5/BT)
      D(20,20)=(C(3,3)*AL/2.,0+4.,0**4*(YB*BL**2+YA*BL**3))*FL**2
     1+0.25/BS*GG
      D(1,18)=-C(1,1)*AL**2/(4.,0*3.14)*FL
      D(1,19)=-C(1,2)*AL**2/(8.,0*3.14)*FL
  130 D(1,20)=-C(1,3)*AL**2/(8.,0*3.14)*FL
      D(3,18)=-C(1,2)*AL**2/(8.,0*3.14)*FL
      D(3,19)=-C(2,2)*AL**2/(4.,0*3.14)*FL
      D(3,20)=-C(2,3)*AL**2/(8.,0*3.14)*FL
      D(18,20)=(C(1,3)*AL/2.,0-2.,0*4.,0**4*BL*BT*YB)*FL**2
  135 1-0.5/BS*GG
      D(18,19)=C(1,2)*AL/2.,0*FL**2
      D(19,20)=C(2,3)*AL/2.,0*FL**2
      FLL=AL/(31.4)
      D(21,21)=(C(1,1)*AL/2.,0+5.,0**4*(YB*BT**2+YA*BT**3))*FLL**2
  140 1+0.25/BS*GG
      D(22,22)=(C(2,2)*AL/2.,0+2.,0*5.,0**4*YA*BS**3)*FLL**2
     1+GG*(0.5/BT+0.5/BL)
      D(23,23)=(C(3,3)*AL/2.,0+5.,0**4*(YB*BL**2+YA*BL**3))*FLL**2
     1+0.25/BS*GG
  145 D(1,21)=C(1,1)*AL**2/(5.,0*3.14)*FLL
      D(1,22)=C(1,2)*AL**2/31.4*FLL
      D(1,23)=C(1,3)*AL**2/31.4*FLL
      D(3,21)=C(1,2)*AL**2/31.4*FLL
      D(3,22)=C(2,2)*AL**2/(3.14*5.,0)*FLL
  150 D(3,23)=C(2,3)*AL**2/31.4*FLL
      D(21,23)=(C(1,3)*AL/2.,0-2.,0*5.,0**4*BT*BL*YB)*FLL**2
     1-0.5/BS*GG
      D(21,22)=C(1,2)*AL/2.,0*FLL**2
      D(22,23)=C(2,3)*AL/2.,0*FLL**2
  155 DO 21 M=1,4
      DO 32 I=1,23
      DO 33 J=1,23
      IF(I.GT.J)D(I,J)=D(J,I)
      IF(I.EQ.J) D(I,J)=2.,0*D(I,J)
  160 33 CONTINUE
      32 CONTINUE
      DO 71 I=1,23
      Z(I)=0.,0
      F(1,I)=D(1,I)+BT/(2.,0*BS)*D(3,I)
  165 F(2,I)=D(2,I)-BI/BL*D(5,I)
      F(3,I)=D(4,I)+2.,0*BS/BL*D(5,I)
      F(4,I)=D(6,I)-BI/BL*D(8,I)
      F(5,I)=D(7,I)+2.,0*BS/BL*D(8,I)
      F(6,I)=D(9,I)+BT/(2.,0*BS)*D(3,I)
  170 F(7,I)=D(10,I)-BT/BL*D(5,I)
      F(8,I)=D(11,I)+D(3,I)
```

Terms in Energy matrix — continued.

```
      PROGRAM FRED      76/76   OPT=1 TRACE                FTN 4.5+420      09/09/75  14.44.55S      P =
AGE   4

      F(9,I)=D(12,I)-2.,0*BS/BL*D(5,I)
      F(10,I)=D(13,I)+BL/(2.,0*BS)*D(3,I)
      F(11,I)=D(14,I)-D(5,I)
  175 F(12,I)=D(15,I)-BT/BL*D(17,I)
      F(13,I)=D(16,I)+2.,0*BS/BL*D(17,I)
      F(14,I)=D(18,I)-BT/BL*D(20,I)
      F(15,I)=D(19,I)+2.,0*BS/BL*D(20,I)
      F(16,I)=D(21,I)-BT/BL*D(23,I)
  180 F(17,I)=D(22,I)+2.,0*BS/BL*D(23,I)
   71 CONTINUE
      IF(M.EQ.1) N=17
      IF(M.EQ.2.OR.M.EQ.3) N=16
      IF(M.EQ.4) N=15
```

```
      DO 22 I=1,23
      IF(M.EQ.1) GOTO 22
      IF(M.EQ.3) GOTO 89
      IF(M.EQ.4) GOTO 87
      F(2,I)=F(2,I)-2.5*BT/BS*D(22,I)
     1-5.0*BT/BL*D(23,I)
      F(3,I)=F(3,I)+5.0*D(22,I)
     1+10.0*BS/BL*D(23,I)
      F(4,I)=F(4,I)-1.25*BT/BS*D(22,I)
     1-2.5*BT/BL*D(23,I)
      F(5,I)=F(5,I)+2.5*D(22,I)
     1+5.0*BS/BL*D(23,I)
      F(7,I)=F(7,I)-2.5*BT/BS*D(22,I)-5.0*BT/BL*D(23,I)
      F(9,I)=F(9,I)-5.0*D(22,I)-10.0*BS/BL*D(23,I)
      F(11,I)=F(11,I)-BL/(2.0*BS)*(5.0*D(22,I)+10.0*BS/BL*D(23,I))
      F(14,I)=F(14,I)+0.625*BT/BS*D(22,I)
     1+1.25*BT/BL*D(23,I)
      F(15,I)=F(15,I)-1.25*D(22,I)
     1-2.5*BS/BL*D(23,I)
      F(16,I)=F(16,I)+BT*0.5/BS*D(22,I)
     1+BT/BL*D(23,I)
      GOTO 22
   89 F(2,I)=F(2,I)+2.5*BT/BS*D(22,I)
     1+5.0*BT/BL*D(23,I)
      F(3,I)=F(3,I)-5.0*D(22,I)
     1-10.0*BS/BL*D(23,I)
      F(7,I)=F(7,I)+2.5*BT/BS*D(22,I)+5.0*BT/BL*D(23,I)
      F(9,I)=F(9,I)+5.0*D(22,I)+10.0*BS/BL*D(23,I)
      F(11,I)=F(11,I)+BL/(2.0*BS)*(5.0*D(22,I)+10.0*BS/BL*D(23,I))
      F(12,I)=F(12,I)-5.0/6.0*BT/BS*D(22,I)
     1-5.0/3.0*BT/BL*D(23,I)
      F(13,I)=F(13,I)+1.67*D(22,I)
     1+3.3*BS/BL*D(23,I)
      F(16,I)=F(16,I)+BT/(2.0*BS)*D(22,I)
     1+BT/BL*D(23,I)
      GOTO 22
   87 DD(I)=D(19,I)+2.0*BS/BL*D(20,I)
      F(2,I)=F(2,I)+BT/(2.0*BS)*4.0*DD(I)
      F(3,I)=F(3,I)-4.0*DD(I)
      F(4,I)=F(4,I)+BT/(2.0*BS)*1.5*(D(16,I)+2.0*BS/BL*D(17,I))
      F(5,I)=F(5,I)-1.5*(D(16,I)+2.0*BS/BL*D(17,I))
      F(7,I)=F(7,I)+BT/(2.0*BS)*DD(I)*4.0
      F(9,I)=F(9,I)+4.0*DD(I)
      F(11,I)=F(11,I)+BL/(2.0*BS)*DD(I)*4.0

      F(12,I)=F(12,I)+BT/(2.0*BS)*(D(16,I)+2.0*BS/BL*D(17,I))
      F(13,I)=F(14,I)+BT/(2.0*BS)*DD(I)
      F(14,I)=F(16,I)
      F(15,I)=F(17,I)
   22 CONTINUE
      DO 24 I=1,N
      IF(M.EQ.2) FA(I)=F(I,22)+2.0*BS/BL*F(I,23)
      IF(M.EQ.3) FB(I)=F(I,22)+2.0*BS/BL*F(I,23)
      IF(M.EQ.1) GOTO 74
      IF(M.EQ.2) GOTO 75
   74 FA(I)=0.0
      IF(M.EQ.3) GOTO 76
   75 FB(I)=0.0
      IF(M.EQ.4) GOTO 77
   76 FC(I)=0.0
      FD(I)=0.0
   77 IF(M.EQ.4) FC(I)=F(I,19)+2.0*BS/BL*F(I,20)
      IF(M.EQ.4) FD(I)=F(I,18)+2.0*BS/BL*F(I,17)
      X(I)=F(I,1)+BT/(2.0*BS)*F(I,3)
      X(I+N)=F(I,2)-BT/BL*F(I,5)-FA(I)*2.5*BT/BS+FB(I)*2.5*BT/BS
     1+2.0*BT/BS*FC(I)
      X(I+2*N)=F(I,4)+2.0*BS/BL*F(I,5)+5.0*FA(I)-5.0*FB(I)
     1-4.0*FC(I)
      X(I+3*N)=F(I,6)-BT/BL*F(I,8)-1.25*BT/BS*FA(I)
     1+1.5*BT/(2.0*BS)*FD(I)
      X(I+4*N)=F(I,7)+2.0*BS/BL*F(I,8)+2.5*FA(I)
     1-1.5*FD(I)
      X(I+5*N)=F(I,9)+BT/(2.0*BS)*F(I,3)
      X(I+6*N)=F(I,10)-BT/BL*F(I,5)
     1-2.5*BT/BS*(FA(I)-FB(I))+BT/(2.0*BS)*FC(I)*4.0
      X(I+7*N)=F(I,11)+F(I,3)
      X(I+8*N)=F(I,12)-2.0*BS/BL*F(I,5)
     1-5.0*(FA(I)+FB(I))+4.0*FC(I)
      X(I+9*N)=F(I,13)+BL/(2.0*BS)*F(I,3)
      X(I+10*N)=F(I,14)-F(I,5)+BL/(2.0*BS)*FC(I)*4.0
     1-5.0*BL/(2.0*BS)*(FA(I)-FB(I))
      IF(M.EQ.4) GOTO 66
      GOTO 67
   66 X(I+11*N)=F(I,15)-BT/BL*F(I,17)+BT/(2.0*BS)*FD(I)
      X(I+12*N)=F(I,16)-BT/BL*F(I,20)+BT/(2.0*BS)*FC(I)
      X(I+13*N)=F(I,21)-BT/BL*F(I,23)
      X(I+14*N)=F(I,22)+2.0*BS/BL*F(I,23)
      GOTO 68
   67 X(I+11*N)=F(I,15)-BT/BL*F(I,17)-5.0/6.0*BT/BS*FB(I)
      X(I+12*N)=F(I,16)+2.0*BS/BL*F(I,17)+1.67*FB(I)
      X(I+13*N)=F(I,18)-BT/BL*F(I,20)+0.625*BT/BS*FA(I)
         X(I+14*N)=F(I,19)+2.0*BS/BL*F(I,20)-1.25*FA(I)
      X(I+15*N)=F(I,21)-BT/BL*F(I,23)+BT/(2.0*BS)*(FA(I)+FB(I))
      IF(M.EQ.1) X(I+16*N)=F(I,22)+2.0*BS/BL*F(I,23)
   68 Y(I)=F(I,3)*0.25/BS
   24 CONTINUE
   79 DO 25 I=1,N
      DO 26 J=1,N
      X(I+(J-1)*N)=0.001*X(I+(J-1)*N)
   26 CONTINUE
   25 CONTINUE
      CALL XINVI(N,X,0,DET)
```

Elimination of dependent variables

Solution for up to four intermediate purlins

Matrix to solve for independent variables

```
      DO 38 LL=1,N
      DO 37 K=1,N
      Z(LL)=Z(LL)+U(LL+N*(K-1))*Y(K)
   37 CONTINUE
  290 38 CONTINUE
      DO 36 LL=1,N
      Z(LL)=Z(LL)*0.001
   36 CONTINUE
      IF(M.EQ.1) Z(22)=Z(17)
  295 IF(M.EQ.4) Z(22)=Z(15)
      IF(M.EQ.4) Z(21)=Z(14)
      IF(M.EQ.4) Z(18)=Z(13)
      IF(M.NE.4) Z(21)=Z(10)
      IF(M.NE.4) Z(19)=Z(15)
  300 IF(M.NE.4) Z(18)=Z(14)
      IF(M.NE.4) Z(16)=Z(13)
      Z(15)=Z(12)
      Z(14)=Z(11)
      Z(13)=Z(10)
  305 Z(12)=Z(9)
      Z(11)=Z(8)
      Z(10)=Z(7)
      Z(9)=Z(6)
      Z(7)=Z(5)
  310 Z(6)=Z(4)
      Z(4)=Z(3)
      IF(M.EQ.3)Z(22)=2.5*BT/BS*(Z(2)+0.2*Z(21)-0.33*Z(15)
     1)+1.67*Z(16)-5.*Z(4)
     1+5.0*Z(12)+BL/(2.*BS)*Z(14)*5.*Z(10)*2.5*BT/BS
  315 IF(M.EQ.2) Z(22)=5.*Z(4)+2.5*Z(7)-1.25*Z(19)-2.5*BT/BS*(
     1Z(2)+0.5*Z(6)-0.25*Z(18)-0.2*Z(21))
     1-5.0*Z(12)-BL/(2.*BS)*Z(14)*5.-2.5*BT/BS*Z(10)
      IF(M.EQ.4)Z(19)=Z(18)*BT/(2.0*BS)-4.0*(Z(4)-Z(12))
     1+BT*2.0/BS*(Z(2)+Z(10))+Z(14)*BL/(2.0*BS)*4.0
  320 IF(M.EQ.4)  Z(16)=Z(15)*BT/(2.0*BS)-1.5*Z(7)+BT/(2.*BS)*1.5*Z(6)
      Z(3)=BT/(2.0*BS)*Z(1)-0.25/BS+Z(9)*BT/(2.0*BS)+Z(11)+Z(13)
     1*BL/(2.*BS)
      Z(5)=-BT/BL*Z(2)+2.0*BS/BL*Z(4)-Z(14)*BT/BL
     1-Z(12)*2.0*BS/BL-Z(14)
  325 Z(8)=-BT/BL*Z(6)+2.0*BS/BL*Z(7)
      Z(17)=-BT/BL*Z(15)+2.0*BS/BL*Z(16)
      Z(20)=-BT/BL*Z(18)+2.0*BS/BL*Z(19)
      Z(23)=-BT/BL*Z(21)+2.0*BS/BL*Z(22)
      Z(24)=0.0
  330 AF=0.0
      DO 34 I=1,23
      DO 35 J=1,23
      IF(I.GT.J) GOTO 35
      IF(I.EQ.J) D(I,J)=0.5*D(I,J)
  335 AF=AF+D(I,J)*Z(I)*Z(J)
   35 CONTINUE
   34 CONTINUE
      Z(1)=Z(1)*AL/2.0
      Z(2)=Z(2)*AL/6.28
  340 Z(3)=Z(3)*AL/2.0
      Z(4)=Z(4)*AL/6.28
      Z(5)=Z(5)*AL/6.28
```

"Displacement" parameters for every trough fixing analysis

Solving for dependent parameters

Total energy expression


```
      Z(6)=Z(6)*AL/12.56
      Z(7)=Z(7)*AL/12.56
  345 Z(8)=Z(8)*AL/12.56
      Z(15)=Z(15)*AL/18.84
      Z(16)=Z(16)*AL/18.84
      Z(17)=Z(17)*AL/18.84
      Z(18)=Z(18)*AL/(8.0*3.14)
  350 Z(19)=Z(19)*AL/(8.0*3.14)
      Z(20)=Z(20)*AL/(8.0*3.14)
      Z(23)=Z(23)*AL/31.4
      Z(22)=Z(22)*AL/31.4
      Z(21)=Z(21)*AL/31.4
  355 CX=0.5/AF
      CX1=(2.0*BL+2.0*BT+4.0*BS)/(1*G*AL)
      CX=CX-CX1
      AK=CX*EY*T**3*AL**3/(0.144*ALA**5)
      AKHAR(M)=AK**.144*SQRT(ALA**3)/(AL*SQRT(T))
  360 AMB=2.0*M/ALA*(2.0*BT+P)*BL
      AMC=M*(2.0/ALA*(2.0*MT+P)*(P+RL)-(P+BT))
      AM1=(P+BT)*M*BL/(ALA*BS)
      AM2=(P+BT)*(P+BL)*M/(ALA*BS)-P*M/(2.0*BS)
      BM1=2.0*M*BL/ALA
  365 BM2=-2.0*M*MT/ALA
```

K and $\bar{K}$ values

```
      D1=AMB/3.0*((BI**2.0*BS)*AM1+AM2*BS)*AMC/3.0
     1+(BS*AM1+AM2*(BT**2.0*BS))
      D2=AMB/3.0*((BL**2.0*BS)*BM1+BM2*BS)*AMC/3.0
     1+(BS*BM1+BM2*(BT**2.0*BS))
370   FLEX1=288.0*((D1**2.0*BS+D2*1.0*BT)/(EY*AL**3*T**3)
      AMB=(B+BT)**2.0*B*BL/ALA
      AMC=2.0*(B+BT)*(B+BL)/ALA-B
      DEF1=BI**2*((BL/3.0*B+2.0*B*BS+BT)-(BS+BT)**2/(B.67*BS+BT))
     1/(EY*T**3/12.0*AL*B.13)
378   DEF2=(AMB**2*(BI**2.0*B*BS)+AMC**2*(BT**2.0*BS)+AMB+AMC**2.0*BS)
     1/(EY*T**3/12.0)**2.0*B/AL
      VSD=72.0*D1/(EY*T**3*AL**2)
      APA=VSD/(DEF1+DEF2)
      AMB=B/ALA*BI
380   AMC=BT*B/ALA
      DEF3=((AMB/3.0*((BI**2.0*BS)*AMB+BS*AMC)+AMC/3.0*(BS*AMB
     1+(BT**2.0*BS)*AMC))/(EY*T**3/12.0))*12.0/AL
      FFLEX=2.0*APA*(4.0*BS*DEF2+2.0*BT*DEF3)/AL
      BFD=FFLEX/FLEX1
388   AN=FLOAT(M)
      AKBARR(M)=AKBAR(M)*(1.0-BFD)
      CX=SQRT(ALA**5/T**5)*AKBARR(M)/(EY*AL**2)
      WRITE(2,133)AKBAR(M),AKBARR(M),CX,AN
133   FORMAT(4E15.6//)
390   DO 55 NL=1,8
      ANL=FLOAT(NL)/8.0
      DT(NL)=Z(1)*ANL+Z(2)*SIN(3.14*ANL)+Z(6)*SIN(6.28*ANL)+
     1Z(15)*SIN(9.42*ANL)+Z(18)*SIN(12.56*ANL)+Z(21)*SIN(18.84*ANL)
      DS(NL)=Z(3)*ANL+Z(4)*SIN(3.14*ANL)+Z(7)*SIN(6.28*ANL)+
398   1Z(16)*SIN(9.42*ANL)+Z(19)*SIN(12.56*ANL)+Z(22)*SIN(18.84*ANL)
      DB(NL)=Z(5)*SIN(3.14*ANL)+Z(8)*SIN(6.28*ANL)+
     1Z(17)*SIN(9.42*ANL)+Z(20)*SIN(12.56*ANL)+Z(23)*SIN(18.84*ANL)
      DT(NL)=DT(NL)*ALA*CX
      DS(NL)=-DS(NL)*AL**2*CX
```

Evaluates 'punch-prop' restraint for every tough fastening

```
PROGRAM FRED      76/76  OPT=1 TRACE          FTN 4.5+420      09/09/76  15.22.35      P =
AGF   8
```

Plate displacements

```
400   DB(NL)=DB(NL)*ALA*CX
   55 CONTINUE
      WRITE(2,188)(DT(NL),NL=1,8)
      WRITE(2,188)(DS(NL),NL=1,8)
      WRITE(2,188)(DB(NL),NL=1,8)
408   188 FORMAT(8E15.6//)
      21 CONTINUE
      L=AL
      AK1=2.0
      AK2=2.0
410   DDD=H**2*(0.67*BS+BT)
      VS=0.5*H*BL*(BS+BT)
      Z1=BL**2/ALA
      Z2=BL/ALA*(BL+B)
      Z3=BL/ALA*(BL+B+2.0*BT)
418   Z4=(1.0-BL/ALA)*BL
      ZA1=BL
      ZA2=BL+B
      ZA3=BL+B+2.0*BT
      ZA4=BL+2.0*B+2.0*BT
420   ZB1=BL
      ZB2=BL
      ZB3=BL
      ZB4=BL
      ZC1=BL*(1.0-BL/ALA)
428   ZC2=BL/ALA*(BL+B+2.0*BT)
      ZC3=BL/ALA*(BL+B)
      ZC4=BL**2/ALA
      ZD1=0.0
      ZD2=H/2.0
438   ZD3=H/2.0
      ZD4=0.0
      D11=AK1*0.5*SOMP(ZA1,ZA2,ZA3,ZA4,ZA1,ZA2,ZA3,ZA4,BL,BS,BT)+
     1AK1*2.5*ZA4**2*BL*B.67+
     1B.5*SOMP(Z1,Z2,Z3,Z4,Z1,Z2,Z3,Z4,BL,BS,BT)
438   D12=B.5*AK1*SOMP(ZB1,ZB2,ZB3,ZB4,ZA1,ZA2,ZA3,ZA4,BL,BS,BT)+
     1B.5*AK1*ZA4*ZB4*BL*B.67+
     1B.5*SOMP(ZC1,ZC2,ZC3,ZC4,Z1,Z2,Z3,Z4,BL,BS,BT)
      D21=B.5*AK2*SOMP(ZB1,ZB2,ZB3,ZB4,ZA1,ZA2,ZA3,ZA4,BL,BS,BT)+
     1B.5*AK2*ZA4*ZB4*BL*B.67+
448   1B.5*SOMP(ZC1,ZC2,ZC3,ZC4,Z1,Z2,Z3,Z4,BL,BS,BT)
      D22=B.5*SOMP(ZC1,ZC2,ZC3,ZC4,ZC1,ZC2,ZC3,ZC4,BL,BS,BT)+
     1AK2*B.5*ZB4**2*BL*B.67+
     1AK2*B.5*SOMP(ZB1,ZB2,ZB3,ZB4,ZB1,ZB2,ZB3,ZB4,BL,BS,BT)
      P1=VS*(D22-D12)/(D11*D22-D12*D21)
448   P2=VS*(D21-D11)/(D12*D21-D11*D22)
      IF(P1.LT.B.B) GOTO 72
      IF(P2.LT.B.B) GOTO 78
      GOTO 73
   72 P1=B.B
458   P2=VS/D22
      GOTO 73
   78 P2=B.B
      P1=VS/D11
   73 B=P1*2.0*SOMP(Z1,Z2,Z3,Z4,ZD1,ZD2,ZD3,ZD4,BL,BS,BT)/DDD
468     1+P2*2.0*SOMP(ZC1,ZC2,ZC3,ZC4,ZD1,ZD2,ZD3,ZD4,BL,BS,BT)/DDD
      GG=EY/2.6*B.33*T**3
      V=BL/H*(BS+BT)/(B.67*BS+BT)
      AK=EY*T**3/(12.0*H**2*(1.13*BS+2.0*BT))
```

Evaluates 'punch-prop' restraint for alternate tough fastening

```
      GA=HL**3/3.0+HT**3/6.0+(HL+2.0*V*BS)**2*BT/2.0
     1+BS/8.0+((3.0*BL+2.0*V*BS-BT)**2+(BL+2.0*V*BS+BT)**2
     1+1.0/3.0*(HL-2.0*V*BS+BT)**2+1.0/3.0*(BL+2.0*V*BS+BT)**2)
  480 GA=GA*EY*1*9.0/L
      GC=-HT*(BL+2.0*V*PS)**2+BT**3/3.0+BS/4.0*((-3.0*BL-2.0*V*BS+BT)*
     1(PL+2.0*V*BS+HT)+(-BL-2.0*V*BS-BT)*(3.0*HL+2.0*V*BS-BT)
     1+2.0/3.0*(HT+HL-2.0*V*BS)*(HT+HL+2.0*V*BS))
      GC=GC*EY*1*9.0/L
  485 GB=BL**3/3.0+HT**3/6.0+(BL+2.0*V*BS)**2*BT/2.0
     1+BS/8.0*((HL+2.0*V*BS+BT)**2+(3.0*BL+2.0*V*BS-BT)**2
     1+1.0/3.0*(HL-2.0*V*BS+BT)**2+1.0/3.0*(BL+2.0*V*BS+BT)**2)
      GB=GB*EY*1*9.0/L
      VS=(2.0*(P+HT)*HL/ALA)**2*(BL+2.0*BS)/3.0+(2.0*HL*BT/ALA)**2*
  490 1(HT+2.0*BS)/3.0+(2.0*(P+BT)*HL/ALA)*2.0*BT*HL/ALA*2.0*BS/3.0
      GD=L/(8.0*VS)*(L/6.28)**2*((BT+BL)/(2.0*BS))**2*EY*T**3/10.0
      E(1,1)=AK*L/6.0+(P.5/BL*V**2+0.25/BS)*6.0/L*GG
      E(1,2)=-AK*L**2/(9.8*2.0)
      E(1,3)=AK*L**2/(9.8*8.0)
  495 E(1,4)=-E(1,2)
      E(1,6)=-AK*L**2/(9.8*16.0)
      E(1,5)=-E(1,3)
      E(1,7)=-E(1,6)
      E(2,2)=AK*L**3/(9.8*16.0)+L*GG*(0.5/BL*V**2+P.25/BS)/4.0+GA+GD
  500 E(3,3)=AK*L**3/(9.8*64.0)+L*GG*(0.5/BL*V**2+P.25/BS)/4.0+4.0*GA+
     110.25*GD
      E(6,6)=AK*L**3/(9.8*16.0*9.0)+L*GG*(0.5/BL*V**2+P.25/BS)/4.0+
     19.0*GA+1.0/9.0*GD
      E(4,4)=E(2,2)+GB-GA
  505 E(5,5)=E(3,3)+4.0*GB-4.0*GA
      E(7,7)=E(6,6)+9.0*(GB-GA)
      E(2,4)=-2.0*E(2,2)+GC+2.0*GD+2.0*(GA+GD)
      E(3,5)=-2.0*E(3,3)+4.0*GC+P.5*GD+2.0*(4.0*GA+P.25*GD)
      E(6,7)=-2.0*E(6,6)+9.0*GC+2.0/9.0*GD+2.0*(9.0*GA+1.0/9.0*GD)
  510 DAT=4.0*E(3,3)*E(5,5)-E(3,5)**2
      DOT=4.0*E(6,6)*E(7,7)-E(6,7)**2
      DO 10 M=5,7
      IF(M.EQ.5) GOTO 94
      GOTO 91
  515 94 DET=4.0*E(2,2)*E(4,4)-E(2,4)**2
      Z(1)=(-2.0*E(1,2)*E(4,4)+E(2,4)*E(1,4))/DET
      Z(3)=(+E(1,2)*E(2,4)-2.0*E(2,2)*E(1,4))/DET
      Z(2)=(-2.0*E(1,3)*E(5,5)+E(3,5)*E(1,5))/DAT
      Z(4)=(-2.0*E(3,3)*E(1,5)+E(1,3)*E(3,5))/DAT
  520 Z(5)=(-2.0*E(7,7)*E(1,6)+E(1,7)*E(6,7))/DOT
      Z(6)=(-2.0*E(6,6)*E(1,7)+E(1,6)*E(6,7))/DOT
      GOTO 98
   91 IF(M.EQ.6) GOTO 95
      GOTO 92
  525 95 W(1)=2.0*E(2,2)+8.0*E(3,3)
      W(2)=E(2,4)
      W(3)=-2.0*E(3,5)
      W(4)=E(2,4)
      W(5)=2.0*E(4,4)
  530 W(6)=0.0
      W(7)=-2.0*E(3,5)
      W(8)=0.0
      W(9)=2.0*E(6,6)
```

Energy method terms for alternate trough festuring.

Solution for up to three independent variables


```
      Y1=2.0*E(1,3)-E(1,2)
  535 Y2=-E(1,4)
      Y3=-E(1,5)
      A1=Y3/W(9)
      A2=-W(3)/W(9)
      A3=Y2/W(5)
  540 A4=-W(2)/W(5)
      Z(1)=(Y1-W(7)*A1-W(4)*A3)/(W(7)*A2+W(4)*A4+W(1))
      Z(4)=A1+A2*Z(1)
      Z(3)=A3+A4*Z(1)
      Z(2)=-2.0*Z(1)
  545 Z(5)=(-2.0*E(7,7)*E(1,6)+E(1,7)*E(6,7))/DOT
      Z(6)=(-2.0*E(6,6)*E(1,7)+E(1,6)*E(6,7))/DOT
      GOTO 98
   92 IF(M.EQ.7) GOTO 96
      GOTO 98
  550 96 W(1)=2.0*E(2,2)+18.0*E(6,6)
      W(3)=3.0*E(6,7)
      W(7)=3.0*E(6,7)
      W(9)=2.0*E(7,7)
      Y1=-E(1,2)-3.0*E(1,6)
  555 Y3=-E(1,7)
      A1=Y3/W(9)
      A2=-W(3)/W(9)
      A3=Y2/W(5)
      A4=-W(2)/W(5)
  560 Z(1)=(Y1-W(7)*A1-W(4)*A3)/(W(7)*A2+W(4)*A4+W(1))
      Z(5)=3.0*Z(1)
      Z(3)=A3+A4*Z(1)
```

```
      Z(6)=A1+A2*Z(1)
      Z(2)=(-2.*F(1,3)*E(5,5)+F(3,5)*E(1,5))/DAT
      Z(4)=(-2.*F(1,3)*E(3,5)+E(1,5)*E(1,3)*E(3,5))/DAT
   98 C=E(1,1)+E(1,2)*Z(1)+E(1,3)*Z(2)+E(1,4)*Z(3)+E(1,6)*Z(4)
     1+E(2,2)*Z(1)**2+E(3,3)*Z(2)**2+E(4,4)*Z(3)**2+E(5,6)*Z(4)**2
     1+E(2,4)*Z(1)*Z(3)+E(3,6)*Z(2)*Z(4)
     1+E(6,6)*Z(5)**2+E(7,7)*Z(6)**2+E(6,7)*Z(5)*Z(6)
     1+E(1,6)*Z(5)+E(1,7)*Z(6)
      CX=(ALA/L)**2*0.5/U
      CK=CX*EY*L**2/(6WRI(ALA**7/T**5))
      AK=FLOAT(K)
      Z(1)=L/6.28*Z(1)
      Z(2)=L/12.56*Z(2)
      Z(3)=L/6.28*Z(3)
      Z(4)=L/12.56*Z(4)
      Z(5)=L/(6.28*3.0)*Z(5)
      Z(6)=L/(6.28*3.0)*Z(6)
      ABO=CX*L/ALA
      Z(1)=Z(1)*ABO
      Z(2)=Z(2)*ABO
      Z(3)=Z(3)*ABO
      Z(4)=Z(4)*ABO
      Z(5)=Z(5)*ABO
      Z(6)=Z(6)*ABO
      IF(AN.EQ.5.0) GOTO 57
      IF(AN.EQ.7.0) GOTO58
      IF(AN.EQ.6.0) GOTO 59
   57 AKBAR(5)=CK+AKBAR(1)


      AKBARR(5)=CK*(1.0-R)+AKBAR(1)
      GOTO 60
   59 AKBAR(6)=CK+AKBAR(1)*0.5+AKBAR(2)*0.5
      AKBARR(6)=CK*(1.0-R)+AKBAR(1)*0.5+AKBAR(2)*0.5
      GOTO 60
   58 AKBAR(7)=CK+AKBAR(1)*0.5+AKBAR(3)*0.5
      AKBARR(7)=CK*(1.0-R)+AKBAR(1)*0.5+AKBAR(3)*0.5
   60 CX=SQRT(ALA**5/T**5)*AKBARR(M)/(EY*L**2)
      WRITE(2,133)AKBAR(M),AKBARR(M),CX,AN
      DO 56 NL=1,8
      ANL=FLOAT(NL)/8.0
      UB1(NL)=ABO*ANL+Z(2)*SIN(3.14*ANL)+Z(4)*SIN(6.28*ANL)+
     1Z(6)*SIN(9.42*ANL)
      UB2(NL)=Z(1)*SIN(3.14*ANL)+Z(3)*SIN(6.28*ANL)+Z(5)*SIN(9.42*ANL)
   56 CONTINUE
      WRITE(2,188)(UB1(I),I=1,8)
      WRITE(2,188)(UB2(I),I=1,8)
   10 CONTINUE
      GOTO 88
   51 STOP
      END
```

Energy expression

Evaluates K and $\bar{K}$ values for alternate trough fastening

Plate displacements

```
      FUNCTION SOMP(A1,A2,A3,A4,B1,B2,B3,B4,BL,BS,BT)
      SOMP=A1*B1*(BL+2.0*BS)/3.0+A2*B2*(2.0*BS+2.0*B1)/3.0+
     1(A1*B2+B1*A2)*BS/3.0+A3*B3*(2.0*BS+2.0*BT)/3.0+(A2*B3+A3*B2)*BT
     1/3.0+A4*B4/3.0*(BL+2.0*BS)+(A4*B3+A3*B4)*BS/3.0
    5 RETURN
      END
```

Integrates cross-sectional bending moments

SUBROUTINE XINVT 76/76 OPT=1 TRACE FTN 4.5+420 09/09/76 10.40.55S P =
IGE 1

```
    1 SUBROUTINE XINV1(IP,B,C,DET)
      DIMENSION B(289),C(289)
      IF(IP.EQ.1)GO TO 9
      IW=IP*IP
    5 DO 2 I=1,IW
    2 C(I)=0
      DO 3 I=1,IP
    3 C(I+IP*(I-1))=1.0
      IW=IP-1
   10 DO 5 IQ=1,IW
      K=IP-IQ+1
      AP=B(K+IP*(K-1))
      IK=K-1
      DO 5 I=1,IK
   15 AT=B(I+IP*(K-1))/AP
      DO 5 J=1,IP
      B(I+IP*(J-1))=B(I+IP*(J-1))-B(K+IP*(J-1))*AT
    5 C(I+IP*(J-1))=C(I+IP*(J-1))-C(K+IP*(J-1))*AT
C     MATRIX NOW REDUCED TO UPPER TRIANGLE FORM
   20 DO 6 IQ=1,IW
      AP=B(IQ+IP*(IQ-1))
      IK=IQ+1
      DO 6 I=IK,IP
      AT=B(I+IP*(IQ-1))/AP
   25 DO 6 J=1,IP
      B(I+IP*(J-1))=B(I+IP*(J-1))-B(IQ+IP*(J-1))*AT
    6 C(I+IP*(J-1))=C(I+IP*(J-1))-C(IQ+IP*(J-1))*AT
C     MATRIX NOW REDUCED TO DIAGONAL FORM
      DET=1.0
   30 DO 7 I=1,IP
      DO 12 J=1,IP
   12 C(I+IP*(J-1))=C(I+IP*(J-1))/B(I+IP*(I-1))
    7 DET=DET*B(I+IP*(I-1))
      GO TO 8
   35 C(1)=1.0/B(1)
    9 DET=B(1)
    8 RETURN
      END
```

Solves for independent displacement parameter (17)

OUTPUT FOR PROFILE SHEAR DISTORTION

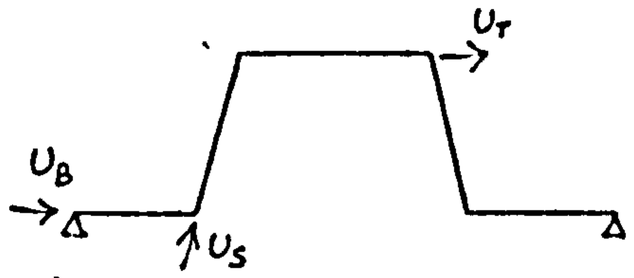

Plate displacements for every trough fastening.

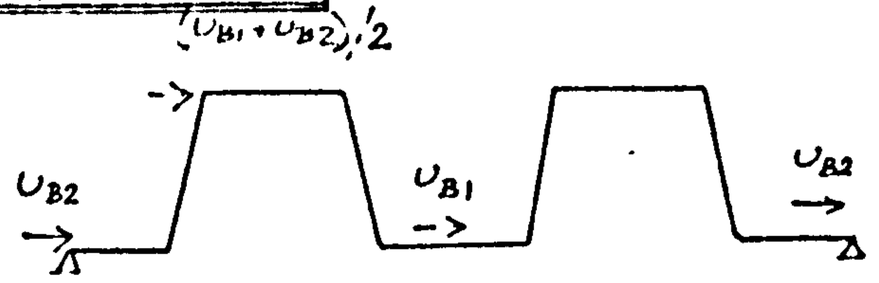

Concertina plate displacements to be added to the every trough fastening displacement to give the deflection due to alternate trough fastening

N=1 - Every trough fastening, no intermediate purlins;
N=2 - " " " , 2 " "
N=3 - " " " , 3 " "
N=4 - " " " , 4 " "

N=5 -- alternate trough fastening
N=6 - " " " 2 intermediate purlins
N=7 - " " " 3 " "

.300000F+02 .100000F+02 .190000F+02 .380000E+02 .670000F+00 .207000E+03 .600104E+04

DATA b_L b_S b_T h t E AL

.219302F+00 .173490F+00 .174000F-04 .100000E+01 $\bar{K}$ - value for no purlin - prop restraint

$\bar{K}$ $\bar{K}(1-r)$ CX N $\bar{K}(1-r)$ - value for purlins - prop restraint

.562113F-02 .107322F-01 .169868F-01 .217934E-01 .269105E-01 .337924E-01 .392584F-01 .447931E-01

U_T Top plate displacements from centre line to outer face for 1 kN shear force

.242700F-02 .577299F-03 .601823F-02 .101457E-01 .113400F-01 .103577F-01 .273594E-01 .588868F-01

U_S Side plate displacements

.550406F-02 .102264E-01 .170703F-01 .218591E-01 .298241E-01 .377702E-01 .270305E-01 .110504E-03

U_B Bottom plate displacements

.150852F+00 .124041F+00 .124835E-04 .200000E+01 CX - sheet flexibility mm/kN/mm

Two intermediate purlins

.360704F-02 .657488E-03 .107142F-01 .136961E-01 .170451E-01 .220408E-01 .257683E-01 .300146E-01

.317305F-02 .100341E-01 .990007E-02 .988298E-02 .733709E-02 .509464E-02 .191431F-01 .304802E-01

.114242E-02 -.132738E-03 .361841E-02 .944697E-02 .182188F-01 .262095E-01 .167773E-01 .666689E-04

.111249F+00 .879777F-01 .885404E-05 .300000E+01 Three intermediate purlins

.186506F-02 .403802E-03 .634389E-02 .854486E-02 .109479E-01 .138374E-01 .168904E-01 .198032E-01

.553678E-03 .222283E-02 .757019E-02 .107911E-01 .864791E-02 .605466E-03 .102537E-01 .258432E-01

.225863E+02 .326815E-03 .480244E-03 .442762E-03 .659809E-02 .135108E-01 .130439E-01 .662895E-04

.833307E-01 .658095E-21 .663209E-05 .400000E+01 Four intermediate purlins

.117782E-02 .237667E-03 .420152E-02 .549719E-02 .707801E-02 .957888E-03 .114912E-01 .132253E-01

.218693E-02 .265018E-03 .298433E-02 .725492E-03 .917887E-02 .602933E-03 .810502E-02 .170440E-01

-.717137E-03 .635787E-03 .212087E-02 -.172180E-03 .423152E-03 .662758E-02 .755567E-02 .377598E-04

$\bar{K}$ $\bar{K}(1-r)$ Cx N Alternate trough fastening

.807504E+00 .734860E+00 .739257E-04 .500000E+01

U_{B1} Centre trough displacements from centre line to outer face

.456825E-01 .900810E-01 .132106E+00 .171809E+00 .211317E+00 .254107E+00 .302453E+00 .355141E+00

U_{B2} Outer trough displacements

-.241770E-01 -.219804E-01 .163102E-01 .762499E-01 .125716E+00 .132827E+00 .854753E-01 .374350E-03

.619783E+00 .542882E+00 .566280E-04 .600000E+01 Two intermediate purlins

.275247E-01 .554012E-01 .836790E-01 .112571E+00 .143109E+00 .177381E+00 .214134E+00 .258195E+00

-.187776E-01 -.190908E-01 -.748530E-02 .185010E-01 .386004E-01 .453431E-01 .704103E-01 .134815E-03

.956775E+00 .508170E+00 .511429E-04 .700000E+01 Three intermediate purlins

.340840E-01 .627571E-01 .864075E-01 .110374E+00 .130106E+00 .171984E+00 .204955E+00 .236369E+00

-.787885E-02 -.143930E-01 -.135107E-01 -.303704E-04 .213058E-01 .350830E-01 .271177E-01 .129491E-03

STRENGTH OF DIAPHRAGMS

```
0005          MASTER STRENGTH
0006          REAL N
0007          DIMENSION VF(8),VS(8),VO(8)
0008       88 READ(1,101) CX,AIY,EY,A,N
0009          IF(CX,EQ,0,0) GOTO 89
0010          READ(1,101) ANE,ANS,SE,SS
0011      100 FORMAT(5F8,0)
0012          ANE=,0F67*A/ANE
0013          READ(1,102) G,H,AJ
0014      102 FORMAT(3F8,0)
0015      101 FORMAT(4F8,0)
0016          WRITE(2,113) CX,AIY,EY,A,N
0017      113 FORMAT(5E15,6//)
0018          WRITE(2,110) ANE,ANS,SE,SS
0019      110 FORMAT(4E15,6//)
0020          WRITE(2,120) G,H,AJ
0021      120 FORMAT(3E15,6//)
0022          EG=EY*AIY/(G*AJ*4,0/H**2)
0023          CS=CX*0,25*H**2/(G*AJ*N)
0024       90 X1=N*CS*0,5/(A*SE/ANE)
0025          X2=1,0/(EY*AIY*A*SE/ANE)
0026          DC=0,0
0027          Y1=-X1**2+X2
0028          IF(Y1,LT,0,0) GOTO 69
0029          GOTO 70
0030       69 DC=1,0
0031          Y1=X1**2-X2
0032          Y1=SQRT(Y1)
0033          A1=SQRT(X1+Y1)
0034          A2=SQRT(X1-Y1)
0035          GOTO 71
0036       70 Y1=SQRT(Y1)
0037          A1=(X1+SQRT(X1**2+Y1**2))*0,5
0038          A1=SQRT(A1)
0039          A2=(-X1+SQRT(X1**2+Y1**2))*0,5
0040          A2=SQRT(A2)
0041       71 CA1=COS(A1*A*0,5)
0042          SA1=SIN(A1*A*0,5)
0043          CH1=COSH(A1*A*0,5)
0044          CA2=COS(A2*A*0,5)
0045          CH2=COSH(A2*A*0,5)
0046          SH1=SINH(A1*A*0,5)
0047          SH2=SINH(A2*A*0,5)
0048          SA2=SIN(A2*A*0,5)
0049          IF(DC,EQ,1,0) GOTO 72
0050          GOTO 73
0051       72 BA=-A1**2*SH1/(A2**2*SH2)
0052          ATS=CX*EY*AIY*A1**2*N
0053          BTS=CX*EY*AIY*A2**2*BA*N
0054          ATE=(1,0-A1**2*EG)
0055          BTE=(1,0-A2**2*EG)*BA
0056          AB=(BTE-BTS)/(ATE-ATS)
0057          FE=2,0/A**2*(A*0,5/A1*CH1-SH1/A1**2+AB*(A*0,5/A2*CH2-SH2/A2**2))
0058          FS=SH1+AB*SH2
0059          VS1=A1+A2*BTS/ATS
0060          VS2=A1*CH1+A2*CH2*BTS/ATS
0061          VMAX=SH1+BTE/ATE*SH2
0062            VMAXO=SH1+BA*SH2
0063          DSHEAR=ATS*SH1+BTS*SH2
0064          FEJ=(CH1-1,0)/(A1*A)+AB*(CH2-1,0)/(A2*A)-FE
0065          GOTO 74
0066       73 A12=A1**2+A2**2
0067          BA=(-(A1**2-A2**2)*SH1*CA2+2,0*A1*A2*CH1*SA2)/
0068         1((A1**2-A2**2)*CH1*SA2+2,0*A1*A2*SH1*CA2)
0069          ATE=1,0-EG*(X1+Y1*BA)
0070          BTE=BA-EG*(-Y1+BA*X1)
0071          ATS=CX*EY*AIY*(-X1-BA*Y1)*N
0072          BTS=CX*EY*AIY*(Y1-BA*X1)*N
0073          ATS=-ATS
0074          BTS=-BTS
0075          AB=(BTE-BTS)/(ATE-ATS)
0076          B1=0,5*A*CH1*CA2*(A1-A2*AB)/A12
0077          B2=0,5*A*SH1*SA2*(A2+A1*AB)/A12
0078          B3=CH1*SA2*(-2,0*A1*A2+(A2**2-A1**2)*AB)/A12**2
0079          B4=SH1*CA2*(A2**2-A1**2+2,0*A1*A2*AB)/A12**2
0080          FE=2,0/A**2*(B1+B2+B3+B4)
0081          FS=SH1*CA2+AB*CH1*SA2
0082          AI1=(A2*SH1*SA2+A1*(CH1*CA2-1,0))/A12
0083          AI2=(-A2*(CH1*CA2-1,0)+A1*SH1*SA2)/A12
0084          FEJ=2,0/A**2*(A**0,5*(AI1+AI2*AB))-FE
0085          VS1=A1+BTS/ATS*A2
0086          VS2=A1*CH1*CA2-A2*SH1*SA2+BTS/ATS*(SA2*SH1*A1+A2*CH1*CA2)
0087          VMAX=SH1*CA2+BTE/ATE*CH1*SA2
0088          VMAXO=SH1*CA2+BA*CH1*SA2
0089          DSHEAR=ATS*SH1*CA2+BTS*CH1*SA2
0090       74 AN=ANE*N/SE
0091          BK1=1,0/(AN*A/12,0+ANS/SS*A)
0092          BK2=-(FE*AN+2,0*ANS/SS*FS)*BK1
```

Input data

CX – Sheet flexibility, mm/kgs/mm
AIY – purlin 'taken' inertia, mm^4
ET – Young's modulus, kgs/mm^2
A – panel width or sheet width, mm
G – Shear modulus, kgs/mm^2
H – purlin depth, mm
AJ – Torsional stiffness, mm^4
SE – fastener slip, mm/kgs
SS – seam fastener slip
ANS – number of seam fastners
ANE – sheet – purlin fastenings
(= 1 for every trough fastening)
(= 2 for alternate trough fastening)
N – number of purlins

Differential equation solution depending on nature of roots

Solution of differential equation constants by boundary conditions

```
0093                BK3=CX*(1,0+AN*BK1*A/24,0)
0094                BK4=-VS1*ATS+CX*(ATE-ATS)*(AN*FE3+BK2*A/24,0*AN)
0095                AD=(BK3/CX-ANS/SS*BK1*A)/((ATE-ATS)*ANS/SS*(2,0*FS+BK2*A)
0096               1-ATS*VS2/CX-BK4/CX)
0097                FE=(ATE-ATS)*FE*AD+(BK1+BK2*(ATE-ATS)*AD)*A/12,0
0098                FS=FS*(ATE-ATS)*AD+(BK1+BK2*(ATE-ATS)*AD)*A/2,0
0099                D=BK1+BK3+AD*(BK2*(ATE-ATS)+BK4)
0100                DEL=2,0*ATE*VMAX*AD+D*A
0101                DEL3=(BK3+BK4*AD)*A/DEL
0102                DSHEAR=DSHEAR*AD*2,0+DEL3*DEL
0103                DELEND=DEL-DSHEAR
0104                FE=FE/DELEND
0105                FS=FS/DELEND
0106                AFF=12,0*FE*A
0107                G=FE
0108                SSF=1,0+(A1*ATS+A2*BTS)*AD/CX
0109                BD=2,0/A*AD*(ATE*VMAX-VMAXO)+D
0110                DEL4=BD*A/DEL
0111                DO 55 I=1,8
0112                ANN=FLOAT(I)
0113                AA1=A1*A*0,5*ANN/8,0
0114                AA2=A2*A*0,5*ANN/8,0
0115                IF(DC,EQ,1) GOTO 46
0116                VE(I)=AD*(SINH(AA1)*COS(AA2)*ATE+BTE*COSH(AA1)*SIN(AA2))
0117               1+D*ANN/8,0*A*0,5
0118               1-CX*ANN*A/16,0
0119                VO(I)=AD*(SINH(AA1)*COS(AA2)+BA*COSH(AA1)*SIN(AA2))
0120               1+DEL4*DEL/A*ANN/8,0*A*0,5
0121               1-CX*ANN*A/16,0
0122                VS(I)=AD*(SINH(AA1)*COS(AA2)*ATS+COSH(AA1)*SIN(AA2)*BTS)
0123               1+DEL3*DEL/A*ANN/8,0*A*0,5
0124               1-CX*ANN*A/16,0
0125                GOTO 55
0126              46 VE(I)=AD*(SINH(AA1)*ATE+SINH(AA2)*BTE)+D*ANN/8,0*A*0,5
0127                1-CX*ANN*A/16,0
0128                VO(I)=AD*(SINH(AA1)+BA*SINH(AA2))+DEL4*DEL/A*ANN/8,0*A*0,5
0129                1-CX*ANN*A/16,0
0130                VS(I)=AD*(SINH(AA1)*ATS+BTS*SINH(AA2))+DEL3*DEL/A*ANN/8,0*A*0,5
0131                1-CX*ANN*A/16,0
0132               55 CONTINUE
0133                WRITE(2,116)G,AFF,DC,DELEND,SSF
0134              116 FORMAT(5E15,6//)
0135                WRITE(2,121)(VE(I),I=1,8)
0136                WRITE(2,121)(VO(I),I=1,8)
0137                WRITE(2,121)(VS(I),I=1,8)
0138              121 FORMAT(8E15,6//)
0139               92 GOTO 88
0140               89 STOP
0141                  END
```

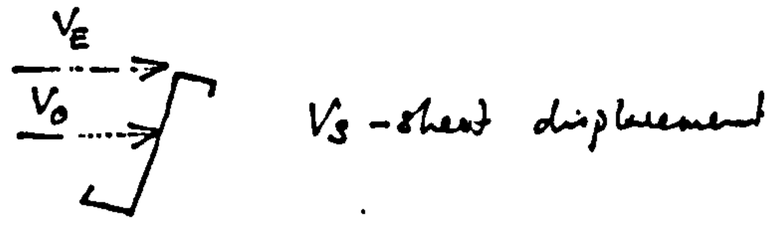

V_S - sheet displacement

CX	A1Y	EY	A	N
0,240000E-03	0,154400E 06	0,247000E 03	0,152000E 04	0,200000E 01

ANE (input as 2)	ANS	SE	SS
0,509200E 01	0,210000E 02	0,350000E 00	0,350000E 00

G	H	AJ
0,800000E 02	0,100000E 01	0,100000E 04

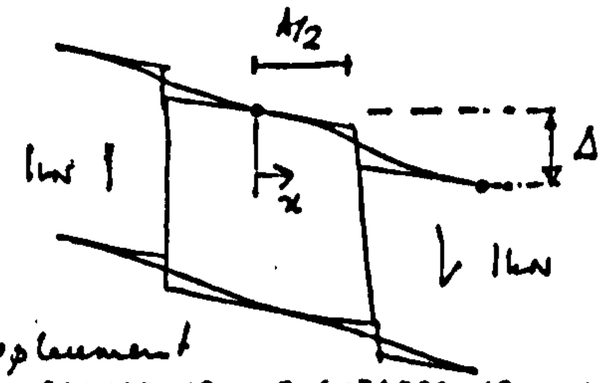

G	A_{EFF}	V_C	Δ	F
0,535041E-01	0,975914E 03	0,000000E 00	0,162452E-01	0,100695E 01

Purlin to flange displacement

0,201879E-03	0,496630E-03	0,975050E-03	0,172146E-02	0,280457E-02	0,426141E-02	0,607188E-02	0,812258E-02

Purlin centroid displacement

0,202908E-03	0,498667E-03	0,978028E-03	0,172521E-02	0,280875E-02	0,426540E-02	0,607465E-02	0,812258E-02

Sheet displacement

0,131738E-03	0,260778E-03	0,381114E-03	0,480094E-03	0,535083E-03	0,510343E-03	0,354587E-03	0,000000E 00
$x =$ $A/16$	$A/8$	$3A/16$	$A/4$	$5A/16$	$3/8\ A$	$7A/16$	$A/2$

F is central sheet shear force, kN

G is effect of sheet-purlin fastenings : for linear purlin movements is 0.0833 (1/

A_{eff} is the effective sheet width (= A x 12 x g)

Δ is the net displacement per sheet which equals $Cx.A + \frac{1}{\sqrt{\frac{SE}{SS}} + N.g.ANE}$

V_C = 0 for imaginary roots, or 1 for real roots

V_E, V_O and V_S are only due to fastener slip, and sheet flexibility is omitted.

OPENINGS IN DIAPHRAGMS

```
      MASTER OPENINGS
      DIMENSION X(25),P(25),Z(7),Y(5)
      DIMENSION F1(10),F2(10),FJ(10)
      DIMENSION VO(10),VE(10),VS(10),W(4),U(4)
      DIMENSION ACX(6),AAI(6),AAJ(6),DEL(10),ESIGMA(10),FEMAX(10)
   88 READ(1,100)AIY,AJ,H,B,A,CX1,CX2,AN
  100 FORMAT(8F10.0)
      IF(AIY.EQ.0.0) GOTO 99
      WRITE(2,101) AIY,AJ,H,B,A,CX1,CX2,AN
  101 FORMAT(8E15.6//)
      AIY=AIY*AN
      AJ=AJ*AN
      READ(1,109)SE,D,EY,G
  109 FORMAT(4F10.0)
      WRITE(2,110) SE,D,EY,G
      ASE=D*SE/AN
  110 FORMAT(4E15.6//)
      DC=0.0
      FG=EY*AIY*H**2*0.25/(G*AJ)
      CS=CX2+0.25*H**2/(G*AJ)
      CT=CX1+0.25*H**2/(G*AJ)
      X1=CS*0.5/ASE
      U1=CT*0.5/ASE
      X2=1.0/(EY*AIY*ASE)
      Y1=-X1**2+X2
      V1=-U1**2+X2
      IF(Y1.LT.0.0) GOTO 69
      GOTO 70
   69 DC=1.0
      Y1=X1**2-X2
      Y1=SQRT(Y1)
      A1=SQRT(X1-Y1)
      A2=SQRT(X1+Y1)
      GOTO 71
   70 Y1=SQRT(Y1)
      A1=(X1+SQRT(X1**2+Y1**2))*0.5
      A1=SQRT(A1)
      A2=(-X1+SQRT(X1**2+Y1**2))*0.5
      A2=SQRT(A2)
   71 IF(V1.LT.0.0) GOTO 72
      GOTO 73
   72 IF(DC.EQ.1.0) DC=2.0
      V1=U1**2-X2
      V1=SQRT(V1)
      B1=SQRT(U1-V1)
      B2=SQRT(U1+V1)
      GOTO 74
   73 V1=SQRT(V1)
      B1=(U1+SQRT(U1**2+V1**2))*0.5
      B1=SQRT(B1)
      B2=(-U1+SQRT(U1**2+V1**2))*0.5
      B2=SQRT(B2)
   74 CA1=COS(A1*A)
      SA1=SIN(A1*A)
      CH1=COSH(A1*A)
      CA2=COS(A2*A)
      CH2=COSH(A2*A)
      SH1=SINH(A1*A)
      SH2=SINH(A2*A)
      SA2=SIN(A2*A)
      DO 36 I=1,7
      Z(I)=0.0
   36 CONTINUE
      CB1=-COS(B1*B)
      CB2=-COS(B2*B)
      CK1=-COSH(B1*B)
      CK2=-COSH(B2*B)
      SB1=SIN(B1*B)
      SB2=SIN(B2*B)
      SK1=SINH(B1*B)
      SK2=SINH(B2*B)
      VS1=-A2*SH1*SA2+A1*CH1*CA2
      VS2=A2*CH1*CA2+A1*SH1*SA2
      IF(B.NE.0.0) GOTO 49
      X(1)=U1*B2-V1*B1
      X(2)=-CX1*EY*AIY*V1
      X(3)=-2.0*B1*B2
      X(4)=B2
      X(5)=0.0
      X(6)=-V1*B2-U1*B1
      X(7)=CX1*EY*AIY*U1
      X(8)=B1**2-B2**2
      X(9)=-B1
      X(10)=1.0
      GOTO 50
```

Input data

AIY — purlin lateral inertia, mm⁴

AJ — purlin torsional stiffness, mm⁴

H — member depth, mm

B — width of stiff portion, mm
(this is zero for a single opening)

A — opening width, mm

CX1 — flexibility of stiff portion, mm/kN/mm

CX2 — flexibility of portion including the opening

AN — number of purlins

SE — slip of sheet-purlin fasteners, mm/kN

D — pitch of sheet-purlin fasteners mm

EY — Young's Modulus, kN/mm²

G — Shear Modulus, kN/mm²

Works out roots of differential equation depending on whether they are real or imaginary.

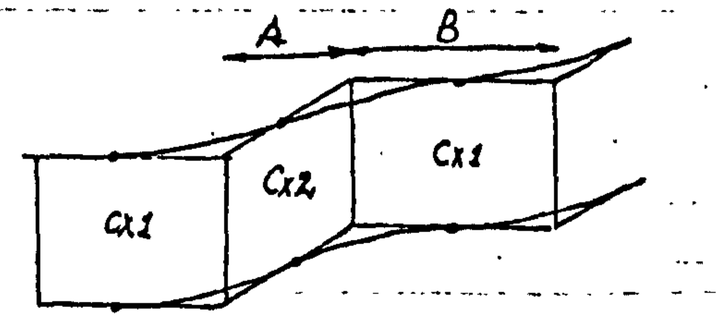

Periodic distribution of openings

If B=0.0, then the solution is for a single opening

```
0091          49 US1=-B2*SK1*SB2+B1*CK1*CB2
0092             US2=B2*CK1*CB2+B1*SK1*SB2
0093             X(1)=+(U1*US1-V1*US2)
0094             X(2)=+EY*AIY*CX1*(U1*SK1*CB2-V1*CK1*SB2)
0095             X(3)=+(B1**2-B2**2)*SK1*CB2-2,0*B1*B2*CK1*SB2
0096             X(4)=US1
0097             X(5)=SK1*CB2
0098             X(6)=+(V1*US1+U1*US2)
0099             X(7)=+EY*AIY*CX1*(V1*SK1*CB2+U1*CK1*SB2)
0100             X(8)=+2,0*B1*B2*SK1*CB2+(B1**2-B2**2)*CK1*SB2
0101             X(9)=US2
0102             X(10)=CK1*SB2
0103          50 X(11)=-(X1*VS1-Y1*VS2)
0104             X(12)=-EY*AIY*CX2*(X1*SH1*CA2-Y1*CH1*SA2)
0105             X(13)=-(A1**2-A2**2)*SH1*CA2+2,0*A1*A2*CH1*SA2
0106             X(14)=-VS1
0107             X(15)=-SH1*CA2
0108             X(16)=-(Y1*VS1+X1*VS2)
0109             X(17)=-EY*AIY*CX2*(Y1*SH1*CA2+X1*CH1*SA2)
0110             X(18)=-2,0*A1*A2*SH1*CA2-(A1**2-A2**2)*CH1*SA2
0111             X(19)=-VS2
0112             X(20)=-CH1*SA2
0113             X(21)=0,0
0114             X(22)=1,0
0115             X(23)=0,0
0116             X(24)=0,0
0117             X(25)=1,0
0118             Y(1)=0,0
0119             IF(B,NE,0,0) Y(2)=CX1*B+CX2*A
0120             IF(B,EQ,0,0) Y(2)=CX2*A
0121             Y(3)=0,0
0122             Y(4)=CX2-CX1
0123             Y(5)=Y(2)
0124             IF(DC,EQ,1,0,OR,DC,EQ,2,0) GOTO 81
0125             GOTO 82
0126          81 X(15)=-SH1
0127             X(11)=-A1**3*CH1
0128             X(12)=-CX2*EY*AIY*A1**2*SH1
0129             X(13)=-A1**2*SH1
0130             X(14)=-A1*CH1
0131             X(16)=-A2**3*CH2
0132             X(17)=-CX2*EY*AIY*A2**2*SH2
0133             X(18)=-A2**2*SH2
0134             X(19)=-A2*CH2
0135             X(20)=-SH2
0136             IF(DC,EQ,1,0) GOTO 82
0137             IF(B,EQ,0,0) GOTO 79
0138             X(1)=-B1**3*CK1
0139             X(2)=-CX1*EY*AIY*B1**2*SK1
0140             X(3)=-B1**2*SK1
0141             X(4)=-B1*CK1
0142             X(5)=-SK1
0143             X(6)=-B2**3*CK2
0144             X(7)=-CX1*EY*AIY*B2**2*SK2
0145             X(8)=-B2**2*SK2
0146             X(9)=-B2*CK2
0147             X(10)=-SK2
0148             GOTO 82
0149          79 X(1)=-B1**3
0150             X(2)=CX1*EY*AIY*B1**2
0151             X(3)=B1**2
0152             X(4)=-B1
0153             X(5)=1,0
0154             X(6)=-B2**3
0155             X(7)=CX1*EY*AIY*B2**2
0156             X(8)=B2**2
0157             X(9)=-B2
0158             X(10)=1,0
0159          82 EY=207,0
0160             CALL XINVT(5,X,P,DET)
0161             DO 38 L=1,5
0162             DO 37 K=1,5
0163             Z(L)=Z(L)+P(L+5*(K-1))*Y(K)
0164          37 CONTINUE
0165          38 CONTINUE
0166             Z(6)=Z(5)
0167             Z(5)=CX2
0168          97 Z(7)=CX2*A+CX1*B
0169             VO(1)=-Z(6)
0170             VO(2)=Z(3)*SINH(A1*A*0,25)*COS(A2*A*0,25)
0171            1+Z(4)*COSH(A1*A*0,25)*SIN(A2*A*0,25)+Z(5)*A*0,25-Z(6)
0172             VO(3)=Z(3)*SINH(A1*A*0,5)*COS(A2*A*0,5)
0173            1+Z(4)*COSH(A1*A*0,5)*SIN(A2*A*0,5)+Z(5)*A*0,5-Z(6)
0174             VO(4)=Z(3)*SINH(A1*A*0,75)*COS(A2*A*0,75)
0175            1+Z(4)*COSH(A1*A*0,75)*SIN(A2*A*0,75)+Z(5)*0,75*A-Z(6)
0176             VO(5)=Z(3)*SINH(A1*A)*COS(A2*A)
0177            1+Z(4)*COSH(A1*A)*SIN(A2*A)+Z(5)*A-Z(6)
0178             VO(6)=Z(2)
0179             VO(7)=EXP(-B1*A*0,25)*(Z(2)*COS(B2*A*0,25)+Z(1)*SIN(B2*A*0,25))
0180            1+CX1*A*0,25
```

Evaluates boundary conditions & solve for constants of sixth order differential equation.

Four solutions are required for

1. Periodic openings ---> Real roots
2. Single opening ---> Imaginary roots.

Displacements of portion

Imaginary roots

```
0181            VU(8)=EXP(-B1*A*0,5)*(Z(2)*COS(B2*A*0,5)+Z(1)*SIN(B2*A*0,5))
0182           1+CX1*A*0,5
0183            VU(9)=EXP(-B1*A*0,75)*(Z(2)*COS(B2*A*0,75)+Z(1)*SIN(B2*A*0,75))
0184           1+CX1*A*0,75
0185            VU(10)=EXP(-B1*A)*(Z(2)*COS(B2*A)+Z(1)*SIN(B2*A))
0186           1+CX1*A
0187            W(1)=Z(1)-EG*(U1*Z(1)+V1*Z(2))
0188            W(2)=Z(2)-EG*(-V1*Z(1)+U1*Z(2))
0189            W(3)=Z(3)-EG*(X1*Z(3)+Y1*Z(4))
0190            W(4)=Z(4)-EG*(-Y1*Z(3)+X1*Z(4))
0191            VE(1)=-Z(6)
0192            VE(2)=W(3)*SINH(A1*A*0,25)*COS(A2*A*0,25)
0193           1+W(4)*COSH(A1*A*0,25)*SIN(A2*A*0,25)+CX2*A*0,25-Z(6)
0194            VE(3)=W(3)*SINH(A1*A*0,5)*COS(A2*A*0,5)
0195           1+W(4)*COSH(A1*A*0,5)*SIN(A2*A*0,5)+CX2*A*0,5-Z(6)
0196            VE(4)=W(3)*SINH(A1*A*0,75)*COS(A2*A*0,75)
0197           1+W(4)*COSH(A1*A*0,75)*SIN(A2*A*0,75)+CX2*A*0,75-Z(6)
0198            VE(5)=W(3)*SINH(A1*A)*COS(A2*A)
0199           1+W(4)*COSH(A1*A)*SIN(A2*A)+CX2*A-Z(6)
0200            VE(6)=W(2)
0201            VE(7)=EXP(-B1*A*0,25)*(W(2)*COS(B2*A*0,25)+W(1)*SIN(B2*A*0,25))
0202           1+CX1*A*0,25
0203            VE(8)=EXP(-B1*A*0,5)*(W(2)*COS(B2*A*0,5)+W(1)*SIN(B2*A*0,5))
0204           1+CX1*A*0,5
0205            VE(9)=EXP(-B1*A*0,75)*(W(2)*COS(B2*A*0,75)+W(1)*SIN(B2*A*0,75))
0206           1+CX1*A*0,75
0207            VE(10)=EXP(-B1*A)*(W(2)*COS(B2*A)+W(1)*SIN(B2*A))
0208           1+CX1*A
0209            U(1)=CX1*EY*AIY*(U1*Z(1)+V1*Z(2))
0210            U(2)=CX1*EY*AIY*(-V1*Z(1)+U1*Z(2))
0211            U(3)=CX2*EY*AIY*(X1*Z(3)+Y1*Z(4))
0212            U(4)=CX2*EY*AIY*(-Y1*Z(3)+X1*Z(4))
0213            VS(1)=-Z(6)
0214            VS(2)=U(3)*SINH(A1*A*0,25)*COS(A2*A*0,25)
0215           1+U(4)*COSH(A1*A*0,25)*SIN(A2*A*0,25)+CX2*A*0,25-Z(6)
0216            VS(3)=U(3)*SINH(A1*A*0,5)*COS(A2*A*0,5)
0217           1+U(4)*COSH(A1*A*0,5)*SIN(A2*A*0,5)+CX2*A*0,5-Z(6)
0218            VS(4)=U(3)*SINH(A1*A*0,75)*COS(A2*A*0,75)
0219           1+U(4)*COSH(A1*A*0,75)*SIN(A2*A*0,75)+CX2*A*0,75-Z(6)
0220            VS(5)=U(3)*SINH(A1*A)*COS(A2*A)
0221           1+U(4)*COSH(A1*A)*SIN(A2*A)+CX2*A-Z(6)
0222            VS(6)=U(2)
0223            VS(7)=EXP(-B1*A*0,25)*(U(2)*COS(B2*A*0,25)+U(1)*SIN(B2*A*0,25))
0224           1+CX1*A*0,25
0225            VS(8)=EXP(-B1*A*0,5)*(U(2)*COS(B2*A*0,5)+U(1)*SIN(B2*A*0,5))
0226           1+CX1*A*0,5
0227            VS(9)=EXP(-B1*A*0,75)*(U(2)*COS(B2*A*0,75)+U(1)*SIN(B2*A*0,75))
0228           1+CX1*A*0,75
0229            VS(10)=EXP(-B1*A)*(U(2)*COS(B2*A)+U(1)*SIN(B2*A))
0230           1+CX1*A
0231            IF(B,EQ,0,0) GOTO 33
0232            VS(10)=0,0
0233            VE(10)=0,0
0234            VO(10)=0,0
0235            VO(9)=Z(1)*SINH(B1*B*0,25)*COS(B2*B*0,25)*(-1,0)
0236           1-Z(2)*COSH(B1*B*0,25)*SIN(B2*B*0,25)-CX1*0,25*B
0237            VO(8)=-Z(1)*SINH(B1*B*0,5)*COS(B2*B*0,5)
0238           1-Z(2)*COSH(B1*B*0,5)*SIN(B2*B*0,5)-CX1*0,5*B
0239            VO(7)=-Z(1)*SINH(B1*B*0,75)*COS(B2*B*0,75)
0240           1-Z(2)*COSH(B1*B*0,75)*SIN(B2*B*0,75)-CX1*B*0,75
0241            VO(6)=-Z(1)*SINH(B1*B)*COS(B2*B)
0242           1-Z(2)*COSH(B1*B)*SIN(B2*B)-CX1*B
0243            VE(9)=W(1)*SINH(B1*B*0,25)*COS(B2*B*0,25)*(-1,0)
0244           1-W(2)*COSH(B1*B*0,25)*SIN(B2*B*0,25)-CX1*0,25*B
0245            VE(8)=-W(1)*SINH(B1*B*0,5)*COS(B2*B*0,5)
0246           1-W(2)*COSH(B1*B*0,5)*SIN(B2*B*0,5)-CX1*0,5*B
0247            VE(7)=-W(1)*SINH(B1*B*0,75)*COS(B2*B*0,75)
0248           1-W(2)*COSH(B1*B*0,75)*SIN(B2*B*0,75)-CX1*B*0,75
0249            VE(6)=-W(1)*SINH(B1*B)*COS(B2*B)
0250           1-W(2)*COSH(B1*B)*SIN(B2*B)-CX1*B
0251            VS(9)=U(1)*SINH(B1*B*0,25)*COS(B2*B*0,25)*(-1,0)
0252           1-U(2)*COSH(B1*B*0,25)*SIN(B2*B*0,25)-CX1*0,25*B
0253            VS(8)=-U(1)*SINH(B1*B*0,5)*COS(B2*B*0,5)
0254           1-U(2)*COSH(B1*B*0,5)*SIN(B2*B*0,5)-CX1*0,5*B
0255            VS(7)=-U(1)*SINH(B1*B*0,75)*COS(B2*B*0,75)
0256           1-U(2)*COSH(B1*B*0,75)*SIN(B2*B*0,75)-CX1*B*0,75
0257            VS(6)=-U(1)*SINH(B1*B)*COS(B2*B)
0258           1-U(2)*COSH(B1*B)*SIN(B2*B)-CX1*B
0259         33 FMAX=(W(3)-U(3))*SINH(A1*A)*COS(A2*A)+(W(4)-U(4))*COSH(A1*A)*
0260           1SIN(A2*A)
0261            FMAX=FMAX/0,15
0262             SFORCE1=1,0+(U(3)*(A1*CH1*CA2-A2*SH1*SA2)+U(4)*(CH1*CA2+SH1*SA2))
0263           1/CX2
0264            SFORCE3=0,0
```

Prohm displacements

V_0 — centroid

V_E — top flange

V_S — sheet

Single opening.

Imaginary roots

Periodic openings

```
      IF(B,NE,0,0) SFORCE3=1,0+(U(1)*B1+U(2)*B2)/CX1
      SFORCE2=1,0+(U(3)*A1+U(4)*A2)/CX2
      SIGMA=Z(3)*((A1**2-A2**2)*SH1*CA2-2,0*A1*A2*CH1*SA2)+
     1Z(4)*((A1**2-A2**2)*CH1*SA2+2,0*A1*A2*SH1*CA2)
      SIGMA=SIGMA*EY*1000,0*50,0
      IF(DC,EQ,1,0,OR,DC,EQ,2,0) GOTO 91
      GOTO 92
   91 U(1)=CX1*EY*AIY*B1**2*Z(1)
      U(2)=CX1*EY*AIY*B2**2*Z(2)
      U(3)=CX2*EY*AIY*A1**2*Z(3)
      U(4)=CX2*EY*AIY*A2**2*Z(4)
      W(1)=Z(1)*(1,0-EG*B1**2)
      W(2)=Z(2)*(1,0-EG*B2**2)
      W(3)=Z(3)*(1,0-EG*A1**2)
      W(4)=Z(4)*(1,0-EG*A2**2)
      VO(2)=Z(3)*SINH(A1*A*0,25)+Z(4)*SINH(A2*A*0,25)+Z(5)*A*0,25-Z(6)
      VO(3)=Z(3)*SINH(A1*A*0,5)+Z(4)*SINH(A2*A*0,5)+Z(5)*A*0,5-Z(6)
      VO(4)=Z(3)*SINH(A1*A*0,75)+Z(4)*SINH(A2*A*0,75)+Z(5)*A*0,75-Z(6)
      VO(5)=Z(3)*SINH(A1*A)+Z(4)*SINH(A2*A)+Z(5)*A-Z(6)
      VE(2)=W(3)*SINH(A1*A*0,25)+W(4)*SINH(A2*A*0,25)+CX2*A*0,25-Z(6)
      VE(3)=W(3)*SINH(A1*A*0,5)+W(4)*SINH(A2*A*0,5)+CX2*A*0,5-Z(6)
      VE(4)=W(3)*SINH(A1*A*0,75)+W(4)*SINH(A2*A*0,75)+CX2*A*0,75-Z(6)
      VE(5)=W(3)*SINH(A1*A)+W(4)*SINH(A2*A)+CX2*A-Z(6)
      VS(2)=U(3)*SINH(A1*A*0,25)+U(4)*SINH(A2*A*0,25)+CX2*A*0,25-Z(6)
      VS(3)=U(3)*SINH(A1*A*0,5)+U(4)*SINH(A2*A*0,5)+CX2*A*0,5-Z(6)
      VS(4)=U(3)*SINH(A1*A*0,75)+U(4)*SINH(A2*A*0,75)+CX2*A*0,75-Z(6)
      VS(5)=U(3)*SINH(A1*A)+U(4)*SINH(A2*A)+CX2*A-Z(6)
      IF(DC,EQ,1,0) GOTO 34
      VS(6)=U(1)+U(2)
      VS(7)=U(1)*EXP(-B1*A*0,25)+U(2)*EXP(-B2*A*0,25)
     1+CX1*A*0,25
      VS(8)=U(1)*EXP(-B1*A*0,5)+U(2)*EXP(-B2*A*0,5)
     1+CX1*A*0,5
      VS(9)=U(1)*EXP(-B1*A*0,75)+U(2)*EXP(-B2*A*0,75)
     1+CX1*A*0,75
      VS(10)=U(1)*EXP(-B1*A)+U(2)*EXP(-B2*A)
     1+CX1*A
      VE(6)=W(1)+W(2)
      VE(7)=W(1)*EXP(-B1*A*0,25)+W(2)*EXP(-B2*A*0,25)
     1+CX1*A*0,25
      VE(8)=W(1)*EXP(-B1*A*0,5)+W(2)*EXP(-B2*A*0,5)
     1+CX1*A*0,5
      VE(9)=W(1)*EXP(-B1*A*0,75)+W(2)*EXP(-B2*A*0,75)
     1+CX1*A*0,75
      VE(10)=W(1)*EXP(-B1*A)+W(2)*EXP(-B2*A)
     1+CX1*A
      VO(6)=Z(1)+Z(2)
      VO(7)=Z(1)*EXP(-B1*A*0,25)+Z(2)*EXP(-B2*A*0,25)
     1+CX1*A*0,25
      VO(8)=Z(1)*EXP(-B1*A*0,5)+Z(2)*EXP(-B2*A*0,5)
     1+CX1*A*0,5
      VO(9)=Z(1)*EXP(-B1*A*0,75)+Z(2)*EXP(-B2*A*0,75)
     1+CX1*A*0,75
      VO(10)=Z(1)*EXP(-B1*A)+Z(2)*EXP(-B2*A)
     1+CX1*A
      IF(B,EQ,0,0) GOTO 34
      VO(10)=0,0
      VE(10)=0,0
      VS(10)=0,0
      VO(9)=-Z(1)*SINH(B1*B*0,25)-Z(2)*SINH(B2*B*0,25)-CX1*0,25*B
      VO(8)=-Z(1)*SINH(B1*B*0,5)-Z(2)*SINH(B2*B*0,5)-CX1*0,5*B
      VO(7)=-Z(1)*SINH(B1*B*0,75)-Z(2)*SINH(B2*B*0,75)-CX1*B*0,75
      VO(6)=-Z(1)*SINH(B1*B)-Z(2)*SINH(B2*B)-CX1*B
      VE(9)=-W(1)*SINH(B1*B*0,25)-W(2)*SINH(B2*B*0,25)-CX1*0,25*B
      VE(8)=-W(1)*SINH(B1*B*0,5)-W(2)*SINH(B2*B*0,5)-CX1*0,5*B
      VE(7)=-W(1)*SINH(B1*B*0,75)-W(2)*SINH(B2*B*0,75)-CX1*B*0,75
      VE(6)=-W(1)*SINH(B1*B)-W(2)*SINH(B2*B)-CX1*B
      VS(9)=-U(1)*SINH(B1*B*0,25)-U(2)*SINH(B2*B*0,25)-CX1*0,25*B
      VS(8)=-U(1)*SINH(B1*B*0,5)-U(2)*SINH(B2*B*0,5)-CX1*0,5*B
      VS(7)=-U(1)*SINH(B1*B*0,75)-U(2)*SINH(B2*B*0,75)-CX1*B*0,75
      VS(6)=-U(1)*SINH(B1*B)-U(2)*SINH(B2*B)-CX1*B
   34 FMAX=(W(3)-U(3))*SINH(A1*A)+(W(4)-U(4))*SINH(A2*A)
      FMAX=FMAX/0,15
      SFORCE1=1,0+(U(3)*A1*CH1+U(4)*A2*CH2)/CX2
      SFORCE2=1,0+(U(3)*A1+U(4)*A2)/CX2
      SFORCE3=0,0
      IF(B,NE,0,0) SFORCE3=1,0+(U(1)*B1+U(2)*B2)/CX1
      SIGMA=(Z(3)*A1**2*SINH(A1*A)+Z(4)*A2**2*SINH(A2*A))*EY*50,0*1000,0
   92 EY=207,0
      WRITE(2,103)(VO(I),I=1,10),DC
      WRITE(2,103)(VE(I),I=1,10),Z(7)
      WRITE(2,103)(VS(I),I=1,10),Z(7)
  103 FORMAT(11E11,3//)
      WRITE(2,102) FMAX,SIGMA,SFORCE2,SFORCE1,SFORCE3
  102 FORMAT(5E15,6//)
      IF(AIY,NE,0,0) GOTO 88
   99 STOP
      END
```

Real roots
Single opening

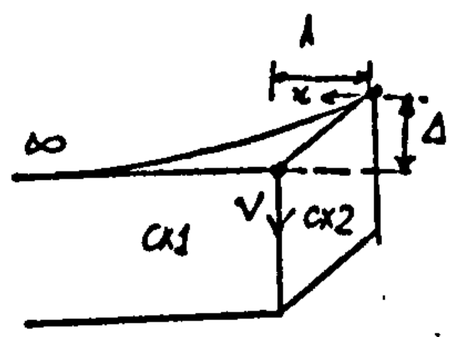

Single opening displacement

Real roots
Reentrant openings

Evaluate stresses and fastener forces.

```
0353            SUBROUTINE XINVT(IP,B,C,DET)
0354            DIMENSION B(25),C(25)
0355            IF(IP.EQ.1)GO TO 9
0356            I=IP*IP
0357            DO 2 I=1,I
0358          2 C(I)=0
0359            DO 3 I=1,IP
0360          3 C(I+IP*(I-1))=1.0
0361            I=IP-1
0362            DO 5 IQ=1,I
0363            K=IP-IQ+1
0364            AP=B(K+IP*(K-1))
0365            IK=K-1
0366            DO 5 I=1,IK
0367            AT=B(I+IP*(K-1))/AP
0368            DO 5 J=1,IP
0369            B(I+IP*(J-1))=B(I+IP*(J-1))-B(K+IP*(J-1))*AT
0370          5 C(I+IP*(J-1))=C(I+IP*(J-1))-C(K+IP*(J-1))*AT
0371      C     MATRIX NOW REDUCED TO UPPER TRIANGLE FORM
0372            DO 6 IQ=1,I
0373            AP=B(IQ+IP*(IQ-1))
0374            IK=IQ+1
0375            DO 6 I=IK,IP
0376            AT=B(I+IP*(IQ-1))/AP
0377            DO 6 J=1,IP
0378            B(I+IP*(J-1))=B(I+IP*(J-1))-B(IQ+IP*(J-1))*AT
0379          6 C(I+IP*(J-1))=C(I+IP*(J-1))-C(IQ+IP*(J-1))*AT
0380      C   MATRIX NOW REDUCED TO DIAGONAL FORM
0381            DET=1.0
0382            DO 7 I=1,IP
0383            DO 12 J=1,IP
0384         12 C(I+IP*(J-1))=C(I+IP*(J-1))/B(I+IP*(I-1))
0385          7 DET=DET*B(I+IP*(I-1))
0386            GO TO 8
0387          9 DET=B(1)
0388            C(1)=1.0/B(1)
0389         10 FORMAT(21H LOCAL DETERMINANT = ,E10.4)
0390          8 RETURN
0391            END
```

Solves for differential equation constants

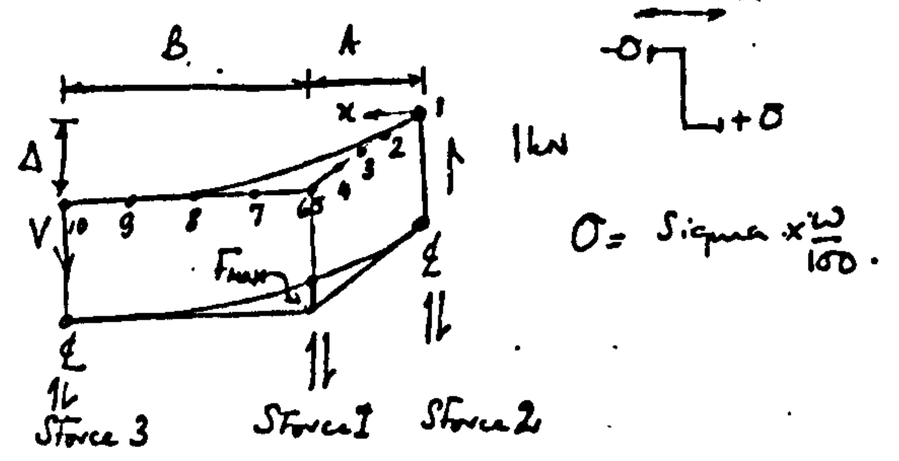

$O = Sigma \times \frac{3}{100}$.

$V_c = 0$ – imaginary roots
1 – one root imaginary, the other is real.
2 – real roots.

V_{free} – central deflection for I = 0
F_{max} – max. sheet-purlin fastener force, kN
Sigma – bending stress N/mm^2.
Force – sheet shear forces, kN

```
      AIY            AJ             H              B              A             CX1            CX2            AN
 0,2000000E 07  0,8000000E 05  0,1000000E 01  0,0000000E 00  0,5000000E 03  0,1000000E-04  0,4500000E-03  0,1000000E 01

      SE             D             ET             G
 0,1500000E 00  0,1500000E 03  0,2070000E 03  0,8000000E 02
```

Purlin displacements from centre of opening in increments of A/4

Single opening case

```
-0,117E 00 -0,824E-01 -0,498E-01 -0,216E-01 -0,295E-04 -0,295E-04  0,131E-01  0,196E-01  0,218E-01  0,213E-01 | 0,000E 0
  X=0    ,   A/4    ,   A/2    ,   3/4 A  ,    A     ,    A     ,  5/4 A    ,  3/2 A   ,  7/4 A   ,  2A      | V_E
-0,117E 00 -0,824E-01 -0,498E-01 -0,216E-01 -0,200E-04 -0,200E-04  0,131E-01  0,196E-01  0,218E-01  0,213E-01 | 0,225E 0
 Δmax                                                                                                         | V_S
-0,117E 00 -0,861E-01 -0,563E-01 -0,284E-01 -0,245E-02 -0,245E-02 -0,505E-03  0,135E-02  0,300E-02  0,400E-02 | 0,225E 0
```

V0 | Pc
V_E | V'free
V_S | V_free

```
   Fmax, kN      Sigma, N/mm²    Force 2, kN     Force 1        Force 3
 0,162009E-01  -0,612750E 01   0,554807E 00   0,996129E 03   0,000000E 00
```

```
      AIY            AJ             H              B              A             CX1            CX2            AN
 0,5000000E 06  0,2000000E 05  0,1000000E 01  0,1000000E 04  0,5000000E 03  0,1000000E-04  0,4500000E-03  0,4000000E 01

      SE             D             ET             G
 0,1500000E 00  0,1500000E 03  0,2070000E 03  0,8000000E 02
```

Periodic opening case

Purlin displacements from centre of openings

```
-0,163E 00 -0,128E 00 -0,958E-01 -0,671E-01 -0,439E-01 -0,439E-01 -0,987E-02 -0,741E-02 -0,457E-02  0,000E 00 | 0,100E 0
  X=0    ,   A/4    ,   A/2    ,   3/4 A  ,    A     ,    A     ,  A+B/4    ,  A+B/2   ,  A+3/4B  ,  A+B      | V_E
-0,163E 00 -0,128E 00 -0,958E-01 -0,671E-01 -0,439E-01 -0,439E-01 -0,987E-02 -0,741E-02 -0,457E-02  0,000E 00 | 0,243E 0
 Δmax                                                                                                         | V_S
-0,163E 00 -0,129E 00 -0,957E-01 -0,617E-01 -0,198E-01 -0,198E-01 -0,140E-01 -0,894E-02 -0,447E-02  0,000E 00 | 0,243E 0
```

V0 | Pc
V_E | V_free
V_S | V_free

```
   Fmax, kN      Sigma, N/mm²    Force 2, kN     Force 1        Force 3
-0,160733E 00  -0,455538E 01   0,604721E 00   0,922369E 00   0,100270E 01
```

HOLES IN FOLDED PLATES

```
0005        MASTER WORKOUT
0006        REAL K
0007        DIMENSION VE(7)
0008     88 READ(1,100)B,AIY,CX,SE,PF,P,W,TH
0009        IF(B.EQ.0.0) GOTO 89
0010        EY=207.0
0011        TH=TH*3.14/180.0
0012    100 FORMAT(8F10.0)
0013        WRITE(2,101) B,AIY,CX,SE,PF,P,W,TH
0014    101 FORMAT(8E15.6//)
0015        SLIP=PF*SE/(2.0*(SIN(TH))**2)
0016        CX=CX/(2.0*(SIN(TH))**2)
0017        AK=W*B**2/(EY*AIY)*(-1.0)
0018        X1=+(CX*P*SLIP/(EY*AIY))*0.5/SLIP
0019        X2=(1.0-CX*P)/(EY*AIY*SLIP)
0020        Y1=-X1**2+X2
0021        Y1=SQRT(Y1)
0022        A1=(X1+SQRT(X1**2+Y1**2))*0.5
0023        A1=SQRT(A1)
0024        A2=(-X1+SQRT(X1**2+Y1**2))*0.5
0025        A2=SQRT(A2)
0026        A12=A1**2+A2**2
0027        BO=AK*(B*A1/3.0+0.5)/A12
0028        BG=-2.0*(1.0+2.0*A1*B)/A12
0029        AO=AK*(B*(A1**2-A2**2)/6.0+A1/2.0)/(A2*A12)
0030        AG=2.0*(A1+B*(A1**2-A2**2))/(A2*A12)*(-1.0)
0031         BA=-CX*EY*AIY*Y1
0032        BB=CX*AIY*EY*X1
0033        AA=CX*AIY*EY*X1
0034        AB=CX*EY*AIY*Y1
0035        IF(P.NE.0.0) GOTO 79
0036        WO=A2*AO*(1.0-AA)-A2*AB*BO+BO*A1*(1.0-BB)-A1*BA*AO
0037        WG=A2*AG*(1.0-AA)-A2*AB*BG+BG*(1.0-BB)*A1-A1*BA*AG
0038        G=W*B*A12*SLIP/WG-WO/WG
0039        AC=AO+AG*G
0040        BC=BO+BG*G
0041        D=BC-2.0*B**2*G+AK/24.0*B**2
0042        D1=-AK*B*B/24.0+2.0*G*B*B+D
0043        SIGMA=2.0*G*EY*1000.0*50.0
0044        GOTO 80
0045     79 K=SQRT(P/(EY*AIY))
0046        BF=(K**2*COS(K*B)+2.0*A1*K*SIN(K*B))/A12
0047        BFO=-(2.0*A1*B+1.0)*W/(P*A12)
0048        AFO=-((A1**2-A2**2)*B+A1)*W/(P*A2*A12)
0049        AF=(K**2*A1*COS(K*B)+K*SIN(K*B)*(A1**2-A2**2))/(A2*A12)
0050        F=(BFO*(-A1**3+3.0*A1*A2**2)+AFO*(3.0*A1**2*A2-A2**3))/
0051       1(K**3*SIN(K*B)-BF*(-A1**3+3.0*A1*A2**2)-AF*(3.0*A1**2*A2-A2**3))
0052        AC=AF*F+AFO
0053        BC=BF*F+BFO
0054        D=BC-F*COS(K*B)-W*B**2*0.5/P
0055     80 FMAX=(BC-(BA*AC+BB*BC))/SE*SIN(TH)
0056        Z=(B/3.14)**2*SQRT(1.0/(EY*AIY*SLIP))
0057        PE=9.8*EY*AIY/B**2
0058        DO 20 IP1=1,100
0059        P1=FLOAT(IP1)/100.0
0060        P2=Z*(1.0+COS(3.14*SQRT(P1)))
0061        PA=ABS(P1-P2)
0062        IF(PA.LT.0.03) GOTO 21
0063     20 CONTINUE
0064     21 PCRIT=P2*PE
0065        IF(P.NE.0.0) SIGMA=(W/P-F*K**2)*EY*50.0*1000.0
0066        VE(1)=D
0067        VE(2)=-AK*B**2/(24.0*3.0**4)+2.0*G*B**2/9.0+D
0068        VE(3)=-AK*B**2/(24.0*1.5**4)+8.0*G*B**2/9.0+D
0069        IF(P.NE.0.0) VE(1)=D+F
0070        IF(P.NE.0.0) VE(2)=D+F*COS(K*B*0.33)+W*0.5/P*(0.33*B)**2
0071         IF(P.NE.0.0) VE(3)=D+F*COS(K*B*0.67)+W*0.5/P*(0.67*B)**2
0072        VE(4)=BC
0073        VE(5)=EXP(-A1*B*0.33)*(AC*SIN(A2*B*0.33)+BC*COS(A2*B*0.33))
0074        VE(6)=EXP(-A1*B*0.67)*(AC*SIN(A2*B*0.67)+BC*COS(A2*B*0.67))
0075        VE(7)=EXP(-A1*B)*(AC*SIN(A2*B)+BC*COS(A2*B))
0076        WRITE(2,102)(VE(I),I=1,7)
0077        WRITE(2,103)PCRIT,PE,SIGMA,FMAX
0078    102 FORMAT(7E15.6//)
0079    103 FORMAT(4E15.6//)
0080        GOTO 88
0081     89 STOP
0082        END
```

Input data :

B — half opening width, mm
AIY — vertical fold line inertia, mm⁴
CX — sheet flexibility, mm/kN/mm
SE — fastener slip, mm/kN
PF — fastener pitch, mm.
P — fold line axial force, kN
W — local load on fold line, kN/mm
TH — plate slope to horizontal, degrees

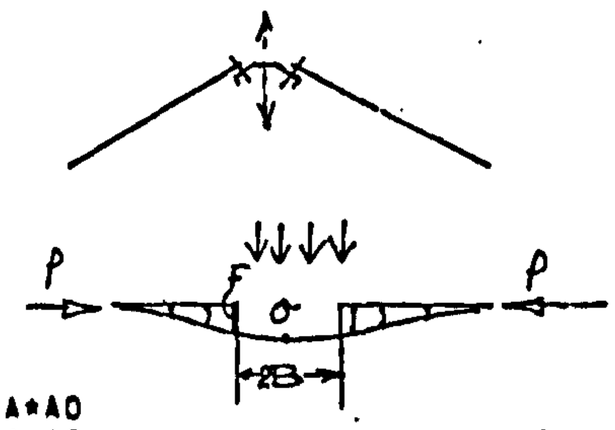

Solves boundary conditions of differential equation

Works out critical buckling load of fold line.

Evaluates fold line displacements

B	AIY	CX	SE	PF	P	W	TH rads.
0,500000E 03	0,500000E 06	0,300000E-03	0,150000E 00	0,150000E 03	0,100000E 03	0,300000E-02	0,610556E 00.

Fold line displacements from centre of hole at increments of B/3

0,952758E 00	0,895712E 00	0,733005E 00	0,518425E 00	0,314651E 00	0,151968E 00	0,712380E-01

Buckling Load, kN; π^2EI/B^2 ; σ, Max. stress N/mm² ; F, Max fastener force, kN

0,137583E 04	0,405720E 04	-0,442869E 02	0,189331E 01

Actual stress = $\sigma \times \frac{W}{100}$ N/mm².

VARIATIONS IN FOLDED PLATE STIFFNESS

```
0005            MASTER FOLDSTIFFEN
0006            REAL L,K1,K2,K3,K
0007            DIMENSION  DEL(50),X(50,50),W(50),Q(50)
0008            DIMENSION  S(50),P(50),E(50),C(50),Y(50)
0009            DIMENSION AA(50),BB(50),CC(50),DD(50),EE(50),FF(50)
0010         88 READ(1,100) M
0011        100 FORMAT(I2)
0012            READ(1,101)L,EI,EY,T,BL,D
0013        101 FORMAT(6F10.0)
0014            READ(1,102)(P(I),I=1,M)
0015        102 FORMAT(9F8.0)
0016            READ(1,103)K1,K2,K3,D1,D2,CMIN
0017        103 FORMAT(6F8.0)
0018            WRITE(2,104)L,EI,EY,T,BL,D
0019        104 FORMAT(6E15.6//)
0020            WRITE(2,105)K1,K2,K3,D1,D2,CMIN,M
0021        105 FORMAT(6E15.6,I2//)
0022            DO 30 I=1,M
0023            S(1)=P(1)
0024            IF(I.EQ.1) GOTO 49
0025            S(I)=S(I-1)+P(I)
0026            E(I)=EI*EY
0027         49 IF(S(I).GT.L/2.0) GOTO 30
0028         30 CONTINUE
0029            K=K1
0030            DO 31 I=1,M
0031            IF(I.EQ.1) GOTO 54
0032            Q(I)=(1.0-(S(I)+S(I-1))/L)
0033         54 Q(1)=(1.0-S(1)/L)
0034            IF(S(I).GT.D1)K=K2
0035            IF(S(I).GT.D2)K=K3
0036            C(I)=K*(D/T)**2*SQRT(D/T)/(EY*BL**2)+CMIN*S(I)*2.0/L
0037            DEL(1)=C(1)*P(1) *Q(1)
0038            IF(I.EQ.1) GOTO 35
0039            DEL(I)=DEL(I-1)+C(I)*P(I)*Q(I)
0040            Y(I)=-Q(I)
0041            W(I)=0.0
0042         35 DO 32 J=1,M
0043            X(I,J)=0.0
0044         32 CONTINUE
0045         31 CONTINUE
0046            X(1,1)=-(E(1)/P(1)**3+E(2)/(P(2)*P(1)**2)+1.0/(C(1)*P(1)))
0047            X(1,2)=E(2)/(P(2)*P(1)**2)
0048            X(2,1)=(2.0*E(1)/(P(1)*P(2)**2)+E(2)/P(2)**3+1.0/(C(2)*P(2)))
0049            X(2,2)=-(2.0*E(2)/P(2)**3+E(3)/(P(3)*P(2)**2)+1.0/(C(2)*P(2)))
0050            X(2,3)=E(3)/(P(3)*P(2)**2)
0051            X(M,M)=-(2.0*E(M)/P(M)**3+E(M-1)/(P(M)**3)+1.0/
               1(C(M)*P(M)))
0052            X(M,M-1)=(1.0*E(M-1)/(P(M-1)*P(M)**2)+E(M)/P(M)**3*2.0
               1+1.0/(C(M)*P(M)))
0053            X(M,M-2)=-1.0/(P(M-1)*P(M)**2)*E(M-1)
0054            X(M,M+1)=E(M)/P(M)**3
0055            DO 33 I=3,M-1
0056            X(I,I)=-(2.0*E(I)/P(I)**3+E(I+1)/(P(I+1)*P(I)**2)
0057           1+1.0/(C(I)*P(I)))
0058            X(I,I-1)=1.0*E(I-1)/(P(I-1)*P(I)**2)+E(I)/P(I)**3*2.0
0059           1+1.0/(C(I)*P(I))
0060            X(I,I-2)=-E(I-1)/(P(I-1)*P(I)**2)
0061            X(I,I+1)=E(I+1)/(P(I+1)*P(I)**2)
0062         33 CONTINUE
0063            DO 61 I=2,M
0064            IF(I.GT.2) AA(I)=-X(I,I-2)/X(I,I)
0065            BB(I)=-X(I,I-1)/X(I,I)
0066            CC(I)=-X(I,I+1)/X(I,I)
0067            FF(I)=Y(I)/X(I,I)
0068            DD(1)=-X(1,2)/X(1,1)
0069            EE(1)=Y(1)/X(1,1)
0070            DD(2)=CC(2)/(1.0-DD(1)*BB(2))
0071            EE(2)=(BB(2)*EE(1)+FF(2))/(1.0-DD(1)*BB(2))
0072            IF(I.EQ.2) GOTO 61
0073            DD(I)=CC(I)/(1.0-DD(I-1)*(AA(I)+DD(I-2)+BB(I)))
0074            EE(I)=(AA(I)*EE(I-2)+(AA(I)*DD(I-2)+BB(I))*EE(I-1)+FF(I))/
               1(1.0-DD(I-1)*(AA(I)*DD(I-2)+BB(I)))
0075         61 CONTINUE
```

Input data

M - number of elements up to roof centre line
L - roof length, mm
EI - fold line inertia in plane of roof
EY - Young's modulus, kg/mm²
T - sheet thickness, mm
BL - panel depth, mm
D - corrugation pitch
P(I) - width of elements
K1 - $\bar{K}$ of first fastening range from edge
K2 - $\bar{K}$ of second fastening range from edge
K3 - $\bar{K}$ of third fastening range from edge
D1 - length of fastening from edge with K1 value, mm
D2 - length of fastening from edge with K2 value, mm
CMIN - minor flexibilities such as seam slip, shear strain etc mm/kg/mm

$$C_i = \frac{\bar{K}_i \cdot D^{2.5}}{EY \cdot T^{2.5} \cdot BL^2} \cdot Q_i + CMIN \cdot Q_i$$

Finite difference Solution

$$-EI \frac{d^3v}{dx^3} + \frac{1}{c_i} \frac{dv}{dx} = Q$$

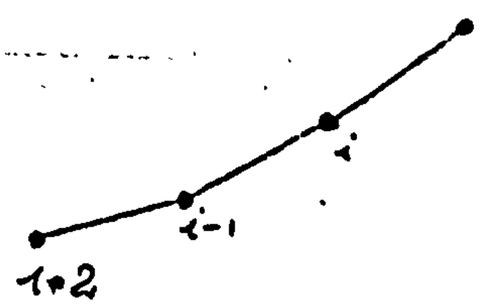

```
0079              W(M)=(EE(M)+DD(M)*EE(M-1))/(1.0-DD(M)*DD(M-1))
0080              DO 62 I=2,M
0081              J=M+2-I
0082              W(J-1)=DD(J-1)*W(J)+EE(J-1)
0083           62 CONTINUE                          Solves for fold line displacements
0084              DO 34 I=1,M
0085           34 CONTINUE
0086              WRITE(2,110)(W(I),I=1,M)
0087              WRITE(2,110)(DEL(I),I=1,M)
0088          110 FORMAT(10E12.3//)
0089              GOTO 88
0090           89 STOP
0091              END
```

L	EI	EY	T	BL	D
0.216000E 05	0.238000E 07	0.207000E 03	0.570000E 00	0.205000E 04	0.178000E 03

k1	k2	k3	D1	D2	CMIN H
0.660000E-01	0.110000E 00	0.750000E 00	0.400000E 04	0.900000E 04	0.140000E-0422

0.124E-01 0.603E-01 0.117E 00 0.172E 00 0.225E 00 0.275E 00 0.323E 00 0.371E 00 0.433E 00 0.494E 00

0.552E 00 0.604E 00 0.652E 00 0.694E 00 0.732E 00 0.765E 00 0.794E 00 0.823E 00 0.869E 00 0.911E 00

0.938E 00 0.944E 00 — Displacements along roof to centre at each element node. — Shear displacement only

0.642E-01 0.126E 00 0.184E 00 0.240E 00 0.293E 00 0.343E 00 0.391E 00 0.435E 00 0.503E 00 0.560E 00

0.624E 00 0.676E 00 0.724E 00 0.767E 00 0.804E 00 0.836E 00 0.863E 00 0.885E 00 0.992E 00 0.107E 01

0.110E 01 0.111E 01 — Free displacement along roof for zero fold line inertia.

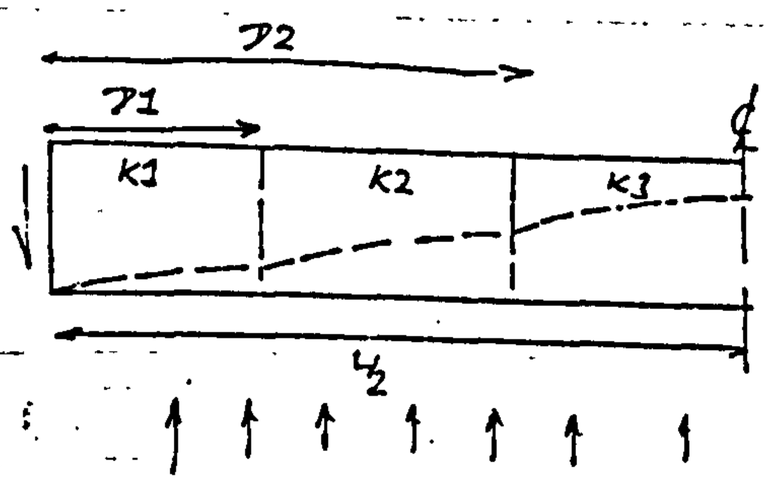

All displacements for 1 kN end shear force